Imperial College London

Early events in *Aspergillus fumigatus* infection: A chronicle of host-pathogen interactions

Timothy Charles Cairns

A thesis submitted to fulfil the requirements for a Doctor of Philosophy degree from Imperial College London, Faculty of Medicine

September 2011

Department of Microbiology
Imperial College London

This thesis is dedicated to my parents

Abstract

Host-pathogen interactions have critical implications for the establishment of disease and for determining adaptive immune responses of the host.

This study has conducted global *Aspergillus fumigatus* transcriptional analyses throughout the initiation of murine infection using a wild-type and an attenuated Δ*laeA* isolate. A novel data analysis protocol was applied from which three time-series datasets were generated between 4, 8 and 14 hours post infection. This approach identified distinct temporal gene expression profiles during disease initiation whereby numerous secreted enzymes, including proteases and antigens, were upregulated between 4 and 8 hours, while a striking upregulation of genes in secondary metabolism clusters and subtelomeric loci was observed between 8 and 14 hours.

In order to test the role of several upregulated secondary metabolite genes on host-pathogen interactions and virulence, two isolates mutated in non-ribosomal peptide synthetase encoding genes (Δ*ftmA*, Δ*pes3*), and mutants of a hybrid non-ribosomal-polyketide synthase (Δ*psoA*) and a putative secondary metabolite transcription factor (Δ*regA*) were analysed in murine models of infection. These analyses suggest fumitremorgin C, pseurotin A and, putatively, a pigment augment *A. fumigatus* virulence. In contrast, the *pes3* gene product favours pathogen clearance, possibly by facilitating recognition of host innate immunity.

There was no evidence to support the view that defective secondary metabolism is causative of the attenuated virulence phenotype observed for the LaeA mutant. Alternative hypotheses regarding the attenuation of Δ*laeA* include upregulation and downregulation of Th1 and Th2 associated antigens respectively, and deficiencies in plasma membrane transport relative to wild-type isolates.

A hypothesised deficiency in maintenance of genome stability, due to LINE-1 mobilisation in the Δ*laeA* isolate was tested, and subsequently discredited by a discovered lack of isogenicity among the tested strains.

Work presented in this thesis also assesses the use of a mass-spectrometric method for detection of epitope tagged *A. fumigatus* protein in the host.

Declaration of originality

The author of this thesis has been fortunate to collaborate with several people whom have contributed to work presented in this thesis. These people include Dan Chen, Yan Yu, John Varga and Natalie Fedorova from the J. Craig Venter Institute, Rockville, Maryland, U. S. A. Additionally, collaborators from Imperial College London include Geraint Barton, Florian Huber, Laura Alcazar-Fuoli and Hwen-Yee Chea. Finally, Leonardo Potenza from the University of Modena and Reggio Emilia, Italy.

Their contribution to the work presented in this thesis are summarised below:

***A. fumigatus* and host gene expression profiling experiments, Chapter 3, 8 and 10:**

- Dan Chen and Yan Yu conducted RNA amplification, labelling and array hybridisations
- John Varga and Natalie Fedorova conducted *A. fumigatus* microarray data capture and provided MEV and MIDAS files for non-ratiometric and ratiometric array normalisation respectively
- John Varga conducted qRT-PCR experimentation of host innate immune responses
- Geraint Barton wrote a custom R script for non-ratiometric quantile normalisation

Macrophage phagocytosis assays, Chapter 5:

- All macrophage phagocytosis assays were conducted by Laura Alcazar-Fuoli
- Optimisation of the recombineering methodology was conducted by Laura Alcazar-Fuoli

Surface enhanced laser desorption/ionisation time of flight mass spectroscopy, Chapter 6:

- Hwen-yee Chea assisted in SELDI-ToF-MS and in generating epitope tagged *A. fumigatus* strains using plasmid pSK379

ELISPOT assay 7:

- ELISPOT assays were conducted by Leonardo Potenza

Analysis of LINE-1 mobile genetic elements, Chapter 8:

- Florian Huber assisted in LINE-1 bioinformatic analyses and the Southern blot of gDNA grown under hypoxia mimicking conditions

Apart from work that is noted as originating from the input of these people, the author declares that all work contained here-in as deriving from his efforts.

Signed: **Date:**

(Timothy Cairns)

Table of contents

Title **1**

Dedication **2**

Abstract **3**

Declaration of originality **4**

Table of contents **6**

List of abbreviations and Acronyms **15**

List of Figures **18**

List of Tables **23**

Chapter 1: Introduction **30**

1.0 Aspergilli 31

1.1.0 *Aspergillus fumigatus* 32

1.1.2 Aspergillosis 32

1.1.3 Diagnosis and molecular mechanisms of *A. fumigatus* antifungal therapy 34

1.2.0- Environmental adaptation during the initiation of aspergillosis 35

1.2.1 Acquisition of nitrogen in the host 36

1.2.2 Acquisition of iron in the host 38

1.2.3 Acquisition of zinc in the host 38

1.2.4 Alkaline adaptation 39

1.2.5 Surviving hypoxia 39

1.2.6 Thermotolerance 41

1.2.7 Detoxification of reactive oxygen species 41

1.2.8 Secretion stress and the unfolded protein response 42

1.2.9 Antifungal resistance 43

1.3.0 Molecular interactions between *A. fumigatus* and the host 43

1.3.1 Molecular interactions between *A. fumigatus* resting spores and the host 44

1.3.2 Molecular interactions between *A. fumigatus* swollen spores and the host 47

1.3.3 Molecular interactions between *A. fumigatus* hyphae and the host 50

1.4.0 *A. fumigatus* Δ*laeA*: a tool for reverse engineering the molecular basis of attenuation 53

1.4.1 LaeA is a putative methyltransferase which may regulate secondary metabolite biosynthesis and subtelomeric loci by epigenetic mechanisms 54

1.4.2 *A. fumigatus* Δ*laeA* is attenuated in murine models of infection and can be used as a tool to reverse engineer the molecular basis of *A. fumigatus* virulence 56

1.5.0 Microarray technology is a powerful tool to study environmetal adaption and host-pathogen interactions during infection 57
1.5.1 Ratiometric and non-ratiometric array normalisation for analysis of *A. fumigatus* gene expression during early murine infection 58
1.6.1 Existing mass spectrometric tools for studying *A. fumigatus* proteins 67
1.6.2 The advantages of Surface enhanced laser desorption/ionisation time of flight mass spectrometry for pathogen protein detection in the infected murine lung 69
1.7.0 Principle objective of this study 70
1.7.1 Specific objectives of this study 70

Chapter 2: Materials and Methods 73
2.1 Chemicals, enzymes and general reagents 73
2.2 Media 73
2.2.1 Bacterial culture 73
2.2.2 *A. fumigatus* culture 74
2.3.0 General molecular techniques 74
2.3.1 Oligonucleotide primer synthesis 74
2.3.2 Polymerase chain reaction (PCR) 74
2.3.3 Separation of DNA fragments using electrophoresis 74
2.3.4 Generation of competent bacterial cells 75
2.3.5 Bacterial transformation 75
2.3.6 Plasmid extraction from bacterial culture 75
2.3.7 Plasmids 75
2.3.8 Sequencing 75
2.3.9 DNA Cloning Techniques 76
2.3.10 Southern blotting 76
2.3.11 SDS-PAGE 77
2.3.12 Western blotting 77
2.3.13 Reverse transcriptase quantitative PCR (RT-qPCR) 78
2.4.0 *A. fumigatus* techniques 78
2.4.1 Transformation of *A. fumigatus* electrocompetent spores 78
2.4.2 Transformation of *A. fumigatus* protoplasts 79
2.4.3 Extraction of *A. fumigatus* DNA from spores 80
2.4.4 Extraction of *A. fumigatus* DNA from mycelia 80
2.4.5 Protein extraction from *A. fumigatus* mycelia 81
2.4.6 Protein extraction from *A. fumigatu*s supernatant 71

2.4.7 RNA extraction from *A. fumigatus* mycelia 81
2.4.8 *A. fumigatus* phenotypic test 81
2.4.9 *A. fumigatus* germination assay 82
2.4.10 *A. fumigatus* growth assay 82
2.4.11 *A. fumigatus* oxidative stress assay 82
2.5.0 Murine Infections 82
2.5.1 Survival analysis 82
2.5.2 Histopathology 83
2.5.3 qPCR assay for measurement of fungal burden in murine lungs 83
2.5.4 Murine infections for Microarray Experiments 84
2.6.0 Microarray techniques 85
2.6.1 *A. fumigatus* RNA Extraction, amplification and hybridisation 85
2.6.2 *A. fumigatus* microarray data capture 85
2.6.3 Ratiometric microarray normalisation 86
2.6.4 Non-ratiometric microarray normalisation 86
2.6.5 Mus musculus host RNA qRT-PCR Super Array analyses 87
2.7.0 SELDI-ToF-MS Techniques 88
2.7.1 Immobilisation of anti-his antibody and antigen on PG20 chips 88
2.7.2 Surface enhanced laser desorption/ionisation time of flight mass spectrometry 89
2.8.0 Modified recombineering approach for generation of *A. fumigatus* gene disruption cassette 90
2.8.1 Lambda phage infection of BAC clones 90
2.8.2 Recombineering and chemical transformation of BACs gene-disruption biselectable marker 91
2.8.3 BAC extraction from bacterial culture 91

Chapter 3: Time-point specific transcriptional profiling of *A. fumigatus* Af293 and Δ*laeA* mutant during the initiation of murine infection 92
3.1 Overview 92
3.2 Methods 95
3.2.1 *A. fumigatus* strains 95
3.2.2 Murine infection 95
3.2.3 *A. fumigatus* RNA Extraction, amplification and hybridisation 96
3.2.4 *A. fumigatus* microarray scanning and normalisation 95
3.3 Results 98
3.3.1 Experimental design, non-ratiometric data capture and quantile normalisation 98

3.4 *A. fumigatus* Af293 transcriptional profile during the initiation of murine infection 105
3.4.1 Gene expression profiling of the Af293 isolate between 4 and 14 hours in the murine lung 108
3.4.3 Characterisation of differentially expressed genes between 4 and 14 hours: chromosomal loci, lineage specificity and functionality 108
3.4.2 Functional classification of differentially expressed genes between 4 and 14 hours post infection in Af293 123
3.4.3 Characterisation of differentially expressed genes between 4 and 14 hours: chromosomal loci, lineage specificity and functionality 145
3.4.4 Analysis of differentially expressed genes between 4 and 14 hours: comparison to other relevant microarray studies 148
3.4.5 Time-point specific gene expression profiling of the Af293 isolate in the murine lung 152
3.4.6 Functional classification of time-point specifc datasets for Af293 murine infection 167
3.4.7 Characterisation of Af293 time-point specific datasets: chromosomal loci, lineage specificity and functionality 200
3.4.8 Short Time-series Expression Miner profiling of temporal gene expression in Af293 during murine infection 205
3.5. A. *fumigatus* Δ*laeA* transcriptional profile during the initiation of murine infection 211
3.5.1 Gene expression profiling of the Δ*laeA* isolate between 4 and 14 hours in the murine lung 213
3.5.2 Functional classification of differentially expressed genes between 4 and 14 hours post infection in Δ*laeA* 222
3.5.3 Characterisation of differentially expressed genes between 4 and 14 hours: chromosomal loci, lineage specificity and functionality 237
3.5.4 Time-point specific gene expression profiling of the Δ*laeA* isolate in the murine lung 239
3.5.6 Characterisation of Δ*laeA* time-point specific datasets: chromosomal loci, lineage specificity and functionality 279
3.5.7 STEM profiling of temporal gene expression in Δ*laeA* during murine infection 284
3.6.1. Summary 290

Chapter 4: Virulence analyses of *A. fumigatus* NRPS/PKS deletants Δ*psoA*, Δ*ftmA* and Δ*pes3* in neutropenic and corticosteroid treated murine models of infection 307

4.1 Overview 307
4.2 Materials and methods 310
4.2.1 *A. fumigatus* strains 310
4.2.2 Oligonucleotide primers 310
4.2.3 Survival analysis 310
4.2.4 Histopathology 311
4.2.5 qPCR assay for measurement of fungal burden in murine lungs 311
4.3 Results 313
4.3.1 Establishing a qPCR method for measuring *A. fumigatus* burden using the ΔCt method 313
4.3.2 Determination of amplification efficiencies of murine actin and fungal beta tubulin primers 313
4.3.3 A qPCR assay detects statistically significant differences in fungal burden between fully virulent Af293 and attenuated Δ*pabaA* isolates in both neutropenic and corticosteroid treated murine models of infection 316
4.4. Survival, histological and infection burden comparisons of the Af293 clinical isolate with the Af293Δ*psoA* strain in neutropenic and corticosteroid treated murine models of infection 318
4.5 Survival, histological and infection burden comparisons of the Af293 clinical isolate with the Af293Δ*fmtA* strain in neutropenic and corticosteroid treated murine models of infection 323
4.6 Survival, histological and infection burden comparisons of the ATCC46645 clinical isolate with the ATCC46645Δ*pes3* strain in neutropenic and corticosteroid treated murine models of infection 327
4.7 Discussion 331

Chapter 5: Disruption and virulence analysis of the *regA* gene, encoding a putative melanin transcription factor 344
5.1 Overview 344
5.2 Materials and methods 347
5.2.1 *A. fumigatus* strains 347
5.2.2 Phage strain 347
5.2.3 Bacterial strain 347
5.2.4. Plasmids 347
5.2.5 Oligonucleotide primers 348

5.2.6 Modified recombineering approach for generation of a *A. fumigatus regA* disruption cassette 348
5.2.7 Lambda phage infection of BAC clones 349
5.2.8 Recombineering and chemical transformation of BACs with a *regA* gene replacement biselectable marker cassette 349
5.2.9 Fungal transformation using *A. fumigatus* protoplasts 350
5.2.10 Southern blotting 351
5.2.11 Murine infections 352
5.2.12 Histopathology 353
5.2.13 Macrophage phagocytosis assay 353
5.3 Results 354
5.3.1 Construction of *regA* disruption cassette using modified recombineering methodology 354
5.3.2 Gene replacement of *regA* in *A. fumigatus* 356
5.3.3 Δ*regA* displays wild-type resistance to cell wall and oxidative stress but an increased resistance to macrophage phagocytosis 359
5.3.4 *regA* deletion causes a reduction in fungal burden in a corticosteroid, but not neutropenic, murine model of infection 360
5.4 Discussion 365

Chapter 6: Surface enhanced laser desorption/ionisation time of flight mass spectrometry for high through put detection of epitope-tagged fungal proteins in murine BAL fluid 375

6.1 Overview 375
6.2 Materials and methods 377
6.2.1 *A. fumigatus* strains 377
6.2.2 Bacterial strains 377
6.2.3 Plasmids 377
6.2.3.1 pGEM_BLE 377
6.2.3.2 pGEM_TK 377
6.2.3.3 pSK379. 377
6.2.3 Oligonucleotide primers 379
6.2.4 Cloning of PCR inserts into plasmids pGEM_BLE and pGEM_TK for the generation of *A. fumigatus* epitope tag transformation constructs 381
6.2.5 Transformation of *A. fumigatus* electrocompetent spores 382

6.2.6 Cloning inserts into plasmid pSK379 for the construction of epitope tagged transformation vector 383
6.2.7 Fungal transformation using *A. fumigatus* protoplasts 384
6.2.8 Semi-quantitative RT-PCR assay 385
6.2.9 Protein extraction from *A. fumigatus* mycelia 385
6.2.10 Protein extraction from *A. fumigatus* supernatant 386
6.2.11 SDS-PAGE and Western blot analyses of protein extracts 386
6.2.12 Murine infections 387
6.2.13 Lyophilisation of murine BALF 387
6.2.14 Albumin depletion of murine BALF 387
6.2.15 Acetone precipitation of murine BALF 388
6.2.16 Ni-NTA enrichment of murine BALF 388
6.2.17 Immobilisation of anti-his antibody and antigen on PG20 chips 388
6.2.18 Surface enhanced laser desorption/ionisation time of flight mass spectrometry 389
6.3 Results 390
6.3.1 Construction of *A. fumigatus* his-tagged alleles 390
6.3.2 Afu5g00540 his-tagged allele is transcribed during 16 hours in vitro culture 394
6.3.3 SELDI-ToF-MS, but not Western blotting, detects epitope tagged *A. fumigatus* Afu5g00540 protein from in vitro culture 395
6.3.4 SELDI-Tof-MS analysis of in vitro protein 398
6.3.5 SELDI-ToF-MS detection of minute quantities of polyhistidine-tagged bacterial protein diluted with murine BALF 401
6.3.6 Construction of a library of recombinant *A. fumigatus* clones expressing His-tagged candidate alleles 402
6.3.7 Putative SELDI-ToF-MS detection of epitope tagged proteins in BALF from mice infected with a library of *A. fumigatus*_His6 strains 410
6.3.8 SELDI-ToF-MS does not reproducibly detect epitope tagged proteins in BALF from mice infected with single *A. fumigatus*_His6 strains 420
6.4 Discussion .428

Chapter 7: Expression, purification and PBMC responses to two putative *A. fumigatus* allergens 438
7.1 Overview 438
7.2 Materials and methods 440
7.2.1 Bacterial strains 440

7.2.2 Plasmids 440
7.2.3 Oligonucleotide primers 441
7.2.4 Cloning 441
7.2.5 Expression optimisation 441
7.2.6 Coomassie Staining 442
7.2.7 Western Analysis 442
7.2.8 Protein purification 442
7.2.9 Endotoxin removal 443
7.2.10 ELISPOT assay 443
7.3 RESULTS 444
7.3.1 Cloning of Afu2g03830 and Afu5g13300 cDNAs into PRSET A 441
7.3.2 Pilot protein expression utilising pRSET_3830 and pRSET_3300 445
7.3.3 Batch purification of Asp F4 and Asp F10 using NiNTA agarose beads 446
7.3.4 ELISPOT assays using purified recombinant antigens 447
7.4 Discussion 449

Chapter 8: Ratiometric comparisons of *A. fumigatus* Af293 and ΔlaeA during murine infection 451
8.2 Methods 453
8.2.1 *A. fumigatus* strains 453
8.2.2 Murine infection 453
8.2.3 *A. fumigatus* microarray normalisation 453
8.2.4 Mus musculus host RNA qRT-PCR Super Array analyses 454
8.3 Results 456
8.3.1 Comparative histological analyses of Af293 and Δ*laeA* infected lungs 456
8.3.2 Ratiometric gene expression profiling of Δ*laeA* relative to Af293 at 4, 8 and 14 hours post infection 458
8.3.3 Functional classification of differentially expressed genes 479
8.3.4 Characterisation of gens differentially expressed between Δ*laeA* and Af293: chromosomal loci, lineage specificity and functionality 487
8.3.5 Profiling host innate immune responses to Af293 and Δ*laeA* 493
8.3.5 Interrogation of LINE-1 mobilisation in Af293, CEA10 and ATCC46645 isolates 501
8.4 Summary 503

Chapter 9: Discussion and conclusions **516**

Chapter 10: Addendum: Ratiometric and non-ratiometric comparisons of *A. fumigatus* Af293 and Δ*laeA* during the initation of infection **532**

10.1 Overview 532

10.2 Materials and methods 533

10.3 Results 534

10.3.1 Experimental design 534

10.3.2 Time-point specific transcriptional profiling of *A. fumigatus* Af293 during the initiation of murine infection 535

10.3.3 *A. fumigatus* Af293 transcriptional profile during the initiation of murine infection 538

10.3.4 Functional classification of differentially expressed genes between 4 and 14 hours post infection in Af293 565

10.3.5 Characterisation of differentially expressed genes between 4 and 14 hours: chromosomal loci, lineage specificity and functionality 580

10.3.7 Time-point specific gene expression profiling of the Af293 isolate in the murine lung 582

10.3.8 Functional classification of time-point specifc datasets for Af293 murine infection 624

10.3.9 Ratiometric comparisons of *A. fumigatus* Af293 and Δ*laeA* during murine infection 655

10.4 Discussion

Appendix A: Gene expression datasets **702**

References **705**

Acknowledgements **725**

List of Abbreviations and Acronyms

µg	Microgram
µl	Microlitre
µM	Micromolar
ABPA	Allergic bronchopulmonary aspergillosis.
ACM	*Aspergillus* complete media
AIDS	Acquired immune deficiency syndrome
AMM	*Aspergillus* minimal media
ATP	Adenosine triphosphate
ATCC	American type culture collection
BAC	Bacterial artificial chromosome
BALs	Bronchoalveolar lavage
BALFs	Bronchoalveolar lavage fluid
BCA	Bicinchoninic acid
BLAST	Basic local alignment search tool
BSA	Bovine serum albumin
bp	Base pair
cDNA	Complementary DNA
CC	Contingency clusters
CIP	Calf intestinal alkaline phosphatase
CFU	Colony forming unit
CGD	Chromin granulomatous disease
Ct	Threshold cycle
CT	Computerised tomography
CWI	Cell wall integrity
dH_2O	Distilled water
DNA	Deoxyribonucleic acid
ECL	Enhanced chemiluminescence
EDTA	Ethylenediaminetetraacetic acid
ER	Endoplasmic reticulum
gDNA	genomic DNA
GABA	γ-Amino-*n*-butyric acid
GFP	green fluorescent protein
GMS	Grocott's methanamine sliver
GO	Gene ontology
GPI	Glycosylphosphoinositol
GTP	Guanosine-5'-triphosphate
HEPES	4-(2-hydroxyethyl)-1-piperazineethanesulfonic acid
HKG	House-keeping gene
HPLC	High-performance liquid chromatography
g/l	Grams per litre
H and E	Haemotoxylin and eosin
HDACs	Histone acetyltransferases
HOG	High osmolarity glycerol
HSCT	Hematopoietic stem-cell transplantation
Ig	Immunoglobulin
IFN-γ	Interferon gamma
IL	Interleukin
IPA	Invasive pulmonary aspergillosis
IPTG	Isopropyl-beta-D-thiogalactopyranoside
Kb	kilobase

kDa	Kilo dalton
kg	Kilogram
L	Litre
LB	Lysogeny broth
LINEs	Ling interspersed nuclear elements
LOWESS	Locally weighted scatter plot smoothing
LTRs	Long terminal repeat
M	Molar
MA	Microarray
MALDI	Matrix assisted laser desorption/ ionisation
MAPK	Mitogen activated protein kinase
MDR	Multidrug resistance
MFS	Major facilitator superfamily
mg	Milligram
ml	Milliliter
mM	Millimolar
mRNA	Messenger RNA
MS	Mass spectrometry
mw	Molecular weight
n	Number
NETs	Neutrophil extracellular traps
ng	Nanogram
NRPS	Nonribosomal peptide synthetase
OD	Optical density
ORF	Open reading frame
p	P-value
PARs	Protease activated receptors
PAGE	Polyacrylamide Gel Electrophoresis
PBMCs	Peripheral blood mononuclear cell
PBS	Phosphate buffered saline
PAMPs	Pathogen-associated molecular patterns
PRR	Pathogen recognition receptor
PCR	Polymerase chain reaction
PEG	Polyethylene glycol
PKA	Protein Kinase A
PKS	Polyketide synthase
PMN	Polymorphonuclear cells
PNK	Polynucleotide Kinase
PYRT	Pyrithiamine
RIA	Reductive iron assimilation
RNA	Ribonucleic acid
rRNA	Ribosomal RNA
RnaseH	Ribonuclease H
ROS	Reactive oxygen species
Rpm	Rotations per minute
RT-PCR	Reverse transcription polymerase chain reaction
SDS	Sodium dodecyl sulfate
SELDI	Surface-enhanced laser desorption/ionization
SINEs	Short interspersed nuclear elements
SSC	Saline Sodium Citrate
STEM	Short Time-series Expression Miner
TCA	Trichloroacetic acid
TE	Tris EDTA buffer

TLC	Thin layer chromatography
ToF	Time of flight
TOR	Target of
TLR	Toll-like receptor
UV	Ultraviolet
WT	wild-type
X-CGD	X-linked chronic granulomatous disease

List of Figures

	Page
Fig. 1.1: The clinical spectrum of disease caused by *A. fumigatus*.	**33**
Fig. 1.2: Schematic depicting putative host-pathogen interactions during the initiation of *A. fumigatus* murine infection.	**46**
Fig. 1.3: Options for experimental design of microarray experiments investigating Af293 and Δ*laeA* gene expression throughout a 3 time-point time-course.	**59**
Fig. 1.4: Comparison of standard ratiometric (A) and non-ratiometric (B) of dual colour microarrays in a two strain time series experiment.	**62**
Fig. 1.5: Schematic representation of ratio and single channel intensity strategies to analyse the host infecting fungal transcriptome in Af293 and Af293 Δ*laeA.*	**65**
Fig. 3.1: Hybridisations of Af293 and Δ*laeA* replicates throughout the experiment.	**98**
Fig. 3.2: Schematic representation of experimental design and quantile normalisation.	**100**
Fig. 3.3: Box plots depicting nonratiometric intensity distribution before and after double quantile normalisation for Af293 and Δ*laeA* datasets.	**101**
Fig. 3.4: Schematic depicting count and standard deviation filtering for three genes at a single time-point post infection.	**102**
Fig. 3.5: Frequency distribution of relative nSI datasets.	**105**
Fig. 3.6: Venn diagrams depicting comparisons between relative nSI datasets from the Af293 non-ratiometric analysis.	**108**
Fig. 3.7: Histopathological analysis of Af293 during infection.	**109**
Fig. 3.8: Distribution of differentially expressed genes between 4 – 14 hours post infection among the functional cohorts of chromosomal location, signal peptide content, *A. fumigatus* specificity and functional association.	**146**
Fig. 3.9: Distribution of differentially expressed genes from three microarray studies among 4 – 14 hour differentially expressed datasets.	**149**
Fig. 3.10: Schematic depicting time-point specific transcriptional comparisons.	**153**
Fig. 3.11: Distribution of differentially expressed genes between 4 – 8, and 8 - 14 hours post infection among the functional cohorts of chromosomal location,	**201**

signal peptide content, *A. fumigatus* specificity and functional association.

Fig. 3.12: nSI values for genes in the gliotoxin biosynthetic cluster at 4, 8 and 14 hours post infection. **204**

Fig. 3.13: nSI values for NRPS and PKS genes at 4, 8 and 14 hours post infection. **205**

Fig. 3.14: STEM analysis of the Af293 infection time-course. **207**

Fig. 3.15: STEM clustering analysis of differentially expressed genes in the Af293 time-course ordered on the basis of enrichment of genes within location and functionally related cohorts. **210**

Fig. 3.16: Venn diagrams depicting comparisons between relative nSI datasets from the Δ*laeA* non-ratiometric analysis. **213**

Fig. 3.17: Histopathological analysis of Δ*laeA* during the initiation of murine infection. **214**

Fig. 3.18: Distribution of differentially expressed genes between 4 – 14 hours post infection among the functional cohorts of chromosomal location, signal peptide content, *A. fumigatus* specificity and functional association. **237**

Fig. 3.19: Schematic depicting time-point specific transcriptional comparisons. **239**

Fig. 3.20: Distribution of differentially expressed genes between 4 – 8, and 8 - 14 hours post infection among the functional cohorts of chromosomal location, signal peptide content, *A. fumigatus* specificity and functional association. **280**

Fig. 3.21: nSI values for genes in the gliotoxin biosynthetic cluster at 4, 8 and 14 hours post infection. **283**

Fig. 3.22: nSI values for Δ*laeA* NRPS and PKS genes at 4, 8 and 14 hours post infection. **284**

Fig. 3.23: Transcription profile clustering analyses of the Δ*laeA* infection time-course. **285**

Fig. 3.24: STEM clustering analysis of differentially expressed genes in the Δ*laeA* time-course ordered on the basis of enrichment of genes within location and functionally related cohorts. **288**

Fig. 4.1: Ct values from triplicate RT-PCR reactions using murine actin or fungal beta tubulin primers, with fungal gDNA or saline inoculated murine lung gDNA as template. **314**

Fig. 4.2: Graphical representation of *A. fumigatus* beta tubulin and murine actin primer efficiencies. **315**

Fig. 4.3: ΔCt^{norm} values calculated from Af293 or Δ*pabaA* infected mice in **318**

neutropenic and corticosteroid treated models of infection.

Fig. 4.4: Survival, histological and tissue burden comparisons of Δ*psoA* and Af293 in a neutropenic murine model of infection. **320**

Fig. 4.5: Survival, histological and tissue burden comparisons of Δ*psoA* and Af293 in a corticosteroid murine model of infection. **322**

Fig. 4.6: Survival, histological and tissue burden comparisons of Δ*ftmA* and Af293 in a neutropenic murine model of infection. **324**

Fig. 4.7: Survival, histological and tissue burden comparisons of Δ*ftmA* and Af293 in a corticosteroid murine model of infection. **326**

Fig. 4.8: qPCR analyses of fungal burden from ATCC46645 or Δ*pes3* infected mice in neutropenic and corticosteroid treated models of infection. **328**

Fig. 4.9: Histological comparisons of ATCC46645 and Δ*pes3* in corticosteroid treated murine model of aspergillosis at 14 and 24 hours post infection. **329**

Fig. 4.10: Survival comparison of ATCC46645 and Δ*pes3* isolates in a corticosteroid treated murine model of infection. **330**

Fig. 5.1: Construction of *regA* deletion cassette by BAC recombineering. **355**

Fig. 5.2: *regA* gene replacment in *A. fumigatus* using the BAC CC_e12.9 cassette. **357**

Fig. 5.3: Comparison of vegetative growth and germination rates for Ku80 and Δ*regA*. **358**

Fig. 5.4: Percentage survival of Ku80 and Δ*regA* spores following incubation with various concentrations of hydrogen peroxide, and percentage of phagocytosed conidia following incubation with murine macrophages **360**

Fig. 5.5: Fungal burden of Ku80 and Δ*regA* infected murine lung from a neutropenic model of aspergillosis. **361**

Fig. 5.6: Histological comparisons of Ku80 and Δ*regA* infected murine lung in a neutropenic model of aspergillosis at 4 days post infection **361**

Fig. 5.7: Fungal burden of Ku80 and Δ*regA* infected murine lung from a corticosteroid model of aspergillosis. **362**

Fig. 5.8: Histological comparisons of Ku80 and Δ*regA* infected bronchioles in a corticosteroid murine model of aspergillosis at 5 days post infection. **363**

Fig. 5.9: Histological comparisons of Ku80 and Δ*regA* infected alveoli in a corticosteroid murine model of aspergillosis at 5 days post infection. **364**

Fig. 6.1: Cloning strategy for epitope tagging of *A. fumigatus* genes using a split marker methodology. **392**

Fig. 6.2: Schematic depicting locations of confirmation primers before and after a homologous recombination event with the *ble/tk* biselectable marker, and gel electrophoresis image of PCR products using confirmation primers and transformant or Ku80 gDNA as template **393**

Fig. 6.3: Semi quantitative RT-PCR assay to determine Afu5g00540-His_6 transcript abundance relative to *A. fumigatus* beta tubulin following 16 hour in vitro culture in ACM. **395**

Fig. 6.4: SDS-PAGE and Western blot analyses of crude and Ni-NTA purified *A. fumigatus* Afu5g00540_His_6 and Ku80 mycelial extracts. **397**

Fig. 6.5: Spectra from SELDI-ToF-MS analyses of crude or acetone precipitated/Ni-NTA treated protein extracted from Afu5g00540-His_6 or Ku80 from 16 hours in vitro culture. **400**

Fig. 6.6: Spectra from SELDI-ToF-MS analyses of murine BAL fluid spiked with epitope tagged Afu2g03830. **402**

Fig. 6.7: Plasmid maps of pSK379 and an exemplar epitope tag vector (pSK379 Afu4g11800_His_6). **406**

Fig. 6.8: Schematic depicting a homologous recombination event between an exemplar epitope tag vector (pSK379 Afu4g11800_His_6) and the *A. fumigatus* genome. **407**

Fig. 6.9: Gel electrophoresis of PCR reactions using primers AfuX_F and His_R, with transformant or Ku80 gDNA as template. **409**

Fig. 6.10: Spectra between 0 – 20 kDa from SELDI-ToF-MS analysis of Ku80 infected murine BALF extracted 4 hours post infection. **413**

Fig. 6.11: Spectra from SELDI-ToF-MS analyses of library or control infected murine BALF extracted 4 hrs post infection. **414**

Fig. 6.12: Spectra from SELDI-ToF-MS analyses of library or control infected murine BALF extracted 18 hrs post infection. **416**

Fig. 6.13: Spectra from SELDI-ToF-MS analyses of *A. fumigatus*_His_6 or Ku80 infected murine BALF extracted at 4 and 18 hrs. **422**

Fig. 6.14: Spectra from SELDI-ToF-MS analyses of *A. fumigatus*_His_6 or Ku80 infected murine BALF extracted at 4 and 18 hrs. **426**

Fig. 6.15: Spectra from SELDI-ToF-MS analyses of Afu3g14170_His_6 and Afu3g14030_His6 infected murine BALF extracted at 4 and 18 hrs. **427**

Fig. 7.1: Plasmid map of pRSET A. **440**

Fig. 7.2: Coomassie stained SDS-PAGE gels visualising protein extractions **446**

from C41 cells containing pRSET_3830 and pRSET_3300 following IPTG induction.	
Fig. 7.3: Asp F4 and Asp F10 purification under denaturing conditions and verification using western blotting.	**447**
Fig. 7.4: IFN-γ and IL-10 ELISPOT assay on PBMC isolated from a single patient with probably IPA.	**448**
Fig. 8.1: Histopathology of mice infected with Af293 and Δ*laeA*.	**457**
Fig. 8.2: Schematic representation of experimental design and ratiometric normalisation for a single gene throughout the time-course of infection.	**459**
Fig. 8.3: MA plot for Af293 Δ*laeA* 14 hrs versus Af293 14 hrs analysis.	**460**
Fig. 8.4: Box whisker plots depicting the sequential stages of data normalisation.	**461**
Fig. 8.5: Scatter plots depicting variation in $\log_2$ ratios between biological and technical replicates.	**462**
Fig. 8.6: Venn diagrams depicting distribution of differentially expressed genes between the Δ*laeA* and Af293 throughout the time course of infection.	**465**
Fig. 8.7: Distribution of cohorts categorised by chromosomal location, signal peptide content, *A. fumigatus* specificity and functional association among Δ*laeA*:Af293 differentially expressed datasets throughout infection.	**487**
Fig. 8.8: A transcriptional snap shot of the LaeA regulon across the time-course of early infection.	**492**
Fig. 8.9: Schematic depicting normalisation of an exemplar gene for host transcriptional comparisons between Af293 and Δ*laeA* infected animals.	**494**
Fig. 8.10: Gene expression profiling of 6 innate immune genes between saline inoculated, and Af293 and Δ*laeA* infected BALFs.	**495**
Fig. 8.11: Southern blots of *A. fumigatus* gDNA using a 592 bp gDNA fragment common to eleven putative LINE-1 elements.	**501**
Figure 10.1: Hybridisation scheme for replicated Af293/Δ*laeA* competitive hybridisations.	**534**
Figure 10.2: Box plots depicting non-ratiometric spot intensity distribution before and after double quantile normalisation for Af293 and Δ*laeA* datasets.	**536**
Figure 10.3: Frequency distribution of relative nSI datasets.	**537**
Figure 10.4: Venn diagrams depicting comparisons between relative nSI datasets from the Af293 nonratiometric analysis.	**540**
Figure 10.5 Distribution of differentially expressed genes between 4 – 14	**581**

hours post infection among the functional cohorts of chromosomal location, signal peptide content, *A. fumigatus* specificity and functional association.

Figure 10.6: Distribution of differentially expressed genes between 4 – 8, and 8 - 14 hours post infection among the functional cohorts of chromosomal location, signal peptide content, and *A. fumigatus* specificity **656**

Figure 10.7: Box whisker plots depicting the effect of sequential data normalisations. **659**

List of Tables

Table 1.1: Summary of possible stress conditions encountered in the natural niche or during colonisation of the immunocompromised mammal. **36**

Table 2.1: Calibration parameters for protein standards present in ProteinChip All-in-One Protein Standard II (Biorad). **89**

Table 3.1: Summary statistics for the Af293 non-ratiometric analysis **105**

Table 3.2: Summary statistics for Af293 relative nSI datasets. **106**

Table 3.3: Over-represented Gene Ontology terms among genes with increasing expression between 4 and 14 hours in the Af293 infected murine lung. **109**

Table 3.4: Significant GO terms among genes with decreasing expression between 4 and 14 hours in the Af293 infected murine lung. **110**

Table 3.5: 100 genes with greatest nSI increase between 4 and 14 hours post infection. **111**

Table 3.6: 100 genes with greatest nSI decrease between 4 and 14 hours post infection. **116**

Table 3.7: Functional classification of selected genes having differential transcript abundance in Af293 between 4 and 14 hours post infection in the murine lung. **123**

Table 3.8: Distribution and Chi-square analysis of differentially expressed genes categorised by chromosomal location, signal peptide content, *A. fumigatus* specificity and annotation at 4 – 14 hours post infection. **146**

Table 3.9: Distribution and Chi-square analysis of differentially expressed **149**

genes from relevant microarray studies among 4 – 14 hour differentially expressed datasets.

Table 3.10: Classification of 154 genes upregulated during 3 microarray analyses of *A. fumigatus* in the murine lung by chromosomal position, *A. fumigatus* specificity, signal peptide content and functional association. **151**

Table 3.11: Over represented Gene Ontology terms among genes with increasing expression between 4 and 8 hours in the Af293 infected murine lung. **153**

Table 3.12: Over represented Gene Ontology terms among genes with increasing expression between 8 and 14 hours in the Af293 infected murine lung. **153**

Table 3.13: Over represented Gene Ontology terms among genes with decreasing expression between 4 and 8 hours in the Af293 infected murine lung. **154**

Table 3.14: Over represented Gene Ontology terms among genes with decreasing expression between 8 and 14 hours in the Af293 infected murine lung. **154**

Table 3.15: 100 genes with greatest nSI increase between 4 and 8 hours post infection. Genes are reported ranked according to greatest nSI intensity increase between 4 and 8 hours. **155**

Table 3.16: 100 genes with greatest nSI decrease between 4 and 8 hours post infection. **158**

Table 3.17: 100 genes with greatest nSI increase between 8 and 14 hours post infection. **160**

Table 3.18: Top 100 genes with greatest nSI decrease between 8 and 14 hours post infection. **163**

Table 3.19: Functional classification of selected genes having differential transcript abundance in Af293 between 4 and 8 hours post infection in the murine lung. **167**

Table 3.20: Functional classification of selected genes having differential transcript abundance in Af293 between 8 and 14 hours post infection in the murine lung. **182**

Table 3.21: Distribution and Chi-square analysis of differentially expressed genes categorised by chromosomal location, signal peptide content, *A. fumigatus* specificity and annotation at 4 - 8 hours post infection. **203**

Table 3.22: Distribution and Chi-square analysis of differentially expressed genes categorised by chromosomal location, signal peptide content, *A. fumigatus* specificity and annotation at 8 - 14 hours post infection.	**203**
Table 3.23: Significant GO terms among the red cluster during the Af293 time course.	**206**
Table 3.24: Significant GO terms among the green cluster during the Af293 time course.	**207**
Table 3.25: Significant GO terms among profiles 39, 49, 34, 36, 48, 44, and 38 in the Af293 time-course experiment.	**208**
Table 3.26: Summary statistics for the Δ*laeA* non-ratiometric analysis.	**210**
Table 3.27: Summary statistics for Δ*laeA* relative nSI datasets.	**211**
Table 3.28: Over-represented Gene Ontology terms among genes with increasing expression between 4 and 14 hours in the Δ*laeA* infected murine lung.	**214**
Table 3.29: 100 genes with greatest nSI increase between 4 and 14 hours post infection in Δ*laeA*.	**214**
Table 3.30: 100 genes with greatest nSI decrease between 4 and 14 hours post infection.	**218**
Table 3.31: Functional classification of selected genes having differential transcript abundance in Δ*laeA* between 4 and 14 hours post infection in the murine lung	**222**
Table 3.32: Distribution and Chi-square analysis of dfferentially expressed genes categorised by chromosomal location, signal peptide content, *A. fumigatus* specificity and functional association among 4 – 14 hour dataset.	**237**
Table 3.33: Top 100 genes with greatest nSI increase between 4 and 8 hours post infection.	**239**
Table 3.34: Top 100 genes with greatest nSI decrease between 4 and 8 hours post infection.	**241**
Table 3.35: Top 100 genes with greatest nSI increase between 8 and 14 hours post infection.	**244**
Table 3.36: Top 100 genes with greatest nSI decrease between 8 and 14 hours post infection.	**246**
Table 3.37: Functional classification of selected genes having differential transcript abundance in Δ*laeA* between 4 and 8 hours post infection in the murine lung.	**250**

Table 3.38: Functional classification of selected genes having differential transcript abundance in Δ*laeA* between 8 and 14 hours post infection in the murine lung.	**263**
Table 3.39: Distribution and Chi-square analysis of differentially expressed genes categorised by chromosomal location, signal peptide content, *A. fumigatus* specificity and functional association among 4 – 8 hour datasets.	**280**
Table 3.40: Distribution and Chi-square analysis of differentially expressed genes categorised by chromosomal location, signal peptide content, *A. fumigatus* specificity and functional association among 8 – 14 hour differentially expressed datasets.	**281**
Table 3.41: Significant GO terms among the red cluster during the Δ*laeA* time course	**285**
Table 3.42: Significant GO terms among the green cluster during the Δ*laeA* time course.	**286**
Table 3.43: Significant GO terms among profiles 30, 34, 38 and 49 in the Δ*laeA* time-course experiment.	**286**
Table 4.1: Oligonucleotide primer sequences used in this chapter.	**310**
Table 5.1: Oligonucleotide primer sequences used in this chapter	**348**
Table 5.2: Phenotypic plate assay reagents and concentrations to effect cell wall and membrane stress.	**359**
Table 6.1: Oligonucleotide primer sequences used in this chapter.	**378**
Table 6.2: Shortlisted predicted genes for pilot epitope tagging and SELDI-ToF-MS detection.	**390**
Table 6.3: Stage specific gene expression profiles during initiation of infection for 40 genes selected for epitope tagging.	**404**
Table 6.4: Grouping of *A. fumigatus* strains putatively expressing an epitope tag in two libraries for murine infection.	**412**
Table 6.5: Treatment type, molecular mass and intensity of spectral peaks putatively representing epitope tagged protein detection from group A, group B and Ku80 infected BALF.	**419**
Table 7.1: Oligonucleotide primer sequences used in this chapter.	**441**
Table 8.1: Correlation coefficients between experiments.	**463**
Table 8.2: Summary statistics for the Δ*laeA* versus Af293 time course during initiation of murine infection.	**463**
Table 8.3: Number of differentially expressed genes for Δ*laeA* versus Af293	**464**

time-course during initiation of murine infection, based on students t-test.

Table 8.4: Number of differentially expressed genes for Δ*laeA* versus Af293 time course during initiation of murine infection, based on standard deviation corrected data with a fold change of ±1.5 between isolates. **465**

Table 8.5: Genes with increased transcript abundance in Δ*laeA* relative to Af293 throughout the time course of infection **466**

Table 8.6: Genes with decreased transcript abundance in Δ*laeA* relative to the wild type throughout the time course of infection. **471**

Table 8.7: Over-represented Gene Ontology terms among genes with decreased transcript abundance in the Δ*laeA* strain 4 hours post infection. **480**

Table 8.8: Functional classification of selected genes having differential transcript abundance in Δ*laeA* mutant relative to the parental isolate Af293 during initiation of murine infection. **482**

Table 8.9: Distribution and chi square analysis of cohorts categorised by chromosomal location, signal peptide content, *A. fumigatus* specificity and functional association among differentially expressed datasets. **488**

Table 8.10: Infection cluster genes with increased transcript abundance in Δ*laeA* relative to the wild type throughout the time course of infection. **490**

Table 8.11: Infection cluster genes with decreased transcript abundance in Δ*laeA* relative to the wild type throughout the time course of infection. **490**

Table 8.12: Genes with increased transcript abundance in Δ*laeA* infected relative to Af293 infected experimental cohort in neutropenic model **496**

Table 8.13: Genes with decreased transcript abundance in Δ*laeA* infected relative to Af293 infected experimental cohort in neutropenic model **500**

Table 10.1: Summary statistics for the Af293 non-ratiometric analysis. **538**

Table 10.2: Summary statistics for Af293 relative nSI datasets. **539**

Table 10.3: 200 genes with greatest nSI increases between 4 and 14 hours post infection. **541**

Table 10.4: 200 genes with greatest nSI decrease between 4 and 14 hours post infection. **553**

Table 10.5: Functional classification of selected genes having differential transcript abundance in Af293 between 4 and 14 hours post infection in the murine lung. **566**

Table 10.6: Distribution and Chi-square analysis of differentially expressed genes categorised by chromosomal location, signal peptide content, *A.* **582**

fumigatus specificity and annotation at 4 – 14 hours post infection.

Table 10.7: 200 genes with greatest nSI increase between 4 and 8 hours post infection. **582**

Table 10.8: 200 genes with greatest nSI decrease between 4 and 8 hours post infection. **593**

Table 10.9: 200 genes with greatest nSI increase between 8 and 14 hours post infection. **603**

Table 10.10: 200 genes with greatest nSI decrease between 8 and 14 hours post infection. **613**

Table 10.11: Functional classification of selected genes having differential transcript abundance in Af293 between 4 and 8 hours post infection in the murine lung. **625**

Table 10.12: Functional classification of selected genes having differential transcript abundance in Af293 between 8 and 14 hours post infection in the murine lung. **640**

Table 10.13: Distribution and Chi-square analysis of differentially expressed genes categorised by chromosomal location, signal peptide content, *A. fumigatus* specificity and annotation at 4 - 8 hours post infection. **657**

Table 10.14: Distribution and Chi-square analysis of differentially expressed genes categorised by chromosomal location, signal peptide content, *A. fumigatus* specificity and annotation at 8 - 14 hours post infection. **657**

Table 10.15: Summary statistics for the Δ*laeA* versus Af293 time course during initiation of murine infection. **658**

Table 10.16: 100 genes with greatest $\log_2$ ratios (Δ*laeA*:Af293) at 4 hrs post infection. **660**

Table 10.17: 100 genes with lowest $\log_2$ ratios (Δ*laeA*:Af293) at 4 hrs post infection. **664**

Table 10.18: 100 genes with greatest $\log_2$ ratios (Δ*laeA*:Af293) at 8 hrs post infection. **669**

Table 10.19: 100 genes with lowest $\log_2$ ratios (Δ*laeA*:Af293) at 8 hrs post infection. **674**

Table 10.20: 100 genes with greatest $\log_2$ ratios (Δ*laeA*:Af293) at 14 hrs post infection. **679**

Table 10.21: 100 genes with lowest $\log_2$ ratios (Δ*laeA*:Af293) at 14 hrs post infection. **683**

Table 10.22: Functional classification of selected genes with the greatest log_2 ratio increase and decrease in Δ*laeA* mutant relative to Af293 during the initiation of murine infection. **689**

Chapter 1

Introduction

The late 20th century saw the emergence, re-emergence and persistence of human infectious diseases. While the antibiotic revolution initially seemed to have turned the tide against the scourge of bacterial pathogens, antibiotic resistance has lead to almost untreatable infections from prokaryotes. To avoid the catastrophic implications of the post-antibiotic era, research groups are focusing on new drug targets which, in contrast to conventional broad spectrum bactericidal and bacteriostatic agents, are specific to pathogenic species. Rich ground for the identification of such putative drug targets can be found from the study of disease initiating host-pathogen interactions. This is exemplified by the research of several groups which has identified compounds which inhibit the type III secretory system of Gram negative bacterial pathogens (Hudson et al. 2007, Kauppi et al. 2003), which may eventually be adapted into anti-bacterial therapies (Keyser et al. 2008). In addition to the current dilemma of antibiotic resistance, advances in other areas of medicine have paradoxically created entire populations which are at increased risk of infectious disease. Oncology, solid organ transplantation, and antiretroviral therapy have resulted in substantial numbers of immunocompromised individuals. These susceptible groups are hosts for an emerging eukaryotic threat: fungal infections.

Of the predicted 1.5 – 5.1 million fungal species (Hawksworth 2001, O'Brien et al. 2005), 307 have been identified as causing human mycoses (Taylor et al. 2001). The majority of human deaths and disease-affected life years can be attributed to the genera *Candida*, *Cryptococcus*, and *Aspergillus*. The genus *Aspergillus* may contribute between 38 – 80% of fungal disease-associated mortality across Europe, depending on geographical location (Lass-Florl 2009). Approximately 90% of invasive infections attributed to the genus are caused by the opportunistic pathogen *Aspergillus fumigatus* (Latge 1999). Anti-fungal compounds currently used to treat *A. fumigatus* infections target either cell wall or cell membrane biosynthesis. In addition to alarming reports of anti-fungal resistance, these compounds have high levels of toxicity and low efficacy. In a situation somewhat analogous to the development of novel anti-bacterials, *A. fumigatus* drug targets may be identified by the study of disease-initiating host-pathogen interactions.

Much effort has already been invested to elucidate the molecular interactions between *A. fumigatus* and the mammalian host. The role of multiple aggressive and defensive pathogen molecules which facilitate infection or disrupt host immune responses have been characterised.

Notwithstanding this progress, the impact of numerous fungal molecules which are putatively found at the host-pathogen interface have not been determined. With regard to host defence, it is clear that elements of the innate immune system provide early and essential protection against *A. fumigatus* infection, including alveolar macrophages, neutrophils, dendritic cells and soluble pathogen recognition receptors (Balloy et al. 2005, Bozza et al. 2002, Garlanda et al. 2002, Philippe et al. 2003). Interactions between host and pathogen during early infection have critical implications for the activation of either protective or allergic adaptive immunity. Consequently, early host pathogen interactions may define disease outcome.

The disease initiating host-pathogen interface is dynamic. Indeed, *A. fumigatus* germination and cellular differentiation represent essential cellular processes in the establishment of invasive aspergillosis (Tekaia and Latge 2005) which occur over several hours in the mammalian lung. Accordingly, the host must defend against multiple pathogen morphologies. Concurrent to substantial fungal changes in physiology and biochemistry throughout infection, multiple host niches are possibly encountered by the fungi, exemplified by the aerobic alveoli which accommodate the spore, and the likely hypoxic parenchyma surrounding the invasive hyphae (Wezensky and Cramer 2011). Delineating temporal host pathogen interactions will therefore be essential for understanding the complex molecular relationship between *A. fumigatus* and the mammalian host, and perhaps in the development of novel therapeutics. Work conducted in this thesis has employed transcriptomic and proteomic tools to determine host pathogen interactions in various murine models of infection.

1.1.0 Aspergilli

The genus *Aspergillus* (phylum *Ascomycota*) is comprised of nearly 200 species of saprophytic and ubiquitous fungi. The typical niche of *Aspergilli* is soil, where they play an important role in the aerobic decomposition of organic material and in the recycling of nitrogen and carbon. The genus contains scientifically, industrially, agriculturally and medically relevant fungi. The model organism *Aspergillus nidulans* possesses a well characterised sexual cycle and therefore has a developed genetics system (Timberlake and Marshall 1989). *A. nidulans* has been an essential tool for the study of eukaryotic metabolic regulation, development, cell cycle control, chromatin structure, cytoskeletal function, DNA repair, pH control and morphogenesis (Galagan et al. 2005). The genus is a potentially rich source of industrially useful enzymes, which is exemplified by the production of common pharmaceuticals (citric acid) and foodstuffs (sake, miso soup, soy sauce) by *Aspergillus niger* and *Aspergillus oryzae* respectively. In contrast to these utilities *Aspergillus* species are deleterious agricultural contaminants. Several species, most notably *Aspergillus flavus*

and *Aspergillus parasiticus*, are wheat, rice and maize contaminants due to the production of the highly hepatocarcinogenic secondary metabolite aflatoxin. A risk assessment suggests 28% of world wide hepatocellular carcinoma may be attributable to aflatoxin contamination (Liu and Wu 2010). Additionally, Aspergilli cause disease in a variety of organisms. *Aspergillus sydowii* was responsible for the Caribbean-wide, Cnidarian aspergillosis epidemic, which caused up to 70% mortality of the ahermatypic coral *Gorgonia ventalina* (Rosenberg et al. 2007). Species pathogenic to humans include *A. flavus, Aspergillus terreus, A. niger,* and *A. fumigatus*. Of these, *A. fumigatus* causes over 90% of human infections (Latge 1999).

1.1.1 *Aspergillus fumigatus*

A. fumigatus is a ubiquitous saprobe which has been isolated from various marine and terrestrial substrata from all over the world. The normal ecological niche is soil and leaf detritus where it survives on organic debris (Tekaia and Latge 2005). Asexual growth of *A. fumigatus* on Aspergillus complete medium (ACM) typically produces dark green colonies consisting of a dense mass of conidiophores and aerial hyphae. Hyphae are septate, dichotomously branching and form a filamentous mycelium. Conidiophores are columnar, about 300 µm in length, and contain densely packed vesicles which are between 20 – 30 µm in diameter. Vesicles support phialides which are usually 6 – 8 µm in length, from which chains of conidia are basipetally produced. Conidia of *A. fumigatus* are usually between 2.5 – 3 µm in diameter, smooth or echinulate and approximately spherical. The mechanism of conidial dispersal simply relies on air currents. Due to abundant sporulation of the species, *A. fumigatus* spores are one of the most common inhabitants of the air-borne fungal flora (Latge, 1999). In addition to asexual reproduction, *A. fumigatus* undergoes a sexual reproduction via a heterothallic breeding system (O'Gorman, et al 2009). Complimentary mating types Mat-1 and Mat-2 sexually reproduce under limited laboratory conditions to produce cleistothecia containing ascospores (O'Gorman et al. 2009)

1.1.2 Aspergillosis

A. fumigatus causes a variety of life threatening infections depending on the underlying immune status of the host (Figure 1.1). The primary route of infection is via the inhalation of airbourne conidia, which are small enough in diameter to reach the alveoli. Consequently, the lung is the most common site of *A. fumigatus* infection, although other areas, such as the skin (Ben-Ami et al. 2010), eyes (Thomas 2003) and gastointestinal tract (Kami et al. 2002) have been reported.

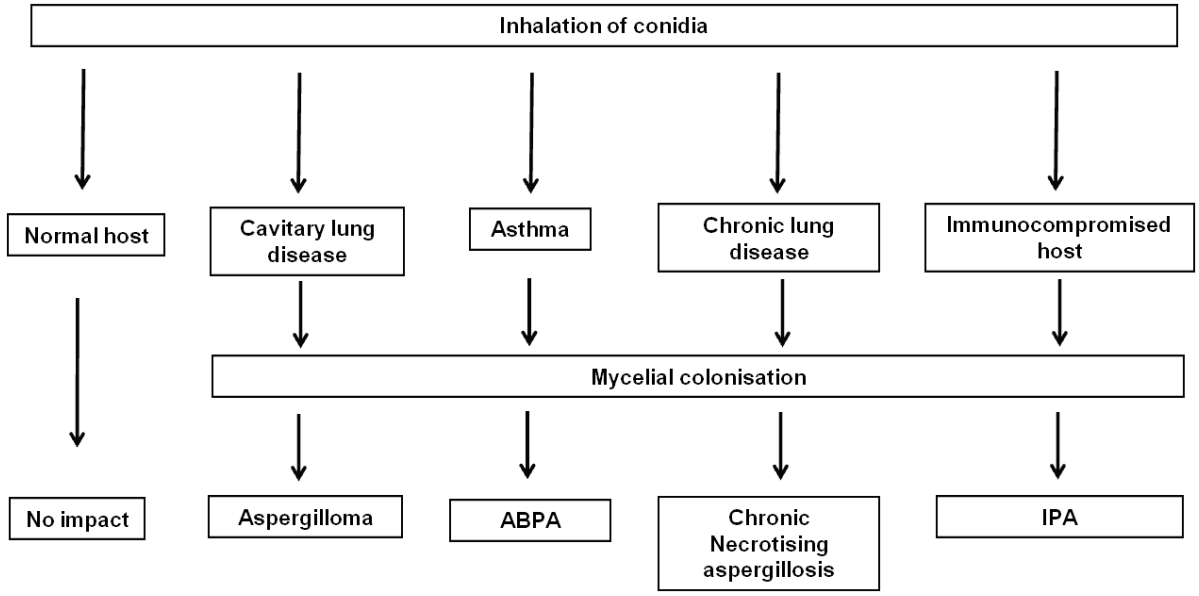


Figure 1.1. The clinical spectrum of disease caused by *A. fumigatus*. Infection develops in individuals with an underlying pulmonary condition following the inhalation of airborne conidia. The extent of mycelial colonisation varies significantly between conditions. ABPA, Allergic bronchopulmonary aspergillosis. IPA, invasive pulmonary aspergillosis. Adapted from (Soubani and Chandrasekar 2002).

Aspergilloma is a spheroid mass of hyphae in an intrathoracic cavity which occurs in 10 - 15% of patients with existing pulmonary damage (Zmeili and Soubani 2007). The condition is associated with a 40% 5 year survival rate with death occurring due to exanguinating hemorrhage (Denning 2001). Chronic Necrotising Aspergillosis (CNA) is a subacute infection associated with pre-existing pulmonary disease or immune dysfunction (Denning 2001). Following mycelial colonisation of a lung lesion, the invasion of cavity wall occurs over months or years, reducing lung function and causing death by hemoptysis. Patients with atopic asthma or cystic fibrosis suffer from various forms of allergic hypersensitivity to *A. fumigatus*, including IgE-mediated asthma, allergic sinusitis and life threatening allergic brochopulmonary aspergillosis (ABPA). The most severe form of *A. fumigatus* allergic disorders is ABPA, for which clinical impacts range from asthma and bronchiectasis to fatal lung destruction. ABPA is estimated to affect 3 million people worldwide (Denning et al. 2010). Invasive pulmonary aspergillosis (IPA) occurs in patients subjected to prolonged neutropenia, corticosteroid treatment, cytotoxic therapy, haematological malignancy and advanced AIDS. Following inhalation, conidia germinate and produce hyphae, which may disseminate throughout the body, infecting organs including the kidneys, heart and brain. It is the most severe disease caused by *A. fumigatus*, and is also the condition investigated in this study. The primary infection route is the lung. The risk level in neutropenic patients is estimated to be 1% per day of neutropenia, and increases to 4% per day if neutropenia lasts over 3 weeks (Zmeili and Soubani, 2007). In allogenic hematopoietic stem-cell transplantation (HSCT) recipients, incidence

may be as high as 15% (Zmeili and Soubani, 2007). IPA can cause mortality rates of 50% and 90% for neutropenic and hematopoietic stem-cell transplantation (HSCT) recipients respectively (Fukuda et al. 2003, Yeghen et al. 2000).

1.1.3 Diagnosis and molecular mechanisms of *A. fumigatus* antifungal therapy

Currently disease diagnosis and antifungal treatment do not adequately address the threat to human health. Existing clinical diagnosis is problematic for both invasive and allergic disease. For patients at risk or showing symptoms of invasive aspergillosis, CT scans are widely used for diagnosis, but are not species specific and rely on the identification of transient lung lesions (Latge 1999). Culture from respiratory tract specimens is vulnerable to false positives by contamination. Serodiagnosis using a galactomannan ELISA has unsatisfactory specificity and positive predictive values (Siemann et al. 1998), and is further complicated by a poor understanding of galactomannan pharmacokinetics in the host. Diagnosis of allergic hypersensitivity caused by *A. fumigatus* is equally problematic, relying on various transient symptoms such as peripheral blood eosinophilia and IgE antibodies against *A. fumigatus.*

Treatment of invasive *A. fumigatus* infections currently relies on the use of several antifungal agents, which include the azoles, polyenes, and echinocandins. Imidazole and triazole compounds (azoles) inhibit ergosterol biosynthesis by blocking 14 α-demethylation of lanosterol (Nagappan and Deresinski 2007). This results in disruption of other membrane bound enzymes, such as those involved in cell wall biosynthesis (Marichal et al. 1985). Azoles bind to the cytochorme P450 Erg11p via the iron atom in the enzyme active site and nitrogen atom in the imidazole or triazole ring. Azoles used to treat *A. fumigatus* infections include voriconazole, itraconazole, fluconazole and most recently posaconazole. In patients treated with voriconazole, 30% suffered visual abnormalities, 20% suffered skin reactions and less than 20% suffered an increase in hepatic enzymes (Jeu et al. 2003).

The polyenes, such as amphotericin B, do not inhibit a fungal enzyme rather, they bind to ergosterol, the sterol component of fungal plasma membranes, and perturb membrane function causing irreparable cell damage. However, the exact mechanism of binding is unclear (Odds et al. 2003). While Amphotercin B is considered one of the most effective agents in treating *A. fumigatus* infections, it has significant side effects, such as nephrotoxicity (Depont et al. 2007).

Echinocandins, such as caspofungin acetate, are fungal secondary metabolites comprising a cyclic hexapeptide with a lipid sidechain. The target for the echinocandins is the protein complex

responsible for the synthesis of cell-wall β-1,3 glucan polysaccharide. The exact mechanism of action is unclear, yet echinocandins bind to the transmembrane protein Fks1 (Odds et al. 2003).
In addition to mammalian toxicity and limited efficacy of antifungals, resistance is becoming an increasing problem. Azole resistance can occur by a variety of mechanisms, such as polymorphisms in the target gene (Denning et al. 2011) or by overexpression of drug efflux pumps such as AfuMDR3 and AfuMDR4 (Nascimento et al. 2003).

1.2.0- Environmental adaptation during the initiation of aspergillosis

A. fumigatus must sense and respond to numerous physical, chemical and biological stressors in its natural niche. It is clear that the ability to adapt to conditions of environmental stress is also an essential virulence attribute for many opportunistic pathogenic fungi, leading some authors to describe these virulence determinants as “dual use” (Casadevall et al. 2003). A better phrase is “multiple use”, seeing as the natural niche of a ubiquitous saprobe is likely to vary considerably. For example, thermotolerance is essential for multiple environments encountered by *A. fumigatus*, such as compost heaps (above 45 °C), the mammalian body (37 °C), tropical soil (e.g. 30 °C) or temperate soil (below 20 °C). Multiple use virulence determinants may include the ability to sense and respond to nutritional deprivation, oxidative stress, hypoxia, alkaline pH, elevated temperature and antifungal treatment (Table 1.1). Study of deletant mutants and more recent global transcriptional and proteomic profiling from *in vitro, ex vivo,* and *in vivo* assays has been essential in elucidating the molecular mechanisms of environmental adaption in the mammalian host.
Environmental adaptation is not generally considered to be a true host-pathogen interaction. For example, the high temperature of the host niche does not physically interact with a pathogen molecule. Nevertheless, environmental adaptation represents critical challenges to host colonisation, and is likely to modify host-pathogen interactions. For example, adaption to nitrogen limiting conditions may require the secretion of numerous proteases which can facilitate infection (Kogan et al. 2004) or cause damage to the host immune system (Behnsen et al. 2010). Accordingly, a comprehensive understanding of host-pathogen interactions must consider *A. fumigatus* environmental adaption to the host.

Putative stress	Natural niche	Mammalian host
Nitrogen limitation	Nitrogen poor soils e.g. areas of denitrification or leeching; competition with microflora	Proteinaceous lung matrix
Iron limitation	General variation in soil iron concentration; competition with microflora	Iron sequestered in host tissue; hypoferremia; neutrophil lactoferrin
Zinc limitation	General variation in soil zinc concentration; competition with microflora	Zinc associated with host proteins
Alkaline pH	Clay soils; chalk soils	Physiological pH
Hypoxia	Compost heaps	Areas of inflammation; host parenchyma
High temperature	Compost heaps; tropical regions	Body temperature
Reactive oxygen species	Mitochondrial metabolism; UV photo-oxidation	Mitochondrial metabolism; phagocytes; neutrophil ROS attack
Secretion	Saprophytism	Saprophytism
Antifungal	DMI antifungals	Antifungal therapy

Table 1.1: Summary of possible stress conditions encountered in the natural niche or during colonisation of the immunocompromised mammal. DMIs: 14 α-demethylation inhibitors.

1.2.1 Acquisition of nitrogen in the host

The utilisation of nitrogen sources is essential for fungal growth, as nucleotides and amino acid molecules both contain this element. *A. fumigatus* may encounter nitrogen rich or replete conditions in the natural niche, for example in agricultural soils supplemented with fertiliser or in regions with bacterial denitrification respectively. Nitrogen may be acquired from primary sources, such as ammonium or nitrate, or from secondary sources, such as amino acids or proteins. The latter are considered poor nitrogen sources, and their utilisation is of particular interest to infection due to the proteinaceous composition of the mammalian lung. Transcriptional comparisons between *A. fumigatus* germlings isolated from the murine lung with developmentally matched laboratory culture have suggested that nitrogen starvation conditions are encountered in the host (McDonagh et al. 2008). Specifically, decreased transcript abundance of genes directing ribosomal protein synthesis, rRNA synthesis, RNA polymerase I and II activity and translation initiation in the murine lung mimic *S. cerevisiae* gene expression following target of rampamycin (TOR) kinase inhibition (Cardenas et al. 1999). TOR kinases are part of a signalling cascade

which sense nitrogen availability in eukaryotic cells, and TOR inhibition with rampamycin mimics conditions of nitrogen starvation.

Two other studies support the hypothesis that nitrogen limitation is a key stress condition encountered in the host. The GATA transcription factor AreA is a positive acting transcription factor in the nitrogen catabolite response (NCR) system, which prevents utilisation of a poor nitrogen source when a rich one is present. Characterisation of Δ*areA* strains in *A. fumigatus* demonstrated wild-type growth rates on primary nitrogen sources, but reduced growth and virulence in murine infections (Hensel et al. 1998). This study suggests nitrogen starvation is encountered in the mammalian lung, and that utilisation of secondary nitrogen sources is an important virulence determinant. A second study has supported the hypothesis that successful nitrogen sensing and utilisation is a virulence determinant in *A. fumigatus* infections. The small GTPase RhbA is a member of the Ras superfamily of proteins, and its corresponding transcript was elevated under nitrogen limiting laboratory conditions (Panepinto et al. 2003). A Δ*rhbA* strain demonstrated reduced growth rate relative to a wild-type isolate when grown on media with nitrate, histidine or proline as a sole nitrogen source (Panepinto et al. 2003). Importantly, a Δ*rhbA* strain was attenuated in a murine model of infection (Panepinto et al. 2003).

Transcriptional comparisons between *A. fumigatus* germlings isolated from the murine lung with developmentally matched laboratory culture suggested that nitrogen limitating conditions may be addressed by increased expression of genes encoding functions associated with amino acid catabolism, transport and secretion of extracellular proteases (McDonagh et al. 2008). *A. fumigatus* secretes a diverse inventory of hydrolytic enzymes into the surrounding environment. Most notably in the context of infection, these include both metalloproteinases, alkaline proteases and elastases, which have been hypothesised to mobilise oligopeptides from the proteinaceous lung matrix and to act as “chemical drills” which clear the way through host tissues for invading hyphae (Ben-ami et al 2010). In addition to global transcriptional profiling, alkaline serine protease Alp1 is detectable in *A. fumigatus* infected human sera and lung as determined by an antibody specific enzymatic immunoassay and immunofluorescence assay respectively (Reichard et al. 1990). These data suggest secreted proteases may be required for nitrogen acquisition. However, virulence analyses of deletant mutants of Alp1 demonstrate wild-type levels of virulence in murine models of infection (Behnsen et al. 2010). Additionally, two groups have characterised the *A. fumigatus* transcription factor PrtT, which is required for extracellular proteolytic activity (Bergmann et al. 2009, Sharon et al. 2009). Interestingly, Δ*ptrT* strains demonstrated wild-type levels of murine virulence, suggesting the PtrT regulated protease activity is not required for murine

virulence. However, it is likely that these data reflect functional redundancy amongst such enzymes, as numerous proteases are likely not regulated by PtrT.

1.2.2 Acquisition of iron in the host

Iron is an essential micronutrient due to its role as a cofactor in many biosynthetic reactions and a catalyst in electron transport systems. Ferric and ferrous iron may be abundant in organic debris as iron oxides and iron hydroxides. In contrast, free iron within the host is low since virtually all iron is associated with proteins. Additionally, infection by microorganisms is responded to by hypoferremia of the host (Beaumier et al. 1984). *A. fumigatus* scavenges iron in low iron environments by siderophore-mediated Fe^{3+} uptake and reductive iron assimilation (RIA). *A. fumigatus* produces the siderophores triacetylfusarinine C (TAFC) and extracellular fusarinine C (FSC) for extracellular iron acquisition. Additionally, the intracellular siderophore ferricrocin is used for conidial and hyphal iron storage. All siderophores are produced from the precursor L-ornithine and require non-ribosomal peptide synthase activity. The first step in siderophore biosynthesis is catalysed by the ornithine-N^5-monooxygenase SidA. Δ*sidA* strains are avirulent in a neutropenic murine model of infection, demonstrating the importance of siderophore mediated iron acquisition in the host (Schrettl et al. 2004). Further analyses of deletant strains have demonstrated both intra and extracellular siderophores as being required for full murine virulence (Schrettl et al. 2007). RIA occurs by the reduction of Fe^{3+} to Fe^{2+} by an uncharacterised membrane protein, and transport of Fe^{2+} into the cell via the putative iron permease FtrA (Schrettl et al. 2004). Δ*ftrA* strains demonstrate wild-type levels of virulence in murine models of infection, suggesting *A. fumigatus* principally employs siderophore-based iron acquisition system in the host niche (Schrettl et al. 2004).

1.2.3 Acquisition of zinc in the host

Zinc is also an essential micronutrient which is a cofactor in numerous enzymatic reactions. Analyses of the *A. fumigatus* genome sequence suggests that three mechanisms of zinc acquisition and/or homeostasis are employed: (1) zinc transporters of the ZIP family, which pump zinc ions from the extracellular space into the cytoplasm; (2) transporters of the CDF family, which transport zinc from the cytoplasm into the lumen of intracellular organelles; (3) the zinc responsive transcriptional activator ZafA (Calera and Haas 2009). Work conducted by Moreno and co-workers has demonstrated *A. fumigatus* ZafA can functionally replace the zinc-responsive transcriptional activator *Zap1* gene from *S. cerevisiae*, and that *zafA* is required for full virulence in a corticosteroid treated murine model of IPA (Moreno et al. 2007). Global transcriptional approaches

and analyses of gene deletion mutants strongly support the hypothesis that the mammalian host is an iron and zinc poor environment which is circumvented by elaborate molecular methods of nutrient acquisition and cellular homeostasis by *A. fumigatus*.

1.2.4 Alkaline adaptation

The pH of soil and organic debris can vary between basic, neutral and acidic conditions. Consequently, *Aspergilli* can grow over a wide pH range, for example, the model organism *A. nidulans* can grow between pH of 2.5 – 9.0 The necessity for pH adaptation by a ubiquitous saprobe might also be required to overcome pH challenges encountered in the host, such as alkaline physiological pH or acidification of the innate immune cell phagolysosome (Thywiben et al. 2011). In *A. nidulans* and *A. fumigatus*, the PacC transcription factor regulates gene expression in response to extracellular pH. At alkaline pH, PacC becomes proteolytically processed and positively or negatively regulates alkaline and acidic response genes (Penalva and Arst 2004). *A nidulans* and *A. fumigatus* Δ*pacC* strains are both severely attenuated in murine models of infection (Bignell et al. 2005), which suggests the PacC regulated transcriptional response to extracellular pH is required for virulence (Loss et al. in prep). However, extensive transcriptional profiling conducted in our laboratory has found numerous genes which are unrelated to alkaline tolerance response are putatively under PacC control during initiation of neutropenic infection, and the impact of these processes on virulence cannot currently be determine (Loss et al. in prep). Notwithstanding these data, transcriptional comparisons between *A. fumigatus* germlings isolated from the murine lung with developmentally matched laboratory culture identified the increased transcript abundance of genes associated with alkaline stress in the mammalian host, and alkaline shift *in vitro* significantly overlaps with the *in vivo* trasncriptome, such as two sodium ATPases (Afu6g03690 and Afu4g09440) and an alkaline phosphatase (Afu3g14030) (McDonagh et al. 2008). It therefore seems likely that physiological pH is a significant challenge to *A. fumigatus* colonisation of the immunocompromised mammal.

1.2.5 Surviving hypoxia

Oxygen availability in compost heaps ranges from aerobic to hypoxic (< 1.5% O_2) (Wang et al. 2007). Similarly, in the host niche both aerobic and hypoxic environments may be encountered in alveolar space and at sites of tissue damage respectively. Two significant studies from the Cramer laboratory have supported the hypothesis that hypoxic conditions are indeed encountered in the

host, and that this may challenge *A. fumigatus* colonisation, modulate host immune responses and impact the efficacy of antifungal drugs (Wezensky and Cramer 2011). The first study by Willger and co-workers demonstrated that the sterol regulatory element-binding protein SrbA (a putative membrane bound transcription factor) is required for cell polarity, hypoxia adaptation and azole drug resistance in *A. fumigatus* (Willger et al. 2008). A Δ*srbA* strain was incapable of growth in hypoxic conditions but demonstrated wild-type growth in normoxic culture. Additionally, Δ*srbA* was avirulent in a neutropenic model of infection and attenuated in a murine model of X-linked chronic granulomatous disease (X-CGD) utilising gp91$^{phox-/-}$ mice. Histopathological analyses was conducted in infected gp91$^{phox-/-}$ mice 24 and 96 hours post infection, which demonstrated germination of Δ*srbA* condia in the lung but reduced growth relative to the wild type isolate. Accordingly, it was hypothesised that reduced virulence of the Δ*srbA* strains was primarily due to its inability to grow in hypoxic microenvironments in the host (Willger et al. 2008). A subsequent study by Grahl and colleagues was able to detect ethanol in *A. fumigatus* infected bronchoalveolar lavage fluids (BALFs) using ^{1}H-NMR, which suggested fermentation may occur *in vivo* in response to hypoxic conditions (Grahl et al. 2011). To further characterise putative hypoxic microenvironments in murine models of infection, the hypoxia marker pimonidazole hydrochloride was utilised. The hypoxia-dependent activation of this compound by cellular mammalian nitroreductases in conditions of ≤1% oxygen leads to the formation of covalent intracellular adducts with thiol groups on proteins, peptides, amino acids, and the marker, which can be visualised using immunofluorescence. This approach visually demonstrated hypoxic conditions at 4 days post infection in corticosteroid, neutropenic and CGD murine models of *A. fumigatus* infection. Interestingly, the largest areas of hypoxic conditions were found in and around lung lesions with high inflammation in both the corticosteroid and CGD models of infection. The authors also demonstrated the alcohol dehydrogenase *alcC* null mutant was unable to ferment glucose *in vitro* and was reduced in fungal burden and inflammation as determined by qPCR and flow cytometry of murine BALFs respectively. These data suggested fermentation in hypoxic areas of the murine lung may be required for fungal growth *in vivo*.

With regard to the hypothesis that hypoxic conditions modulate host immune responses, RT-PCR analyses of corticosteroid treated murine BALF detected increased transcript abundance of hypoxia inducible factor 1 alpha (HIF-1α) 24 hours after *A. fumigatus* infection (Ben-Ami et al. 2009). HIF-1α is a transcription factor which regulates mammalian innate immune cell gene expression in hypoxic environments and is required for macrophage killing of Gram negative bacterial pathogens (Wezensky and Cramer, 2011). These data further support the existence of hypoxic microenvironments in the host, and suggest hypoxia specific host gene expression.

1.2.6 Thermotolerance

As already noted, thermotolerance is essential for survivorship in multiple environments encountered by *A. fumigatus*, such as compost heaps or the mammalian lung. *A. fumigatus* is a mesophile which can thrive at temperatures of 50 °C and resist temperatures up to 75 °C (Beffa et al. 1998). As thermotolerance is likely to be a polygenic trait which may contribute to virulence, global transcriptional and proteomic profiling has been conducted by several groups. In addition to the publication of the *A. fumigatus* genome, work conducted by Nierman and co-workers described transcriptional profiles following shift of *in vitro* growth from 30 °C to 37°C or 47 °C (Nierman et al. 2005). These data demonstrated that numerous heat shock-responsive genes yet few virulence associated genes were employed following heat shock. A more comprehensive analysis of these datasets by Do and co-workers (Do et al. 2009) suggested primary metabolic genes, including those directing carbohydrate, lipid and amino acid metabolism increased in gene expression 120 minutes following heat shock. These data suggest the metabolic adaptation from a mesophillic to thermophillic cellular state. Transcriptional and proteomic profiling conducted by Albrecht and colleagues following *A. fumigatus* heat shock (Albrecht et al. 2010) demonstrated the increased abundance of transcripts and proteins involved in protein chaperone activity, oxidative stress response, signal transduction, and carbohydrate and nitrogen metabolism. Accordingly, *A. fumigatus* heat responses differ from other fungi, most notably by an increase in amino acid biosynthesis, which is repressed in *S. cerevisiae* following heat shock (Albrecht et al. 2008). In support of the role of heat adaption in *A. fumigatus* virulence, deletion of the gene encoding the nuclear protein CgrA caused impaired rates of conidial germination and hyphal growth at 37°C relative to the wild-type (Bhabhra et al. 2004). Moreover, a Δ*cgrA* strain demonstrated reduced virulence in a neutropenic murine model (Bhabhra et al. 2004).

1.2.7 Detoxification of reactive oxygen species

Molecular oxygen readily accepts unpaired electrons to form partially reduced species known as reactive oxygen species (ROS), including superoxide (O_2^-), hydrogen peroxide (H_2O_2), hydroxyl radical (HO^-), peroxyl (ROO^-) and alkoxyl (RO^-) radicals (Riley 1994). ROS may initiate free radical chain reactions which can damage macromolecules including DNA and protein. ROS are encountered in the *A. fumigatus* natural niche from both cellular mitochondrial metabolism and photo-oxidation from ultra-violet radiation. *In vitro*, alveolar macrophages kill *A. fumigatus* conidia in a ROS dependent manner (Philippe et al. 2003). Additionally, neutrophils release ROS, most

likely superoxide radical and hydrogen peroxide during the oxidative burst to kill hyphae and conidia. *A. fumigatus* scavenges ROS via the glutathione redox system and oxidase enzymatic activity (Tekaia and Latge 2005). Additionally, *A. fumigatus* biosynthesises numerous enzymes which catalyse the decomposition of ROS, including superoxide dismutases, catalases and peroxidases. While the exact ROS which causes *A. fumigatus* killing by innate immune cells is unknown, the importance of host ROS is illustrated by the prevalence of IPA in corticosteroid treated and CGD patients, both of which suffer deficiencies in ROS production. Attempts to define the *A. fumigatus* ROS detoxifying mechanisms which presumably are required for virulence have been elusive. For example, proteomic profiling conducted by Lessing and co-workers investigated regulation of the *A. fumigatus* ROS detoxifying system by the transcription factor Afyap1 (Lessing et al. 2007). 29 proteins were found to be directly or indirectly controlled by Afyap1 including catalase Cat1, Cu/Zn superoxide dismutase, a cytochrome C peroxidase and the peroxiredoxin allergen Asp F3. Combining these data with phenotypic characterisation and virulence analyse of the Δ*yap1* in a murine model of infection, the authors demonstrated that the Afyap1 ROS detoxifying proteome is required for protection against H_20_2 but dispensable for virulence in a murine model of infection. Additionally, superoxide dismutases which detoxify the superoxide anion are not required for virulence, as determined by analyses of a triple SOD null in a neutropenic model of infection (Lambou et al. 2010). Histopathological analysis of a mycelial catalase double mutant Δ*cat1*Δ*cat2* in murine models of infection suggested reduced tissue damage and lesions relative to the wild-type at 5 and 13 days post infection (Paris et al. 2003). These data suggest the mycelia catalases Cat1 and Cat2 transiently protect the *A. fumigatus* from host ROS.

1.2.8 Secretion stress and the unfolded protein response

Secretion of hydrolytic enzymes and subsequent absorption of products produced from the enzymatic reactions is fundamental to a saprophytic lifestyle (Cramer 2011). The endoplasmic reticulum (ER) is essential for the folding of proteins into stable tertiary structures before secretion. Rapid translation of secreted proteins can cause stress on the ER, which results in the accumulation of potentially toxic unfolded proteins. In *A. fumigatus*, this stress is compensated by the unfolded protein response (UPR) and endoplasmic reticulum associated pathway (ERAD) which adjust the folding capacity of the ER and dispose of mis-folded proteins respectively. The UPR restores ER homeostasis by sensing surplus unfolded proteins and increasing the biosynthesis of proteins which function to increase folding. The UPR in *A. fumigatus* is regulated by the transcription factor HacA. Deletion of *hacA* causes disruption of cell wall integrity, reduction

in protease secretion, increased susceptibility to antifungals and virulence attenuation in neutropenic and corticosteroid treated murine models of *A. fumigatus* infection (Richie et al. 2009). In the ERAD pathway, incorrectly folded proteins are recognised and transferred across the ER membrane into the cytoplasm, where they are finally degraded by the proteasome (Richie et al 2011). Deletion of the ERAD gene *derA* and *hacA* causes reduced hyphal growth, antifungal resistance and attenuation in a murine model of infection (Richie et al. 2011). Attenuation of the mutants may be due to pleiotropic impacts of gene deletion, yet these studies suggest the UPR and ERAD response to secretion stress may be an essential virulence attribute in *A. fumigatus* infection.

1.2.9 Antifungal resistance

Since the 1990's, 14 α-demethylation inhibitors (DMIs) have been used to combat fungal phytopathogens throughout Europe (Alanio et al. 2011). These antifungals function by inhibiting ergosterol biosynthesis by blocking 14 α-demethylation of lanosterol, which is the same mechanism of the human therapeutics voriconazole, itraconazole and fluconazole. Consequently, it is possible that *A. fumigatus* isolates may encounter certain antifungals in both the environment and during human infection. *A. fumigatus* antifungal resistance may arise by polymorphisms in the target gene (Denning et al. 2011) or by overexpression of drug efflux pumps such as AfuMDR3 and AfuMDR4 (Nascimento et al. 2003). Positive selection for *A. fumigatus* antifungal resistance in the natural niche is of growing concern.

1.3.0 Molecular interactions between *A. fumigatus* and the host

Molecular interactions between host and pathogen can have three potential outcomes: (1) support survivorship of the pathogen or facilitate the infectious process; (2) support survivorship of host cells, tissues, organs or facilitate pathogen killing; (3) have no impact on host, pathogen or the outcome of infection. Numerous studies have investigated molecular interactions between host and pathogen using *in vitro* or *ex vivo* conditions, which either approximate or are relevant to the infection. However, these studies do not address host-pathogen interactions in the dynamic and multifaceted mammalian lung. *A. fumigatus* germination and cellular differentiation represent essential cellular processes in the establishment of invasive aspergillosis (Tekaia and Latge 2005) which occur over several hours in the mammalian lung. Accordingly, the host must defend against resting conidia, swollen conidia, germlings and invasive hyphae. Concurrent to substantial fungal

changes in physiology and biochemistry throughout infection, multiple host niches are possibly encountered by the fungi, which may impact both pathogen associated molecular patterns (PAMPs) and host pattern recognition receptors (PRRs) (Wezensky and Cramer 2011). Moreover, numerous soluble PRR and cell subsets of the host innate and adaptive immune system are active against *A. fumigatus*. A selection of putative host pathogen interactions during the initiation of mammalian infection is shown in Figure 1. Delineating temporal host pathogen interactions within murine models of infection will be essential for understanding the complex molecular relationship between *A. fumigatus* and the mammalian host.

1.3.1 Molecular interactions between *A. fumigatus* resting spores and the host

Host-pathogen interactions occur immediately following the inhalation or experimental inoculation of resting *A. fumigatus* spores. A defining feature of resting *A. fumigatus* conidia is the electron dense outermost cell wall layer, which is composed of proteinaceous microfibrils called rodlets and DHN melanin pigments (Bernard and Latge 2001). In the natural niche, DHN-melanin is likely involved in protection from UV radiation, while the rodlet layer confers hydrophobicity and aerosolisation to the spore, thus aiding dispersal by air currents. In the host, these molecules protect against PRR recognition, phagocytosis and killing by innate immune cells such as alveolar macrophages and neutrophils. Extraction of the rodlet protein RodA and co-incubation with human dendritic cells and murine alveolar macrophages demonstrated the layer is immunologically inert (Aimanianda et al. 2009). Moreover, chemical removal of the rodlet layer or deletion of *rodA* resulted in increased spore phagocytosis by human dendritic cells or murine macrophages. These data collectively demonstrate proteinaceous microfibrils protect the spore PAMPs from immune cell PRR (Aimanianda et al. 2009). The first step of the conidial pigment DHN melanin biosynthesis is catalysed by the polyketide synthase PksP (Langfelder et al. 1998, Tsai et al. 1998). Δ*pksP* strains produce white, smooth conidia, which are more susceptible to oxidative stress, neutrophil phagocytosis, and complement 3 deposition (Tsai et al. 1998). Moreover, Δ*pksP* isolates are attenuated in murine models of IPA (Tsai et al. 1998, Langfelder et al. 1998). DHN-melanin is immunologically inert and may physically protect conidial PAMP from phagocyte PRR, including dectin-1 and TLR-4 (Chai et al. 2010). Additionally, DHN-melanin inhibits the acidification of host immune cell phagolysosomes (Thywiben et al. 2011).

In addition to the electron dense outer layer, the surface of resting conidia contain the negatively charged sugar sialic acid (Warwas et al. 2007) and a cell wall laminin binding protein (Tronchin et al 2002) which may adhere to host lectins. The adherence of resting conidia may exacerbate

existing lung damage for example laminin is exposed upon epithelial injury (Dagenais and Keller 2009). Thus, adhesins of resting conidia may promote *A. fumigatus* colonisation at areas of pre-existing lung damage.

Finally, *A. fumigatus* resting spores are putatively coated with both secondary metabolite toxins and proteases which may facilitate infection, disrupt host immune responses and cause damage to host cells. For example, the secondary metabolite toxins verruculogen, fumagillin, fumigaclavine C, aurasperone C, fumitremorgin C, and trypacidin have been detected using HPLC analyses of resting conidial extracts (Fischer et al. 2000, Khoufache et al. 2007). The alkaline serine protease Alp1 is detectable on the surface of *A. fumigatus* conidia in human lungs as determined by an antibody specific enzymatic immunoassay and immunofluorescence assay (Reichard et al. 1990). This protease degrades proteins C3, C4 and C5 *in vitro* (Behnsen et al. 2010). Intracellular proteomic profiling of resting conidia demonstrated high abundance of a conidial catalase, hemolysin, allergen Asp F13 and rodlet proteins (Teutschbein et al. 2010) which strongly suggests these proteins may direct host interactions with the resting spore. However, a comprehensive analysis of secondary metabolite biosynthesis or protease production by the conidia in the host has not been conducted.

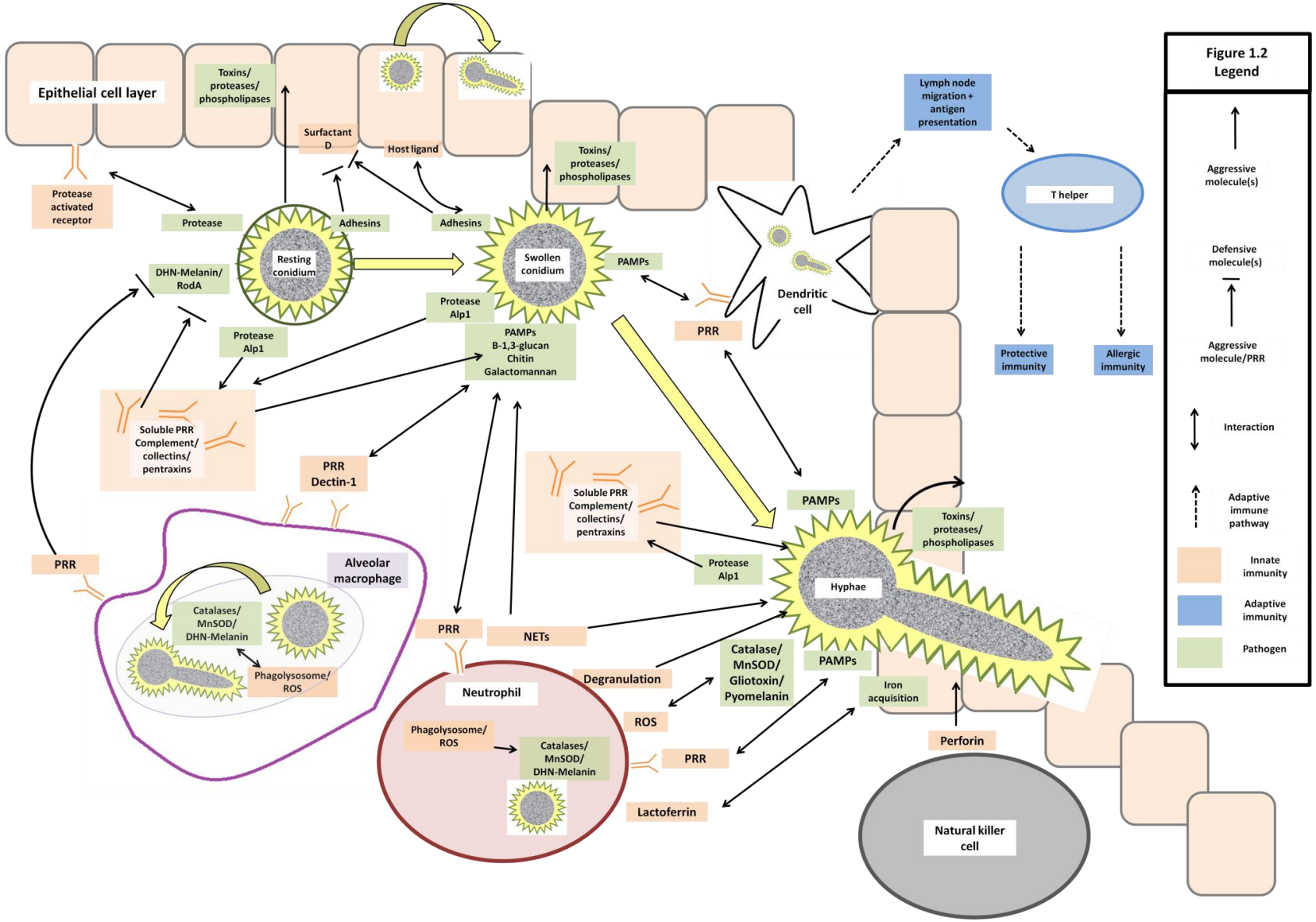


Figure 1.2: Schematic depicting putative host-pathogen interactions during the initiation of *A. fumigatus* murine infection. *A. fumigatus* growth is depicted by yellow arrows. Host epithelial cells, natural killer cells, neutrophils, alveolar macrophages, dendritic cells and T-helper cells are shown. *A. fumigatus* morphology includes the dormant spore, in which the rodlet/DHN melanin layer is depicted by a green circle. Swollen conidia lack this layer, and more PAMPs are exposed to host PRRs. An invading hyphae crossing the host epithelial barrier is shown. For references please refer to the text.

A picture therefore emerges of a highly protected propagule which is able to resist immune cell phagocytosis or killing, adhere to host epithelia, and assault the host with a variety of aggressive molecules. Nevertheless, numerous elements of host innate immunity are active against resting *A. fumigatus* conidia in an immunocompetent mammal. Firstly, conidia which come into contact with mucosa may be physically removed from the airways by epithelial cilia (Paris et al. 1997). Additionally, the mucosa and alveolar epithelium contain numerous soluble PRR with antimicrobial or phagocyte activating properties. For example, the collectins surfactant A and D are produced by lung epithelial cells and secreted into the alveoli. These PRR bind to carbohydrate structures of resting conidia, which promotes agglutination and enhances alveolar macrophage and neutrophil phagocytosis *in vitro* (Madan et al. 1997). Furthermore, C-type lectin surfactant protein D has been shown to reduce adhesion of resting conidia to host epithelial cells *in vitro* (Yang et al. 2000). Intriguingly, intranasal instillation of recombinant surfactant D the day after infection in corticosteroid treated mice significantly increased murine survival, although this may also be attributable to surfactant D interactions with other fungal morphotypes encountered in the lung (Madan et al. 2001). The soluble PRR pentraxin-3 is secreted by a variety of cells including phagocytes and dendritic cells in response to inflammatory mediators (Park and Mehrad 2009). Pentraxin-3 binds to *A. fumigatus* resting condia, putatively to the PAMP conidial galactomannan (Garlanda et al. 2002). Pentraxin-3 binding enhances phagocytosis of alveolar macrophages and dendritic cells (Garlanda et al. 2002). The importance of this molecule in immune defence is highlighted by the increased susceptibility of PTX3- null mice to *A. fumigatus* infection (Garlanda et al. 2002). Additionally PRR complement protein C3 binds and is activated on resting *A. fumigatus* conidia *in vitro* (Kozel et al. 1989) which enhances phagocytosis by alveolar macrophages and neutrophils.

1.3.2 Molecular interactions between *A. fumigatus* swollen spores and the host

A. fumigatus spores germinate in the presence of oxygen, carbon, phosphate, nitrate and water. Early germination is characterised by swelling, isotrophic growth, nuclear decondensation and the shedding of the hydrophobic outer layer of rodlets and pigments. In the context of host pathogen interactions, the loss of this layer exposes numerous cell wall PAMPs to soluble and cell surface host PRRs. The swollen conidial cell wall is composed of various macromolecules which putatively have immune activating properties, including β-1,3 glucan, β-1,4 glucan, α-1,3-glucan, galactomannan, chitin and galactosaminogalactan (Cramer et al. 2011). Consequently swelling is

associated with increased rates of both phagocytosis and killing in innate immune cell phagolysosomes.

Alveolar macrophages are resident lung leukocytes which recognise, phagocytose and kill swollen conidia (Phillippe et al. 2003). Additionally, alveolar macrophages produce proinflammatory chemokines and cytokines which recruit neutrophils to the site of infection. While PAMP/PRR interactions remain to be categorically determined, evidence suggests recognition of swollen conidia occurs by dectin-1 binding β-1,3 glucan (Luther et al. 2007, Steele et al. 2005) and the C type lectin dendritic cell–specific intercellular adhesion molecule 3–grabbing nonintegrin (DC-SIGN) binding galactomannan (Serrano-Gomez et al. 2005). With regard to Toll-like receptor recognition, studies have reported both TLR-2 and TLR-4 dependent (Meier et al. 2003) and independent (Dubourdeau et al. 2006) activation of murine macrophages. It is possible that disparities in these data are due to differences in host cells, *A. fumigatus* isolates and surrogate markers of alveolar macrophage recognition between experiments (Park and Mehrad, 2009). Nevertheless, loss of the rodlet layer results in increased rates of alveolar macrophage phagocytosis and killing. The exact mechanism of alveolar macrophage killing is not fully understood. Phillippe and co-workers suggested conidial killing occurs in the alveolar macrophage phagolysosome by ROS (Phillippe et al. 2003). In this study, macrophages isolated from congenic p47*phox*$^{-/-}$ mice, which lack the cytosolic subunit of the multi-protein NADPH oxidase complex, showed dramatic reduction in macrophage killing. Additionally, treatment of wild-type macrophages with the NADPH oxidase inhibitors diphenylene iodonium chloride and phenylarside oxide significantly reduced conidial killing. A second study published the same year demonstrated that treatment of human alveolar macrophages with bafilomycin A, an inhibitor of vacuolar-type H+ ATPase activity and phagolysosomal acidification, greatly reduced conidial killing (Ibrahim-Granet et al. 2003). Additionally, acidification of the phagolysosome was monitored with an acidotrophic probe, which demonstrated conidial killing was correlated with acidification. Accordingly, it seems likely that ROS and acidification are key elements of alveolar macrophage conidial killing, although the exact ROS which effect killing or other mechanisms such as anti microbial peptides remain to be determined.

Neutrophils are recruited to the site of infection from the blood stream approximately 3 – 6 hours after infection by chemokines and activated complement components. While neutrophils are the main cell population which destroy invasive hyphae (Latge 1999), they also effect multiple responses to *A. fumigatus* conidia, including phagocytosis (Levitz S. M. and Diamond 1985), extracellular degranulation (Levitz and Farrell 1990) and the production of neutrophil extracellular traps (Bruns et al. 2010b, McCormick et al. 2010). The relative contribution of each killing

mechanism to host defence is not clear, but all three may synergistically contribute to *A. fumigatus* conidial killing. Neutrophil PRRs have not been definitively identified, but it is likely dectin 1, TLR 2 and TLR 4 are involved in recognition of swollen conidia (Bellocchio et al. 2004, Werner et al. 2009). Given the likely importance of ROS in microbial phagolysosomal killing it seems highly probable that ROS contribute to killing of phagocytosed conidia via oxidative burst and intracellular degranulation. This is indirectly supported by the prevalence of IPA in CGD patients and the susceptibility of p91*phox*$^{-/-}$ deficient mice to *A. fumigatus* (Morgenstern et al. 1997). A study conducted by Henriet and co-workers used a luminol-enhanced chemiluminescence assay to demonstrated that *A. fumigatus* conidia generate greater ROS production by neutrophils than *A. nidulans* (Henriet et al. 2011), which supports neutrophil killing of *A. fumigatus* conidia by ROS. Additionally, mice deficient in phagosome hydrolytic enzymes elastase and cathepsin G are susceptible to an intravenous model of murine infection (Tkalcevic et al. 2000), indicating conidial killing in the phagolysosomes may be caused by protease activity. However, the precise mechanism of conidial killing in the neutrophil phagolysosome remains unknown.

Additionally, neutrophils may degranulate and release cytotoxic molecules into the extracellular region when stimulated with swollen conidia *in vitro* (Levitz and Farrell 1990). Extracellular degranulation may kill by oxidative or nonoxidative mechanisms, and inhibit *A. fumigatus* iron acquisition by the production of lactoferrin (Levitz and Farrell 1990). Neutrophil extracellular traps (NETS), are DNA fibres covered in antimicrobial cytosolic and granule proteins which do not effect killing but physically prevent dissemination of conidia from the site of infection (Bruns et al. 2010b, McCormick et al. 2010).

Dendritic cells are located on epithelial barriers in the lung and phagocytose conidia more rapidly following swelling and loss of the rodlet layer (Aimanianda et al. 2009). After phagocytosis, dendritic cells migrate to the lymph nodes where they present antigens to T-helper cells (Bozza et al. 2002). Accordingly, dendritic cells are a crucial link between innate and adaptive immune responses to *A. fumigatus* infection (Romani 2004). Dectin-1 is expressed on dendritic cells and recognises β-1,3 glucan on *A. fumigatus* germ tubes (Mezger et al. 2008a). Accordingly, it is likely to also act as a PRR for swollen conidia. Immature dendritic cells recognise conidial galactomannan by the C type lectin DC-SIGN (Serrano-Gomez et al. 2005). Dendritic cells which phagocytose conidia elicit protective Th1 immunity against *A. fumigatus* (Bozza et al. 2002). Finally, swollen conidia adhere more readily to lung epithelial cells than resting conidia (Osherov 2009) which can prompt epithelial cell phagocytosis. While the majority of conidia are killed in phagolysosomes, a minority have been shown to germinate causing epithelial cell death.

With regard to identifying prompt aggressive or protective molecules released by the germinated spore, global transcriptional profiling of swollen conidia identified 244 genes which were upregulated following *in vitro* exposure to human neutrophils (Sugui et al. 2008). These data strongly suggest a reprogramming of metabolic pathways towards fatty acid degradation, and found some support for the increased expression of genes required for iron acquisition. Proteases are required for epithelial cell damage throughout germination as determined by a time series experiment (Kogan et al. 2004). However, some studies are limited to analysis of either resting conidia or hyphal morphologies. For example, proteomic profiling conducted by Teutschbein and colleagues compared protein profiles between resting spores and germinated hyphae, but not swollen conidia (Teutschbein et al. 2010). Secondary metabolite profiling which identified verruculogen in resting spores using HPLC analyses did not investigate swollen conidia (Khoufache et al. 2007). Secondary metabolites (e.g. verruculogen), proteases (e.g. Alp1) and ROS detoxifying molecules (e.g. conidial catalase) may be secreted from the spore throughout resting and germinating phases. However, gene expression comparisons between resting and swollen *A. fumigatus* conidia have demonstrated substantial changes in transcription between the two morphologies (Lamarre et al. 2008). Genes differentially expressed during germination included cell wall biosynthetic genes, numerous transporters and genes directing respiratory metabolism and protein synthesis (Lamarre et al. 2008). Accordingly, it is highly probable that differences in genes required for ROS detoxification, and other molecules associated with the host-pathogen interface may be differentially expressed between resting and swollen conidia during infection.

1.3.3 Molecular interactions between *A. fumigatus* hyphae and the host

Following isotrophic swelling, a germ tube is produced and hyphal growth occurs by polar extension, forming septate invasive hyphae. This cellular differentiation results in substantial physiological and biochemical changes, and is a defining feature in the establishment of IPA (Tekaia and Latge 2005). Indeed, hyphae invade and colonise the local lung architecture causing necrosis characteristic of the disease. Although some host-spore interactions are retained into the hyphal phase, numerous interactions are modified, or novel interactions introduced into the milieu. This can be attributed to both changes in *A. fumigatus* morphology and the development of innate and adaptive immune responses.

Complement component C3 binds *A. fumigatus* hyphae *in vitro* and activates the alternative pathway, which may opsonise hyphae and enhance binding by neutrophils (Behnsen et al. 2010). Surfactant D also binds putative carbohydrate moieties on hyphae, which may enhance neutrophil binding (Geunes-Boyer et al. 2010). No study has been conducted to determine the interaction between surfactant A and *A. fumigatus* hyphae. In contrast to the swollen conidia, pentraxin 3 does not bind to hypha, which is most likely due to alterations in galactomannan on the hyphal surface (Garlanda et al. 2002).

In contrast to the essential role that alveolar macrophages play in phagocytosing and killing *A. fumigatus* conidia, these cells are unable to phagocytose hyphae due to their size. Nevertheless, a macrophage-hyphae interaction occurs in the corticosteroid treated murine model of aspergillosis, where drug treatment facilitates polarised growth and hyphal production in the macrophage phagolysosome *ex vivo* (Phillippe et al. 2003). Polarised growth is probably enabled due to the inhibition of macrophage ROS by corticosteroids (Phillippe et al. 2003). Hyphal growth eventually results in outgrowth from the cell and death of the macrophage. This observation may account for the susceptibility of corticosteroid treated patients to IPA and also highlights the variability of host pathogen interactions between different immunosuppressive regimes.

Neutrophils are the main cell population which destroy invasive hyphae (Latge 1999). The filaments are too large to phagocytose; accordingly, neutrophils adhere to the external hyphal surface and use extracellular killing mechanisms. Few studies have specifically investigated the PRR which mediates neutrophil adherence to hyphal morphotypes but it is likely dectin-1, TLR-2 and TLR-4 are required (Romani 2004, Bellochio et al. 2004). Comparable to the extracellular killing of conidia, hyphae are destroyed by extracellular degranulation (Levitz and Farrell 1990) and entrapped in NETS which prevent growth and physically prevent dissemination of hyphae (Bruns et al. 2010b, McCormick et al. 2010). It is possible that degranulation may cause hyphal damage by both oxidative and non-oxidative means.

Dendritic cells internalise germlings by the PRR dectin-1 (Mezger et al. 2008a) and hyphae by complement receptor 3 and the FC receptor (Bozza et al. 2002). Migration to the lymph nodes and presentation of hyphae is associated with allergic Th2 response and the secretion of cytokines IL-4 and IL-10 (Bozza et al. 2002). In addition to the well established roles of alveolar macrophages and neutrophils in host protection, recent work suggests natural killer cells may also be an important component of the innate immune system with regards to defence against *A. fumigatus* infection (Schmidt et al. 2011). Natural killer cells are lymphocytes located in the vascular and

interstitial compartments of the lung. They play a major role in killing virus infected cells by releasing perforin and granzyme, which cause apoptosis. Natural killer cells have recently been shown to kill *A. fumigatus* hyphae but not conidia *in vitro* via the production of the cytotoxic protein perforin (Schmidt et al. 2010). The relative contribution of natural killer cells to protective immunity against *A. fumigatus* remains to be determined.

Numerous *in vitro* studies have analysed conditions which approximate or are relevant to *A. fumigatus* hyphae in the host niche, which may identify defensive or aggressive molecules produced by this morphotype during infection. Two dimensional gel electrophoresis and matrix assisted laser desorption/ ionisation time of flight mass spectroscopy (MALDI-ToF) identified 64 proteins from *A. fumigatus* mycelial supernatant (Wartenberg et al. 2011). These proteins include alkaline serine protease Alp1, autophagic serine protease Alp2, 5 peptidases, elastinolytic metalloproteinase Mep1, 2 superoxide dismutases, two catalases, several cell wall proteins and a hemolysin, which may attack or defend against the host immune system during infection. HPLC and TLC analyses have detected numerous secondary metabolite toxins from *A. fumigatus* mycelial culture supernatant, including the fumitrimorgin precursor brevianamide F, gliotoxin (Bok et al. 2006b, Maiya et al. 2006) and numerous unknown metabolites (Bok and Keller 2004). Gliotoxin inhibits the ROS burst of neutrophils, induces host apoptotic cell death by activating a proapoptotic Bcl-2 family member protein, and is required for virulence in murine models of infection (Bok et al. 2006b, Pardo et al. 2006, Sugui et al. 2007a). Transcriptional, proteomic and metabolic analyses have also demonstrated the biosynthesis of the cytotoxic cyclic peptide pseurotin A in hypoxic, but not normoxic culture which may be produced in hypoxic lung regions (Vodisch et al. 2011). Proteases may be secreted by hyphae which may facilitate infection or activate protease activated receptors (PARS). Extracellular phospholipase activity has been demonstrated from mycelial supernatant (Birch et al. 2004) suggesting these enzymes may be secreted by the invasive hyphae in the lung. Lung surfactant is composed of 90% phospholipids. Accordingly, extracellular phospholipase activity of the hyphae may cause tissue damage (Birch et al. 2004). This is supported by the attenuation of *C. albicans* phospholipase B deletants, which are attenuated in a murine model of infection (Leidich et al. 1998). Crude hyphal extract (CHE) induced IFN-γ, IL-4, and IL-17 responses in PBMC from 20 healthy individuals (Chaudhary et al. 2010). T cell responses to *A. fumigatus* hyphal antigens demonstrate they are potent activators of the adaptive immune system.

While these studies provide insights into *A. fumigatus* responses to *in vitro* disease relevant conditions they do not address pathogen gene expression in the multifaceted and dynamic host niche. Transcriptional comparisons between *A. fumigatus* germlings isolated from the murine lung

with developmentally matched laboratory culture represent a vital insight into the response of *A. fumigatus* hyphae to the host niche (McDonagh et al. 2008). These data demonstrate key environmental challenges to host colonisation relative to laboratory growth were alkaline stress, iron limitation and nitrogen starvation (McDonagh et al. 2008). Additionally, hundreds of genes which are putatively involved in host-hyphal interactions were identified, including secreted proteases, cutinases, lipases and phospholipases. Additionally genes directing the biosynthesis of numerous secondary metabolites, GPI-anchored proteins, cell wall proteins and antigens had increased transcriptional abundance in the host. This study also demonstrated genes preferentially employed in the murine lung were more likely to reside in subtelomeric regions, which are enriched in mobile genetic elements and undergo frequent chromosomal rearrangements (Nierman et al. 2005). These regions have consequently been suggested to expand the gene content of the *A. fumigatus* genome, and may help explain the evolutionary basis of *A. fumigatus* virulence. Work by McDonagh and colleagues therefore demonstrates how global transcriptional profiling from the murine niche can address numerous hypothesis with regard to host pathogen interactions and environmental adaptation, while also providing insights into the evolutionary mechanisms of virulence acquisition. Accordingly, the technical expertise developed by McDonagh and co-workers was employed to study host pathogen interactions at three time points following murine infection in this study.

1.4.0 *A. fumigatus* Δ*laeA*: a tool for reverse engineering the molecular basis of attenuation

Gene expression profiling of the virulent Af293 clinical isolate has be used to elucidate the transcriptional basis of *A. fumigatus* virulence in the murine host (McDongah et al. 2008). Using a comparable strategy, gene expression profiling of an attenuated strain may be used to determine the transcriptional basis of attenuation. An outstanding pilot candidate for such an analysis is a *A. fumigatus* Δ*laeA* strain, which was constructed by Nancy Keller's laboratory (Bok and Keller 2004). *A. fumigatus* Δ*laeA* strains are attenuated in neutropenic and corticosteroid treated murine models of infection (Bok et al. 2005, Sugui et al. 2007b). Δ*laeA* strains demonstrate wild-type growth rates and are able to germinate in the murine lung. Accordingly, the attenuation of these isolates is not due to a simple inability to adapt to the host niche. Indeed, LaeA deletion results in pleiotropic impacts which may synergistically contribute to the reduced virulence phenotype, including an altered conidial morphology and the reduced production of numerous secondary metabolite toxins.

Most importantly, LaeA controls transcription of 9.5% of the *A. fumigatus* genome *in vitro* (Perrin et al. 2007) and numerous genes which reside in subtelomeric loci (McDonagh et al. 2008) via epigenetic mechanisms (Reyes-Dominguez et al. 2010). Transcriptional comparisons between Δ*laeA* and a wild-type comparator during the initiation of infection may determine the relative contribution of subtelomeric loci and epigenetic gene regulation towards virulence. A short summary of current knowledge regarding LaeA is given below.

1.4.1 LaeA is a putative methyltransferase which may regulate secondary metabolite biosynthesis and subtelomeric loci by epigenetic mechanisms

In eukaryotic genomes, genes involved in functional related pathways often cluster at proximal genomic locations (Keller and Hohn 1997). The *A. fumigatus* genome contains 23 clusters which putatively direct the biosynthesis of secondary metabolites (Perrin et al. 2007). The discovery (Butchko et al. 1999) and characterisation (Bok and Keller 2004) of the *A. nidulans* nuclear LaeA protein was a significant achievement with regard to understanding the regulatory mechanisms governing secondary metabolite biosynthesis in *Aspergilli*.

The putative methyltransferase LaeA was initially discovered by Butchko and co-workers (Butchko et al. 1999). These investigators were interested in regulation of the positively acting transcription factor AlfR, which is required for sterigmatocystin biosynthesis in *A. nidulans*. The authors used UV mutagenesis and a novel assay to determine AlfR regulators. By disrupting a gene in the SC biosynthetic pathway, an intermediate metabolite (Norsolorinic acid, NOR) accumulating strain was produced. NOR is a bright orange piment. Following UV mutagenesis of the NOR^- strain, normally pimented strains were identified, which putatively contained mutations in genes required for sterigmatocystin biosynthesis. 83 such isolates were identified, and through classical genetic analysis 23 mutations were found to be unlinked to the sterigmatocystin gene cluster. 3 of these strains were unable to express *aflR* under a variety of conditions. In a later study, one of the *A. nidulans aflR* expression mutants was transformed with an *A. nidulans* genomic cosmid library, and norsolorinic acid-producing transformants identified (Bok et al. 2004). Retrieval of the cosmid which complemented the mutant enabled the identification of a the gene *laeA,* which stands for loss of *aflR* expression. GFP tagging demonstrated LaeA localised mainly in the nucleus. The gene was found to contain 3 putative *aflR* binding sites and an S-adenosylmethionine binding site. S-adenosylmethionine is substrate involved in methyl group transfers. The authors noted the absence of a double E loop domain associated with histone methyltransferases, and suggest

LaeA may be a DNA methyl transferase. In the same study, *laeA* deletants were constructed in *A. nidulans* and *A. fumigatus.* Northern analysis of *A. nidulans* Δ*laeA* demonstrated reduced expression of genes in the sterigmatocystin, penicillin and lovastatin clusters throughout a time series of *in vitro* growth. Moreover, TLC analyses of mycelila culture supernatants demonstrated the reduced production of sterigmatocystin and gliotoxin in *A. nidulans* Δ*laeA* and *A. fumigatus* Δ*laeA* respectively. The authors suggested LaeA is a global regulator of secondary metabolite biosynthesis which may regulate gene expression by epigentic control of chromatin.

The first direct evidence that LaeA plays a role in regulating *A. nidulans* secondary metabolite biosynthesis by controlling the metabolically dependent, reversible formation of heterochromatin was provided by Reyes-Dominguez and co-workers (Reyes-Dominguez et al. 2010). In the model proposed by these authors, transcriptionally silent heterochromatin is formed by the histone deactylase HdaA, the H3K9 specific methylase ClrD and heterochromatin protein HepA. HdaA directs the hypoacetylation of H3 and H4 (Lee et al. 2009), which facilitates methylation by ClrD. H3K9 methylation is recognised by HepA, which results in DNA methylation and the formation of heterochromatin. LaeA is hypothesised to reverse the formation of heterochromatin by DNA or H3K9 methylation activity. This model was based on several observations: (1) deletion of *hepA* results in upregulation of numerous secondary metabolite gene clusters, but not genes immediately outside the cluster; (2) chromosome immunoprecipitation demonstrated HepA occupancy at the sterigmatocystin cluster decreases during transcriptional activation, but not on adjacent genes; (3) deletion of *clrD* resulted in increased expression of several secondary metabolite genes, but not those adjacent to the cluster; (4) HepA occupancy of AflR is greatly increased in Δ*laeA* relative to the wild-type. Work conducted by Bayram and colleagues has shown LaeA forms part of the heterotrimeric velvet complex which co-ordinates light, fungal development and secondary metabolism in *A. nidulans* (Bayram et al. 2008).

Transcriptional comparisons between *A. fumigatus* Af293 and an Af293 Δ*laeA* strain during *in vitro* culture supported the role of LaeA as a global regulator of secondary metabolite biosynthesis (Perrin et al. 2007). 13 out of 23 secondary metabolite clusters were defined as LaeA regulated, based on the definition that either a PKS, NRPS, or more than 50% of the genes in the cluster demonstrated decreased transcript abundance in the Δ*laeA* strain. 9.5% of the *A. fumigatus* genome was differentially expressed between Δ*laeA* and wild-type isolates. Comparison of this dataset with genes preferentially employed during infection (McDonagh et al. 2008) identified numerous genes which were putatively under LaeA control and putatively required for murine infection, including gliotoxin, pseurotin A and a secondary metabolite cluster with an unknown product. Moreover, 40 of these genes were found to reside in subtelomeric loci, indicating LaeA

may regulate these regions during the intiation of infection (McDonagh et al. 2008). Identification of genes which are differentially expressed in the Δ*laeA* strain during infection relative to the wild-type might identify genes which contribute to the attenuated phenotype. It is hypothesised that these genes may biosynthesise proteins or small molecular mass molecules which are involved in host-pathogen interactions.

1.4.2 *A. fumigatus* Δ*laeA* is attenuated in murine models of infection and can be used as a tool to reverse engineer the molecular basis of *A. fumigatus* virulence

Secondary metabolites which may be employed to improve survivorship in the natural niche are hypothesised to be critical for survival in the immunocompromised mammal (Keller et al. 2005). In keeping with this hypothesis, LaeA deletant strains are attenuated in neutropenic and corticosteroid treated murine models of infection (Bok et al. 2005). However, the molecular basis of Δ*laeA* attenuation is not clear. In the study conducted by Bok and colleagues, murine survival in Δ*laeA* infected animals was associated with a reduction in pulmonary gliotoxin (Bok et al. 2005). Additionally, Δ*laeA* demonstrated wild-type growth rates but scanning electron microscopy revealed spores of Δ*laeA* were smooth, in contrast to the echinulate spores of the wild-type (Bok et al. 2005). Δ*laeA* conidia were more susceptible to alveolar macrophage phagocytosis, and mycelial supernatant from Δ*laeA* causes less neutrophil damage than the wild-type (Bok et al. 2005). Accordingly, it was hypothesised that Δ*laeA* may be attenuated due to modification of the spore architecture, reduced rates of secondary metabolite toxin production, unknown factors, or synergystic contribution of all these elements to virulence (Bok et al. 2005). Two subsequent studies have utilised Δ*laeA* as a tool to reverse engineer the molecular basis of *A. fumigatus* attenuation.

The laboratory of Dr Kwong-Chung has been interested in the role of microbial pigments in *A. fumigatus* virulence (Tsai et al. 1998). Investigators from this laboratory previously demonstrated deletion of the DHN-melanin polyketide synthase *pksP* resulted in smooth, white conidia (Tsai et al. 1998). The observation that Δ*laeA* strains had smooth yet normally pigmented conidia (Bok et al. 2005) suggested pigmentation and spore architecture may be controlled by different factors under LaeA regulation. Accordingly, Sugui and co-workers deleted *laeA* in the clinical isolates Af293 and B5233. RT-PCR and HPLC from Δ*laeA in vitro* cultures demonstrated a reduction in gliotoxin gene transcription and metabolite biosynthesis in both strain backgrounds. In contrast to work conducted in the Af293 background, LaeA deletants in the B5233 strain had echinulate

spores. B5233 Δ*laeA* demonstrated reduced virulence in a corticosteriod treated murine model of infection. Accordingly, the authors hypothesised that LaeA plays an essential role in virulence but not in conidial morphogenesis. These data suggested that in the B5233 isolate, attenuation of *laeA* deletants was likely related to decrease in secondary, metabolite toxins in the host niche.

Dagnenais and colleagues utilised Af293 Δ*laeA* as a tool to reverse engineer conidial susceptability to phagocytosis (Dagenais et al. 2010). Blocking conidial PAMPs with laminarin and mannan did not alter the difference in macrophage phagocytosis between wild-type and Δ*laeA*, indicating differences in phagocytosis were not likely due to alteration in PAMPs. Formaldehyde fixing of Δ*laeA* spores had no significant impact on rates of phagocytosis, which suggested secreted factors could not explain the difference in phagocytosis. However, extraction of the rodlet layer demonstrated a 60% decrease in the protective protein RodA from Δ*laeA* spores. Additionally, phagocytosis with germinated spores demonstrated comparable rates of phagocytosis. Accordingly, it was determinded that the increased rates of Δ*laeA* phagocytosis are due to a reduction in the conidial rodlet layer, and that this may contribute to the attenuation of Af293 Δ*laeA.* Work reported in this thesis describes the analysis of global gene expression profiling in Δ*laeA* and its fully virulent wild-type isolate in the murine lung in order to provide insights into the transcriptional basis of Af293 virulence and Δ*laeA* attenuation.

1.5.0 Microarray technology is a powerful tool to study environmetal adaption and host-pathogen interactions during infection

DNA microarray technology is a powerful approach which has been previously employed to study global gene expression of *A. fumigatus* under a number of laboratory conditions, which either approximate or are relevant to host colonisation. *In vitro* and *ex vivo* transcriptional profiling following heat shock (Nierman et al. 2005), antifungal treatment (Cagas et al. 2011, Gautam et al. 2008), exposure to human neutrophils (Sugui et al. 2008), following exit of spore dormancy (Lamarre et al. 2008) or between planktonic and biofilm growth states (Bruns et al. 2010a) provide insights into *A. fumigatus* responses to disease relevant conditions, yet do not address pathogen gene expression in the multifaceted and dynamic host niche. Our group has published the first global analyses of the *A. fumigatus* infecting transcriptome, which identified genes preferentially employed at a single time-point of murine infection relative to laboratory culture (McDonagh et al. 2008). This analysis identified pH, iron starvation and nitrogen limitation as key challenges to host colonisation, and revealed the induction of multiple secondary metabolite loci and a biased distribution of induced genes in subtelomeric regions of chromosomes. Similar *in vitro* reference

experiments have proved critical in elucidating the transcriptional basis of fungal pathogenesis for other mammalian and plant pathogens (Kamper et al. 2006, Mosquera et al. 2009, Walker et al. 2009). However, single time-point analyses are inherently limited with regard to delineating pathogen transcriptional changes which are temporally regulated. Indeed, *A. fumigatus* germination and cellular differentiation represent essential cellular process in the establishment of invasive aspergillosis (Tekaia and Latge 2005) which occur over several hours in the murine lung. Concurrent to substantial fungal changes in physiology and biochemistry throughout infection, multiple host niches are encountered, exemplified by the aerobic alveoli which accomodate the spore, and the likely hypoxic parenchyma surrounding the invasive hyphae (Wezensky and Cramer 2011). Delineating temporal transcription changes will therefore be essential for understanding gene expression in the host.

1.5.1 Ratiometric and non-ratiometric array normalisation for analysis of *A. fumigatus* gene expression during early murine infection

Two distinct objectives were served by a single microarray experiment; (1) defining time-point specific changes in gene expression in Af293 and Δ*laeA*; (2) deviation of the Δ*laeA* host infecting transcriptome from that of Af293. With regard to the methodology which is developed during this experiment, its use as a tool for the study of *A. fumigatus* infection is greatly enhanced if it is easily adaptable to the comparison of other isolates, models of disease or time-points. This presents a challenge for microarray experimental design, which aims to gain maximal insight into both time-point and strain variables from expensive and labour intensive microarray experiments, while remaining amenable to extensions (such as the inclusion of another strain of interest) following the completion of this work. Common experimental set ups, such as reference or loop designs both have positive and negative attributes with regard to maximising data and inclusion of subsequent experiments (Figure 1A and B).

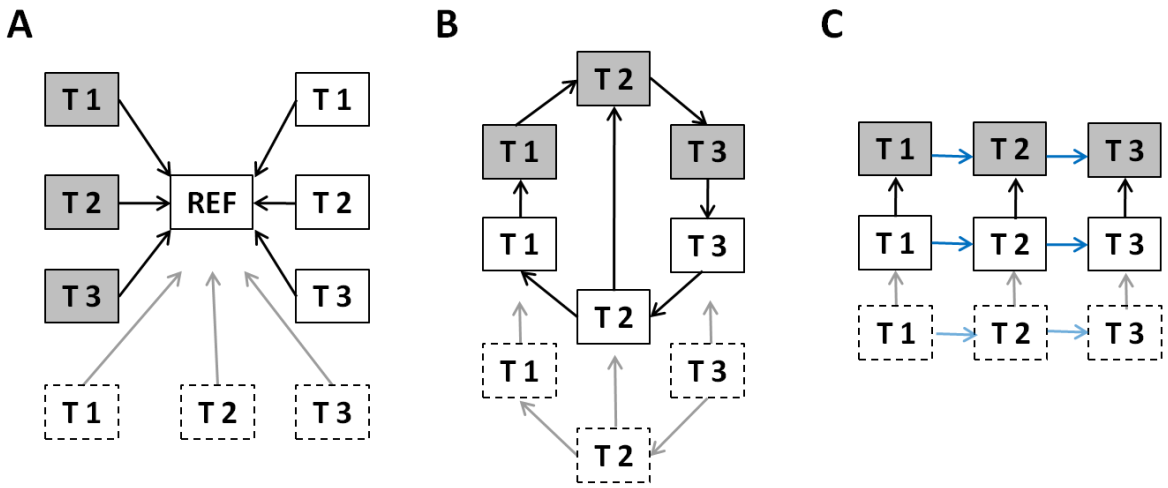


Figure 1.3: Options for experimental design of microarray experiments investigating Af293 and Δ*laeA* gene expression throughout a 3 time-point time-course. Unshaded and shaded boxes represent Af293 and Δ*laeA* RNA samples respectively. Black arrows represent co-hybridisation on a dye swap pair of arrays, for which a dye swap replication was performed. Three time points (T1 – T3) and a reference sample (REF) are shown. Blue arrows represent possible pair wise comparisons using the channel intensity approach proposed by t Hoen (2004) and Bossers (2010a). Chequered boxes and faint grey/blue arrows indicate extension of the experiment following completion of this study. **A.** Common reference design in which samples are competitively hybridised against a reference. The design is amenable to the inclusion of other samples, but is inefficient as half the data comes from the reference. **B.** Loop design. The set up is more efficient, as samples are always hybridised with a biologically relevant sample. The approach is not amenable to extension, as a sub loop of 10 arrays is required (5 co-hybridisations with dye swaps). **C.** Combined approach using both ratio and non-ratiometric intensity analyses. Differences between strains are directly compared at each time point by standard ratio analyses, and intensity approach is used to analyse gene expression profiles between the time-points. 6 arrays are required per replicate allowing a maximum amount of replication with a given set of arrays. Additionally, extension of the experiment to include another strain requires only 6 arrays.

A previous study conducted by Thewes and co-workers concurrently investigated two strains at different time-points of *C. albicans* murine infection using a reference approach (Thewes et al. 2007). Thewes and colleagues compared gene expression of the invasive SC5314 and non-invasive ATCC10231 *C. albicans* strains at 30 minutes, 3 hours and five hours post infection in a murine model of haematogenously generated candidiasis. For both strains, RNA samples at each time-point were co-hybridised with RNA from SC5314 grown in YPD. The ratio of signal intensity was a relative measure of gene expression between the time-point and the common reference, and was used to identify transcriptional changes between the time-points of disease. Differences between SC5314 and ATCC10231 were subsequently identified by comparing gene expression data at each time-point (i.e. 3 hours ATCC10231 with 3 hours SC5314). The use of a reference sample is also common in single time-point analyses of host infection, including *A. fumigatus*, *C. albicans*, *M. grisea,* and *U. maydis* (Kamper et al. 2006, McDonagh et al. 2008, Mosquera et al. 2009, Walker et al. 2009). There are several advantages to this approach- it is easy to extend the study and incorporate other conditions by simply hybridising a novel sample to the original reference. Additionally, technical error (for example minor changes in hybridisation conditions) and

array variation (such as differences in spot size, concentration or background signal) are reduced between conditions as the reference and experimental sample are co-hybridised. However, common reference sampling is inefficient, for example when compared to loop designs (Figure 1.3) as half the data is from a single sample. Additionally, as a consequence of the low RNA quantities obtained from the host niche, reference samples are taken from laboratory culture. This has far reaching consequences for the interpretation of gene expression, as transcript abundance will vary relative to the growth conditions employed. For example, a universal challenge to host colonisation is the lack of available iron, which is an essential co-factor for many cellular processes. Consequently, mechanisms of iron assimilation are essential virulence factors in *A. fumigatus, C. albicans,* and *C. neoformans* infection (Jung et al. 2009, Ramanan and Wang 2000, Schrettl et al. 2007). Despite this common challenge to infection, transcriptional analyses showed *A. fumigatus* and *C. albicans* employ genes for iron acquisition in the host (McDonagh et al. 2008, Thewes et al. 2007) whereas *C. neoformans* did not (Hu et al. 2008). It is highly likely that these observations are due to the differences in iron content of the reference sample growth media, as the latter study used *C. neofromans* grown in low iron media (LIM).

A loop design in which samples are hybridised sequentially throughout a time-course is one way of negating the use of a common reference sample (Figure 1.3B). This approach is more efficient as samples are always co-hybridised with a sample extracted from the host niche. Yet for time series experiments with few time-points, appropriate to the interest of this study, this approach is vulnerable to technical failure- if a single array is of poor quality, two or possibly three time-point comparisons are affected (Figure 1.3). Loop designs are also not amenable to the inclusion of additional conditions following the experiment, as they require the construction of a sub-loop (Figure 1.3B).

To circumvent the disadvantages of reference and loop designs ‘t Hoen and colleagues investigated an intensity based approach to analyse gene expression from two colour microarrays ('t Hoen et al. 2004). In standard experiments, the ratio of signal intensity is a relative measure of transcript abundance between two samples which are co-hybridised. The intensity approach treats both colour channels as independent measures of gene expression, which allows pair-wise comparisons to be made between channels from any array without the need for co-hybridisation (Figure 1.4). To validate this method, the authors firstly compared spot intensities from two differently labelled and co-hybridized RNA samples (Cy3 and Cy5) with equivalent spots from two singly labelled experiments (Cy3 or Cy5). Intensities between these hybridisation conditions showed high concordance, and no statistically significant differences in intensity were reported.

This demonstrated that cDNAs in co-hybridised arrays do not compete for oligonucleotide binding sites, an essential prerequisite for analysing channels separately. Spot intensities were not impacted by any of several other variations in hybridisation design, including co-hybridisation with a common reference, unlabelled RNA or a self-sample. Ratio calculations from both ratio (co-hybridised) and intensity approaches (calculated *in silico* between arrays) correlated well ($R > 0.8$). The authors noted that signal intensities from targets labelled in the same colour were better correlated than the signal intensities from the opposite colour. This observation reinforces the importance of dye swap experiments in analysis using non-ratiometric intensity as a measure of transcript abundance.

Bosser and colleagues further demonstrated the advantages to intensity based analysis of dual colour microarrays (Bossers et al. 2010a). These authors noted that the use of oligonucleotide arrays, as opposed to previous cDNA platforms, had greatly reduced variation between arrays, such as spot concentration. They found analyses using a spot intensity model were highly reproducible between technical replicates. The authors also demonstrated, as did t'Hoen and colleagues, that *in silico* ratio calculations reconstructed from inter-array intensities were well correlated to ratio calculations when the same samples were co-hybridised ($R > 0.94$). Although both studies referred to these types of analyses as "intensity based" this is actually a misnomer as all microarray data are ultimately based on intensity. Therefore, the term "non-ratiometric" is used for the remainder of this work. Nevertheless these studies suggest that inter-array pair-wise comparisons between any intensity channels from a dual colour platform can be compared provided the experimental design adequately controls for dye bias with appropriate dye swap experiments and the platform uses oligonucleotide probes. This allows for interrogation of both time-point specific changes in gene expression in Af293 and Δ*laeA*, and deviation of the Δ*laeA* host infecting transcriptome from that of Af293, with a minimal number of arrays, while also being amenable to inclusion of other experiments (Figure 1.4C).

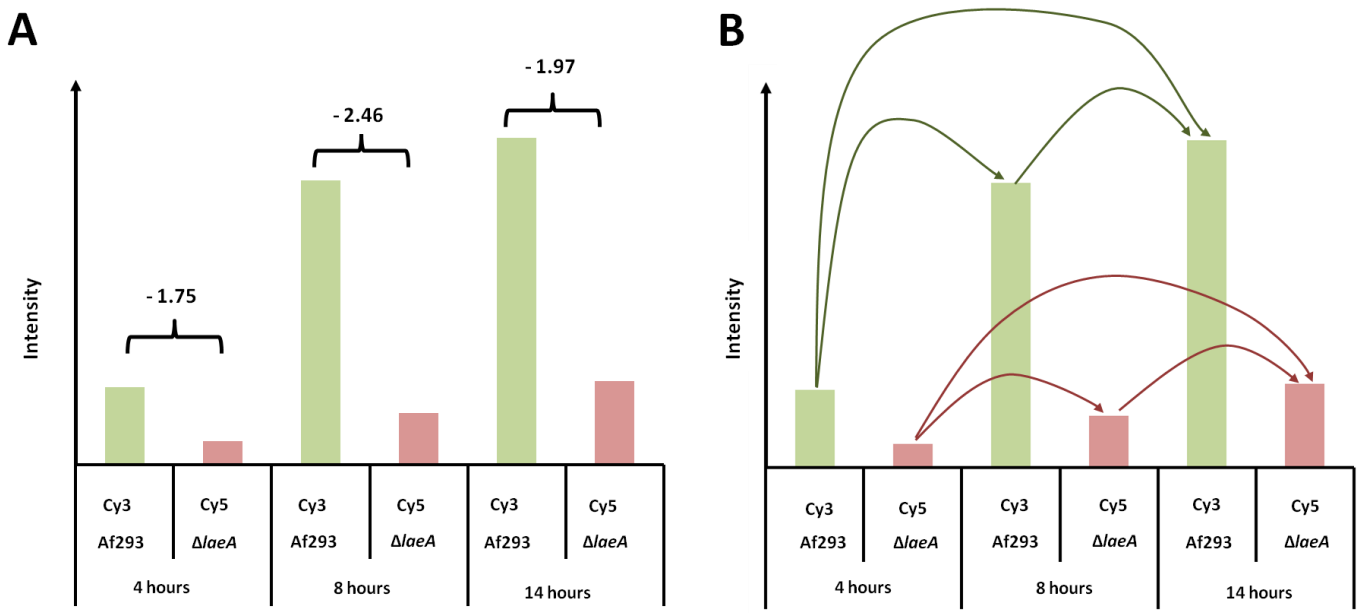


Figure 1.4: Comparison of standard ratiometric (A) and non-ratiometric (B) of dual colour microarrays in a two strain time series experiment. Transcript abundance of a single exemplar gene (elastinolytic metalloproteinase Mep, Afu8g07080) from a single array at each time-point is shown. **A.** In a ratiometric analysis, intensity of Cy3 and Cy5 is used to calculate expression of Δ*laeA* relative to Af293. **B.** In non-ratiometric approach proposed by t'Hoen (2004) and Bossers (2010a), single channels are treated as single colour experiments, allowing for pair wise comparisons between time-points without co-hybridisation. Green and red arrows show possible strain specific analysis of gene expression across the time course using this method.

A final criterion to facilitate single channel analysis of dual colour microarrays is an appropriate method for inter-array normalisation to reduce inter-array technical differences. Considering that the non-ratiometric intensity approach treats each channel as a single colour experiment, methodologies for inter-array normalisation from single channel experiments are considered.

One approach is to normalise arrays to constitutively expressed genes. For example, Affymetrix Genechip® Human Genome Arrays include a set of 100 human "maintenance genes" which have theoretically stable expression levels in a variety of conditions (Affymetrix, UK). The house-keeping set includes glyceraldehyde 3 phosphate dehydrogenase (GAPDH), beta actin and the transcription factor interferon-stimulated gene factor 3 (ISGF-3). The constitutive expression of these genes facilitates normalisation by scaling, so the average intensity value of the house-keeping set is equal between arrays (Affymetrix). A significant disadvantage to this approach is that transcription of house-keeping genes may vary between experimental conditions (de Jonge et al. 2007). GAPDH or beta actin transcript abundance is unknown during *A. fumigatus* infection, which invalidates this approach for inter-array normalisation.

Scaling using linear regression is a common method for inter-array normalisation of single channel experiments. Firstly, a baseline array is chosen, for example the array with the median of the

median intensities. A normalisation constant is defined by dividing the average intensity of the baseline array by the average intensity of the array to be scaled (Bolstad et al. 2003). Normalisation is achieved by multiplying all probe intensities by the normalisation constant. A large number of variations of this approach are used, for example using median or trimmed mean values to determine the normalisation constant. Non-linear locally weighted scatter plot smoothing (LOWESS) transformation can also be used to reduce variation between single channel arrays of interest relative to a baseline array (Quackenbush 2002). Firstly, a regression line is fitted to MA plots using locally weighted least squares estimate of regression fit. MA plots are used to assess the relation between the Cy3 and the Cy5 channels from a given hybridisation experiment. In these plots the $\log_2$ ratio between red and green channels (Y-axis) is plotted against the sum of red and green channels (X-axis). Un-normalised data have higher spot intensities associated with the green dye (Cy3) and LOWESS normalisation distributes the data more evenly around the X-axis. Secondly, log values are adjusted relative to the regression line. This has the effect of smoothing the MA plot around the M = 0 axis. Both linear and non linear approaches require the use of a baseline array which is inherently problematic- for example, using the median of the baseline may increase a given intensity dataset, whereas using the mean value from the same baseline may decrease the values (Bolstad et al. 2003).

To circumvent problems associated with a baseline array, Bolstad and colleagues implemented quantile normalisation of intensities for inter-array normalisation (Bolstad et al. 2003). In this approach, all arrays in the experiment form the normalising relation. Quantile normalisation employs the following algorithm, described in Bolstad et al. 2003:

1) Given n arrays of length p, form X of dimension p x n where each array is a column

2) sort each column (X) to give X_{sort} based on magnitude of signal intensity

3) take the means across rows of X_{sort} and assign this mean to each element in the row to get X'_{sort}

4) get $X_{normalised}$ by rearranging each column of X'_{sort} to have the same ordering as original X.

Quantile normalisation facilitates inter-array comparisons as all arrays have equivalent distribution of intensities, and intensity datasets are smoothed around the M = 0 axis of an MA plot. This approach has become widely used for single channel experiments, and quantile normalisation

algorithms are available in Bioconductor, Genespring (Agilent) and a Python module available online (Baber et al. 2011).

Quantile normalisation of non-ratiometric intensity from dual colour arrays has been used by two groups. Nota and colleagues investigated the transcriptional response of the soil arthropod, *Folsomia candida* to multiple heavy metals, with a view to identifying gene expression profiles which were diagnostic of soil contamination (Nota et al. 2010). Hierarchical clustering between all samples was essential to ascertain gene expression that could differentiate between treatments, an analysis not suited to ratiometric analysis. The study employed 16 treatments, replicated 4 times, equating to a total of 64 samples. Biological replicates were therefore co-hybridised on dual colour arrays (n = 32), from which non-ratiometrics (n = 64) were quantile normalised across all hybridisations and $\log_2$ transformed. Clustering revealed 188 genes which were able to discriminate between treatments. The inefficient and irrelevant use of a reference sample was avoided by use of separate intensity channels.

A second study used non-ratiometric analysis from two colour arrays to study transcriptional changes in the prefrontal cortex during the progression of Alzheimer's disease (Bossers et al. 2010b). 49 samples, grouped into 7 time-points, were analysed using 102 channels from 52 arrays (45 duplicate and 4 triplicate channels). Inter-array intensities were quantile normalised and $\log_2$ transformed followed by transcript fold change calculations over seven time-points of disease. Four significant gene clusters, (as defined by comparable temporal profiles throughout disease progression) were identified using this approach. A combination of standard ratiometric and non-ratiometric methods allows both time-point specific changes in gene expression in Af293 and Δ*laeA* and deviation of the Δ*laeA* host infecting transcriptome from that of Af293 to be determined in parallel from a minimum number of arrays, whilst also being easily adapted to include additional isolates, models of disease or time-points (Figure 1C). A non-ratiometric approach is ideal for extending the microarray study, as it is simple to apply quantile normalisation across every intensity channel, including a new microarray. As a consequence, array outputs (i.e. differentially expressed gene lists) are not compared, but rather the entire experiment re-normalised to include the new data, enabling full statistical analysis in the context of the entire dataset.

Accordingly, array experiments were designed so that hybridisations between Af293 and Δ*laeA* facilitated ratiometric analyses between the strains directly at specific time-points (4, 8 and 14 hours), and quantile normalised non-ratiometric intensities allowed changes in gene expression in Af293 and Δ*laeA* between each time-point (Figure 1.5). While it would be equally possible to co-

hybridise between time points and use quantile normalised non-ratiometric intensity between strains, this would require the use of two additional arrays (Figure 1C).

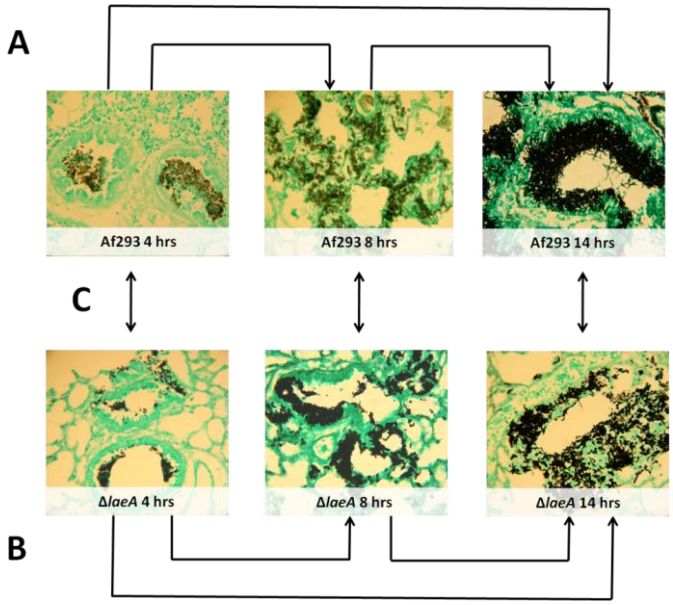


Figure 1.5: Schematic representation of ratio and single channel intensity strategies to analyse the host infecting fungal transcriptome in Af293 and Af293 Δ*laeA*. A. To assess temporal modulation of Af293 gene expression between time-points, quantile normalised non-ratiometric normalisation was applied. **B.** To assess temporal modulation of Δ*laeA* gene expression between time-points, quantile normalised non-ratiometric normalisation was applied. **C.** Rationmetric analysis of Δ*laeA* transcript profile relative to the parental isolate Af293 directly compared transcript abundance between the mutant and the parental isolate at each time point.

1.6.0 Application of Surface enhanced laser desorption/ionisation time of flight mass spectrometry for detection of epitope tagged fungal proteins in murine bronchoalveolar lavage fluid

Transcriptional comparisons between *A. fumigatus* germlings isolated from the murine lung with developmentally matched laboratory culture have identified numerous genes which are preferentially employed in the host (McDonagh et al. 2008). The products of many of these genes, such as secreted proteases, cutinases, lipases, phospholipases, GPI-anchored proteins, cell wall proteins and antigens are putatively involved in host-pathogen interactions. The detection of these proteins in an infection model would enable strong hypotheses to be draw about the role they might play in disease. This is best illustrated by the alkaline serine protease Alp1. This protein is present in *A. fumigatus* infected human as determined by an antibody specific immunofluorescence assay (Reichard et al. 1990). Interestingly, this study reported Alp1 release from both conidial and hyphal elements, suggesting this protein is present before and after

germination. Alp1 transcription was also reported 3, 7 and 10 days post infection in a murine model utilising a alp::LacZ reporter gene fusion (Smith et al. 1994). More recently, this enzyme was found to degrade multiple elements of the host complement system, including C3, C4, C5, and C1q, and the anitbody IgG (Behnsen et al. 2010). Without detection of Alp1 *in vivo*, these data of complement degradation might have been irrelevant to disease. However, irrespective of the virulence phenotype deemed of the mutant (Smith et al. 1994, Behnsen et al. 2010) one can hypothesise with some confidence that that Alp1 plays a role in host pathogen interactions, at least via complement degradation, and that this is sustained throughout morphological development in the mammalian lung. In a similar sense, detection of a gene product which, when deleted, impacts infection would provide evidence linking the gene function to a specific time-point, or throughout sustained periods of disease. For example, analyses of tissue damage caused by a double mycelial catalase mutant Δ*cat1*Δ*cat2*, using histology from a neutropenic rat model found restricted hyphal growth and reduced lesions relative to the wild-type at 5 and 13 days post infection (Paris et al. 2003). The authors noted that tissue damage and fungal development in the mutant at 13 days matched that of the WT at 5 days, and therefore suggested the mycelial catalases transiently protect the *A. fumigatus* from ROS at some time-point before day 5. However, questions still remain regarding the role of these enzymes during infection: are they protecting *A. fumigatus* throughout 5 days, or at specific time points, perhaps relating to fungal development or host ROS attack? Detection of the catalases in the rat lung would provide causal evidence to complement observations inferred from the tissue damage effect, enabling the formation of hypotheses which address the temporal nature of the host pathogen interactions.

In addition to enhancing understanding of the basic pathophysiology of aspergillosis, detection of fungal proteins within the murine lung would provide a platform for the development of clinical diagnostics. The early time-points addressed in this study have two main advantages for this purpose. Firstly, biomarkers from disease initiation will enable the most prompt diagnosis. Secondly, identification of biomarkers specific to time-points before and after germination in the lung would enable the distinction between invasive infection from normal carriage of spores. This study therefore sets out to develop a methodology for Surface enhanced laser desorption/ionisation time of flight mass spectrometry (SELDI-ToF-MS) for detection of epitope tagged fungal proteins in murine bronchoalveolar lavage fluid.

1.6.1 Existing mass spectrometric tools for studying *A. fumigatus* proteins

While study of proteins in the *A fumigatus* infected murine niche is limited, the power of modern methods for the analyses of macromolecules have been harnessed by the fungal community to address a wide range of basic and translational research issues (Doyle 2011). Although the aims of these studies are diverse, common criteria essential for a proteomic tool are clearly identifiable; namely, a sensitive and accurate method for molecule detection and identification, with high reproducibility and relatively low cost. Mass spectrometric (MS) methods involve the formation, manipulation and measurement of charged molecules, and present the obvious candidate to fulfil many of these research requirements. Consequently MS has become a common analytical method for examination of the fungal proteome, most often following two-dimensional gel electrophoresis or liquid chromatography.

For example, Lessing and co-workers investigated regulation of the *A. fumigatus* reactive oxygen intermediate detoxification by the transcription factor Af*yap1* using such analyses (Lessing et al. 2007). Following deletion of Af*yap1*, wild type and deletion strains were challenged with H_20_2, and differentially expressed proteins identified by two-dimensional fluorescent-difference gel electrophoresis (DIGE) and Matrix Assisted Laser Desorption/Ionization Time-of-Flight (MALDI-TOF) mass spectrometry. DIGE defined protein changes between samples by differential labelling with fluorescent dyes (Cy3 and Cy5) followed by two-dimensional electrophoresis and fluorescence intensity quantification of spots. Proteins of interest were then characterised by MALDI-ToF, in which ionisation of the protein analyte were achieved by a laser beam (Karas and Hillenkamp 1988). ToF MS followed ionisation, and proteins were identified by software specifically designed to compare mass spectra against protein databases, such as the MASCOT interface (Matrix Science, United Kingdon). Using these methods, 29 proteins were found to be directly or indirectly controlled by Af*yap1* including catalase Cat1, Cu/Zn superoxide dismutase, a cytochrome C peroxidase and Allergen Asp F3. Combining these data with phenotypic characterisation and virulence analyse of the ΔAf*yap1* in a murine model of infection, the authors demonstrated that the Af*yap1* ROI detoxifying proteome is required for protection against H_20_2 but dispensable for virulence. In another study, quantitative 2D-PAGE and MALDI-ToF-MS were used to demonstrate the presence of the gliotoxin oxidoreductase (GliT) in 21 hour cultures following addition of exogenous gliotoxin (Schrettl et al. 2010). Further analyses of this gene, including deletion and virulence assays in an invertebrate *G. mellonella* model demonstrated GliT is essential for protection against exogenous gliotoxin but not required for invertebrate infection. 2D-DIGE and MALDI-ToF were used to dissect the *A. fumigatus* heat shock response at 5 sequential

time points following a shift from 30° to 48° of 16 hour cultures (Albrecht et al. 2010). 64 differentially expressed proteins were identified, which were involved in protein folding, oxidative stress, signal transduction, transcription, translation, carbohydrate and nitrogen metabolism. As noted above, this study reported transcriptional profiling in parallel with low levels of concordance between proteomic analyses. However, these data demonstrate the analytical power of MS methods in analysing the fungal proteome.

Nonetheless, due to several unique challenges encountered from infected host samples, no technology employed by the fungal community to date is wholly appropriate for protein detection in the host. Firstly, the extensive fungal morphological changes throughout spore adherence, germination, tissue penetration and subsequent disease progression occur in parallel with host cellular and molecular immune responses. This is further complicated by interest in different models of infection, such as corticosteroid treated, neutropenic or allergic animals which radically alter the host niche. This is in contrast to controlled laboratory proteomic experiments, where a single variable is often modified. To assess the different fungal protein profile within different models and at defining time-points of disease, a high throughput tool would be desirable. Secondly, the use of infected host samples means pathogen proteins will be at low concentrations within a complex mix of host proteins. Such issues of concentration and host contamination are often circumvented in transcriptional studies by physical removal of host tissues and fungal mRNA amplification (McDonagh et al. 2008, Mosquera et al. 2009, Thewes et al. 2007). As no analogous technique is available for proteomic studies, samples are usually treated with labour intensive liquid chromatography or PAGE separation prior to MS analyses.

As discussed in the previous section, the field has assembled a wealth of information on activities required by *A. fumigatus* to successfully colonise its immunocompromised host. This inherently presents a challenge to proteomic study as large numbers of putative fungal proteins are predicted to be present in the host niche at various stages of infection. When one considers recent transcriptional insights (McDonagh et al. 2008) combined with *in vitro, in vivo*, *ex vivo* and *in silico* predictions of function, hundreds and possibly thousands of fungal proteins present themselves. In a rapidly developing field, where new insights into potential virulence molecules are discovered every year, a targeted tool able to rapidly assess specific hypotheses on protein content in the host is required.

1.6.2 The advantages of Surface enhanced laser desorption/ionisation time of flight mass spectrometry for pathogen protein detection in the infected murine lung

Surface enhanced laser desorption/ionisation (SELDI) ToF-MS is a recently developed form of laser desorption/ionisation MS where the sample surface plays an active role in the extraction, cleaning, and/or amplification of the sample of interest (Tang et al. 2004). This is of particular interest for the study of protein in biological samples, which will include many homeostatic or contaminating proteins such as albumin and IgG. SELDI ToF MS was first described by Hutchens and Yip in 1993, who designed an active chip surface with a view to studying *in situ* modifications to protein structure by MS (Hutchens and Yip 1993). In this proof of principle study, they designed a class of DNA probe surfaces which were used as affinity devices to capture human lactoferrin from infant urine. The active capture of protein target from complex biological fluids improved the quality of the observed spectra, and lowered the detection thresholds for analytes (Hutchens and Yip 1993). Indeed, the authors reported detection of attomolar concentrations of protein. Clearly, the principle of active chip-based purification directly prior to MS was amenable to multiple purposes, and SELDI has been commercially available since 1997 as Protein Chip® from BioRad. Surfaces for active capture include chemical (immobilized metal ion affinity chromatography beads, ionic, hydrophobic) or biological (DNA, enzyme, ligand, antibody) affinity probes (Tang et al. 2004). These have been applied in clinical proteomics for the discovery biomarkers of HIV (Zhang et al. 2002) trypanosomiasis (Papadopoulos et al. 2004) and *M. tuberculosis* infection (Agranoff et al. 2006). SELDI combined with poly or monoclonal antibody capture has been used to detect the secretion of β-defensins in human gingival cervicular fluid (Diamond et al. 2001), high density lipoproteins in human plasma (Levels et al. 2007) and the hormonal transporter transthyretin in human blood and urine (Schweigert et al. 2004). The authors noted the speed and ease of the technique, the elimination of prior HPLC analyses, small sample volume and active enhancement using antigen based capture of trace proteins were ideal for detection in complex biological fluids.

It was hypothesised that SELDI-ToF-MS could be used as a tool to detect *A. fumigatus* proteins from the murine lung using the following methodology: (1) construct *A. fumigatus* strains expressing polyhistidine tagged alleles; (2) use these strains in a high dose murine infection model; (3) use an anti-his antibody immobilised to the SELDI chip surface to selectively bind epitope tagged protein from infected murine BALF; (4) detect protein using SELDI-ToF-MS according to the predicted protein mass.

1.7.0 Principle objective of this study:

To determine disease initiating host pathogen interactions in murine models of infection using transcriptional and proteomic tools.

1.7.1 Specific objectives of this study:

1) Use transcriptional profiling at three time points of murine infection to elucidate pathogen environmental adaptation, identify putative *A. fumigatus* molecules which interact with the host, and determine murine innate immune responses to invasive infection

Host-pathogen interactions during the initiation of infection have critical implications for the outcome of disease. It is likely that various *A. fumigatus* morphotypes and micro-environments encountered in the host drastically impact host-pathogen interactions, and therefore outcome of infection. Understanding is currently limited with regard to host-pathogen interactions throughout key time-points of infection. To determine the transcriptional basis of infection at key time-points of disease, the following objectives were achieved:

- global transcriptional profiling of a fully virulent Af293 isolate at 4, 8 and 14 hours post infection in a murine model has been used to identify environmental challenges to host colonisation, while simultaneously identifying a subset of *A. fumigatus* molecules which putatively interact with the host. A non-ratiometric array normalisation methodology was developed, which represents a powerful strategy for maximising biological interpretation from data intensive microarray experiments.

- comparative gene expression analyses of Af293 and the attenuated Δ*laeA* strain have been used to reverse engineer the transcriptional basis of *A. fumigatus* attenuation in the Δ*laeA* mutant

- host innate immune responses to the differentially virulent Af293 and Δ*laeA* isolates at the invasive time-point of infection were measured at the level of transcription

2) Characterise the role of various secondary metabolite molecules in neutropenic and corticosteroid treated murine models of aspergillosis

Transcriptional profiling strongly suggests the employment of numerous secondary metabolites during disease initiation, which putatively have protective or toxic effects during host colonisation. Four deletant strains were analysed in both neutropenic and corticosteroid treated murine models of infection.

- A semi-quantitative qPCR assay was developed for quantification of *A. fumigatus* fungal burden in infected tissue

- The virulence of Δ*psoA*, Δ*ftmA* and Δ*pes3* were compared to wild-type isolates using murine survival assays, histopathology and infection burden quantification

- A modified recombineering methodology was used for gene disruption

- The gene *regA* which putatively biosynthesises the melanin transcription factor RegA was disrupted using the recombineering methodology

- the Δ*regA* strain was characterised with regards to virulence using histopathology and infection burden quantification

3) Detection of epitope tagged fungal proteins from murine BALF using SELDI-ToF-MS

Gene expression analyses suggests numerous pathogen proteins interact with the host. In order to determine which *A. fumigatus* proteins are present in the host niche, the following strategy was proposed: (1) construct *A. fumigatus* strains expressing polyhistidine tagged alleles; (2) use these strains in a high dose murine infection model; (3) utilise an anti-his antibody immobilised to the SELDI chip surface to selectively bind epitope tagged protein from infected murine BALF; (4) detect protein using SELDI-ToF-MS according to the predicted protein mass.

A) Pilot detection of epitope tagged protein from *in vitro* culture
   - Generate epitope tagged *A. fumigatus* clones expressing His-tagged alleles based on published transcription profiling conducted from the murine lung (McDonagh et al 2008).
   - Optimise SELDI-ToF-MS detection of epitope tagged protein from *in vitro* culture

B) Detection of epitope tagged *A. fumigatus* protein from murine bronchoalveolar lavage fluid

- Generate a library of epitope tagged *A. fumigatus* clones expressing His-tagged alleles based on transcriptional profiling conducted in this thesis
- Utilise recombinant *A. fumigatus* strains in a high dose murine model of infection
- SELDI-ToF-MS detection of epitope tagged *A. fumigatus* protein from host BALF

Chapter 2

Materials and methods

2.1 Chemicals, enzymes and general reagents

Chemicals and other reagents were purchased from Fisher Chemicals (UK) or Sigma-Aldrich (UK) unless otherwise stated. Enzymes for cloning, including restriction enzymes, ligases, kinases and phosphatases were purchased from New England Biolabs (UK). Taq DNA polymerases were purchased from Invitrogen (UK), New England Biolabs (UK), KAPABiosystems (UK) and Clontech (UK). All protocols were conducted using manufacture's guidelines, unless otherwise stated.

2.2 Media

All ingredients were purchased from Sigma-Aldrich (UK) or Oxoid Ltd (UK) unless otherwise stated. All media were sterilised by autoclaving at 121°C for 15 minutes.

2.2.1 Bacterial culture

XL-10 (Stratagene) and C41 (Miroux and Walker 1996) *E. coli* were grown in Lysogeny Broth (LB) medium (1% (w/v) tryptone, 0.5% (w/v) yeast extract, 1% (w/v) NaCl) at 37°C, 180 RPM. Solid LB was produced by addition of 2% (w/v) agar prior to autoclaving. Where required, the media was supplemented with 100 µg/ml ampicillin after autoclaving. For β-galactosidase assays, plates were supplemented with 0.5 mM isopropyl β-D-1-thiogalactopyranoside (IPTG) and 80 µg/ml bromo-chloro-indolyl-galactopyranoside (X-Gal) in accordance with the p-GEM®-T Easy protocol. Bacterial cultures and plates were stored for up to 1 week at 4°C. For longer term storage, strains were stored in 25% (w/v) glycerol at -80°C.

2.2.2 *A. fumigatus* culture

A. fumigatus strains used in this study are listed in each respective chapter. Solid and liquid media used identical recipes, except 1% (w/v) agar was added to solid media. Liquid cultures were agitated by orbital shaking at 150 RPM unless otherwise stated. *A. fumigatus* strains were routinely cultured at 37°C in Aspergillus Complete Media (ACM) (1% (w/v) glucose, 0.1% (w/v)

yeast extract, 0.1% (w/v) casamino acids, 0.2% (w/v) peptone, 75 mg/l adenine, 20 ml/l Aspergillus salt solution, 10 ml/l vitamin solution) or Aspergillus Minimal Media (AMM) (20 ml/l Aspergillus salt solution [26 g/l KCl, 26 g/l $MgSO_4$.7H2O, 76 g/l KH_2PO_4], 10 ml/l vitamin solution [400 mg/l 4-aminobenzoic acid, 50 mg/l aneurin, 1 mg/l biotin, 24 g/l mesoinositol, 100 mg/l nicotinic acid, 200 mg/l DL-pantothenic acid (hemicalcium salt), 250 mg/l pyridoxine monohydrochloride, 100 mg/l riboflavin, 1.4 mg/l choline chloride], 20 ml/l 50% glucose, 10 ml/l 500 mM ammonium tartrate). The pH of ACM and AMM were adjusted to 6.5 using 10 M NaOH. Strains were either stored at 4°C for up to 2 weeks on solid agar plates or in 20% (w/v) glycerol at -20°C for long term storage.

2.3.0 General molecular techniques

2.3.1 Oligonucleotide primer synthesis

All oligonucleotide primers were purchased from Sigma-Aldrich (UK). Primers used in this study are summarised in each respective chapter.

2.3.2 Polymerase chain reaction (PCR)

PCRs were performed and optimised according to the manufacture's guidlines. Standard PCRs were conducted using KAPATaq (KAPABiosystems, UK). High fidelity PCRs were conducted using BD Advantage Taq (Clontech, UK), Platinum Taq DNA Polymerase High Fidelity (Invitrogen, UK) or Vent Polymerase (New England Biolabs). For colony PCR from bacteria, initial incubation at 95 °C was extended to 10 minutes. PCR products were purified with QIAquick PCR purification kit (Qiagen, UK) as specified by the manufacturer.

2.3.3 Separation of DNA fragments using electrophoresis

DNA fragments were routinely separated on 1% (w/v) agarose gel. TBE buffer (Tris-Borate 0.1 M, EDTA 1 mM, pH 8.0) was used to prepare and run the gel. 5 µl of SYBR Safe DNA gel stain (Invitrogen) was added to each 50 ml agarose gel. DNA samples were resuspended in the appropriate volume of 6 x loading buffer (10 mM Tris-HCl (pH 7.6), 0.03% bromophenol blue, 60% glycerol, 60 mM EDTA). A 1 Kb DNA ladder (New England Biolabs) was routinely used to determine size of DNA fragments. DNA fragments were visualised using a UV transilluminator AlphaImager (Alpha Innotech).

2.3.4 Generation of competent bacterial cells

A single colony of either Xl-10 (Stratagene) or C41 strains (Miroux and Walker 1996) were grown overnight in 5 mls LB at 37°C with 180 RPM. The following day 5 ml cultures were inoculated into 100 mls LB, which were grown at 37 °C, 180 RPM until the A_{550} of the culture reached 0.48. Cells were then chilled on ice for 5 minutes and centrifuged in a prechilled (4 °C) centrifuge for 5 minutes at 3660 RPM. The supernatant was removed and resuspended in 40 mls of ice cold TfbI (30 mM KAc, 10 mM $CaCl_2$, 50 mM $MnCl_2$, 100 mM KCl, Glycerol 15%, pH 5.8 with 0.2 M acetic acid), chilled on ice for 5 minutes and centrifuged as above. Cells were then resuspended in 4 ml ice-cold TfbII (10 mM MOPs, 10 mM KCl, 10 mM $CaCl_2$, Glycerol 15%, pH to 6.5 with 3 M KOH) and chilled on ice for 15 minutes. Finally cells were aliquoted into cryotubes and stored at -80°C.

2.3.5 Bacterial transformation

1-5 µl of DNA was added to a sterile eppendorf tube, to which 50 µl of either Xl-10 or C41 competent cells were added. The mixture was incubated on ice for 15 minutes, after which cells were heat shocked in a water bath for 45 seconds at 42 °C. 1 ml of LB was then added, and cells were incubated for 1 hour at 37°C with 180 RPM. 100 µl was then plated onto LB agar plates containing the appropriate antibiotic selection, which was incubated overnight at 37 °C.

2.3.6 Plasmid extraction from bacterial culture

Plasmids were extracted from 4 ml overnight *E. coli* LB culture (supplemented with the appropriate antibiotic) with the commercial kit NucleoSpin Plasmid (Macherey-Negen, Germany) according to the manufacturer's instructions.

2.3.7 Plasmids

Full details of the plamids used in this study are summarised in the respective chapters.

2.3.8 Sequencing

Where specified, plasmids were validated by sequencing with the Sanger's method using a 3730 capillary electrophoresis sequencer (Applied Biosystems, Cheshire) at the DNA Core Laboratory, Medical Research Council, Imperial College London. For each reaction, the mix was comprised of

200-400 ng of the plasmid DNA, 2 µl of the primer (20 µM) in a final volume of 10 µl. Sequencing primers were designed for maximal coverage of the region of interest. Sequences were analysed in Chromas (Technelysium Pty Ltd).

2.3.9 DNA Cloning Techniques

DNA polymerase I, Large (Klenow) Fragment (New England Biolabs, UK) was used to blunt end DNA fragments. A maximum of 3 µg of DNA, in a total volume of 40 µl or less, was mixed with 3.5 µl enzyme, 3.3 µl dNTPs (100 µM), 10 µl NEB Buffer 3 and made up to 100 µl total volume using sterile distilled water. Reactions were incubated for 30 minutes at 37 °C. DNA was purified from the reaction mixture using QIAquick PCR purification Kit (Qiagen, UK).

KAPATaq (KAPABiosystems, UK) was used for A-tailing DNA fragments. 7 µl PCR product was mixed with 1 µl dATP (2 mM, in KAPATaq Buffer A), 1 µl sterile distilled water and 1 µl enzyme. Reactions were incubated for 30 minutes at 70 °C. DNA was purified from the reaction mixture using QIAquick PCR purification Kit (Qiagen, UK).

For vector dephosphorlyation, 30 µl of vector from a miniprep extraction was mixed with 5 µl NEB buffer 3, 12 µl sterile distilled water and 3 µl Calf Intestinal Phosphatase (CIP) enzyme. Reactions were incubated at 37°C for a minimum of 4 hours. DNA was purified from the reaction mixture using QIAquick PCR purification Kit (Qiagen, UK).

Ligations were conducted using T4 DNA ligase (New Engloand Biolabs, UK) with vector:insert ratios of 1:3, 1:1 or 3:1. Appropriate volumes of vector and insert were mixed, and 2 µl ligase buffer, 2 µl enzyme and 2 µl PEG4000 were added. Reactions were made up to 20 µl total volume with sterile distilled water and incubated overnight at 16 °C. 5 µl of ligation mixture was transformed into competent *E. coli.*

Restriction enzyme digestion of DNA was conducted using enzymes from New England Biolabs according to manfacturer's guidlines. When required bovine serum albumin (BSA) was added to the reaction at the final concentration of 100 µg/ml. DNA was purified from the reaction mixture using QIAquick PCR purification Kit (Qiagen, UK).

2.3.10 Southern blotting

20 µg *A. fumigatus* gDNA was digested overnight with the appropriate volume of restriction enzyme and digestion reactions were separated on a 1% (w/v) agarose gel. The gel was stained for 30 minutes in 150 ml TBE containing 30 µl of SYBR Safe DNA Gel stain (Invitrogen),

photographed and then depurinated (250 mM HCl), denatured (0.5 M NaOH, 1.5 M NaCl), neutralised (0.5 M Tris-HCl, pH 7.5, 1.5 M NaCl) and equilibrated in 20 x SSC (3 M NaCl, 300 mM sodium citrate, pH 7). The gel was blotted overnight onto a postive nylon membrane (Roche, UK) after which the DNA was fixed to the membrane using the automatic crosslink function on a Stratagene UV Stratalinker 1800. DIG Easy Hyb solution (Roche, UK) was pre-warmed to the probe hybridisation temperature (50 °C) and the membrane prehybridised in DIG Easy Hyb for 1 hour with gentle agitation. DNA probes were amplified from a suitable template using the PCR DIG Probe synthesis kit (Roche, UK) using the manufacture's guidelines. 50 ng of probe was denatured for 10 minutes at 100 °C for 5 minutes in a volume of 25 µl, which was then added to 10 ml prewarmed DIG Easy Hyb solution. The membrane was incubated overnight at 50 °C with continual agitation. The membrane was incubated with low stringency wash buffer (2 x SSC, 0.1% (w/v) SDS) at room temperature, followed by high stringency wash buffer (0.5 x SSC, 0.1% (w/v) SDS) at 65 °C and washed (0.1 M Malic acid, 0.15 M NaCl (pH 7.5), 0.3% (v/v) Tween 20). The membrane was blocked (1% (w/v) blocking solution (Roche, UK) in 0.1 M Malic acid, 0.15 M NaCl, pH 7.5) for 2 hours at room temperatue. The antibody (Anti-Digoxigenin-AP Fab fragments, Roche) was centrifuged at maximum speed for 5 minutes and used at a dilution of 1 in 10000 in 30 ml blocking solution for 30 minutes with gentle agitation. The membrane was then washed in wash buffer and incubated with detection buffer (0.1 M Tris-HCl, 0.1 M NaCl, pH 9.5 for 5 minutes. CPD-Star (Roche, UK) was added to the membrane and incubated at room temperature for 5 minutes. Finally, the membrane was exposed onto Hyper film (Kodax).

2.3.11 SDS-PAGE

Protein samples were run on 10 or 12% SDS-PAGE. For protein visualization, gels were stained in Coomassie stain (0.1% Coomassie Blue R-250, 45% methanol, 10% acetic acid) for an hour, before been left in Coomassie de-stain (10% methanol, 10% acetic acid) overnight.

2.3.12 Western blotting

For Western blotting, gels were transferred to PVDF membrane (Amersham) in transfer buffer (25mM Tris base, 192 mM glycine, 20% methanol) as per manufacturer's instructions using Invitrogen's XCell-SureLock Mini Cell XII Blot module. Membranes were blocked for an hour in 5% (w/v) milk in PBS-Tween (0.001% Tween-20, 137 mM NaCl, 1.47 mM KH_2PO_4, 2.68 mM KCl, 8.1 mM Na_2HPO_4.12H2O) before being incubated with primary antibody diluted in 5% w/v milk for an hour. Membranes were washed 3 x 10 mins with PBS-Tween and incubated in the secondary

antibody for an hour and washed 3 x 10 mins with PBS-Tween. Membranes were developed using ECL solution 1 (12.5 mM luminol/3-aminophthalhydrazide in DMSO, 19.8 mM coumaric acid in DMSO, 5 mM Tris-HCl, pH8.5) and ECL solution 2 (5 mM Tris-HCl, pH8.5, 0.064% (v/v) H_2O_2) in a 1:1 ratio and exposed onto Hyper film (Kodax). During all incubations and washings the membrane was agitated continuously using a rocker.

2.3.13 Reverse transcriptase quantitative PCR (RT-qPCR)

4 µg of RNA was treated using DNase I to remove contaminating gDNA (New England Biolabs, UK). RNA was reverse transcribed into cDNA using manufacture's guidelines from Superscript III™ First Strand cDNA Synthesis kit (Invitrogen): 500 ng DNase treated RNA was incubated with 1 µl oligo$(dT)_{20}$ primers (50 µM), 1 µl dNTPs (10 µM) and the reaction mixture was made up to 10 µl using DEPC treated water. The sample was incubated at 65 °C for 5 minutes, chilled on ice for 1 minute and 10 µl of cDNA synthesis mix was added (2 µl RT Buffer, 2 µl 25 mM $MgCl_2$, 2 µl 0.1 M DTT, 1 µl RNaseOUT™, 1 µl SuperScript III™ reverse transcriptase). The 20 µl sample was then incubated for 10 minutes at 25 °C, 50 minutes at 50 °C and 15 minutes for 85 °C. 1 µl of RNaseH was added and the sample was incubated for 30 minutes at 37 °C. cDNA quality was checked using the Nanodrop ND-1000 spectrophotometer.

Rt-qPCR was performed in triplicate using Sybr Green Jumpstart™Taq ReadyMix™ (Sigma-Aldrich, UK). 5 µl of cDNA was mixed with 1 µl of each primer (10 µM), 10 µl of Sybr Green Jumpstart™Taq ReadyMix™, and 3 µl sterilised distilled water. RT-qPCR was conducted in a Rotor-Gene RG-3000 PCR cycler (Corbett Research, UK) with the following cycling parameters: 95 °C for 5 seconds, 58 °C for 5 seconds, 72 °C for 15 seconds, 78 °C for 5 seconds, which was repeated 40 times. Data were then analysed using the RotorGene 6 software, from which the amplification threshold was manually assigned to generate Ct values. Ct values were normalised as described in the respective chapters.

2.4.0 *A. fumigatus* techniques

2.4.1 Transformation of *A. fumigatus* electrocompetent spores

For preparation of electrocompetent spores, *A. fumigatus* Ku80 or CEA10 strains were grown on solid ACM for 5 days, harvested in sterile H_2O and filtered through Miracloth (Calbiochem). Spores were centrifuged for 10 minutes at 4000 g, washed 5 times with sterile H_2O and enumerated on a haemocytometer. 250 mls YG broth (0.5% Yeast Extract, 2% Glucose) was inoculated with 5 x 10^9

spores and grown at 37°C for 2 - 4 hours until the spores had swollen. Spores were then centrifuged for 10 minutes at 4000 g, washed in cold water, and resuspended in 20 mls YED (1% Yeast Extract, 1% Glucose, 20 mM Hepes, pH 8 with NaOH). Spores were incubated at 30°C for 1 hour, and then resuspended in ice cold EB (10 mM Tris HCl pH 7.5, 270 mM Sucrose, 1 mM LiAc). 2 µg of DNA containing the transformation cassette was resuspended in 10 µl dH_2O and mixed with 50 µl of electrocompetent spores. The transformation mixture was pulsed with the following parameters: 1 Kv, 400 Ohms, 25 F. Following electroporation, 1 mls of cold YED was added, cooled on ice for 15 minutes and then incubated for 1.5 hours at 30°C. The mixture was plated onto AMM, left overnight at room temperature and then overlayed with AMM containing the drug selection. Finally plates were left for 48 hours at 4 °C before being incubated at 37 °C.
Transformants were subcultured on AMM supplemented with the appropriate selection and grown for 5 days. Transformants were analysed using the techniques specified in each respective chapter.

2.4.2 Transformation of *A. fumigatus* protoplasts

Protoplast transformation was based on the protocol described by Szewczyk and co-workers (Szewczyk et al. 2006). *A. fumigatus* was grown for 5 days on ACM plates. Spores were harvested in sterile water, filtered twice through Miracloth (Calbiochem) and washed twice with sterile water. 1 x 10^8 spores were inoculated into 20 mls ACM broth and grown for 16 hours at 30 °C with 150 rpm. Hyphae were isolated by filtration through Miracloth and rinsed with ACM broth. Hyphae were resuspended in 8 mls ACM, to which 8 mls of protoplasting solution (KCl, 12.8% Vineflow, Novo Nordisk) was added. Protoplasting was microscopically monitored, and the solution was incubated for 3 - 4 hours at 30 °C with 100 rpm. To remove undigested hyphal material, the protoplasting solution was layered onto 30 mls 1.2 M sucrose and centrifuged at 2000*g*. Protoplasts were collected at the top of the sucrose cushion and gently resuspended in 0.6 M KCl and centrifuged at 2000*g.* The pellet was washed three times in 0.6 M KCl, once in KCl 0.6 M, 50 mM $CaCl_2$, and resuspended in a volume of KCl 0.6 M, 50 mM $CaCl_2$ appropriate for transformation.
2 - 5 µg of DNA containing the selection cassette containing the gene of interest was mixed with 100 µl of protoplasts. The solution was mixed by vortexing and 50 µl PEG solution was added. The mixture was incubated in an ice water bath for 25 minutes, after which 1 ml of PEG was added and the sample was left at room temperature for an additional 25 minutes. 150 µl of protoplast/DNA solution was added to 10 mls AMM media containing 10 ul of pyrithiamine (0.5 mg/ml), which was overlayed onto a plate containing 15 mls of AMM with 15 ul pyrithiamine (0.5 mg/ml). Plates were incubated at room temperature for 24 hours and then incubated at 37°C for

72 – 144 hours. Transformants were subcultured on AMM supplemented with the appropriate selection and grown for 5 days. Transformants were analysed using techniques specified in each respective chapter.

2.4.3 Extraction of *A. fumigatus* DNA from spores

Spores were picked using a loop and added to 200 µl breaking buffer (2% Triton X-100, 1% SDS, 100 mM NaCl, 10 mM Tris-HCl pH 8.0, 1 mM EDTA pH 8.0). 300 mg of glass beads (0.4-0.6mm diameter, Sartorius UK) were added and incubated for 30 minutes at 70 °C, with vortexing every 10 minutes. 200 µl chloroform:isoamylalcohol 25:24:1 was added and further vortexed for 5 minutes, before being spun for 8 minutes at max speed. The supernatant was precipitated with equal volume of isopropanol and incubated overnight at 4 °C. Following centrifugation at 13000 rpm for 10 minutes the pellet was washed in 70% (v/v) ethanol and air-dried before resuspension in 20 µl TE containing RNace-It™ ribonuclease cocktail (Stratagene). 2 µl of DNA solution was used in PCR reactions unless otherwise stated.

2.4.4 Extraction of *A. fumigatus* DNA from mycelia

For large scale gDNA preparations, gDNA was extracted from *A. fumigatus* mycelia. 5 x 10^6 *A. fumigatus* spores were inoculated into 60 mls ACM and grown overnight at 37°C with 150 RPM. Mycelia were harvested through Miracloth (Calbiochem), washed twice with sterile water, pat dried and snap frozen in liquid nitrogen. 250 mg of mycelia was grinded in liquid nitrogen using a pestle and mortar, to which 750 µl of Aspergillus extraction buffer was added (300 mM Tris-HCl, 375 mM NaCl, 37.5 mM EDTA, 2% (v/v) sarkosyl). 750 µl of phenolcholoroform: isoamylalcohol 24:1 (Sigma) was added and samples mixed on a tube rotator for 15 minutes at 4 °C. Samples were then centrifuged at 13000 RPM for 1 hour, and the supernatant mixed with 400 µl chloroform. The samples were shaken for 30 seconds, incubated on ice for 5 minutes and centrifuged at 13000 RPM for 15 minutes at 4 °C. The supernatant was then removed, mixed with 400 µl chloroform, shaken for 30 seconds, incubated on ice for 5 minutes and centrifuged at 13000 RPM for 15 minutes at 4 °C. The supernatant was then mixed with an equal volume of isopropanol and precipitated at 4 °C for 4 hours. The sample was then centrifuged at 13000 RPM for 15 minutes and the pellet was washed in 70% ethanol and air-dried. The pellet was resuspended in 100 µl TE to which 2 µl of RNace-It ribonuclease cocktail (Stratagene) was added and the samples were incubated at 37°C for 1 hour. Finally, the DNA was stored at -20 °C.

2.4.5 Protein extraction from *A. fumigatus* mycelia

5 x 10^6 *A. fumigatus* spores were inoculated into 60 mls ACM and grown for the specific time at 37°C with 150 RPM. 250 mg of frozen mycelia was added to a 2 ml Eppendorf tube containing a metal bead and 1 ml of buffer A50 (25mM HEPES pH 7.5, 50 mM KCl, 5mM $MgCl_2$, 0.1mM EDTA, 0.5 mM DTT, 1mM PeFa-Bloc, 1 μM Pepstatin, 0.6 μM Leupeptin, 10% glycerol $^{v}/_{v}$). Mycelial samples were homogenised in a Fast Prep-24 (MP Biomedicals, United Kingdom) using 6 x 10 second bursts at power setting number 4. Homogenised mycelia were mixed on a tube rotator for 90 minutes at 4 °C. Samples were then centrifuged at 13000 rpm for 30 minutes at 4 °C, after which the supernatant was isolated and stored at -80 °C. Protein concentrations were measured using BCA assay (Thermo Scientific, UK).

2.4.6 Protein extraction from *A. fumigatus* supernatant

Mycelia were separated from 50 mls liquid media of 16, 24, 36 and 48 hour cultures by filtration through Miracloth (Calbiochem). 3 volumes of ice cold acetone was added and proteins were precipitated over night at - 20°C. Proteins were isolated by centrifugation at 13,000 rpm for 20 minutes at 4°C and resuspended in PBS. Protein concentrations were measured using BCA assay (Thermo Scientific, UK).

2.4.7 RNA extraction from *A. fumigatus* mycelia

5 x 10^6 *A. fumigatus* spores were inoculated into 60 mls ACM and grown for the specific time at 37°C with 150 RPM. Mycelia were isolated from liquid culture by filtration through miracloth (Calbiochem), rinsed with sterile water and snap frozen in liquid nitrogen. Frozen mycelia were ground using a pestle and mortar in liquid nitrogen. RNA was extracted from ground mycelia using RNeasy kit (Qiagen, UK) following the manufacturer's guidelines.

2.4.8 *A. fumigatus* phenotypic test

A. fumigatus conidia were harvested in sterile distilled water and filtered through Miracloth (Calbiochem). Spores were counted using a haemocytometer and resuspended at a concentration of 2 x 10^6 cfu/ml in sterile distilled water prior to serial dilutions of 1 x 10^4, 1 x 10^3, 1 x 10^2, 1 x 10^1 spores. Each serial dilution was spotted onto AMM plates 3 times containing the appropriate chemical. Spots were allowed to air dry and then incubated for 2 days at 37°C.

2.4.9 *A. fumigatus* germination assay

A. fumigatus conidia were harvested in sterile distilled water and filtered through Miracloth (Calbiochem). Spores were counted using a haemocytometer and 60 mls of AMM was inoculated with 5 x 10^6 spores and incubated at 37°C with 150 RPM. Germination rates were microscopically monitored using a Nikon Eclipse 80i microscope and a haemocytometer. Germination was measured as the percentage of spores which had germinated from total counted.

2.4.10 *A. fumigatus* growth assay

A. fumigatus conidia were harvested in sterile distilled water and filtered through Miracloth (Calbiochem). Spores were counted using a haemocytometer and 60 mls AMM was inoculated with 5 x 10^6 spores and incubated at 37°C with 150 RPM. Mycelial were harvested by filtration through Miracloth (Calbiochem) at specified time-points, pat dried and incubated in a Whatman Paper (VWR, UK) envelope at 37°C for 1 week, after which mycelial dry weight was calculated.

2.4.11 *A. fumigatus* oxidative stress assay

A. fumigatus conidia were harvested in sterile distilled water and filtered through Miracloth (Calbiochem). Spores were counted using a haemocytometer and resuspended at 5 x 10^5 spores/ml in AMM containing 0.0 M, 0.05 M, 0.1 M, 0.2 M and 0.4 M hydrogen peroxide. Spores were incubated for 30 minutes, followed by 1:50 dilution in sterile water and duplicate plating. Colony forming units (CFUs) were enumerated and surviving colonies reported as a percentage value of the CFUs counted from the 0.0 M hydrogen peroxide control.

2.5.0 Murine Infections

2.5.1 Survival analysis

Murine infections were performed under UK Home Office Project Licence PPL/70/6487 in Central Biomedical Services centre, Imperial College London. Outbred male mice (strain CD1, 18 – 22 g, Harlan Ortech) were housed in individually vented cages. Two immunosuppressive regimes were used. For a neutropenic model, mice received cyclophosphamide (150 mg/kg, Endoxana, Asta Medica) by intraperitoneal injection on days -3 and -1, +2 and then every third day. A single dose

of hydrocortisone acetate (112.5 mg/kg, Hydrocortistab, Sovereign Medical) was administered on day -1. For the hydrocortisone treated model, mice received subcutaneous doses of hydrocortisone acetate (112.5 mg/kg, Hydrocortistab, Sovereign Medical) on days -3, -1, +2 and then every third day. *A. fumigatus* spores were grown on ACM, supplemented with 1% (w/v) glucose and 5 mM ammonium tartrate, for 5 days prior to infection. Spores were harvested on the day of infection, using sterile saline (Baxter Healthcare Ltd, UK), and filtered through MIRACLOTH. Conidial suspensions were centrifuged for 10 minutes at 5000 rpm, washed twice with sterile saline, counted using a haemocytometer and resuspended at a concentration of 1.25 x 10^7 or 1.75 x 10^8 cfu/ml for neutropenic and hydrocortisone models respectively. Mice were anesthetized by halothane inhalation and infected by intranasal instillation of 5 x 10^5 or 7 x 10^6 conidia in 40 µl of saline for neutropenic and hydrocortisone models respectively. Viable counts from administered inocula were determined following serial dilution by plating on ACM and growth at 37 °C. Mice were weighed every 24 hours from Day -3 and visual inspections made twice daily. The end point for survival experimentation was a 20% reduction in body weight measured from the day of infection, at which point mice were culled.

2.5.2 Histopathology

Mice for histology were culled by neck dislocation at designated time points following infection. Whole lungs were extracted and fixed in 4% v/v formaldehyde (Sigma-Aldrich). Lungs were embedded in paraffin prior to sectioning and stained with hemotoxylin and eosin (H&E) or Grocott's Methenamine Silver (GMS). Slides were visualised using a Nikon Eclipse 80i microscope and photographed without magnification using a Nikon Coolpix 990 digital camera.

2.5.3 qPCR assay for measurement of fungal burden in murine lungs

In order to assess fungal burden as a quantitative virulence criterion, quantitative PCR (qPCR) was performed on total genomic DNA extracted from homogenized whole lungs. Mice were treated identically as for survival analyses, but the *A. fumigatus* spore inoculum concentration was reduced to 7.5 x 10^5 or 2 x 10^7 cfu/ml for neutropenic and corticosteroid cohorts respectively. For neutropenic and hydrocortisone acetate treated mice, lungs were extracted from mice culled on day + 4 or day + 5 respectively. Lungs were weighed, and 1 volume of sterile saline was added. Lungs were homogenised using an X120 electric tissue homogeniser (Bennett Scientific Limited) and 250 µl of homogenate was added to 180 µl of buffer ATL (Qiagen) and DNA extracted using DNeasy Blood and Tissue Kit (Qiagen). Fungal burden was assessed by quantitative PCR

amplification using the oligonucleotides BT-F (GAGCCCTTTTCCGACCTGAT) and BT-R (GGAACTCCTCCCGGATCTTG) to amplify the beta tubulin (Afu7g00250) locus from the *A. fumigatus* genome, and the oligonucleotides Actin-F (CGAGCACAGCTTCTTTGCAG) and Actin-R (CCCATGGTGTCCGTTCTGA) to amplify the murine actin locus (NM_007393). Quantification of both gene targets was performed in triplicate qPCR reactions. qPCR was performed using Sybr Green Jumpstart™Taq ReadyMix™ (Sigma-Aldrich, UK). 5 µl of gDNA extracted from murine lung was used as a template in 20 µl qPCR reactions. qPCR was conducted in a Rotor-Gene RG-3000 PCR cycler (Corbett Research, UK) with the following cycling parameters: 95 °C for 5 seconds, 58 °C for 5 seconds, 72 °C for 15 seconds, 78 °C for 5 seconds, which was repeated 40 times. Data were then analysed using the RotorGene 6 software, from which the amplification threshold was manually assigned to generate Ct values. A modified mathematical model (incorporating adjustment for fungal inoculum) for relative quantification of *A. fumigatus* actin, and murine beta-tubulin was adopted for each mouse sample using the formula RATIO = $(E_{target})^{\Delta Ct(\text{fungal actin} - \text{murine tubulin})}$ where *E*= efficiency of amplification of target gene and is equal to 1.88, based on efficiency calculations using the Ct slope method (Schmittgen and Livak 2008). RATIO values were $\log_{10}$ transformed and corrected for inoculum size, and reciprocal values were plotted ($1/\log_{10} RATIO_C$). The statistical significance of variances between fungal burdens was calculated using a nonparametric Mann-Whitney t-test. Genomic DNA, isolated from animals infected with an attenuated *A. fumigatus* p-amino benzoic acid auxotroph, Δ*pabaA* was used as a positive control for attenuation (Brown et al 2000).

2.5.4 Murine infections for Microarray Experiments

Mice were immunosuppressed accordingly to the neutropenic model of infection, i.e intraperitoneal injections of cyclophosphamide (150 mg/kg) on days –3 and –1 and by a single subcutaneous dose of hydrocortisone acetate (112.5 mg/kg) on day –1 (Schrettl et al. 2004). Immunocompetent control mice for host transcriptional profiling were housed in identical conditions but were not subjected to injections. *A. fumigatus* spores were harvested as for survival analyses, and resuspended at a concentration of $2.5x10^9$ spores/ml. Mice were anaesthetised by isofluorane inhalation and infected by intranasal instillation of $1x10^8$ conidia in 40 µl of saline solution. Non infected control mice for host transcriptional profiling were anaesthetised as above and inoculated with 40 µl sterile saline. The determination of viable counts for the administered inocula was performed as for the survival analyses. For the transcriptional time course comparison between Af293 and the Af293 Δ*laeA* mutant, groups of 7 mice were culled at 4, 8 and 14 hours post infection by neck dislocation. Bronchoalveolar lavage (BAL) was performed using 3-4 aliquots of 37° sterile saline per mouse. BAL fluids (BALFs) were snap frozen in liquid nitrogen. Mice were

processed sequentially to ensure that the maximum time lapse between neck dislocation and BALF snap freezing was 3 minutes. Designated mice (n = 2) were used for Af293 Δ*laeA* histological analyses at each time point. Mice were culled and lungs fixed as described above

For host transcriptional profiling, groups of 7 mice were infected with Af293 and Af293 Δ*laeA* strains in both neutropenic and immunocompetent models of infection as described above. BALFs were extracted at 14 hours post infection. Crude host response BALF samples were stored at -80° and sent for analyses at the JCVI on dry ice.

2.6.0 Microarray techniques

2.6.1 *A. fumigatus* RNA Extraction, amplification and hybridisation

BALF samples were centrifuged at 14,000 rpm for 5 minutes and the pellet was washed with 500 µl ice cold water to lyse host cells. BALFs were pooled, resuspended in 450 µl ME-RLC buffer (Qiagen) and ground in liquid nitrogen with a pestle and mortar. RNA was then extracted using RNeasy® Kit (QIAGEN). The quality of RNA used for microarray analysis was checked by Nanodrop ND-1000 Spectrophotometer (Nanodrop, Wilmington, USA). RNA with an A260/280 and an A260/230 ratio > 1.9 was used for the experiments. RNA samples were doubly amplified prior to labelling with Cy3 or Cy5 fluorescent dye at the J. Craig Venter Institute (JCVI, Rockville, Maryland, USA, as described previously (McDonagh 2008). Protocols for direct labelling and hybridisation of cDNA probes can be found on the JCVI website (http://pfgrc.jcvi.org/index.php/microarray/protocols.html).

2.6.2 *A. fumigatus* microarray data capture

Fungal RNA was doubly amplified from BALFs (McDonagh et al. 2008) prior to array hybridisation. Washed slides were scanned and data captured using GenePix 4000b (Axon Instruments, Foster City, CA) semiconfocal microarray scanner and associated GenePix Pro 3.0 software. Scans were performed at a pixel size of 10 µm with 2 lines average. Overall red to green channel intensities were balanced as near as possible to a ratio of 1:1 by altering photo-mutiplier tube (PMT) gains. Images were saved as .TIF files and TIGR Spotfinder (Saeed et al, 2003) was used to quantitate fluorescent intensities. Poor quality spots were identified manually and flagged. After Spotfinder analysis, results were exported as TIGR software compatible MEV files following local background subtraction.

2.6.3 Ratiometric microarray normalisation

MEV files were loaded into the JCVI MIDAS normalisation programme where they were normalised by block locally-weighted scatter plot smoothing (LOWESS). After LOWESS, the flip-dye pairs were combined a consistency check was applied to remove any spots that do not fall within a specified deviation of the array-wide average log2 ratio of the fluorescence values for spot on both slides. Following the flip-dye consistency check values underwent inter-slide standard deviation regularisation by averaging the values of the replicate spots for each gene. MIDAS output files were loaded into Genespring 11.0 software package (Agilent) and intensity values were averaged at each time point. All subsequent statistical testing and data analysis were performed in Genespring 11.0.

2.6.4 Non-ratiometric microarray normalisation

A separate channel intensity approach was applied to the dual colour microarrays in order to extract strain specific intensity values throughout the time-course (t'Hoen et al. 2004, Bossers et al. 2010a). From MEV files (n = 18) intensity channels (n = 36) were separated and grouped into strain and stage specific channel cohorts (n = 6). Triplicate oligonucleotide spots for each gene were averaged to give a single spot intensity value (aSI) for each gene per channel. Quantile normalisation (Bolstad et al 2002) was applied to aSI values within stage and strain cohorts using a custom script in the R programming language. A second quantile normalisation was applied across aSI values from every array. Following quantile normalisation, data was $\log_2$ transformed, to give aSI*norm* values. For each gene, aSI*norm* were averaged within the strain and time specific channel cohorts, producing a single normalised intensity value (nSI) per gene for either Af293 or Δ*laeA* at each stage. Genes were filtered based on two quality control criteria. Genes with < 3 aSI values were removed. Secondly, genes for which aSI*norm* values varied more than a standard deviation of 1.5 were filtered. Only genes with nSI values at all three time points were considered in the final Af293 or Δ*laeA* datasets.

To determine temporal gene expression profiles throughout the time-course of infection, nSI ratios were calculated between stages. Differentially expressed transcripts were defined according to distribution within the nSI ratio dataset, with upper and lower quartiles considered increased and decreased respectively. In order to distinguish magnitude of transcriptional change between time-points, increased and decreased gene sets were subdivided into thirds, and the upper, intermediate and lower genes defined as high, moderate, and low changes respectively. GO

enrichment of differentially expressed genes was performed using Genespring GX 11.02 (Aligent). Clustering was performed using the STEM program (Short Time-series Expression Miner) designed for short time-series microarray experiments (Ernst and Bar-Joseph 2006).

2.6.5 *Mus musculus* host RNA qRT-PCR Super Array analyses

Groups of 7 mice from immunocompetent or neutropenic models were infected with 1 x 10^8 spores from either Af293 Δ*laeA*, the parental isolate or a sterile saline control. Mice were culled 14 hours post infection and BALFs extracted as described above. Samples were sent on dry ice to our collaborators at the JCVI where groups of BALFs were pooled and RNA extracted using TRIzol (Invitrogen). DNA was removed using Turbo DNase (Ambion) before a final TRIzol purification. Poly A RNA was doubly amplified by Message Amp II aRNA amplification kit (Ambion). cDNA was synthesized using RT² First Strand Kit (SABiosciences) and analysed by QRT-PCR (RotorGene) with Mouse Innate and Adaptive Immune Responses RT² Profiler™ PCR array, Mouse Inflammatory Response and Autoimmunity RT² Profiler™ PCR array and a custom array featuring a further 45 genes of *M. musculus* innate immunity (SABiosciences). Data were loaded into SABiosciences analysis portal with each array treated as a separate experiment (http://pcrdataanalysis.sabiosciences.com/pcr/arrayanalysis.php). Experimental design and normalisation measures are discussed in the results section.

CT values for genes of interest (GOI) were normalised to the most transcriptionally stable housekeeping gene (HKG) across the 6 murine cohorts by calculating ΔCt values (Ct(GOI) - Ct(HKG)). Hypoxanthine guanine phosphoribosyl transferase 1 (Mm.299381) was used for the Mouse Innate and Adaptive Immune Responses RT² Profiler™ PCR array and Mouse Inflammatory Response and Autoimmunity RT² Profiler™ PCR array. For the custom array, the arithmetic mean of glyceraldehyde-3-phosphate dehydrogenase (Mm.343110) and beta actin (Mm.343110) was used.

To facilitate comparisons of gene expression across the infection cohorts and two immunosuppressive regimes, the immunocompetent saline infected mice were used as a common reference sample and fold regulation was calculated relative to this group. Genes where CT values were undetected in either the control or test group were removed. Additionally, genes where values in both samples were greater than the linear limit of the manufacturer's recommended RT-PCR quantification threshold were considered erroneous and omitted. Finally, genes where a CT value in either the control or test sample was greater than the linear limit were

retained, following the adjustment of the non-linear value to the linear detection threshold (i.e. a CT of 35).

Fold changes (2^(-ΔΔCt)) were determined for every gene in each test cohort relative to the common reference, where 2^(-ΔΔCt) is the normalized gene expression (2^(- ΔCt)) in the test sample divided by the normalized gene expression (2^(- ΔCt)) in the control. Fold changes were converted to fold regulation, where for positive values fold-regulation equals fold-change, and for negative values fold-regulation equals the negative inverse of the fold-change.

Values were exported as an Excel file, where fold changes were $\log_2$ transformed to reduce variations in sample standard deviation and allow comprehensive cut offs between cohorts. These values were considered the final datasets for each qRT-PCR array experiment. Log_2 converted fold changes were compared between groups and gene expression was considered different when a 3 fold or greater difference was observed. Genes represented on duplicate or triplicate arrays had to pass the fold cut off in every replicate or they were omitted. Fold change values of replicates that passed filtering were averaged. A full list of genes represented on each array is available in supplementary materials.

2.7.0 SELDI-ToF-MS Techniques

2.7.1 Immobilisation of anti-his antibody and antigen on PG20 chips

The PG20 chip contains 8 spots to which protein G is covalently bound. Consequently, most antibodies capable of binding protein G can be used with PG20 chips. The anti-his antibody (GE Healthcare, UK) used in this study is an IgG2a monoclonal antibody, which has high binding affinity to protein G (ProteinChip® Antibody Capture Kit Instruction Manual). ProteinChip® Antibody Capture Kit (Biorad, USA) was used to immobilise the anti-his antibody to the PG20 array surface following the manufacture's guidelines. 2 µl of 0.2 mg/ml anti-his antibody was added to spots on the chip and incubated in a humidity chamber overnight at 4 ºC. The chip was washed once in 8 mls wash buffer (0.5% Triton X-100 in PBS) for 10 minutes, and twice in 8 mls PBS for a total of 10 minutes. The array was air dried for 5 minutes. To cross-link the anti-his antibody to Protein G, 1 µl of cross linking reagent (Bissulfosuccinimidyl suberate, 0.5 mg/ml) was added to each spot and the chip was incubated in a humidity chamber at room temperature for 30 minutes. 1 µl of deactivation buffer (0.5 M ethanolamine in PBS, pH 8.0) was added to each spot, which was incubated on a rocker for 15 minutes at room temperature. The chip was then

incubated for 10 minutes in wash buffer and twice in PBS for a total of 10 minutes. For antigen capture, 2 µl of the sample was added a spot on the array, which was incubated for one hour (Increased to 3 hours for murine BALFs) at room temperature. The array was washed once with wash buffer for 10 minutes, twice with PBS for a total of 10 minutes, and briefly rinsed twice with 1 mM HEPES. The array was then air dried for 10 minutes. 0.5 µl of energy absorbing molecules (Sinapinic acid, 5 mg/ml) was added to each spot and left to air dry. This was repeated once, and the PG20 arrays were then read using ProteinChip SELDI reader.

2.7.2 Surface enhanced laser desorption/ionisation time of flight mass spectrometry

All Time-of-flight spectra were generated using a PBS II ProteinChip SELDI Reader (Ciphergen, USA) at laser intensities of 230 or 260, with a high mass of 200 kDa and detector sensitivity 9. Each spot on the array was analysed from position 20 to 80. Every protein array included a universal control sample (100 ng his-tagged recombinant bacterial protein). The PBS II ProteinChip SELDI Reader was routinely calibrated prior to sample detection using ProteinChip All-in-One Protein Standard II (Biorad), which contains 7 protein standards of various molecular mass (Table 2.1). For calibration, mass range of the protein standards was split into high and low ranges, and spectral peaks were aligned with < 0.3% deviation from the molecular mass of the protein standards (Table 2.1).

Protein standard	Molecular mass, Da	Calibration group	Maximum/ minimum calibration range, Da
Hirudin, recombinant	6964	Low mass	6984/ 6943
Cytochrome C (bovine)	12230	Low mass	12266/ 12193
Myoglobin (equine)	16951	Low mass	17001/ 16900
Carbonic anhydrase (bovine red blood cells)	29023	Low/ high mass	29110/ 28936
Enolase (*S. cerevisiae*)	46671	High mass	46811/ 46531
Albumin (bovine)	66433	High mass	66632/ 66234
IgG (bovine)	147300	High mass	147741/ 146859

Table 2.1: Calibration parameters for protein standards present in ProteinChip All-in-One Protein Standard II (Biorad).

Spectra were analysed using Ciphergen ProteinChip® Software. Individual spectra were baseline subtracted, from which peaks between 1 – 100 kDa with a signal-to-noise ratio above 3 were manually annotated.

2.8.0 Modified recombineering approach for generation of *A. fumigatus* gene disruption cassette

Lambda phage was prepared according to the method described previously (Maniatis 1982) with minor modifications. LE392λ bacteria (Chan et al. 2007) were inoculated in 10 mls LB supplemented with 12.5 ug/ml tetracycline and grown overnight at 32 °C, 180 rpm. The 10 ml culture was then inoculated to 200 mls LB, supplemented with 12.5 µg/ml tetracycline, and incubated at 32 °C with 180 rpm for approximately 2.5 hours until the OD was 1.2. Cultures were incubated at 42°C for 15 minutes with 180 rpm, and at 39 °C for 2 hours with 180 rpm. The 200 ml culture was split into 4 x 50 ml falcon tubes and centrifuged for 20 min. Pellets were dissolved in a total of 2 ml of TMG buffer (10 mM Tris-HCl pH 7.4, 10 mM MgCl2). 5 drops of chloroform were added, incubated for 15 min at room temperature and kept at 4 °C until use. For phage titration, LE392 (virus free isolate) were growth in LB overnight at 37°C. Cultures were then spun at 3000 rpm for 5 minutes. The supernatant was discarded and the pellet was resuspended in 10 ml of 10 mM $MgSO_4$. 5 serial dilutions (1:100) of the lambda phage were prepared in eppendorf tubes, each containing 500 µl of TMG buffer. 100 µl of each phage dilution was incubated in a water bath at 37°C for 15 minutes to remove chloroform. 100 µl of LE392-$MgSO_4$ were then added to each tube and incubated at room temperature for 15 minutes. 3 ml of 0.8% TYE agar was added to each tube, inverted fives and overlayed on 1.2% TYE plates. Plates were incubated overnight at 37°C. The following day, titration was calculated according to the formula: phage/ml = (number plaques/plate) x (1/ ml plated) x dilution factor.

2.8.1 Lambda phage infection of BAC clones

Appropriate BACs with sufficient coverage of the gene of interest were picked from a library of end-sequenced, indexed *A. fumigatus* BAC clones (Pain et al. 2004) and inoculated into 5 mls LB supplemented with 12.5 µg/ml chloramphenicol. Cultures were grown overnight at 37°C, 180 rpm. 1 ml of cells were centrifuged for 5 minutes at 5000 RPM, washed once with 10 mM $MgSO_4$ and resuspended in 100 µl 10 mM $MgSO_4$. 1 µl of lambda phage suspension containing over 1 million phage was added to the cells, which were incubated at 32 °C, 180 RPM for 20 minutes. 1 ml of LB

was added, and incubated for 1 hour at 32 °C, 180 RPM. 100 µl of infected cells were plated on LB supplemented with 12.5 µg/ml tetracycline and grown overnight at 32 °C.

2.8.2 Recombineering and chemical transformation of BACs gene-disruption biselectable marker

One colony was picked from infected cell plates and inoculated into 1 ml LB supplemented with 12.5 µg/ml chloramphenicol and tetracycline, which was grown overnight at 32 °C, 180 RPM. 25 µl, 35 µl, 45 µl and 55 µl volumes of overnight culture were resuspended in LB to a total volume of 1 ml and incubated for 2 hours at 32 °C, 180 RPM in 5 ml Universal tubes. Cells were transferred to 1.5 ml eppendorf tubes and incubated for 15 minutes at 42 °C in a water bath. Subsequently, samples were incubated for 2 minutes on ice, centrifuged at maximum speed for 3 minutes and washed with 1 ml 100 mM $MgCl_2$. Cells were then washed with 1 ml 100 mM $CaCl_2$ three times and resuspended in 50 µl 100 mM $CaCl_2$ containing 3 µg of the pyrT/zeocin PCR amplicon. Cells were heat shocked at 42 °C for 2 minutes and tubes were incubated on ice for 8 minutes, after which 1 ml LB was added and samples incubated for 1.5 hours. Samples were plated on LB supplemented with 25 µg/ml zeocin and grown overnight at 32 °C. Colonies were screened for chloramphenicol and zeocin resistance by overnight growth in LB supplemented with 12.5 µg/ml chloramphenicol and 25 µg/ml zeocin.

2.8.3 BAC extraction from bacterial culture

In order to extract BACs from cell culture, chloramphenicol and zeocin resistance clones were inoculated into 50 mls LB supplemented with 12.5 µg/ml chloramphenicol and grown for 18 hours at 30 °C, 150 RPM. Cultures were centrifuged and the pellet resuspended in 1 ml resuspension buffer (Qiagen). Cells were lysed using 500 µl lysis buffer (Qiagen) and the reaction neutralised using 750 µl neutralisation buffer (Qiagen). Reactions were spun on maximum speed for 30 minutes and the supernatant precipitated with an equal volume of isopropanol for 5 hours. Samples were then centrifuged at maximum speed for 10 minutes, washed once in 1 ml ethanol before being air dried and resuspended in 200 µl water. BACs were diluted 1:10 and 1 µl used as template in PCR reactions. For *A. fumigatus* transformation, 60 µl recombined BACs were digested overnight with the appropriate restriction enzyme in a total volume of 70 µl. Digests were heat inactivated before transformation.

Chapter 3

Time-point specific transcriptional profiling of *A. fumigatus* Af293 and Δ*laeA* mutant during the initiation of murine infection

3.1 Overview

The discovery (Butchko et al. 1999) and characterisation (Bok and Keller 2004) of the *A. nidulans* nuclear LaeA protein was a significant achievement with regard to understanding the regulatory mechanisms governing chemical diversity (Bok and Keller 2004, Bok et al. 2006a), reproduction (Bayram et al. 2008) and virulence (Bok et al. 2005, Sugui et al. 2007) of *Aspergillus* species. In the model organism *A. nidulans*, formation of transcriptionally silent heterochromatin is mediated by hypoacetylation of histones 3 and 4 by the histone deacetylase HdaA, which facilitates methylation by the H3K9 specific methylase ClrD and subsequent recruitment of the heterochromatin protein HepA (Reyes-Dominguez et al. 2010). LaeA reverses the formation of heterochromatin, most likely via methyltransferase activity, to activate multiple secondary metabolite loci (Reyes-Dominguez et al. 2010). HPLC analyses of LaeA deletants relative to wild-type isolates demonstrate reduced biosynthesis of multiple secondary metabolites in laboratory culture, including sterigmatocystin and gliotoxin in *A. nidulans* and *A. fumigatus* respectively (Bok et al. 2004, Bok et al. 2005). *In vitro* transcriptional profiling has supported the role of LaeA as a global regulator of secondary metabolite biosynthesis, with 13 out of 22 secondary metabolite clusters mis-expressed in a LaeA deletant strain (Perrin et al. 2007). In keeping with the hypothesis that melanising (Langfelder et al. 1998, Tsai et al. 1998), iron scavenging (Schrettl et al. 2007) and toxic (Bok et al. 2006b, Sugui et al. 2007a), secondary metabolites likely to improve survivorship in the natural niche are also critical for survival in the immunocompromised mammal, LaeA null strains are attenuated for virulence in neutropenic (Bok et al. 2005) and corticosteroid treated (Sugui et al. 2007b) murine models of infection.

In addition to the putative and well characterised roles of LaeA regulated secondary metabolites in virulence, other molecular modulations in Δ*laeA* strains may synergistically contribute, or indeed define, the observed virulence phenotype. For example, the link between increased susceptibility to macrophage phagocytosis and modified cell wall architecture of the

Δ*laeA* spore (Dagenais et al. 2010). As determined by Dagenais and co-workers, Δ*laeA* spores are susceptible to macrophage phagocytosis due to a reduction in RodA content in the spore cell wall, a protein which forms protective microfibrils that prevent immune recognition. These studies highlight how LaeA deletant strains may be used as a tool to reverse engineer the molecular basis of *A. fumigatus* attenuation.

In a comparable approach, work reported in this Chapter describes global gene expression profiling of Δ*laeA* and a fully virulent projenitor in the murine lung in order to provide insights into the transcriptional basis of Δ*laeA* attenuation. DNA microarray technology is a powerful approach which has been previously employed to study global gene expression of *A. fumigatus* under a number of laboratory conditions, which either approximate or are relevant to host colonisation. *In vitro* and *ex vivo* transcriptional profiling following heat shock (Nierman et al. 2005), antifungal treatment (Cagas et al. 2011, Gautam et al. 2008), exposure to human neutrophils (Sugui et al. 2008), following exit of spore dormancy (Lamarre et al. 2008) or between planktonic and biofilm growth states (Bruns et al. 2010a) provide insights into *A. fumigatus* responses to disease-relevant conditions, yet do not address pathogen gene expression in the multifaceted and dynamic host niche. The Bignell group published the first global analyses of the *A. fumigatus* infecting transcriptome, which identified genes preferentially employed at a single time-point of murine infection relative to laboratory culture (McDonagh et al. 2008). This analysis identified pH, iron starvation and nitrogen limitation as key challenges to host colonisation, and revealed the upregulation of genes directing multiple secondary metabolite biosynthesis and those residing in subtelomeric chromosomal regions in the host. Similar *in vitro* reference experiments have proved critical in elucidating the transcriptional basis of fungal pathogenesis for other mammalian and plant pathogens (Kamper et al. 2006, Mosquera et al. 2009, Walker et al. 2009). However, single time-point analyses are inherently limited with regard to delineating pathogen transcriptional changes which occur at defined time-points of infection. Indeed, *A. fumigatus* germination and cellular differentiation represent essential cellular processes in the establishment of invasive aspergillosis (Tekaia and Latge 2005) which occur over several hours in the murine lung. Concurrent to substantial changes in fungal physiology and metabolism throughout infection, multiple host niches are likely to be encountered, such as the aerobic alveoli which initially accomodates the spore, and the likely hypoxic parenchyma surrounding the invasive hyphae (Wezensky and Cramer 2011). Delineating the temporal basis of *A. fumigatus* transcription is therefore essential for understanding gene expression in the host.

In this Chapter global gene expression profiling was conducted using Af293 and a Δ*laeA* isolate at three time-points of early host infection. In addition, this Chapter describes development of a non-ratiometric normalisation methodology which is rapid, relatively cost- and labour- efficient,

and easily extendable. The development of such a methodology represents a powerful tool for a research community in which numerous regulators of virulence continue to be discovered (Bignell et al. 2005, Cramer et al. 2008, Gravelat et al. 2010, Moreno et al. 2007).

3.2 Methods

3.2.1 *A. fumigatus* strains

A. fumigatus strains used for the experimentation described in this Chapter are a clinical isolate provided by M. A. Anderson. Throughout Chapter 3 and 8, this isolate was incorrectly identified as clinical isolate Af293. For a discussion regarding strain isogenecity please see section 8.3.5. Throughout this Chapter, this clinical isolate is referred to as Af293.

To address the obvious limitations of utilising non-isogenic strains in the comparative analyses described in Chapters 3 and 8, the infection experiments were repeated with a genotypically confirmed Af293 isolate, which are reported in Chapter 10.

The Af293 Δ*laeA* mutant used in this Chapter was kindly provided by our collaborator Nancy Keller.

3.2.2 Murine infection

Murine infections were conducted under UK Home Office Project Licence PPL/70/6487 in a dedicated facility at Imperial College London. Outbred male mice (strain CD1, 18 – 22 g, Harlan Ortech) were housed in individually ventilated cages and allowed water and food *ad libitum*. Water was supplemented with 1 g/L tetracycline hydrochloride (Sigma-Aldrich) and 64 mg/L ciprofloxacin as prophylaxis against bacterial infection. For a neutropenic model of infection, immunosuppression of mice was performed by intraperitoneal injections of cyclophosphamide (150 mg/kg) on days –3 and –1 and by a single subcutaneous dose of hydrocortisone acetate (112.5 mg/kg) on day –1 (Schrettl et al. 2004). *A. fumigatus* spores were grown on ACM, supplemented with 1% (w/v) glucose and 5 mM ammonium tartrate, for 5 days prior to infection. Spores were harvested on the day of infection, using sterile saline (Baxter Healthcare Ltd, UK), and filtered through MIRACLOTH. Conidial suspensions were centrifuged for 10 minutes at 5000 RPM, washed twice with sterile saline, counted using a haemocytometer and resuspended at a concentration of $2.5x10^9$ cfu/ml. Mice were anaesthetised by isofluorane inhalation and infected by intranasal instillation of $1x10^8$ conidia in 40 µl of saline solution. The determination of viable counts for the administered inocula was performed using serial dilution on ACM plates supplemented with 1% (w/v) glucose and 5 mM ammonium tartrate and incubated for 3 days at 37°C. Mice were weighed every 24 hours from day -3 and inspected twice daily.

Groups of 7 mice were culled at 4, 8 and 14 hours post infection by neck dislocation. Bronchoalveolar lavage (BAL) was performed using three to four 250 µl aliquots of 37°C sterile saline per mouse. BAL fluids (BALFs) were snap frozen in liquid nitrogen. Mice were processed sequentially to ensure that the maximum time lapse between neck dislocation and BALF snap freezing was 3 minutes. Designated mice (n = 2) were used for Af293 Δ*laeA* histological analyses at each time-point, for which mice were culled as described above. Whole lungs were extracted and fixed in 4% v/v formaldehyde (Sigma-Aldrich). Lungs were embedded in paraffin prior to sectioning and stained with hemotoxylin and eosin (H&E) or Grocott's Methenamine Silver (GMS). These were compared with Af293 infected histological samples from the Bignell laboratory library.

3.2.3 *A. fumigatus* RNA Extraction, amplification and hybridisation

BALF samples were centrifuged at 14,000 RPM for 5 minutes and the pellet was washed with 500 µl ice cold water to lyse host cells. BALFs were pooled, resuspended in 450 µl ME-RLC buffer (Qiagen) and ground in liquid nitrogen with a pestle and mortar. RNA was then extracted using RNeasy® Kit (QIAGEN). The quality of RNA used for microarray analysis was checked by Nanodrop ND-1000 Spectrophotometer (Nanodrop, Wilmington, USA). RNA with an A260/280 and an A260/230 ratio > 1.9 was used for the experiments. RNA samples were doubly amplified prior to labelling with Cy3 or Cy5 fluorescent dye at the J. Craig Venter Institute (JCVI, Rockville, Maryland, USA, as described previously (McDonagh et al. 2008). Protocols for direct labelling and hybridisation of cDNA probes can be found on the JCVI website (http://pfgrc.jcvi.org/index.php/microarray/protocols.html). Double amplified, labelled RNA from BALFs was co-hybridised (Δ*lae*A:Af293) on each array and a dye swap replication of every hybridisation was performed. Two biological, and one technical replication of the experiment was performed.

3.2.4 *A. fumigatus* microarray scanning and normalisation

Washed slides were scanned and data were captured using a GenePix 4000b (Axon Instruments, Foster City, CA) semiconfocal microarray scanner and associated GenePix Pro 3.0 software. Scans were performed at a pixel size of 10 µm with 2 lines average. Overall red to green channel intensities were balanced as near as possible to a ratio of 1:1 by altering photo-mutiplier tube (PMT) gains. Images were saved as .TIF files and TIGR Spotfinder (Saeed et al. 2003) was used

to quantitate fluorescence intensities. Poor quality spots were identified manually and flagged. After Spotfinder analysis, results were exported as TIGR software-compatible MEV files following local background subtraction.

A non-ratiometric approach was applied in order to extract strain specific intensity values at each time–point ('t Hoen et al. 2004, Bossers et al. 2010a). For a full discussion of this approach please see the Introduction (section 1.5.1) and Results (section 3.3.1). Triplicate amplicon spots for each gene were averaged to give a single spot intensity value (aSI) for each gene per channel. Quantile normalisation (Bolstad et al. 2003) was applied to aSI values by time-point and by strain using a custom script in the R programming language. A second quantile normalisation was applied to effect inter-array normalisation of aSIs. Following quantile normalisation, data was $\log_2$ transformed, to give aSI*norm* values. For each gene and strain, aSI*norm* were averaged producing a single normalised intensity value (nSI) per gene for either Af293 or Δ*laeA* at each time-point. Genes were filtered based on two quality control criteria. Genes with < 3 aSI values were removed. Secondly, genes for which aSI*norm* values varied more than a standard deviation of 1.5 were filtered. Only genes with nSI values for all three time-points were considered in the final Af293 or Δ*laeA* datasets.

To determine temporal gene expression profiles throughout the time-course of infection, the change in nSI ratios were calculated between time-points. Genes in the upper and lower quartiles of the nSI ratio datasets were considered increased and decreased in transcript abundance respectively. In order to distinguish magnitude of transcriptional change between time-points, increased and decreased gene sets were subdivided into thirds, and the upper, intermediate and lower genes defined as high, moderate, and low changes respectively. GO enrichment of differentially expressed genes was performed using Genespring GX 11.02 (Aligent). Grouping of genes into comparable expression profiles was performed using the STEM program (Short Time-series Expression Miner) designed for short time-series microarray experiments (Ernst and Bar-Joseph 2006).

3.3 Results

3.3.1 Experimental design, non-ratiometric data capture and quantile normalisation

Groups of seven mice were infected with either Af293 or Δ*laeA* and culled at 4, 8 and 14 hours post infection for BALF sampling. For each strain BALFs were pooled and RNA was extracted. RNA was then amplified and reverse transcribed into labelled cDNA (see Methods). Two biological replicates were conducted. A technical replicate was included by co-hybridisation of Af293 and Δ*laeA* cDNA from the first and second biological replicates respectively (Figure 3.1). A total of 6 arrays were used to analyse each time-point, consisting of dye swap experiments for both biological and the single technical replicate (Figure 3.1).

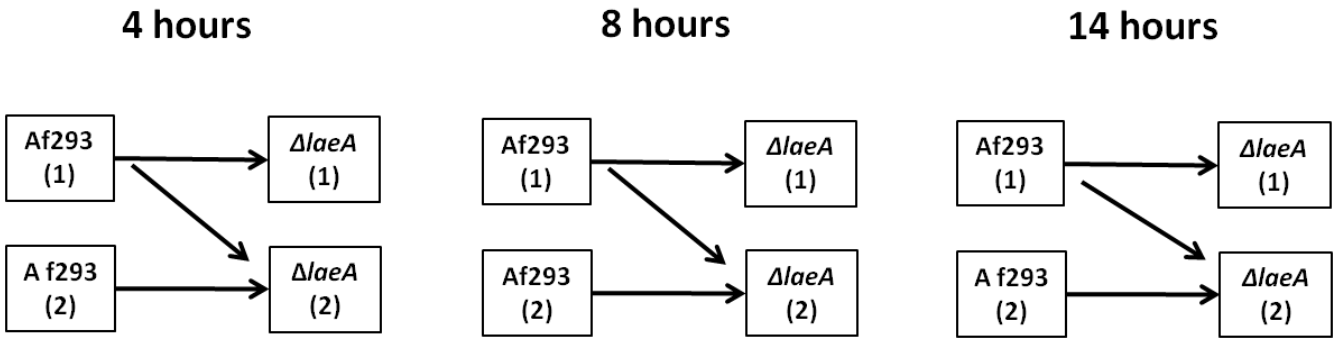


Figure 3.1: Hybridisations of Af293 and Δ*laeA* replicates throughout the experiment. Black arrows indicate co-hybridisations between samples on a dye swap pair of arrays. Diagonal lines depict the technical replicate. Duplicate biological replicates of Af293 and Δ*laeA* were co-hybridised at each time-point. Numbers in parentheses indicate the replicate number.

Data were captured from slides using TIGR spotfinder, and data exported as MEV files. From MEV files (n = 18) intensity channels (n = 36) were grouped into strain and time-point specific cohorts (n = 6, Figure 3.2A). On the custom *A. fumigatus* arrays used in this experiment, triplicate oligonucleotide spots represent each gene. These spots are identified by a unique gene identification (UID) number. Mean UID spot values were calculated to give an average spot intensity value (aSI) for each gene per channel (Figure 3.2A). Quantile normalisation was conducted on aSI data within time-point and strain cohorts, followed by a second quantile normalisation across the entire dataset (Figure 3.2C). Following quantile normalisation, all arrays have identical distribution, and inter-array variance is reduced (Figure 3.3). Following quantile normalisation, data was $\log_2$ transformed, to give aSI*norm* values. For each gene, aSI*norm* were

averaged within the strain and time specific channel cohorts, producing a single normalised intensity value (nSI) per gene for either Af293 or Δ*laeA* at each time-point (Figure 3.3D). Figure 3.6 depicts distribution of intensity data points in each channel before and after each quantile normalisation. Genes were filtered based on two quality control criteria (Figure 3.4). Genes with < 3 aSI values were removed (count filtering). Secondly, genes for which aSI*norm* values varied more than a standard deviation of 1.5 were filtered. Table 3.1 and Table 3.26 show the number of values filtered by count and standard deviation filtering for Af293 and Δ*laeA* respectively. Finally, only genes with nSI values at all three time-points were considered in final datasets.

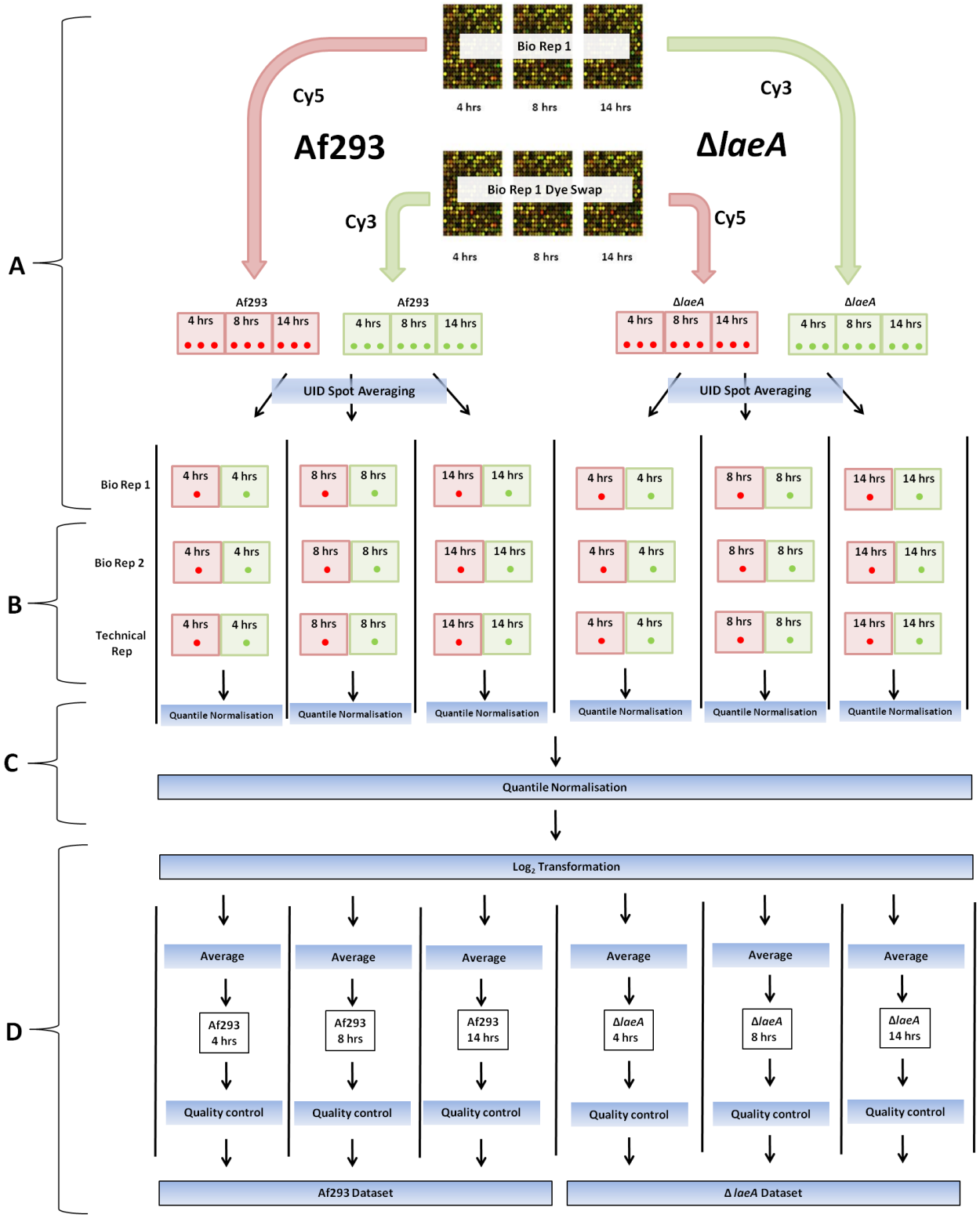


Figure 3.2: Schematic representation of experimental design and quantile normalisation. A. UID spot intensity values from Cy3 (red) or Cy5 (green) channels corresponding to either Af293 or Δ*laeA* RNA samples were separated from dye swap arrays. Each ORF is represented by triplicate UID spots on each array, which were averaged. **B.** Averaged spots from 3 experimental replicates, including dye swaps, were grouped into strain and time-point specific cohorts (n = 6, cohorts separated by vertical black lines). **C.** Quantile normalisation was applied by strain and by time-point, followed by inter-array quantile normalisation. **D.** The dataset was $\log_2$ transformed, and double quantile normalised intensity values at each time-point (n = 6) were averaged for Af293 or Δ*laeA*. Intensity values were excluded if they failed count and standard deviation quality control.

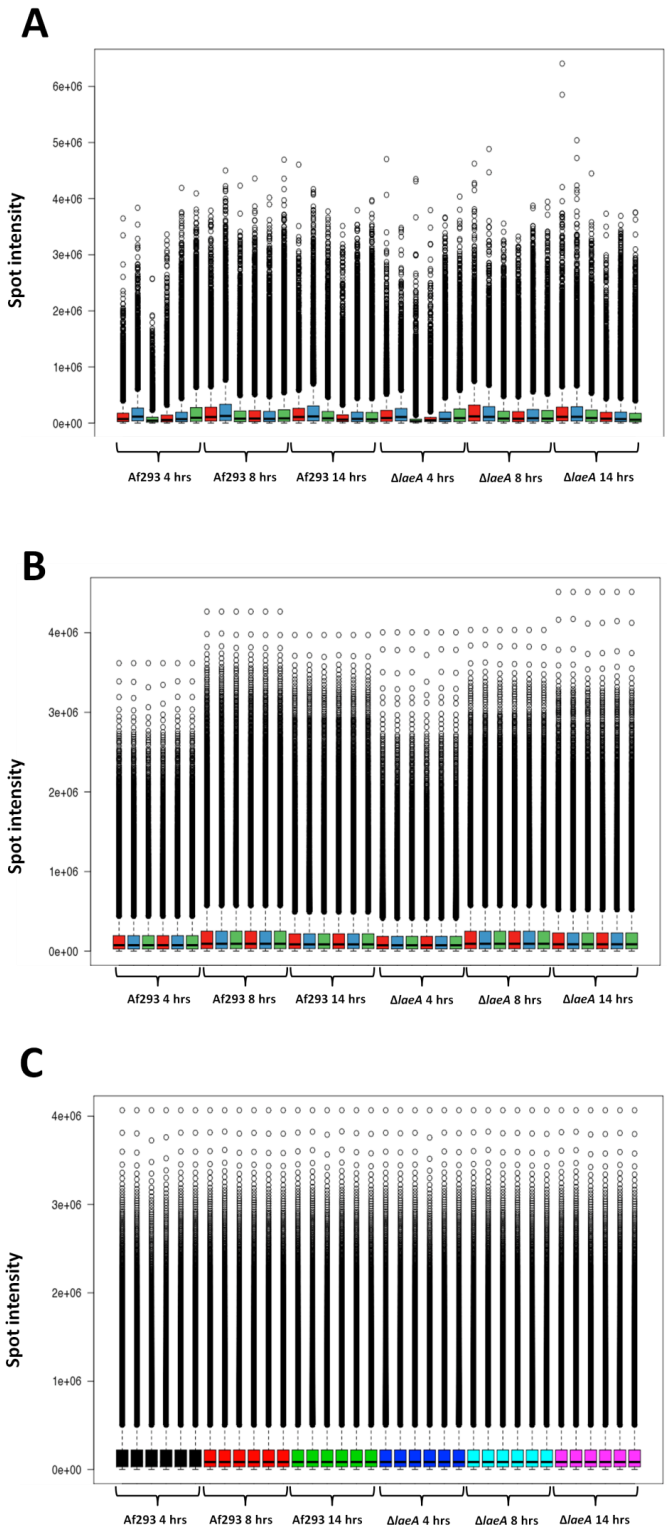


Figure 3.3: Box plots depicting non-ratiometric spot intensity distribution before and after double quantile normalisation for Af293 and Δ*laeA* datasets. Data points represent intensity values (*y* axis) for a single ORF averaged from triplicate UID spots on each array. **A.** Distribution of raw spot intensity values for every intensity channel (n = 36). Channels from biological rep 1 (red) biological rep 2 (blue) and the technical replicate (green) were grouped into strain and time-point cohorts. **B.** Distribution of spot intensity values following the first quantile normalisation within time-point and strain cohorts. Following normalisation, intensity channels have identical distribution within groups. **C.** Distribution of spot intensities following quantile normalisation across all intensity channels in the experiment. Following the second quantile normalisation, all channels have identical intensity distribution. Strain and time-point specific cohorts are highlighted in various colours.

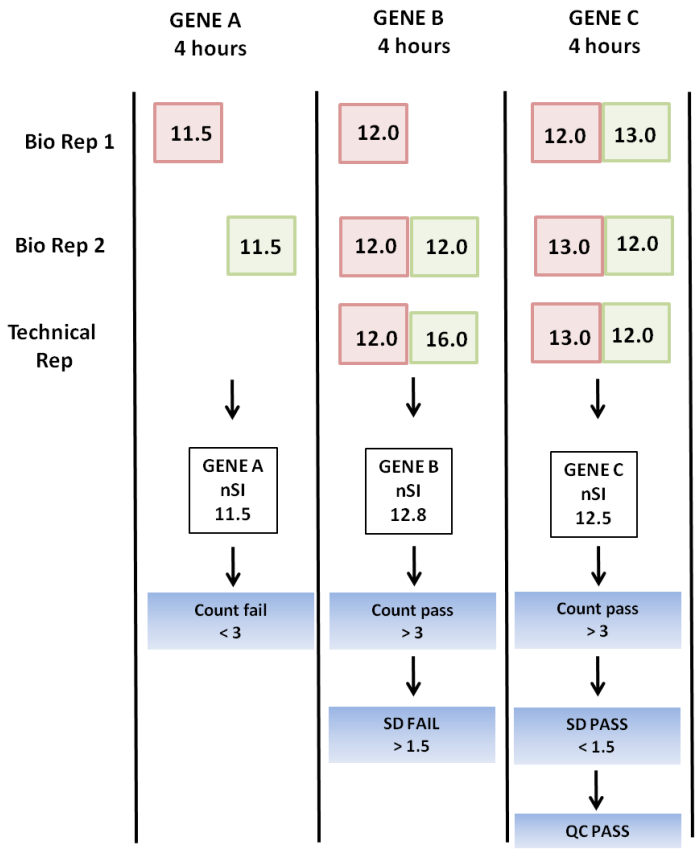


Figure 3.4: Schematic depicting count and standard deviation filtering for three genes at a single time-point post infection. Red and green boxes represent aSI*norm* values from Cy5 or Cy3 channels respectively. Hypothetical values for 3 genes (A, B and C) at 4 hours post infection. aSI*norm* values were averaged to give nSI values are shown (black boxes). Blue boxes show filtering steps. For gene A, due to prior removal of spots in Spotfinder Software (see Methods), < 3 aSI values are counted. Gene B passes count filtering, but fails standard deviation filtering due to unacceptable variation between aSI*norm* values. Gene C passes both filtering steps.

Datasets for Af293 and Δ*laeA* consisted of nSI values for 7896 and 7819 genes respectively, out of a possible 9516. To determine temporal transcriptional profiles throughout infection, differences in nSI ratios were calculated between time-points. nSI ratios reported relative to an earlier time-point (either 4 hours or 8 hours) and are directional in terms of the temporal gene profile, i.e. > 1 if the gene increases and < 1 if the gene decreases between time-points. From relative nSI values, differentially expressed transcripts between time-points were defined.

The most appropriate method for identifying differential expression can be viewed as a compromise between acceptance of false negative and false positive error rates (Quackenbush 2002). This study is interested in *A. fumigatus* physiological and biochemical changes directed by many genes. Consequently stringent control of false positives in which small gene lists are produced with high confidence by rigorous statistical analyses would greatly limit interpretation of

the dataset. Additionally, differential gene expression defined by *t*-statistical methods is less reproducible than approaches based on fold change or gene distribution. This is exemplified by a study conducted by Tan and co-workers, who investigated variation in gene expression between different array platforms. From identical experimental samples, the authors identified differentially expressed genes from three commercially available microarrays. Using various *t*-statistics, including Bonferroni corrected ANOVA models, 117, 67 and 34 genes were found to be differentially expressed by Amersham, Agilent and Affymetrix arrays respectively, of which only 4 were common to all platforms (Tan et al. 2003). Concern over the reproducibility of microarray technology (Ioannidis 2005, Marshall 2004) prompted a second analysis of the Tan *et al* dataset by a second group (Shi et al. 2005). This study reported improved concordance between the three technologies, provided stringent *t*-statistics were replaced with fold-change ranking. This approach found 39 genes common to the three platforms (Shi et al. 2005). Such controversy in the most appropriate definition of differential expression motivated initiation of the Microarray Quality Control project (MAQC) in 2005 (Shi et al. 2008a). The first report from MAQC, published in Nature Biotechnology (2006) analysed commercially available reference RNA samples with 1329 microarrays from over 40 laboratories and 20 array platforms (MAQC-Consortium 2006). This extensive study supported the findings of Shi et al, namely differentially expressed genes lists between groups, array platforms and technical replicates were much more reproducible (and therefore biologically representative) when fold-change ranking was used in conjunction with a non-stringent p value, as opposed to stringent *t*-statistical approaches (Shi et al. 2008b).

Considering this study intends to establish a methodology which can be extended to other microarray experiments from the host niche, reproducible identification of differentially expressed genes between expriments is of paramount importance. In light of the biological and methodological objectives of this study, differential gene expression within the nSI ratio datasets was defined based on gene distribution, with upper and lower quartiles used to identify increase or decrease in transcript abundance between time-points respectively. All relative nSI datasets were normally distributed around median values which did not deviate more than 0.018 from 1 (Figure 3.5). Increased and decreased gene sets were subdivided into three groups which represented high, moderate, and low changes between time-points.

In addition to this ranking of temporal gene expression, a one-way ANOVA test was applied between time-points with the null hypothesis that average nSI values for each gene do not differ between time-points. False discovery corrected p values are reported but were not used to filter genes from the datasets.

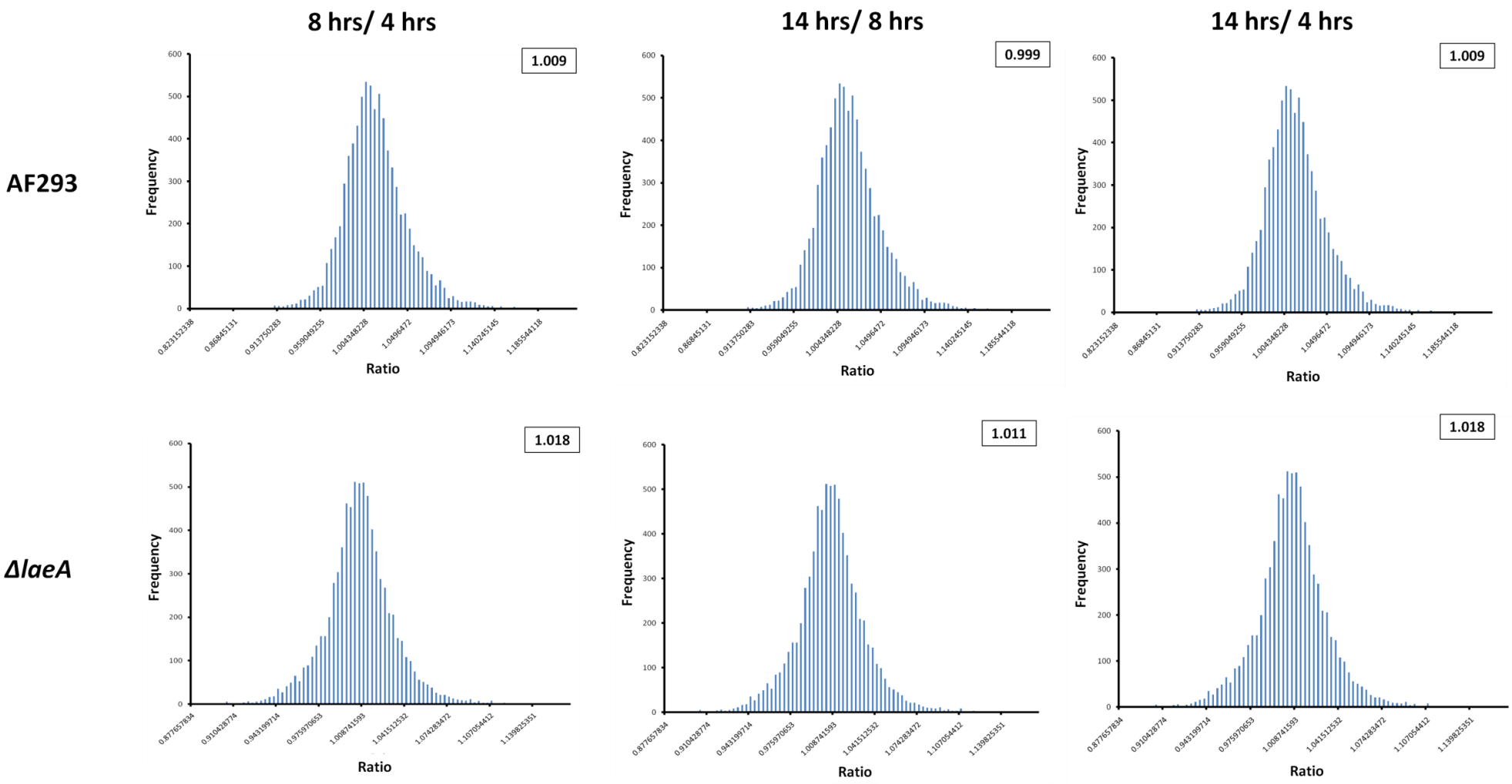


Figure 3.5: Frequency distribution of relative nSI datasets. nSI values were divided for each gene between time-points to give relative values of expression. A value of 1 therefore indicates no change between time-points. Median values are shown in black boxes. Upper and lower quartiles were considered increased and decreased gene expression between time-points respectively.

3.4 *A. fumigatus* Af293 transcriptional profile during the initiation of murine infection

As summarised in Table 3.1, fluorescent intensities for 8510, 8143 and 8549 out of a possible 9516 represented ORFs passed quality control filtering for 4, 8 and 14 hour time-points respectively. Genes without expression values at all three time-points (due to quality control filtering) were omitted from the dataset, resulting in a total of 7896 gene expression profiles. To determine the temporal basis of transcriptional changes during infection, relative nSI values were calculated between time-points and the upper and lower quartiles of the relative nSI datasets were considered up and down expressed transcripts (n = 1974) respectively. Increased and decreased gene sets were subdivided into three groups of high, moderate, and low transcriptional changes between time-points (n = 658) respectively. Table 3.2 summaries upper and lower quartile values at each time-point, and maximal and minimal relative nSI values between time-points.

	4 hrs	8 hrs	14
Count fail	703	934	651
Standard deviation fail	222	38	235
Retained genes	8510	8143	8549
Average nSI	16.15	16.28	16.27
Median nSI	16.13	16.38	16.34
Standard deviation	1.82	1.88	1.83
Minimum nSI value	11.77	11.93	11.81
Maximum nSI value	21.27	21.31	21.32

Table 3.1: Summary statistics for the Af293 non-ratiometric analysis. The number of genes failing count and standard deviation quality control filtering are shown. The total number of genes with expression values common to every time-point and thus retained for analysis was 7896.

	nSI			Relative nSI		
	4 hrs	8 hrs	14 hrs	8 vs 4 hrs	14 vs 8 hrs	4 vs 14 hrs
Lower quartile	14.57	14.8	14.82	0.991	0.987	0.99
Upper quartile	17.62	17.79	17.76	1.03	1.013	1.031
Median	16.09	16.43	16.38	1.009	0.999	1.009
Average	16.18	16.37	16.37	1.012	1.001	1.013
Standard deviation	1.84	1.85	1.8	0.033	0.023	0.036

Table 3.2: Summary statistics for Af293 relative nSI datasets. Relative nSI values were calculated for 7896 genes. Upper and lower quartiles (n = 1974) were used to define up and down expressed genes respectively.

Distribution of the up and down expressed datasets is summarised in 2 and 3-way Venn diagram in Figure 3.6. Comparisons between lists of differentially expressed genes between the 4 – 8 and 8 – 14 hours time-points revealed 417 and 287 genes with increased and decreased transcript abundance, respectively.. These identified genes also featured in the 4 - 14 hour dataset (Figure 3.6B). Consequently, the 4 – 14 hour comparison is inclusive of all gene expression changes and therefore constitutes the most appropriate cohort for interrogating transcriptional changes across the entire time-course. 4 – 8 and 8 – 14 hour comparisons were used to identify time-point specific transcriptional changes.

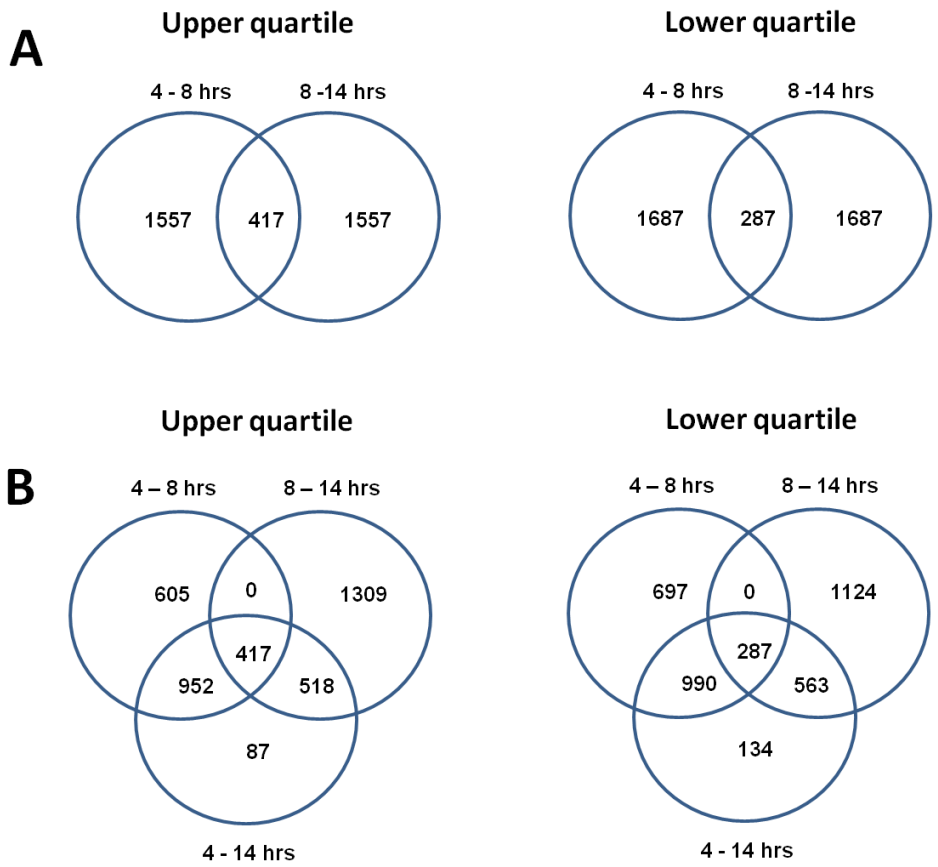


Figure 3.6: Venn diagrams depicting comparisons between relative nSI datasets from the Af293 non-ratiometric analysis. **A.** 2 way Venn diagram depicting comparisons between time-point specific datasets. **B**. Three-way Venn diagram depicting coparisons between all nSI datasets. Upper and lower quartiles (n =1974) were used to define genes with increase and decrease in expression respectively.

3.4.1 Gene expression profiling of the Af293 isolate between 4 and 14 hours in the murine lung

Initial interpretations of gene expression profiles were conducted across the entire time course of infection, between which spores germinate and produce primary germ tubes (Figure 3.7). Gene ontology analysis was conducted using Genespring GX 11.02 to indentify over represented terms in increased or decreased datasets. GO terms satisfying an arbitrarily imposed corrected p value cut off of ≤ 0.2 with respect to their occurence in the *A. fumigatus* genome are reported (Table 3.3 and 3.4). The 100 genes having the greatest increase and 100 genes having the greatest decrease between 4 and 14 hours are reported in Tables 3.5 and 3.6.

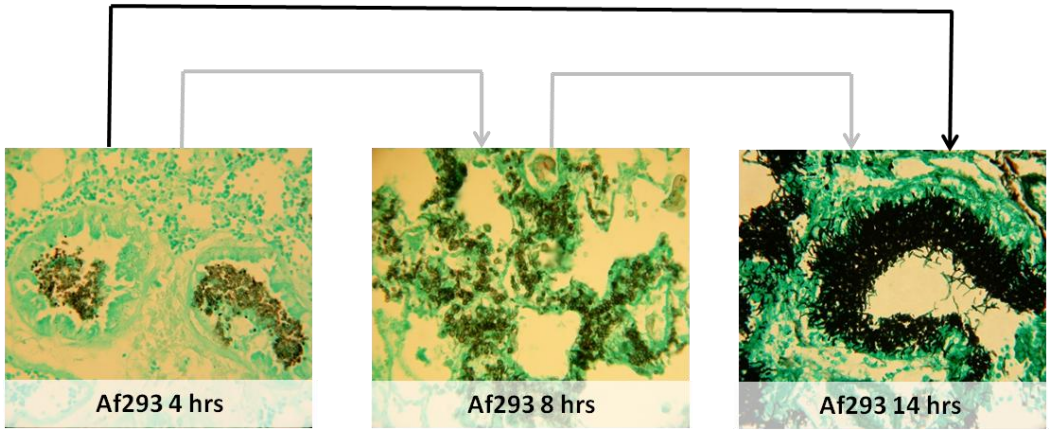


Figure 3.7: Histopathological analysis of Af293 during infection. Lungs were paraffin-embedded and stained with Grocott's Methenamine Silver. Solid black arrow represents relative nSI comparisions conducted between 4 and 14 hours. Faint grey arrows represent time-point specific comparisions which are discussed later in this Chapter. At 4 hrs, spores were ungerminated. At 8 hrs, germination had occurred in approximately 60% of spores. At 14 hours, >90% of Af293 spores had germinated, and germ tube penetration through surrounding host tissue and airways was observed

GO ACCESSION	GO Term	p-value	corrected p-value	Count in Selection	% Count in Selection	Count in Total	% Count in Total
GO:0007186	G-protein coupled receptor protein signaling pathway	3.12E-06	0.014	13	13	20	0.43
GO:0046999	regulation of conjugation	4.14E-06	0.014	13	13	18	0.39
GO:0032005	signal transduction involved in conjugation with cellular fusion	4.14E-06	0.014	13	13	18	0.39
GO:0000750|GO:0007330|GO:0030454	pheromone-dependent signal transduction involved in conjugation with cellular fusion	4.14E-06	0.014	13	13	18	0.39
GO:0031137	regulation of conjugation with cellular fusion	4.14E-06	0.014	13	13	18	0.39
GO:0043900	regulation of multi-organism process	4.14E-06	0.014	13	13	18	0.39
GO:0007165	signal transduction	5.21E-06	0.015	26	26	122	2.63
GO:0000041	transition metal ion transport	1.06E-05	0.026	5	5	55	1.18
GO:0005935	cellular bud neck	1.14E-05	0.026	12	12	24	0.52
GO:0030427|GO:0000134|GO:0030483	site of polarized growth	2.86E-05	0.048	12	12	28	0.60
GO:0007166	cell surface receptor linked signal transduction	2.86E-05	0.048	13	13	28	0.60
GO:0005933	cellular bud	2.86E-05	0.048	12	12	28	0.60
GO:0007154	cell communication	3.21E-05	0.050	26	26	133	2.86
GO:0051704|GO:0051706	multi-organism process	4.03E-05	0.059	14	14	109	2.35
GO:0005886|GO:0005904	plasma membrane	6.18E-05	0.084	65	65	330	7.10
GO:0006811	ion transport	7.64E-05	0.095	5	5	137	2.95
GO:0000749|GO:0007328|GO:0030434	response to pheromone during conjugation with cellular fusion	7.97E-05	0.095	14	14	27	0.58
GO:0005874	microtubule	1.03E-04	0.115	1	1	22	0.47
GO:0065007	biological regulation	1.07E-04	0.115	26	26	641	13.80
GO:0019236	response to pheromone	1.49E-04	0.146	14	14	31	0.67
GO:0006812|GO:0006819	cation transport	1.50E-04	0.146	5	5	111	2.39
GO:0010033	response to organic substance	2.05E-04	0.189	14	14	47	1.01
GO:0016723	oxidoreductase activity, oxidizing metal ions, NAD or NADP as acceptor	2.36E-04	0.200	1	1	13	0.28

Table 3.3: Over-represented Gene Ontology terms among genes with increasing expression between 4 and 14 hours in the Af293 infected murine lung. GO terms significantly enriched with respect to their occurrence in the *A. fumigatus* Af293 genome are reported (Bonferroni corrected p-values ≤ 0.2)

GO ACCESSION	GO Term	p-value	corrected p-value	Count in Selection	% Count in Selection	Count in Total	% Count in Total
GO:0006396|GO:0006394	RNA processing	2.78E-09	5.23E-05	37	58.73016	232	4.994618
GO:0044085	cellular component biogenesis	2.85E-08	2.68E-04	48	76.19048	315	6.781486
GO:0016070	RNA metabolic process	4.87E-08	3.05E-04	39	61.90476	380	8.18084
GO:0022613	ribonucleoprotein complex biogenesis	9.59E-08	4.51E-04	40	63.49206	181	3.896663
GO:0042254|GO:0007046	ribosome biogenesis	2.81E-07	0.001059	40	63.49206	169	3.638321
GO:0010467	gene expression	5.40E-06	0.014513	37	58.73016	579	12.46502
GO:0065003	macromolecular complex assembly	5.04E-06	0.014513	8	12.69841	135	2.906351
GO:0022607	cellular component assembly	1.21E-05	0.028511	8	12.69841	158	3.401507
GO:0034470	ncRNA processing	1.81E-05	0.037885	33	52.38095	140	3.013994
GO:0034660	ncRNA metabolic process	2.06E-05	0.038853	34	53.96825	167	3.595264
GO:0016072	rRNA metabolic process	3.07E-05	0.05261	34	53.96825	113	2.432723
GO:0006364|GO:0006365	rRNA processing	4.23E-05	0.064128	33	52.38095	111	2.389666
GO:0044428	nuclear part	4.77E-05	0.064128	9	14.28571	477	10.26911
GO:0043933|GO:0034600	macromolecular complex subunit organization	4.45E-05	0.064128	8	12.69841	174	3.745963
GO:0000785|GO:0005717	chromatin	7.16E-05	0.089852	9	14.28571	27	0.58127
GO:0006139	nucleobase, nucleoside, nucleotide and nucleic acid metabolic process	1.14E-04	0.118812	40	63.49206	672	14.46717
GO:0042273	ribosomal large subunit biogenesis	1.48E-04	0.1465	5	7.936508	39	0.839613
GO:0070271	protein complex biogenesis	1.92E-04	0.150324	8	12.69841	63	1.356297
GO:0000790	nuclear chromatin	1.84E-04	0.150324	9	14.28571	26	0.559742
GO:0006461	protein complex assembly	1.92E-04	0.150324	8	12.69841	63	1.356297
GO:0044260|GO:0034960	cellular macromolecule metabolic process	2.57E-04	0.193607	39	61.90476	1101	23.70291

Table 3.4: Significant GO terms among genes with decreasing expression between 4 and 14 hours in the Af293 infected murine lung. GO terms significantly enriched (Bonferroni corrected p-values ≤ 0.2) with respect to their occurrence in the *A. fumigatus* genome are reported.

Table 3.5: 100 genes with greatest nSI increase between 4 and 14 hours post infection. Genes are reported ranked according to greatest nSI intensity increase between 4 and 14 hours where 1 is the greatest. A one-way ANOVA was conducted on nSI values between time-points, with the null hypothesis that nSI values do not change between time-points. FDR correct *p*-values from this analysis are reported for each gene.

ORF	Description	Rank	*p-value*	GO Biological Process
Afu6g09690	glutathione S-transferase GliG	1	0.006	
Afu6g09670	cytochrome P450 oxidoreductase GliC	2	0.007	oxidoreductase activity///metabolic process
Afu4g13970	conserved hypothetical protein	3	0.003	
Afu6g09680	O-methyltransferase GliM	4	0.034	S-adenosylmethionine-dependent methyltransferase activity///O-methyltransferase activity
Afu4g14070	glycosyl transferase, putative	5	0.043	transferase activity, transferring glycosyl groups
Afu6g09730	cytochrome P450 oxidoreductase GliF	6	0.012	oxidoreductase activity///metabolic process
Afu8g00610	cell surface protein Mas1, putative	7	0.03	
Afu6g03350	acetyltransferase, GNAT family, putative	8	0.004	N-acetyltransferase activity///metabolic process
Afu6g08490	inorganic diphosphatase, putative	9	0.008	phosphate metabolic process///inorganic diphosphatase activity///cytosol
Afu3g00520	SIR2 family histone deacetylase, putative	10	0.001	chromatin silencing at telomere///cytoplasm///NAD-dependent histone deacetylase activity
Afu5g14230	C6 transcription factor, putative	11	0.036	DNA binding///nucleus///zinc ion binding
Afu7g07010	hypothetical protein	12	0.001	
Afu6g00290	aminotransferase, putative	13	0.001	arylformamidase activity///cytoplasm///mitochondrion///NAD biosynthetic process
Afu6g09710	MFS gliotoxin efflux pump GliA	14	0.052	transporter activity///transport
Afu6g06360	mating alpha-pheromone PpgA	15	0.002	mating pheromone activity///extracellular region///pheromone-dependent signal transduction involved in conjugation with cellular fusion///conjugation with cellular fusion
Afu4g10340	C6 finger domain protein, putative	16	0.007	DNA binding///zinc ion binding

Afu7g05490	hypothetical protein	17	0.009	
Afu2g17330	serine peptidase, family S28, putative	18	0.001	
Afu3g09060	hypothetical protein	19	0.013	
Afu4g14180	hypothetical protein	20	0.008	
Afu2g00580	hypothetical protein	21	0.003	
Afu2g08820	hypothetical protein	22	0.003	
Afu6g00430	IgE-binding protein	23	0.008	
Afu1g01300	GPI anchored protein, putative	24	0.003	
Afu6g09650	membrane dipeptidase GliJ	25	0.005	
Afu7g08280	hypothetical protein	26	0.004	
Afu7g00200	conserved hypothetical protein	27	0.019	
Afu1g01310	carboxylesterase, putative	28	0.008	
Afu5g14240	ThiJ/PfpI family protein	29	0.002	
Afu2g00230	NADH oxidoreductase Amid, putative	30	0.004	oxidoreductase activity///"DNA damage response, signal transduction resulting in induction of apoptosis"///electron carrier activity///nucleus///mitochondrion///coenzyme binding
Afu4g14090	UDP-glucose 4-epimerase	31	0.011	cellular component unknown///molecular function unknown///galactose metabolic process
Afu7g06780	hypothetical protein	32	0.006	
Afu2g03280	hypothetical protein	33	0.003	
Afu1g14560	alpha-mannosidase	34	0.007	
Afu5g09020	WSC domain protein, putative	35	0.004	membrane fraction///transmembrane receptor activity///cell wall organization///response to heat///Rho protein signal transduction///actin cytoskeleton organization
Afu7g01930	sexual development protein EsdC, putative	36	0.062	GTP binding
Afu6g09740	thioredoxin reductase GliT	37	0.008	secondary metabolic process

Afu3g08110	cell wall protein, putative	38	0.027	
Afu6g00650	hypothetical protein	39	0.018	
Afu1g13140	G protein complex alpha subunit GpaA	40	0.008	response to pheromone during conjugation with cellular fusion///pheromone-dependent signal transduction involved in conjugation with cellular fusion///pathogenesis///heterotrimeric G-protein GTPase activity///signal transduction///heterotrimeric G-protein complex///response to stress
Afu4g10120	C6 finger domain protein, putative	41	0.003	DNA binding///zinc ion binding
Afu2g14490	endoglucanase, putative	42	0.027	
Afu3g09960	aureobasidin resistance protein Aur1	43	0.017	inositol phosphoceramide synthase activity///sphingolipid metabolic process///Golgi apparatus
Afu2g14420	cutinase, putative	44	0.043	
Afu5g11190	hypothetical protein	45	0.038	
Afu7g06810	L-amino acid oxidase LaoA, putative	46	0.004	
Afu5g02650	hypothetical protein	47	0.032	
Afu6g03470	ABC multidrug transporter, putative	48	0.051	ATP-binding cassette (ABC) transporter activity///integral to plasma membrane///transport
Afu3g14920	LaeA-like methyltransferase, putative	49	0.132	
Afu7g01990	conserved hypothetical protein	50	0.015	
Afu4g00750	hypothetical protein	51	0.03	
Afu3g09260	hypothetical protein	52	0.01	
Afu6g09640	aminotransferase GliI	53	0.027	secondary metabolic process///transaminase activity
Afu6g13740	hypothetical protein	54	0.018	
Afu2g01430	hypothetical protein	55	0.015	
Afu3g03450	cytochrome P450 pisatin demethylase, putative	56	0.09	oxidoreductase activity///metabolic process
Afu2g11900	pyruvate dehydrogenase kinase	57	0.003	kinase activity///biological process unknown///mitochondrion

Afu6g13380	hypothetical protein	58	0.012	
Afu3g01990	DUF636 domain protein	59	0.123	
Afu1g05370	conserved hypothetical protein	60	0.025	
Afu1g17270	ferric-chelate reductase (Fre2), putative	61	0.061	ferric-chelate reductase activity///transition metal ion transport///plasma membrane
Afu1g02760	cell cycle inhibitor Nif1, putative	62	0.003	
Afu6g12420	SprT family metallopeptidase, putative	63	0.039	
Afu2g12320	conserved hypothetical protein	64	0.002	
Afu2g00870	hypothetical protein	65	0.089	
Afu5g08640	hypothetical protein	66	0.128	
Afu8g05300	RNA polymerase II subunit 7	67	0.18	transcription from RNA polymerase II promoter///DNA-directed RNA polymerase activity///"DNA-directed RNA polymerase II, core complex"
Afu2g11110	nuclear condensin complex subunit Smc2, putative	68	0.005	nuclear condensin complex///double-stranded DNA binding///mitotic sister chromatid segregation///DNA secondary structure binding///ATPase activity///AT DNA binding///mitotic chromosome condensation
Afu5g07590	hypothetical protein	69	0.027	
Afu3g01490	alcohol dehydrogenase, putative	70	0.004	cellular component unknown///oxidoreductase activity///metabolic process///zinc ion binding
Afu6g00630	MFS transporter, putative	71	0.001	transporter activity///transport///integral to membrane
Afu5g10950	hypothetical protein	72	0.046	
Afu8g05680	serine/threonine protein kinase, putative	73	0.011	protein serine/threonine kinase activity///DNA-dependent DNA replication///nucleus///protein amino acid phosphorylation///spindle pole
Afu3g01500	integral membrane protein	74	0.043	
Afu6g13800	integral membrane protein, putative	75	0.011	
Afu4g14730	GNAT family acetyltransferas	76	0.032	N-acetyltransferase activity///metabolic process

	e, putative			
Afu4g11270	hypothetical protein	77	0.079	
Afu1g16760	acetyltransferase, GNAT family family	78	0	
Afu2g03730	Ctr copper transporter family protein	79	0.032	copper uptake transmembrane transporter activity///copper ion import///integral to plasma membrane
Afu5g01620	extracellular proline-rich protein	80	0.003	
Afu5g08770	hypothetical protein	81	0.02	
Afu1g12620	MFS toxin efflux pump (AflT), putative	82	0.009	response to drug///multidrug transport///multidrug efflux pump activity
Afu1g05920	hypothetical protein	83	0.028	
Afu7g08580	dynamin GTPase, putative	84	0.315	membrane fraction///vacuolar transport///protein retention in Golgi apparatus///GTPase activity///peroxisome organization///protein targeting to vacuole
Afu6g00640	integral membrane protein	85	0.031	
Afu4g08730	conserved hypothetical protein	86	0.041	
Afu5g14660	GABA permease, putative	87	0.02	plasma membrane///choline transmembrane transporter activity///choline transport
Afu6g08470	glycerol kinase, putative	88	0.073	cytoplasm///glycerol kinase activity///glycerol metabolic process
Afu1g05950	integral membrane protein	89	0.012	
Afu8g05950	hypothetical protein	90	0.115	
Afu2g00130	solid-state culture specific protein, putative	91	0.003	
Afu4g10220	homeobox transcription factor (RfeB), putative	92	0.023	transcription factor activity///transcription///nucleus///cellular response to phosphate starvation///histidine biosynthetic process///purine base biosynthetic process
Afu6g12110	salicylate synthetase, putative	93	0.138	cytoplasm///anthranilate synthase activity///tryptophan biosynthetic process
Afu5g00200	conserved hypothetical protein	94	0.057	

Afu2g17300	glutathione S-transferase	95	0.017	glutathione metabolic process///glutathione transferase activity///endoplasmic reticulum
Afu3g08710	protein kinase domain-containing protein	96	0.034	protein kinase activity
Afu7g06820	galactose oxidase, putative	97	0.031	
Afu1g10220	hypothetical protein	98	0.066	
Afu2g11920	hypothetical protein	99	0.077	
Afu4g00610	aryl-alcohol dehydrogenase, putative	100	0.068	

Table 3.6: 100 genes with greatest nSI decrease between 4 and 14 hours post infection. Genes are reported ranked according to greatest nSI decrease between 4 and 14 hours where 1 is the greatest. A one-way ANOVA was conducted on nSI values between time-points, with the null hypothesis that nSI values do not change between time-points. FDR correct *p*-values from this analysis are reported for each gene.

ORF	Description	Rank	p-value	GO_BiologicalProcess
Afu2g05360	C6 transcription factor, putative	1	0.002	transcription factor activity///regulation of transcription
Afu6g02980	small nuclear ribonucleoprotein U2, A'	2	0.386	pectin catabolic process///pseudohyphal growth///extracellular region///polygalacturonase activity
Afu1g16420	GPI anchored protein, putative	3	0.07	
Afu2g17600	polyketide synthetase PksP	4	0.029	pathogenesis///polyketide synthase activity///pigment biosynthetic process
Afu3g09410	reverse transcriptase	5	0.035	
Afu7g07190	reverse transcriptase/protease/endonuclease Pol, putative	6	0.249	
Afu2g05350	major facilitator superfamily protein superfamily	7	0.096	transporter activity///transport
Afu5g10290	oxidoreductase, short-chain dehydrogenase/reductase family	8	0.031	fructose-bisphosphate aldolase activity///glycolysis
Afu8g06870	hypothetical	9	0.441	hexose transport///mannose

	protein			transmembrane transporter activity///fructose transmembrane transporter activity///plasma membrane///glucose transmembrane transporter activity
Afu8g02630	endonuclease/reverse transcriptase/RNaseH, putative	10	0.142	pectin catabolic process///pseudohyphal growth///extracellular region///polygalacturonase activity
Afu6g11670	basic amino acid transporter, putative	11	0.1	
Afu5g09140	polysaccharide deacetylase family protein	12	0.189	aerobic respiration///amidase activity///mitochondrion
Afu3g11920	dihydrodipicolinate synthetase family protein	13	0.011	catalytic activity///metabolic process
Afu6g08410	conserved hypothetical protein	14	0.201	
Afu6g11700	conserved hypothetical protein	15	0.138	
Afu5g08600	hypothetical protein	16	0.306	homoserine metabolic process///homoserine O-acetyltransferase activity///cytoplasm///methionine biosynthetic process
Afu7g05440	hypothetical protein	17	0.411	cytoplasm///transcription factor activity///nucleus///biological process unknown
Afu2g01240	beta-D-fructofuranoside fructohydrolase	18	0.083	extracellular region///cytoplasm///beta-fructofuranosidase activity///sucrose catabolic process
Afu7g06420	TOS4, putative	19	0.152	NADPH dehydrogenase activity///cytoplasm///nucleus///biological process unknown
Afu4g13900	polyphenol monooxygenase, putative	20	0.274	nicotinamide mononucleotide permease activity///nicotinamide mononucleotide transport///integral to plasma membrane
Afu3g11760	MFS transporter, putative	21	0.35	transporter activity///transport///integral to membrane
Afu5g10710	monosaccharide transporter	22	0.213	
Afu8g06040	extracellular exo-polygalacturonase, putative	23	0.066	
Afu3g11510	O-acetyltransferase, putative	24	0.415	cellular component unknown///acetyltransferase activity///biological process unknown
Afu3g15120	hypothetical protein	25	0.305	

Afu2g14120	C6 finger domain protein, putative	26	0.082	
Afu4g00220	metallo-beta-lactamase domain protein	27	0.427	
Afu3g02500	protein kinase, putative	28	0.05	cytoplasm///protein kinase activity
Afu6g08530	hypothetical protein	29	0.125	cellular component unknown///mitotic sister chromatid separation///molecular function unknown
Afu5g07850	hypothetical protein	30	0.629	
Afu2g16170	DNA-directed RNA polymerase III RPC4, putative	31	0.149	
Afu5g09130	homoserine O-acetyltransferase	32	0.286	
Afu1g06490	hypothetical protein	33	0.211	
Afu3g12770	putative nucleoside-diphosphate-sugar epimerase	34	0	
Afu2g02290	hypothetical protein	35	0.004	structural constituent of ribosome///translation///mitochondrial small ribosomal subunit
Afu3g03860	3-hydroxyacyl-CoA dehydrogenase, putative	36	0.001	
Afu8g06130	LEA domain protein	37	0.028	
Afu2g04290	cytochrome P450 monooxygenase, putative	38	0.488	oxidoreductase activity///metabolic process
Afu6g09260	sister chromatid separation protein (Src1), putative	39	0.65	protein histidine kinase activity///two-component sensor activity///protein amino acid phosphorylation
Afu5g07910	phosphatase family protein	40	0.531	
Afu6g04100	extracellular exo-polygalacturonase, putative	41	0.004	
Afu2g17920	hypothetical protein	42	0.469	
Afu4g00730	C6 transcription factor, putative	43	0.075	
Afu2g16300	dihydroxy acid dehydratase,	44	0.481	dihydroxy-acid dehydratase activity///branched chain family amino

	putative			acid biosynthetic process///mitochondrion
Afu4g10160	cytochrome P450 monooxygenase , putative	45	0.501	carbohydrate metabolic process///transcription factor activity///"regulation of transcription, DNA-dependent"///nucleus
Afu2g09150	adenosine deaminase	46	0.413	cytoplasm///adenine catabolic process///nucleus///adenine deaminase activity
Afu2g00200	catalase, putative	47	0.239	oxygen and reactive oxygen species metabolic process///peroxisomal matrix///response to oxidative stress///catalase activity
Afu2g04970	Kelch repeats protein, putative	48	0.287	cytoplasm///biological process unknown///molecular function unknown
Afu1g11590	quinate 5-dehydrogenase	49	0.239	3-dehydroquinate synthase activity///3-phosphoshikimate 1-carboxyvinyltransferase activity///cytoplasm///shikimate 5-dehydrogenase activity///shikimate kinase activity///aromatic amino acid family biosynthetic process///3-dehydroquinate dehydratase activity
Afu2g15480	hypothetical protein	50	0.226	
Afu7g06520	NADH-dependent flavin oxidoreductase, putative	51	0.202	
Afu8g00230		52	0.031	
Afu6g11100	sensor histidine kinase/response regulator, putative	53	0.117	basic amino acid transmembrane transporter activity///plasma membrane///basic amino acid transport
Afu3g15040	xenobiotic compound monooxygenase , DszA family	54	0.117	
Afu3g11900	oxidoreductase, zinc-binding	55	0.004	alcohol metabolic process///soluble fraction///alcohol dehydrogenase (NADP+) activity///cellular aldehyde metabolic process
Afu5g07860	decapping enzyme Dcp1, putative	56	0.017	endocytosis///inositol-polyphosphate 5-phosphatase activity///membrane fraction///cell wall organization///dephosphorylation
Afu1g08970	conserved hypothetical protein	57	0.329	endoplasmic reticulum///biological process unknown///molecular function unknown
Afu1g04550	HMG box protein, putative	58	0.426	
Afu1g09180	hypothetical protein	59	0.095	
Afu2g17730	MFS multidrug transporter, putative	60	0.34	integral to plasma membrane///multidrug transporter activity///response to toxin

Afu3g04230	transcription initiation factor IIF subunit alpha, putative	61	0.349	transcription factor TFIIF complex///transcription initiation from RNA polymerase II promoter///general RNA polymerase II transcription factor activity
Afu2g13210	DnaJ domain protein	62	0.59	nucleus///biological process unknown///mitochondrion///chaperone regulator activity
Afu4g09470	hypothetical protein	63	0.12	oxidoreductase activity///metabolic process
Afu5g10690	fructose-bisphosphate aldolase, putative	64	0.068	membrane///transporter activity///transport
Afu3g03810	hypothetical protein	65	0.061	
Afu1g11430	hypothetical protein	66	0.052	
Afu5g11000	conserved hypothetical protein	67	0.134	pre-mRNA splicing factor activity///"nuclear mRNA splicing, via spliceosome"///cytoplasm///U2 snRNP
Afu2g09170	DUF814 domain protein, putative	68	0.032	cytoplasm///biological process unknown///molecular function unknown
Afu2g03740	exosome complex endonuclease 1/ribosomal RNA processing protein, putative	69	0.493	3'-5'-exoribonuclease activity///nuclear exosome (RNase complex)///cytoplasmic exosome (RNase complex)///mRNA catabolic process///35S primary transcript processing
Afu1g16730	TruD domain protein	70	0.094	pseudouridine synthase activity///pseudouridine synthesis///nucleus
Afu3g00400	hypothetical protein	71	0.509	
Afu1g10100	3-oxoacyl-(acyl-carrier-protein) reductase	72	0.011	
Afu1g14210	putative nucleoside-diphosphate-sugar epimerase	73	0.004	
Afu4g12850	C6 transcription factor (AmyR), putative	74	0.373	integral to endoplasmic reticulum membrane///ER-associated protein catabolic process///molecular function unknown
Afu4g13780	calnexin	75	0.202	
Afu4g07370	conserved hypothetical protein	76	0.433	
Afu1g17000	sin3-associated polypeptide, 18kD	77	0.202	
Afu2g14950	exonuclease, putative	78	0.178	ribonuclease H activity///DNA replication///nucleus///RNA processing///3'-5' exonuclease activity

Afu8g04920	LEA domain protein	79	0.936	
Afu3g12780	C6 transcription factor, putative	80	0.007	
Afu2g14680	hypothetical protein	81	0.51	
Afu5g04410	feruloyl esterase, putative	82	0.461	
Afu3g02780	multidrug transporter, putative	83	0.333	integral to plasma membrane///multidrug transporter activity///response to toxin
Afu5g09150	amidase, putative	84	0.002	sporulation (sensu Saccharomyces)///peroxisomal matrix///fatty acid catabolic process///"2,4-dienoyl-CoA reductase (NADPH) activity"
Afu3g10320	Zinc finger, C3HC4 type (RING finger) domain protein	85	0.626	
Afu8g07210	FluG family protein	86	0.196	hydroxymethylglutaryl-CoA synthase activity///endoplasmic reticulum///mitochondrion///ergosterol biosynthetic process
Afu3g11930	NAD binding Rossmann fold oxidoreductase, putative	87	0.008	
Afu3g12810	transcriptional corepressor of histone genes (Hir3), putative	88	0.478	gene silencing///nucleosome assembly///nucleosome///transcription corepressor activity
Afu7g07170	CAIB/BAIF family enzyme	89	0.091	
Afu4g06880	MSF transporter, putative	90	0.121	
Afu4g00710	C6 transcription factor, putative	91	0.075	
Afu4g01480	HHE domain protein	92	0.239	plasma membrane///transporter activity///transport
Afu3g14010	DNA replication licensing factor Mcm2, putative	93	0.335	pre-replicative complex///DNA replication initiation///chromatin binding///cytoplasm///ATP-dependent DNA helicase activity///DNA unwinding during replication///nucleus///pre-replicative complex assembly
Afu5g00960	MFS transporter, putative	94	0.274	
Afu8g00330	phytanoyl-CoA dioxygenase family protein	95	0.092	
Afu8g00350	hydroxymethylgl	96	0.209	

	utaryl-CoA synthase			
Afu2g09120	SNF2 family helicase, putative	97	0.098	chromatin assembly or disassembly///nucleus///DNA-dependent ATPase activity
Afu1g14190	DUF614 domain protein	98	0.201	
Afu6g13150	hypothetical protein	99	0.285	
Afu2g15650	DUF323 domain protein	100	0.377	

3.4.2 Functional classification of differentially expressed genes between 4 and 14 hours post infection in Af293

Differentially expressed genes were grouped into functional categories based on GO Terms and by reference to the *A. fumigatus* literature. A summary of up and down expressed functional categories between 4 and 14 hours is given in Table 3.7.

Table 3.7: Functional classification of selected genes having differential transcript abundance in Af293 between 4 and 14 hours post infection in the murine lung. Increased (red) and decreased (green) are shown for each functional category. Both increasing and decreasing transcripts are sub divided into expression cohorts which are either high, moderate, and low with respect to their expression change. Genes within functional categories ranked according to greatest nSI intensity changes between 4 and 14 hours. A one-way ANOVA was conducted on nSI values between time-points, from which FDR correct *p*-values are reported for each gene.

Functional Category	ORF	Description	Rank	p-value	Magnitude	ORF	Description	Rank	p-value	Magnitude
Cell wall	Afu1g07110	related to export control protein CHS7	196	0.003	UP HIGH	Afu4g12900	alpha-1,6-mannosyltransferase subunit (Ecm39), putative	218	0.025	DOWN HIGH
	Afu1g12040	chitin biosynthesis protein (Chs7), putative	221	0.001	UP HIGH	Afu7g01540	endo-1,4-beta-glucanase	225	0.026	DOWN HIGH
	Afu6g09310	class V chitinase, putative	271	0.332	UP HIGH	Afu2g14910	alpha-1,6-mannosyltransferase subunit, putative	671	0.723	DOWN MOD
	Afu5g14060	Rho GTPase Rho4, putative	301	0.129	UP HIGH	Afu7g05140	class III chitinase, putative	820	0.471	DOWN MOD
	Afu3g10340	Rho GTPase Rho 2, putative	312	0.399	UP HIGH	Afu3g03870	endo-1,4-beta-glucanase, putative	875	0.584	DOWN MOD
	Afu1g15440	alpha-1,3-glucan synthase, putative	331	0.007	UP HIGH	Afu3g03080	endo-1,3(4)-beta-glucanase, putative	1473	0.856	DOWN LOW
	Afu1g00310	class V chitinase, putative	343	0.134	UP HIGH	Afu2g15910	aminonitrophenyl propanediol resistance protein	1687	0.871	DOWN LOW
	Afu3g12600	beta-glucosidase 1	475	0.082	UP HIGH	Afu5g00760	chitin synthase C	1859	0.895	DOWN LOW
	Afu2g13440	chitin synthase E	534	0.337	UP HIGH					
	Afu2g14360	GPI anchored glucanase, putative	583	0.202	UP HIGH					
	Afu5g03960	class V chitinase Chi100	641	0.215	UP HIGH					
	Afu8g05020	beta-N-acetylhexosaminidase NagA, putative	653	0.461	UP HIGH					
	Afu5g03760	class III chitinase	704	0.023	UP MOD					

		ChiA1							
	Afu6g12400	1,3-beta-glucan synthase catalytic subunit FksP	763	0.003	UP MOD				
	Afu6g09780	class V chitinase, putative	789	0.243	UP MOD				
	Afu5g08580	alpha-1,6-mannosyltransferase subunit (Och1), putative	804	0.378	UP MOD				
	Afu5g14030	endo-1,3(4)-beta-glucanase, putative	947	0.375	UP MOD				
	Afu2g01170	1,3-beta-glucanosyltransferase Gel1	1134	0.547	UP MOD				
	Afu3g11280	class V chitinase, putative	1349	0.429	UP LOW				
	Afu5g08550	Rho guanyl nucleotide exchange factor (Rom2), putative	1364	0.426	UP LOW				
	Afu8g00700	class III chitinase ChiA2	1397	0.565	UP LOW				
	Afu6g11390	1,3-beta-glucanosyltransferase Gel2	1492	0.032	UP LOW				
	Afu6g14540	endo-1,3(4)-beta-glucanase, putative	1508	0.516	UP LOW				
	Afu3g07110	class III chitinase, putative	1518	0.493	UP LOW				
	Afu2g03980	alpha-1,3-glucanase, putative	1815	0.426	UP LOW				
	Afu1g01380	alpha-1,6-mannosyltransferase subunit (Hoc1), putative	1824	0.156	UP LOW				
Ergosterol biosynthesis	Afu2g00320	sterol delta 5,6-desaturase, putative	128	0.202	UP HIGH	Afu4g12040	oxidosqualene:lanosterol cyclase	1095	0.314	DOWN MOD
	Afu2g17400	C-3 sterol dehydrogenase/C-4 decarboxylase	172	0.07	UP HIGH	Afu7g02480	oxysterol binding protein (Osh1), putative	1400	0.249	DOWN LOW
	Afu7g00300	squalene-hopene-cyclase, putative	240	0.006	UP HIGH	Afu4g06380	sterol carrier protein, putative	1555	0.786	DOWN LOW

	Afu5g07780	squalene monooxygenase Erg1	316	0.026	UP HIGH	Afu3g11750	oxysterol binding protein (Osh5), putative	1624	0.524	DOWN LOW
	Afu8g02440	C-4 methyl sterol oxidase, putative	375	0.102	UP HIGH					
	Afu7g00260	squalene-hopene-cyclase, putative	531	0.286	UP HIGH					
	Afu1g03950	cytochrome P450 sterol C-22 desaturase, putaitve	705	0.084	UP MOD					
	Afu8g01070	Lathosterol oxidase, putative	907	0.233	UP MOD					
	Afu1g03150	c-14 sterol reductase	1014	0.397	UP MOD					
	Afu1g06040	sterol o-acyltransferase (APE2), putaitve	1090	0.277	UP MOD					
	Afu5g04080	oxidosqualene:lanosterol cyclase	1117	0.6	UP MOD					
	Afu4g07780	mevalonate kinase	1158	0.386	UP MOD					
	Afu4g06890	14-alpha sterol demethylase Cyp51A	1233	0.537	UP MOD					
Microtubule	Afu2g07550	serine/threonine protein kinase (Ark1), putative	147	0.107	UP HIGH	Afu1g12820	gamma-tubulin complex component GCP6, putative	484	0.67	DOWN HIGH
	Afu3g11860	microtubule associated protein EB1, putative	279	0.064	UP HIGH	Afu4g07630	microtubule associated protein (Ytm1), putative	998	0.338	DOWN MOD
	Afu2g14280	kinesin family protein (KlpA), putative	353	0.077	UP HIGH	Afu4g07630	microtubule associated protein (Ytm1), putative	998	0.338	DOWN MOD
	Afu1g02550	tubulin alpha-1 subunit	414	0.217	UP HIGH	Afu2g15750	gamma-tubulin complex component GCP4, putative	1379	0.798	DOWN LOW
	Afu7g01400	kinesin family protein (BimC), putative	452	0.043	UP HIGH	Afu5g02730	gamma-tubulin complex component GCP5, putative	1533	0.247	DOWN LOW
	Afu2g14730	kinesin family protein	610	0.228	UP HIGH					
	Afu2g03150	kinesin family protein	627	0.086	UP HIGH					
	Afu3g12820	kinesin family protein	747	0.292	UP MOD					
	Afu5g11810	cytoplasmic dynein heavy chain	810	0.101	UP MOD					
	Afu1g10910	tubulin beta, putative	1070	0.416	UP MOD					
	Afu2g14990	tubulin alpha-2	1149	0.076	UP MOD					

		subunit								
	Afu6g12840	kinesin family protein	1382	0.725	UP LOW					
	Afu2g16260	microtubule associated protein (Ase1), putative	1632	0.319	UP LOW					
Cell polarity	Afu5g14060	Rho GTPase Rho4, putative	301	0.129	UP HIGH	Afu4g10490	related to protein transport protein SEC6	1264	0.38	DOWN MOD
	Afu5g07710	nuclear migration protein (ApsA), putative	386	0.006	UP HIGH	Afu1g04360	exocyst complex component sec3, putative	1271	0.566	DOWN MOD
	Afu2g01000	LIM domain protein	437	0.084	UP HIGH					
	Afu1g05130	PH domain protein	597	0.034	UP HIGH					
	Afu7g04300	RhoGAP and Fes/CIP4 domain protein	731	0.095	UP MOD					
	Afu5g03080	septin	795	0.057	UP MOD					
	Afu2g02520	cell polarity protein (Tea1), putative	970	0.128	UP MOD					
	Afu6g02620	conserved hypothetical protein	1024	0.688	UP MOD					
	Afu7g05340	conserved hypothetical protein	1115	0.016	UP MOD					
	Afu2g03710	cell polarity protein, putative	1128	0.094	UP MOD					
	Afu1g05610	protein phosphotase 2a 65kd regulatory sububit	1537	0.44	UP LOW					
	Afu3g10250	phosphoprotein	1568	0.298	UP LOW					
	Afu2g12390	protein kinase regulator (Mob1), putative	1643	0.388	UP LOW					
	Afu1g08850	septin	1896	0.659	UP LOW					
Ion transport	Afu2g03730	Ctr copper transporter family protein	79	0.032	UP HIGH	Afu2g08070	CorA family metal ion transporter, putative	564	0.542	DOWN HIGH
	Afu2g07630	vacuolar H+\Ca2+ exchanger	396	0.446	UP HIGH	Afu6g02550	magnesium ion transporter (Mrs2), putative	839	0.771	DOWN MOD
	Afu6g02810	Ctr copper transporter family family	371	0.172	UP HIGH	Afu8g01890	Na+/H+ exchanger family protein, putative	1055	0.279	DOWN MOD

	Afu1g01550	high affinity zinc ion transporter, putative	427	0.029	UP HIGH	Afu2g17170	Na+/H+ antiporter Nha1	1069	0.784	DOWN MOD
	Afu7g06570	zinc/cadmium resistance protein	520	0.216	UP HIGH	Afu4g00930	CorA family metal ion transporter, putative	1543	0.253	DOWN LOW
	Afu3g10690	calcium-translocating P-type ATPase(PMCA-type),putative	695	0.564	UP MOD	Afu5g06220	sodium/hydrogen exchanger 3	1845	0.906	DOWN LOW
	Afu1g02930	Ca2+ binding protein (calmodulin), putative	719	0.35	UP MOD	Afu1g14250	potassium channel, putative	1848	0.777	DOWN LOW
	Afu4g12620	copper-transporting ATPase, putative	901	0.039	UP MOD					
	Afu4g09560	ZIP Zinc transporter, putative	981	0.211	UP MOD					
	Afu2g03860	plasma membrane low affinity zinc ion transporter, putative	991	0.347	UP MOD					
	Afu1g16340	potassium transporter, putative	1201	0.633	UP MOD					
	Afu1g16340	potassium transporter, putative	1201	0.633	UP MOD					
	Afu8g01480	potassium channel, putative	1333	0.394	UP LOW					
	Afu8g01480	potassium channel, putative	1333	0.394	UP LOW					
	Afu5g03550	plasma membrane H(+)ATPase, putative	1440	0.297	UP LOW					
	Afu6g07050	sodium-hydrogen antiporter, putative	1512	0.68	UP LOW					
	Afu1g02480	plasma membrane ATPase, putative	1774	0.554	UP LOW					
	Afu6g14240	calcium sensor (NCS-1), putative	1778	0.025	UP LOW					
	Afu1g16130	copper-transporting ATPase, putative	1814	0.121	UP LOW					
Iron acquisition	Afu1g17270	ferric-chelate reductase (Fre2), putative	61	0.061	UP HIGH	Afu4g14640	low affinity iron transporter, putative	602	0.611	DOWN HIGH
	Afu6g13750	ferric-chelate reductase, putative	209	0.011	UP HIGH	Afu6g12870	mitochondrial ABC-type iron exporter (Atm1), putative	817	0.333	DOWN MOD

	Afu2g05730	siderochrome-iron transporter (MirC), putative	292	0.234	UP HIGH					
	Afu3g03400	siderophore biosynthesis acetylase AceI, putative	847	0.121	UP MOD					
	Afu3g03440	MFS family siderophore transporter, putative	937	0.075	UP MOD					
	Afu3g13670	siderochrome-iron transporter, putative	1193	0.196	UP MOD					
	Afu7g06060	siderochrome-iron transporter (Sit1), putative	1262	0.052	UP MOD					
Antigen	Afu4g00610	aryl-alcohol dehydrogenase, putative	100	0.068	UP HIGH	Afu4g09090	thioredoxin, putative	697	0.063	DOWN MOD
	Afu1g14550	Mn superoxide dismutase MnSOD	132	0.003	UP HIGH	Afu1g06830	60s Acidic ribosomal protein superfamily	1348	0.298	DOWN LOW
	Afu2g03830	allergen Asp F4	142	0.332	UP HIGH	Afu2g03720	peptidyl-prolyl cis-trans isomerase	1429	0.857	DOWN LOW
	Afu4g11800	alkaline serine protease Alp1	161	0.004	UP HIGH	Afu5g09580	conidial hydrophobin Hyp1/RodA	1441	0.828	DOWN LOW
	Afu1g09670	HLH transcription factor (GlcD gamma), putative	230	0.026	UP HIGH	Afu2g06150	disulfide isomerase, putative	1636	0.397	DOWN LOW
	Afu5g13300	aspartic endopeptidase Pep1	420	0.075	UP HIGH	Afu2g11850	large subunit ribosomal protein L3	1666	0.861	DOWN LOW
	Afu1g16190	cell wall glucanase Crf1	424	0.095	UP HIGH	Afu3g02940	allergen, putative	1856	0.84	DOWN LOW
	Afu4g06670	allergen Asp F7	467	0.076	UP HIGH					
	Afu4g09580	major allergen Asp F2	513	0.038	UP HIGH					
	Afu8g05020	beta-N-acetylhexosaminidase NagA, putative	653	0.461	UP HIGH					
	Afu1g02820	Y20 protein	697	0.223	UP HIGH					
	Afu6g06770	enolase	1125	0.053	UP MOD					

	Afu6g11330	histidine acid phosphatase, putative	1335	0.38	UP LOW					
	Afu2g12630	allergen Asp F13	1795	0.65	UP LOW					
	Afu6g02280	allergen Asp F3	1956	0.296	UP LOW					
Secreted proteases	Afu2g17330	serine peptidase, family S28, putative	18	0	UP HIGH	Afu4g09030	aminopeptidase	112	0.004	DOWN HIGH
	Afu6g12420	SprT family metallopeptidase, putative	63	0.039	UP HIGH					
	Afu8g07080	elastinolytic metalloproteinase Mep	125	0	UP HIGH					
	Afu4g11800	alkaline serine protease Alp1	161	0.004	UP HIGH					
	Afu3g00650	aminopeptidase Y, putative	241	0.023	UP HIGH					
	Afu5g03400	SH3 domain protein (Cyk3), putative	394	0.322	UP HIGH					
	Afu5g13300	aspartic endopeptidase Pep1	420	0.075	UP HIGH					
	Afu4g14000	tripeptidyl peptidase A	515	0.283	UP HIGH					
	Afu1g02700	zinc metallopeptidase, putative	982	0.343	UP MOD					
	Afu2g01250	serine peptidase, family S28, putative	1010	0.047	UP MOD					
	Afu1g04950	serine/threonine protein phosphatase pp1	1283	0.146	UP MOD					
Secretion peptide encoding genes	Afu6g09670	cytochrome P450 oxidoreductase GliC	2	0.007	UP HIGH	Afu6g02980	extracellular exo-polygalacturonase, putative	2	0.004	UP HIGH
	Afu8g00610	cell surface protein Mas1, putative	7	0.03	UP HIGH	Afu1g16420	GPI anchored protein, putative	3	0.07	UP HIGH
	Afu6g06360	mating alpha-pheromone PpgA	15	0.002	UP HIGH	Afu2g05350	major facilitator superfamily protein superfamily	7	0.096	UP HIGH
	Afu6g00430	IgE-binding protein	23	0.008	UP HIGH	Afu8g02630	extracellular exo-polygalacturonase, putative	10	0.066	UP HIGH
	Afu1g01300	GPI anchored protein, putative	24	0.003	UP HIGH	Afu2g01240	beta-D-fructofuranoside fructohydrolase	18	0.083	UP HIGH
	Afu1g01310	carboxylesterase, putative	28	0.008	UP HIGH	Afu2g17920	hypothetical protein	42	0.469	UP HIGH

	Afu1g14560	alpha-mannosidase	34	0.007	UP HIGH	Afu1g08970	conserved hypothetical protein	57	0.329	UP HIGH
	Afu3g09960	aureobasidin resistance protein Aur1	43	0.017	UP HIGH	Afu4g09470	cytochrome P450 monooxygenase, putative	63	0.501	UP HIGH
	Afu2g14420	cutinase, putative	44	0.043	UP HIGH	Afu4g12850	calnexin	74	0.202	UP HIGH
	Afu7g06810	L-amino acid oxidase LaoA, putative	46	0.004	UP HIGH	Afu4g09030	aminopeptidase	112	0.004	UP HIGH
	Afu4g00750	hypothetical protein	51	0.03	UP HIGH	Afu3g08070	GMC oxidoreductase, putative	122	0.117	UP HIGH
	Afu3g09260	hypothetical protein	52	0.01	UP HIGH	Afu8g01900	hypothetical protein	126	0.483	UP HIGH
	Afu1g12350	extracellular fruiting body protein, putative	131	0.03	UP HIGH	Afu2g11130	NOT2 family protein	135	0.465	UP HIGH
	Afu7g00970	GPI-anchored serine-threonine rich protein	193	0.03	UP HIGH	Afu7g04720	alpha-1,2-mannosidase, putative	139	0.461	UP HIGH
	Afu4g13750	Deuterolysin metalloprotease, putative	194	0.032	UP HIGH	Afu2g14220	conserved hypothetical protein	157	0.139	UP HIGH
	Afu2g10130	phase-specific adhesin, putative	201	0.038	UP HIGH	Afu1g10800	thioesterase family protein	164	0.042	UP HIGH
	Afu3g14980	extracellular chitosanase CsnC, putative	252	0.02	UP HIGH	Afu6g10040	fructosyl amine: oxygen oxidoreductase	177	0.249	UP HIGH
	Afu6g09310	class V chitinase, putative	271	0.332	UP HIGH	Afu4g10150	alpha-glucosidase	183	0.43	UP HIGH
	Afu4g01290	endo-chitosanase, pseudogene	272	0.084	UP HIGH	Afu2g08500	carboxylesterase, putative	210	0.41	UP HIGH
	Afu2g14480	oxidoreductase, FAD-binding, putative	276	0.053	UP HIGH	Afu4g12900	alpha-1,6-mannosyltransferase subunit (Ecm39), putative	218	0.025	UP HIGH
Pathogenesis	Afu1g13140	G protein complex alpha subunit GpaA	40	0.008	UP HIGH	Afu2g17600	polyketide synthetase PksP	4	0.029	DOWN HIGH
	Afu8g07080	elastinolytic metalloproteinase Mep	125	0	UP HIGH	Afu8g02380	FAD-dependent monooxygenase, putative	107	0.489	DOWN HIGH
	Afu2g03830	allergen Asp F4	142	0.332	UP HIGH	Afu5g09580	conidial hydrophobin Hyp1/RodA	1441	0.828	DOWN LOW
	Afu1g15440	alpha-1,3-glucan synthase, putative	331	0.007	UP HIGH	Afu5g09250	transcription factor (Snd1/p100), putative	1700	0.613	DOWN LOW
	Afu5g06070	ABC multidrug transporter Mdr1	459	0.079	UP HIGH	Afu7g05060	MgtC/SapB family membrane protein	1743	0.831	DOWN LOW

	Afu1g12930	G protein complex alpha subunit GpaB	484	0.052	UP HIGH	Afu3g10000	cAMP-dependent protein kinase regulatory subunit PkaR	1911	0.604	DOWN LOW
	Afu2g13440	chitin synthase E	534	0.337	UP HIGH					
	Afu2g07680	L-ornithine N5-oxygenase SidA	539	0.092	UP HIGH					
	Afu3g00590	Asp-hemolysin	814	0.416	UP MOD					
	Afu2g17560	1,3,6,8-tetrahydroxynaphthalene reductase	1214	0.2	UP MOD					
	Afu5g00600	NPP1 domain protein, putative	1935	0.068	UP LOW					
Secondary metabolism	Afu8g00540	hybrid polyketide synthase/nonribosomal peptide synthase, putative	307	0.4	UP HIGH	Afu2g17600	polyketide synthetase PksP	4	0.029	DOWN HIGH
	Afu3g01410	polyketide synthase, putative	478	0.455	UP HIGH	Afu3g12940	C6 transcription factor, putative	194	0.67	DOWN HIGH
	Afu5g00350	nonribosomal peptide synthetase, putative	961	0.759	UP MOD	Afu1g17710	C6 transcription factor, putative	288	0.701	DOWN HIGH
	Afu6g03480	nonribosomal peptide synthetase, putative	973	0.425	UP MOD	Afu3g12920	nonribosomal peptide synthase (GliP), putative	376	0.575	DOWN HIGH
	Afu3g12890	C6 transcription factor (GliZ), putative	1160	0.09	UP MOD	Afu8g00420	C6 finger transcription factor, putative	978	0.82	DOWN MOD
	Afu5g12730	nonribosomal peptide synthase, putative	1248	0.36	UP MOD	Afu8g00490	polyketide synthase, putative	1467	0.921	DOWN LOW
	Afu8g00370	polyketide synthase, putative	1413	0.286	UP LOW	Afu4g14590	C6 transcription factor, putative	1496	0.903	DOWN LOW
	Afu6g12050	nonribosomal peptide synthase, putative	1433	0.248	UP LOW	Afu3g13600	C6 transcription factor, putative	1607	0.874	DOWN LOW
	Afu4g14680	C6 transcription factor, putative	1593	0.492	UP LOW	Afu4g14440	nonribosomal peptide synthase, putative	1753	0.888	DOWN LOW
	Afu1g17640	melanin biosynthesis transcription factor RegA	1825	0.483	UP LOW					
Gliotoxin	Afu6g09690	glutathione S-transferase GliG	1	0.006	UP HIGH	Afu6g09580	hypothetical protein	960	0.584	DOWN MOD
	Afu6g09670	cytochrome P450 oxidoreductase GliC	2	0.007	UP HIGH	Afu6g09600	peptidase, putative	988	0.331	DOWN MOD

	Afu6g09680	O-methyltransferase GliM	4	0.034	UP HIGH	Afu6g09590	zinc-containing alcohol dehydrogenase, putative	1603	0.837	DOWN LOW
	Afu6g09730	cytochrome P450 oxidoreductase GliF	6	0.012	UP HIGH	Afu6g09760	toxin biosynthesis cytochrome P450 oxidoreductase, putative	1618	0.894	DOWN LOW
	Afu6g09710	MFS gliotoxin efflux pump GliA	14	0.052	UP HIGH					
	Afu6g09650	membrane dipeptidase GliJ	25	0.005	UP HIGH					
	Afu6g09740	thioredoxin reductase GliT	37	0.008	UP HIGH					
	Afu6g09640	aminotransferase GliI	53	0.027	UP HIGH					
Pseurotin A supercluster	Afu8g00610	cell surface protein Mas1, putative	7	0.03	UP HIGH	Afu8g00230	phytanoyl-CoA dioxygenase family protein	52	0.092	DOWN HIGH
	Afu8g00540	hybrid polyketide synthase/nonribosomal peptide synthase, putative	307	0.4	UP HIGH	Afu8g00330	endonuclease/reverse transcriptase/RNaseH, putative	95	0.142	DOWN HIGH
	Afu8g00280	short-chain dehydrogenase, putative	327	0.404	UP HIGH	Afu8g00350	conserved hypothetical protein	96	0.558	DOWN HIGH
	Afu8g00240	cytochrome P450 monooxygenase, putative	330	0.355	UP HIGH	Afu8g00110	oxidoreductase, 2OG-Fe(II) oxygenase family, putative	187	0.074	DOWN HIGH
	Afu8g00360	NlpC/P60-like cell-wall peptidase, putative	887	0.461	UP MOD	Afu8g00220	cytochrome P450, putative	250	0.516	DOWN HIGH
	Afu8g00680	glycosyl transferase, group 2 family protein	1122	0.24	UP MOD	Afu8g00720	amino acid transporter, putative	321	0.002	DOWN HIGH
	Afu8g00460	methionine aminopeptidase, type I, putative	1263	0.615	UP MOD	Afu8g00390	O-methyltransferase, putative	428	0.784	DOWN HIGH
	Afu8g00470	conserved hypothetical protein	1309	0.281	UP MOD	Afu8g00710	secreted antimicrobial peptide, putative	911	0.731	DOWN MOD
	Afu8g00260	F-box domain and ankyrin repeat protein	1351	0.349	UP LOW	Afu8g00310	LINE-1 class reverse transcriptase, RNaseH, putative	942	0.722	DOWN MOD
	Afu8g00700	class III chitinase ChiA2	1397	0.565	UP LOW	Afu8g00420	C6 finger transcription factor, putative	978	0.82	DOWN MOD
	Afu8g00370	polyketide synthase, putative	1413	0.286	UP LOW	Afu8g00550	SirN-like methyltransferase, putative	1099	0.732	DOWN MOD
	Afu8g00290	conserved hypothetical protein	1545	0.668	UP LOW	Afu8g00450		1103	0.302	DOWN MOD

	Afu8g00300	conserved hypothetical protein	1738	0.639	UP LOW	Afu8g00150	conserved hypothetical protein	1119	0.384	DOWN MOD
	Afu8g00440	steroid monooxygenase, putative	1884	0.689	UP LOW	Afu8g00490	polyketide synthase, putative	1464	0.921	DOWN LOW
						Afu8g00570	alpha/beta hydrolase, putative	1499	0.81	DOWN LOW
Secondary metabolite cluster 5	Afu3g01490	alcohol dehydrogenase, putative	70	0.004	UP HIGH	Afu3g01330	class II aldolase/adducin domain protein	767	0.515	DOWN MOD
	Afu3g01500	integral membrane protein	74	0.043	UP HIGH	Afu3g01300	hypothetical protein	856	0.471	DOWN MOD
	Afu3g01580	GMC oxidoreductase, putative	432	0.112	UP HIGH	Afu3g01370	MFS transporter, putative	1131	0.082	DOWN MOD
	Afu3g01410	polyketide synthase, putative	478	0.455	UP HIGH	Afu3g01540	MFS monocarboxylate transporter, putative	1524	0.867	DOWN LOW
	Afu3g01440	DUF1212 domain membrane protein	707	0.032	UP MOD	Afu3g01460	salicylate hydroxylase, putative	1844	0.649	DOWN LOW
	Afu3g01590	hypothetical protein	754	0.132	UP MOD					
	Afu3g01350	proteinase, putative	860	0.598	UP MOD					
	Afu3g01390	hypothetical protein	1374	0.536	UP LOW					
	Afu3g01400	ABC multidrug transporter, putative	1585	0.774	UP LOW					
	Afu3g01480	conserved hypothetical protein	1638	0.586	UP LOW					
Secondary metabolite cluster 13	Afu4g14730	GNAT family acetyltransferase, putative	76	0.032	UP HIGH	Afu4g14570	metallo-beta-lactamase domain protein, putative	132	0.078	DOWN HIGH
	Afu4g14380	conserved hypothetical protein	744	0.092	UP MOD	Afu4g14780	cytochrome P450 monooxygenase, putative	184	0.511	DOWN HIGH
	Afu4g14660	conserved hypothetical protein	1272	0.202	UP MOD	Afu4g14430		224	0.61	DOWN HIGH
	Afu4g14410	hypothetical protein	1439	0.5	UP LOW	Afu4g14530	glutathione S-transferase, putative	356	0.579	DOWN HIGH
	Afu4g14650	ribokinase	1521	0.094	UP LOW	Afu4g14640	low affinity iron transporter, putative	602	0.611	DOWN HIGH
	Afu4g14670	MFS quinate transporter, putative	1550	0.3	UP LOW	Afu4g14460	hypothetical protein	676	0.733	DOWN MOD
	Afu4g14680	C6 transcription factor, putative	1593	0.492	UP LOW	Afu4g14760	ABC multidrug transporter, putative	728	0.419	DOWN MOD

	Afu4g14850	extracellular 3-ketosteroid 1-dehydrogenase, putative	1662	0.604	UP LOW	Afu4g14480	hypothetical protein	849	0.647	DOWN MOD
	Afu4g14520	toxin biosynthesis protein, putative	1687	0.179	UP LOW	Afu4g14600	UPF0075 domain protein	1104	0.867	DOWN MOD
	Afu4g14830	cytochrome P450 monooxygenase, putative	1745	0.71	UP LOW	Afu4g14590	C6 transcription factor, putative	1496	0.903	DOWN LOW
	Afu4g14630	FAD binding domain protein	1846	0.786	UP LOW	Afu4g14440	nonribosomal peptide synthase, putative	1753	0.888	DOWN LOW
	Afu4g14820	transferase family protein	1952	0.722	UP LOW					
Ribosome biogenesis and RNA metabolism	Afu1g17120	elongation factor-1 gamma	237	0.152	UP HIGH	Afu5g11000	small nuclear ribonucleoprotein U2, A'	67	0.386	DOWN HIGH
	Afu3g08160	eukaryotic translation initiation factor eIF4A, putative	572	0.239	UP HIGH	Afu2g08520	50S ribosomal protein L14	331	0.563	DOWN HIGH
	Afu6g08430	conserved hypothetical protein	748	0.24	UP MOD	Afu4g06350	rna binding protein	375	0.607	DOWN HIGH
	Afu8g02750	nucleolar protein CgrA	757	0.305	UP MOD	Afu1g04840	RNP domain protein	448	0.561	DOWN HIGH
	Afu3g08580	glycine-rich RNA-binding protein, putative	874	0.03	UP MOD	Afu1g10990	ribosomal RNA processing protein, putative	487	0.636	DOWN HIGH
	Afu3g09820	C2H2 transcription factor, putative	868	0.315	UP MOD	Afu2g12890	small nucleolar ribonucleoprotein complex subunit, putative	547	0.789	DOWN HIGH
	Afu3g10030	forkhead domain protein	1165	0.471	UP MOD	Afu3g05840	RNA-binding protein rnp24, putative	553	0.469	DOWN HIGH
	Afu6g02520	Eukaryotic initiation factor 1A, putative	1420	0.138	UP LOW	Afu1g06770	Ribosomal protein S26e	587	0.132	DOWN HIGH
	Afu3g07680	ran GTPase activating protein 1 (RNA1 protein)	1670	0.675	UP LOW	Afu1g02680	small nucleolar ribonucleoprotein complex subunit Dip2, putative	591	0.034	DOWN HIGH
	Afu3g06790	RNA-directed RNA polymerase (Sad-1), putative	1960	0.481	UP LOW	Afu3g11410	RNA Polymerase II CTD phosphatase Fcp1, putative	606	0.759	DOWN HIGH
						Afu3g10380	RNA polymerase III transcription factor, putative	640	0.045	DOWN HIGH
						Afu1g15020	40S ribosomal protein S5	759	0.655	DOWN MOD

Afu4g07540	small nucleolar ribonucleoprotein complex subunit, putative	782	0.085	DOWN MOD
Afu1g07350	RNA12 protein, putative	803	0.565	DOWN MOD
Afu2g16880	ribosomal protein L37a	896	0.313	DOWN MOD
Afu5g05930	RNA processing factor 1	898	0.82	DOWN MOD
Afu3g13320	40S ribosomal protein S0, putative	932	0.102	DOWN MOD
Afu7g02080	RNA polymerase I subunit Rpa43, putative	958	0.232	DOWN MOD
Afu1g06290	small nucleolar ribonucleoprotein complex subunit (SOF1), putative	973	0.387	DOWN MOD
Afu1g05080	ribosomal protein P0	977	0.125	DOWN MOD
Afu1g11670	small nuclear ribonucleoprotein (LSM8), putative	1012	0.686	DOWN MOD
Afu2g05110	small nuclear ribonucleoprotein SmD1, putative	1019	0.65	DOWN MOD
Afu5g07390	ribosomal large subunit assembly protein (Sqt1), putative	1072	0.089	DOWN MOD
Afu1g03390	60S ribosomal protein L12	1087	0.079	DOWN MOD
Afu8g04960	small nuclear ribonucleoprotein SmG, putative	1142	0.565	DOWN MOD
Afu2g07970	ribosomal protein L19	1196	0.5	DOWN MOD
Afu4g07640	ribosomal protein S13	1211	0.346	DOWN MOD
Afu6g02440	60s ribosomal protein L24, putative	1228	0.543	DOWN MOD
Afu2g10500	ribosomal protein S9	1232	0.616	DOWN MOD
Afu8g04400	RNA binding protein, putative	1252	0.337	DOWN MOD
Afu3g12300	Ribosomal L22e protein family	1259	0.739	DOWN MOD

Afu7g01330	RNA binding complex component (TraX), putative	1290	0.363	DOWN MOD
Afu1g06830	60s Acidic ribosomal protein superfamily	1348	0.298	DOWN LOW
Afu2g16370	Ribosomal protein L32	1370	0.613	DOWN LOW
Afu1g06340	60S ribosomal protein L27	1449	0.65	DOWN LOW
Afu5g03090	small nucleolar ribonucleoprotein complex subunit (Pwp2), putative	1484	0.249	DOWN LOW
Afu3g09620	RNA recognition motif. (a.k.a. RRM, RBD, or RNP domain) protein	1550	0.723	DOWN LOW
Afu6g10370	RNA lariat debranching enzyme, putative	1588	0.898	DOWN LOW
Afu1g10510	60S ribosomal protein L35, putative	1643	0.544	DOWN LOW
Afu2g02270	ribosomal protein S14p/S29e	1661	0.787	DOWN LOW
Afu2g08130	ribosomal protein L41	1673	0.545	DOWN LOW
Afu4g07440	Ribosomal protein L36e, putative	1704	0.366	DOWN LOW
Afu6g08040	RNP domain protein	1713	0.156	DOWN LOW
Afu2g05930	small nucleolar ribonucleoprotein complex subunit, putative	1736	0.802	DOWN LOW
Afu6g04810	RNA polymerase II transcription mediator complex subunit (Med6), putative	1741	0.852	DOWN LOW
Afu1g14410	60s ribosomal protein yl17-b	1766	0.69	DOWN LOW

						Afu3g06310	RNA binding protein	1798	0.846	DOWN LOW
						Afu1g12590	RNA-binding La domain protein	1804	0.763	DOWN LOW
						Afu1g11130	60S ribosomal protein yl16a	1838	0.659	DOWN LOW
						Afu2g10440	ribosomal protein S14.e	1915	0.737	DOWN LOW
						Afu2g15210	small nuclear ribonucleoprotein (LSM2), putative	1952	0.711	DOWN LOW
						Afu1g04530	Ribosomal L18ae protein family	1959	0.708	DOWN LOW
						Afu5g13470	60S acidic ribosomal protein, putative	1965	0.704	DOWN LOW
						Afu2g13090	RNA polymerase II subunit 3	1966	0.941	DOWN LOW
						Afu1g04280	Ribosomal protein S7p/S5e, putative	1969	0.26	DOWN LOW
Sugar transport	Afu3g01700	maltose permease	463	0.17	UP HIGH	Afu8g06870	MFS sugar transporter, putative	9	0.022	DOWN HIGH
	Afu3g01670	MFS hexose transporter, putative	506	0.235	UP HIGH	Afu1g16390	MFS hexose transporter, putative	219	0.186	DOWN HIGH
	Afu3g14170	high-affinity hexose transporter	931	0.298	UP MOD	Afu3g02890	MFS sugar transporter, putative	227	0.286	DOWN HIGH
	Afu6g14500	MFS sugar transporter, putative	1188	0.262	UP MOD	Afu8g02010	MFS sugar transporter, putative	296	0.455	DOWN HIGH
	Afu4g06630	MFS monosaccharide transporter, putative	1251	0.471	UP MOD	Afu8g01180	MFS sugar transporter, putative	311	0.715	DOWN HIGH
	Afu7g05830	MFS sugar transporter, putative	1298	0.375	UP MOD	Afu8g05710	MFS sugar transporter Stl1, putative	625	0.079	DOWN HIGH
	Afu1g11050	MFS sugar transporter, putative	1564	0.36	UP LOW	Afu7g06380	maltase	733	0.22	DOWN MOD
	Afu3g03320	MFS monocarboxylate transporter, putative	1904	0.559	UP LOW	Afu7g00950	MFS monosaccharide transporter, putative	1063	0.613	DOWN MOD

	Afu7g00220	plasma membrane hexose transporter, putative	1950	0.735	UP LOW	Afu4g00800	MFS monosaccharide transporter, putative	1386	0.633	DOWN LOW
						Afu6g01860	MFS lactose permease, putative	1460	0.781	DOWN LOW
						Afu7g05100	hexose transporter protein	1663	0.374	DOWN LOW
Amino acid transport	Afu5g14660	GABA permease, putative	87	0.02	UP HIGH	Afu3g11490	GABA permease, putative	314	0.262	DOWN HIGH
	Afu5g09300	amino acid transporter, putative	129	0.251	UP HIGH	Afu8g00720	amino acid transporter, putative	321	0.002	DOWN HIGH
	Afu5g00710	GABA permease, putative	519	0.492	UP HIGH	Afu5g01510	amino acid transporter	691	0.806	DOWN MOD
	Afu1g09120	amino acid permease, putative	547	0.128	UP HIGH	Afu2g17790	amino acid transporter, putative	746	0.087	DOWN MOD
	Afu3g01820	amino acid permease	825	0.235	UP MOD	Afu7g00440	GABA permease, putative	781	0.658	DOWN MOD
	Afu2g01370	GABA permease, putative	922	0.144	UP MOD	Afu5g02790	amino acid permease	1101	0.754	DOWN MOD
	Afu1g14700	allantoate transporter, putative	1129	0.598	UP MOD	Afu1g12310	GABA permease GabA	1668	0.834	DOWN LOW
	Afu6g04990	amino acid transporter, putative	1181	0.23	UP MOD					
	Afu8g06090	amino acid permease, putative	1260	0.239	UP MOD					
	Afu5g09440	amino acid permease, putative	1280	0.599	UP MOD					
	Afu2g11220	proline permease, putative	1479	0.732	UP LOW					
	Afu8g07200	neutral amino acid permease	1752	0.565	UP LOW					
	Afu3g00120	amino acid transporter, putative	1791	0.803	UP LOW					
Protein and carbohydrate glycosylation	Afu4g14070	glycosyl transferase, putative	5	0.043	UP HIGH	Afu1g10780	glycine cleavage system T protein	256	0.045	DOWN HIGH
	Afu8g06980	glycosyl hydrolase, putative	661	0.579	UP MOD	Afu1g02140	glycogen debranching enzyme, putative	531	0.268	DOWN HIGH
	Afu4g13770	glycosyl hydrolase, putative	865	0.524	UP MOD	Afu6g05120	glycogen synthase kinase-3, putative	533	0.252	DOWN HIGH
	Afu5g00670	glycosyl hydrolase	900	0.612	UP MOD	Afu4g11730	glycerol dehydrogenase (GldB),	975	0.152	DOWN

		family 35, putative					putative			MOD
	Afu8g00680	glycosyl transferase, group 2 family protein	1122	0.24	UP MOD	Afu2g03270	glycosyl hydrolase, putative	1006	0.505	DOWN MOD
	Afu4g13400	glycosyltransferase family 28, putative	1230	0.323	UP MOD	Afu3g02040	glycosyl hydrolase, putative	1444	0.934	DOWN LOW
	Afu4g00390	glycosyl hydrolase, putative	1284	0.61	UP MOD	Afu7g02290	ER glycosyl hydrolase (Edem), putative	1506	0.907	DOWN LOW
	Afu3g03620	glycosyl transferase, putative	1421	0.106	UP LOW	Afu1g02150	glycerol 3-phosphate dehydrogenase (GfdA), putative	1691	0.825	DOWN LOW
	Afu8g02070	glycosyl transferase, putative	1787	0.618	UP LOW	Afu1g08810	glycerol-3-phosphate dehydrogenase, mitochondrial	1723	0.493	DOWN LOW
						Afu1g09930	glycerol dehydrogenase (GCY1), putative	1728	0.604	DOWN LOW
						Afu8g02320	glycosyl transferase, group 2 family protein domain protein	1752	0.891	DOWN LOW
						Afu3g00700	glycosyl hydrolase, putative	1858	0.906	DOWN LOW
						Afu6g12010	glycosyl hydrolase, family 3, putative	1882	0.948	DOWN LOW
Transposition associated	Afu1g10020	reverse transcriptase, RNaseH	480	0.377	UP HIGH	Afu3g09410	reverse transcriptase	5	0.035	DOWN HIGH
	Afu6g09940	transposase	486	0.09	UP HIGH	Afu7g07170	reverse transcriptase/protease/endonuclease Pol, putative	89	0.249	DOWN HIGH
	Afu3g06810	possible transposase	587	0.179	UP HIGH	Afu4g01630	reverse transcriptase, putative	418	0.815	DOWN HIGH
	Afu7g02160	DDE superfamily endonuclease/transposase	673	0.461	UP MOD	Afu2g03570	transposase	530	0.471	DOWN HIGH
	Afu3g09440	reverse transcriptase, RNaseH, putative	723	0.565	UP MOD	Afu8g06290	LINE-1 class reverse transcriptase, RNaseH, putative	563	0.719	DOWN HIGH
	Afu1g00940	Tc1-mariner class transposase, putative	792	0.602	UP MOD	Afu4g00820	reverse transcriptase, RNaseH	608	0.704	DOWN HIGH

	Afu7g06870	Tf1-like reverse transcriptase, integrase, putative	908	0.489	UP MOD	Afu6g14660	reverse transcriptase, RNaseH	808	0.731	DOWN MOD
	Afu1g05480	transposase	1063	0.566	UP MOD	Afu8g00310	LINE-1 class reverse transcriptase, RNaseH, putative	942	0.722	DOWN MOD
	Afu7g07070	LINE-1 class reverse transcriptase, RNaseH, putative	1079	0.556	UP MOD	Afu6g09470	reverse transcriptase, RNaseH, putative	1009	0.829	DOWN MOD
	Afu5g13900	transposase	1174	0.038	UP MOD	Afu7g06930	reverse transcriptase, RNaseH	1437	0.836	DOWN LOW
	Afu7g03810	possible transposase	1317	0.053	UP LOW	Afu7g08210	reverse transcriptase, putative	1567	0.84	DOWN LOW
	Afu3g10430	transposase	1401	0.002	UP LOW	Afu7g00100	LINE-1 class reverse transcriptase, RNaseH, putative	1824	0.92	DOWN LOW
	Afu5g04110	Fot1 family transposase, putative	1422	0.529	UP LOW					
	Afu5g06180	possible transposase	1514	0.335	UP LOW					
	Afu1g08780	transposase	1706	0.048	UP LOW					
	Afu6g03650	possible transposase	1720	0.182	UP LOW					
	Afu3g01740	transposase	1810	0.027	UP LOW					
	Afu1g00140	Fot5 transposase, putative	1821	0.197	UP LOW					
	Afu7g02580	transposase	1870	0.509	UP LOW					
	Afu3g03090	transposase	1957	0.38	UP LOW					
Transcription factors	Afu5g14230	C6 transcription factor, putative	11	0.036	UP HIGH	Afu2g05360	C6 transcription factor, putative	1	0.002	DOWN HIGH
	Afu2g10550	C2H2 transcription factor (RfeC), putative	150	0.081	UP HIGH	Afu2g14120	C6 finger domain protein, putative	26	0.082	DOWN HIGH
	Afu4g01390	C6 transcription factor, putative	297	0.164	UP HIGH	Afu4g10160	C6 transcription factor (AmyR), putative	45	0.373	DOWN HIGH
	Afu8g01140	C6 transcription factor, putative	302	0.063	UP HIGH	Afu5g12020	C6 transcription factor (NirA), putative	405	0.614	DOWN HIGH
	Afu4g01010	C6 transcription factor, putative	347	0.079	UP HIGH	Afu3g02320	C2H2 finger domain protein (Kin17), putative	451	0.51	DOWN HIGH
	Afu6g14350	C6 transcription factor, putative	382	0.25	UP HIGH	Afu1g01560	C6 finger domain protein, putative	583	0.206	DOWN HIGH
	Afu8g05270	C6 transcription factor, putative	451	0.261	UP HIGH	Afu5g01460	C6 finger domain protein, putative	663	0.296	DOWN MOD
	Afu3g11250	C2H2 transcription	551	0.169	UP HIGH	Afu6g11250	C2H2 finger domain protein,	770	0.816	DOWN

		factor (Swi5), putative					putative		MOD
	Afu1g13750	C2H2 transcription factor (Rpn4), putative	564	0.035	UP HIGH	Afu1g02860	C2H2 transcription factor, putative	882	0.664	DOWN MOD
	Afu2g10400	C6 transcription factor, putative	576	0.143	UP HIGH	Afu8g00420	C6 finger transcription factor, putative	978	0.82	DOWN MOD
	Afu1g14750	C2H2 transcription factor (Sfp1), putative	580	0.181	UP HIGH	Afu3g04180	C2H2 finger domain protein, putative	1127	0.873	DOWN MOD
	Afu6g12160	C6 transcription factor, putative	602	0.086	UP HIGH	Afu5g13790	C6 transcription factor (Acr-2), putative	1166	0.8	DOWN MOD
	Afu7g00410	C6 transcription factor, putative	634	0.03	UP HIGH	Afu6g02690	C2H2 finger domain protein, putative	1198	0.561	DOWN MOD
	Afu5g01270	C6 transcription factor, putative	701	0.558	UP MOD	Afu8g04300	C2H2 finger domain protein, putative	1207	0.664	DOWN MOD
	Afu3g00690	C6 transcription factor, putative	822	0.305	UP MOD	Afu3g11990	C6 transcription factor (Mut3), putative	1232	0.426	DOWN MOD
	Afu2g05380	C6 transcription factor, putative	1006	0.237	UP MOD	Afu1g09190	C6 finger domain protein, putative	1247	0.604	DOWN MOD
	Afu1g06900	C2H2 transcription factor (Crz1), putative	1026	0.119	UP MOD	Afu4g01470	C6 finger domain protein, putative	1319	0.834	DOWN LOW
	Afu7g06320	C6 transcription factor, putative	1062	0.235	UP MOD	Afu1g14060	C2H2 finger domain protein, putative	1373	0.614	DOWN LOW
	Afu1g17150	C6 transcription factor, putative	1075	0.562	UP MOD	Afu2g15260	C6 transcription factor (Leu3), putative	1454	0.884	DOWN LOW
	Afu4g12560	C6 transcription factor, putative	1105	0.343	UP MOD	Afu1g05150	C2H2 transcription factor (TFIIIA), putative	1455	0.687	DOWN LOW
	Afu3g12890	C6 transcription factor (GliZ), putative	1160	0.09	UP MOD	Afu6g01910	C2H2 finger domain protein, putative	1481	0.73	DOWN LOW
	Afu2g17220	C2H2 transcription factor (AmdX), putative	1392	0.101	UP LOW	Afu3g05320	C2H2 finger domain protein, putative	1560	0.641	DOWN LOW
	Afu3g08010	C2H2 transcription factor (Ace1), putative	1611	0.079	UP LOW	Afu8g07230	C6 finger domain protein, putative	1620	0.731	DOWN LOW
	Afu2g11780	C2H2 transcription factor (Crea), putative	1636	0.542	UP LOW	Afu2g03460	C6 transcription factor (Leu3), putative	1654	0.469	DOWN LOW
	Afu3g06740	C6 transcription factor (Gal4), putative	1916	0.25	UP LOW	Afu2g10770	C2H2 transcription factor (Con7), putative	1867	0.849	DOWN LOW

.

Trends favoured among differentially regulated biological processes are apparent from these analyses. Appropriate to extensive cellular differentiation between the spore and primary germ tube (Figure 3.7), genes directing cellular budding and polarized growth were upregulated (Tables 3.3 and 3.7). These included three septins (Afu5g03080, Afu1g08850, Afu7g05370) two cell polarity proteins, including the *S. cerevisiae* homologue tea1 (Afu2g02520) and a protein phosphatase involved in actin filament organisation (Afu1g05610). Microtubules appear to be of particular importance during polar growth of filamentous fungi relative to budding yeast (Harris 2006). Accordingly, microtubule biosynthesis was enriched among genes increasing between 4-14 hours, including alpha and beta tubulins and multiple kinesin family proteins (Tables 3.3 and 3.7). Polarity signalling genes are essential for directing growth, with mutants displaying aberrant morphologies of conidia, germ tube and cellular polarisation. Four Rho GTPases, a Rho GTPAse activator and two RAS GTPases were upregulated between 4 – 14 hours. This highly conserved class of signalling proteins play a crucial role in polarity establishment, cell wall integrity, septum formation and actin dynamics in *A. niger* (Kwon et al. 2011). Twenty six genes associated with cell wall remodelling were upregulated during infection including a beta-glucosidase (Afu3g12600) two alpha-1,3-glucanases (Afu1g15440, Afu2g03980), two mannosyl transferases (Afu1g01380, Afu5g08580) two chitin synthases (Afu1g12040, Afu2g13440) and eight chitinases. Additionally, seventeen GPI-anchored genes, including the 1,3-beta-glucanosyltransferases Gel1 (Afu2g01170) and Gel2 (Afu6g11390) were upregulated. A *gel2* mutant or *gel1* and *gel2* double deletion mutant demonstrates hyperpolarised phalidades, reduced melanin in conidia and reduced virulence (Mouyna et al. 2005). These data highlight the importance of polar extension and cell wall remodelling during the establishment of *A. fumigatus* infection.

GO terms representing metal ion, cation and transition metal transport increased between 4 and 14 hours (Table 3.3). In concordance with the importance of iron acquisition in microbial pathogenesis and the dependence of *A. fumigatus* virulence on siderophore biosynthesis (Schrettl et al. 2004, Schrettl et al. 2007), seven genes involved in iron mobilisation and transport were increased between 4 and 14 hours. These included three siderochrome iron transporters (Afu2g05730, Afu3g13670, Afu7g06060), an MFS siderophore transporter (Afu3g03440), a siderophore acetylase (Afu3g03440) and two ferric-chelate reductases (Afu1g17270, Afu6g13750). Multiple genes involved in the uptake, mobilisation and utilisation of other crucial ions are also up-regulated, including three zinc ion transporters (Afu1g01550, Afu2g03860, Afu4g09560), two plasma membrane ATPases (Afu5g03550, Afu1g02480), a potassium channel (Afu8g01480), potassium transporter (Afu1g16340), a calcium binding protein (Afu1g02930)

calcium sensor (Afu6g14240), calcium translocating ATPase (Afu3g10690) and four copper transporters (Afu4g12620, Afu1g16130, Afu6g02810, Afu2g03730).

During infection, *A. fumigatus* must respond to environmental stresses, such as pH or nutrient limitation to maintain an optimal intracellular state. Accordingly, signal transduction was a significantly enriched functional category increasing between 4 and 14 hours (n = 26 genes). This included two MAPKKK (Afu5g06420, Afu1g10940), a MAPKK Ste7 (Afu3g05900) a MAPK (Afu5g09100), two serine/threonine kinases (Afu2g04680, Afu6g13160), a GTPase (Afu6g12340) and multiple genes associated with G protein receptor signalling (Table 3.7).

Extracellular proteases have been putatively identified as *A. fumigatus* virulence factors due to necessity for acquisition of carbon and nitrogen from the proteinaceous lung matrix and the breakdown of lung parenchyma during hyphal penetration. In keeping with these hypotheses, this analysis found sixteen genes encoding proteases with a putative signal peptide as upregulated between the conidal and hyphal time-points in the murine lung. These included three carboxypeptidases (Afu1g00420, Afu5g01200, Afu5g07330), an alkaline serine protease Alp1 (Afu4g11800), an antigenic dipeptidyl-peptidase Dpp4 (Afu4g09320), a serine peptidase (Afu2g01250), an elastinolytic metalloproteinase Mep (Afu8g07080) and four aspartic endopeptidases, including Pep1 (Afu5g13300 Afu2g15950, Afu4g07040, Afu3g01220). Secreted fungal proteases have also been implicated in allergic disorders by effecting protease activated receptor (PAR) activation of proinflammatory cytokines (Hershenson 2007). Transcript abundance of other known (n = 8) and predicted (n = 7) antigens also increased, including Asp F2, F3, F4, F7, F9, and F10 (Table 3.7, (Banerjee and Kurup 2003). These data suggest that antigenic processing and presentation from the invasive hyphae may illicit a greater Th2-dominated immune response than that of the conidia.

A striking feature of the dataset was the high increase in transcription of the gliotoxin secondary metabolite cluster (Table 3.5 and 3.7). The aminotransferase GliI (Afu6g09640), membrane dipeptidase GliJ (Afu6g09650), cytochrome P450 oxidoreductase GliC (Afu6g09670), O-methyltransferase GliM (Afu6g09680), glutathione S-transferase GliG (Afu6g09690), MFS gliotoxin efflux pump GliA (Afu6g09710), cytochrome P450 oxidoreductase GliF (Afu6g09730) and thioredoxin reductase GliT (Afu6g09740) all showed increased transcription between 4 and 14 hours. This cluster was found to be highly upregulated in the murine lung relative to laboratory culture, and gene deletants aberrant in glitoxin production are attenuated in a corticosteroid treated murine model of infection (McDonagh et al. 2008, Bok et al. 2006, Sugui et al. 2007).

These data suggest the transcription of this key virulence determinant begins before 14 hours, and further validates both the relevance of transcriptional studies in general, and the specific normalisation methods used for this study. Genes directing the biosynthesis of a putative conidial pigment (Chapter 5) and those within the pseurotin A and fumitremorgin B supercluster on chromosome 8 were also increased in transcript abundance during infection (Table 3.7). Transcriptional profiles of secondary metabolite clusters are considered in more detail in the time-point specific analysis (Tables 3.19 and 3.20). Intriguingly, genes putatively involved in transposition were both highly increased and decreased between 4 and 14 hours (Table 3.7).

Functional categories representing protein biosynthesis and ribosome biogenesis and assembly were significantly enriched among transcripts decreasing in abundance during infection (Table 3.4 and Table 3.7). Transcriptional analysis of the exit from dormancy of *A. fumigatus* conida grown in nutrient rich media found increased expression of genes required for translation (Lamarre et al. 2008). In the present study, the observed reduction in primary anabolic processes is likely due to encountered stress and nutrient limitation in the host. Transcriptional comparisons between *A. fumigatus* germlings isolated from the murine lung with developmentally matched laboratory culture suggested that relative to laboratory culture amino acid and sugar catabolism played a role in addressing stress or starvation (McDonagh et al. 2008). Nine amino acid permeases, three amino acid transporters and nine sugar transporters, including three hexose transporters (Afu7g00220, Afu3g14170, Afu3g01670) and a maltose permease (Afu3g01700) increased during infection. Additionally, seven beta-glucosidases and two glucohydrolases increased in transcript abundance between time-points.

3.4.3 Characterisation of differentially expressed genes between 4 and 14 hours: chromosomal loci, lineage specificity and functionality

Given the previously observed over-representation of transcripts encoded by genes of subtelomeric loci (including *A. fumigatus* specific genes, signal peptide encoding genes, and secondary metabolite clusters) during infection relative to laboratory growth (McDonagh et al. 2008), distribution of genes demonstrating increased or decreased transcript abundance between 4 and 14 hours was investigated with respect to these cohorts. Additionally, we hypothesised that contingency cluster loci, which contain physically linked genes that demonstrate co-ordinated up and down regulation during infection, might also be identified by non-ratiometric analyses. A full list of the enhanced GO terms used in this study is available in Appendix A. Statistical significance

of enrichment was measured by Chi square analyses, with the null hypothesis that equal numbers of increased and decreased genes would be expected to occur in each cohort (Figure 3.8 and Table 3.8). Transposition associated genes which were identified manually from the genome annotation in this study (n = 68) were also investigated with respect to their distribution in upregulated and decreasing datasets.

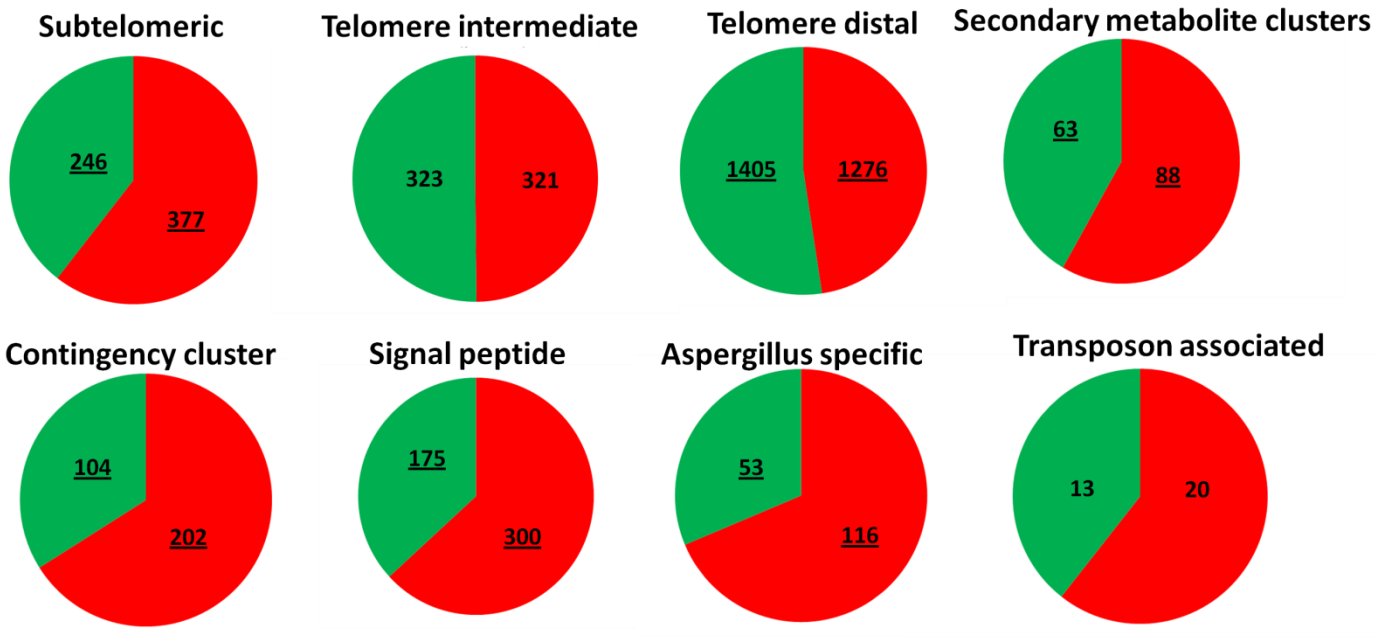


Figure 3.8: Distribution of differentially expressed genes between 4 – 14 hours post infection among the functional cohorts of chromosomal location, signal peptide content, *A. fumigatus* specificity and functional association. Distribution of increased (red) and decreased (green) genes at subtelomeric loci (0 – 300 Kb from telomere, n =1509); telomere intermediate loci (301 - 600 Kb from telomere, n = 1634); telomere distal loci (> 600 Kb from telomere, n =6494). Secondary metabolite clusters (n = 337); Contingency clusters (n = 594); signal peptide cohort (n = 1103); *A. fumigatus* specific genes (n = 596) and; Transposon associated genes (n = 68). Underlined values significantly deviate from the null hypothesis that an equal number of upregulated or downregulated genes will occur in each cohort, as tested by Chi-square analysis**.**

	Number of genes	Differentially expressed	Up (observed)	Down (observed)	Up (expected)	Down (expected)	Chi-square	p-value
0-300 kb	1509	623	377	246	311.5	311.5	27.5	< 0.0001
301- 600 kb	1634	644	321	323	322	322	0.06	0.9372
>600 kb	6373	2681	1276	1405	1340.5	1340.5	6.20	0.0127
Signal P	1103	475	300	175	237.5	237.5	32.8	< 0.0001
Secondary metabolism	337	151	88	63	75.5	75.5	0.04	0.0420
Contingency cluster	594	306	202	104	153	153	31.38	< 0.0001
Aspergillus specific	596	169	116	53	84.5	84.5	23.48	< 0.0001
Transposition associated	68	33	20	13	16.5	16.5	1.48	0.2230

Table 3.8: Distribution and Chi-square analysis of differentially expressed genes categorised by chromosomal location, signal peptide content, *A. fumigatus* specificity and annotation at 4 – 14 hours post infection. Chi-square analysis with one degree of freedom was used to test the distribution of upper and lower quartiles with respect to cohorts of interest to this study, with the null hypothesis that even numbers of upregulated or downregulated genes occur in each group.

Comparison of *A. fumigatus* transcription in the murine lung relative to laboratory culture found genes preferentially employed during infection occur at subtelomeric loci and at contiguous clusters on chromosomes. As a consequence of the nutrient rich reference sample used, these data could represent a general response to the nutrient limitations of the host rather than an infection specific phenomenon. Genes inhabiting subtelomeric loci represent 16% of the *A. fumigatus* genome (McDonagh et al. 2008), yet 19% of genes in the upper quartile were found at these regions. Moreover, distribution was significantly enriched in the upregulated dataset using Chi square analyses ($p < 0.0001$, Table 3.8). Similar positional enrichment is observed at contingency clusters which constitute 6.2% of the genome and 10.2% and 5.4% of the upper and lower quartile respectively ($p < 0.0001$, Chi-square Table 3.8).

Eighty eight genes of a total 337 directing the biosynthesis of secondary metabolites were increased during infection, which was a significant enrichment relative to 66 genes decreasing using Chi-square analyses ($p = 0.042$, Table 3.8). Genes specific to *A. fumigatus* are of great interest as they might include functions which account for the prominence of *A. fumigatus* as a pathogen amongst the Aspergilli. *A. fumigatus* specific genes were more likely to increase than decrease in transcript abundance (Figure 3.8). These data support the hypothesis that transcription during *A. fumigatus* colonisation of the murine lung preferentially occurs at subtelomeric, contingency cluster and secondary metabolite loci.

3.4.4 Analysis of differentially expressed genes between 4 and 14 hours: comparison to other relevant microarray studies

The Bignell research group has performed three analyses of global *A. fumigatus* gene expression which are relevant to this study. As previously described, McDonagh et al. (2008) compared gene expression in the murine lung with developmentally matched germlings from laboratory culture. A second experiment used a reference hybridisation design to compare *A. fumigatus* ATCC46645 gene expression across three time-points of infection (Bertuzzi et al. unpublished). Specifically, this study analysed *A. fumigatus* transcription using RNA extracted from BALF samples harvested at 4, 8 and 16 hours relative to RNA extracted from spores. Thirdly, an *in vitro* study investigated the *A. fumigatus* response to alkaline shift (Loss et al. 2011 in preparation). Gene expression was sampled at 5, 15, 30, 45 and 60 minutes following 14 hour growth in AMM pH 5 and subsequent transfer to AMM pH 8. Genes having increasing or decreasing transcript abundance between 4 and 14 hours from the present study were compared to both up and down regulated gene lists from the afore-mentioned studies (Figure 3.9).

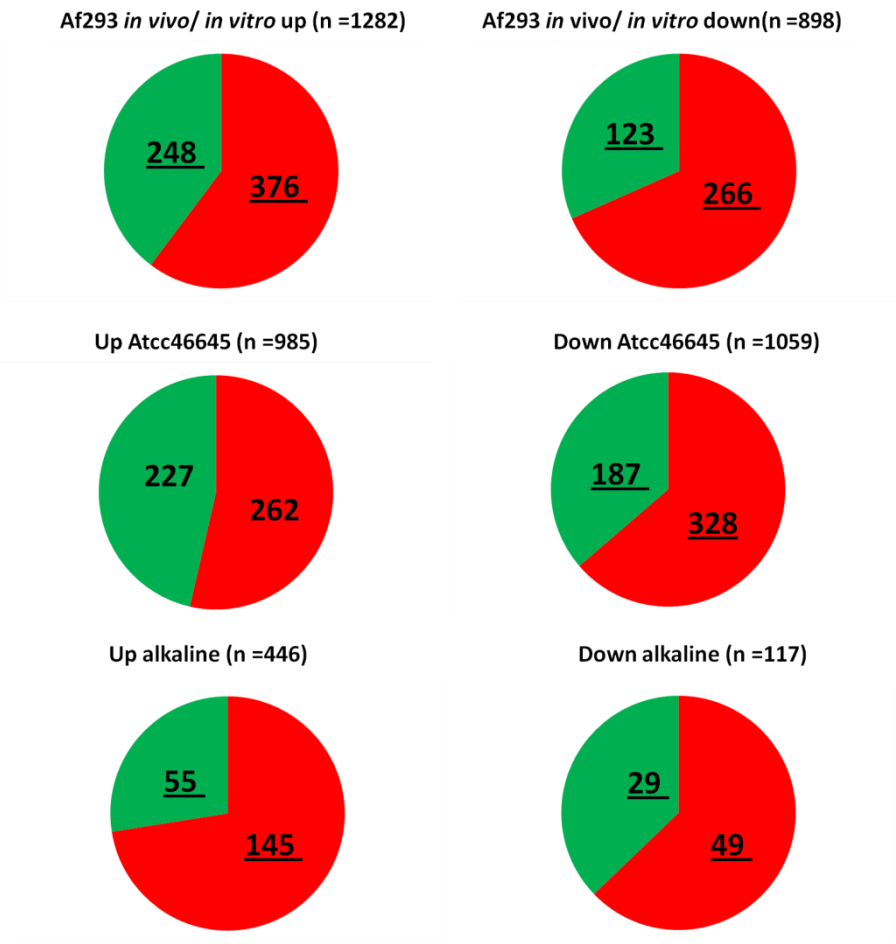


Figure 3.9: Distribution of differentially expressed genes from three microarray studies among 4 – 14 hour differentially expressed datasets Distribution of genes in upper (red) and lower (green) quartiles amongst differentially expressed genes from three microarray studies. Af293 *in vivo*/*in vitro* gene expression values were from murine lung relative to developmentally matched laboratory culture (McDonagh et al 2008). For the ATCC46645 dataset, transcriptional profiles were from 16 hours post infection relative to RNA from spore reference sample (Bertuzzi et al unpublished data). For the alkaline response dataset, genes up or down regulated following 5, 15 30, 45 and 60 minutes after alkaline shift were included. Underlined values significantly deviate from the null hypothesis that an equal number of upregulated or downregulated genes will occur in each cohort, as determined by Chi-square analysi

Experiment and reference	Data-set	Number of genes	Differentially expressed (this study)	Up (observed)	Down (observed)	Up (expected)	Down (expected)	Chi-square	*p-value*
Murine/Lab Af293 (McDonagh et al. 2008)	Up	1282	624	376	248	312	312	26.25	< 0.0001
	Down	898	389	266	123	194.5	194.5	52.56	< 0.0001
Murine/ spore ATCC46645 (Bertuzzi et al. unpublished)	Up	985	489	262	227	244.5	244.5	2.50	0.1135
	Down	1059	515	328	187	227.5	227.5	88.79	< 0.0001
Alkaline shift (Loss et al. 2011 in preparation)	Up	446	200	145	55	100	100	40.50	< 0.0001
	Down	117	78	49	29	39	39	5.12	0.0235

Table 3.9: Distribution and Chi-square analysis of differentially expressed genes from relevant microarray studies among 4 – 14 hour differentially expressed datasets (this study). Chi-square analysis with one degree of freedom was used to test the distribution of upper and lower quartiles with respect to genomic locations and inclusion in signal peptide and *A. fumigatus* specific cohorts, with the null hypothesis that even numbers of upregulated or downregulated genes occur in group.

Low levels of concordance were found between previous array experiments and this analysis (Figure 3.9, Table 3.9). While there was a subset of genes commonly increased and decreased during all analyses, numerous genes showed reverse expression profiles between experiments.
In addition to the general noise associated with microarray experiments, disparities between experiments can be attributable to several factors. For example, the down expressed dataset for the Af293 *in vivo*/*in vitro* experiment (McDonagh et al. 2008) was significantly enriched with genes increasing between 4 – 14 hours (Figure 3.9). Numerous genes directing cellular differentiation, and cell wall/ ergosterol biosynthesis were found in this cohort. This is consistent with disparities in the experimental design, as this study considers developmental changes during infection which were excluded from single time-point comparison with an *in vitro* sample reference (McDonagh et al. 2008).

Similar enrichment of genes with increasing profiles between 4 – 14 hours was observed in the down regulated dataset from the ATCC46645 time-series experiment. This included genes directing cell wall biosynthesis, signal transduction and 16 transcription factors, including *crzA* (Afu1g06900). Two disparities between the experiments may explain these observations. Firstly, ATCC46645 and Af293 wild-type isolates may employ distinct transcriptional reponses to the host niche. The clinical *A. fumigatus* isolates CEA10 and Af293 are known to have discontinuous genomic variation, with approximately 2% of genes specific to each strain (Fedorova et al. 2008).

ATCC46645 is an unsequenced isolate, and consequently the degree of genomic variation from the Af293 isolate employed in this study is unknown. Secondly, the use of *in vitro* spores as a reference sample will impact calculated transcript abundance relative to the subsequent time-points of infection as 25% of genes have stored mRNA transcripts in dormant conidia (Lamarre et al. 2008). The discrepancies between the above array experiments are considered fully in the discussion.

154 genes were common to upregulated datasets from all three murine experiments (McDonagh et al. 2008, Bertuzzie et al. unpublished data), which demonstrated enrichment of multiple genes directing known and putative virulence factors. This included 18 genes for secondary metabolite biosynthesis, of which 7 were from the gliotoxin cluster. Interestingly, a polyketide synthase found within a cluster with an unknown product was upregulated in all experiments (Afu3g01410). Additionally genes for iron acquisition (Afu3g03440, Afu3g03400, Afu1g17270, Afu6g13750), other transition metal transport (Afu1g01550, Afu4g09560), protection from oxidative stress (Afu1g14550), secreted proteases (Afu4g09320, Afu3g01220, Afu8g07080), multidrug efflux pumps (Afu6g03320, Afu1g12620), predicted antigens (Afu6g11330, Afu4g09580, Afu4g00610) and cell wall proteins (Afu8g00610, Afu2g05150, Afu3g08110) and a single reverse transcriptase were upregulated during infection. Intriguingly, 37 genes with unknown function were common to all upregulated datasets. The relative contribution of these gene products to infection remains to be determined. Genes common to all murine array experiments maintained positional enrichment at subtelomeric, metabolite and contingency cluster loci, yet no enrichment of *A. fumigatus* specific genes was observed (Table 3.10).

Cohort	Number of genes	Expected	Observed
0-300 kb	1509	24	52
301- 600 kb	1634	26	29
>600 kb	6373	103	73
Signal P	1103	18	41
Secondary metabolism	337	5	18
Contingency cluster	594	10	83
Aspergillus specific	596	10	5
Transposition associated	68	1	1

Table 3.10: Classification of 154 genes upregulated during 3 microarray analyses of *A. fumigatus* in the murine lung by chromosomal position, *A. fumigatus* specificity, signal peptide content and functional association. 154 transcripts which increased in Af293 in the murine lung relative to developmentally matched laboratory culture (McDonagh et al. 2008), between dormant spores and 16 hours post infection for wild-type isolate ATCC46645 (Bertuzzie et al. unpublished data) and between 4 and 14 hours (this study) were investigated with regard to chromosomal locus, signal peptide content and transposition-associated genes. Numbers of expected genes were predicted based on frequency % within the entire *A. fumigatus* genome.

3.4.5 Time-point specific gene expression profiling of the Af293 isolate in the murine lung

During *A. fumigatus* spore adherence, germination and tissue penetration extensive physiological and biochemical changes occur in the context of a rapidly changing host environment. To determine gene expression profiles specific to each time-point of infection, relative nSI datasets between 4 – 8 and 8 – 14 hours post infection were analysed (Figure 3.10).

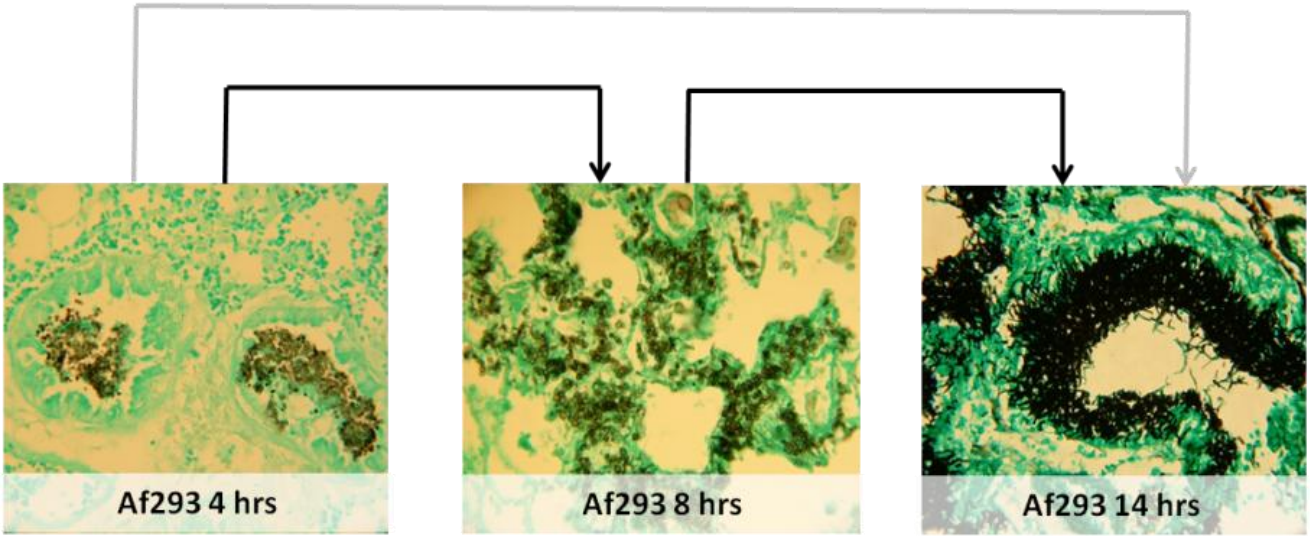


Figure 3.10: Schematic depicting time-point specific transcriptional comparisions. Black arrows depict strain specific comparisons conducted between 4 and 8, and 8 and 14 hours post infection. Faint grey arrow depicts analysis discussed in the previous section.

Gene ontology analysis was conducted using Genespring GX 11.02 to indentify over represented terms in increased (n = 1974, Tables 3.11 and 3.12) or decreased datasets (n = 1974, Tables 3.13 and 3.14) between 4 – 8 and 8 - 14 hours. GO terms satisfying an arbitrarily imposed *p*-value cut-off of 0.2 with respect to their occurence in the *A. fumigatus* genome are reported. The 100 genes having the greatest increase or decrease between 4 and 8 hours are reported in Tables 3.15 and 3.16. The 100 genes having the greatest increase or decrease between 8 and 14 hours are reported in Tables 3.17 and 3.18.

GO ACCESSION	GO Term	p-value	corrected p-value	Count in Selection	% Count in Selection	Count in Total	% Count in Total
GO:0051704|GO:0051706	multi-organism process	1.68E-07	0.00	35	58.33	109	2.35
GO:0009405	pathogenesis	1.35E-06	0.01	24	40.00	42	0.90
GO:0030148	sphingolipid biosynthetic process	1.45E-05	0.08	10	16.67	14	0.30
GO:0046467	membrane lipid biosynthetic process	1.45E-05	0.08	10	16.67	14	0.30
GO:0007186	G-protein coupled receptor protein signaling pathway	6.12E-05	0.16	12	20.00	20	0.43
GO:0007165	signal transduction	4.96E-05	0.16	29	48.33	122	2.63
GO:0031137	regulation of conjugation with cellular fusion	8.28E-05	0.16	12	20.00	18	0.39
GO:0032005	signal transduction involved in conjugation with cellular fusion	8.28E-05	0.16	12	20.00	18	0.39
GO:0043900	regulation of multi-organism process	8.28E-05	0.16	12	20.00	18	0.39
GO:0000750|GO:0007330	pheromone-dependent signal transduction involved in conjugation with cellular fusion	8.28E-05	0.16	12	20.00	18	0.39
GO:0046999	regulation of conjugation	8.28E-05	0.16	12	20.00	18	0.39

Table 3.11: Over represented Gene Ontology terms among genes with increasing expression between 4 and 8 hours in the Af293 infected murine lung. GO terms significantly enriched with respect to their occurrence in the *A. fumigatus* Af293 genome are reported (Bonferroni corrected p-values ≤ 0.2).

GO ACCESSION	GO Term	p-value	corrected p-value	Count in Selection	% Count in Selection	Count in Total	% Count in Total
GO:0016021	integral to membrane	5.13E-08	9.04E-04	74	46.54	259	5.58
GO:0031224	intrinsic to membrane	1.90E-07	0.00	74	46.54	266	5.73
GO:0044264	cellular polysaccharide metabolic process	1.10E-06	0.01	11	6.92	73	1.57
GO:0016798	hydrolase activity, acting on glycosyl bonds	1.95E-06	0.01	22	13.84	115	2.48
GO:0006073	cellular glucan metabolic process	3.10E-06	0.01	11	6.92	52	1.12
GO:0044042	glucan metabolic process	4.70E-06	0.01	11	6.92	53	1.14
GO:0004553|GO:0016800	hydrolase activity, hydrolyzing O-glycosyl compounds	3.97E-06	0.01	20	12.58	95	2.05

GO:0005886|GO:0005904	plasma membrane	4.84E-06	0.01	90	56.60	330	7.10
GO:0005976	polysaccharide metabolic process	8.73E-06	0.02	12	7.55	121	2.60
GO:0009277	fungal-type cell wall	3.54E-05	0.06	24	15.09	62	1.33
GO:0005618	cell wall	4.88E-05	0.08	24	15.09	63	1.36
GO:0030312	external encapsulating structure	6.65E-05	0.10	24	15.09	64	1.38
GO:0005887	integral to plasma membrane	8.01E-05	0.11	34	21.38	99	2.13

Table 3.12: Over represented Gene Ontology terms among genes with increasing expression between 8 and 14 hours in the Af293 infected murine lung. GO terms significantly enriched with respect to their occurrence in the *A. fumigatus* Af293 genome are reported (Bonferroni corrected p-values ≤ 0.2).

GO ACCESSION	GO Term	p-value	corrected p-value	Count in Selection	% Count in Selection	Count in Total	% Count in Total
GO:0006396|GO:0006399	RNA processing	2.01E-06	0.035871	2	100	232	4.994618

Table 3.13: Over represented Gene Ontology terms among genes with decreasing expression between 4 and 8 hours in the Af293 infected murine lung. GO terms significantly enriched with respect to their occurrence in the *A. fumigatus* Af293 genome are reported (Bonferroni corrected p-values ≤ 0.2).

GO ACCESSION	GO Term	p-value	corrected p-value	Count in Selection	% Count in Selection	Count in Total	% Count in Total
GO:0005737	cytoplasm	2.61E-07	0.002853	244	97.21116	2075	44.67169
GO:0005622	intracellular	2.65E-07	0.002853	251	100	2984	64.24112
GO:0044424	intracellular part	5.21E-07	0.003734	244	97.21116	2962	63.76749

Table 3.14: Over represented Gene Ontology terms among genes with decreasing expression between 8 and 14 hours in the Af293 infected murine lung. GO terms significantly enriched with respect to their occurrence in the *A. fumigatus* Af293 genome are reported (Bonferroni corrected p-values ≤ 0.2).

Table 3.15: 100 genes with greatest nSI increase between 4 and 8 hours post infection. Genes are reported ranked according to greatest nSI intensity increase between 4 and 8 hours. Position of the gene in the 8 – 14 hours increasing dataset is also shown. A one-way ANOVA was conducted on nSI values between time-points, with the null hypothesis that nSI values do not change between time-points. FDR correct *p*-values from this analysis are reported for each gene. Genes transcripts highlighted in red increased uniquely between 4 and 8 hours

ORF	Description	**Rank 4 – 8 hours**	**Rank 8 – 14 hours**	**p-value 4 - 8 hours**	**p-value 8 - 14 hours**
Afu8g00610	cell surface protein Mas1, putative	1	6945	0.021	0.869
Afu6g00430	IgE-binding protein	2	5033	0.01	0.925
Afu7g05490	hypothetical protein	3	3579	0.009	0.985
Afu6g12420	SprT family metallopeptidase, putative	4	6889	0.027	0.853
Afu6g06470	heat shock protein HSP30, putative	5	7524	0.005	0.639
Afu3g00520	SIR2 family histone deacetylase, putative	6	897	0.006	0.723
Afu3g02550	conserved hypothetical protein	7	7781	0.008	0.497
Afu4g10340	C6 finger domain protein, putative	8	1165	0.017	0.845
Afu5g01200	carboxypeptidase S1, putative	9	7881	0.005	0.152
Afu5g02650	hypothetical protein	10	4398	0.012	0.939
Afu4g08730	conserved hypothetical protein	11	6612	0.026	0.924
Afu5g08640	hypothetical protein	12	5536	0.07	0.964
Afu5g09020	WSC domain protein, putative	13	2218	0.023	0.933
Afu2g17330	serine peptidase, family S28, putative	14	757	0.012	0.753
Afu2g08180	flotillin domain protein	15	7860	0.004	0.329
Afu2g12320	conserved hypothetical protein	16	4614	0.008	0.948
Afu7g08410	Tc1-mariner transposase, putative	17	7413	0.014	0.781
Afu5g09070	hypothetical protein	18	7621	0.001	0.381
Afu4g14180	hypothetical protein	19	525	0.012	0.624
Afu7g01990	conserved hypothetical protein	20	2956	0.021	0.948
Afu3g09060	hypothetical protein	21	488	0.046	0.783
Afu3g01500	integral membrane protein	22	4589	0.033	0.983
Afu5g05610	cell cycle control protein Cwf14, putative	23	6285	0.005	0.81
Afu6g00290	aminotransferase, putative	24	317	0.005	0.314
Afu7g07010	hypothetical protein	25	303	0.038	0.657
Afu5g13300	aspartic endopeptidase Pep1	26	7771	0.005	0.451
Afu6g03350	acetyltransferase, GNAT family, putative	27	147	0.019	0.266
Afu2g03280	hypothetical protein	28	935	0.012	0.822
Afu4g01160	von Willebrand domain protein	29	6557	0.023	0.867
Afu3g08110	cell wall protein, putative	30	1067	0.06	0.887
Afu4g14000	tripeptidyl peptidase A	31	7789	0.053	0.701
Afu4g13970	conserved hypothetical protein	32	30	0.037	0.236

Afu2g12680	conserved hypothetical protein	33	5115	0.018	0.938
Afu2g00580	hypothetical protein	34	278	0.014	0.263
Afu3g12140	hypothetical protein	35	6229	0.018	0.882
Afu4g09310	hypothetical protein	36	7589	0.012	0.432
Afu8g05680	serine/threonine protein kinase, putative	37	2998	0.014	0.933
Afu3g06880	SDP3	38	7629	0.107	0.574
Afu6g06360	mating alpha-pheromone PpgA	39	204	0.004	0.143
Afu1g04250	hypothetical protein	40	6358	0.041	0.907
Afu2g02440	conserved hypothetical protein	41	6109	0.046	0.894
Afu7g06780	hypothetical protein	42	637	0.046	0.834
Afu2g11110	nuclear condensin complex subunit Smc2, putative	43	2395	0.001	0.869
Afu2g07550	serine/threonine protein kinase (Ark1), putative	44	5471	0.157	0.915
Afu8g05120	hypothetical protein	45	7863	0.181	0.702
Afu5g13870	mlo3 protein	46	6430	0.084	0.914
Afu1g13140	G protein complex alpha subunit GpaA	47	839	0.088	0.787
Afu1g05920	hypothetical protein	48	2834	0.076	0.974
Afu6g08490	inorganic diphosphatase, putative	49	83	0.05	0.325
Afu2g01430	hypothetical protein	50	1580	0.162	0.933
Afu5g14230	C6 transcription factor, putative	51	122	0.056	0.659
Afu6g09310	class V chitinase, putative	52	7106	0.092	0.879
Afu5g09050	hypothetical protein	53	5446	0.035	0.82
Afu3g00180	short chain dehydrogenase, putative	54	7047	0.35	0.891
Afu5g01620	extracellular proline-rich protein	55	2433	0.004	0.925
Afu5g01230	RTA1 domain protein, putative	56	7876	0.036	0.43
Afu5g12900	GATA transcription factor (Ams2), putative	57	6772	0.014	0.902
Afu2g17320	conserved hypothetical protein	58	4712	0.005	0.959
Afu7g08280	hypothetical protein	59	277	0.027	0.334
Afu8g05300	RNA polymerase II subunit 7	60	1694	0.112	0.938
Afu6g08180	hypothetical protein	61	5668	0.044	0.824
Afu6g04500	FOG1 protein	62	7802	0.082	0.616
Afu1g13050	C2H2 transcription factor, putative	63	4731	0.065	0.948
Afu2g00230	NADH oxidoreductase Amid, putative	64	365	0.068	0.673
Afu4g06950	related to (VAMP)-associated protein	65	7238	0.083	0.833
Afu3g00650	aminopeptidase Y, putative	66	6404	0.008	0.78
Afu4g11800	alkaline serine protease Alp1	67	4850	0.007	0.936
Afu2g06080	GTPase activating protein (Gyp1), putative	68	2873	0.055	0.967

Afu5g11190	hypothetical protein	69	837	0.057	0.845
Afu6g07410	hypothetical protein	70	2822	0.035	0.976
Afu4g09830	indoleamine 2,3-dioxygenase pyrrole 2,3-dioxygenase)	71	2919	0.059	0.956
Afu3g07900	conserved hypothetical protein	72	5114	0.017	0.849
Afu2g03730	Ctr copper transporter family protein	73	1832	0.008	0.914
Afu1g01300	GPI anchored protein, putative	74	174	0.037	0.031
Afu2g10110	hypothetical protein	75	5728	0.07	0.933
Afu7g06750	phosphoglycerate mutase family protein, putative	76	6713	0.021	0.733
Afu2g08900	voltage-gated chloride channel (ClcA), putative	77	3279	0.014	0.952
Afu6g09320	LysM domain protein, putative	78	4673	0.067	0.964
Afu1g02760	cell cycle inhibitor Nif1, putative	79	1135	0.021	0.783
Afu2g02080	C2H2 finger domain protein, putative	80	3063	0.034	0.937
Afu3g14920	LaeA-like methyltransferase, putative	81	763	0.169	0.914
Afu3g00810	cholestenol delta-isomerase, putative	82	7747	0.043	0.594
Afu5g08740	DHHC zinc finger membrane protein	83	6836	0.112	0.898
Afu6g14010	GPI anchored protein, putative	84	5981	0.097	0.787
Afu1g14560	alpha-mannosidase	85	338	0.005	0.518
Afu2g17400	C-3 sterol dehydrogenase/C-4 decarboxylase	86	4488	0.03	0.973
Afu3g11370	mitochondrial large ribosomal subunit L49, putative	87	6752	0.111	0.864
Afu4g10120	C6 finger domain protein, putative	88	470	0.202	0.824
Afu6g12160	C6 transcription factor, putative	89	7562	0.024	0.714
Afu3g09960	aureobasidin resistance protein Aur1	90	591	0.067	0.821
Afu4g06790	ubiquinol-cytochrome c reductase complex 14 kDa protein	91	7015	0.05	0.628
Afu3g10340	Rho GTPase Rho 2, putative	92	6556	0.205	0.882
Afu5g12770	metallo-beta-lactamase family protein	93	7602	0.023	0.287
Afu2g14490	endoglucanase, putative	94	458	0.08	0.792
Afu2g17300	glutathione S-transferase	95	1647	0.031	0.845
Afu5g10950	hypothetical protein	96	1202	0.012	0.882
Afu3g10690	calcium-translocating P-type ATPase(PMCA-type),putative	97	7610	0.144	0.852
Afu3g15210	endo-1,4-beta-xylanase, putative	98	7823	0.104	0.746
Afu1g12770	conserved hypothetical protein	99	2617	0.079	0.933
Afu6g08200	m-phase inducer phosphatase	100	2384	0.157	0.947

Table 3.16: 100 genes with greatest nSI decrease between 4 and 8 hours post infection. Genes are reported ranked according to greatest nSI decrease between 4 and 8 hours. Position of each gene in the 8 – 14 hours decreasing dataset is also shown. A one-way ANOVA was conducted on nSI values between time-points, with the null hypothesis that nSI values do not change between time-points. FDR correct *p*-values from this analysis are reported for each gene. Genes highlighted in green decreased uniquely between 4 and 8 hours

ORF	Description	Rank 4 – 8 hours	Rank 8 – 14 hours	p-value 4 - 8 hours	p-value 8 - 14 hours
Afu3g09410	reverse transcriptase	1	7882	0.004	0.377
Afu7g07190		2	7753	0.009	0.281
Afu8g00330	endonuclease/reverse transcriptase/RNaseH, putative	3	7875	0.002	0.182
Afu7g07150		4	7862	0.024	0.119
Afu7g01700	hypothetical protein	5	7734	0.135	0.481
Afu1g17050	hypothetical protein	6	7751	0.186	0.728
Afu1g06490	hypothetical protein	7	6738	0.059	0.887
Afu7g07180		8	7729	0.05	0.34
Afu5g07910	hypothetical protein	9	6729	0.204	0.914
Afu4g14860		10	7876	0.097	0.432
Afu1g16420	GPI anchored protein, putative	11	906	0.18	0.767
Afu4g00220	metallo-beta-lactamase domain protein	12	6291	0.382	0.915
Afu4g14760	ABC multidrug transporter, putative	13	7838	0.07	0.276
Afu4g01630	reverse transcriptase, putative	14	7769	0.327	0.746
Afu3g15120	hypothetical protein	15	5760	0.32	0.925
Afu2g05360	C6 transcription factor, putative	16	10	0.003	0.263
Afu2g15550	molybdenum cofactor biosynthesis protein Gephyrin, putative	17	7400	0.27	0.774
Afu7g07170	reverse transcriptase/protease/endonuclease Pol, putative	18	7016	0.184	0.882
Afu7g05440	TOS4, putative	19	4413	0.281	0.992
Afu3g04230	transcription initiation factor IIF subunit alpha, putative	20	6400	0.241	0.887
Afu7g07160		21	7441	0.069	0.637
Afu1g17710	C6 transcription factor, putative	22	7605	0.331	0.709
Afu8g00350	conserved hypothetical protein	23	6885	0.252	0.88
Afu5g00690	hypothetical protein	24	7379	0.464	0.82
Afu4g09470	cytochrome P450 monooxygenase, putative	25	5943	0.354	0.954
Afu3g00550	hypothetical protein	26	7660	0.197	0.776
Afu3g00400	hypothetical protein	27	6054	0.391	0.933
Afu6g09490		28	7831	0.054	0.13
Afu8g06130	FluG family protein	29	5160	0.17	0.933
Afu2g14120	C6 finger domain protein, putative	30	4331	0.104	0.992
Afu7g04720	alpha-1,2-mannosidase, putative	31	6988	0.209	0.749
Afu7g07000	fumarylacetoacetate hydrolase family protein	32	7853	0.261	0.56
Afu2g16300	dihydroxy acid dehydratase, putative	33	4923	0.262	0.984
Afu7g06420	NADH-dependent flavin oxidoreductase, putative	34	2898	0.157	0.964
Afu6g03880	hypothetical protein	35	7796	0.376	0.804

Afu8g01060	hypothetical protein	36	6580	0.046	0.871
Afu1g11430	hypothetical protein	37	5389	0.059	0.925
Afu3g02500	protein kinase, putative	38	3783	0.092	0.993
Afu2g00200	catalase, putative	39	4732	0.213	0.941
Afu5g10290	fructose-bisphosphate aldolase, putative	40	812	0.04	0.888
Afu8g00230	phytanoyl-CoA dioxygenase family protein	41	4606	0.06	0.985
Afu2g15270	conserved hypothetical protein	42	7701	0.41	0.701
Afu3g02720	MFS transporter, putative	43	6459	0.071	0.835
Afu1g14190	DUF614 domain protein	44	5871	0.131	0.925
Afu4g06880	conserved hypothetical protein	45	5561	0.47	0.948
Afu2g17920	hypothetical protein	46	3946	0.421	0.995
Afu2g04290	cytochrome P450 monooxygenase, putative	47	3664	0.499	0.994
Afu5g10070	dehydrogenase	48	7878	0.049	0.54
Afu4g10160	C6 transcription factor (AmyR), putative	49	3558	0.408	0.979
Afu3g15040	xenobiotic compound monooxygenase, DszA family	50	3844	0.082	0.993
Afu8g02380	FAD-dependent monooxygenase, putative	51	5779	0.522	0.942
Afu2g14150	endo-arabinanase, putative	52	7507	0.599	0.911
Afu1g11590	quinate 5-dehydrogenase	53	3648	0.212	0.986
Afu2g14140	hypothetical protein	54	7697	0.112	0.331
Afu3g03810	hypothetical protein	55	4119	0.069	0.997
Afu3g12770	putative nucleoside-diphosphate-sugar epimerase	56	2883	0	0.876
Afu1g01170	hypothetical protein	57	6718	0.282	0.736
Afu2g05350	major facilitator superfamily protein superfamily	58	412	0.115	0.869
Afu8g02280	C6 transcription factor, putative	59	6810	0.069	0.781
Afu8g00630	conserved hypothetical protein	60	7550	0.372	0.734
Afu8g04920	LEA domain protein	61	4458	0.006	0.982
Afu6g01920	xenobiotic compound monooxygenase, DszA family	62	6044	0.037	0.883
Afu3g12070	conserved hypothetical protein	63	5300	0.258	0.957
Afu6g09260	sensor histidine kinase/response regulator, putative	64	2791	0.266	0.959
Afu6g08410	hypothetical protein	65	932	0.189	0.917
Afu3g08510		66	7343	0.553	0.845
Afu2g14220	conserved hypothetical protein	67	5971	0.134	0.915
Afu4g09460	NACHT domain protein	68	5746	0.463	0.641
Afu5g06440	ubiquitin C-terminal hydrolase family protein	69	7560	0.27	0.883
Afu6g06880	conserved hypothetical protein	70	5144	0.022	0.933
Afu4g00730	HHE domain protein	71	2732	0.336	0.954
Afu3g11590	Taz1-interacting factor 1 (TAF1), putative	72	6900	0.24	0.859
Afu2g17230	NACHT domain protein	73	6230	0.277	0.822
Afu1g17000	sin3-associated polypeptide, 18kD	74	4107	0.256	0.997
Afu3g03850	hypothetical protein	75	6409	0.23	0.887

Afu8g02630	extracellular exo-polygalacturonase, putative	76	697	0.214	0.635
Afu4g09200	hypothetical protein	77	7284	0.112	0.544
Afu5g10430	MSF multidrug transporter, putative	78	5633	0.074	0.896
Afu5g09650	small monomeric GTPase (Gtr1), putative	79	4907	0.448	0.985
Afu2g11630	P-factor mating pheromone (Map2), putative	80	7090	0.493	0.883
Afu6g08530	sister chromatid separation protein (Src1), putative	81	1688	0.54	0.964
Afu7g06210	hypothetical protein	82	7788	0.582	0.796
Afu3g00970	hypothetical protein	83	4691	0.382	0.977
Afu1g00270	hypothetical protein	84	7880	0.288	0.131
Afu2g14350	AT DNA binding protein, putative	85	7474	0.396	0.733
Afu3g14670	MFS transporter, putative	86	7832	0.129	0.237
Afu4g14130	ABC multidrug transporter, putative	87	7224	0.342	0.594
Afu4g13900	MFS transporter, putative	88	900	0.341	0.882
Afu6g00540	conserved hypothetical protein	89	6737	0.562	0.893
Afu6g02980	extracellular exo-polygalacturonase, putative	90	4	0.164	0.277
Afu1g09790	histone transcription regulator Hir1, putative	91	5141	0.392	0.96
Afu3g14010	DNA replication licensing factor Mcm2, putative	92	3759	0.315	0.984
Afu1g11390	cytochrome P450, putative	93	6464	0.306	0.925
Afu1g14000	hypothetical protein	94	5346	0.353	0.943
Afu5g08410	PQ loop repeat protein	95	7802	0.5	0.723
Afu6g10160	hypothetical protein	96	5742	0.151	0.933
Afu1g14640	hypothetical protein	97	7334	0.007	0.263
Afu6g11650	short-chain dehydrogenase/reductase family protein, putative	98	5379	0.195	0.946
Afu3g06600	siroheme synthase, putative	99	5895	0.101	0.927
Afu1g10100	3-oxoacyl-(acyl-carrier-protein) reductase	100	2861	0.019	0.857

Table 3.17: 100 genes with greatest nSI increase between 8 and 14 hours post infection. Genes are reported ranked according to greatest nSI increase between 8 and 14 hours. Position of each gene in the 4 – 8 hour increasing dataset is also shown. A one-way ANOVA was conducted on nSI values between between time-points, with the null hypothesis that nSI values do not change between time-points. FDR correct *p*-values from this analysis are reported for each gene. Gene transcripts highlighted in red increased uniquely between 8 and 14 hours

ORF	Description	Rank 4 – 8 hours	Rank 8 – 14 hours	p-value 4 - 8 hours	p-value 8 - 14 hours
Afu6g09690	glutathione S-transferase GliG	1406	1	0.545	0
Afu6g09670	cytochrome P450 oxidoreductase GliC	356	2	0.09	0.037
Afu6g09680	O-methyltransferase GliM	2000	3	0.664	0.092
Afu6g09710	MFS gliotoxin efflux pump GliA	3044	4	0.87	0.195
Afu2g13370	55 kDa type II phosphatidylinositol 4-kinase	7771	5	0.44	0.084
Afu6g09730	cytochrome P450 oxidoreductase	399	6	0.175	0.13

	GliF				
Afu4g14070	glycosyl transferase, putative	257	7	0.541	0.466
Afu4g01100	hypothetical protein	7222	8	0.719	0.671
Afu7g01930	sexual development protein EsdC, putative	1264	9	0.486	0.37
Afu6g09740	thioredoxin reductase GliT	1227	10	0.198	0.264
Afu2g08820	hypothetical protein	477	11	0.361	0.214
Afu6g13740	hypothetical protein	1700	12	0.586	0.03
Afu2g11120	hypothetical protein	2835	13	0.562	0.17
Afu6g09650	membrane dipeptidase GliJ	476	14	0.139	0.152
Afu3g09410	reverse transcriptase	7896	15	0.004	0.377
Afu7g06680	AAA family ATPase, putative	6151	16	0.795	0.325
Afu1g00270	hypothetical protein	7813	17	0.288	0.131
Afu4g00610	aryl-alcohol dehydrogenase, putative	2304	18	0.726	0.288
Afu5g10070	dehydrogenase	7849	19	0.049	0.54
Afu5g01930	hypothetical protein	3144	20	0.76	0.105
Afu4g14860		7887	21	0.097	0.432
Afu8g00330	endonuclease/reverse transcriptase/RNaseH, putative	7894	22	0.002	0.182
Afu7g05760	hypothetical protein	7732	23	0.194	0.173
Afu1g00690	hypothetical protein	6982	24	0.81	0.718
Afu6g09500	DnaJ domain protein	7735	25	0.396	0.084
Afu4g08890	aldo-keto reductase family protein, putative	4659	26	0.961	0.136
Afu3g00130	conserved hypothetical protein	2009	27	0.564	0.406
Afu2g17410	hypothetical protein	7322	28	0.797	0.788
Afu2g11280	hypothetical protein	2906	29	0.863	0.718
Afu4g13970	conserved hypothetical protein	32	30	0.037	0.236
Afu5g00700	hypothetical protein	5861	31	0.902	0.583
Afu8g06980	glycosyl hydrolase, putative	6391	32	0.678	0.616
Afu7g06600	NADPH-dependent FMN reductase, putative	7426	33	0.567	0.826
Afu3g11910		4469	34	0.942	0.428
Afu7g07150		7893	35	0.024	0.119
Afu1g02260	hypothetical protein	7588	36	0.478	0.188
Afu8g00540	hybrid polyketide synthase/nonribosomal peptide synthase, putative	4170	37	0.914	0.639
Afu6g00650	hypothetical protein	419	38	0.163	0.152
Afu6g00180	hypothetical protein	4569	39	0.958	0.538
Afu8g01350	hypothetical protein	3697	40	0.888	0.473
Afu2g05120	hypothetical protein	4057	41	0.918	0.262
Afu3g01180	sarcosine oxidase, putative	2735	42	0.46	0.063
Afu1g01650	C6 finger domain protein, putative	6847	43	0.61	0.525
Afu7g07000	fumarylacetoacetate hydrolase family protein	7865	44	0.261	0.56
Afu6g00630	MFS transporter, putative	898	45	0.425	0.168
Afu1g01310	carboxylesterase, putative	243	46	0.092	0.304

Afu4g12410	HMG box protein, putative	5350	47	0.974	0.236
Afu3g09240	CAIB/BAIF family enzyme	2249	48	0.64	0.424
Afu7g01820	C6 transcription factor, putative	7734	49	0.553	0.598
Afu1g13980	conserved hypothetical protein	5348	50	0.971	0.54
Afu4g13770	glycosyl hydrolase, putative	6415	51	0.874	0.595
Afu7g00960	extracellular cysteine-rich protein, putative	7029	52	0.762	0.776
Afu8g01460	hypothetical protein	7755	53	0.694	0.784
Afu1g09120	amino acid permease, putative	5097	54	0.994	0.119
Afu8g05270	C6 transcription factor, putative	4402	55	0.941	0.262
Afu2g00250	conserved hypothetical protein	5533	56	0.94	0.624
Afu6g10190	hypothetical protein	7789	57	0.551	0.469
Afu1g14140	DUF409 domain protein	7579	58	0.775	0.802
Afu4g14760	ABC multidrug transporter, putative	7884	59	0.07	0.276
Afu7g06820	galactose oxidase, putative	1003	60	0.276	0.237
Afu3g03450	cytochrome P450 pisatin demethylase, putative	549	61	0.357	0.686
Afu3g03670	ABC multidrug transporter, putative	3200	62	0.787	0.624
Afu3g13560	toxin biosynthesis protein, putative	6303	63	0.867	0.607
Afu5g08800	hypothetical protein	1786	64	0.57	0.287
Afu3g14670	MFS transporter, putative	7811	65	0.129	0.237
Afu6g09490		7869	66	0.054	0.13
Afu6g03470	ABC multidrug transporter, putative	423	67	0.051	0.563
Afu8g04060		3590	68	0.767	0.604
Afu7g04050	hypothetical protein	7761	69	0.111	0.282
Afu3g12220	ABC transporter, putative	7140	70	0.596	0.263
Afu1g10160	conserved hypothetical protein	6664	71	0.845	0.741
Afu6g07890	related to yeast zds family proteins, putative	7587	72	0.312	0.845
Afu7g01130	hypothetical protein	7518	73	0.309	0.157
Afu6g09560	conserved hypothetical protein	6869	74	0.685	0.544
Afu6g11770	hypothetical protein	7686	75	0.677	0.704
Afu7g04930	alkaline serine protease (PR1), putative	1562	76	0.729	0.703
Afu1g17270	ferric-chelate reductase (Fre2), putative	489	77	0.292	0.633
Afu3g09660	hypothetical protein	6648	78	0.76	0.812
Afu5g14240	ThiJ/PfpI family protein	171	79	0.037	0.182
Afu5g00920	transesterase (LovD), putative	4701	80	0.943	0.729
Afu3g00120	amino acid transporter, putative	7256	81	0.726	0.784
Afu5g14320	hypothetical protein	7045	82	0.774	0.303
Afu6g08490	inorganic diphosphatase, putative	49	83	0.05	0.325
Afu4g14090	UDP-glucose 4-epimerase	184	84	0.066	0.287
Afu5g08880	hypothetical protein	7612	85	0.283	0.51
Afu6g10580	antigenic CFEM domain protein, putative	3932	86	0.908	0.442
Afu5g01470	peroxisomal copper amine oxidase	7608	87	0.618	0.612
Afu5g00160	MFS polyamine transporter, putative	7377	88	0.471	0.676

Afu1g03190	hypothetical protein	7311	89	0.665	0.458
Afu1g11320	class II DAHP synthetase family protein	7630	90	0.072	0.421
Afu2g13030	phenylalanyl-tRNA synthetase alpha subunit (PodG), putative	6714	91	0.908	0.84
Afu5g01030	glyceraldehyde 3-phosphate dehydrogenase (Ccg-7), putative	1084	92	0.436	0.31
Afu8g05460	bZIP transcription factor, putative	1808	93	0.526	0.432
Afu1g00120	hypothetical protein	3400	94	0.907	0.727
Afu5g08410	PQ loop repeat protein	7802	95	0.5	0.723
Afu4g09160	ankyrin repeat protein	7486	96	0.262	0.624
Afu1g05840	hypothetical protein	1410	97	0.517	0.282
Afu5g06940	dipeptidyl peptidase III	5238	98	0.981	0.439
Afu5g01270	C6 transcription factor, putative	5112	99	0.994	0.69
Afu6g13810	hypothetical protein	1141	100	0.138	0.383

Table 3.18: Top 100 genes with greatest nSI decrease between 8 and 14 hours post infection. Genes are reported ranked according to greatest nSI decrease between 8 and 14 hours. Position of each gene in the 4 – 8 hour decreasing dataset is also shown. A one-way ANOVA was conducted on nSI values between time-points, with the null hypothesis that nSI values do not change between time-points. FDR correct *p*-values from this analysis are reported for each gene. Genes highlighted in green decreased uniquely between 8 and 14 hours.

ORF	Description	Rank 4 – 8 hours	Rank 8 – 14 hours	p-value 4 - 8 hours	p-value 8 - 14 hours
Afu2g13210	DnaJ domain protein	6045	1	0.779	0.583
Afu8g01260	hypothetical protein	7682	2	0.11	0.076
Afu2g15650	DUF323 domain protein	5606	3	0.672	0.429
Afu6g02980	extracellular exo-polygalacturonase, putative	90	4	0.164	0.277
Afu2g02010	transmembrane protein UsgS	7770	5	0.01	0.092
Afu5g09130	polysaccharide deacetylase family protein	2899	6	0.998	0.331
Afu6g11700	hypothetical protein	1652	7	0.925	0.365
Afu4g08320	tyrosyl-tRNA synthetase, mitochondrial precursor (tyrosine--tRNA ligase) (tyrrs)	5699	8	0.605	0.477
Afu4g14780	cytochrome P450 monooxygenase, putative	5150	9	0.786	0.714
Afu2g05360	C6 transcription factor, putative	16	10	0.003	0.263
Afu6g05140	sterol delta 5,6-desaturase ERG3	7486	11	0.564	0.72
Afu2g17600	polyketide synthetase PksP	270	12	0.54	0.546
Afu3g00820	putative exported protein	7547	13	0.051	0.041
Afu5g13620	ubiquitin C-terminal hydrolase, putative	6496	14	0.622	0.738
Afu3g02970	aspergillopepsin, putative	7778	15	0.012	0.092
Afu5g01200	carboxypeptidase S1, putative	7888	16	0.005	0.152
Afu3g14140	metacaspase CasB	7434	17	0.235	0.365
Afu2g09790	glucose-6-phosphate isomerase	6660	18	0.469	0.443
Afu1g03830	prefoldin subunit 2, putative	5755	19	0.841	0.81
Afu5g07400	phenylacetyl-CoA ligase PclA, putative	4237	20	0.843	0.327
Afu5g01230	RTA1 domain protein, putative	7841	21	0.036	0.43

Afu1g04160	aspartate aminotransferase, putative	7500	22	0.043	0.182
Afu2g09150	adenosine deaminase	1665	23	0.893	0.562
Afu5g04410	hypothetical protein	2461	24	0.979	0.792
Afu2g10480	conserved hypothetical protein	5827	25	0.604	0.263
Afu3g12260	hypothetical protein	7550	26	0.154	0.302
Afu5g10710	conserved hypothetical protein	839	27	0.785	0.42
Afu3g08330	ATP-dependent Clp protease, proteolytic subunit ClpP	3833	28	0.755	0.496
Afu8g01780	nitrilase, putative	7194	29	0.351	0.367
Afu5g11080	MSF multidrug transporter, putative	7176	30	0.346	0.696
Afu5g15000	arsenate reductase (ArsC), putative	7751	31	0.066	0.119
Afu3g06540	3'-phosphoadenosine-5'-phosphosulfate reductase	4679	32	0.867	0.651
Afu5g00760	chitin synthase C	6898	33	0.303	0.407
Afu8g05120	hypothetical protein	7852	34	0.181	0.702
Afu1g16090	arsenate reductase (ArsC), putative	7649	35	0.097	0.395
Afu3g12800	conserved hypothetical protein	6779	36	0.528	0.72
Afu2g08180	flotillin domain protein	7882	37	0.004	0.329
Afu3g08350	Sec20 family	6285	38	0.694	0.723
Afu2g16890	conserved hypothetical protein	4662	39	0.904	0.639
Afu6g07500	DNA excision repair protein Rad2	4956	40	0.657	0.263
Afu5g01350	major facilitator superfamily	5095	41	0.366	0.334
Afu1g12880	epoxide hydrolase, putative	7107	42	0.336	0.287
Afu3g13240	aldose 1-epimerase, putative	4919	43	0.591	0.263
Afu2g16800	lectin family integral membrane protein, putative	7459	44	0.089	0.024
Afu3g04180	C2H2 finger domain protein, putative	6368	45	0.615	0.733
Afu2g13090	RNA polymerase II subunit 3	6873	46	0.092	0.772
Afu1g15430	lipase/esterase, putative	7460	47	0.044	0.538
Afu5g12100	pmt2 methyltransferase	6646	48	0.649	0.624
Afu6g04630	conserved hypothetical protein	4396	49	0.691	0.432
Afu5g11130	PAXNEB protein superfamily	6241	50	0.755	0.705
Afu7g02210	conserved hypothetical protein	6224	51	0.4	0.723
Afu8g06040	hypothetical protein	708	52	0.829	0.82
Afu5g08600	homoserine O-acetyltransferase	528	53	0.726	0.74
Afu1g16270	xylitol dehydrogenase XdhB, putative	5638	54	0.632	0.57
Afu5g10160	actVA 4 protein	3753	55	0.9	0.776
Afu5g09600	2-nitropropane dioxygenase family oxidoreductase, putative	7367	56	0.269	0.473
Afu2g02830	hypothetical protein	5725	57	0.786	0.81
Afu5g00640	peroxisomal dehydratase, putative	7171	58	0.309	0.624
Afu4g09030	aminopeptidase	2431	59	0.901	0.263
Afu1g14120	nuclear segregation protein (Bfr1), putative	5988	60	0.486	0.277
Afu3g10320	Zinc finger, C3HC4 type (RING finger) domain protein	1899	61	0.933	0.828
Afu5g08460	SET domain protein	4238	62	0.766	0.223
Afu2g12630	allergen Asp F13	7747	63	0.053	0.389

Afu5g03840	oxidoreductase, short chain dehydrogenase/reductase family	5691	64	0.632	0.342
Afu8g04710	xylosidase	7192	65	0.392	0.758
Afu5g10690	monosaccharide transporter	1325	66	0.819	0.277
Afu4g08210	GNAT family acetyltransferase (Nat4), putative	5859	67	0.636	0.641
Afu2g08150	NEDD8-like protein (RubA), putative	7718	68	0.148	0.386
Afu5g03270	hypothetical protein	6504	69	0.395	0.3
Afu8g06870	MFS sugar transporter, putative	338	70	0.277	0.381
Afu1g11670	small nuclear ribonucleoprotein (LSM8), putative	5998	71	0.582	0.287
Afu1g07580	cell polarity protein (Alp11), putative	7269	72	0.47	0.723
Afu5g01240	general amidase-B	6710	73	0.124	0.095
Afu3g15210	endo-1,4-beta-xylanase, putative	7799	74	0.104	0.746
Afu2g13600	mitochondrial pyruvate dehydrogenase kinase, putative	2084	75	0.828	0.641
Afu3g14680	lysophospholipase Plb3	7182	76	0.074	0.018
Afu6g11670	conserved hypothetical protein	336	77	0.606	0.583
Afu4g06380	sterol carrier protein, putative	6439	78	0.31	0.194
Afu5g07850	decapping enzyme Dcp1, putative	739	79	0.052	0.19
Afu3g13200	1,3-beta-glucanosyltransferase, putative	6657	80	0.293	0.325
Afu8g02090	nucleotide-sugar transporter family protein	7081	81	0.368	0.422
Afu1g12110	NADH:ubiquinone oxidoreductase (NADH dehydrogenase),14 kDa	6836	82	0.209	0.311
Afu5g10450	hypothetical protein	7036	83	0.09	0.152
Afu2g16250	COP9 signalosome subunit 5 (CsnE), putative	4541	84	0.824	0.553
Afu5g13110	conserved hypothetical protein	3046	85	0.982	0.81
Afu3g02270	mycelial catalase Cat1	7377	86	0.025	0.354
Afu1g14310	poly(A)-binding protein-dependent poly(A) ribonuclease, putative	4360	87	0.734	0.442
Afu1g07740	LEM3/CDC50 family protein	7576	88	0.091	0.583
Afu6g10040	fructosyl amine: oxygen oxidoreductase	2816	89	0.992	0.283
Afu4g10150	alpha-glucosidase	2924	90	0.996	0.386
Afu3g00680	copper amine oxidase	4583	91	0.593	0.327
Afu6g04100	conserved hypothetical protein	862	92	0.691	0.686
Afu7g05870	proteasome component Pre8, putative	6891	93	0.318	0.789
Afu1g13560	hypothetical protein	2031	94	0.858	0.262
Afu6g04500	FOG1 protein	7835	95	0.082	0.616
Afu5g08570	cAMP-dependent protein kinase catalytic subunit, putative	7093	96	0.555	0.72
Afu3g11210	YagE family protein	7426	97	0.299	0.545
Afu6g13020	AP-3 adaptor complex subunit sigma, putative	4127	98	0.858	0.325
Afu5g11540	related to ribosomal protein S5	7229	99	0.275	0.794
Afu5g14190	beta-glucanase, putative	6994	100	0.336	0.355

3.4.6 Functional classification of time-point specifc datasets for Af293 murine infection

Differentially expressed genes were grouped into functional categories based on GO Terms and by reference to the *A. fumigatus* literature. A summary of up and down expressed functional categories identified for 4 – 8 and 8 – 14 hours post infection are reported in Tables 3.19 and 3.20 respectively.

Table 3.19: Functional classification of selected genes having differential transcript abundance in Af293 between 4 and 8 hours post infection in the murine lung. Increased (red) and decreased (green) are shown for each functional category. Both increasing and decreasing transcripts are sub divided into expression cohorts which are either high, moderate, or low with respect to their expression change. Genes within functional categories are ranked according to greatest nSI intensity changes between 4 and 8 hours. FDR correct *p*-values from a one-way ANOVA are reported for each gene .

Functional category	ORF	Description	Rank	FDR P-value	Magnitude	ORF	Description	Rank	FDR P-value	Magnitude
Cell wall	Afu6g09310	class V chitinase, putative	52	0.092	UP HIGH	Afu3g03870	endo-1,4-beta-glucanase, putative	159	0.183	DOWN HIGH
	Afu5g14060	Rho GTPase Rho4, putative	318	0.079	UP HIGH	Afu3g03080	endo-1,3(4)-beta-glucanase, putative	263	0.225	DOWN HIGH
	Afu3g12600	beta-glucosidase 1	369	0.044	UP HIGH	Afu4g12900	alpha-1,6-mannosyltransferase subunit (Ecm39), putative	377	0.089	DOWN HIGH
	Afu5g08550	Rho guanyl nucleotide exchange factor (Rom2), putative	880	0.151	UP MOD	Afu3g07160	class V chitinase, putative	678	0.79	DOWN MOD
	Afu5g00760	chitin synthase C	999	0.303	UP MOD	Afu1g03350	alpha-1,3-glucanase, putative	756	0.737	DOWN MOD
	Afu5g03940	alpha-1,3-glucanase, putative	1355	0.473	UP LOW	Afu5g02280	endo-1,3(4)-beta-glucanase, putative	843	0.796	DOWN MOD
	Afu3g11280	class V chitinase, putative	1694	0.515	UP LOW	Afu2g11270	alpha-1,3-glucan synthase, putative	926	0.794	DOWN MOD
	Afu5g11990	alpha-1,3-mannosyltransferase (Alg3), putative	1956	0.71	UP LOW	Afu7g05140	class III chitinase, putative	976	0.564	DOWN MOD
						Afu8g02040	glycosyl transferase, putative	1374	0.701	DOWN LOW
						Afu4g09940	polysaccharide deacetylase family protein	1657	0.529	DOWN LOW
						Afu2g05340	1,3-beta-glucanosyltransferase, putative	1750	0.811	DOWN LOW
						Afu2g12850	1,3-beta-glucanosyltransferase Gel3	1963	0.898	DOWN LOW
Ergosterol	Afu2g17400	C-3 sterol dehydrogenase/C-4 decarboxylase	86	0.03	UP HIGH	Afu4g14770	squalene-hopene-cyclase, putative	896	0.735	DOWN MOD
	Afu5g07780	squalene monooxygenase Erg1	162	0.066	UP HIGH	Afu1g11140	Sterol desaturase family	905	0.685	DOWN MOD
	Afu4g06890	14-alpha sterol	225	0.098	UP HIGH	Afu1g05720	c-14 sterol reductase	914	0.843	DOWN

		demethylase Cyp51A							MOD
	Afu8g01070	Lathosterol oxidase, putative	317	0.036	UP HIGH	Afu7g02480	oxysterol binding protein (Osh1), putative	1395	0.449	DOWN LOW
	Afu6g05140	sterol delta 5,6-desaturase ERG3	411	0.564	UP HIGH					
	Afu4g07780	mevalonate kinase	458	0.24	UP HIGH					
	Afu1g03950	cytochrome P450 sterol C-22 desaturase, putaitve	500	0.08	UP HIGH					
	Afu5g04080	oxidosqualene:lanosterol cyclase	818	0.416	UP MOD					
	Afu1g03150	c-14 sterol reductase	1066	0.23	UP MOD					
	Afu2g03790	oxysterol binding protein (Osh7), putative	1348	0.03	UP LOW					
	Afu4g06380	sterol carrier protein, putative	1458	0.31	UP LOW					
	Afu2g15030	C-3 sterol dehydrogenase/C-4 decarboxylase	1936	0.148	UP LOW					
Antigen	Afu5g13300	aspartic endopeptidase Pep1	26	0.005	UP HIGH	Afu6g11030	RNA recognition motif. (a.k.a. RRM, RBD, or RNP domain) protein	1334	0.666	DOWN LOW
	Afu4g11800	alkaline serine protease Alp1	67	0.007	UP HIGH					
	Afu2g03830	allergen Asp F4	104	0.288	UP HIGH					
	Afu2g12630	allergen Asp F13	150	0.053	UP HIGH					
	Afu1g09670	HLH transcription factor (GlcD gamma), putative	231	0.07	UP HIGH					
	Afu4g06670	allergen Asp F7	472	0.112	UP HIGH					
	Afu6g11330	histidine acid phosphatase, putative	550	0.213	UP HIGH					
	Afu1g02820	Y20 protein	569	0.193	UP HIGH					
	Afu6g02280	allergen Asp F3	865	0.236	UP MOD					
	Afu6g06770	enolase	1182	0.164	UP MOD					
	Afu5g02330	major allergen Asp F1	1596	0.119	UP LOW					
	Afu5g09580	conidial hydrophobin Hyp1/RodA	1762	0.675	UP LOW					
	Afu2g09030	secreted dipeptidyl peptidase	1806	0.698	UP LOW					
	Afu5g02040	extracellular lipase, putative	1938	0.379	UP LOW					

Ion transport	Afu3g10690	calcium-translocating P-type ATPase(PMCA-type),putative	97	0.144	UP HIGH		Afu1g11110	calcium channel pore-forming subunit (Cch1), putative	592	0.599	DOWN HIGH
	Afu5g15000	arsenate reductase (ArsC), putative	146	0.066	UP HIGH		Afu8g01890	Na+/H+ exchanger family protein, putative	904	0.409	DOWN MOD
	Afu6g02810	Ctr copper transporter family family	221	0.157	UP HIGH		Afu1g14250	potassium channel, putative	1101	0.622	DOWN MOD
	Afu1g16090	arsenate reductase (ArsC), putative	248	0.097	UP HIGH		Afu5g06220	sodium/hydrogen exchanger 3	1530	0.872	DOWN LOW
	Afu1g02930	Ca2+ binding protein (calmodulin), putative	255	0.106	UP HIGH		Afu2g09460	potassium transporter	1907	0.692	DOWN LOW
	Afu1g05760	arsenite efflux transporter (ArsB), puative	681	0.225	UP MOD						
	Afu1g16120	arsenic resistance protein ArsH, putative	710	0.104	UP MOD						
	Afu1g10880	P-type calcium ATPase, putative	855	0.135	UP MOD						
	Afu5g15030	arsenic resistance protein ArsH	862	0.218	UP MOD						
	Afu3g11350	arsenite translocating ATPase (arsA), putative	1421	0.355	UP LOW						
	Afu4g09560	ZIP Zinc transporter, putative	1445	0.384	UP LOW						
	Afu6g14240	calcium sensor (NCS-1), putative	1538	0.017	UP LOW						
	Afu8g01480	potassium channel, putative	1541	0.506	UP LOW						
	Afu3g08180	Ctr copper transporter family protein	1690	0.417	UP LOW						
	Afu1g16130	copper-transporting ATPase, putative	1914	0.259	UP LOW						
Iron aquisition	Afu2g07680	L-ornithine N5-oxygenase SidA	322	0.096	UP HIGH		Afu4g14640	low affinity iron transporter, putative	929	0.722	DOWN MOD
	Afu2g07670	palmitoyltransferase (SidR), putative	326	0.321	UP HIGH						
	Afu3g13670	siderochrome-iron transporter, putative	1252	0.267	UP LOW						
Secondary metabolite	Afu3g14700	polyketide synthase, putative	1360	0.329	UP MOD		Afu1g17710	C6 transcription factor, putative	22	0.331	DOWN HIGH
	Afu7g00160	polyketide synthase, putative	1403	0.545	UP LOW		Afu3g12920	nonribosomal peptide synthase (GliP), putative	177	0.426	DOWN HIGH
	Afu5g12730	nonribosomal peptide synthase, putative	1817	0.225	UP LOW		Afu8g00490	polyketide synthase, putative	208	0.586	DOWN HIGH
	Afu5g14460	polyketide synthase, putative	1823	0.622	UP LOW		Afu4g14270	polyketide synthase, putative	228	0.604	DOWN HIGH

						Afu8g00420	C6 finger transcription factor, putative	271	0.595	DOWN HIGH
						Afu3g12940	C6 transcription factor, putative	331	0.634	DOWN HIGH
						Afu1g01010	polyketide synthase, putative	580	0.656	DOWN HIGH
						Afu6g09630	C6 finger domain protein GliZ	643	0.57	DOWN HIGH
						Afu3g03350	nonribosomal peptide synthase, putative	644	0.512	DOWN HIGH
						Afu5g00150	nonribosomal peptide synthetase, putative	686	0.454	DOWN MOD
						Afu4g14590	C6 transcription factor, putative	820	0.823	DOWN MOD
						Afu4g14440	nonribosomal peptide synthase, putative	877	0.716	DOWN MOD
						Afu3g15270	nonribosomal peptide synthetase, putative	1054	0.618	DOWN MOD
						Afu6g08560	nonribosomal peptide synthase (NRPS), putative	1076	0.832	DOWN MOD
						Afu3g01510	C6 transcription factor, putative	1525	0.743	DOWN LOW
						Afu3g02670	nonribosomal peptide synthetase, putative	1770	0.857	DOWN LOW
Gliotoxin						Afu6g09760	toxin biosynthesis cytochrome P450 oxidoreductase, putative	275	0.523	DOWN HIGH
						Afu6g09580	hypothetical protein	509	0.193	DOWN HIGH
						Afu6g09590	zinc-containing alcohol dehydrogenase, putative	559	0.462	DOWN HIGH
						Afu6g09630	C6 finger domain protein GliZ	643	0.57	DOWN HIGH
						Afu6g09600	peptidase, putative	782	0.314	DOWN MOD
						Afu6g09530	hypothetical protein	866	0.541	DOWN MOD
Pseurotin A Supercluster	Afu8g00610	cell surface protein Mas1, putative	1	0.021	UP HIGH	Afu8g00330	endonuclease/reverse transcriptase/RNaseH, putative	3	0.002	DOWN HIGH
	Afu8g00460	methionine aminopeptidase, type I, putative	565	0.411	UP HIGH	Afu8g00350	conserved hypothetical protein	23	0.252	DOWN HIGH
	Afu8g00940	MFS drug transporter, putative	707	0.376	UP MOD	Afu8g00230	phytanoyl-CoA dioxygenase family protein	41	0.06	DOWN HIGH

	Afu8g00260	F-box domain and ankyrin repeat protein	836	0.329	UP MOD	Afu8g00630	conserved hypothetical protein	60	0.372	DOWN HIGH
	Afu8g00890	glucose transporter	968	0.364	UP MOD	Afu8g00310	LINE-1 class reverse transcriptase, RNaseH, putative	127	0.308	DOWN HIGH
	Afu8g00470	conserved hypothetical protein	1015	0.227	UP MOD	Afu8g00490	polyketide synthase, putative	208	0.586	DOWN HIGH
	Afu8g00950	hypothetical protein	1097	0.349	UP MOD	Afu8g00220	cytochrome P450, putative	266	0.548	DOWN HIGH
	Afu8g00680	glycosyl transferase, group 2 family protein	1238	0.337	UP MOD	Afu8g00420	C6 finger transcription factor, putative	271	0.595	DOWN HIGH
	Afu8g00990	F-box domain protein	1629	0.661	UP LOW	Afu8g00390	O-methyltransferase, putative	332	0.798	DOWN HIGH
	Afu8g00700	class III chitinase ChiA2	1763	0.632	UP LOW	Afu8g00550	SirN-like methyltransferase, putative	405	0.376	DOWN HIGH
	Afu8g00560	cytochrome P450, putative	1911	0.564	UP LOW	Afu8g00150	conserved hypothetical protein	764	0.529	DOWN MOD
	Afu8g00650	LPS glycosyltransferase, putative	1971	0.64	UP LOW	Afu8g00200	O-methyltransferase, putative	822	0.438	DOWN MOD
						Afu8g00620	dimethylallyl tryptophan synthase, putative	927	0.318	DOWN MOD
						Afu8g00730	transcription regulator (RTG2), putative	982	0.151	DOWN MOD
						Afu8g00180	conserved hypothetical protein	1073	0.85	DOWN MOD
						Afu8g00530	alpha/beta hydrolase, putative	1214	0.84	DOWN MOD
						Afu8g00570	alpha/beta hydrolase, putative	1285	0.778	DOWN MOD
						Afu8g00660	solute transporter, putative	1680	0.909	DOWN LOW
						Afu8g00640	glycosyl transferase, putative	1886	0.619	DOWN LOW
Microtubule	Afu3g11860	microtubule associated protein EB1, putative	149	0.046	UP HIGH	Afu6g14220	kinesin family protein (KinA), putative	1042	0.308	DOWN MOD
	Afu2g14280	kinesin family protein (KlpA), putative	189	0.065	UP HIGH					
	Afu1g02550	tubulin alpha-1 subunit	226	0.077	UP HIGH					
	Afu7g01400	kinesin family protein (BimC), putative	320	0.056	UP HIGH					
	Afu1g10910	tubulin beta, putative	459	0.203	UP HIGH					
	Afu6g12840	kinesin family protein	1136	0.669	UP MOD					
	Afu4g06710	kinase-related protein	1566	0.481	UP LOW					

	Afu2g14990	tubulin alpha-2 subunit	1699	0.201	UP LOW					
Secreted proteases	Afu3g00650	aminopeptidase Y, putative	9	0.008	UP HIGH	Afu3g11400	aspartic endopeptidase Pep2	525	0.204	DOWN HIGH
	Afu5g01200	carboxypeptidase S1, putative	26	0.005	UP HIGH					
	Afu4g11800	alkaline serine protease Alp1	31	0.007	UP HIGH					
	Afu8g07080	elastinolytic metalloproteinase Mep	66	0.001	UP HIGH					
	Afu5g13300	aspartic endopeptidase Pep1	67	0.005	UP HIGH					
	Afu1g00420	carboxypeptidase S1, putative	103	0.075	UP HIGH					
	Afu6g00310	serine carboxypeptidase (CpdS), putative	194	0.027	UP HIGH					
	Afu2g03510	pheromone processing carboxypeptidase (Sxa2), putative	336	0.339	UP HIGH					
	Afu6g14420	disintegrin-like metalloproteinase, putative	754	0.216	UP MOD					
	Afu2g01250	serine peptidase, family S28, putative	774	0.027	UP MOD					
	Afu5g07330	carboxypeptidase S1, putative	801	0.371	UP MOD					
	Afu8g04120	carboxypeptidase S1, putative	1048	0.299	UP LOW					
	Afu2g09030	secreted dipeptidyl peptidase	1346	0.698	UP LOW					
	Afu4g14000	tripeptidyl peptidase A	1806	0.053	UP LOW					
	Afu3g12210	carboxypeptidase Y, putative	1807	0.198	UP LOW					
Signal peptide encoding genes	Afu6g00430	IgE-binding protein	2	0.01	UP HIGH	Afu1g17050	hypothetical protein	6	0.186	DOWN HIGH
	Afu3g08110	cell wall protein, putative	30	0.06	UP HIGH	Afu1g16420	GPI anchored protein, putative	11	0.18	DOWN HIGH
	Afu2g12680	conserved hypothetical protein	33	0.018	UP HIGH	Afu3g00550	hypothetical protein	26	0.197	DOWN HIGH
	Afu6g06360	mating alpha-pheromone PpgA	39	0.004	UP HIGH	Afu2g17920	hypothetical protein	46	0.421	DOWN HIGH
	Afu2g02440	conserved hypothetical protein	41	0.046	UP HIGH	Afu2g14150	endo-arabinanase, putative	52	0.599	DOWN HIGH
	Afu6g09310	class V chitinase, putative	52	0.092	UP HIGH	Afu2g05350	major facilitator superfamily	58	0.115	DOWN

Afu5g01620	extracellular proline-rich protein	55	0.004	UP HIGH
Afu3g07900	conserved hypothetical protein	72	0.017	UP HIGH
Afu1g01300	GPI anchored protein, putative	74	0.037	UP HIGH
Afu7g06750	phosphoglycerate mutase family protein, putative	76	0.021	UP HIGH
Afu3g00810	cholestenol delta-isomerase, putative	82	0.043	UP HIGH
Afu6g14010	GPI anchored protein, putative	84	0.097	UP HIGH
Afu1g14560	alpha-mannosidase	85	0.005	UP HIGH
Afu3g09960	aureobasidin resistance protein Aur1	90	0.067	UP HIGH
Afu2g14490	endoglucanase, putative	94	0.08	UP HIGH
Afu3g03060	cell wall protein (PhiA), putative	115	0.011	UP HIGH
Afu2g10130	phase-specific adhesin, putative	116	0.068	UP HIGH
Afu3g02970	aspergillopepsin, putative	119	0.012	UP HIGH
Afu8g05160	peroxisomal membrane protein (Pex13), putative	135	0.013	UP HIGH
Afu1g12350	extracellular fruiting body protein, putative	151	0.037	UP HIGH
Afu4g01290	endo-chitosanase, pseudogene	153	0.149	UP HIGH
Afu2g14420	cutinase, putative	268	0.238	UP HIGH
Afu2g14540	endoglucanase, putative	493	0.43	UP HIGH
Afu3g02270	mycelial catalase Cat1	520	0.025	UP HIGH
Afu8g02530	extracellular lipase, putative	572	0.27	UP HIGH
Afu4g06640	acid sphingomyelinase	838	0.038	UP MOD
Afu3g11280	class V chitinase, putative	1694	0.515	UP LOW
Afu8g00700	class III chitinase ChiA2	1763	0.632	UP LOW

	protein superfamily			HIGH
Afu2g14220	conserved hypothetical protein	67	0.134	DOWN HIGH
Afu2g11630	P-factor mating pheromone (Map2), putative	80	0.493	DOWN HIGH
Afu2g08500	carboxylesterase, putative	106	0.346	DOWN HIGH
Afu1g15670	laccase	107	0.13	DOWN HIGH
Afu3g00610	glucoamylase	141	0.361	DOWN HIGH
Afu3g03870	endo-1,4-beta-glucanase, putative	159	0.183	DOWN HIGH
Afu1g08970	conserved hypothetical protein	166	0.408	DOWN HIGH
Afu3g08990	hypothetical protein	209	0.296	DOWN HIGH
Afu1g10800	thioesterase family protein	225	0.065	DOWN HIGH
Afu3g03930	cytochrome P450, putative	247	0.488	DOWN HIGH
Afu3g03080	endo-1,3(4)-beta-glucanase, putative	263	0.225	DOWN HIGH
Afu2g00350	acetylornithine deacetylase (ArgE), putative	273	0.493	DOWN HIGH
Afu2g01240	beta-D-fructofuranoside fructohydrolase	281	0.393	DOWN HIGH
Afu2g15450	hypothetical protein	294	0.724	DOWN HIGH
Afu3g08070	GMC oxidoreductase, putative	314	0.283	DOWN HIGH
Afu4g01200	extracellular guanyl-specific ribonuclease, putative	319	0.391	DOWN HIGH
Afu4g06590	hypothetical protein	342	0.289	DOWN HIGH
Afu3g14910	extracellular signalling protein (factor C), putative	378	0.305	DOWN HIGH
Afu2g00780	MFS multidrug transporter, putative	438	0.553	DOWN HIGH
Afu3g09230	carboxylesterase, putative	705	0.827	DOWN MOD
Afu3g13550	2-dehydropantoate 2-reductase, putative	1541	0.744	DOWN LOW
Afu3g00480	RTA1 domain protein, putative	1582	0.649	DOWN LOW

	Afu5g02040	extracellular lipase, putative	1938	0.379	UP LOW		Afu2g00820	extracellular GDSL-like lipase/acylhydrolase, putative	1593	0.549	DOWN LOW
Ribosome biogenesis and RNA metabolism	Afu1g14110	RNA polymerase subunit	274	0.151	UP HIGH		Afu7g01460	ribosomal protein S5	190	0.265	DOWN HIGH
	Afu1g02510	RNA-binding protein, putative	303	0.114	UP HIGH		Afu6g10370	RNA lariat debranching enzyme, putative	217	0.115	DOWN HIGH
	Afu5g09060	RNA binding protein, putative	392	0.165	UP HIGH		Afu5g07640	RNA 3'-terminal phosphate cyclase, putative	435	0.599	DOWN HIGH
	Afu5g08350	ribosomal protein S16	680	0.182	UP MOD		Afu3g11410	RNA Polymerase II CTD phosphatase Fcp1, putative	470	0.695	DOWN HIGH
	Afu1g10310	RNase L inhibitor of the ABC superfamily, putative	906	0.318	UP MOD		Afu3g11220	ribonuclease T2, putative	769	0.808	DOWN MOD
	Afu5g04240	RNA binding protein Nrd1, putative	989	0.548	UP MOD		Afu2g16040	rRNA biogenesis protein RRP5, putative	886	0.138	DOWN MOD
	Afu2g13090	RNA polymerase II subunit 3	1024	0.092	UP MOD		Afu1g07600	ribonuclease HI large subunit	971	0.366	DOWN MOD
	Afu6g08610	RNA methylase family protein, putative	1063	0.3	UP MOD		Afu5g08430	RO10	1132	0.461	DOWN MOD
	Afu4g13450	RNA methyltransferase, TrmH family family	1419	0.564	UP LOW		Afu7g02080	RNA polymerase I subunit Rpa43, putative	1168	0.166	DOWN MOD
	Afu1g09410	ribosomal protein L17	1581	0.292	UP LOW		Afu3g09620	RNA recognition motif. (a.k.a. RRM, RBD, or RNP domain) protein	1188	0.53	DOWN MOD
	Afu5g08310	RNA and export factor binding protein 2-I	1722	0.448	UP LOW		Afu1g02950	RNA recognition motif. (a.k.a. RRM, RBD, or RNP domain) protein	1196	0.805	DOWN MOD
	Afu1g15810	RNA splicing factor (Pad-1), putative	1901	0.559	UP LOW		Afu5g07390	ribosomal large subunit assembly protein (Sqt1), putative	1252	0.088	DOWN MOD
	Afu5g09670	RNase III domain protein	1952	0.138	UP LOW		Afu7g01330	RNA binding complex component (TraX), putative	1294	0.3	DOWN MOD
	Afu2g16370	Ribosomal protein L32	1963	0.36	UP LOW		Afu6g04320	RNA binding protein	1296	0.778	DOWN MOD
							Afu6g11030	RNA recognition motif. (a.k.a. RRM, RBD, or RNP domain) protein	1334	0.666	DOWN LOW
							Afu2g13570	ribosome biogenesis protein (Bms1), putative	1335	0.853	DOWN LOW
							Afu2g07970	ribosomal protein L19	1402	0.529	DOWN

										LOW
						Afu5g11150	ribonuclease P protein subunit p29	1444	0.601	DOWN LOW
						Afu5g05930	RNA processing factor 1	1549	0.727	DOWN LOW
						Afu2g03260	RNA-binding protein, putative	1688	0.917	DOWN LOW
						Afu6g02440	60s ribosomal protein L24, putative	1705	0.798	DOWN LOW
						Afu8g04400	RNA binding protein, putative	1719	0.596	DOWN LOW
						Afu1g03390	60S ribosomal protein L12	1741	0.606	DOWN LOW
						Afu1g05630	40s ribosomal protein s3	1857	0.873	DOWN LOW
Carbohydrate transport	Afu1g12240	MFS peptide transporter, putaitve	223	0.065	UP HIGH	Afu8g01180	MFS sugar transporter, putative	194	0.582	DOWN HIGH
	Afu8g02090	nucleotide-sugar transporter family protein	816	0.368	UP MOD	Afu5g12950	MFS quinate transporter, putative	620	0.216	DOWN HIGH
	Afu4g06630	MFS monosaccharide transporter, putative	924	0.312	UP MOD	Afu1g11830	MFS quinate transporter (QutD), putative	1185	0.644	DOWN MOD
	Afu3g14170	high-affinity hexose transporter	950	0.354	UP MOD	Afu3g03700	Sugar transporter subfamily	1281	0.305	DOWN MOD
	Afu3g12170	MFS sugar transporter, putative	1620	0.189	UP LOW	Afu7g00950	MFS monosaccharide transporter, putative	1550	0.813	DOWN LOW
	Afu3g00200	hexose transporter protein	1841	0.452	UP LOW	Afu2g14590	MFS monosaccharide transporter, putative	1610	0.366	DOWN LOW
						Afu4g00800	MFS monosaccharide transporter, putative	1796	0.785	DOWN LOW
Amino acid transport	Afu4g07760	Transmembrane amino acid transporter protein family	446	0.095	UP HIGH	Afu7g00440	GABA permease, putative	382	0.346	DOWN HIGH
	Afu2g13630	amino transferase	570	0.265	UP HIGH	Afu3g11490	GABA permease, putative	555	0.384	DOWN HIGH
	Afu6g04990	amino acid transporter, putative	845	0.205	UP MOD	Afu1g12310	GABA permease GabA	923	0.3	DOWN MOD
	Afu2g15470	neutral amino acid permease	947	0.574	UP MOD	Afu4g06230	general amino acid permease (Agp2), putative	1000	0.854	DOWN MOD
	Afu2g01370	GABA permease, putative	988	0.219	UP MOD	Afu4g10090	GABA permease, putative	1012	0.434	DOWN MOD
	Afu5g09440	amino acid permease, putative	1098	0.499	UP MOD					
	Afu2g11220	proline permease, putative	1307	0.607	UP MOD					
	Afu5g00930	amino acid permease,	1443	0.529	UP LOW					

		putative								
	Afu1g10770	neutral amino acid permease, putative	1507	0.093	UP LOW					
Carbohydrate / protein glycosylation	Afu4g00390	glycosyl hydrolase, putative	152	0.093	UP HIGH	Afu3g02040	glycosyl hydrolase, putative	115	0.509	DOWN HIGH
	Afu4g13400	glycosyltransferase family 28, putative	199	0.061	UP HIGH	Afu6g12010	glycosyl hydrolase, family 3, putative	456	0.755	DOWN HIGH
	Afu8g00680	glycosyl transferase, group 2 family protein	1238	0.337	UP MOD	Afu3g07860	glycosyl transferase, putative	614	0.606	DOWN HIGH
	Afu8g02070	glycosyl transferase, putative	1336	0.485	UP LOW	Afu8g02320	glycosyl transferase, group 2 family protein domain protein	668	0.736	DOWN MOD
	Afu6g08080	glycosyl hydrolase, family 15	1924	0.155	UP LOW	Afu3g00700	glycosyl hydrolase, putative	803	0.761	DOWN MOD
						Afu8g02040	glycosyl transferase, putative	1374	0.701	DOWN LOW
						Afu4g13770	glycosyl hydrolase, putative	1482	0.874	DOWN LOW
						Afu8g06980	glycosyl hydrolase, putative	1506	0.678	DOWN LOW
						Afu2g03270	glycosyl hydrolase, putative	1531	0.685	DOWN LOW
						Afu6g11820	Glycosyl hydrolase family 10	1681	0.895	DOWN LOW
						Afu2g00680	glycosyl hydrolase, putative	1729	0.888	DOWN LOW
						Afu8g00640	glycosyl transferase, putative	1886	0.619	DOWN LOW
Transposition associated genes	Afu7g08410	Tc1-mariner transposase, putative	17	0.014	UP HIGH	Afu3g09410	reverse transcriptase	1	0.004	DOWN HIGH
	Afu6g09940	transposase	262	0.081	UP HIGH	Afu8g00330	endonuclease/reverse transcriptase/RNaseH, putative	3	0.002	DOWN HIGH
	Afu1g00940	Tc1-mariner class transposase, putative	426	0.578	UP HIGH	Afu4g01630	reverse transcriptase, putative	14	0.327	DOWN HIGH
	Afu1g10020	reverse transcriptase, RNaseH	432	0.36	UP HIGH	Afu7g07170	reverse transcriptase/protease/endo nuclease Pol, putative	18	0.184	DOWN HIGH
	Afu7g02160	DDE superfamily endonuclease/transposase	638	0.483	UP HIGH	Afu7g06930	reverse transcriptase, RNaseH	121	0.36	DOWN HIGH
	Afu5g13900	transposase	1035	0.078	UP MOD	Afu8g00310	LINE-1 class reverse transcriptase, RNaseH, putative	127	0.308	DOWN HIGH

	Afu3g10430	transposase	1813	0.008	UP LOW		Afu4g00820	reverse transcriptase, RNaseH	185	0.445	DOWN HIGH
	Afu3g01740	transposase	1922	0.01	UP LOW		Afu3g09420	transposase, putative	311	0.615	DOWN HIGH
							Afu5g00270	LINE-1 class reverse transcriptase, RNaseH, putative	459	0.786	DOWN HIGH
							Afu8g01040	reverse transcriptase, RNaseH	687	0.787	DOWN MOD
							Afu8g06290	LINE-1 class reverse transcriptase, RNaseH, putative	954	0.791	DOWN MOD
							Afu5g03620	endonuclease/transposase	1022	0.072	DOWN MOD
							Afu7g00100	LINE-1 class reverse transcriptase, RNaseH, putative	1282	0.881	DOWN MOD
							Afu7g08210	reverse transcriptase, putative	1355	0.811	DOWN LOW
							Afu6g14660	reverse transcriptase, RNaseH	1418	0.888	DOWN LOW
							Afu2g18080	LINE-1 class reverse transcriptase, RNaseH, putative	1821	0.937	DOWN LOW
							Afu6g10920	mariner class transposase, putative	1970	0.791	DOWN LOW
Pathogenesis	Afu5g13300	aspartic endopeptidase Pep1	26	0.005	UP HIGH		Afu8g02380	FAD-dependent monooxygenase, putative	51	0.522	DOWN HIGH
	Afu4g11800	alkaline serine protease Alp1	67	0.007	UP HIGH		Afu5g08890	homoaconitase LysF	951	0.297	DOWN MOD
	Afu8g07080	elastinolytic metalloproteinase Mep	103	0.001	UP HIGH		Afu7g05060	MgtC/SapB family membrane protein	1925	0.843	DOWN LOW
	Afu2g03830	allergen Asp F4	104	0.288	UP HIGH						
	Afu2g13440	chitin synthase E	160	0.147	UP HIGH						
	Afu2g07680	L-ornithine N5-oxygenase SidA	322	0.096	UP HIGH						
	Afu8g02750	nucleolar protein CgrA	327	0.095	UP HIGH						
	Afu3g02270	mycelial catalase Cat1	520	0.025	UP HIGH						
	Afu6g02280	allergen Asp F3	865	0.236	UP MOD						
	Afu3g00590	Asp-hemolysin	982	0.4	UP MOD						
	Afu5g00600	NPP1 domain protein, putative	1014	0.169	UP MOD						

	Afu3g12960	cytochrome P450 monooxigenase (GliC), putative	1019	0.565	UP MOD					
	Afu6g06770	enolase	1182	0.164	UP MOD					
	Afu2g04200	4-hydroxyphenylpyruvate dioxygenase, putative	1317	0.042	UP LOW					
	Afu5g05480	Rheb GTPase RhbA	1334	0.297	UP LOW					
	Afu2g17560	1,3,6,8-tetrahydroxynaphthalene reductase	1530	0.311	UP LOW					
	Afu5g02330	major allergen Asp F1	1596	0.119	UP LOW					
	Afu2g12200	cAMP-dependent protein kinase catalytic subunit PkaC1	1657	0.361	UP LOW					
	Afu5g09580	conidial hydrophobin Hyp1/RodA	1762	0.675	UP LOW					
Signal transduction	Afu5g09020	WSC domain protein, putative	13	0.023	UP HIGH	Afu3g02500	protein kinase, putative	38	0.092	DOWN HIGH
	Afu6g04500	FOG1 protein	62	0.082	UP HIGH	Afu6g09260	sensor histidine kinase/response regulator, putative	64	0.266	DOWN HIGH
	Afu3g10340	Rho GTPase Rho 2, putative	92	0.205	UP HIGH	Afu1g05010	MFS transporter, putative	268	0.425	DOWN HIGH
	Afu2g02760	protein-tyrosine phosphatase, putative	122	0.03	UP HIGH	Afu2g11730	Protein kinase domain-containing protein	515	0.832	DOWN HIGH
	Afu5g12210	G-protein complex beta subunit SfaD	163	0.166	UP HIGH	Afu6g11190	protein kinase (VPS15), putative	691	0.105	DOWN MOD
	Afu3g12400	G protein complex alpha subunit (GanA), putative	201	0.261	UP HIGH	Afu1g04330	Ser/Thr protein phosphatase family protein	785	0.214	DOWN MOD
	Afu3g05770	RAS small monomeric GTPase, putative	304	0.032	UP HIGH	Afu1g06920	serine/threonine protein kinase, putative	808	0.799	DOWN MOD
	Afu5g14060	Rho GTPase Rho4, putative	318	0.079	UP HIGH	Afu5g08620	Ser/Thr protein phosphatase family	1072	0.46	DOWN MOD
	Afu6g03160	NACHT domain protein	328	0.058	UP HIGH	Afu3g13210	protein kinase domain-containing protein	1160	0.707	DOWN MOD
	Afu1g14890	cpdP protein, putative	519	0.243	UP HIGH	Afu2g00910	Pfs, NB-ARC and TPR domain protein	1187	0.81	DOWN MOD
	Afu1g05210	G-protein complex gamma subunit Ste18	576	0.086	UP HIGH	Afu4g07400	sensor histidine kinase/response regulator, putative	1237	0.687	DOWN MOD
	Afu5g07430	Rho guanyl nucleotide exchange factor, putative	616	0.116	UP HIGH	Afu2g14650	protein kinase domain-containing protein	1396	0.891	DOWN LOW
	Afu1g06900	C2H2 transcription factor (Crz1), putative	623	0.115	UP HIGH	Afu4g00320	sensor histidine kinase/response regulator,	1488	0.134	DOWN LOW

Afu1g07630	zinc knuckle domain protein (Byr3), putative	645	0.286	UP HIGH
Afu2g03510	pheromone processing carboxypeptidase (Sxa2), putative	754	0.339	UP MOD
Afu3g10240	Ccr4-Not transcription complex subunit (NOT1), putative	797	0.346	UP MOD
Afu5g08550	Rho guanyl nucleotide exchange factor (Rom2), putative	880	0.151	UP MOD
Afu3g14170	high-affinity hexose transporter	950	0.354	UP MOD
Afu7g04300	RhoGAP and Fes/CIP4 domain protein	1033	0.231	UP MOD
Afu1g10940	MAP kinase kinase kinase, putative	1082	0.165	UP MOD
Afu6g08350	retrograde regulation protein 2	1289	0.288	UP MOD
Afu4g10010	cdc37 protein	1460	0.057	UP LOW
Afu1g09560	protein transport protein (LST8), putative	1465	0.599	UP LOW
Afu2g11100	AMFR protein, putative	1523	0.089	UP LOW
Afu3g06300	Rho GTPase Rac, putative	1574	0.166	UP LOW
Afu2g12200	cAMP-dependent protein kinase catalytic subunit PkaC1	1657	0.361	UP LOW
Afu3g12550	sensor histidine kinase/response regulator, putative	1659	0.594	UP LOW
Afu5g11970	protein kinase c, putative	1695	0.509	UP LOW
Afu2g07540	TOR signalling pathway protein TipA, putative	1739	0.507	UP LOW
Afu5g08420	SHO1 protein	1747	0.346	UP LOW
Afu2g05740	Rho GTPase ModA, putative	1748	0.469	UP LOW
Afu6g10330	GTP binding protein (SPG1), putative	1857	0.444	UP LOW
Afu6g11010	cell morphogenesis protein (PAG1), putative	1884	0.638	UP LOW
Afu5g09320	signal transduction protein (Syg1), putative	1933	0.449	UP LOW

	putative			
Afu8g05980	protein kinase, putative	1672	0.769	DOWN LOW
Afu2g16620	protein kinase, putative	1777	0.854	DOWN LOW
Afu4g00800	MFS monosaccharide transporter, putative	1796	0.785	DOWN LOW
Afu2g17130	protein kinase regulator Ste50	1807	0.92	DOWN LOW
Afu5g03160	protein kinase, putative	1938	0.752	DOWN LOW

	Afu2g15050	Rho GTPase activator (Lrg11), putative	1968	0.738	UP LOW					
Sphingolipid biosynthesis	Afu2g10460	conserved hypothetical protein	286	0.095	UP HIGH	Afu6g08370	neutral sphingomyelinase	623	0.107	DOWN HIGH
	Afu5g02760	fatty acid elongase (Gns1), putative	379	0.001	UP HIGH	Afu1g10980	sphingosine kinase (SphK), putative	1039	0.774	DOWN MOD
	Afu6g00300	serine palmitoyltransferase 1, putative	599	0.006	UP HIGH					
	Afu6g10460	ceramide synthase membrane component (Lag1), putative	792	0.078	UP MOD					
	Afu1g16710	fatty acid elongase (Gig30), putative	802	0.579	UP MOD					
	Afu6g04680	MIPC synthase subunit (SurA), putative	1037	0.164	UP MOD					
	Afu5g14050	PAP2 domain protein	1354	0.065	UP LOW					
	Afu6g12390	serine palmitoyl CoA transferase subunit LcbA	1564	0.527	UP LOW					
	Afu1g11150	3-ketosphinganine reductase (Tsc10), putative	1834	0.463	UP LOW					
Transcription factors	Afu4g10340	C6 finger domain protein, putative	8	0.017	UP HIGH	Afu2g05360	C6 transcription factor, putative	16	0.003	DOWN HIGH
	Afu5g14230	C6 transcription factor, putative	51	0.056	UP HIGH	Afu1g17710	C6 transcription factor, putative	22	0.331	DOWN HIGH
	Afu1g13050	C2H2 transcription factor, putative	63	0.065	UP HIGH	Afu2g14120	C6 finger domain protein, putative	30	0.104	DOWN HIGH
	Afu4g10120	C6 finger domain protein, putative	88	0.202	UP HIGH	Afu4g10160	C6 transcription factor (AmyR), putative	49	0.408	DOWN HIGH
	Afu2g10550	C2H2 transcription factor (RfeC), putative	220	0.246	UP HIGH	Afu5g06800	C6 transcription factor, putative	168	0.337	DOWN HIGH
	Afu6g09350	C6 finger domain protein, putative	345	0.098	UP HIGH	Afu2g15260	C6 transcription factor (Leu3), putative	258	0.499	DOWN HIGH
	Afu2g10850	C6 finger domain protein, putative	496	0.172	UP HIGH	Afu8g00420	C6 finger transcription factor, putative	271	0.595	DOWN HIGH
	Afu1g06900	C2H2 transcription factor (Crz1), putative	623	0.115	UP HIGH	Afu5g12020	C6 transcription factor (NirA), putative	539	0.722	DOWN HIGH
	Afu4g12470	bZIP transcription factor CpcA	662	0.128	UP MOD	Afu6g09630	C6 finger domain protein GliZ	643	0.57	DOWN HIGH
	Afu1g14750	C2H2 transcription factor (Sfp1), putative	810	0.27	UP MOD	Afu7g04890	C6 transcription factor, putative	654	0.508	DOWN HIGH
	Afu1g13750	C2H2 transcription factor (Rpn4), putative	866	0.273	UP MOD	Afu3g11990	C6 transcription factor (Mut3), putative	666	0.253	DOWN MODERATE

Afu3g11250	C2H2 transcription factor (Swi5), putative	910	0.384	UP MOD
Afu1g08770	C6 finger domain protein, putative	983	0.255	UP MOD
Afu2g07480	C6 finger domain protein, putative	1057	0.135	UP MOD
Afu8g05800	C6 finger domain protein, putative	1067	0.008	UP MOD
Afu3g12660	C6 finger domain protein, putative	1212	0.276	UP MOD
Afu2g04250	C6 finger domain protein, putative	1220	0.35	UP MOD
Afu4g11850	C6 finger domain protein, putative	1225	0.384	UP MOD
Afu3g00490	C6 finger domain protein, putative	1329	0.533	UP LOW
Afu2g08040	C6 finger domain protein, putative	1362	0.424	UP LOW
Afu3g09820	C2H2 transcription factor, putative	1368	0.562	UP LOW
Afu3g00210	C6 finger domain protein, putative	1446	0.561	UP LOW
Afu2g16160	C6 finger domain protein, putative	1549	0.243	UP LOW
Afu3g11330	bZIP transcription factor (AtfA), putative	1746	0.31	UP LOW
Afu3g06740	C6 transcription factor (Gal4), putative	1770	0.275	UP LOW
Afu1g16460	bZIP transcription factor (LziP), putative	1804	0.2	UP LOW
Afu8g05460	bZIP transcription factor, putative	1808	0.526	UP LOW
Afu2g17220	C2H2 transcription factor (AmdX), putative	1882	0.191	UP LOW
Afu3g08010	C2H2 transcription factor (Ace1), putative	1926	0.175	UP LOW

Afu4g00710	C6 transcription factor, putative	696	0.396	DOWN MODERATE
Afu5g01460	C6 finger domain protein, putative	710	0.097	DOWN MODERATE
Afu7g01810	C6 transcription factor, putative	721	0.289	DOWN MODERATE
Afu1g11620	C6 transcription factor (QutA), putative	723	0.56	DOWN MODERATE
Afu4g01470	C6 finger domain protein, putative	794	0.667	DOWN MODERATE
Afu4g14590	C6 transcription factor, putative	820	0.823	DOWN MODERATE
Afu1g15230	C6 transcription factor, putative	845	0.761	DOWN MODERATE
Afu8g04540	C6 transcription factor, putative	849	0.122	DOWN MODERATE
Afu3g01510	C6 transcription factor, putative	1525	0.743	DOWN LOW
Afu1g16220	C6 transcription factor, putative	1572	0.856	DOWN LOW
Afu3g11970	C2H2 transcription factor PacC, putative	1580	0.612	DOWN LOW
Afu1g15470	C6 transcription factor (UaY), putative	1626	0.76	DOWN LOW
Afu8g07180	C6 transcription factor, putative	1639	0.579	DOWN LOW
Afu5g14290	C6 transcription factor, putative	1740	0.73	DOWN LOW
Afu1g15850	C6 transcription factor, putative	1753	0.829	DOWN LOW
Afu6g07130	C6 transcription factor, putative	1793	0.402	DOWN LOW
Afu4g01510	C6 transcription factor, putative	1836	0.528	DOWN LOW
Afu1g09190	C6 finger domain protein, putative	1873	0.689	DOWN LOW

Table 3.20: Functional classification of selected genes having differential transcript abundance in Af293 between 8 and 14 hours post infection in the murine lung. Increased (red) and decreased (green) are shown for each functional category. Both increasing and decreasing transcripts are sub divided into expression cohorts which are either high, moderate, or low with respect to their expression change. Genes within funcation categories ranked according to greatest nSI intensity changes between 8 and 14 hours. FDR correct *p*-values from a one-way ANOVA are reported for each gene.

Functional category	ORF	Description	Rank	FDR P-value	Magnitude
Cell wall	Afu2g14360	GPI anchored glucanase, putative	103	0.358	UP HIGH
	Afu5g03960	class V chitinase Chi100	141	0.258	UP HIGH
	Afu1g00310	class V chitinase, putative	142	0.622	UP HIGH
	Afu5g14030	endo-1,3(4)-beta-glucanase, putative	231	0.534	UP HIGH
	Afu6g14540	endo-1,3(4)-beta-glucanase, putative	309	0.44	UP HIGH
	Afu7g08510	extracellular alpha-1,3-glucanase/mutanase, putative	783	0.393	UP MOD
	Afu2g06160	mutanase	794	0.689	UP MOD
	Afu6g09780	class V chitinase, putative	838	0.857	UP MOD
	Afu3g03080	endo-1,3(4)-beta-glucanase, putative	885	0.871	UP MOD
	Afu3g03870	endo-1,4-beta-glucanase, putative	902	0.641	UP MOD
	Afu3g07160	class V chitinase, putative	1063	0.914	UP MOD
	Afu4g13360	endo-1,3(4)-beta-glucanase, putative	1181	0.412	UP MOD
	Afu8g06030	alpha-1,3-glucanase, putative	1188	0.881	UP MOD
	Afu5g00760	chitin synthase C	33	0.407	DOWN HIGH
	Afu3g13200	1,3-beta-glucanosyltransferase, putative	80	0.325	DOWN HIGH
	Afu5g14190	beta-glucanase, putative	100	0.355	DOWN HIGH
	Afu2g14910	alpha-1,6-mannosyltransferase subunit, putative	151	0.673	DOWN HIGH
	Afu2g15910	aminonitrophenyl propanediol resistance protein	368	0.32	DOWN HIGH
	Afu5g03940	alpha-1,3-glucanase, putative	640	0.791	DOWN HIGH
	Afu6g09310	class V chitinase, putative	791	0.879	DOWN MOD
	Afu1g04260	endo-1,3-beta-glucanase Engl1	1240	0.842	DOWN MOD
	Afu2g13440	chitin synthase E	1304	0.857	DOWN MOD
	Afu3g10340	Rho GTPase Rho 2, putative	1341	0.882	DOWN LOW
	Afu8g02130	1,3-beta-glucanosyltransferase, putative	1352	0.82	DOWN LOW
	Afu1g01380	alpha-1,6-mannosyltransferase subunit (Hoc1), putative	1365	0.686	DOWN LOW
	Afu5g11990	alpha-1,3-mannosyltransferase (Alg3), putative	1433	0.872	DOWN LOW

	Afu5g02280	endo-1,3(4)-beta-glucanase, putative	1421	0.92	UP LOW		Afu2g13430	chitin synthase, putative	1693	0.93	DOWN LOW
	Afu8g02040	glycosyl transferase, putative	1458	0.914	UP LOW		Afu3g07110	class III chitinase, putative	1766	0.875	DOWN LOW
	Afu8g05620	chitin synthase activator (Chs3), putative	1492	0.939	UP LOW		Afu2g01170	1,3-beta-glucanosyltransferase Gel1	1927	0.948	DOWN LOW
	Afu1g03350	alpha-1,3-glucanase, putative	1563	0.899	UP LOW						
	Afu2g03980	alpha-1,3-glucanase, putative	1650	0.716	UP LOW						
	Afu7g08350	alpha-1,3-glucanase, putative	1835	0.882	UP LOW						
Ergosterol	Afu1g11140	Sterol desaturase family	173	0.703	UP HIGH		Afu6g05140	sterol delta 5,6-desaturase ERG3	11	0.72	DOWN HIGH
	Afu4g14770	squalene-hopene-cyclase, putative	1280	0.916	UP MOD		Afu4g06380	sterol carrier protein, putative	78	0.194	DOWN HIGH
	Afu3g05880	oxysterol binding protein (Osh3), putative	1535	0.914	UP LOW		Afu4g12040	oxidosqualene:lanosterol cyclase	334	0.38	DOWN HIGH
	Afu1g05720	c-14 sterol reductase	1545	0.946	UP LOW		Afu4g06890	14-alpha sterol demethylase Cyp51A	391	0.787	DOWN HIGH
							Afu2g03790	oxysterol binding protein (Osh7), putative	874	0.633	DOWN MOD
							Afu3g11750	oxysterol binding protein (Osh5), putative	1170	0.721	DOWN MOD
							Afu8g01070	Lathosterol oxidase, putative	1198	0.849	DOWN MOD
							Afu4g07780	mevalonate kinase	1332	0.857	DOWN LOW
							Afu2g15030	C-3 sterol dehydrogenase/C-4 decarboxylase	1415	0.716	DOWN LOW
Antigen	Afu4g00610	aryl-alcohol dehydrogenase, putative	18	0.288	UP HIGH		Afu2g12630	allergen Asp F13	63	0.389	DOWN HIGH
	Afu7g05740	malate dehydrogenase, NAD-dependent	1519	0.678	UP LOW		Afu5g09580	conidial hydrophobin Hyp1/RodA	111	0.739	DOWN HIGH
							Afu5g13300	aspartic endopeptidase Pep1	126	0.451	DOWN HIGH
							Afu2g03720	peptidyl-prolyl cis-trans isomerase	221	0.776	DOWN HIGH
							Afu5g02040	extracellular lipase, putative	389	0.152	DOWN HIGH
							Afu5g02330	major allergen Asp F1	393	0.787	DOWN

										HIGH
						Afu2g06150	disulfide isomerase, putative	761	0.276	DOWN MOD
						Afu2g11850	large subunit ribosomal protein L3	834	0.893	DOWN MOD
						Afu4g09090	thioredoxin, putative	887	0.395	DOWN MOD
						Afu3g10460	nuclear transport factor 2	934	0.3	DOWN MOD
						Afu6g02280	allergen Asp F3	1292	0.865	DOWN MOD
						Afu6g11330	histidine acid phosphatase, putative	1380	0.78	DOWN LOW
						Afu2g10100	60S acidic ribosomal protein P2	1700	0.922	DOWN LOW
						Afu1g06830	60s Acidic ribosomal protein superfamily	1792	0.733	DOWN LOW
Ion transport	Afu5g05980	calcium/calmodulin dependent protein kinase, putative	304	0.884	UP HIGH	Afu6g06740	endoplasmic reticulum calcium ATPase, putative	300	0.662	DOWN HIGH
	Afu2g01460	ZIP Zinc transporter, putaitve	836	0.905	UP MOD	Afu2g17170	Na+/H+ antiporter Nha1	317	0.304	DOWN HIGH
	Afu1g16340	potassium transporter, putative	925	0.689	UP MOD	Afu1g10880	P-type calcium ATPase, putative	585	0.643	DOWN HIGH
	Afu2g03860	plasma membrane low affinity zinc ion transporter, putative	1032	0.723	UP MOD	Afu5g05840	calcium channel MID1	1344	0.8	DOWN LOW
	Afu1g11110	calcium channel pore-forming subunit (Cch1), putative	1038	0.902	UP MOD	Afu7g03880	sodium/calcium exchanger protein	1563	0.785	DOWN LOW
	Afu2g13060	calcineurin binding protein, putative	1166	0.544	UP MOD	Afu7g03880	sodium/calcium exchanger protein	1563	0.785	DOWN LOW
	Afu6g07050	sodium-hydrogen antiporter, putative	1427	0.938	UP LOW	Afu4g13540	potassium uptake transporter, putative	1900	0.442	DOWN LOW
	Afu2g09460	potassium transporter	1768	0.799	UP LOW					
Iron aquisition	Afu3g03440	MFS family siderophore transporter, putative	549	0.563	UP HIGH	Afu2g12610	ferrodoxin-NADP(+) reductase	238	0.381	DOWN HIGH
	Afu3g03400	siderophore biosynthesis acetylase AceI, putative	956	0.739	UP MOD	Afu5g00260	ferric-chelate reductase, putative	1172	0.91	DOWN MOD
	Afu7g06060	siderochrome-iron transporter (Sit1),	1162	0.38	UP MOD					

		putative								
	Afu5g03800	high-affinity iron permease CaFTR2	1229	0.869	UP MOD					
Secondary metabolite	Afu8g00540	hybrid polyketide synthase/nonribosomal peptide synthase, putative	37	0.639	UP HIGH					
	Afu4g14270	polyketide synthase, putative	230	0.624	UP HIGH					
	Afu6g12050	nonribosomal peptide synthase, putative	261	0.409	UP HIGH					
	Afu5g00150	nonribosomal peptide synthetase, putative	263	0.591	UP HIGH					
	Afu3g02570	polyketide synthase, putative	529	0.426	UP HIGH					
	Afu6g03480	nonribosomal peptide synthetase, putative	610	0.753	UP HIGH					
	Afu8g00490	polyketide synthase, putative	668	0.874	UP MOD					
	Afu3g03350	nonribosomal peptide synthase, putative	787	0.624	UP MOD					
	Afu6g08560	nonribosomal peptide synthase (NRPS), putative	824	0.914	UP MOD					
	Afu6g09610	nonribosomal peptide synthase, putative	927	0.81	UP MOD					
	Afu3g15270	nonribosomal peptide synthetase, putative	1297	0.877	UP MOD					
	Afu3g02670	nonribosomal peptide synthetase, putative	1379	0.882	UP LOW					
	Afu8g00170	nonribosomal peptide synthetase, putative	1576	0.784	UP LOW					
	Afu8g00370	polyketide synthase, putative	1840	0.898	UP LOW					
Gliotoxin	Afu6g09680	O-methyltransferase GliM	3	0.092	UP HIGH	Afu6g09620	hypothetical protein	1521	0.673	DOWN LOW
	Afu6g09710	MFS gliotoxin efflux pump GliA	4	0.195	UP HIGH					
	Afu6g09630	C6 finger domain protein GliZ	683	0.565	UP MOD					
	Afu6g09760	toxin biosynthesis cytochrome P450 oxidoreductase, putative	867	0.723	UP MOD					

	Afu6g09610	nonribosomal peptide synthase, putative	927	0.81	UP MOD				
	Afu6g09590	zinc-containing alcohol dehydrogenase, putative	1583	0.876	UP LOW				
Pseurotin A Supercluster	Afu8g00330	endonuclease/reverse transcriptase/RNaseH, putative	22	0.182	UP HIGH	Afu8g00650	LPS glycosyltransferase, putative	369	0.787	DOWN HIGH
	Afu8g00540	hybrid polyketide synthase/nonribosomal peptide synthase, putative	37	0.639	UP HIGH	Afu8g00710	secreted antimicrobial peptide, putative	379	0.767	DOWN HIGH
	Afu8g00280	short-chain dehydrogenase, putative	120	0.72	UP HIGH	Afu8g00450		492	0.594	DOWN HIGH
	Afu8g00240	cytochrome P450 monooxygenase, putative	169	0.726	UP HIGH	Afu8g00610	cell surface protein Mas1, putative	952	0.869	DOWN MOD
	Afu8g00630	conserved hypothetical protein	347	0.734	UP HIGH	Afu8g00130	hypothetical protein	966	0.879	DOWN MOD
	Afu8g00620	dimethylallyl tryptophan synthase, putative	381	0.221	UP HIGH	Afu8g00460	methionine aminopeptidase, type I, putative	1599	0.925	DOWN LOW
	Afu8g00300	conserved hypothetical protein	566	0.84	UP HIGH	Afu8g00430	conserved hypothetical protein	1787	0.925	DOWN LOW
	Afu8g00310	LINE-1 class reverse transcriptase, RNaseH, putative	660	0.686	UP MOD					
	Afu8g00490	polyketide synthase, putative	668	0.874	UP MOD					
	Afu8g00440	steroid monooxygenase, putative	750	0.511	UP MOD					
	Afu8g00360	NlpC/P60-like cell-wall peptidase, putative	903	0.807	UP MOD					
	Afu8g00530	alpha/beta hydrolase, putative	905	0.891	UP MOD					
	Afu8g00350	conserved hypothetical protein	1012	0.88	UP MOD					
	Afu8g00200	O-methyltransferase, putative	1248	0.834	UP MOD					
	Afu8g00420	C6 finger transcription	1409	0.918	UP LOW					

		factor, putative							
	Afu8g00180	conserved hypothetical protein	1516	0.938	UP LOW				
	Afu8g00660	solute transporter, putative	1554	0.93	UP LOW				
	Afu8g00170	nonribosomal peptide synthetase, putative	1576	0.784	UP LOW				
	Afu8g00550	SirN-like methyltransferase, putative	1775	0.89	UP LOW				
	Afu8g00410	methionine aminopeptidase, type II, putative	1792	0.941	UP LOW				
	Afu8g00290	conserved hypothetical protein	1837	0.938	UP LOW				
	Afu8g00370	polyketide synthase, putative	1840	0.898	UP LOW				
	Afu8g00640	glycosyl transferase, putative	1879	0.914	UP LOW				
Microtubule	Afu2g16260	microtubule associated protein (Ase1), putative	244	0.583	UP HIGH				
	Afu2g03150	kinesin family protein	479	0.287	UP HIGH				
	Afu6g14220	kinesin family protein (KinA), putative	1273	0.701	UP MOD				
Secreted proteases	Afu3g11400	aspartic endopeptidase Pep2	520	0.262	UP HIGH	Afu5g01200	carboxypeptidase S1, putative	16	0.152	DOWN HIGH
	Afu2g15950	aspartic endopeptidase, putative	611	0.809	UP HIGH	Afu4g14000	tripeptidyl peptidase A	108	0.701	DOWN HIGH
	Afu3g01220	aspartic-type endopeptidase, putative	694	0.615	UP MOD	Afu5g13300	aspartic endopeptidase Pep1	126	0.451	DOWN HIGH
	Afu8g00360	NlpC/P60-like cell-wall peptidase, putative	903	0.807	UP MOD	Afu2g03510	pheromone processing carboxypeptidase (Sxa2), putative	689	0.727	DOWN MOD
	Afu1g08940	pheromone processing carboxypeptidase Kex1	1385	0.696	UP LOW	Afu3g12210	carboxypeptidase Y, putative	1140	0.835	DOWN MOD
	Afu4g07270	serine carboxypeptidase, putative	1452	0.832	UP LOW	Afu3g00650	aminopeptidase Y, putative	1493	0.78	DOWN LOW
						Afu6g00310	serine carboxypeptidase	1587	0.704	DOWN

									(CpdS), putative			LOW
								Afu8g04120	carboxypeptidase S1, putative	1827	0.918	DOWN LOW
Signal peptide encoding genes	Afu6g09670	cytochrome P450 oxidoreductase GliC	2	0.037	UP HIGH			Afu3g00820	putative exported protein	13	0.041	DOWN HIGH
	Afu4g14070	glycosyl transferase, putative	7	0.466	UP HIGH			Afu3g02970	aspergillopepsin, putative	15	0.092	DOWN HIGH
	Afu8g06980	glycosyl hydrolase, putative	32	0.616	UP HIGH			Afu3g13240	aldose 1-epimerase, putative	43	0.263	DOWN HIGH
	Afu1g01310	carboxylesterase, putative	46	0.304	UP HIGH			Afu2g16800	lectin family integral membrane protein, putative	44	0.024	DOWN HIGH
	Afu1g13980	conserved hypothetical protein	50	0.54	UP HIGH			Afu2g12630	allergen Asp F13	63	0.389	DOWN HIGH
	Afu4g13770	glycosyl hydrolase, putative	51	0.595	UP HIGH			Afu3g15210	endo-1,4-beta-xylanase, putative	74	0.746	DOWN HIGH
	Afu6g10580	antigenic CFEM domain protein, putative	86	0.442	UP HIGH			Afu3g14680	lysophospholipase Plb3	76	0.018	DOWN HIGH
	Afu2g14420	cutinase, putative	119	0.354	UP HIGH			Afu3g13200	1,3-beta-glucanosyltransferase, putative	80	0.325	DOWN HIGH
	Afu3g01910	cellobiohydrolase, putative	125	0.704	UP HIGH			Afu3g02270	mycelial catalase Cat1	86	0.354	DOWN HIGH
	Afu1g04430	conserved hypothetical protein	133	0.264	UP HIGH			Afu1g14310	poly(A)-binding protein-dependent poly(A) ribonuclease, putative	87	0.442	DOWN HIGH
	Afu8g07250	pectin methylesterase family protein	136	0.701	UP HIGH			Afu1g07740	LEM3/CDC50 family protein	88	0.583	DOWN HIGH
	Afu6g00250	GPI anchored protein, putative	140	0.604	UP HIGH			Afu1g12870	conserved hypothetical protein	135	0.381	DOWN HIGH
	Afu5g03960	class V chitinase Chi100	141	0.258	UP HIGH			Afu2g01240	beta-D-fructofuranoside fructohydrolase	142	0.262	DOWN HIGH
	Afu1g00310	class V chitinase, putative	142	0.622	UP HIGH			Afu3g00810	cholestenol delta-isomerase, putative	150	0.594	DOWN MOD
	Afu3g14030	alkaline phosphatase	702	0.262	UP MODERATE			Afu1g16250	alpha-glucosidase B	681	0.432	DOWN MOD
	Afu1g17570	urea active transporter, putative	703	0.264	UP MODERATE			Afu2g03510	pheromone processing carboxypeptidase (Sxa2), putative	689	0.727	DOWN MOD
	Afu3g10820	metalloreductase, putative	745	0.538	UP MODERATE			Afu3g10490	DNA damage response protein (Dap1), putative	692	0.277	DOWN MOD
	Afu8g06490	conserved hypothetical protein	762	0.043	UP MODERATE			Afu1g03790	mannosylphosphorylation protein (Mnn4), putative	705	0.583	DOWN MOD

	Afu2g01710	GPI anchored protein, putative	765	0.81	UP MODERATE		Afu2g00890	hypothetical protein	729	0.168	DOWN MOD
	Afu5g01830	extracellular endoglucanase, putative	766	0.867	UP MODERATE		Afu2g11130	NOT2 family protein	736	0.907	DOWN MOD
Ribosome biogenesis and RNA metabolism	Afu7g01460	ribosomal protein S5	154	0.202	UP HIGH		Afu2g13090	RNA polymerase II subunit 3	46	0.772	DOWN HIGH
	Afu5g07640	RNA 3'-terminal phosphate cyclase, putative	512	0.845	UP HIGH		Afu2g16370	Ribosomal protein L32	121	0.263	DOWN HIGH
	Afu2g13570	ribosome biogenesis protein (Bms1), putative	543	0.82	UP HIGH		Afu1g10310	RNase L inhibitor of the ABC superfamily, putative	154	0.447	DOWN HIGH
	Afu6g10370	RNA lariat debranching enzyme, putative	642	0.893	UP HIGH		Afu3g10380	RNA polymerase III transcription factor, putative	193	0.214	DOWN HIGH
	Afu3g03050	RNAse III, putative	918	0.892	UP MOD		Afu1g07350	RNA12 protein, putative	241	0.662	DOWN HIGH
	Afu1g02950	RNA recognition motif. (a.k.a. RRM, RBD, or RNP domain) protein	1242	0.849	UP MOD		Afu6g08610	RNA methylase family protein, putative	258	0.236	DOWN HIGH
	Afu1g11440	RNA export mediator Gle1, putative	1386	0.739	UP LOW		Afu4g13450	RNA methyltransferase, TrmH family family	320	0.742	DOWN HIGH
	Afu8g04820	ribonuclease P complex subunit p30, putative	1825	0.93	UP LOW		Afu5g08350	ribosomal protein S16	403	0.611	DOWN HIGH
							Afu1g15020	40S ribosomal protein S5	417	0.791	DOWN HIGH
							Afu1g10990	ribosomal RNA processing protein, putative	445	0.783	DOWN HIGH
							Afu3g05840	RNA-binding protein rnp24, putative	567	0.694	DOWN HIGH
							Afu6g07360	ribosomal protein S8	629	0.442	DOWN HIGH
							Afu5g08310	RNA and export factor binding protein 2-I	650	0.776	DOWN HIGH
							Afu3g12300	Ribosomal L22e protein family	670	0.741	DOWN MOD
							Afu4g12170	ribosomal protein L2	722	0.258	DOWN MOD
							Afu4g07640	ribosomal protein S13	748	0.443	DOWN MOD

Afu1g04980	RNA polymerase III transcription factor TFIIIC subunit (Tfc4), putative	773	0.919	DOWN MOD
Afu6g12660	40s ribosomal protein	792	0.287	DOWN MOD
Afu1g06770	Ribosomal protein S26e	868	0.481	DOWN MOD
Afu1g03110	60S ribosomal protein L29, putative	946	0.723	DOWN MOD
Afu1g05080	ribosomal protein P0	997	0.318	DOWN MOD
Afu1g14110	RNA polymerase subunit	1062	0.726	DOWN MOD
Afu1g06340	60S ribosomal protein L27	1162	0.784	DOWN MOD
Afu3g12280	RNA binding complex component (Translin), putative	1254	0.263	DOWN MOD
Afu6g04560	40S ribosomal protein S9, mitochondrial precursor	1262	0.237	DOWN MOD
Afu2g16880	ribosomal protein L37a	1348	0.832	DOWN LOW
Afu5g05450	ribosomal protein S3Ae, putative	1432	0.749	DOWN LOW
Afu2g13720	RNA-polymerase I	1443	0.914	DOWN LOW
Afu6g04810	RNA polymerase II transcription mediator complex subunit (Med6), putative	1462	0.606	DOWN LOW
Afu3g13320	40S ribosomal protein S0, putative	1501	0.583	DOWN LOW
Afu3g10730	Ribosomal protein S7e	1576	0.581	DOWN LOW
Afu2g10500	ribosomal protein S9	1613	0.877	DOWN LOW
Afu6g02450	ribosomal S30/ubiquitin fusion	1680	0.653	DOWN LOW
Afu2g10100	60S acidic ribosomal protein P2	1700	0.922	DOWN LOW
Afu1g09410	ribosomal protein L17	1717	0.624	DOWN LOW
Afu7g04490	Ribosomal protein S28e	1770	0.802	DOWN LOW
Afu1g06830	60s Acidic ribosomal protein	1792	0.733	DOWN

									superfamily		LOW
								Afu2g02270	ribosomal protein S14p/S29e	1797	0.909 DOWN LOW
								Afu1g15810	RNA splicing factor (Pad-1), putative	1849	0.899 DOWN LOW
								Afu5g04240	RNA binding protein Nrd1, putative	1893	0.941 DOWN LOW
Carbohydrate transport	Afu1g11050	MFS sugar transporter, putative	578	0.588	UP HIGH			Afu7g05550	sugar transporter family protein	254	0.237 DOWN HIGH
	Afu6g11920	maltose permease	614	0.85	UP HIGH			Afu8g01340	MFS sugar transporter, putative	347	0.822 DOWN HIGH
	Afu7g05100	hexose transporter protein	691	0.018	UP MOD			Afu8g05710	MFS sugar transporter Stl1, putative	469	0.329 DOWN HIGH
	Afu2g10910	maltose permease	899	0.481	UP MOD			Afu1g12240	MFS peptide transporter, putaitve	647	0.394 DOWN HIGH
	Afu6g14500	MFS sugar transporter, putative	1007	0.798	UP MOD			Afu3g12170	MFS sugar transporter, putative	1459	0.613 DOWN LOW
	Afu1g03280	maltose permease, putative	1224	0.915	UP MOD			Afu5g14540	MFS monosaccharide transporter, putative	1486	0.869 DOWN LOW
	Afu7g00220	plasma membrane hexose transporter, putative	1249	0.914	UP MOD			Afu5g06210	sucrose transporter, putative	1542	0.909 DOWN LOW
	Afu7g05830	MFS sugar transporter, putative	1475	0.594	UP LOW			Afu7g01490	MFS peptide transporter, putative	1715	0.777 DOWN LOW
	Afu5g00280	MFS sugar transporter, putative	1669	0.93	UP LOW						
Amino acid transport	Afu1g09120	amino acid permease, putative	54	0.119	UP HIGH			Afu2g15470	neutral amino acid permease	683	0.787 DOWN MOD
	Afu3g00120	amino acid transporter, putative	81	0.784	UP HIGH			Afu4g01570	neutral amino acid permease	1617	0.427 DOWN LOW
	Afu4g10090	GABA permease, putative	268	0.31	UP HIGH						
	Afu6g00410	amino acid permease, putative	516	0.701	UP HIGH						
	Afu8g06090	amino acid permease, putative	699	0.771	UP MOD						
	Afu3g01820	amino acid permease	710	0.726	UP MOD						
	Afu4g06230	general amino acid permease (Agp2), putative	1039	0.925	UP MOD						
	Afu8g01450	GABA permease, putative	1405	0.421	UP LOW						
	Afu8g00800	amino acid transporter, putative	1649	0.902	UP LOW						

Carbohydrate / protein glycosylation	Afu8g06980	glycosyl hydrolase, putative	32	0.616	UP HIGH		Afu4g00390	glycosyl hydrolase, putative	164	0.821	DOWN HIGH
	Afu4g13770	glycosyl hydrolase, putative	51	0.595	UP HIGH		Afu4g13400	glycosyltransferase family 28, putative	336	0.704	DOWN HIGH
	Afu5g00670	glycosyl hydrolase family 35, putative	145	0.78	UP HIGH		Afu6g08080	glycosyl hydrolase, family 15	1824	0.853	DOWN LOW
	Afu3g02040	glycosyl hydrolase, putative	363	0.842	UP HIGH						
	Afu3g07860	glycosyl transferase, putative	403	0.727	UP HIGH						
	Afu6g12010	glycosyl hydrolase, family 3, putative	1116	0.915	UP MOD						
	Afu3g03620	glycosyl transferase, putative	1270	0.726	UP MOD						
	Afu8g02040	glycosyl transferase, putative	1458	0.914	UP LOW						
	Afu8g02320	glycosyl transferase, group 2 family protein domain protein	1736	0.883	UP LOW						
	Afu8g00640	glycosyl transferase, putative	1879	0.914	UP LOW						
Transposition associated genes	Afu3g09410	reverse transcriptase	15	0.377	UP HIGH		Afu7g08410	Tc1-mariner transposase, putative	484	0.781	DOWN HIGH
	Afu8g00330	endonuclease/reverse transcriptase/RNaseH, putative	22	0.182	UP HIGH		Afu4g14880	reverse transcriptase, RNaseH, putative	1818	0.927	DOWN LOW
	Afu4g01630	reverse transcriptase, putative	128	0.746	UP HIGH		Afu6g09470	reverse transcriptase, RNaseH, putative	1862	0.929	DOWN LOW
	Afu8g01040	reverse transcriptase, RNaseH	252	0.77	UP HIGH		Afu6g09470	reverse transcriptase, RNaseH, putative	1862	0.929	DOWN LOW
	Afu7g06930	reverse transcriptase, RNaseH	388	0.853	UP HIGH						
	Afu3g09440	reverse transcriptase, RNaseH, putative	459	0.893	UP HIGH						
	Afu5g06180	possible transposase	580	0.262	UP HIGH						
	Afu8g00310	LINE-1 class reverse transcriptase, RNaseH, putative	660	0.686	UP MOD						
	Afu5g00270	LINE-1 class reverse transcriptase, RNaseH, putative	672	0.9	UP MOD						

	Afu3g09420	transposase, putative	680	0.727	UP MOD					
	Afu4g00780	Fot5 transposase, putative	798	0.71	UP MOD					
	Afu7g07170	reverse transcriptase/proteas e/endonuclease Pol, putative	881	0.882	UP MOD					
	Afu1g05030	possible transposase	951	0.582	UP MOD					
	Afu7g07070	LINE-1 class reverse transcriptase, RNaseH, putative	1058	0.883	UP MOD					
	Afu5g09820	mariner class transposase, putative	1081	0.728	UP MOD					
	Afu1g00140	Fot5 transposase, putative	1200	0.673	UP MOD					
	Afu6g10920	mariner class transposase, putative	1276	0.72	UP MOD					
	Afu4g00820	reverse transcriptase, RNaseH	1402	0.81	UP LOW					
	Afu5g03620	endonuclease/transp osase	1446	0.528	UP LOW					
	Afu7g03810	possible transposase	1525	0.624	UP LOW					
	Afu1g14760	possible transposase	1533	0.59	UP LOW					
	Afu5g02810	mariner class transposase, putative	1609	0.645	UP LOW					
	Afu5g04110	Fot1 family transposase, putative	1666	0.891	UP LOW					
	Afu6g02880	possible transposase	1674	0.892	UP LOW					
	Afu5g02980	mariner class transposase, putative	1735	0.694	UP LOW					
	Afu1g04650	transposase	1851	0.735	UP LOW					
	Afu3g12540	mariner class transposase, putative	1856	0.672	UP LOW					
	Afu6g03650	possible transposase	1956	0.88	UP LOW					
Pathogenesis	Afu3g14810	pathogenicity associated protein PEP2, putative	235	0.704	UP HIGH	Afu3g02270	mycelial catalase Cat1	86	0.354	DOWN HIGH
	Afu5g06070	ABC multidrug transporter Mdr1	239	0.152	UP HIGH	Afu5g09580	conidial hydrophobin Hyp1/RodA	111	0.739	DOWN HIGH
	Afu3g07150	succinate-semialdehyde dehydrogenase,	700	0.13	UP MOD	Afu5g13300	aspartic endopeptidase Pep1	126	0.451	DOWN HIGH

		putative								
	Afu6g09610	nonribosomal peptide synthase, putative	927	0.81	UP MOD		Afu5g02330	major allergen Asp F1	393	0.787	DOWN HIGH
	Afu5g08890	homoaconitase LysF	1500	0.491	UP LOW		Afu3g12960	cytochrome P450 monooxigenase (GliC), putative	464	0.845	DOWN HIGH
	Afu6g04820	para-aminobenzoate synthase PabaA	1703	0.883	UP LOW		Afu5g05480	Rheb GTPase RhbA	811	0.496	DOWN MOD
							Afu2g12200	cAMP-dependent protein kinase catalytic subunit PkaC1	999	0.82	DOWN MOD
							Afu2g04200	4-hydroxyphenylpyruvate dioxygenase, putative	1236	0.263	DOWN MOD
							Afu6g02280	allergen Asp F3	1292	0.865	DOWN MOD
							Afu2g13440	chitin synthase E	1304	0.857	DOWN MOD
							Afu2g08360	orotidine 5'-phosphate decarboxylase PyrG	1460	0.739	DOWN LOW
							Afu6g13970	FAD-dependent monooxygenase (PaxM), putative	1604	0.942	DOWN LOW
							Afu5g00600	NPP1 domain protein, putative	1696	0.869	DOWN LOW
							Afu8g02750	nucleolar protein CgrA	1774	0.882	DOWN LOW
							Afu1g01890	enoyl-CoA hydratase/isomerase family protein	1886	0.39	DOWN LOW
Signal transduction	Afu3g07680	ran GTPase activating protein 1 (RNA1 protein)	419	0.734	UP HIGH		Afu3g03740	protein kinase, putative	448	0.784	DOWN HIGH
	Afu1g12680	Rho GTPase activator (Rga1), putative	1507	0.78	UP HIGH		Afu2g03510	pheromone processing carboxypeptidase (Sxa2), putative	689	0.727	DOWN MOD
	Afu5g08950	RAS small monomeric GTPase (Rsr1), putative	1511	0.659	UP MOD		Afu2g03360	polarized growth protein (Boi2), putative	720	0.738	DOWN MOD
							Afu5g05750	protein kinase, putative	1139	0.693	DOWN MOD
							Afu5g09100	MAP kinase, putative	1186	0.933	DOWN MOD
							Afu5g11840	protein kinase, putative	1360	0.922	DOWN LOW

								Afu3g07530	pH signal transduction protein PalI, putative	1375	0.867	DOWN LOW
								Afu6g08590	protein kinase, putative	1421	0.902	DOWN LOW
								Afu3g11080	MAP kinase kinase kinase (Bck1), putative	1436	0.869	DOWN LOW
								Afu3g14290	protein kinase, putative	1670	0.877	DOWN LOW
								Afu1g12940	MAP kinase (Osm1), putative	1699	0.624	DOWN LOW
								Afu1g11930	protein kinase, putative	1822	0.869	DOWN LOW
Sphingolipid biosynthesis								Afu1g16710	fatty acid elongase (Gig30), putative	624	0.917	DOWN HIGH
								Afu5g02760	fatty acid elongase (Gns1), putative	781	0.354	DOWN MOD
								Afu2g02310	sur7 protein, putative	1489	0.845	DOWN LOW
								Afu6g04680	MIPC synthase subunit (SurA), putative	1585	0.815	DOWN LOW
								Afu2g10460	conserved hypothetical protein	1588	0.894	DOWN LOW
								Afu6g12390	serine palmitoyl CoA transferase subunit LcbA	1622	0.924	DOWN LOW
								Afu6g09980	patched sphingolipid transporter (Ncr1), putative	1842	0.862	DOWN LOW
Transcription factors	Afu1g01650	C6 finger domain protein, putative	43	0.525	UP HIGH			Afu2g05360	C6 transcription factor, putative	10	0.263	DOWN HIGH
	Afu7g01820	C6 transcription factor, putative	49	0.598	UP HIGH			Afu3g04180	C2H2 finger domain protein, putative	45	0.733	DOWN HIGH
	Afu8g05270	C6 transcription factor, putative	55	0.262	UP HIGH			Afu5g13790	C6 transcription factor (Acr-2), putative	134	0.624	DOWN HIGH
	Afu8g05460	bZIP transcription factor, putative	93	0.432	UP HIGH			Afu6g11520	C6 transcription factor, putative	143	0.42	DOWN HIGH
	Afu5g01270	C6 transcription factor, putative	99	0.69	UP HIGH			Afu1g10280	C2H2 finger domain protein (Gli3), putative	153	0.439	DOWN HIGH
	Afu6g09630	C6 finger domain protein GliZ	683	0.565	UP MODERATE			Afu1g16830	C6 transcription factor, putative	802	0.744	DOWN MOD
	Afu2g17860	C6 transcription factor, putative	773	0.704	UP MODERATE			Afu3g00210	C6 finger domain protein, putative	841	0.914	DOWN MOD
	Afu4g09710	C6 sexual development transcription factor Pro1	1094	0.822	UP MODERATE			Afu5g10130	bZIP transcription factor, putative	954	0.93	DOWN MOD
	Afu1g03860	C6 transcription factor	1129	0.885	UP			Afu6g12920	C2H2 finger domain protein,	1033	0.699	DOWN

	(AmdR), putative			MODERATE
Afu7g04820	C6 transcription factor, putative	1146	0.787	UP MODERATE
Afu2g10550	C2H2 transcription factor (RfeC), putative	1232	0.9	UP MODERATE
Afu1g02860	C2H2 transcription factor, putative	1314	0.849	UP MODERATE
Afu5g12060	C2H2 transcription factor, putative	1321	0.263	UP LOW
Afu3g11250	C2H2 transcription factor (Swi5), putative	1465	0.9	UP LOW
Afu3g11970	C2H2 transcription factor PacC, putative	1508	0.678	UP LOW
Afu4g06530	bZIP transcription factor (MetR), putative	1517	0.938	UP LOW
Afu3g12890	C6 transcription factor (GliZ), putative	1542	0.762	UP LOW
Afu6g08790	C6 transcription factor (PrnA), putative	1559	0.929	UP LOW
Afu1g13750	C2H2 transcription factor (Rpn4), putative	1643	0.888	UP LOW
Afu4g12470	bZIP transcription factor CpcA	1737	0.893	UP LOW

	putative			MOD
Afu2g12070	C6 transcription factor, putative	1049	0.784	DOWN MOD
Afu6g07530	bZIP transcription factor, putative	1109	0.512	DOWN MOD
Afu1g16220	C6 transcription factor, putative	1149	0.901	DOWN MOD
Afu2g03180	C6 finger domain protein, putative	1392	0.845	DOWN LOW
Afu2g15030	C-3 sterol dehydrogenase/C-4 decarboxylase	1415	0.716	DOWN LOW
Afu8g02710	C6 transcription factor, putative	1532	0.913	DOWN LOW
Afu3g02070	C2H2 transcription factor, putative	1606	0.872	DOWN LOW
Afu3g09130	C6 transcription factor, putative	1620	0.86	DOWN LOW
Afu4g11110	C2 domain protein	1686	0.893	DOWN LOW
Afu5g00290	C6 transcription factor, putative	1703	0.643	DOWN LOW
Afu3g01100	C2H2 finger domain protein, putative	1763	0.853	DOWN LOW

Commonalities in gene functions over-represented at each time-point are identifiable. Acquisition and utilisation of crucial metal ions is evident in both time-point-specific and shared cohorts (Tables 3.7, 3.19 and 3.20). Transcriptional regulators were comparably increased and decreased in expression at both time-points analysed. Of note was the increase of virulence associated transcription factors *crzA* (Afu1g06900) between 4 – 8 hours, and *pacC* (Afu3g11970), *gliZ* (Afu6g09630) and *stuA* (Afu2g07900) between 8 – 14 hours. Transcription of genes putatively involved in transposition was a common feature of all datasets (Tables 3.19 and 3.20). However, increase of genes likely to be associated with mobile genetic elements between 8 - 14 hours was highly significant as determined by Chi Square analysis (Table 3.22).

Biological processes distinctive of each time-point are also apparent. Transcription of multiple genes associated with pathogenesis increased between 4 and 8 hour time-points, when the spore is adhering to the lung epithelium. These genes included conidial hydrophobin *rodA* (Afu5g09580), an *Aspergillus*-hemolysin (Afu3g00590), mycelial catalase *cat1* (Afu3g02270) and IgE-binding protein (Afu6g00430). A prominent feature of pathogenesis related genes, and the 4 – 8 hour time-point generally, was the increase in transcription of known or predicted antigens (n = 14). This included allergens Asp F1, F3, F4, F7, F10 and F13. In contrast, the latter time-point of infection had only two predicted antigens increasing (an aryl-alcohol dehydrogenase, Afu4g00610 and malate dehydrogenase Afu7g05740) and only three were common to both time-points (Tables 3.19 and 3.20). Increased transcription of protease enzymes were similarly distributed between the early and later time-points of infection, with 27 and 11 genes assigned respectively. The 4 - 8 hour time-point included three of the major *A. fumigatus* proteases, Mep (Afu8g07080), Alp1 (Afu4g11800) and Pep1 (Afu5g13300, Table 3.19). *Ex vivo* analyses have shown that actin disruption and membrane blebbing in a human epithelial cell line is caused by secreted proteases from conidia and culture filtrates (Kogan et al. 2004). These data support the role for antigen and protease mediated host disruption from the earliest time-points when the spore is adhering to the lung epithelia.

GO analysis showed genes directing sphingolipid biosynthesis were significantly enriched in genes increasing between 4-8 hours post infection. 11 such genes were indentified, including 3 serine palmitoyltransferases (Afu6g00300, Afu6g12390, Afu1g11890), a 3-ketosphinganine reductase (Afu1g11150) and a mannose-inositol-P-ceramide (MIPC) synthase subunit (Afu6g04680). Sphingolipids are integral components of the eukaryotic cell membrane and may play roles in development and virulence of pathogenic fungi. Membrane sphingolipid biosynthesis is required for cell cycle progression and cell polarity in *A. nidulans* (Cheng et al. 2001).

Additionally, sphingolipids are associated with virulence in fungal pathogens by involvement in lipid signalling networks in *C. neoformans* (Luberto et al. 2001) and by mediating host-pathogen interactions in *C. alibcans* (Rouabhia et al. 2011).

Signal transduction was particularly enriched at the 4 – 8 hour time-point (n = 47 genes) relative to transcriptional changes across the entire time course (n = 26 genes) or between 8-14 hours (Tables 3.7, 3.19 and 3.20). In concordance with the spore responding to the host niche, genes involved in several important *A. fumigatus* signalling pathways increased, including 3 GTPase activating proteins (Afu2g06080, Afu4g10600, Afu3g09900), 5 Rho GTPases (Afu2g15050, Afu2g05740, Afu3g06300, Afu3g10340, Afu5g14060) 2 MAPKKK (Afu5g06420, Afu1g10940), a MAPKK (Afu3g05900), a MAPK (Afu5g09100), two cAMP-dependent protein kinase catalytic subunits (Afu2g12200, Afu5g08570) and a putative cAMP-dependent protein kinase (Afu1g06400). Interestingly, genes putatively involved in sexual reproduction and cellular conjugation were enriched at this time-point, including the sexual development transcription factor SteA (Afu5g06190), and the mating alpha pheromone PpgA (Afu6g06360, Table 3.11). GO terms enriched among decreasing genes throughout infection were limited (Tables 3.13 and 3.14), yet supported trends from the 4 – 14 hour comparison which found genes directing RNA processing were down at the earliest time-point. This included 79 genes directing RNA splicing factors, nuclear riboproteins and RNA helicases, amongst others.

During the 8 – 14 hour time-point of infection genes with increasing expression were enriched in GO processes related to cellular polysaccharide metabolism and the fungal cell wall (Table 3.14). The *A. fumigatus* cell wall is composed mainly of polysaccharides including β-1,3-glucan, chitin, galactomannan, β-1,3/ β-1,4-glucan and α-1,3-glucan. During transition from a resting conidia to germinating conidia and hyphae there are extensive changes to the cell wall, requiring both hydrolase and synthase activities. Genes associated with cell wall biosynthesis were found at all time-points of infection. For example, Rho and RAS GTPases, and the 1,3-beta-glucan synthase catalytic subunit FksP (Afu6g12400) increased between 4 - 8 hours and their transcription subsequently remained at a mainly constant level. In accordance with the extensive cell wall growth during germ tube production between 8 – 14 hours, polysaccharide metabolic processes were particularly prominent at this time-point (Table 3.14).

3.4.7 Characterisation of Af293 time-point specific datasets: chromosomal loci, lineage specificity and functionality

Functional enrichment of increased and decreased datasets was investigated among gene categories of interest by Chi-square analyses, with the null hypothesis that equal numbers of upregulated and downregulated genes occur in each cohort (Figure 3.11, Table 3.21)

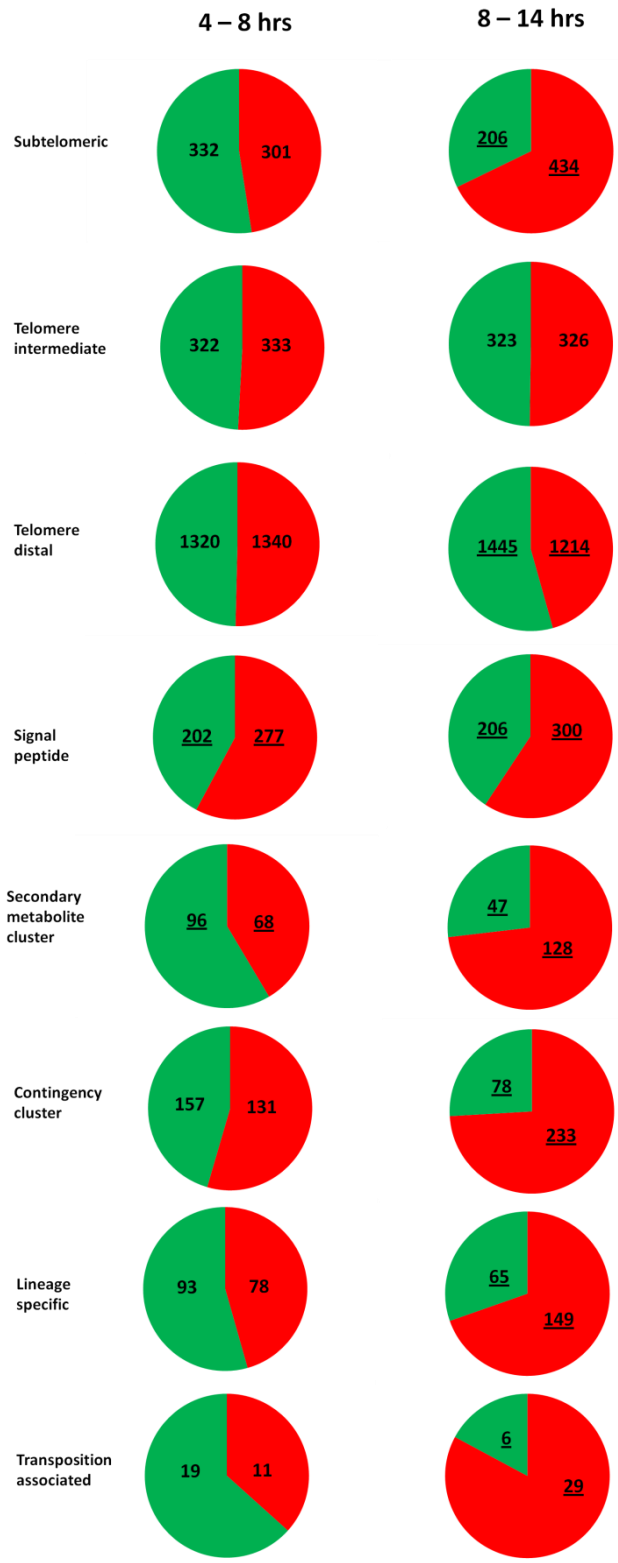


Figure 3.11: Distribution of differentially expressed genes between 4 – 8, and 8 - 14 hours post infection among the functional cohorts of chromosomal location, signal peptide content, *A. fumigatus* specificity and functional association. Distribution of genes in increasing (red) and decreasing (green) datasets among gene cohorts of interest to this study. Underlined values significantly deviate from the null hypothesis that an equal number of upregulated or downregulated genes will occur in each cohort, as tested by Chi-square analysis.

	Number of genes	Differentially expressed	Up (observed)	Down (observed)	Up (expected)	Down (expected)	Chi-square	p-value
0-300 kb	1509	633	301	332	316.5	316.5	1.51	0.2179
301- 600 kb	1634	654	333	322	327	327	0.18	0.6658
>600 kb	6373	2640	1340	1320	1330	1330	0.15	0.5820
Signal P	1103	479	277	202	239.5	239.5	11.74	0.0006
Secondary metabolism	337	164	68	96	82	82	4.78	0.0288
Infection cluster	594	288	157	131	144	144	2.34	0.1255
Aspergillus specific	596	171	78	93	85.5	85.5	1.31	0.2513
Transposition	68	28	11	19	14	14	2.13	0.1191

Table 3.21: Distribution and Chi-square analysis of differentially expressed genes categorised by chromosomal location, signal peptide content, *A. fumigatus* specificity and annotation at 4 - 8 hours post infection. Chi square analysis with one degree of freedom was used to test the distribution of upper and lower quartiles with respect to cohorts of interest to this study, with the null hypothesis that even numbers of upregulated or downregulated genes occur in each group.

	Number of genes	Differentially expressed	Up (observed)	Down (observed)	Up (expected)	Down (expected)	Chi-square	p-value
0-300 kb	1509	640	434	206	320	320	81.22	< 0.0001
301- 600 kb	1634	649	326	323	324.5	324.5	0.01	0.9063
>600 kb	6373	2659	1214	1445	1329.5	1329.5	20.06	< 0.0001
Signal P	1103	506	300	206	253	253	17.46	< 0.0001
Secondary metabolism	337	175	128	47	87.5	87.5	37.49	< 0.0001
Infection cluster	594	301	223	78	150.5	150.5	69.85	< 0.0001
Aspergillus specific	596	214	149	65	107	107	32.97	< 0.0001
Transposition associated	68	35	29	6	17.5	17.5	15.11	<0.0001

Table 3.22: Distribution and Chi-square analysis of differentially expressed genes categorised by chromosomal location, signal peptide content, *A. fumigatus* specificity and annotation at 8 - 14 hours post infection. Chi square analysis with one degree of freedom was used to test the distribution of upper and lower quartiles with respect to cohorts of interest to this study, with the null hypothesis that even numbers of upregulated or downregulated genes occur in each group.

A trend towards reduction in secondary metaoblite expression was noticed at 4 – 8 hours post infection (Table 3.19 and Figure 3.11). This tendency was not focused at specific clusters. Interestingly, the virulence factor PskP, which is required for DHN-melanin biosynthesis decreased between each time-point of infection. In contrast, the general trend towards increase in secondary metabolite gene expression at 8 - 14 hours was particularly pronounced at specific loci, most notably the gliotoxin biosynthetic cluster (Table 3.12). NRPS and PKS genes directing the biosynthesis of many secondary metabolites, including Fumitremorgin C and Pseurotin A showed similar expression profiles (Figure 3.13).

Analyses of time-point specific datasets with regard to chromosomal distribution found that enrichment of preferentially expressed genes at subtelomeric loci and contingency clusters occurred only between 8 and 14 hours (Figure 3.11). While subtelomeric and contingency loci constitute 16% and 3.2% of the genome, 21.9% and 11.3% of increased genes between 8 – 14 hours are found at these loci respectively. Additionally, analysis of time-point specific datasets with regard to lineage specificity found enrichment of preferentially expressed genes between 8 and 14 hours only (Figure 3.11).

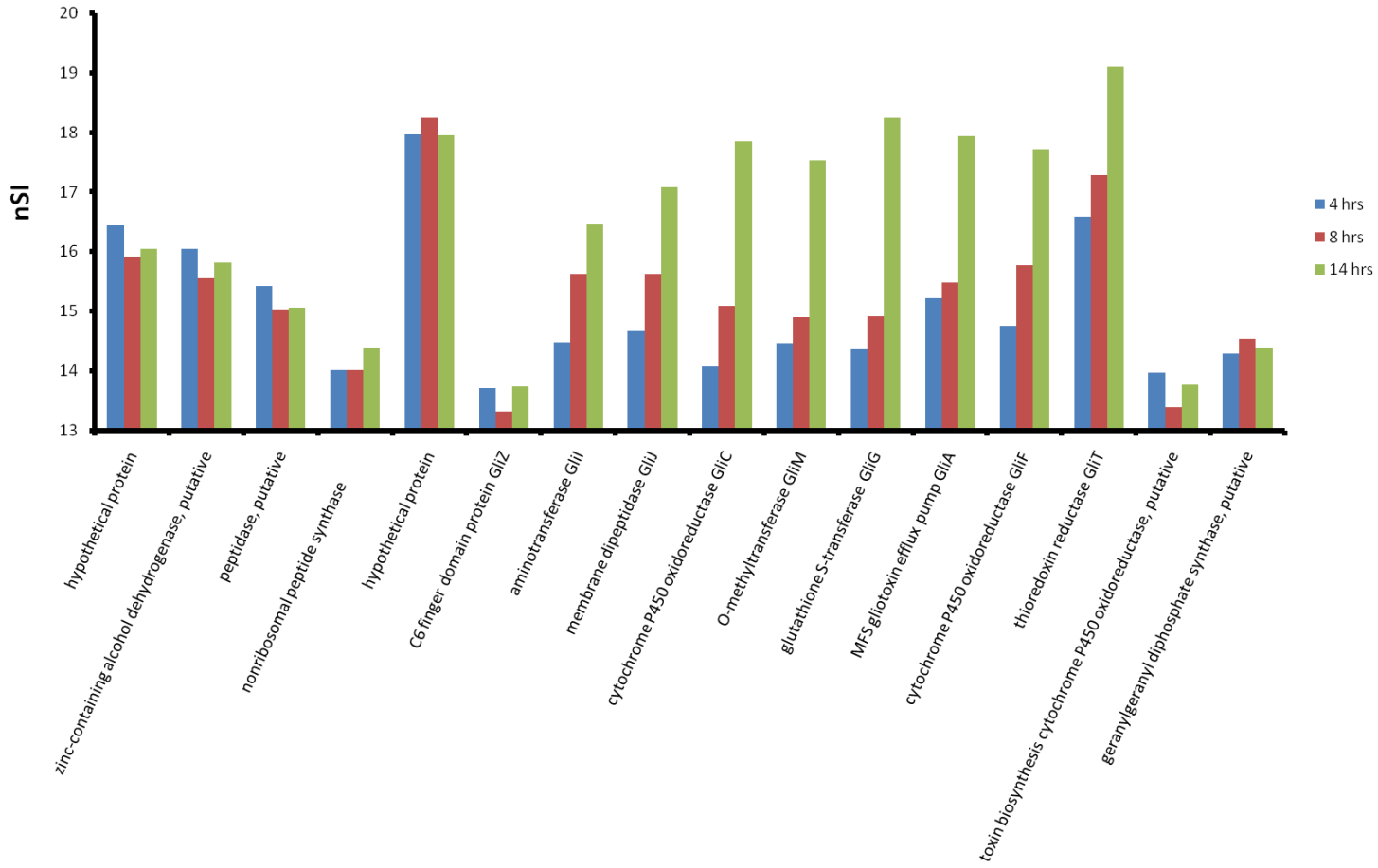


Figure 3.12: nSI values for genes in the gliotoxin biosynthetic cluster at 4, 8 and 14 hours post infection. nSI for genes putatively in the gliotoxin biosynthetic cluster as annotated by Perrin et al. 2007 is shown. Expression for the the NRPS *gliP* failed quality control filtering. Increase in transcript abundance was most notable between 8 and 14 hours.

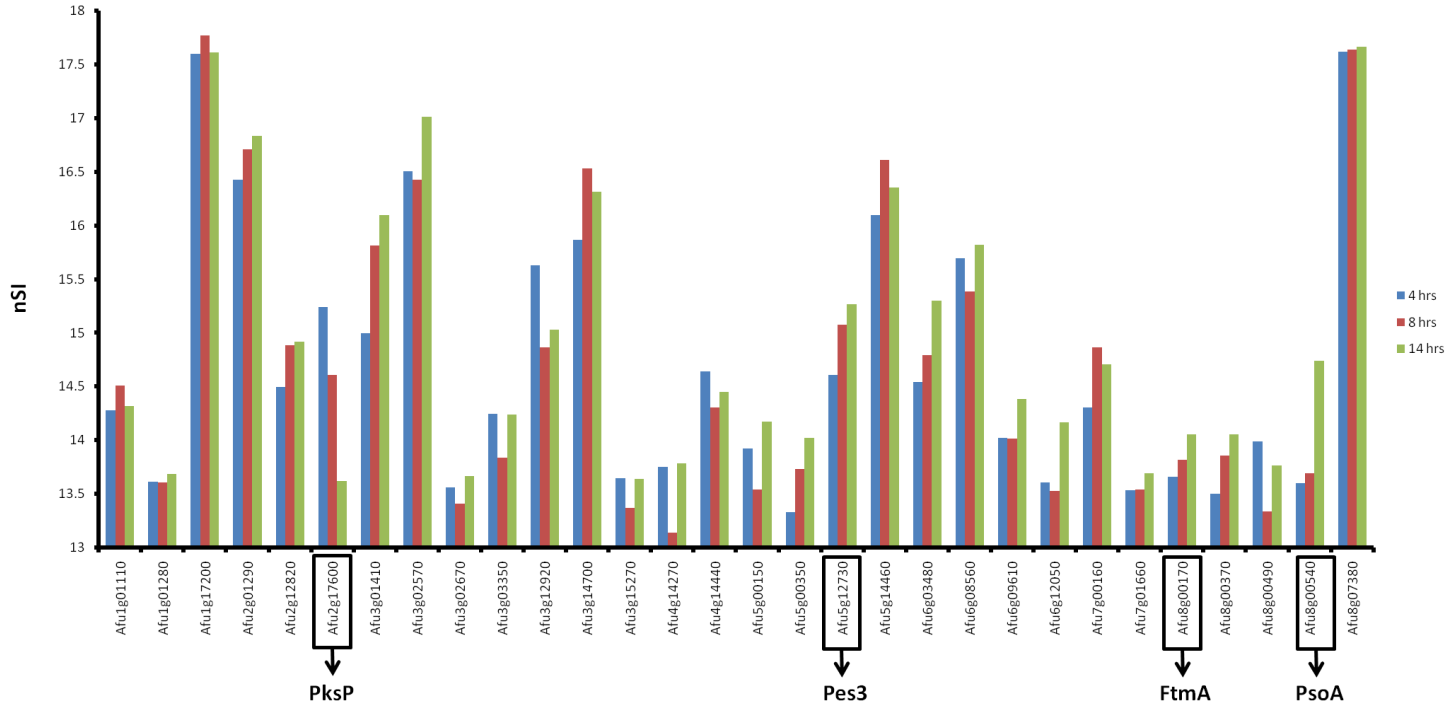


Figure 3.13: nSI values for NRPS and PKS genes at 4, 8 and 14 hours post infection. nSI for 30 putative NRPS and PKS are shown. A general trend towards greatest transcript abundance at 14 hours is noticeable. Genes highlighted are the DHN-melanin gene *pksP*, and three genes which are studied in Chapter 4 of this thesis.

3.4.8 Short Time-series Expression Miner profiling of temporal gene expression in Af293 during murine infection

In order to assign gene functionality to specific temporal expression profiles, the Af293 infection time-course was analysed using Short Time-series Expression Miner (STEM) software. This program defines a set of distinct and representative model temporal profiles independently of the data which denote potential profiles of gene change throughout the experiment (Ernst and Bar-Joseph 2006). A gene's observed expression profile is assigned to a model profile provided it is significantly similar based on a correlation coefficient. The number of genes expected to be assigned to each profile is computed by random permutations. Finally, statistical analyses of the number of observed genes against the number randomly predicted enables the identification of profiles which occure more frequently than would be expected by chance, thereby inferring functional relatedness of the genes in that cohort and/or regulatory significance of the genes' expression signature.

STEM is integrated with Gene Ontology, enabling analyses of enriched GO terms amongst statistically significant profiles. In addition, gene cohorts may be manually annotated, enabling clustering and enrichment analyses of groups external to GO. Manually annotated groups included secondary metabolite genes (Perrin et al. 2007), contingency clusters, subtelomeric, telomere intermediate, signal peptide, and *A. fumigatus* specific datasets (McDonagh et al. 2008), predicted antigens and manually annotated genes associated with transposition. nSI values were imported into STEM and normalised against the first time-point, so that profiles were plotted by calculating the difference between nSI values at 8 or 14 hours relative to nSI at 4 hours.

STEM output profiles for the Af293 time course analyses are shown in Figure 3.14. Each box is an expression profile, which is coloured when statistically significant enrichment is observed (FDR corrected $p > 0.05$) with respect to the number of genes assigned relative to the number predicted randomly. Multiple profiles which have the similar expression are grouped into clusters, which are highlighted with the same colour. Model profiles are indicated by a single black line, and the temporal expression of genes assigned to the profile are indicated by red lines. 15 profiles, grouped into 4 clusters, are significantly enriched according to STEM analysis. These clusters generally contain transcription profiles which increase at both of the 8 and 14 hour time-points (green), increase and then plateau (red), increase and then decrease (purple) and decrease (yellow). GO analysis was used to determine over-represented functional categories in each cluster for which a corrected *p*-value cut-off of 0.2 was applied. Both red and green clusters reported enrichment under these conditions (Tables 3.23 and 3.24).

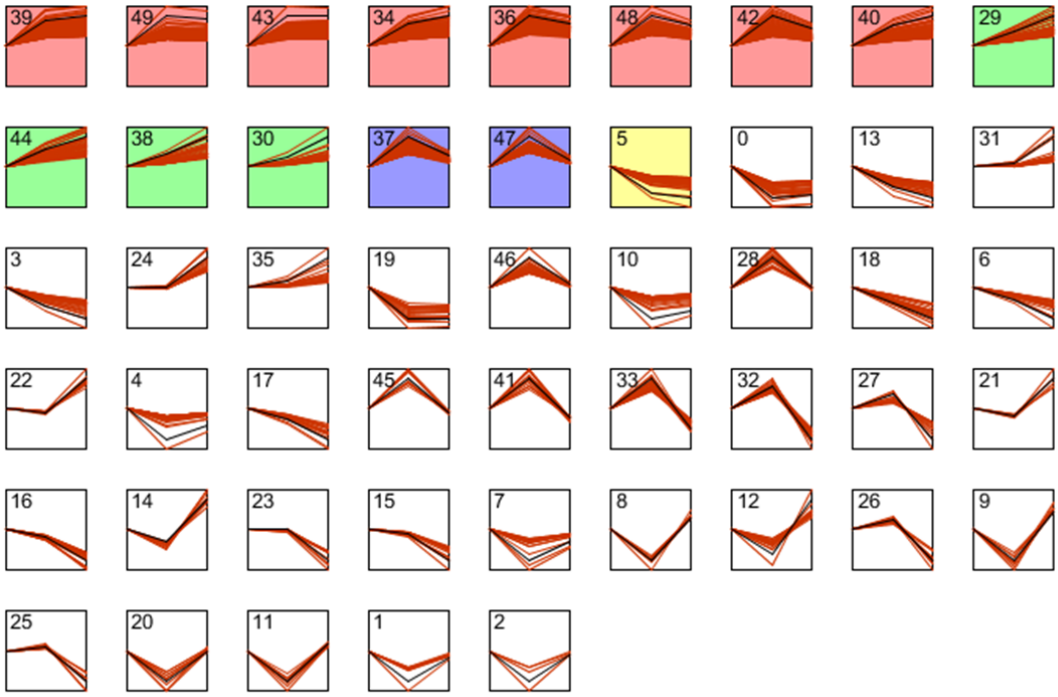


Figure 3.14: STEM analysis of the Af293 infection time-course. Statistically significant profiles are coloured and grouped into 4 clusters. Model profiles are shown with a single black line. Genes assigned to each profile are shown in red.

Category Name	Genes in Category	Genes Assigned	Genes Expected	Genes Enriched	*p*-value	Corrected p-value
pheromone-dependent signal transduction involved in conjugation with cellular fusion	16	11	2.9	8.1	1.30E-05	0.004
heterotrimeric G-protein GTPase activity	5	5	0.9	4.1	2.10E-04	0.044
heterotrimeric G-protein complex	5	5	0.9	4.1	2.10E-04	0.044
pathogenesis	41	17	7.5	9.5	4.70E-04	0.074
response to stress	43	17	7.9	9.1	9.10E-04	0.142

Table 3.23: Significant GO terms among the red cluster during the Af293 time course. Bonferroni corrected *p*-value represents the probability of observing the number of genes from the specific GO term from randomly assigned entities.

Category Name	Genes in Category	Genes Assigned	Genes Expected	Genes Enriched	*p*-value	Corrected p-value
plasma membrane	119	15	5.1	9.9	1.50E-04	1.00E-02
Signal peptide	516	38	22.3	15.7	5.00E-04	0.038
Contingency cluster	288	24	12.5	11.5	1.20E-03	0.084
cellular iron ion homeostasis	21	5	0.9	4.1	1.70E-03	0.106

Table 3.24: Significant GO terms among the green cluster during the Af293 time course. Bonferroni corrected *p*-value represents the probability of observing the number of genes from the specific GO term from randomly assigned entities.

Trends among biological processes favoured during infection are apparent from STEM analyses. Signal transduction, pathogenesis, iron homeostasis, signal peptide genes and contingency cluster loci increase in transcript abundance during infection. Significant GO terms for individual profiles also supported the above trends, with several additional functional categories reported. In profile 49, 10 genes associated with the *A. fumigatus* endoplasmic reticulum were observed (Table 3.25), which is supportive of increased demand for carriage of cell wall components to the hyphae and secretion of extracellular enzymes during infection (Richie et al. 2009). Profile 34 demonstrated enrichment of 6 transcription factors, including CpcA (Afu4g12470), which putatively regulates *A. fumigatus* amino acid biosynthesis and is required for virulence in a murine model of infection (Krappmann et al 2004). Additionally, individual profiles were investigated with respect to enrichment of functional categories using GO analyses (Table 3.25).

Category Name	#Genes Category	#Genes Assigned	#Genes Expected	#Genes Enriched	p-value	Corrected p-value
Profile 39						
nucleus	508	19	5.6	13.4	5.20E-06	0.003
cytoplasm	652	21	7.1	13.9	1.60E-05	0.01
Subtelomeric	541	18	5.9	12.1	4.20E-05	0.025
Signal peptide	516	17	5.6	11.4	7.60E-05	0.046
Semi-subT	784	22	8.6	13.4	8.00E-05	0.048
Profile 49						
response to stress	43	6	1.3	4.7	1.40E-03	0.094
endoplasmic reticulum	115	10	3.4	6.6	1.80E-03	0.104
Profile 34						
Subtelomeric	541	21	4.9	16.1	4.90E-08	3.00E-05
Contingency cluster	288	13	2.6	10.4	3.30E-06	0.002
transcription factor activity	61	6	0.6	5.4	2.00E-05	0.012
Signal peptide	516	15	4.7	10.3	1.00E-04	0.063
nucleus	508	14	4.6	9.4	3.00E-04	0.18
Profile 36						
cytoplasm	652	22	7	15	3.80E-06	0.002
AFFC specific	94	7	1	6	7.40E-05	0.044
Signal peptide	516	16	5.5	10.5	1.90E-04	0.116
Profile 48						
nucleus	508	18	3.8	14.2	1.10E-07	6.60E-05
cytoplasm	652	16	4.9	11.1	5.20E-05	0.031
Profile 44						
Signal peptide	516	16	3.2	12.8	2.50E-07	1.50E-04
Profile 38						
plasma membrane	119	7	0.7	6.3	1.20E-05	0.007

Table 3.25: Significant GO terms among profiles 39, 49, 34, 36, 48, 44, and 38 in the Af293 time-course experiment. GO enrichment analysis for significant STEM profiles was conducted. Bonferroni corrected *p*-value represents the probability of observing the number of genes from the specific GO term from randomly assigned entities.

Model profiles were also ordered based on enrichment of functional categories, enabling identification of temporal profiles most closely associated with specific groups of interest. These data strongly support the upregulation of subtelomeric regions, with all 11 profiles assigned to this cohort increasing in transcript abundance during infection. Moreover, 6 profiles (14, 12, 35, 21, 24 and 22) suggest these regions are upregulated between 8 and 14 hours.

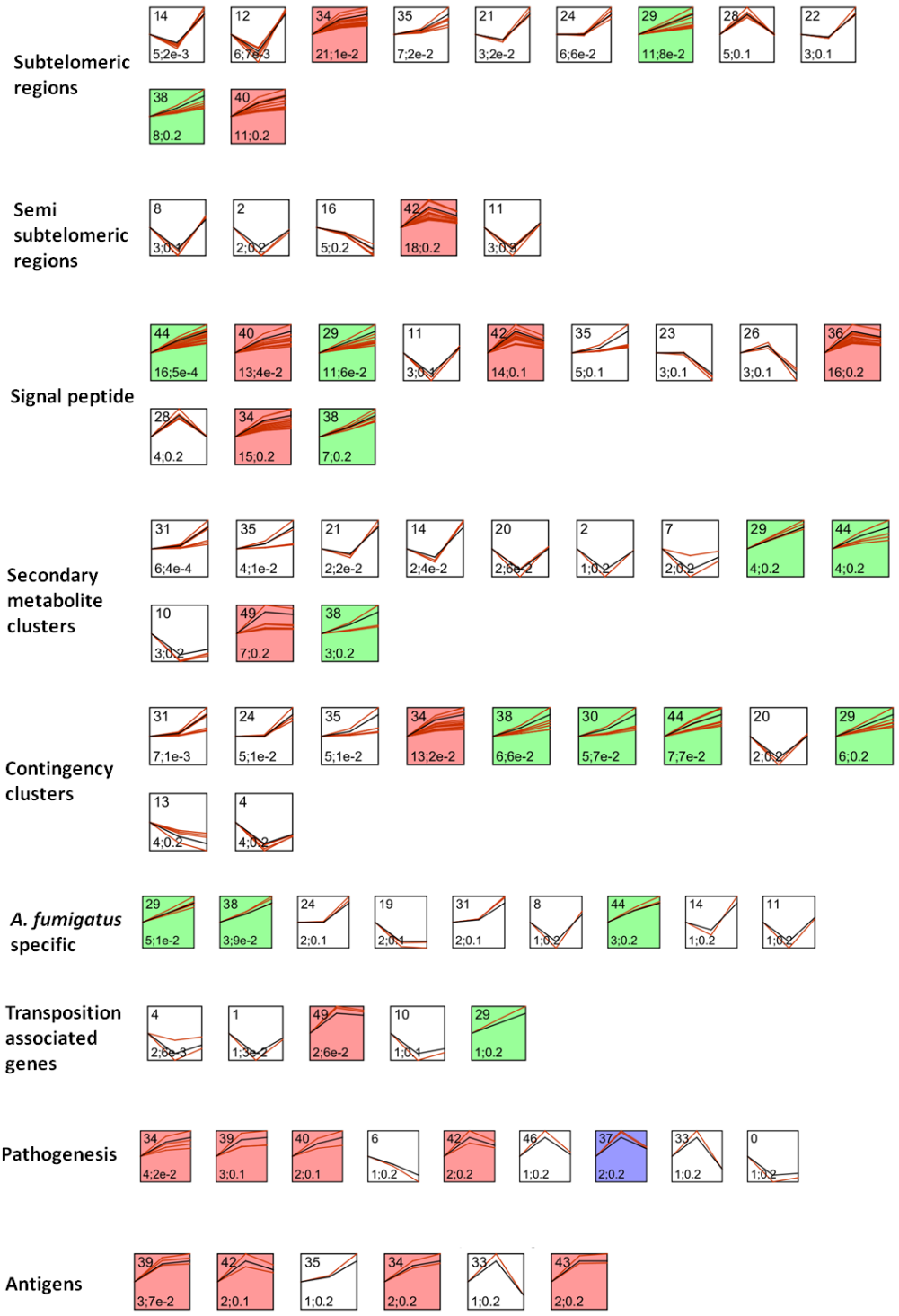


Figure 3.15: STEM clustering analysis of differentially expressed genes in the Af293 time-course ordered on the basis of enrichment of genes within location and functionally related cohorts. Values in the top left corner denote the profile number. Numbers in the bottom left show the number of genes specific to that cohort found in the profile, followed by the p-value representing the probability of observing the number of genes from randomly assigned entities. Model profiles remain coloured or white based on significant or non significant enrichment from the initial analysis respectively. In the bottom left corner is the number of genes belonging to the cohort of interest is shown, followed by the *p*-value for enrichment in the respective profiles. Profiles passing an 0.2 p value cut-off are shown. In this analysis red lines show expression profiles only of genes from the cohort of interest.

3.5. *A. fumigatus* Δ*laeA* transcriptional profile during the initiation of murine infection

As summarised in Table 3.26, fluorescence intensities for 8498, 8471 and 8480 out of a possible 9516 represented ORFs passed quality control filtering for 4, 8 and 14 hour time-points respectively. Genes without expression values at all three time-points (due to quality control filtering) were omitted from the dataset, resulting in a total of 7819 gene expression profiles (Table 3.26). To determine the temporal basis of transcriptional changes in Δ*laeA* during infection, relative nSI values and differentially expressed transcripts were defined as for Af293. Table 3.27 summaries upper and lower quartile values at each time-point (n = 1955), and maximal and minimal relative nSI values between time-points.

	4 hrs	8 hrs	14 hrs
Count fail	632	941	725
Standard deviation fail	305	23	230
Retained spots	8498	8471	8480
Average	16.21	16.28	16.26
Median	16.13	16.39	16.29
Standard deviation	1.81	1.89	1.84
Minimum value	12.21	11.76	11.07
Maximum value	21.19	21.29	21.20

Table 3.26: Summary statistics for the Δ*laeA* non-ratiometric analysis. The numbers of genes failing count and standard deviation quality control filtering are shown. The total number of genes common to every time-point was 7819.

	4 hrs	8 hrs	14 hrs	8 hrs vs 4 hrs	14 hrs vs 8 hrs	14 hrs vs 4 hrs
Lower quartile	14.74	14.74	14.74	0.9899	0.98329	0.98215
Upper quartile	17.74	17.81	17.77	1.0183	1.01134	1.01887
Median	16.13	16.43	16.27	1.0039	0.99698	0.99938
Average	16.28	16.35	16.31	1.0041	0.99783	1.0019
St dev	1.80	1.87	1.83	0.0262	0.02357	0.03218

Table 3.27: Summary statistics for Δ*laeA* relative nSI datasets. Relative nSI values were calculated between time-points for 7819 genes with intensity values at each time-point. Upper and lower quartiles (n = 1955) were used to define up and down expressed genes respectively.

Distribution of the up and down expressed datasets is summarised in 2 and 3-way Venn diagram in Figure 3.16. Comparisons between 4 - 8 hour and 8 - 14 hour up and down expressed cohorts showed 419 and 320 genes with increased and decreased transcript abundance, respectively, throughout the time-course of analysis. (Figure 3.16A). These genes also featured in the 4 - 14 hour dataset (Figure 3.16B). Consequently, the 4 – 14 hour comparison is inclusive of gene expression changes shared by both time-points (Figure 3.16) and therefore constitutes the most appropriate comparison for interrogating transcriptional changes across the entire time-course. 4 – 8 and 8 - 14 hour comparisons were used to identify time-point specific transcriptional changes.

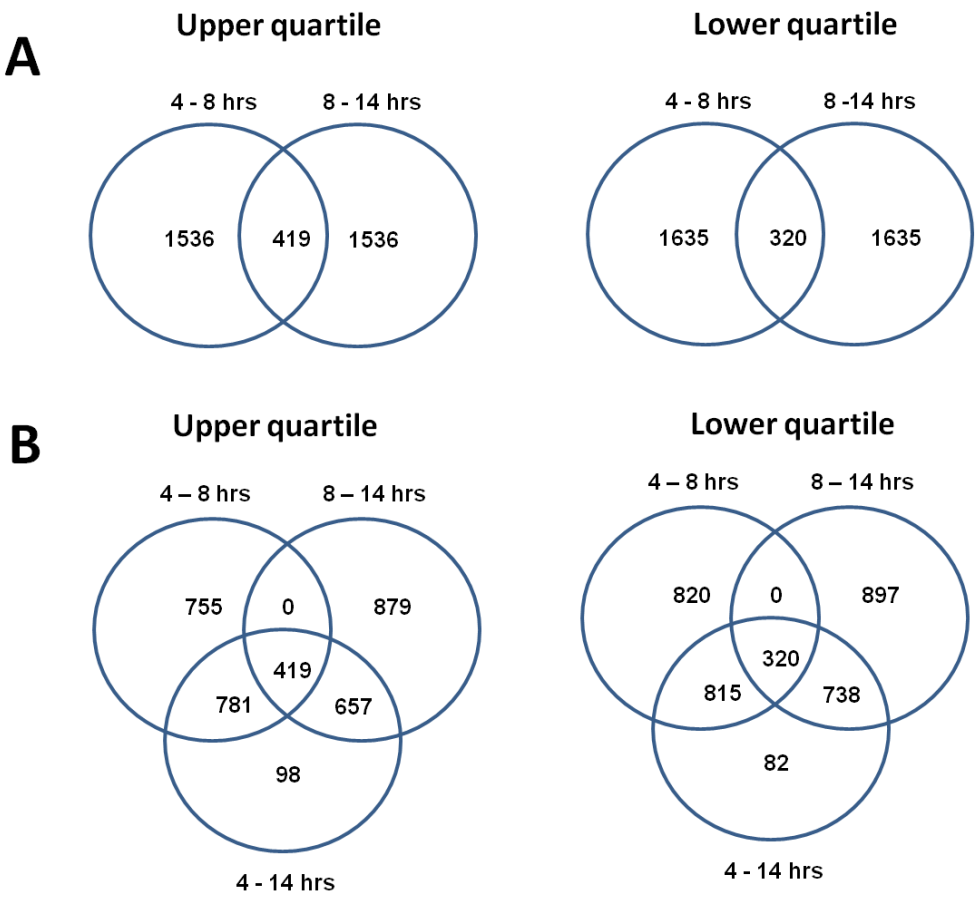


Figure 3.16: Venn diagrams depicting comparisons between relative nSI datasets from the Δ*laeA* non-ratiometric analysis. A. 2 way Venn diagram depicting distribution between time-point specific datasets. **B**. Three-way Venn diagram depicting distribution among all nSI datasets. Upper and lower quartiles (n =1955) were used to define genes with increase and decrease in expression respectively.

3.5.1 Gene expression profiling of the Δ*laeA* isolate between 4 and 14 hours in the murine lung

Initial interpretations of gene expression profiles were conducted across the entire time-course of infection (Figure 3.17). Gene ontology analysis was conducted using Genespring GX 11.02 to identify over-represented terms among increased or decreased datasets (Table 3.28). Significant GO terms based on a corrected *p*-value cut-off of 0.2 were only obtained for genes increasing during infection. The top 100 genes having the greatest increase or decrease between 4 and 14 hours are reported in Tables 3.29 and 3.30.

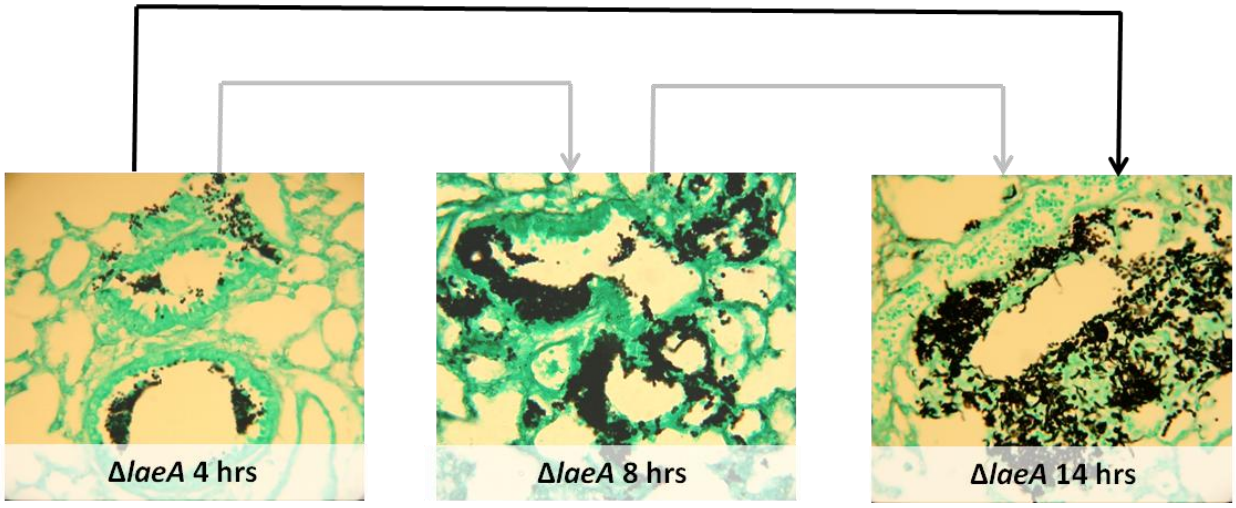


Figure 3.17: Histopathological analysis of *ΔlaeA* during the initiation of murine infection. Lungs were paraffin-embedded and stained with Grocott's Methenamine Silver. Solid black arrow represents transcriptional comparison conducted between 4 and 14 hours. Faint grey arrows represent time-point specific comparisons which are discussed later in this Chapter. At 4 hrs, ungerminated spores were adhering to lung epithelial cells. At 8 hrs, germination had occurred in approximately 10% of spores. At 14 hours, approximately 60% of *ΔlaeA* spores has germinated, and germ tube production through surrounding host tissue and airways was observed.

GO ACCESSION	GO Term	p-value	corrected p-value	Count in Selection	% Count in Selection	Count in Total	% Count in Total
GO:0046914	transition metal ion binding	1.72E-05	0.1205	70	98.6	204	4.4
GO:0046872	metal ion binding	3.84E-05	0.1205	70	98.6	212	4.6
GO:0043169	cation binding	3.84E-05	0.1205	70	98.6	212	4.6
GO:0043167	ion binding	3.84E-05	0.1205	70	98.6	212	4.6
GO:0008270	zinc ion binding	1.31E-05	0.1205	70	98.6	199	4.3
GO:0015082	di-, tri-valent inorganic cation transmembrane transporter activity	4.08E-05	0.1205	1	1.4	41	0.9
GO:0022891	substrate-specific transmembrane transporter activity	6.63E-05	0.1713	1	1.4	328	7.1

Table 3.28: Over-represented Gene Ontology terms among genes with increasing expression between 4 and 14 hours in the *ΔlaeA* infected murine lung. GO terms significantly enriched with respect to their occurrence in the *A. fumigatus* Af293 genome are reported (Bonferroni corrected p-values ≤ 0.2).

Table 3.29: 100 genes with greatest nSI increase between 4 and 14 hours post infection in Δ*laeA*. Genes are reported ranked according to greatest nSI intensity increase between 4 and 14 hours. A one-way ANOVA was conducted on nSI values between time-points, with the null hypothesis that nSI values do not change between time-points. FDR correct *p*-values from this analysis are reported for each gene.

ORF	Description	Rank	*p-value*	GO_BiologicalProcess
Afu6g09670	cytochrome P450 oxidoreductase GliC	1	0.012	oxidoreductase activity///metabolic process
Afu6g09730	cytochrome P450 oxidoreductase GliF	2	0.002	oxidoreductase activity///metabolic process
Afu6g09690	glutathione S-transferase GliG	3	0.000	
Afu6g09680	O-methyltransferase GliM	4	0.008	S-adenosylmethionine-dependent methyltransferase activity///O-methyltransferase activity
Afu6g09650	membrane dipeptidase GliJ	5	0.000	
Afu2g14540	endoglucanase, putative	6	0.000	
Afu7g06790	putative allantoate permease of the major facilitator superfamily	7	0.056	endoplasmic reticulum///ion transmembrane transporter activity///biological process unknown
Afu8g01480	potassium channel, putative	8	0.066	cellular potassium ion homeostasis///potassium channel activity///plasma membrane
Afu6g09740	thioredoxin reductase GliT	9	0.000	secondary metabolic process
Afu2g09450	carboxylic acid transport protein	10	0.034	lactate transmembrane transporter activity///lactate transport///plasma membrane
Afu2g10130	phase-specific adhesin, putative	11	0.003	
Afu3g03670	ABC multidrug transporter, putative	12	0.134	ATP-binding cassette (ABC) transporter activity///ATP binding///transport
Afu3g03950	endoglucanase, putative	13	0.034	
Afu8g06830	endoglucanase, putative	14	0.007	

Afu2g14420	cutinase, putative	15	0.000	
Afu5g14420	hypothetical protein	16	0.083	
Afu2g12680	conserved hypothetical protein	17	0.023	
Afu4g09830	indoleamine 2,3-dioxygenase pyrrole 2,3-dioxygenase)	18	0.006	cytoplasm///"tryptophan 2,3-dioxygenase activity"///NAD biosynthetic process
Afu2g13270	alcohol dehydrogenase, putative	19	0.040	alcohol metabolic process///cytoplasm///zinc ion binding///alcohol dehydrogenase (NAD) activity
Afu6g09640	aminotransferase GliI	20	0.011	secondary metabolic process///transaminase activity
Afu5g03010	conserved hypothetical protein	21	0.037	
Afu2g14490	endoglucanase, putative	22	0.040	
Afu7g04930	alkaline serine protease (PR1), putative	23	0.415	protein catabolic process///cellular component unknown///peptidase activity
Afu5g01620	extracellular proline-rich protein	24	0.005	
Afu4g00390	glycosyl hydrolase, putative	25	0.165	
Afu2g14360	GPI anchored glucanase, putative	26	0.066	
Afu8g05910	pectate lyase, putative	27	0.031	
Afu8g00610	cell surface protein Mas1, putative	28	0.000	
Afu8g06450	Rieske 2Fe-2S family protein, putative	29	0.071	
Afu5g09440	amino acid permease, putative	30	0.118	
Afu3g13640	extracellular serine-rich protein	31	0.323	
Afu2g11220	proline permease, putative	32	0.220	plasma membrane///neutral amino acid transmembrane transporter activity///neutral amino acid transport///amino acid permease activity
Afu3g01230	sugar transporter-like protein	33	0.087	membrane///transporter activity///transport
Afu3g14980	extracellular chitosanase CsnC, putative	34	0.134	cell wall organization
Afu6g06620	YIP3-like protein	35	0.040	COPII-coated vesicle///ER to Golgi vesicle-mediated transport///molecular function unknown
Afu3g08110	cell wall protein, putative	36	0.003	
Afu3g07410	isoamyl alcohol oxidase	37	0.111	
Afu3g14170	high-affinity hexose transporter	38	0.240	response to glucose stimulus///plasma membrane///glucose transmembrane transporter activity///signal transduction///glucose binding///receptor activity
Afu3g00620	zinc-containing alcohol dehydrogenase, putative	39	0.040	oxidoreductase activity///cellular component unknown///zinc ion binding///metabolic process
Afu2g15950	aspartic endopeptidase, putative	40	0.236	protein catabolic process///aspartic-type endopeptidase activity///extracellular region
Afu2g17650	DUF907 domain protein	41	0.002	cytoplasm///biological process unknown///molecular function unknown
Afu3g13670	siderochrome-iron transporter, putative	42	0.323	siderophore-iron transport///siderophore-iron (ferrioxamine) uptake transmembrane

				transporter activity///integral to membrane///cellular iron ion homeostasis
Afu4g10340	C6 finger domain protein, putative	43	0.117	DNA binding///zinc ion binding
Afu1g01540	Endonuclease/Exonuclease/phosphatase family family	44	0.340	
Afu3g13110	extracellular serine-threonine rich protein	45	0.003	
Afu4g00610	aryl-alcohol dehydrogenase, putative	46	0.062	aryl-alcohol oxidase activity
Afu3g03580	Transferase family superfamily	47	0.388	
Afu6g00290	aminotransferase, putative	48	0.182	arylformamidase activity///cytoplasm///mitochondrion///NAD biosynthetic process
Afu3g02090	beta-xylosidase	49	0.097	carbohydrate metabolic process///"hydrolase activity, hydrolyzing O-glycosyl compounds"
Afu1g06470	neutral/alkaline nonlysosomal ceramidase, putative	50	0.483	
Afu7g06810	L-amino acid oxidase LaoA, putative	51	0.060	
Afu8g07080	elastinolytic metalloproteinase Mep	52	0.135	pathogenesis///endopeptidase activity
Afu2g00500	conserved hypothetical protein	53	0.087	
Afu3g01580	GMC oxidoreductase, putative	54	0.012	oxidoreductase activity///metabolic process
Afu4g09840	kynureninase	55	0.176	cytoplasm///nucleus///kynureninase activity///tryptophan catabolic process to kynurenine///NAD biosynthetic process
Afu6g13750	ferric-chelate reductase, putative	56	0.183	ferric-chelate reductase activity///transition metal ion transport///integral to membrane
Afu4g10070	class I alpha-mannosidase	57	0.015	protein amino acid N-linked glycosylation///endoplasmic reticulum///"mannosyl-oligosaccharide 1,2-alpha-mannosidase activity"
Afu1g10020	reverse transcriptase, RNaseH	58	0.471	
Afu8g05680	serine/threonine protein kinase, putative	59	0.007	DNA-dependent DNA replication///protein serine/threonine kinase activity///protein amino acid phosphorylation///nucleus///spindle pole
Afu1g10030	hypothetical protein	60	0.075	
Afu4g08440	Patatin-like serine hydrolase, putative	61	0.450	lipid particle///molecular function unknown
Afu3g00650	aminopeptidase Y, putative	62	0.236	proteolysis///aminopeptidase activity
Afu8g06560	DUF895 domain membrane protein	63	0.337	
Afu2g00760	pectate lyase A	64	0.003	
Afu2g17320	conserved hypothetical protein	65	0.087	
Afu5g12470	oxidoreductase, 2OG-Fe(II) oxygenase family	66	0.217	
Afu5g07530	hypothetical protein	67	0.040	
Afu1g06330	conserved hypothetical protein	68	0.220	molecular function unknown
Afu8g02200	proline permease	69	0.176	amino acid transport///plasma membrane///amino acid permease activity///amino acid transmembrane transporter activity
Afu6g13760	alpha-1,2-mannosidase, putative	70	0.166	

	subfamily			
Afu3g01500	integral membrane protein	71	0.067	
Afu5g14810	pyruvate decarboxylase, putative	72	0.082	glucose catabolic process to ethanol///cytoplasm///nucleus///pyruvate metabolic process///pyruvate decarboxylase activity
Afu2g07630	vacuolar H+\/Ca2+ exchanger	73	0.286	calcium ion transport///calcium:hydrogen antiporter activity///fungal-type vacuole///calcium ion transmembrane transporter activity///cellular calcium ion homeostasis///vacuolar membrane
Afu4g01290	endo-chitosanase, pseudogene	74	0.310	
Afu3g12430	guanine nucleotide exchange factor, putative	75	0.483	regulation of exit from mitosis///cellular bud///guanyl-nucleotide exchange factor activity
Afu1g09260	acetyltransferase, GNAT family family	76	0.078	
Afu5g01990	BYS1 domain protein, putative	77	0.058	
Afu3g03330	mitochondrial enoyl reductase, putative	78	0.180	aerobic respiration///fatty acid biosynthetic process///mitochondrion///enoyl-[acyl-carrier-protein] reductase activity
Afu2g13030	phenylalanyl-tRNA synthetase alpha subunit (PodG), putative	79	0.549	translation///phenylalanine-tRNA ligase activity///mitochondrion
Afu4g13300	hypothetical protein	80	0.498	
Afu3g06290	regulatory protein leu3, putative	81	0.625	
Afu8g04060		82	0.205	beta-N-acetylglucosaminidase activity///N-acetylglucosamine catabolic process
Afu3g13080	hypothetical protein	83	0.044	
Afu3g10820	metalloreductase, putative	84	0.211	ferric-chelate reductase activity///copper ion import///plasma membrane///iron ion transport
Afu6g09710	MFS gliotoxin efflux pump GliA	85	0.286	transporter activity///transport
Afu5g13050	kinesin family protein	86	0.001	kinesin complex///microtubule motor activity///establishment of mitotic spindle orientation///cytoplasmic microtubule///microtubule depolymerization///nuclear microtubule
Afu5g14230	C6 transcription factor, putative	87	0.389	DNA binding///nucleus///zinc ion binding
Afu8g06440	fructosyl amino acid oxidase, putative	88	0.075	
Afu5g02670	ThiJ/PfpI family protein	89	0.594	
Afu1g17280	hypothetical protein	90	0.040	
Afu4g12030	hypothetical protein	91	0.300	
Afu1g11140	Sterol desaturase family	92	0.571	
Afu6g12420	SprT family metallopeptidase, putative	93	0.035	
Afu5g02320	hypothetical protein	94	0.595	
Afu6g03410		95	0.175	
Afu2g15130	ABC multidrug transporter, putative	96	0.028	response to drug///drug transport///xenobiotic-transporting ATPase activity///plasma membrane
Afu6g08470	glycerol kinase, putative	97	0.083	cytoplasm///glycerol kinase activity///glycerol metabolic process
Afu2g08060	involucrin repeat protein, putative	98	0.385	

Afu1g17380	3-oxoacyl-(acyl-carrier-protein) reductase, putative	99	0.409
Afu5g00290	C6 transcription factor, putative	100	0.307

Table 3.30: 100 genes with greatest nSI decrease between 4 and 14 hours post infection. Genes are reported ranked according to greatest nSI decrease between 4 and 14 hours. A one-way ANOVA was conducted on nSI values between time-points, with the null hypothesis that nSI values do not change between time-points. FDR correct *p*--values from this analysis are reported for each gene.

ORF	Description	Rank	p-value	GO_BiologicalProcess
Afu1g10930	ammonium transporter	1	0.186	pseudohyphal growth///plasma membrane///ammonium transport///ammonium transmembrane transporter activity
Afu5g06930	hypothetical protein	2	0.375	
Afu3g09410	reverse transcriptase	3	0.130	
Afu2g17600	polyketide synthetase PksP	4	0.007	pathogenesis///pigment biosynthetic process///polyketide synthase activity
Afu5g10290	fructose-bisphosphate aldolase, putative	5	0.411	fructose-bisphosphate aldolase activity///glycolysis
Afu1g10990	ribosomal RNA processing protein, putative	6	0.432	
Afu1g16540	WD40 domain protein	7	0.002	
Afu1g10300	hypothetical protein	8	0.333	
Afu6g04750	conserved hypothetical protein	9	0.479	adenyl-nucleotide exchange factor activity///translation///cytosolic ribosome (sensu Eukaryota)///cytosol
Afu6g10950		10	0.522	
Afu4g14770	squalene-hopene-cyclase, putative	11	0.055	lipid particle///plasma membrane///endoplasmic reticulum///ergosterol biosynthetic process///lanosterol synthase activity
Afu7g06950	oxidoreductase, putative	12	0.346	
Afu1g04550	HMG box protein, putative	13	0.457	
Afu3g12930	dimethylallyl tryptophan synthase (GliD), putative	14	0.032	tryptophan dimethylallyltransferase activity///alkaloid biosynthetic process///secondary metabolic process
Afu5g01680	MFS transporter, putative	15	0.381	integral to plasma membrane
Afu8g01810	conserved hypothetical protein	16	0.377	
Afu5g02940	choline transport protein Ctr, putative	17	0.389	plasma membrane///choline transport///choline transmembrane transporter activity
Afu7g01120		18	0.409	
Afu8g07020	salicylate hydroxylase, putative	19	0.655	cellular aromatic compound metabolic process///monooxygenase activity
Afu4g13900	MFS transporter, putative	20	0.232	nicotinamide mononucleotide transport///nicotinamide mononucleotide permease activity///integral to plasma membrane
Afu5g03280	hypothetical protein	21	0.264	

Afu2g05360	C6 transcription factor, putative	22	0.469	transcription factor activity///regulation of transcription
Afu3g09920	hypothetical protein	23	0.509	
Afu1g17320	endo-arabinanase, putative	24	0.500	
Afu1g01290	cytochrome P450 monooxygenase, putative	25	0.138	
Afu8g00690	hypothetical protein	26	0.695	
Afu1g13810	hypothetical protein	27	0.066	
Afu3g09120	hypothetical protein	28	0.341	
Afu2g05100	Hypothetical protein	29	0.565	S-adenosylmethionine-dependent methyltransferase activity///cytoplasm///nucleus///biological process unknown
Afu8g01020	HET domain protein	30	0.141	programmed cell death
Afu1g12270	hypothetical protein	31	0.517	
Afu2g14060	NADH-cytochrome b5 reductase	32	0.621	cytochrome-b5 reductase activity///microsome///electron transport
Afu1g16420	GPI anchored protein, putative	33	0.087	
Afu3g03190	MFS transporter, putative	34	0.389	multidrug transport///plasma membrane///integral to plasma membrane///multidrug transporter activity
Afu2g17760	integral membrane protein	35	0.698	
Afu1g01500	short-chain dehydrogenase/reductase family protein, putative	36	0.165	
Afu5g12760	CCCH zinc finger protein	37	0.512	
Afu5g01130	hypothetical protein	38	0.323	
Afu5g00680	CRAL/TRIO domain protein	39	0.175	phosphatidylinositol transporter activity///phospholipid transport///Golgi to plasma membrane transport///cytosol
Afu2g09300	hypothetical protein	40	0.717	
Afu1g09160	hypothetical protein	41	0.331	
Afu4g01570	neutral amino acid permease	42	0.375	
Afu1g12850	nitrate transporter (nitrate permease)	43	0.389	nitrate transmembrane transporter activity///nitrate transport///integral to plasma membrane
Afu3g02840	isopropanol dehydrogenase, putative	44	0.383	
Afu4g13880	ankyrin repeat protein	45	0.271	
Afu1g14650	WD repeat protein	46	0.055	nucleus///biological process unknown///molecular function unknown
Afu7g05870	proteasome component Pre8, putative	47	0.438	proteasome core complex///ubiquitin-dependent protein catabolic process///endopeptidase activity
Afu5g01760	nucleolar RNA methyltransferase (Nop2), putative	48	0.104	S-adenosylmethionine-dependent methyltransferase activity///RNA methyltransferase activity///nucleolus///rRNA processing
Afu1g11680		49	0.485	
Afu5g01460	C6 finger domain protein, putative	50	0.346	zinc ion binding
Afu3g01930	conserved hypothetical protein	51	0.390	
Afu4g14780	cytochrome P450 monooxygenase, putative	52	0.759	oxidoreductase activity///metabolic process
Afu1g02780	L-asparaginase	53	0.484	endoplasmic reticulum///asparagine catabolic process///cellular response to

				nitrogen starvation///nuclear envelope///cell wall-bounded periplasmic space///asparaginase activity
Afu5g10210	hypothetical protein	54	0.466	
Afu4g13730	hypothetical protein	55	0.417	
Afu3g03930	cytochrome P450, putative	56	0.460	oxidoreductase activity///metabolic process
Afu4g14570	metallo-beta-lactamase domain protein, putative	57	0.258	catalytic activity///metabolic process
Afu3g03350	nonribosomal peptide synthase, putative	58	0.521	
Afu4g14530	glutathione S-transferase, putative	59	0.501	regulation of nitrogen utilization///soluble fraction///transcription corepressor activity
Afu3g13370	ubiquitin-like protein (HubA), putative	60	0.637	ubiquitin-dependent protein catabolic process///protein tagging activity///protein binding
Afu5g09150	oxidoreductase, short-chain dehydrogenase/reductase family	61	0.304	sporulation (sensu Saccharomyces)///fatty acid catabolic process///peroxisomal matrix///"2,4-dienoyl-CoA reductase (NADPH) activity"
Afu1g01980	IgE binding protein, putative	62	0.489	
Afu4g14510	hypothetical protein	63	0.639	
Afu3g08860	Transcriptional regulator ATRX related protein	64	0.680	
Afu7g07170	reverse transcriptase/protease/endonuclease Pol, putative	65	0.308	
Afu6g14080		66	0.528	
Afu4g08710	short chain dehydrogenase, putative	67	0.129	fatty acid catabolic process
Afu6g07660	hypothetical protein	68	0.519	
Afu1g12200	conserved hypothetical protein	69	0.490	
Afu4g14130	ABC multidrug transporter, putative	70	0.583	peptide pheromone export///ATP-binding cassette (ABC) transporter activity///integral to plasma membrane
Afu8g07210	hydroxymethylglutaryl-CoA synthase	71	0.375	hydroxymethylglutaryl-CoA synthase activity///endoplasmic reticulum///mitochondrion///ergosterol biosynthetic process
Afu5g10050	cytochrome P450 monooxygenase, putative	72	0.514	oxidoreductase activity///metabolic process
Afu4g00740	hypothetical protein	73	0.459	
Afu4g08890	aldo-keto reductase family protein, putative	74	0.179	cellular component unknown///aldo-keto reductase activity///cellular aldehyde metabolic process
Afu3g13650	integral membrane protein	75	0.602	
Afu2g00290	hypothetical protein	76	0.689	
Afu4g00700	oxidoreductase, zinc-binding	77	0.418	cytoplasm///nucleus///alcohol dehydrogenase (NADP+) activity
Afu4g13930	CRAL/TRIO domain protein	78	0.782	phosphatidylinositol transporter activity///cell wall organization///phospholipid transport///cytoplasm///cytosol///microsome
Afu7g00830	alpha/beta hydrolase, putative	79	0.521	hydrolase activity///metabolic process
Afu1g16090	arsenate reductase (ArsC), putative	80	0.526	response to arsenic///arsenite transport///cytoplasm///arsenate reductase activity

Afu7g06250	DSBA-like thioredoxin domain protein	81	0.359	
Afu2g00710	alpha-amylase, putative	82	0.500	extracellular region///alpha-amylase activity///polysaccharide catabolic process
Afu3g03290	hypothetical protein	83	0.028	
Afu8g00230	phytanoyl-CoA dioxygenase family protein	84	0.265	
Afu1g11230	HMG-CoA reductase	85	0.604	hydroxymethylglutaryl-CoA reductase (NADPH) activity///mitochondrial matrix///ergosterol biosynthetic process///endoplasmic reticulum membrane///nuclear envelope
Afu4g01280	hypothetical protein	86	0.321	
Afu3g12120	fatty acid oxygenase PpoC, putative	87	0.680	
Afu3g02800	lipase/esterase, putative	88	0.774	
Afu6g11250	C2H2 finger domain protein, putative	89	0.550	
Afu5g07910	hypothetical protein	90	0.697	
Afu5g04000	conserved hypothetical protein	91	0.389	ubiquitin-dependent protein catabolic process///chaperone activity///nucleus///protein complex assembly///proteasome complex
Afu7g00500	hypothetical protein	92	0.633	
Afu3g11900	oxidoreductase, zinc-binding	93	0.455	alcohol metabolic process///soluble fraction///alcohol dehydrogenase (NADP+) activity///cellular aldehyde metabolic process
Afu8g00920	UDP-glucose dehydrogenase Uxs2p	94	0.451	
Afu3g03690	hypothetical protein	95	0.375	
Afu2g05430	Uridine kinase	96	0.286	pyrimidine salvage///cytoplasm///uridine kinase activity///nucleus
Afu3g08630	coactivator bridging factor 1 (Mbf1), putative	97	0.131	DNA binding
Afu5g10650	pyridoxamine phosphate oxidase, putative	98	0.490	cellular component unknown///pyridoxamine-phosphate oxidase activity///fatty acid metabolic process
Afu3g13960	hypothetical protein	99	0.581	
Afu5g07980	hypothetical protein	100	0.527	

3.5.2 Functional classification of differentially expressed genes between 4 and 14 hours post infection in Δ*laeA*

Differentially expressed genes were grouped into functional categories based on GO Terms and by reference to the *A. fumigatus* literature. A summary of up and down expressed functional categories between 4 and 14 hours is given in Table 3.31.

Table 3.31: Functional classification of selected genes having differential transcript abundance in Δ*laeA* between 4 and 14 hours post infection in the murine lung. Increased (red) and decreased (green) genes are shown for each functional category. Both increasing and decreasing transcripts are sub-divided into expression cohorts which are either high, moderate, and low with respect to their expression change. Genes within functional categories ranked according to greatest nSI intensity changes between 4 and 14 hours. A one-way ANOVA was conducted on nSI values between time-points, from which FDR correct *p*-values are reported for each gene.

Functional category	ORF	Description	Rank	p-value	Magnitude	ORF	Description	Rank	p-value	Magnitude
Cell wall	Afu5g03940	alpha-1,3-glucanase, putative	26	0.527	UP HIGH	Afu5g02280	endo-1,3(4)-beta-glucanase, putative	189	0.722	DOWN HIGH
	Afu8g01410	class V chitinase ChiB1	280	0.572	UP HIGH	Afu5g14030	endo-1,3(4)-beta-glucanase, putative	368	0.36	DOWN HIGH
	Afu5g03760	class III chitinase ChiA1	285	0.108	UP HIGH	Afu3g03870	endo-1,4-beta-glucanase, putative	416	0.527	DOWN HIGH
	Afu2g13440	chitin synthase E	297	0.572	UP HIGH	Afu6g09310	class V chitinase, putative	603	0.721	DOWN HIGH
	Afu8g05020	beta-N-acetylhexosaminidase NagA, putative	316	0.557	UP HIGH	Afu6g09780	class V chitinase, putative	614	0.722	DOWN HIGH
	Afu1g12040	chitin biosynthesis protein (Chs7), putative	360	0.097	UP HIGH	Afu6g12410	1,3-beta-glucanosyltransferase, putative	667	0.633	DOWN MOD
	Afu2g14360	GPI anchored glucanase, putative	476	0.066	UP HIGH	Afu6g14540	endo-1,3(4)-beta-glucanase, putative	711	0.677	DOWN MOD
	Afu6g12400	1,3-beta-glucan synthase catalytic subunit FksP	714	0.385	UP MOD	Afu4g12900	alpha-1,6-mannosyltransferase subunit (Ecm39), putative	1151	0.519	DOWN MOD
	Afu5g08580	alpha-1,6-mannosyltransferase subunit (Och1), putative	882	0.67	UP MOD	Afu2g06160	mutanase	1245	0.634	DOWN MOD
	Afu7g08510	extracellular alpha-1,3-glucanase/mutanase, putative	949	0.298	UP MOD	Afu3g07110	class III chitinase, putative	1403	0.869	DOWN LOW
	Afu6g11390	1,3-beta-glucanosyltransferase Gel2	1011	0.24	UP MOD	Afu5g03960	class V chitinase Chi1	1418	0.863	DOWN LOW
	Afu2g13430	chitin synthase, putative	1046	0.629	UP MOD	Afu8g02130	1,3-beta-glucanosyltransferase, putative	1446	0.792	DOWN LOW
	Afu8g05630	chitin synthase F	1103	0.782	UP MOD	Afu2g14910	alpha-1,6-mannosyltransferase subunit, putative	1528	0.857	DOWN LOW
	Afu6g14040	glycosyl transferase, putative	1227	0.554	UP MOD	Afu2g03980	alpha-1,3-glucanase, putative	1556	0.86	DOWN LOW
	Afu7g08350	alpha-1,3-glucanase, putative	1438	0.793	UP LOW	Afu7g05140	class III chitinase, putative	1701	0.797	DOWN LOW
	Afu1g04260	endo-1,3-beta-glucanase Engl1	1477	0.786	UP LOW	Afu8g05620	chitin synthase activator (Chs3), putative	1705	0.894	DOWN LOW
	Afu2g05340	1,3-beta-glucanosyltransferase, putative	1481	0.782	UP LOW	Afu1g05290	endo-1,3(4)-beta-glucanase, putative	1725	0.847	DOWN LOW

	Afu6g14480	alpha-1,3-mannosyltransferase, putative	1505	0.817	UP LOW					
	Afu1g15440	alpha-1,3-glucan synthase, putative	1623	0.734	UP LOW					
	Afu5g11990	alpha-1,3-mannosyltransferase (Alg3), putative	1788	0.818	UP LOW					
	Afu4g06870	N-glycosyl-transferase	1892	0.749	UP LOW					
	Afu5g14190	beta-glucanase, putative	1900	0.683	UP LOW					
Ergosterol	Afu1g11140	Sterol desaturase family	92	0.571	UP HIGH	Afu4g14770	squalene-hopene-cyclase, putative	11	0.55	DOWN HIGH
	Afu5g04080	oxidosqualene:lanosterol cyclase	198	0.637	UP HIGH	Afu1g11230	HMG-CoA reductase	85	0.64	DOWN HIGH
	Afu2g01160	C-4 methyl sterol oxidase, putative	310	0.604	UP HIGH	Afu5g00110	squalene-hopene-cyclase, putative	369	0.664	DOWN HIGH
	Afu7g00260	squalene-hopene-cyclase, putative	403	0.375	UP HIGH	Afu5g14350	c-24(28) sterol reductase	718	0.87	DOWN MOD
	Afu4g09190	S-adenosyl-methionine-sterol-C- methyltransferas	716	0.678	UP MOD	Afu4g06890	14-alpha sterol demethylase Cyp51A	1303	0.797	DOWN MOD
	Afu7g04880	UDP-glucose,sterol transferase	871	0.754	UP MOD	Afu1g07140	c-24(28) sterol reductase	1517	0.822	DOWN LOW
	Afu8g02440	C-4 methyl sterol oxidase, putative	1295	0.748	UP MOD					
	Afu4g07780	mevalonate kinase	1541	0.647	UP LOW					
	Afu7g02480	oxysterol binding protein (Osh1), putative	1704	0.554	UP LOW					
	Afu2g17400	C-3 sterol dehydrogenase/C-4 decarboxylase	1871	0.833	UP LOW					
Microtubule	Afu2g03150	kinesin family protein	1261	0.749	UP MOD	Afu4g07630	microtubule associated protein (Ytm1), putative	281	0.374	DOWN HIGH
	Afu5g11810	cytoplasmic dynein heavy chain	1567	0.61	UP LOW	Afu1g02550	tubulin alpha-1 subunit	428	0.679	DOWN HIGH
Cell polarity	Afu2g01000	LIM domain protein	342	0.028	UP HIGH	Afu1g12820	gamma-tubulin complex component GCP6, putative	1716	0.99	DOWN LOW
	Afu5g07710	nuclear migration protein (ApsA), putative	566	0.818	UP HIGH	Afu4g06710	kinase-related protein	1941	0.92	DOWN LOW
	Afu7g05340	conserved hypothetical protein	729	0.695	UP MOD	Afu2g14990	tubulin alpha-2 subunit	1955	0.843	DOWN LOW
	Afu5g03080	septin	776	0.519	UP MOD					

	Afu2g12390	protein kinase regulator (Mob1), putative	858	0.673	UP MOD					
	Afu1g05610	protein phosphotase 2a 65kd regulatory sububit	1076	0.763	UP MOD					
	Afu2g03710	cell polarity protein, putative	1512	0.749	UP LOW					
	Afu1g04950	serine/threonine protein phosphatase pp1	1713	0.757	UP LOW					
Ion transport	Afu8g01480	potassium channel, putative	8	0.066	UP HIGH	Afu1g16090	arsenate reductase (ArsC), putative	80	0.526	DOWN HIGH
	Afu2g07630	vacuolar H+VCa2+ exchanger	73	0.286	UP HIGH	Afu5g15000	arsenate reductase (ArsC), putative	470	0.68	DOWN HIGH
	Afu2g03730	Ctr copper transporter family protein	124	0.437	UP HIGH	Afu1g11110	calcium channel pore-forming subunit (Cch1), putative	472	0.661	DOWN HIGH
	Afu1g01550	high affinity zinc ion transporter, putative	133	0.07	UP HIGH	Afu6g06740	endoplasmic reticulum calcium ATPase, putative	539	0.545	DOWN HIGH
	Afu1g02480	plasma membrane ATPase, putative	319	0.323	UP HIGH	Afu6g07050	sodium-hydrogen antiporter, putative	1430	0.861	DOWN LOW
	Afu1g16130	copper-transporting ATPase, putative	531	0.444	UP HIGH	Afu7g06570	zinc/cadmium resistance protein	1601	0.782	DOWN LOW
	Afu4g09560	ZIP Zinc transporter, putative	768	0.524	UP MOD					
	Afu1g14250	potassium channel, putative	849	0.639	UP MOD					
	Afu2g17170	Na+/H+ antiporter Nha1	995	0.604	UP MOD					
	Afu5g15030	arsenic resistance protein ArsH	1089	0.568	UP MOD					
	Afu1g02930	Ca2+ binding protein (calmodulin), putative	1247	0.834	UP MOD					
	Afu6g02550	magnesium ion transporter (Mrs2), putative	1265	0.801	UP MOD					
	Afu4g12620	copper-transporting ATPase, putative	1363	0.297	UP LOW					
	Afu3g10690	calcium-translocating P-type ATPase(PMCA-type),putative	1406	0.862	UP LOW					
	Afu1g05760	arsenite efflux transporter (ArsB), puative	1412	0.854	UP LOW					
	Afu6g02810	Ctr copper transporter family family	1494	0.638	UP LOW					
Iron acquisition	Afu3g13670	siderochrome-iron transporter, putative	42	0.323	UP HIGH	Afu7g04730	siderochrome-iron transporter, putative	1053	0.664	DOWN MOD

	Afu6g13750	ferric-chelate reductase, putative	56	0.183	UP HIGH	Afu3g03390	siderophore biosynthesis lipase/esterase, putative	1070	0.112	DOWN MOD
	Afu3g03640	siderochrome-iron transporter (MirB), putative	534	0.561	UP HIGH					
	Afu4g14640	low affinity iron transporter, putative	1095	0.484	UP MOD					
	Afu2g05730	siderochrome-iron transporter (MirC), putative	1189	0.846	UP MOD					
	Afu3g03440	MFS family siderophore transporter, putative	1630	0.438	UP LOW					
Antigen	Afu4g00610	aryl-alcohol dehydrogenase, putative	46	0.062	UP HIGH	Afu2g03720	peptidyl-prolyl cis-trans isomerase	701	0.88	DOWN MOD
	Afu6g11330	histidine acid phosphatase, putative	201	0.389	UP HIGH	Afu5g09210	alkaline serine protease Alp2	885	0.68	DOWN MOD
	Afu1g14550	Mn superoxide dismutase MnSOD	272	0.089	UP HIGH	Afu5g02040	extracellular lipase, putative	1208	0.796	DOWN MOD
	Afu8g05020	beta-N-acetylhexosaminidase NagA, putative	280	0.557	UP HIGH	Afu5g09580	conidial hydrophobin Hyp1/RodA	1232	0.811	DOWN MOD
	Afu5g13300	aspartic endopeptidase Pep1	349	0.661	UP HIGH	Afu4g09090	thioredoxin, putative	1591	0.526	DOWN LOW
	Afu4g09580	major allergen Asp F2	384	0.09	UP HIGH					
	Afu2g03830	allergen Asp F4	809	0.798	UP MOD					
	Afu1g09670	HLH transcription factor (GlcD gamma), putative	961	0.639	UP MOD					
	Afu2g09030	secreted dipeptidyl peptidase	1023	0.724	UP MOD					
	Afu5g04170	molecular chaperone HSP90	1451	0.86	UP LOW					
	Afu4g06670	allergen Asp F7	1499	0.807	UP LOW					
Secreted protease	Afu2g15950	aspartic endopeptidase, putative	40	0.236	UP HIGH					
	Afu8g07080	elastinolytic metalloproteinase Mep	52	0.135	UP HIGH					
	Afu3g00650	aminopeptidase Y, putative	62	0.236	UP HIGH					
	Afu2g17330	serine peptidase, family S28, putative	128	0.003	UP HIGH					
	Afu2g03510	pheromone processing carboxypeptidase (Sxa2), putative	242	0.34	UP HIGH					

	Afu4g13750	Deuterolysin metalloprotease, putative	291	0.633	UP HIGH						
	Afu5g13300	aspartic endopeptidase Pep1	349	0.661	UP HIGH						
	Afu5g07330	carboxypeptidase S1, putative	490	0.634	UP HIGH						
	Afu4g09320	antigenic dipeptidyl-peptidase Dpp4	751	0.484	UP MOD						
	Afu3g01220	aspartic-type endopeptidase, putative	896	0.58	UP MOD						
	Afu2g09030	secreted dipeptidyl peptidase	1023	0.724	UP MOD						
	Afu4g07040	aspartic-type endopeptidase (CtsD), putative	1050	0.483	UP MOD						
	Afu6g14420	disintegrin-like metalloproteinase, putative	1101	0.286	UP MOD						
	Afu1g00420	carboxypeptidase S1, putative	1275	0.385	UP MOD						
	Afu4g14000	tripeptidyl peptidase A	1404	0.749	UP LOW						
	Afu1g08940	pheromone processing carboxypeptidase Kex1	1449	0.385	UP LOW						
Signal peptide encoding genes	Afu2g14540	endoglucanase, putative	6	0	UP HIGH		Afu1g17320	endo-arabinanase, putative	24	0.5	UP HIGH
	Afu8g01480	potassium channel, putative	8	0.066	UP HIGH		Afu1g16420	GPI anchored protein, putative	33	0.087	UP HIGH
	Afu2g10130	phase-specific adhesin, putative	11	0.003	UP HIGH		Afu1g02780	L-asparaginase	53	0.484	UP HIGH
	Afu2g14420	cutinase, putative	15	0	UP HIGH		Afu3g03930	cytochrome P450, putative	56	0.46	UP HIGH
	Afu2g14360	GPI anchored glucanase, putative	26	0.066	UP HIGH		Afu1g01980	IgE binding protein, putative	62	0.489	UP HIGH
	Afu8g05910	pectate lyase, putative	27	0.031	UP HIGH		Afu3g13650	integral membrane protein	75	0.602	UP HIGH
	Afu8g00610	cell surface protein Mas1, putative	28	0	UP HIGH		Afu2g00710	alpha-amylase, putative	82	0.5	UP HIGH
	Afu3g13640	extracellular serine-rich protein	31	0.323	UP HIGH		Afu8g00920	UDP-glucose dehydrogenase Uxs2p	94	0.451	UP HIGH
	Afu3g14980	extracellular chitosanase CsnC, putative	34	0.134	UP HIGH		Afu5g00120	cytochrome P450 oxidoreductase/alkane hydroxylase, putative	115	0.673	UP HIGH
	Afu3g08110	cell wall protein, putative	36	0.003	UP HIGH		Afu1g17050	hypothetical protein	116	0.743	UP HIGH
	Afu3g02090	beta-xylosidase	49	0.097	UP HIGH		Afu2g15450	hypothetical protein	120	0.717	UP HIGH
	Afu1g06470	neutral/alkaline nonlysosomal ceramidase,	50	0.483	UP HIGH		Afu1g04870	urea transporter (Dur3), putative	125	0.291	UP HIGH

		putative								
	Afu7g06810	L-amino acid oxidase LaoA, putative	51	0.06	UP HIGH	Afu3g02930	extracellular soluble lytic transglycosylase, putative	140	0.105	UP HIGH
	Afu3g00650	aminopeptidase Y, putative	62	0.236	UP HIGH	Afu6g02980	extracellular exo-polygalacturonase, putative	141	0.3	UP HIGH
	Afu2g00760	pectate lyase A	64	0.003	UP HIGH	Afu1g15250	autophagy protein Atg27, putative	144	0.611	UP HIGH
	Afu6g13760	alpha-1,2-mannosidase, putative subfamily	70	0.166	UP HIGH	Afu6g08700	beta glucosidase, putative	147	0.438	UP HIGH
	Afu4g01290	endo-chitosanase, pseudogene	74	0.31	UP HIGH	Afu3g00550	hypothetical protein	171	0.583	UP HIGH
	Afu3g02270	mycelial catalase Cat1	143	0.262	UP HIGH	Afu3g02790	amidohydrolase family protein, putative	183	0.677	UP HIGH
	Afu1g04340	SH3 and Ded_cyto domain protein, putative	145	0.433	UP HIGH	Afu6g07480	endoglucanase C	185	0.625	UP HIGH
	Afu3g00320	endo-1,4-beta-xylanase (XlnA), putative	150	0.593	UP HIGH	Afu7g06720	tannase, putative	191	0.633	UP HIGH
	Afu4g13990	hypothetical protein	157	0.09	UP HIGH	Afu1g17320	endo-arabinanase, putative	24	0.5	UP HIGH
	Afu1g01300	GPI anchored protein, putative	166	0.581	UP HIGH	Afu1g16420	GPI anchored protein, putative	33	0.087	UP HIGH
	Afu2g05150	cell wall galactomannoprotein Mp2	167	0.002	UP HIGH	Afu1g02780	L-asparaginase	53	0.484	UP HIGH
	Afu1g14560	alpha-mannosidase	169	0.002	UP HIGH	Afu3g03930	cytochrome P450, putative	56	0.46	UP HIGH
	Afu2g11920	hypothetical protein	173	0.519	UP HIGH	Afu1g01980	IgE binding protein, putative	62	0.489	UP HIGH
	Afu4g12380	hypothetical protein	183	0.648	UP HIGH	Afu3g13650	integral membrane protein	75	0.602	UP HIGH
	Afu3g12170	MFS sugar transporter, putative	186	0.385	UP HIGH	Afu2g00710	alpha-amylase, putative	82	0.5	UP HIGH
	Afu3g00310	extracellular phytase, putative	194	0.272	UP HIGH	Afu8g00920	UDP-glucose dehydrogenase Uxs2p	94	0.451	UP HIGH
	Afu5g00540	extracellular signaling protein FacC, putative	196	0.375	UP HIGH	Afu5g00120	cytochrome P450 oxidoreductase/alkane hydroxylase, putative	115	0.673	UP HIGH
	Afu3g08870	conserved hypothetical protein	197	0.639	UP HIGH	Afu1g17050	hypothetical protein	116	0.743	UP HIGH
Pathogensis	Afu8g07080	elastinolytic metalloproteinase Mep	52	0.135	UP HIGH	Afu2g17600	polyketide synthetase PksP	4	0.7	DOWN HIGH
	Afu3g02270	mycelial catalase Cat1	143	0.262	UP HIGH	Afu8g02380	FAD-dependent monooxygenase, putative	190	0.597	DOWN HIGH
	Afu7g05060	MgtC/SapB family membrane protein	175	0.68	UP HIGH	Afu6g13970	FAD-dependent monooxygenase (PaxM), putative	270	0.697	DOWN HIGH
	Afu5g06070	ABC multidrug transporter Mdr1	254	0.105	UP HIGH	Afu3g14810	pathogenicity associated protein PEP2, putative	777	0.725	DOWN MOD
	Afu2g04200	4-hydroxyphenylpyruvate dioxygenase, putative	258	0.031	UP HIGH	Afu5g09580	conidial hydrophobin Hyp1/RodA	1232	0.811	DOWN MOD

	Afu2g13440	chitin synthase E	285	0.572	UP HIGH				
	Afu5g13300	aspartic endopeptidase Pep1	349	0.661	UP HIGH				
	Afu2g17560	1,3,6,8-tetrahydroxynaphthalene reductase	693	0.61	UP MOD				
	Afu2g08360	orotidine 5'-phosphate decarboxylase PyrG	748	0.698	UP MOD				
	Afu2g03830	allergen Asp F4	809	0.798	UP MOD				
	Afu6g09610	nonribosomal peptide synthase, putative	889	0.717	UP MOD				
	Afu1g01890	enoyl-CoA hydratase/isomerase family protein	897	0.385	UP MOD				
	Afu3g11250	C2H2 transcription factor (Swi5), putative	1124	0.752	UP MOD				
	Afu3g00590	Asp-hemolysin	1678	0.81	UP LOW				
	Afu6g04820	para-aminobenzoate synthase PabaA	1714	0.715	UP LOW				
	Afu1g15440	alpha-1,3-glucan synthase, putative	1788	0.734	UP LOW				
Secondary metabolite	Afu8g00540	hybrid polyketide synthase/nonribosomal peptide synthase, putative	178	0.093	UP HIGH	Afu2g17600	polyketide synthetase PksP	4	0.7	DOWN HIGH
	Afu1g17640	melanin biosynthesis transcription factor RegA	265	0.046	UP HIGH	Afu3g03350	nonribosomal peptide synthase, putative	58	0.521	DOWN HIGH
	Afu3g13600	C6 transcription factor, putative	294	0.527	UP HIGH	Afu4g14440	nonribosomal peptide synthase, putative	122	0.625	DOWN HIGH
	Afu6g09610	nonribosomal peptide synthase, putative	889	0.717	UP MOD	Afu4g14590	C6 transcription factor, putative	293	0.581	DOWN HIGH
	Afu3g01410	polyketide synthase, putative	967	0.813	UP MOD	Afu8g00170	nonribosomal peptide synthetase, putative	433	0.432	DOWN HIGH
	Afu3g12890	C6 transcription factor (GliZ), putative	1080	0.639	UP MOD	Afu3g02530	polyketide synthase, putative	572	0.843	DOWN HIGH
	Afu5g12730	nonribosomal peptide synthase, putative	1158	0.35	UP MOD	Afu3g12920	nonribosomal peptide synthase (GliP), putative	602	0.734	DOWN MOD
	Afu6g12050	nonribosomal peptide synthase, putative	1485	0.68	UP LOW	Afu8g00490	polyketide synthase, putative	671	0.727	DOWN MOD
	Afu3g02670	nonribosomal peptide synthetase, putative	1528	0.744	UP LOW	Afu8g00420	C6 finger transcription factor, putative	1101	0.753	DOWN MOD
	Afu3g01510	C6 transcription factor, putative	1552	0.724	UP LOW	Afu6g09630	C6 finger domain protein GliZ	1514	0.757	DOWN LOW

	Afu4g14400	C2H2 finger domain protein, putative	1923	0.385	UP LOW		Afu1g17710	C6 transcription factor, putative	1940	0.888	DOWN LOW
Gliotoxin	Afu6g09670	cytochrome P450 oxidoreductase GliC	1	0.012	UP HIGH		Afu6g09770	geranylgeranyl diphosphate synthase, putative	1192	0.743	DOWN MOD
	Afu6g09730	cytochrome P450 oxidoreductase GliF	2	0.002	UP HIGH		Afu6g09760	toxin biosynthesis cytochrome P45 oxidoreductase, putative	1394	0.792	DOWN LOW
	Afu6g09690	glutathione S-transferase GliG	3	0	UP HIGH		Afu6g09630	C6 finger domain protein GliZ	1514	0.757	DOWN LOW
	Afu6g09680	O-methyltransferase GliM	4	0.008	UP HIGH		Afu6g09530	hypothetical protein	1603	0.734	DOWN LOW
	Afu6g09650	membrane dipeptidase GliJ	5	0	UP HIGH						
	Afu6g09740	thioredoxin reductase GliT	9	0	UP HIGH						
	Afu6g09640	aminotransferase GliI	20	0.011	UP HIGH						
	Afu6g09710	MFS gliotoxin efflux pump GliA	85	0.286	UP HIGH						
	Afu6g09610	nonribosomal peptide synthase, putative	889	0.717	UP MOD						
Pseurotin A supercluster	Afu8g00610	cell surface protein Mas1, putative	28	0	UP HIGH		Afu8g00690	hypothetical protein	26	0.695	DOWN HIGH
	Afu8g00540	hybrid polyketide synthase/nonribosomal peptide synthase, putative	178	0.093	UP HIGH		Afu8g00230	phytanoyl-CoA dioxygenase family protein	84	0.265	DOWN HIGH
	Afu8g00600	conserved hypothetical protein	203	0.24	UP HIGH		Afu8g00550	SirN-like methyltransferase, putative	180	0.548	DOWN HIGH
	Afu8g00260	F-box domain and ankyrin repeat protein	427	0.597	UP MOD		Afu8g00110	oxidoreductase, 2OG-Fe(II) oxygenase family, putative	330	0.648	DOWN HIGH
	Afu8g00760	cytochrome P450, putative	537	0.68	UP MOD		Afu8g00660	solute transporter, putative	372	0.824	DOWN HIGH
	Afu8g00300	conserved hypothetical protein	559	0.796	UP MOD		Afu8g00170	nonribosomal peptide synthetase, putative	433	0.432	DOWN HIGH
	Afu8g00460	methionine aminopeptidase, type I, putative	571	0.718	UP MOD		Afu8g00720	amino acid transporter, putative	449	0.83	DOWN HIGH
	Afu8g00530	alpha/beta hydrolase, putative	618	0.922	UP LOW		Afu8g00330	endonuclease/reverse transcriptase/RNaseH, putative	504	0.698	DOWN HIGH
	Afu7g01400	kinesin family protein (BimC), putative	966	0.389	UP HIGH		Afu8g00140	MFS transporter, putative	572	0.843	DOWN HIGH
	Afu2g14280	kinesin family protein (KlpA), putative	997	0.501	UP HIGH		Afu8g00130	hypothetical protein	647	0.757	DOWN MOD
	Afu2g15750	gamma-tubulin complex component GCP4, putative	1185	0.708	UP HIGH		Afu8g00710	secreted antimicrobial peptide, putative	688	0.721	DOWN MOD

	Afu2g14730	kinesin family protein	1195	0.615	UP HIGH	Afu8g00570	alpha/beta hydrolase, putative	714	0.81	DOWN MOD
	Afu2g07550	serine/threonine protein kinase (Ark1), putative	1468	0.7	UP HIGH	Afu8g00390	O-methyltransferase, putative	803	0.678	DOWN MOD
						Afu8g00490	polyketide synthase, putative	841	0.727	DOWN MOD
						Afu8g00450		890	0.781	DOWN MOD
						Afu8g00200	O-methyltransferase, putative	933	0.561	DOWN MOD
						Afu8g00420	C6 finger transcription factor, putative	1101	0.753	DOWN MOD
						Afu8g00220	cytochrome P45, putative	1137	0.792	DOWN MOD
						Afu8g00290	conserved hypothetical protein	1259	0.86	DOWN MOD
						Afu8g00440	steroid monooxygenase, putative	1867	0.729	DOWN LOW
						Afu8g00640	glycosyl transferase, putative	1882	0.876	DOWN LOW
						Afu8g00310	LINE-1 class reverse transcriptase, RNaseH, putative	1888	0.776	DOWN LOW
Ribosome biogenesis and RNA processing	Afu8g05300	RNA polymerase II subunit 7	262	0.685	UP HIGH	Afu1g10990	ribosomal RNA processing protein, putative	6	0.432	DOWN HIGH
	Afu2g13570	ribosome biogenesis protein (Bms1), putative	664	0.519	UP MOD	Afu1g02950	RNA recognition motif. (a.k.a. RRM, RBD, or RNP domain) protein	328	0.523	DOWN HIGH
	Afu2g13720	RNA-polymerase I	973	0.721	UP MOD	Afu4g07640	ribosomal protein S13	406	0.375	DOWN HIGH
	Afu1g02510	RNA-binding protein, putative	1064	0.725	UP MOD	Afu8g04960	small nuclear ribonucleoprotein SmG, putative	418	0.375	DOWN HIGH
	Afu3g11220	ribonuclease T2, putative	1115	0.797	UP MOD	Afu2g05110	small nuclear ribonucleoprotein SmD1, putative	434	0.544	DOWN HIGH
	Afu1g04280	Ribosomal protein S7p/S5e, putative	1615	0.176	UP LOW	Afu2g02270	ribosomal protein S14p/S29e	435	0.737	DOWN HIGH
	Afu4g13450	RNA methyltransferase, TrmH family family	1642	0.801	UP LOW	Afu5g11000	small nuclear ribonucleoprotein U2, A'	629	0.781	DOWN HIGH
	Afu5g09060	RNA binding protein, putative	1780	0.68	UP LOW	Afu1g02680	small nucleolar ribonucleoprotein complex subunit Dip2, putative	664	0.34	DOWN MOD
	Afu6g04810	RNA polymerase II transcription mediator complex subunit (Med6), putative	1883	0.825	UP LOW	Afu4g07540	small nucleolar ribonucleoprotein complex subunit, putative	666	0.236	DOWN MOD
						Afu3g05840	RNA-binding protein rnp24, putative	721	0.449	DOWN MOD

						Afu5g08310	RNA and export factor binding protein 2-I	815	0.81	DOWN MOD
						Afu2g15210	small nuclear ribonucleoprotein (LSM2), putative	822	0.633	DOWN MOD
						Afu1g04840	RNP domain protein	828	0.647	DOWN MOD
						Afu3g12300	Ribosomal L22e protein family	840	0.68	DOWN MOD
						Afu3g10380	RNA polymerase III transcription factor, putative	878	0.499	DOWN MOD
						Afu6g04320	RNA binding protein	999	0.631	DOWN MOD
						Afu6g04560	4S ribosomal protein S9, mitochondrial precursor	1057	0.24	DOWN MOD
						Afu1g03110	6S ribosomal protein L29, putative	1291	0.486	DOWN LOW
						Afu6g07360	ribosomal protein S8	1322	0.758	DOWN LOW
						Afu5g13470	6S acidic ribosomal protein, putative	1414	0.39	DOWN LOW
						Afu3g10730	Ribosomal protein S7e	1421	0.582	DOWN LOW
						Afu8g04400	RNA binding protein, putative	1432	0.414	DOWN LOW
						Afu4g07440	Ribosomal protein L36e, putative	1480	0.554	DOWN LOW
						Afu1g15020	4S ribosomal protein S5	1482	0.717	DOWN LOW
						Afu2g16370	Ribosomal protein L32	1531	0.522	DOWN LOW
						Afu7g01330	RNA binding complex component (TraX), putative	1671	0.7	DOWN LOW
						Afu3g06310	RNA binding protein	1768	0.841	DOWN LOW
						Afu1g05080	ribosomal protein P	1807	0.494	DOWN LOW
						Afu3g13320	4S ribosomal protein S, putative	1827	0.667	DOWN LOW
						Afu6g10370	RNA lariat debranching enzyme, putative	1830	0.918	DOWN LOW
						Afu5g07640	RNA 3'-terminal phosphate cyclase, putative	1844	0.898	DOWN LOW
Carbohydrate transport	Afu3g01230	sugar transporter-like protein	33	0.087	UP HIGH	Afu7g00950	MFS monosaccharide transporter, putative	145	0.2	DOWN HIGH

	Afu3g14170	high-affinity hexose transporter	38	0.24	UP HIGH	Afu8g02010	MFS sugar transporter, putative	153	0.49	DOWN HIGH
	Afu8g01340	MFS sugar transporter, putative	120	0.291	UP HIGH	Afu5g12950	MFS quinate transporter, putative	463	0.68	DOWN HIGH
	Afu3g12170	MFS sugar transporter, putative	186	0.385	UP HIGH	Afu8g05710	MFS sugar transporter Stl1, putative	634	0.262	DOWN HIGH
	Afu5g02840	sugar transporter family protein, putative	260	0.55	UP HIGH	Afu2g14590	MFS monosaccharide transporter, putative	663	0.47	DOWN MOD
	Afu5g14540	MFS monosaccharide transporter, putative	275	0.286	UP HIGH	Afu6g01860	MFS lactose permease, putative	1051	0.779	DOWN MOD
	Afu7g06380	maltase	288	0.542	UP HIGH	Afu8g01180	MFS sugar transporter, putative	1495	0.847	DOWN LOW
	Afu3g01700	maltose permease	568	0.638	UP HIGH					
	Afu2g10910	maltose permease	590	0.45	UP HIGH					
	Afu6g14500	MFS sugar transporter, putative	732	0.483	UP MOD					
	Afu3g01670	MFS hexose transporter, putative	950	0.437	UP MOD					
	Afu3g03700	Sugar transporter subfamily	1173	0.753	UP MOD					
	Afu6g11920	maltose permease	1312	0.355	UP LOW					
	Afu1g11050	MFS sugar transporter, putative	1394	0.761	UP LOW					
	Afu3g00200	hexose transporter protein	1464	0.757	UP LOW					
	Afu7g05830	MFS sugar transporter, putative	1503	0.78	UP LOW					
	Afu5g00280	MFS sugar transporter, putative	1718	0.833	UP LOW					
	Afu3g02890	MFS sugar transporter, putative	1863	0.846	UP LOW					
Amino acid transport	Afu5g09440	amino acid permease, putative	30	0.118	UP HIGH	Afu4g01570	neutral amino acid permease	42	0.375	DOWN HIGH
	Afu2g11220	proline permease, putative	32	0.22	UP HIGH	Afu8g00720	amino acid transporter, putative	449	0.83	DOWN HIGH
	Afu5g14660	GABA permease, putative	107	0.023	UP HIGH	Afu2g15470	neutral amino acid permease	1242	0.838	DOWN MOD
	Afu1g14700	allantoate transporter, putative	515	0.461	UP HIGH	Afu6g00410	amino acid permease, putative	1712	0.834	DOWN LOW
	Afu2g13630	amino transferase	645	0.572	UP HIGH					

	Afu2g17790	amino acid transporter, putative	873	0.595	UP MOD				
	Afu1g12310	GABA permease GabA	1465	0.793	UP LOW				
	Afu6g04990	amino acid transporter, putative	1504	0.785	UP LOW				
	Afu4g07760	Transmembrane amino acid transporter protein family	1619	0.723	UP LOW				
	Afu7g00440	GABA permease, putative	1639	0.783	UP LOW				
Carbohydrate / protein glycosylation	Afu4g00390	glycosyl hydrolase, putative	25	0.165	UP HIGH	Afu1g02150	glycerol 3-phosphate dehydrogenase (GfdA), putative	287	0.637	DOWN HIGH
	Afu8g06980	glycosyl hydrolase, putative	721	0.8	UP MOD	Afu8g02320	glycosyl transferase, group 2 family protein domain protein	487	0.68	DOWN HIGH
	Afu8g02070	glycosyl transferase, putative	955	0.462	UP MOD	Afu2g00680	glycosyl hydrolase, putative	977	0.78	DOWN MOD
	Afu6g12010	glycosyl hydrolase, family 3, putative	1329	0.655	UP LOW	Afu1g02140	glycogen debranching enzyme, putative	1877	0.697	DOWN LOW
	Afu3g03620	glycosyl transferase, putative	1954	0.765	UP LOW	Afu8g00640	glycosyl transferase, putative	1882	0.876	DOWN LOW
Transposition associated genes	Afu1g10020	reverse transcriptase, RNaseH	58	0.471	UP HIGH	Afu3g09410	reverse transcriptase	3	0.13	DOWN HIGH
	Afu1g00940	Tc1-mariner class transposase, putative	636	0.704	UP HIGH	Afu7g07170	reverse transcriptase/protease/endonuclease Pol, putative	65	0.38	DOWN HIGH
	Afu5g13900	transposase	868	0.346	UP MOD	Afu8g00330	endonuclease/reverse transcriptase/RNaseH, putative	504	0.698	DOWN HIGH
	Afu3g10430	transposase	874	0.131	UP MOD	Afu5g00270	LINE-1 class reverse transcriptase, RNaseH, putative	525	0.68	DOWN HIGH
	Afu6g09940	transposase	902	0.456	UP MOD	Afu1g00960	LINE-1 class reverse transcriptase, RNaseH, putative	920	0.698	DOWN MOD
	Afu1g08780	transposase	1188	0.304	UP MOD	Afu6g14660	reverse transcriptase, RNaseH	944	0.661	DOWN MOD
	Afu3g01740	transposase	1221	0.527	UP MOD	Afu3g09440	reverse transcriptase, RNaseH, putative	997	0.737	DOWN MOD
	Afu3g03090	transposase	1289	0.68	UP MOD	Afu7g08210	reverse transcriptase, putative	1117	0.724	DOWN MOD
	Afu6g03650	possible transposase	1620	0.607	UP LOW	Afu7g06930	reverse transcriptase, RNaseH	1185	0.782	DOWN MOD
	Afu7g08410	Tc1-mariner transposase, putative	1644	0.826	UP LOW	Afu8g06290	LINE-1 class reverse transcriptase, RNaseH, putative	1587	0.721	DOWN LOW
	Afu7g02580	transposase	1679	0.782	UP LOW	Afu8g00310	LINE-1 class reverse transcriptase, RNaseH, putative	1813	0.776	DOWN LOW

	Afu6g10870	transposase	1684	0.529	UP LOW		Afu3g15370	LINE-1 class reverse transcriptase, RNaseH, putative	1814	0.74	DOWN LOW
	Afu2g01420	transposase	1824	0.883	UP LOW		Afu3g11670	DDE superfamily endonuclease/transposase, pseudogene	1842	0.939	DOWN LOW
	Afu2g04990	transposase	1942	0.629	UP LOW		Afu6g00780	LINE-1 class reverse transcriptase, RNaseH, putative	1888	0.792	DOWN LOW
	Afu5g08340	transposase	1950	0.678	UP LOW						
Transcription factors	Afu4g10340	C6 finger domain protein, putative	43	0.117	UP HIGH		Afu2g05360	C6 transcription factor, putative	22	0.469	DOWN HIGH
	Afu5g14230	C6 transcription factor, putative	87	0.389	UP HIGH		Afu5g01460	C6 finger domain protein, putative	50	0.346	DOWN HIGH
	Afu5g00290	C6 transcription factor, putative	100	0.307	UP HIGH		Afu6g11250	C2H2 finger domain protein, putative	89	0.55	DOWN HIGH
	Afu1g13050	C2H2 transcription factor, putative	115	0.549	UP HIGH		Afu5g09890	C6 finger domain protein, putative	150	0.308	DOWN HIGH
	Afu8g04180	C2H2 zinc finger protein	129	0.644	UP HIGH		Afu5g09740	C6 transcription factor, putative	363	0.579	DOWN HIGH
	Afu6g14350	C6 transcription factor, putative	181	0.291	UP HIGH		Afu6g07010	C6 transcription factor, putative	413	0.807	DOWN HIGH
	Afu6g03010	C2H2 finger domain protein (Zms1), putative	189	0.68	UP HIGH		Afu5g02270	C6 transcription factor, putative	443	0.279	DOWN HIGH
	Afu6g09350	C6 finger domain protein, putative	213	0.074	UP HIGH		Afu8g01990	C6 transcription factor, putative	452	0.576	DOWN HIGH
	Afu7g00410	C6 transcription factor, putative	251	0.331	UP HIGH		Afu4g11850	C6 finger domain protein, putative	523	0.527	DOWN HIGH
	Afu1g03860	C6 transcription factor (AmdR), putative	774	0.695	UP MOD		Afu5g12020	C6 transcription factor (NirA), putative	1113	0.611	DOWN MOD
	Afu1g14280	C6 finger domain protein, putative	792	0.486	UP MOD		Afu1g02010	C2H2 finger domain protein, putative	1159	0.611	DOWN MOD
	Afu3g12780	C6 transcription factor, putative	804	0.484	UP MOD		Afu8g01240	C6 transcription factor, putative	1171	0.479	DOWN MOD
	Afu1g13510	C6 transcription factor (FacB), putative	819	0.588	UP MOD		Afu4g09710	C6 sexual development transcription factor Pro1	1172	0.717	DOWN MOD
	Afu3g09820	C2H2 transcription factor, putative	1370	0.765	UP LOW		Afu8g07180	C6 transcription factor, putative	1244	0.783	DOWN LOW
	Afu2g04150	C6 transcription factor, putative	1372	0.711	UP LOW		Afu7g05080	C6 transcription factor, putative	1277	0.874	DOWN LOW
	Afu2g04250	C6 finger domain protein, putative	1401	0.597	UP LOW		Afu1g16830	C6 transcription factor, putative	1296	0.74	DOWN LOW
	Afu1g13750	C2H2 transcription factor (Rpn4), putative	1403	0.597	UP LOW		Afu6g11110	C6 zinc cluster transcription factor, putative	1361	0.857	DOWN LOW

Commonalities among gene cohorts increasing and decreasing between 4 and 14 hours are observed in the Δ*laeA* and Af293 transcriptomes (Table 3.7 and 3.31). Genes required for the acquisition of iron increased in transcript abundance between time-points, including siderochrome transporters MirB, MirC and Sit1 (Afu3g03640, Afu2g05730, Afu7g06060) a ferric-chelate reductase (Afu6g13750) and a low affinity iron transporter (Afu4g14640). Genes required for the uptake and transport of copper (Afu2g03730, Afu1g16130, Afu4g12620), zinc (Afu4g09560, Afu1g01550, Afu6g00470), potassium (Afu1g14250, Afu8g01480, Afu5g02290) and calcium (Afu3g10690, Afu3g02740, Afu3g09550, Afu7g01030) also increased between the time-points.
Induction of genes directing cellular differentiation (n = 20), ergosterol biosynthesis (n = 10) and cell wall biogenesis (n = 22) was observed (Table 3.31). In accordance with wild-type environmental sensing and signal transduction, increase in expression of two MAPKKK (Afu1g10940, Afu5g06420), two MAPKK (Afu1g05800, Afu1g15950) a MAPK (Afu5g09100), three GTPase activating proteins (Afu2g06080, Afu3g12870, Afu6g04000) and multiple serine/thronine kinases was observed.

In agreement with the general suppression of protein biosynthesis and ribosome biogenesis observed in Af293, 13 ribosomal proteins decreased in expression over the time-course, whereas only 2 increased. These data suggest iron acquisition, ion transport, cellular development, environmental sensing and the metabolic state of the cells are comparable between Δ*laeA* and Af293 isolates. 16 secreted proteases were upregulated during infection (Table 3.31) with the notable omission of the alkaline serine protease Alp1, which was highly upregulated in Af293 (Table 7). In addition, genes directing the biosynthesis of 11 putative antigenic proteins were upregulated, including Asp F2, F4, F7 and F10. This was somewhat less than that observed in Af293 (n = 15) for which expression of Asp F3 and Asp F9 increased. As observed for the Af293 isolate, genes involved in gliotoxin biosynthesis were highly upregulated between the time-points studied (Table 3.31).

3.5.3 Characterisation of differentially expressed genes between 4 and 14 hours: chromosomal loci, lineage specificity and functionality

Distribution of genes demonstrating increased or decreased transcript abundance between 4 and 14 hours in Δ*laeA* were investigated with respect to subtelomeric loci, *A. fumigatus* specific genes, signal peptide encoding genes, and secondary metabolite clusters during infection relative to laboratory growth (McDonagh et al. 2008). Statistical significance of enrichment was measured by Chi-square analyses, with the null hypothesis that equal numbers of increased and decreased genes occur in each cohort (Figure 3.18 and Table 3.32). Transposition associated genes were also investigated with respect to their distribution in increasing and decreasing datasets.

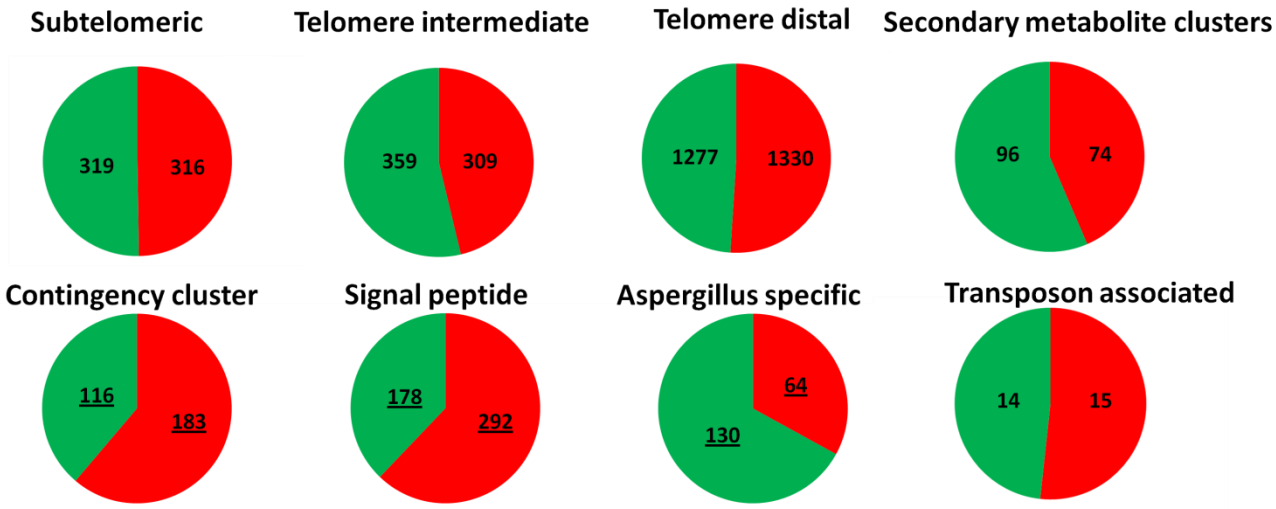


Figure 3.18: Distribution of differentially expressed genes between 4 – 14 hours post infection among the functional cohorts of chromosomal location, signal peptide content, *A. fumigatus* specificity and functional association. Distribution of increased (red) and decreased (green) genes at subtelomeric loci (0 – 300 Kb from telomere, n =1509); telomere intermediate loci (301 - 600 Kb from telomere, n = 1634); telomere distal loci (> 600 Kb from telomere, n =6494). Secondary metabolite clusters (n = 337); Contingency clusters (n = 594); signal peptide cohort (n = 1103); *A. fumigatus* specific genes (n = 596) and; transposon associated genes (n = 68). Underlined values significantly deviate from the null hypothesis that an equal number of upregulated or downregulated genes will occur in each cohort, as tested by Chi-square analysis.

	Number of genes	Differentially expressed	Up (observed)	Down (observed)	Up (expected)	Down (expected)	Chi-square	p-value
0-300 kb	1509	635	316	319	317.5	317.5	0.01	0.9052
301- 600 kb	1634	668	309	359	334	334	3.74	0.053
>600 kb	6373	2607	1330	1277	1303.5	1303.5	1.07	0.2993
Secondary metabolism	337	170	74	96	85	85	2.84	0.0915
Infection cluster	594	299	183	116	149.5	149.5	15.01	< 0.0001
Signal P	1103	470	292	178	235	235	7.86	< 0.0001
Aspergillus specific	596	194	64	130	97	97	22.45	< 0.0001
Transposition associated	68	29	15	14	14.5	14.5	0.034	0.8527

Table 3.32: Distribution and Chi-square analysis of dfferentially expressed genes categorised by chromosomal location, signal peptide content, *A. fumigatus* specificity and functional association among 4 – 14 hour dataset. Chi-square analysis with one degree of freedom was used to test the distribution of upper and lower quartiles with respect to cohorts of interest to this study, with the null hypothesis that even numbers of upregulated or downregulated genes occur in each group.

Similar preferential empolyment of contingency cluster loci and signal peptide cohorts was observed in the Δ*laeA* and Af293 strains (Figure 3.18). However, enrichment of upregulated genes at secondary metabolite clusters and subtelomeric loci was not observed in Δ*laeA* between 4 and 14 hours post infection. Additionally, *A. fumigatus* specific gene sets significantly increased and decreased for Af293 and Δ*laeA* isolates respectively. A total of 96 secondary metabolite genes were decreased during infection, which was approaching significantly more than those which increased (n = 74, p = 0.09, Figure 3.18 and Tabl 3.32). These included four four nonribosomal peptide synthases (Afu3g12920, Afu3g03350, Afu4g14440, Afu8g00170) and three polyketide synthases (Afu3g02530, Afu8g00490, Afu2g17600).

3.5.4 Time-point specific gene expression profiling of the Δ*laeA* isolate in the murine lung

To determine gene expression profiles specific to each time-point of infection in the Δ*laeA* isolate, transcription was compared between 4 – 8 and 8 – 14 hours post infection (Figure 3.19). Gene ontology analyses did not report significant enrichment of any functional categories with a corrected p-value ≤ 0.2 (data not shown). The 100 genes having the greatest increase or decrease between 4 and 8 hours are reported in Tables 3.33 and 3.35. The 100 genes having the greatest increase or decrease between 8 and 14 hours are reported in Tables 3.34 and 3.36.

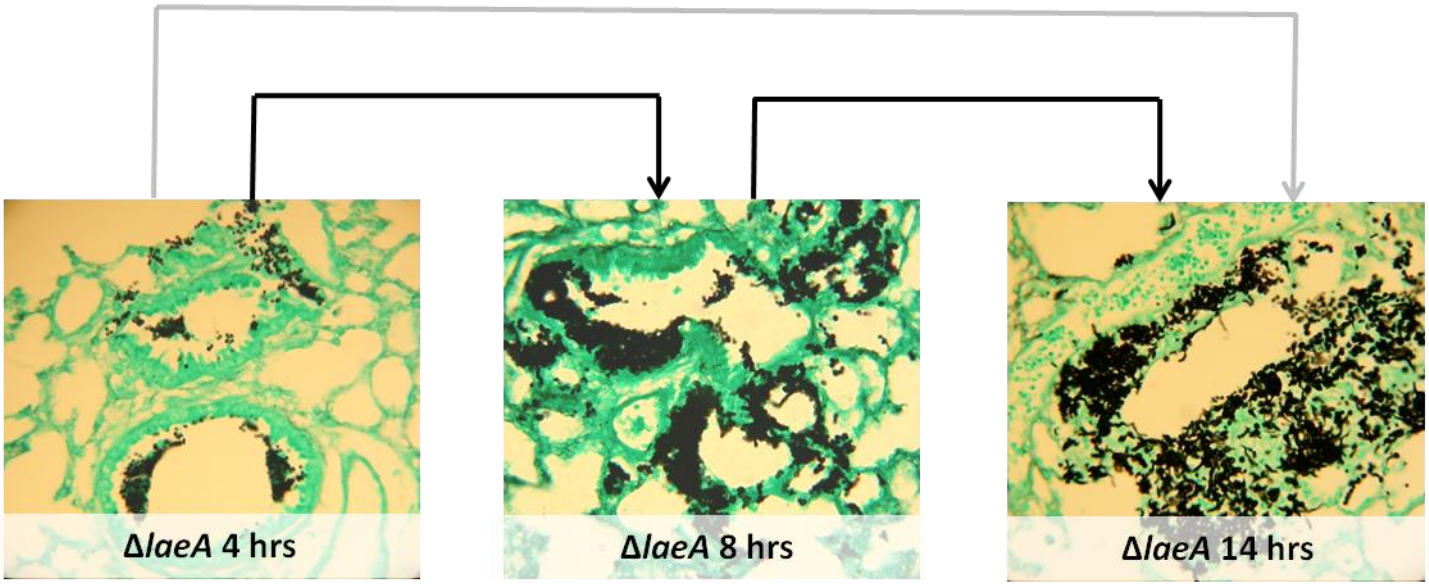


Figure 3.19: Schematic depicting time-point specific transcriptional comparisons. Black arrows depict strain specific comparisons conducted between 4 and 8, and 8 and 14 hours post infection. Faint grey arrow depicts analysis discussed in the previous section.

Table 3.33: Top 100 genes with greatest nSI increase between 4 and 8 hours post infection in Δ*laeA*. Genes are reported ranked according to greatest nSI intensity increase between 4 and 8 hours. Position of the gene in the 8 – 14 hours increasing dataset is also shown. **A one-way ANOVA was conducted on nSI values between** time-point**s, with the null hypothesis that nSI values do not change between** time-point**s. FDR correct *p*-values from this analysis are reported for each gene . Genes highlighted in red increased uniquely between 4 and 8 hours**

ORF	Description	Rank 4 – 8 hours	Rank 8 – 14 hours	p-value 4 - 8 hours	p-value 8 - 14 hours
Afu2g12680	conserved hypothetical protein	1	6041	0.012	0.887
Afu8g00610	cell surface protein Mas1, putative	2	5458	0.002	0.849
Afu5g01620	extracellular proline-rich protein	3	4847	0.015	0.894
Afu2g14540	endoglucanase, putative	4	417	0.004	0.652
Afu2g13270	alcohol dehydrogenase, putative	5	2756	0.009	0.983
Afu7g00990	integral membrane protein	6	7609	0.238	0.813
Afu3g08110	cell wall protein, putative	7	2884	0.012	0.975
Afu6g09730	cytochrome P450 oxidoreductase GliF	8	6	0.035	0.059
Afu2g14420	cutinase, putative	9	581	0.009	0.594
Afu3g00520	SIR2 family histone deacetylase, putative	10	7734	0.015	0.507
Afu2g17610	sulfatase domain protein	11	7773	0.011	0.529
Afu3g01500	integral membrane protein	12	4869	0.009	0.914
Afu6g00430	IgE-binding protein	13	7676	0.007	0.057
Afu3g13110	extracellular serine-threonine rich protein	14	2261	0.022	0.85
Afu8g06830	endoglucanase, putative	15	249	0.026	0.534
Afu5g14240	ThiJ/PfpI family protein	16	6134	0.474	0.906
Afu6g12880	hypothetical protein	17	6196	0.606	0.828
Afu6g00680	hypothetical protein	18	5916	0.019	0.837
Afu8g05910	pectate lyase, putative	19	706	0.071	0.843
Afu2g15950	aspartic endopeptidase, putative	20	1551	0.167	0.917
Afu5g03010	conserved hypothetical protein	21	420	0.298	0.713
Afu2g10130	phase-specific adhesin, putative	22	140	0.411	0.507
Afu6g09690	glutathione S-transferase GliG	23	4	0.089	0.002
Afu2g14490	endoglucanase, putative	24	425	0.176	0.258
Afu1g10020	reverse transcriptase, RNaseH	25	2706	0.535	0.986
Afu2g17320	conserved hypothetical protein	26	3130	0.23	0.982
Afu6g09740	thioredoxin reductase GliT	27	34	0.005	0.2
Afu6g12250	succinyl-CoA:3-ketoacid-coenzyme A transferase (ScoT), putative	28	5794	0.53	0.894
Afu6g09670	cytochrome P450 oxidoreductase GliC	29	3	0.272	0.069
Afu3g00690	C6 transcription factor, putative	30	7508	0.673	0.882
Afu4g09840	kynureninase	31	1927	0.261	0.851
Afu5g02320	hypothetical protein	32	4016	0.576	0.99
Afu5g14420	hypothetical protein	33	169	0.013	0.639
Afu2g00580	hypothetical protein	34	7754	0.094	0.385
Afu4g14180	hypothetical protein	35	4338	0.309	0.983
Afu1g05920	hypothetical protein	36	5433	0.3	0.91

Afu4g00390	glycosyl hydrolase, putative	37	276	0.089	0.797
Afu2g00720	aldehyde dehydrogenase, putative	38	5093	0.395	0.88
Afu1g01540	Endonuclease/Exonuclease/phosphatase family family	39	803	0.119	0.883
Afu6g12420	SprT family metallopeptidase, putative	40	3366	0.015	0.995
Afu6g00690	conserved hypothetical protein	41	6579	0.238	0.879
Afu4g11320	hypothetical protein	42	3515	0.252	0.998
Afu4g01290	endo-chitosanase, pseudogene	43	2446	0.568	0.96
Afu3g02550	conserved hypothetical protein	44	7715	0.003	0.222
Afu3g00320	endo-1,4-beta-xylanase (XlnA), putative	45	4893	0.643	0.983
Afu7g06810	L-amino acid oxidase LaoA, putative	46	965	0.172	0.567
Afu5g13650	hypothetical protein	47	7050	0	0.781
Afu2g04260	transcription factor, putative	48	4221	0.222	0.974
Afu3g03950	endoglucanase, putative	49	81	0.391	0.559
Afu4g13750	Deuterolysin metalloprotease, putative	50	6513	0.291	0.887
Afu5g01990	BYS1 domain protein, putative	51	2148	0.158	0.922
Afu5g09290	NAD-dependent 15-hydroxyprostaglandin dehydrogenase	52	5658	0.527	0.913
Afu8g05680	serine/threonine protein kinase, putative	53	1450	0.015	0.804
Afu2g08770	RING finger domain protein, putative	54	3234	0.472	0.991
Afu5g08830	HEX1	55	2821	0.223	0.975
Afu6g00290	aminotransferase, putative	56	686	0.181	0.85
Afu5g08640	hypothetical protein	57	7809	0.717	0.704
Afu6g00770	extracellular arabinanase, putative	58	6953	0.079	0.85
Afu2g17650	DUF907 domain protein	59	444	0.045	0.377
Afu4g13760	hypothetical protein	60	7468	0.114	0.807
Afu2g09450	carboxylic acid transport protein	61	20	0.167	0.258
Afu4g09830	indoleamine 2,3-dioxygenase pyrrole 2,3-dioxygenase)	62	104	0.088	0.277
Afu4g10340	C6 finger domain protein, putative	63	439	0.494	0.724
Afu6g09650	membrane dipeptidase GliJ	64	8	0.172	0.128
Afu3g12250	protein-tyrosine phosphatase, putative	65	3449	0.218	0.999
Afu5g07530	hypothetical protein	66	1437	0.2	0.832
Afu1g17380	3-oxoacyl-(acyl-carrier-protein) reductase, putative	67	2302	0.551	0.881
Afu6g13750	ferric-chelate reductase, putative	68	878	0.182	0.883
Afu2g11900	pyruvate dehydrogenase kinase	69	5848	0.114	0.877
Afu1g14730	cell division cycle protein 20 (CDC20), putative	70	6184	0.103	0.884
Afu3g00810	cholestenol delta-isomerase, putative	71	7711	0.118	0.427
Afu5g09070	hypothetical protein	72	6711	0.1	0.782
Afu8g01260	hypothetical protein	73	7811	0.431	0.457
Afu1g11250	amidohydrolase, putative	74	6637	0.751	0.713
Afu7g04970	metalloreductase, putative	75	3284	0.528	0.991
Afu2g09500	universal stress protein family domain protein	76	2850	0.345	0.986
Afu3g03670	ABC multidrug transporter, putative	77	36	0.454	0.639
Afu3g14980	extracellular chitosanase CsnC, putative	78	207	0.249	0.682
Afu3g02270	mycelial catalase Cat1	79	2934	0.114	0.967

Afu5g14660	GABA permease, putative	80	2070	0.148	0.887
Afu7g00200	conserved hypothetical protein	81	7458	0.74	0.88
Afu2g01720	conserved hypothetical protein	82	2061	0.049	0.887
Afu2g14280	kinesin family protein (KlpA), putative	83	6294	0.238	0.258
Afu1g02270	ars binding protein 2	84	4972	0.261	0.875
Afu8g06880	pectin methylesterase, putative	85	3775	0.273	0.99
Afu4g08730	conserved hypothetical protein	86	7742	0.321	0.507
Afu5g12270	rRNA processing protein (Ebp2), putative	87	6568	0.706	0.852
Afu2g11770	hypothetical protein	88	4539	0.026	0.892
Afu4g08830	telomere length regulator protein (Rif1), putative	89	2672	0.572	0.974
Afu5g07610		90	5332	0.252	0.951
Afu3g10820	metalloreductase, putative	91	1342	0.158	0.894
Afu2g00500	conserved hypothetical protein	92	437	0.538	0.764
Afu4g09310	hypothetical protein	93	7756	0.22	0.438
Afu2g10540	hypothetical protein	94	6928	0.743	0.894
Afu1g02760	cell cycle inhibitor Nif1, putative	95	5164	0.291	0.951
Afu2g11220	proline permease, putative	96	133	0.706	0.497
Afu5g04080	oxidosqualene:lanosterol cyclase	97	3487	0.623	0.999
Afu2g00570	GNAT family acetyltransferase, putative	98	7286	0.658	0.883
Afu2g09070	DUF221 domain protein, putative	99	3365	0.716	0.995
Afu7g00580	conserved hypothetical protein	100	1964	0.127	0.85

Table 3.34: Top 100 genes with greatest nSI decrease between 4 and 8 hours post infection in Δ*laeA*. Genes are reported ranked according to greatest nSI intensity decrease between 4 and 8 hours. Position of the gene in the 8 – 14 hours increasing dataset is also shown. A FDR correct *p*-values from this analysis are reported for each gene. Genes highlighted in green decreased uniquely between 4 and 8 hours

ORF	Description	Rank 4 – 8 hours	Rank 8 – 14 hours	p-value 4 - 8 hours	p-value 8 - 14 hours
Afu5g06930	hypothetical protein	1	4852	0.398	0.986
Afu2g00550	conserved hypothetical protein	2	7809	0.642	0.554
Afu1g01290	cytochrome P450 monooxygenase, putative	3	6251	0.089	0.704
Afu6g04750	conserved hypothetical protein	4	3663	0.706	0.990
Afu1g17050	hypothetical protein	5	7505	0.528	0.880
Afu3g03930	cytochrome P450, putative	6	7024	0.512	0.883
Afu5g07910	hypothetical protein	7	7343	0.641	0.718
Afu1g17320	endo-arabinanase, putative	8	5739	0.550	0.896
Afu4g13930	CRAL/TRIO domain protein	9	7180	0.746	0.905
Afu3g12930	dimethylallyl tryptophan synthase (GliD), putative	10	2911	0.015	0.920
Afu2g00710	alpha-amylase, putative	11	6918	0.443	0.510

Afu7g07000	fumarylacetoacetate hydrolase family protein	12	7557	0.631	0.718
Afu3g09410	reverse transcriptase	13	878	0.346	0.810
Afu4g00740	hypothetical protein	14	6424	0.405	0.764
Afu3g02800	lipase/esterase, putative	15	6595	0.638	0.920
Afu4g00220	metallo-beta-lactamase domain protein	16	6806	0.612	0.852
Afu3g06510	hypothetical protein	17	7411	0.648	0.872
Afu4g14130	ABC multidrug transporter, putative	18	6013	0.609	0.868
Afu4g08890	aldo-keto reductase family protein, putative	19	6081	0.045	0.899
Afu6g07660	hypothetical protein	20	5864	0.572	0.907
Afu7g06740	endoglucanase, putative	21	6458	0.572	0.850
Afu3g00550	hypothetical protein	22	6986	0.454	0.856
Afu1g15190	hypothetical protein	23	7662	0.264	0.694
Afu7g01120		24	1704	0.607	0.883
Afu5g09090	ATP binding protein, putative	25	7459	0.536	0.764
Afu3g13650	integral membrane protein	26	5643	0.638	0.915
Afu6g10950		27	841	0.648	0.913
Afu5g01470	peroxisomal copper amine oxidase	28	6643	0.754	0.907
Afu7g04620	hypothetical protein	29	6946	0.347	0.736
Afu4g14440	nonribosomal peptide synthase, putative	30	6038	0.612	0.900
Afu1g11230	HMG-CoA reductase	31	5343	0.659	0.915
Afu5g13230	MFS monocarboxylic acid transporter, putative	32	5998	0.638	0.894
Afu8g01980	hypothetical protein	33	7751	0.676	0.704
Afu2g17920	hypothetical protein	34	6499	0.757	0.898
Afu4g06880	conserved hypothetical protein	35	6747	0.678	0.885
Afu5g01210	amine oxidase, flavin-containing superfamily	36	7553	0.538	0.563
Afu3g10990		37	6893	0.675	0.796
Afu2g17660	C4-dicarboxylate transporter/malic acid transport protein, putative	38	6006	0.534	0.863
Afu7g06950	oxidoreductase, putative	39	599	0.637	0.673
Afu1g11320	class II DAHP synthetase family protein	40	7355	0.580	0.639
Afu3g02790	amidohydrolase family protein, putative	41	6093	0.675	0.887
Afu1g03190	hypothetical protein	42	7379	0.584	0.752
Afu8g01650	hypothetical protein	43	7810	0.648	0.192
Afu2g17530	conidial pigment biosynthesis oxidase Arb2/brown2	44	7565	0.561	0.600
Afu1g10990	ribosomal RNA processing protein, putative	45	345	0.673	0.718
Afu7g01700	hypothetical protein	46	6417	0.501	0.887
Afu5g00370	amino acid permease, putative	47	7227	0.553	0.883
Afu8g01230	conserved transmembrane protein	48	7276	0.528	0.774
Afu3g02930	extracellular soluble lytic transglycosylase, putative	49	5344	0.291	0.966
Afu6g11690		50	7532	0.522	0.756
Afu7g08260	hypothetical protein	51	6203	0.235	0.881
Afu6g14540	endo-1,3(4)-beta-glucanase, putative	52	7338	0.502	0.732

Afu3g06160	hypothetical protein	53	7264	0.794	0.903
Afu2g12830	UDP-glucoronosyl and UDP-glucosyl transferase family	54	7559	0.502	0.609
Afu8g07250	pectin methylesterase family protein	55	7488	0.705	0.798
Afu4g08390	hypothetical protein	56	7139	0.311	0.828
Afu1g02260	hypothetical protein	57	7125	0.659	0.856
Afu3g01870	hypothetical protein	58	7006	0.630	0.751
Afu2g00850	conserved hypothetical protein	59	7259	0.675	0.732
Afu1g10160	conserved hypothetical protein	60	7612	0.638	0.744
Afu6g11630	FAD-dependent isoamyl alcohol oxidase, putative	61	5649	0.623	0.907
Afu7g01500	hypothetical protein	62	7772	0.460	0.424
Afu1g16870	hypothetical protein	63	7686	0.705	0.406
Afu3g02840	isopropanol dehydrogenase, putative	64	2381	0.638	0.914
Afu4g14530	glutathione S-transferase, putative	65	2775	0.667	0.856
Afu3g10870	hypothetical protein	66	5341	0.530	0.958
Afu8g02400	geranylgeranyl pyrophosphate synthetase, putative	67	7601	0.648	0.559
Afu7g00830	alpha/beta hydrolase, putative	68	3425	0.638	0.945
Afu8g00550	SirN-like methyltransferase, putative	69	5214	0.577	0.951
Afu2g13660	hypothetical protein	70	6838	0.612	0.824
Afu4g14770	squalene-hopene-cyclase, putative	71	281	0.652	0.741
Afu3g01930	conserved hypothetical protein	72	2318	0.553	0.922
Afu4g01420	hypothetical protein	73	6587	0.754	0.914
Afu1g16420	GPI anchored protein, putative	74	1568	0.291	0.752
Afu3g03690	hypothetical protein	75	3722	0.494	0.978
Afu6g00170	hypothetical protein	76	7710	0.734	0.577
Afu4g06470		77	6298	0.710	0.875
Afu2g03940	hypothetical protein	78	7815	0.727	0.497
Afu3g03290	hypothetical protein	79	3191	0.311	0.949
Afu3g15120	hypothetical protein	80	7130	0.781	0.881
Afu4g09270	ankyrin repeat protein	81	7560	0.794	0.764
Afu4g01120	hypothetical protein	82	6926	0.794	0.878
Afu5g14740	fucose-specific lectin	83	7367	0.195	0.851
Afu7g06250	DSBA-like thioredoxin domain protein	84	2993	0.553	0.915
Afu8g01460	hypothetical protein	85	7525	0.794	0.883
Afu1g01780	alcohol dehydrogenase, putative	86	7596	0.521	0.350
Afu8g00920	UDP-glucose dehydrogenase Uxs2p	87	3447	0.608	0.914
Afu4g13900	MFS transporter, putative	88	588	0.584	0.732
Afu2g12270		89	6898	0.579	0.856
Afu2g17410	hypothetical protein	90	7776	0.811	0.722
Afu5g00120	cytochrome P450 oxidoreductase/alkane hydroxylase, putative	91	3901	0.748	0.986
Afu7g07170	reverse transcriptase/protease/endonuclease Pol, putative	92	2461	0.537	0.951
Afu2g05380	C6 transcription factor, putative	93	6981	0.360	0.732

Afu1g05010	MFS transporter, putative	94	3566	0.675	0.947
Afu1g00800	hypothetical protein	95	7577	0.764	0.813
Afu4g00560	NAD binding Rossmann fold oxidoreductase, putative	96	6606	0.591	0.856
Afu6g02330	hypothetical protein	97	6525	0.523	0.881
Afu3g02530	polyketide synthase, putative	98	6742	0.797	0.866
Afu3g13370	ubiquitin-like protein (HubA), putative	99	2087	0.751	0.924
Afu3g03030	catechol dioxygenase, putative	100	7416	0.670	0.835

Table 3.35: Top 100 genes with greatest nSI increase between 8 and 14 hours post infection in Δ*laeA*. Genes are reported ranked according to greatest nSI increase between 8 and 14 hours. Position of each gene in the 4 – 8 hour increasing dataset is also shown. A one-way ANOVA was conducted on nSI values between time-points, with the null hypothesis that nSI values do not change between time-points. FDR correct *p*-values from this analysis are reported for each gene . Genes highlighted in red increased uniquely between 8 and 14 hours

ORF	Description	Rank 4 – 8 hours	Rank 8 – 14 hours	p-value 4 - 8 hours	p-value 8 - 14 hours
Afu8g01480	potassium channel, putative	4978	1	0.986	0.004
Afu6g09680	O-methyltransferase GliM	441	2	0.762	0.013
Afu6g09670	cytochrome P450 oxidoreductase GliC	29	3	0.272	0.069
Afu6g09690	glutathione S-transferase GliG	23	4	0.089	0.002
Afu2g03940	hypothetical protein	7742	5	0.727	0.497
Afu6g09730	cytochrome P450 oxidoreductase GliF	8	6	0.035	0.059
Afu7g04930	alkaline serine protease (PR1), putative	1942	7	0.936	0.539
Afu6g09650	membrane dipeptidase GliJ	64	8	0.172	0.128
Afu7g06790	putative allantoate permease of the major facilitator superfamily	125	9	0.193	0.155
Afu8g01650	hypothetical protein	7777	10	0.648	0.192
Afu2g00550	conserved hypothetical protein	7818	11	0.642	0.554
Afu2g13370	55 kDa type II phosphatidylinositol 4-kinase	7327	12	0.797	0.385
Afu3g01180	sarcosine oxidase, putative	7554	13	0.794	0.176
Afu6g09640	aminotransferase GliI	350	14	0.496	0.060
Afu3g00620	zinc-containing alcohol dehydrogenase, putative	1063	15	0.795	0.042
Afu6g03410		4297	16	0.992	0.122
Afu4g08440	Patatin-like serine hydrolase, putative	2391	17	0.957	0.521
Afu1g09260	acetyltransferase, GNAT family family	2938	18	0.855	0.220
Afu5g01340	lysophospholipase, putative	6250	19	0.864	0.011
Afu2g09450	carboxylic acid transport protein	61	20	0.167	0.258
Afu5g00550	endoglycoceramidase, putative	7431	21	0.794	0.500
Afu3g02090	beta-xylosidase	1181	22	0.768	0.137
Afu4g01100	hypothetical protein	7637	23	0.764	0.732
Afu1g06470	neutral/alkaline nonlysosomal ceramidase, putative	1116	24	0.797	0.547

Afu8g06470	N,N-dimethylglycine oxidase	4172	25	0.981	0.198
Afu5g14810	pyruvate decarboxylase, putative	1909	26	0.845	0.128
Afu6g00350	hypothetical protein	7287	27	0.803	0.741
Afu8g01310	metalloreductase, putative	6836	28	0.794	0.688
Afu4g01480	MSF transporter, putative	4524	29	0.997	0.412
Afu5g14580	Pfs, NACHT and Ankyrin domain protein	7361	30	0.848	0.724
Afu2g14450	hypothetical protein	3255	31	0.944	0.556
Afu4g12410	HMG box protein, putative	7672	32	0.496	0.033
Afu1g00290	hypothetical protein	6935	33	0.754	0.688
Afu6g09740	thioredoxin reductase GliT	27	34	0.005	0.200
Afu2g05120	hypothetical protein	5113	35	0.978	0.258
Afu3g03670	ABC multidrug transporter, putative	77	36	0.454	0.639
Afu3g01230	sugar transporter-like protein	314	37	0.638	0.377
Afu3g14170	high-affinity hexose transporter	419	38	0.623	0.724
Afu6g09450	NB-ARC domain protein	5576	39	0.936	0.520
Afu2g13030	phenylalanyl-tRNA synthetase alpha subunit (PodG), putative	1795	40	0.920	0.684
Afu8g06450	Rieske 2Fe-2S family protein, putative	244	41	0.176	0.385
Afu8g01210	enoyl-CoA hydratase/isomerase family protein	6485	42	0.800	0.087
Afu8g01350	hypothetical protein	7408	43	0.710	0.611
Afu2g17410	hypothetical protein	7730	44	0.811	0.722
Afu6g09710	MFS gliotoxin efflux pump GliA	1822	45	0.854	0.539
Afu2g05330	vacuolar H+\Ca2+ exchanger	6329	46	0.840	0.438
Afu5g09440	amino acid permease, putative	232	47	0.675	0.080
Afu7g01500	hypothetical protein	7758	48	0.460	0.424
Afu6g06620	YIP3-like protein	316	49	0.754	0.457
Afu5g14320	hypothetical protein	6646	50	0.867	0.285
Afu1g07050	armadillo repeat protein	3310	51	0.950	0.688
Afu1g14370	hypothetical protein	5865	52	0.917	0.507
Afu5g11170	nucleosome remodeling complex ATPase subunit (Snf2h), putative	5799	53	0.925	0.563
Afu5g01270	C6 transcription factor, putative	6686	54	0.914	0.732
Afu3g03480	cytochrome P450 monooxygenase, putative	6156	55	0.887	0.218
Afu6g03010	C2H2 finger domain protein (Zms1), putative	3971	56	0.976	0.738
Afu1g06920	serine/threonine protein kinase, putative	6230	57	0.876	0.519
Afu3g07410	isoamyl alcohol oxidase	291	58	0.550	0.507
Afu1g11750		7005	59	0.535	0.133
Afu1g11140	Sterol desaturase family	1592	60	0.809	0.639
Afu6g10800	carboxylesterase, putative	6269	61	0.901	0.629
Afu5g02670	ThiJ/PfpI family protein	1478	62	0.920	0.646
Afu1g12410	salicylate hydroxylase	2440	63	0.874	0.006
Afu1g13460	conserved hypothetical protein	6332	64	0.932	0.732
Afu5g01090	UPF0075 domain protein	1715	65	0.771	0.220
Afu8g06980	glycosyl hydrolase, putative	6806	66	0.797	0.720
Afu3g06290	regulatory protein leu3, putative	1267	67	0.899	0.773
Afu2g14360	GPI anchored glucanase, putative	139	68	0.454	0.258

Afu8g01980	hypothetical protein	7787	69	0.676	0.704
Afu4g09480	extracellular endo-1,4-beta-xylanase, putative	3897	70	0.972	0.732
Afu7g00110	lipase, putative	5604	71	0.938	0.854
Afu5g12490	stress response protein rds1p	5289	72	0.927	0.290
Afu2g18050	FAD binding oxidoreductase, putative	6670	73	0.881	0.605
Afu5g10970		6293	74	0.934	0.772
Afu7g00410	C6 transcription factor, putative	4351	75	0.992	0.058
Afu4g13990	hypothetical protein	2586	76	0.870	0.369
Afu2g09890	conserved hypothetical protein	5632	77	0.856	0.462
Afu2g17380	hypothetical protein	6920	78	0.832	0.752
Afu5g13780	stress response protein (Rds1), putative	6221	79	0.898	0.397
Afu4g00680	aquaglyceroporin, putative	7550	80	0.638	0.664
Afu3g03950	endoglucanase, putative	49	81	0.391	0.559
Afu4g12030	hypothetical protein	1241	82	0.794	0.483
Afu3g13670	siderochrome-iron transporter, putative	258	83	0.673	0.639
Afu2g08240	C6 transcription factor, putative	7714	84	0.794	0.621
Afu2g17930	integral membrane protein	4526	85	0.999	0.704
Afu6g03150	hypothetical protein	5575	86	0.964	0.774
Afu5g02390	Auxin Efflux Carrier superfamily	6209	87	0.866	0.060
Afu5g14230	C6 transcription factor, putative	1032	88	0.780	0.710
Afu3g03580	Transferase family superfamily	292	89	0.773	0.258
Afu2g07920	cytochrome P450, putative	5981	90	0.887	0.412
Afu3g13640	extracellular serine-rich protein	121	91	0.638	0.639
Afu6g03420	trehalose synthase, putative	2061	92	0.873	0.385
Afu3g00600	hypothetical protein	2288	93	0.868	0.718
Afu1g12970	conserved hypothetical protein	5757	94	0.912	0.774
Afu3g01250	short-chain dehydrogenase/reductase family protein, putative	3156	95	0.957	0.695
Afu5g12940	arylsulfatase, putative	1416	96	0.797	0.277
Afu3g11910		1311	97	0.718	0.659
Afu1g02180	hypothetical protein	6030	98	0.859	0.387
Afu3g09010		7518	99	0.745	0.774
Afu7g08220	hypothetical protein	1635	100	0.844	0.377

Table 3.36: Top 100 genes with greatest nSI decrease between 8 and 14 hours post infection in Δ*laeA*. Genes are reported ranked according to greatest nSI decrease between 8 and 14 hours. Position of each gene in the 4 – 8 hour decreasing dataset is also shown. A one-way ANOVA was conducted on nSI values between time-points, with the null hypothesis that nSI values do not change between time-points. FDR correct *p*-values from this analysis are reported for each gene . Genes highlighted in red increased uniquely between 8 and 14 hours

ORF	Description	Rank 4 – 8 hours	Rank 8 – 14 hours	p-value 4 - 8 hours	p-value 8 - 14 hours
Afu8g01810	conserved hypothetical protein	4472	1	0.997	0.385
Afu1g04550	HMG box protein, putative	5678	2	0.956	0.521
Afu6g00390	aminotransferase, putative	186	3	0.597	0.197

Afu2g08210	conserved hypothetical protein	826	4	0.762	0.312
Afu1g10930	ammonium transporter	7475	5	0.813	0.2
Afu6g09310	class V chitinase, putative	293	6	0.675	0.486
Afu5g10290	fructose-bisphosphate aldolase, putative	6913	7	0.83	0.547
Afu5g01680	MFS transporter, putative	6659	8	0.822	0.424
Afu8g01260	hypothetical protein	73	9	0.431	0.457
Afu7g02210	conserved hypothetical protein	470	10	0.729	0.377
Afu5g08640	hypothetical protein	57	11	0.717	0.704
Afu3g08860	Transcriptional regulator ATRX related protein	3230	12	0.954	0.576
Afu8g06770	conserved hypothetical protein	1569	13	0.238	0.6
Afu3g14000	mlo2 protein	1378	14	0.813	0.107
Afu2g17600	polyketide synthetase PksP	7345	15	0.438	0.007
Afu7g00710	oxalate/formate antiporter, putative	1828	16	0.83	0.258
Afu1g16540	WD40 domain protein	7190	17	0.096	0.022
Afu4g06890	14-alpha sterol demethylase Cyp51A	270	18	0.616	0.198
Afu2g00290	hypothetical protein	3503	19	0.96	0.481
Afu1g16090	arsenate reductase (ArsC), putative	3476	20	0.95	0.41
Afu3g00430	high-affinity glucose transporter, putative	230	21	0.553	0.507
Afu3g00180	short chain dehydrogenase, putative	271	22	0.158	0.251
Afu3g14400	hypothetical protein	1237	23	0.494	0.42
Afu3g09920	hypothetical protein	6550	24	0.909	0.427
Afu3g07570	conserved hypothetical protein	383	25	0.717	0.639
Afu2g09150	adenosine deaminase	967	26	0.861	0.639
Afu4g07010	hydrolase, TatD family protein, putative	2951	27	0.914	0.369
Afu4g01570	neutral amino acid permease	5723	28	0.936	0.194
Afu5g12770	metallo-beta-lactamase family protein	104	29	0.472	0.123
Afu1g06350	virulence related protein (Cap20), putative	641	30	0.768	0.114
Afu4g11930	Formamidopyrimidine-DNA glycosylase, putative	761	31	0.828	0.175
Afu4g06610	hypothetical protein	1020	32	0.794	0.031
Afu3g12810	transcriptional corepressor of histone genes (Hir3), putative	2589	33	0.94	0.521
Afu2g17070	DUF298 domain protein	2614	34	0.851	0.268
Afu2g07820	MOSC domain protein	3097	35	0.757	0.507
Afu5g09150	oxidoreductase, short-chain dehydrogenase/reductase family	5413	36	0.944	0.639
Afu6g13850	GTPase activating protein (Evi5), putative	807	37	0.797	0.6
Afu6g06470	heat shock protein HSP30, putative	153	38	0.308	0.813
Afu3g10370	conserved hypothetical protein	680	39	0.839	0.639
Afu1g12270	hypothetical protein	6476	40	0.864	0.715
Afu2g01850	phytanoyl-CoA dioxygenase family protein	855	41	0.844	0.734
Afu2g09300	hypothetical protein	6121	42	0.955	0.813
Afu2g16350	thioesterase family protein	2286	43	0.813	0.621
Afu6g01990	conserved hypothetical protein	3831	44	0.96	0.417
Afu1g03260	tartrate MFS transporter, putative	207	45	0.771	0.781

Afu4g14780	cytochrome P450 monooxygenase, putative	5910	46	0.971	0.868
Afu2g17610	sulfatase domain protein	11	47	0.011	0.529
Afu5g10650	pyridoxamine phosphate oxidase, putative	4511	48	0.993	0.639
Afu3g03660	esterase superfamily protein	751	49	0.824	0.258
Afu3g01300	hypothetical protein	1064	50	0.748	0.507
Afu8g02010	MFS sugar transporter, putative	3736	51	0.936	0.296
Afu7g08360	hypothetical protein	2980	52	0.866	0.128
Afu2g14910	alpha-1,6-mannosyltransferase subunit, putative	479	53	0.773	0.449
Afu5g08310	RNA and export factor binding protein 2-I	941	54	0.748	0.639
Afu5g01370	conserved hypothetical protein	2062	55	0.887	0.513
Afu2g12250	DNA replication factor C subunit Rfc5, putative	2878	56	0.936	0.554
Afu4g09500	pfkb family carbohydrate kinase superfamily	997	57	0.799	0.72
Afu7g00120	metallo-beta-lactamase domain protein	162	58	0.705	0.724
Afu8g02260	neutral amino acid permease	318	59	0.794	0.575
Afu1g13810	hypothetical protein	6897	60	0.915	0.676
Afu4g08710	short chain dehydrogenase, putative	5901	61	0.874	0.252
Afu6g05140	sterol delta 5,6-desaturase ERG3	135	62	0.705	0.732
Afu2g16250	COP9 signalosome subunit 5 (CsnE), putative	678	63	0.794	0.382
Afu4g09310	hypothetical protein	93	64	0.22	0.438
Afu7g05870	proteasome component Pre8, putative	6473	65	0.912	0.718
Afu2g00580	hypothetical protein	34	66	0.094	0.385
Afu4g01580	ankyrin repeat protein	1608	67	0.886	0.539
Afu2g12240	hypothetical protein	407	68	0.794	0.62
Afu1g09160	hypothetical protein	6631	69	0.856	0.184
Afu4g11500	3-ketosteroid reductase	1011	70	0.844	0.756
Afu5g01460	C6 finger domain protein, putative	6456	71	0.856	0.409
Afu5g11130	PAXNEB protein superfamily	1339	72	0.885	0.665
Afu7g05810	29kD B ribonucleoprotein, putative	2592	73	0.813	0.015
Afu3g08540	Ca2+ binding modulator protein (Alg2), putative	4123	74	0.957	0.716
Afu6g10520	3-oxoacyl-acyl carrier protein reductase	357	75	0.648	0.194
Afu2g05290	isoflavone reductase family protein	2052	76	0.794	0.629
Afu5g10210	hypothetical protein	6559	77	0.815	0.675
Afu4g08730	conserved hypothetical protein	86	78	0.321	0.507
Afu2g14850	enoyl-CoA hydratase/isomerase family protein	5069	79	0.93	0.772
Afu7g01740	sugar transporter, putative	2750	80	0.885	0.735
Afu8g07210	hydroxymethylglutaryl-CoA synthase	6186	81	0.889	0.489
Afu6g10040	fructosyl amine: oxygen oxidoreductase	596	82	0.572	0.271
Afu6g00220	fungal specific transcription factor, putative	1943	83	0.84	0.46
Afu2g02450	Leucine Rich Repeat domain protein	140	84	0.54	0.19
Afu4g07360	5-methyltetrahydropteroyltriglutamate--homocysteine S-methyltransferase	5580	85	0.961	0.752
Afu3g00520	SIR2 family histone deacetylase, putative	10	86	0.015	0.507
Afu5g07780	squalene monooxygenase Erg1	102	87	0.307	0.22

Afu1g12850	nitrate transporter (nitrate permease)	6742	88	0.657	0.673
Afu1g03910	hypothetical protein	213	89	0.647	0.491
Afu7g04500	ATP phosphoribosyltransferase	5311	90	0.935	0.639
Afu6g12160	C6 transcription factor, putative	327	91	0.557	0.507
Afu2g13210	DnaJ domain protein	394	92	0.806	0.732
Afu1g15430	lipase/esterase, putative	1462	93	0.705	0.271
Afu1g10300	hypothetical protein	7625	94	0.639	0.738
Afu3g02220	DUF427 domain protein	609	95	0.764	0.639
Afu3g09350	prefoldin subunit 6, putative	805	96	0.794	0.6
Afu4g08210	GNAT family acetyltransferase (Nat4), putative	799	97	0.753	0.554
Afu2g12170	hypothetical protein	1474	98	0.794	0.724
Afu2g05430	Uridine kinase	5848	99	0.798	0.497
Afu3g14340	mitotic spindle checkpoint protein (Mad2), putative	390	100	0.643	0.386

3.5.5 Functional classification of time-point specifc datasets for Af293 murine infection

Differentially expressed genes between each time-point were grouped into functional categories based on GO Terms and by reference to the *A. fumigatus* literature. A summary of up and down expressed functional categories identified for 4 – 8 and 8 – 14 hours post infection are reported in Tables 3.37 and 3.38 respectively.

Table 3.37: Functional classification of selected genes having differential transcript abundance in Δ*laeA* between 4 and 8 hours post infection in the murine lung. Increased (red) and decreased (green) genes are shown for each functional category. Both increasing and decreasing transcripts are sub divided into expression cohorts which are either high, moderate, and low with respect to their expression change. Genes within functional categories are ranked according to greatest nSI intensity changes between 4 and 8 hours. FDR correct *p*-values from a one-way ANOVA are reported for each gene.

Functional category	ORF	Description	Rank	p-value	Magnitude		ORF	Description	Rank	p-value	Magnitude
Cell wall	Afu1g15440	alpha-1,3-glucan synthase, putative	199	0.176	UP HIGH		Afu6g14540	endo-1,3(4)-beta-glucanase, putative	52	0.502	DOWN HIGH
	Afu6g09310	class V chitinase, putative	293	0.675	UP HIGH		Afu6g09780	class V chitinase, putative	290	0.744	DOWN HIGH
	Afu5g03760	class III chitinase ChiA1	351	0.026	UP HIGH		Afu3g03870	endo-1,4-beta-glucanase, putative	448	0.675	DOWN HIGH
	Afu5g14060	Rho GTPase Rho4, putative	442	0.675	UP HIGH		Afu5g03960	class V chitinase Chi100	528	0.813	DOWN HIGH
	Afu2g14910	alpha-1,6-mannosyltransferase subunit, putative	479	0.773	UP HIGH		Afu5g14030	endo-1,3(4)-beta-glucanase, putative	639	0.659	DOWN HIGH
	Afu3g10340	Rho GTPase Rho 2, putative	616	0.762	UP HIGH		Afu4g13360	endo-1,3(4)-beta-glucanase, putative	762	0.753	DOWN MOD
	Afu6g12400	1,3-beta-glucan synthase catalytic subunit FksP	635	0.056	UP HIGH		Afu2g03980	alpha-1,3-glucanase, putative	921	0.827	DOWN MOD
	Afu1g04260	endo-1,3-beta-glucanase Engl1	853	0.764	UP MOD		Afu8g06030	alpha-1,3-glucanase, putative	1049	0.827	DOWN MOD
	Afu1g01380	alpha-1,6-mannosyltransferase subunit (Hoc1), putative	994	0.453	UP MOD		Afu2g11270	alpha-1,3-glucan synthase, putative	1279	0.803	DOWN LOW
	Afu2g01170	1,3-beta-glucanosyltransferase Gel1	1012	0.453	UP MOD		Afu8g05620	chitin synthase activator (Chs3), putative	1326	0.917	DOWN LOW
	Afu3g12600	beta-glucosidase 1	1084	0.733	UP MOD		Afu7g05140	class III chitinase, putative	1366	0.86	DOWN LOW
	Afu8g00700	class III chitinase ChiA2	1098	0.798	UP MOD		Afu3g07160	class V chitinase, putative	1380	0.924	DOWN LOW
	Afu2g01870	chitin synthase A	1212	0.675	UP MOD		Afu1g03350	alpha-1,3-glucanase, putative	1393	0.873	DOWN LOW
	Afu6g11390	1,3-beta-glucanosyltransferase Gel2	1271	0.371	UP MOD		Afu2g12850	1,3-beta-glucanosyltransferase Gel3	1466	0.887	DOWN LOW
	Afu6g14040	glycosyl transferase,	1516	0.762	UP LOW		Afu2g06160	mutanase	1481	0.819	DOWN

		putative								LOW
	Afu8g05630	chitin synthase F	1573	0.882	UP LOW	Afu8g02130	1,3-beta-glucanosyltransferase, putative	1589	0.906	DOWN LOW
	Afu2g01450	alpha-1,6 mannosyltransferase subunit (Mnn9), putative	1596	0.856	UP LOW	Afu5g03530	class III chitinase, putative	1746	0.868	DOWN LOW
	Afu5g11990	alpha-1,3-mannosyltransferase (Alg3), putative	1676	0.89	UP LOW					
	Afu3g14420	chitin synthase G	1721	0.771	UP LOW					
	Afu3g11280	class V chitinase, putative	1751	0.768	UP LOW					
	Afu7g01540	endo-1,4-beta-glucanase	1804	0.82	UP LOW					
	Afu5g00760	chitin synthase C	1870	0.83	UP LOW					
	Afu2g15910	aminonitrophenyl propanediol resistance protein	1915	0.831	UP LOW					
Ergosterol	Afu5g04080	oxidosqualene:lanosterol cyclase	97	0.623	UP HIGH	Afu1g11230	HMG-CoA reductase	31	0.659	DOWN HIGH
	Afu5g07780	squalene monooxygenase Erg1	102	0.307	UP HIGH	Afu5g14350	c-24(28) sterol reductase	316	0.799	DOWN HIGH
	Afu6g05140	sterol delta 5,6-desaturase ERG3	135	0.705	UP HIGH	Afu5g00110	squalene-hopene-cyclase, putative	332	0.746	DOWN HIGH
	Afu8g02440	C-4 methyl sterol oxidase, putative	252	0.623	UP HIGH	Afu2g02220	UDP-glucose:sterol glycosyltransferase	1443	0.825	DOWN LOW
	Afu4g06890	14-alpha sterol demethylase Cyp51A	270	0.616	UP HIGH					
	Afu1g03150	c-14 sterol reductase	295	0.371	UP HIGH					
	Afu7g04880	UDP-glucose,sterol transferase	404	0.482	UP HIGH					
	Afu2g17400	C-3 sterol dehydrogenase/C-4 decarboxylase	425	0.789	UP HIGH					
	Afu8g01070	Lathosterol oxidase, putative	544	0.586	UP HIGH					
	Afu4g06380	sterol carrier protein, putative	774	0.572	UP MOD					
	Afu4g09190	S-adenosyl-methionine-sterol-C-methyltransferas	922	0.797	UP MOD					
	Afu4g07780	mevalonate kinase	1134	0.757	UP MOD					

	Afu2g15030	C-3 sterol dehydrogenase/C-4 decarboxylase	1227	0.76	UP MOD					
	Afu7g02480	oxysterol binding protein (Osh1), putative	1284	0.52	UP MOD					
	Afu1g05720	c-14 sterol reductase	1289	0.895	UP MOD					
Antigen	Afu2g12630	allergen Asp F13	130	0.291	UP HIGH		Afu5g09210	alkaline serine protease Alp2	1010	0.809	DOWN MOD
	Afu5g02330	major allergen Asp F1	174	0.753	UP HIGH						
	Afu4g09580	major allergen Asp F2	363	0.097	UP HIGH						
	Afu2g03830	allergen Asp F4	430	0.803	UP HIGH						
	Afu2g09030	secreted dipeptidyl peptidase	452	0.67	UP HIGH						
	Afu1g09670	HLH transcription factor (GlcD gamma), putative	628	0.694	UP HIGH						
	Afu6g02280	allergen Asp F3	1456	0.708	UP LOW						
	Afu4g06670	allergen Asp F7	1538	0.693	UP LOW						
	Afu5g04170	molecular chaperone HSP90	1896	0.92	UP LOW						
Ion transport	Afu1g02930	Ca2+ binding protein (calmodulin), putative	123	0.693	UP HIGH		Afu1g11110	calcium channel pore-forming subunit (Cch1), putative	437	0.767	DOWN HIGH
	Afu2g03860	plasma membrane low affinity zinc ion transporter, putative	180	0.026	UP HIGH		Afu2g01460	ZIP Zinc transporter, putaitve	736	0.771	DOWN MOD
	Afu3g10690	calcium-translocating P-type ATPase(PMCA-type),putative	529	0.813	UP HIGH		Afu7g06570	zinc/cadmium resistance protein	779	0.777	DOWN MOD
	Afu4g09560	ZIP Zinc transporter, putative	537	0.55	UP HIGH		Afu6g07050	sodium-hydrogen antiporter, putative	1306	0.917	DOWN LOW
	Afu2g17170	Na+/H+ antiporter Nha1	987	0.652	UP MOD		Afu2g09460	potassium transporter	1534	0.797	DOWN LOW
	Afu7g03880	sodium/calcium exchanger protein	1028	0.553	UP MOD						
	Afu5g03550	plasma membrane H(+)ATPase, putative	1654	0.642	UP LOW						
Iron aquisition	Afu3g03640	siderochrome-iron transporter (MirB), putative	144	0.575	UP HIGH		Afu6g12870	mitochondrial ABC-type iron exporter (Atm1), putative	1810	0.839	DOWN LOW
	Afu2g05730	siderochrome-iron transporter (MirC), putative	850	0.813	UP MOD						
	Afu7g04730	siderochrome-iron transporter, putative	1412	0.621	UP LOW						

	Afu7g06060	siderochrome-iron transporter (Sit1), putative	1652	0.608	UP LOW					
	Afu5g00260	ferric-chelate reductase, putative	1379	0.862	UP LOW					
Secondary metabolism	Afu7g00160	polyketide synthase, putative	215	0.706	UP HIGH		Afu4g14440	nonribosomal peptide synthase, putative	30	0.612	DOWN HIGH
	Afu3g01410	polyketide synthase, putative	508	0.813	UP HIGH		Afu3g02530	polyketide synthase, putative	98	0.797	DOWN HIGH
	Afu8g00370	polyketide synthase, putative	1053	0.638	UP MOD		Afu1g17710	C6 transcription factor, putative	182	0.658	DOWN HIGH
	Afu3g14700	polyketide synthase, putative	1900	0.813	UP LOW		Afu4g14590	C6 transcription factor, putative	206	0.642	DOWN HIGH
	Afu3g02670	nonribosomal peptide synthetase, putative	1924	0.804	UP LOW		Afu8g00170	nonribosomal peptide synthetase, putative	295	0.538	DOWN HIGH
							Afu8g00490	polyketide synthase, putative	360	0.757	DOWN HIGH
							Afu3g12920	nonribosomal peptide synthase (GliP), putative	502	0.772	DOWN HIGH
							Afu6g09630	C6 finger domain protein GliZ	560	0.794	DOWN HIGH
							Afu8g00420	C6 finger transcription factor, putative	567	0.771	DOWN HIGH
							Afu6g03430	C6 finger domain protein, putative	837	0.813	DOWN MOD
							Afu4g14720	C6 transcription factor, putative	852	0.813	DOWN MOD
							Afu5g00150	nonribosomal peptide synthetase, putative	868	0.757	DOWN MOD
							Afu6g03480	nonribosomal peptide synthetase, putative	966	0.845	DOWN MOD
							Afu3g02570	polyketide synthase, putative	1071	0.803	DOWN MOD
							Afu3g15270	nonribosomal peptide synthetase, putative	1075	0.803	DOWN MOD
							Afu4g00210	polyketide synthase, putative	1137	0.176	DOWN MOD
Gliotoxin	Afu6g09580	hypothetical protein	1049	0.764	UP MOD		Afu6g09630	C6 finger domain protein GliZ	560	0.794	DOWN HIGH
Pseurotin A Supercluster	Afu8g00610	cell surface protein Mas1, putative	2	0.002	UP HIGH		Afu8g00550	SirN-like methyltransferase, putative	69	0.577	DOWN HIGH
	Afu8g00460	methionine aminopeptidase, type I, putative	746	0.727	UP MOD		Afu8g00230	phytanoyl-CoA dioxygenase family protein	147	0.182	DOWN HIGH
	Afu8g00370	polyketide synthase,	1053	0.638	UP MOD		Afu8g00660	solute transporter, putative	198	0.82	DOWN

		putative								HIGH
	Afu8g00700	class III chitinase ChiA2	1098	0.798	UP MOD	Afu8g00630	conserved hypothetical protein	275	0.753	DOWN HIGH
	Afu8g00260	F-box domain and ankyrin repeat protein	1138	0.641	UP MOD	Afu8g00170	nonribosomal peptide synthetase, putative	295	0.538	DOWN HIGH
	Afu8g00590	fatty acid desaturase, putative	1223	0.845	UP MOD	Afu8g00200	O-methyltransferase, putative	326	0.586	DOWN HIGH
						Afu8g00490	polyketide synthase, putative	360	0.757	DOWN HIGH
						Afu8g00280	short-chain dehydrogenase, putative	465	0.81	DOWN HIGH
						Afu8g00130	hypothetical protein	490	0.74	DOWN HIGH
						Afu8g00110	oxidoreductase, 2OG-Fe(II) oxygenase family, putative	505	0.783	DOWN HIGH
						Afu8g00450		514	0.813	DOWN HIGH
						Afu8g00390	O-methyltransferase, putative	557	0.822	DOWN HIGH
						Afu8g00420	C6 finger transcription factor, putative	567	0.771	DOWN HIGH
						Afu8g00220	cytochrome P450, putative	594	0.844	DOWN HIGH
						Afu8g00570	alpha/beta hydrolase, putative	642	0.856	DOWN HIGH
						Afu8g00290	conserved hypothetical protein	738	0.816	DOWN MOD
						Afu8g00180	conserved hypothetical protein	890	0.83	DOWN MOD
						Afu8g00640	glycosyl transferase, putative	1250	0.811	DOWN LOW
						Afu8g00440	steroid monooxygenase, putative	1291	0.675	DOWN LOW
						Afu8g00150	conserved hypothetical protein	1668	0.917	DOWN LOW
Microtubule	Afu2g14280	kinesin family protein (KlpA), putative	83	0.238	UP HIGH	Afu8g00530	alpha/beta hydrolase, putative	1741	0.956	DOWN LOW
	Afu7g01400	kinesin family protein (BimC), putative	168	0.323	UP HIGH	Afu2g14990	tubulin alpha-2 subunit	1818	0.919	DOWN LOW
	Afu2g07550	serine/threonine protein kinase (Ark1), putative	229	0.753	UP HIGH					
	Afu2g15750	gamma-tubulin complex component GCP4, putative	625	0.753	UP HIGH					

	Afu1g10910	tubulin beta, putative	823	0.017	UP MOD					
	Afu2g03150	kinesin family protein	1158	0.678	UP MOD					
	Afu3g11860	microtubule associated protein EB1, putative	1337	0.757	UP LOW					
	Afu3g12820	kinesin family protein	1901	0.869	UP LOW					
Secreted proteases	Afu4g13750	Deuterolysin metalloprotease, putative	50	0.291	UP HIGH		Afu3g11400	aspartic endopeptidase Pep2	836	0.764	DOWN MOD
	Afu2g03510	pheromone processing carboxypeptidase (Sxa2), putative	120	0.638	UP HIGH						
	Afu2g09030	secreted dipeptidyl peptidase	452	0.67	UP HIGH						
	Afu6g14420	disintegrin-like metalloproteinase, putative	495	0.307	UP HIGH						
	Afu4g14000	tripeptidyl peptidase A	500	0.716	UP HIGH						
	Afu1g00420	carboxypeptidase S1, putative	523	0.146	UP HIGH						
	Afu3g12210	carboxypeptidase Y, putative	1519	0.753	UP LOW						
Secretion peptide encoding genes	Afu2g12680	conserved hypothetical protein	1	0.012	UP HIGH		Afu1g17050	hypothetical protein	5	0.528	DOWN HIGH
	Afu8g00610	cell surface protein Mas1, putative	2	0.002	UP HIGH		Afu3g03930	cytochrome P450, putative	6	0.512	DOWN HIGH
	Afu5g01620	extracellular proline-rich protein	3	0.015	UP HIGH		Afu1g17320	endo-arabinanase, putative	8	0.550	DOWN HIGH
	Afu2g14540	endoglucanase, putative	4	0.004	UP HIGH		Afu2g00710	alpha-amylase, putative	11	0.443	DOWN HIGH
	Afu3g08110	cell wall protein, putative	7	0.012	UP HIGH		Afu3g00550	hypothetical protein	22	0.454	DOWN HIGH
	Afu2g14420	cutinase, putative	9	0.009	UP HIGH		Afu3g13650	integral membrane protein	26	0.638	DOWN HIGH
	Afu6g00430	IgE-binding protein	13	0.007	UP HIGH		Afu2g17920	hypothetical protein	34	0.757	DOWN HIGH
	Afu3g13110	extracellular serine-threonine rich protein	14	0.022	UP HIGH		Afu5g01210	amine oxidase, flavin-containing superfamily	36	0.538	DOWN HIGH
	Afu8g06830	endoglucanase, putative	15	0.026	UP HIGH		Afu3g02790	amidohydrolase family protein, putative	41	0.675	DOWN HIGH
	Afu6g00680	hypothetical protein	18	0.019	UP HIGH		Afu2g17530	conidial pigment biosynthesis oxidase Arb2/brown2	44	0.561	DOWN HIGH

	Afu8g05910	pectate lyase, putative	19	0.071	UP HIGH		Afu3g02930	extracellular soluble lytic transglycosylase, putative	49	0.291	DOWN HIGH
	Afu2g15950	aspartic endopeptidase, putative	20	0.167	UP HIGH		Afu6g14540	endo-1,3(4)-beta-glucanase, putative	52	0.502	DOWN HIGH
	Afu5g03010	conserved hypothetical protein	21	0.298	UP HIGH		Afu8g07250	pectin methylesterase family protein	55	0.705	DOWN HIGH
	Afu2g10130	phase-specific adhesin, putative	22	0.411	UP HIGH		Afu6g11630	FAD-dependent isoamyl alcohol oxidase, putative	61	0.623	DOWN HIGH
	Afu2g14490	endoglucanase, putative	24	0.176	UP HIGH		Afu1g16420	GPI anchored protein, putative	74	0.291	DOWN HIGH
	Afu6g09670	cytochrome P450 oxidoreductase GliC	29	0.272	UP HIGH		Afu4g01120	hypothetical protein	82	0.794	DOWN HIGH
	Afu5g14420	hypothetical protein	33	0.013	UP HIGH		Afu8g00920	UDP-glucose dehydrogenase Uxs2p	87	0.608	DOWN HIGH
	Afu4g14180	hypothetical protein	35	0.309	UP HIGH		Afu5g00120	cytochrome P450 oxidoreductase/alkane hydroxylase, putative	91	0.748	DOWN HIGH
	Afu4g00390	glycosyl hydrolase, putative	37	0.089	UP HIGH		Afu6g14390	extracelular cellulose binding protein (Cip2), putative	104	0.180	DOWN HIGH
	Afu1g01540	Endonuclease/Exonuclease/phosphatase family family	39	0.119	UP HIGH		Afu5g03280	hypothetical protein	109	0.658	DOWN HIGH
	Afu6g00690	conserved hypothetical protein	41	0.238	UP HIGH		Afu1g02780	L-asparaginase	124	0.705	DOWN HIGH
	Afu4g01290	endo-chitosanase, pseudogene	43	0.568	UP HIGH		Afu1g01980	IgE binding protein, putative	133	0.043	DOWN HIGH
	Afu3g00320	endo-1,4-beta-xylanase (XlnA), putative	45	0.643	UP HIGH		Afu2g15450	hypothetical protein	135	0.804	DOWN HIGH
	Afu7g06810	L-amino acid oxidase LaoA, putative	46	0.172	UP HIGH		Afu6g01800	endoglucanase, putative	160	0.497	DOWN HIGH
	Afu3g03950	endoglucanase, putative	49	0.391	UP HIGH		Afu4g06590	hypothetical protein	166	0.584	DOWN HIGH
	Afu4g13750	Deuterolysin metalloprotease, putative	50	0.291	UP HIGH		Afu7g05180	defensin domain protein, putative	168	0.494	DOWN HIGH
	Afu5g01990	BYS1 domain protein, putative	51	0.158	UP HIGH		Afu7g01130	hypothetical protein	171	0.544	DOWN HIGH
	Afu6g00770	extracellular arabinanase, putative	58	0.079	UP HIGH		Afu1g17570	urea active transporter, putative	175	0.705	DOWN HIGH
	Afu2g17650	DUF907 domain protein	59	0.045	UP HIGH		Afu5g02340	hypothetical protein	184	0.714	DOWN HIGH
Ribosome biogenesis and RNA	Afu4g13450	RNA methyltransferase, TrmH family family	268	0.675	UP HIGH		Afu1g02950	RNA recognition motif. (a.k.a. RRM, RBD, or RNP domain) protein	291	0.584	DOWN HIGH

metabolism										
	Afu6g04810	RNA polymerase II transcription mediator complex subunit (Med6), putative	504	0.576	UP HIGH	Afu7g01460	ribosomal protein S5	455	0.697	DOWN HIGH
	Afu5g09060	RNA binding protein, putative	758	0.648	UP MOD	Afu5g11150	ribonuclease P protein subunit p29	732	0.63	DOWN MOD
	Afu2g13720	RNA-polymerase I	767	0.794	UP MOD	Afu3g06310	RNA binding protein	992	0.804	DOWN MOD
	Afu1g10310	RNase L inhibitor of the ABC superfamily, putative	778	0.679	UP MOD	Afu3g10730	Ribosomal protein S7e	1095	0.747	DOWN MOD
	Afu5g08310	RNA and export factor binding protein 2-I	941	0.748	UP MOD	Afu2g10500	ribosomal protein S9	1262	0.716	DOWN LOW
	Afu1g02510	RNA-binding protein, putative	973	0.581	UP MOD	Afu7g04490	Ribosomal protein S28e	1348	0.874	DOWN LOW
	Afu1g11670	small nuclear ribonucleoprotein (LSM8), putative	1179	0.804	UP MOD	Afu1g15020	40S ribosomal protein S5	1419	0.827	DOWN LOW
	Afu8g04820	ribonuclease P complex subunit p30, putative	1360	0.675	UP LOW	Afu2g16370	Ribosomal protein L32	1478	0.813	DOWN LOW
	Afu1g09410	ribosomal protein L17	1566	0.867	UP LOW	Afu1g14410	60s ribosomal protein yl17-b	1520	0.739	DOWN LOW
	Afu5g08430	RO10	1712	0.86	UP LOW	Afu2g03260	RNA-binding protein, putative	1539	0.917	DOWN LOW
	Afu3g09620	RNA recognition motif. (a.k.a. RRM, RBD, or RNP domain) protein	1780	0.794	UP LOW	Afu5g13470	60S acidic ribosomal protein, putative	1540	0.753	DOWN LOW
						Afu2g08130	ribosomal protein L41	1545	0.642	DOWN LOW
						Afu1g10510	60S ribosomal protein L35, putative	1556	0.716	DOWN LOW
						Afu6g10370	RNA lariat debranching enzyme, putative	1569	0.757	DOWN LOW
						Afu2g08520	50S ribosomal protein L14	1767	0.95	DOWN LOW
						Afu5g03090	small nucleolar ribonucleoprotein complex subunit (Pwp2), putative	1768	0.771	DOWN LOW
Carbohydrate transport	Afu6g14500	MFS sugar transporter, putative	169	0.759	UP HIGH	Afu8g01180	MFS sugar transporter, putative	301	0.757	DOWN HIGH
	Afu3g01700	maltose permease	172	0.465	UP HIGH	Afu5g12950	MFS quinate transporter, putative	788	0.717	DOWN MOD
	Afu8g02090	nucleotide-sugar transporter family	499	0.747	UP HIGH	Afu1g03280	maltose permease, putative	1058	0.895	DOWN MOD

		protein								
	Afu7g05550	sugar transporter family protein	1102	0.794	UP MOD	Afu1g16390	MFS hexose transporter, putative	1132	0.798	DOWN MOD
	Afu3g01670	MFS hexose transporter, putative	1164	0.87	UP MOD	Afu6g01860	MFS lactose permease, putative	1287	0.895	DOWN LOW
	Afu1g12240	MFS peptide transporter, putaitve	1253	0.795	UP MOD	Afu5g00280	MFS sugar transporter, putative	1531	0.901	DOWN LOW
	Afu8g06870	MFS sugar transporter, putative	1480	0.794	UP LOW					
	Afu3g00200	hexose transporter protein	1779	0.789	UP LOW					
Amino acid transport	Afu5g14660	GABA permease, putative	80	0.148	UP HIGH	Afu4g10090	GABA permease, putative	524	0.647	DOWN HIGH
	Afu5g02790	amino acid permease	362	0.797	UP HIGH	Afu3g00120	amino acid transporter, putative	577	0.813	DOWN HIGH
	Afu2g13630	amino transferase	510	0.675	UP HIGH	Afu8g00800	amino acid transporter, putative	1271	0.812	DOWN LOW
	Afu4g07760	Transmembrane amino acid transporter protein family	741	0.693	UP MOD	Afu2g15470	neutral amino acid permease	1327	0.917	DOWN LOW
	Afu6g04990	amino acid transporter, putative	788	0.462	UP MOD	Afu3g01820	amino acid permease	1740	0.827	DOWN LOW
	Afu8g07200	neutral amino acid permease	829	0.622	UP MOD	Afu1g09120	amino acid permease, putative	1770	0.87	DOWN LOW
	Afu1g12310	GABA permease GabA	1392	0.84	UP LOW					
Carbohydrate and protein glycosylation	Afu8g02070	glycosyl transferase, putative	1294	0.706	UP MOD	Afu8g02320	glycosyl transferase, group 2 family protein domain protein	225	0.727	DOWN HIGH
	Afu6g11820	Glycosyl hydrolase family 10	1574	0.879	UP LOW	Afu2g00680	glycosyl hydrolase, putative	571	0.771	DOWN HIGH
	Afu6g12010	glycosyl hydrolase, family 3, putative	1877	0.751	UP LOW	Afu3g07860	glycosyl transferase, putative	644	0.76	DOWN HIGH
						Afu8g06980	glycosyl hydrolase, putative	1014	0.797	DOWN MOD
						Afu3g00700	glycosyl hydrolase, putative	1044	0.845	DOWN MOD
						Afu8g00640	glycosyl transferase, putative	1250	0.811	DOWN LOW
						Afu4g11730	glycerol dehydrogenase (GldB), putative	1451	0.609	DOWN LOW
Transposition associated processes	Afu1g10020	reverse transcriptase, RNaseH	25	0.535	UP HIGH	Afu7g07170	reverse transcriptase/protease/endonuclease Pol, putative	92	0.537	DOWN HIGH
	Afu1g00940	Tc1-mariner class	257	0.777	UP HIGH	Afu3g09440	reverse transcriptase, RNaseH,	464	0.753	DOWN

		transposase, putative					putative			HIGH
	Afu7g08410	Tc1-mariner transposase, putative	1088	0.753	UP MOD	Afu7g08210	reverse transcriptase, putative	724	0.803	DOWN MOD
	Afu6g09330	transposase	1385	0.818	UP LOW	Afu7g06870	Tf1-like reverse transcriptase, integrase, putative	899	0.864	DOWN MOD
	Afu3g11670	DDE superfamily endonuclease/transposase, pseudogene	1420	0.917	UP LOW	Afu4g01630	reverse transcriptase, putative	924	0.76	DOWN MOD
	Afu6g00780	LINE-1 class reverse transcriptase, RNaseH, putative	1579	0.794	UP LOW	Afu7g06930	reverse transcriptase, RNaseH	1034	0.844	DOWN MOD
	Afu3g01740	transposase	1864	0.679	UP LOW	Afu5g06180	possible transposase	1180	0.797	DOWN MOD
	Afu7g00100	LINE-1 class reverse transcriptase, RNaseH, putative	1875	0.777	UP LOW	Afu7g07070	LINE-1 class reverse transcriptase, RNaseH, putative	1226	0.869	DOWN MOD
	Afu1g00880	reverse transcriptase, RNaseH, putative	1888	0.675	UP LOW	Afu1g04650	transposase	1331	0.716	DOWN LOW
	Afu6g03650	possible transposase	1919	0.813	UP LOW	Afu3g09420	transposase, putative	1598	0.875	DOWN LOW
						Afu6g10920	mariner class transposase, putative	1721	0.873	DOWN LOW
						Afu3g14810	pathogenicity associated protein PEP2, putative	268	0.686	DOWN HIGH
Pathogensis	Afu3g02270	mycelial catalase Cat1	79	0.114	UP HIGH	Afu6g13970	FAD-dependent monooxygenase (PaxM), putative	390	0.844	DOWN HIGH
	Afu5g02330	major allergen Asp F1	174	0.753	UP HIGH					
	Afu1g15440	alpha-1,3-glucan synthase, putative	199	0.176	UP HIGH					
	Afu2g03830	allergen Asp F4	430	0.803	UP HIGH					
	Afu2g08360	orotidine 5'-phosphate decarboxylase PyrG	484	0.757	UP HIGH					
	Afu1g01890	enoyl-CoA hydratase/isomerase family protein	684	0.457	UP MOD					
	Afu5g09250	transcription factor (Snd1/p100), putative	949	0.676	UP MOD					
	Afu6g02280	allergen Asp F3	1456	0.708	UP LOW					
	Afu2g07680	L-ornithine N5-oxygenase SidA	1505	0.544	UP LOW					
	Afu3g00590	Asp-hemolysin	1658	0.864	UP LOW					
	Afu5g05480	Rheb GTPase RhbA	1894	0.858	UP LOW					

Signal transduction	Afu2g03510	pheromone processing carboxypeptidase (Sxa2), putative	120	0.638	UP HIGH	Afu1g05010	MFS transporter, putative	94	0.675	DOWN HIGH
	Afu6g03160	NACHT domain protein	126	0.026	UP HIGH	Afu3g13210	protein kinase domain-containing protein	188	0.727	DOWN HIGH
	Afu5g09020	WSC domain protein, putative	150	0.351	UP HIGH	Afu3g02500	protein kinase, putative	251	0.433	DOWN HIGH
	Afu2g02760	protein-tyrosine phosphatase, putative	163	0.264	UP HIGH	Afu3g00780	cAMP receptor (Car4), putative	383	0.679	DOWN HIGH
	Afu1g14890	cpdP protein, putative	187	0.538	UP HIGH	Afu2g00910	Pfs, NB-ARC and TPR domain protein	558	0.693	DOWN HIGH
	Afu1g09560	protein transport protein (LST8), putative	218	0.757	UP HIGH	Afu6g09260	sensor histidine kinase/response regulator, putative	747	0.794	DOWN MOD
	Afu5g14060	Rho GTPase Rho4, putative	442	0.675	UP HIGH	Afu5g08950	RAS small monomeric GTPase (Rsr1), putative	1349	0.638	DOWN LOW
	Afu3g12550	sensor histidine kinase/response regulator, putative	513	0.794	UP HIGH	Afu1g06920	serine/threonine protein kinase, putative	1590	0.876	DOWN LOW
	Afu3g10340	Rho GTPase Rho 2, putative	616	0.762	UP HIGH	Afu3g07680	ran GTPase activating protein 1 (RNA1 protein)	1823	0.906	DOWN LOW
	Afu4g11450	Rho guanyl nucleotide exchange factor, putative	624	0.705	UP HIGH					
	Afu3g12400	G protein complex alpha subunit (GanA), putative	664	0.767	UP MOD					
	Afu5g07430	Rho guanyl nucleotide exchange factor, putative	669	0.623	UP MOD					
	Afu5g12210	G-protein complex beta subunit SfaD	687	0.723	UP MOD					
	Afu1g06900	C2H2 transcription factor (Crz1), putative	914	0.675	UP MOD					
	Afu7g02570	HET-C domain protein	978	0.656	UP MOD					
	Afu5g03160	protein kinase, putative	1150	0.705	UP MOD					
	Afu2g17130	protein kinase regulator Ste50	1225	0.836	UP MOD					
	Afu5g11840	protein kinase, putative	1304	0.84	UP LOW					
	Afu1g12680	Rho GTPase activator (Rga1), putative	1375	0.79	UP LOW					
	Afu1g11930	protein kinase, putative	1644	0.768	UP LOW					
	Afu4g10010	cdc37 protein	1646	0.553	UP LOW					

	Afu3g10240	Ccr4-Not transcription complex subunit (NOT1), putative	1657	0.822	UP LOW					
	Afu1g04330	Ser/Thr protein phosphatase family protein	1669	0.605	UP LOW					
	Afu2g11100	AMFR protein, putative	1726	0.758	UP LOW					
	Afu2g03360	polarized growth protein (Boi2), putative	1840	0.693	UP LOW					
	Afu6g13160	serine/threonine protein kinase, putative	1872	0.753	UP LOW					
Sphingolipid biosynthesis	Afu1g16850	sur2 protein	698	0.818	UP MOD		Afu1g10980	sphingosine kinase (SphK), putative	1708	0.946	DOWN LOW
	Afu6g00300	serine palmitoyltransferase 1, putative	721	0.096	UP MOD						
	Afu2g10460	conserved hypothetical protein	728	0.782	UP MOD						
	Afu1g16710	fatty acid elongase (Gig30), putative	1595	0.892	UP LOW						
	Afu5g02760	fatty acid elongase (Gns1), putative	1855	0.705	UP LOW						
	Afu6g04680	MIPC synthase subunit (SurA), putative	1343	0.659	UP LOW						
Transcription factors	Afu3g00690	C6 transcription factor, putative	30	0.673	UP HIGH		Afu2g05380	C6 transcription factor, putative	93	0.360	DOWN HIGH
	Afu4g10340	C6 finger domain protein, putative	63	0.494	UP HIGH		Afu2g08240	C6 transcription factor, putative	106	0.794	DOWN HIGH
	Afu3g06740	C6 transcription factor (Gal4), putative	129	0.245	UP HIGH		Afu3g03920	C6 transcription factor, putative	113	0.710	DOWN HIGH
	Afu5g00290	C6 transcription factor, putative	173	0.608	UP HIGH		Afu5g06800	C6 transcription factor, putative	127	0.708	DOWN HIGH
	Afu6g09350	C6 finger domain protein, putative	196	0.143	UP HIGH		Afu7g01820	C6 transcription factor, putative	131	0.757	DOWN HIGH
	Afu8g05800	C6 finger domain protein, putative	243	0.096	UP HIGH		Afu7g00210	C6 transcription factor, putative	768	0.793	DOWN MOD
	Afu1g14280	C6 finger domain protein, putative	727	0.404	UP MOD		Afu3g02750	C6 transcription factor, putative	806	0.771	DOWN MOD
	Afu5g02800	C6 transcription factor, putative	772	0.767	UP MOD		Afu6g03430	C6 finger domain protein, putative	837	0.813	DOWN MOD
	Afu2g10400	C6 transcription factor, putative	785	0.762	UP MOD		Afu3g14840	C6 transcription factor, putative	840	0.867	DOWN MOD

Afu1g10280	C2H2 finger domain protein (Gli3), putative	811	0.675	UP MOD	Afu4g14720	C6 transcription factor, putative	852	0.813	DOWN MOD
Afu1g15680	C6 finger domain protein, putative	834	0.792	UP MOD	Afu8g06010	C6 transcription factor, putative	870	0.675	DOWN MOD
Afu1g06900	C2H2 transcription factor (Crz1), putative	914	0.675	UP MOD	Afu1g01650	C6 finger domain protein, putative	889	0.794	DOWN MOD
Afu6g02850	C6 finger domain protein, putative	916	0.803	UP LOW	Afu8g01990	C6 transcription factor, putative	1357	0.864	DOWN LOW
Afu3g01640	C6 finger domain protein, putative	1268	0.659	UP LOW	Afu5g01460	C6 finger domain protein, putative	1364	0.856	DOWN LOW
Afu6g08550	C6 transcription factor, putative	1288	0.739	UP LOW	Afu6g02690	C2H2 finger domain protein, putative	1525	0.863	DOWN LOW
Afu3g05760	C6 transcription factor (Fcr1), putative	1300	0.887	UP LOW	Afu5g12020	C6 transcription factor (NirA), putative	1537	0.839	DOWN LOW
Afu2g17220	C2H2 transcription factor (AmdX), putative	1320	0.753	UP LOW	Afu8g04290	C2H2 finger domain protein, putative	1612	0.864	DOWN LOW
Afu5g02690	C6 transcription factor, putative	1341	0.804	UP LOW	Afu3g11990	C6 transcription factor (Mut3), putative	1616	0.773	DOWN LOW
Afu7g06320	C6 transcription factor, putative	1369	0.78	UP LOW	Afu8g01240	C6 transcription factor, putative	1617	0.861	DOWN LOW
Afu1g17460	C6 transcription factor, putative	1424	0.848	UP LOW	Afu1g01560	C6 finger domain protein, putative	1624	0.844	DOWN LOW

Table 3.38: Functional classification of selected genes having differential transcript abundance in Δ*laeA* between 8 and 14 hours post infection in the murine lung. Increased (red) and decreased (green) genes are shown for each functional category. Both increasing and decreasing transcripts are sub divided into expression cohorts which are either high, moderate, and low with respect to their expression change. Genes within functional categories are ranked according to greatest nSI intensity changes between 8 and 14 hours. FDR correct *p*-values from a one-way ANOVA are reported for each gene.

Functional category	ORF	Description	Rank	p-value	Magnitude	ORF	Description	Rank	P-value	Magnitude
Cell wall	Afu8g05020	beta-N-acetylhexosaminidase NagA, putative	101	0.664	UP HIGH	Afu6g09310	class V chitinase, putative	6	0.486	DOWN HIGH
	Afu5g08580	alpha-1,6-mannosyltransferase subunit (Och1), putative	326	0.639	UP HIGH	Afu2g14910	alpha-1,6-mannosyltransferase subunit, putative	53	0.449	DOWN HIGH
	Afu6g14540	endo-1,3(4)-beta-glucanase, putative	482	0.732	UP HIGH	Afu1g15440	alpha-1,3-glucan synthase, putative	472	0.6	DOWN HIGH
	Afu1g11460	1,3-beta-glucanosyltransferase Bgt1	644	0.83	UP HIGH	Afu5g00760	chitin synthase C	507	0.72	DOWN HIGH
	Afu2g05340	1,3-beta-glucanosyltransferase, putative	1079	0.79	UP MOD	Afu5g14060	Rho GTPase Rho4, putative	514	0.664	DOWN HIGH
	Afu7g08350	alpha-1,3-glucanase, putative	1279	0.854	UP MOD	Afu2g15910	aminonitrophenyl propanediol resistance protein	515	0.312	DOWN HIGH
	Afu5g14190	beta-glucanase, putative	1385	0.796	UP LOW	Afu4g12900	alpha-1,6-mannosyltransferase subunit (Ecm39), putative	767	0.605	DOWN MOD
	Afu3g07160	class V chitinase, putative	1625	0.915	UP LOW	Afu2g01870	chitin synthase A	1099	0.513	DOWN MOD
	Afu7g08510	extracellular alpha-1,3-glucanase/mutanase, putative	1641	0.718	UP LOW	Afu3g14420	chitin synthase G	1244	0.738	DOWN MOD

	Afu4g13360	endo-1,3(4)-beta-glucanase, putative	1889	0.929	UP LOW	Afu2g01170	1,3-beta-glucanosyltransferase Gel1	1320	0.704	DOWN LOW
						Afu1g07110	related to export control protein CHS7	1356	0.788	DOWN LOW
						Afu3g10340	Rho GTPase Rho 2, putative	1380	0.513	DOWN LOW
						Afu3g07110	class III chitinase, putative	1605	0.896	DOWN LOW
						Afu8g00700	class III chitinase ChiA2	1678	0.883	DOWN LOW
Ergosterol	Afu7g00260	squalene-hopene-cyclase, putative	292	0.128	UP HIGH					
	Afu7g00300	squalene-hopene-cyclase, putative	1686	0.883	UP LOW					
	Afu3g05520	oxysterol binding protein (Orp8), putative	1792	0.872	UP LOW					
Antigen	Afu8g05020	beta-N-acetylhexosaminidase NagA, putative	101	0.664	UP HIGH	Afu2g12630	allergen Asp F13	161	0.639	DOWN HIGH
	Afu5g13300	aspartic endopeptidase Pep1	278	0.838	UP HIGH	Afu5g02330	major allergen Asp F1	316	0.872	DOWN HIGH
	Afu6g11430	aldehyde dehydrogenase, putative	1267	0.008	UP MOD	Afu5g09580	conidial hydrophobin Hyp1/RodA	859	0.783	DOWN MOD
						Afu6g02280	allergen Asp F3	1442	0.704	DOWN LOW
						Afu3g10460	nuclear transport factor 2	1554	0.567	DOWN LOW
						Afu4g09090	thioredoxin, putative	1569	0.718	DOWN LOW
						Afu2g06150	disulfide isomerase, putative	1691	0.813	DOWN LOW
Ion transport	Afu8g01480	potassium channel, putative	1	0.004	UP HIGH	Afu1g16090	arsenate reductase (ArsC), putative	20	0.41	DOWN HIGH

	Afu1g02480	plasma membrane ATPase, putative	199	0.393	UP HIGH	Afu5g15000	arsenate reductase (ArsC), putative	164	0.507	DOWN HIGH
	Afu2g01460	ZIP Zinc transporter, putaitve	461	0.838	UP HIGH	Afu6g06740	endoplasmic reticulum calcium ATPase, putative	285	0.674	DOWN HIGH
	Afu5g15030	arsenic resistance protein ArsH	782	0.732	UP MOD	Afu2g03860	plasma membrane low affinity zinc ion transporter, putative	310	0.639	DOWN HIGH
	Afu4g12620	copper-transporting ATPase, putative	1156	0.65	UP MOD	Afu1g02930	Ca2+ binding protein (calmodulin), putative	473	0.784	DOWN HIGH
	Afu6g02550	magnesium ion transporter (Mrs2), putative	1189	0.881	UP MOD	Afu3g11350	arsenite translocating ATPase (arsA), putative	984	0.827	DOWN MOD
	Afu2g09460	potassium transporter	1481	0.751	UP LOW	Afu7g03880	sodium/calcium exchanger protein	1319	0.752	DOWN LOW
	Afu1g16340	potassium transporter, putative	1582	0.86	UP LOW	Afu3g08180	Ctr copper transporter family protein	1692	0.881	DOWN LOW
	Afu1g05760	arsenite efflux transporter (ArsB), puative	1678	0.943	UP LOW					
	Afu6g02810	Ctr copper transporter family family	1864	0.881	UP LOW					
Iron utilisation	Afu4g14640	low affinity iron transporter, putative	908	0.519	UP MOD	Afu7g04730	siderochrome-iron transporter, putative	137	0.513	DOWN HIGH
Secondary metabolism	Afu6g03430	C6 finger domain protein, putative	259	0.646	UP HIGH	Afu7g00160	polyketide synthase, putative	304	0.861	DOWN HIGH
	Afu6g03480	nonribosomal peptide synthetase, putative	387	0.507	UP HIGH	Afu3g02590	C6 transcription factor, putative	1640	0.881	DOWN LOW
	Afu1g17710	C6 transcription factor, putative	438	0.816	UP HIGH					
	Afu6g12050	nonribosomal peptide synthase, putative	734	0.6	UP MOD					
	Afu3g01510	C6 transcription factor, putative	764	0.694	UP MOD					

	Afu6g09610	nonribosomal peptide synthase, putative	838	0.875	UP MOD					
	Afu5g00150	nonribosomal peptide synthetase, putative	865	0.78	UP MOD					
	Afu5g12730	nonribosomal peptide synthase, putative	1070	0.639	UP MOD					
	Afu3g02530	polyketide synthase, putative	1078	0.866	UP MOD					
	Afu3g02570	polyketide synthase, putative	1676	0.856	UP LOW					
	Afu4g14440	nonribosomal peptide synthase, putative	1782	0.9	UP LOW					
Gliotoxin	Afu6g09610	nonribosomal peptide synthase, putative	838	0.875	UP MOD	Afu6g09580	hypothetical protein	808	0.657	DOWN MOD
						Afu6g09600	peptidase, putative	1682	0.855	DOWN LOW
Pseurotin A Supercluster	Afu8g00630	conserved hypothetical protein	180	0.704	UP HIGH	Afu8g00720	amino acid transporter, putative	148	0.004	DOWN HIGH
	Afu8g00280	short-chain dehydrogenase, putative	268	0.738	UP HIGH	Afu8g00590	fatty acid desaturase, putative	370	0.6	DOWN HIGH
	Afu8g00530	alpha/beta hydrolase, putative	335	0.62	UP HIGH	Afu8g00710	secreted antimicrobial peptide, putative	442	0.639	DOWN HIGH
	Afu8g00360	NlpC/P60-like cell-wall peptidase, putative	1256	0.85	UP MOD	Afu8g00310	LINE-1 class reverse transcriptase, RNaseH, putative	1036	0.725	DOWN MOD
	Afu8g00180	conserved hypothetical protein	1454	0.922	UP LOW	Afu8g00700	class III chitinase ChiA2	1678	0.883	DOWN LOW
	Afu8g00300	conserved hypothetical protein	1516	0.909	UP LOW					

	Afu8g00620	dimethylallyl tryptophan synthase, putative	1574	0.878	UP LOW						
	Afu8g00410	methionine aminopeptidase, type II, putative	1901	0.881	UP LOW						
	Afu8g00200	O-methyltransferase, putative	1936	0.87	UP LOW						
Microtubule	Afu2g14730	kinesin family protein	354	0.798	UP HIGH		Afu1g10910	tubulin beta, putative	407	0.258	DOWN HIGH
	Afu5g02730	gamma-tubulin complex component GCP5, putative	1603	0.704	UP LOW		Afu4g06710	kinase-related protein	1132	0.873	DOWN MOD
	Afu5g11810	cytoplasmic dynein heavy chain	1338	0.652	UP LOW		Afu3g12820	kinesin family protein	1348	0.369	DOWN LOW
Secreted protease	Afu3g01220	aspartic-type endopeptidase, putative	240	0.6	UP HIGH		Afu3g12210	carboxypeptidase Y, putative	1572	0.813	DOWN LOW
	Afu5g13300	aspartic endopeptidase Pep1	278	0.838	UP HIGH		Afu4g13750	Deuterolysin metalloprotease, putative	1307	0.887	DOWN LOW
	Afu3g11400	aspartic endopeptidase Pep2	463	0.6	UP HIGH						
	Afu4g09320	antigenic dipeptidyl-peptidase Dpp4	778	0.798	UP MOD						
	Afu4g07040	aspartic-type endopeptidase (CtsD), putative	994	0.716	UP MOD						
	Afu8g00360	NlpC/P60-like cell-wall peptidase, putative	1256	0.85	UP MOD						
	Afu1g08940	pheromone processing carboxypeptidase Kex1	1905	0.813	UP LOW						
Signal peptide encoding genes	Afu8g01480	potassium channel, putative	1	0.004	UP HIGH		Afu8g01810	conserved hypothetical protein	1	0.385	DOWN HIGH

Afu6g09670	cytochrome P450 oxidoreductase GliC	3	0.069	UP HIGH		Afu6g09310	class V chitinase, putative	6	0.486	DOWN HIGH
Afu5g00550	endoglycoceramidase, putative	21	0.5	UP HIGH		Afu4g06890	14-alpha sterol demethylase Cyp51A	18	0.198	DOWN HIGH
Afu3g02090	beta-xylosidase	22	0.137	UP HIGH		Afu3g10370	conserved hypothetical protein	39	0.639	DOWN HIGH
Afu1g06470	neutral/alkaline nonlysosomal ceramidase, putative	24	0.547	UP HIGH		Afu2g05290	isoflavone reductase family protein	76	0.629	DOWN HIGH
Afu8g01310	metalloreductase, putative	28	0.688	UP HIGH		Afu6g10040	fructosyl amine: oxygen oxidoreductase	82	0.271	DOWN HIGH
Afu3g03480	cytochrome P450 monooxygenase, putative	55	0.218	UP HIGH		Afu1g17390	hypothetical protein	103	0.064	DOWN HIGH
Afu1g11140	Sterol desaturase family	60	0.639	UP HIGH		Afu3g00810	cholestenol delta-isomerase, putative	109	0.427	DOWN HIGH
Afu8g06980	glycosyl hydrolase, putative	66	0.72	UP HIGH		Afu3g07650	pectin methyl esterase, putative	125	0.781	DOWN HIGH
Afu2g14360	GPI anchored glucanase, putative	68	0.258	UP HIGH		Afu1g06200	Mn2+ homeostasis protein (Per1), putative	132	0.237	DOWN HIGH
Afu4g09480	extracellular endo-1,4-beta-xylanase, putative	70	0.732	UP HIGH		Afu6g00430	IgE-binding protein	144	0.057	DOWN HIGH
Afu5g12490	stress response protein rds1p	72	0.29	UP HIGH		Afu8g00720	amino acid transporter, putative	148	0.004	DOWN HIGH
Afu2g18050	FAD binding oxidoreductase, putative	73	0.605	UP HIGH		Afu2g12630	allergen Asp F13	161	0.639	DOWN HIGH
Afu4g13990	hypothetical protein	76	0.369	UP HIGH		Afu2g00820	extracellular GDSL-like lipase/acylhydrolase, putative	163	0.688	DOWN HIGH
Afu5g13780	stress response protein (Rds1), putative	79	0.397	UP HIGH		Afu4g08200	GPI transamidase component PIG-U, putative	166	0.652	DOWN HIGH
Afu3g03950	endoglucanase, putative	81	0.559	UP HIGH		Afu6g06640	FK506 suppressor Sfk1, putative	179	0.724	DOWN HIGH

Afu6g03150	hypothetical protein	86	0.774	UP HIGH		Afu3g09140	endo 1,5-alpha-arabinase	222	0.343	DOWN HIGH
Afu5g02390	Auxin Efflux Carrier superfamily	87	0.06	UP HIGH		Afu1g03150	c-14 sterol reductase	223	0.19	DOWN HIGH
Afu3g13640	extracellular serine-rich protein	91	0.639	UP HIGH		Afu2g02440	conserved hypothetical protein	224	0.704	DOWN HIGH
Afu8g05020	beta-N-acetylhexosaminidase NagA, putative	101	0.664	UP HIGH		Afu1g09150	rhomboid family protein, putative	235	0.66	DOWN HIGH
Afu1g01300	GPI anchored protein, putative	121	0.752	UP HIGH		Afu3g00820	putative exported protein	236	0.128	DOWN HIGH
Afu6g14620	fungal alpha-L-arabinofuranosidase, putative	129	0.677	UP HIGH		Afu2g16800	lectin family integral membrane protein, putative	246	0.538	DOWN HIGH
Afu3g00610	glucoamylase	131	0.554	UP HIGH		Afu1g07740	LEM3/CDC50 family protein	252	0.639	DOWN HIGH
Afu2g00760	pectate lyase A	132	0.1	UP HIGH		Afu4g07210	mitochondrial acetolactate synthase small subunit, putative	273	0.785	DOWN HIGH
Afu1g14560	alpha-mannosidase	139	0.121	UP HIGH		Afu3g07900	conserved hypothetical protein	286	0.724	DOWN HIGH
Afu2g10130	phase-specific adhesin, putative	140	0.507	UP HIGH		Afu5g02330	major allergen Asp F1	316	0.872	DOWN HIGH
Afu5g02950	conserved hypothetical protein	152	0.566	UP HIGH		Afu6g07480	endoglucanase C	333	0.804	DOWN HIGH
Afu6g00450	feruloyl esterase, putative	153	0.521	UP HIGH		Afu2g11080	glucosyltransferase (Die2), putative	339	0.258	DOWN HIGH
Afu6g09790	LysM domain protein, putative	156	0.764	UP HIGH		Afu3g08070	GMC oxidoreductase, putative	389	0.669	DOWN HIGH
Afu3g00630	conserved hypothetical protein	160	0.517	UP HIGH		Afu3g00740	2-dehydropantoate 2-reductase, putative	406	0.819	DOWN HIGH

Ribosome biogenesis and RNA metabolism	Afu2g13570	ribosome biogenesis protein (Bms1), putative	170	0.684	UP HIGH	Afu5g08310	RNA and export factor binding protein 2-I	54	0.639	DOWN HIGH
	Afu3g11220	ribonuclease T2, putative	302	0.813	UP HIGH	Afu2g05110	small nuclear ribonucleoprotein SmD1, putative	218	0.576	DOWN HIGH
	Afu7g01460	ribosomal protein S5	483	0.684	UP HIGH	Afu1g11670	small nuclear ribonucleoprotein (LSM8), putative	319	0.594	DOWN HIGH
	Afu5g11150	ribonuclease P protein subunit p29	515	0.513	UP HIGH	Afu1g09410	ribosomal protein L17	383	0.385	DOWN HIGH
	Afu5g03090	small nucleolar ribonucleoprotein complex subunit (Pwp2), putative	1308	0.639	UP LOW	Afu6g07360	ribosomal protein S8	417	0.694	DOWN HIGH
	Afu1g04280	Ribosomal protein S7p/S5e, putative	1847	0.845	UP LOW	Afu1g10310	RNase L inhibitor of the ABC superfamily, putative	447	0.811	DOWN HIGH
						Afu1g04840	RNP domain protein	502	0.738	DOWN HIGH
						Afu4g07540	small nucleolar ribonucleoprotein complex subunit, putative	512	0.258	DOWN HIGH
						Afu3g12300	Ribosomal L22e protein family	545	0.738	DOWN HIGH
						Afu6g04560	40S ribosomal protein S9, mitochondrial precursor	596	0.038	DOWN HIGH
						Afu5g11000	small nuclear ribonucleoprotein U2, A'	597	0.881	DOWN HIGH
						Afu3g13320	40S ribosomal protein S0, putative	724	0.692	DOWN MOD
						Afu4g13450	RNA methyltransferase, TrmH family family	839	0.826	DOWN MOD
						Afu5g08350	ribosomal protein S16	953	0.887	DOWN MOD

						Afu2g15210	small nuclear ribonucleoprotein (LSM2), putative	1026	0.694	DOWN MOD
						Afu1g11440	RNA export mediator Gle1, putative	1247	0.898	DOWN MOD
						Afu8g04820	ribonuclease P complex subunit p30, putative	1253	0.781	DOWN MOD
						Afu4g12170	ribosomal protein L2	1283	0.432	DOWN MOD
						Afu2g16040	rRNA biogenesis protein RRP5, putative	1422	0.37	DOWN LOW
						Afu6g04810	RNA polymerase II transcription mediator complex subunit (Med6), putative	1424	0.704	DOWN LOW
						Afu5g07390	ribosomal large subunit assembly protein (Sqt1), putative	1460	0.718	DOWN LOW
						Afu3g09620	RNA recognition motif. (a.k.a. RRM, RBD, or RNP domain) protein	1474	0.878	DOWN LOW
						Afu1g03110	60S ribosomal protein L29, putative	1548	0.752	DOWN LOW
						Afu8g04400	RNA binding protein, putative	1549	0.639	DOWN LOW
						Afu4g06350	rna binding protein	1639	0.881	DOWN LOW
						Afu1g05080	ribosomal protein P0	1825	0.639	DOWN LOW
Carbohydrate transport	Afu5g00280	MFS sugar transporter, putative	363	0.258	UP HIGH	Afu8g02010	MFS sugar transporter, putative	51	0.296	DOWN HIGH
	Afu2g10910	maltose permease	375	0.438	UP HIGH	Afu7g00950	MFS monosaccharide transporter, putative	101	0.339	DOWN HIGH
	Afu6g11920	maltose permease	941	0.519	UP MOD	Afu8g05710	MFS sugar transporter Stl1, putative	363	0.171	DOWN HIGH
	Afu1g16390	MFS hexose transporter, putative	960	0.845	UP MOD	Afu7g05550	sugar transporter family protein	607	0.713	DOWN HIGH

	Afu3g03700	Sugar transporter subfamily	976	0.866	UP MOD	Afu2g14590	MFS monosaccharide transporter, putative	697	0.513	DOWN MOD
	Afu1g03280	maltose permease, putative	1019	0.887	UP MOD	Afu8g02090	nucleotide-sugar transporter family protein	731	0.865	DOWN MOD
	Afu8g01180	MFS sugar transporter, putative	1041	0.864	UP MOD	Afu8g06870	MFS sugar transporter, putative	837	0.819	DOWN MOD
	Afu1g11050	MFS sugar transporter, putative	1092	0.856	UP MOD	Afu1g12240	MFS peptide transporter, putaitve	1268	0.873	DOWN MOD
	Afu3g02890	MFS sugar transporter, putative	1158	0.881	UP MOD	Afu6g14500	MFS sugar transporter, putative	1761	0.9	DOWN LOW
	Afu7g05830	MFS sugar transporter, putative	1425	0.85	UP LOW					
Amino acid transport	Afu1g14700	allantoate transporter, putative	277	0.669	UP HIGH	Afu4g01570	neutral amino acid permease	28	0.194	DOWN HIGH
	Afu4g10090	GABA permease, putative	541	0.519	UP HIGH	Afu8g00720	amino acid transporter, putative	148	0.004	DOWN HIGH
	Afu2g17790	amino acid transporter, putative	642	0.622	UP HIGH	Afu5g02790	amino acid permease	652	0.507	DOWN MOD
	Afu3g00120	amino acid transporter, putative	661	0.878	UP MOD	Afu8g07200	neutral amino acid permease	1651	0.849	DOWN LOW
	Afu1g09120	amino acid permease, putative	718	0.563	UP MOD					
	Afu8g00800	amino acid transporter, putative	1463	0.821	UP LOW					
	Afu8g06090	amino acid permease, putative	1602	0.887	UP LOW					
	Afu7g00440	GABA permease, putative	1888	0.928	UP LOW					
Carbohydrate/ protein glycosylation	Afu8g06980	glycosyl hydrolase, putative	66	0.72	UP HIGH	Afu1g02150	glycerol 3-phosphate dehydrogenase (GfdA), putative	172	0.66	DOWN HIGH

	Afu3g07860	glycosyl transferase, putative	1558	0.936	UP LOW	Afu6g11820	Glycosyl hydrolase family 10	522	0.764	DOWN HIGH
	Afu3g00700	glycosyl hydrolase, putative	1843	0.88	UP LOW					
Transposition associated	Afu4g01630	reverse transcriptase, putative	341	0.879	UP HIGH	Afu6g14660	reverse transcriptase, RNaseH	202	0.556	DOWN HIGH
	Afu1g04650	transposase	401	0.35	UP HIGH	Afu3g11670	DDE superfamily endonuclease/transposase, pseudogene	275	0.844	DOWN HIGH
	Afu5g06180	possible transposase	691	0.621	UP MOD	Afu6g00780	LINE-1 class reverse transcriptase, RNaseH, putative	324	0.632	DOWN HIGH
	Afu5g13900	transposase	851	0.533	UP MOD	Afu5g00270	LINE-1 class reverse transcriptase, RNaseH, putative	393	0.748	DOWN HIGH
	Afu7g02580	transposase	871	0.778	UP MOD	Afu3g15370	LINE-1 class reverse transcriptase, RNaseH, putative	460	0.609	DOWN HIGH
	Afu7g06870	Tf1-like reverse transcriptase, integrase, putative	879	0.906	UP MOD	Afu8g06290	LINE-1 class reverse transcriptase, RNaseH, putative	641	0.752	DOWN HIGH
	Afu3g10430	transposase	959	0.537	UP MOD	Afu1g00960	LINE-1 class reverse transcriptase, RNaseH, putative	681	0.609	DOWN MOD
	Afu3g03090	transposase	1022	0.715	UP MOD	Afu6g09470	reverse transcriptase, RNaseH, putative	854	0.645	DOWN MOD
	Afu2g04990	transposase	1032	0.31	UP MOD	Afu8g00310	LINE-1 class reverse transcriptase, RNaseH, putative	1036	0.725	DOWN MOD
	Afu6g10870	transposase	1049	0.577	UP MOD	Afu1g00570	Tc1-mariner transposase, putative	1180	0.51	DOWN MOD
	Afu2g01420	transposase	1160	0.895	UP MOD	Afu4g14870	LINE-1 class reverse transcriptase, RNaseH, putative	1515	0.772	DOWN LOW
	Afu1g08780	transposase	1187	0.171	UP MOD	Afu2g18080	LINE-1 class reverse transcriptase, RNaseH, putative	1524	0.849	DOWN LOW
	Afu6g10110	transposase	1285	0.328	UP MOD	Afu8g01040	reverse transcriptase, RNaseH	1622	0.85	DOWN LOW
	Afu1g05030	possible transposase	1299	0.732	UP MOD					

	Afu2g03570	transposase	1456	0.894	UP LOW						
	Afu5g09820	mariner class transposase, putative	1461	0.88	UP LOW						
	Afu6g10920	mariner class transposase, putative	1523	0.864	UP LOW						
	Afu3g09420	transposase, putative	1632	0.883	UP LOW						
	Afu4g06450	possible transposase	1693	0.611	UP LOW						
	Afu6g02880	possible transposase	1704	0.886	UP LOW						
	Afu5g02810	mariner class transposase, putative	1896	0.861	UP LOW						
	Afu5g08340	transposase	1897	0.823	UP LOW						
	Afu5g02980	mariner class transposase, putative	1928	0.878	UP LOW						
	Afu1g14760	possible transposase	1946	0.878	UP LOW						
Pathogenesis	Afu7g05060	MgtC/SapB family membrane protein	105	0.373	UP HIGH		Afu5g02330	major allergen Asp F1	316	0.872	DOWN HIGH
	Afu5g13300	aspartic endopeptidase Pep1	278	0.838	UP HIGH		Afu5g09250	transcription factor (Snd1/p100), putative	384	0.302	DOWN HIGH
	Afu3g11250	C2H2 transcription factor (Swi5), putative	732	0.878	UP MOD		Afu1g15440	alpha-1,3-glucan synthase, putative	472	0.6	DOWN HIGH
	Afu6g09610	nonribosomal peptide synthase, putative	838	0.875	UP MOD		Afu5g09580	conidial hydrophobin Hyp1/RodA	859	0.783	DOWN MOD
	Afu3g07150	succinate-semialdehyde dehydrogenase, putative	1360	0.781	UP LOW		Afu8g02750	nucleolar protein CgrA	1082	0.809	DOWN MOD
	Afu1g12930	G protein complex alpha subunit GpaB	1621	0.914	UP LOW		Afu6g02280	allergen Asp F3	1442	0.704	DOWN LOW
	Afu3g14810	pathogenicity associated protein PEP2, putative	1919	0.92	UP LOW						

Signal transduction	Afu1g06920	serine/threonine protein kinase, putative	57	0.519	UP HIGH	Afu3g14290	protein kinase, putative	133	0.694	DOWN HIGH
	Afu2g11730	Protein kinase domain-containing protein	106	0.66	UP HIGH	Afu1g09560	protein transport protein (LST8), putative	213	0.718	DOWN HIGH
	Afu2g04680	serine/threonine kinase Ste20	322	0.639	UP HIGH	Afu3g12400	G protein complex alpha subunit (GanA), putative	221	0.78	DOWN HIGH
	Afu1g13250	1-phosphatidylinositol-4,5-bisphosphate phosphodiesterase 1, putative	494	0.836	UP HIGH	Afu3g03740	protein kinase, putative	264	0.732	DOWN HIGH
	Afu2g00910	Pfs, NB-ARC and TPR domain protein	587	0.764	UP HIGH	Afu5g14060	Rho GTPase Rho4, putative	514	0.664	DOWN HIGH
	Afu5g09100	MAP kinase, putative	653	0.906	UP MOD	Afu1g04700	related to aimless RasGEF, putative	631	0.88	DOWN HIGH
	Afu8g05980	protein kinase, putative	698	0.81	UP MOD	Afu6g03160	NACHT domain protein	640	0.251	DOWN HIGH
	Afu1g10940	MAP kinase kinase kinase, putative	824	0.849	UP MOD	Afu2g14650	protein kinase domain-containing protein	1149	0.222	DOWN MOD
	Afu3g02500	protein kinase, putative	828	0.871	UP MOD	Afu2g05740	Rho GTPase ModA, putative	1379	0.539	DOWN LOW
	Afu3g05770	RAS small monomeric GTPase, putative	1020	0.813	UP MOD	Afu3g10340	Rho GTPase Rho 2, putative	1380	0.513	DOWN LOW
	Afu3g13210	protein kinase domain-containing protein	1076	0.781	UP MOD	Afu2g11100	AMFR protein, putative	1434	0.856	DOWN LOW
	Afu6g06360	mating alpha-pheromone PpgA	1219	0.852	UP MOD	Afu1g05210	G-protein complex gamma subunit Ste18	1697	0.83	DOWN LOW
	Afu6g08590	protein kinase, putative	1486	0.883	UP LOW					
	Afu4g00320	sensor histidine kinase/response regulator, putative	1510	0.795	UP LOW					
	Afu5g05750	protein kinase, putative	1531	0.912	UP LOW					

	Afu5g09320	signal transduction protein (Syg1), putative	1609	0.798	UP LOW					
	Afu5g08950	RAS small monomeric GTPase (Rsr1), putative	1610	0.731	UP LOW					
	Afu4g07400	sensor histidine kinase/response regulator, putative	1616	0.88	UP LOW					
	Afu1g12930	G protein complex alpha subunit GpaB	1621	0.914	UP LOW					
	Afu6g11190	protein kinase (VPS15), putative	1697	0.727	UP LOW					
	Afu6g08350	retrograde regulation protein 2	1869	0.906	UP LOW					
Sphingolipid biosynthesis							Afu5g02760	fatty acid elongase (Gns1), putative	183	0.751	DOWN HIGH
							Afu6g10460	ceramide synthase membrane component (Lag1), putative	1270	0.865	DOWN MOD
Transcription factors	Afu5g01270	C6 transcription factor, putative	54	0.732	UP HIGH		Afu5g01460	C6 finger domain protein, putative	71	0.409	DOWN HIGH
	Afu7g00410	C6 transcription factor, putative	75	0.058	UP HIGH		Afu6g12160	C6 transcription factor, putative	91	0.507	DOWN HIGH
	Afu2g08240	C6 transcription factor, putative	84	0.621	UP HIGH		Afu2g05360	C6 transcription factor, putative	160	0.674	DOWN HIGH
	Afu5g14230	C6 transcription factor, putative	88	0.710	UP HIGH		Afu5g02270	C6 transcription factor, putative	230	0.328	DOWN HIGH
	Afu8g04180	C2H2 zinc finger protein	109	0.684	UP HIGH		Afu5g09740	C6 transcription factor, putative	268	0.704	DOWN HIGH

Afu6g08550	C6 transcription factor, putative	676	0.554	UP MOD
Afu8g02640	C6 transcription factor, putative	689	0.577	UP MOD
Afu2g17800	C6 transcription factor, putative	692	0.770	UP MOD
Afu1g03860	C6 transcription factor (AmdR), putative	693	0.554	UP MOD
Afu6g12130	C6 transcription factor, putative	716	0.433	UP MOD
Afu7g04820	C6 transcription factor, putative	726	0.741	UP MOD
Afu3g11250	C2H2 transcription factor (Swi5), putative	732	0.864	UP MOD
Afu2g08040	C6 finger domain protein, putative	1503	0.592	UP MOD
Afu1g10080	C2H2 transcription factor, putative	1519	0.724	UP MOD
Afu1g11620	C6 transcription factor (QutA), putative	1813	0.813	UP LOW
Afu2g04250	C6 finger domain protein, putative	1817	0.538	UP LOW
Afu2g10550	C2H2 transcription factor (RfeC), putative	1832	0.557	UP LOW

Afu3g02070	C2H2 transcription factor, putative	832	0.853	DOWN MOD
Afu1g16830	C6 transcription factor, putative	900	0.733	DOWN MOD
Afu1g16830	C6 transcription factor, putative	995	0.489	DOWN MOD
Afu1g10280	C2H2 finger domain protein (Gli3), putative	1014	0.312	DOWN MOD
Afu1g10280	C6 transcription factor, putative	1061	0.704	DOWN MOD
Afu5g06460	C6 finger domain protein, putative	1064	0.85	DOWN MOD
Afu8g05750	C6 finger domain protein, putative	1072	0.813	DOWN MOD
Afu5g09890	C6 finger domain protein, putative	1358	0.85	DOWN LOW
Afu8g01140	C6 transcription factor, putative	1425	0.823	DOWN LOW
Afu3g02320	C2H2 finger domain protein (Kin17), putative	1472	0.838	DOWN LOW
Afu1g16220	C6 transcription factor, putative	1491	0.887	DOWN LOW
Afu6g14580	C6 finger domain protein, putative	1502	0.788	DOWN LOW

Afu2g05830	C6 finger domain protein, putative	1853	0.813	UP LOW	Afu1g17460	C6 transcription factor, putative	1597	0.868	DOWN LOW
Afu6g05160	C2H2 transcription factor (Azf1), putative	1856	0.402	UP LOW	Afu2g16230	C2H2 finger domain protein, putative	1623	0.609	DOWN LOW
Afu3g11990	C6 transcription factor (Mut3), putative	1863	0.856	UP LOW	Afu3g02590	C6 transcription factor, putative	1640	0.881	DOWN LOW

Time-point specific trends in gene expression were similar to those observed for the Af293 isolate. Pathogenesis associated genes increased between 4 – 8 hours, including an aspergillus haemolysin (Afu3g00590), mycelia catalase (Afu3g02270), metalloproteinase Mep (Afu8g07080), Asp F4 (Afu2g03830) and Asp F1 (Afu5g02330). Genes encoding known and putative antigens increased in transcript abundance at this time-point. Genes directing sphingolipid biosynthesis also increased between 4 – 8 hours (n = 6), although fewer in number than observed for the Af293 isolate (n = 11). Genes involved in signal transduction were also employed from the earliest time-point, with some additional genes upregulated between 8 – 14 hours. As observed in Af293, fungal cell wall biosynthetic genes were upregulated at both time-points, but were notably more common between 8 – 14 hours (Tables 3.19, 3.20, 3.37 and 3.38).

3.5.6 Characterisation of Δ*laeA* time-point specific datasets: chromosomal loci, lineage specificity and functionality

Relative distribution of upregulated and downregulated datasets were investigated among gene categories of interest, where significant enrichment of either was defined by Chi-square analyses, with the null hypothesis that equal numbers of upregulated and downregulated genes occur in each cohort (Table 3.39, 3.40 Figure 3.28).

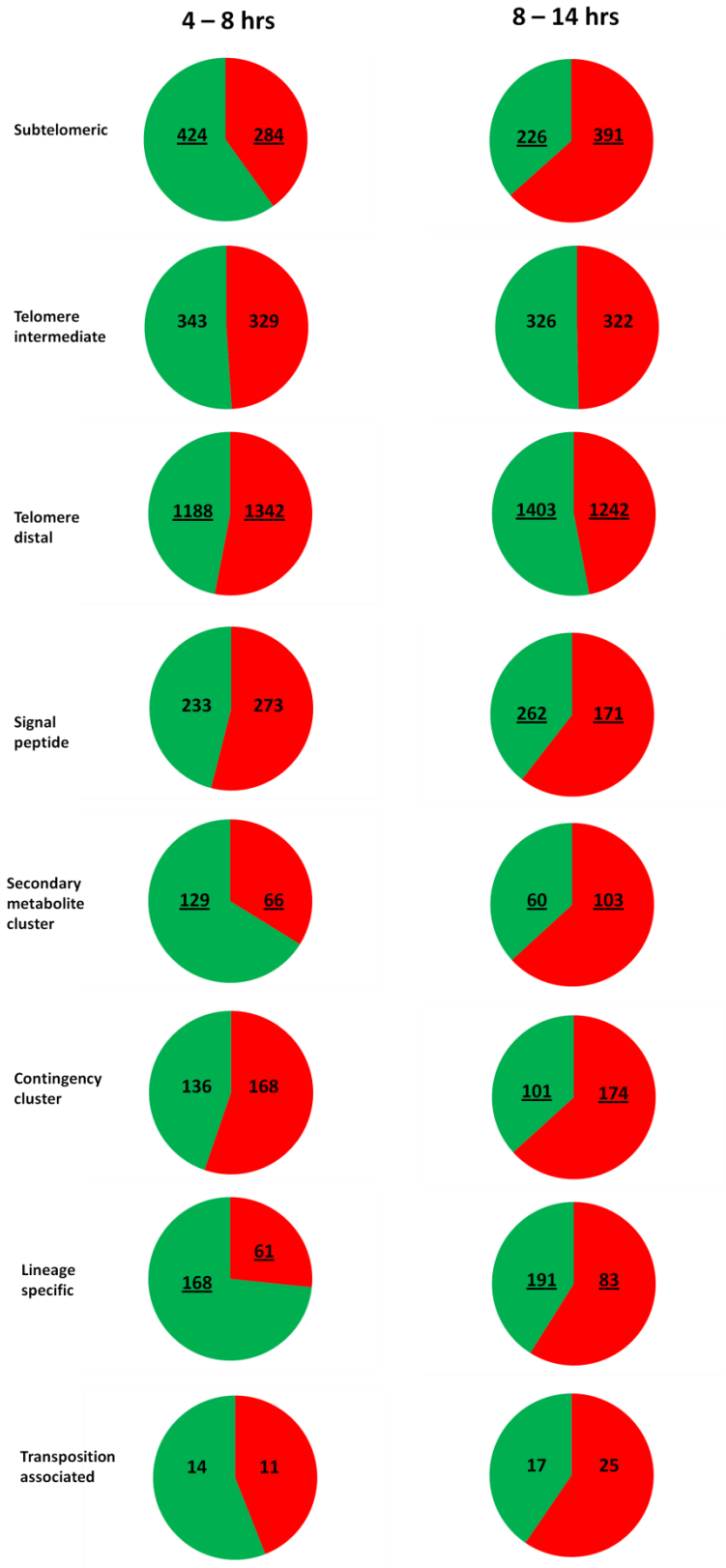


Figure 3.20: Distribution of differentially expressed genes between 4 – 8, and 8 - 14 hours post infection among the functional cohorts of chromosomal location, signal peptide content, *A. fumigatus* specificity and functional association. Distribution of genes in increasing (red) and decreasing (green) datasets among gene cohorts of interest to this study. Underlined values significantly deviate from the null hypothesis that an equal number of upregulated or downregulated genes will occur in each cohort, as tested by Chi-square analysis.

Upregulated genes were significantly enriched relative to downregulated genes among subtelomeric, signal peptide, secondary metabolite and contingency cluster cohorts between 8 – 14 hours (Figure 3.20). However, the number of upregulated genes within all these datasets was lower than in Af293 at the same time-point (Figure 3.11). Interestingly, the observed increase in 29 transposon-associated genes observed for Af293 at the 8 – 14 hours was somewhat lessened in the Δ*laeA* strain (n = 25), which also saw greater numbers of putative mobile elements downregulated (Table 3.38).

	Number of genes	Differentially expressed	Up (observed)	Down (observed)	Up (expected)	Down (expected)	Chi-square	p-value
0-300 kb	1509	708	284	424	354	354	27.68	< 0.0001
301- 600 kb	1634	672	329	343	336	336	0.29	0.5892
>600 kb	6373	2530	1342	1188	1265	1265	9.37	0.0022
Signal P	1103	506	273	233	253	253	3.16	0.0754
Secondary metabolism	337	195	66	129	97.5	97.5	20.35	< 0.0001
Infection cluster	594	304	168	136	152	152	3.36	0.0665
Aspergillus specific	596	229	61	168	114.5	114.5	49.99	< 0.0001
Transposition associated	68	25	11	14	12.5	12.5	0.36	0.5485

Table 3.39: Distribution and Chi-square analysis of differentially expressed genes categorised by chromosomal location, signal peptide content, *A. fumigatus* specificity and functional association among 4 – 8 hour datasets. Chi-square analysis with one degree of freedom was used to test the distribution of upper and lower quartiles with respect to cohorts of interest to this study, with the null hypothesis that even numbers of upregulated or downregulated genes occur in each group.

	Number of genes	Differentially expressed	Up (observed)	Down (observed)	Up (expected)	Down (expected)	Chi-square	p-value
0-300 kb	1509	617	391	226	308.5	308.5	44.12	< 0.0001
301- 600 kb	1634	648	322	326	324	324	0.025	0.8751
>600 kb	6373	2645	1242	1403	1322.5	1322.5	9.8	0.0017
Signal P	1103	433	262	171	216.5	216.5	19.12	< 0.0001
Secondary metabolism	337	163	103	60	81.5	81.5	11.34	0.0008
Infection cluster	594	275	174	101	137.5	137.5	19.37	< 0.0001
Aspergillus specific	596	202	119	83	101	101	6.41	0.0113
Transposition associated	68	42	25	17	21	21	1.52	0.217

Table 3.40: Distribution and Chi-square analysis of differentially expressed genes categorised by chromosomal location, signal peptide content, *A. fumigatus* specificity and functional association among 8 – 14 hour differentially expressed datasets. Chi-square analysis with one degree of freedom was used to test the distribution of upper and lower quartiles with respect to cohorts of interest to this study, with the null hypothesis that even numbers of upregulated or downregulated genes occur in each group.

The general trend towards increase in secondary metabolite gene expression at 8 - 14 hours was particularly pronounced at specific loci, most notably the gliotoxin biosynthetic cluster, which was also noticed in Af293 (Figure 3.21). NRPS and PKS genes directing the biosynthesis of many secondary metabolites, including the hybrid NRPS/PKS *psoA* (Afu8g00540) showed similar expression profiles (Figure 3.22).

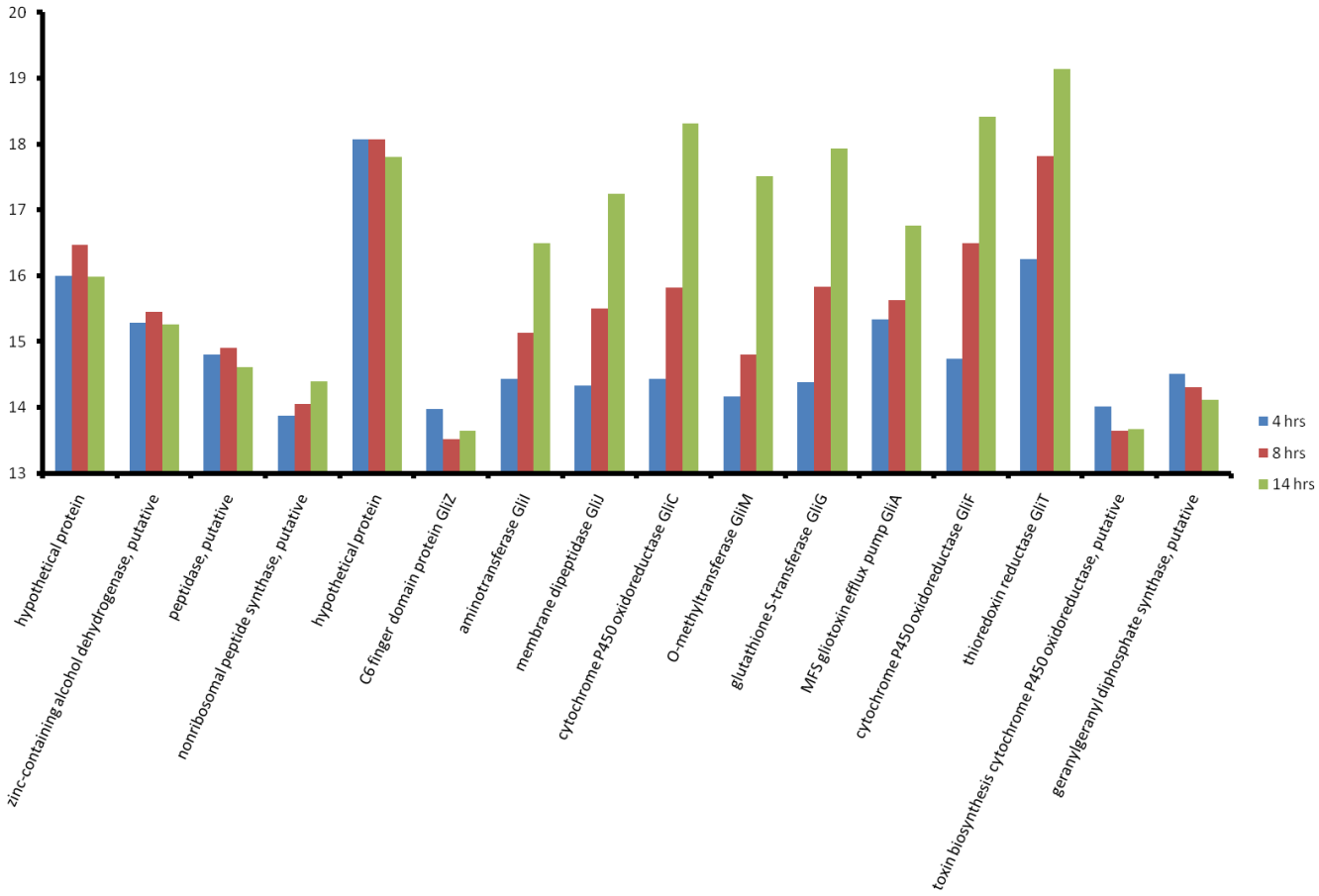


Figure 3.21: nSI values for genes in the gliotoxin biosynthetic cluster at 4, 8 and 14 hours post infection. nSI for genes putatively in the gliotoxin biosynthetic cluster as annotated by Perrin et al. 2007 is shown. Expression for the the NRPS *gliP* failed quality control filtering. Increase in transctript abundance was most notable between 8 and 14 hours.

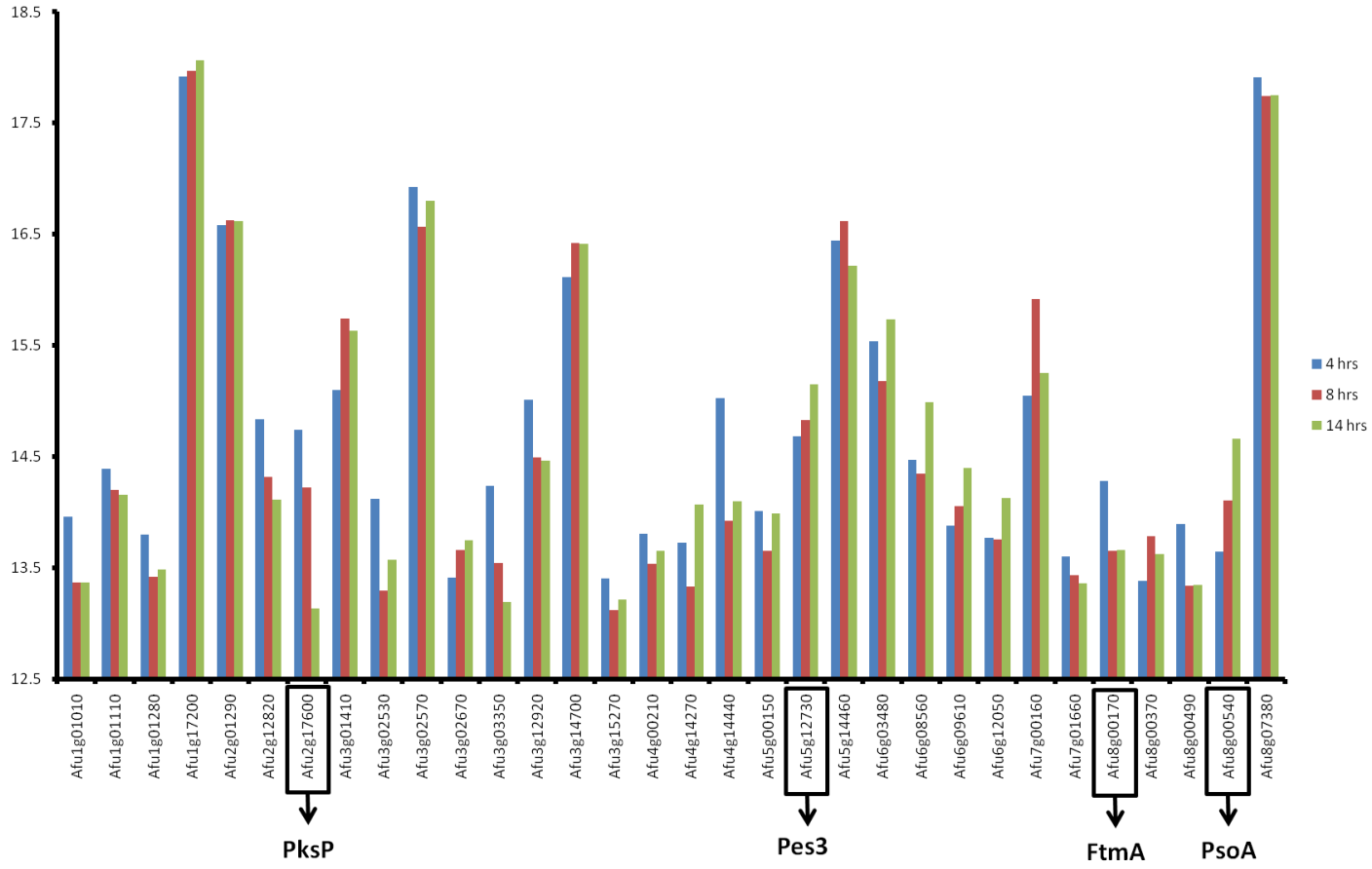


Figure 3.22: nSI values for Δ*laeA* NRPS and PKS genes at 4, 8 and 14 hours post infection. nSI for 30 putative NRPS and PKS are shown. Several genes are upregulated between 8 - 14 hours. Genes highlighted is the DHN-melanin gene PksP, and three genes which are studied in Chapter 4 of this thesis.

3.5.7 STEM profiling of temporal gene expression in Δ*laeA* during murine infection

In order to assign gene functionality to specific temporal expression profiles, the Δ*laeA* infection time-course was analysed using using STEM software. STEM output profiles are shown in Figure 3.23. 13 profiles, grouped into 3 clusters are significantly enriched according to this analysis. GO analyses was used to determine over-represented functional categories in each cluster for which a p value cut-off of 0.2 was applied. Both red and green clusters reported enrichment under these conditions (Tables 3.41 and 3.42).

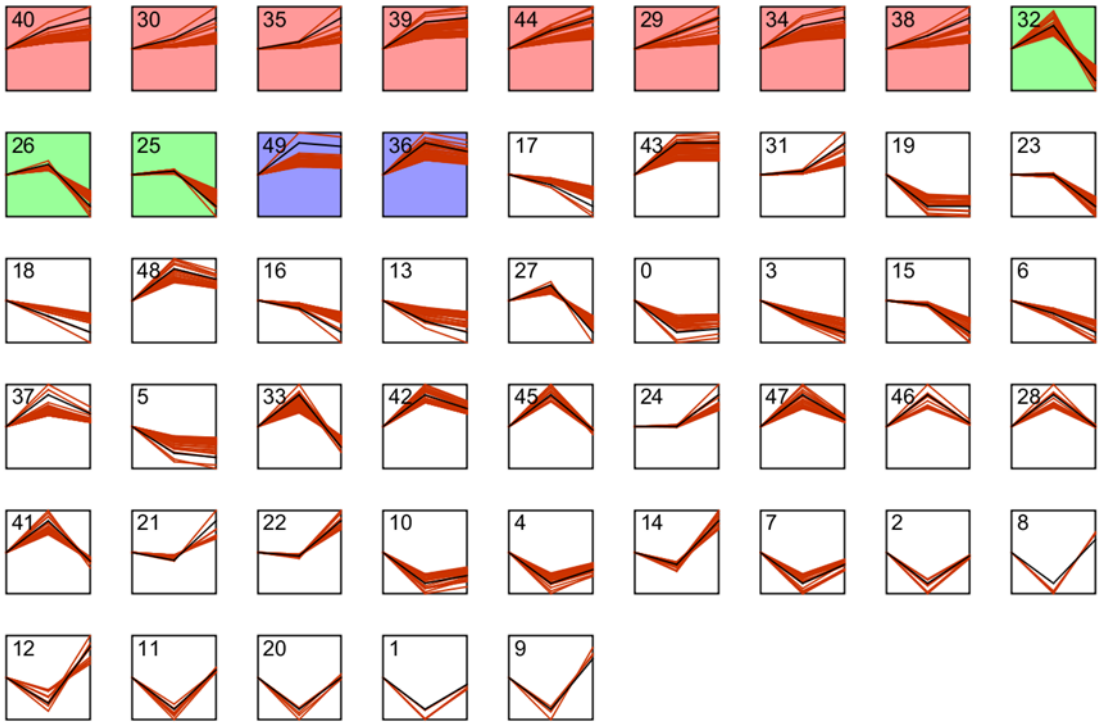


Figure 3.23: Transcription profile clustering analyses of the Δ*laeA* infection time-course. Statistically significant profiles are coloured and grouped into 4 clusters. Model profiles are shown with a single black line. Genes assigned are shown in red.

Category Name	#Genes Category	#Genes Assigned	#Genes Expected	#Genes Enriched	p-value	Corrected p-value
Contingency cluster	284	42	24.5	17.5	2.60E-04	0.046
integral to plasma membrane	48	12	4.1	7.9	5.70E-04	0.08
plasma membrane	122	21	10.5	10.5	1.50E-03	0.2

Table 3.41: Significant GO terms among the red cluster during the Δ*laeA* time course. Bonferroni corrected *p*-value represents the probability of observing the number of genes from the specific GO term from randomly assigned entities.

Category Name	#Genes Category	#Genes Assigned	#Genes Expected	#Genes Enriched	p-value	Corrected p-value	Fold
molecular function unknown	398	26	15	11	3.30E-03	0.162	1.7

Table 3.42: Significant GO terms among the green cluster during the Δ*laeA* time course. Bonferroni corrected *p*-value represents the probability of observing the number of genes from the specific GO term from randomly assigned entities.

Additionally, individual profiles were investigated with respect to enrichment of functional categories using GO analyses (Table 3.43).

Category Name	#Genes Category	#Genes Assigned	#Genes Expected	#Genes Enriched	p-value	Corrected p-value
Profile 30						
transcription factor activity	59	5	0.3	4.7	1.60E-05	0.009
Contingency clusters	284	8	1.5	6.5	1.50E-04	0.089
Profile 34						
plasma membrane	122	5	1.4	3.6	0.01	0.1
Profile 38						
Contingency cluster	284	7	2.6	4.4	0.01	0.11
Profile 49						
plasma membrane	122	6	1.7	4.3	7.10E-03	0.112

Table 3.43: Significant GO terms among profiles 30, 34, 38 and 49 in the Δ*laeA* time-course experiment. GO enrichment analysis for significant STEM profiles was conducted with functional categories satisfying a 0.2 corrected p-value cut-off reported**.**

In addition to plasma membrane and contingency cluster enrichment, this analysis reported the over-representation of transcription factor activity (n = 5). This included a putative melanin biosynthesis regulator RegA, which is found in a secondary metabolite cluster in the subtelomeric region of chromosome 1. Model profiles were also ordered based on enrichment of functional categories, enabling identification of temporal profiles most closely associated with specific groups of interest (Figure 3.24).

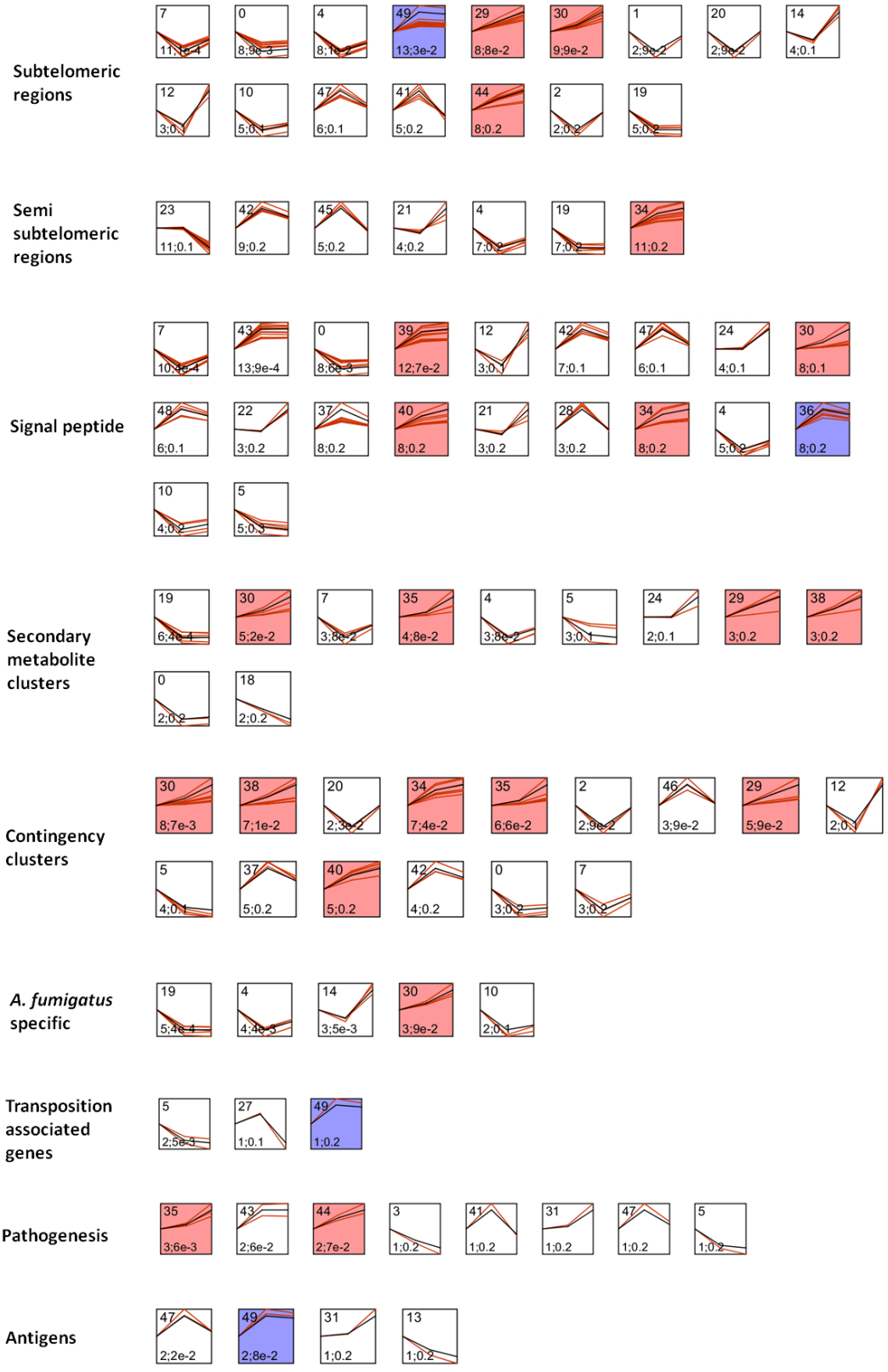


Figure 3.24: STEM clustering analysis of differentially expressed genes in the Δ*laeA* time-course ordered on the basis of enrichment of genes within location and functionally related cohorts. Values in the top left corner denote the profile number. The bottom left corner is the number of genes belonging to the cohort of interest, followed by the *p*-value for enrichment in the respective profiles. Profiles passing an 0.2 *p*-value cut-off are shown. In this analysis red lines show expression profiles only of genes from the cohort of interest.

Comparable expression profiles of contingency cluster, pathogenesis related and putative antigens were observed between Af293 and Δ*laeA* with the majority of transcripts within these cohorts increasing. In addition, the variable expression profiles of transposition associated genes were observed in both strains. The co-ordinated upregulation of genes directing gliotoxin biosynthesis between 8 and 14 hours was maintain in the LaeA deletant, with 9 genes from the cluster distributed between profiles 29, 30, 35 and 38.

3.6.1. Summary

This study aimed to define transcriptional changes throughout the multitime-point *A. fumigatus* infection process and the basis of aberrant gene expression in an *A. fumigatus* Δ*laeA* mutant in the host. Critically, Af293 and Δ*laeA* were selected to enable the elucidation of the transcriptional basis of *A. fumigatus* virulence and attenuation respectively. Consequently array experiments were designed such that co-hybridisations with Af293 and Δ*laeA* cDNAs facilitated comparative analyses of the strains directly at specific time-points (Chapter 8), and non-ratiometric normalisation enabled strain specific information to be analysed across the time course (this Chapter). The latter approach has been used to identify environmental challenges to host colonisation, and ascertain putative pathogen molecules which interact with the host throughout early infection. In addition, this Chapter describes the development of a non-ratiometric normalisation protocol which is rapid, relatively cost and labour efficient, and easily extendable to the study of other clinical or recombinant isolates.

Non-ratiometric analysis of microarray data employed in this Chapter treats individual intensity channels from a dual colour array as single channel experiments ('t Hoen et al. 2004, Bossers et al. 2010a). This strategy was employed for two main reasons. Firstly, the non-ratiometric method enables interrogation of both strain (e.g. Af293 4hrs vs Δ*laeA* 4hrs) and time-point variables (e.g. Af293 4 hrs/Af293 8 hours) with a minimal number of arrays. This maximises the number of technical and biological replicates which can be conducted from a given number of microarray slides. Secondly, adaptation of the non-ratiometric method to analyse other isolates or time-points of infection requires less arrays than loop designs, and is more data efficient than a common reference design. Accordingly, the non-ratiometric approach developed in this Chapter is a tool which is intended to be expanded to other isolates, time-points and murine models of infection following the completion of this study.

The need for normalisation between time-points arises due to the variation in sample preparation, production of arrays and processing of arrays, which can bias gene expression profiles, thus impeding or distorting biological interpretation (Bolstad et al. 2003). The most appropriate normalisation method for any array experiment is a controversial issue, which must consider strengths and weaknesses of the method employed. With regard to the non-ratiometric array analyses, two normalisation strategies were considered. For initial experiments not reported in this thesis, intensities on every array were scaled to constitutively expressed genes which have theoretically stable expression levels, such as gpdA (Afu5g01970) or beta tubulin (Afu7g00250).

This approach mimics that of Affymetrix Genechip® Human Genome Arrays, which are scaled to intensity values of 100 “house-keeping” genes. However, this strategy was found to introduce significant bias to intensity datasets, as the choice of house-keeping gene altered gene expression profiles between time-points. This is likely due to the differential expression of putative house-keeping genes throughout infection. Indeed, a study has questioned the constitutive expression of Affymetrix Genechip® Human Genome Array house-keeping genes (de Jonge et al. 2007). Accordingly, scaling to constitutively expressed genes was discontinued.

In a second approach, quantile-normalisation of spot intensities was applied to facilitate inter-array comparisons throughout the time course (Figure 3.2 and 3.3). During quantile normalisation, the lowest signal from each array is replaced by the average of all of the lowest signals, the second lowest on each array is replaced by the average of all of the second lowest, and so forth (Bolstad et al 2003). Quantile normalisation facilitates inter-array comparisons as the algorithm forces all arrays to have equal intensity distribution. A possible disadvantage is the assumption that the distributions of spot intensities are identical between arrays, which may not be the case in the upper tails of the intensity distribution (Bolstad et al. 2003). Consequently, for spots of highest intensity, differences between time-points may be underestimated using quantile normalisation. Nevertheless, the significant advantage to quantile normalisation is the avoidance of a baseline array, which is required for both linear regression and non linear (e.g. LOWESS) normalisation. With regard to technical performance, quantile normalisation performed in this study required low computational power and was fast. Quantile normalisation has become widely used for single channel experiments since its initial publication by Bolstad and co-workers, and the utility of this approach is evidenced by the readily available algorithms in Bioconductor, Genespring (Agilent) and a Python module available online (Bolstad et al. 2003, Baber et al. 2010). Moreover, quantile normalisation was used in two studies which utilised a non-ratiometric approach to analyse dual colour microarrays (Bossers et al. 2010b, Nota et al. 2010).

The most appropriate method for identifying differential expression can be viewed as a compromise between acceptance of false negative and false positive error rates (Quackenbush 2002). It was hypothesised that cellular differentiation and adaptation to the murine lung during early infection would result in extensive transcriptional changes between time-points. This hypothesis is supported by *in vitro* microarray studies, which do not take into account the multifaceted host niche yet identify several hundred differentially expressed genes, for example between planktonic and biofilm growth (n = 740), following heat shock (n = 726), or culture with or without amphotericin B (n = 295) (Bruns et al. 2010a, Do et al. 2009, Gautam et al. 2008).

Moreover, comparative transcriptional profiling between *A. fumigatus* germlings isolated from the murine lung with developmentally matched laboratory culture has identified thousands of differentially expressed genes (n = 2178).

To accommodate the expected dearth of growth-associated gene expression change, without biasing conclusions on infection-related changes, the use of an arbitrary cut-off was avoided, in favour of studying upper and lower quartiles. Accordingly, half the genes which passed quality control filtering were defined as differentially expressed, equating to 3948 and 3910 for Af293 and Δ*laeA* respectively. A disadvantage to this approach is the acceptance of high numbers of false positives, i.e. identifying a gene as differentially expressed when actually it has similar transcript levels between time-points. False positives would be considerably reduced by analyses using fold cut-offs and false discovery corrected *t*-statistics reported by other studies (McDonagh et al. 2008).

In general, the acceptance of false positives can be viewed as appropriate to the aims of this study, which is interested in *A. fumigatus* physiological and biochemical changes directed by many genes. Consequently stringent control of false positives in which small gene lists are produced with high confidence by rigorous statistical analyses would greatly limit interpretation of the dataset. Nevertheless, to limit the inclusion and impact of false positives, several steps were taken. Firstly, quality control was conducted to omit nSI values which were not compiled from sufficient replicates (count filtering), or which varied unacceptably between technical and biological replicates (standard deviation filtering). These quality control approaches were stringent, with an average of 940 ORFs (9.9% of total dataset) removed from each time-point in the experiment. Secondly, differential expression between time-points was divided into high, moderate and low categories, which in addition to aiding biological interpretation of the datasets can be used as a measure of confidence in differential gene expression, i.e. a gene with “high” expression change can be considered less likely to be a false positive than a gene with “low” expression change. The utility of these categories is highlighted by the analyses of putative secondary metabolite gene deletants (Chapters 4 and 5), epitope tagging of 24 putative proteins (Chapter 6) and the expression and purification of two putative allergens (Chapter 7) conducted in this thesis, all of which focused on gene expression changes which were defined as “high”. Finally, FDR corrected p values from a one-way ANOVA were reported, but not used to filter genes from the final datasets. While it is most common for studies analysing the host infecting fungal transcriptome to use fold change and *t*-tests to define differential expression (Kamper et al. 2006, McDonagh et al. 2008, Mosquera et al. 2009, Walker et al. 2009), other authors have relied on fold changes alone

(Thewes et al. 2007). Readers wishing to determine a subset of genes differentially expressed between time-points with highest confidence can easily interrogate the dataset based on the *p*-values from the one way ANOVA, which are currently being complied into MIAME format for publication.

Transcriptional profiling has proved an essential tool in elucidating the molecular basis of host environmental adaptation for both animal and plant fungal pathogens (Cairns et al. 2010, Hu et al. 2008, Kamper et al. 2006, Mosquera et al. 2009, Thewes et al. 2007, Walker et al. 2009). Work described in this Chapter presents a key insight into challenges to host colonisation, and how they are overcome by the different morphologies of *A. fumigatus*. This section discusses gene expression in the wild-type isolate. *A. fumigatus* growth and differentiation is a defining feature of IPA. Germination and hyphal production is a prerequisite for extensive pulmonary necrosis and dissemination characteristic of this disease (Tekaia and Latge 2005). Accordingly, identification of conserved genes required for growth which are upregulated during infection offers a potential strategy for elucidating novel antifungal drug targets which impede growth or effect cell death (Hu et al. 2007). This study has identified numerous genes with increased transcript abundance in the murine lung which are associated with *A. fumigatus* growth, including those directing establishment of cell polarity, microtubule biosynthesis, cell wall remodelling, and ergosterol biosynthesis. This discussion will consider transcriptional analyses of the fully virulent Af293 isolate before examining gene expression in Δ*laeA*. Additionally, a full discussion regarding growth and differentiation *in vivo* and *in vitro* is considered in the final discussion (Chapter 9).

A. fumigatus hyphae grow via polar extension, in which addition of new materials occurs at the tips of hyphae. The spore and invasive hyphae represent isotrophic and polar morphologies respectively. Accordingly, transcriptional comparisons between 4 and 14 hour time-points identified numerous genes associated with the establishment of cell polarity, including septins (Afu5g03080, Afu1g08850, Afu7g05370), cell polarity proteins and a protein phosphatase involved in actin filament organisation (Afu1g05610). Transcript for the putative nuclear migration protein AspA (Afu5g07710) greatly increased between 4 and 14 hours. Deletion of the *aspA* homologue in *A. nidulans* results in the restriction of nuclei into primary buds, resulting in developmental arrest (Fischer and Timberlake 1995). A similar transcriptional increase was observed for the putative cell wall polarity protein *tea1* (Afu2g02520). Intriguingly, the putative Rho GTPase Rho4 (Afu5g14060) was also upregulated between 4 and 14 hours post infection. Rho4 is a component of a highly conserved class of signalling proteins which play a crucial role in polarity establishment, cell wall integrity, septum formation and actin dynamics in *A. niger* (Kwon et al. 2011).

The microtubule cytoskeleton is a fundamental component of eukaryotic cells, and plays essential roles in establishment of spatial organisation, spindle organisation, cell division and polarised cell growth. The transcriptional profile of the invading fungus clearly reveals numerous genes and biological processes associated with the establishment of cell polarity. The inhibition of these processes via novel antifungals may represent a potential strategy for impeding the establishment of infection. Comparison of differentially expressed genes from this study, with the dataset generated from developmentally matched germlings (McDonagh et al. 2008) was enriched with cell polarity and cell wall biosynthetic genes. These data support the general premise that time-series experimentation are more representative of key aspects of host colonisation.

Twenty six genes associated with cell wall remodelling were upregulated between 4 – 14 hours. Of particular note was the moderate increase in transcript abundance of the putative echinocandin drug target, the 1,3-beta-glucan synthase catalytic subunit FksP (Afu6g12400). This observation validates the use of transcriptional profiling for the identification of putative *A. fumigatus* antifungal targets. Inspection of the time-point specific datasets clearly showed a preference for genes associated with cell wall biosynthesis between 8 – 14 hours, at the time-point when extensive cell wall remodelling occurs during hyphal production. During the 8 – 14 hour stage of infection genes with increasing expression were enriched in GO processes related to cellular polysaccharide metabolism and the fungal cell wall (Table 3.12). The *A. fumigatus* cell wall is composed mainly of polysaccharides including β-1,3-glucan, chitin, galactomannan, β-1,3/ β-1,4-glucan and α-1,3-glucan. Conversion from a resting conidia to germinating conidia and hyphae involves extensive change to the cell wall, requiring both hydrolase and synthase activities. The contribution of many of these genes to cell wall integrity and therefore the establishment of infection remains to be determined.

With regard to fatty acid and lipid biosynthesis, ergosterol is an important component of the fungal membrane which regulates membrane fluidity, distribution of integral membrane proteins and control of cell cycle (Alcazar-Fuoli et al. 2008). Ergosterol biosynthesis is essential for growth, as evidenced by inviability of a 14 α-demethylase Erg11A and Erg11B double deletant (Hu et al. 2007) and the molecular inhibition of this pathway using azole antifungals (Nagappan and Deresinski 2007). Transcriptional comparisons between 4 and 14 hour time-points identified 12 genes involved in ergosterol biosynthesis as employed during infection, including the drug target Erg11A (Afu4g06890). This observation further validates the use of transcriptional profiling for the identification of putative *A. fumigatus* antifungal targets.

Significant themes among genes having decreased transcript abundance during infection include ribosome biogenesis, RNA metabolism and protein biosynthesis. Comparative profiling by McDonagh and co-workers attributed reduction of similar *A. fumigatus* processes in the host to a TOR kinase mediated mechanism, a signalling cascade which links protein synthesis and cellular growth to nutrient availability (McDonagh et al. 2008). While comparisons of differentially expressed genes from this study with the dataset of *S. cerevisiae* following rampamycin upregulated TOR inhibition revealed poor concordance (data not shown) elevation of certain genes throughout infection was suggestive of nutrient limitation.

Analyses of genes differentially expressed between 4 – 14 hours demonstrate upregulation of the cross pathway control transcription factor CpcA. The cross pathway control system is a signal transduction cascade which regulates fungal nitrogen metabolism with respect to amino acid homeostasis. The system includes a dimeric kinase which perceives amino acid starvation to activate the transcription factor CpcA (Krappmann et al. 2004). Under amino acid replete conditions, such as histidine starvation, CpcA becomes expressed at high levels which activates many genes involved in biosynthesis of amino acids (Natarajan et al. 2001). In *A. fumigatus cpcA* is required for wild-type growth in conditions of tryptophan starvation, and is required for full virulence in a murine model of infection (Krappman et al. 2004). The transcriptional profile of *cpcA* is therefore consistent with conditions of nitrogen starvation in the host, and requirement for the cross pathway control system for murine virulence. A striking feature of the dataset was the employment of numerous secreted protease and peptidase enzymes, particularly between 4 and 8 hours. These enzymes may be utilised to acquire nitrogen from the proteinaceous lung matrix. Further supporting the challenge of nitrogen limitation to host colonisation was the employment of numerous genes associated with amino acid transport.

In support of the fundamental role of iron acquisition in *A. fumigatus* virulence (Schrettl et al. 2004, Schrettl et al. 2007) numerous genes associated with iron homeostasis and acquisition demonstrated increased transcript abundance during infection. *A. fumigatus* scavenges iron in low iron environments by siderophore-mediated Fe^{3+} uptake and reductive iron assimilation (RIA). Three genes required for siderophore biosynthesis were upregulated between 4 and 8 hours, including the L-ornithine N5-oxygenase *sidA* (Afu2g07680), palmitoyltransferase *sidR* (Afu2g07670), and a putative siderochrome-iron transporter (Afu3g13670). Between 8 an 14 hours, a further 3 siderophore associated genes demonstrated increased transcript abundance, including a MFS family siderophore transporter (Afu3g03440), siderophore biosynthesis acetylase SidF (Afu3g03400) and siderochrome-iron transporter Sit1 (Afu7g06060).

In the postulated siderophore biosynthesis pathway, SidA catalyses the biosynthesis of N^5-hydroxy-L-ornithine from L-ornithine (Schrettl et al. 2004). N^5-hydroxy-L-ornithine is the precursor to the extracellular siderophore triacetylfusarinine C (TAFC) and the intracellular siderophore ferricrocin (Schrettl et al. 2004). SidF converts N^5-hydroxy-L-ornithine to N^5-*cis*anhydromevalonyl-N^5-hydroxy-L-ornithine and is required for TAFC biosynthesis (Schrettl et al. 2004). Δ*sidA* and Δ*sidF* are avirulent, and attenuated, in neutropenic murine models of infection respectively (Schrettl et al. 2004, Schrettl et al. 2007). Thus, the physiological relevance and normalisation protocols employed in this study are valid with respect to identifying environmental adaption essential for *A. fumigatus* virulence. Interestingly, the high affinity iron permease *ftrA* (Afu5g03800) involved in RIA was moderately increased between 8 – 14, although this mechanism of iron acquisition is not required for virulence (Schrettl et al. 2004). Multiple genes involved in the uptake, mobilisation and utilisation of other crucial ions also increased in transcript abundance, including three zinc ion transporters (Afu1g01550, Afu2g03860, Afu4g09560), a calcium binding protein (Afu1g02930) calcium sensor (Afu6g14240), calcium translocating ATPase (Afu3g10690) and four copper transporters (Afu4g12620, Afu1g16130, Afu6g02810, Afu2g03730). Consequently, transcriptional analyses of the initiation of *A. fumigatus* infection are suggestive of a nutrient limited niche wherein processes which likely support nutrient acquisition in the soil facilitate colonisation of the immunocompromised host.

Genes which are putatively involved in alkaline adaptation were not a striking feature of increasing or decreasing datasets throughout the time course of murine infection. This is best demonstrated by comparisons between the 4 vs 14 hour datasets with an *in vitro* alkaline adaptation dataset (Loss et al. 2011 in preparation, Table 3.9). Loss and co-workers investigated the transcriptional profile of mycelia following shift from pH 5.0 to 8.0. This identified 446 and 117 genes with increased and decreased transcript abundance respectively. Comparisons of these datasets with 4 – 14 hour *in vivo* profiling revealed low concordance, with only 145 and 29 genes upregulated and downregulated in both experiments respectively. Nevertheless, some concordance between the datasets is identifiable, most notably in genes associated with cell membrane transport, a process greatly impacted by external pH due to the reliance of many transporters on the membrane proton gradient. A possible explanation of the lack of alkaline responsive genes identified by this study is the first time-point analysed, i.e. 4 hours post infection. Work conducted by Loss and co-workers demonstrated extensive transcriptional responses to alkaline stress within 1 hour. Accordingly, all time-points of infection profiled in this study are likely in the context of an established alkaline stress response. The relevance of alkaline stress to host colonisation is strongly supported by transcriptional comparisons between *A. fumigatus* germlings isolated from

the murine lung with developmentally matched laboratory culture, which identified the increased transcript abundance of genes associated with alkaline stress in the mammalian host (McDonagh et al. 2008), and the necessity of alkaline responsive transcriptional regulator PacC for wild-type *A. fumigatus* virulence (Bertuzzi et al. unpublished).

Work conducted by Grahl and co-workers utilised the hypoxia marker pimonidazole hydrochloride to visually demonstrate hypoxic conditions were associated with fungal lung lesions and inflammation in murine models of *A. fumigatus* infection (Grahl et al. 2011). In the high dose infection model employed in this study, considerable inflammation occurs, especially at the latest invasive time-point. Accordingly, it is reasonable to hypothesise that hypoxic conditions are encountered in this model, most notably at 14 hours post infection. Under anaerobic conditions, fermentative metabolism may be used to produce energy. Ethanol is detectable in *A. fumigatus* lungs by NMR (Grahl et al. 2011). However, there was limited transcriptional support of fermentative metabolism in this study. While numerous putative pyruvate decarboxylases and alcohol dehydrogenases were employed throughout infection, comparable numbers were also found to decrease. Close inspection of genes required for ergosterol biosynthesis between 4 – 8 and 8 – 14 hours reveals the majority of genes were upregulatied (n = 12) and downregulated (n = 9) at each stage respectively (Tables 3.19 and 3.20). Thus, numerous genes within the ergosterol biosynthetic pathway (n = 9) decreased between 8 – 14 hours. This may be explained by the increasingly inflamed, and thus hypoxic conditions, of the host which results in downregulation of the oxygen dependent biosynthetic ergosterol pathway (Todd et al. 2006). In *Schizosaccharomyces pombe*, oxygen dependent sterol synthesis and hypoxia adaptation are linked through the membrane bound SREBP transcription factor Sre1. Under hypoxic conditions, ergosterol biosynthesis is reduced causing the proteolytic processing of Sre1 which activates numerous genes associated with adaptation to hypoxia (Hughes et al. 2005, Todd et al. 2006). The *C. neoformans* SREBP homologue, Sre1p, plays an important role in hypoxia adaptation and is required for full virulence (Chang et al. 2007). In *A. fumigatus*, a decrease in ergosterol biosynthesis may be used as a surrogate measure of oxygen supply by the SREBP transcription factor SrbA (Willger et al. 2008). This SREBP has been shown to be essential for hypoxia adaptation and virulence in a murine model of X-linked chronic granulomatous disease (X-CGD) utilising gp91$^{phox-/-}$ mice (Willger et al. 2008). Thus, reduction in transcript abundance of genes required for ergosterol biosynthesis between 8 and 14 hours may support the existence of hypoxic conditions at the invasive and inflammed time-points of infection. This further highlights the potential of inhibiting hypoxia adaptation as a therapeutic strategy (Wezensky and Cramer 2011).

Upregulation of genes required for the detoxification of reactive oxygen species was reported throughout infection, including the mycelial catalase Cat1 (Afu3g02270), a putative catalase (Afu2g00200), a superoxide dismutase (Afu1g14550) and the peroxiredoxin Asp F3 (Afu6g02280). With regard to secretory stress, STEM analysis reported the increase of 10 genes associated with the *A. fumigatus* endoplasmic reticulum, which is supportive of increased demand for carriage of cell wall components to the hyphae and secretion of extracellular enzymes during infection (Richie et al. 2009). Genes which are putatively involved in thermotolerance were not a striking feature of increasing or decreasing datasets throughout the time course of murine infection. These data may be explained by the rapid adaptation of the inhaled and dormant spore to mammalian body temperature. As demonstrated by Nierman and colleagues, extensive transcriptional reprogramming occurs following heat stress within 180 minutes (Nierman et al. 2005). An interesting observation was the moderate increase of the nucleolar protein CgrA (Afu8g02750) between 4 – 14 hours post infection. This transcription factor is required for adaptation to 37°C growth and virulence (Bhabhra et al. 2004).

Secreted proteases have long been postulated as putative *A. fumigatus* virulence factors (Behnsen et al. 2010, Bergmann et al. 2009, Reichard et al. 1990, Sharon et al. 2009, Smith et al. 1994). This study shows a striking transcriptional increase of secreted proteases between 4 – 8 hours post infection (Table 3.19). These data are agree with the findings of *ex vivo* assays which demonstrated a role of secreted proteases in spore epithelial damage and immune attack (Kogan et al. 2004, Behnsen et al. 2010).

In addition to proteases or peptidases, *A. fumigatus* secretes a diverse range of hydrolytic enzymes likely to facilitate saprophytic nutrient acquisition. Transcriptional comparisons between 4 and 8 hours post infection suggested increased transcript abundance of 277 genes encoding a putative signal peptide, including four 1,3-beta-glucanosyltransferases, two alpha-1,2-mannosyltransferases, 3 cell wall proteins, 13 GPI anchored proteins, 5 chitinases, 3 lipases, a cutinase, extracellular signalling protein FacC protein, a lipophospholipase and an acid sphingomyelinase (Table 3.19). All these enzymes putatively interact with the mammalian host during the early time-points of infection and thus may represent aggressive or defensive pathogen molecules which facilitate infection, or activate host defence mechanisms. Clearly, cell wall and GPI-anchored proteins may act as PAMPs, and thus mediate immune recognition by host PRRs. Lipases catalyse the hydrolysis and synthesis of triacylglycerols and may facilitate infection by nutrient acquisition, mediating adhesion, degradation of host cells or tissue, and initiation of inflammatory immune reponses. Lipases are required for full virulence in murine models of

Candida albicans infection (Gacser et al. 2007). The putatively secreted acid sphingomyelinase (Afu4g06640) moderately increased between 4 – 8 hours. Sphingomyelinases degrade sphingomyelin, a lipid component of mammalian cell membranes. An acid sphingomyelinase from *Pseudomonas aeruginosa* is haemolytic to human erythrocytes, cytotoxic to human neutrophils, macrophages and endothelial cells, and prevents angiogenesis in a zebra fish model (Vasil et al. 2009). Extracellular cutinases are likely supportive of the *A. fumigatus* saprophytic lifestyle, where it breaks down organic debris from decaying plant matter. Cutinases degrade cutin, a polyester found on plant leaves. These enzymes may play a role in host attack; characterisation of two secreted cutinases of *Mycobacterium tuberculosis* has demonstrated these enzymes effect phospholipase activity and are able to induce macrophage phagocytosis *in vitro* (Schué et al. 2010). Chitinases are endo-ß-1,4-N-acetylglucosamidases which degrade chitin, a component of helminth exoskeleton and fungal cell walls. Chitinases are well characterised components of plant and more recently mammalian immunity (De Wit et al. 2009, Zhu et al. 2004). Nevertheless these enzymes might be detrimental to the mammalian host. Inhibition of mammalian chitinase reduces both tissue inflammation and airway hyperresponsiveness in mice (Zhu et al. 2004). Acid mammalian chitinase is produced primarily in asthmatic individuals and contributes to Th2 type allergy (Elias et al. 2005).

Consequently, secreted *A. fumigatus* chitinases may contribute to an unfavourable Th2 immune response. Additionally, 14 putative antigens demonstrated increased transcript abundance at this time-point, including allergenS Asp F1, Asp F3, Asp F4, Asp F7, Asp F10 and Asp F13. These proteins may facilitate infection by eliciting an unfavourable Th2 immune response (Banerjee and Kurup 2003). It has been hypothesised that secondary metabolite toxins are released by *A. fumigatus* spores (Dagenais et al. 2010). This is certainly true *in vitro*, for example, the secondary metabolite toxins verruculogen, fumagillin, fumigaclavine C, aurasperone C, fumitremorgin C, and trypacidin have been detected using HPLC analyses of resting conidial extracts (Khoufache et al. 2007). Upregulation of secondary metabolite genes was not a defining feature of the 4 – 8 hour dataset, with the majority of secondary metabolite genes slightly reduced in expression between these time-points. Accordingly, the spore transcriptome appears to direct expression of encoding damaging hydrolytic enzymes and immunogenic molecules rather than toxic metabolites.

Other pathogenesis associated molecules increased in transcript abundance between 4 and 8 hours post infection. The mycelial catalase Cat1 (Afu3g02270) might provide protection against host ROS attack. Additionally, a hemolysin (Afu3g00590) might cause toxicity and lyses host blood cells, although mutants having deletions of this gene are fully virulent in a murine model of

infection (Wartenberg et al. 2011). An interesting observation was the increase in transcript abundance of genes directing sphingolipid biosynthesis. In *C. albicans*, sphingolipid plays a role in pathogen adhesion, as evidenced by disruption of the sphingolipid biosynthetic gene *ipt1*, which reduced adhesion to gingival epithelial cells, prevented TLR activation and beta-defensin expression in an *ex vivo* assay (Rouabhia et al. 2011). The role of *A. fumigatus* sphingolipids in spore adhesion is not known.

Thus, a picture emerges of the infecting *A. fumigatus* spore preparing to secrete numerous enzymes and allergens which may be highly damaging to the mammalian host and illicit unfavourable Th2 immune responses. In contrast, changes to the pathogen cell wall, GPI anchored protein expression, and Th1 stimulating antigens may facilitate host immune recognition. In the case of the immunocompromised mammal, the balance is in favour of the pathogen, which is able to germinate into invasive hyphae.

A striking feature of the dataset comparing 8 hour and 14 hour morphologies in the murine lung was the increased expression of numerous genes directing the biosynthesis of secondary metabolites (n = 128). A direct link between regulation of *A. fumigatus* secondary metabolism and development has been demonstrated (Keller et al. 2005). In *A. nidulans*, this occurs via the heterotrimeric velvet complex, a component of which is the putative nuclear methyltransferase LaeA (Bayram et al. 2008). Clusters directing the biosynthesis of the epipolythiodioxopiperazine gliotoxin, the cyclic dipeptide pseurotin A and four uncharacterised secondary metabolites are preferentially upregulated during infection relative to laboratory culture (McDonagh et al. 2008). Of the 10 genes displaying the greatest upregulation between 8 and 14 hours, 6 of these were found to reside in the gliotoxin biosynthetic cluster (Table 3.17). Gliotoxin inhibits the ROS burst of neutrophils, induces host apoptotic cell death by activating a proapoptotic Bcl-2 family member protein, and is required for virulence in murine models of infection (Sugui et al. 2007, Pardo. et al 2006, Bok et al. 2006). 14 NRPS or PKS genes also increased between these 8 and 14 hours post infection. These included the hybrid NRPS/PKS *psoA* which is required for the biosynthesis pseurotin A, a dipeptide which is to cytotoxic to lung epithelial cells and secreted in hypoxic *in vitro* conditions (Maiya et al. 2007, Schmeda-Hirschmann et al. 2008, Vodisch et al. 2011). The putative brevianamide F synthetase *ftmA* (Afu8g00170, Maiya et al. 2006) catalyses the biosynthesis of the diketopiperazine brevianamide F by the condensation of amino acids L-tryptophan and L-proline (Maiya et al. 2006). Brevianamide F is the precursor for fumitremorgins and tryprostatins, (Grundmann et al. 2008, Kato et al. 2009) which act on the central nervous system to induce tremors and titanic spasms in mice (Yamazaki et al. 1979). Numerous other PKS or NRPS genes

from uncharacterised clusters also increased. The role of these putative secondary metabolites during infection remains unknown, and is partially addressed in two subsequent Chapters of this thesis.

Secreted proteases, other hydrolytic enzymes, antigens, and other pathogen associated molecules identified in the 4 – 8 hour comparison likely remain relevant at the hyphal time-point as evidenced by the elevated or constitutive expression of these genes between 8 – 14 hours. Finally, a preference for genes associated with cell wall remodelling was noted between 8 – 14 hours, which is consistent with extensive modifications and synthesis of the hyphal cell wall. These modifications might have critical implications for host-pathogen interactions. For example, in contrast to swollen conidia, pentraxin 3 does not bind to hyphae, which is most likely due to alterations in galactomannan on the hyphal surface (Garlanda et al. 2002). Additionally, dendritic cells internalise germlings using dectin-1 (Mezger et al. 2008) and hyphae by complement receptor 3 and the FC receptor (Bozza et al. 2002). In addition, the cell wall represents a cellular structure with protective qualities against host attack, for example protection from host ROS (Latge 1999). Therefore, transcriptional profiling conducted in this Chapter represents a chronicle of pathogen processes, many of which putatively initiate host-pathogen interactions during *A. fumigatus* infection.

Transcriptional comparisons between *A. fumigatus* germlings isolated from the murine lung with developmentally matched laboratory culture found that genes which are preferentially employed in the murine lung are more likely to reside in subtelomeric regions or in contiguous contingency clusters (McDonagh et al. 2008). These are defined as areas within 300 Kb of the chromosome ends. Subtelomeres are enriched in mobile genetic elements, secondary metabolite clusters, catabolite genes and transport genes, and undergo frequent chromosomal rearrangements (Federova et al. 2008). In support of the importance of subtelomeric genes during host adaptation, transcriptional profiling between 8 – 14 hours reported in this Chapter demonstrated a predominance of genes residing in subtelomeric loci among upregulated cohorts. This locational bias was not observed in the 4 – 8 hour transcriptional analysis. Virulence-associated genes are often located in pathogen subtelomeres, and include those directing antigenic variation in *Trypanosoma brucei* and *Plasmodium falciparum*, surface glycoproteins of *Candida glabrata* (De las Penas et al. 2003), and secondary metabolites in *U. maydis* (Bolker et al. 2008). The subtelomeres are characterized by repeat sequences of various lengths, enabling high levels of ectopic recombination, a phenomenon which is augmented by telomere grouping at the nuclear periphery (Barry et al. 2003). Moreover, repeat sequences can cause DNA polymerase slip which

results in chromosomal rearrangements (Viguera et al. 2001). Additionally, many subtelomeres are enriched with retrotransposons and other mobile genetic elements, which can lead to local insertions, deletions, duplications and inversions (Volff 2006). A prominent feature of the 8 – 14 hour dataset was the increased transcript abundance of numerous transposition associated genes, which has been reported in other studies following *A. fumigatus* germination (Bertuzzi et al. unpublished, Lamarre et al. 2008).

With respect to the evolution of *A. fumigatus* pathogenecity, several hypotheses have been postulated, including horizontal gene transfer of secondary metabolite clusters (Walton 2000). Data presented in this Chapter support the gene duplication, diversification and differential gene loss (DDL) hypothesis suggested by Federova and co-workers (Federova et al. 2008) that emphasises subtelomeres as “gene factories” which cause expansion of the gene content of the *A. fumigatus* genome. Employment of these regions during early murine infection strongly suggests that DDL at subtelomeric regions may play a driving role in the evolution of *A. fumigatus* virulence, as opposed to other mechanism such as horizontal gene transfer of toxic metabolite clusters (Walton 2000) or diversification of virulence associated genes by sexual reproduction (O’Gorman et al. 2009).

This study also identified the involvement of contingency gene clusters between 8 – 14 hours in the murine lung. In eukaryotic genomes, genes involved in functionally related pathways often cluster at proximal genomic locations (Keller and Hohn 1997). While the majority of non-metabolite contingency clusters are not functionaly related (McDonagh et al. 2008), their co-ordinated employment is suggestive of epigenetic control mechanims during the initiation of infection. These data further re-inforce the importance of these loci during infection. Indeed, a methodology developed with collaborators and presented in this thesis (Chapter 5) is an ideal tool for the deletion of *A. fumigatus* contingency clusters.

Transcriptional analysis of the Δ*laeA* isolate enables the formation of hypotheses regarding the molecular basis of *A. fumigatus* attenuation, and the importance of LaeA gene regulation during the establishment of infection. This is considered more fully in comparative transcriptional profiling conducted in Chapter 8. Attenuation of Δ*laeA* isolates have been associated with reduced toxin production (Bok et al. 2005, Sugui et al. 2007b) and RodA content of the conidia (Dagenais et al. 2010). Inspection of the six datasets generated in this study paints an extremely complex picture with regard to attenuation of Δ*laeA* which finds that Δ*laeA* aberrantly expresses several genes which might synergistically contribute to the observed virulence phenotype of the isolate.

Commonalities among gene increases between 4 and 14 hours are observed between the Δ*laeA* and Af293 isolates including genes reqired for iron, copper and zinc acquisition, cellular differentiation, ergosterol biosynthesis and cell wall biogenesis (Table 3.28). In accordance with wild-type environmental sensing and signal transduction in Δ*laeA*, increase in expression of multiple MAP kinases, GTPase activating proteins and serine/thronine kinases was observed. In agreement with the general suppression of protein biosynthesis and ribosome biogenesis observed in AF293, 13 ribosomal proteins decreased in expression over the time-course, whereas only 2 increased. Thus, data suggest iron acquisition, ion transport, cellular differentiation, environmental sensing and the metabolic state of the cell is comparable between Δ*laeA* and Af293 isolates. Thus, it seems unlikely attenuation of Δ*laeA* can be attributed to these factors.

Given the striking upregulation of antigens and secreted proteases in Af293 between 4 and 8 hours, these genes were carefully examined in Δ*laeA*. A reduction in the number of secreted proteases upregulated between 4 and 8 hours was observed in Δ*laeA* (n = 7) relative to (n = 15). This included an alkaline serine protease Alp1, which degrads host complement *in vitro* (Behnsen et al. 2010). The reduced expression of these genes might explain the histopathological finding that infected tissue contains less invasive hyphae following infection with a Δ*laeA* mutant. Slightly more antigen transcripts increased in Af293 (n = 14) compared to Δ*laeA* (n = 9) between 4 and 8 hours, including an extracellular lipase (Afu5g02040), enolase (Afu6g06770) and a histidine acid phosphatase (Afu6g11330). While these may contribute to an unfavourable Th2 response to Af293 (Banerjee and Kurup 2003, Romani 2005) transcriptional profiles of other antigens (e.g. Asp F1, Asp F2, Asp F3) were comparable between isolates.

There was a slight reduction in the number of secondary metabolite genes upregulated during infection in Δ*laeA* relative to Af293. For example, between 8 and 14 hours 103 and 128 genes increased in these strains respectively. These were not focused at specific gene clusters. Moreover, few NRPS or PKS genes were differentially expressed between the two isolates. One exception was the putative brevianamide F synthetase *ftmA* (Afu8g00170) which increased and decreased throughout the time-course in Af293 and Δ*laeA* respectively. Differential expression of *ftmA* might therefore contribute to Δ*laeA* attenuation.

While non-ratiometric normalisation does not take into account absolute transcript intensities between isolates, data presented here suggests that metabolite clusters are not regulated by LaeA

during initiation of infection. This is surprising, given the putative function of LaeA as a global regulator of secondary metabolite loci (Bayram et al. 2008, Reyes-Dominguez et al. 2010 Perrin et al. 2007). Chi-square analysis of secondary metabolite genes demonstrated that these loci are upregulated in Δ*laeA* between 8 and 14 hours, albeit to a lesser degree than observed in Af293. Aspergillus secondary metabolism is has been strongly correlated with developmental stage and with alterations in environmental factors including temperature, light, pH or carbon and nitrogen sources (Yu and Keller 2005). This study and other *A. fumigatus* transcriptional profiling (McDonagh et al. 2008) suggest secondary metabolites are transcribed most abundantly at the hyphal time-point of infection. Thus, the general reduction in secondary metabolite gene transcript in Δ*laeA* relative to Af293 is likely related to the slower development of Δ*laeA* in the host rather than a specific LaeA regulatory phenomenon.

The most well studied secondary metabolite of *A. fumigatus* is the epipolythiodioxopiperazine gliotoxin. The *A. fumigatus* LaeA deletant utilised in this study is impaired in gliotoxin production and multiple unknown secondary metabolites as determined by thin layer chromatography (TLC) analyses of laboratory culture (Bok et al. 2004, Bok et al. 2005). Transcriptional comparisons between Af293 and Δ*laeA* *in vitro* demonstrated reduced transcript levels among the majority of genes in the gliotoxin cluster in the Δ*laeA* strain, including the NRPS *gliP* (Perrin et al. 2007). Accordingly, the attenuation of Δ*laeA* strains in murine models has been attributed to reduced toxin production during infection, especially gliotoxin (Bok et al. 2005, Sugui et al. 2007b). It was therefore surprising to note the upregulation of numerous genes directing gliotoxin biosynthesis in the Δ*laeA* strain throughout murine infection. In the Af293 isolate, gliotoxin genes increased between 8 and 14 hours. In Δ*laeA*, genes within this cluster increased at both time-points. Notwithstanding this difference, a general concordance in gliotoxin biosynthetic gene expression was observed between Δ*laeA* and Af293. Several studies have dissected the role of individual genes in *A. fumigatus* gliotoxin production (Bok et al. 2006b, Gardiner et al. 2005, Schrettl et al. 2010) and the putative regulation of these genes by LaeA (Sugui et al. 2007b, Perrin et al. 2007). The NRPS *gliP* catalyses the first step in gliotoxin biosynthesis (Gardiner et al. 2005). It is required for gliotoxin production *in vitro* and deletant strains are attenuated in a corticosteriod treated model of infection (Sugui et al. 2007a). RT-PCR analyses of *gliP* expression following 24, 48 and 72 hour culture demonstrated decreased transcript abundance of *gliP* in a Δ*laeA* deletant strain relative to the wild type (Sugui et al. 2007b). A role for LaeA in regulating *gliP* is supported by global transcriptional comparisons between Δ*laeA* and Af293 following 25 °C growth for 60 hours (Perrin et al. 2007). In this Chapter, expression values for *gliP* were removed from both Af293 and Δ*laeA* datasets due to quality control filtering. However, analysis of available spots from

pre-filtered datasets suggests *gliP* expression is comparable between isolates and remains at a constant level throughout infection.

Numerous secondary metabolite clusters contain transcription factors which putatively regulate expression of genes within the cluster. *gliZ* is a transcription factor which is required for *in vitro* gliotoxin production, wild-type virulence in a corticosteroid murine model of infection, and the expression of aminotransferase *gliI* during 72 hour *in vitro* culture at 25°C (Bok et al. 2006b). Work described in this Chapter has demonstrated *gliZ* was not differentially expressed between isolates and decreased slightly in Af293 and Δ*laeA* between 4 – 14 hours respectively. *gliI* is highly increased in transcript abundance for both Af293 and Δ*laeA* strains between 4 and 14 hours post infection.

Epipolythiodioxopiperazines are toxic to fungi and must be exported from the cell. Schrettl and colleagues have demonstrated that the thioredoxin reductase *gliT* (Afu6g09740) is required for secretion and protection against exogenous gliotoxin (Schrettl et al. 2010). In the model proposed by these authors, the MFS gliotoxin efflux pump *gliA* (Afu6g09710) also mediates secretion of this metabolite (Schrettl et al. 2010). These two genes are among the 100 greatest increased transcripts between 4 and 14 hours in both Af293 and Δ*laeA* datasets indicating gliotoxin secretion is not impaired in Δ*laeA* during the initiation of infection. Other genes putatively involved in methylation and oxidation of intermediates during gliotoxin biosynthesis demonstrated highly similar expression between isolates. For example, the O-methyltransferase GliM (Afu6g09680), cytochrome P450 oxidoreductase GliC (Afu6g09670), glutathione S-transferase GliG (Afu6g09690) and cytochrome P450 oxidoreductase GliF (Afu6g09730) were among the top 10 greatest increased genes between 4 and 14 hours in both Af293 and Δ*laeA* datasets. Thus, during the initiation of murine infection in both Af293 and Δ*laeA* strains, key genes within the gliotoxin cluster are upregulated.

This contrasts with LCMS analyses which were unable to detect gliotoxin in the lung of Δ*laeA* infected mice (Bok et al. 2005). Bok and colleagues analysed infected neutropenic murine lung using LCMS which detected gliotoxin in wild-type but not in Δ*laeA* infected samples (Bok et al. 2005). However, the authors did not state the numbers of animals from which lung homogenate was analysed using LCMS. This considerably limits the interpretation of these data given the likely high variability among mice in models of *A. fumigatus* infection. A later study utilising lung homogenate from 5 corticosteroid treated mice used LCMS to demonstrate gliotoxin is produced by Δ*laeA* isolates in the host, albeit in a reduced amount relative to the wild-type (Bok et al. 2006). Thus, gliotoxin might be undetectable, or present at reduced concentrations in Δ*laeA* infected mice

simply due to a more rapid elimination of the fungus from the host niche, rather than a specific regulatory phenomenon of LaeA. These data are consistent with transcriptional profiling conducted in this Chapter.

Finally, during the initiation of Δ*laeA* murine infection the gliotoxin cluster appears to be in a region of transcriptionally active euchromatin. In the model organism *A. nidulans*, formation of heterochromatin is mediated by hypoacetylation of histones 3 and 4 by the histone deacetylase HdaA, which facilitates methylation by the H3K9 specific methylase ClrD and subsequent recruitment of the heterochromatin protein HepA (Reyes-Dominguez et al. 2010). LaeA is hypothesised to reverse the formation of heterochromatin, most likely via methyltransferase activity thus activating multiple secondary metabolite loci (Reyes-Dominguez et al. 2010). Transcriptional profiling in this Chapter suggests other proteins besides LaeA may determine the epigenetic state of secondary metabolite loci. Moreover, it further highlights the difficulties of extrapolating *in vitro* hypotheses into the infectious setting. These hypothesis are further explored in Chapter 8 and Chapter 9.

Chapter 4

Virulence analyses of *A. fumigatus* NRPS/PKS deletants Δ*psoA*, Δ*ftmA* and Δ*pes3* in neutropenic and corticosteroid treated murine models of infection

4.1 Overview

Fungal secondary metabolites are small molecular weight compounds which are dispensable for fungal growth and demonstrate restricted taxonomic distribution (Keller et al. 2005). Evidence suggests these molecules are employed for numerous purposes which benefit survival in the natural niche, including the elimination of bacteria, fungi, amoebae, plants, or insects; or which act as metal transporting or protective molecules, or differentiation effectors (Demain and Fang 2000). The vast diversity of fungal secondary metabolite structure and bioactivity is contrasted by the sparse knowledge of *A. fumigatus* gene cluster products (Brakhage and Schroeckh 2011). Accordingly, there is great potential for known and uncharacterised fungal secondary metabolites to benefit human health by their applications as novel therapeutics. Conversely, these molecules may contribute to contamination of foodstuffs, or augment virulence in human mycoses. In support of the latter hypothesis, transcriptional profiling described in Chapter 3 has demonstrated that hundreds of genes directing the biosynthesis of secondary metabolites, including siderophores and gliotoxin, increase in transcript abundance during colonisation of the immunocompromised mammal. Siderophores and gliotoxin are of particular note, as both these secondary metabolites are required for full virulence in murine models of aspergillosis (Bok et al. 2006b, Schrettl et al. 2007, Sugui et al. 2007a). Gene expression profiling also suggests the employment of other metabolite clusters, for which the product is either unknown, or the significance with regard to infection has not been investigated (McDonagh et al. 2008).

For example, the hybrid PKS/NRPS *psoA* (Afu8g00540) is essential for the biosynthesis of the cyclic peptide pseurotin A in *A. fumigatus* (Maiya et al. 2007). Gene expression analyses demonstrated increased *psoA* transcript abundance in Af293 and Δ*laeA* strains during the initiation of infection (Chapter 3). Comparative transcriptome analysis between germlings isolated from the murine host and developmentally matched *in vitro* culture showed *psoA* was preferentially employed during infection (McDonagh et al. 2008). Additionally, recent transcriptional, proteomic and metabolic analyses have demonstrated pseurotin A biosynthesis in hypoxic, but not normoxic culture (Vodisch et al. 2011). These data suggest pseurotin A may be produced *in vivo* due to the

low oxygen levels encountered in the lung parenchyma (Vodisch et al. 2011, Wezensky and Cramer 2011). In keeping with the diverse bioactivity of fungal secondary metabolites (Keller et al 2005) pseurotin A inhibits IgE production of murine B-cells *in vitro* (Ishikawa et al. 2009) is neuritogenic (Komagata et al. 1996) and inhibits chitin synthase activity (Wenke et al. 1993). Most notably in the context of murine virulence, pseurotin A isolated from *Penicillium janczewskii* demonstrated toxicity to lung fibroblasts (Schmeda-Hirschmann et al. 2008). It was therefore hypothesised that pseurotin A may contribute to *A. fumigatus* virulence in murine infections.

With regard to reverse engineering the transcriptional basis of *A. fumigatus* attenuation, it was hypothesised that genes differentially expressed between Δ*laeA* and wild-type comparator during early infection may biosynthesise products which contribute to *A. fumigatus* virulence. One such gene identified from expression profiling conducted in Chapter 3 was the putative brevianamide F synthetase *ftmA* (Afu8g00170, Maiya et al. 2006), for which transcript abundance increased and decreased during early infection in the Af293 and Δ*laeA* strains respectively. Intriguingly, *in vitro* transcriptional profiling demonstrated a decrease in *ftmA* gene expression in a Δ*laeA* strain relative to a wild-type comparator (Perrin et al. 2007). These data suggest *ftmA* expression may be epigenetically regulated by LaeA. FtmA is a dimodular NRPS which forms the diketopiperazine brevianamide F by the condensation of amino acids L-tryptophan and L-proline (Maiya et al. 2006). Brevianamide F is the precursor for fumitremorgin B, fumitremorgin C, tryprostatin A and tryprostatin B biosynthesis in *A. fumigatus* (Grundman et al. 2008, Kato et al. 2009). Fumitremorgins and tryptostatins are mycotoxins which act on the central nervous system to induce tremors and titanic spasms in mice (Yamazaki 1979), and may contribute to extrinsic allergic alveolitis of agricultural workers (Land et al. 1987). Given the differential transcription of *ftmA* in fully virulent Af293 and attenuated Δ*laeA* strain during early infection, and the mycotoxic activity of both fumitremorgins and tryprostatins, *ftmA* might be required for full murine virulence.

In parallel to this study, our collaborators from Sean Doyle's laboratory at the National University of Ireland deleted the largest NRPS, *pes3*, in the *A. fumigatus* genome (Afu5g12730). Δ*pes3* strains demonstrated an increase in virulence in *G. mellonella* model of infection relative to a wild-type isolate (O'Hanlon et al. 2011). Additionally, stimulation of murine macrophages with *A. fumigatus* Δ*pes3* resulted in reduced cytokine production when compared to a wild-type comparator (O'Hanlon et al. 2011). O'Hanlon and co-workers hypothesised that this is due to a structural alteration in *A. fumigatus* Δ*pes3*, which abrogates a pathogen associated molecular pattern (PAMP), thereby leading to defective recognition by innate immune receptors (O'Hanlon et al. 2011). Gene expression profiling conducted in Chapter 3 demonstrated an increase in *pes3*

transcript abundance for both Af293 and Δ*laeA* strains during the initiation of murine infection. Accordingly, Δ*pes3* might impact host pathogen interactions and virulence in murine models of infection.

In work described in this Chapter, *A. fumigatus* Δ*psoA*, Δ*ftmA* and Δ*pes3* mutants and isogenic progenitors have been characterised with regard to virulence, tissue invasion, and fungal burden in murine models of infection. The immune status of the host is critical with regard to fully understanding host pathogen interactions and virulence, as evidenced by the attenuation of *ΔgliP* and *ΔgliZ* strains in corticosteroid treated, but not neutropenic models of aspergillosis (Bok et al. 2006b, Cramer et al. 2006, Sugui et al. 2007a). Accordingly, Δ*psoA*, Δ*pes3* and Δ*ftmA* mutants were tested in neutropenic and corticosteroid treated models of infection. In order to determine fungal burden from infected tissue, a highly sensitive and reproducible semi-quantitative qPCR assay was developed.

4.2 Materials and methods

4.2.1 *A. fumigatus* strains

Strains used in this Chapter included the genotypically confirmed Af293 clinical isolate, provided by Nancy Keller. Strains Δ*ftmA* and Δ*psoA* were constructed in the Af293 background using the *A. fumigatus pyrG*$^{-}$ mutant and *A. nidulans pyrG* gene disruption cassettes (Maiya et al. 2006, Maiya et al. 2007). Both strains were kindly provided by Professor Geoffrey Turner (University of Sheffield, Department of Molecular Biology and Biotechnology). Δ*pes3* was constructed in the ATCC46645 background using a pyrithiamine disruption cassette (O'Hanlon et al. 2011). Both these isolates were provided by Professor Sean Doyle (Department of Biology, National University of Ireland). Δ*pabaA* was constructed in the Af237 background (Brown J. S. et al. 2000) and provided by Professor David Holden (Centre for Molecular Microbiology and Infection, Imperial College London).

4.2.2 Oligonucleotide primers

Oligonucleotide primers used in this Chapter are listed in Table 4.1.

Table 4.1: Oligonucleotide primer sequences used in this chapter

Primer	Orientation	Sequence
BT-F	Forward	GAGCCCTTTTCCGACCTGAT
BT-R	Reverse	GGAACTCCTCCCGGATCTTG
Actin-F	Forward	CGAGCACAGCTTCTTTGCAG
Actin-R	Reverse	CCCATGGTGTCCGTTCTGA

4.2.3 Survival analysis

Murine infections were performed under UK Home Office Project Licence PPL/70/6487 in the Central Biomedical Services Centre, Imperial College London. Outbred male mice (strain CD1, 18 – 22 g, Harlan Ortech) were housed in individually vented cages. Two immunosuppressive regimes were used. For a neutropenic model, mice received cyclophosphamide (150 mg/kg, Endoxana, Asta Medica) by intraperitoneal injection on days -3 and -1, +2 and every subsequent third day. A single dose of hydrocortisone acetate (112.5 mg/kg, Hydrocortistab, Sovereign

Medical) was administered on day -1. For the hydrocortisone treated model, mice received subcutaneous doses of hydrocortisone acetate (112.5 mg/kg, Hydrocortistab, Sovereign Medical) on days -3, -1, +2 and every subsequent third day. *A. fumigatus* spores were grown on ACM, supplemented with 1% (w/v) glucose and 5 mM ammonium tartrate, for 5 days prior to infection. Spores were harvested on the day of infection, using sterile saline (Baxter Healthcare Ltd, UK), and filtered through MIRACLOTH. Conidial suspensions were centrifuged for 10 minutes at 5000 rpm, washed twice with sterile saline, counted using a haemocytometer and resuspended at a concentration of 1.25×10^7 or 1.75×10^8 cfu/ml for neutropenic and hydrocortisone models respectively. Mice were anesthetized by halothane inhalation and infected by intranasal instillation of 5×10^5 or 7×10^6 conidia in 40 µl of saline for neutropenic and hydrocortisone models respectively. Viable counts from administered inocula were determined following serial dilution by plating on ACM and growth at 37 °C. Mice were weighed every 24 hours from Day -3 and visual inspections made twice daily. The end point for survival experimentation was a 20% reduction in body weight measured from the day of infection, at which point mice were culled.

4.2.4 Histopathology

Mice for histology were culled by neck dislocation. Whole lungs were extracted and fixed in 4% v/v formaldehyde (Sigma-Aldrich). Lungs were embedded in paraffin prior to sectioning and stained with hemotoxylin and eosin (H&E) or Grocott's Methenamine Silver (GMS).

4.2.5 qPCR assay for measurement of fungal burden in murine lungs

In order to assess fungal burden as a quantitative virulence criterion, quantitative PCR (qPCR) was performed on total genomic DNA extracted from homogenized whole lungs. Mice were treated identically to those used for survival analyses, but the *A. fumigatus* spore inoculum was reduced to 7.5×10^5 or 2×10^7 cfu/ml for neutropenic and corticosteroid cohorts respectively. For neutropenic and hydrocortisone acetate treated mice, lungs were extracted from mice culled on day + 4 or day + 5 respectively. Lungs were weighed, and 1 volume of sterile saline was added. Lungs were homogenised using an X120 electric tissue homogeniser (Bennett Scientific Limited) and 250 µl of homogenate was added to 180 µl of buffer ATL (Qiagen) and DNA extracted using DNeasy Blood and Tissue Kit (Qiagen). Fungal burden was assessed by quantitative PCR amplification using the oligonucleotides BT-F (GAGCCCTTTTCCGACCTGAT) and BT-R (GGAACTCCTCCCGGATCTTG) to amplify the beta tubulin (Afu7g00250) locus from the *A. fumigatus* genome, and the oligonucleotides Actin-F (CGAGCACAGCTTCTTTGCAG) and Actin-R

(CCCATGGTGTCCGTTCTGA) to amplify the murine actin locus (NM_007393). Quantification of both gene targets was performed in triplicate qPCR reactions. qPCR was performed using Sybr Green Jumpstart™Taq ReadyMix™ (Sigma-Aldrich, UK). 5 µl of gDNA extracted from murine lung was used as a template in 20 µl qPCR reactions. qPCR was conducted in a Rotor-Gene RG-3000 PCR cycler (Corbett Research, UK) with the following cycling parameters: 95 °C for 5 seconds, 58 °C for 5 seconds, 72 °C for 15 seconds, 78 °C for 5 seconds, which was repeated 40 times. Data were then analysed using the RotorGene 6 software, from which the amplification threshold was manually assigned to generate Ct values. A modified mathematical model (incorporating adjustment for fungal inoculum) for relative quantification of *A. fumigatus* actin, and murine beta-tubulin was adopted for each mouse sample using the formula RATIO = $(E_{target})^{\Delta Ct(\text{fungal actin} - \text{murine tubulin})}$ where *E*= efficiency of amplification of target gene and is equal to 1.88, based on efficiency calculations using the Ct slope method (Pfaffl 2001). RATIO values were $\log_{10}$ transformed and corrected for inoculum size, and reciprocal values were plotted ($1/\log_{10} RATIO_C$). The statistical significance of variances between fungal burdens was calculated using a nonparametric Mann-Whitney t-test. Genomic DNA, isolated from animals infected with an attenuated *A. fumigatus* p-amino benzoic acid auxotroph, Δ*pabaA* was used as a positive control for attenuation (Brown et al. 2000).

4.3 Results

4.3.1 Establishing a qPCR method for measuring *A. fumigatus* burden using the ΔCt method

The burden of a pathogen in host tissue is a quantitative virulence criterion which can be used to assess virulence or effectiveness of drug treatment (Bowman et al. 2001). For animals infected with unicellular organisms, such as *C. albicans*, pathogen burden can be reproducibly quantified by tissue homogenisation, plating and CFU counting (Walsh et al. 1987). CFU counts have been used as a measure of *A. fumigatus* virulence to supplement survival data (Bok et al. 2005). However, this method of burden quantification is not accurate for tissues infected with multicellular hyphae, as these cells cannot be effectively disseminated on agar plates by spreading and hyphae are multinucleate thereby constituting multiple CFUs (Bowman et al. 2001). For the *A. fumigatus* assay described in this Chapter, both murine and *A. fumigatus* gDNA were concomitantly quantified by qPCR and burden determined using a method based on ΔCt calculations (Pfaffl 2001, Schmittgen and Livak 2008).

4.3.2 Determination of amplification efficiencies of murine actin and fungal beta tubulin primers

In qPCR, the Ct value is defined as the PCR cycle at which the fluorescent signal of the reporter dye crosses an arbitrarily placed threshold (Schmittgen and Livak 2008). The numerical value of the Ct is therefore inversely related to the amount of amplicon in the reaction. qPCR data may be presented in absolute or relative values (Schmittgen and Livak 2008). ΔCt is defined as the difference in Ct values between a target and internal control gene gene, in this case fungal beta tubulin and murine actin. ΔCt is therefore calculated by: Ct beta tubulin – Ct murine actin. As this method measures both murine and fungal gDNA concentrations, it controls for variation in template concentration between samples. For a full consideration of the benefits of using this assay, please see the discussion section.

Primers were designed to amplify a 234 bp region of *A. fumigatus* beta tubulin (Afu7g00250) locus or a 147 bp region of the murine actin locus (NM_007393, Table 4.1). BLAST analyses of the predicted PCR amplicons were conducted on both genomes and primers were chosen which minimised the chances of non-specific product amplification. To confirm that beta-tubulin and actin primers only amplified a product from *A. fumigatus* and murine templates respectively, triplicate

qPCR reactions using Actin-F and Actin-R were conducted with 100 ng *A. fumigatus* gDNA as template. Additionally, triplicate PCRs using primers BT-F and BT-R and saline infected, murine gDNA as template were conducted. Ct values from Af293 *in vitro* gDNA and unspiked saline inoculated murine lung were restricted to PCRs using fungal beta tubulin and murine actin primers respectively (Figure 4.1).

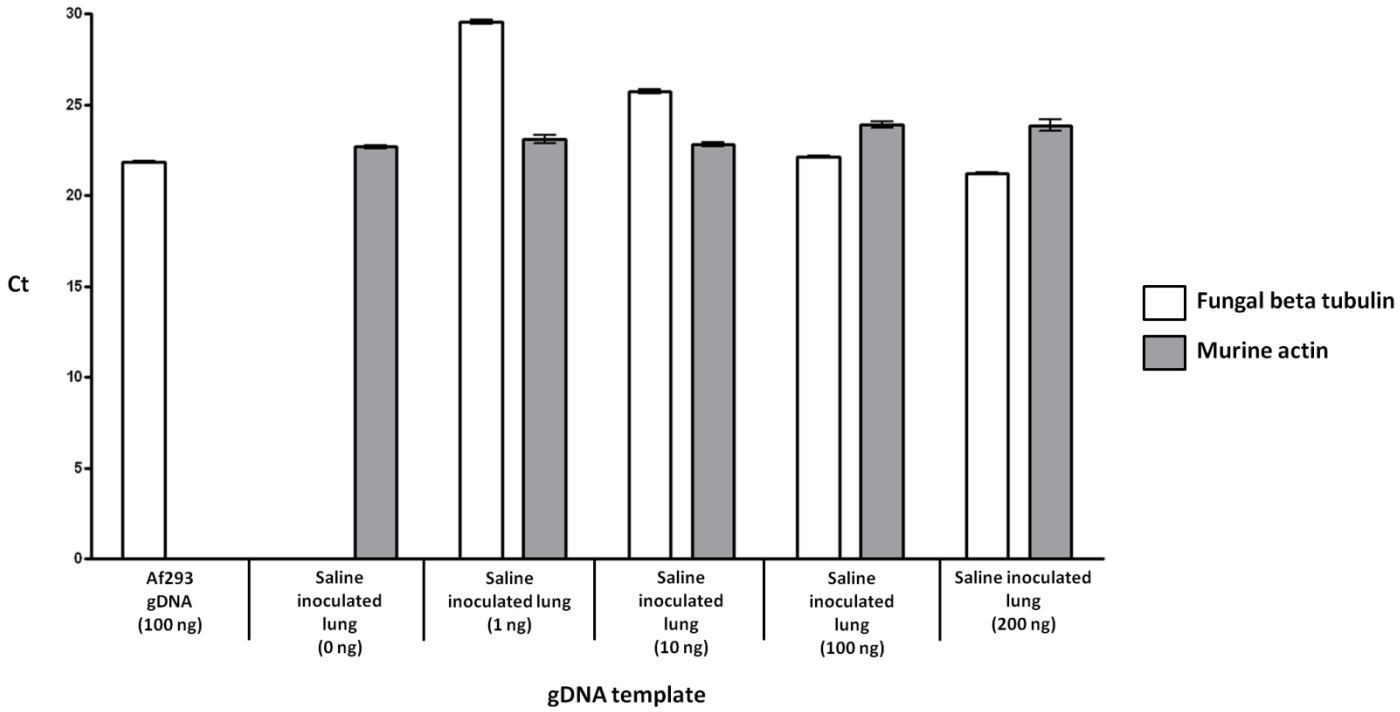


Figure 4.1: Ct values from triplicate RT-PCR reactions using murine actin or fungal beta tubulin primers, with fungal gDNA or saline inoculated murine lung gDNA as template. Templates included Af293 gDNA extracted from *in vitro A. fumigatus* culture, or gDNA extracted from a saline inoculated murine lung, which was spiked with increasing concentrations of Af293 gDNA. Numbers in parentheses indicate the total concentration of fungal gDNA per reaction. Ct values from Af293 *in vitro* gDNA and unspiked saline inoculated murine lung were restricted to PCRs using fungal beta tubulin (open bars) and murine actin (dark grey bars) respectively. This indicated beta-tubulin and actin primers only amplified a product from *A. fumigatus* and murine templates respectively. Error bars represent standard error from triplicate RT-PCR reaction.

For effective ΔCt calculations, both primer pairs should amplify the target amplicon with approximately the same efficiency (Schmittgen and Livak 2008). Primer efficiency should equate approximately to 2, as there should be a doubling of each PCR product per cycle. In order to determine beta tubulin primer efficiency, gDNA from saline infected murine gDNA was spiked with different concentrations of *A. fumigatus* gDNA (Figure 4.1 and 4.2A). This was used as a template in qPCR reactions utilising the beta tubulin primers (Figure 4.2A). In order to determine murine

actin primer efficiency, gDNA from three *A. fumigatus* Af293 infected lungs was serially diluted and used as templates for qPCR quantification utilising the actin primers (Figure 4.2B). Primer efficiencies were calculated using the Ct slope method. Ct values were plotted against log transformed template concentration (Schmittgen and Livak 2008) and primer efficiencies were calculated based on the following calculation (Pfaffl 2001):

$E = 10^{[-1/\text{slope}]}$

Where E = amplification efficiency
Slope = gradient from Ct vs template concentration graph

Using this method, the primer efficiencies for murine actin and fungal beta tubulin were calculated as 1.825 and 1.880 respectively. Efficiency between murine actin and fungal beta tubulin primers are therefore sufficiently similar for ΔCt quantifications, based on the recommendations that efficiencies differ by no more than 10% (Schmittgen and Livak 2008).

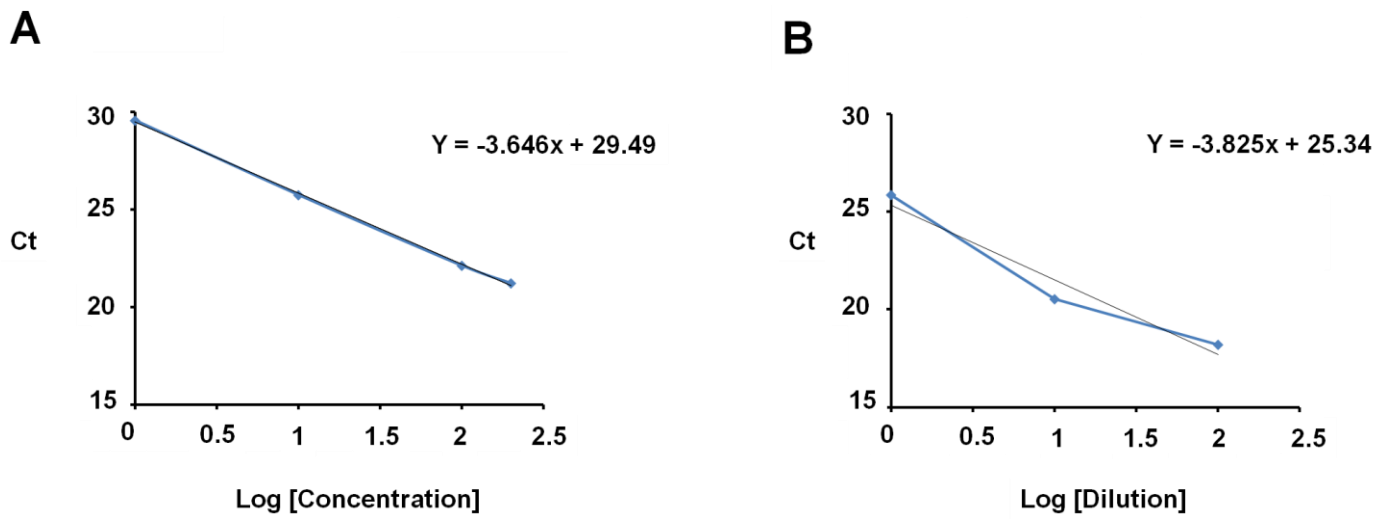


Figure 4.2: Graphical representation of *A. fumigatus* beta tubulin and murine actin primer efficiencies. For *A. fumigatus* beta tubulin primers (A), *A. fumigatus* gDNA was spiked at 1 ng, 10 ng, 100 ng and 200 ng concentrations into naive murine gDNA which was used as template for qPCR reactions. For murine actin primers (B), murine gDNA from 3 mice were diluted by 10 or 100 with sterile saline. Undiluted and diluted samples were used as templates for qPCR reactions. Both *A. fumigatus* and murine templates therefore were measured at three orders of magnitude. Ct values were averaged from triplicate qPCR reactions and plotted against log transformed concentration. The line of best fit is indicated in grey, and the straight line equation shown in the top right of the graph.

4.3.3 A qPCR assay detects statistically significant differences in fungal burden between fully virulent Af293 and attenuated Δ*pabaA* isolates in both neutropenic and corticosteroid treated murine models of infection.

In order to verify that the assay could detect differences in fungal burden between a fully virulent and attenuated isolate, cohorts of 5 mice undergoing each of the two immunosuppressive regimes (neutropenic and corticosteroid) were infected with Af293 or Δ*pabaA*. The *pabaA* gene encodes a *para*-aminobenzoic acid synthetase, which is required for biosynthesis of folate, an essential cofactor in DNA synthesis (Brown et al. 2000). An *A. fumigatus* Δ*pabaA* mutant cannot germinate in the murine lung and is avirulent in a neutropenic murine model of infection (Brown et al. 2000). Mice infected with Δ*pabaA* were therefore used as a positive control for attenuation. Mice infected with the fully virulent Af293 isolate were used as a positive control for virulence. gDNA was extracted (see methods) and 3 - 5 µl of each gDNA template were used in triplicate qPCR reactions with either fungal beta tubulin or murine actin primers. A single gDNA sample from the Δ*pabaA* corticosteroid treated model was omitted from analyses due to a contamination issue. ΔCt values (Ct beta tubulin – Ct murine actin) were calculated for each triplicate reaction and averaged to give a single ΔCt value for each murine gDNA sample. From ΔCt values, the ratio of fungal gDNA to murine gDNA was summarised thus:

$$\text{Ratio} = (E)^{\Delta Ct}$$

where E = mean efficiency of amplification of target genes (Figure 4.2). Ratio values were $\log_{10}$ transformed. $\log_{10}$ transformed values were corrected for inoculum size according to vital counts of administered inocula, which had been calculated on the day of infection by duplicate dilution, plating and enumeration. Corrected ratios were termed Ratio^{C}. As the numerical value of the Ct is inversely related to the amount of target gDNA in the reaction, reciprocal values were calculated ($1/\text{Ratio}^{C}$) and reported as ΔCt^{norm} (Figure 4.3B and 4.3D). To assess the impact of the dose correction step, the data were treated identically, but with dose correction omitted (Figure 4.3A and 4.3C). The statistical significance of variances between fungal burdens was calculated using a nonparametric Mann-Whitney t-test with the null hypothesis that ΔCt^{norm} do not differ between groups. The null hypothesis was rejected when $p \leq 0.05$.

Using this approach, statistically significant differences in fungal burden were reported between Af293 and Δ*pabaA* in both neutropenic and corticosteroid treated murine models of infection

(Figure 4.3). The murine actin amplicon was detectable in all samples. However, fungal beta tubulin was not detected from 4 gDNA templates (Figure 4.3). This was explained by: (1) the fungal burden was cleared by the host to levels which were not detectable by the qPCR assay; (2) the gDNA extraction eliminated the fungal gDNA. Given that 3 of the samples which did not amplify fungal beta tubulin were from the Δ*pabaA* strain (Figure 4.3) which is unable to germinate in the host (Brown et al 2000), it was considered likely that *A. fumigatus* had been cleared from these lungs to levels which were not detectable by the PCR assay. To ascertain differences in concentration of administered inocula between Af293 and Δ*pabaA*, inocula were serially diluted, plated and enumerated. Log_{10} transformed $(E)^{\Delta Ct}$ were mathematically corrected for differences in inocula concentration by the following calculation:

Dose corrected $Log_{10}(E)^{\Delta Ct} = Log_{10}(E)^{\Delta Ct}$ (CFU/ml Af293/ CFU/ml Δ*pabaA*)

ΔCt^{norm} values following dose correction are shown in Figure 4.3B and 4.3D. Both uncorrected and dose corrected ΔCt^{norm} values demonstrate that the parameters employed in the murine infection and qPCR assay are appropriate for detection of infection burden differences between the fully virulent and attenuated isolates.

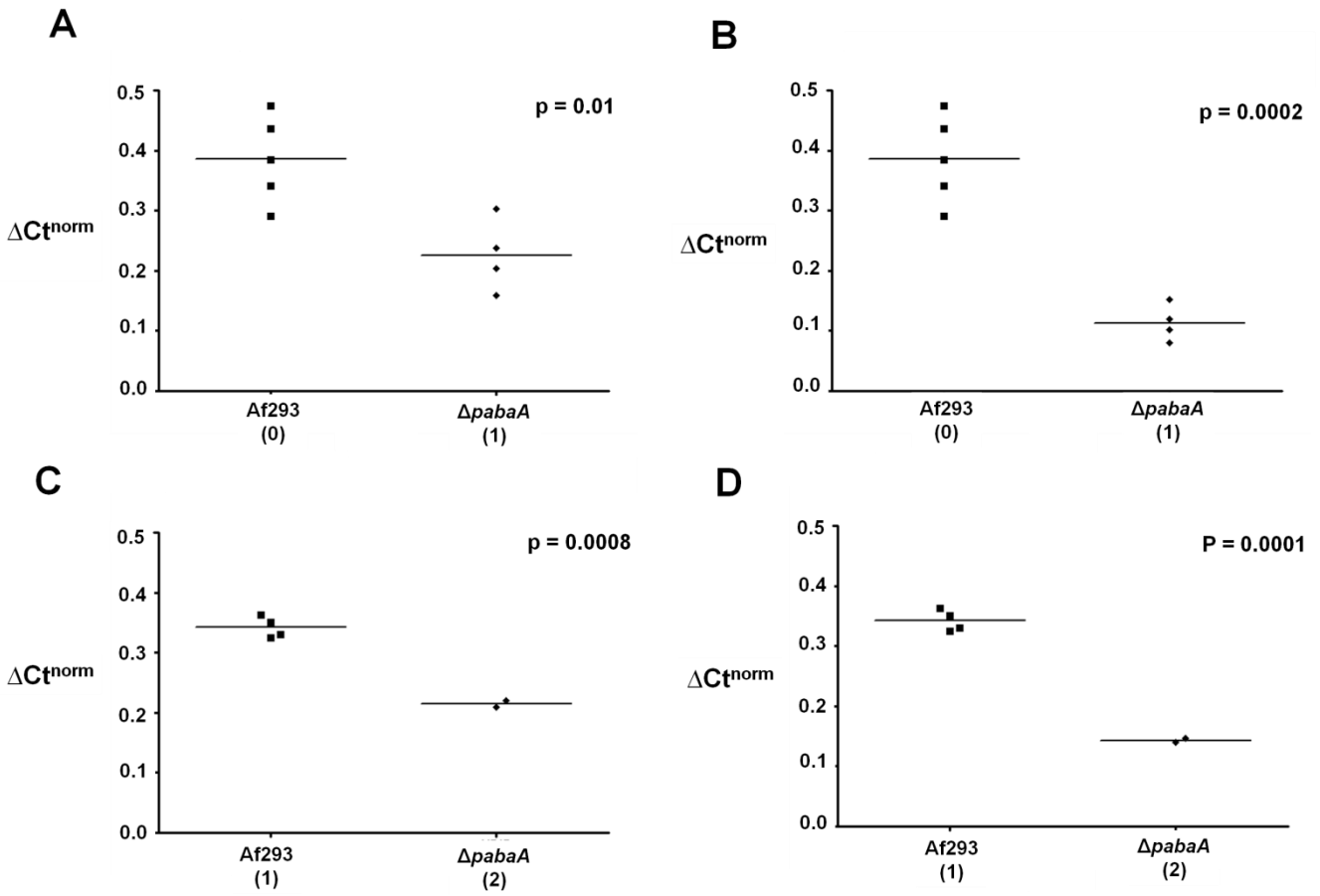


Figure 4.3: ΔCt^{norm} values calculated from Af293 or Δ*pabaA* infected mice in neutropenic and corticosteroid treated models of infection. ΔCt^{norm} values from neutropenic mice are shown without dose correction (A) and following dose correction (B). ΔCt^{norm} values from corticosteroid mice are shown with dose correction (C) and following dose correction (D). Horizontal lines depict the average ΔCt^{norm} value. Numbers in parentheses indicate the number of gDNA samples which amplified murine actin but did not amplify fungal beta tubulin. P values from nonparametric Mann-Whitney t-test are shown. All samples significantly deviate from the null hypothesis that ΔCt^{norm} values are not statistically different between Af293 and Δ*pabaA* infected lungs.

4.4. Survival, histological and infection burden comparisons of the Af293 clinical isolate with the Af293Δ*psoA* strain in neutropenic and corticosteroid treated murine models of infection.

An *A. fumigatus* Δ*psoA* strain was kindly given to our laboratory by Professor Geoffery Turner (University of Sheffield, Department of Molecular Biology and Biotechnology). The virulence of the Δ*psoA* strain was compared to the Af93 isogenic progenitor (Maiya et al. 2007) using survival, histological and infection burden assays in both neutropenic (Figure 4.4) and corticosteroid (Figure 4.5) models of infection.

Two biological replicates of survival analyses were conducted in the neutropenic model (Figure 4.4A and 4.4B). Both reported statistically significant reduction of virulence in Δ*psoA* relative to the

wild-type comparator (p = 0.01 and p = 0.0008, Kaplan-Meier plot and log rank analyses). Consolidation of replicate data into a single survival analyses demonstrated Δ*psoA* is reduced in virulence relative to Af293 in the neutropenic model, with median survival times of 4 and 6 days for Af293 and Δ*psoA* respectively (p = 0.0002, Kaplan-Meier plot and log rank analyses, Figure 4.4C). Histological samples from Af293 and Δ*psoA* infected mice were taken 4 days post infection. A reduction in Δ*psoA* burden and tissue inflammation was clearly discernable relative to Af293 infected lungs (Figure 4.4D, 4.4E, 4.4H and 4.4I). Δ*psoA* hyphae were mainly observed in the bronchioles, and hyphal penetration of lung epithelium was generally reduced compared to Af293 (Figure 4.4F and 4.4J). In Af293 infected lung, hyphal penetration of epithelia cells caused significant necrosis, with the destruction of host cells clearly visible in areas of invasion (Figure 4.4G). Conversely, areas of Δ*psoA* hyphal penetration showed intact epithelial cell layers (Figure 4.4K).

For infection burden analysis, 5 mice were infected with 3 x 10^4 Δ*psoA* spores which were culled on day 4 and fungal burden was quantified relative to murine beta tubulin using the ΔCt method described in section 4.3.3. ΔCt values were compared to the Af293 wild-type and Δ*pabaA* values reported in section 4.3.3, which were used as positive controls for virulent and attenuated isolates respectively. A single Δ*psoA* template did not amplify a beta tubulin target, suggesting the host had cleared *A. fumigatus* burden to levels below the detection limit of the assay (Figure 4.4L and 4.4M). ΔCt^{norm} values from Δ*psoA* infected mice were approaching significant reduction of burden without mathematical correction for dose differences between experiments (p = 0.0507, nonparametric Mann-Whitney t-test). Correction for differences in inoculum concentration relative to the wild-type dose suggested a significant reduction in fungal burden in Δ*psoA* relative to Af293 (p = 0.0237). Additionally, the Δ*psoA* burden was significantly greater than the avirulent Δ*pabaA* strain (p = 0.0042, Figure 4.4M).

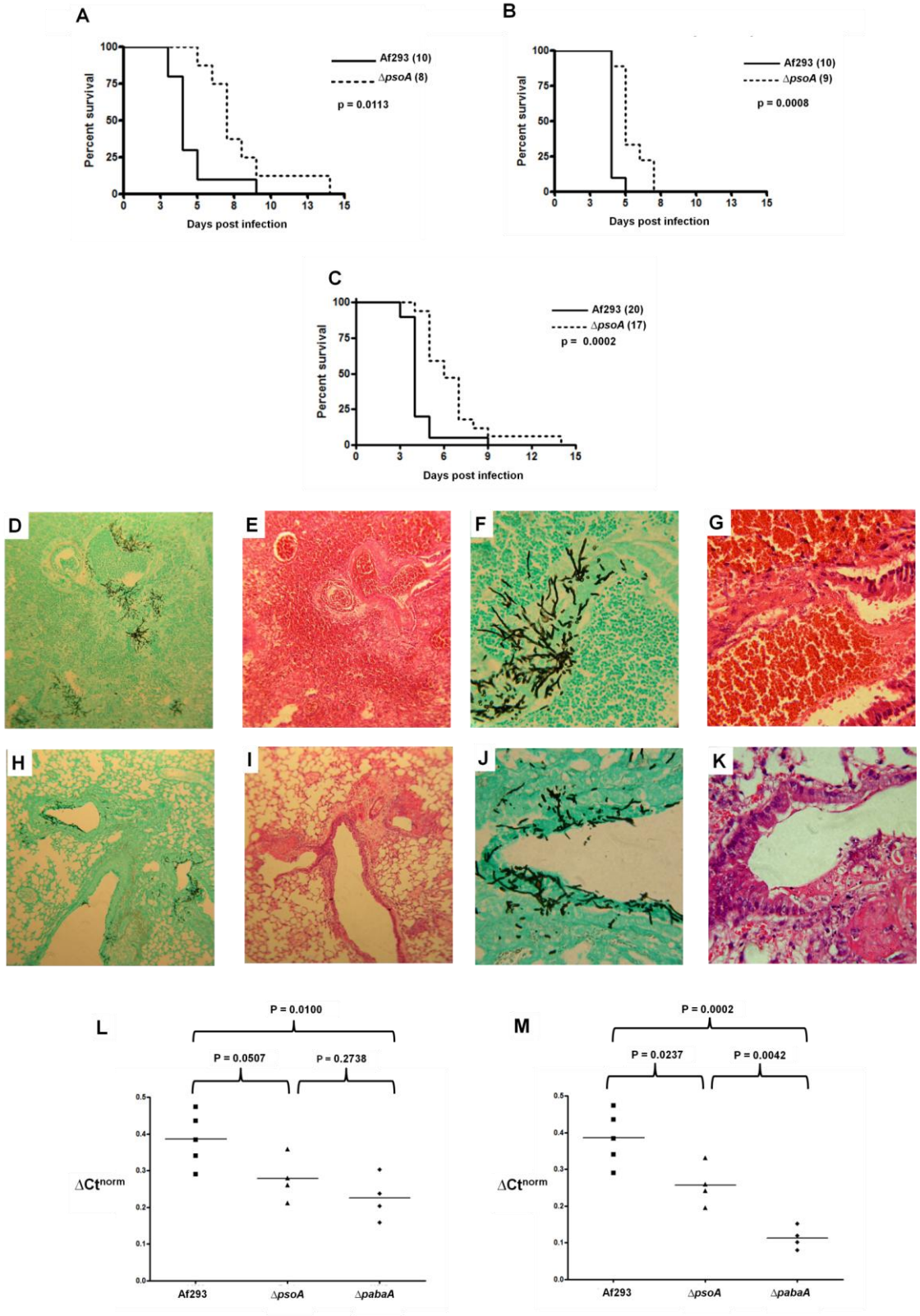


Figure 4.4: Survival, histological and tissue burden comparisons of Δ*psoA* and Af293 in a neutropenic murine model of infection. Survival analysis was conducted using two biological replicates. Numbers in parentheses indicate the number of animals per cohort. Replicate 1 (A) and replicate 2 (B) both demonstrate significant reduction in Δ*psoA* (dotted line) virulence relative to Af293 (solid line) using Kaplan-Meier log rank analyses. *P* values are shown for each survival comparison. Combination of both biological replicates into a single analysis demonstrated attenuation of Δ*psoA* relative to the wild-type (C, *P* = 0.0002). Histological comparisons from day +5 for Af293 (D – G) and Δ*psoA* infected lungs (H – K) using GMS staining (green images) and H&E staining (red images) are shown. Relative to Af293 sections (D and E), a reduction in Δ*psoA* burden (H) and tissue inflammation (I) was clearly discernable. Δ*psoA* hyphae were mainly observed in the bronchioles (J), and hyphal penetration of lung epithelium was generally reduced compared to Af293 (F). In Af293 infected lung, hyphal penetration of epithelia cells caused significant necrosis, with the destruction of host cells clearly visible in areas of invasion (F and G). Conversely, areas of Δ*psoA* hyphal penetration showed intact epithelial cell layers (J and K). Fungal burden was measured by qPCR from cohorts of five animals (L and M). ΔCt^{norm} values are shown without dose correction (L) and following dose correction (M). *P* values from nonparametric Mann-Whitney t-test are shown. Dose corrected Δ*psoA* values demonstrate a reduction and increase in burden relative to Af293 and Δ*pabaA* respectively.

Two biological replicates of survival analyses were conducted in the corticosteroid model (Figure 4.5A and 4.5B). Poor concordance was observed between replicates for the parental Af293 isolate. Median survival times were 3 and 5 days for replicate 1 and 2 respectively, which was statistically different (p = 0.0177). Consequently, experimental replicates 1 and 2 reported significant Δ*psoA* attenuation (p = 0.0055) and comparable virulence (p = 0.2515) with regard to the wild-type respectively. Consolidation of replicate data into a single survival analyses suggested Δ*psoA* is reduced in virulence relative to Af293 in the corticosteroid model, with median survival times of 3.5 and 5 for Af293 and Δ*psoA* respectively (p = 0.0184, Kaplan-Meier log rank analyses, Figure 4.5C). However, due to poor replication of the wild-type infection, survival analyses were considered inconclusive.

Histological samples from Af293 and Δ*psoA* infected mice were taken 5 days post infection. For both strains, limited germination of conidia was observed in environments of extensive host inflammation and immune cell recruitment (Figure 4.5D, 4.5E, 4.5H and 4.5I). These observations are consistent with examination of corticosteroid *A. fumigatus* infection reported by other groups (Balloy et al 2005). Histological examination suggested fungal burden and tissue inflammation were comparable between Δ*psoA* and Af293 infected lungs (Figure 4.5D, 4.5E, 4.5H and 4.5I). Additionally, tissue penetration and epithelial cell necrosis were limited in both isolates (4.5F, 4.5G, 4.5J and 4.5K).

5 mice were infected with 8 x 10^5 Δ*psoA* spores which were culled on day 5 and fungal burden was quantified relative to murine beta tubulin using the ΔCt method described in section 4.3.3. ΔCt values were compared to the Af293 wild-type and Δ*pabaA* values reported from the corticosteroid lung in section 4.3.3. A single Δ*psoA* template did not amplify a beta tubulin target, which suggested the host had cleared *A. fumigatus* burden to levels below the detection limit of the assay (Figure 4.5L and 4.5M). ΔCt^{norm} values from Δ*psoA* infected mice were approaching significant reduction of burden relative to the wild-type without mathematical correction for dose differences between experiments (p = 0.0703, nonparametric Mann-Whitney t-test). Correction for differences in inoculum concentration relative to the wild-type suggested a significant reduction in fungal burden in Δ*psoA* relative to Af293 (p = 0.0002). Interestingly, Δ*psoA* burden was not significantly different to the avirulent Δ*pabaA* strain (p = 0.1795, Figure 4.4M).

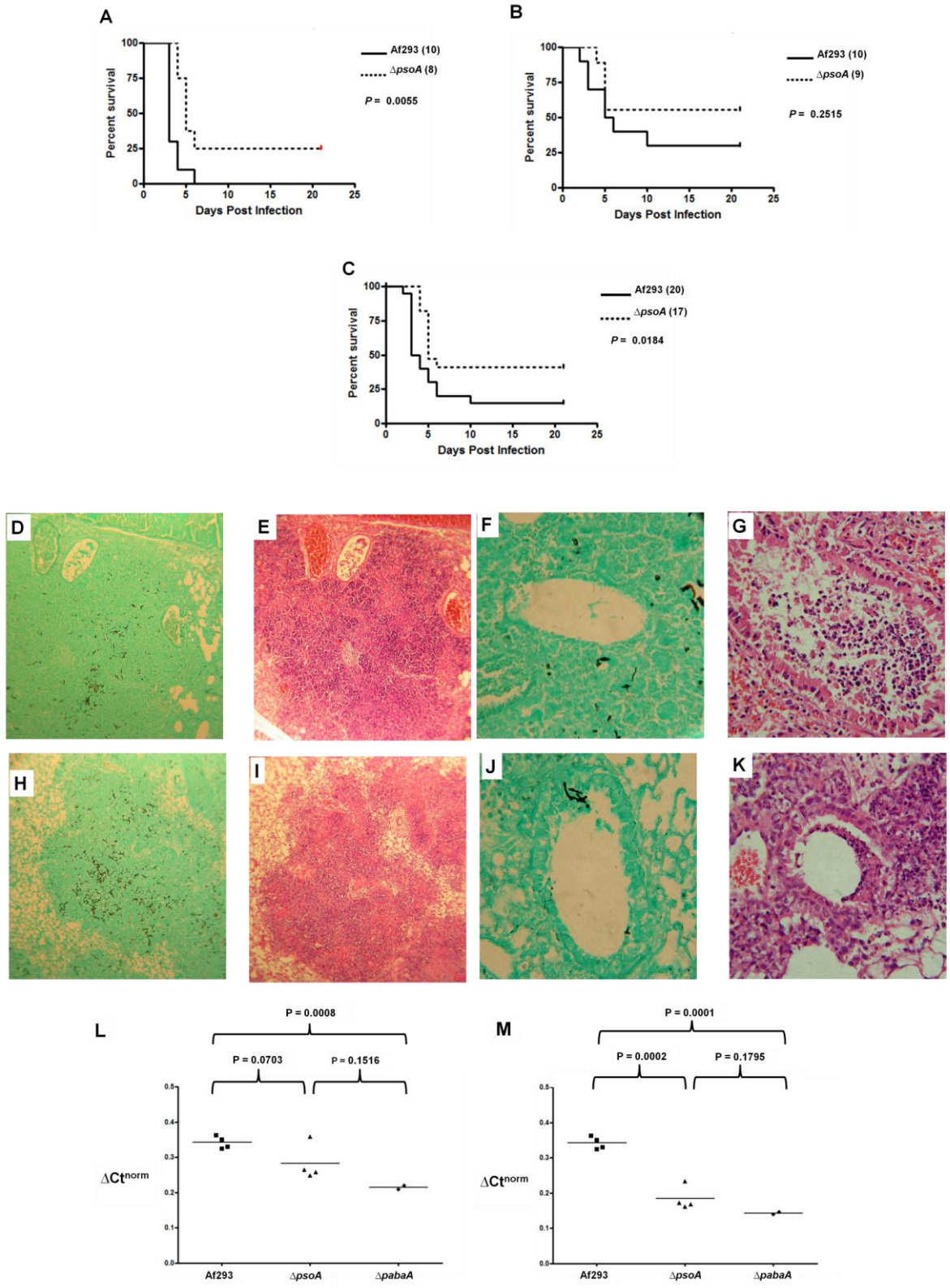


Figure 4.5: Survival, histological and tissue burden comparisons of Δ*psoA* and Af293 in a corticosteroid murine model of infection. Survival analysis was conducted using two biological replicates. Numbers in parentheses indicate the number of animals per cohort. Replicate 1 (A) demonstrates significant reduction in Δ*psoA* (dotted line) virulence relative to Af293 (solid line) using Kaplan-Meier log rank analyses. Replicate 2 (B) demonstrates comparable virulence between isolates. *P* values are shown for each survival comparison. Combination of both biological replicates into a single analysis suggests attenuation of Δ*psoA* relative to the wild-type (C, *P* = 0.018). Histological comparisons from lungs extracted on day +5 for Af293 (D – G) and Δ*psoA* infected lungs (H – K) using GMS staining (green images) and H&E staining (red images) are shown. For both strains, limited germination of conidia was observed in environments of extensive host inflammation and immune cell recruitment (Figure 5D, 5E, 5H and 5I). Fungal burden and tissue inflammation were comparable between Δ*psoA* and Af293 infected lungs (Figure 5D, 5E, 5H and 5I). Additionally, tissue penetration and epithelial cell necrosis were limited in both isolates (5F, 5G, 5J and 5K). Fungal burden was measure by qPCR from cohorts of 5 animals (L and M). ΔCt^{norm} values are shown without dose correction (L) and following dose correction (M). *P* values from nonparametric Mann-Whitney t-test are shown. Dose corrected Δ*psoA* values demonstrate a reduction in burden relative to Af293 (*P* = 0.0002). Burden between Δ*pabaA* and Δ*psoA* were comparable.

4.5 Survival, histological and infection burden comparisons of the Af293 clinical isolate with the Af293Δ*fmtA* strain in neutropenic and corticosteroid treated murine models of infection.

An *A. fumigatus* Δ*ftmA* strain was kindly provided by Professor Geoffery Turner (University of Sheffield, Department of Molecular Biology and Biotechnology). The virulence of the Δ*ftmA* strain was compared to the Af293 isogenic progenitor (Maiya et al. 2006) using survival, histological and infection burden assays in both neutropenic (Figure 4.6) and corticosteroid (Figure 4.7) models of infection. Spore concentrations of administered inocula for murine infections are given in Table 2.

Two biological replicates of survival analyses were conducted in the neutropenic model (Figure 4.6A and 4.6B). In both replicates, virulence was comparable between Δ*ftmA* and Af293 (Figure 4.6A and 4.6B). However, consolidation of replicate data into a single survival analyses reported median survival times of 4 and 5 days for Af293 and Δ*ftmA* respectively. This slight reduction in virulence of the Δ*ftmA* strain was approaching statistical significance ($p = 0.055$, Figure 4.6C).

Histological samples from Af293 and Δ*ftmA* infected mice were taken 5 days post infection. While *A. fumigatus* germination, growth and tissue penetration were comparable between isolates, frequency of pulmonary lesions in major airways was reduced in Δ*ftmA* (Figure 4.6D and 4.6H). It was therefore hypothesised from histological observations that the infectious burden would be reduced in the Δ*ftmA* strain. Tissue inflammation were comparable between infected lungs (4.6E and 4.6I). Hyphal morphology, tissue penetration and epithelial cell damage were comparable between the isolates (Figure 4.6F, 4.6F, 4.6J, 4.6K).

5 mice were infected with 3×10^4 Δ*ftmA* spores which were culled on day 4 and fungal burden was quantified. ΔCt values were compared to the Af293 wild-type and Δ*pabaA* values reported in section 4.3.3 (Figure 4.6L and 4.6M). ΔCt^{norm} values from Δ*ftmA* infected mice were significantly reduced relative to Af293 without mathematical correction for dose differences between experiments ($p = 0.026$, nonparametric Mann-Whitney t-test). Correction for differences in inoculum concentration relative to the wild-type dose supported a significant reduction in fungal burden in Δ*ftmA* relative to Af293 ($p = 0.0002$). Additionally, the Δ*ftmA* fungal burdens were not significantly greater than the avirulent Δ*pabaA* strain ($p = 0.0117$, Figure 4.6M).

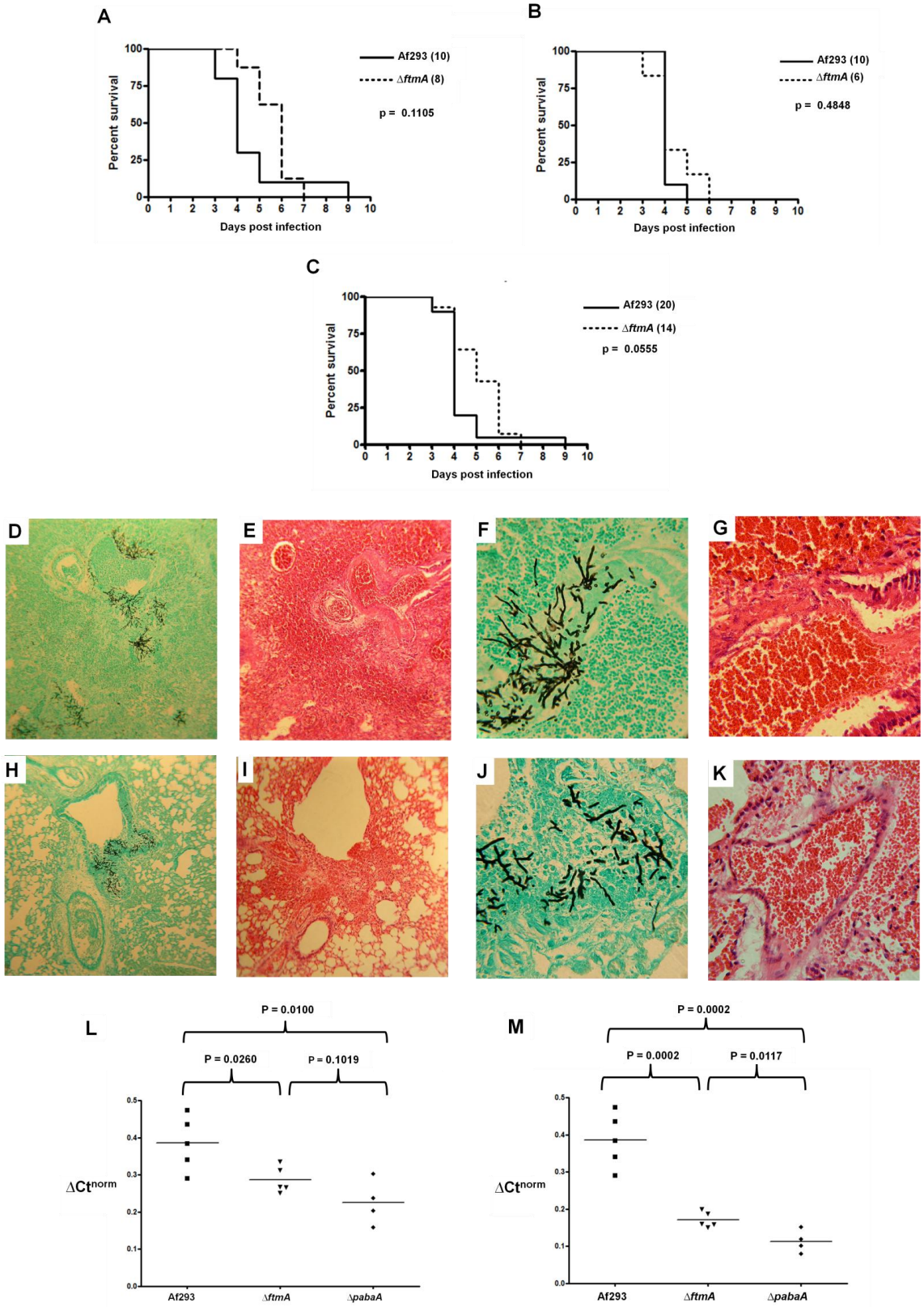


Figure 4.6: Survival, histological and tissue burden comparisons of Δ*ftmA* and Af293 in a neutropenic murine model of infection. Survival analysis was conducted using two biological replicates. Numbers in parentheses indicate the number of animals per cohort. Replicate 1 (A) and replicate 2 (B) both demonstrate comparable virulence between Δ*ftmA* (dotted line) and Af293 (solid line) using Kaplan-Meier log rank analyses. *P* values are shown for each survival comparison. Combination of both biological replicates into a single analysis suggested Δ*ftmA* virulence was slightly reduced, relative to the wild-type which was approaching significant (C, $P = 0.055$). Histological comparisons from day +5 for Af293 (D – G) and Δ*ftmA* infected lungs (H – K) using GMS staining (green images) and H&E staining (red images) are shown. Frequency of pulmonary lesions in major airways was reduced in Δ*ftmA* (Figure 6D and 6H). Tissue inflammation were comparable between infected lungs (6E and 6I). In both strains invasive hyphae penetrated lung epithelia and caused necrosis of host cells (Figure 6F, 6F, 6J, 6K). Fungal burden was measured by qPCR from cohorts of 5 animals (L and M). ΔCt^{norm} values are shown without dose correction (L) and following dose correction (M). *P* values from nonparametric Mann-Whitney t-test are shown. Δ*ftmA* ΔCt^{norm} values demonstrate a reduction in burden relative to Af293 with and without dose correction. Δ*ftmA* burden was greater than Δ*pabaA* but this was not statistically significant.

Two biological replicates of Δ*ftmA* survival analyses were conducted in the corticosteroid model (Figure 4.7A and 4.7B). As already noted, poor concordance was observed between replicates for the parental Af293 isolate. Consequently, experimental replicates 1 and 2 reported significant Δ*ftmA* attenuation (p = 0.0011) and comparable virulence (p = 0.8765) with regard to the wild-type respectively. Consolidation of replicate data into a single survival analysis suggested Δ*fmtA* is not significantly reduced in virulence relative to Af293 in the corticosteroid model, with median survival of 3 and 9 days for Af293 and Δ*ftmA* respectively (p = 0.0646, Kaplan-Meier log rank analyses, Figure 4.7C).

Histological samples from Af293 and Δ*ftmA* infected mice were taken 5 days post infection. For both strains, limited germination of conidia was observed in environments of extensive host inflammation and immune cell recruitment (Figure 4.7D, 4.7E, 4.7H and 4.7I) which was also observed in Δ*psoA* infected lung. Histological examination suggested fungal burden and tissue inflammation were comparable between Δ*ftmA* and Af293 infected lungs (Figure 4.7D, 4.7E, 4.7H and 4.7I). Additionally, tissue penetration and epithelial cell necrosis were limited in both isolates (4.7F, 4.7G, 4.7J and 4.7K).

5 mice were infected with 8 x 10^5 Δ*ftmA* spores which were culled on day 5 and fungal burden was quantified relative to murine beta tubulin using the ΔCt method. ΔCt values were compared to the Af293 wild-type and Δ*pabaA* values reported from the corticosteroid lung in section 4.3. A single Δ*ftmA* template did not amplify a beta tubulin target, which suggested the host had cleared *A. fumigatus* burden to levels below the detection limit of the assay (Figure 4.7L and 4.7M). ΔCt^{norm} values from Δ*ftmA* infected mice suggested a significant reduction of burden relative to the wild-type without mathematical correction for dose differences between experiments (p = 0.0276, nonparametric Mann-Whitney t-test). Correction for differences in inoculum concentration relative to the wild-type suggested the reduction in fungal burden was not statistically significant in the Δ*ftmA* strain relative to Af293 (p = 0.0558). Δ*ftmA* burden was significantly greater than the avirulent Δ*pabaA* strain (p = 0.0035, Figure 4.7M).

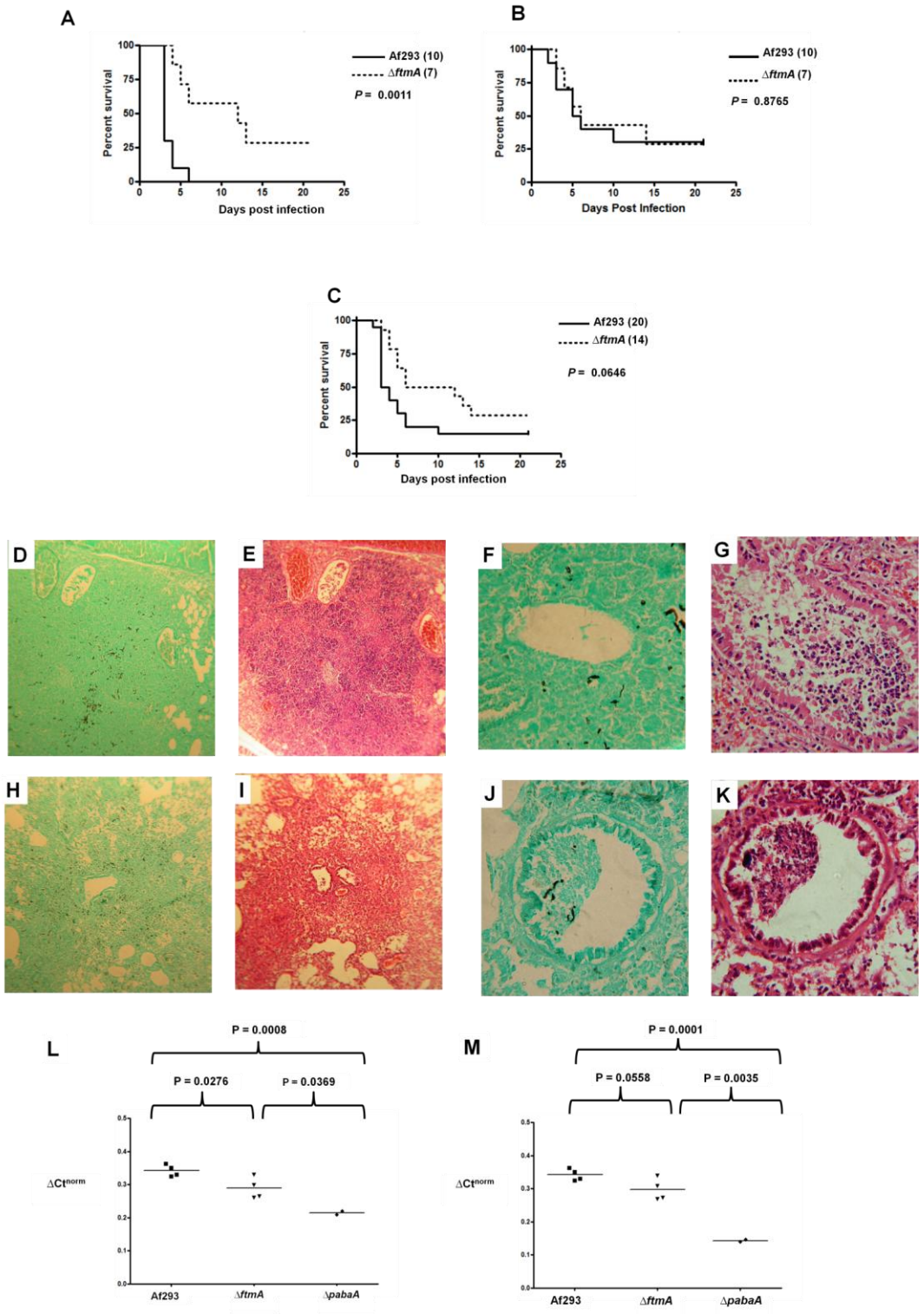


Figure 4.7: Survival, histological and tissue burden comparisons of Δ*ftmA* and Af293 in a corticosteroid murine model of infection. Survival analysis was conducted using two biological replicates. Numbers in parentheses indicate the number of animals per cohort. Replicate 1 (A) demonstrates significant reduction in Δ*ftmA* (dotted line) virulence relative to Af293 (solid line) using Kaplan-Meier log rank analyses. Replicate 2 (B) demonstrates comparable virulence between isolates. *P* values are shown for each survival comparison. Combination of both biological replicates into a single analysis suggests Δ*ftmA* is slightly reduces in virulence relative to the wild-type and that this is approaching statistical significance (C, *P* = 0.064). Histological comparisons from lungs extracted on day +5 for Af293 (D – G) and Δ*ftmA* infected lungs (H – K) using GMS staining (green images) and H&E staining (red images) are shown. For both strains, limited germination of conidia was observed in environments of extensive host inflammation and immune cell recruitment (Figure 5D, 5E, 5H and 5I). Fungal burden and tissue inflammation were comparable between Δ*ftmA* and Af293 infected lungs (Figure 5D, 5E, 5H and 5I). Additionally, tissue penetration and epithelial cell necrosis were limited in both isolates (5F, 5G, 5J and 5K). Fungal burden was measure by qPCR from cohorts of 5 animals (L and M). ΔCt^{norm} values are shown without dose correction (L) and following dose correction (M). *P* values from nonparametric Mann-Whitney t-test are shown. Fungal burden was decreased in the Δ*ftmA* strain relative to Af293 which was significant without dose correction (L). With dose correction the reduction in fungal burden was approaching significance (M). Δ*ftmA* values demonstrate an increase in burden relative to Δ*pabaA* in both dose corrected and non-dose corrected analyses (L and M).

4.6 Survival, histological and infection burden comparisons of the ATCC46645 clinical isolate with the ATCC46645Δ*pes3* strain in neutropenic and corticosteroid treated murine models of infection.

Virulence analyses of Δ*psoA* and Δ*ftmA* presented in the preceding sections have shown concordance between survival and qPCR analyses. Indeed, these data suggest infection burden may be a more sensitive virulence criterion than murine survival (for full consideration, please see the discussion section). In addition, infection burden analysis reduces experimental cost and animal use. Therefore, virulence of an *A. fumigatus* Δ*pes3* strain was assessed initially using the qPCR approach. *A. fumigatus* Δ*pes3* and the ATCC46645 wild-type background strains were provided by Professor Sean Doyle (Department of Biology, National University of Ireland). Mice were inoculated with 3 x 10^4 or 8 x 10^5 spores for neutropenic and corticosteroid cohorts respectively. Mice were culled on day 4 and 5 for neutropenic and corticosteroid models. In the corticosteroid treated cohort, two mice were culled from the Δ*pes3* group on days 3 and 4 due to end point weight loss. ΔCt^{norm} values are reported from both models without dose correction (8A and 4.8C) and following dose correction (4.8B and 4.8D). Doses were corrected relative to ATCC46645 inoculum concentration.

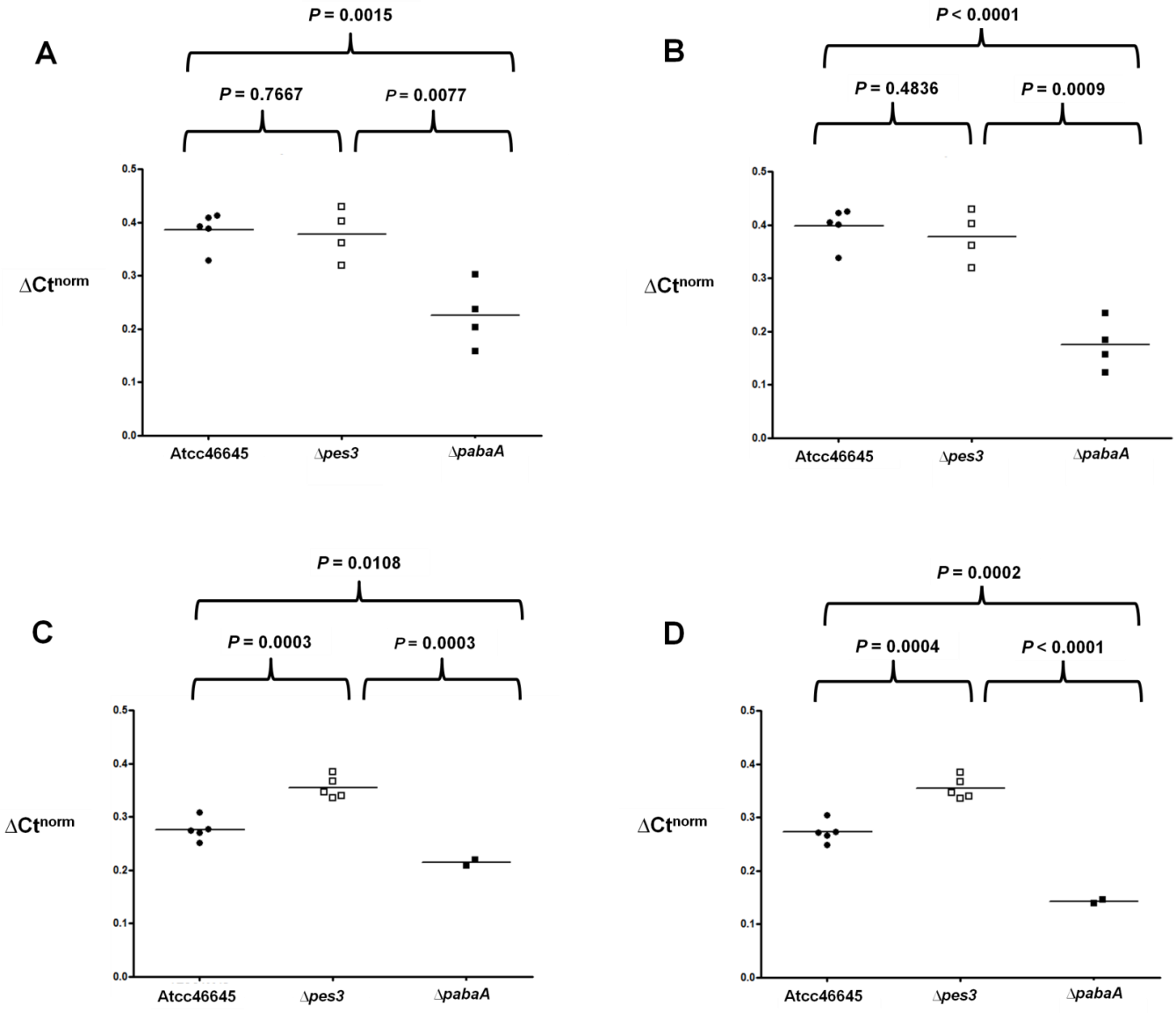


Figure 4.8: qPCR analyses of fungal burden from ATCC46645 or Δ*pes3* infected mice in neutropenic and corticosteroid treated models of infection. ΔCt^{norm} values from neutropenic mice are shown without dose correction (A) and following dose correction (B). ΔCt^{norm} values from corticosteroid mice are also shown with dose correction (C) and following dose correction (D). Horizontal lines depict the average ΔCt^{norm} value. *P* values from nonparametric Mann-Whitney t-test are shown. All lungs demonstrated significantly greater fungal burden than Δ*pabaA* infected animals. In the neutropenic model, burden of ATCC46645 and Δ*pes3* lungs were comparable. In corticosteroid treated mice, Δ*pes3* demonstrated greater fungal burden relative to ATCC46645 with and without dose correction.

ΔCt^{norm} values from ATCC46645 and Δ*pes3* cohorts in both models were significantly greater than the attenuated Δ*pabaA* isolate (Figure 4.8). In the neutropenic model, ΔCt^{norm} values were comparable between ATCC46645 and Δ*pes3* (Figure 4.8A and 4.8B). In the corticosteroid treated model, ΔCt^{norm} values were statistically greater from Δ*pes3* infected lungs relative to the ATCC46645 wild type, with or without dose correction (Figure 4.8C and 4.8D). These data

demonstrate an increase in *A. fumigatus* burden in Δ*pes3* infected mice, which suggests Pes3 deletion results in hypervirulence in murine models of infection.

In order to assess the basis of increased fungal burden in Δ*pes3* infected mice, histological analysis was used in a high dose model (1 x 10^7) to study the progression of infection at 14 and 24 hours post-infection. A significant benefit of these time-points is that immune cell recruitment is in the initiating stages. Consequently images are not saturated with host cells which impede visualisation of *A. fumigatus*. The most striking difference between wild-type and Δ*pes3* infected lungs was the earlier germination of the Δ*pes3* spores (Figure 4.9A and 4.9E). At 14 hours, approximately 70% of the Δ*pes3* spores had germinated, observed in both major airways and alveoli (Figure 4.9E). In contrast, less than 5% of the ATCC46645 spores throughout the lung had germinated (Figure 4.9A). At 24 hours post-infection the observed disparate germination was restricted to areas of high inflammation. A trend was clearly discernable towards more extensive germ tube production in Δ*pes3* infected animals relative to the wild-type (Figure 4.9C and 4.9G). At both stages of infection, a slight reduction in inflammation was noted in the Δ*pes3* strain, although this was most pronounced at 14 hours post infection (Figure 4.9B and 4.9F).

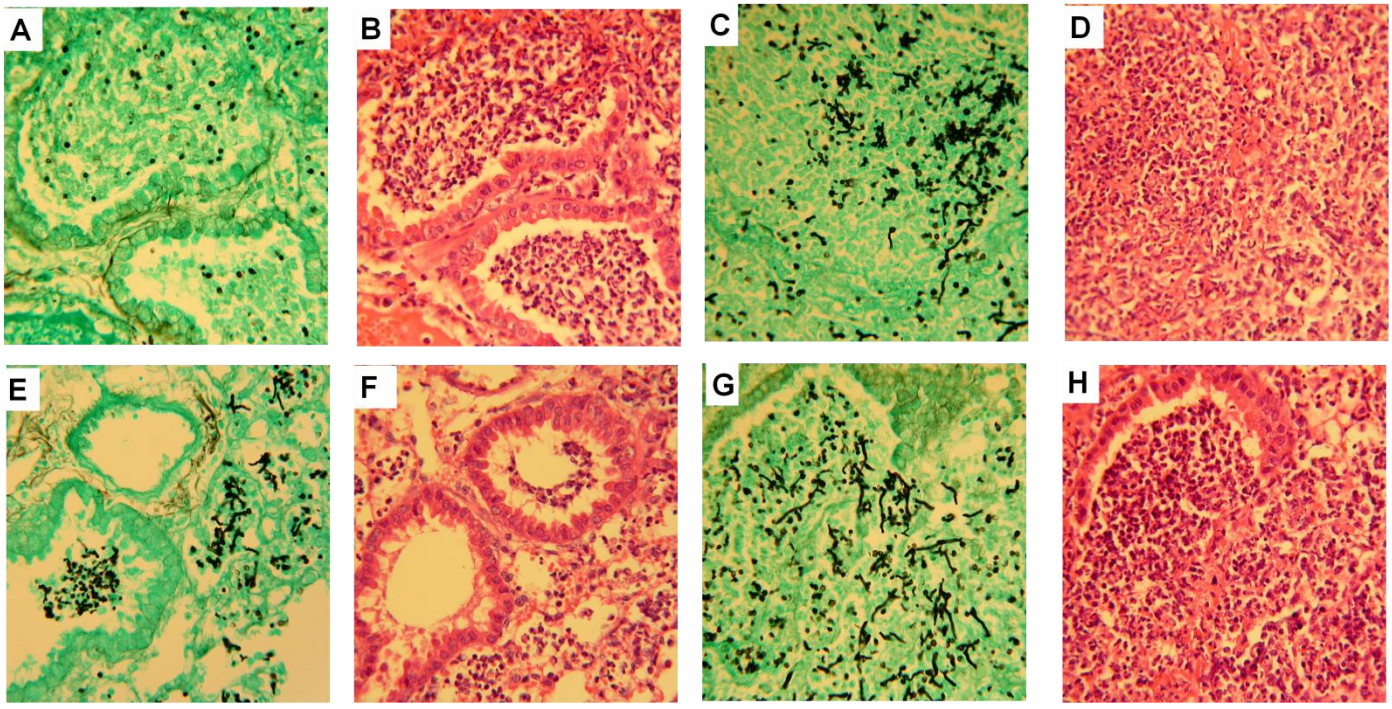


Figure 4.9: Histological comparisons of ATCC46645 and Δ*pes3* in corticosteroid treated murine model of aspergillosis at 14 and 24 hours post infection. Lung sections were stained using GMS (green images) and H&E (red images). Mice were infected with ATCC46645 and culled at 14 hours (A and B) and 24 hours (C and D). Additionally, mice were infected with Δ*pes3* and culled at 14 hours (E and F) and 24 hours (G and H). At 14 hours, less than 5% of the ATCC46645 spores throughout the lung had germinated (Figure 9A). In contrast, approximately 70% of the Δ*pes3* spores had germinated (E), which were observed in both major airways and alveoli. At 24 hours, trend was observed towards more extensive germ tube production in Δ*pes3* infected animals (G) relative to the wild-type (C). At both stages of infection, a slight reduction in inflammation was noted in the Δ*pes3* strain, although this was most pronounced at 14 hours post infection (Figure 9B and 9F).

Virulence of the Δ*pes3* mutant was compared to that of the parental wild type strain in a corticosteriod murine model of infection. 10 mice for each strain were immunosuppressed as described in the methods section and intranasally inoculated with 7 x 10^6 conidia. While a tendency towards an increase in virulence was observed for Δ*pes3*, this was not significant by log rank analysis (p = 0.32, Figure 4.10).

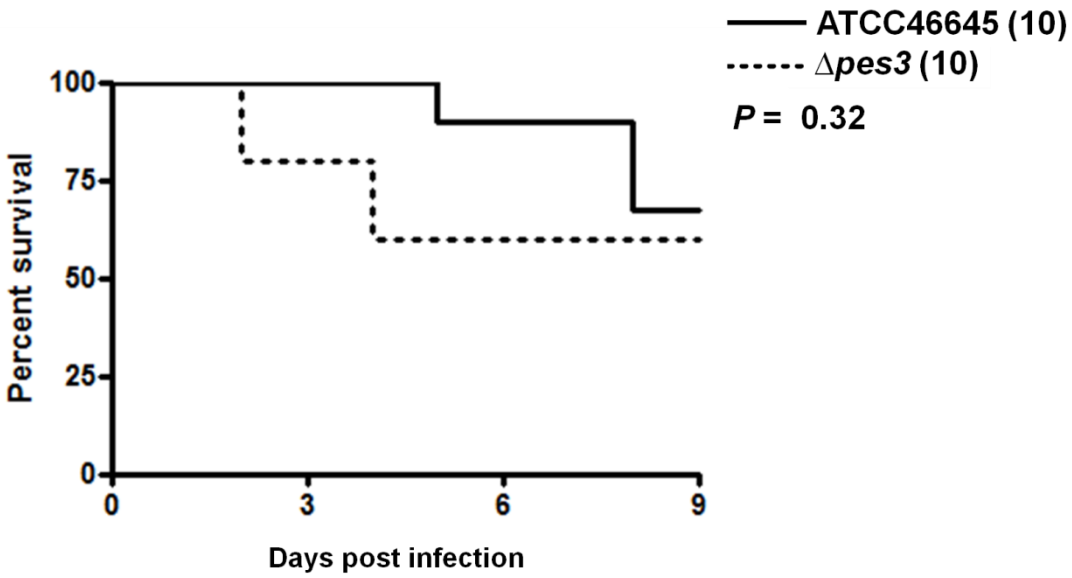


Figure 4.10: Survival comparison of ATCC46645 and Δ*pes3* isolates in a corticosteroid treated murine model of infection. Mice were immunosuppressed with hydrocortisone acetate and infected with 7 x 10^6 conidia. There was a trend towards increased virulence in the Δ*pes3* strain, but this was not significant by Kaplan-Meier log rank analyses (p = 0.32).

4.7 Discussion

Murine survival assays are the most common method for assessing virulence of *A. fumigatus* isolates (Clemons and Stevens 2005). Typically, cohorts of animals are concomitantly infected with a deletant mutant or an isogeneic progenitor, and weight loss is utilised as a predictive marker for mortality. Comparison of survival between the two infected cohorts enables the virulence of the deletant to be assessed relative to the isogenic progenitor. A significant limitation of these assays is their inability to detect modifications in host-pathogen interactions which might contribute to virulence but do not manifest as differences in murine weight loss. For example, the *A. fumigatus* alcohol dehydrogenase *alcC* has been demonstrated to impact the progression of IPA in a corticosteroid treated murine model of infection despite comparable levels of virulence relative to the progenitor strain in survival analysis (Grahl et al. 2011). The impact of *alcC* deletion was determined by histopathology, which demonstrated an increase of inflammation in lungs infected with Δ*alcC* relative to the wild-type. Additionally, flow cytometry of BALF demonstrated neutrophils were more abundant in Δ*alcC* infected samples.

When compared to survival analysis, the burden of a pathogen in host tissue is a more sensitive virulence criterion which can be used to assess virulence or effectiveness of drug treatment (Bowman et al. 2001). When comparing mutants and wild-type isolates, a reduction of infectious burden in mutant infected lungs might suggest attenuation, for example from impairment in the infectious process or reduced protection against host immune attack. Conversely, an increase in pathogen burden might imply increased growth rate in the host, or defective pathogen clearance. These data may then be interpreted as an augmentation of virulence, perhaps by enhanced aggressive or defensive pathogen strategies.

CFU counts have been published as a measure of *A. fumigatus* virulence. For example, Bok and colleagues enumerated *A. fumigatus* CFUs from homogenised Af293 or Δ*laeA* infected lungs to supplement survival data (Bok et al. 2005). The time-point analysed by Bok et al was 7 days post infection, when fungal morphology consists of extensive mycelium of filamentous hyphae. This method of burden quantification is not accurate for several reasons: (1) hyphae cannot be effectively disseminated on agar plates by spreading; (2) speading may cause cell breakage, and therefore death; (3) hyphae are multinucleate, thereby consist of multiple CFUs. To circumvent problems associated with survival analyses and CFU counting, several groups have investigated and developed infection burden assays of *A. fumigatus* mammalian infection models using qPCR

(Bowman et al. 2001, Vallor et al. 2008). These assays measure *A. fumigatus* burden in absolute terms and report infectious load as conidial equivalents.

For example, work conducted by Bowman and colleagues quantified *A. fumigatus* 18s RNA copy number from infected tissue, from which conidial equivalents were calculated using a standard curve which had been generated *in vitro* (Bowman et al. 2001). In a disseminated murine model of aspergillosis, assessment of tissue burden was concomitantly measured by CFU counts and qPCR analysis of infected kidney. Additionally, these data were cross-referenced to survival analysis in the same model. Mortality was first observed at day 4, and continued to increase until 7 days post infection, after which time none of the animals survived. The *A. fumigatus* burden in the kidneys of infected animals when measured at 4 and 7 days following CFU enumeration did not change significantly from the initial value determined at day 1. In contrast, qPCR determination of conidial equivalents suggested a near 10,000-fold increase in tissue burden between 4 and 7 days post infection. Thus, qPCR is more sensitive and accurate than CFU counting (Bowman et al. 2001). However, a disadvantage to this method is that gDNA in each sample is only measured using a single PCR target. Accordingly, the template for each reaction cannot be standardised by template concentration and is standardised by volume. The approach does not therefore experimentally account for differences among sample gDNA concentrations. Work described in this Chapter has found that total gDNA extracted from murine lungs might differ by as much as 100% between samples using a commercial gDNA extraction kit (data not shown). Thus, the gDNA extraction step is a potential source of significant variation in absolute measurements of *A. fumigatus* tissue burden using qPCR, and the gDNA content between samples, notwithstanding procedural variance, must differ.

To address this issue, an assay was developed to concomitantly quantify murine and *A. fumigatus* gDNA target by qPCR, and fungal burden was determined using a method based on ∆Ct calculations (Pfaffl 2001, Schmittgen and Livak, 2008). This strategy was based on three hypotheses: (1) murine gDNA concentration would vary as a factor of gDNA extraction efficiency; (2) fungal gDNA concentration would vary as a factor of gDNA extraction efficiency; (3) fungal gDNA concentration would vary relative to murine gDNA concentration based on the abundance of *A. fumigatus* in the murine lung. Therefore relative quantification of murine actin and fungal beta tubulin in every gDNA sample enables control for gDNA extraction efficiency and provides a relative measure of host and pathogen gDNA. Fungal burden is reported as ΔCt^{norm} values. ΔCt^{norm} are a mathematically modified ratio of fungal beta tubulin: murine actin which is indicative of the total fungal content per whole lung.

Several control experiments were conducted to ensure the assay could reproducibly and accurately measure fungal burden in the murine lung. In order to confirm that beta-tubulin and actin primers specifically amplified targets from *A. fumigatus* and murine templates respectively, qPCR reactions were conducted utilising both primer pairs with gDNA templates extracted from Af293 mycelium and saline inoculated murine lung. qPCR-mediated amplicon detection in gDNA from Af293 *in vitro* culture, and saline inoculated murine lung was restricted to PCRs using fungal beta tubulin and murine actin primers respectively (Figure 4.1). Thus, non-specific amplification was not observed for fungal and murine qPCR targets with actin and beta tubulin primers. For accurate ΔCt calculations, both primer pairs should amplify the target amplicon with efficiencies that do not deviate more than 10% from each other (Schmittgen and Livak, 2008). Primer amplification efficiencies for murine actin and fungal beta tubulin were calculated as 1.825 and 1.880 respectively. The relative amplification efficiency of the primer pairs was therefore deemed sufficiently matched for accurancy of ΔCt quantification (Schmittgen and Livak, 2008).

Finally, in a proof of principle experiment, the assay demonstrated reduction of *A. fumigatus* burden in lungs infected with an attenuated Δ*pabaA* isolate relative to a fully virulent Af293 strain in both neutropenic and corticosteroid models of infection (Figure 4.3). The Af293 isolate is fully virulent in both corticosteroid treated and neutropenic survival models of infection. Although the Δ*pabaA* isolate has only been demonstrated to be avirulent in a neutropenic model of murine survival (Brown et al. 2000), it was hypothesised that the inability of this isolate to germinate in the murine lung would reduce virulence relative to the wild-type in the corticosteroid model.

With regard to optimisation of the murine infections, inocula were reduced relative to those used for survival studies in order to limit the loss of animals prior to day +5. For neutropenic and corticosteroid treated models, lungs were extracted from mice culled on day + 4 or day + 5 respectively, which equated to median survival times of Af293 infected mice in each model. It was hypothesised that these time points represent a state of established *A. fumigatus* infection from which differences in fungal burden would be detectable. When compared to survival experiments, the infection burden assay uses less animals, which are required for a shorter time, and receive a reduced *A. fumigatus* inoculum. Thus, infection burden performs favourably with regard to ethics, cost and labour. Moreover, the data obtained from this study suggest that quantification of fungal burden might be a more sensitive virulence criterion than survival. Statistically significant reductions and increases in fungal burden relative to wild-type isolates were detectable for Δ*ftmA* and Δ*pes3* strains respectively (Figure 4.6 and 4.8). In contrast, survival analyses using these isolates demonstrated comparable levels of virulence. Survival anaysis can only detect marked

differences in virulence whereby the net effect of host and pathogen contributions to disease outcome are measured among a group of individuals. In the case of the qPCR assay a single virulence criterion is assessable and every animal provides significance data. Thus, fewer animals are required for the detection of smaller differences in virulence.

An additional advantage to the assay developed in this study when compared to other qPCR assays is the use of fungal beta tubulin for quantification of fungal burden. BLAST analyses of Af293 and A1163 genomes demonstrated a single copy of the beta tubulin gene employed in this study. Additionally, qPCR using identical concentrations of template from A1163, ATCC46645 and Af293 gDNA resulted in comparable Ct values (data not shown), indicating the copy number of beta tubulin does not differ between isolates. Thus, comparisons of fungal burden can be made between wild type isolates. In contrast, Bowman and colleagues utilised the 18s RNA gene which is present in multiple copies in the *A. fumigatus* genome which occur in a tandem array (Bowman et al. 2001). While this might improve sensitivity of a PCR assay, screening of 8 *A. fumigatus* clinical isolates found between 38 – 91 18s RNA copies for each strain (Herrera et al. 2009). Accordingly, standardisation would be required for accurate inter-strain comparisons of fungal burden.

While dose of administered inocula is constant within strains cohorts, it might vary between strain cohorts. To address this issue, inocula were enumerated by serial dilution and plating, and $Log_{10}(E)^{\Delta Ct}$ values corrected according to dose differences between mutants and their progenitor isolate. Throughout this study, both uncorrected and dose corrected ΔCt^{norm} values are given. In both neutropenic and corticosteroid models, uncorrected ΔCt^{norm} values suggested fungal burden in the Δ*psoA* mutant relative to the wild type was approaching a significant reduction ($p = 0.05$ and $p = 0.07$ respectively). Following dose correction, this reduction in both models was deemed significant ($p = 0.02$ and $p = 0.0002$ respectively Figures 4.4 and 4.5). Uncorrected ΔCt^{norm} values from corticosteroid treated mice suggested a significant reduction in Δ*ftmA* infectious burden ($p = 0.02$, Figure 4.7) relative to the wild-type. Dose correction suggested infectious burden was reduced in Δ*ftmA*, but this was not deemed statistically significant ($p = 0.055$). Thus, dose correction dose not drastically impact interpretation of fungal burden data, but may help to reduce experimental variation between infected cohorts. Finally, this approach is cheaper than the utilisation of a galactomannan ELISA or a TaqMan probe, both of which have been utilised in experimental models of IPA (Vallor et al. 2008). The utility of this assay as a tool for analyses of murine virulence is supported by its recent use in several peer reviewed studies (Bergmann et al. 2009, Bhatti et al. 2011, O'Hanlon et al. 2011). Using this approach, hypervirulence (O'Hanlon et

al. 2011, this study), hypovirulence (this study) and wild-type virulence (Bergmann et al. 2009, Bhatti et al. 2011) have been demonstrated in various murine models of infection.

Several limitations must be considered when utilising this assay. Firstly, the assay cannot distinguish between live or dead fungi. Killed *A. fumigatus* cells are able to illicit immune responses, and therefore may contribute to the pathogenesis of IPA. For example, Morgenstern and co-workers demonstrated increased neutrophil recruitment and proinflammatory cytokine production occurs in an X-linked mouse model of CGD following intratracheal inoculation with heat killed hyphae (Morgenstern et al. 1997). In contrast, dead *A. fumigatus* morphologies will presumably cause reduced tissue invasion and dissemination. These considerations are not addressed by qPCR assessments of fungal burden. A potential source of variation when using the qPCR assay developed in this Chapter is that the mass of the lung may vary with the mass of the animal. Increased murine lung mass would decrease the ΔCt^{norm} values, and may impact interpretation of fungal burden if one cohort has a significantly increased lung mass when compared to another. In this study, the majority of mice weighed between 25 and 30 g and the average mass of the lung was not found to vary significantly between cohorts. For example, in the pilot study utilising Af293 (n = 5) and Δ*pabaA* (n = 5) in the neutropenic model, average lung mass was 0.27 and 0.22 g respectively (standard deviation = 0.05 and 0.07 respectively). Nevertheless, potential variation in weight between mice must be considered in future applications of this assay, and addressed by reallocation of mice to appropriate cohorts if a significant difference in animal mass is observed.

Additionally, the qPCR assay does not consider host responses, which are a critical factor in IPA (Romani 2004). In a corticosteroid treated model of infection, the majority of lung damage is attributed to the host inflammatory response (Balloy et al. 2005). Models of IPA must therefore consider differential host responses between wild-type and mutant isolates. This is supported by a study by Grahl and co-workers, who demonstrated differential inflammatory responses to Δ*alcC* and the isogenic progenitor by histopathological and flow cytometric analysis of infected lungs and murine BALF respectively (Grahl et al. 2011). Thus, the fungal burden assay developed in this thesis represents a useful tool for analysing a virulence criterion, yet it cannot be considered the only necessary measure of fungal virulence. The benefits of the assay can be considered greatest when combined with both survival and histological analyses. This approach was conducted to assess virulence of *A. fumigatus* Δ*psoA*, Δ*ftmA* and Δ*pes3* mutants relative to their wild-type comparators.

Pseurotin A is a cyclic peptide putatively biosynthesised by a 5 gene cluster in the left subtelomeric region of chromosome 8. Genes in the cluster include two hydrolases (Afu8g00530, Afu8g00570) a methyltransferase (Afu8g00550), and P450 monooxygenase (Afu8g00560) and the hybrid PKS/NRPS *psoA* (Afu8g00540) (Maiya et al. 2007). *psoA* is required for the biosynthesis of pseurotin A in *A. fumigatus* (Maiya et al. 2007). Several observations suggest that pseurotin A is produced the murine pulmonary cavity. Gene expression studies described in Chapter 3 demonstrated increased *psoA* transcript abundance in Af293 and Δ*laeA* strains during the initiation of murine infections (Table 3.17). Secondly, comparative transcriptional analysis of germlings isolated from the murine host and developmentally matched *in vitro* culture showed *psoA* was preferentially employed during infection (McDonagh et al. 2008). Hypoxic conditions are encountered in the neutropenic host (Grahl et al. 2011), and transcriptional, proteomic and metabolic analyses have demonstrated pseurotin A is biosynthesised in hypoxic, but not normoxic culture (Vodisch et al. 2011).

To assess the hypothesis that *psoA* might contribute to *A. fumigatus* virulence, the deletant mutant was assessed with regard to virulence, fungal burden and tissue invasion in murine models of infection. In the neutropenic model, two independent survival comparisons (Figure 4.4) of Δ*psoA* and the wild-type isolate Af293 reported significant attenuation of the mutant (p = 0.01 and p = 0.0008, Kaplan-Meier log rank analyses). Consolidation of the datasets produced the same result, whereby Δ*psoA* is attenuated relative to Af293 in the neutropenic model, with median survival of 4 and 6 days for Af293 and Δ*psoA* respectively (p = 0.0002). These data suggest *psoA* is required for wild-type virulence in a neutropenic murine model. In support of this hypothesis, dose corrected qPCR analyses of infection burden demonstrated a reduction in *A. fumigatus* burden in Δ*psoA* infected lungs relative to Af293 (p = 0.02). These data suggest impairment either in the infectious process or protection against host immune attack. Interestingly, Δ*psoA* burden was significantly greater than the avirulent Δ*pabaA* strain (p = 0.004), which is consistent with germination and some growth of Δ*psoA* in the lung.

In order to determine the basis of attenuation and decreased fungal burden in Δ*psoA* infected animals, the histopathological basis of IPA was studied at 4 days post infection. A reduction of host inflammation in Δ*psoA* infected lungs was clearly discernable, with host inflammatory cells localised around major airways which harboured *A. fumigatus*. In contrast, the Af293 infected lung demonstrated extensive areas of inflammation that were observed throughout regions surrounding the bronchioles and alveoli. Three hypotheses are consistent with these observations; (1) pseurotin A or an intermediate metabolite interacts with the host in Af293 infected animals,

causing significant inflammation; (2) Δ*psoA* is less invasive which elicits a muted immune response; (3) both of the above. In support of the second hypothesis, Δ*psoA* hyphae were mainly observed in the bronchioles, and hyphal penetration of lung epithelium was generally reduced compared to Af293 (Figure 4.4). Moreover, in Af293 infected lung, hyphal penetration of epithelia cells caused significant necrosis, with the destruction of host cells clearly visible in areas of invasion. In contrast, areas of Δ*psoA*-epithelial interaction generally exhibited an intact epithelial layer with minimal necrosis. Accordingly, it was hypothesised that reduced cytotoxicity of Δ*psoA* to host epithelial cells might limit or reduce invasion of the airways. This might be a contributing factor to the mutant phenotype, reduced fungal burden and consequently muted inflammatory response in neutropenic mice.

Lung epithelial cells constitute the main physical barrier to *A. fumigatus* infection (Latge 1999). *Ex vivo* assays have focused on the role of secreted proteases in spore epithelial damage and immune attack (Kogan et al. 2004). Data presented here suggest that the secondary metabolite toxin pseurotin A or an intermediate metabolite thereof might facilitate epithelial cell damage by hyphae, and that this might have critical implications for the establishment of infection. This hypothesis is supported by transcriptional analyses, which show that expression of genes required for pseurotin A biosynthesis is greatest at the invasive stage (Chapter 3, McDonagh et al. 2008).
Pseurotin A has pleiotropic effects on host cells *in vitro.* Ishikawa and co-workers screened B-cells isolated from spleens of naive mice with Pseurotin A purified from *A. fumigatus in vitro* culture (Ishikawa et al. 2009). ELISA analysis of B-cell IgE production demonstrated IgE was strongly inhibited by challenge with Pseurotin A. Screening of microbial metabolites which induce cellular differentiation in a rat pheochromocytoma cell line by Komagata and co-workers demonstrated pseurotin A is neuritogenic (Komagata et al. 1996). These authors isolated pseurotin A from 4 day culture of the ascomycete *Diheterospora chlamydospora* using silica gel chromatography. Pseurotin A induced neutrite outgrowth in the rat cell line. Furthermore, pseurotin A inhibits chitin synthase activity (Wenke et al. 1993). Pseurotin A isolated from *Penicillium janczewskii* demonstrated low toxicity (IC_{50} ≤ 1000 µM) to lung fibroblasts (Schmeda-Hirschmann et al. 2008). Although these data are conducted from *in vitro* studies which do not address the multifaceted host niche, they tentatively support the hypotheses that pseurotin A might act as an aggressive and cytotoxic molecule, but are suggestive of pleiotrophic effects *in vivo*. An important consideration when analysing NRPS or PKS deletants in murine models of infection is that it is speculative to comment on the molecule which modulates virulence in the host niche. For example, the hybrid PKS/NRPS *psoA* putatively catalyses the first step in pseurotin A biosynthesis (Maiya et al. 2007). However, the pseurotin A biosynthetic pathway likely involves at least 3

intermediates, putatively including azaspirene (Maiya et al. 2007). Azaspirene is a bioactive molecule, which has been shown to inhibit angiogenesis *in vitro* (Asami et al. 2008). Angiogenesis is the formation of new blood vessels from existing blood vessels, and might represent an important host strategy for the prevention of thrombosis and tissue infarction during IPA (Ben-Ami et al. 2009). Thus, while it is tempting to speculate on the aggressive role of pseurotin A in a neutropenic model of infection, this study cannot identify the precise host-pathogen interaction. Indeed, it is possible that deletion of *psoA* has pleiotrophic effects on the establishment of IPA which synergistically contribute to the observed reduction in virulence.

The immune status of the host is critical with regard to fully understanding host pathogen interactions and virulence, as evidenced by the attenuation of *ΔgliP* and *ΔgliZ* strains in corticosteroid treated, but not neutropenic models of aspergillosis (Bok et al. 2006b, Cramer et al. 2006, Sugui et al. 2007a). Transcript abundance of both the NRPS/PKS *psoA* (Afu8g00540) and the neighbouring methyltransferase gene (Afu8g00550) are elevated in a corticosteroid treated murine model of infection (Alcazar-Fuoli et al. in writing). Therefore it was hypothesised that *psoA* might be required for virulence in a corticosteroid model of infection. To assess this hypothesis, the deletant mutant was assessed with regard to virulence, fungal burden and tissue invasion in a murine corticosteroid model of infection.

The reproducibility of the corticosteroid survival assay employed in this study was unsatisfactory for the parental Af293 isolate. The poor reproducibility is difficult to explain, given that weight and inoculum concentration were comparable between replicates. It is possible that this model is generally more variable as the main cause of damage is the host response (Balloy et al 2005). Median survival times from two biological replicates were 3 and 5 days (Figure 4.5), inferring a statistically significant difference in virulence (p = 0.01). Consequently, biologically replicated survival analyses produced conflicting results of both significant Δ*psoA* attenuation (p = 0.005) and comparable virulence (p = 0.251). In both replicates, a trend towards reduced virulence relative to the Af293 isolate in Δ*psoA* infected animals was observed. Additionally, consolidation of these data suggested Δ*psoA* is attenuated relative to Af293 in the corticosteroid model, with median survival times of 3.5 and 5 for Af293 and Δ*psoA* respectively (p = 0.01). These data suggest Δ*psoA* might be attenuated in this model. Survival analyses are being repeated at the time of writing this thesis.

Dose corrected qPCR analyses of infection burden reported a reduction in *A. fumigatus* burden in Δ*psoA* infected lungs relative to Af293 (p = 0.0002). These data suggest impairment either in the

infectious process or protection against host immune attack. In order to determine the basis of the likely attenuation and decreased fungal burden in Δ*psoA* infected animals, the histopathological basis of IPA was studied at 5 days post infection. Histological examination suggested fungal burden and development were comparable between Δ*psoA* and Af293 infected lungs, with both isolates characterised by germlings or small hyphae surrounded by extensive host inflammatory cells. The disparity between qPCR and histopathological assessments of infection burden in this model highlights difficulties in assessing the extent of fungal growth in corticosteroid treated lungs by histology as the airways are characterised by extensive inflammation. These cells physically mask the fungus, making assessment of burden difficult using light microscopy. Thus, the qPCR analysis is considered a more reliable measure of *A. fumigatus* load in the corticosteroid infected lung (Figure 4.5).

Histopathology also demonstrated tissue inflammation and epithelial cell necrosis was comparable between Δ*psoA* and Af293 infected lungs. Thus, the following contradictory results have been reported with regard to the virulence of Δ*psoA* in a corticosteroid model of IPA: (1) notwithstanding unsatisfactory replication, survival analyses suggest attenuation of Δ*psoA* relative to the wild-type; (2) qPCR analyses demonstrate a reduction of fungal burden in the Δ*psoA* infected lung; (3) histopathology suggests comparable progression of infection and inflammation.

These data highlight the difficulty in interpreting data from murine models of IPA. Although the mechanistic basis of reduced Δ*psoA* fungal burden and attenuation remains elusive, insights into the role of pseurotin A or another metabolite intermediate can be gleaned from the assays conducted in this model. In contrast to the neutropenic animals, a reduction in fungal burden was reported in Δ*psoA* relative to Af293 infected animals, despite comparable levels of epithelial necrosis. These data implicate a product or products from the pseurotin A biosynthetic pathway in more than one host-pathogen interaction. Moreover, this supports the hypothesis that the pseurotin A biosynthetic pathway has pleotrophic effects on virulence, and suggests these interactions might be specific to the host niche. In this instance, it appears that fungal burden might perform favourably as a measurement of fungal virulence.

ftmA encodes a dimodular NRPS which forms the diketopiperazine brevianamide F by the condensation of amino acids L-tryptophan and L-proline (Maiya et al. 2006). Brevianamide F is the precursor for fumitremorgin B, fumitremorgin C, tryprostatin A and tryprostatin B biosynthesis in *A. fumigatus* (Grundmann et al. 2008, Kato et al. 2009). *ftmA* transcript abundance increased and decreased in Af293 and Δ*laeA* isolates respectively during the initiation of murine infection

(Chapter 3). Fumitremorgins and tryptostatins are mycotoxins which act on the central nervous system to induce tremors and titanic spasms in mice (Yamazaki et al. 1979). Accordingly, it was hypothesised that *ftmA* might be required for full murine virulence.

Two independent survival comparisons of Δ*ftmA* and the wild-type isolate Af293 in a neutropenic model reported comparable virulence between strains, although a trend towards greater survival in Δ*ftmA* infected cohorts was observed (p = 0.11 and p = 0.48). Consolidation of both biological replicates into a single survival analysis demonstrated that Δ*ftmA* approaches a significant reduction in virulence relative to Af293, with median survival times of 5 and 4 days respectively (p = 0.055). These data suggest inclusion of more mice or additional replicates might report a significant attenuation of the Δ*ftmA* strain.

Dose corrected qPCR analyses demonstrated a reduction in *A. fumigatus* burden in Δ*ftmA* infected cohort relative to Af293 (p = 0.0002). These data were supported by histopathological analyses, where a trend towards fewer pulmonary lesions in major airways was observed in Δ*ftmA* infected lungs. In contrast, at local areas of infection hyphal growth, tissue penetration, inflammation and angioinvasion were comparable between isolates. The wild-type progression of local pulmonary lesions, yet decrease in their frequency throughout the lung, suggests a gross reduction in the initial infectious challenge, possibly caused by heightened susceptibility of Δ*ftmA* to ciliary beat. Ciliated cells line the nose, trachea, and lower airways and physically remove pathogens in from the airways to the intestinal tract. *In vitro* assays have suggested several *A. fumigatus* mycotoxins inhibit the ciliary beat of human epithelial cells, including fumagillin, gliotoxin, helvolic acid and other unknown secondary metabolites (Amitani et al. 1995). In an intranasal model of *Staphylococcus aureus* infection, chemical inhibition of murine ciliary beat resulted in greater infectious burden at 5 days post infection (Kimura et al. 1999). Therefore, ciliary beat might play a substantial role in removing *A. fumigatus* from the lower and upper airways in the intranasal model employed in this study. It is possible that a secondary metabolite produced from the brevianamide F precursor might inhibit ciliary beat in Af293 infected lungs throughout infection. If so, infection with Δ*ftmA* would lead to increased ciliary beat and pathogen clearance, resulting in the observed gross reduction in *A. fumigatus* pulmonary challenge and *A. fumigatus* burden. However, this hypothesis is entirely speculative and substantial additional analyses are required to determine the molecular basis of Δ*ftmA* reduction in the murine lung.

Notwithstanding the molecular basis of Δ*ftmA* attenuation, data presented here suggest that reduced biosynthesis of *ftmA* in Δ*laeA* relative to Af293 during murine infection (Chapter 3, Perrin

et al. 2007) might synergistically contribute to reduced virulence of the Δ*laeA* mutant (Bok et al. 2005, Sugui et al. 2007b)

Two survival analyses demonstrated attenuation ($p = 0.001$) and comparable virulence ($p = 0.876$) of Δ*ftmA* with regard to the wild-type respectively due to poor concordance between wild-type replicates. Consolidation of biological replicates into a single survival analyses suggested Δ*fmtA* approaches significantly reduced virulence relative to Af293 in the corticosteroid model ($p = 0.06$). Dose corrected qPCR analyses of infection burden demonstrated a trend towards reduced fungal burden in Δ*ftmA* infected lungs relative to Af293 although this was not statistically significant ($p = 0.055$). Histological samples from Af293 and Δ*ftmA* infected mice were taken 5 days post infection which demonstrated comparable fungal morphology and tissue inflammation between isolates. Thus, the role of *ftmA* during IPA in a corticosteroid model of infection seems minimal.

The NRPS Pes3 (Afu5g12730) resides in a 5 gene cluster, including a hypothetical protein (Afu5g12700), TPR domain protein (Afu5g12710), ABC multidrug transporter (Afu5g12720) and MFS multidrug transporter (Afu5g12740). These annotations provide no clue as to the putative product. Characterization of a *pes3* disruption mutant has recently been reported by our collaborators from Professor Sean Doyle's laboratory at the National University of Ireland (O'Hanlon et al. 2011). Comparative LC-MS analyses of Δ*pes3* or wild-type metabolite extracts from *in vitro* growth were unable to assign a secreted metabolite to *pes3*, despite detectable gene expression under several laboratory conditions. Interestingly, germ tubes of Δ*pes3* aggregated and scanning electron microscopy of the germlings demonstrated the loss of a distinctive rod like structure on the cell wall. Thus, the authors hypothesised that *pes3* encodes a structural peptide. Interestingly, stimulation of murine bone-derived macrophages with germlings demonstrated a diminished cytokine response following Δ*pes3* stimulation relative to the wild-type, with Il-6, IL-10 and TNF-α protein levels reduced. Furthermore, *pes3* deletion caused hypervirulence in a *G. mellonella* model of infection. Accordingly, it is possible that *pes3* deletion results in modulation of a PAMP which abrogates immune recognition of *A. fumigatus* (O'Hanlon et al. 2011). Gene expression profiling conducted in Chapter 3 demonstrated an increase in *pes3* transcript abundance for both Af293 and Δ*laeA* strains during the initiation of murine infection. Accordingly, it was hypothesized that *pes3* might impact upon host pathogen interactions and virulence in murine models of infection. To further explore the role of *pes3* during IPA, virulence of an *A. fumigatus* Δ*pes3* strain was assessed relative to the ATCC46645 wild-type using qPCR quantification of fungal burden. This approach was employed in the first instance due to the favourable performance of the qPCR assay over survival comparisons (see preceding sections). In a

neutropenic model, ΔCt^{norm} values were comparable between ATCC46645 and Δ*pes3.* In the corticosteroid treated model, ΔCt^{norm} values were significantly greater from Δ*pes3* infected lungs (*p* = 0.0002). These data demonstrate an increase in *A. fumigatus* burden in Δ*pes3* infected mice, which suggests Pes3 deletion results in hypervirulence in a corticosteriod murine model of infection. In light of the difficulties in assessing fungal burden in the highly inflamed corticosteroid treated lung, early time-points and a high dose were employed to histopathoplogically assess Δ*pes3* burden. It was hypothesised that histopathological analyses at earlier time-points would result in a less developed immune response, which would result in easy assessment of fungal morphology. Additionally, high dosage maximises the fungal content of the lung, thus facilitating easy comparison between the mutant and wild-type.

This approach provided clear support for the increase in fungal burden reported with qPCR. The most striking difference between wild-type and Δ*pes3* infected lungs was the earlier germination of the Δ*pes3* spores at 14 hours post infection. At 24 hours post infection, a trend was clearly discernable towards more extensive germ tube production in Δ*pes3* infected animals relative to the wild-type. Nevertheless, these differences did not manifest as differences in survival as determined by comparative analyses of Δ*pes3* and ATCC46645 in a corticosteroid model of infection.

qPCR and histopathological data suggest augmentation of virulence in the Δ*pes3* isolate, possibly by a defective immune response and/or enhanced *A. fumigatus* aggressive/defensive strategies in the mutant. O'Hanlon and co-workers hypothesised that *pes3* deletion results in a modulation of a PAMP in the vicinity of the cell wall, which abrogates immune recognition of *A. fumigatus* (O'Hanlon et al. 2011). While data presented here, and published in the O'Hanlon manuscript, might support this view, other explanations cannot currently be excluded. Firstly, only a slight reduction of inflammation was observed in Δ*pes3* infected lungs, which suggests inflammation defining PAMPs are maintained in the mutant. The term "immunologically silenced" is therefore potentially misleading when referring to Δ*pes3*. An alternative explanation is that the Δ*pes3* mutant is resistant to killing by the host. This might feasibly result from either or both of (a) an aberrancy in the local cytokine environment or (b) the enhanced *in vivo* growth rate of the Δ*pes3* mutant, which might outgrow macrophages and thereby avoid killing or possibly only transiently display a PAMP. Additionally, 2D-PAGE and LC-MS proteomic profiling of germlings identified 25 proteins which were differentially expressed in the Δ*pes3* mutant. For example, *A. fumigatus* allergen Asp F22 (Afu6g06770) concentration was greater in Δ*pes3* culture relative to the wild-type. The

hypothesis that these proteins might contribute to Δ*pes3* hypervirulence cannot currently be excluded.

Chapter 5

Disruption and virulence analysis of the *regA* gene, encoding a putative melanin transcription factor

5.1 Overview

Transcriptional profiling described in Chapter 3 has demonstrated the stage specific upregulation of two gene clusters which direct the biosynthesis of DHN-Melanin (Afu2g17510 – Afu2g17600) and pyomelanin (Afu2g04200 – Afu2g04262) during the initiation of murine aspergillosis (Langfelder et al. 1998, Schmaler-Ripcke et al. 2009, Tsai et al. 1998). Additionally, a 13 gene cluster putatively involved in melanin production (Afu1g17640 – Afu1g17740) was found to be preferentially upregulated between 8 and 14 hours post infection. The transcriptional profile of these clusters suggests *A. fumigatus* melanin pigments might impact host-pathogen interactions and fungal virulence during murine infection. The location of melanin at the exterior surface of *A. fumigatus* conidia, combined with its ability to scavenge reactive oxygen species, has resulted in much interest in the roles of melanin in biochemical protection, masking PAMPS from host PRRs and, as a consequence, affecting the activation of immune defences. Melanins are hydrophobic, negatively charged, high molecular weight pigments, which are formed by the oxidative polymerisation of phenolic or indolic compounds (Gomez and Nosanchuk 2003). Melanins have been shown to be important virulence determinants for fungal pathogens of animals and plants, including *C. neoformans* (Kwon-Chung et al. 1982, Wang et al. 1995) *Wangiella dermatitidis* (Feng et al. 2001), *Sporothrix schenckii* (Romero-Martinez et al. 2000)*, C. lagenarium* (Takano et al. 1995)*, M. grisea* (Howard and Valent 1996) and *A. fumigatus* (Langfelder et al. 1998, Tsai et al. 1998).

A. fumigatus is able to produce both 1,8-dihydroxynapthalene (DHN) melanin and pyomelanin using the polyketide biosynthetic pathway and the tyrosine degradation pathway respectively (Schmaler-Ripcke et al. 2009, Tsai et al. 1999, Tsai et al. 1998). The genes directing the biosynthesis of these pigments are physically clustered (Tsai et al. 1999, Schmaler-Ripcke et al. 2009). In the DHN melanin polyketide biosynthetic pathway, 1,3,6,8 tetrahydroyxnapthalene (1,3,6,8-THN) is synthesised from acetyl CoA and malonyl CoA precursors by the polyketide synthase *pksP* (Afu2g17600). 1,3,6,8-THN is reduced to form scytalone and subsequently

dehydrated to produce 1,3,8-trihydroxynapthalene (1,3,8-THN). 1,3,8-THN is then reduced and dehydrated to form 1,8-dihydroxynapthalene (1,8-DHN). Finally 1,8-DHN undergoes oxidative polymerisation to produce DHN melanin. Studies,utilising Δ*pksP* strains, have demonstrated DHN melanin is required for murine virulence (Tsai et al. 1998, Langerfeld et al. 1998), that it physically protects conidial PAMPs from immune cell recognition (Chai et al. 2010) and that it inhibits the acidification of host immune cell phagolysosomes (Thywiben et al. 2011). Gene expression profiling from the Af293 clinical isolate between 4 – 8 hours and 8 – 14 hours during the initiation of murine infection identified a decrease in *pksP* transcript abundance during murine infection (Chapter 3). Conversely, 5 genes including the scytalone dehydratase *arp1*, 1,3,6,8-tetrahydroxynaphthalene reductase *arp2* and pigment biosynthesis gene *ayg1* were upregulated, most notably between 8 and 14 hours. These data support the observation that *pksP* is transcribed most abundantly in conidia (Langerfelder et al. 2001) and the hypothesis that intermediates or branch products of the melanin pathway may be more important than the pigment itself in modulating *A. fumigatus* virulence (Tsai et al. 1999, Chai et al. 2010).

In the tyrosine degradation pathway described by Schmaler-Ripcke and co-workers (2009), pyomelanin is produced from phenylalanine, which is converted to tyrosine via a phenylalanine hydroxylase. Tyrosine is converted to homogentisic acid by a 4-hydroxyphenylpyruvate dioxygenase. Subsequently homogentisic acid is oxidised to benziquinoneacetate, which undergoes polymerisation to form pyomelanin. Pyomelanin deficient mutants have increased hyphal susceptibility to ROS (Schmaler-Ripcke et al. 2009) and pyomelanin is produced under conditions of cell wall stress, suggesting it may act as a defensive molecule (Valiante et al. 2009). Intriguingly, key genes within this biosynthetic cluster demonstrated an increase and decrease in transcript abundance during early and later time points of murine infection respectively. Most notably, the 4-hydroxyphenylpyruvate dioxygenase *hppD,* which is essential for pyomelanin biosynthesis (Schmaler-Ripcke et al. 2009). These data may suggest the employment of pyomelanin as a defensive molecule between 4 and 8 hours post infection but not at later stages or that, from a developmental viewpoint, pyomelanin biosynthesis is important at later stages of growth.

Given the well characterised role of microbial pigments as virulence factors (Liu and Nizet 2009), and the observed stage specific transcriptional upregulation of two melanin clusters during *A. fumigatus* infection, it was intriguing to note the increases in transcript abundance of genes from a putative melanin biosynthetic cluster between 8 and 14 hours post infection. This cluster contains 13 genes and is located in the subtelomeric region of chromosome 1. The cluster contains a

putative polyketide synthase, two putative transcription factors, a salicylate hydroxylase and a cytochrome P450 oxidoreductase. Of particular note is the presence of the putative transcription factor, *regA*, which is a 2719 bp gene with a Zn_2Cys_6 binuclear DNA binding domain. *regA* is a homologue of the DHN melanin regulators *pig1* of *M. grisea* and *cmr1* of *Collectotrichum lagenarium* and *Cochliobolus heterostrophus* (Eliahu et al. 2007, Tsuji et al. 2000). These transcription factors have been shown to be essential for DHN melanin production at specific developmental stages. For example, in *C. heterostrophus, cmr1* is located in a three gene cluster including the polyketide synthase *pks18* and the hydroxynapthalene reductase *brn2*. *cmr1* regulates key steps of DHN melanin biosynthesis by positively controlling transcription of the hydroxynapthalene reductases *brn1*, *brn2*, and the scatalone dehydratase *scd1* during hyperosmotic stress and late stationary growth phase (Eliahu et al. 2007). *Cmr1* deletion leads to a visible loss of pigmentation of conidia and hyphae, but wild-type appressoria formation and maize virulence (Eliahu et al. 2007). *M. grisea* ∆*pig1* and *C. lagenarium* ∆*cmr1* strains were also able to produce melanin in appressoria but not vegetative hyphae, suggesting the developmental regulation of melanin by these transcription factors (Tsuji et al. 2000).

regA transcript abundance was greatly increased at between 8 and 14 hours post infection in both Af293 and ∆*laeA* strains. Additionally, the putative salicylate hydroxylase, C6 transcription factor and zinc binding enoyl reductase within the cluster increased at this time point. No genes within the cluster decreased in transcript abundance between 8 – 14 hours, suggesting a possible link between developmental stage and expression. Additionally, transcriptional comparisons between germlings isolated from the murine host and developmentally matched *in vitro* culture showed 4 genes from this cluster were preferentially upregulated during infection (McDonagh et al. 2008). Finally, genes within the *regA* cluster showed significant increases in transcript abundance throughout early time points of infection in a corticosteroid model of pulmonary aspergillosis (Alcazar-Fuoli, in preparation). It was hypothesised that *regA* might transcriptionally activate the biosynthesis of a melanin pigment during early murine infection, and that this molecule might protect *A. fumigatus* from stress conditions encountered in the host niche, or act as a toxic molecule to the host.

In work described in this Chapter, *A. fumigatus regA* was deleted and the mutant was characterised in phenotypic assays and two murine models of aspergillosis. Data presented here suggest *regA* does not control melanin biosynthesis *in vitro*, but might play a protective role in a corticosteroid treated murine model of infection.

5.2 Materials and methods

5.2.1 *A. fumigatus* strains

The *A. fumigatus* strain used in this chapter is the *akuB*^{KU80} strain (da Silva Ferreira et al. 2006).

5.2.2 Phage strain

The replication deficient phage (λ *cI*$_{857}$ *ind1* Cro$_{TYR26amber}$ *P*$_{GLN59amber}$ *rex*< >*tetra*) was used for recombineering experiments (Chan et al. 2007).

5.2.3 Bacterial strain

The phage was maintained in *E. coli* LE392 (Promega, UK).

Bacterial artificial chromosomes (BACs) were maintained in *E. coli* DH10B (Invitrogen, UK).

5.2.4. Plasmids

pBSM10.

Vector BSM10 contains a biselectable marker consisting of a Zeocin resistance cassette for selection in *E. coli* and a pyrithiamine resistance gene for selection in A*. fumigatus*. This vector was constructed by Dr Elaine Bignell. The zeocin cassette was amplified using the primers Zeo1F and Zeo1R from the plasmid pCDA21 (Chaveroche et al. 2000), and the resulting PCR product was blunt ended and inserted into the SmaI site of pUC19 to produce plasmid pZ3. The pyrithiamine resistance marker was obtained by PCR amplification from the plasmid pPTRII (Kubodera et al. 2002) with primers PtrAF and PtrAR, and was cloned into the pZ3 Sal I site.

5.2.5 Oligonucleotide primers

Table 5.1: Oligonucleotide primer sequences used in this chapter.

Primer	Orientation	Sequence
BT-F	Forward	GAGCCCTTTTCCGACCTGAT
BT-R	Reverse	GGAACTCCTCCCGGATCTTG
Actin-F	Forward	CGAGCACAGCTTCTTTGCAG
Actin-R	Reverse	CCCATGGTGTCCGTTCTGA
640_F	Forward	CCCCTTGACATAGGGTAATAAT GTGCTTTCGCATTGTTCCACCC ATGGCCCCCCCGCGTTCGGAG CTGCGTTAGCTAGGCTTCTAG AGCGGCCGCGATAT
640_R	Reverse	TTATTTGCTGGCATCTCGCAAC TTCTCAAGAAGATGGACCAAG TTATCCACCAGTGGCGGAGTC TGTTTAGAAGTTTCATATGGCC TCTTGCATCTTTG
640_INT_F	Forward	ATTCGGCTCTGCATATCACC
640_INT_R	Reverse	TGAATGATAGGCGTCCTTCC
5'_640	Forward	TCCAGGATCTTCGCATAGGT
3'_640	Reverse	GACCGAGTTGACTCGGATCT

5.2.6 Modified recombineering approach for generation of a *A. fumigatus regA* disruption cassette

Lambda phage was prepared according to the method described by Maniatis et al (1982) with minor modifications. LE392λ bacteria (Chan et al. 2007) were inoculated in 10 mls LB supplemented with 12.5 ug/ml tetracycline and grown overnight at 32 °C, 180 rpm. The 10 ml culture was then inoculated to 200 mls LB, supplemented with 12.5 µg/ml tetracycline, and incubated at 32 °C with 180 rpm for approximately 2.5 hours until the OD was 1.2. Cultures were incubated at 42°C for 15 minutes with 180 rpm, and at 39 °C for 2 hours with 180 rpm. The 200 ml culture was split into 4 x 50 ml falcon tubes and centrifuged for 20 min. Pellets were dissolved in a total of 2 ml of TMG buffer (10 mM Tris-HCl pH 7.4, 10 mM MgCl2). 5 drops of chloroform were added, incubated for 15 min at room temperature and kept at 4 °C until use. For phage titration, LE392 (virus free isolate) were grown in LB overnight at 37°C. Cultures were then spun at 3000 rpm for 5 minutes. The supernatant was discarded and the pellet was resuspended in 10 ml of 10 mM $MgSO_4$. 5 serial dilutions (1:100) of the lambda phage were prepared in eppendorf tubes,

each containing 500 µl of TMG buffer. 100 µl of each phage dilution was incubated in a water bath at 37°C for 15 minutes to remove chloroform. 100 µl of LE392-$MgSO_4$ were then added to each tube and incubated at room temperature for 15 minutes. 3 ml of 0.8% TYE agar was added to each tube, inverted five times and overlaid onto 1.2% TYE plates. Plates were incubated overnight at 37°C. The following day, titration was calculated according to the formula: phage/ml = (number plaques/plate) x (1/ ml plated) x dilution factor.

5.2.7 Lambda phage infection of BAC clones

BAC AfB28_mq1_17e12 was picked from a library of end-sequenced, indexed *A. fumigatus* BAC clones (Pain et al. 2004) and inoculated into 5 mls of LB supplemented with 12.5 µg/ml chloramphenicol. Cultures were grown overnight at 37°C, 180 rpm. 1 ml of cells were centrifuged for 5 minutes at 5000 RPM, washed once with 10 mM $MgSO_4$ and resuspended in 100 µl 10 mM $MgSO_4$. 1 µl of lambda phage suspension containing over 1 million phage was added to the cells, which were incubated at 32 °C, 180 RPM for 20 minutes. 1 ml of LB was added, and incubated for 1 hour at 32 °C, 180 RPM. 100 µl of infected cells were plated on LB supplemented with 12.5 µg/ml tetracycline and grown overnight at 32 °C.

5.2.8 Recombineering and chemical transformation of BACs with a *regA* gene replacement biselectable marker cassette

One colony was picked from infected cell plates and inoculated into 1 ml LB supplemented with 12.5 µg/ml chloramphenicol and tetracycline, which was grown overnight at 32 °C, 180 RPM. 25 µl, 35 µl, 45 µl and 55 µl volumes of overnight culture were resuspended in LB to a total volume of 1 ml and incubated for 2 hours at 32 °C, 180 RPM in 5 ml universal tubes. Cells were transferred to 1.5 ml eppendorf tubes and incubated for 15 minutes at 42 °C in a water bath. Subsequently, samples were incubated for 2 minutes on ice, centrifuged at maximum speed for 3 minutes and washed with 1 ml 100 mM $MgCl_2$. Cells were then washed with 1 ml 100 mM $CaCl_2$ three times and resuspended in 50 µl 100 mM $CaCl_2$ containing 3 µg of the ptrA/zeo PCR amplicon. Cells were heat shocked at 42 °C for 2 minutes and tubes were incubated on ice for 8 minutes, after which 1 ml LB was added and samples incubated for 1.5 hours. Samples were plated on LB supplemented with 25 µg/ml zeocin and grown overnight at 32 °C. Colonies were screened for chloramphenicol and zeocin resistance by overnight growth in LB supplemented with 12.5 µg/ml chloramphenicol and 25 µg/ml zeocin. In order to extract BACs from cell culture, chloramphenicol

and zeocin resistant clones were inoculated into 50 mls LB supplemented with 12.5 µg/ml chloramphenicol and grown for 18 hours at 30 °C, 150 RPM. Cultures were centrifuged and the pellet resuspended in 1 ml resuspension buffer (Qiagen). Cells were lysed using 500 µl lysis buffer (Qiagen) and the reaction neutralised using 750 µl neutralisation buffer (Qiagen). Reactions were spun on maximum speed for 30 minutes and the supernatant precipitated with an equal volume of isopropanol for 5 hours. Samples were then centrifuged at maximum speed for 10 minutes, washed once in 1 ml ethanol before being air dried and resuspended in 200 µl water.

For gene replacement verification, recombined BACs were diluted 1:10 and 1 µl used as a template in PCR reactions. For transformation, 60 µl recombined BACs were digested overnight with SacI in a total volume of 70 µl. Digests were heat inactivated before transformation.

5.2.9 Fungal transformation using *A. fumigatus* protoplasts

Protoplast transformation was based on the protocol described by Szewczyk and co-workers (Szewczyk et al. 2006). *A. fumigatus* Ku80 was grown for 5 days on ACM plates. Spores were harvested in sterile water, filtered twice through Miracloth (Calbiochem) and washed twice with sterile water. 1 x 10^8 spores were inoculated into 20 mls ACM broth and grown for 16 hours at 30 °C with 150 rpm. Hyphae were isolated by filtration through Miracloth and rinsed with ACM broth. Hyphae were resuspended in 8 mls ACM, to which 8 mls of protoplasting solution (KCl, 12.8% Vineflow, Novo Nordisk) was added. Protoplasting was visually monitored, and the solution was incubated for 3 - 4 hours at 30 °C with 100 rpm. To remove undigested hyphal material, the protoplasting solution was layered onto 30 mls 1.2 M sucrose and centrifuged at 2000*g*. Protoplasts were collected at the top of the sucrose cushion and gently resuspended in 0.6 M KCl and centrifuged at 2000*g.* The pellet was washed three times in 0.6 M KCl, once in KCl 0.6 M, 50 mM $CaCl_2$, and resuspended in a volume of KCl 0.6 M, 50 mM $CaCl_2$ appropriate for transformation. 60 µl of SacI digested BAC was heat inactivated and mixed with 100 µl of protoplasts. The solution was mixed by vortexing and 50 µl PEG solution was added. The mixture was incubated in an ice water bath for 25 minutes, after which 1 ml of PEG was added and the sample was left at room temperature for an additional 25 minutes. 150 µl of protoplast/DNA solution was added to 10 mls AMM media containing 10 ul of pyrithiamine (0.5 mg/ml), which was overlayed onto a plate containing 15 mls of AMM with 15 ul pyrithiamine (0.5 mg/ml). Plates were incubated at room temperature for 24 hours and then incubated at 37°C for 72 – 144 hours. Transformants were subcultured on AMM supplemented with 0.5 mg pyrithyamine and grown for 5

days. Spores were picked using a loop and added to 200 µl breaking buffer (2% Triton X-100, 1% SDS, 100 mM NaCl, 10 mM Tris-HCl pH 8.0, 1 mM EDTA pH 8.0). 300 mg of glass beads (0.4-0.6mm diameter, Sartorius UK) were added and incubated for 30 minutes at 70 °C, with vortexing every 10 minutes. 200 µl chloroform:isoamylalcohol 25:24:1 was added and further vortexed for 5 minutes, before being spun for 8 minutes at max speed. The supernatant was precipitated with equal volume of isopropanol and incubated overnight at 4 °C. Following centrifugation at 13000 rpm for 10 minutes the pellet was washed in 70% (v/v) ethanol and air-dried before resuspension in 20 µl TE containing RNace-It™ ribonuclease cocktail (Stratagene).

5.2.10 Southern blotting

20 µg *A. fumigatus* gDNA was digested overnight with the appropriate volume of SacI (New England Biolabs, UK) and digestion reactions were separated on a 1% (w/v) agarose gel. The gel was stained for 30 minutes in 150 ml TBE containing 30 µl of SYBR Safe DNA Gel stain (Invitrogen), photographed and then depurinated (250 mM HCl), denatured (0.5 M NaOH, 1.5 M NaCl), neutralised (0.5 M Tris-HCl, pH 7.5, 1.5 M NaCl) and equilibrated in 20 x SSC (3 M NaCl, 300 mM sodium citrate, pH 7). The gel was blotted overnight onto a postive nylon membrane (Roche, UK) after which the DNA was fixed to the membrane using the automatic crosslink function on a Stratagene UV Stratalinker 1800. DIG Easy Hyb solution (Roche, UK) was pre-warmed to the probe hybridisation temperature (50 °C) and the membrane was prehybridised in DIG Easy Hyb for 1 hour with gentle agitation. Zeocin probes were amplified from plasmid BSM10 using the PCR DIG Probe synthesis kit (Roche, UK) using the manufacturer's guidelines. 50 ng of probe was denatured for 10 minutes at 100 °C for 5 minutes in a volume of 25 µl, which was then added to 10 ml prewarmed DIG Easy Hyb solution. The membrane was incubated overnight at 50°C with continual agitation. The membrane was incubated with low stringency wash buffer (2 x SSC, 0.1% (w/v) SDS) at room temperature, followed by high stringency wash buffer (0.5 x SSC, 0.1% (w/v) SDS) at 65 °C and washed (0.1 M Malic acid, 0.15 M NaCl (pH 7.5), 0.3% (v/v) Tween 20). The membrane was blocked (1% (w/v) blocking solution (Roche, UK) in 0.1 M Malic acid, 0.15 M NaCl, pH 7.5) for 2 hours at room temperatue. The antibody (Anti-Digoxigenin-AP Fab fragments, Roche) was centrifuged at maximum speed for 5 minutes and used at a dilution of 1 in 10000 in 30 ml blocking solution for 30 minutes with gentle agitation. The membrane was then washed in wash buffer and incubated with detection buffer (0.1 M Tris-HCl, 0.1 M NaCl, pH 9.5 for 5 minutes. CPD-Star (Roche, UK) was added to the membrane and incubated at room temperature for 5 minutes. Finally, the membrane was exposed onto Hyper film (Kodax).

5.2.11 Murine infections

Murine infections were conducted under UK Home Office Project Licence PPL/70/6487 in a dedicated facility at Imperial College London. Outbred male mice (strain CD1, 18 – 22 g, Harlan Ortech) were housed in individually ventilated cages and allowed water and food *ad libitum*. Water was supplemented with 1 g/L tetracycline hydrochloride (Sigma-Aldrich) and 64 mg/L ciprofloxacin as prophylaxis against bacterial infection. Neutropenia was induced by intraperitoneal injections of cyclophosphamide (150 mg/kg) on days –3 and –1 and by a single subcutaneous dose of hydrocortisone acetate (112.5 mg/kg) on day –1 (Schrettl et al. 2004). *A. fumigatus* spores were grown on ACM, supplemented with 1% (w/v) glucose and 5 mM ammonium tartrate, for 5 days prior to infection. Spores were harvested on the day of infection, using sterile saline (Baxter Healthcare Ltd, UK), and filtered through Miracloth (Calbiochem). Conidial suspensions were centrifuged for 10 minutes at 5000 rpm, washed twice with sterile saline, counted using a haemocytometer and resuspended at a concentration of $2.5x10^9$ cfu/ml. Mice were anaesthetised by isofluorane inhalation and infected by intranasal instillation of conidia in 40 µl of saline solution. The concentration of conidia for each experiment is indicated in the Results section of this chapter. The determination of viable counts for the administered inocula was performed using serial dilution on ACM plates supplemented with 1% (w/v) glucose and 5 mM ammonium tartrate and incubated for 3 days at 37°C. Mice were weighed every 24 hours from day -3 and inspected twice daily.

For neutropenic and hydrocortisone acetate treated mice, lungs were extracted from mice culled on day + 4 or day + 5 respectively. Lungs were weighed, and 1 volume of sterile saline was added. Lungs were homogenised using an X120 electric tissue homogeniser (Bennett Scientific Limited) and 250 µl of homogenate was added to 180 µl of buffer ATL (Qiagen) and DNA extracted using DNeasy Blood and Tissue Kit (Qiagen). Fungal burden was assessed by quantitative PCR amplification using the oligonucleotides BT-F (GAGCCCTTTTCCGACCTGAT) and BT-R (GGAACTCCTCCCGGATCTTG) to amplify the beta tubulin (Afu7g00250) locus from the *A. fumigatus* genome, and the oligonucleotides Actin-F (CGAGCACAGCTTCTTTGCAG) and Actin-R (CCCATGGTGTCCGTTCTGA) to amplify the murine actin locus (NM_007393). Quantification of both gene targets was performed in triplicate qPCR reactions. qPCR was performed using Sybr Green Jumpstart™Taq ReadyMix™ (Sigma-Aldrich, UK). 5 µl of gDNA extracted from murine lung was used as a template in 20 µl qPCR reactions. qPCR was conducted in a Rotor-Gene RG-3000 PCR cycler (Corbett Research, UK) with the following cycling parameters: 95 °C for 5 seconds, 58 °C for 5 seconds, 72 °C for 15 seconds, 78 °C for 5 seconds, which was repeated 40 times. Data were then analysed using the RotorGene 6 software, from which the amplification threshold was manually assigned to generate Ct values. A modified

mathematical model (incorporating adjustment for fungal inoculum) for relative quantification of *A. fumigatus* actin, and murine beta-tubulin was adopted for each mouse sample using the formula RATIO = $(E_{target})^{\Delta Ct(\text{fungal actin} - \text{murine tubulin})}$ where *E*= efficiency of amplification of target gene and is equal to 1.88, based on efficiency calculations using the Ct slope method (Schmittgen and Livak 2008). RATIO values were $\log_{10}$ transformed and corrected for inoculum size, and reciprocal values were plotted ($1/\log_{10}$ $RATIO_C$). The statistical significance of variances between fungal burdens was calculated using a nonparametric Mann-Whitney t-test. Genomic DNA, isolated from animals infected with an attenuated *A. fumigatus* p-amino benzoic acid auxotroph, Δ*pabaA*, was used as a positive control for attenuation (Brown et al. 2000).

5.2.12 Histopathology

Mice for histology were culled by neck dislocation. Whole lungs were extracted and fixed in 4% v/v formaldehyde (Sigma-Aldrich). Lungs were embedded in paraffin prior to sectioning and stained with hemotoxylin and eosin (H&E) or Grocott's Methenamine Silver (GMS).

5.2.13 Macrophage phagocytosis assay

The murine macrophage cell line RAW 264.7 was used for a phagocytosis assay. RAW 264.7 macrophages were grown in RPMI media supplemented with 10% fetal bovine serum and L-Glutamine–Penicillin–Streptomycin solution (L-glutamine 200 mM, penicillin 10,000 units, streptomycin 10 mg/ml, Sigma, UK) at 37°C in an atmosphere of 5 % CO_2. The day before the infection, macrophages were adjusted to a cell density of 5 x 10^5 cells per ml. 1 ml of cells was added to 24 well Multiwell (BD Falcon) plates and allowed to adhere overnight at 37°C in an atmosphere of 5% CO_2. Ku80 and Δ*regA* strains were cultivated on ACM for 5 days at 37°C. Spores were harvested, and adjusted to a concentration of 1x10^7 cells/ml in RPMI. Media was removed from macrophages on the 24 well plates and 1ml RPMI added. 1x10^6 *A. fumigatus* spores were added so the macrophages were challenged with 1 conidia per cell, and incubated for 2 hours at 37°C in an atmosphere of 5% CO_2. Next, the medium of each well was removed and washed three times with PBS. The supernatant and the three washes were pooled and plated in appropriate dilutions onto ACM agar plates. CFU were counted and compared to the number of CFU without RAW 264.7 cells, and reported as a percentage of that value.

5.3 Results

5.3.1 Construction of *regA* disruption cassette using modified recombineering methodology

A *regA* (Afu1g17640) disruption cassette was constructed using a recombineering based approach for systematic gene deletion based on the protocol described by Chan and co-workers (2007). From a library of end-sequenced, indexed *A. fumigatus* BAC clones, a candidate with appropriate coverage of the *regA* region was retrieved (Figure 5.1A). The BAC AfB28_mq1_17e12 insert spanned the entire Afu1g17640 gene with 12326 and 1442 bp of 5' and 3' flanking regions respectively. A zeocin (zeo)/ and pyrithiamine (PtrA) biselectable marker was amplified from the unpublished plasmid BSM10 with primers 640_F and 640_R (Table 5.1). Primer 640_F contains 80 bp which are homologous to 5' UTR immediately before the *regA* gene start codon. Primer 640_R contains 80 bp which are homologous to the *regA* coding sequence immediately before the gene stop codon (Figure 5.1B, Table 5.1). Following lambda infection of BAC AfB28_mq1_17e12, homologous recombination with the PCR-generated biselectable marker was mediated by heat induction (Figure 5.1C).

In order to confirm *regA* gene disruption, a BAC was extracted from a chloramphenicol and zeocin resistant clone and used as a template in three PCR reactions (Figure 5.1D and 5.1E). Firstly, presence of the 1.9 Kb pyrithiamine cassette was confirmed using primers Pyrt_F and Pyrt_R. Secondly, the integration of the biselectable cassette within the *regA* coding region was confirmed using primers 5'640 and Pyrt_R. A third PCR reaction which also confirmed integration of the biselectable cassette within the *regA* coding region utilised primers 3'640 and Pyrt_F. Gel electrophoresis analysis showed PCR products of the predicted size when the recombined BAC was used as template. The recombined BAC was named CC_e12.9 (Figure 5.1D). Finally, BAC CC_e12.9 was linearised with SacI, liberating a 12.9 kb deletion cassette (Figure 5.1D). SacI digests were heat inactivated and used for subsequent *A. fumigatus* transformations.

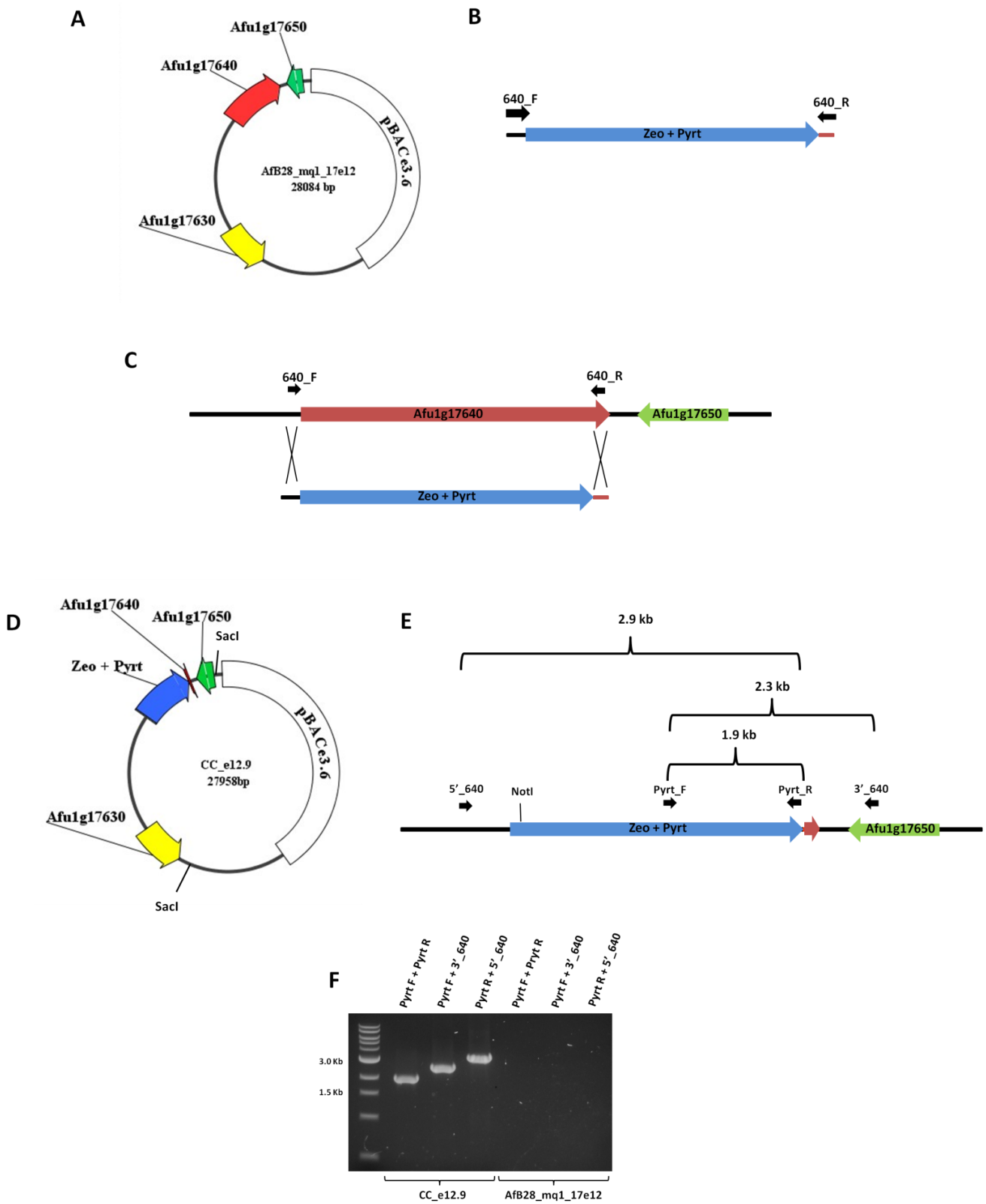


Figure 5.1: Construction of *regA* deletion cassette by BAC recombineering. The BAC AfB28_mq1_17e12 insert spanned the entire Afu1g17640 gene with 12326 and 1442 bp of 5' and 3' flanking regions respectively (A). For a gene disruption amplicon, a zeocin (Zeo)/ and pyrithiamine (Pyrt) biselectable marker was amplified from the plasmid pBSM10 using primers 640_F and 640_R (B). Primer 640_F contains 80 bp which are homologous to the 5' UTR immediately upstream of the *regA* start codon. Primer 640_R contains 80 bp which are homologous to the *regA* coding sequence immediately downstream of the stop codon. During recombineering, homologous recombination occurs between the 80 bp flanking regions of the amplicon and BAC AfB28_mq1_17e12 (C) to give BAC CC_e12.9 (D). SacI restriction sites used to liberate the disruption cassette are shown. BACs from chloramphenicol and zeocin resistant clones were used as templates for PCR reactions using primers Pyrt_F/Pyrt_R, Pyrt_F/3'_640, and 5'_640/Pyrt_R (E and F). *regA* gene replacement was demonstrated where PCR products of the expected size were amplified from the putatively recombined BAC but not the unrecombined control BAC (F).

5.3.2 Gene replacement of *regA* in *A. fumigatus*.

A *regA* mutant strain (Δ*regA*) was generated by protoplast transformation with the BAC deletion cassette. Putative transformants were grown on AMM + Pyrt and genomic DNA was extracted (see Methods). In order to distinguish transformants having appropriate gene replacements from those having wild-type or ectopic integrations, two approaches were used. Firstly, a 3903 bp region containing the *regA* gene was amplified using primers 5'_640 and 3'_640. Amplicons from wild-type gDNA do not contain a NotI restirction site (Figure 5.2A). However, amplicons from Δ*regA* contain a NotI restriction site due to the introduction of the biselectable cassette (Figure 5.2B). Amplicons from putative transformants and Ku80 strain were digested with NotI. Gel electrophoresis of digestion reactions identified a single transformant from which band patterns suggested *regA* gene replacement with the biselectable cassette (Figure 5.2C). Absence of the wild-type 3903 bp fragment in this digest suggested homologous recombination had occurred at the target locus without an ectopic recombination event (Figure 5.2C). The deletion of *regA* was confirmed by PCR using primers 640_INT_F and 640_INT_R with gDNA from Ku80 or the putative transformant as template (Figure 5.2C). Primers 640_INT_F and 640_INT_R amplify a 1.55 kb product from within the *regA* coding region. *regA* deletion was demonstrated by the presence of a 1.55 kb PCR product (Figure 5.2C). A single integration event was verified by Southern blot probing with a 600 bp fragment of the zeocin cassette, which produced a single fragment of the expected size (Figure 5.2B).

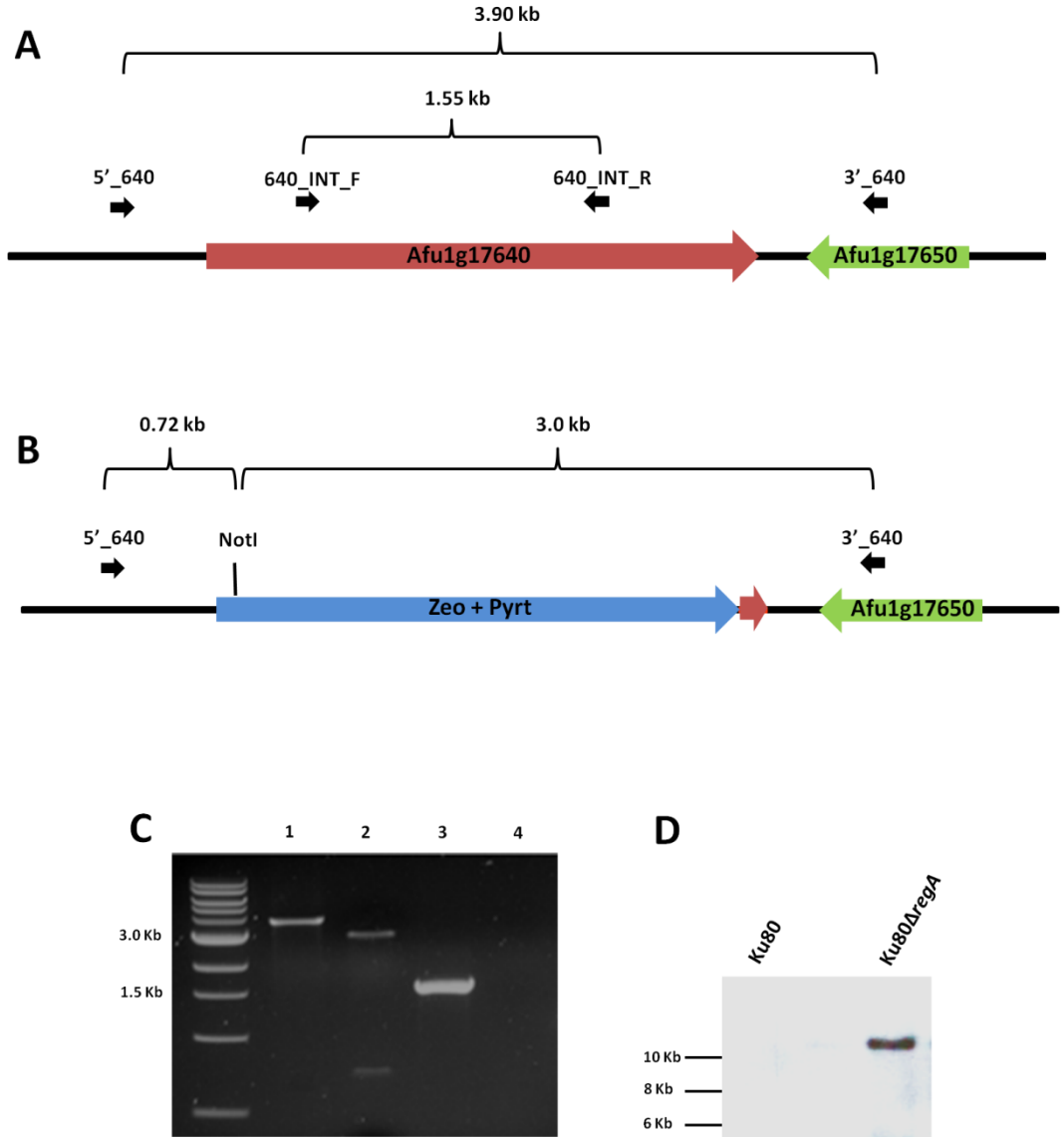


Figure 5.2: *regA* gene replacement in *A. fumigatus* using the BAC CC_e12.9 cassette. (A) Schematic representation of wild-type *regA* region with locations of primer pairs 5'_640/ 3'_640 and 640_INT_F/ 640_INT_R depicted. Sizes of PCR products using these primer pairs and Ku80 gDNA as template are shown. A NotI restriction site is absent in this region in the wild-type. (B) Schematic representation of the *regA* region following a homologous recombination event with the BAC CC_e12.9 disruption cassette. Primers 640_INT_F and 640_INT_R do not amplify a product from gDNA following a homologous recombination event. A notI restriction site is introduced by the introduction of the zeocin cassette. Sizes of fragments following notI digestion are shown. (C) Primers 5'_640 and 3'_640 were used to amplify the *regA* region from Ku80 and putative Δ*regA* transformant gDNA. PCR amplicons from Ku80 and Δ*regA* were NotI digested and analysed using gel electrophoresis, which demonstrated wild-type banding patterns in the Ku80 (lane 1) and introduction of the NotI site by the zeocin cassette in the transformant strain (lane 2). PCR using primers 640_INT_F and 640_INT_R demonstrated a product of the expected 1.55 kb size from Ku80 gDNA template (lane 3) but no product from Δ*regA* transformant (lane 4), suggesting Δ*regA* gene replacement. (D) Southern blot analyses of Ku80 and Δ*regA* transformant gDNA which was digested with SacI. Blots were probed with a 600 bp fragment of the zeocin cassette as described in section 5.3.1. *regA* deletion is indicated by a single SacI fragment of 12.6 Kb observed for Δ*regA* gDNA.

Alterations in germination and vegetative growth rate by gene disruption may impact virulence of *A. fumigatus* in murine models of infection. For example, double deletion of the chitin sythase genes *chsC* and *chsG* reduced conidial growth rates and virulence (Mellado et al. 1996) and growth rate analyses of 9 *A. fumigatus* strains using a spectrophotometric method found correlation with growth rate and LD_{90} values in a neutropenic murine model of infection (Paisley et al. 2005). Therefore prior to virulence analyses, germination and vegetative growth rates were compared between Ku80 and Δ*regA* strains. For vegetative growth analyses, 60 mls AMM was inoculated with 5 x 10^6 spores from either Ku80 or Δ*regA* and incubated at 37°C with 150 RPM. Mycelial dry weight was measured over a 136 hour period (Figure 5.3A). Triplicate biological replicates were conducted. Filamentous growth rates in liquid culture were similar between the *regA* mutant and Ku80 strain (Figure 3A). For comparisons of spore germination rates, 60 mls AMM was inoculated as above and germination rates microscopically monitored. Triplicate biological replicates were conducted, for which the germination was measured as the percentage of spores which had germinated from total counted (Figure 4B). Radial growth rates on AMM and ACM plates were identical (data not shown).

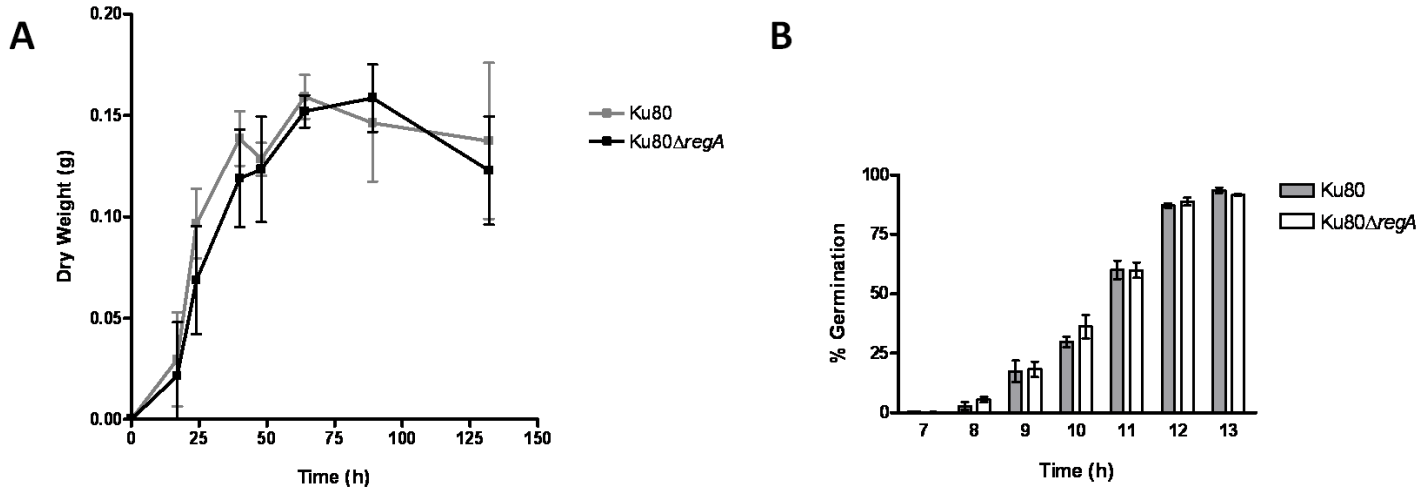


Figure 5.3: Comparison of vegetative growth and germination rates for Ku80 and Δ*regA*. (A) Dry weights from vegetative growth over 136 h are shown. No significant differences were observed between strains. (B) Germinated spores were reported as a percentage of the total counted. Germination rates of *A. fumigatus* wild-type and Δ*regA* strains demonstrate that both germinate at comparable rates. Germination was first recorded in both strains at 7 h. For both analyses the mean ± standard error of 3 biological replicates is shown.

5.3.3 Ku80Δ*regA* displays wild-type resistance to cell wall and oxidative stress but an increased resistance to macrophage phagocytosis

It was reasoned that deletion of a putative regulator of conidial melanin might result in modifications to the spore cell wall architecture and/or resistance to oxidative stress. To determine if *regA* deletion resulted in susceptibility to cell wall stress, Δ*regA* and Ku80 spores were subjected to phenotypic assays. Each strain was spotted at concentrations of 1 x 10^4, 1 x 10^3, 1 x 10^2 and 1 x 10^1 onto duplicate plates containing cell wall or membrane stressors (Table 5.2). No differences were observed in radial growth rates or colony morphology between Ku80 and Δ*regA* strain for cell wall or membrane stress (data not shown).

Phenotypic test	Reagent	Concentration
Cell wall stress	Calcofluor White	100, 200 µg/ml
	Congo Red	5, 10, 15 µg/ml
	Caffeine	2, 5 mM
	High temperature (50°C)	N/A
Membrane stress	SDS	0.01, 0.02 % (w/v)

Table 5.2: Phenotypic plate assay reagents and concentrations to effect cell wall and membrane stress. Δ*regA* and Ku80 spores were spotted at concentrations of 1 x 10^4, 1 x 10^3, 1 x 10^2 and 1 x 10^1 onto duplicate plates containing cell wall or membrane stressors. No difference was observed in radial growth rate or colony morphology between strains (data not shown).

To determine if *regA* deletion resulted in spore susceptibility to oxidative stress, Δ*regA* or Ku80 spores were harvested and resuspended at 5 x 10^5 spores/ml in AMM containing 0.0 M, 0.05 M, 0.1 M, 0.2 M and 0.4 M hydrogen peroxide. Spores were incubated for 30 minutes, followed by 1:50 dilution in sterile water and duplicate plating. CFUs were enumerated and surviving colonies reported as a percentage value of the CFUs counted from the 0.0 M hydrogen peroxide control (Figure 5.4A). No differences were observed between survival of the wild-type and Δ*regA* strain following hydrogen peroxide stress (Figure 5.4A). In order to determine if *regA* deletion caused modification to conidial PAMPs, a macrophage phagocytosis assay was conducted. Murine alveolar macrophages were co-incbated with spores from either Ku80 or Δ*regA*, and the percentage of unphagocytosed cells was calculated relative to macrophage free controls (Figure 5.4B). These data demonstrate comparable rates of phagocytosis between Δ*regA* and Ku80 isolates.

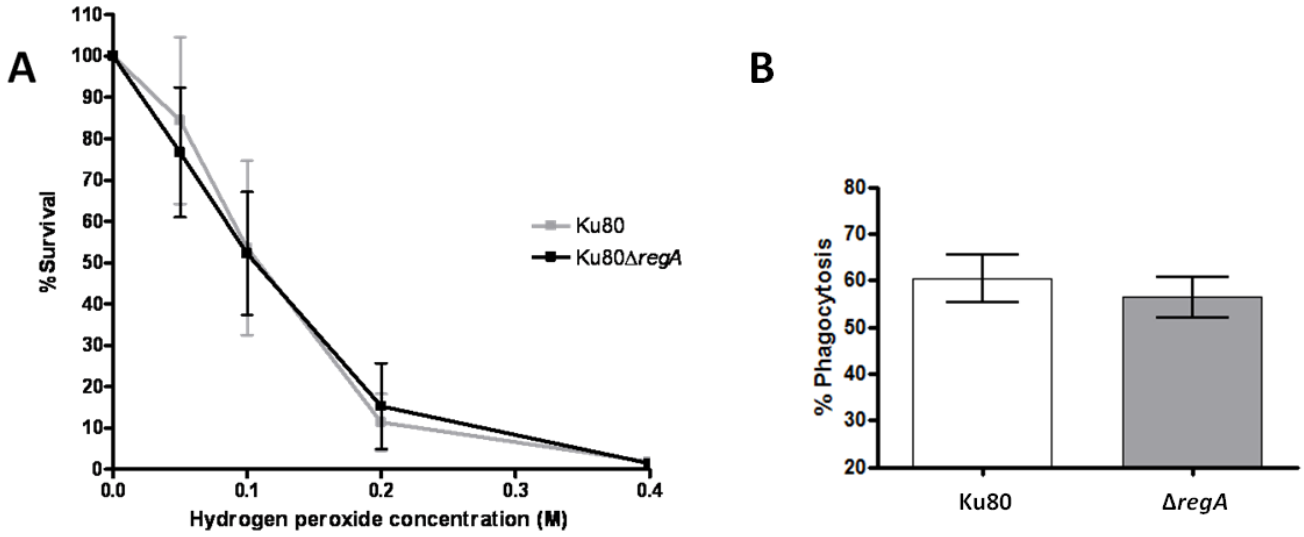


Figure 5.4: Percentage survival of Ku80 and Δ*regA* spores following incubation with various concentrations of hydrogen peroxide, and percentage of phagocytosed conidia following incubation with murine macrophages. For the hydrogen peroxide assay, 5 x 10^5 spores/ml in MM containing 0.0 M, 0.05 M, 0.1 M, 0.2 M and 0.4 M hydrogen peroxide. Spores were incubated for 30 minutes, followed by 1:50 dilution in sterile water and duplicate plating. CFUs were enumerated and surviving colonies reported as a percentage value of the CFUs counted from the 0.0 M hydrogen peroxide control.

5.3.4 *regA* deletion causes a reduction in fungal burden in a corticosteroid, but not neutropenic, murine model of infection

Two murine models of pulmonary aspergillosis were used to assess comparative virulence of the *A. fumigatus* Ku80 and Δ*regA* mutant, by analysis of fungal burden. Groups of n = 5 neutropenic or corticosteroid-treated animals were infected with 3 x 10^4 or 5 x 10^6 conidia, respectively. Two independent biological replicates were conducted. Inoculum viable counts were determined following dilution and duplicate plating onto ACM, and CFUs enumerated for dose correction as described in Chapter 4. Fungal burden was quantified, relative to murine actin, by quantitative PCR using genomic DNA isolated from homogenised murine lung harvested from animals sacrificed on day +3 and day + 4 for corticosteroid or neutropenic models respectively. A single animal from either Ku80 or Δ*regA* infected mice was used from the first biological replicate for histological analyses. Dose corrected ΔCt^{norm} values from neutropenic mice infected with Δ*regA* or Ku80 were comparable for biological replicates 1 and 2 respectively (Figure 5.5A and 5.5B). Consolidation of replicate data into a single analysis demonstrated infectious burden does not significantly differ between Ku80 and Δ*regA* in neutropenic mice (Figure 5.5C). Histological comparisons of Ku80 and Δ*regA* infected murine lung in neutropenic mice demonstrated

comparable hyphal development, tissue penetration, inflammation and epithelial necrosis (Figure 5.6).

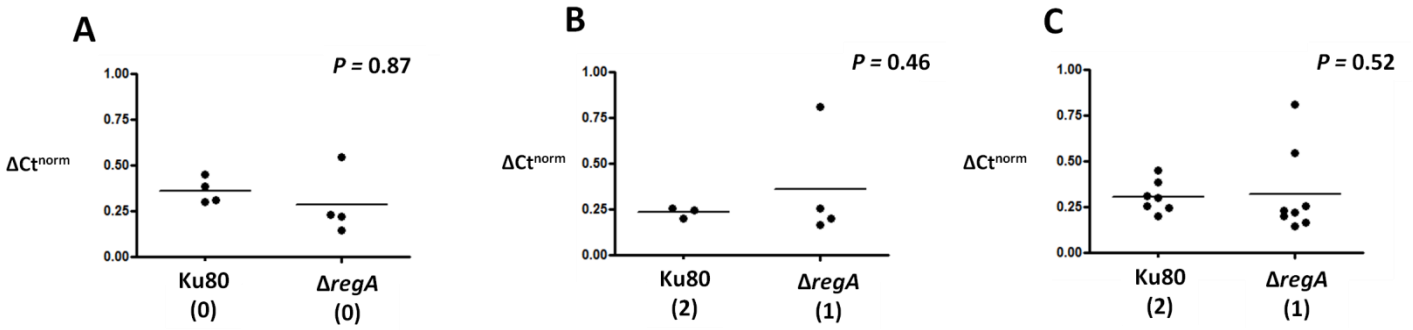


Figure 5.5: Fungal burden of Ku80 and Δ*regA* infected murine lung from a neutropenic model of aspergillosis. ΔCt^{norm} values from neutropenic mice are shown following dose correction for biological replicate 1 (A), replicate 2 (B), and with both replicates combined into a single analysis (C). Horizontal lines depict the average ΔCt^{norm} value. Numbers in parenthesis indicate the number of gDNA samples which amplified murine actin but did not amplify fungal beta tubulin. P values from nonparametric Mann-Whitney t-test are shown.

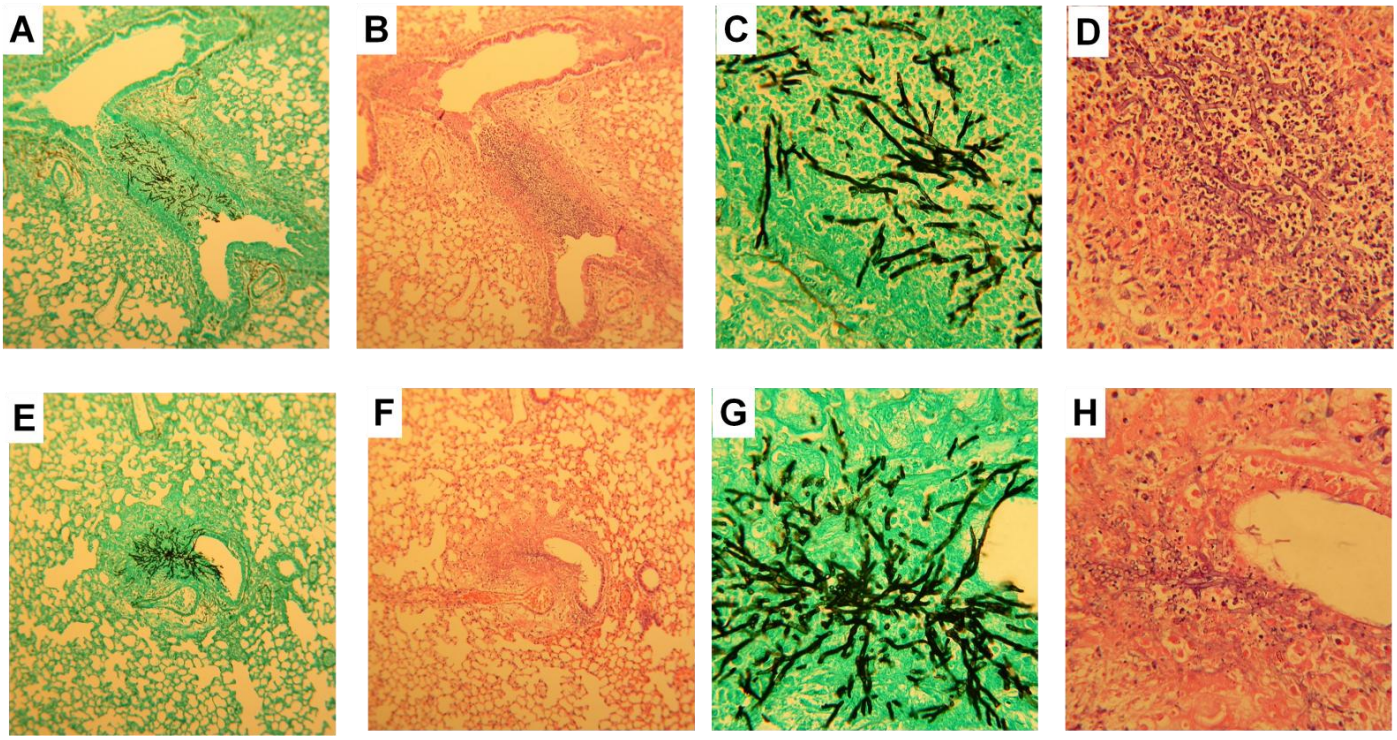


Figure 5.6: Histological comparisons of Ku80 and Δ*regA* infected murine lung in a neutropenic model of aspergillosis at 4 days post infection. Lung sections were stained using GMS (green images) and H&E (red images). Mice were infected with Ku80 (A – D) and Δ*regA* strains (E – H). In either instance, hyphae had germinated in the bronchioles (A and E). Inflammation was localised to areas surrounding *A. fumigatus* hyphae, with the surrounding alveoli clear of immune cell recruitment (B and F). Hyphae were developmentally comparable between the isolates, and had penetrated host epithelial layers (C and G). Tissue necrosis of epithelial cells occurred for both of Ku80 and Δ*reg* infections. .

Dose corrected ΔCt^{norm} values from corticosteroid treated mice infected with Δ*regA* were lower than Ku80 in both biological replicates (Figure 5.6A and 5.6B). The observed reduction was approaching significance in the first replicate (*P* = 0.06). Consolidation of replicate data into a single analysis suggested infectious burden is significantly lower in Δ*regA* infected mice relative to Ku80 wild-type (*P* = 0.01, Figure 5.5C). These data suggest a slight, but significant, reduction in fungal burden in mice infected with the Δ*regA* strain relative to the Ku80 isolate.

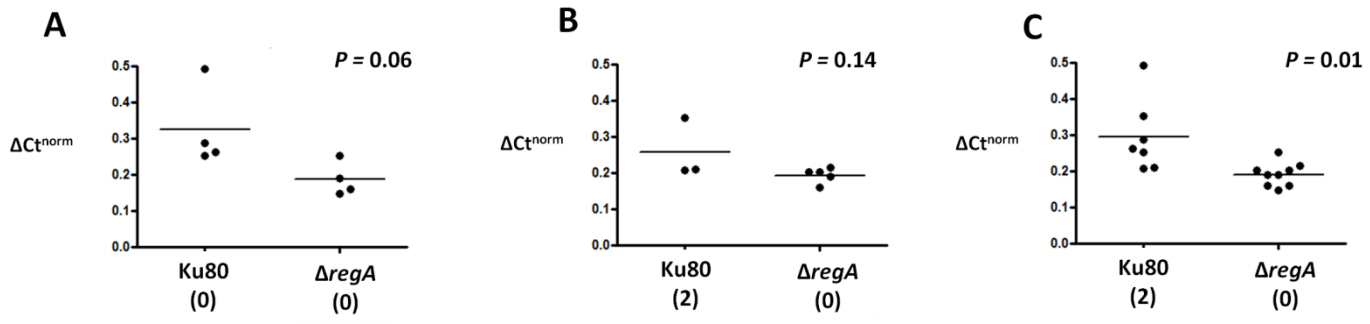


Figure 5.7: Fungal burden of Ku80 and Δ*regA* infected murine lung from a corticosteroid model of aspergillosis. ΔCt^{norm} values from corticosteroid treated mice are shown following dose correction for biological replicate 1 (A), replicate 2 (B), and with both replicates combined into a single analysis (C). Horizontal lines depict the average ΔCt^{norm} value. Numbers in parentheses indicate the number of gDNA samples which amplified murine actin but did not amplify fungal beta tubulin. P values from nonparametric Mann-Whitney t-test are shown.

Histological comparisons of Ku80 and Δ*regA* infected lungs in corticosteroid treated mice showed a decrease in inflammation of tissue surrounding infected bronchioles in the Δ*regA* strain (Figure 5.7A, B, D and E). Hyphal development in major airways for both strains was comparable, as was localised immune cell recruitment (Figure 5.7 C, D, F, G). In lung alveoli, similar levels of inflammation were noted between isolates, but greater hyphal development was observed in the Ku80 lung (Figure 5.8).

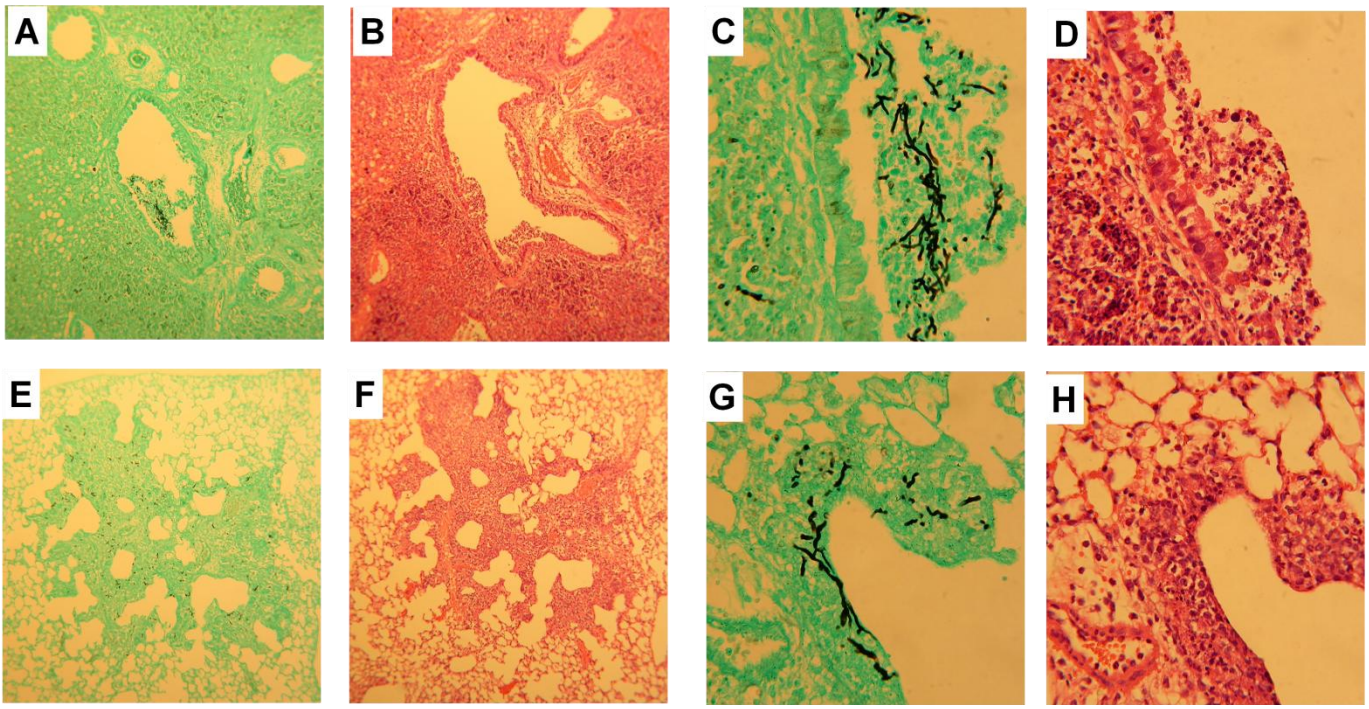


Figure 5.8: Histological comparisons of Ku80 and Δ*regA* infected bronchioles in a corticosteroid murine model of aspergillosis at 5 days post infection. Lung sections were stained using GMS (green images) and H&E (red images). Mice were infected with Ku80 (A – D) and Δ*regA* strains (E – H). Inflammation around major airways in Ku80 infected lungs extended into the surrounding alveoli (A and B). Conversely, a trend was noticed where inflammation was limited around the bronchioles in Δ*regA* infected mice, an example of which is shown (E and F). Hyphal development was comparable in the bronchioles between Ku80 and Δ*regA* (C and G) as was local inflammation (D and H).

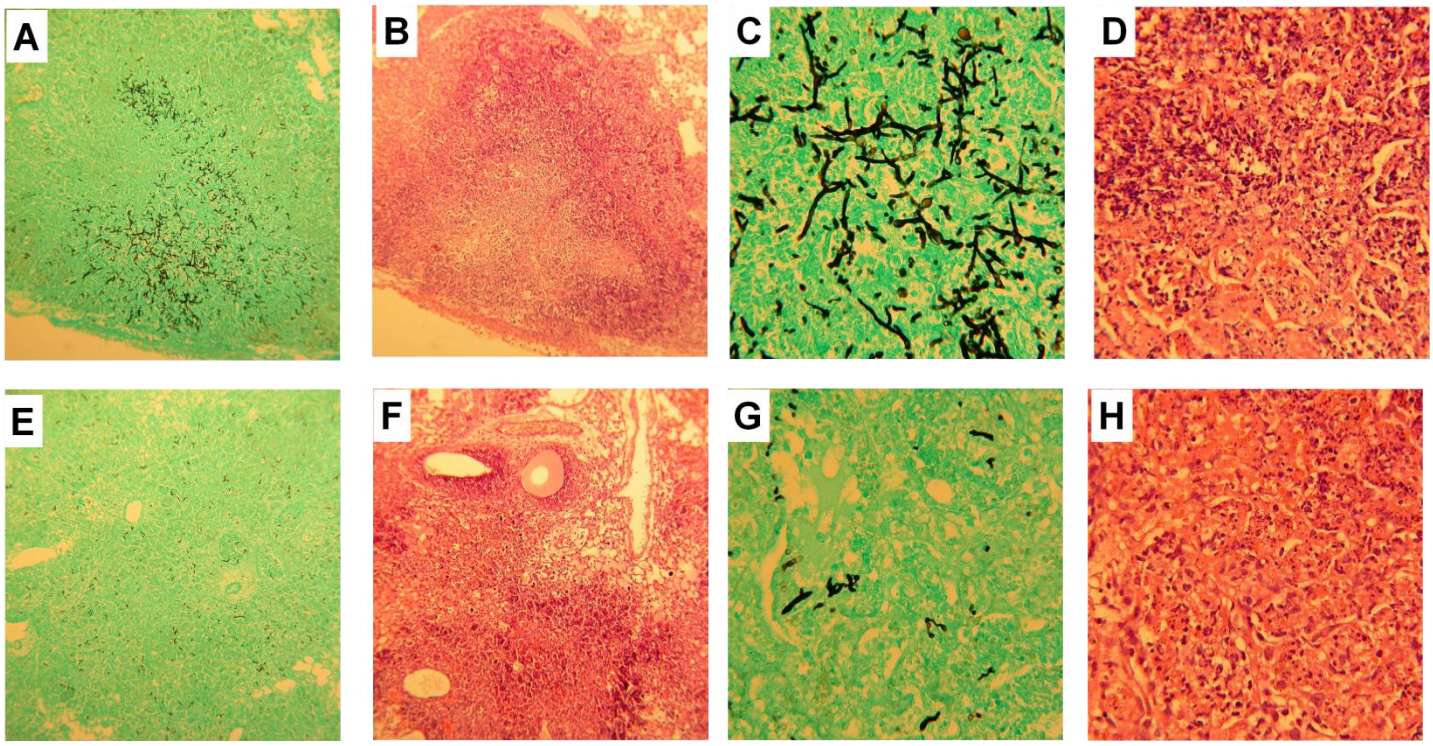


Figure 5.9: Histological comparisons of Ku80 and Δ*regA* infected alveoli in a corticosteroid murine model of aspergillosis at 5 days post infection. Lung sections were stained using GMS (green images) and H&E (red images). Mice were infected with Ku80 (A – D) and Δ*regA* strains (E – H). In sections of lung alveoli, a trend was noticed for more extensive hyphal development in Ku80 relative to Δ*regA* (A and E) with comparable levels of inflammation (B and F). Areas of extensive hyphal development were noted in Ku80 infected (C), but not Δ*regA* infected mice (G). Levels of inflammation were comparable between lungs infected with both isolates (D and H).

5.4 Discussion

These experiments attempted to define the role of a putative *A. fumigatus* pigment with regard to host-pathogen interactions and virulence. In the context of fungal disease, melanins are some of the most comprehensively studied molecules. *In vitro* and *in vivo* analyses suggest these pigments may play protective roles for human pathogens *C. neoformans* (Kwong-Chung et al. 1982, Wang et al. 1995), *W. dermatitidis* (Feng et al. 2001), *S. schenskii* (Romero-Martinez et al. 2000) and *A. fumigatus* (Tsai el al. 1998, Langfelder el al. 1998). Melanin is also required for full virulence of fungal plant pathogens, such as *C. lagenarium* (Takano et al. 1995), *C. heterostrophus* (Eliahu et al. 2007) and *M. grisea* (Howard and Valent 1996). In fungi, there are two main kinds of melanin, DHN-melanin (named from one of the pathway intermediates, 1,8-dihydroxynaphthalene) and DOPA-melanin (named from one of the precursors, L-3,4-dihydroxyphenylalanine). Due to hydroquinone and semi quinine chemical groups, melanin pigments are able to act as electron donors and acceptors and therefore may produce and scavenge reactive oxygen intermediates (Riley 1994). Melanin provides protection to fungi from various environmental stresses, such as antifungal agents (Paolo et al. 2006), UV light (Wang and Casadevall 1994), extreme temperatures (Rosas and Casadevall 1997) and reactive oxygen species (Goncalves and Pombeiro-Sponchiado 2005). Thus, the role which these pigments play during infection is diverse.
In phytopathogens, the function of melanin is related to appressorial formation and host invasion. TEM demonstrated that the *M. grisea* appressorium has a layer of melanin between the cell wall and the cell membrane (Howard and Ferrari 1989). Non-melanised appressoria were sensitive to plasmolysation by low solute concentrations (Howard and Ferrari 1989). Analysis of naturally occurring and mutagenically-derived pigment mutants in a rice infection model demonstrated normal adhesion, but greatly reduced infection (Howard and Ferrari 1989). Wild-type infection could be restored by addition of the melanin intermediate scytalone to mutant cultures prior to rice infection. Thus, the *M. grisea* melanin layer is putatively required for turgor generation, and acts as a barrier to the efflux of solute from the appressorium. Thus, melanin enables approessorial turgor pressure which is used to force a penetration peg through leaf cuticle layer. The role of melanin in *C. lagenarium* and *C. heterostrophus* virulence is likely to be similar (Takano et al 1995. and Eliahu et al. 2007).

DOPA melanin is a virulence factor which may protect *C. neoformans* from a variety of challenges encountered in the mammalian host. Although melanin is not constitutively expressed *in vitro*, it is highly likely that *C. neoformans* melanises during infection. To support this hypothesis Rosas and colleagues protease treated, denatured (guanidine thiocyanate), and acid digested (HCl) infected

murine kidney and brain tissues, which results in the complete solubilisation of fungal and host cells with the exception of melanin particles (Rosas et al. 2000). SEM of the solubilised sample revealed melanin envelopes which retained the shape of infecting cells, thus demonstrating that melanisation occurs in the host. *In vivo* melanisation may protect invading *C. neoformans* from host effector cells (Wang et al. 1995). Wang and colleagues generated a melanin deficient mutant by UV mutagenesis, which was attenuated for virulence in a murine model of infection. Melanised cells were also found to be more resistant to phagocytosis and killing by murine macrophages.
In vitro analyses suggest DHN-melanin plays a protective role in the human pathogen *S. schenskii*, which causes cutaneous mycosis (Romero-Martinez et al. 2000). White and other abnormally pigmented mutants were generated by UV mutagenesis, which demonstrated increased susceptibility to UV radiation, H_2O_2, and susceptibility to killing by human monocytes and murine alveolar macrophages. These data indicate a protective role of melanin in *S. schenskii* infection, although the molecular mechanism of this protection is unclear. Additionally, deletion of the *pskP* homologue *wdpks1* in *W. dermatitidis* resulted in a loss of visible melanin, susceptibility to phagocytosis and killing by human neutrophils, and attenuation in an immunocompetent intravenous model of *W. dermatitidis* infection (Feng et al. 2001). The seemingly protective role of melanin in human fungal pathogens may be explained by several hypothesis; (1) melanin may physically protect PAMPs from host PRR, or modify cell wall architecture so that PAMPs are shielded; (2) the negative charge of melanin may reduce cell wall charge, thus abrogating binding by PRR; (3) melanin or an pathway intermediate may be toxic to host cells; (4) melanin may quench ROS during phagolysosomal attack.

A defining feature of resting *A. fumigatus* conidia is the electron dense outermost cell wall layer, which is composed of rodlet microfibrils and DHN melanin pigments (Latge 2001). Several studies have addressed the role of melanin in *A. fumigatus* virulence. Evidence that DNH-melanin was synthesised via a polyketide synthase pathway was provided by Tsai et al, who analysed a cosmid which was complementary to a reddish-pink (RP3) conidial-colour mutant of *A. fumigatus* (Tsai et al. 1998). This cosmid contained a truncated *pksP* gene. Sequence analysis of *pksP* suggested that the gene was a polyketide synthase, and the subsequent deletion of this gene resulted in a white conidial phenotype. TLC analysis of flaviolin, scytalone, and 1,3,6,8-THN metabolites from the DHN-melanin pathway demonstrated that treatment of wild-type growth media with tricyclazole, which blocks the first reduction step in melanin biosynthesis (conversion of 1,3,6,8-THN to scytalone) resulted in the accumulation of flaviolin, an autoxidative product of 1,3,6,8-THN. Similar treatment of the Δ*pksP* isolate did not produce flaviolin, indicating the first reduction step in DHN melanin biosynthesis was absent in the mutant. Thus, *pksP* catalyses the conversion of

1,3,6,8-THN to scytalone, which is the first step in melanin biosynthesis. SEM of the Δ*pksP* isolate demonstrated smooth conidia, which were more susceptible to neutrophil phagocytosis and C3 deposition. Moreover, Δ*pksP* was attenuated in an intravenous murine model of infection, which was supported by work conducted by another group (Langfelder et al. 1998).

DHN-melanin plays an essential role in *A. fumigatus* cell wall structure, and thus may impact PAMPS or adhesins on the spore surface. Environmental isolates with mutations in various genes of the DHN-melanin pathway demonstrate increased electronegative charge of the conidial surface and significant modulations to the cell wall, most notably loss of the rodlet layer (Pihet et al. 2009). Chai and colleagues have demonstrated that DHN-melanin may physically protect conidial PAMPs from PRRs (Chai et al. 2010). In a macrophage stimulation assay, a Δ*pksP* isolate was found to elicit a greater cytokine response relative to the wild-type, with Il-6, TNF-α and IFN-γ elevated when co-incubated with the mutant. Additionally, macrophage stimulation with purified *A. fumigatus* melanin extracted from *in vitro* spores did not elicit a cytokine response, indicating that DHN-melanin is immunologically inert. Selective inhibition of dectin-1, TLR-4 and mannose receptors by co-incubation of spores and macrophages with laminarin, lipopolysaccharide or exogenous mannose respectively did not alter cytokine responses following stimulation with wild-type conidia, yet reduced Δ*pskP* cytokine responses to wild-type levels. Thus, the authors hypothesised that melanin may shield fungal PAMPs from host phagocytic cells and modulate the host proinflammatory cytokine response. Nevertheless, the presence of immonologically active intermediates in the wild-type isolate could not be excluded by this study. Additionally, *A. fumigatus* DHN-melanin inhibits the acidification of host immune cell phagolysosomes (Thywiben et al. 2011). Acidification of the host phagolysosomes may be an important element of phagosome killing (Ibrahim-Granet et al. 2003). Thywiben and colleagues compared phagolysosomal acidification following engulfment of Δ*pksP* and wild-type progenitor, demonstrating marked reduction of acidification in wild-type containing phagolysosomes (Thywiben et al. 2011). Protease treatment, denaturation and acid digestion was used to isolate intact melanin envelopes from cells (melanin “ghosts”) which were then used in phagolysosomal assays. Both wild-type conidia and extracted melanin envelopes demonstrated comparable phagolysosomal acidification, indicating melanin is responsible for inhibiting this method of immune attack. Δ*rodA* isolates did not inhibit acidification of the phagolysosome, excluding this important surface molecule in acidification inhibition. With regard to the evolution of *A. fumigatus* virulence, related species which lack the DHN-melanin cluster, i.e. *A. flavus*, *A. nidulans*, and *A. terreus* were analysed in the phagolysosomal assay. *A. fumigatus* and *A. flavus* were most effective in inhibiting the acidification of phagolysosomes, with 26 and 12% of spores from these species contained in

acidified phagolysosomes respectively. In contrast, about 48 and 66% of conidia of *A. nidulans* and *A. terreus* were located in acidified phagolysosomes respectively. Thus, the authors speculated that specific melanisation of *A. fumigatus* and *A. flavus* may contribute to the prominence of these species as the etiological agents of disease relative to other *Aspergilli*.
A second form of melanin, pyomelanin, is produced by *A. fumigatus* via the tyrosine degradation pathway (Schmaler-Ripcke et al. 2009). Although not as well characterised as DHN-melanin, pyomelanin deficient mutants have increased hyphal susceptibility to oxidative stress (Schmaler-Ripcke et al. 2009), which may be a protective molecule under conditions of cell wall stress (see below). Thus, the roles of *A. fumigatus* pigments in virulence are diverse, and have critical implications for virulence. Additionally, as shown by Thywiben et al. (2011), melanin clusters may provide clues as to the evolutionary basis of *A. fumigatus* virulence.

In this study the putative pigment biosynthesis transcriptional regulator, *regA*, was deleted in an attempt to further understand the role of melanin in *A. fumigatus* infection. Deletion of *regA* did not lead to any visible change to *A. fumigatus* pigmentation, yet histopathology and a qPCR assay of fungal burden presented in this study demonstrate that Δ*regA* deletion causes reduced fungal burden, most notably in the region of the alveoli, in a corticosteroid treated model of infection. Additionally, a trend towards reduced inflammation was observed in Δ*regA* infected mice in this model. Differences in virulence between Δ*regA* and the wild-type comparator were not observed in a neutropenic model, which suggests a modulation of *A. fumigatus*-neutrophil interactions in the Δ*regA* strain. Given the limited phenotypic analysis conducted thus far, it is not possible to distinguish the mechanistic basis which might be due to loss of a defensive molecule, abrogated biosynthesis of a toxic metabolite, or modification of a PAMP leading to heightened immune recognition. Considering both pyomelanin and DHN-melanin are putative cell wall components which confer resistance to various physical and biological stressors, Δ*regA* was characterised with regard to cell wall integrity. While no phenotype was observed by using physical (e.g. congo red) or biological (i.e. macrophage phagocytosis) assays, time constraints prevented extensive phenotypic analyses. Following the submission of this thesis, susceptibility to cell wall-active antifungals will be tested. Additionally, Δ*regA* resistance to UV radiation is currently being assessed in order to determine if protection is conferred by the *regA* cluster product. Additionally, in order to accurately determine melanin content of spores and hyphae, melanin concentration from conidia and hyphae will be measured by a method based on those used by Chai and colleagues (Chai et al. 2009), where cells are enzymatically lysed to form protoplasts, denatured using 4.0 M guanidine thiocyanate and boiled in 6.0 M HCL for 1 h to obtain pure melanin, which can simply be weighed. Scanning and transmission electron microscopy would be useful to

determine the cell wall architecture of conidia and hyphae, as evidenced by several studies which have used SEM and TEM to study the melanin layer of conidia (Pihet et al. 2009, Tsai et al. 1998) or the hyphal surface following disruption of a secondary metabolite gene (O'Hanlon et al. 2011). Perhaps the most important tools for identifying the metabolite biosynthesised by the *regA* gene cluster are HPLC and LCMS metabolite profiling, which have been instrumental in elucidating the DNH-melanin pathway and other secondary metabolites (Tsai et al. 1998). However, Preliminary phenotypic analyses suggest that the RegA cluster might be silent *in vitro*, and become active in the host. While elaborate methods for the activation of secondary metabolite clusters have been successful, such as co-incubation with other microbes (Schroeckh et al. 2009) or epigenetic manipulations (Williams et al. 2008), work conducted by Bergman and colleagues suggests that overexpression of pathyway specific regulatory factors such as RegA is a particularly promising approach for *in vitro* activation and subsequent study of the cluster product (Bergmann S. et al. 2010). The authors postulated that overexpression of putative pathway regulators facilitates concerted expression of the entire cluster. This was demonstrated for a cryptic 7 gene secondary metabolite cluster of *A. nidulans*, which contained a hybrid NRPS/PKS gene (*apdA*), and a putative transcription factor regulator (*apdR*) which were not expressed under *in vitro* conditions. An overexpression strain was constructed where *apdR* was cloned under control of the inducible alcohol dehydrogenase promoter *alcAp*. All genes within the cluster were transcribed in the overexpression strain, but only under inducing conditions. HPLC analysis of fermentative culture under batch conditions led to the discovery of the secondary metabolites aspyridone A and B. Thus, overexpression of *regA* represents a very attractive strategy for determining the product of this cluster. This will greatly enhance understanding of the role of this gene cluster in the corticosteroid treated animal.

Transcriptional evidence presented in Chapter 3 and gleaned from other *A. fumigatus* microarray experiments suggests that the pigment clusters are preferentially upregulated *in vivo*. *regA* transcript abundance was greatly increased between 8 and 14 hours post infection in Af293 (Chapter 3) in contrast to *in vitro* studies, which demonstrated *regA* transcript abundance significantly decreased between 0 and 30 minutes incubation in YPD (Lamarre et al. 2007). Transcripts of the putative salicylate hydroxylase, C6 transcription factor and zinc binding enoyl reductase genes, also present within the cluster increased at 8 – 14 hours post infection, while no genes within the cluster decreased in transcript abundance at this time-point. Thus, a possible link between developmental stage and *regA* gene cluster expression cannot be excluded. Comparative transcriptional profiling between germlings isolated from the host niche with developmentally matched laboratory culture demonstrated higher transcript abundance of 4 genes

within the cluster, including a short chain dehydrogenase (Afu1g17650), histidinol dehydrogenase (Afu1g17660), salicylate hydroxylase (Afu1g17670) and MFS transporter (Afu1g17680) in the host (McDonagh et al. 2008). Similar expression profiles have been observed in an identical experimental design but with corticosteroid treated mice (Alcazar-Fuoli, in preparation). Given that in these studies comparisons are made between developmentally matched germlings it is likely that specific environmental cues in the host and not *in vitro* may result in the upregulation of this cluster rather than a developmental cue.

With regard to DHN-melanin biosynthesis in the host, *pskP* transcript abundance decrease between 4 – 8 and 8 – 14 hours post infection in the host (Chapter 3). This was surprising, given that murine infection experiments utilising a *pksP-egfp*-expressing strain demonstrated expression of this gene in germlings isolated from BALFs 24 hours post infection (Langfelder et al. 2001). The single time-point analysed by Langfelder et al. combined with the transcriptional decrease of *pksP* between 4 – 14 hours suggest that while *pksP* transcript is highest at the conidial stage of infection, it remains expressed in the neutropenic host up until 24 hours post infection (Langfelder et al. 2001, Chapter 3). In any case, 5 genes including the scytalone dehydratase *arp1*, 1,3,6,8-tetrahydroxynaphthalene reductase *arp2* and pigment biosynthesis gene *ayg1* were upregulated, most notably between 8 and 14 hours which suggests that that intermediates or branch products of the melanin pathway may be important during infection.

Additionally, genes within the pyomelanin biosynthetic cluster demonstrated an increase and decrease in transcript abundance during early and later time points of murine infection respectively, which may suggest the employment of pyomelanin as a defensive molecule between 4 and 8 hours. The upregulation of DHN-melanin, pyomelanin, and the *regA* cluster (Chapter 3, McDonagh et al. 2008, Alcazar-Fuoli, in preparation) combined with the impact of these genes on fungal virulence (Tsai et al. 1998, Langerfelder et al. 1998, this study) suggests that melanisation might be a strategy which improves survivorship in the host niche. Upregulation of melanin specific genes is in contrast to the general assumption that the main role of pigments is the constitutive expression of DHN-melanin as a protective layer on the dormant spore. Data presented here suggest melanisation may have critical implications throughout the latter stages of IPA, which is reminiscent of human and plant pathogens *C. neoformans* and *M. grisea* which preferentially melanise during infection (Howard and Ferrari 1990, Kwong-Chung et al. 1982, Wang et al. 1995). The discovery that *A. fumigatus* and *A. flavus* are the most potent inhibitors of phagolysosomal acidification relative to other *Aspergillus* species led Thywiben and colleagues to speculate that melanisation specific to *A. fumigatus* and *A. flavus* may contribute to the prominence of these

species as etiological agents of disease (Thywiben et al. 2011). The authors noted that the DHN-melanin cluster is only present in *A. fumigatus* and suggest it may be a species specific virulence determinant. Analysis of the distribution of the *regA* cluster within *Aspergillus* species demonstrates it is highly conserved amongst the genus. *regA* homologues are present in *A. nidulans*, *A. terreus*, *A. oryzae*, *A flavus* and *N. fischeri*, which suggests the contribution of this cluster to mammalian infection might be maintained in other *Aspergillus* species. This is supported by transcriptional comparisons between *A. flavus* germlings isolated from the murine lung at 14 hours post infection with developmentally matched germlings from laboratory culture (Cairns et al. unpublished data). The *A. flavus regA* homologue (AFLA_073870) was the highest upregulated transcription factor in the host relative to *in vitro* growth, indicating *regA* upregulation *in vivo* is conserved amongst other species.

In addition to elucidating the molecular basis of host-pigment interactions, we hypothesise that further characterisation of Δ*regA* may provide a functional link between signal transduction and virulence in *A. fumigatus*. Given the well established role of fungal pigments in pathogenesis, several studies have attempted to elucidate the signal transduction cascades which regulate their expression. For example, the *C. neoformans* G-protein α subunit *gpa1* which is involved in cAMP signalling was deleted by Alspaugh and colleagues (Alspaugh et al. 1997), which caused inhibition of capsule formation and mating. Additionally, in response to glucose starvation, the Δ*gpa1* isolate was unable to produce melanin, which is strongly induced under these conditions in wild-type strains. Addition of exogenous cAMP to low glucose culture restored melanin production in Δ*gpa1*. With regard to pathogenesis, Δ*gpa1* demonstrated reduced virulence relative to the progenitor strain as determined by cerebrospinal fluid CFU counts in a rabbit model of cryptococcal meningitis. D'Souza and co-workers disrupted the *pka1* gene, which encodes the major cAMP-dependent protein kinase catalytic subunit in *C. neoformans* (D'Souza et al. 2001). The Δ*pka1* isolate was sterile and demonstrated reduced melanin and capsule production *in vitro*. Moreover, Δ*pka1* was attenuated in a murine model infection. Although the inability of Δ*gpa1* and Δ*pka1* to produce the *C. neoformans* capsule means that attenuation cannot be attributed to cAMP regulation of melanin alone, these data provide a link between cAMP signalling, melanisation and virulence. In *M. grisea,* deletion of the *mac1* gene, which encodes adenylate cyclase, abrogates appressoria formation, indicating that cAMP response pathway regulates appressorium morphogenesis (Choi and Dean 1997). Given that melanin is an essential component of the appressoria, one can speculate that cAMP signalling regulates melanin biosynthesis in *M. grisea*.
In *A. fumigatus*, pyomelanin biosynthesis is regulated by a MAP kinase signalling pathway (Valiante et al. 2009). These authors deleted the protein kinase MpkA, and demonstrated the

deletant was sensitive to various cell wall or membrane stressors, including SDS, caffeine, congo red, calcafluor white and enzymatic degradation. Western blot analysis demonstrated MpkA is directly activated by two other protein kinases, Bck1 and Mkk2 under cell wall stress. Following addition of L-tyrosine to *in vitro* culture, spectrophotomeric monitoring combined with a homogentisate dioxygenase assay (which measures activity of a key enzyme in pyomelanin biosynthesis, HmgA) demonstrated that pyomelanin production was markedly reduced in Δ*mpkA* isolates relative to the wild-type. Thus, the authors postulate that pyomelanin formation occurs in response to cell wall stress via a cell wall integrity MAPK module. Liebmann and colleagues investigated the link between cAMP signalling, *pksP* expression, and virulence in *A. fumigatus*. Deletion of the *pkaC1* gene encoding a protein kinase A catalytic subunit caused a reduction in growth rate and sporulation *in vitro*. Additionally, *A. fumigatus pkaC1* deletion strains carrying a *pksP*p-*lacZ* gene fusion were generated, which demonstrated reduced *pksP* expression in the Δ*pkaC1* background from 24 hour *in vitro* culture. While the Δ*pkaC1* was attenuated in a low dose neutropenic murine model of infection, this is likely due to poor growth of the mutant rather than any *pksP* regulatory phenomenon.

These studies highlight how elucidating signal transduction cascades and their melanising gene targets in pathogenic fungi, including *A. fumigatus*, may enable a better understanding of virulence. However, a significant limitation to the current model of cAMP or MAP kinase melanin regulation in *A. fumigatus*, and indeed other fungi, is the limited knowledge regarding downstream transcription factors involved in regulating melanin biosynthetic genes. The *regA* homologue *cmr1* in *C. heterostrophus* is under control of the MAP kinase signalling cascade. *C. heterostrophus* MAP kinase deletants Δ*chk1* and Δ*mps1* display white, non-pigmented conidia (Eliahu et al. 2007). Eliahu and co-workers demonstrated the transcription factor *cmr1* is required for melanin biosynthesis and virulence in the maize pathogen *C. heterostrophus*. In this species, deletants of *cmr1* have a light orange-pink colour, due to accumulation of a melanin intermediate. Moreover, RT-PCR analyses demonstrated Cmr1 is essential for expression of both scytalone dehydratase (*scd1*) and two hydroxynaphthalene reductases (*brn1* and *brn2*) during *in vitro* growth. Additionally, in Δ*chk1* and Δ*mps1* mutants, melanin biosynthetic genes, and *cmr1* transcript abundance were greatly reduced relative to wild-type isolates in 3 and 5 day old culture. Thus, the authors hypothesised that melanin is regulated via MAP kinases Chk1 and Mps1 regulation of Cmr1. This hypothesis is supported by the partial clustering of genes required for melanin biosynthesis in *C. heterostrophus (cmr1, brn1,* and polyketide synthase *pks18*), which suggests Cmr1 is a pathway specific transcription factor analogous to *gliZ*.

Further support for the role of *cmr1* in melanin transcriptional regulation is provided by a study conducted by Tsuji and co-workers, who demonstrated *cmr1* homologues in the cucumber pathogen *C. lagenarium* controls melanin biosynthesis via regulation of a 1,3,8-trihydroxynaphthalene reductase and scatalone dehydratase during mycelial growth (Tsuji et al. 2000). Similarly, the *regA* homologue *pig1* in *M. grisea* controls melanin biosynthesis during late stage hyphal growth (Tsuji et al. 2000). Thus, future characterisation of the *A. fumigatus* Δ*regA* mutant, has the potential to link signal transduction, melanin biosynthesis and virulence during *A. fumigatus* infection.

In this study, a *regA* disruption cassette was constructed using a recombineering approach for systematic gene deletion based on the protocol described by Chan and co-workers (2007). These authors developed reagents and protocols for simultaneous construction of numerous knock-out vectors targeting genes in mice. It was anticipated that adaptation of the recombineering approach for *A. fumigatus* vector construction would facilitate high-throughput deletion of *A. fumigatus* genes. This methodology would be most appropriate for future study of host-pathogen interactions, given the identification of hundreds of genes which putatively biosynthesise molecules which interact with the host (Chapter 3). Although high-throughput production of numerous disruption vectors was beyond the scope of this study, generation of the *regA* disruption cassette and subsequent construction of the *A. fumigatus* Δ*regA* mutant represents proof of principle for the technology. The recombineering protocol optimised in this study relies on two main reagents. Firstly, a library of end-sequenced, indexed *A. fumigatus* BAC clones was generously provided by Dr Paul Bowyer, University of Manchester. This BAC library was constructed to give an insight into the *A. fumigatus* genome (Pain et al. 2004). In the study by Pain and co-workers, chromosomal DNA was partially digested and fragments were cloned into plasmid pBACe3.6. The average insert size is 75 Kb, and end-sequencing enables identification of clones which cover a region of interest. Appropriate to the aims of this study, the BAC AfB28_mq1_17e12 insert spanned the entire Afu1g17640 gene with 12326 and 1442 bp of 5' and 3' flanking regions respectively.

The second reagent is a replication defective λ phage which mediates heat-inducible homologous recombination (Chan et al. 2007). In recombineering, the first step is usually to transform the BAC DNA into recombineering-competent *E. coli* cells. This step is not necessary with the replication defective phage, as any *E. coli* can be infected without damage to the host cell (Chan et al. 2007). Three genes encoded by the phage mediate homologous recombination (Court et al. 2002). The exonuclease *Exo* acts on linear double stranded DNA to generate 3' single strand overhangs. The

single stranded binding protein *beta* binds to these overhangs and stimulates complimentary strand annealing. Finally, the *Gam* gene inhibits DNA degradation by the host.

A zeocin and pyrithiamine biselectable marker was amplified with 80 bp homologous to the region to be disrupted, and homologous recombination with the biselectable marker and BAC AfB28_mq1_17e12 was mediated by heat induction. Subsequently, the recombined BAC was digested to give a linear disruption cassette, which was utilised for *A. fumigatus* transformation. A significant advantage of this approach is the speed at which disruption vectors can be constructed. For example, generation of *regA* disruption BAC, CC_e12.9 took one week. This is in stark contrast to preliminary attempts to generate a similar disruption cassette using fusion PCR based on the method described by Szewczyk and co-workers, which involved several classical cloning steps and was ultimately unsuccessful despite numerous optimisation attempts (Szewczyk et al. 2006). A potential disadvantage to this approach is that some genes may not be covered by a BAC insert in the library. Nevertheless, the adaptation of this approach to a 96 well format is a significant step towards high-throughput *A. fumigatus* gene deletion (Alcaza-Fuoli et al, in writing). Work conducted by Dr Alcazar-Fuoli has demonstrated this approach is amenable to deletion of large segmentss of the *A. fumigatus* genome. Indeed, the entire pseurotin A cluster has been deleted using this methodology (Alcaza-Fuoli, in preparation). An additional benefit is improved frequency of homologous recombination due to the large size of the deletion cassettes. High-throughput analysis of *A. fumigatus* genes represents a major challenge in the post-genome era. A significant advancement towards this objective was the construction of the Ku80 mutant, which undergoes much higher rates of homologous recombination than wild-type isolates (da Silva Ferreira et al. 2006). Work described in this chapter has provided proof of principle for a recombineering based approach to deletion vector construction, which is a promising method for simultaneous construction of dozens of deletion cassettes. The utility of such high-throughput strategies is highlighted by work conducted in *S. cerevisiae* for rapid gene knockout construction in *Neurospora* (Colot et al. 2006). This method takes advantage of recombinational cloning in yeasts, thus circumventing traditional cloning. Construction of 103 transcription factor knock-outs was achieved in a single study, which is in contrast to a total of 21 *Neurospora* transcription factors which had been characterised prior to the high-throughput approach (Colot et al. 2006).

Chapter 6

Surface enhanced laser desorption/ionisation time of flight mass spectrometry for high through put detection of epitope-tagged fungal proteins in murine BAL fluid

6.1 Overview

The temporal study of pathogen gene expression during the initiating stages of disease presents a wealth of information regarding *A. fumigatus* host niche colonisation. Transcriptional profiling presented in Chapter 3 of this thesis suggests numerous genes which encode putative signal peptides increase in transcript abundance during the initiation of murine infection. These predicted proteins include antigens, toxins, proteases and other molecules which may attack the host and/or modulate immune responses. Much research interest has recently focused on fungal effectors, which are proteins secreted by pathogens to suppress or evade host immunity (reviewed in de Wit et al. 2009). These include secreted protease inhibitors of *Cladosporium fulvum*, metalloproteases of *M. grisea* and several putative proteins with unknown function in other agriculturally important phytopathogens (Orbach et al. 2000, Shabab et al. 2008). Given the extensive arsenal of putatively secreted proteins in the host, it was hypothesised that molecules identified as differentially regulated (Chapter 3) may act as *A. fumigatus* effectors.

The potential significance of fungal proteins as biomarkers of infection, and facilitators of disease progression drives the need for high throughput analyses of pathogen protein in the host. While transcriptional profiling is a powerful tool for analysis of host pathogen interactions, multiple post transcriptional events and inherent noise from high throughput gene expression studies can disrupt the association between an mRNA molecule and the corresponding protein. Functional genomic investigations of the *A. fumigatus* proteome have found various levels of concordance and highlighted the complexity of the transcription/translation relationship, while emphasising the complimentary nature of both analyses (Albrecht et al. 2010, Bruns et al. 2010a, Cagas et al. 2011, Gautam et al. 2008). While global approaches using existing technologies such as 2D-PAGE combined with MALDI-ToF-MS may be useful in this respect, they constitute labour intensive processes which are not amenable to addressing multiple stages of disease, or the pressing need to analyse multiple models, such a corticosteroid or neutropenic animals. Furthermore, these types of global approaches do not allow specific hypothesis testing of individual candidates, for example, if a cell wall protein is present during early spore adhesion to

the host, or a catalase is biosynthesised in response to later neutrophil attack. Addressing these questions with specific antibodies against candidate proteins is again labour intensive and expensive. Of great use would be a quick, flexible means to detect the presence of a protein in an infection model. Previous studies have used green fluorescent protein (GFP) tagging (Langfelder et al. 2001), immunogold electron microscopy (Markaryan et al 1994) and immunohistochemistry (Reichard et al. 1994) in order to visualise *A. fumigatus* protein in murine models of infection. In this study, an innovative approach to protein detection was optimised to exploit the sensitivity of mass spectrometric methods. Surface enhanced laser desorption/ionisation (SELDI) ToF-MS is a recently developed form of laser desorption/ionisation MS where the sample surface plays an active role in the extraction and/or cleaning of the sample of interest. SELDI combined with poly or monoclonal antibody capture has been used to detect the secretion of β-defensins in human gingival cervicular fluid (Diamond et al. 2001), high density lipoproteins in human plasma (Levels et al. 2007) and the hormonal transporter transthyretin in human blood and urine (Schweigert et al. 2004). The technique is fast, sensitive and eliminates prior HPLC analyses. Consequently, it was hypothesised that the SELDI-ToF-MS platform would be ideal for detection of *A. fumigatus* proteins in the host.

In order to optimise such a tool, recent advances in *A. fumigatus* molecular biology, antigen capture and SELDI-ToF-MS were implemented with a view to detecting fungal proteins in murine BALFs. This chapter can be broadly divided into two sections firstly, a pilot study aiming to provide proof of principle for epitope tagging and recombinant protein detection *in vitro*, and secondly, the first implementation of SELDI-ToF-MS as a tool to study a library of recombinant his-tagged proteins at two stages of *A. fumigatus* infection in the murine host.

6.2 Materials and methods

6.2.1 *A. fumigatus* strains

A fumigatus strains used in this chapter are the clinical isolate CEA10 and the *akuB*^{KU80} strain (Silva Ferreria et al. 2006).

6.2.2 Bacterial strains

The bacterial strain used was *E. coli* Xl-10 (Stratagene). Bacterial strains were routinely grown overnight in Luria broth (LB) composed of 0.5% (w/v) NaCl, 0.5% (w/v) yeast extract and 1% bactotryptone. For solid medium, 2% (w/v) agar was added to LB.

6.2.3 Plasmids

6.2.3.1 pGEM_BLE

pGEM_BLE is derived from pSK259 which was generated by Sven Krappman. Prior to this study, a 2596 bp portion of pSK259 (Krappman et al. 2005) was cloned into the NdeI site of pGEM®-T EASY vector (Promega). The cloned fragment contains 1991 bp of the *gpdA* promoter and a 300 bp non-functional portion of the *ble/tk* cassette (Loss, 2009).

6.2.3.2 pGEM_TK

pGEM_TK is derived from pSK259 which was generated by Sven Krappman. Prior to this study, a 2409 portion of pSK259 was cloned into the NdeI site of pGEM®-T EASY vector (Promega). The cloned fragment contains a 1467 bp non-functional sequence of the *ble/tk* cassette. A portion of the *ble* cassette contained in plasmids pGEM_BLE and pGEM_TK overlaps by 259 bp, facilitating recombination between the two regions during *A. fumigatus* transformation. Reconstitution of the *ble/tk* cassette confers phleomycin resistance and FUDR sensitivity by means of the *ble* and *tk* (herpes simplex virus type 1 thymidine kinase) genes respectively (Loss, 2009).

6.2.3.3 pSK379.

pSK379, generated by Sven Krappmann contains a pyrithiamine resistance gene (*ptrA*) and a *his2A* cassette to promote targeted integration of heterologous DNA into an intergenic region of the recipient strain genome.

6.2.3 Oligonucleotide primers

Oligonucleotide primers used in this chapter are listed in Table 6.1

Table 6.1: Oligonucleotide primer sequences used in this chapter. Oligonucleotides encoding a polyhistidine tag are shown in bold text. Sequence encoding the gene stop codon is shown in bold and underlined text.

Primer	Orientation	Sequence
Afu5g14190_5'_F	Forward	GTCGTCTACCGATTCCCAAA
Afu5g14190_5'_R	Reverse	**CTA**GTGGTGATGGTGATGATG-AGGTTCAGGCGGATAAACCA
Afu5g14190_3'_F	Forward	ATGGCCAGCAACAGGGTG
Afu5g14190_3'_R	Reverse	TTTTCGAAGCTGGCAACTGA
Afu1g17510_5'_F	Forward	ACTTTCGATGTGGTCCATCGG
Afu1g17510_5'_R	Reverse	**CTA**GTGGTGATGGTGATGATG-TGCGAAACCCCACCATTTAA
Afu1g17510_3'_F	Forward	TTGTTCGACATGGTTGCTTCA
Afu1g17510_3'_R	Reverse	AAGTTCGCCTATGTGGAGAGA
Afu2g05150_5'_F	Forward	AGACCTCTACCCCCTGTGAGA
Afu2g05150_5'_R	Reverse	**CTA**GTGGTGATGGTGATGATG- CAGCAACAGTGCAAATGCAG
Afu2g05150_3'_F	Forward	CGAGCATGGAATGAGATGGA
Afu2g05150_3'_R	Reverse	TCTTGGTTAGACGGATGCAA
Afu5g00540_5'_F	Forward	TCCCGTTTTGTATTAAGTGCC
Afu5g00540_5'_R	Reverse	**CTA**GTGGTGATGGTGATGATG-TATCAGCGCGTTCTTGTAAA
Afu5g00540_3'_F	Forward	TGACCTTGTGAGGAGCTTGA
Afu5g00540_3'_R	Reverse	TCGATTCTAGCAGCAGGACTT
BLE-A	Reverse	TCCGGAAGTTCGTGGACA
TK-B	Forward	AAGTTGACCAGTGCCGTTCC
5'_510_Confirmation_F	Forward	GTTGAGGATACTGCCGGAAAG
3'_510_Confirmation_R	Reverse	CTTTCCGGCAGTATCCTCAAC
5'_540_Confirmation_F	Forward	CAGTGTCGCTAGGTTGATCC
3'_540_Confirmation_R	Reverse	GGATCAACCTAGCGACACTG
540_Rt-PCR_F	Forward	GGGTCGACGTTGAAATTTGC
540_Rt-PCR_R	Reverse	GATGGTGATGATGTATCAGCGC

BT-F	Forward	GAGCCCTTTTCCGACCTGAT
BT-R	Reverse	GGAACTCCTCCCGGATCTTG
Afu4g09580_F	Forward	TGGTTTGAGTTTCGTTTTGC
Afu4g09580_R	Reverse	**CTAGTGGTGATGGTGATGATG**CGAGATCCGGACTGTCCTTAC
Afu1g17180_F	Forward	TATTCGGCTTTGTGGGTCAT
Afu1g17180_R	Reverse	**CTAGTGGTGATGGTGATGATG**CGAGCTAGGCGTCCATGGCT
Afu5g01990_F	Forward	CGATGGGGACCATAAGTGAC
Afu5g01990_R	Reverse	**CTAGTGGTGATGGTGATGATG**ACAACCCTCTGCACAAAGTG
Afu3g14170_F	Forward	TCCTTTGAGTGCCAACTGC
Afu3g14170_R	Reverse	**CTAGTGGTGATGGTGATGATG**GACGGTCTCGGTAGTAGCAGC
Afu8g01110_F	Forward	AAGTTTATTTCGCGTCCTTACA
Afu8g01110_R	Reverse	CTAGTGGTGATGGTGATGATG TACATCTCCCCCAATATTAC
Afu8g06560_F	Forward	TCCTTCAACAGCCCTCAAGT
Afu8g06560_R	Reverse	**CTAGTGGTGATGGTGATGATG**GGCCACGGCCTTCTCGGGGT
Afu3g03280_F	Forward	CCTACCTGGACAAGTAAGTTGC
Afu3g03280_R	Reverse	**CTAGTGGTGATGGTGATGATG**GACCAAACGAATTCCGTTCC
Afu4g00390_F	Forward	CGAGAATCAATTTCTGGGTGA
Afu4g00390_R	Reverse	CTAGTGGTGATGGTGATGATG CGACAAGAGAGTTCTCTTCA
Afu8g04380_F	Forward	ACTTGAACACCGCATCCTTC
Afu8g04380_R	Reverse	**CTAGTGGTGATGGTGATGATG**TGCGGCAACCCATTGGGGACA
Afu1g17190_F	Forward	ACTCGCAGCTACCCTCGTTA
Afu1g17190_R	Reverse	**CTAGTGGTGATGGTGATGATG**TTTTTCCTTTATTGCTGCCG
Afu4g06640_F	Forward	GCCACAAGAAACCGACAAAT
Afu4g06640_R	Reverse	**CTAGTGGTGATGGTGATGATG**GATATACAGCTCAGCCCGCT
Afu2g03990_F	Forward	GAGGAGGGTAGGGCTCAATC
Afu2g03990_R	Reverse	**CTAGTGGTGATGGTGATGATG**CGCAGCTCGAACGGAACAGT
Afu7g06750_F	Forward	CCCCTATAATGGCAATCAGC
Afu7g06750_R	Reverse	**CTAGTGGTGATGGTGATGATG**ACCATCCAAACCAGGGCATT
Afu5g01910_F	Forward	CAGCATGGCTCCTGTAATCA
Afu5g01910_R	Reverse	**CTAGTGGTGATGGTGATGATG**CTTCTTCACAGTGTCAACAT
Afu4g11800_F	Forward	TTGCTCTCGAACCATGACTG
Afu4g11800_R	Reverse	**CTAGTGGTGATGGTGATGATG**AGCATTGCCATTGTAGGC
Afu5g01620_F	Forward	GTCTTGACAACCTCCCAAGC

Afu5g01620_R	Reverse	**CTAGTGGTGATGGTGATGATG** CACCCGCACTATTCTCCTCT
Afu6g00290_F	Forward	ATGTTTTCCCGAAAGGCATC
Afu6g00290_R	Reverse	**CTAGTGGTGATGGTGATGATG** TTTGCGCTCCGCCAAGGGCAC
Afu4g10610_F	Forward	CCCCGGTCATCTCTGTAGATT
Afu4g10610_R	Reverse	**CTAGTGGTGATGGTGATGATG** CAGAACACTCTCGAAATAAGT
Afu6g05030_F	Forward	TCTAACTCCAATGGCGACTGT
Afu6g05030_R	Reverse	**CTAGTGGTGATGGTGATGATG** CTCCAAAACCGGAGTAACC
Afu2g12680_F	Forward	CGAAGGAGTTGACCATCATAG A
Afu2g12680_R	Reverse	**CTAGTGGTGATGGTGATGATG** ACAGTTGTGAGTCATCCTCAG
Afu7g00580_F	Forward	CATGCACATGGCAAATTCTC
Afu7g00580_R	Reverse	**CTAGTGGTGATGGTGATGATG** GATAATCCATTGTACCAGCCC
Afu8g00610_F	Forward	CTGCAGTTCCACACTGACAA
Afu8g00610_R	Reverse	**CTAGTGGTGATGGTGATGATG** CATCGTAAATGCAGCAGAACC
Afu5g01200_F	Forward	CAGAAAACGACGAGCAGCTA
Afu5g01200_R	Reverse	**CTAGTGGTGATGGTGATGATG** AGTTGAGAAGATGGGCTTCTT C
Afu7g01040_F	Forward	GGATAAGCTGGCGACATCAC
Afu7g01040_R	Reverse	**CTAGTGGTGATGGTGATGATG** ATCCACAAGATACGCAAATGG
Afu2g17320_F	Forward	GGCACTCACGGTTGAAGAGT
Afu2g17320_R	Reverse	**CTAGTGGTGATGGTGATGATG** ATGCGGCTTGACCCATGCGGG
Afu2g17330_F	Forward	CATGCTGAAGTTGGTACAGTC C
Afu2g17330_R	Reverse	**CTAGTGGTGATGGTGATGATG** GAGCACCAGTTGCCGATTTCT C
Afu5g14660_F	Forward	AATTCCCCTCCGTTTCAGAT
Afu5g14660_R	Reverse	**CTAGTGGTGATGGTGATGATG** AATCGAAACCTCCATGACAGG
Afu8g05600_F	Forward	GTGGAAGACTTTGGCCTGAA
Afu8g05600_R	Reverse	**CTAGTGGTGATGGTGATGATG** TGAATCCGTCGGGGGCCGATA
Afu3g01500_F	Forward	GAAAACGAAGGGAAATAGAAC G
Afu3g01500_R	Reverse	**CTAGTGGTGATGGTGATGATG** CTTCGACGGGTCTTCTGCCAA
Afu1g14550_F	Forward	TGATTCCGATGGATGAGAGA
Afu1g14550_R	Reverse	**CTAGTGGTGATGGTGATGAT GCAGCTTCATGAATGGGTGTC C**

Afu2g10130_F	Forward	TGAGCCAAAGAATAAACTGAG C
Afu2g10130_R	Reverse	**CTAGTGGTGATGGTGATGATG** AATAGCGCACTTGTCTTGGAT
Afu1g12350_F	Forward	CAGCAATTCCGCTGTTATGA
Afu1g12350_R	Reverse	**CTAGTGGTGATGGTGATGATG** CGCCGAGTAGAAGGCGTGTCC
Afu3g10960_F	Forward	GCATGATCCGAGGAGACAG
Afu3g10960_R	Reverse	**CTAGTGGTGATGGTGATGATG** GAAGTTGGACGCAGCGTTAAC
Afu8g05610_F	Forward	GACCAAGGATGCAGGATCAC
Afu8g05610_R	Reverse	**CTAGTGGTGATGGTGATGATG** GTTGAAGGTGTCGAAGCAACC
Afu2g12630_F	Forward	TTGAGAGATTTCCCCAATGC
Afu2g12630_R	Reverse	**CTAGTGGTGATGGTGATGATG** TACACCAGAGGCACAGTGGGA
Afu3g03060_F	Forward	TCTTTCCGTTTCCTCGACTG
Afu3g03060_R	Reverse	**CTAGTGGTGATGGTGATGATG** CTGGGTGTAGACACAGCTGTT
Afu5g10270_F	Forward	GCACGTTGGATCATGGATGT
Afu5g10270_R	Reverse	**CTAGTGGTGATGGTGATGATG** CTCTGACTTAATGTCGATACG
His_R	Reverse	CTAGTGGTGATGGTGATGATG

6.2.4 Cloning of PCR inserts into plasmids pGEM_BLE and pGEM_TK for the generation of *A. fumigatus* epitope tag transformation constructs

To construct *A. fumigatus* alleles expressing a polyhistidine epitope tag, plasmids pGEM_BLE and pGEM_TK were utilised. Plasmids pGEM_BLE and pGEM_TK were linearised with NdeI (New England Biolabs, UK) and blunt-ended using DNA polymerase I (New England Biolabs, UK). Blunt ended vectors were dephosphorylated using alkaline phosphatase (New England Biolabs, UK). 5' and 3' PCR fragments from the gene of interest were amplified using BD Advantage™ 2 polymerase (Clontech, USA) from CEA10 gDNA template according to the manufacturer's guidelines. Oligonuclotide primers are listed in Table 1. Note that 5' reverse primers (e.g. Afu5g10270_R) encode a polyhistidine tag immediately before the gene stop codon. PCR fragments were blunt ended and phosphorylated using alkaline phosphatase and T4 polynucleotide kinase (New England Biolabs, UK) respectively. 5' and 3' fragments from the gene of interest were blunt end ligated into plasmids pGEM_BLE and pGEM_TK respectively using T4 DNA ligase (New England Biolabs, UK). The ligation reaction was transformed into competent *E. coli* XL-10 (Stratagene) cells, which were grown overnight on LB plates containing 0.1 mg/ml ampicillin. Plasmids were extracted by miniprep (Sigma-Aldrich, UK) and ligation of the target

flanks into the vector was confirmed using restriction digest mapping. This generated plasmids pGEM_BLE_*x* and pGEM_TK_*y*, where *x* and *y* denote the 5' or 3' target flanks respectively. Linear constructs for *A. fumigatus* transformation were generated by PCR using primer pairs BLE-A and 5'_F, and TK-B and 3'_R (Table 6.1) with plasmids pGEM_BLE_*x* or pGEM_TK_*y* as templates respectively. 10 PCR reactions for each construct were co-purified (Nucleospin) to yield gDNA concentrations of 200 ng/µl. 2 µg of each purified linear construct was used for *A. fumigatus* transformations (Figure 6.1).

6.2.5 Transformation of *A. fumigatus* electrocompetent spores

For preparation of electrocompetent spores, *A. fumigatus* Ku80 or CEA10 strains were grown on solid ACM for 5 days, harvested in sterile H_2O and filtered through Miracloth (Calbiochem). Spores were centrifuged for 10 minutes at 4000 g, washed 5 times with sterile H_2O and enumerated on a haemocytometer. 250 mls YG broth (0.5% Yeast Extract, 2% Glucose) was inoculated with 5×10^9 spores and grown at 37°C for 2 - 4 hours until the spores had swollen. Spores were then centrifuged for 10 minutes at 4000 g, washed in cold water, and resuspended in 20 mls YED (1% Yeast Extract, 1% Glucose, 20 mM Hepes, pH 8 with NaOH). Spores were incubated at 30°C for 1 hour, and then resuspended in ice cold EB (10 mM Tris HCl pH 7.5, 270 mM Sucrose, 1 mM LiAc). 2 µg of both 5' and 3' linear constructs was resuspended in 10 µl dH_2O and mixed with 50 µl of electrocompetent spores. The transformation mixture was pulsed with the following parameters: 1 Kv, 400 Ohms, 25 F. Following electroporation, 1 ml of cold YED was added, cooled on ice for 15 minutes and then incubated for 1.5 hours at 30°C. The mixture was plated onto AMM, left overnight at room temperature and then overlayed with AMM containing phelomycin, giving a final concentration of 250 µg per plate. Finally plates were left for 48 hours at 4°C before being incubated at 37°C.

Transformants were subcultured on AMM supplemented with 250 µg phleomycin and grown for 5 days. Spores were picked using a loop and added to 200 µl breaking buffer (2% Triton X-100, 1% SDS, 100 mM NaCl, 10 mM Tris-HCl pH 8.0, 1 mM EDTA pH 8.0). 300 mg of glass beads (0.4-0.6 mm diameter, Sartorius UK) were added and incubated for 30 minutes at 70°C, with vortexing every 10 minutes. 200 µl chloroform:isoamylalcohol 25:24:1 was added and further vortexed for 5 minutes, before being spun for 8 minutes at max speed. The supernatant was precipitated with an equal volume of isopropanol and incubated overnight at 4°C. Following centrifugation at 13000 rpm for 10 minutes the pellet was washed in 70% (v/v) ethanol and air-dried before resuspension in 20 µl TE containing RNace-It™ ribonuclease cocktail (Stratagene).

Presence of the biselectable marker cassette at the C-termini of genes of interest was confirmed by PCR using forward and reverse confirmation primers, e.g. 5'_540_Confirmation_F and 3'_540_Confirmation_R (Table 6.1) and transformant gDNA as template. Confirmation primers were designed to amplify a chromosomal locus approximately 100 bp up and downstream from the 5' and 3' extremities of the cassette target flanks respectively. Recombination of the biselectable cassette at the target loci is indicated by an increase in PCR product size by 4.6 Kb relative to the Ku80 isogenic background strain.

6.2.6 Cloning inserts into plasmid pSK379 for the construction of epitope tagged transformation vector

To increase the through-put of epitope tagging methodology in later experiments, the biselectable split marker approach was substituted for a strategy using plasmid pSK379 containing a tagged allele of the gene of interest (see section 3.36). The *gpdA* promoter of pSK379 was removed by restriction digest with PmeI, followed by a second digest with PstI (New England Biolabs, UK). The digested vector was blunt ended using DNA polymerase I (New England Biolabs, UK) and dephosphorylated using alkaline phosphatase (New England Biolabs, UK). Genes of interest were amplified from CEA10 genomic DNA using Phusion® Polymerase (New England Biolabs, UK) which produces PCR fragments with blunt ends. Primers were designed to amplify the gene of interest with 1 Kb of 5' UTR to include the native promoter. The reverse primer amplified 18 - 22 bp of the gene C terminus, with a polyhistidine tag encoded before the stop codon. Primer sequences are shown in Table 6.1. PCR fragments were phosphorylated using T4 polynucleotide kinase (New England Biolabs, UK) and blunt end ligated into pSK379 using T4 DNA ligase (New England Biolabs, UK). The ligation reaction was transformed into competent *E. coli* Xl-10 cells (Stratagene), which were grown overnight on LB plates supplemented with 0.1 mg/ ml ampicillin. Plasmids were extracted by miniprep (Sigma-Aldrich, UK) and ligation of the gene of interest into the vector was confirmed using restriction digest mapping, and colony PCR using the gene of interest forward and reverse primers. For *A. fumigatus* transformation, pSK379 containing the gene of interest was extracted from bacterial culture by miniprep and 3 µg of plasmid resuspended in less than 20 µl sterile water.

6.2.7 Fungal transformation using *A. fumigatus* protoplasts

Protoplast transformation was based on the protocol described by Szewczyk and co-workers (Szewczyk et al. 2006). *A. fumigatus* Ku80 was grown for 5 days on ACM plates. Spores were harvested in sterile water, filtered twice through Miracloth (Calbiochem) and washed twice with sterile water. 1 x 10^8 spores were inoculated into 20 mls ACM broth and grown for 16 hours at 30°C with 150 rpm. Hyphae were isolated by filtration through Miracloth and rinsed with ACM broth. Hyphae were resuspended in 8 mls ACM, to which 8 mls of protoplasting solution (KCl, 12.8 % Vineflow, Novo Nordisk) was added. Protoplasting was visually monitored, and the solution was incubated for 3 - 4 hours at 30 °C with 100 rpm. To remove undigested hyphal material, the protoplasting solution was layered onto 30 mls 1.2 M sucrose and centrifuged at 2000*g*. Protoplasts were collected at the top of the sucrose cushion and gently resuspended in 0.6 M KCl and centrifuged at 2000*g.* The pellet was washed three times in 0.6 M KCl, once in KCl 0.6 M, 50 mM $CaCl_2$, and resuspended in a volume of KCl 0.6 M, 50 mM $CaCl_2$ appropriate for transformation.

3 µg of plasmid pSK379 containing the gene of interest was mixed with 100 µl of protoplasts. The solution was mixed by vortexing and 50 µl PEG solution was added. The mixture was incubated in an ice water bath for 25 minutes, after which 1 ml of PEG was added and the sample was left at room temperature for an additional 25 minutes. 150 µl of protoplast/DNA solution was added to 10 mls AMM media containing 10 ul of pyrithiamine (0.5 mg/ml), which was overlayed onto a plate containing 15 mls of AMM with 15 ul pyrithiamine (0.5 mg/ml). Plates were incubated at room temperature for 24 hours and then incubated at 37°C for 72 – 144 hours. Transformants were subcultured on AMM supplemented with 0.5 mg pyrithyamine and grown for 5 days. Spores were picked using a loop and added to 200 µl breaking buffer (2% Triton X-100, 1% SDS, 100 mM NaCl, 10 mM Tris-HCl pH 8.0, 1 mM EDTA pH 8.0). 300 mg of glass beads (0.4-0.6mm diameter, Sartorius UK) were added and incubated for 30 minutes at 70 °C, with vortexing every 10 minutes. 200 µl of chloroform:isoamylalcohol 25:24:1 was added and further vortexed for 5 minutes, before being spun for 8 minutes at max speed. The supernatant was precipitated with an equal volume of isopropanol and incubated overnight at 4 °C. Following centrifugation at 13000 rpm for 10 minutes the pellet was washed in 70% (v/v) ethanol and air-dried before resuspension in 20 µl TE containing RNace-It™ ribonuclease cocktail (Stratagene). *A. fumigatus* transformant gDNA was checked for homologous recombination of the tagged allele into the genome by PCR using the forward primer from the gene of interest and the His_R reverse primer.

6.2.8 Semi-quantitative RT-PCR assay

Ku80 and *A. fumigatus* strains putatively expressing an epitope tagged allele were inoculated into 200 mls ACM broth at a concentration of 5 x 10^5 spores / ml. Cultures were grown for 16 hours at 37°C with 150 rpm. Mycelia were isolated from liquid culture by filtration through miracloth (Calbiochem), rinsed with sterile water and snap frozen in liquid nitrogen. Frozen mycelia were ground using a pestle and mortar in liquid nitrogen. RNA was extracted from ground mycelia using the RNeasy kit (Qiagen, UK).

4 µg of RNA was DNase treated using DNase I (New England Biolabs, UK). To confirm absence of residual DNA contamination following DNase treatment, PCR with primers 540_Rt_PCR_F and 540_Rt_PCR_R (Table 6.1) was conducted using untreated and DNase treated RNA samples as templates. Gel electrophoresis showed presence and absence of the expected 154 bp PCR product for untreated and treated templates respectively, which demonstrated gDNA removal from DNase treated RNA samples. 500 ng of DNase treated RNA was reverse transcribed into cDNA with 50 µM oligo(dT) primers and manufacturer's guidelines using the First Strand cDNA Synthesis kit (GEHealthcare, UK). Rt-PCR primers 540_Rt_PCR_F and 540_Rt_PCR_R were designed to amplify a 154 bp product from the Afu5g00540-His_6 cDNA (Table 6.1). Rt-PCR was performed in triplicate using Sybr Green Jumpstart™Taq ReadyMix™ (Sigma-Aldrich, UK). 5 µl of cDNA from either Afu5g00540-His_6 or Ku80 was used as a template in 20 µl RT-PCR reactions. RT-qPCR was conducted in a Rotor-Gene RG-3000 PCR cycler (Corbett Research, UK) with the following cycling parameters: 95 °C for 5 seconds, 58 °C for 5 seconds, 72 °C for 15 seconds, 78 °C for 5 seconds, which was repeated 40 times. Data were then analysed using the RotorGene 6 software, from which the amplification threshold was manually assigned to generate Ct values. Ct values from reactions using primers 540_Rt_PCR_F and 540_Rt_PCR_R were normalised to that of the house keeping gene (beta tubulin, Afu7g00250).

6.2.9 Protein extraction from *A. fumigatus* mycelia

Mycelia from Ku80 and *A. fumigatus* strains putatively expressing an epitope tagged allele were isolated as for RNA extractions from 16, 24, 36 and 48 hour cultures. 250 mg of frozen mycelia was added to a 2 ml Eppendorf tube containing a metal bead and 1 ml of buffer A50 (25 mM HEPES pH 7.5, 50 mM KCl, 5 mM $MgCl_2$, 0.1mM EDTA, 0.5 mM DTT, 1mM PeFa-Bloc, 1 µM Pepstatin, 0.6 µM Leupeptin, 10% glycerol v/v). Mycelial samples were homogenised in a Fast Prep-24 (MP Biomedicals, United Kingdom) using 6 x 10 second bursts at power setting number 4. Homogenised mycelia were mixed on a tube rotator for 90 minutes at 4°C. Samples were then

centrifuged at 13000 rpm for 30 minutes at 4°C, after which the supernatant was isolated and stored at -80°C. Protein concentrations were measured using BCA assay (Thermo Scientific, UK). His-tagged proteins were enriched from crude protein extracts using Ni-NTA agarose beads (Qiagen) and 5 ml polypropylene columns (Qiagen). 40 µg of *in vitro* protein was resuspended in 4 mls and mixed with 1 ml Ni-NTA agarose beads according to the manufacturer's guidelines, except washing steps were increased (n = 10).

6.2.10 Protein extraction from *A. fumigatus* supernatant

Mycelia were separated from 50 mls liquid media of 16, 24, 36 and 48 hour cultures by filtration through Miracloth (Calbiochem). 3 volumes of ice cold acetone was added and proteins were precipitated over night at - 20°C. Proteins were isolated by centrifugation at 13,000 rpm for 20 minutes at 4°C and resuspended in PBS.

6.2.11 SDS-PAGE and Western blot analyses of protein extracts

Protein samples were run on 12% SDS-PAGE. Gels were stained in Coomassie stain (0.1% Coomassie Blue R-250, 45% methanol, 10% acetic acid) for an hour, before overnight incubation in Coomassie de-stain (10% methanol, 10% acetic acid).

For Western blotting, gels were transferred to PVDF membrane (Amersham) in transfer buffer (25mM Tris base, 192 mM glycine, 20% methanol) as per manufacturer's instructions using Invitrogen's XCell-SureLock Mini Cell XII Blot module. Membranes were blocked for an hour in 5% (w/v) milk in PBS-Tween (0.001% Tween-20, 137 mM NaCl, 1.47 mM KH_2PO_4, 2.68 mM KCl, 8.1 mM $Na_2HPO_4.12H_2O$) before being incubated with primary Anti-his antibody (GE Healthcare, UK) in 5% w/v milk for an hour. Membranes were washed 3 x 10 mins with PBS-Tween and incubated in the secondary antibody (ECL Anti Mouse IgG, GE Healthcare, UK) for an hour and washed 3 x 10 mins with PBS-Tween. Membranes were developed using ECL solution 1 (12.5 mM luminol/3-aminophthalhydrazide in DMSO, 19.8 mM coumaric acid in DMSO, 5 mM Tris-HCl, pH8.5) and ECL solution 2 (5 mM Tris-HCl, pH8.5, 0.064% (v/v) H_2O_2) in a 1:1 ratio and exposed onto Hyper film (Kodax). During all incubations and washings the membrane was agitated continuously using a rocker.

6.2.12 Murine infections

Murine infections were conducted under UK Home Office Project Licence PPL/70/6487 in a dedicated facility at Imperial College London. Outbred male mice (strain CD1, 18 – 22 g, Harlan Ortech) were housed in individually ventilated cages and allowed water and food *ad libitum*. Water was supplemented with 1 g/L tetracycline hydrochloride (Sigma-Aldrich) and 64 mg/L ciprofloxacin as prophylaxis against bacterial infection. Neutropenia was induced by intraperitoneal injections of cyclophosphamide (150 mg/kg) on days –3 and –1 and by a single subcutaneous dose of hydrocortisone acetate (112.5 mg/kg) on day –1 (Schrettl et al. 2004). *A. fumigatus* spores were grown on ACM, supplemented with 1% (w/v) glucose and 5 mM ammonium tartrate, for 5 days prior to infection. Spores were harvested on the day of infection, using sterile saline (Baxter Healthcare Ltd, UK), and filtered through Miracloth (Calbiochem). Conidial suspensions were centrifuged for 10 minutes at 5000 rpm, washed twice with sterile saline, counted using a haemocytometer and resuspended at a concentration of $2.5x10^9$ cfu/ml. Mice were anaesthetised by isofluorane inhalation and infected by intranasal instillation of conidia in 40 µl of saline solution. The concentration of conidia for each experiment is indicated in the Results section of this chapter. The determination of viable counts for the administered inocula was performed using serial dilution on ACM plates supplemented with 1% (w/v) glucose and 5 mM ammonium tartrate and incubated for 3 days at 37°C. Mice were weighed every 24 hours from day -3 and inspected twice daily. Mice were culled at 4 and 18 hours post infection by neck dislocation. Bronchoalveolar lavage (BAL) was performed using several 250 µl aliquots of 37° sterile saline. BAL fluids (BALFs) were snap frozen in liquid nitrogen.BALF protein concentration was measured using BCA assay (Thermo Scientific, UK). Typically, BALF concentrations were between 1 – 2 µg/ml.

6.2.13 Lyophilisation of murine BALF

200 µl of murine BALFs were lyopholised for 7 – 8 hours at – 20 °C and resuspended in 40 µl PBS including protease inhibitor cocktails (Roche, UK).

6.2.14 Albumin depletion of murine BALF

50 µl BALF was albumin depleted using Proteoprep Immunoaffinity Albumin and IgG Depletion Kit (Sigma, UK). Samples were resuspended in 50 µl.

6.2.15 Acetone precipitation of murine BALF

For acetone precipitation, 1.5 mls of ice cold acetone was added to 500 µl BALF, which was precipitated overnight at – 20 °C. Samples were centrifuged at 13000 rpm for 30 minutes at 4 °C, where the pellet was air dried for 20 minutes and resuspended in 500 µl of PBS.

6.2.16 Ni-NTA enrichment of murine BALF

His-tagged proteins were enriched from murine BALFs using Ni-NTA agarose beads (Qiagen) and 1 ml polypropylene columns (Qiagen). 300 µl acetone precipitated BALF was resuspended in 100 µl Ni-NTA agarose beads according to the manufacturer's guidelines, except washing steps were increased (n = 10).

6.2.17 Immobilisation of anti-his antibody and antigen on PG20 chips

The PG20 chip contains 8 spots to which protein G is covalently bound. Consequently, most antibodies capable of binding protein G can be used with PG20 chips. The anti-his antibody (GE Healthcare, UK) used in this study is an IgG2a monoclonal antibody, which has high binding affinity to protein G (ProteinChip® Antibody Capture Kit Instruction Manual). ProteinChip® Antibody Capture Kit (Biorad, USA) was used to immobilise the anti-his antibody to the PG20 array surface following the manufacturer's guidelines. 2 µl of 0.2 mg/ml anti-his antibody was added to spots on the chip and incubated in a humidity chamber overnight at 4 ºC. The chip was washed once in 8 mls wash buffer (0.5% Triton X-100 in PBS) for 10 minutes, and twice in 8 mls PBS for a total of 10 minutes. The array was air dried for 5 minutes. To cross-link the anti-his antibody to Protein G, 1 µl of cross linking reagent (Bissulfosuccinimidyl suberate, 0.5 mg/ml) was added to each spot and the chip was incubated in a humidity chamber at room temperature for 30 minutes. 1 µl of deactivation buffer (0.5 M ethanolamine in PBS, pH 8.0) was added to each spot, which was incubated on a rocker for 15 minutes at room temperature. The chip was then incubated for 10 minutes in wash buffer and twice in PBS for a total of 10 minutes. For antigen capture, 2 µl of the sample was added a spot on the array, which was incubated for one hour (increased to 3 hours for murine BALFs) at room temperature. The array was washed once with wash buffer for 10 minutes, twice with PBS for a total of 10 minutes, and briefly rinsed twice with 1 mM HEPES. The array was then air dried for 10 minutes. 0.5 µl of energy absorbing molecules (Sinapinic acid, 5 mg/ml) was added to each spot and left to air dry. This was repeated once, and the PG20 arrays were then read using ProteinChip SELDI reader.

6.2.18 Surface enhanced laser desorption/ionisation time of flight mass spectrometry

All time-of-flight spectra were generated using a PBS II ProteinChip SELDI Reader (Ciphergen, USA) at laser intensities of 230 or 260, with a high mass of 200 kDa and detector sensitivity 9. Each spot on the array was analysed from position 20 to 80. Every protein array included a universal control sample (100 ng his-tagged recombinant bacterial protein). The PBS II ProteinChip SELDI Reader was routinely calibrated prior to sample detection using ProteinChip All-in-One Protein Standard II (Biorad), as described in Table 2.1. Spectra were analysed using Ciphergen ProteinChip® Software. Individual spectra were baseline subtracted, from which peaks between 1 – 100 kDa with a signal-to-noise ratio above 3 were manually annotated.

6.3 Results

6.3.1 Construction of *A. fumigatus* his-tagged alleles

Pilot experimentation began prior to gene expression profiling presented in Chapter 3. Therefore, four alleles were chosen for pilot epitope tagging and recombinant protein detection experimentation based on high expression in murine BALFs relative to *in vitro* growth (McDonagh et al. 2008). Of secondary importance to candidate transcriptional profiles was the presence of a signal peptide sequence (n = 3). To limit the likelihood that C-terminal tags would be cleaved off, genes were checked for the absence of a GPI anchor (Table 6.2). It was hypothesised that genes which meet these criteria were most likely to direct the biosynthesis of proteins which were secreted in murine BALF during early murine infection.

Gene	Annotation	Log_2 *in vivo: in vitro* expression values	Protein size (AA)	Signal peptide	Signal peptide probability	Most likely cleavage site	GPI Anchor	His-tagged allele	*In vitro* protein detection
Afu5g14190	Beta-glucanase	7.40	485	Yes	0.999	18-19: AQA-RY	No	×	×
Afu1g17510	Lipase/esterase	5.89	154	No	0.004	-	No	✓	×
Afu2g05150	MP-2 antigenic galactomannoprotein	5.06	591	Yes	1.000	20-21: VLA-TP	No	×	×
Afu5g00540	Extracellular signalling protein FacC	5.00	310	Yes	0.998	17 and 18: VIA-KI	No	✓	✓

Table 6.2: Shortlisted predicted genes for pilot epitope tagging and SELDI-ToF-MS detection. Functions are based on annotation provided by CADRE (http://www.cadre-genomes.org.uk/index.html). Log_2 *in vivo*: *in vitro* ratios are gene expression values of 14 hour germlings from murine lung relative to developmentally matched laboratory culture (McDonagh et al. 2008). Signal peptide probability and cleavage site calculations are from the Signal P 3.0 Server (http://www.cbs.dtu.dk/services/SignalP/). Absence of GPI Anchors were confirmed by The GPI Prediction Server (http://mendel.imp.ac.at/gpi/cgi-bin/gpi_pred.cgi). Ticks and crosses represent success or failure respectively with regard to epitope tagging and protein detection.

A modified split marker approach was used for epitope tagging (Catlett et al. 2005). This facilitates gene tagging by triple homologous recombination between two linear constructs and the chromosomal locus, and overlapping portions of a selectable cassette (Figure 6.1C). The reconstituted biselectable marker cassette confers phleomycin resistance and FUDR sensitivity by means of the *ble* and *tk* (herpes simplex virus type 1 thymidine kinase) genes respectively. Prior to this study, two non functional halves of the *ble/tk* cassette (Krappman et al. 2005) were cloned into

pGEM-T EASY (Promega) to generate acceptor plasmids pGEM-BLE and pGEM-TK. The two non-functional encoded portions of the phelomycin cassette contained in these plasmids overlap by 259 bp, facilitating homologous recombination (Figure 6.1C). To generate target gene flanks, regions up and downstream of the gene stop codon were amplified from CEA10 genomic DNA. For the 5' targeting sequence, primers were designed to amplify 1 Kb upstream from the gene 3' end, with six histidine residues introduced in the reverse primer immediately before the stop codon (Table 6.1). For the 3' targeting sequence, 1 Kb of 3' UTR, no more than 100 bp from the gene stop codon was amplified. 5' and 3' flanking regions were blunt ended using DNA polymerase I (NEB) and ligated into plasmids pGEM-BLE and pGEM-TK respectively (Figure 6.1A and B). This generated plasmids pGEM_BLE_*x* and pGEM_TK_*y*, where *x* and *y* denote the 5' or 3' target flanks for each allele respectively.

Cloning of 5' and 3' targeting sequences into pGEM-BLE and pGEM-TK respectively was successfully completed for the lipase/esterase (Afu1g17510) and the extracellular FacC signalling protein (Afu5g00540, Table 3). 5' targeting sequences for the beta glucanase (Afu5g14190) and MP-2 antigenic galactomannoprotein (Afu2g05150) candidate genes could not be cloned into pGEM-BLE despite multiple optimisations of standard cloning techniques. PCR amplification of the 5' targeting sequence for the MP-2 antigenic galactomannoprotein produced multiple fragments which were not amenable to cloning, a phenomenon likely explained by the presence of coding tandem repeats in the gene (Levdansky et al. 2007). Appropriate for timely proof of principle for SELDI-ToF-MS epitope-tagged protein detection, linear constructs for *A. fumigatus* transformation were generated by PCR using primer pairs BLE-A and 5'_F, and TK-B and 3'_R (Table 6.1) with plasmids pGEM_BLE_*x* or pGEM_TK_*y* as templates respectively.

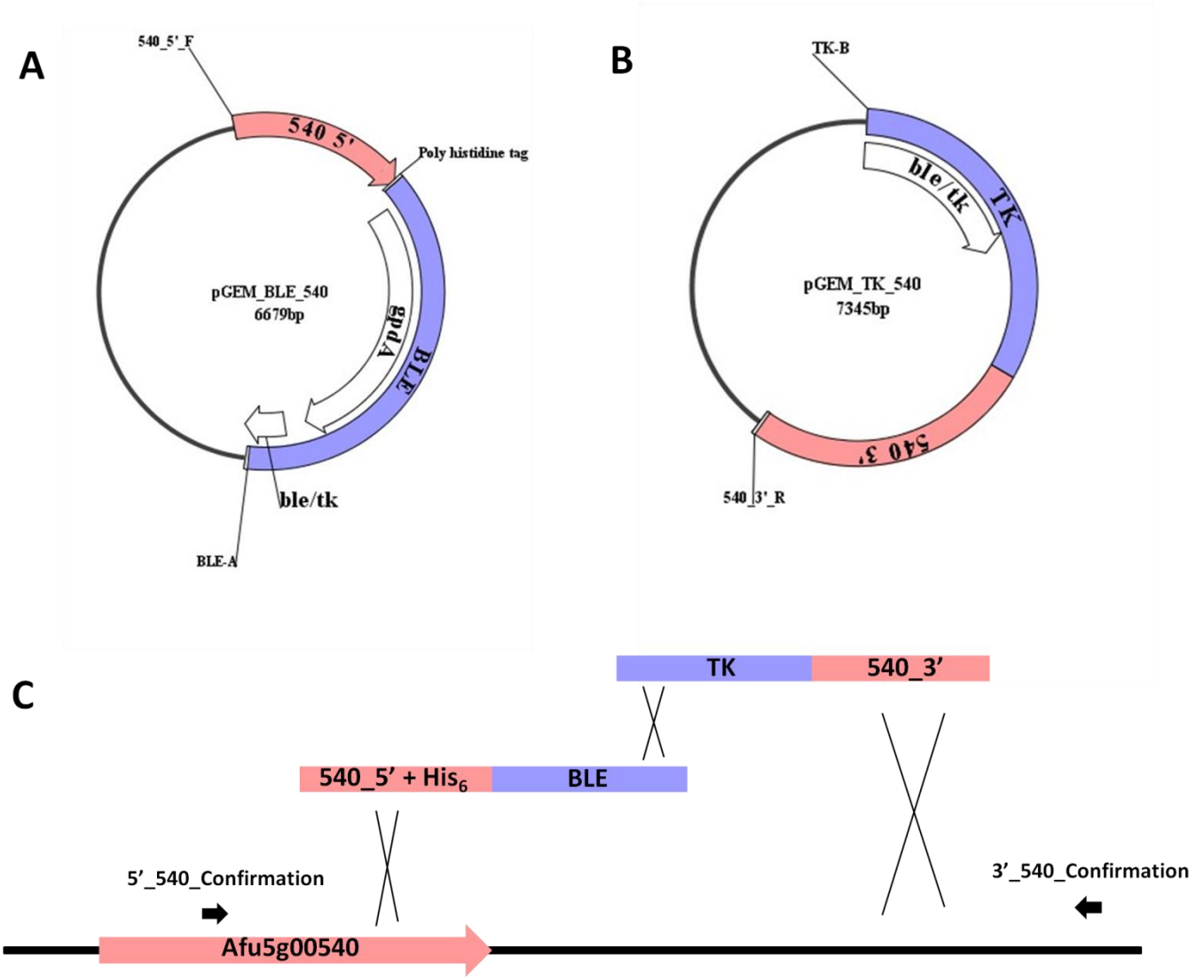


Figure 6.1: Cloning strategy for epitope tagging of *A. fumigatus* genes using a split marker methodology. Plasmids and linear transformation constructs for Afu5g00540 are shown as exemplars. Plasmids pGEM_BLE_540 (A) and pGEM_TK_540 (B) contain the *ble/tk* cassette (purple) and 5' and 3' flanks of the gene of interest respectively (pink). Primer pairs for generation of linear tag constructs are shown. The polyhistidine tag is encoded in the 5' flank immediately before the gene stop codon. A triple homologous recombination event introduces the his-tag via the 5' fragment and inserts a reconstituted biselectable marker cassette downstream of the putative poly A tail (C). Crosses depict recombination between the target gene flanks and the chromosomal locus, or between overlapping sequences of the selectable cassette. Locations of confirmation primers used to confirm homologous recombination are shown.

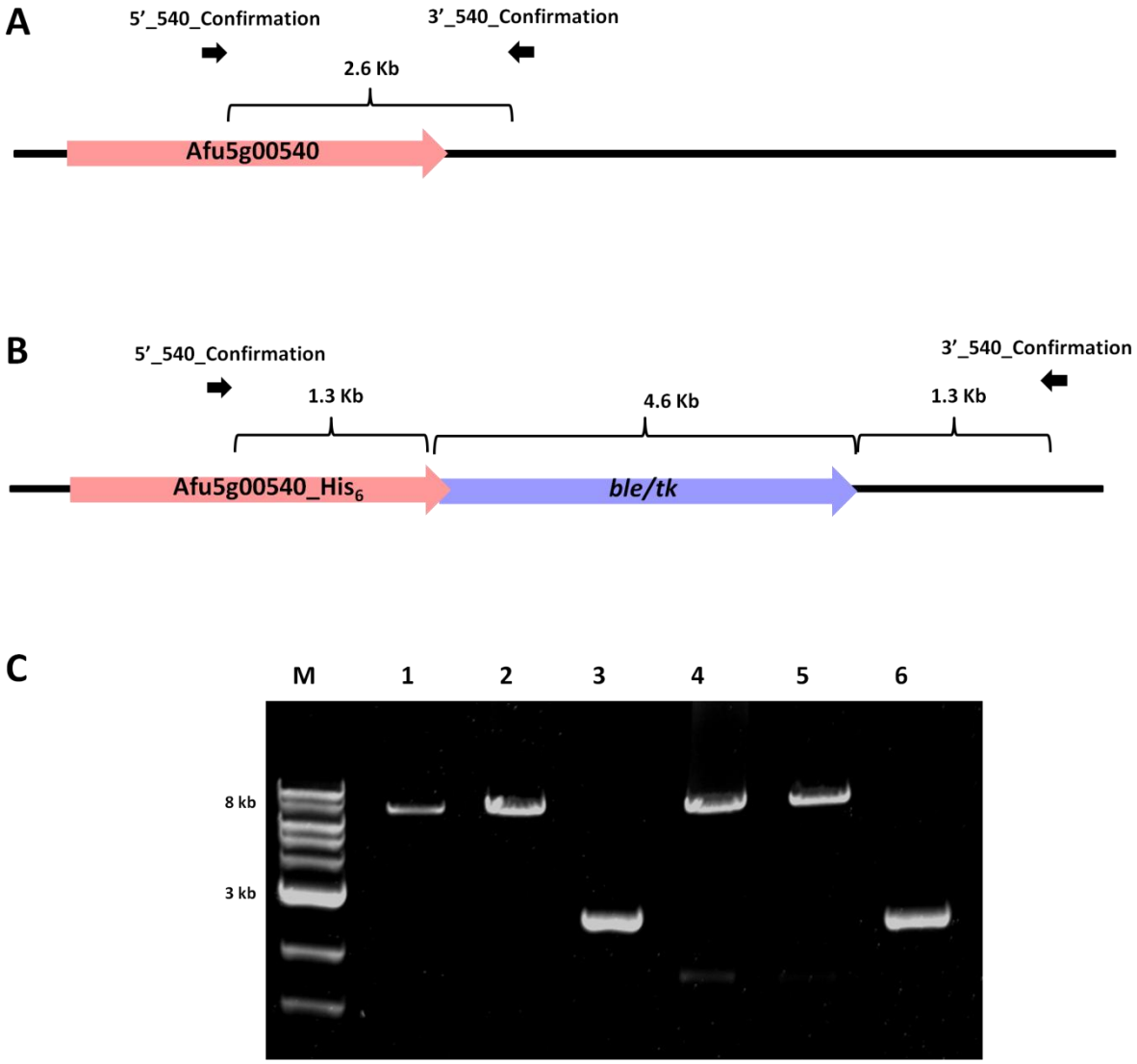


Figure 6.2: Schematic depicting locations of confirmation primers before and after a homologous recombination event with the *ble/tk* biselectable marker, and gel electrophoresis image of PCR products using confirmation primers and transformant or Ku80 gDNA as template. 5' and 3' confirmation primers amplify a 2.6 Kb fragment of the native chromosomal locus (A). The 5' confirmation primer was designed 100 bp upstream of the 5'_540_F primer (Figure 6.1C). The 3' confirmation primer was designed 100 bp downstream of the 3'_540_R primer (Figure 6.1C). Following a homologous recombination event with the *ble/tk* biselectable marker, confirmation primers amplify a 7.2 Kb product (B). PCR using forward and reverse Afu1g17510 confirmation primers and gDNA from transformants (lanes 1 and 2) or Ku80 control (lane 3) as template demonstrated recombination of the cassette at the target locus (C). PCR using forward and reverse Afu5g00540 confirmation primers and gDNA from transformants (lanes 4 and 5) or Ku80 control (lane 6) as template demonstrated recombination of the cassette at the target locus (C).

Linear constructs were co-transformed into *A. fumigatus* CEA10 using electroporation and transformants were selected on AMM containing phelomycin. Putative transformants were picked and screened by PCR using 5' and 3' confirmation primers, which amplify approximately 100 bp up and downstream from the 5' and 3' extremities of the cassettes target gene flanks respectively (Figure 6.2A and 6.2B). PCR using confirmation primers and transformant or Ku80 gDNA as template demonstrated cassette recombination when PCR products of sizes 7.2 Kb and 2.6 Kb were observed respectively (Figure 6.2). Multiple transformation attempts using CEA10 produced

transformants that were phleomycin resistant but did not demonstrate recombination at the native loci when checked with PCR. Subsequent transformations using the *akuB*^{KU80} strain (Silva Ferreria et al. 2006) produced higher numbers of transformants (between 10 and 20 per transformation), which demonstrated homologous recombination rates between 94% - 100%. During the course of this study, Afu1g17510 was re-annotated as a psuedogene. We therefore ceased work with this strain and continued work with the remaining tagged allele, the FacC signalling protein Afu5g00540.

6.3.2 Afu5g00540 his-tagged allele is transcribed during 16 hours *in vitro* culture

In keeping with prompt progression towards recombinant protein detection by SELDI-ToF-MS, it was reasoned that confirmation of a single integration event by Southern blotting was not necessary. Indeed, of greater importance was confirmation of gene expression and the presence of the histidine tag at the transcript 3' terminus. Thus, a semi-quantitative RT-PCR assay was used to confirm expression of the his-tagged transcript prior to protein detection. In order to distinguish between tagged and non-tagged transcripts, primers 540_Rt_PCR_F and 540_Rt_PCR_R were designed to amplify a 154 bp region of cDNA from Afu5g00540-His_6 strains (Table 1). The forward primer was designed 162 bp upstream of the gene stop codon. The reverse primer was homologous to a 22 bp region which spanned 9 bp and 13 bp of the gene locus and polyhistidine tag respectively. Amplification efficiency of primers 540_Rt_PCR_F and 540_Rt_PCR_R was tested by PCR using Afu5g00540-His_6 or Ku80 gDNA as a template. A product of the expected size was amplified from recombinant but not from Ku80 templates (Figure 6.3A).

For a semi quantitative RT-PCR assay, RNA was extracted from Afu5g00540-His_6 or Ku80 strains following growth in ACM for 16 hours. RNA was DNase treated and reverse transcribed into cDNA. To confirm absence of residual DNA contamination following DNase treatment, PCR with primers 540_Rt_PCR_F and 540_Rt_PCR_R was conducted using untreated and DNase treated RNA samples as templates. Gel electrophoresis showed presence and absence of the 154 bp product for untreated and treated templates respectively, which demonstrated gDNA removal from DNase treated RNA samples (data not shown). Expression of the His_6 transcript was detected from triplicate qRT-PCR reactions using the Afu5g00540-His_6 strain. Ku80 was used as a control strain lacking the putatively tagged transcript (Figure 6.3B). Ct values from Ku80 samples did not differ significantly from no-template control reactions using a student's T-test (p = 0.76, Figure 6.3B) and was therefore considered background signal. This was confirmed by gel electrophoresis of the RT-PCR reactions which showed the expected 154 bp product for his-tagged strains but not

for Ku80 or no-template control samples (data not shown). Ct values from Afu5g00540-His_6 cDNA were normalised relative to fungal beta tubulin (Figure 6.3B) which showed Afu5g00540-His_6 transcript abundance was comparable to that of *A. fumigatus* beta tubulin following 16 hours *in vitro* culture (Figure 6.3C).

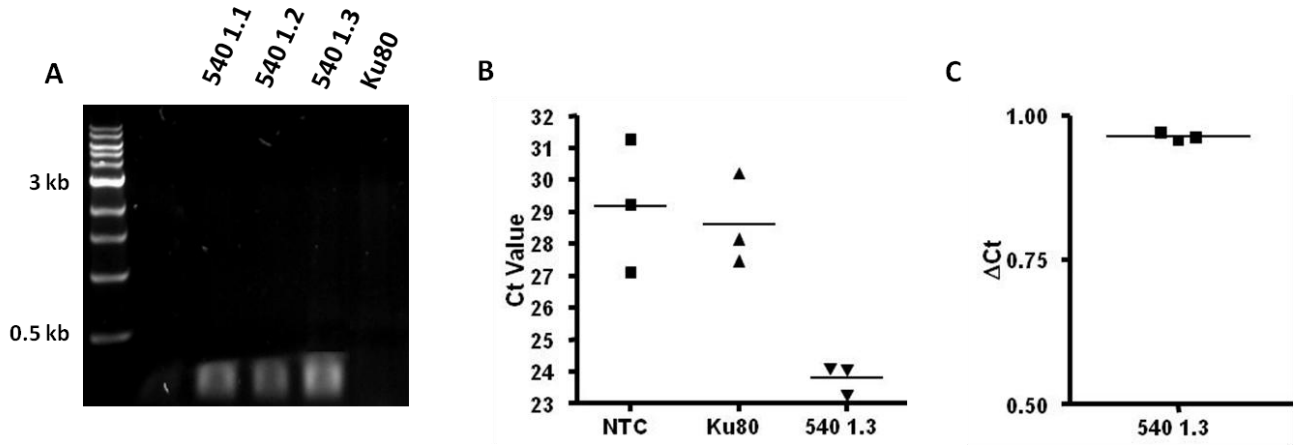


Figure 6.3: Semi quantitative RT-PCR assay to determine Afu5g00540-His_6 transcript abundance relative to *A. fumigatus* beta tubulin following 16 hour *in vitro* culture in ACM. (A) Gel electrophoresis of PCR products showed amplification of a fragment of the expected size (154 bp) which was restricted to PCRs containing gDNA from three Afu5g00540-His_6 transformants. (**B)** Raw Ct values from triplicate qRT-PCR reactions. Ct values from triplicate reactions using Ku80 cDNA as template did not differ significantly from no-template control samples ($p = 0.76$). Ct values from triplicate reactions using Afu5g00540-His_6 cDNA as a template were statistically different from Ku80 ($p = 0.0051$) and no template control samples ($p = 0.012$). (**C)** Afu5g00540-His_6 is expressed at levels slightly less than beta tubulin as determined by Ct analysis.

6.3.3 SELDI-ToF-MS, but not Western blotting, detects epitope tagged *A. fumigatus* Afu5g00540 protein from *in vitro* culture

Afu5g00540_His_6 detection was attempted by Western blotting utilising an anti-his primary antibody in order to provide evidence that the recombinant protein was indeed detectable by the epitope tag. The predicted molecular mass of Afu5g00540_His_6 protein is 34.7 kDa. Western blotting was conducted on protein extracted from Afu5g00540_His_6 and Ku80 mycelia or supernatant extracts (see Methods). Preliminary Western blotting demonstrated that background signal from 40 µg crude protein extracts was excessively high (Figure 6.4A and 6.4B). Attempts to reduce background signal by reducing the protein concentration slightly reduced background

signal but did not identify a his-tagged protein of the expected size which was restricted to Afu5g00540_His_6 protein samples relative to Ku80 controls (data not shown).

It was hypothesised that pigments, lipid droplets, and polysaccharides present in the crude protein extracts could interfere with isoelectric focusing during SDS-PAGE (Kniemeyer et al. 2006) or antigen binding to the epitope tag. Consequently protein samples were precipitated using acetone. In an attempt to reduce background signal observed from Western blot experiments, his-tagged proteins from acetone precipitated samples were selectively bound using Ni-NTA agarose beads (Qiagen), washed 10 times to remove unbound proteins and eluted in 500 µl aliquots. SDS-PAGE showed some reduction of contaminating proteins in acetone precipitated and Ni-NTA purified samples relative to crude extracts (Figure 6.4C). However, Western blotting of the acetone precipitated and Ni-NTA enriched elutions at a range of sample concentrations (15, 30, 40 µg) demonstrated persistent non-specific signal and no enrichment at the expected mass relative to the Ku80 control throughout a time course of *in vitro* growth (Figure 6.4D and data not shown). Identical issues of background saturation were observed for NiNTA purified supernatant (data not shown). A number of possible explanations were considered for these observations: 1) washing steps did not sufficiently remove non-specific protein or Western blotting was not sensitive enough for Afu5g00540_His_6 detection; 2) Acetone precipitation and Ni-NTA agarose bead purification was insufficiently stringent, or eliminated the target protein; 3) the transcript was expressed but not translated; 4) the epitope tag had been cleaved from the protein or was blocked by tertiary structure or unknown post-translational modifications.

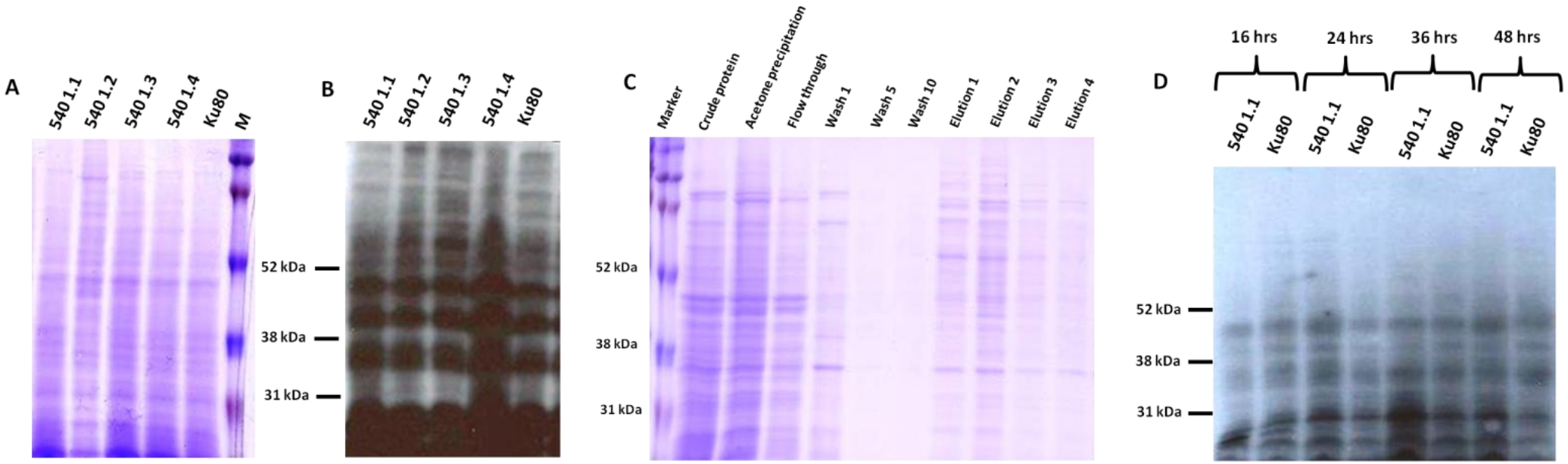


Figure 6.4- SDS-PAGE and Western blot analyses of crude and Ni-NTA purified *A. fumigatus* Afu5g00540_His$_6$ and Ku80 mycelial extracts. **A.** Crude protein extracts (40 µg) from 4 different transformants putatively expressing the Afu5g00540-His$_6$ allele and Ku80 control. Samples were grown in ACM for 16 hours before protein extraction. **B.** Western blotting of 40 µg total crude protein with an anti-his primary antibody targeting the Afu5g00540-His$_6$ epitope tag was saturated with background signal. **C.** Ni-NTA purification of crude protein from Afu5g00540-His$_6$ clone 1.1 from 14 hour growth in ACM. SDS-PAGE gel is representative of Ni-NTA enrichment for all experiments. Washing steps 1-10 removed unbound sample, as evidenced by the absence of protein observed in wash 10. Elutions showed no enrichment of a protein of the expected mass (34.7 kDa) relative to Ku80 controls (data not shown). **D.** Western blotting of 40 µg of Ni-NTA elutions from protein extracted following 16, 24, 36 and 48 hours of growth in ACM broth.

6.3.4 SELDI-Tof-MS analysis of *in vitro* protein

For SELDI-ToF-MS analysis of *in vitro* protein samples, Afu5g00540-His_6 and Ku80 strains were cultured in ACM and protein was extracted at 16 hours. Duplicate biological replicates were conducted. SELDI-ToF-MS performed in this study utilises the PG20 chip (Biorad, USA). PG20 chips contain 8 spots to which protein G is covalently attached. The anti-his antibody (GE Healthcare, UK) used in this study is an IgG2a monoclonal antibody which has high binding affinity to protein G (ProteinChip® Antibody Capture Kit Instruction Manual). 2 µl of 0.2 mg/ml anti-his antibody was immobilised to the PG20 array surface using the ProteinChip® Antibody Capture Kit (see Methods). 2 µl of crude and acetone precipitated/Ni-NTA purified protein samples were selectively bound to the anti-his antibody on the PG20 chips. Chips were analysed using a PBS II ProteinChip SELDI Reader (Ciphergen, USA). Spectra were baseline subtracted, and peaks with a signal to noise ratio above 3 were automatically annotated using Ciphergen Protein Chip® software.

The first biological replicate was analysed in triplicate. SELDI-ToF-MS spectra demonstrated a peak with an average molecular mass of 36946 Da from crude protein extracted from the Afu5g00540-His_6 strain (Figure 6.5A, 6.5B and 6.5C). These data suggest high levels of reproducibility between SELDI-ToF-MS technical replicates. No peak of the equivalent mass was observed in spectra from crude protein extracted from the Ku80 isolate (Figure 6.5D), or from Ni-NTA enriched samples from either strain (data not shown).

To limit the financial cost of preliminary experimentation, the second biological replicate was analysed by a single technical replicate. No peaks equating to proteins between 30 – 40 kDa were identified from Afu5g00540-His_6 or Ku80 crude protein samples (data not shown). However, a peak with a molecular mass of 37332 Da was detected in the acetone precipitated/Ni-NTA enriched protein from Afu5g00540-His_6 (Figure 6.5E). A peak of equivalent molecular mass was not detected from the Ku80 enriched protein (Figure 6.5F). In both biological replicates peaks of approximately the same molecular mass (average 37043 Da, standard deviation 237 Da) were identified in protein samples restricted to the Afu5g00540-His_6 strain. These data are inconsistent with respect to the effectiveness of acetone precipitation and Ni-NTA enrichment, which seemed to eliminate or enrich a putatively epitope tagged protein in the first and second biological replicates respectively. Based on *in silico* calculations, the molecular mass of Afu5g00540-His_6 epitope tagged FacC signalling protein is predicted to be 34762 Da. The average mass of the putative epitope tagged protein observed in SELDI-ToF-MS spectra was therefore 2281 Da greater than *in silico* predictions, possibly due to post-translational modifications. Recent proteomic profiling of the *A. fumigatus* secretome has demonstrated similar discrepancies in

predicted and observed molecular mass of *A. fumigatus* proteins (Kumar et al. 2011). It was therefore hypothesised that the peaks observed in spectra from Afu5g00540-His_6 protein represent detection of epitope tagged FacC signalling protein using SELDI-ToF-MS. *In vitro* detection of epitope tagged protein from independent biological replicates via antibody based capture and SELDI-ToF-MS validated the use of this approach as a detection tool in a murine model of infection.

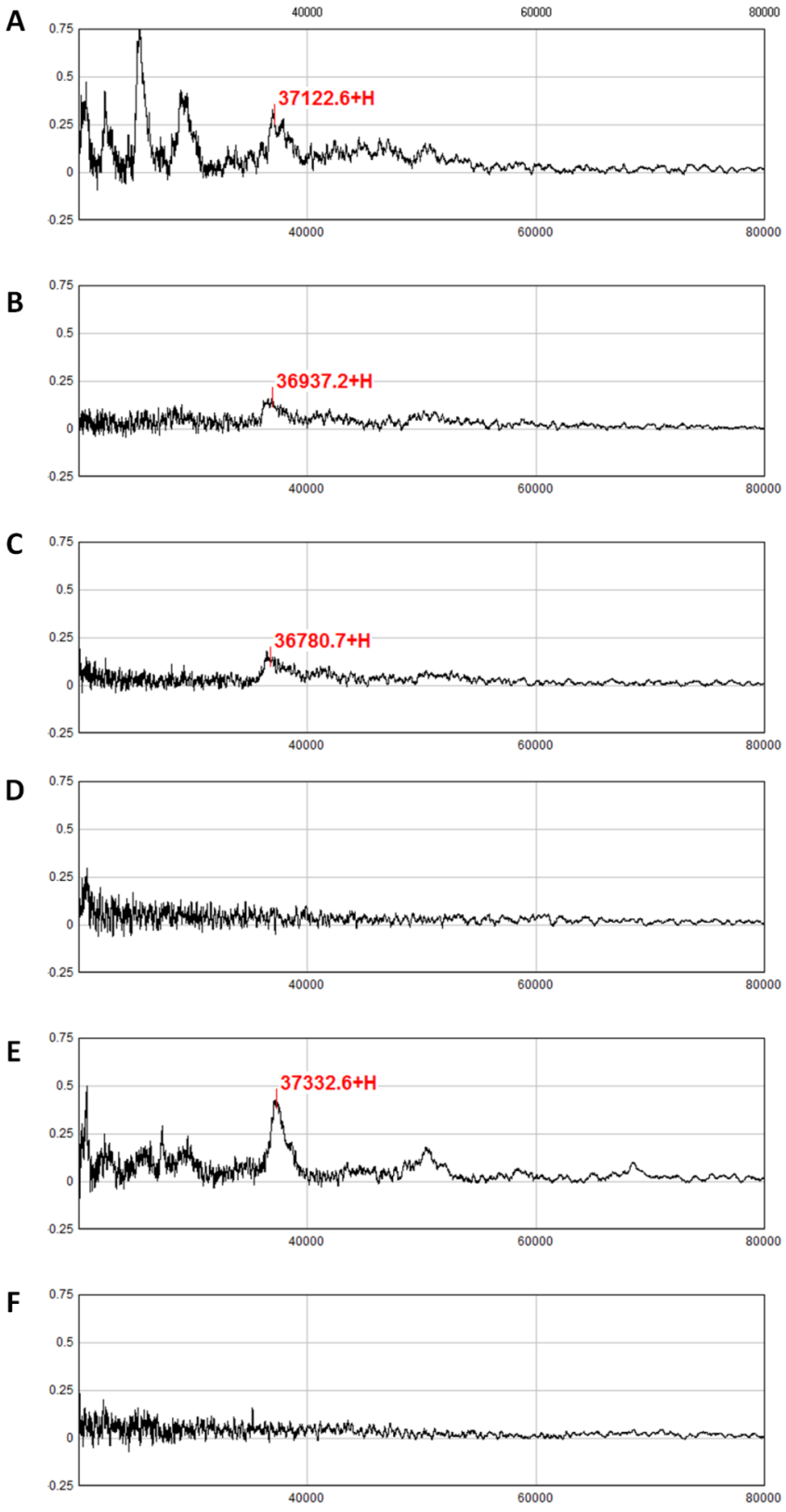


Figure 6.5: Spectra from SELDI-ToF-MS analyses of crude or acetone precipitated/Ni-NTA treated protein extracted from Afu5g00540-His$_6$ or Ku80 from 16 hours *in vitro* culture. Spectra from two biological replicates are shown. From the first biological replicate, peaks were observed at a molecular mass of approximately 36.9 kDa from triplicate SELDI-ToF-MS analyses of crude Afu5g00540-His$_6$ protein (A, B, C). No peak of equivalent mass was observed in triplicate spectra from Ku80 crude protein, an example of which is shown (D). In a second biological replicate, a peak was observed at a molecular mass of 37.3 kDa in acetone precipitated/Ni-NTA treated Afu5g00540-His$_6$ protein (E). No protein of equivalent mass was observed in acetone precipitated/Ni-NTA enriched Ku80 protein (F). Spectra scales show between 20000 – 80000 Da and peak intensity between -0.25 and 0.75.

6.3.5 SELDI-ToF-MS detection of minute quantities of polyhistidine-tagged bacterial protein diluted with murine BALF

In order to determine the minimum concentration of detectable poly-histidine tagged protein in murine BALF using SELDI-ToF-MS, two mice were infected with 1 x 10^8 CEA10 spores and BALF was extracted 14 hours post infection. BALF was pooled and spiked with decreasing concentrations of an N-terminally his-tagged recombinant *A. fumigatus* protein (Allergen Asp F4, Afu2g03830) which had been expressed and purified from *E. coli* culture. The predicted molecular mass of Afu2g03830 is 38.2 kDa. The threshold concentration for detection was 1 ng of epitope tagged protein per 1 µl BALF (Figure 6.6). Peaks at the minimum detectable concentration had an intensity of 0.4 (Figure 6.6C). The optimised SELDI-ToF-MS approach is therefore approximately 50 times more sensitive than Western blots using the same antibody, which have a detection limit of 100 ng according to the manufacturer's guidelines.

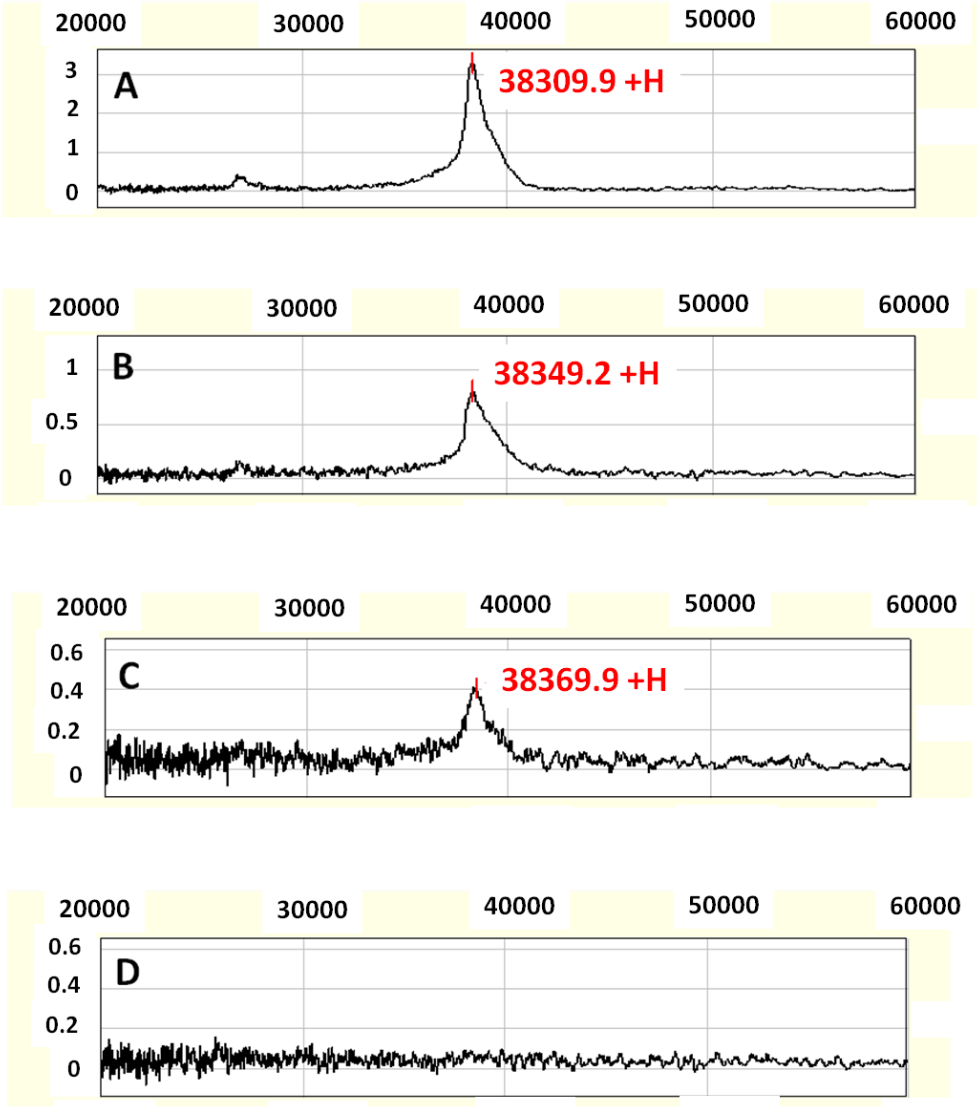


Figure 6.6: Spectra from SELDI-ToF-MS analyses of murine BAL fluid spiked with epitope tagged Afu2g03830. Mice were infected with 1 x 10^8 *A. fumigatus* Af293 and culled at 14 hours post infection and BALF was extracted. BALF were used to dilute recombinant his-tagged protein. A recombinant *A. fumigatus* protein (Afu2g03830) expressed and purified from bacterial culture was serially diluted in BALF. Afu2g03830 has a predicted molecular mass of 38.2 kDa and contains an N-terminal polyhistidine tag. Spectra from BALF containing 100 ng/µl (A), 10 ng/µl (B), 1 ng/µl (C) and 0.1 ng/µl (D) concentrations of Afu2g03830 are shown. A peak of 38.3 kDa was observed in spectra from concentrations equal to or above 1 ng/µl. No peak was observed at higher BALF dilutions (D).

6.3.6 Construction of a library of recombinant *A. fumigatus* clones expressing His-tagged candidate alleles

At this point, on the strength of pilot data and efficacy of SELDI-ToF-MS detections in BALF it was decided to proceed with a shotgun cloning experiment to address detection of several *A. fumigatus* proteins. Forty *A. fumigatus* alleles were selected for epitope tagging based on either transcriptional profiling described in Chapter 3 or increased transcript abundance in the murine

lung relative to laboratory culture (McDonagh et al. 2008). It was hypothesised that genes for which transcript abundance increased with greatest magnitude between 4 – 8 hours were most likely to direct protein biosynthesis during early murine infection. The majority of alleles (n = 35) for epitope tagging were therefore selected based on a high increase in expression between 4 – 8 hours post infection from a preliminary microarray dataset preceding the results presented in Chapter 3. Following comprehensive analyses of the microarray data using the non-ratiometric approach, 34 of the candidate genes demonstrated an increase in transcript abundance between these time points in the clinical isolate Af293. However, 7 and 4 genes demonstrated moderate or low increases respectively between 4 – 8 hours in the final datasets (Table 6.3). A single gene (Afu8g01050) failed quality control in non-ratiometric analyses presented in Chapter 3. An additional 5 genes were chosen for epitope tagging based on high induction in the murine lung relative to developmentally matched laboratory culture (Table 6.3, McDonagh et al. 2008). Additionally, it was hypothesised that genes encoding putative signal peptides were most likely to be secreted into murine BALF. Accordingly, twenty alleles chosen for epitope tagging contained a putative signal peptide and lacked a putative GPI anchor. Temporal gene expression profiles between 4, 8 and 14 hours in the murine lung for the 40 alleles selected for epitope tagging are given in Table 6.3.

Table 6.3: **Stage specific gene expression profiles during initiation of infection for 40 genes selected for epitope tagging.** Expression ranks based on non-ratiometric analyses (Chapter 3) are given for Af293 based on the position of each gene in the 4 – 8 and 8 – 14 hours increasing (red) and decreasing (green) datasets. A one-way ANOVA was conducted on nSI values between time points, with the null hypothesis that nSI values do not change between time points. FDR correct *p*-values from this analysis are reported for each gene. Genes highlighted in bold were chosen due to high expression in the host niche relative to laboratory culture (McDonagh et al. 2008).

ORF	Description	4 vs 8 hours			8 vs 14 hours			Epitope tagged allele transformed into *A. fumigatus*	Signal peptide
		Rank	Change magnitude	FDR *p* value	Rank	Change magnitude	FDR *p* value		
Afu6g00290	aminotransferase, putative	24	Up high	0.005	317	Up high	0.314	✓	×
Afu5g14660	GABA permease, putative	275	Up high	0.076	374	Up high	0.503	×	×
Afu8g06560	DUF895 domain membrane protein	360	Up high	0.008	334	Up high	0.031	×	×
Afu7g00580	conserved hypothetical protein	372	Up high	0.019	572	Up high	0.141	×	✓
Afu2g17330	serine peptidase, family S28, putative	14	Up high	0.012	757	Up moderate	0.753	×	✓
Afu1g14550	Mn superoxide dismutase MnSOD	230	Up high	0.026	947	Up moderate	0.325	✓	×
Afu1g17180	pyridine nucleotide-disulphide oxidoreductase, putative	602	Up high	0.145	1212	Up moderate	0.857	✓	×
Afu1g12350	extracellular fruiting body protein, putative	151	Up high	0.037	1637	Up low	0.871	✓	✓
Afu3g01500	integral membrane protein	22	Up high	0.033	NA	No change	0.983	×	×
Afu2g12680	conserved hypothetical protein	33	Up high	0.018	NA	No change	0.938	×	✓
Afu5g01620	extracellular proline-rich protein	55	Up high	0.004	NA	No change	0.925	✓	✓
Afu2g17320	conserved hypothetical protein	58	Up high	0.005	NA	No change	0.959	×	×
Afu4g11800	alkaline serine protease Alp1	67	Up high	0.007	NA	No change	0.936	✓	✓
Afu8g07080	elastinolytic metalloproteinase Mep	103	Up high	0.001	NA	No change	0.72	×	✓
Afu2g10130	phase-specific adhesin, putative	116	Up high	0.068	NA	No change	1	✓	✓
Afu5g10270	heat shock protein, HSP20 family	113	Up high	0.115	NA	No change	0.985	✓	×
Afu1g17190	long-chain-fatty-acid-CoA ligase, putative	443	Up high	0.181	NA	No change	0.976	✓	×
Afu3g03060	cell wall protein (PhiA), putative	115	Up high	0.011	1454	Down low	0.442	✓	✓
Afu8g00610	cell surface protein Mas1, putative	1	Up high	0.021	952	Down moderate	0.869	×	✓
Afu7g06750	phosphoglycerate mutase family protein, putative	76	Up high	0.021	1184	Down moderate	0.733	✓	✓
Afu5g01200	carboxypeptidase S1, putative	9	Up high	0.005	16	Down high	0.152	×	✓
Afu2g12630	allergen Asp F13	150	Up high	0.053	63	Down high	0.389	✓	✓
Afu4g00390	glycosyl hydrolase, putative	152	Up high	0.093	164	Down high	0.821	×	✓

Afu8g05610	cell wall glucanase (Scw11), putative	724	Up moderate	0.082	771	Up moderate	0.369	×	×
Afu4g09580	major allergen Asp F2	852	Up moderate	0.169	1444	Up low	0.86	✓	✓
Afu3g10960	cell wall protein, putative	1137	Up moderate	0.044	1332	Up low	0.605	×	✓
Afu4g06640	acid sphingomyelinase	838	Up moderate	0.038	NA	No change	0.918	×	✓
Afu3g14170	high-affinity hexose transporter	950	Up moderate	0.354	NA	No change	0.982	✓	×
Afu7g01040	cytidine deaminase, putative	997	Up moderate	0.296	NA	No change	0.979	×	×
Afu5g01910	aldo-keto reductase (AKR), putative	1115	Up moderate	0.001	NA	No change	0.994	×	×
Afu8g05600	hypothetical protein	1536	Up low	0.307	1686	Up low	0.911	✓	×
Afu5g01990	BYS1 domain protein, putative	1468	Up low	0.193	NA	No change	0.933	✓	✓
Afu6g05030	polysaccharide deacetylase family protein	1589	Up low	0.191	NA	No change	0.974	✓	×
Afu8g01110	integral membrane protein, putative	1384	Up low	0.194	273	Down high	0.409	✓	×
Afu8g04380	conserved hypothetical protein	NA	No change	0.079	1959	Up low	0.671	✓	×
Afu7g06380	maltase	NA	No change	0.823	979	Down moderate	0.624	✓	×
Afu3g14030	alkaline phosphatase	91	Down high	0.317	702	Up moderate	0.262	✓	✓
Afu8g01130	alpha-galactosidase C	483	Down high	0.198	NA	No change	0.902	✓	×
Afu6g02980	extracellular exo-polygalacturonase, putative	90	Down high	0.164	4	Down high	0.277	✓	✓

Epitope tagging of *A. fumigatus* alleles using the biselectable marker approach is labour intensive with regard to cloning as two linear constructs are required for each target allele (Figure 6.1). Consequently, the biselectable marker strategy is not amenable to constructing a library of epitope tagged alleles. In parallel to epitope tagging *A. fumigatus* genes using the split marker approach, work conducted by our collaborator Hwen Yee Chea optimised epitope tagging and SELDI-ToF-MS recombinant protein detection using pSK379 (data not shown). This strategy requires less cloning steps, as a single plasmid is required for *A. fumigatus* transformation (Figure 6.7). Therefore, to construct a library of *A. fumigatus* clones expressing his-tagged alleles, the plasmid pSK379 was utilised (Figure 6.7). pSK379 contains the *his2A* sequence, which drives targeted insertion of pSK379 into the *A. fumigatus* genome (Figure 6.8). A pyrithiamine resistance cassette facilitates selection in *A. fumigatus.* Additionally, for selection in bacterial cells, the plasmid carries an ampiciliin resistance cassette (Figure 6.7).

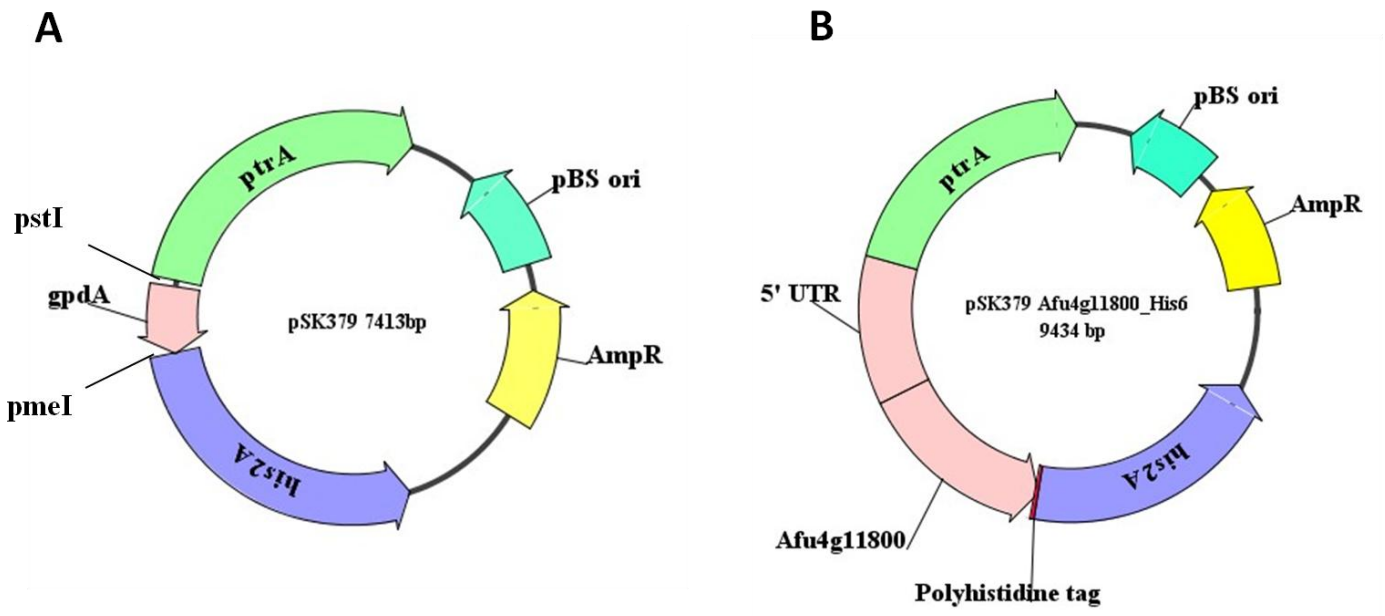


Figure 6.7: Plasmid maps of pSK379 and an exemplar epitope tag vector (pSK379 Afu4g11800_His6). (A) Plasmid pSK379 contains a pyrithiamine resistance cassette. The *his2A* sequence facilitates recombination of the plasmid into an intergenic region of the recipient strain genome. (B) Map of Plasmid pSK379 Afu4g11800_His6 as an exemplar *A. fumigatus* epitope tag transformation vector. The *gpdA* promoter was removed prior to blunt end ligation of the target allele PCR product by restriction digest using pmeI and pstI. The polyhistidine tag is encoded immediately before the Afu4g11800 gene stop codon. Approximately 1000 bp of 5' UTR was cloned to maintain the native promoter region.

For each allele, primers Afu*X*_F and Afu*X*_R (where *X* denotes a specific ORF) were designed to amplify 1000 bp of 5' UTR containing the putative promoter sequence, and the entire coding sequence of the gene with a polyhistidine tag encoded in the reverse primer immediately before the stop codon (Figure 6.7). Primer sequences are given in Table 6.1. To generate epitope tag vectors (Figure 6.7), the *gpdA* promoter was excised from plasmid pSK379 using PmeI and PstI restriction digestion. PCR fragments containing the epitope tagged allele and 1000 bp promoter sequence were blunt end ligated into linearised pSK379, and the ligation mixture transformed into Xl-10 *E. coli*. Ligation of the PCR fragment into pSK379 was confirmed by colony PCR using primers Afu*X*_F and Afu*X*_R and putative *E. coli* transformants as template. Forward orientation of the PCR fragment into pSK379 was confirmed using restriction digest mapping.

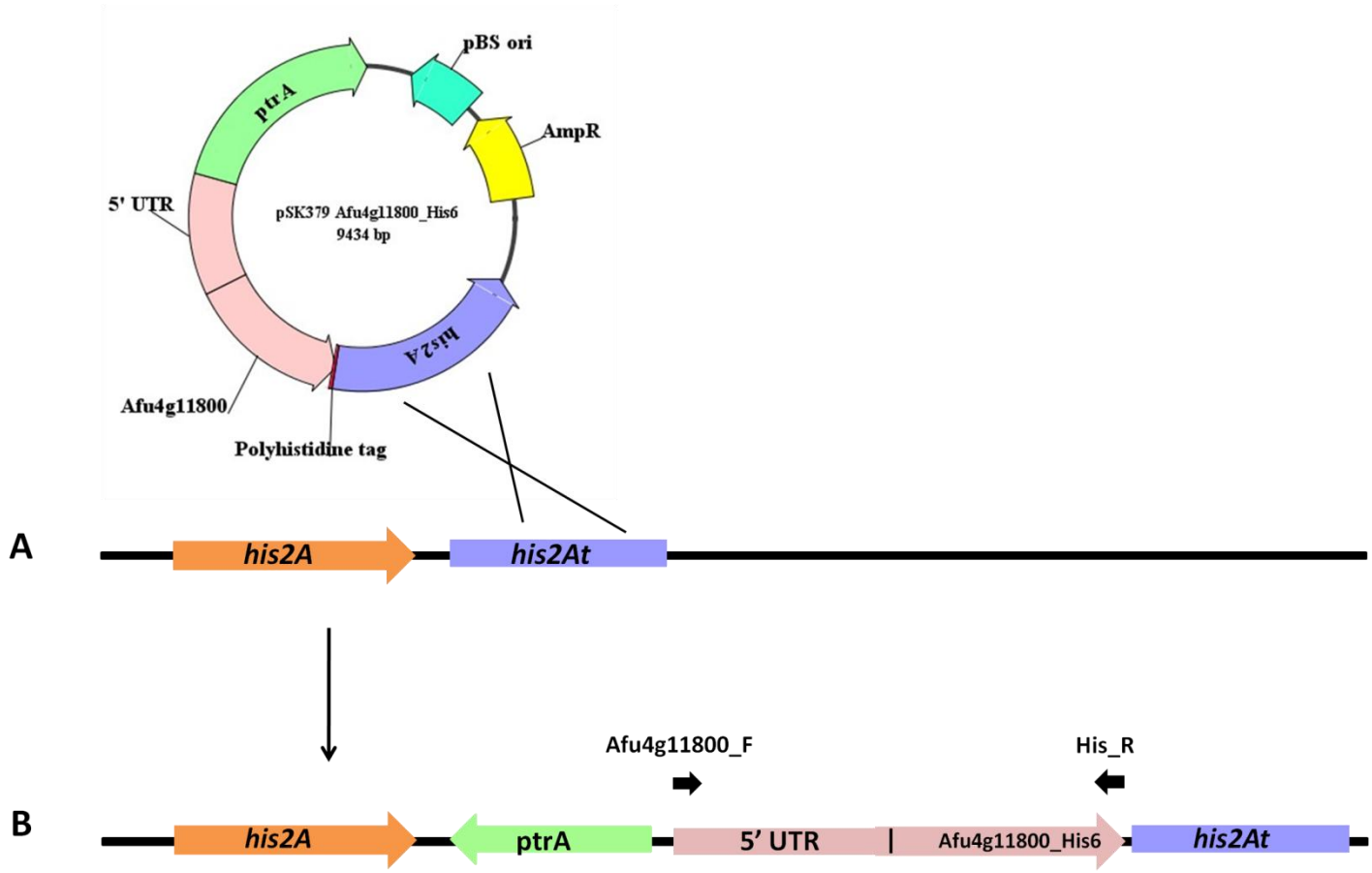


Figure 6.8: Schematic depicting a homologous recombination event between an exemplar epitope tag vector (pSK379 Afu4g11800_His6) and the *A. fumigatus* genome. Epitope tag vectors target the histone 2A locus of the *A. fumigatus* genome. A black cross depicts a single homologous recombination event between the *his2A* sequence in pSK379 and the *his2A* intergenic region of the recipient strain genome (A). Following integration, transformants contain an ectopic copy of the polyhistidine epitope tagged allele and native promoter region (B). Locations of forward (Afu4g11800_F) and reverse (His_R) primers used to confirm homologous recombination are shown. The His_R reverse primer hybridises to 21 bp of the polyhistidine tag and the gene stop codon which is common to all of the constructed epitope tagged alleles (Table 6.1).

For *A. fumigatus* transformation, 3 µg of epitope tag transformation vector was extracted from *E. coli* culture and resuspended in 10 – 20 µl of sterile water. *A. fumigatus* Ku80 transformation was conducted using protoplasts, based on a method described by Szewczyk and co-workers (Szewczyk et al. 2006). Putative transformants were subcultured on AMM supplemented with 500 mg pyrithiamine and gDNA was extracted from spores. Presence of the recombinant allele in the recipient genome was demonstrated by PCR using primers Afu*X*_F and His_R (Figure 6.9) with transformant or Ku80 gDNA as template. Homologous recombination of the cassette with the genome was demonstrated by amplification of a PCR product of the expected size which was restricted to reactions using transformant gDNA as template (Figure 6.9). Using these methods, 24 alleles putatively expressing an epitope tag were transformed into the *A. fumigatus* Ku80 strain (Table 4 and Figure 6.9).

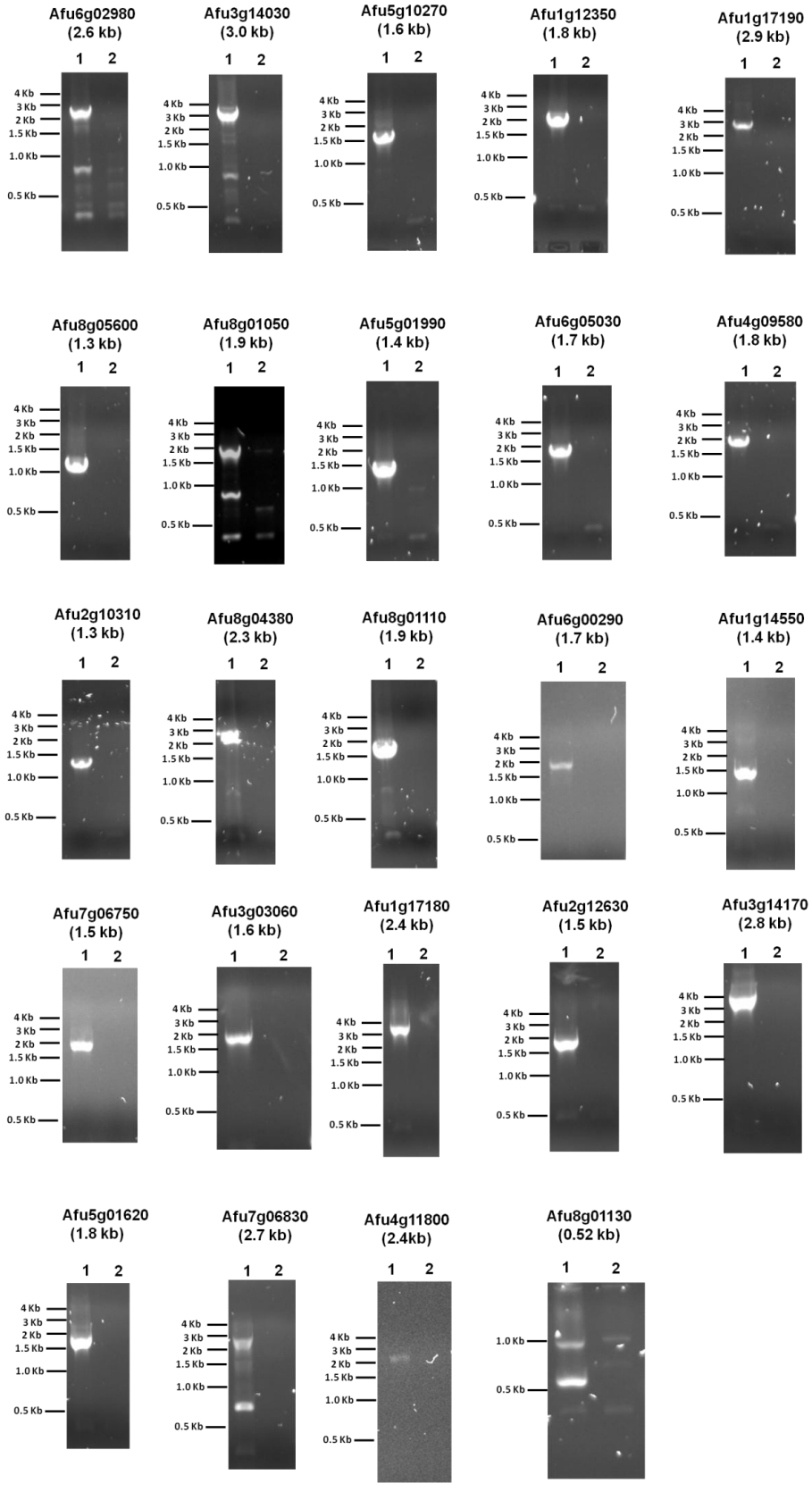


Figure 6.9: Gel electrophoresis of PCR reactions using primers Afu*X*_F and His_R, with transformant or Ku80 gDNA as template. Lanes 1 and 2 show PCRs using transformant or Ku80 gDNA as template respectively. The allele putatively tagged in each transformant strain is shown above the gel. The predicted size of the PCR product from recombinant *A. fumigatus* strains is shown in parentheses. Recombination of the epitope tag vector with the recipient genome is demonstrated by PCR amplification of a product of the predicted size which is restricted to reactions using the transformant gDNA as template.

6.3.7 Putative SELDI-ToF-MS detection of epitope tagged proteins in BALF from mice infected with a library of *A. fumigatus*_His_6 strains

Multiple factors such as short protein half life, low protein concentration or post translational modifications make detection of pathogen protein in the host extremely challenging. It was therefore hypothesised that from infections using twenty four *A. fumigatus*_His_6 strains, only a subset of epitope tagged proteins would be detected in murine BALF. In order to rapidly and efficiently identify epitope tagged proteins which were detectable in the host, two groups of mice were infected with a library of *A. fumigatus*_His_6 strains. It was hypothesised that proteins detected by SELDI-ToF-MS could be identified by matching spectral peaks to the predicted molecular mass of epitope tagged proteins.

Two groups of five mice were infected with mixed inocula of 11 or 12 *A. fumigatus* strains putatively expressing an epitope tagged protein of interest (Table 6.4). Strains were allocated into each group (named A or B) in order to maximise differences between the predicted molecular mass of protein candidates (Table 6.4). For a putative positive control, 5 mice were infected with the *A. fumigatus* strain expressing the Afu4g11800 epitope tagged allele. Afu4g11800 directs the biosynthesis of the alkaline serine protease Alp1. Antibodies specific to this protein are present in *A. fumigatus* infected human sera and lung as determined by an antibody specific enzymatic immunoassay and immunofluorescence assay respectively (Reichard et al. 1990). For a negative control strain lacking an epitope tagged allele, 5 mice were inoculated with *A. fumigatus* Ku80.

In order to maximise the chances of protein detection from infected murine BALF, careful consideration was given to choice of infection model, time-points and sample treatment. It was hypothesised that maximising the burden of *A. fumigatus* in the lung would increase the concentration of putative epitope tagged proteins, and therefore improve the chance of detection. Therefore a high dose infection model was employed in which neutropenic mice were infected with 1×10^8 *A. fumigatus* spores. Mice were culled and BALF extracted at 4 and 18 hours post infection. SELDI-ToF-MS detection of a putative biomarker at these early stages may enable the development of more timely diagnostics for *A. fumigatus* infection. Additionally, defining proteins present in BALF at either 4 or 18 hours post infection may facilitate the differentiation between normal carriage of *A. fumigatus* spores in the lung and an invasive infection. Finally, the 18 hour stage was chosen over earlier invasive time points (e.g. 14 hours) to maximise the infectious burden and possibly the concentration of *A. fumigatus* proteins. Time points later than 18 hours were not considered for ethical reasons.

BALF samples from mice infected with group A, group B, Afu4g11800_His_6, or Ku80 were pooled and then aliquoted for several treatments designed to address challenges to protein detection from the murine host. Firstly, pathogen protein concentration is likely to be very low in BALFs. Accordingly, aliquots of murine BALF were concentrated by a factor of 5 by lyophilisation. To enrich polyhistidine tagged proteins, 300 µl BALF were selectively bound using Ni-NTA agarose beads (Qiagen), washed 10 times to remove unbound proteins and eluted in 100 µl aliquots. To remove polysaccharide, pigment, lipid or salt contaminants, aliquots of BALFs were precipitated in acetone and resuspended in PBS. Finally, host samples may contain a high abundance of protein which may physically prevent antigen binding to the epitope tag. Therefore, aliquots of murine BALF were treated using using Proteoprep Immunoaffinity Albumin and IgG Depletion Kit (Sigma, UK).

2 µl of untreated and treated BALF were selectively bound on PG20 chips with an anti-his anti body and analysed by SELDI-ToF-MS. BALF treatment and SELDI-ToF-MS for infection groups A, B and saline inoculated negative control were technically replicated. Spectra were baseline subtracted, and peaks with a signal to noise ratio above 3 were automatically annotated using Ciphergen Protein Chip® software.

Confidence in a peak representing detection of an epitope tagged protein was increased when it passed the following criteria; 1) the molecular mass of the peak was restricted to the epitope tagged infection groups and absent from the Ku80 control; 2) the intensity of the peak was greater than or equal to 0.4, which was the intensity reported by detection of 1 ng of recombinant bacterial protein in murine BALF; 3) the peak was observed in more than one treatment regime; 4) the peak was observed in two technical replicates; 5) the molecular mass of the peak approximated the predicted mass of one of the putative epitope tagged proteins.

Strain group or control	Strain	Epitope tagged allele description	Predicted protein size (kDa)
A	Afu8g05600_His_6	hypothetical protein	9.2
	Afu2g10130_His_6	phase-specific adhesin, putative	12.7
	Afu2g12630_His_6	allergen Asp F13	15.9
	Afu7g06750_His_6	phosphoglycerate mutase family protein, putative	20.7
	Afu5g10270_His_6	heat shock protein, HSP20 family	23.0
	Afu8g01110_His_6	integral membrane protein, putative	32.7
	Afu1g12350_His_6	extracellular fruiting body protein, putative	33.8
	Afu8g04380_His_6	conserved hypothetical protein	44.5
	Afu1g17180_His_6	pyridine nucleotide-disulphide oxidoreductase, putative	46.2
	Afu7g06380_His_6	Maltase	67.5
	Afu3g14030_His_6	alkaline phosphatase	72.5
B	Afu5g01990_His_6	BYS1 domain protein, putative	16.0
	Afu3g03060_His_6	cell wall protein (PhiA), putative	19.4
	Afu1g14550_His_6	Mn superoxide dismutase MnSOD	23.3
	Afu5g01620_His_6	extracellular proline-rich protein	28.3
	Afu4g09580_His_6	major allergen Asp F2	32.2
	Afu6g05030_His_6	polysaccharide deacetylase family protein	35.3
	Afu8g01050_His_6	Lipase	35.6
	Afu6g00290_His_6	aminotransferase, putative	38.2
	Afu6g02980_His_6	extracellular exo-polygalacturonase, putative	48.4
	Afu3g14170_His_6	high-affinity hexose transporter	57.6
	Afu1g17190_His_6	long-chain-fatty-acid-CoA ligase, putative	64.8
	Afu8g01130_His_6	alpha-galactosidase C	80.8
Positive control	Afu4g11800_His_6	alkaline serine protease Alp1	42.2
Negative control	Ku80	None	N/A

Table 6.4: Grouping of *A. fumigatus* strains putatively expressing an epitope tag in two libraries for murine infection. Strains were allocated into group A or B to maximise the difference in predicted molecular mass of the epitope tagged proteins.

Peaks observed in spectra between 0 – 20000 kDa were detected with intensities between 2 and 15 (Figure 6.10). Spectra were highly comparable between treatments, infection cohorts, technical replicates and time points (Figure 6.10 and data not shown). No peaks representing putative detection of epitope tagged proteins were observed between 0 – 20000 kDa (data not shown).

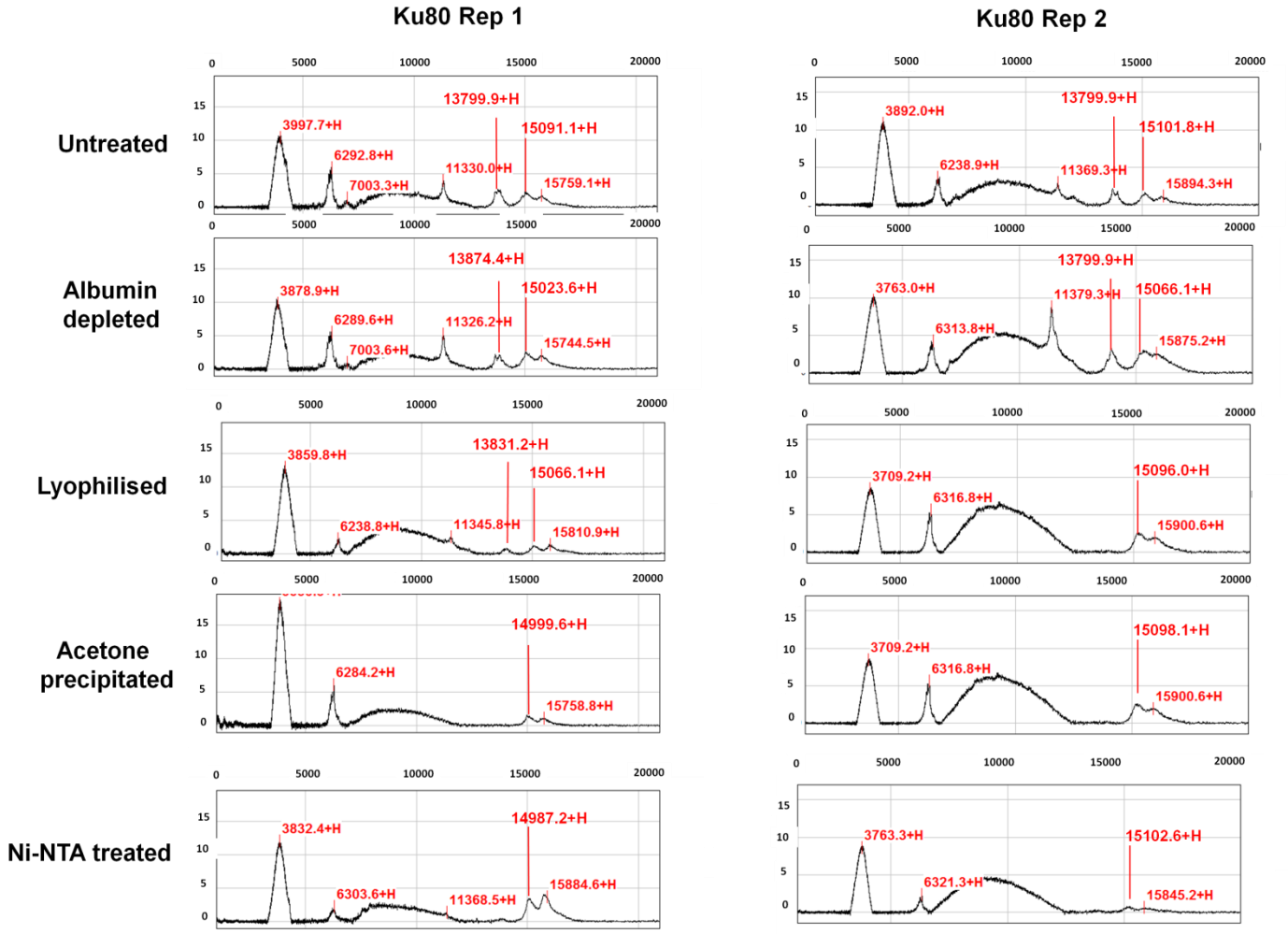


Figure 6.10: Spectra between 0 – 20 kDa from SELDI-ToF-MS analysis of Ku80 infected murine BALF extracted 4 hours post infection. Untreated and treated samples are shown from two technical replicates. These data are representative examples of 0 – 20 kDa spectra from all murine BALF samples.

Peaks observed in spectra between 20 and 100 kDa were detected with intensities below 0.4 (Figures 6.10 and 6.11). The 1 ng/µl detection limit of epitope tagged bacterial protein in murine BALF (Figure 6.4) reported a peak with an intensity of 0.4. Therefore, intensities for the majority of peaks observed in murine BALF from *A. fumigatus* infected cohorts were below the previously determined detection threshold.

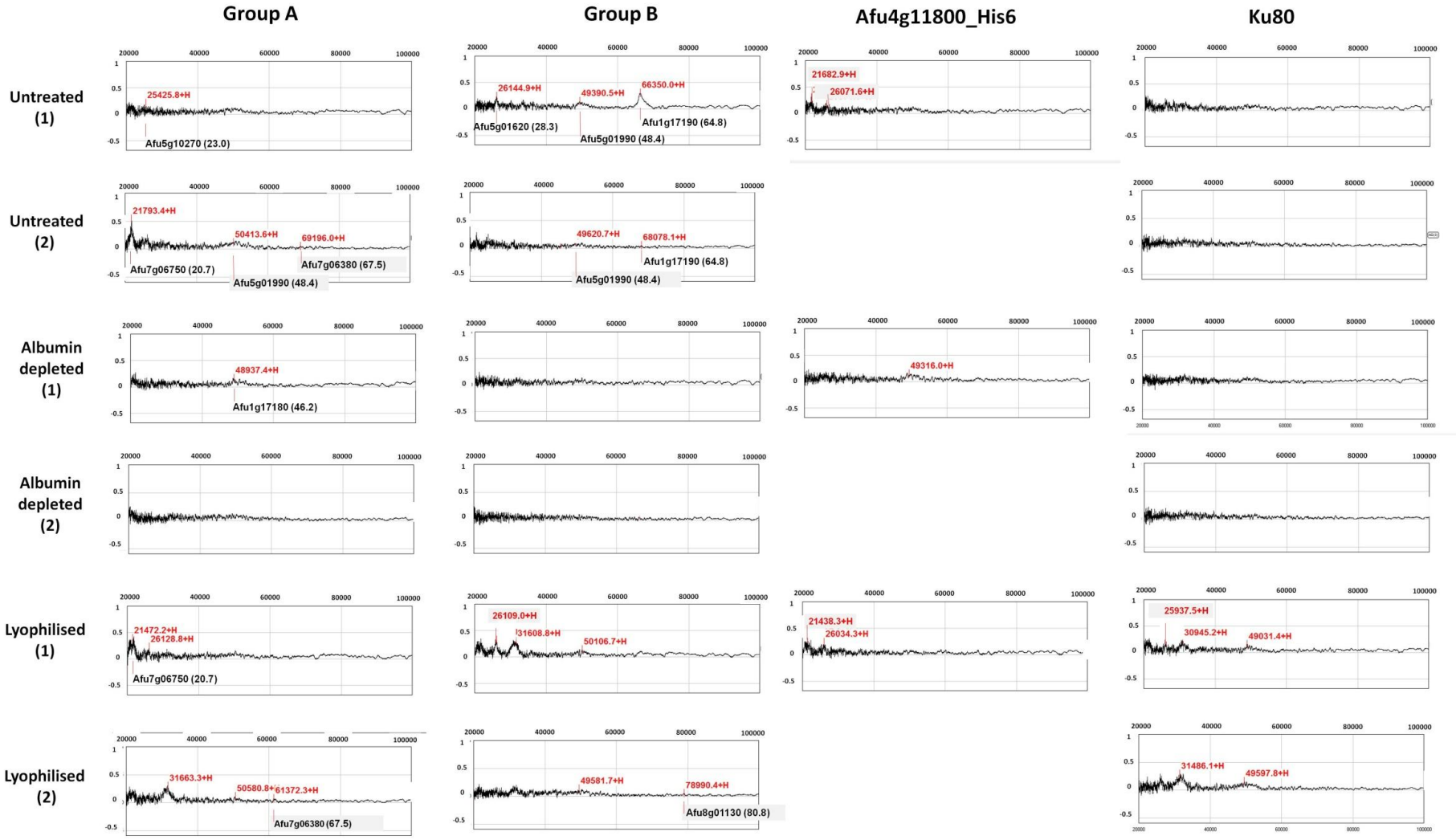
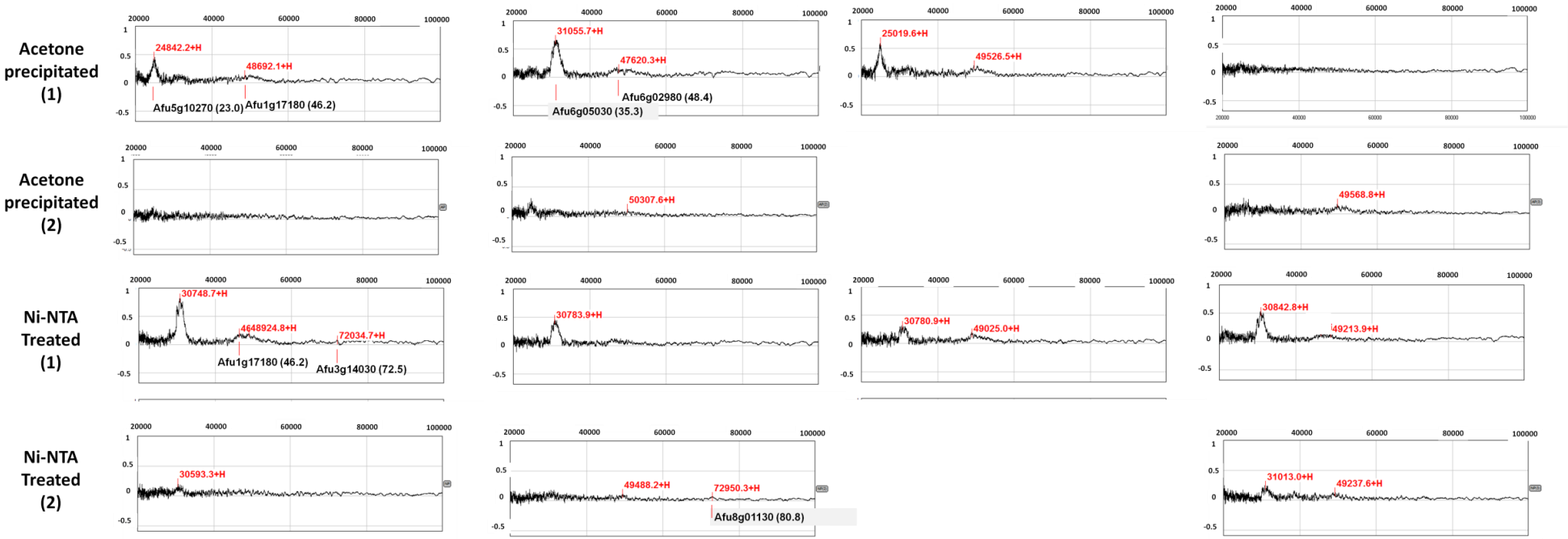


Figure 6.11: Spectra from SELDI-ToF-MS analyses of library or control infected murine BALF extracted 4 hrs post infection. Mice were infected with inocula of either mixed *A. fumigatus*_His_6 (groups A or B) or positive control (Afu4g11800_His_6) or Ku80 strain. Spectra from untreated, albumin depleated, lyopholised, acetone precipitated or Ni-NTA agarose treated BALF are shown. Numbers 1 and 2 in parentheses below treatment description refer to technical replicate number. Peaks with a signal to noise ratio greater than or equal to 3 are signified by a red line, and molecular mass indicated in red text (kDa). Peaks identified in group A or B which are not observed in the comparable Ku80 control spectra were assigned the ORF number of the putative epitope tagged protein which was closest to the peak molecular mass (black text beneath spectra trace). Shown in parentheses is the predicted molcular mass of the assigned protein (kDa). Spectra scales show between 20000 – 100000 Da and peak intensity between 1 and -0.5.

Figure 6.11 continued



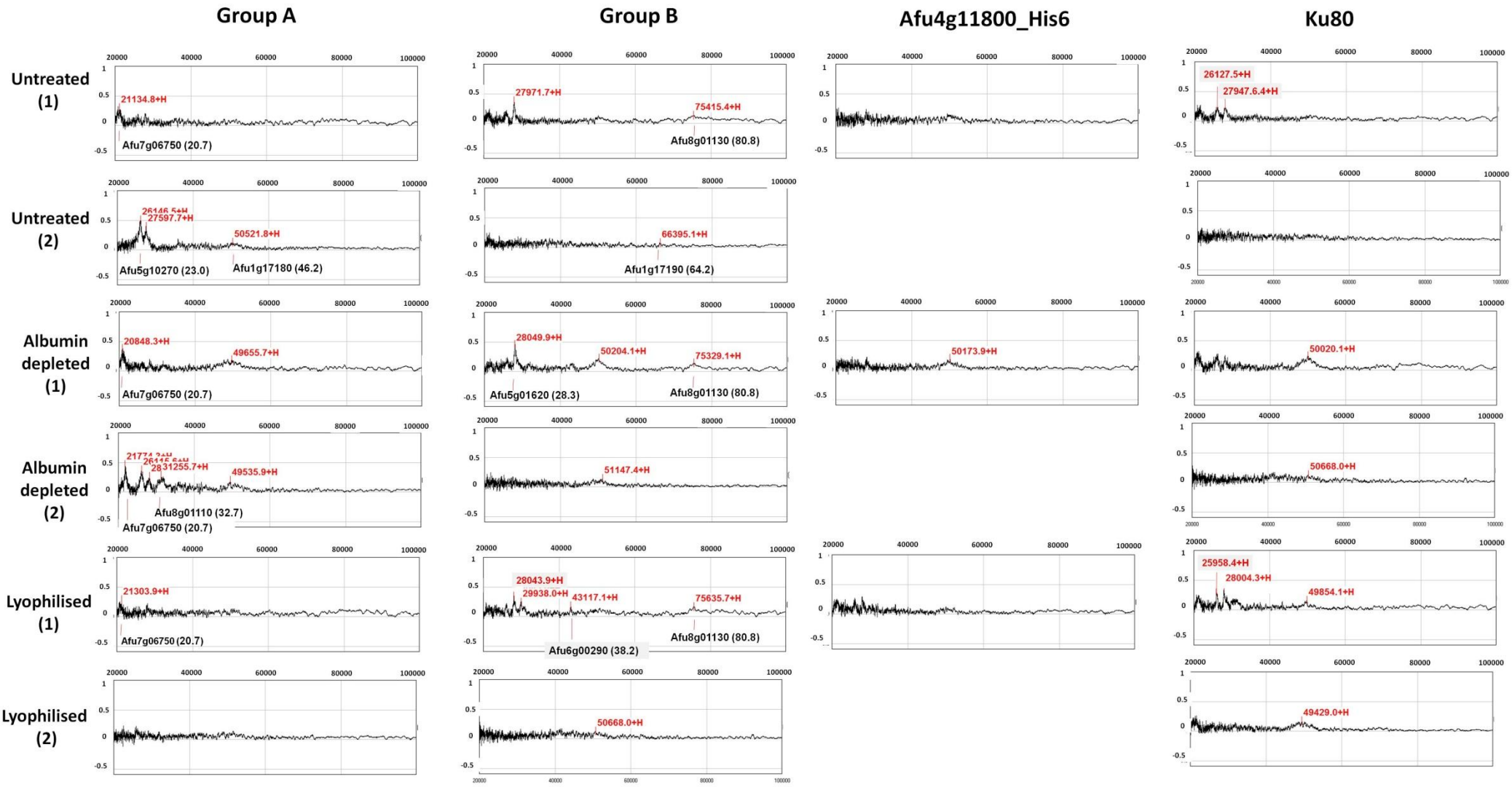
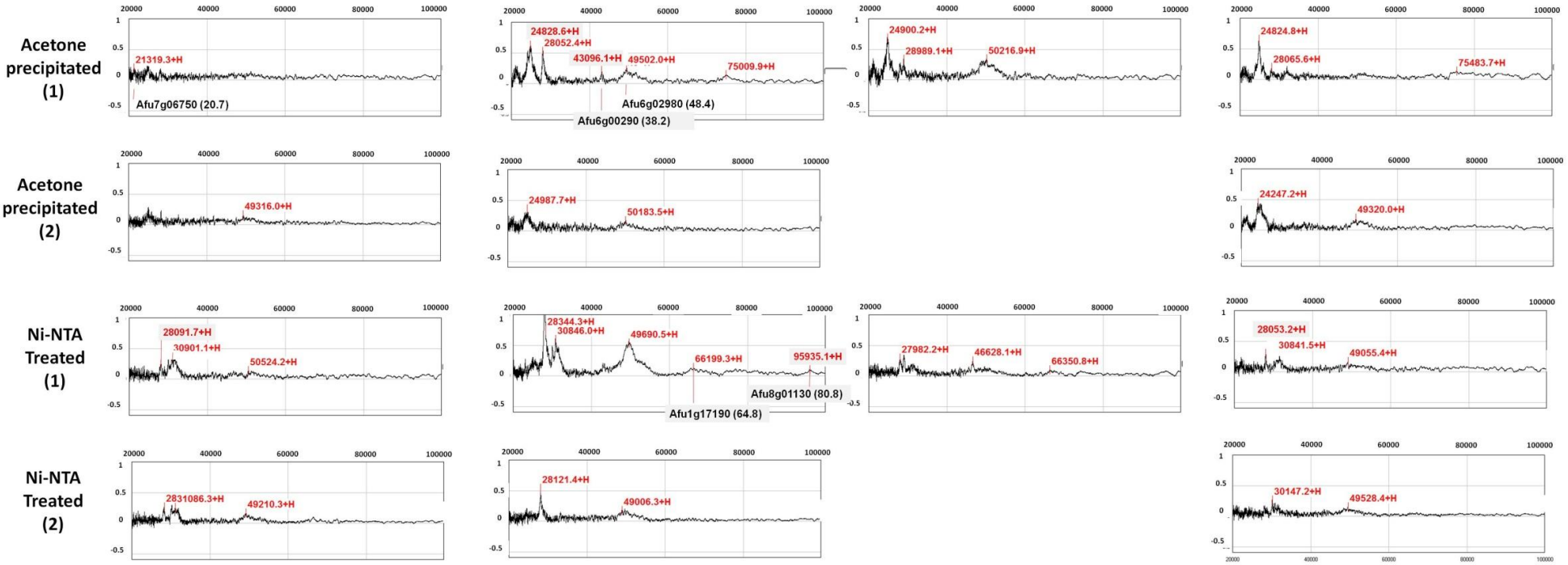


Figure 6.12: Spectra from SELDI-ToF-MS analyses of library or control infected murine BALF extracted 18 hrs post infection. Groups of mice were infected with inocula of either mixed *A. fumigatus*_His_6 (groups A or B) or positive control (Afu4g11800_His_6) or Ku80 strain. Spectra from untreated, albumin depleated, lyopholised, acetone precipitated or Ni-NTA agarose treated BALF are shown. Numbers 1 and 2 in parentheses below treatment description refer to technical replicate number. Peaks with a signal to noise ratio greater than or equal to 3 are signified by a red line, and molecular mass indicated in red text (kDa). Peaks identified in group A or B which are not observed in the comparable Ku80 control spectra were assigned the ORF number of the putative epitope tagged protein which was closest to the peak molecular mass (black text beneath spectra trace). Shown in parentheses is the predicted molcular mass of the assigned protein (kDa). Spectra scales show between 20000 – 100000 Da and peak intensity between 1 and -0.5.

Figure 6.12 continued



Albumin depletion, lyophilisation, acetone precipitation and Ni-NTA enrichment did not significantly increase either peak intensity or abundance (Figure 6.11 and 6.12). However, a slight trend was noticeable towards greater peak intensity in lyophilised, acetone precipitated and Ni-NTA enriched BALF. Ku80 infected BALF was used as a negative control to define *A. fumigatus* infected protein profiles in the absence of epitope tagged protein.

Spectra from BALF infected with the putative positive control expressing the epitope tagged alkaline serine protease *alp*1 allele did not show a peak of the expected 42.2 kDa size in any sample at either 4 or 18 hours. The most notable peak had a molecular mass of 46.6 kDa in the Ni-NTA enriched sample 18 hours post infection (Figure 6.12). A peak of this mass was absent from all Ku80 spectra. However, due to the discrepancy between the peak molecular mass and the predicted molecular mass of Alp1, and the absence of this peak in other positive control spectra, it was hypothesised that this peak did not demonstrate detection of epitope tagged Alp1 protein in BALF.

Accordingly, technical reproduction of SELDI-ToF-MS was only conducted with Ku80, group A and group B infected BALF. In contrast to the high levels of reproducibility using SELDI-ToF-MS reported by other authors (Diamond et al. 2001, Levels et al. 2007) and between spectra at lower molecular weights (Figure 6.9), peaks observed between 20 and 100 kDa demonstrate very poor concordance between technical replicates (Figures 6.11 and 6.12). For example, the spectrum from untreated 18 hour BALF from infection group A showed a single peak with a signal to noise ratio above 3 at 21.1 kDa in the first replicate. In the second technical replicate, no peak of 21.1 kDa was observed. Additionally, three peaks with a signal to noise ratio above 3 were observed with molecular masses of 26.1, 27.5 and 50.2 kDa (Figure 6.11).

It is difficult to explain the lack of concordance between replicates. Positive controls using 100 ng of recombinant histidine tagged bacterial protein (molecular mass 38.2 kDa) were conducted on each PG20 chip. These controls showed high reproducibility with regard to both peak molecular mass and intensity (data not shown). It is possible that variation in BALF protein profiles was introduced during technical replication of acetone precipitation, lyophilisation, albumin depletion or Ni-NTA treatments. However, low concordance between spectra from technically replicated, untreated BALF suggests that poor reproducibility is not due to these treatments. One possible explanation is that there was a degree of sample degradation during the 7 day storage period between technical replication. Consequently, during subsequent experiments BALF extraction, treatments and SELDI-ToF-MS were completed within 72 hours.

Notwithstanding poor technical reproduction, putative peaks which may represent the detection of epitope tagged *A. fumigatus* proteins were identified from these data (Figures 6.11, 6.12 and Table 6.5). A peak with a molecular mass of approximately 21 kDa was observed in seven (out of a total of twenty) spectra from group A infected BALF (Table 6.5). This peak was observed in two treatments from BALF extracted at 4 hours, and four treatments from BALF extracted at 18 hours post infection. A peak of equivalent molecular mass with a signal to noise ratio above 3 was not observed in any Ku80, or group B infected BALF sample. The molecular mass of the 21 kDa peak observed in group A spectra approximate the predicted molecular mass of the putatively epitope tagged phosphoglycerate mutase family protein (Afu7g06750, molecular mass 20.7 kDa) from the group A infection library. Interestingly this gene encodes a putative signal peptide, and gene expression profiling showed high transcript increase between 4 – 8 hours post infection (Table 6.3). Additionally, these data suggest a degree of replication is achievable using this assay.

			Group A infected BALF		**Ku80 Infected BALF**		
Time point	**Treatment**	**Replicate**	**Mass of peak (kDa)**	**Peak intensity**	**Mass of peak (kDa)**	**Peak intensity**	**Putative protein detected**
4 hrs	Untreated	2	21793.4	0.5	×	×	Epitope tagged Afu7g06750
	Lyophilised	1	21472.2	0.5	×	×	
18 hrs	Untreated	1	21134.8	0.4	×	×	
	Albumin depleted	1	20848.3	0.5	×	×	
	Albumin depleted	2	21774.3	0.5	×	×	
	Lyophilised	1	21303.9	0.3	×	×	
	Acetone precipitated	1	21319.3	0.2	×	×	
			Group B infected BALF		**Ku80 Infected BALF**		
4 hrs	Untreated	1	66350.0	0.3	×	×	Murine albumin
18 hrs	Untreated	1	66359.1	0.1	×	×	
18 hrs	Untreated	1	75415.4	0.2	×	×	Unknown host protein
	Albumin depleted	1	75329.1	0.2	×	×	
	Lyophilised	1	75635.7	0.2	×	×	
	Acetone precipitated	1	75009.9	0.2	75483.7	0.2	
18hrs	Untreated	1	27971.7	0.4	27947.6	0.3	Epitope tagged Afu5g01620
	Albumin depleted	1	28049.9	0.5	×	×	
	Lyophilised	1	28043.9	0.4	28004.3	0.4	
	Acetone precipitated	1	28052.4	0.6	28052.4	0.2	
	Ni-NTA treated	1	28344.3	1.2	28053.2	0.3	
	Ni-NTA treated	2	28121.4	0.6	×	×	

Table 6.5: Treatment type, molecular mass and intensity of spectral peaks putatively representing epitope tagged protein detection from group A, group B and Ku80 infected BALF. Time-points and treatement type are shown. A cross in the Ku80 column denotes that no peak above a signal to noise ratio of 3 was observed in the Ku80 spectra at the corresponding mass. Shown in the far left column is the putative protein which may have been detected.

SELDI-ToF-MS analysis of group B infected BALF did not reproducibly demonstrate any peaks distinct from those present in Ku80 control samples (Figures 6.11 and 6.12). For example, peaks at approximately 75.2 kDa were observed in four spectra from 18 hour group B infected BALF. However, a peak of 75.4 kDa was also observed in an acetone precipitated Ku80 control spectra, suggesting peaks at this molecular mass may be detection of host or untagged *A. fumigatus* protein (Table 6.5). A peak with a molecular mass of approximately 28.0 kDa was observed in 5 treatment regimes from group B infected, 18 hour BALF. Peaks with approximately the same mass were observed in Ku80 controls (Table 6.5). Notably however, both replicates of Ni-NTA treated BALF produced a peak at this size with greater intensity than that observed for Ku80 controls. It was hypothesised that greater peak intensity may be due to Ni-NTA binding of epitope tagged extracellular proline-rich protein (Afu5g01620, molecular mass 28.3 kDa) from group B infected BALF. Afu5g01620 encodes a putative signal peptide, and gene expression profiling showed high transcript increase between 4 – 8 hours post infection (Table 6.3).

6.3.8 SELDI-ToF-MS does not reproducibly detect epitope tagged proteins in BALF from mice infected with single *A. fumigatus*_His_6 strains

Spectra from BALF infected with a pooled library of *A. fumigatus* strains putatively expressing an epitope tag showed low peak intensity, poor technical reproduction and low concordance between treatments (section 6.3.7). Therefore, confidence in any peak representing epitope tagged protein detection was low. Accordingly, it was considered possible that infection using *A. fumigatus* Afu7g06750_His_6 and Afu5g01620_His_6 strains (Table 6.4) may not result in positive detection. In order to comprehensively determine if any of the 24 putatively epitope tagged proteins were detectable in murine BALF, each *A. fumigatus*_His_6 strain was used to infect two mice, from which BALFs were extracted at either 4 or 18 hours post infection. BALFs were lyophilised or acetone precipitated in order to maximise peak intensity. 2 µl of treated BALF was selectively bound on PG20 chips with an anti-his antibody and analysed by SELDI-ToF-MS. Spectra between 20 and 100 kDa are shown in Figure 6.13. Spectra between 1 and 20 kDa are shown for strains where the predicted molecular mass of the epitope tagged protein is below 20 kDa (Figure 6.14).

Two peaks were observed which approximated the predicted mass of the putative epitope tagged protein (Figure 6.13). The spectrum from Afu3g14030_His_6 (molecular mass 72.5 kDa) infected, acetone precipitated murine BALF from 4 hours post infection showed a peak at 77.9 kDa. Additionally, the spectrum from Afu3g14170_His_6 (molecular mass 57.6 kDa) infected, acetone precipitated murine BALF from 18 hours post infection showed a peak at 55.0 kDa (Figure 6.13).

Biological repeats were conducted using these two strains, from which BALF were acetone precipitated and analysed using SELDI-ToF-MS. Peaks observed in spectra from the first replicate were not observed in spectra from repeat experimentation (Figure 6.15). An important constraint to this analysis was the low number of mice employed. Secondly, vital counts demonstrated that due to experimental error a lower dose was employed in the second experiment (1×10^7) relative to the first (1×10^8).

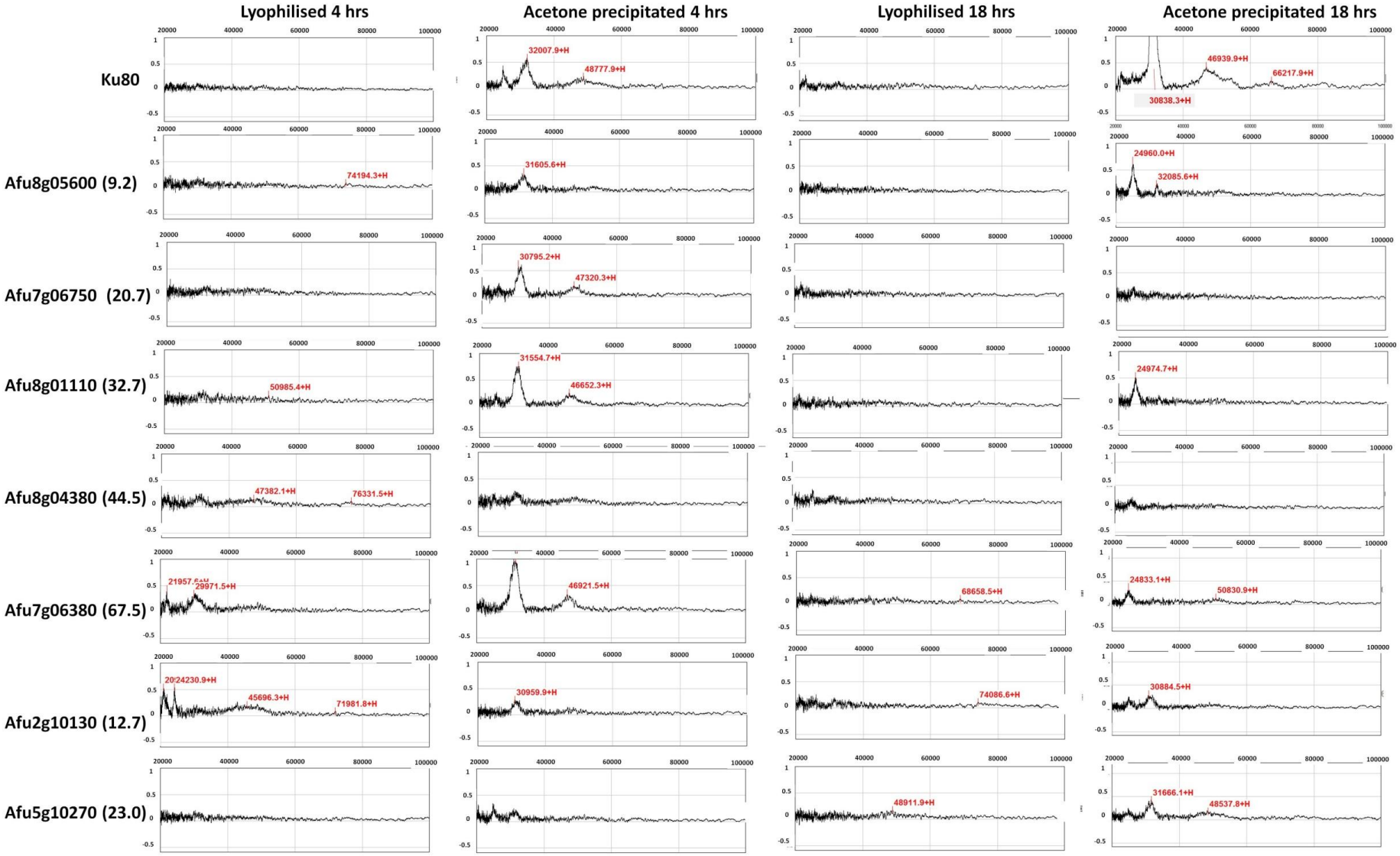


Figure 6.13: Spectra from SELDI-ToF-MS analyses of *A. fumigatus*_His_6 or Ku80 infected murine BALF extracted at 4 and 18 hrs. Single mice were infected with inocula from individual *A. fumigatus*_His_6 or Ku80 strains. Spectra from both 4 and 18 hour time points and lyophilised and acetone precipitated BALF are shown. Strains are identified by the gene number of the putatively epitope tagged allele. Numbers in parentheses indicate the predicted protein size (kDa). Peaks with a signal to noise ratio greater than or equal to 3 are signified by a red line, and molecular mass indicated in red text (kDa). Spectra scales show between 20000 – 100000 Da and peak intensity between 1 and -0.5.

Figure 6.13 continued

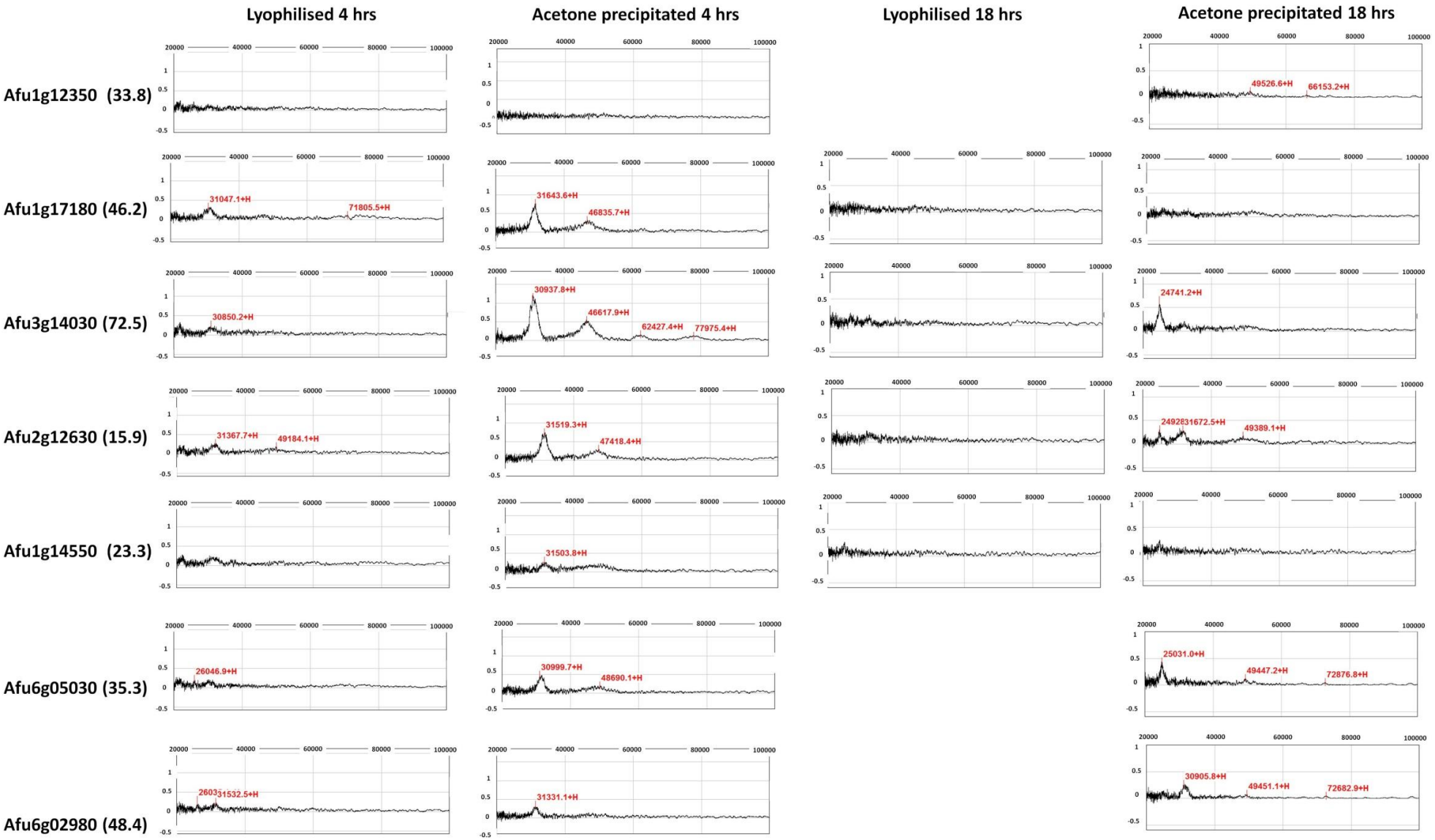


Figure 6.13 continued

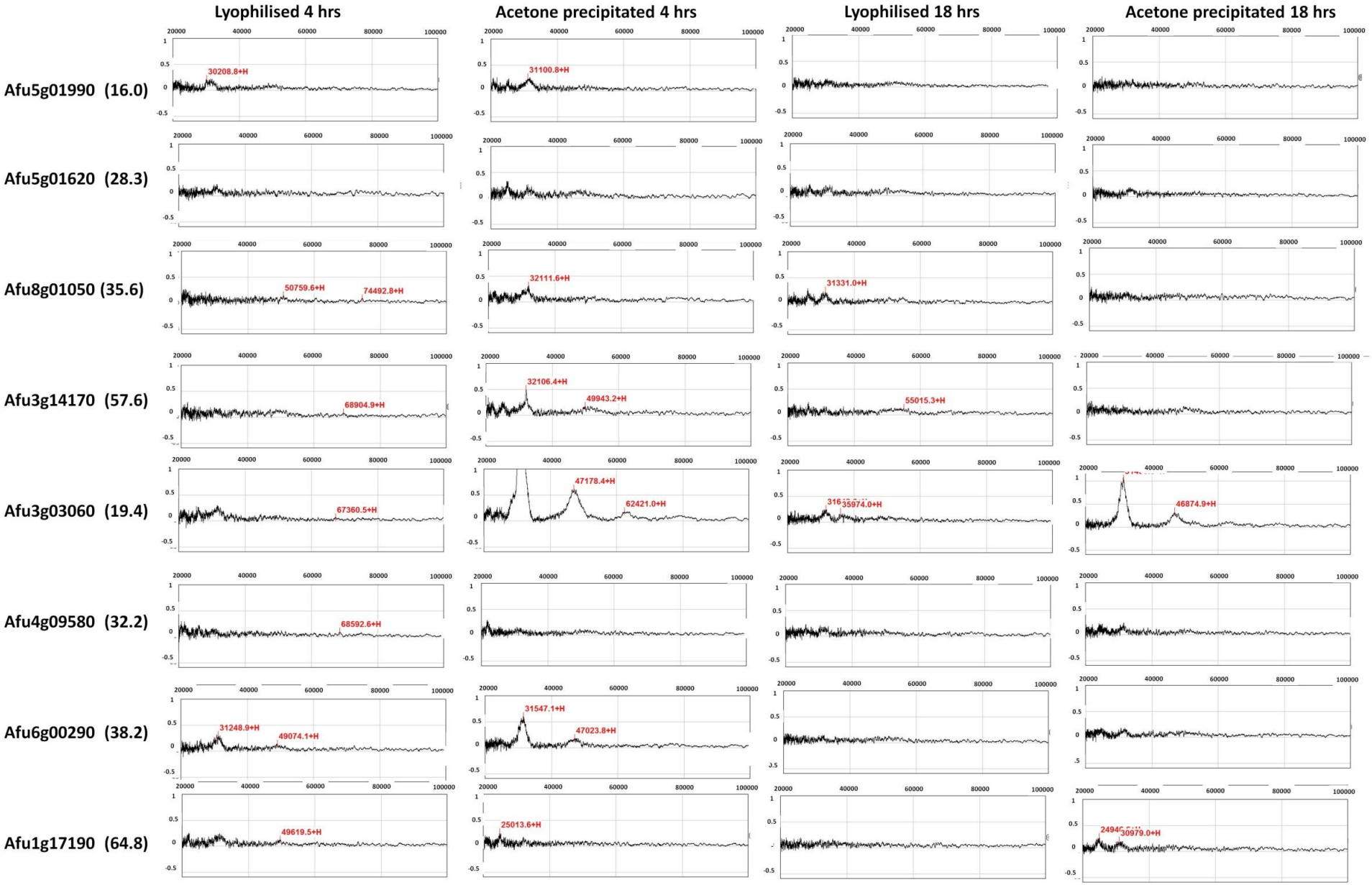
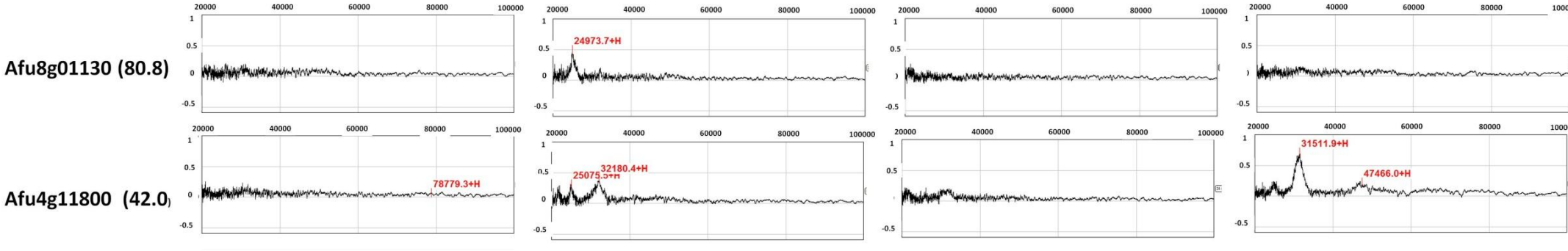


Figure 6.13 continued



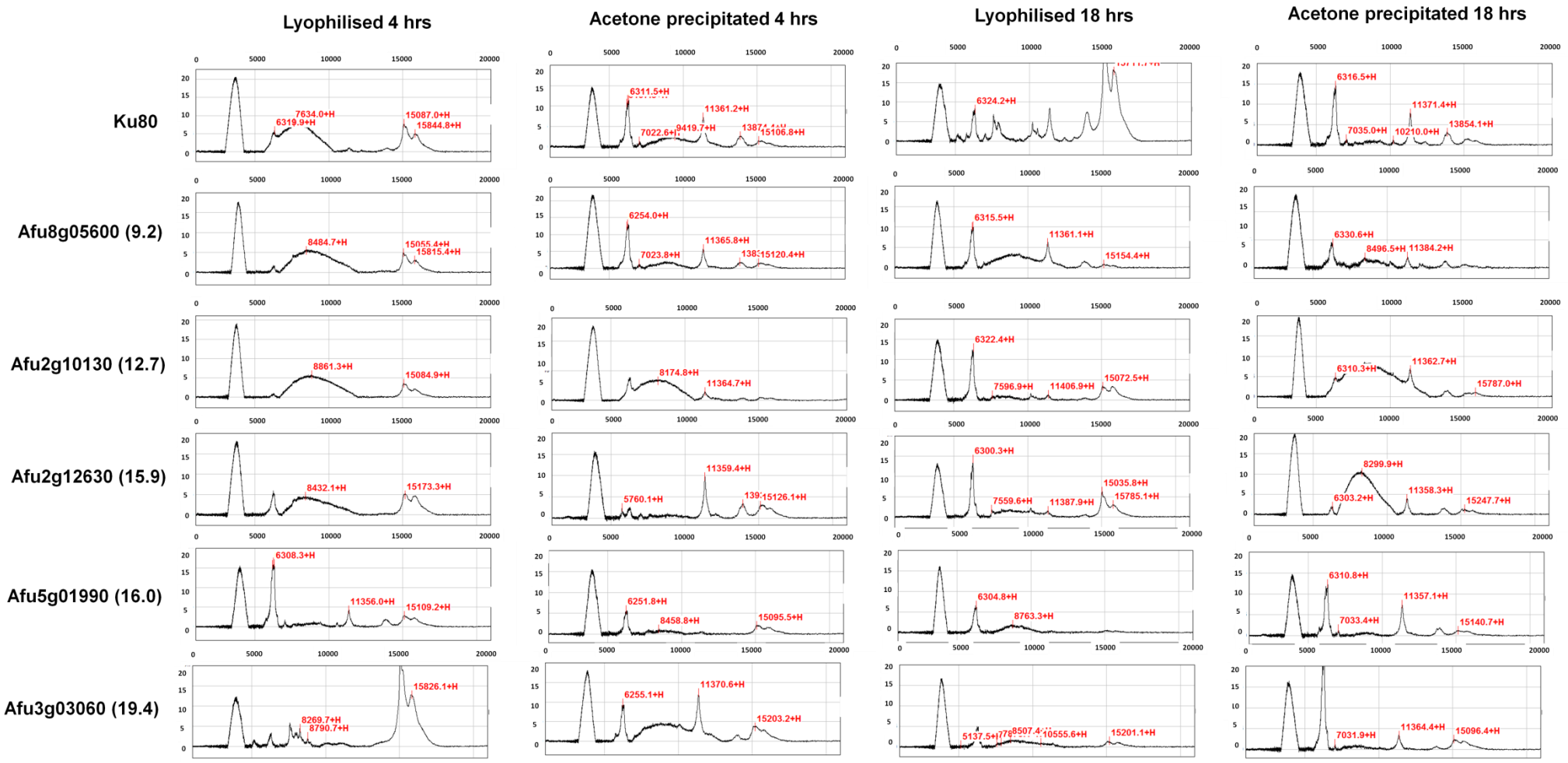


Figure 6.14: Spectra from SELDI-ToF-MS analyses of *A. fumigatus*_His$_6$ or Ku80 infected murine BALF extracted at 4 and 18 hrs. Single mice were infected with inocula from individual *A. fumigatus*_His$_6$ or Ku80 strains. Spectra from both 4 and 18 hour time points and lyophilised and acetone precipitated BALF are shown. Strains are identified by the gene number of the putatively epitope tagged allele. Numbers in parentheses indicate the predicted protein size (kDa). Peaks with a signal to noise ratio greater than or equal to 3 are signified by a red line, and molecular mass indicated in red text (kDa). Spectra scales show between 1000 – 20000 Da and peak intensity between 20 and -0.5.

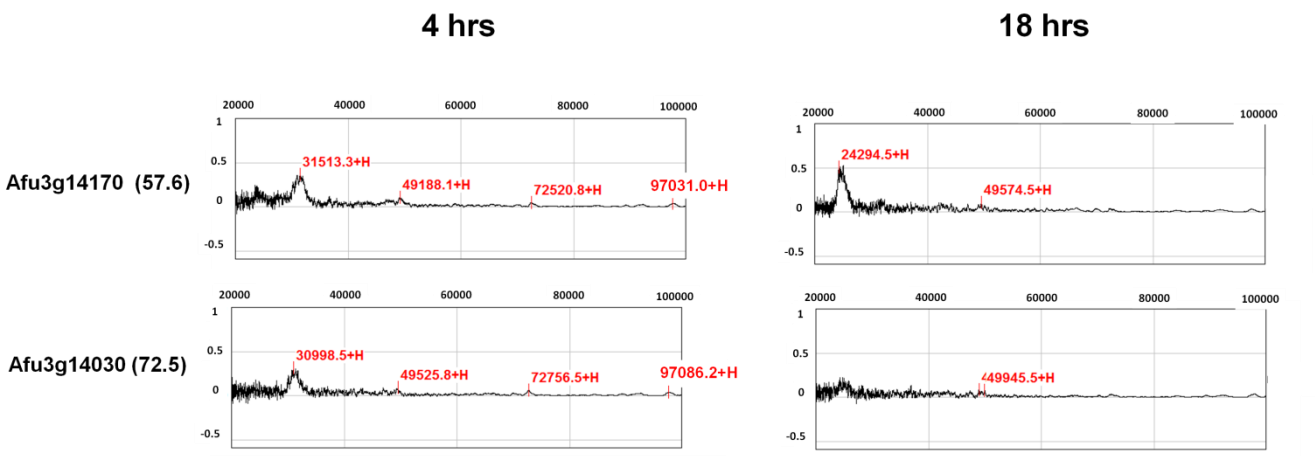


Figure 6.15: Spectra from SELDI-ToF-MS analyses of Afu3g14170_His$_6$ and Afu3g14030_His$_6$ infected murine BALF extracted at 4 and 18 hrs. Single mice were infected with inocula from individual *A. fumigatus*_His$_6$ strains. Spectra from both 4 and 18 hour acetone precipitated BALF are shown. Strains are identified by the gene number of the putatively epitope tagged allele. Numbers in parentheses indicate the predicted protein size (kDa). Peaks with a signal to noise ratio greater than or equal to 3 are signified by a red line, and molecular mass indicated in red text (kDa). Spectra scales show between 20000 – 100000 Da and peak intensity between 1 and -0.5.

6.4 Discussion

In light of this study's interest in host pathogen interactions, special consideration has been given to putative *A. fumigatus* cell surface molecules, such as those biosynthesised by the *pes3* and *regA* secondary metabolite clusters (Chapters 4 and 5), and also to putatively secreted proteins. The latter molecules play highly diverse roles in the molecular events during initiation of fungal disease. Much effort has recently been invested into elucidating the role of secreted protein effectors, which are a component of the pathogen armamentarium that are utilised to suppress or evade host immune responses (reviewed in de Wit et al. 2009). When present in the host-pathogen molecular milieu, they have critical implications for the outcome of disease, as evidenced by secreted virulence factors which are encoded by bacterial (Fontana et al. 2011), fungal (Rooney 2005) and oomycete (Birch et al. 2008) pathogens. Conversely, effector-triggered immunity represents a significant component of innate immune response, most notably in plants. Work presented in this chapter can be viewed as an attempt to identify putative host effectors during *A. fumigatus* infection.

Much data regarding fungal effectors comes from the study of phytopathogens. The plant immune system is dualistic in nature, consisting of a basal system which recognises conserved PAMPs, and the *R* system in which the products of resistance genes mediate resistance against effectors. Effectors putatively overcome plant basal immunity, for example the effector protein Avr2 of *Cladosporium fulvum* (Dixon et al. 1996), Avrlm1 of *Laptosphaeria maculans* (Gout et al. 2006), and Avr1 of *Fusarium oxysporum* f.sp. *lycopersici* (Houterman et al. 2008). Corresponding *R* genes in plants renders fungal pathogens possessing the effector gene avirulent. Work conducted to elucidate the molecular mechanism of *C. fulvum* Avr2 illustrates the profound impact of secreted effectors on disease initiation and host pathogen interactions. In the tomato apoplast, numerous host proteins including β-1,3-glucanases, chitinases, and serine proteases attack *C. fulvum* by degradation of cell wall components. Shabab and colleagues investigated the role of host proteases and pathogen protease inhibitors in the establishment of *C. fulvum* tomato infection (Shabab et al. 2008). In this study, stimulation of a host immune response with a PAMP analogue greatly enhanced the protease activity of the host apoplastic space. 2D-DIGE and MALDI-ToF-MS identified the presence of 5 putative proteases, and RT-PCR suggested two, PIP1 and RCR3, were significantly induced following PAMP stimulation of the host. A protease inhibition assay was utilised, where overexpression strains producing 5 putative proteases were co-incubated with recombinant Avr2. Incubation with the putative effector significantly reduced the protease activity of PIP1 and RCR3 overexpression extracts. Moreover, coimmunoprecipitation assays demonstrated Avr2 physically interacts with both PIP1 and RCR3 (Rooney et al. 2005,

Shabab et al. 2008). Heterologous expression of Avr2 in *Arabidopsis thaliana* enhanced susceptibility to fungal pathogens, including strains of *C. fulvum* that lack functional Avr2 (van Esse et al. 2008). Additionally, an RNA silenced Avr2 isolate was attenuated in a tomato infection model, indicating that inhibition of host proteases by Avr2 is required for *C. fulvum* virulence. Paradoxically, when the resistance gene Cf-2 is present in the host, Avr2 behaves as an avirulence factor (Rooney et al. 2005). The plant extracellular leucine-rich repeat receptor protein (Cf-2) putatively recognises the Rcr3-Avr2 complex to activate host hypersensitive responses. Thus, in phytopathogens, secreted effectors are defining features of the molecular host-pathogen interface, and may determine disease outcome.

With regard mammalian disease, numerous prokaryotic pathogens secrete a myriad of effectors which mimic, block, or alter host-signaling cascades to allow bacterial survival (reviewed in (Mattoo et al. 2007)). For example, host RhoGTPase activity is inhibited by the *Yersinia* effector YopT (Shao et al. 2002) which cleaves RhoGTPases near their carboxyl termini, releasing them from the membrane and causing subsequent disruption of actin cytoskeleton in host cells. Additionally, bacterial effectors can modify host PRRs to gain entry into the host. For example, the type II-secreted invasin protein, InvA, of *Yersina* sp. interacts with multiple integrin receptors expressed on host cells, leading to the activation of the RhoGTPases Rac-1 and subsequent internalisation via cytoskeletal rearrangements (Owen et al. 2007). While it is unlikely the opportunistic pathogen *A. fumigatus* posses the plethora of effectors secreted by obligate bacterial pathogens such as *Yersinia* sp., work conducted by Fontana and colleagues have demonstrated secreted effectors in the opportunistic bacterial pathogen *Legionella pneumophila* (Fontana et al. 2011). *L. pneumophila* is able to replicate in alveolar macrophages, and multiplies within a specialised vacuole, which is facilitated by bacterial effector proteins translocated into the host cytoplasm via the Dot/Icm type IV secretion system (Isberg et al. 2009). Fontana and co-workers used host transcriptional comparisons between macrophages infected with either a fully virulent, or attenuated *L. pneumophilia* isolate to demonstrate increased transcript abundance of 166 genes in the virulent infected macrophages, many of which were not normally associated with innate responses to *L. pneumophilia.* These included *Il23a* and *Gem* (which encodes a small GTPase). Infection of *Myd88*$^{-/-}$ macrophages, which are deficient in TLR signalling still displayed high transcriptional increase of *Il23a* and *Gem*, indicating PRRs did not account for the increased expression of these genes. Treatment of macrophages with various cell stresses was used in an attempt to induce *Il23a* and *Gem* expression. Thapsigargin and tunicamycin, which inhibit host translation, were found to strongly induce *Il23a* and *Gem*. Next, a mutant strain in which five putative secreted effectors (Δ*5*) was constructed. These effectors putatively block host translation

by modification of the mammalian elongation factor. Infection of macrophages with a *Δ5* isolate demonstrated *Il23a* and *Gem* transcriptional responses were significantly reduced relative to wild-type. As *Il23a* and *Gem* expression are both positively regulated by the NF-κB signalling cascade. Analysis of the transcriptional basis of the NF-κB signalling cascade demonstrated infection with *Δ5* permitted normal translation of the NF-κB inhibitor IκB. Conversely, expression of the 5 *L. pneumophila* effectors correlates with sustained loss of inhibitors of the NF-κB transcription factor. Thus, in wild-type isolates, the *L. pneumophila* effectors inhibit protein synthesis, which leads to activation of the NF-κB signalling cascade. Given that the natural niche of *L. pneumophilia* is amoebae, it seems unlikely that these effector proteins evolved specifically to manipulate the mammalian immune system. Indeed, the authors postulate that innate responses to translation inhibition represents a host strategy for detecting *L. pneumophila*. These data highlight the complex molecular basis of effector-triggered immunity, and suggests opportunistic mammalian pathogens may produce effectors in the host, notwithstanding that their primary role of these proteins is not virulence related. This may be especially true of saprobes such as *A. fumigatus* which secrete a cocktail of hydrolytic and other enzymes into the environment to gain nutrients. Transcriptional comparisons between 4 and 8 hours post infection in Af293 suggested increased transcript abundance of 277 genes encoding a putative signal peptide (Chapter 3). These genes encoded proteases, cell wall proteins, chitinases, lipases, cutinases, extracellular signalling proteins, lipophospholipases and an acid sphingomyelinase. The role of these molecules in modulating host pathogen interactions via effector functions is unknown.

Of fundamental importance to understanding host-pathogen interactions and pathogen effectors is identifying which pathogen molecules are present in the host niche at defining stages of disease. In addition, protein discovery in the host may facilitate the development of novel diagnostics. The first proteomic analysis of *A. fumigatus* developed 2D-DIGE for analysing pathogen proteins *in vitro* (Kniemeyer et al. 2006). Since then, several proteomic studies have investigated *A. fumigatus* responses to laboratory conditions which approximate or are relevant to mammalian infection, including antibiotic exposure (Cagas et al. 2011, Gautam et al. 2008) heat shock (Albrecht et al. 2010) and biofilm formation (Bruns et al. 2010a). While these studies provide insights into *A. fumigatus* proteomic responses to single disease relevant conditions, they do not address pathogen protein biosynthesis in the multifaceted and dynamic host niche. One strategy to define host-pathogen protein interactions in the host is to conduct global proteomic analyses from *in vivo* samples using techniques such as LCMS or 2D-DIGE. These approaches are cost and labour intensive and consequently are not suited to studying multiple time-points or models of infection. Of great use would be a rapid tool for the targeted detection of specific *A. fumigatus*

proteins in the host niche. In an attempt to optimise such a tool, twenty five *A. fumigatus* strains putatively expressing a poly-histidine tagged genes were constructed and used to infect mice in a high dose model of invasive aspergillosis. SELDI-ToF-MS was employed in an attempt to detect recombinant protein in the BALF.

SELDI-ToF-MS combined with poly or monoclonal antibody capture has been used to detect several proteins from samples extracted from human tissue. Diamond and colleagues optimised a SELDI-ToF-MS platform for accurate detection of the antimicrobial peptides β-defensins hBD1 and HBD2 in human gingival cervicular fluid (Diamond et al. 2001). Both normal phase and ProteinChip arrays were used, which capture proteins from the sample based on hydrophobicity and immobilised anti-hBD1 or anti-hBD2 antibodies respectively. For normal phase and ProteinChip arrays, SELDI-ToF-MS detection limits of synthetic β-defensins diluted in sterile saline were 0.0025 ng/μl. However, detection of β-defensins hBD1 or hBD2 from human gingival cervicular fluid was only achieved with the ProteinChip array and immobilised anti-hBD1 or anti-hBD2 antibodies. These data suggest the anti-body capture with ProteinChip array may be more sensitive than other SELDI-ToF-MS array chips for protein detection from host tissues. Levels and colleagues used SELDI-ToF-MS to profile human high density lipoprotein, the molecular composition of which is modified during vascular disease (Levels et al. 2007). Thus, the authors hypothesised SELDI-ToF-MS may be used to detect biomarkers of vascular dysfunction. High density lipoprotein was captured from human plasma using two specific anti-bodies covalently bound to ProteinChip arrays. Concentrations of protein, or the detection threshold were not determined. However, spectra clearly differentiated between normal and diseased samples, and the authors concluded SELDI-ToF-MS was an appropriate tool for high throughput profiling of high density lipoprotein in patient sera. The authors also reported (but did not show) high reproducibility between technical replicates.

Schweigert and co-workers investigated the molecular variants of the hormone transporter transthyretin in human plasma and urine (Schweigert et al. 2004). Using ProteinChip arrays to which an anti-transthyretin antibody was immobilised were combined with SELDI-ToF-MS analysis, which found that transthyretin in the urine of pregnant women reproducibly produced smaller immunoreactive fragments than normal individuals. The authors suggest SELDI-ToF-MS was a rapid and accurate method for characterising the molecular variants of transthyretin, which may be a marker which is able to determine between metabolism in healthy and diseased individuals. These studies suggest that SELDI-ToF-MS is an accurate, sensitive and reproducible assay for the analysis of proteins from complex biological fluids.

With regard to the analysis of minute concentrations of pathogen protein in host samples, the SELDI-ToF-MS platform has several advantages over other mass spectrometric techniques. Most notably, in SELDI-ToF-MS the chip surface plays an active role in the extraction and cleaning of the sample of interest (Tang et al. 2004). Protein chips may incorporate broad binding characteristics, such as cationic, anionic, IMAC or hydrophobic surfaces, or specific affinity probes, such as DNA, enzyme or antibody receptors. Molecules with affinity to the biochemical chip surface are selectively bound to the chip, and other molecules which may be present in the sample are removed by a series of washing steps. This is in contrast to MALDI-ToF-MS, where the sample bearing surface and matrix compound is inactive, and simply present the analyte for MS analyses. In this study, epitope tagged proteins were targeted from murine BALF using an anti-his antibody immobilised to the chip surface. The exclusion of contaminating host and fungal proteins from Tof-MS analyses was a major motivation for using this platform. In addition, SELDI-ToF-MS is highly sensitive. For example, SELDI-ToF-MS is able to detect attomolar concentrations of lactoferrin from infant urine using DNA probe surfaces (Hutchens and Yip 1993). Spiking experiments using recombinant bacterial protein in murine BALF supported both the selective antibody capture of epitope tagged protein to the chip and sensitivity of the platform. 1 ng of recombinant protein per 1 µl BALF was detectable (Figure 6.6). Moreover, SELDI-ToF-MS detected recombinant epitope tagged *A. fumigatus* protein from *in vitro* culture, which was not possible using Western blotting. However, no epitope tagged protein was reproducibly detectable by SELDI-ToF-MS analysis of BALF. Spectral peaks putatively detecting epitope tagged phosphoglycerate mutase family protein (Afu7g06750), extracellular proline rich protein (Afu5g01620), alkaline phosphatase (Afu3g14030) and a high affinity hexose transporter (Afu3g14170) were not observed in biological replicates. In general, spectral peaks above a molecular mass of 20 kDa demonstrated very poor concordance between technical replicates. Thus it was concluded that anti-his immune capture and SELDI-ToF-MS detection of poly-histidine epitope tagged fungal proteins was not reproducible.

A number of explanations may be offered as to why the strategy for protein detection was unsuccessful in this study. Firstly, it is possible genes may increase in transcript abundance but the protein may not be translated. Gene expression profiling described in Chapter 3 is inherently limited to the study of genes and their expression, rather than post transcriptional events. This is highlighted by recent functional genomic studies which concomitantly investigated the *A. fumigatus* transcriptome and proteome, and reported large discrepancies between mRNA and protein abundance. For example, Gautam and colleagues found 293 genes and 48 proteins differentially expressed following amphotericin B exposure (Gautam et al. 2008). However, only

13 were common to both analyses. Bruns and co-workers found a weak correlation between transcriptional and proteomic comparisons between planktonic and biofilm grown mycelia, with several gene categories, such as heat shock proteins, demonstrating reverse regulation depending on the sampling method (Bruns et al. 2010a). Other studies analysing heat shock response (Albrecht et al. 2010) and caspofungin exposure (Cagas et al. 2011) in *A. fumigatus* have reported similar differences between mRNA and protein abundance. This variation is likely due to a combination of complex post transcriptional modification, protein half life and inherent methodological noise (Greenbaum et al. 2003). This is further complicated by common stress conditions in eukaryotes causing repression of translation initiation and accumulation of mRNA in the nucleus (Hilgers et al. 2006).

Nevertheless, several studies suggest various members of the 24 epitope tagged proteins may be translated in the host. For example, 64 proteins were detectable using MALDI-ToF-MS proteomic profiling of TCA precipitated *A. fumigatus* secretome from 72 hour culture (Wartenberg et al. 2011). This included the cell wall protein PhiA (Afu3g03060) and the allergenic cerato-platanin allergen Asp F13 (Afu2g12630). Antibodies specific to this protein are present in *A. fumigatus* infected human sera and lung as as determined by an antibody specific enzymatic immunoassay and immunofluorescence assay respectively (Reichard et al. 1990). Mn superoxide dismutase allergen Asp F6 (Afu1g14550) is detectable by MALDI-ToF-MS of hyphal extracts and is recognised by IgE of ABPA patients (Schwienbacher et al. 2005). Similar IgE binding was observed for Asp F2 (Afu4g09580) and Asp F13 (Banerjee et al. 1996, Chow et al. 2000). Therefore, while it is likely translation of some epitope tagged proteins may not have occurred within the time-points analysed in this study, this is unlikely to explain the lack of detection for all 24 epitope tagged proteins.

A second possibility is that the polyhistidine tag was either cleaved by post translational modifications or physically masked by protein tertiary structure. Epitope tagging at the C-terminus should reduce the chances of this occurring compared to internal tagging; nevertheless, optimal placement of the polyhistidine tag is protein specific and often requires optimisation (Terpe 2003). Movement of the polyhistidine tag to the N terminus is a strategy which often solves purification complications attributed to protein tertiary structure. The high-throughput experimentation conducted in this thesis could not accommodate the determination of optimal epitope tagging for each of the 24 proteins. While the detection of C-terminal epitope tagged proteins from *in vitro* culture using SELDI-ToF-MS was considered promising for the utility of the technique, the cleavage or physical masking of the polyhistidine-tag likely rendered some of the candidate

proteins undetectable. This is assuming the tags were expressed at all, which was not experimentally confirmed with Western analysis. Western blots were not used to confirm functionality of the tags, as Western and SELDI-ToF-MS were unable and able to detect epitope tagged protein extracted from *in vitro* culture respectively (Figure 6.5 and 6.6).

The polyhistidine-tag was used as it is cheap, non-immunogenic, amenable to purification using immobilised metal-affinity chromatography (IMAC), contains few amino acid residues and is effective at physiological pH. Polyhistidine epitopes have been used for heterologous protein tagging and purification from *A. nidulans* (Roth and Dersch 2010). Other tags may be too large, for example the glutathione-s-transferase (GST) epitope tag is composed of 220 amino acids, which would almost certainly disrupt secretion. Although outside the scope of this study, other tags could have been utilised that may have conferred advantages over the polyhistidine epitope. IMAC utilising Ni-NTA beads has lower specificity than other epitope tags and their respective affinity methods (Waugh 2005). For example, the FLAG-epitope is an octapeptide which can be utilised to purify protein with high specificity using a commercially available anti-FLAG antibody and ANTI-FLAG® M2 Affinity Gel (Sigma-Aldrich, UK). Western analyses of crude mycelial and supernatant extracts demonstrated high non-specific binding of *A. fumigatus* protein to Ni-NTA resin (Figure 6.5). Thus, improving specificity by utilising a FLAG epitope may have enhanced detection. However, the ANTI-FLAG® M2 Affinity Gel (Sigma-Aldrich, UK) is approximately 10 times more expensive than Ni-NTA agarose.

A third possibility which may have reduced the likelihood of detection is that some fungal proteins remained intracellular. To address this possibility, 12 out of 24 alleles were selected which lacked a GPI-anchor sequence and contained a putative N-terminal signal peptide. With regard to intracellular proteins, it was reasoned that murine immune activity would lyse spores or hyphae, thus releasing intracellular proteins. Nevertheless, it is possible that epitope tagged proteins may have remained intracellular and thus inaccessible to the anti-his antibody.

A general limitation to the approach utilised in this study is the extremely low concentration of *A. fumigatus* proteins present in the host. As already noted, SELDI-ToF-MS was chosen due to the high sensitivity of the platform. A high dose infection model was employed in which neutropenic mice were infected with 1×10^8 *A. fumigatus* spores. It was reasoned that this would maximise the concentration of fungal protein in BALFs. Mice were culled and BALF extracted at 4 and 18 hours post infection. The 18 hour stage was chosen over earlier invasive time points (e.g. 14 hours) to maximise the infectious burden and therefore concentration of proteins in BALFs. Additionally

these time-points were chosen in order to identify proteins which differentiated between normal carriage of *A. fumigatus* spores in the lung and an invasive infection. In an attempt to maximise epitope tagged protein and minimise non-specific protein binding to the chip BALFs were lyophilised, acetone precipitated, albumin and IgG depleted and Ni-NTA purified. Nevertheless, *in vitro* spiking experiments suggested 1 ng/µl was the detection threshold of the SELDI-ToF-MS platform. Although the concentration of *A. fumigatus* proteins in BALF is unknown, some, or possibly all may have been biosynthesised at concentrations below the detection threshold.

The ability of SELDI-ToF-MS to detect his-tagged protein from *in vitro* samples demonstrates the platform theoretically should be able to detect epitope tagged proteins from *in vivo* BALF. Indeed, this study cannot rule out that a spectral peak from BALF samples represents successful protein detection. It is possible that the lack of concordance between biological replicates may be due to significant variation in the germination and development of disease between mice, coupled with the fact that only a small population of replicates was used. This is a common problem in murine models of IPA (Warn, personal communication). Indeed, where detection appeared to have been successful, a larger cohort of animals might have helped improve reproducibility of the assay. In summary, it is likely that the above challenges synergistically contributed to the failure of this platform to achieve the specified objectives. Work conducted in this study has not generated sufficient data to comment on which challenge was the most problematic.

Several studies have detected *A. fumigatus* proteins in mammalian models or clinical cases of IPA. Markaryan and colleagues used immunogold labelling and transmission scanning electron microscopy to visualise secretion of metalloproteinase (Afu8g07080) in a murine model of infection (Markaryan et al. 1994). Neutropenic mice were inoculated with 1 x 10^7 spores, and culled at 8 and 20 hours post infection. Histology slides were probed with an anti-metalloproteinase primary antibody followed by a secondary antibody conjugated with gold. Metalloproteinase secretion was visualised with a transmission electron microscope, and was found on the surface of both conidial and hyphal morphologies. Although shortlisted for epitope tagging, generation of an *A. fumigatus* Afu8g07080-His_6 isolate was unsuccessful (Table 6.3). Nevertheless, the highly similar dose (1 x 10^7 in both) and time-points (e.g. 18 hours and 20 hours post infection) employed between this study and that of Markaryan and co-workers suggest secreted proteins are likely present in the host and detectable by immunological methods. A second study detected an alkaline serine protease in the lung from a fatal case of human IPA (Reichard et al. 1990). Immunohistochemistry using an anti-Alp1 primary antibody suggested both conidia and hyphae secreted this protein *in vivo*. Additionally, ELISA analysis demonstrated

antibodies specific to this protein are present in human sera from IPA patients. These data were the rationale for using Afu4g11800_His_6 as a positive control. Finally, GFP-tagging has been used to visualise *A. fumigatus* protein biosynthesis *in vivo*. For example, PksP (Afu2g17600) which is required for melanin biosynthesis and murine virulence (Tsai el al. 1998, Langfelder el al. 1998) has been detected using an *egfp*-containing gene fusion. Neutropenic mice were inoculated with 1 x 10^7 spores from the *pksP-egfp*-expressing strain, and BALFs extracted 24 hours post infection. Microscopic examination of fungal hyphae isolated in BALFs showed germlings were biosynthesising PksP in the host 24 hours post infection. Given that the authors of these studies do not measure (or report) protein concentration detection limits for the assays described, the minimum concentration of the fungal proteins in the host in each model remains unknown. These data would be extremely valuable with regard to this study, as it would enable determination of whether protein concentrations are above the minimum theoretical limit of detection for the SELDI-ToF-MS platform (0.1 ng/µl, Figure 6.6). In general, immunohistochemical and immunogold detection suggest that proteins are sufficiently abundant in the host for detection with an anti-body.

With regard to the future application of SELDI-ToF-MS to the study of *A. fumigatus* and IPA, Kniemeyer and colleagues have described SELDI-ToF-MS as “one of the most important proteomic technologies for the high-throughput analysis of complex protein samples” (Kniemeyer et al. 2009). Work conducted in this study is not exhaustive of the application of SELDI-ToF-MS in the study of *A. fumigatus* infection. Alternative chip surface chemistry, combined with later time-points of infection, may be useful tools for the study of IPA and *A. fumigatus*. Gonzales and co-workers used SELDI-ToF-MS to conduct protein expression profiling of a neutropenic rabbit model of IPA (Gonzales et al. 2010). In this study, proteins from serum and BALF were captured on an anionic exchange chip over a time-course of infection. The authors demonstrated a distinct protein signature following *A. fumigatus* infection relative to non-infected controls at 5 days post infection. Additionally, SELDI-ToF-MS could distinguish between animals infected with *A. fumigatus* and *Pseudomonas aeruginosa*. Using the SELDI-ToF-MS spectrum to verify the molecular mass of differentially expressed protein, SDS-PAGE and LC-MS analyses demonstrated elevated levels of haptoglobin, apolipoprotein A1, transthyretin and C-reactive protein (Gonzales et al. 2010). In addition to the potential use in diagnosis, these proteins have interesting implications for host-pathogen interactions. For example, lipoproteins have been shown to inhibit the activity of *A. fumigatus* hemolysin (Fukuchi et al. 1996). In a second study, Pinel and colleagues utilised SELDI-ToF-MS and weak cation exchange (CM10), reverse phase (H50) and silicate surface (NP20) chips to analyse *A. fumigatus* and *Aspergillus lentulus* protein extracts (Pinel et al. 2011).

Mycelial, conidial and culture supernatant demonstrated reproducibly different protein profiles. Moreover, the authors were able identify spectral peaks which distinguished *A. fumigatus* from *A. lentulus*. These studies, in addition to proteomic profiling of other organisms, demonstrate the likely value of SELDI-ToF-MS for future study of *A. fumigatus* host pathogen interactions (Agranoff et al. 2006, Papadopoulos et al. 2004).

The use of mass spectrometric methods for the analysis of host pathogen interactions was predicted by Latge and Calderone, who wrote “the development of mass spectrometry systems and transcriptome analysis should lead to the identification of fungal molecules that are released at the earliest time of infection” (Latgé and Calderone 2002). This study has not been able to reproducibly detect fungal molecules in the host using SELDI-ToF-MS. Nevertheless, further study of the *A. fumigatus* isolates which putatively express the epitope tagged alleles is currently underway. Immunohistochemistry is being conducted on lung tissue from Afu4g11800_His_6 (Alp1 positive control) and Ku80 (negative control) infected animals. Immunohistochemistry also addresses the possibility that *A. fumigatus* effectors may ultimately be intra-cellular, in either pathogen or host epithelial or immune cells.

Chapter 7

Expression, purification and PBMC responses to two putative *A. fumigatus* allergens

7.1 Overview

Fungal infections induce expansion and differentiation of naive, pathogen-specific CD4 T cells into populations which either facilitate or impede pathogen clearance (Romani 2004). CD4 T-helper cells (Th cells) become activated against *A. fumigatus* once they are presented with peptide antigens expressed on APC (Bozza et al. 2002). Once activated, T-cells differentiate and secrete numerous cytokines, which have a diverse impact on innate and adaptive immunity. In response to *A. fumigatus* infection, Th cells can differentiate into Th1, Th2 and Th17 subtypes. Th1 cells are characterised by their production of IFN-γ, and primarily contribute to cellular immunity, for example IFN-γ activation of macrophages. Transcriptional comparisons between neutropenic and immunocompetent mice following *A. fumigatus* infection demonstrated a Th1 T-cell response was associated with survival (Armstrong-James et al. 2009). Administration of exogenous Th1 cytokine IFN-γ is currently being investigated as immunotherapy for invasive fungal infections (Armstrong-James et al. 2010). Th17 differentiation may be protective, for example by IL-17 enhancement of neutrophil recruitment (Rivera et al. 2011). However, a Th17 response may also result in pulmonary hyperreactivity, as evidenced by the increase in soluble IL-17A in asthmatic patients, and the suppression of allergic responses in IL-17 deficient mice (Linden et al. 2005, Nakae et al. 2002). Th2 like lymphocytes are characterised by the production of IL-4, IL-5, IL-9 and IL-13, and result in an allergic response associated with poor disease outcome (Romani 2004). The importance of T-cell differentiation with regard to *A. fumigatus* infection is highlighted by studies which demonstrate inhibition of TNF-α (Th1) and IL-4 (Th2) cytokines results in susceptibility and resistance to IPA in murine models respectively (Cenci et al. 1997, Cenci et al. 1999, Mehrad et al. 1999).

However, the molecular events which determine a Th1, Th2 or Th17 phenotype are currently poorly characterised. Identification of immunodominant antigens may enable the development of immunotherapies and be utilised as diagnostic tools (Armstrong-James et al. 2010, Potenza et al. 2007). Antigens produced by *A. fumigatus* which elicit a Th2 response in atopic individuals have

been described as allergens (Banerjee and Kurup 2003). These include a diverse range of proteins which are highly abundant from *in vitro* hyphal culture (Vodisch et al. 2009), including a superoxide dismutase (Afu1g14550), ribosomal protein (Afu2g10100), cell wall glucanase (Afu1g16190) and aspartic endopeptidase (Afu5g13300). These proteins have been described as "Asp F" allergens due to their recognition by IgE from atopic individuals (Banerjee and Kurup 2003), and it has been assumed they naturally evoke a Th2 response. However, work conducted by Chaudhary and co-workers has challenged the concept that these proteins are strictly associated with Th2 differentiation (Chaudhary et al. 2010). ELISPOT analyses of human PBMC from 20 healthy individuals which were stimulated with recombinant allergens Asp F3, Asp F6, Asp F9, Asp F 11, Asp F 12, Asp F17 and Asp F22 demonstrated Th1 cytokine responses. Accordingly, it seems that both Th1 and Th2 responses are possible following exposure to the *A. fumigatus* antigens tested by Chaudhary and co-workers.

Transcriptional profiling conducted in chapter 3 demonstrated increased transcript abundance of numerous putative antigens and allergens during the initiation of murine infection. Of particular note was the increase in transcripts for allergens Asp F4 (Afu2g03830) and Asp F10 (Afu5g13300) between 4 and 8 hours post infection for both Af293 and Δ*laeA* isolates. Both these proteins were not amenable to recombinant expression in the study conducted by Chaudhary and colleagues (Chaudhary et al. 2010). Asp F4 encodes a protein with unknown function, whereas Asp F10 encodes a secreted protease.

In addition to activation of T-cells via dendritic cell antigen presentation, proteases may directly activate inflammatory responses via protease activated receptors (PARs) expressed on airway epithelium, mast cells, eosinophils, alveolar macrophages and lymphocytes (Hershenson 2007). Accordingly, it was hypothesised that Asp F4 and Asp F10 may represent *A. fumigatus* antigens which are biosynthesised in the lung following germination and elicit allergic Th2 responses.

Anti-*Aspergillus* T-cell ELISPOT assays have been used to characterise healthy human *Aspergillus* T-cell responses to recombinant antigens, and identify haematology patients with invasive aspergillosis (Chaudhary et al. 2010, Potenza et al. 2007). In this chapter, putative allergens Asp F4 and Asp F10 were cloned, expressed and purified using an *E. coli* expression system. These proteins were analysed in a pilot ELISPOT assay from PBMC isolated from patients with probable IPA.

7.2 Materials and methods

7.2.1 Bacterial strains

E. coli Xl-10 (Stratagene) was used for cloning experimentation and maintenance of plasmid stocks. For protein expression and purification, C41 *E. coli* cells (Miroux and Walker 1996) were used. Bacterial strains were routinely grown overnight in Luria broth (LB) composed of 0.5% (w/v) NaCl, 0.5% (w/v) yeast extract and 1% bactotryptone. For solid medium, 2% (w/v) agar was added to LB.

7.2.2 Plasmids

pRSET A

Plasmid pRSET A (Invitrogen, UK) was used for cloning and protein expression. pRSET A contains an ampicillin resistance gene for bacterial selection, pUC origin for high copy replication and an N-terminal polyhistidine tag for protein purification using metal-chelating resins.

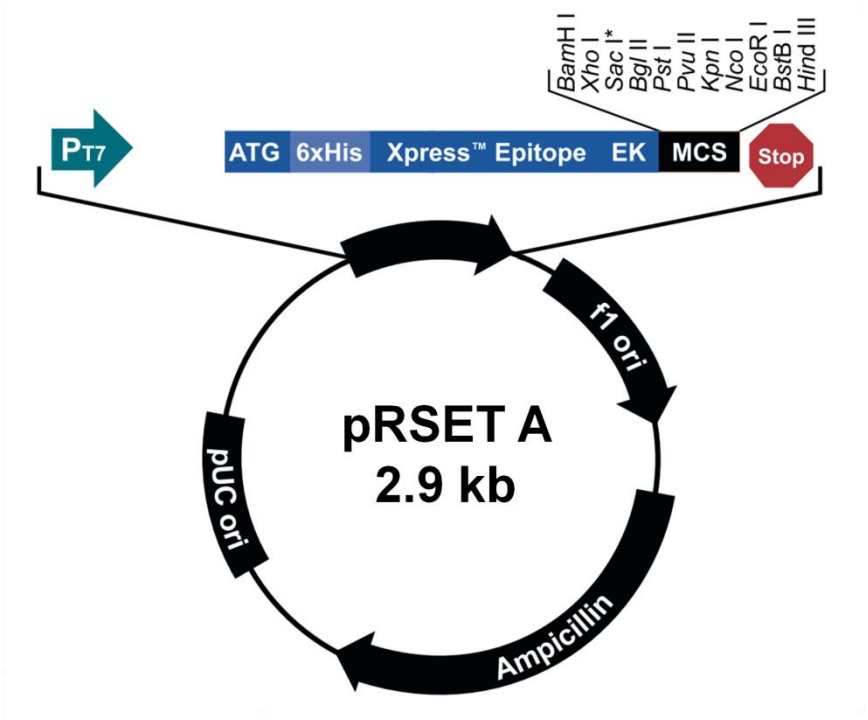


Figure 7.1: Plasmid map of pRSET A. The complete ORFs for allergens Asp F4 (Afu2g03830) and Asp F10 (Afu5g13300) were amplified from an *A. fumigatus* cDNA library and cloned into the pRSET A multiple cloning site (MCS). The T7 promoter (pT7) enables dose-dependent regulation of heterologous gene expression. The N-terminal Xpress™ epitope tag allows detection of the protein by the Xpress™ antibody. The N-terminal polyhistidine tag permits purification of the recombinant proteins using metal-chelating resin. The enterokinase (EK) cleavage site enables efficient cleavage of the tag. PCR productes were amplified with the native stop codon Image downloaded from www.invitrogen.com

7.2.3 Oligonucleotide primers

Table 7.1: Oligonucleotide primer sequences used in this chapter. Oligonucleotides encoding a restriction site are shown in bold text.

Primer	Orientation	Sequence	Restriction site
Asp F4 F	Forward	NNN-**GGATCC**-CAGCTCAAGAATTCGATGCT	BamHI
Asp F4 R	Reverse	NNN-**AAGCTT**-CTCCTTGTAGTCGAGGTTGA	HindIII
Asp F10 F	Forward	NNN- **GGATCC**-GTCGTCTTTAGCAAAGTCA	BamHI
Asp F10 R	Reverse	NNN-**GAATTC**-CTATGCCTGAGGGGCGAAGC	EcoRI
T7 promoter primer	Forward	TAATACGACTCACTATAGGG	N/A
T7 reverse primer	Reverse	TATGCTAGTTATTGCTCAG	N/A

7.2.4 Cloning

Genes selected for expression were amplified from a comprehensive *A. fumigatus* cDNA library using BD Advantage Taq following manufacturer's guidelines (Clontech). Primers were designed with restriction sites for cohesive in-frame ligation of PCR products into the multiple cloning site of the PRSET A plasmid (Invitrogen). Primer sequences are summarised in Table 1. The ligation was transformed into competent XL-10 cells and the plasmids were extracted by mini-prep (Clontech). Plasmids were checked by restriction digest analysis and were sequenced to identify amplification errors. Successful plasmids were transformed into competent C41 cells for high level expression.

7.2.5 Expression optimisation

Cells were grown overnight at 37°C in LB containing 100 µg/ml ampicillin. Cells were then diluted to an OD_{580} of 0.1 and grown at 37°C with shaking to an OD_{580} of 0.4-0.6. Expression was induced using 50 µM, 200 µM, 350 µM and 500µM IPTG (Sigma) at 25 °C, 30 °C and 37 °C. Samples of 1.5 ml were taken hourly over an induction period of 5 hours. Samples were then centrifuged to pellet the cells and extracted in bacterial protein extraction reagent (BPER, Pierce) or 8 M urea and vortexed for 1 minute. Samples were then centrifuged at 13000 rpm for 10 minutes. The supernatant was transferred to a new tube and 15 µl samples were added to 5 µl SDS-PAGE loading buffer (60 mM Tris-HCl, pH6.8, 25% (v/v) glycerol, 2% (v/v) SDS, 10% (v/v) b-

mercaptoethanol, 0.1% (w/v) bromophenol blue) and boiled for 5 minutes. Samples were then run on 10% SDS-PAGE gels in XCell-SureLock Mini Cell electrophoresis tank (Invitrogen) with SDS-PAGE running buffer (25 mM Tris-HCl, 192 mM glycine, 0.1% (v/v) SDS) at 150V until samples reached the end of the gel.

7.2.6 Coomassie Staining

Gels were stained in Coomassie stain (0.1% (w/v) Coomassie Blue R-250, 45% (v/v) methanol, 10% (v/v) acetic acid) for an hour, before been left in Coomassie de-stain (10% (v/v) methanol, 10 % (v/v) acetic acid) overnight. The coomassie de-stain was replaced with fresh de-stain in the morning and allowed to de-stain for a further 2-3 hours before been viewed.

7.2.7 Western Analysis

Cells were grown overnight at 37°C in LB containing 100 µg/ml ampicillin. Cells were then diluted to an OD_{580} of 0.1 and grown at 37°C with shaking to an OD_{580} of 0.4-0.6. Expression was induced using 50 µM, 200 µM, 350 µM and 500µM IPTG (Sigma) at 37°C for 5 hours. Protein samples were extracted using BPER and run on 10% SDS-PAGE gels as described above. Gels were transferred to nitrocellulose membrane, from Amersham, in transfer buffer (25mM Tris base, 192mM glycine, 20% (v/v) methanol) as per manufacturer's instructions using Invitrogen's XCell-SureLock Mini Cell XII Blot module. Membranes were blocked for a minimum of an hour in 5% (w/v) milk, from Marvel, in PBS-Tween (0.001% (v/v) Tween-20, 137 mM NaCl, 1.47 mM KH_2PO_4, 2.68 mM KCl, 8.1 mM Na_2HPO_4.12H2O) before being incubated with primary antibody in 5% (w/v) milk PBS-Tween for an hour. Membranes were washed 3x 10 mins with PBS-Tween and incubated in the secondary antibody (in PBS-Tween) for an hour and washed 3 x 10 mins with PBS-Tween. Membranes were developed using homemade ECL solution 1 (12.5 mM luminol/3-aminophthalhydrazide in DMSO, 19.8 mM coumaric acid in DMSO, 5 mM Tris-HCl, pH8.5) and ECL solution 2 (5 mM Tris-HCl, pH8.5, 0.064% (v/v) H_2O_2) in a 1:1 ratio and exposed onto Hyper film from Kodax. During all incubations and washings the membrane was agitated continuously using a rocker.

7.2.8 Protein purification

Cells were induced in 250 ml cultures under pre-defined optimum conditions. After a 5 hour induction period, cells were centrifuged at 4500 rpm and the pellet resuspended in 5mls equilibrium buffer (50mM NaH_2PO_4 pH 8.0, 300mM NaCl, 1mM DTT) containing an appropriate volume of mini EDTA free protease inhibitor cocktail (Roche). Cells were lysed using a pre-cooled French press or sonicated. Samples were then centrifuged at 4 °C for 30 minutes at 16000 rpm and the supernatant added to 1 ml of Ni-NTA agarose (Qiagen) for column purification using 5ml polypropylene columns (Qiagen) according to QIAexpressionist™ (Qiagen) guidelines.

7.2.9 Endotoxin removal

Bacterial endotoxins were removed from purified recombinant proteins using ProteoSpin Endotoxin Removal Micro Kit (Norgen BioTech Corp, Canada) following manufacturers guidelines.

7.2.10 ELISPOT assay

Preliminary ELISPOT assays with recombinant proteins were conducted by Dr Potenza (Department of Oncology, Haematology and Respiratory Diseases, University of Modena and Reggio Emilia, Italy) according to a previously described method (Potenza et al. 2007). Written permission from four patients with probable IPA was obtained, and PBMCs were collected. PBMCs were separated using Ficoll-Hypaque gradient centrifugation and then cultured in a 96-well polyvinylidene difluoride-bached plate coated with either anti IFN-γ, anti IL-10 or anti IL-4 monoclonal antibodies. Cells were stimulated with recombinant Asp F4, Asp F10, or negative controls consisting of protein extracted from untransformed C41 *E. coli*. Cells were cultured for 16 hours and cells enumerated using an automated ELISPOT counter (AID-GmbH, Germany). Sample were considered positive if all the following are fulfilled: (1) the presence of at least 20 spot forming cells (SFCs); (2) the presence of more than 5 SFCs in the sample compared with the negative control; (3) the presence of a stimulation index of ≥2 (defined as the ratio of the number of SFCs in the sample to that in the negative control). Test controls were run in conjection with Polymyxin immobilized in the wells of a microtiter plate served as a high affinity adsorbent for lipopolysaccharide (LPS) antigens.

RESULTS

Cloning of Afu2g03830 and Afu5g13300 cDNAs into PRSET A

The plasmid pRSET A (Invitrogen) was utilised to express and purify recombinant Afu2g03830 (Asp F4) and Afu5g13300 (Asp F10). pRSET A is a pUC-derived expression vector designed for high-level protein expression and purification of from cloned genes in *E. coli*. Cloning into the multiple cloning site of pRSET A positions cDNA inserts downstream and inframe of an N-terminal polyhistidine tag which functions as a metal binding domain. Afu2g03830 cDNA was amplified by PCR using Platinum HiFi polymerase (Invitrogen) using primers Asp F4 F and Asp F4 R (Table 6.1) and a comprehensive *A. fumigatus* cDNA library as template. 5 PCR reactions were co-purified using using QIAquick PCR purification Kit (Qiagen, UK). Reverse primers contained the native stop codon to minimise modifications in protein sequence which would be added to the C-terminus by additional DNA in PRSET A. Forward and reverse primers contained BamHI and HindIII restriction sites for cohesive end ligation into PRSET A. Sequential restriction digests using BamHI and HindIII were conducted for the Afu2g03830 cDNA product and pRSET A, and DNA was purified from the reaction mixtures using QIAquick PCR purification Kit (Qiagen, UK). Digested cDNA and vector were ligated in a 3:1 vector:insert ratio, and 5 µl of the reaction mixture was transformed into XL-10 as described in Materials and Methods section 2.3.9. Plasmids were extracted by miniprep (Macherey-Negen, Germany) and ligation of the target flanks into the vector confirmed using BamHI and HindIII restriction digest. Analyses of the digest with gel electrophoresis demonstrated liberation of a PCR product of 969 bp, indicating ligation of the Afu2g03830 cDNA into the vector. The resulting plasmid was named pRSET_3830 and the correct orientation, frame and insert sequence was verified by sequencing using the T7 reverse primer and T7 promoter primer.

Afu5g13300 cDNA was amplified by PCR using Platinum HiFi polymerase (Invitrogen) using primers Asp F10 F and Asp F10 R (Table 7.1) and a comprehensive *A. fumigatus* cDNA library as template. 5 PCR reactions were co-purified using using QIAquick PCR purification Kit (Qiagen, UK). Reverse primers contained the native stop codon to minimise modifications in protein sequence which would be added to the C-terminus by additional DNA in PRSET A. Forward and reverse primers contained BamHI and EcoRI restriction sites for cohesive end ligation into pRSET A. Sequential restriction digests using BamHI and EcoRI were conducted for the Afu5g13300 cDNA product and pRSET A, and DNA was purified from the reaction mixtures using QIAquick PCR purification Kit (Qiagen, UK). Digested cDNA and vector were ligated in a 3:1 vector:insert ratio, and 5 µl of the reaction mixture was transformed into XL-10 as described in Materials and Methods section 2.3.9. Plasmids were extracted by miniprep (Macherey-Negen, Germany) and

ligation of the target flanks into the vector confirmed using BamHI and EcoRI restriction digest. Analyses of the digest with gel electrophoresis demonstrated liberation of a PCR product of 1188 bp, indicating ligation of the Afu5g13300 cDNA into the vector. The resulting plasmid was named pRSET_3300 and the correct orientation, frame and insert sequence was verified by sequencing using the T7 reverse primer and T7 promoter primer.

Pilot protein expression utilising pRSET_3830 and pRSET_3300

Once verified by sequencing, plasmids pRSET_3830 and pRSET_3300 were transformed into competent C41 *E. coli* cells (Miroux and Walker 1996). Prior to full scale purification utilising 200 litre cultures, optimum conditions for protein purification were determined. C41 *E. coli* containing pRSET_3830 or pRSET_3300 were inoculated into 5 mls LB supplemented with 100 µg/ml ampicillin and grown overnight at 37°C. Cells were then diluted to an OD_{580} of 0.1 and grown at 37°C with shaking to an OD_{580} of 0.4 - 0.6. Expression was induced using 50 µM, 200 µM, 350 µM and 500µM IPTG (Sigma). Samples were incubated at 37°C with 180 RPM. 1.5 ml aliquots were taken hourly over 7 hours. Aliquots were then centrifuged to pellet the cells, which were lysed using bacterial protein extraction reagent (BPER, Pierce) or 8 M urea. Samples were then centrifuged at 13000 rpm for 10 minutes. The supernatant was transferred to a new tube and 15 µl samples were boiled for 5 minutes and then run on 10% SDS-PAGE gels. Proteins on SDS-PAGE gels were visualised using Coomassie staining (Figure 7.2).

Proteins of the predicted size were only observed in pilot extractions utilising 8 M urea (Figure 7.2 and data not shown) indicating both proteins are insoluble. Optimal parameters which produced the highest concentration of protein from C41 cells containing pRSET_3830 and pRSET_3300 were 200 µM/ml IPTG induction followed by a minimum of 4 hours expression (Figure 1 and data not shown). Protein concentration did not increase following 5 hours, but more contaminating proteins or some degradation were seen at later time points. Therefore, for full scale protein expression experiments, C41 cells containing pRSET_3830 and pRSET_3300 were expressed for 5 hours.

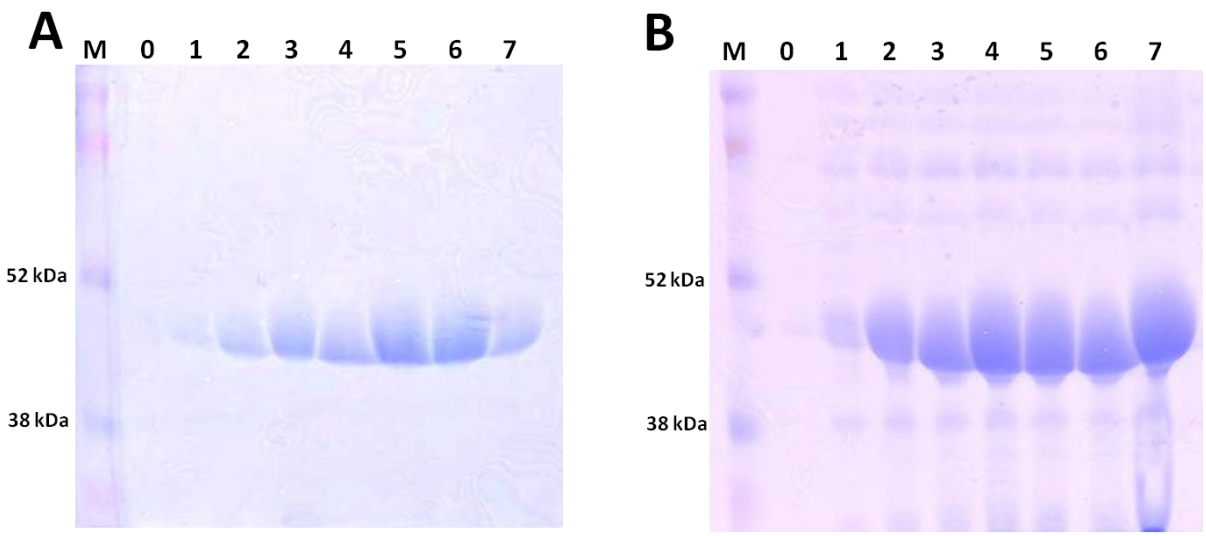


Figure 7.2: Coomassie stained SDS-PAGE gels visualising protein extractions from C41 cells containing pRSET_3830 and pRSET_3300 following IPTG induction. 50 ml cultures of C41 cells containing pRSET_3830 (A) or pRSET_3300 (B) were induced using 200 µM IPTG and expressed at 37°C for 7 hours. Proteins were extracted from 1.5 ml aliquots using 8 M urea, and 15 µl run on SDS-PAGE, which was visualised by Coomassie staining. Lane numbers indicate the duration of expression in hours. The predicted size of the recombinant proteins are 38.3 kDa and 43.5 kDa for pRSET_3830 or pRSET_3300 respectively. A protein of approximately the predicted size was observed in proteins extracted from both pRSET_3830 and pRSET_3300 cultures. The concentration of both proteins increased from 0 - 5 hrs.

Batch purification of Asp F4 and Asp F10 using NiNTA agarose beads

Ni-NTA Agarose Beads (Qiagen) were used for batch purification from 200 ml expression cultures. PAGE showed contaminants were eliminated from the cell lysate by two washing steps (Figure 1A). Proteins were eluted (100 mM NaH_2PO_4, 10 mM Tris HCl, 8 M urea) 4 times in elution buffers at pH 4.5 and 5.9. Both conditions eluted high concentrations of protein with no visible contaminants visible by PAGE analyses. Untransformed cells were treated identically for negative controls (Figure 7.3B). BSA protein quantification showed typical protein concentrations were 700-2000 µg/ml. Western blotting confirmed the presence of the polyhis-tag in the eluted samples (Figure 7.3C). Aliquots of these proteins were used as positive controls for SELDI-ToF-MS anti-his capture (see Chapter 6), which confirmed the sizes of Asp F4 and Asp F10 as 38.2 and 43.5 kDa respectively.

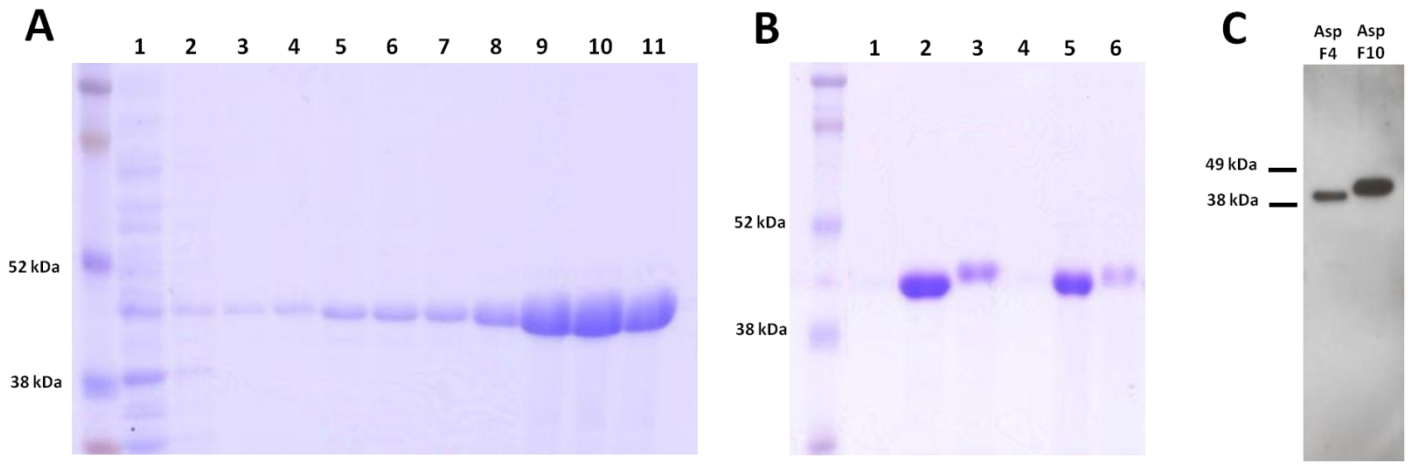


Figure 7.3: Asp F4 and Asp F10 purification under denaturing conditions and verification using Western blotting. A. Batch purification of Asp F4 from 200 ml expression cultures using Ni-NTA Agarose Beads (Qiagen). Contaminants from crude cell lysate (Lane 1) were removed by two washing steps (lanes 2 and 3). Subsequent elutions at pH 4.5 (4-7) and pH 5.9 (8-11) showed lack of non-specific protein in the samples. **B.** PAGE analysis of purified protein (10 µl) from an untransformed negative control (lanes 1 and 4) and Asp F4 (lanes 2 and 5) and Asp F10 (lanes 3 and 6) prior to use in ELISA assays. **C.** Western blot analyses of elutions (10 µg) from NiNTA purification using an antibody directed against the poly-histidine epitope of the recombinant protein

7.3.5 ELISPOT assays using purified recombinant antigens

Analyses of PBMCs stimulated with recombinant Asp F4, Asp F10, negative control and conidial control were conducted as described in section 7.2.10. SFC from IFN-γ, IL-10 and IL-4 are shown in Figure 7.4. SFC were only observed from a single patient out of a total of four with probable IPA.

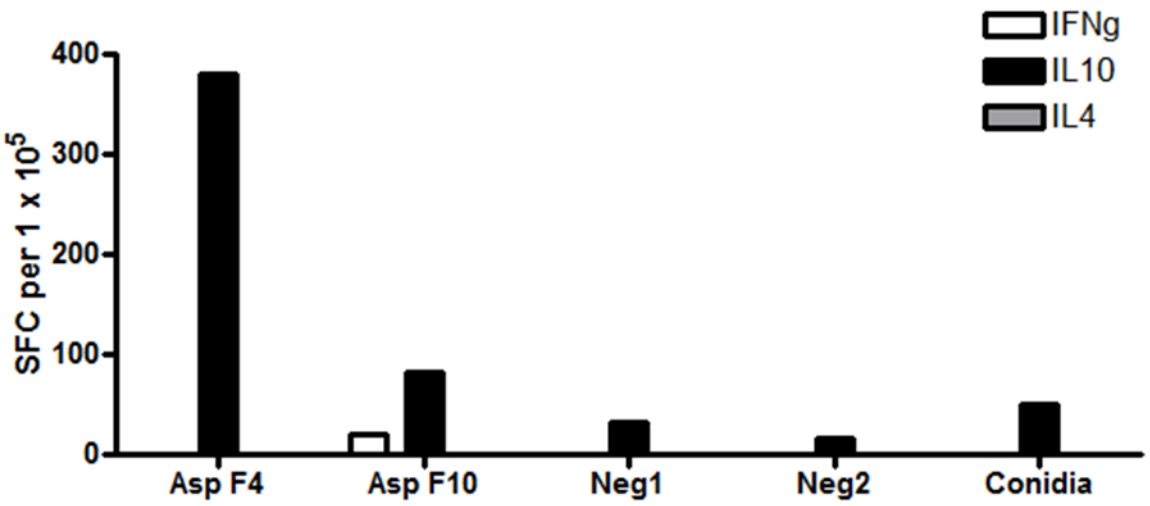


Figure 7.4: IFN-γ, IL-10 and IL-4 ELISPOT assay on PBMC isolated from a single patient with probable IPA. Blood was collected from 4 patients with probable IPA which was stimulated with recombinant Asp F4 or Asp F10 for 16 hours. Additionally, cells were treated with a negative control consisting of protein extracted and purified from non-transformed *E. coli* culture. No IL-4 SFC were observed.

These initial data must be interpreted with caution, as only a single patient demonstrated IL-10 or IFN-γ producing cells in response to the antigens. Additionally, SFC were observed in the negative control consisting of bacterial cell extracts, indicating that some LPS have contaminated the samples, or that residual bacterial proteins in the sample may account for some SFC. Nevertheless, it is notable that in the case of the patient where responses were detected, IL-10 and IFN-γ producing T-cells to Asp F4 and Asp F10 at a level exceeding that provoked by exposure to bacterial cell extracts only, or even *A. fumigatus* conidia. There is, therefore, reason to suggest that the recombinant antigens have the potential to perform better than non-standardised spore extracts, which may possibly reflect the stage-specific expression of these antigens in the host. We therefore hypothesise that further standardisation of the assay and analysis of larger patient cohort is warranted, which is in progress at the time of writing this thesis.

.

7.4 Discussion

Host immune responses to putative *A. fumigatus* antigens are of potential use from both a diagnostic and therapeutic perspective. For example, Potenza and colleagues investigated *Aspergillus* specific T-cells from in putative IPA patients and healthy controls in order to diagnose infection. T-cells were isolated from PBMC which were challenged with heat killed conidia and cytokine responses analysed using ELISPOT (Potenza et al. 2007). Negative control patients demonstrated a Th1 response, with IFN-γ SFC demonstrating Th1 producing T-cells. In contrast IPA patients demonstrated a elevated Th2 response, which was characterised by high numbers of IL-10 producing cells.

With regard to developing immunotherapy against IPA, Perrucchio and colleagues generated donor T-cell clones specific for *A. fumigatus* by treatment with heat killed conidia (Perruccio et al. 2005). Nonrecipient reactive, pathogen-specific $CD4^+$ were adoptively transferred to allo-SCT patients, which resulted in protective high IFN-γ and low IL-10 phenotype relative to untreated controls. Quantity of pathogen-specific T cells remained stable over the study (12 weeks), and immunotherapy was associated with control of *Aspergillus* infection. Work conducted by Tramsen and colleagues has developed a methodology for the rapid generation of anti-*Aspergillus* T-cells, which might be used for adoptive immunotherapy (Tramsen et al. 2009). This has significant advantages over the approach of Potanza and colleagues, as the time to generate anti-*Aspergillus* T-cells took 13 days instead of 25 (Potanza et al. 2007, Tramsen et al. 2009). White blood cells from healthy donors were isolated and stimulated with water soluble *A. fumigatus* conidial extracts. After this, activated cells were isolated by an IFN-γ capture system and clonally expanded. Restimulation of activated T-cells with *A. fumigatus* loaded dendritic cells resulted in a Th1 response, as determined by high IFN-γ production in the absence of IL-10 or IL-4. Thus the authors hypothesised that these anti-aspergillus T-cells may protomote a favourable Th1 response following adoptive transfer. Nevertheless, between these two studies different *A. fumigatus* morphologies were used for antigen stimulation, i.e. heat killed conidia (Perrucchio et al. 2005) and water soluble extract from late stage hyphal growth (Tramsen et al. 2009). Considering both spore and hyphae are encountered by the host immune system, T-cell stimulation and adoptive transfer might benefit from using an antigen which is constitutively expressed by both fungal morphologies *in vivo*. Moreover, Chaudhary and colleagues found antigens isolated from crude preparations generated weak T-cell responses relative to recombinant protein as determined by ELISPOT analysis (Chaudhary et al. 2010). Of interest therefore is the generation of anti-*A. fumigatus* T-cells using recombinant protein which is

putatively biosynthesised by both conidial and hyphal morphologies during infection. One such candidate is allergen Asp F4 (Afu2g03830) which increases between 4 – 8 hours in the host, and remains at this level between 8 – 14 hours (Chapter 3). While transcript abundance of Asp F10 increases between 4 – 8 hours post infection, it is downregulated between 8 – 14 hours. Nevertheless, we hypothesised that it may still be an important element with regard to host-pathogen interactions and adaptive immunity during IPA. To investigate these hypotheses, preliminary ELISPOT assays from PBMC isolated from patients with possible IPA (Figure 7.4) were conducted, which were unsatisfactory as differential cytokine production between recombinant protein and negative controls were only observed for a single patient (Figure 7.4). Additionally, some SFCs were observed in the negative controls, indicating possible LPS contamination. Further standardisation of the assay is currently being completed. Preliminary data suggest that Asp F4 may elicit a strong Th2 response. Although this makes it an unlikely candidate for any immunotherapy, it would be interesting to test healthy PBMCs against this antigen. If there was a differential T-cell response to this antigen (i.e. a Th1 response), this antigen may have potential in diagnosis of IPA. These data also further suggest that proteins transcribed between 4 – 8 hours post infection may contribute to an unfavourable Th2 adaptive response.

CHAPTER 8

Ratiometric comparisons of *A. fumigatus* Af293 and Δ*laeA* during murine infection

8.1 Overview

The microarray experimental design utilised in this thesis permits both ratiometric and non-ratiometric analyses of the Af293 and Δ*laeA* host-infecting fungal transcriptome. It was hypothesised that each approach would reveal specific aspects of the transcriptional basis of *A. fumigatus* host-pathogen interactions. While non-ratiometric normalisation elucidates temporal transcriptional changes throughout infection, ratiometric analyses conducted in this Chapter represents the most appropriate method for determining differential gene expression between isolates at defined time-points of infection.

With regard to determining host responses to *A. fumigatus* infection, gene expression profiling of murine immunity represents a powerful tool which is able to simultaneously profile a diverse range of mammalian defensive strategies. For example, comparative transcriptional profiling of *A. fumigatus* infected lungs from neutropenic and immunocompetent mice by Armstrong-James and co-workers identified modulation of innate immune processes which were associated with murine death and survival respectively (Armstong-James et al. 2009). These authors demonstrated elevated INF-α was associated with survival. In contrast, death from *A. fumigatus* infection is associated with increased levels of interleukin-5, interleukin-17a transcript and TNF-α. These data are consistent with the current paradigm that cellular immunity and a Th1 response is effective at *A. fumigatus* killing, whereas a allergic immunity and inflammation facilitate infection (Romani 2004). Such transcriptional approaches are higher throughput than ELISA based analyses of host cytokines, notwithstanding the fact that mRNA is assessed rather than protein (Brieland et al. 2001, Park and Mehrad 2009). Therefore, transcriptional analysis of the host presents a promising strategy for dissecting differential host responses to Af293 or Δ*laeA*.

In this chapter, comparative gene expression profiling was conducted between Af293 and a Δ*laeA* isolate at three time-points of early host infection. In addition, work presented in this chapter details qRT-PCR analyses of host innate immune responses to each isolate during an invasive stage of disease. These data highlight the importance of host innate immune responses during

the initiation of infection and suggest Δ*laeA* may be attenuated due to the elicitation of a Th1 response which promotes pathogen clearance.

8.2 Methods

8.2.1 *A. fumigatus* strains

A. fumigatus strains used in this chapter are a clinical isolate (please see section 8.3.5 and 8.4) and the Af293Δ*laeA* mutant kindly provided by our collaborator Nancy Keller. The clinical isolate is referred to as Af293. Both strains were stored as glycerol stocks.

8.2.2 Murine infection

Ratiometric analyses conducted in this Chapter utilised the same microarray experiments described in Chapter 3. Murine infections, RNA extractions and microarray data capture are described in sections 3.2.2, 3.2.3 and 3.2.4 respectively.

For host transcriptional profiling, both neutropenic and immunocompetent regimes were utilised. Groups of 7 neutropenic mice were inoculated with 2.5 x 10^9 cfu/ml of Af293 or Δ*laeA* spores (see section 3.2.2). In order to determine the transcriptional effect of cyclophosphomide treatment, a cohort of 7 neutropenic animals were inoculated with sterile saline. Immunocompetent mice were housed in identical conditions but were not subjected to injections, and were intranasally inoculated with 40 µl sterile saline. Saline inoculated immunocompetent mice served as a reference from which gene expression in other cohorts were normalised (see results section). BALFs were extracted at 14 hours post infection. Crude host response BALF samples were stored at -80° and sent for analyses at the JCVI on dry ice.

8.2.3 *A. fumigatus* microarray normalisation

Microarray images were saved as .TIF files and TIGR Spotfinder (Saeed et al. 2003) was used to quantitate fluorescent intensities. Poor quality spots were identified manually and flagged. After Spotfinder analysis, results were exported as TIGR software compatible MEV files following local background subtraction. MEV files were loaded into the JCVI MIDAS normalisation programme where they were normalised by block locally-weighted scatter plot smoothing (LOWESS).
After LOWESS, the flip-dye pairs were combined and a consistency check was applied to remove any spots that did not fall within a specified deviation of the array-wide average $\log_2$ ratio of the fluorescence values for spots on both slides. Following the flip-dye consistency check values underwent inter-slide standard deviation regularisation by averaging the values of the replicate

spots for each gene. MIDAS output files were loaded into Genespring 11.0 software package (Agilent) and intensity values were averaged at each time point. All subsequent statistical testing and data analysis were performed in Genespring 11.0. Genes for which log_2 ratios deviated more than 1.5 stanrd deviations between biological or technical replicates were omitted.

8.2.4 *Mus musculus* host RNA qRT-PCR Super Array analyses

Groups of 7 neutropenic mice were infected with 1 x 10^8 spores from either Δ*laeA*, the Af293 or a sterile saline control. Immunocompetent mice were inoculated with sterile saline. Mice were culled 14 hours post infection and BALFs extracted as described above. Samples were sent on dry ice to our collaborators at the JCVI where groups of BALFs were pooled and RNA extracted using TRIzol (Invitrogen). DNA was removed using Turbo DNase (Ambion) before a final TRIzol purification. Poly A RNA was doubly amplified by Message Amp II aRNA amplification kit (Ambion). cDNA was synthesized using RT² First Strand Kit (SABiosciences) and analysed by QRT-PCR (RotorGene) with Mouse Innate and Adaptive Immune Responses RT² Profiler™ PCR array, Mouse Inflammatory Response and Autoimmunity RT² Profiler™ PCR array and a custom array featuring a further 45 genes of *M. musculus* innate immunity (SABiosciences). Data were loaded into SABiosciences analysis portal with each array treated as a separate experiment (http://pcrdataanalysis.sabiosciences.com/pcr/arrayanalysis.php). Experimental design and normalisation measures are discussed in the results section and depicted in Figure 7.10.

CT values for genes of interest (GOI) were normalised to the most transcriptionally stable housekeeping gene (HKG) across the 4 murine cohorts by calculating ΔCt values (Ct(GOI) - Ct(HKG)). Hypoxanthine guanine phosphoribosyl transferase 1 (Mm.299381) was used for the Mouse Innate and Adaptive Immune Responses RT² Profiler™ PCR array and Mouse Inflammatory Response and Autoimmunity RT² Profiler™ PCR array. For the custom array, the arithmetic mean of glyceraldehyde-3-phosphate dehydrogenase (Mm.343110) and beta actin (Mm.343110) was used.

To facilitate comparisons of gene expression across the infection cohorts and two immunosuppressive regimes, the immunocompetent saline infected mice were used as a common reference sample and fold regulation was calculated relative to this group. Genes where Ct values were undetected in either the control or test group were removed. Additionally, genes where values in both samples were greater than the linear limit of the manufacturer's recommended RT-PCR quantification threshold were considered erroneous and omitted. Finally, genes where a Ct

value in either the control or test sample was greater than the linear limit were retained, following the adjustment of the non-linear value to the linear detection threshold (i.e. a Ct of 35).

Fold changes (2^(-ΔΔCt)) were determined for every gene in each test cohort relative to the common reference, where 2^(-ΔΔCt) is the normalized gene expression (2^(- ΔCt)) in the test sample subtracted from the normalized gene expression (2^(- ΔCt)) in the control. Fold changes were converted to fold regulation, where for values greater than 1, fold-regulation equals fold-change, and for values below 1, fold-regulation equals the negative inverse of the fold-change.

Values were exported as an Excel file, where fold changes were $\log_2$ transformed to reduce variations in sample standard deviation and allow comprehensive cut offs between cohorts (Figure 7.10). These values were considered the final datasets for each qRT-PCR array experiment. Log_2 converted fold changes were compared between groups and gene expression was considered different when a 3 fold or greater difference was observed. Genes represented on duplicate or triplicate arrays had to pass the fold cut off in every replicate or they were omitted. Fold change values of replicates that passed filtering were averaged. A full list of genes represented on each array is available in supplementary materials.

8.3 Results

8.3.1 Comparative histological analyses of Af293 and Δ*laeA* infected lungs

Three groups of 7 neutropenic mice per biological replicate were intranasally inoculated with 1 x 10^8 spores for either Af293 Δ*laeA* or the parental isolate (Figure 8.1). Mice were culled at 4, 8 and 14 hours post infection. Rates of germination, hyphal production, pulmonary lesions and inflammation were monitored using histological analyses in two designated mice at each time point. The Δ*laeA* strain showed reduced rates of germination at 8 hours, and less extensive hyphal production and tissue penetration at 14 hours (Figure 8.1). Additionally, hyphae were found primarily within the bronchioles and larger airways in Δ*laeA* infected lung when compared to Af293. Δ*laeA* infected mice showed marked reduction in inflammation and the severity of pulmonary lesions. A trend toward a reduction in epithelial necrosis was observed at 8 and 14 hours.

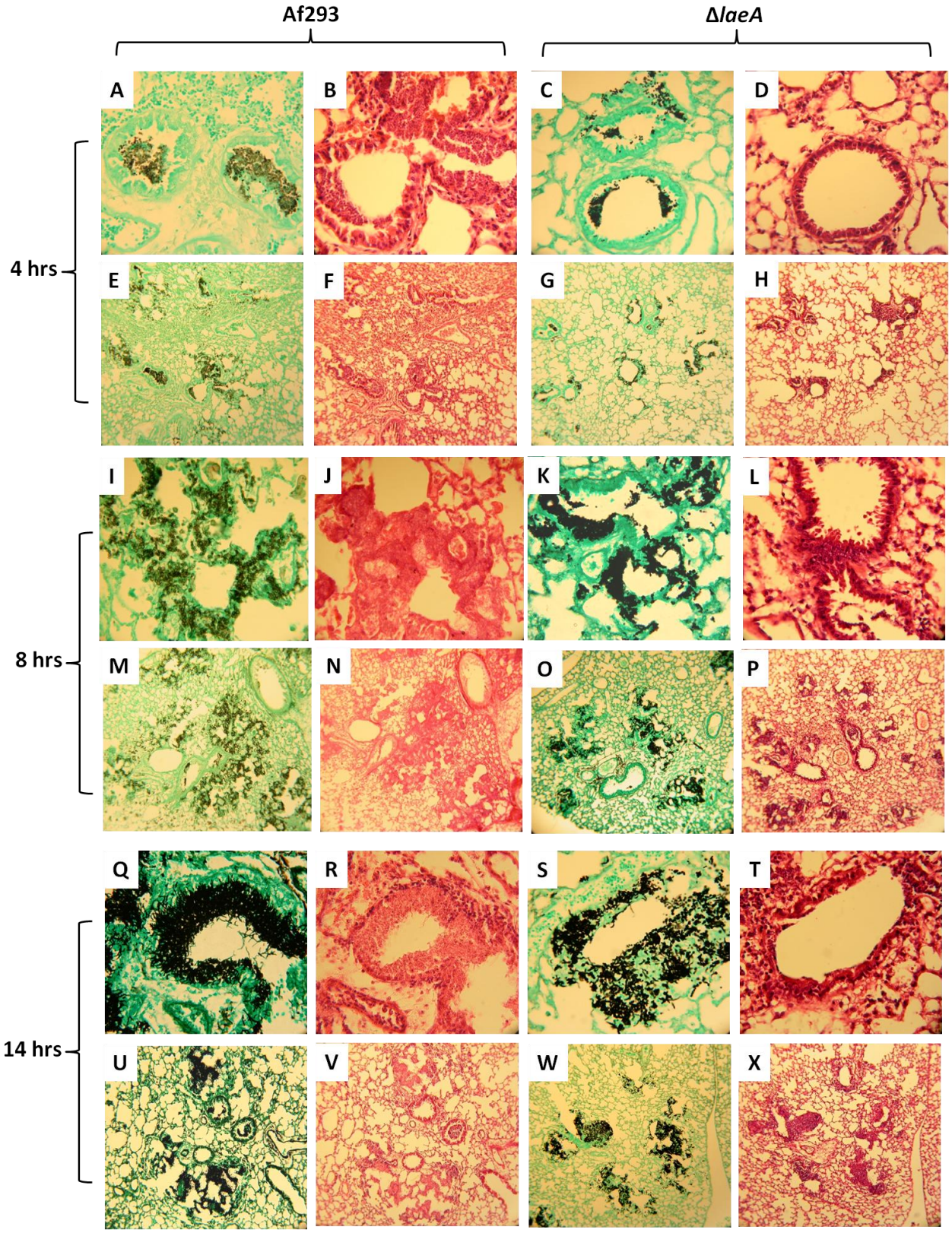


Figure 8.1: Histopathology of mice infected with Af293 and Δ*laeA*.
At 4 hrs, spores were developmentally matched and adhering to lung epithelial cells in both isolates (A and C). In small airways, a trend towards higher inflammation was noted in Af293 (B) compared with Δ*laeA* (D). At 8 hrs germination occurred in both isolates, with higher percentage (approximately 60 %) in Af293 relative to Δ*laeA* (<10 %, panels I and K). Inflammation and epithelial necrosis in Δ*laeA* infected lungs was greater at 8 hrs (L) than 4 hrs (D) but was considerably less than Af293 infected lung comparisons (J). At 14 hours, >90% of Af293 spores has germinated, and germ tube production was pronounced. LaeA showed lower levels of germinated spores (60%), less extensive hyphal production, and were found primarily within the bronchioles (W). Increased inflammation was observed in Af293, and greater levels of epithelial cell necrosis (R). Throughout all stages of infection, large areas of inflammation were noted throughout the Af293 infected lung (F, N and V). Inflammation in Δ*laeA* was limited to local areas of infection which were mainly restricted to the bronchioles (H, P and X).

8.3.2 Ratiometric gene expression profiling of Δ*laeA* relative to Af293 at 4, 8 and 14 hours post infection.

In order to directly compare transcript abundance of the two strains at each time point, double amplified RNA from BALFs was co-hybridised (Δ*lae*A:Af293) on microarrays. Two biological replicates were conducted. A technical replicate was included by co-hybridisation of Af293 and Δ*laeA* cDNA from the first and second biological replicates respectively. A total of 6 arrays were used to analyse each time-point, including dye swap experiments for both biological and the single technical replicate. A schematic depicting microarray hybridisations is given in Figure 1.5. The entire ratiometric normalisation protocol is shown in Figure 8.2. Spot intensities for each array were captured using TIGR Spotfinder, and data were exported as MEV files (Figure 8.2A). Background intensity was subtracted and poor quality spots were manually flagged and removed. Intra-array normalisation of intensity channel values was performed using a LOWESS algorithm in TIGR Microarray Data Analysis System (MIDAS). Figure 8.3 shows microarray (MA) plots before and after LOWESS normalisation for two biological replicate hybridisation experiments at 14 hours post infection. MA plots are used to assess the relation between the Cy3 and the Cy5 channels from a given hybridisation experiment. In these plots the $\log_2$ ratio between red and green channels (Y-axis) is plotted against the sum of red and green channels (X-axis). Un-normalised data have higher spot intensities associated with the green dye (Cy3) and LOWESS normalisation distributes the data more evenly around the X-axis (Figure 8.3).

Following LOWESS normalisation a flip-dye consistency check was applied to corresponding spots from each dye swap replicate (Figure 8.2B). The flip-dye consistency check eliminates fluorescence intensity values which fall outside of a specified deviation of the array-wide average $\log_2$ ratio. Low numbers of spots from the entire experiment (649 out of 215433) failed the dye consistency check, indicating minimal bias of intensity channels. Spot values from flip-dye duplicates were then averaged and exported into Genespring 11.0 (Figure 8.2C). Triplicate intensity values for every gene on each array were averaged. From these values, $\log_2$ ratios of intensity were calculated and reported Δ*laeA*:Af293. Finally, $\log_2$ ratios from two biological and one technical replicate were averaged, to produce a final expression value per gene at each time-point (Figure 8.2C).

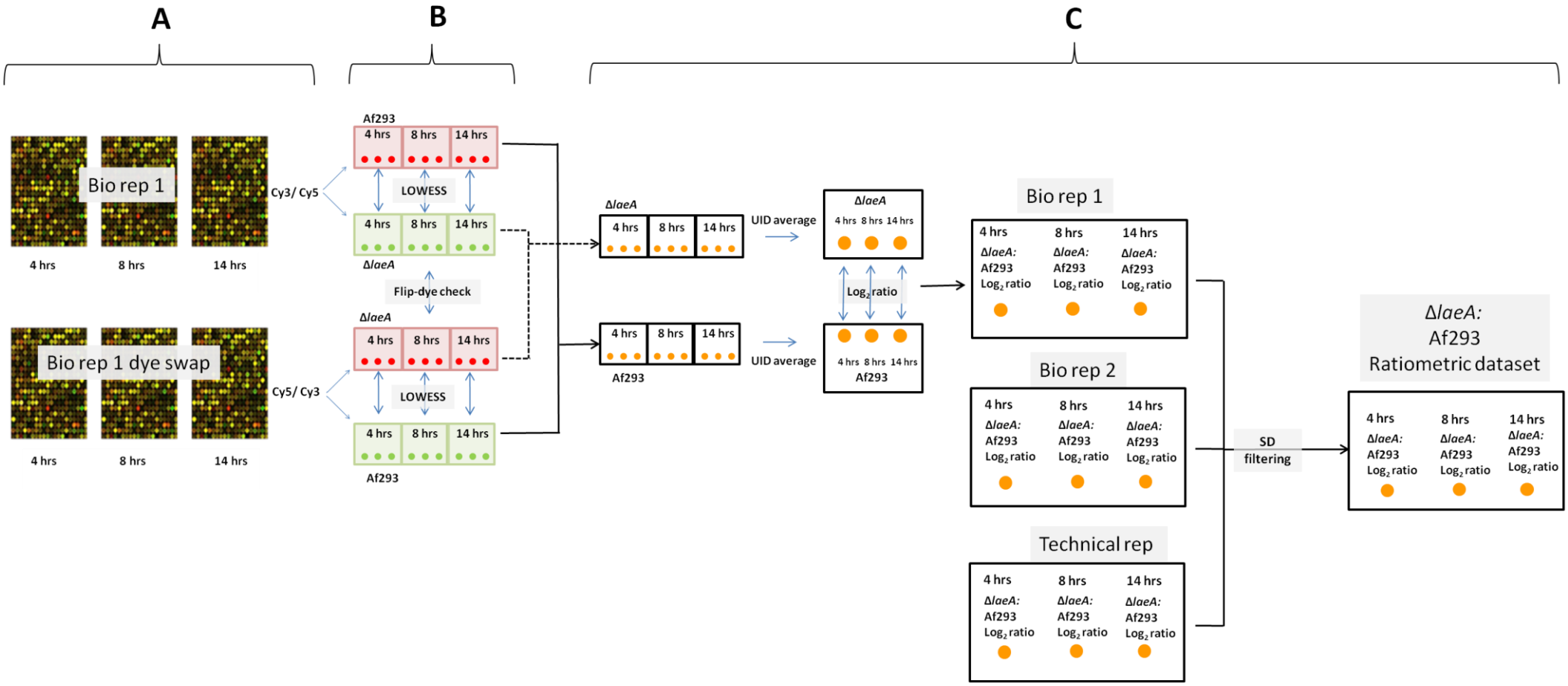


Figure 8.2: Schematic representation of experimental design and ratiometric normalisation for a single gene throughout a comparative time-course of infection study. (A) cDNA from Af293 and Δ*laeA* were co-hybridised in duplicate with dye swap. Data were captured from slides using TIGR Spotfinder, and exported as MEV files. Background intensity was subtracted and poor quality spots were manually flagged and removed. **(B)** Fluorescence intensities for each spot were exported into TM4 MIDAS software. A gene is represented by three spots on each array. Intensity channels were LOWESS normalised and a flip dye consistency check was applied on dye swap duplicates. Next, fluorescence intensity values of dye swap replicates were averaged. **(C)** Datasets were exported into Genespring 11.0. Triplicate spots were averaged to give a single fluorescence intensity value for each array and $\log_2$ ratios were calculated Δ*laeA*:Af293. $\log_2$ ratios from biological replicate 1, biological replicate 2, and the technical replicates were then averaged. Robust gene expression values were defined as those where $\log_2$ ratios which did not vary more than a standard deviation of 1.5 between biological and technical replicate arrays. Thus standard deviation filtering was applied to remove genes with standard deviation >1.5 at each time-point.

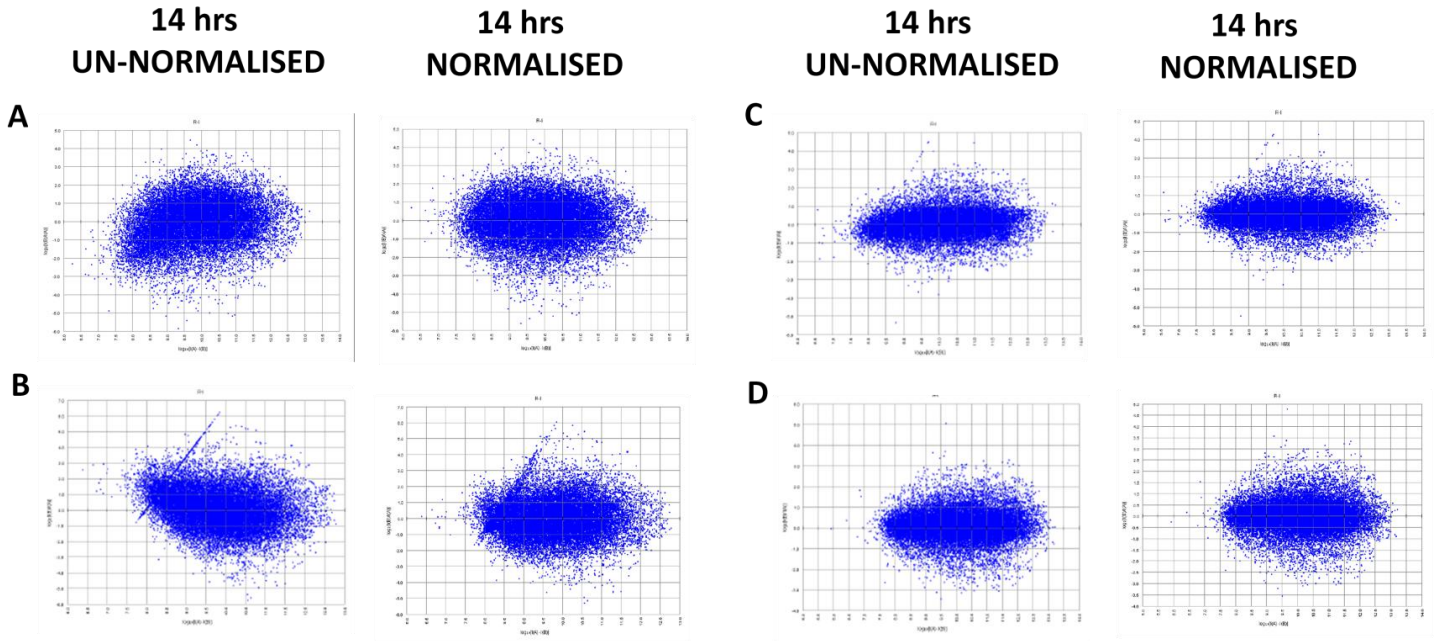


Figure 8.3: MA plot for Af293 Δ*laeA* 14 hrs versus Af293 14 hrs analysis. Dye swap experiments for biological replicate 1 (A and B) and biological replicate 2 (C and D) before and after LOWESS normalisation in MIDAS software are shown.

Figure 8.4 depicts box plots summarising data adjustments at each stage of the normalisation process. A reduction in variance among $\log_2$ ratios is effected between the 18 un-normalised MEV input files (Figure 8.4A) and 9 LOWESS, flip dye checked MIDAS files (Figure 8.4B). Averaging between the replicate experiments (Figure 8.4C) further reduces $\log_2$ ratio variation between time-points. This helps to reduce technical (non-biological) variation throughout the experiment.

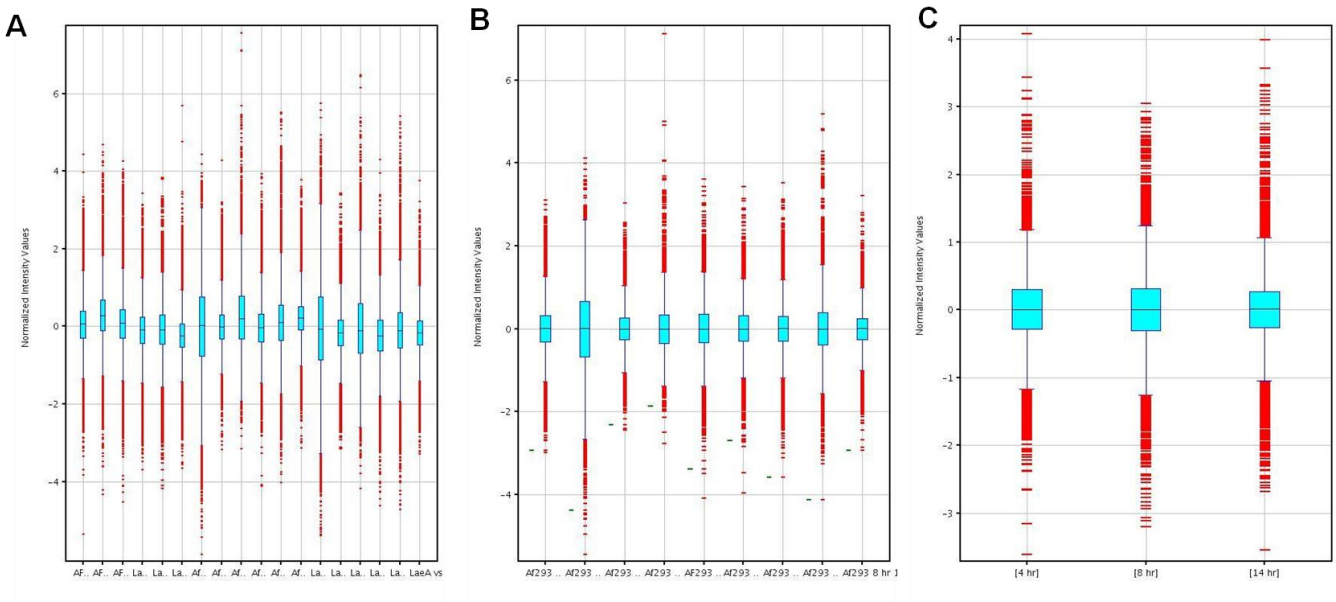


Figure 8.4: Box whisker plots depicting the effect of sequential data normalisations. Un-normalised, background subtracted MEV files (A) show greatest variation between samples. Variance among data distributions is effected by LOWESS normalisation and flip-dye checking (B) and after averaging of replicates at each time point (C). Sample medians are depicted in the middle of the box, which also display the 25th quartile and the 75th quartile. The whiskers are 1.5 times the interquartile and red points outside the whiskers are outliers.

The amount of variation between biological and technical replicates was investigated to measure the reproducibility of the experimentation. Figure 8.5 shows scatter plot comparisons of $\log_2$ ratios between biological (A) and technical (B) replicates after MIDAS normalisation. Scatter plots of $\log_2$ ratios between biological and technical replicates demonstrated greatest variation between biological replicates. This is consistent with the experimental design, as the technical replicate consisted of by co-hybridisation of Af293 and Δ*laeA* cDNA from the first and second biological replicates respectively. All sample comparisons showed robust reproducibility based on correlation coefficients (Table 8.1), which were within the 0.75 to 0.99 range required for deriving biologically meaningful information, based on reports of analytical studies published to date (McDonagh et al. 2008).

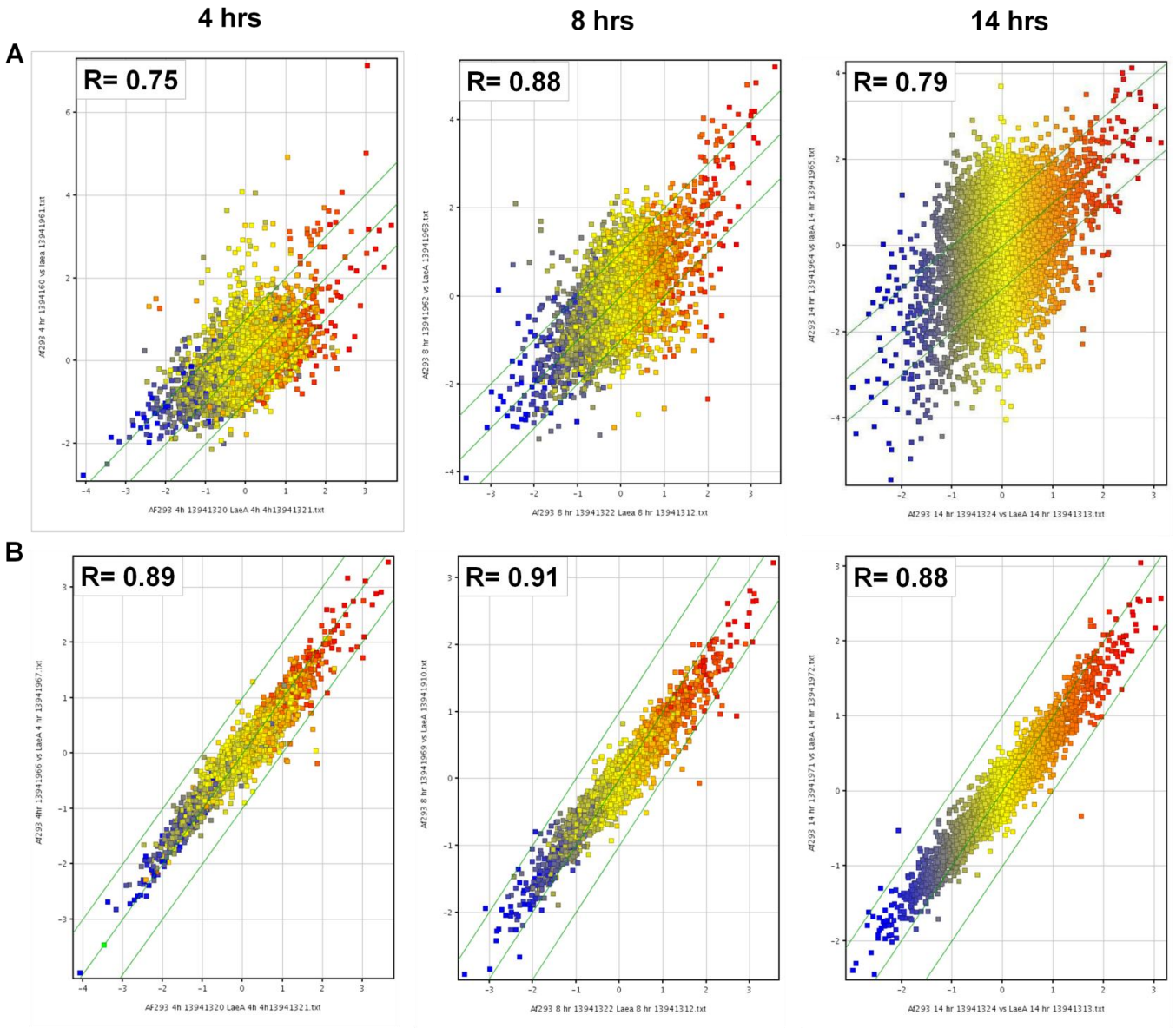


Figure 8.5: Scatter plots depicting variation in log_2 ratios between biological and technical replicates. (A) Log_2 ratios from biological replicate 1 (Y-axis) plotted against log_2 ratios from biological replicate 2 (X-axis) throughout the time-course is shown at each time point. **(B)** Log_2 ratios from technical replicate (Y-axis) plotted against biological replicate 2 (X-axis). Red, blue and yellow colours corresponding to up, down and equally expressed genes respectively. Correlation coefficients are shown in the top left corner of each plot.

Time point		4 hrs			8 hrs			14 hrs		
	Replicate	Bio rep 1	Bio rep 2	Technical	Bio rep 1	Bio rep 2	Technical	Bio rep 1	Bio rep 2	Technical
4 hrs	Bio rep 1	1	0.75	0.82	0.85	0.76	0.82	0.73	0.78	0.82
	Bio rep 2	0.75	1	0.89	0.87	0.96	0.84	0.79	0.94	0.8
	Technical	0.82	0.89	1	0.93	0.89	0.95	0.8	0.88	0.93
8 hrs	Bio rep 1	0.85	0.87	0.93	1	0.88	0.91	0.87	0.87	0.89
	Bio rep 2	0.76	0.96	0.89	0.88	1	0.88	0.8	0.95	0.83
	Technical	0.82	0.84	0.95	0.91	0.88	1	0.78	0.88	0.96
14 hrs	Bio rep 1	0.73	0.79	0.8	0.87	0.8	0.78	1	0.79	0.77
	Bio rep 2	0.78	0.94	0.88	0.87	0.95	0.88	0.79	1	0.88
	Technical	0.82	0.8	0.93	0.89	0.83	0.96	0.77	0.88	1

Table 8.1: Correlation coefficients between experiments. Correlation coefficients between $\log_2$ ratios were used to ascertain reproducibility between biological and technical replicates. Correlation coefficients above 0.75 indicate replicates are sufficiently similar for deriving biological information (Nygaard and Hovig 2006).

Fluorescence signals from 8404, 8416 and 8443 out of a possible 9516 represented ORFs passed quality control and flagging for analyses at 4, 8 and 14 hours respectively (summarised in Table 8.2).

	4 hr	8 hr	14 hr
Observations	8404	8416	8443
Missing Values	374	362	335
Minimum	-3.60	-3.54	-3.19
Maximum	4.09	3.99	3.05
Mean	0.00986	-0.00303	-0.00347
Median	0.00576	0.01136	0.00981
Standard deviation	0.54	0.54	0.60
Outliers	422	511	422

Table 8.2: Summary statistics for the Δ*laeA* versus Af293 time course during initiation of murine infection. Statistics are based on Genespring 11.0 files. Thus, $\log_2$ ratios depicted are averaged from biological replicates 1, 2 and the technical replicate. Mean and median $\log_2$ ratios approximate zero, which are consistent with the hypothesis that the majority of genes are not differentially expressed between isolates.

Preliminary interrogations of the dataset were conducted using student t-tests. Differentially expressed transcripts at each time point were defined as having $\log_2$ (Δ*lae*A:Af293) ratios greater than an arbitrary threshold of ±1.5. A t-test was applied, whereby the null hypothesis states that a given sample mean does significantly differ between strains. Transcripts passed as statistically significant with a corrected *p*-value < 0.05. This identified 243 differentially expressed genes (2.5%

of the *A. fumigatus* genome) which are summarised in Table 8.3. However, it was reasoned that given the stringency of the approach, biologically meaningful data might have been lost.

	Up	Down	Differentially Expressed
Total	119	124	243
4 hrs	50	53	103
8 hrs	66	79	145
14 hrs	88	52	140

Table 8.3: Number of differentially expressed genes for Af293 Δ*laeA* versus Af293 time-course during initiation of murine infection, based on students t-test. Differentially expressed transcripts at each time point were defined as having $\log_2$ (Δ*lae*A:Af293) ratios greater than an arbitrary threshold of ±1.5. A t-test against zero was applied, with the null hypothesis that a gene was not differently expressed between strains. Transcripts passed as statistically significant with a corrected *p*-value ≤ 0.05.

A method was therefore adopted which analysed fold change between isolates after removal of genes with unacceptably high variation between replicates. This approach has been used for *in vivo* comparisons of *C. albicans* isolates during murine liver infection (Thewes et al. 2007). Robust gene expression values were defined as those whose normalised value which did not vary more than a standard deviation of 1.5 between the biological and technical replicates (Figure 8.4C). This criterion filtered 29, 14 and 71 genes with unacceptably high variation at 4, 8 and 14 hours respectively. Differentially expressed transcripts at each time point were defined as having $\log_2$ ratios (Δ*lae*A:Af293) greater than an arbitrary threshold of ±1.5. Using this method, 293 genes (3.0% of the *A. fumigatus* genome) were differentially expressed between Δ*laeA* and Af293 throughout the time-course. Venn diagrams depicted in Figure 8.6 demonstrate distribution of differentially expressed genes between Δ*laeA* and Af293 at each stage of infection. All 243 genes with significant *p*-values from the student t-test were featured in the standard deviation corrected dataset, indicating that this approach is statistically robust. We therefore used the SD corrected dataset for all downstream analyses. Genes with increased and decreased transcript abundance are listed in tables 8.5 and 8.6 respectively.

	Up	Down	Differentially Expressed
Total	130	163	243
4 hrs	65	60	125
8 hrs	83	86	169
14 hrs	103	107	210

Table 8.4: Number of differentially expressed genes for Af293 Δ*laeA* versus Af293 time course during initiation of murine infection, based on standard deviation corrected data with a fold change of ±1.5 between isolates. Following standard deviation filtering, differentially expressed transcripts at each time point were defined as having $\log_2$ (Δ*lae*A:Af293) ratios greater than an arbitrary threshold of ±1.5.

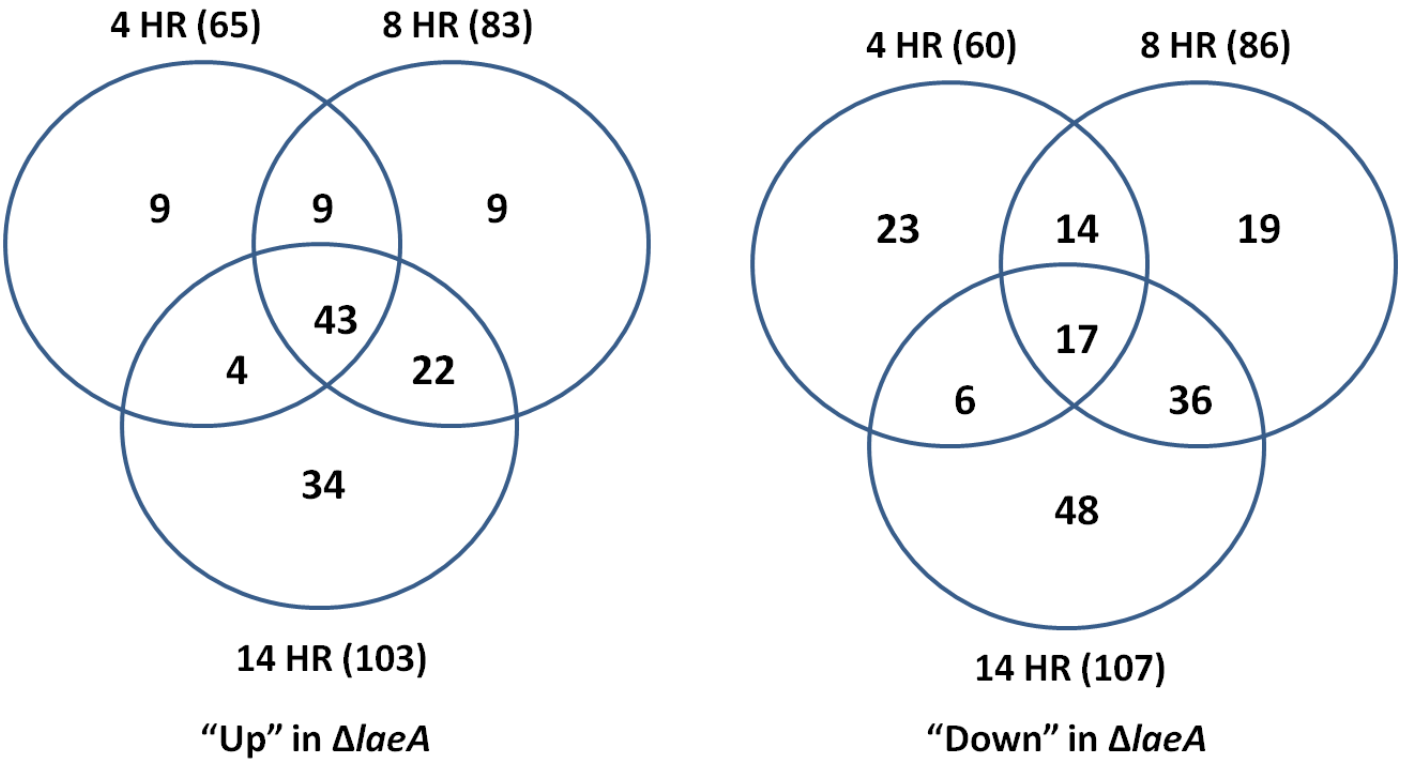


Figure 8.6: Venn diagrams depicting distribution of differentially expressed genes between the Δ*laeA* and Af293 throughout the time course of infection. 43 and 17 genes demonstrated increased and decreased transcript abundance at all stages of infection respectively.

Table 8.5: Genes with increased transcript abundance in Δ*laeA* relative to Af293 throughout the time course of infection. Time points highlighted in red pass standard deviation correction filtering and a 1.5 log_2 ratio cut-off. Values which failed this filter are left un-shaded

ORF	4 hrs	8 hrs	14 hrs	Description	Functional classification
Afu2g01170	2.02	2.18	1.71	1,3-beta-glucanosyltransferase Gel1	cell wall organization///fungal-type cell wall///1,3-beta-glucanosyltransferase activity///biological process unknown///molecular function unknown
Afu3g02480	1.59	2.70	2.33	C6 transcription factor, putative	regulation of transcription
Afu8g00610	2.35	1.85	2.02	cell surface protein Mas1, putative	-
Afu3g11670	1.73	1.88	1.85	DDE superfamily endonuclease/transposase, pseudogene	-
Afu7g00270	2.56	2.61	2.81	FAD binding monooxygenase, putative	cellular aromatic compound metabolic process///monooxygenase activity
Afu4g14390	3.13	3.33	3.06	Fot5 transposase, putative	-
Afu2g18080	1.83	2.53	1.96	LINE-1 class reverse transcriptase, RNaseH, putative	-
Afu3g09430	2.01	2.50	2.02	LINE-1 class reverse transcriptase, RNaseH, putative	-
Afu3g15370	2.08	2.33	1.81	LINE-1 class reverse transcriptase, RNaseH, putative	-
Afu4g14870	1.98	2.32	1.72	LINE-1 class reverse transcriptase, RNaseH, putative	-
Afu5g00270	2.39	3.24	2.24	LINE-1 class reverse transcriptase, RNaseH, putative	-
Afu6g00780	2.04	2.27	1.77	LINE-1 class reverse transcriptase, RNaseH, putative	-
Afu7g00100	2.73	3.57	2.56	LINE-1 class reverse transcriptase, RNaseH, putative	-
Afu8g00310	1.84	2.56	1.73	LINE-1 class reverse transcriptase, RNaseH, putative	-
Afu8g06290	2.18	2.67	1.91	LINE-1 class reverse transcriptase, RNaseH, putative	-
Afu3g03740	2.15	2.14	1.89	protein kinase, putative	-
Afu6g14660	2.12	2.49	1.90	reverse transcriptase, RNaseH	-
Afu6g09470	1.71	2.49	1.93	reverse transcriptase, RNaseH, putative	-
Afu3g01030	1.66	2.11	2.79	RTA1 domain protein, putative	biological process unknown///molecular function unknown///integral to

					membrane
Afu6g03370	1.72	1.77	1.85	short-chain dehydrogenase/reductase, putative///oxidoreductase, short-chain dehydrogenase/reductase family	lipid particle///cytoplasm///endoplasmic reticulum///acylglycerone-phosphate reductase activity///phosphatidic acid biosynthetic process
Afu7g00260	1.97	2.51	2.37	squalene-hopene-cyclase, putative	lipid particle///squalene-hopene cyclase activity///plasma membrane///hopanoid biosynthetic process///endoplasmic reticulum///lanosterol synthase activity///ergosterol biosynthetic process
Afu5g06130	2.75	2.47	2.21	succinyl-CoA synthetase alpha subunit, putative	tricarboxylic acid cycle///succinate-CoA ligase (ADP-forming) activity///mitochondrion///succinyl-CoA metabolic process
Afu6g14130	1.87	1.96	1.65	ubiquitin conjugating enzyme, putative	ubiquitin-protein ligase activity///ER-associated protein catabolic process///endoplasmic reticulum///ubiquitin conjugating enzyme activity
Afu7g08400	2.68	3.13	2.48	ankyrin repeat protein	-
Afu7g08640	2.05	2.16	1.76	BTB/POZ domain protein	-
Afu1g00230	1.63	2.26	1.95	conserved hypothetical protein	-
Afu3g13750	1.84	2.17	1.92	conserved hypothetical protein	-
Afu5g10960	2.80	2.43	1.79	conserved hypothetical protein	-
Afu5g12090	1.59	2.14	1.90	conserved hypothetical protein	cellular component unknown///biological process unknown///molecular function unknown
Afu6g03330	2.78	2.42	1.93	conserved hypothetical protein	-
Afu7g02160	3.45	3.09	2.93	DDE superfamily endonuclease/transposase	-
Afu3g11180	1.62	1.91	1.65	DNA binding protein	-
Afu3g12410	2.00	2.06	1.97	DNA binding protein	-
Afu1g00210	3.13	3.31	2.64	hypothetical protein	-
Afu6g09460	2.66	3.99	2.84	hypothetical protein	-
Afu6g11780	2.61	2.06	2.70	hypothetical protein	-
Afu7g08520	2.88	3.19	2.77	hypothetical protein	-
Afu7g08570	2.89	3.04	2.52	hypothetical protein	-
Afu7g08630	1.97	2.26	1.91	hypothetical protein	-
Afu8g02250	1.88	2.03	1.73	hypothetical protein	-
Afu6g00510	1.68	2.19	1.82	NADP-dependent alcohol dehydrogenase	alcohol metabolic process///soluble fraction///alcohol dehydrogenase (NADP+) activity
Afu5g14820	2.07	2.17	2.43	replication factor C subunit	leading strand

					elongation///DNA replication factor C complex///DNA clamp loader activity///sister chromatid cohesion///mismatch repair///nucleus///ATPase activity
Afu3g03100	1.79	2.14	2.14	hypothetical protein	-
Afu3g04290	2.56	2.55	1.48	-	-
Afu8g01040	2.08	2.51	1.54	reverse transcriptase, RNaseH	-
Afu7g08620	1.72	2.33	1.45	hypothetical protein	-
Afu3g00180	2.69	2.15	1.23	short chain dehydrogenase (AtsC), putative///short chain dehydrogenase, putative	-
Afu6g00430	2.47	1.79	0.99	IgE-binding protein	-
Afu4g08530	1.73	1.72	1.21	WD repeat protein	-
Afu5g14860	1.62	1.71	1.48	cytochrome P450	-
Afu8g06390	1.61	1.69	1.17	hypothetical protein	-
Afu1g01930	1.61	1.65	1.26	MFS multidrug transporter, putative	-
Afu1g00530	3.25	2.96	2.50	thermoresistant gluconokinase family protein	-
Afu8g05780	1.19	1.78	2.25	NACHT and Ankyrin domain protein	-
Afu5g01340	1.50	1.76	2.58	lysophospholipase Plb2///lysophospholipase, putative	-
Afu1g00760	1.43	2.39	1.85	hypothetical protein	-
Afu5g09770	1.56	2.29	2.39	hypothetical protein	-
Afu3g13180	1.26	1.59	1.81	hypothetical protein	-
Afu4g14630	1.50	1.69	2.23	FAD binding domain protein	-
Afu8g06180	1.45	1.94	1.65	DOC family protein	-
Afu8g06140	1.53	1.92	1.69	sensor histidine kinase/response regulator, putative	-
Afu4g00820	1.43	2.76	1.81	reverse transcriptase, RNaseH	-
Afu1g02480	1.50	1.74	2.25	plasma membrane ATPase, putative///P-type ATPase, putative	-
Afu8g06210	1.38	1.76	1.95	metalloreductase transmembrane component, putative	-
Afu1g17110	0.86	1.87	1.73	long chain fatty alcohol oxidase, putative	-
Afu8g01390	1.28	1.68	1.81	glycosyl hydrolase, putative///glycosyl hydrolase, family 15	-
Afu1g00500	4.09	2.90	2.85	FMN dependent dehydrogenase, putative	-
Afu3g14980	0.49	1.81	1.85	extracellular chitosanase CsnC, putative	-
Afu2g14540	0.52	1.70	1.68	endoglucanase, putative	-
Afu3g01420	1.46	1.97	1.68	DUF341 domain	-

				oxidoreductase, putative///DUF341 family oxidoreductase, putative	
Afu2g00470	1.22	1.60	1.60	C6 transcription factor, putative	-
Afu3g06540	1.44	2.01	1.77	3'-phosphoadenosine-5'-phosphosulfate reductase Met16, putative///3'-phosphoadenosine-5'-phosphosulfate reductase	-
Afu1g17380	0.80	1.60	1.91	3-oxoacyl-(acyl-carrier-protein) reductase, putative	-
Afu3g04080	1.52	2.13	1.65	hypothetical protein	-
Afu7g04950	1.84	0.98	1.55	lipase, putative	-
Afu7g07070	1.61	1.58	1.38	LINE-1 class reverse transcriptase, RNaseH, putative	-
Afu2g02390	1.69	1.19	1.30	hypothetical protein	-
Afu2g02940	1.60	1.06	1.01	hypothetical protein	-
Afu6g14010	1.62	1.55	1.37	GPI anchored protein, putative	-
Afu7g06920	1.79	1.39	1.14	conserved hypothetical protein	-
Afu6g13670	1.75	0.71	0.87	conserved hypothetical protein	endoplasmic reticulum///biological process unknown///molecular function unknown
Afu6g10650	1.65	1.47	1.25	ATP citrate lyase, subunit 1, putative	ATP citrate synthase activity
Afu1g10930	2.07	0.19	-0.84	ammonium transporter///ammonium transporter (Mep2), putative	pseudohyphal growth///plasma membrane///ammonium transport///ammonium transmembrane transporter activity
Afu4g12050	1.10	1.68	1.37	thermoresistant gluconokinase///thermoresistant gluconokinase family protein	cytoplasm///biological process unknown///molecular function unknown
Afu1g17670	1.04	1.92	0.99	salicylate hydroxylase, putative	cellular aromatic compound metabolic process///monooxygenase activity
Afu5g03540	1.31	1.59	1.04	pyridine nucleotide-disulphide oxidoreductase, class II, putative	-
Afu3g02110	1.27	1.73	1.57	MFS efflux transporter, putative///MFS multidrug transporter, putative	membrane///transporter activity///transport
Afu1g00120	1.37	1.69	1.20	hypothetical protein	-
Afu2g01260	0.89	1.64	1.18	HLH transcription factor, SrbA	transcription factor activity///nucleus
Afu8g02030	1.27	1.69	1.45	conserved hypothetical protein	-
Afu7g08330	0.96	1.82	1.31	-	-
Afu3g11680	1.45	1.68	1.34	-	-
Afu3g00620	0.80	1.15	1.85	zinc-containing alcohol dehydrogenase, putative	cellular component unknown///oxidoreductase activity///metabolic process///zinc ion binding

Afu6g10900	0.39	0.89	1.64	UV-endonuclease UVE-1	-
Afu6g03420	0.60	0.55	1.79	trehalose synthase, putative	-
Afu8g04550	1.44	1.48	1.83	sulfonate biosynthesis enzyme, putative	-
Afu4g01020	0.88	1.13	1.74	sensor histidine kinase/response regulator, putative	protein histidine kinase activity///two-component sensor activity///protein amino acid phosphorylation
Afu3g00250	1.49	1.31	2.33	salicylate hydroxylase, putative	oxidoreductase activity///metabolic process///FAD binding
Afu5g14810	1.29	1.21	2.46	pyruvate decarboxylase, putative	cytoplasm///glucose catabolic process to ethanol///nucleus///pyruvate metabolic process///pyruvate decarboxylase activity
Afu4g08120	1.02	1.16	1.64	protease inhibitor (Tfs1), putative	peptidase inhibitor activity///regulation of proteolysis///soluble fraction///lipid binding
Afu2g11220	1.10	1.31	2.10	proline permease, putative	plasma membrane///neutral amino acid transmembrane transporter activity///neutral amino acid transport///amino acid permease activity
Afu2g04320	0.47	1.25	1.71	NADH-dependent flavin oxidoreductase, putative	NADPH dehydrogenase activity///cytoplasm///nucleus/// biological process unknown
Afu8g01340	0.55	1.03	1.72	MFS sugar transporter, putative	alpha-glucoside:hydrogen symporter activity///alpha-glucoside transport///membrane fraction
Afu6g05280	1.15	0.76	1.64	mei2 protein	-
Afu4g14640	0.73	1.37	2.02	low affinity iron transporter, putative	iron ion transmembrane transporter activity///low-affinity iron ion transport///integral to plasma membrane///intracellular copper ion transport
Afu5g14800	0.92	1.22	1.62	lactate dehydrogenase	-
Afu7g05050	-0.03	0.89	1.82	hypothetical protein	-
Afu2g14330	0.78	0.95	1.74	hypothetical protein	-
Afu5g14080	1.10	0.89	1.71	hypothetical protein	-
Afu5g00240	0.99	1.15	1.62	hypothetical protein	-
Afu4g00450	0.64	0.93	1.62	hypothetical protein	-
Afu4g00730	-0.12	0.14	1.72	HHE domain protein	-
Afu6g12240	1.31	1.39	1.66	Glycerophosphoryl diester phosphodiesterase family family	-
Afu4g13120	0.94	1.00	1.73	glutamine synthetase	glutamine biosynthetic process///cytoplasm///glutamate-ammonia ligase activity///nitrogen compound metabolic process
Afu6g00450	1.13	1.46	2.13	feruloyl esterase, putative	-
Afu3g01810	0.51	0.68	1.79	F-box domain protein	-
Afu7g08580	1.33	1.45	1.60	dynamin GTPase, putative	membrane fraction///vacuolar

					transport///protein retention in Golgi apparatus///GTPase activity///peroxisome organization///protein targeting to vacuole
Afu8g00600	0.47	1.52	1.84	conserved hypothetical protein///NAD dependent epimerase/dehydratase family protein	nucleotide-sugar metabolic process///NAD or NADH binding
Afu6g11670	0.59	1.53	2.35	conserved hypothetical protein	-
Afu6g03210	1.26	1.00	1.91	conidiation-specific protein 10	-
Afu2g04880	0.86	1.14	1.66	cell wall biogenesis protein, putative///DUF77 domain protein	cell wall organization///cytoplasm///nucleus///molecular function unknown
Afu7g06900	1.17	1.51	1.79	branched-chain amino acid aminotransferase, putative	-
Afu3g02090	0.11	0.75	1.98	beta-xylosidase, putative///beta-xylosidase	carbohydrate metabolic process///"hydrolase activity, hydrolyzing O-glycosyl compounds"
Afu5g09440	1.04	1.32	2.30	amino acid permease, putative	-
Afu7g04930	0.69	0.33	1.71	alkaline serine protease (PR1)/allergen F18-like///alkaline serine protease (PR1), putative	peptidase activity///cellular component unknown///protein catabolic process
Afu6g03410	1.00	0.50	1.60	-	-
Afu8g05770	2.03	1.50	2.27	hypothetical protein	-
Afu1g00290	1.59	1.18	1.93	hypothetical protein	-
Afu5g00250	1.68	1.57	1.65	hypothetical protein	-
Afu3g14540	2.22	1.10	1.78	heat shock protein Hsp30/Hsp42, putative///"heat shock protein HSP30, putative"	-

Table 8.6: Genes with decreased transcript abundance in Δ*laeA* relative to the wild type throughout the time course of infection. Time points highlighted in green pass standard deviation correction filtering and a 1.5 $\log_2$ ratio cut off. Values which failed this filter are left un-shaded

ORF	4 hrs	8 hrs	14 hrs	Description	Functional classification
Afu7g06140	-1.78	-2.05	-1.91	beta-D-glucoside glucohydrolase	-
Afu4g09920	-1.90	-2.06	-2.08	conserved hypothetical protein	-
Afu8g07080	-2.20	-2.67	-1.95	elastinolytic metalloproteinase Mep	endopeptidase activity///pathogenesis
Afu3g03280	-1.80	-1.79	-2.30	FAD binding monooxygenase, putative	-
Afu4g00370	-2.13	-2.54	-2.31	general amidase, putative	cellular component unknown///amidase activity///biological process unknown
Afu3g01580	-2.07	-1.69	-2.20	GMC oxidoreductase, putative	oxidoreductase activity///metabolic process

Afu1g17660	-2.26	-1.87	-1.92	histidinol dehydrogenase, putative	histidinol dehydrogenase activity///cell///histidine biosynthetic process
Afu3g03810	-3.60	-2.67	-2.88	hypothetical protein	-
Afu1g03330	-2.64	-3.54	-3.19	hypothetical protein	-
Afu7g06240	-1.98	-2.62	-1.88	hypothetical protein	-
Afu7g08300	-1.66	-2.19	-2.14	hypothetical protein	-
Afu4g14610	-1.82	-1.60	-1.62	MFS sugar transporter, putative	membrane///transporter activity///transport
Afu6g09970	-1.70	-1.96	-2.08	oxidoreductase, short chain dehydrogenase/reductase family	-
Afu1g16930	-2.06	-2.26	-2.17	phosphatidylserine decarboxylase, putative	Golgi membrane///phosphatidylserine decarboxylase activity///fungal-type vacuole membrane///phosphatidylcholine biosynthetic process
Afu5g14690	-1.87	-1.62	-1.78	phosphorylase, putative	-
Afu6g00160	-2.16	-2.46	-2.49	Ser/Thr protein phosphatase family protein	phosphate metabolic process///fungal-type vacuole///phosphoric ester hydrolase activity
Afu2g13620	-2.08	-1.94	-1.71	thiamine pyrophosphate enzyme, putative	-
Afu5g02940	-1.88	-2.48	-2.82	choline transport protein Ctr, putative	plasma membrane///choline transmembrane transporter activity///choline transport
Afu7g06380	-2.28	-2.44	-1.36	maltase	alpha-glucosidase activity///cellular component unknown///maltose catabolic process
Afu3g12900	-2.04	-2.44	-2.70	MFS transporter, putative///monocarboxylate transporter (Mch4), putative	fungal-type vacuole membrane///monocarboxylic acid transmembrane transporter activity///transporter activity///transport
Afu3g03640	-2.65	-2.14	-1.50	siderochrome-iron transporter (MirB), putative///MFS siderochrome iron transporter MirB	siderophore-iron transport///siderophore-iron (ferrioxamine) uptake transmembrane transporter activity///cellular iron ion homeostasis///integral to membrane
Afu7g07050	-1.63	-2.11	-1.36	hypothetical protein	-
Afu5g00420	-1.87	-2.06	-2.62	MFS transporter, putative	drug transport///drug transporter activity///transporter activity///transport///integral to membrane
Afu7g00410	-1.74	-1.95	-1.53	C6 transcription factor, putative	DNA binding///zinc ion binding
Afu6g05030	-1.74	-1.84	-1.22	polysaccharide deacetylase family protein	-
Afu3g11790	-2.36	-1.79	-1.57	galactose-proton symport, putative	myo-inositol transport///membrane///myo-inositol transmembrane transporter activity
Afu2g05360	-3.14	-1.70	-1.38	C6 transcription factor, putative	transcription factor activity///regulation of

					transcription
Afu8g06470	-2.21	-1.62	-0.30	N,N-dimethylglycine oxidase///N,N-dimethylglycine oxidase, putative	aminomethyltransferase activity
Afu2g09450	-2.38	-1.62	-0.92	carboxylic acid transport protein	lactate transmembrane transporter activity///lactate transport///plasma membrane
Afu1g15330	-2.21	-1.61	-1.53	T10O22.24	-
Afu3g00730	-1.66	-1.60	-3.10	conserved hypothetical protein	-
Afu5g15070	-1.42	-2.35	-1.63	AhpC/TSA family thioredoxin peroxidase, putative	-
Afu5g01910	-1.52	-2.27	-2.48	aldo-keto reductase (AKR), putative	-
Afu6g02030	-1.02	-1.68	-1.82	aminotransferase, putative	-
Afu8g01710	-0.83	-1.74	-2.04	antigenic thaumatin domain protein, putative	-
Afu6g14490	-1.10	-1.60	-1.59	beta-glucosidase, putative	-
Afu6g13770	-1.14	-1.68	-1.66	C6 finger domain protein, putative	-
Afu3g12890	-1.45	-1.71	-1.62	C6 transcription factor GliZ-like, putative///C6 transcription factor (GliZ), putative	-
Afu5g14230	-0.33	-1.63	-1.70	C6 transcription factor, putative	-
Afu6g12160	-0.85	-2.13	-2.16	C6 transcription factor, putative	-
Afu2g09350	-0.92	-1.60	-2.12	endo-beta-1,6-glucanase, putative	-
Afu7g08660	-1.05	-1.78	-1.63	Fot1 family transposase, putative	-
Afu3g05620	-1.12	-1.87	-1.71	Fot1 family transposase, putative	-
Afu1g00140	-1.51	-2.10	-2.14	Fot5 transposase, putative	-
Afu1g01300	-0.81	-1.68	-2.20	GPI anchored protein, putative	-
Afu6g08490	-0.61	-2.59	-3.06	inorganic diphosphatase, putative	-
Afu5g02700	-0.30	-1.68	-1.92	MFS multidrug transporter, putative///multidrug resistant protein	-
Afu4g14670	-1.06	-1.96	-1.61	MFS quinate transporter, putative	-
Afu5g09910	-1.34	-1.89	-2.76	pnitroreductase family protein, putative///nitroreductase family protein, putative	-
Afu4g00660	-1.39	-1.68	-1.68	sensor histidine kinase/response regulator, putative	-
Afu3g00720	-1.38	-1.89	-2.92	DUF500 and UBA/TS-N domain protein	-
Afu8g06560	-1.15	-1.62	-1.85	DUF895 domain membrane protein	-
Afu7g05010	-1.50	-1.90	-1.86	glyoxalase family protein	-
Afu3g13740	-1.54	-2.30	-2.64	HSP70 family protein	-

Afu8g06590	-0.35	-1.69	-1.76	hypothetical protein	-
Afu7g00400	-0.84	-1.76	-1.65	hypothetical protein	-
Afu7g07040	-1.18	-1.85	-1.67	hypothetical protein	-
Afu5g00190	-1.23	-1.86	-1.69	hypothetical protein	-
Afu8g06960	-1.39	-1.89	-1.70	hypothetical protein	-
Afu5g08640	-0.81	-1.94	-2.15	hypothetical protein	-
Afu1g01430	-1.11	-2.03	-2.42	hypothetical protein	-
Afu3g11880	-0.84	-2.12	-2.21	hypothetical protein	-
Afu7g08280	-0.56	-2.36	-2.54	hypothetical protein	-
Afu6g06360	-0.11	-1.62	-1.77	mating alpha-pheromone PpgA	-
Afu6g00260	-1.11	-2.02	-1.87	phosphatidylserine decarboxylase family protein	-
Afu5g04070	-1.44	-1.62	-1.94	Spo11///meiosis-specific topoisomerase Spo11, putative	-
Afu7g08230	-0.96	-1.82	-1.65	-	-
Afu7g08540	-1.60	-1.47	-1.18	ankyrin repeat protein	-
Afu2g17880	-1.77			C6 finger domain protein, putative	DNA binding
Afu7g01030	-1.72	-1.48	-1.55	calcium transporting ATPase (Pmc1), putative///Calcium-transporting ATPase 1 (PMC1), putative	calcium ion transport///fungal-type vacuole membrane///cellular calcium ion homeostasis///calcium-transporting ATPase activity
Afu6g11420	-1.89	-1.27	-1.35	conserved hypothetical protein	-
Afu1g17480	-1.61	-1.34	-1.57	conserved hypothetical protein	-
Afu2g16300	-1.59	-0.86	-0.93	dihydroxy acid dehydratase, putative	dihydroxy-acid dehydratase activity///branched chain family amino acid biosynthetic process///mitochondrion
Afu5g00480	-1.80	-1.48	-1.19	exoinulinase InuD///fructan beta-fructosidase, putative	extracellular region///cytoplasm///beta-fructofuranosidase activity///sucrose catabolic process
Afu5g10290	-1.71	-1.02	-1.42	fructose-bisphosphate aldolase, putative	fructose-bisphosphate aldolase activity///glycolysis
Afu8g06440	-1.65	-1.11	-0.20	fructosyl amino acid oxidase, putative	-
Afu3g03830	-1.72	-0.50	-0.59	hypothetical protein	-
Afu7g04050	-1.66	-0.85	-1.18	hypothetical protein	-
Afu8g04920	-1.79	-1.48	-1.02	LEA domain protein	-
Afu7g06390	-1.67	-1.00	-0.68	maltose permease///MFS maltose permease MalP	alpha-glucoside:hydrogen symporter activity///alpha-glucoside transport///membrane fraction
Afu3g14170	-1.85	-1.58	-0.84	MFS glucose transporter, putative///high-affinity hexose transporter	response to glucose stimulus///plasma membrane///glucose transmembrane transporter activity///signal transduction///glucose binding///receptor activity

Afu2g08120	-1.84	-1.09	-1.07	MFS monosaccharide transporter (Hxt8), putative	hexose transport///mannose transmembrane transporter activity///fructose transmembrane transporter activity///plasma membrane///glucose transmembrane transporter activity
Afu8g06870	-1.90	-0.74	0.08	MFS sugar transporter, putative	hexose transport///mannose transmembrane transporter activity///fructose transmembrane transporter activity///plasma membrane///glucose transmembrane transporter activity
Afu3g03700	-1.71	-1.34	-1.21	MFS sugar transporter, putative///Sugar transporter subfamily	hexose transport///mannose transmembrane transporter activity///fructose transmembrane transporter activity///plasma membrane///glucose transmembrane transporter activity
Afu3g01370	-2.06	-0.94	-0.94	MFS transporter, putative	pantothenate transport///plasma membrane///transporter activity
Afu6g13780	-1.59	-1.27	-1.06	multidrug resistant protein, putative///MFS multidrug transporter, putative	integral to plasma membrane///multidrug transporter activity///response to toxin
Afu3g09150	-1.76	-1.47	-1.55	oxidoreductase, short chain dehydrogenase/reductase family///oxidoreductase, short chain dehydrogenase/reductase family protein, putative	fatty acid catabolic process
Afu8g06450	-1.66	-1.40	0.07	Rieske 2Fe-2S family protein, putative	-
Afu6g03200	-1.71	-0.69	-0.92	solute symporter family transporter	plasma membrane///urea transmembrane transporter activity///urea transport
Afu6g03170	-1.77	-1.26	-0.81	-	-
Afu4g06640	-0.90	-1.82	-1.56	acid sphingomyelinase, putative///acid sphingomyelinase	cyclopropane-fatty-acyl-phospholipid synthase activity///lipid biosynthetic process
Afu1g04160	-1.45	-1.81	-0.24	aspartate aminotransferase, putative	aspartate biosynthetic process///aspartate catabolic process///asparagine biosynthetic process from oxaloacetate///cytoplasm///L-aspartate:2-oxoglutarate aminotransferase activity///peroxisome///glutamate metabolic process///nitrogen compound metabolic process
Afu5g01200	-0.39	-2.28	-1.18	carboxypeptidase S1, putative	carboxypeptidase C activity///fungal-type vacuole///biological process unknown

Afu6g13180	-1.17	-1.59	-1.07	CECR1 family adenosine deaminase, putative	-
Afu2g09890	-1.31	-1.68	-1.12	conserved hypothetical protein	-
Afu4g14660	-1.00	-2.23	-1.53	conserved hypothetical protein	-
Afu1g13400	-0.87	-1.68	-1.50	conserved hypothetical protein///nuclear protein, putative	nucleus///biological process unknown///molecular function unknown
Afu2g09070	-0.87	-1.64	-1.56	DUF221 domain protein, putative	cellular component unknown///biological process unknown///molecular function unknown
Afu3g01990	-0.77	-1.65	-1.34	DUF636 domain protein	-
Afu2g08180	-0.40	-1.84	-1.54	flotillin domain protein	membrane
Afu1g17490	-1.29	-1.66	-1.38	glucokinase regulator family protein, putative	-
Afu6g06470	-0.68	-2.05	-2.24	heat shock protein HSP30, putative	-
Afu5g00650	-0.77	-1.59	-1.41	hypothetical protein	-
Afu6g11700	-1.36	-1.69	-0.32	hypothetical protein	-
Afu5g09050	-1.42	-1.78	-1.22	hypothetical protein	-
Afu8g07160	-1.25	-1.99	-1.17	hypothetical protein	-
Afu7g08470	-1.27	-2.01	-1.58	peroxisomal copper amine oxidase, putative	-
Afu4g14650	-1.11	-2.15	-1.36	ribokinase	ribokinase activity///cytoplasm///nucleus/// ATP binding///D-ribose metabolic process
Afu3g00750	-1.40	-1.65	-1.30	short-chain dehydrogenase/reductase, putative	oxidoreductase activity///metabolic process
Afu5g10090	-1.26	-1.24	-1.65	3-demethylubiquinone-9 3-methyltransferase, putative	-
Afu1g16760	-0.84	-0.96	-2.21	acetyltransferase, GNAT family family	-
Afu4g11800	-0.20	-1.53	-1.59	alkaline serine protease Alp1	proteolysis///extracellular region///serine-type peptidase activity///pathogenesis
Afu6g14480	-0.92	-1.24	-2.27	alpha-1,3-mannosyltransferase, putative	cellular component unknown///mannosyltransferase activity///cell wall mannoprotein biosynthetic process///protein amino acid O-linked glycosylation
Afu1g16770	-0.41	-0.64	-1.67	amidase///amidase family protein, putative	aerobic respiration///amidase activity///mitochondrion
Afu6g00290	-0.72	-1.20	-1.82	aminotransferase, putative	arylformamidase activity///cytoplasm///mitochondrion///NAD biosynthetic process
Afu3g09240	-0.48	-0.59	-1.68	CAIB/BAIF family enzyme	-
Afu2g13060	-1.16	-1.35	-1.60	calcineurin binding protein, putative	-
Afu6g02950	-0.34	-0.84	-1.73	Catalytic LigB subunit of aromatic ring-opening dioxygenase, putative	-
Afu1g05370	-0.17	-0.90	-1.61	conserved hypothetical protein	-

Afu2g04190	-1.03	-1.36	-1.61	conserved hypothetical protein	-
Afu4g13970	0.04	-1.39	-1.67	conserved hypothetical protein	-
Afu7g00200	-0.25	-1.03	-1.68	conserved hypothetical protein	-
Afu1g15690	-0.29	-1.15	-1.81	conserved hypothetical protein	-
Afu2g02500	-0.89	-1.20	-1.83	conserved hypothetical protein	-
Afu4g13380	-1.17	-1.49	-1.83	conserved hypothetical protein	-
Afu5g01030	0.76	-0.49	-2.01	glyceraldehyde 3-phosphate dehydrogenase, putative///glyceraldehyde 3-phosphate dehydrogenase (Ccg-7), putative	lipid particle///fungal-type cell wall///cytoplasm///cytosol///gluconeogenesis///glycolysis///glyceraldehyde-3-phosphate dehydrogenase (phosphorylating) activity
Afu7g00380	-0.54	-1.07	-1.80	GNAT family acetyltransferase, putative	-
Afu2g01380	-1.15	-1.38	-1.86	GNAT family acetyltransferase, putative///GNAT family N-acetyltransferase, putative	N-acetyltransferase activity///metabolic process
Afu7g01930	-0.05	-0.45	-1.82	GTP-binding protein EsdC///sexual development protein EsdC, putative	GTP binding
Afu2g00240	-1.56	-1.41	-1.59	hypothetical protein	-
Afu2g05700	-0.54	-1.20	-1.65	hypothetical protein	-
Afu2g16340	-0.14	-1.42	-1.66	hypothetical protein	-
Afu6g13380	-0.62	-0.93	-1.67	hypothetical protein	-
Afu2g08820	-0.16	-0.63	-1.69	hypothetical protein	-
Afu5g13650	-1.05	-1.25	-1.72	hypothetical protein	-
Afu3g01240	-1.11	-1.39	-1.97	hypothetical protein	-
Afu2g02490	-1.41	-1.48	-2.00	hypothetical protein	-
Afu3g01610	-1.26	-1.10	-2.02	hypothetical protein	-
Afu7g00540	-1.48	-0.82	-1.84	integral membrane protein	-
Afu5g03780	-0.61	-0.86	-1.61	L-PSP endoribonuclease family protein Brt1, putative///L-PSP endoribonuclease family protein (Brt1), putative	cytoplasm///nucleus///cytosol///endoribonuclease activity///mRNA catabolic process
Afu6g03320	-0.42	-0.93	-2.14	MFS drug transporter, putative///MFS multidrug transporter, putative	response to drug///multidrug transport///multidrug efflux pump activity
Afu1g12620	-0.05	-1.10	-1.65	MFS toxin efflux pump (AflT), putative	response to drug///multidrug transport///multidrug efflux pump activity
Afu5g09940	-1.05	-0.84	-1.72	MFS transporter of unkown specificity	cellular component unknown///biological process unknown///molecular function unknown
Afu2g04070	-0.67	-0.96	-1.61	MFS transporter, putative	transporter activity///transport///integral to membrane
Afu7g01790	-1.33	-1.57	-1.92	MFS transporter, putative///C4-dicarboxylate transporter/malic acid	sulfite transmembrane transporter activity///plasma membrane///sulfite transport

				transport protein	
Afu2g04270	-0.94	-1.42	-1.91	mitochondrial inner membrane translocase subunit (TIM17), putative	protein transporter activity///mitochondrial translocation///mitochondrial inner membrane presequence translocase complex
Afu2g04060	-0.81	-1.11	-1.63	NADH:flavin oxidoreductase/NADH oxidase family protein	oxidoreductase activity///NADPH dehydrogenase activity///metabolic process///coenzyme binding
Afu5g05640	-0.31	-0.49	-1.64	RTA1 domain protein, putative	-
Afu2g01250	-0.61	-1.52	-1.70	serine peptidase, family S28, putative	-
Afu2g00130	0.16	-1.32	-2.16	solid-state culture specific protein, putative	-
Afu1g06040	-0.36	-1.12	-1.62	sterol o-acyltransferase (APE2), putaitve	sterol metabolic process///sterol O-acyltransferase activity///endoplasmic reticulum
Afu3g07150	-1.48	-1.12	-1.72	succinate-semialdehyde dehydrogenase, putative	response to oxidative stress///succinate-semialdehyde dehydrogenase [NAD(P)+] activity///cytoplasm///glutamate catabolic process
Afu1g00570	-0.91	-1.46	-1.73	Tc1-mariner transposase, putative	-
Afu3g08860	-0.41	-0.76	-1.62	Transcriptional regulator ATRX related protein	-
Afu5g04060	-1.21	-1.38	-1.67	ubiquitin conjugating enzyme (UbcH), putative	protein ubiquitination///ubiquitin cycle///ER-associated protein catabolic process///endoplasmic reticulum///ubiquitin conjugating enzyme activity
Afu5g03750	-0.60	-0.94	-1.64	WW domain protein	-
Afu5g02490	-1.38	-1.49	-2.03	zinc-binding oxidoreductase, putative	oxidoreductase activity///metabolic process///zinc ion binding
Afu2g04280	-1.71	-1.38	-1.74	asparaginase, putative	-
Afu3g09140	-1.68	-1.40	-1.85	endo 1,5-alpha-arabinase	-
Afu2g07750	-1.65	-1.49	-1.66	haloacid dehalogenase, type II	-
Afu1g15530	-1.68	-1.30	-1.65	lactam utilization protein LamB, putative	-
Afu6g14500	-1.87	-1.66	-1.71	MFS sugar transporter, putative	hexose transport///mannose transmembrane transporter activity///fructose transmembrane transporter activity///plasma membrane///glucose transmembrane transporter activity
Afu8g00770	-1.74	-1.53	-1.69	sugar transporter family protein	lactate transmembrane transporter activity///lactate transport///plasma membrane

8.3.3 Functional classification of differentially expressed genes

Gene ontology analysis was conducted using Genespring GX 11.0 to indentify over represented terms among upregulated or downregulated gene cohorts. Table 8.7 shows the GO terms which satisfy an arbitrarily imposed *p*-value cut off of 0.05 among the down regulated genes at 4 hours post infection with respect to their occurrence in the *A. fumigatus* genome. No other significant GO terms were reported.

GO ACCESSION	GO Term	p-value	corrected p-value	Count in Selection	% Count in Selection	Count in Total	% Count in Total
GO:0005215|GO:0005478	transporter activity	2.59E-09	5.22E-06	11	78.57143	545	11.73305
GO:0022857|GO:0005386|GO:0015646	transmembrane transporter activity	7.12E-09	7.18E-06	8	57.14286	371	7.987083
GO:0022891	substrate-specific transmembrane transporter activity	1.40E-08	9.38E-06	8	57.14286	328	7.061356
GO:0022892	substrate-specific transporter activity	6.13E-08	3.09E-05	8	57.14286	368	7.922497
GO:0051119	sugar transmembrane transporter activity	6.11E-07	2.46E-04	5	35.71429	46	0.990312
GO:0015144	carbohydrate transmembrane transporter activity	1.14E-06	3.85E-04	5	35.71429	51	1.097955
GO:0005355|GO:0015579	glucose transmembrane transporter activity	2.72E-06	5.48E-04	5	35.71429	33	0.710441
GO:0016020	membrane	2.65E-06	5.48E-04	12	85.71429	845	18.19161
GO:0015149	hexose transmembrane transporter activity	2.72E-06	5.48E-04	5	35.71429	33	0.710441
GO:0015145	monosaccharide transmembrane transporter activity	2.72E-06	5.48E-04	5	35.71429	33	0.710441
GO:0005886|GO:0005904	plasma membrane	9.22E-06	0.00169	10	71.42857	330	7.104414
GO:0008643|GO:0006861|GO:0008644	carbohydrate transport	1.82E-05	0.003056	4	28.57143	48	1.033369
GO:0005353|GO:0015585|GO:0019192	fructose transmembrane transporter activity	3.84E-05	0.004294	4	28.57143	28	0.602799
GO:0006810|GO:0015457|GO:0015460	transport	3.16E-05	0.004294	9	64.28571	798	17.17976
GO:0008645	hexose transport	3.84E-05	0.004294	4	28.57143	28	0.602799
GO:0015578|GO:0015589	mannose transmembrane transporter activity	3.84E-05	0.004294	4	28.57143	28	0.602799
GO:0015749	monosaccharide transport	3.84E-05	0.004294	4	28.57143	28	0.602799
GO:0051234	establishment of localization	3.71E-05	0.004294	9	64.28571	808	17.39505
GO:0051179	localization	4.93E-05	0.005226	9	64.28571	826	17.78256
GO:0015129	lactate transmembrane transporter activity	1.46E-04	0.014032	2	14.28571	3	0.064586
GO:0015727	lactate transport	1.46E-04	0.014032	2	14.28571	3	0.064586
GO:0015711	organic anion transport	4.83E-04	0.04425	2	14.28571	5	0.107643

Table 8.7: Over-represented Gene Ontology terms among genes with decreased transcript abundance in the *ΔlaeA* strain at 4 hours post infection. Table lists processes significantly over-represented, relative to their occurrence in the *A. fumigatus* genome. Analysis was carried out in Genespring 11.0.

Over represented GO terms at 4 hrs post infection were exclusively related to transport, whereby putative fructose, glucose, mannose and lactate transporters were significantly downregulated in Δ*lae*A. Other transporters including a Pmc1 like calcium transporting ATPase (Afu7g01030), putative aflatoxin MFS efflux pump (Afu1g12620), the siderochrome-iron transporter MirB (Afu3g03640) and three putative drug transporters (Afu6g03320, Afu5g02700, Afu6g13780). Interestingly, a homologue of the *S. cerevisiae* low glucose sensor Snf3, is also down expressed at this time point (high-affinity hexose transporter, Afu3g14170). Differentially expressed genes were grouped into functional categories based on GO Terms and by reference to the *A. fumigatus* literature. A summary of up and down regulated functional categories between 4 and 14 hours is given in Table 8.8.

Table 8.8: Functional classification of selected genes having differential transcript abundance in Δ*laeA* mutant relative to the parental isolate Af293 during initiation of murine infection.

	Increased transcript abundance in Δ*laeA*					Decreased transcript abundance in Δ*laeA*				
Functional classification	**ORF**	**Description**	**4 hrs**	**8 hrs**	**14 hrs**	**ORF**	**Description**	**4 hrs**	**8 hrs**	**14 hrs**
Cell wall	Afu2g01170	1,3-beta-glucanosyltransferase Gel1	2.02	2.18	1.71	Afu6g14480	alpha-1,3-mannosyltransferase, putative	-	-	-2.27
	Afu8g00610	cell surface protein Mas1, putative	2.35	1.85	2.02	Afu1g01300	GPI anchored protein, putative	-	-1.68	-2.20
	Afu2g14540	endoglucase, putative	-	1.70	1.68					
	Afu3g14980	extracellular chitosase CsnC, putative	-	1.81	1.85					
	Afu2g04880	cell wall biogenesis protein, putative///DUF77 domain protein	-	-	1.66					
Ergosterol	Afu7g00260	squalene-hopene-cyclase, putative	1.97	2.51	2.37	Afu1g06040	sterol o-acyltransferase (APE2), putaitve	-	-	-1.62
Antigens						Afu4g11800	alkaline serine protease Alp1	-	-	-1.59
Iron acquisition	Afu4g14640	low affinity iron transporter, putative	-	-	2.02	Afu3g03640	siderochrome-iron transporter (MirB), putative///MFS siderochrome iron transporter MirB	-2.65	-2.14	-
Ion transport/ homeostasis						Afu2g13060	calcineurin binding protein, putative	-	-	-1.60
						Afu7g01030	calcium transporting ATPase (Pmc1), putative///Calcium-transporting ATPase 1 (PMC1), putative	-1.72	-	-
Secondary metabolite cluster	Afu1g17670	salicylate hydroxylase, putative	-	1.92	-	Afu1g17660	histidinol dehydrogese, putative	-2.26	-1.87	-1.92
	Afu3g01420	DUF341 domain oxidoreductase, putative///DUF341 family oxidoreductase, putative	-	1.97	1.68	Afu3g01370	MFS transporter, putative	-2.06	-	-
	Afu3g13750	conserved hypothetical protein	1.84	2.17	1.92	Afu3g01580	GMC oxidoreductase, putative	-2.07	-1.69	-2.20
	Afu4g14390	Fot5 transposase, putative	3.13	3.33	3.06	Afu3g03280	FAD binding monooxygese, putative	-1.80	-1.79	-2.30
	Afu4g14630	FAD binding domain protein	-	1.69	2.23	Afu3g12890	C6 transcription factor GliZ-like, putative///C6 transcription factor (GliZ), putative	-	-1.71	-1.62
	Afu4g14640	low affinity iron transporter, putative	-	-	2.02	Afu3g12900	MFS transporter, putative///monocarboxylate	-2.04	-2.44	-

							transporter (Mch4), putative			
	Afu6g03330	conserved hypothetical protein	2.78	2.42	1.93	Afu3g13740	HSP70 family protein	-	-2.30	-2.64
	Afu6g03370	short-chain dehydrogese/reductase, putative///oxidoreductase, short-chain dehydrogese/reductase family	1.72	1.77	1.85	Afu4g14610	MFS sugar transporter, putative	-1.82	-1.60	-1.62
	Afu6g03410		-	-	1.60	Afu4g14650	ribokise	-	-2.15	-
	Afu6g03420	trehalose synthase, putative	-	-	1.79	Afu4g14660	conserved hypothetical protein	-	-2.23	-
	Afu8g00310	LINE-1 class reverse transcriptase, RseH, putative	1.84	2.56	1.73	Afu4g14670	MFS quite transporter, putative	-	-1.96	-1.61
	Afu8g00600	conserved hypothetical protein///D dependent epimerase/dehydratase family protein	-	-	1.84	Afu6g03320	MFS drug transporter, putative///MFS multidrug transporter, putative	-	-	-2.14
	Afu8g00610	cell surface protein Mas1, putative	2.35	1.85	2.02					
Secreted proteases						Afu4g11800	alkaline serine protease Alp1	-	-	-1.59
						Afu5g01200	carboxypeptidase S1, putative	-	-2.28	-
						Afu8g07080	elastinolytic metalloproteise Mep	-2.20	-2.67	-1.95
						Afu2g01250	serine peptidase, family S28, putative	-	-	-1.70
Other secreted enzymes	Afu8g00610	cell surface protein Mas1, putative	2.35	1.85	2.02	Afu7g06140	beta-D-glucoside glucohydrolase	-1.78	-2.05	-1.91
	Afu2g01170	1,3-beta-glucanosyltransferase Gel1	2.02	2.18	1.71	Afu3g09140	endo 1,5-alpha-arabise	-1.68		-1.85
	Afu2g14540	endoglucase, putative	-	1.70	1.68	Afu2g09350	endo-beta-1,6-glucase, putative	-	-1.60	-2.12
	Afu3g14980	extracellular chitosase CsnC, putative	-	1.81	1.85	Afu1g01300	GPI anchored protein, putative	-	-1.68	-2.20
	Afu3g02090	beta-xylosidase, putative///beta-xylosidase	-	-	1.98	Afu4g06640	acid sphingomyelise, putative///acid sphingomyelise	-	-1.82	-
	Afu7g04950	lipase, putative	1.84	-	-	Afu8g01710	antigenic thaumatin domain protein, putative	-	-1.74	-2.04
	Afu7g08400	ankyrin repeat protein	2.68	3.13	2.48	Afu5g00480	exoinulise InuD///fructan beta-fructosidase, putative	-1.80	-	-
	Afu8g02030	conserved hypothetical protein	-	1.69	-	Afu7g00540	integral membrane protein	-	-	-1.84
	Afu6g00450	feruloyl esterase, putative	-	-	2.13	Afu6g06360	mating alpha-pheromone PpgA		- 1.62488	-1.77
	Afu6g12240	Glycerophosphoryl diester phosphodiesterase family	-	-	1.66	Afu5g05640	RTA1 domain protein, putative	-	-	-1.64

		family								
	Afu6g14010	GPI anchored protein, putative	1.62	-	-	Afu6g00160	Ser/Thr protein phosphatase family protein	-2.16	-2.46	-2.49
	Afu6g00430	IgE-binding protein	2.47	1.79	-	Afu2g17880	C6 finger domain protein, putative	-1.77	-	-
	Afu5g03540	pyridine nucleotide-disulphide oxidoreductase, class II, putative	-	1.59	-	Afu6g03200	solute symporter family transporter	-1.71	-	-
Transport	Afu3g02110	MFS efflux transporter, putative///MFS multidrug transporter, putative	-	1.73	-	Afu6g03320	MFS drug transporter, putative///MFS multidrug transporter, putative	-	-	-2.14
	Afu4g14640	low affinity iron transporter, putative	-	-	2.02	Afu4g14670	MFS quite transporter, putative	-	-1.96	-1.61
	Afu5g09440	amino acid permease, putative	-	-	2.30	Afu4g14610	MFS sugar transporter, putative	-1.82	-1.60	-1.62
	Afu1g10930	ammonium transporter///ammonium transporter (Mep2), putative	2.07	-	-	Afu3g01370	MFS transporter, putative	-2.06	-	-
	Afu1g01930	MFS multidrug transporter, putative	1.61	1.65	-	Afu3g12900	MFS transporter, putative///monocarboxylate transporter (Mch4), putative	-2.04	-2.44	-
	Afu8g01340	MFS sugar transporter, putative	-	-	1.72	Afu7g01030	calcium transporting ATPase (Pmc1), putative///Calcium-transporting ATPase 1 (PMC1), putative	-1.72	-	-
	Afu1g02480	plasma membrane ATPase, putative///P-type ATPase, putative	-	1.74	2.25	Afu5g02940	choline transport protein Ctr, putative	-1.88	-2.48	-
	Afu2g11220	proline permease, putative	-	-	2.10	Afu2g09450	carboxylic acid transport protein	-2.38	-1.62	-
						Afu3g11790	galactose-proton symport, putative	-2.36	-1.79	-
						Afu3g14170	MFS glucose transporter, putative///high-affinity hexose transporter	-1.85	-	-
						Afu2g08120	MFS monosaccharide transporter (Hxt8), putative	-1.84	-	-
						Afu5g02700	MFS multidrug transporter, putative///multidrug resistant protein	-	-1.68	-1.92
						Afu8g06870	MFS sugar transporter, putative	-1.90	-	-
						Afu6g14500	MFS sugar transporter, putative	-1.87	-	-1.71
						Afu3g03700	MFS sugar transporter, putative///Sugar transporter subfamily	-1.71	-	-

						Afu1g12620	MFS toxin efflux pump (AflT), putative	-	-	-1.65
						Afu5g09940	MFS transporter of unkown specificity	-	-	-1.72
						Afu2g04070	MFS transporter, putative	-	-	-1.61
						Afu5g00420	MFS transporter, putative	-1.87	-2.06	
						Afu7g01790	MFS transporter, putative///C4-dicarboxylate transporter/malic acid transport protein	-	-	-1.92
						Afu6g13780	multidrug resistant protein, putative///MFS multidrug transporter, putative	-1.59	-	-
						Afu3g03640	siderochrome-iron transporter (MirB), putative///MFS siderochrome iron transporter MirB	-2.65	-2.14	-
						Afu8g00770	sugar transporter family protein	-1.74	-	-1.69
Transposition	Afu4g14390	Fot5 transposase, putative	3.13	3.33	3.06	Afu7g08660	Fot1 family transposase, putative	-	-1.78	-1.63
	Afu8g00310	LINE-1 class reverse transcriptase, RseH, putative	1.84	2.56	1.73	Afu3g05620	Fot1 family transposase, putative	-	-1.87	-1.71
	Afu7g02160	DDE superfamily endonuclease/transposase	3.45	3.09	2.93	Afu1g00140	Fot5 transposase, putative	-	-2.10	-2.14
	Afu3g11670	DDE superfamily endonuclease/transposase, pseudogene	1.73	1.88	1.85	Afu1g00570	Tc1-mariner transposase, putative	-	-	-1.73
	Afu2g18080	LINE-1 class reverse transcriptase, RseH, putative	1.83	2.53	1.96					
	Afu3g09430	LINE-1 class reverse transcriptase, RseH, putative	2.01	2.5	2.02					
	Afu3g15370	LINE-1 class reverse transcriptase, RseH, putative	2.08	2.33	1.81					
	Afu4g14870	LINE-1 class reverse transcriptase, RseH, putative	1.98	2.32	1.72					
	Afu5g00270	LINE-1 class reverse transcriptase, RseH, putative	2.39	3.24	2.24					
	Afu6g00780	LINE-1 class reverse transcriptase, RseH, putative	2.04	2.27	1.77					
	Afu7g00100	LINE-1 class reverse transcriptase, RseH, putative	2.73	3.57	2.56					
	Afu8g06290	LINE-1 class reverse transcriptase, RseH, putative	2.18	2.67	1.91					
	Afu7g07070	LINE-1 class reverse transcriptase, RseH, putative	1.61	-	-					

	Afu6g14660	reverse transcriptase, RseH	2.12	2.49	1.9					
	Afu8g01040	reverse transcriptase, RseH	2.08	2.51						
	Afu4g00820	reverse transcriptase, RseH		2.76	1.81					
	Afu6g09470	reverse transcriptase, RseH, putative	1.71	2.49	1.93					
Transcription factors	Afu3g02480	C6 transcription factor, putative	1.59	2.7	2.33	Afu2g17880	C6 finger domain protein, putative	-1.77		
	Afu2g00470	C6 transcription factor, putative	-	1.60	1.60	Afu3g12890	C6 transcription factor GliZ-like, putative///C6 transcription factor (GliZ), putative	-	-1.71	-1.62
	Afu2g01260	HLH transcription factor, putative	-	1.64	-	Afu6g13770	C6 finger domain protein, putative	-	-1.68	-1.66
						Afu7g00410	C6 transcription factor, putative	-1.74	-1.95	-
						Afu2g05360	C6 transcription factor, putative	-3.14	-1.70	-
						Afu5g14230	C6 transcription factor, putative	-	-1.63	-1.70
						Afu6g12160	C6 transcription factor, putative	-	-2.1286	-2.16
						Afu3g08860	Transcriptiol regulator ATRX related protein	-	-	-1.62

8.3.4 Characterisation of genes differentially expressed between Δ*laeA* and Af293: chromosomal loci, lineage specificity and functionality

Given the previously identified significant over-representation of transcripts encoded by differentially expressed genes of subtelomeric loci, *A. fumigatus* specific genes, signal peptide encoding genes, and secondary metabolite clusters during infection relative to laboratory growth (McDonagh et al. 2008) and throughout infection (Chapter 3) distribution of differentially expressed genes was investigated with respect to these functional cohorts (Figure 8.7). Statistical significance of enrichment was measured by Chi squared analyses (Table 8.9), with the null hypothesis that equal numbers of increased and decreased genes occur in each cohort.

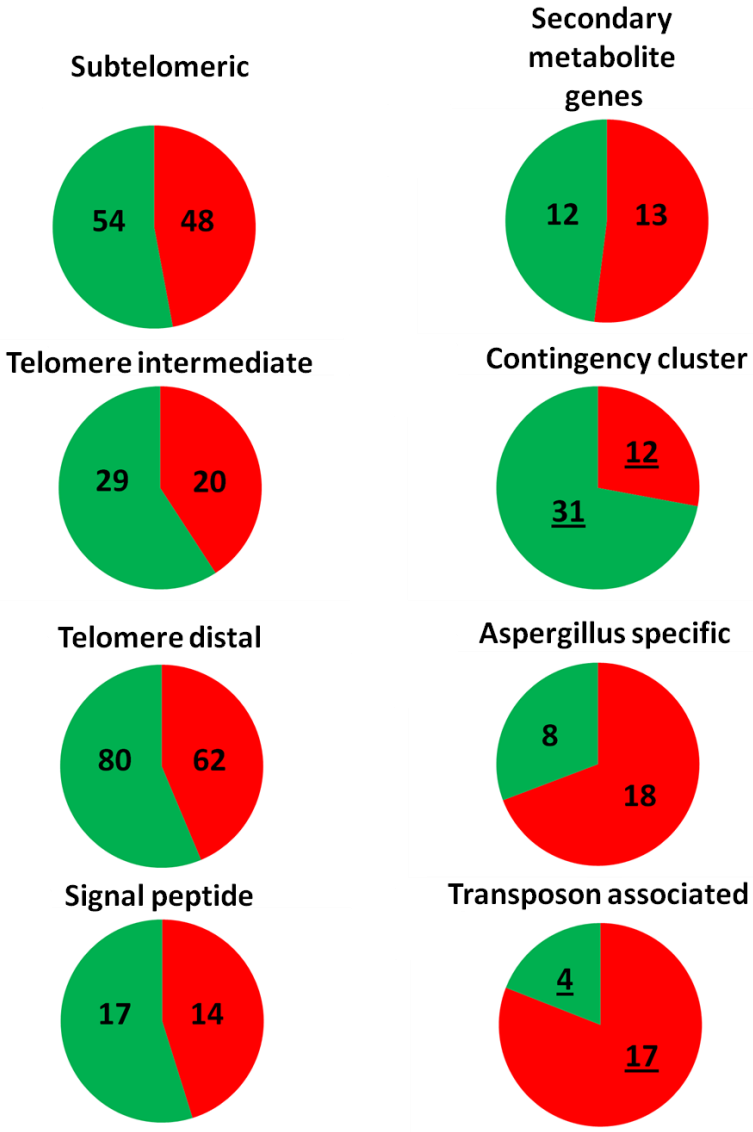


Figure 8.7: Distribution of differentially expressed genes among functional cohorts of chromosomal location, signal peptide content, *A. fumigatus* specificity and functional association. Distribution of upregulated (red) and downregulated (green) genes at subtelomeric loci (0 – 300 Kb from telomere, n =1509); telomere intermediate loci (301 - 600 Kb from telomere, n = 1634); telomere distal loci (> 600 Kb from telomere, n =6494). Secondary metabolite clusters (n = 337); Contingency clusters (n = 594); signal peptide cohort (n = 1103); *A. fumigatus* specific genes (n = 596) and; Transposon associated genes (n = 68). Underlined values significantly deviate from the null hypothesis that an equal number of induced or repressed genes will occur in each cohort, as tested by Chi-square analysis.

	Number of genes	Differentially expressed	Up (observed)	Down (observed)	Up (expected)	Down (expected)	Chi square	p value
0-300 kb	**1509**	**102**	**48**	**54**	**51**	**51**	**0.35**	**0.552**
301- 600 kb	**1634**	**49**	**20**	**29**	**24.5**	**24.5**	**1.65**	**0.199**
>600 kb	**6373**	**142**	**62**	**80**	**71**	**71**	**2.28**	**0.131**
Signal P	**1103**	**31**	**14**	**17**	**15.5**	**15.5**	**0.29**	**0.59**
Secondary metabolism	**337**	**25**	**13**	**12**	**12.5**	**12.5**	**0.04**	**0.841**
Contingency cluster	**594**	**43**	**12**	**31**	**21.5**	**21.5**	**8.39**	**0.004**
Aspergillus specific	**596**	**26**	**18**	**8**	**13**	**13**	**3.84**	**0.05**
Transposition associated	**68**	**21**	**17**	**4**	**10.5**	**10.5**	**9.04**	**0.005**

Table 8.9: Distribution and chi squared analysis of differentially expressed genes categorised by chromosomal location, signal peptide content, *A. fumigatus* specificity and functional association. Chi squared analysis with one degree of freedom was used to test the distribution of differentially expressed genes with respect to cohorts of interest to this study, with the null hypothesis that even numbers of induced or repressed genes occur in each group.

43 genes differentially expressed in Δ*lae*A relative to the wild-type are located at contingency clusters throughout the time-course (Table 8.10 and 8.11). Of these, 72% (31 genes) were decreased in at least one stage of infection. While only 6% of the total *A. fumigatus* gene repertoire is found in contingency clusters, 19% of the total Δ*lae*A downregulated cohort was within these loci, indicating that LaeA effects positive control of transcription in these virulence associated regions. There was no observed enrichment at any specific cluster, with differentially expressed genes being sparsely distributed at 28 different contingency clusters (Tables 8.10 and 8.11). Figure 8.8 depicts the LaeA regulon throughout the initiation of infection with regard to choromosomal locus.

Table 8.10: Infection cluster genes with increased transcript abundance in Δ*laeA* relative to the wild type throughout the time course of infection. Time points highlighted in red pass standard deviation correction filtering and a 1.5 log_2 ratio cut off. Values which failed this filter are left unshaded

Infection cluster No.	Location of cluster	No Genes in Infection Cluster	Distance to telomere	Annotation	Description	4 hrs	8 hrs	14 hrs
16	Afu1g17590-Afu1g17680	6	Proximal	Afu1g17670	salicylate hydroxylase, putative	1.04	1.92	0.99
28	Afu2g14330-Afu2g14480	9	Distal	Afu2g14330	hypothetical protein	0.78	0.95	1.74
31	Afu3g01030-Afu4g01070	34	Proximal	Afu3g01030	RTA1 domain protein, putative	1.66	2.11	2.79
40	Afu4g00980-Afu4g01070	8	Proximal	Afu4g01020	sensor histidine kinase/response regulator, putative	0.88	1.13	1.74
47	Afu5g01240-Afu5g01420	10	Intermediate	Afu5g01340	lysophospholipase Plb2///lysophospholipase, putative	1.50	1.76	2.58
57	Afu6g03140-Afu6g03250	10	Distal	Afu6g03210	conidiation-specific protein 10	1.26	1.00	1.91
58	Afu6g03320-Afu6g03940	12	Distal	Afu6g03330	conserved hypothetical protein	2.78	2.42	1.93
				Afu6g03370	short-chain dehydrogenase/reductase, putative///oxidoreductase, short-chain dehydrogenase/reductase family	1.72	1.77	1.85
67	Afu7g04910-Afu7g05070	5	Distal	Afu7g04950	lipase, putative	1.84	0.98	1.55
69	Afu7g06750-Afu7g06920	7	Intermediate	Afu7g06920	conserved hypothetical protein	1.79	1.39	1.14
72	Afu8g00240-Afu8g00620	21	Proximal	Afu8g00600	conserved hypothetical protein///NAD dependent epimerase/dehydratase family protein	0.47	1.52	1.84
				Afu8g00610	cell surface protein Mas1, putative	2.35	1.85	2.02

Table 8.11: Infection cluster genes with decreased transcript abundance in Δ*laeA* relative to the wild type throughout the time course of infection. Time points highlighted in green pass standard deviation correction filtering and a 1.5 log_2 ratio cut off. Values which failed this filter are left unshaded

Infection cluster No.	Location of cluster	No. Genes in Infection Cluster	Distance to telomere	Annotation	Description	4 hrs	8 hrs	14 hrs
12	Afu1g16670 - Afu1g16770	5	Intermediate	Afu1g16760	acetyltransferase, GNAT family family	-0.84	-0.96	-2.21
				Afu1g16770	amidase///amidase family protein, putative	-0.41	-0.64	-1.67
15	Afu1g17470 - Afu1g17530	5	Proximal	Afu1g17480	conserved hypothetical protein	-1.61	-1.34	-1.57
				Afu1g17490	glucokinase regulator family protein, putative	-1.29	-1.66	-1.38
16	Afu1g17590 -	6	Proximal	Afu1g17660	histidinol dehydrogenase,	-2.26	-1.87	-1.92

	Afu1g17680				putative			
17	Afu2g00120 - Afu2g00260	6	Proximal	Afu2g00130	solid-state culture specific protein, putative	0.16	-1.32	-2.16
				Afu2g00240	hypothetical protein	-1.56	-1.41	-1.59
25	Afu2g07750 - Afu2g07840	5	Distal	Afu2g07750	haloacid dehalogenase, type II	-1.65	-1.49	-1.66
31	Afu3g01030 - Afu4g01070	34	Intermediate	Afu3g01240	hypothetical protein	-1.11	-1.39	-1.97
				Afu3g01370	MFS transporter, putative	-2.06	-0.94	-0.94
				Afu3g01580	GMC oxidoreductase, putative	-2.07	-1.69	-2.20
				Afu3g01610	hypothetical protein	-1.26	-1.10	-2.02
33	Afu3g03200 - Afu3g03450	14	Distal	Afu3g03280	FAD binding monooxygenase, putative	-1.80	-1.79	-2.30
34	Afu3g03600 - Afu3g03870	12	Distal	Afu3g03640	siderochrome-iron transporter (MirB), putative///MFS siderochrome iron transporter MirB	-2.65	-2.14	-1.50
				Afu3g03700	MFS sugar transporter, putative///Sugar transporter subfamily	-1.71	-1.34	-1.21
				Afu3g03810	hypothetical protein	-3.60	-2.67	-2.88
37	Afu3g11650 - Afu3g11790	5	Distal	Afu3g11790	galactose-proton symport, putative	-2.36	-1.79	-1.57
38	Afu4g00240 - Afu4g00430	7	Proximal	Afu4g00370	general amidase, putative	-2.13	-2.54	-2.31
44	Afu4g13900 - Afu4g14200	14	Proximal	Afu4g13970	conserved hypothetical protein	0.04	-1.39	-1.67
45	Afu5g00480 - Afu5g00580	8	Proximal	Afu5g00480	exoinulinase InuD///fructan beta-fructosidase, putative	-1.80	-1.48	-1.19
50	Afu5g10090 - Afu5g10350	10	Distal	Afu5g10090	3-demethylubiquinone-9 3-methyltransferase, putative	-1.26	-1.24	-1.65
				Afu5g10290	fructose-bisphosphate aldolase, putative	-1.71	-1.02	-1.42
52	Afu5g13640 - Afu5g13770	7	Intermediate	Afu5g13650	hypothetical protein	-1.05	-1.25	-1.72
54	Afu6g00120 - Afu6g00190	5	Proximal	Afu6g00160	Ser/Thr protein phosphatase family protein	-2.16	-2.46	-2.49
57	Afu6g03140 - Afu6g03250	10	Distal	Afu6g03200	solute symporter family transporter	-1.71	-0.69	-0.92
58	Afu6g03320 - Afu6g03940	12	Distal	Afu6g03320	MFS drug transporter, putative///MFS multidrug transporter, putative	-0.42	-0.93	-2.14
63	Afu7g00110 - Afu7g00200	8	Proximal	Afu7g00200	conserved hypothetical protein	-0.25	-1.03	-1.68
64	Afu7g00370 - Afu7g00460	5	Proximal	Afu7g00380	GNAT family acetyltransferase, putative	-0.54	-1.07	-1.80
66	Afu7g00970	12	Proximal	Afu7g01030	calcium transporting	-1.72	-1.48	-1.55

	- Afu7g01100				ATPase (Pmc1), putative///Calcium-transporting ATPase 1 (PMC1), putative			
68	Afu7g06120 - Afu7g06180	6	Intermediate	Afu7g06140	beta-D-glucoside glucohydrolase	-1.78	-2.05	-1.91
70	Afu7g07010 - Afu7g08250	5	Intermediate	Afu7g07040	hypothetical protein	-1.18	-1.85	-1.67

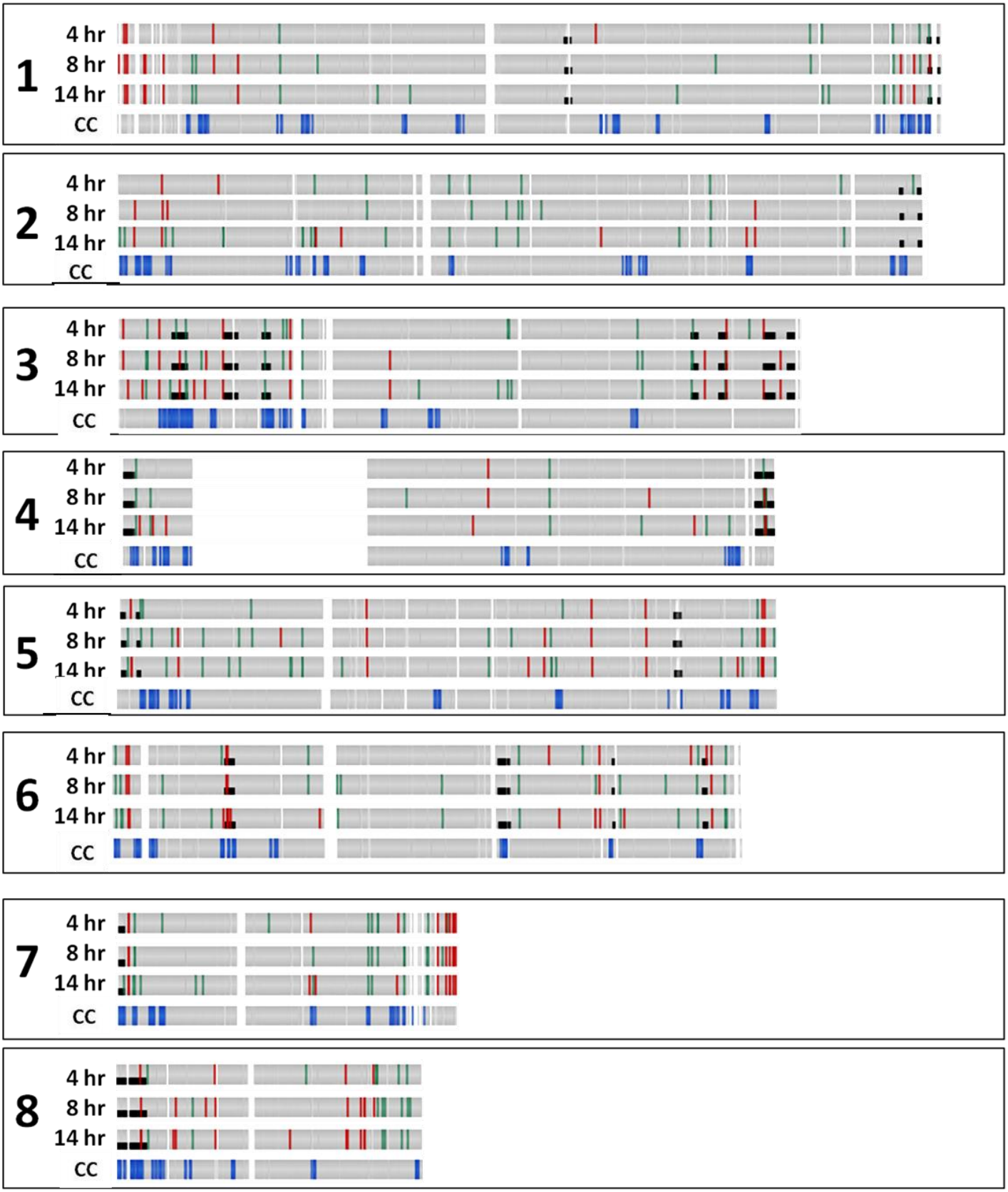


Figure 8.8: A transcriptional snap shot of the LaeA regulon across the time-course of early infection. Genes up and down expressed (> 1.5) in the Δ*lae*A strain are shown in red and green respectively. Secondary metabolite gene clusters are underlined in black. Chromosomal snap shots are shown at the three time points (4, 8 and 14 hr). The CC chromosome depicts locations of contingency clusters, which are shown in blue (McDonagh et al 2008). The blank section of chromosome 4 represents a region of ribosomal DNA.

8.3.5 Profiling host innate immune responses to Af293 and Δ*laeA*

To elucidate host transcriptional responses underlying differential virulence of the Af293 and Δ*laeA* isolates, expression of genes directing host innate immunity, following infection with the wild-type or Δ*laeA* was analysed at 14 hours post infection. The immunocompetent saline infected animals served as a reference against which gene expression in Af293, Δ*laeA* or saline infected neutropenic mice was studied. This experimental design (Figure 8.9) enabled the impact of cyclophosphamide alone to be established. A total of 168 genes of the murine innate immune system were represented on three qRT-PCR arrays. 10 genes with critical implications for host-pathogen interactions, such as TLR-4 and IL-10 were represented on all three arrays. A further 22 were represented on two arrays, and the remaining 136 genes on one.

A common reference experimental design was adopted, whereby gene expression relative to immunocompetent, saline inoculated animals was reported. Figure 8.10 details the experimental design and the normalisation steps which were applied. In order to facilitate comparisons between cohorts, Ct values representing transcript abundance from genes of interest (GOI) were normalised to the most transcriptionally stable housekeeping gene (HKG) across the 4 murine cohorts by calculating ΔCt values (Ct(GOI) - Ct(HKG)). Fold changes (2^(-ΔΔCt)) were determined for every gene in each test cohort relative to the common reference, where 2^(-ΔΔCt) is the normalized gene expression (2^(- ΔCt)) in the test sample subtracted from the normalized gene expression (2^(- ΔCt)) in the control. Fold changes were $\log_2$ transformed to reduce variations in sample standard deviation. To indentify differences in innate immune responses between strains in each cohort, $\log_2$ transformed fold-regulation values were compared between experimental groups. Genes with elevated or decreased transcripts were defined having a difference of greater than ±3 in transformed fold regulation between isolates. Gene expression was therefore investigated as the magnitude of change relative to the control group between infection cohorts.

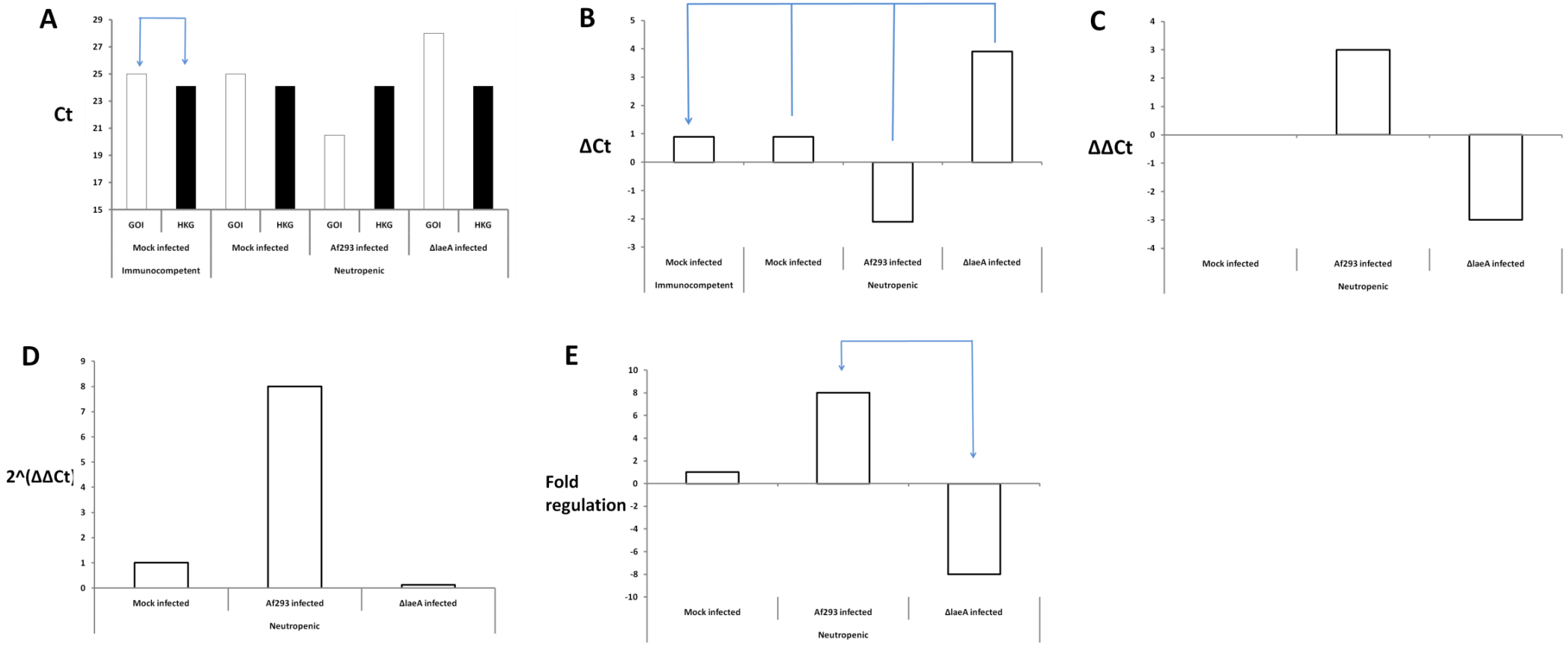


Figure 8.9: Schematic depicting normalisation of an exemplar gene for host transcriptional comparisons between Af293 and Δ*laeA* infected animals. Neutropenic mice were infected with Af293, Δ*laeA* or sterile saline. Immunocompetent mice were inoculated with sterile saline. Animals were culled at 14 hours post infection, and BALFs extracted. Transcript abundance was analysed relative to the immunocompetent saline-infected control cohort using qRT-PCR arrays. **(A)** Raw Ct values from a gene of interest (GOI) were normalised (blue arrows) against constitutively expressed house-keeping genes (HKG) on each array to give ΔCt values. (B) ΔCt values from three experimental cohorts were normalised against ΔCt values in the saline-infected, immunocompetent control group (blue arrows). (C) ΔΔCt values for the 3 cohorts are shown. (D) Fold change of the gene of interest relative to the gene expression in the control cohort was calculated by 2^(ΔΔCt). (E) Fold-regulation was calculated from fold change. Fold-change values greater than one indicate up-regulation. Fold-change values less than one indicate down-regulation. Fold regulation values were $\log_2$ transformed and fold regulation between cohorts investigated (blue arrows). Genes were defined as differentially expressed between cohorts when a 3 fold or greater difference was observed

Interrogation of the host responses in the neutropenic murine model demonstrated both reduced (n = 37) and increased (n = 4) transcript abundance in Δ*laeA* infected animals relative to Af293. However, at this stage in the analysis, the majority of data are only available from one technical replicate (Tables 8.12 and 8.13). Figure 8.10 showns gene expression for 6 differentially expressedgenes where duplicated and triplicated measurements are available.

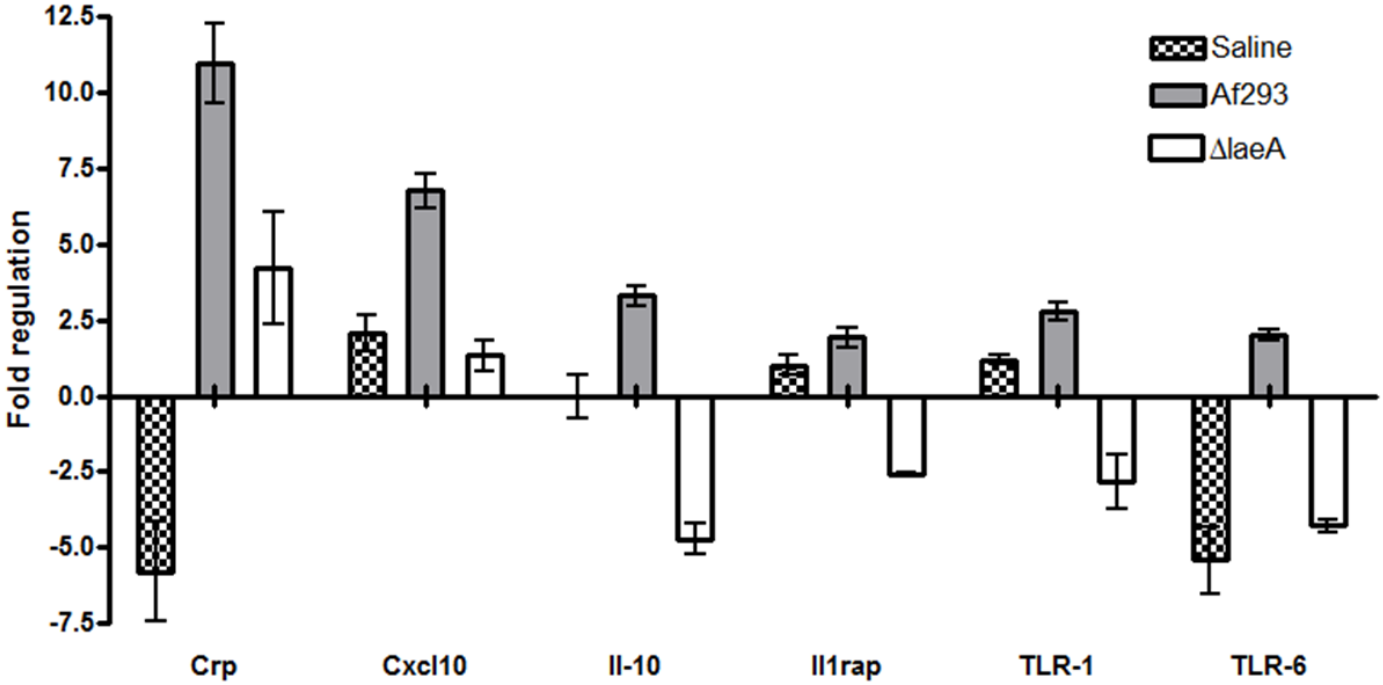


Figure 8.10: Gene expression of innate immune genes as measured from mRNA extracted from saline inoculated, Af293 and Δ*laeA* infected BALFs. Averaged $\log_2$ transformed fold regulation values of 6 murine innate immunity genes was calculated relative to transcript abundance in immunocompetent saline infected mice. Crp, C-reactive protein Mm.28767; CXCL10, Chemokine (C-X-C motif) ligand 10 Mm.877; IL-10, Interleukin 10 Mm.874; Il1rap, Interleukin 1 receptor accessory protein Mm.253424; TLR-1, Toll like receptor 1 Mm.273024; TLR-6, toll-like receptor 6 Mm.42146. A fold difference greater than 3 was observed between Af293 and Δ*laeA* for all transcripts. Error bars represent standard deviation from triplicate (Il10) and duplicate (Crp, Tlr1, Tlr6, CXCL10) measurements. Relative expression in the neutropenic saline group is used to determine impacts of immunosuppression on transcript levels.

Table 8.12: Murine genes demonstrating decreased transcript abundance in Δ*laeA* infected mice relative to Af293 infected mice								
ORF	**Gene Symbol**	**Description**	**Replication on arrays**	**Neutropenic saline log2**	**Af293 log 2**	**Δ*laeA* Log2**	**Difference between Af293 and Δ*laeA***	**Functional classification**
Mm.197638	C8a	Complement component 8, alpha polypeptide	1	-3.69	2.23	-3.38	5.61	Complement activation
Mm.867	Ccl12	Chemokine (C-C motif) ligand 12	1	0.35	6.30	-0.78	7.08	Chemotaxis
Mm.424740	Ccl19	Chemokine (C-C motif) ligand 19	1	1.32	1.61	-4.76	6.37	Chemotaxis
Mm.7275	Ccl25	Chemokine (C-C motif) ligand 25	1	1.35	1.06	-5.43	6.49	Chemotaxis, leukocyte migration
Mm.284248	Ccl5	Chemokine (C-C motif) ligand 5	1	1.57	1.50	-4.62	6.12	Chemotaxis, on Th1 and macrophages
Mm.42029	Ccl8	Chemokine (C-C motif) ligand 8	1	2.14	5.29	-1.34	6.63	Chemotaxis
Mm.271833	Cd40	CD40 antigen	1	-0.34	1.18	-4.06	5.24	B cell activation and IL-12 activation
Mm.3064	Cfp	Complement factor properdin	1	2.28	2.61	-1.44	4.05	Alternative pathway complement activation
Mm.239516	Clec7a	C-type lectin domain family 7, member a	1	4.15	6.75	3.46	3.29	Dectin 1/ Positive regulator of TNF
Mm.218571	Colec12	Collectin sub-family member 12	1	2.60	2.97	-3.27	6.24	PRR, phagocytosis
Mm.28767	Crp	C-reactive protein, pentraxin-related	2	-5.82	10.96	4.21	6.76	Classical complement activation
Mm.877	CXCL10	Chemokine (C-X-C motif) ligand 10	2	2.07	6.77	1.33	5.43	Chemotaxis leukocyte chemotaxis
Mm.1401	Cxcr4	Chemokine (C-X-C motif) receptor 4	1	2.37	2.20	-1.01	3.21	Regulation of chemotaxis and programmed cell death
Mm.4138	Dmbt1	Deleted in malignant brain tumors 1	1	3.84	4.04	-1.99	6.03	Epithelial cell differentiation/ PRR for phosphorylated ligans
Mm.1658	Flt3l	FMS-like tyrosine kinase 3 ligand	1	2.29	2.15	-1.07	3.22	Positive regulation of NK cell proliferation
Mm.318567	Hdac4	Histone deacetylase 4	1	1.49	1.43	-3.71	5.14	Negative regulation of glycolysis and transcription
Mm.549	Ifngr1	Interferon gamma receptor 1	1	3.12	3.88	-1.35	5.23	Blood coagulation/ signal transduction

								((Natural killer cell mediated cytotoxicity from KEGG))
Mm.277886	Ikbkb	Inhibitor of kappaB kinase beta	1	-1.76	0.30	-3.13	3.43	regulation of I-kappaB kinase/NF-kappaB cascade / anti-apoptosis/ I-kappaB phosphorylation
Mm.874	Il10	Interleukin 10	3	-0.01	3.31	-4.72	4.60	inflammatory response/ negative regulation of apoptosis/ negative regulation of B cell proliferation/ negative regulation of chronic inflammatory response to antigenic stimulus/ negative regulation of interleukin-12 and interleukine 6 production/ negative regulation of tumor necrosis factor production/ positive regulation of B cell apoptosis/ suppresses Th17 cytokines
MGI:96539	Il12a	interleukin 12a	1		3.50	-1.65	5.15	positive regulation of T cell proliferation, positive regulation of interferon-gamma production, positive regulation of lymphocyte proliferation, positive regulation of natural killer cell mediated cytotoxicity
Mm.20466	Il18rap	Interleukin 18 receptor accessory protein	1	-1.38	1.55	-2.42	3.97	Il receptor activty
Mm.29261	Il1f5	Interleukin 1 family, member 5 (delta)	1	-2.68	-1.23	-7.76	6.53	negative regulation of receptor activity
Mm.253424	Il1rap	Interleukin 1 receptor accessory	2	1.01	1.92	-2.57	4.49	interleukin-2 biosynthetic process

		protein						
Mm.2856	Il6ra	Interleukin 6 receptor, alpha	1	0.67	3.87	-1.02	4.89	Interleukine 6 receptor
Mm.337035	Il8ra	Interleukin 8 receptor, alpha	1	0.33	1.14	-7.79	8.93	cytokine-mediated signaling pathway/ chemotaxis
Mm.218846	Lbp	Lipopolysaccharide binding protein	1	4.50	4.05	-0.48	4.53	Gram negative bacterial binding/ acute-phase response/ opsonization/ positive regulation of interleukin-6 production and Il8/ positive regulation of macrophage activation/ positive regulation of neutrophil chemotaxis/ positive regulation of toll-like receptor 4 signaling pathway/ positive regulation of tumor necrosis factor biosynthetic process
Mm.311337	Mapk14	Mitogen-activated protein kinase 14	1	-0.41	2.39	-3.70	6.09	Response to lipopolysaccharide/positive regulation of oxygen and reactive oxygen species metabolic process/ positive regulation of erythrocyte differentiation
Mm.21855	Pglyrp1	Peptidoglycan recognition protein 1	1	1.26	4.20	0.71	3.49	apoptosis/ defense response to Gram-positive bacterium/ PRR signalling pathway/ signal transduction
Mm.293614	Ppbp	Pro-platelet basic protein	1	-2.67	-3.35	-6.44	3.09	Cytokine-cytokine receptor interaction, organism-specific biosystem (from KEGG) / platlet activation (from KEGG)
Mm.2786	Proc	Protein C	1	-0.98	4.46	-5.49	9.95	negative regultion of apoptosis and

								blood coagulation
Mm.89389	Ptafr	Platelet-activating factor receptor	1	-2.86	6.04	-1.35	7.39	chemotaxis/ cytokine production/ response to lipopolysaccharide/ signal transduction/ receptor activity
MGI:97798	Ptgs2	prostaglandin-endoperoxide synthase 2	1	-8.30	0.34	-5.23	5.57	Positive regulator of fever and apoptosis
Mm.439692	Serpina1a	Serine (or cysteine) peptidase inhibitor, clade A, member 1a	1	-3.65	8.55	4.25	4.30	Complement and coagulation cascades, organism-specific biosystem (from KEGG) / platlet activation (KEGG)/ response to cytokine stimulus
Mm.220821	Stab1	Stabilin 1	1	1.93	3.07	-2.63	5.70	cell adhesion/ bacterial binding
Mm.273024	Tlr1	Toll-like receptor 1	2	1.20	2.79	-2.85	5.64	activation of NF-kappaB-inducing kinase activity/ cellular response to triacyl bacterial lipopeptide/ macrophage activation/ positive regulation of interleukin-6 biosynthetic process/ positive regulation of tumor necrosis factor biosynthetic process
Mm.42146	Tlr6	Toll-like receptor 6	2	-5.44	1.98	-4.28	6.27	cellular response to diacyl bacterial lipopeptide/ positive regulation of I-kappaB kinase/NF-kappaB cascade/ positive regulation of JUN kinase activity
Mm.307668	Tnfsf14	Tumor necrosis factor (ligand) superfamily, member 14	1	0.42	1.67	-6.26	7.93	T cell costimulation/ release of cytoplasmic sequestered NF-kappaB

Table 8.13: Genes with increased transcript abundance in Δ*laeA* infected relative to Af293 infected experimental cohort in neutropenic model

ORF	Gene Name	Description	Replication on arrays	Neutropenic saline log_2	Af293 log_2	Δ*laeA* Log_2	Difference between Af293 and Δ*laeA*	Functional classification
Mm.795	Csf1	Colony stimulating factor 1 (macrophage)	1	-1.34	2.85	6.89	4.04	Positive regulator of mononuclear cell proliferation
MGI:1339751	Csf3	colony stimulating factor 3 (granulocyte)	1	-	1.99	6.38	4.39	Granulocyte differentiation
Mm.112765	Ripk2	Receptor (TNFRSF)-interacting serine-threonine kinase 2	1	2.37	3.72	7.00	3.28	cellular response to lipopolysaccharide/ T cell proliferation/ apoptosis/ positive regulation of I-kappaB kinase/NF-kappaB cascade/ positive regulation of T-helper 1 cell differentiation/ positive regulation of chemokine production
MGI:1914296	Tbc1d7	TBC1 domain family, member 7	1	-0.31	-1.41	2.36	3.78	positive regulation of protein ubiquitination

8.3.5 Interrogation of LINE-1 mobilisation in Af293, Cea10 and ATCC46645 isolates

Southern blotting was employed to interogate the hypothesis that LINE-1 mobilisation might differ in *A. fumigatus* Af293 and Δ*laeA*. It was hypothesised that increased transcription of multiple genes associated with transposition in Δ*laeA* during infection may result in novel insertion events in the Δ*laeA* genome, thereby explaining the pleiotropic and spatially diverse impact of LaeA regulation. Mycelial gDNA was extracted from 24 hour culture, HindIII digested and probed using a 592 bp gDNA fragment which was conserved in 11 putative LINE-1 elements (Afu2g18080, Afu3g09430, Afu3g15370, Afu4g14370, Afu4g14870, Afu5g00270, Afu5g00370, Afu6g00780, Afu6g00780, Afu8g00310, Afu8g06290). Southern blots from the Af293 and Δ*laeA* isolate are shown in Figure 8.11A, which suggested increased copy number of the LINE-1 probe.

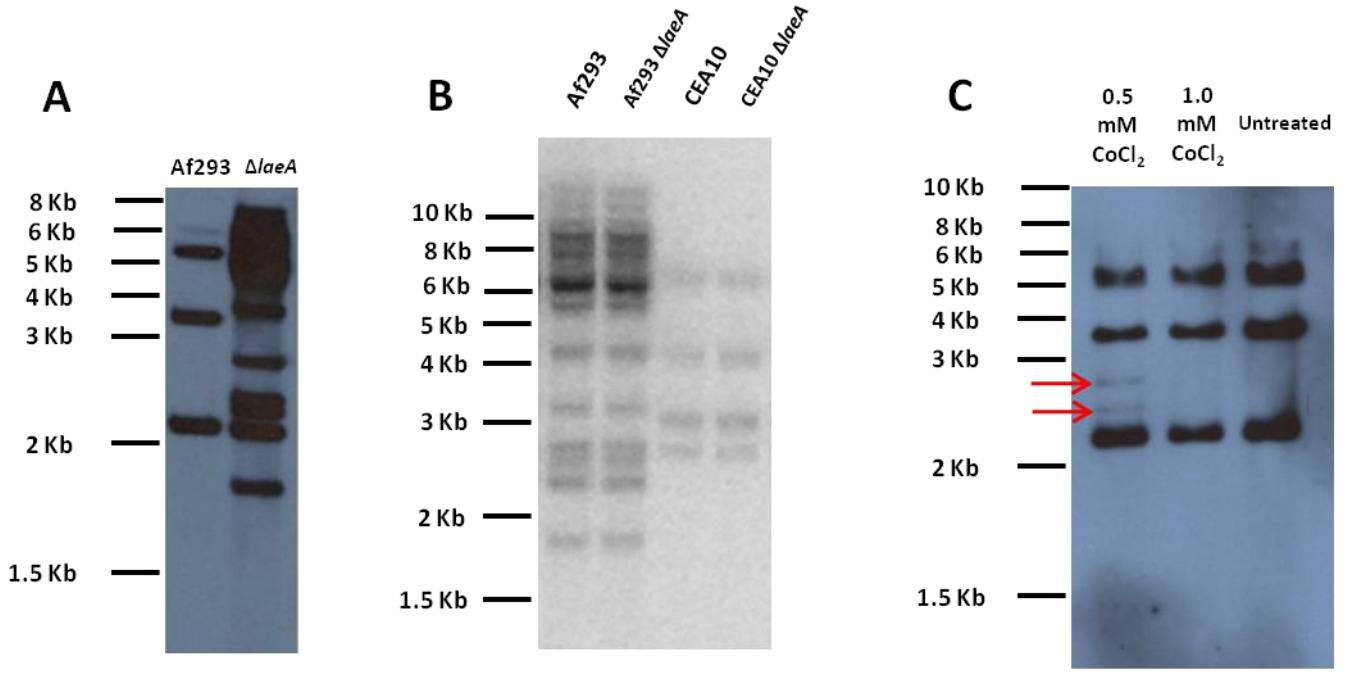


Figure 8.11: Southern blots of *A. fumigatus* gDNA using a 592 bp gDNA fragment common to eleven putative LINE-1 elements. gDNA was extracted from 24 hour mycelial culture and HindIII digested. Subsequently, gDNA was probed using a 592 bp gDNA fragment which was common to LINE-1 elements. *A. fumigatus* isolates included those used in this chapter (A), and those from Nancy Keller's laboratory (B). These data suggest that strains used throughout this thesis were infact Af293 Δ*laeA* and a non-isogenic wild-type comparator. Additionally, the clinical isolate *A. fumigatus* ATCC46645 was grown on ACM supplemented with 0.5 mM and 1 mM $CoCl_2$, which were grown for 48 hours. Spores were then harvested and inoculated into ACM broth, with the respective $CoCl_2$ concentrations for 24 hours and processed for Southern blotting (C). Putative bands which may equate to LINE-1 insertion are highlighted in red.

In parallel to this experiment, and in order to confirm the phenotype inmultiple genetic backgrounds, our collaborators in Nancy Keller's laboratory (University of Wisconsin, USA) conducted identical experiments with Af293 and CEA10 isolates and the isogenic Δ*laeA* strains (Figure 8.11B). These data demonstrated that comparable LINE-1 copy numbers were evident among the tested isolates and isogenic Δ*laeA* strains. A further unexpected finding was that the distinctive LINE-1 banding pattern of the Af293 and CEA10 isolates suggested that strains used throughout this thesis were not isogenic wild-type comparators. This has critical implications for the data presented in this study and is addressed in full in the Addendum of this thesis. Importantly however, this experiment has identified increased LINE-1 copy numbers in the Af293 genome relative to that of CEA10, demonstrating that LINE-1 elements may indeed be active in certain genetic backgrounds.

Given that transposable elements mobilise under hypoxic conditions *S. pombe* (Sehgal et al. 2007) and hypoxic conditions represent a challenge to host colonisation in murine models of IPA, the effect of hypoxia on putative LINE-1 transposition was investigated. As an anaerobic incubator was not available, the hypoxia-mimicking agent $CoCl_2$ was used. Colony radial growth was reduced on plates containing 0.5 mM and 1 mM $CoCl_2$. The clinical isolate *A. fumigatus* ATCC46645 was grown on ACM supplemented with 0.5 mM and 1 mM $CoCl_2$, which were grown for 48 hours. Spores were then harvested and inoculated into ACM broth, with the respective $CoCl_2$ concentrations for 24 hours and processed for Southern blotting. Two bands were observed which were resticted to gDNA extracted from mycelia grown in 0.5 mM $CoCl_2$ (Figure 8.11C, red arrows). These bands were not observed in other conditions. Southern blots were repeated twice with the same results. These data putatively suggest mobilisation of a LINE-1 element occurs during *A. fumigatus* growth under hypoxia mimicking conditions.

8.4 Summary

Aside from the obvious drawbacks of comparing non-isogenic strains in the comparative analyses described in this thesis, several interesting observations are forthcoming: (1) biologically relevant information are derivable from the experimental and analytical analyses conducted during this study; (2) LINE-1 gene expression varies between clinical isolates; (3) in the small cohort of strains thus far studied, heightened LINE-1 copy number correlates with expression of LINE-1 genes (thus vindicating the biological relevance of the initial hypothesis).

The ratiometric analysis described in this Chapter has used a common array normalisation strategy where $\log_2$ ratios are reported as a measure of gene expression in Δ*lae*A relative to Af293. Agreement was observed between the output arising from non-ratiometric and ratiometric normalisation methodologies, whereby *in silico* calculations of $\log_2$ ratios derived from the quantile normalised spot intensity datasets were highly concordant with $\log_2$ ratios calculated from this study (data not shown). This can be viewed as a further corroboration of the validity of the quantile normalisation method. The utility of both approaches is demonstrated by differential expression profiles which are detected in either non-ratiometric or ratiometric datasets. For example, no genes of the gliotoxin biosynthetic gene were found to be differentially expressed using ratiometric normalisation, yet the non-ratiometric approach identified a temporal programming of transcriptional regulation of key genes within the cluster between 8 and 14 hours in both tested isolates. Additionally, the significantly heightened of LINE-1 reverse transcriptases in the Δ*lae*A isolate was only identifiable by ratiometric comparisons. Therefore, both analytical methods have strengths and limitations, and the ideal analysis constitutes interrogation of both outputs.

The putative nuclear methyl transferase LaeA has been described as a global regulator of secondary metabolite biosynthesis in Aspergilli, and has been reported to regulate cluster and subtelomeric gene expression at the level of chromatin remodelling (Lee et al. 2009, Reyes-Dominguez et al. 2010, Shwab et al. 2007). An important component of chromatin is the nucleosome, an octamer of histone proteins enveloped by approximately 150 bp of DNA. In transcriptionally silent heterochromatic regions, DNA is packed into nucleosomes where gene promoter and flanking regions are inaccessible to RNA polymerases. The amino acid termini of histone proteins can be differentially acetylated or methylated by histone deacteylases, histone acetyltransferases or methyltransferases. Differential amino-terminal modifications generate synergistic or antagonistic interactions for chromatin associated proteins, which ultimately define the heterochomatic or euchromatic architecture (Jenuwein and Allis 2001). In eukaryotic genomes,

genes involved in functionally related pathways often cluster at proximal genomic locations (Keller and Hohn 1997). The existence of these clusters suggests they confer a benefit to the organism and are therefore positively selected, since processess such as gene translocation and cross over events would presumably physically disperse genes throughout the genome. Phylogenetic analyses have suggested horizontal gene transfer from beta-lactam producing prokaryotes to *Aspergillus* species seems to have occured for the isopenicillin-N-synthetase (IPNS) gene cluster of *A. nidulans* (Buades and Moya 1996). However secondary metabolite gene clustering may facilitate co-ordinated expression of genes by epigenetic regulatory mechanisms. Such global mechanisms may be used to suppress the biosynthesis of energetically costly metabolites during unfavourable conditions, such as early vegetative growth. Additionally, epigenetic regulation may activate metabolite production under environmental conditions to improve survivorship, for example during late stage vegetative growth, or during infection. Transcriptional comparisions between hyphae isolated from the murine host and developmentally matched laboratory culture identified numerous non-metabolite clusters which were co-expressed during infection (McDonagh et al. 2008), suggesting that virulence essential epigenetic regulatory phenomena might occur at loci additional to secondary metabolite clusters. This observation is supported by the the epigenetic regulation of virulence related non-metabolite clusters in other pathogenic fungi. For example, a 4 gene subtelomeric cluster of GPI anchored adhesins in *C. glabrata*, which are essential for virulence, are epigentically silenced by the histone deacetylase Sir3p (De las Penas et al. 2003), and clusters of antigenic variation genes in *Plasmodium falciparum* are epigenetically regulated by the histone deacetylase PfSir2 (Freitas-Junior et al. 2005). Thus, secondary metabolite and other non-metabolite clusters might be epigenetically controlled during *A. fumigatus* infection. The *in vivo* transcriptional profiling of Δ*laeA* will facilitate the assessment and prioritisation of of LaeA-regulated epigenetic mechanisms during the establishment of murine disease.

Data presented in this chapter demonstrate that only twenty five secondary metabolite biosynthetic genes were differentially expressed in Δ*lae*A relative to the wild-type, equating to 8.5% of the total dataset. Moreover, enrichment of differentially expressed genes at specific metabolite clusters was not observed, which is consistent with observations made from non-ratiometric analyses (Chapter 3) where increased transcript abundance of secondary metabolite genes is evident in the transcriptome of both isolates between 8 and 14 hours post infection. Given the putative function of LaeA as an epigenetic regulator of *A. fumigatus* gene expression at telomeres (Perrin et al. 2007, McDonagh et al. 2008) the dataset was interrogated with regard to these loci. Positional bias at sub-telomeres was not observed in genes which were differentially expressed between the

isolates. Comparable transcriptional profiles of secondary metabolite clusters and subtelomeric genes between Af293 and Δ*laeA* isolates, combined with their preferential employment between 8 and 14 hours during Δ*laeA* infection (Chapter 3) suggest LaeA-independent transcriptional regulation of these genetic loci *in vivo*. Additionally, these data suggest that secondary metabolite clusters (e.g. gliotoxin) and the subtelomeres in Δ*laeA* represent regions of transcriptionally active euchromatin.

In the current model of LaeA epigenetic regulation transcriptionally silent heterochromatin is formed by the histone deactylase HdaA, the H3K9 specific methylase ClrD and the heterochromatin protein HepA. HdaA directs the hypoacetylation of H3 and H4 (Lee et al. 2009), which facilitates methylation by ClrD. H3K9 methylation is recognised by HepA, which results in DNA methylation and the formation of heterochromatin. LaeA is hypothesised to reverse the formation of heterochromatin by DNA or H3K9 methylation activity. Several studies support this model. For example, Lee and colleagues characterised an *A. fumigatus* Δ*hdaA* mutant, and used western analysis to demonstrate that histone proteins H3 and H4 were hyperacteylated in the Δ*hdaA* background (Lee et al. 2009). TLC profiling of secondary metabolites following 72 hour liquid culture demonstrated increased production of secondary metabolites in the Δ*hdaA* isolate. RT-PCR of NRPS and PKS genes demonstrated increased transcript abundance in the Δ*hdaA* strain. These data are supported by a study in *A. nidulans* (Shwab et al. 2007) which demonstrated increased levels of sterigmatocystin and penicillin biosynthetic gene clusters in Δ*hdaA* relative to a wild-type isolate following 72 hours *in vitro* culture. Additionally, transcript abundance of genes within sterigmatocystin and penicillin clusters increased in Δ*hdaA*, whereas expression of genes adjacent to these clusters remained unaffected. Taken together, these studies suggest HdaA functions by hypoacetylation of H3 and H4 at specific secondary metabolite loci in order to increase metabolite biosynthesis. Removal of the acetyl group by HdaA enables methylation by ClrD (Palmer et al. 2008). These authors deleted *clrD* in *A. fumigatus,* and used immunoblotting to demonstrate that H3 mono- and tri-methylation was greatly reduced in Δ*clrD* relative to the wild-type. This histone modification is recognized by one of the principal components of heterochromatin, the heterochromation protein HepA (Reyes-Dominguez et al. 2010). Both HepA occupancy of AflR and H3K9 methylation are greatly increased in Δ*laeA* relative to the wild-type, indicating LaeA limits the extent of key modifications in the formation of heterochromatin (Reyes-Dominguez et al. 2010).

Transcriptional profiling described in this chapter does not directly challenge this paradigm, but is suggestive of differences in secondary metabolite gene regulation between *in vitro* and *in vivo*

studies. Firstly, in the current model of LaeA gene regulation the reversal of heterochromatin seems to be a prerequisite for gene expression. This hypothesis is based on the loss of secondary metabolites production from *in vitro* cultured Δ*laeA* strains (Bok et al. 2004, Bok et al. 2005) and the increased production of metabolites following deletion of *hdaA* (Shwab et al. 2007, Lee et al. 2009)*, clrD* (Palmer et al. 2008) and *hepA* (Reyes-Dominguez et al. 2010). More specifically, chromatin immunoprecipitation analysis of the *A. nidulans* sterigmatocystin cluster demonstrates loss of HepA concentration at the loci decreases as genes become expressed (Reyes-Dominguez. et al 2010). Upregulation of secondary metabolite clusters and subtelomeres during infection (Chapter 3) and comparable expression between Af293 and Δ*laeA* (this chapter) suggests these regions are likely euchromatic in Δ*laeA* during early disease. Thus, other proteins may reverse the formation of heterochromatin during infection. This hypothesis is supported by transcriptional data which demonstrated LaeA transcript abundance did not increase in either isolate throughout the time course (Chapter 3) or differ between isolates. Fascinatingly, in Af293, a LaeA-like methlytransferase (Afu3g14920) was highly and moderately increased between 4 - 8 and 8 – 14 hours respectively. A similar expression profile for this gene was observed in Δ*laeA*. An additional LaeA-like methlytransferase moderately increased in Af293 between 8 and 14 hours (Afu2g04380). PFAM analysis of Afu3g14920 and Afu2g04380 peptide sequences demonstrate both have putative methyltransferase domains.

Aspergillus secondary metabolism is strongly correlated with growth arrest and sexual or asexual reproduction (Keller et al. 2005). In *A. nidulans*, the light-regulated developmental factor VeA forms part of the heterotrimeric velvet complex with LaeA and VelB (Bayram et al. 2008). This complex regulates both sexual development and secondary metabolism through VelB and LaeA activity respectively. LaeA is therefore at the molecular boundary between development and secondary metabolite production (Bayram et al. 2008). While the correlation of metabolite production and LaeA regulation with vegetative growth is well established, no study has investigated the role of LaeA gene regulation during early germination.

In addition to epigenetic control mechanisms, the co-regulation of secondary metabolite cluster loci occurs by two classes of transcription factors, which either mediate environmental adaptation (e.g. PacC) or are specific to a biosynthetic pathway (GliZ). Fungal secondary metabolite regulation is responsive to general environmental factors including temperature, light, pH or carbon and nitrogen sources (Yu and Keller 2005). *In vivo* or *in vitro* environmental signals are perceived at the plasma membrane by G-protein-coupled receptors and transduced intracellularly by various signal transduction pathways, including the MAP kinase pathway, protein kinase A

pathway and cell integrity pathway (Bayram and Braus 2011). Transcriptional regulatory proteins relevant to host colonisation are the targets of these signal transduction cascades, including the nitrogen metabolism transcription factor AreA or pH response transcription factor PacC, which putatively regulate aflatoxin and penicillin biosynthesis in *A. parasiticus* and *A. nidulans* respectively (Chang et al. 2000, Then Bergh and Brakhage 1998). The interaction between these environmental adaption transcription factors and LaeA is unknown.

Regulation of secondary metabolite production is further complicated by in-cluster transcription factors, such as *gliZ* or *regA*, which putatively control expression of the cluster. For example, *gliZ* is required for *in vitro* gliotoxin production, wild-type virulence in a corticosteroid murine model of infection, and the expression of aminotransferase *gliI* during 72 hour *in vitro* culture at 25°C (Bok et al. 2006). Thus, disparities in environmental conditions and *A. fumigatus* developmental stage likely explain differences in LaeA secondary metabolite regulation reported in this chapter with those reported *in vitro*.

A striking feature of genes with elevated transcript abundance in Δ*laeA* relative to Af293 was the number of genes putatively involved in transposition. Southern blotting supported the notion that elevated mobilisation of LINE-1 elements occurs in Δ*laeA*, but demonstrated that this is due to increased copy number in the non-isogenic comparator rather than a regulatory mechinism of LaeA. Nevertheless, these data suggest that LINE-1 transcription, and mobilisation events are more significantly active in Af293 than other clinical isolates, such as CEA10 and ATCC46645. This is intriuging, given that LINE-1 mobile genetic elements are autonomous replicating elements which may have pleiotrophic impacts with regard to gene expression, genome organisation and evolution of eukaryotic organisms.

Mobile genetic elements are divided into class 1 and class 2 subtypes, which include retrotransposons and DNA transposons respectively. DNA transposons encode a transposase enzyme, which cuts the transposon from the chromosome and catalyses the reinsertion at another locus. Retrotransposons are the most common type of mobile genetic element in eukaryotes and replicate via an RNA intermediate. These elements may transpose via replicative or conservative mechanisms in which the mobile element is copied or excised from DNA prior to transposition respectively. Retrotransposons include long interspersed nucleotide elements (LINEs), short interspersed nucleotide elements (SINEs), long terminal repeats (LTRs) and non-LTR transposons.

Extensive bioinformatic analyses not reported in this thesis revealed a conserved 5.8 kb LINE-1 structure common to at least 8 LINE-1 elements, consisting of the following: (1) 14 bp of 5' and 3' direct terminal repeat regions; (2) 160 bp of 5' UTR; (3) 1491 bp encoding a putative 497 amino acid protein with no predicted function; (4) 3819 bp encoding 1273 amino acid protein with an endonuclease domain, reverse transcriptase domain, and RNase H I domain; (5) 340 bp 3'UTR including approximately 34 bp poly A tail. This structure is consistent with the functional human LINE-1 element which mobilises via target primed reverse transcription and a ribonucleoprotein complex consisting of ORF1 protein, ORF2 protein, LINE-1 RNA and gDNA (reviewed in Babushok and Kazazian, 2007). Briefly, LINE-1 elements integrate into the genome when ORF2p protein nicks DNA at the insertion site creating a free 3'hydroxyl group. LINE-1 ORF2p then uses LINE-1 RNA as template and the exposed 3' hydroxyl group as a primer to reverse transcribe the LINE-1 transcript directly into the genome. ORF2p then nicks the top of the DNA strand and the insertion is resolved by second strand synthesis.

Transposition has been demonstrated for DNA transposons in *A. niger,* for example the *Vader* element (Amutan et al. 1996). However, in *A. fumigatus*, only inactive mobile genetic elements have been described, including the retrotransposons *afut2, taf1*, and the DNA transposon *afut1* (Monroy and Sheppard 2005, Neuveglise et al. 1996, Paris and Latge 2001). All of these elements demonstrate repeat induced point (RIP) mutations, a homology-based process that mutates repetitive DNA, causing G:C and A:T transitions. This frequently leads to epigenetic silencing of the mutated sequences through DNA methylation (Galagan and Selker 2004). Evidence of RIP silencing, and truncation, was observed in several LINE-1 elements which were putatively upregulated in Δ*laeA*. Given the high level of sequence homology in the 3' region of all 13 LINE-1 elements, it is likely that these mutated elements are transcriptionally silent, and their putative upregulation in the Δ*laeA* isolate is due to homologous cDNA which originated from transcription of an active LINE-1 element. Thus, it is currently not certain which LINE-1 elements are transcribed or putatively mobilisable. Nevertheless, a conserved sequence lacking truncation and RIP mutation was observed for three LINE-1 elements (Afu8g01040, Afu8g00310, Afu3g09430), all of which were upregulated in Δ*laeA* during infection.

Several lines of evidence suggest that LINE-1 mobilisation might be associated with fungal development. Lamarre and co-workers reported increased transcript abundance of several LTR transposons following 30 minutes incubation in YPD, although these elements were not identifiable from interrogation of their published datasets (Lamarre et al. 2008). *In vivo* profiling of the ATCC46645 mutant relative to ATCC46645Δ*pacC* during the initiation of murine infection

demonstrated decreased transcript abundance of numerous LINE-1 elements, including the intact Afu8g01040, Afu8g00310, Afu3g09430 in the mutant (Bertuzzi et al. unpublished data). While this might plausibly be attributable to direct PacC-mediated regulatory phenomenon, increased transcript abundance in ATCC46645 might also be due to the abrogation of Δ*pacC* germination in the host. Indeed, transposon transcriptional increases became detectable between 8 – 14 hours in the murine lung.

Nevertheless, putative *in vitro* mobilisation of LINE-1 elements might be promptable in by hypoxia mimicking conditions, suggesting that environmental stress encountered in the host may induce transposition. In *S. pombe*, transposons were shown to be transcriptionally upregulated by heat and peroxide stress, but not by heavy metal or osmotic stress (Chen et al. 2003). Shegal and colleagues have show that the sterol regulatory element-binding protein (SREBP) Sre1 directly activates transcription of an entire family (Tf2) of retrotransposons (Sehgal et al. 2007). These LTRs function as oxygen-dependent promoters that are capable of directing low oxygen transcription of adjacent DNA sequences. While any impact on gene expression by the putative LINE-1 elements remains to be established, DNA transposons PbIa and PbIb in *A. nidulans* regulate expression of the subtelomeric penicillin cluster, as evidenced by decreased penicillin biosynthesis following deletion of the transposons (Shaaban et al. 2010).

Given the role of mobile genetic elements in evolution, gene expression and genome stability, it is intriguing to note considerable increase in copy number and transcription in Af293 relative to other clinical isolates. A putative explanation for the high abundance of LINE-1 elements was derived from recent experiments which demonstrate that Af293 is infected with a microvirus (Coutts, personal communication). Mycoviruses are able to suppress RNA silencing in *A. nidulans* (Hammond et al. 2008), a process which is triggered by double stranded RNA and which therefore might protect the host genome against viruses and mobile genetic elements (Plasterk 2002). Nevertheless, to further address this hypothesis, the presence or absence of mycoviral infection of ATCC46645 and CEA10 must be established, as well as the impact of *de novo* virus interactions into sterile isolates.

With regard to reverse engineering the molecular basis of Δ*laeA* attenuation, comparable expression of secondary metabolite genes suggest that abberant host-secondary metabolite interactions were unlikely to explain the attenuated phenotype of Δ*laeA*, with the possible exception of expression of the NRPS *ftmA* (Chapter 4). The ratiometric datasets were therefore interrogated for other putative *A. fumigatus* functions which may define the host-pathogen

interface. Four putatively secreted proteases demonstrated decreased transcript abundance in Δ*laeA* relative to Af293 at various stages throughout early murine infection including an alkaline serine protease Alp1 (Afu4g11800), an elastinolytic metalloproteise Mep (Afu8g07080), a putative serine peptidase (Afu2g01250) and a serine peptidase (Afu2g01250). Three of these were down regulated in the mutant at 14 hours post infection. The decreased expression of putatively secreted proteases at 14 hours in the host niche may reduce tissue invasion (Ben-Ami and Lewis, 2010), complement degradation (Behnsen et al 2010) Th2 activation (Banergee and Kurup 2003) or protease activated receptor stimulation (Hershenson 2007) by the Δ*laeA* strain. Histopathological analyses revealed a reduction in epithelial necrosis and tissue penetration in tissues infected with the Δ*laeA* isolate at this stage, which may be attributed to reduced protease breakdown of the lung parenchyma. Interestingly supernatant from a 72 hour Δ*laeA in vitro* culture demonstrates reduced cytotoxicity to human neutrophils relative to wild-type supernatant (Bok et al 2005). Although the authors suggested that this was due to reduced concentration of secondary metabolites in Δ*laeA* culture, reduction in secreted protease mediated host attack was not investigated. However, virulence analyses a *prtA* mutant, which encodes a transcription factor that positively regulates expression of numerous secreted proteases in murine models of infection (Bergmann et al 2009, Sharon et al 2009) suggests functional redundancy of secreted proteases in the host likely means they do not define attenuation of the Δ*laeA*.

Several other secreted enzymes which may modulate host-pathogen interactions were differentially expressed between the isolates, including the increased transcript abundance of an IgE-binding protein (Afu6g00430), lipase (Afu7g04950) and an extracellular chitosase CsnC (Afu3g14980). The biosynthesis of IgE-binding proteins by *A. fumigatus* is a key stimulus for the development of Th2 and allergic host reponses (Kurup et al. 2002). The decreased transcript abundance of potentially aggressive secreted enzymes in Δ*laeA* relative to Af293 was also observed, including an acid sphingomyelise (Afu4g06640) and an antigenic thaumatin domain protein (Afu8g01710). Given the transcriptional upregulation of the acid sphingomyelinase in Af293 between 4 and 8 hours post infection (Chapter 3), the reduction in expression relative to Δ*laeA* at 8 hours, and the haemolytic or cytotoxic actions of sphingomyelinases from other pulmonary pathogens (Vasil et al. 2009) further characterisation of this molecule with regards to host-pathogen interactions is strongly warranted.

The *A. fumigatus* cell wall plays a critical role in host-pathogen interactions, as polysaccharide moieties, including β-glucan, chitin, galactomannan and α-glucan are all candidate PAMPs for host PRRs. It was therefore interesting to note the increased transcript abundance of 5 cell wall or cell

surface associated genes in Δ*laeA* throughout infection. These genes included 1,3-beta-glucanosyltransferase Gel1 (Afu2g01170), cell surface protein Mas1 (Afu8g00610) and cell wall biogenesis protein (Afu2g04880). Moreover, the cell wall associated proteins alpha-1,3-mannosyltransferase (Afu6g14480) and GPI anchored protein (Afu1g01300) were decreased in Δ*laeA* at 14 hours post infection. The importance of cell wall PAMPs is evidenced by the soluble PRR pentraxin 3, which is only able to bind conidial morphotypes, which is most likely due to alterations in galactomannan on the hyphal surface (Garlanda et al. 2002). Chai and co-workers have recently demonstrated that polysaccharide components of the fungal cell wall can modulate host innate immune responses through TLR-2 and TLR-4 signalling pathways (Chai et al. 2011). These authors activated PBMC TLR-2 and TLR-4 signalling pathways using ligands Pam3Cys and lipopolysaccharide respectively. Il-6 was used to measure TLR signalling following incubation of activated PBMCs with several cell wall polysaccharides, including β-glucan, chitin, galactomannan and α-glucan. β-glucan and galactomannan reduced PBMC Il-6 production via TLR-4 pathway while, α-glucan inhibited both TLR-2 and TLR-4 Il-6 production. Thus, differential transcription of genes associated with cell wall carbohydrates in Δ*laeA* relative to Af293 *in vivo* may have critical implications for Δ*laeA* PAMPs and pathogen modulations of the host immune responses. Certainly, Δ*laeA* conidia have modifications to the cell wall which impact host pathogen interactions *in vitro*. For example, SEM has demonstrated Af293 Δ*laeA* spores are smooth, and lack the echinulate rodlet layer on the conidial surface (Bok et al. 2005). Dagenais and co-workers have demonstrated increased phagocytosis of Δ*laeA* spores by macrophages is due to the loss of the rodlet layer (Dagenais et al. 2010). These authors recognition blocked of cell wall PRR β-glucan and mannan with laminarin and exogenous mannan respectively, and found differences in phagocytosis between wild-type and Δ*laeA* spores were not affected. Comparable rates of macrophage phagocytosis were only observed following removal of the wild-type rodlet layer by sonication, or by allowing Δ*laeA* spores to swell. Nevertheless, no studies have investigated modification of cell wall PRR of Δ*laeA* hyphae. Differential expression of 6 genes between Δ*laeA* and Af293 at 14 hours post infection suggests hyphal PRR and immunomodulatory polysaccharides may be differently biosynthesised in the Δ*laeA* isolate during infection.

For example, increased expression of *gel1* may increase survivorship in Δ*laeA* infected animals as this PAMP may stimulate Th1 protective immunity. The GPI-anchored 1,3-beta-glucanosyltransferase Gel1 was upregulated in Δ*laeA* relative to Af293 at all time-points post infection. Bozza and colleagues have demonstrated that recombinant Gel1 stimulates protective immunity in an experimental murine model of vaccination and in human specific $CD4^+$ T-cells (Bozza et al. 2009). Bozza et al immunised mice with recombinantly expressed Gel1 and

assessed protection against IPA. Protection was assessed in a neutropenic model in terms of survival, local fungal growth and dissemination, and pattern of Th cell activation. The following was observed in Gel1 treated mice relative to non-treated controls: (1) median survival time increased; (2) growth in the lung and dissemination to the brain decreased; (3) IFN-γ, IL-10, IL-17A protein concentrations increased in lung homogenates 3 days following infection; (4) IL-4 protein concentrations decreased in lung homogenates 3 days following infection. These authors associated increased IFN-γ, IL-10, IL-17A in Gel1 vaccinated animals with a protective Th1 or Treg response which led to increased survival. Gel1 was also assessed with regard to Th activation and cytokine production by human T cell clones. In this experiment, PBMC were isolated from healthy donors and pulsed with heat inactivated conidia, Gel1 or a non-treated control, after which $CD4^+$ T-cell supernatants were isolated and assayed for cytokine content. This demonstrated increased production of IFN-γ and IL-10 in both Gel1 and conidia pulsed cells relative to untreated controls. However, the Th2 cytokine IL-4 increased in conidia but not Gel1 treated samples relative to non-treated controls. Thus, the authors hypothesised that Gel1 elicited a protective immune response leading to favourable disease outcome. In the pulmonary pathogen *Coccidioides posadasii*, subcutaneous administration of a recombinantly expressed gel1 homologue increased survival and reduced fungal burden relative to non-immunised mice (Delgado et al. 2003). Thus, it seems Gel1 elicits a protective immune response for at least two important pulmonary pathogens. The increased expression of this molecule in Δ*laeA* relative to Af293 may account for the attenuation of the isolate by facilitating a protective Th1 or Treg response.

A striking feature of the comparative transcriptional profile between the strains was the decreased transcript abundance of numerous transporters in Δ*laeA*, most notably at 4 hrs post infection. These included drug (MFS drug transporter Afu6g03320), ion (calcium transporting ATPase Pmc1, Afu7g01030), sugar (MFS sugar transporter Afu4g14610), iron (siderochrome-iron transporter MirB, Afu3g03640) and toxin (MFS toxin efflux pump AflT, Afu1g12620) transporters. Such a reduction in cell membrane transport at the very early stage of infection might be indicative of defective pH adaptation of Δ*laeA*, as many membrane transporters rely on the symport of protons which consequently impacts pH of the cytoplasm. This hypothesis was in part supported by an increase in the *S. cerevisiae* Pma1 homologue (Afu1g02480) at 8 and 14 hours in Δ*laeA*. In yeast, Pma1 is an H+ ATPase and the primary proton pump of the plasma membrane. It generates an electrochemical proton gradient, thus providing energy for secondary solute transport systems. However, *in vitro* phenotypic analyses demonstrated Δ*laeA* was not sensitive to pH (data not

shown). Nevertheless, a general state of elevated pH stress may contribute to the attenuation of Δ*laeA* in the lung.

Several transcription factors demonstrated increased (n = 3) and decreased (n = 8) transcript abundance in Δ*laeA*. The regulatory role of these transcription factors is currently unknown. Of interest was the decrease of the *gliZ*-like transcription factor, which resides on an uncharacterised secondary metabolite cluster on chromosome 3 (Afu3g12890).

Throughout the initiation of infection *A. fumigatus* stimulates and is confronted by a diverse range of host innate immune responses including physical barriers, soluble PRRs, and various cell subsets. In this chapter, qRT-PCR analysis was used as a tool to characterise the early transcriptional pulmonary immune response to Af293 and Δ*laeA* infection relative to an immunocompetent control cohort. Although several genes demonstrated increased transcript abundance in Δ*laeA* relative to Af293 infected BALFs (n = 4) the majority of differentially expressed genes were downregulated in samples which had been challenged with the mutant (n = 37). This might indicate a reduction in the general innate immune response to Δ*laeA*, an observation which is supported by histological analysis from 14 hours post infection.

Interrogation of genes for which expression was measured by technical qRT-PCR replicates reveals increased transcript abundance of two inflammation associated genes, C-reactive protein and CXCL-10 in Af293 BALFs relative to Δ*laeA*. C-reactive protein (CRP) is a member of the pentraxin family of soluble PRRs, the plasma concentration of which increases during mammalian inflammatory states. *In vitro* profiling has demonstrated C-reactive protein enhances human neutrophil phagocytosis of swollen, but not dormant conidia of *Aspergillus fumigatus* (Richardson et al. 1991). The role of this protein *in vivo* has not been investigated in *A. fumigatus*, but other pentraxins have critical implications for host defences to *A. fumigatus* infection. For example, the soluble PRR pentraxin-3 binds to *A. fumigatus* resting condia, putatively to the PAMP conidial galactomannan (Garlanda et al. 2002). Pentraxin-3 binding enhances phagocytosis of alveolar macrophages and dendritic cells and pentraxin 3 null mice are highly susceptible to *A. fumigatus* infection (Garlanda et al. 2002). CXCL-10 is an inflammatory mediator in murine models of IPA (Ramaprakash et al. 2009). This cytokine promotes dendritic cell and macrophage migration *in vitro* and patients with proven or probably IPA have high levels of CXCL-10 in serum (Mezger et al. 2008b).

An intriguing finding when comparing host transcription between Af293 and Δ*laeA* infected BALFs was the increased and decreased transcript abundance of IL-10 relative to the immunocompetent control respectively. IL-10 is a 35 kDa cytokine which is secreted by Th2 lymphocytes, macrophages, mast cells and B-cells. IL-10 has pleiotropic impacts on the host innate and adaptive immune system including downregulation of Th1 cytokines (e.g. INF-γ, THN-α), inhibition of Th1 $CD4^+$ differentiation, inhibition of nitric oxide production and suppression of macrophage function and proliferation (Borish and Steinke 2003). During late stages of *A. fumigatus* infection, IL-10 produced by T-regulatory cells may limit inflammation, and expression of IL-10 is associated with poor disease outcome (Romani 2004). Early investigations into IL-10 with regard to fungal pathogenesis demonstrated treatment with this cytokine reduced *C. albicans* killing by mouse peritoneal macrophages (Cenci et al. 1993). The first study regarding IL-10 and host phagocytic defences to *A. fumigatus* was conducted by Roilides and co-workers, who demonstrated that this cytokine has multiple impacts upon the function of murine mononuclear cells *in vitro* (Roilides et al. 1997). Comparisons between untreated and IL-10 treated phagocytes demonstrated reduced ROS production and hyphal damage in treated cells, as determined by spectrophotometric assessments of ROS production and an MTT assay of hyphal damage. Additionally, a phagocytosis assay demonstrated IL-10 significantly increased phagocytosis but not killing of conidia. The authors therefore proposed the "sanctuary" hypothesis, in which IL-10 results in increased levels of intracellular fungal burden, and reduced hyphal damage facilitates outgrowth from the macrophage. Additional studies have supported the detrimental role of IL-10 in IPA, as ELISA comparisons of IL-10 concentrations in BALF between immunocompetent and neutropenic mice challenged with *A. fumigatus* demonstrated significantly increased IL-10 concentrations in the neutropenic cohort (Cenci et al. 1998). Moreover, neutralisation of IL-10 with an anti-Il10 mAb increased median survival time and decreased fungal burden relative to untreated animals (Cenci et al .1998). Thus, enhanced levels of IL-10 may facilitate progression of IPA via inhibition of phagocyte killing. The importance of this cytokine with regards to host defence is highlighted by studies which demonstrate that $IL\text{-}10^{-/-}$ mice are significantly more resistant to *A. fumigatus* infection than wild-type animals (Clemons et al. 2000). Additionally, comparisons of serum from 8 humans with diagnosed IPA demonstrated increased IL-10 serum levels when compared to healthy controls (Roilides et al. 2001). Notwithstanding these data, it is unclear whether enhanced concentration of IL-10 causes or results from progression of IPA. Therefore, increased abundance of IL-10 in Af293 relative to Δ*laeA* infected BALFs may simply be due to the enhanced virulence of the wild-type. Conversely, enhanced stimulation of IL-10 by an unknown mechanism during Af293 infection may hold the key to the differential virulence of the two isolates.

This latter hypothesis is partially supported by differential expression of TLR-1 and TLR-6, which increased and decreased in transcript abundance in Af293 and Δ*laeA* infected animals relative to the immunocompetent control respectively. TLR-1 and TLR-6 are receptors which form heterodimers with TLR-2, and these complexes recognise specific PAMPs. For example, the TLR-2/TLR-6 complex recognises lipoteichoic acid on the cell wall of Gram positive bacteria, whereas TLR-2/TLR-1 recognise triacyl lipopeptides (Takeda et al. 2002, Triantafilou et al. 2006). Circumstantial evidence supports a role of these receptors in defence against *A. fumigatus,* as screening of allogeneic hematopoietic stem cell transplant recipients revealed an association of TLR-1 and TLR-6 polymorphisms with susceptibility to IPA (Kesh et al. 2005). Netea and co-workers profiled the role of TLR-1 and TLR-6 receptors in response to *C. albicans* infection (Netea et al. 2008). Survival between wild-type, TLR-$1^{-/-}$ and TLR-$6^{-/-}$ mice was comparable in a disseminated model of candidiasis. Nevertheless, splenocytes isolated from primed TLR-$6^{-/-}$ mice and co-incubated with *C. albicans* blastocytes released significantly less IL-10 and more IFN-γ than cells isolated from wild-type or TLR-$1^{-/-}$ mice. Thus, in *C. albicans* infection, TLR-6 is involved in the stimulation of the anti-inflammatory Th2-type cytokine IL-10, resulting in a skewed proinflammatory profile in TLR-6 knock-out mice. Increased transcription of IL-10 in the Af293 lung relative to Δ*laeA* may therefore be attributed to TLR-6 activation in Af293 infected animals. Given that TLR-1 and TLR-6 recognise lipopeptide moieties of bacteria (Takeda et al. 2002), differential expression of these ligands is suggestive of a lipopolysaccharide PAMP which is present and absent in Af293 and Δ*laeA* respectively. Conversely, TLR-6 is a PRR for the PAMP zymosan of *S. cerevisiae*, which is a β-1,3-glucan. Additionally, macrophage activation by *Tinospora cordifolia* (1,4)-α-d-glucan is TLR-6 dependent (Nair et al. 2006). Thus, carbohydrate or peptide PAMPs presented by Af293 but not Δ*laeA* may account for differences in TLR-6 expression. This might have critical implications for IL-10 activation, and ultimately, disease outcome.

Chapter 9

Discussion and conclusions

Establishment of IPA is dependent on the exit of spore dormancy, isotrophic swelling and the production of germ tubes and invasive hyphae. The development of *A. fumigatus* in the host is markedly different from growth *in vitro*. During infection conidiation does not occur, whereas during growth in rich medium developmental competence is achieved between 9 - 10 hours (Sheppard et al. 2005). *A. fumigatus* development in the immunocompromised mammal is a critical aspect of infection, as genes which co-ordinate growth and differentiation often regulate the expression of key virulence factors through the same signal transduction cascades. For example, members of the Asm1p, Phd1p, Sok2p, Efg1p, and StuAp (APSES) family of fungal proteins regulate morphogenesis and virulence in ascomycetes. In *C. albicans*, the transcription factor Efg1 is a component of the Ras-protein kinase A pathway (Stoldt et al. 1997). The deletion of *efg1* results in rod-like, pseudohyphal cells, whereas overexpression leads to enhanced filamentous growth (Stoldt et al. 1997). *efg1*Δ/*efg1*Δ mutants have reduced capacity to *invade and damage* oropharyngeal epithelial cells *ex vivo,* and are attenuated in an intravenous model of disseminated candidiasis (Park et al. 2005). Deletion of the APSES transcription factor *mstu1* in *M. grisea* results in reduced conidiation and mycelial growth (Nishimura et al. 2009) whereby a gene deletion mutant was found to be delayed in appressorial formation and demonstrated reduced penetration of an onion epithelial layer relative to the wild-type. In *A. fumigatus*, StuA regulates development and the expression of several virulence related genes, including those directing gliotoxin, pseurotin A biosynthesis, a mycelial catalase and an IgE binding protein (Sheppard et al. 2005).

These observations pose interesting questions with regard to virulence of *A. fumigatus* and development. Do disparities between development in the host and laboratory culture account for the production of virulence factors *in vivo*, or can the production of aggressive and defensive molecules which interact with the host simply be attributed to *A. fumigatus* growth and differentiation? These questions were in part answered by McDonagh and co-workers, who compared gene expression between developmentally matched hyphae isolated from the host niche and laboratory culture (McDonagh et al. 2008). This study demonstrated several genes associated with virulence were upregulated during host colonisation, for example gliotoxin and secreted proteases. Thus, environmental cues encountered in the host niche appeared to be more important than developmental regulators such as StuA, in the regulation of virulence genes *in vivo*.

The time-course of infection presented in Chapter 3 can potentially complement the study by McDonagh and colleagues, given that time-series analyses enable dissection of the host-infecting transcriptome prior to the invasive hyphal stage. Presumably, upregulation of several functional categories between spore and hyphae in the host, such as microtubule and cell polarity genes, are related simply to the establishment of polar hyphal extension. Nevertheless, interrogation of published (Lamarre et al. 2008, Sheppard et al. 2005, Twumasi-Boateng et al. 2009), and unreported datasets (Alcazar-Fuoli et al. unpublished) which profile growth throughout several developmental stages *in vitro*, with the *in vivo* time-series presented in this thesis provides some illuminating insights into the relationship between development and virulence. Upregulated and downregulated datasets have obtained from experiments comparing gene expression between: (1) dormant conidia and conidia incubated in YPD, at 37°C, for 30 minutes (Lamarre et al. 2008); (2) dormant conidia and germlings following growth in YPD, at 37°C, for 24 hours (Alcazar-fuoli. et al unpublished data); (3) conidia incubated from 1 hour in YPD at 37°C with hyphae isolated from 24 hours (Twumasi-Boateng et al. 2009). These datasets were compared with the non-ratiometric comparisons from the wild-type isolate between 4 - 8 and 8 - 14 hour time-points in the host (Chapter 3).

Strong themes among genes having decreased transcript abundance during infection include ribosome biogenesis, RNA metabolism and protein biosynthesis. For example, 28 mitochondrial genes were downregulated between 4 and 8 hours post infection (Chapter 3). This is in contrast to all *in vitro* datasets (Twumasi-Boateng et al. 2009, Lamarre et al. 2008, Sheppard et al. 2005, Alcazar-Fuoli et al. unpublished), which demonstrated a trend towards protein synthesis. Numerous genes associated with these processes demonstrate upregulation and downregulation *in vitro* and *in vivo* respectively, for example a 40S ribosomal protein S5 (Afu1g15020), a 60S ribosomal protein L12 (Afu1g03390), a mitochondrial DNA-directed RNA polymerase (Afu2g15610), mitochondrial export translocase (Afu5g03640), mitochondrial large ribosomal subunit L30 (Afu2g16970) and a mitochondrial large ribosomal subunit protein (Afu1g11940). Thus, the trend towards immediate protein synthesis reported from germinating conidia and hyphae seems to be specific to growth in rich medium. These data may further support the hypothesis of McDonagh and colleagues, who suggested nutrient starvation is a significant environmental stress encountered in the host (McDonagh et al. 2008).

Comparisons between genes upregulated between 4 – 14 hours in the host (Chapter 3) with those upregulated following 24 hour growth in YPD (Twumasi-Boateng et al. 2009, Alcazar-Fuoli et al. unpublished) revealed numerous genes directing cell wall biosynthesis (e.g. 1,3-beta-glucan synthase catalytic subunit FksP Afu6g12400, 1,3-beta-glucanosyltransferase Gel1 Afu2g01170,

1,3-beta-glucanosyltransferase Gel2 Afu6g11390), cell division (e.g. cell division cycle protein Afu1g14730, cell division protein kinase Afu1g13600, cell polarity protein Tea1 Afu2g02520) and microtubule biosynthesis (microtubule associated protein Ase1 Afu2g16260, microtubule associated protein EB1 Afu3g11860). These data are consistent with *in vivo* and *in vitro* cell division and cell wall remodelling between spore and hyphal morphologies. These functional categories were notably absent from the study by Lamarre and co-workers, presumably because the study analysed the spore at just 30 minutes germination (Lamarre et al. 2008).

With regard to infection, many virulence associated genes are upregulated during both *in vivo* and *in vitro* growth. For example, Asp F7 (Afu4g06670) is upregulated in the host between 4 and 14 hours (Chapter 3), following 30 minutes incubation in YPD (Lamarr et al. 2008) and following transition to invasive hyphae (Alcazar-Fouli et al. unpublished). Other virulence associated genes demonstrate upregulation *in vivo* and *in vitro*, including a mycelial catalase (Afu3g02270), the p-amino benzoic acid synthase *pabaA* (Afu6g04820), allergen Asp F4 (Afu2g03830), a superoxide dismutase MnSOD (Afu1g14550) and an IgE-binding protein (Afu6g00430). These data suggest that transcriptional upregulation of certain virulence-associated genes within the host might be soley due their dependency on fungal development rather than in response to specific cues encountered in the host.

Nevertheless, several virulence associated genes are upregulated *in vivo* but not *in vitro*. The upregulation of secreted proteases between 4 – 8 hours post infection appears to be a striking example of potentially aggressive pathogen strategies which are limited to the host niche. For example, *alp1* (Afu4g11800), *mep1* (Afu8g07080), and *pep1* (Afu7g04930) were all highly upregulated in the host, yet are not differentially expressed in any *in vitro* dataset. The virtual absence of any protease upregulation *in vitro* may be due to the nitrogen-replete growth media utilised in these studies. Nevertheless, these data demonstrate the preferential use of these enzymes in the host, and highlight them as potential contributors to the early host-pathogen interface. The relevance of iron limitation as a significant challenge to host colonisation was also reinforced by this analysis, with several genes associated with iron acquisition upregulated only in the host, for example siderochrome-iron transporters *sit1* (Afu7g06060), *mirC* (Afu2g05730) and a siderochrome-iron transporter (Afu3g13670). Upregulation of other molecules associated with host pathogen interactions and virulence was limited to the host niche, for example a haemolysin (Afu6g02280), an acid sphingomyelinase (Afu4g06640) and two lipases (Afu1g02580, Afu7g04950). Thus, developmental regulators may play a critical role in the establishment of IPA, yet environmental factors in the host putatively upregulate virulence associated genes.

A defining feature of 8 – 14 hour dataset was the increased transcript abundance of genes directing secondary metabolite biosynthesis. Several studies have demonstrated a strong link between fungal development and secondary metabolism, for example the melanisation of appressoria in *M. grisea* and *C. lagenarium*, and sporulation and aflatoxin production in *A. parasiticus* (Eliahu et al. 2007, Reiss 1982, Tsuji et al. 2000). In *A. nidulans,* LaeA is a component of the heterotrimeric velvet complex which co-ordinates light, fungal development and secondary metabolism (Bayram et al. 2008).

Interrogation of upregulated datasets in the first 30 minutes of *in vitro* growth reveals few genes involved in secondary metabolite biosynthesis (n = 8, total 598, Lamarre et al. 2008), which is consistent with the hypothesis that secondary metabolites are not biosynthesised during periods of extensive *A. fumigatus* primary metabolism. In contrast, genes upregulated following 24 hour growth (Twumasi-Boateng et al. 2009) demonstrate clear enrichment at specific metabolite clusters, including the *psoA* and *ftmA* supercluster (Afu8g00100 – Afu8g00720), an uncharacterised epipolythiodioxopiperazine-like toxin cluster (Afu3g12870 - Afu3g12990) and the gliotoxin cluster (Afu6g09580 – Afu6g09770). In addition to the study of the Af293 clinical isolate, the authors investigated the transcriptome of a Δ*stuA* strain during growth in YPD. StuA is a member of the APSES family of fungal proteins, and was demonstrated to regulate morphogenesis, and a Δ*stuA* mutant demonstrates significant morphological aberrancies, including conidiophores which lack stalks, and greatly reduced conidia relevant to the progenitor isolate (Sheppard et al. 2005). In a Δ*stuA* isolate, differential expression of genes residing in the above secondary metabolite loci was not observed throughout *in vitro* growth (Sheppard et al. 2005, Twumasi-Boateng et al. 2009). The authors therefore hypothesised that StuA positively regulates transcription of these clusters, which might link development and secondary metabolism in *A. fumigatus*. Comparison of genes mis-expressed in the Δ*stuA* isolate with genes increasing in the host between 8 – 14 hours infection revealed numerous genes of the three metabolite clusters putatively under StuA control, including three genes from a putative epipolythiodioxopiperazine-like toxin cluster (Afu3g12890, Afu3g12910, Afu3g12930), five genes from the gliotoxin cluster (Afu6g03480, Afu6g09630, Afu6g09640, Afu6g09650, Afu6g12050) and five genes from the *psoA*/*ftmA* cluster, including *psoA* (Afu8g00540) and an uncharacterised NRPS (Afu8g00490). Therefore we hypothesise that the developmental regulator *stuA* may positively regulate these regions during infection. In support of this hypothesis, *stuA* (Afu2g07900) transcript abundance was greatly increased in the murine lung between 8 – 14 hours.

In contrast, a correlation between upregulation of secondary metabolite gene expression and development was not supported by comparisons between dormant conidia and hyphae from 24

hours culture in the study by Alcazar-Fuoli and colleagues. Only 8 such genes increase between these time-points which were not enriched at any specific metabolite loci. These data are consistent with work conducted by McDonagh and colleagues which suggested these loci, amongst other secondary metabolite clusters, were upregulated in the host (McDonagh et al. 2008). The marked differences in secondary metabolite gene expression between the Alcazar-Fuoil and Twumasi-Boateng studies are surprising given the similarities in experimental design.

These initial interrogations into what constitute a substantial body of novel datasets demonstrate that there is clearly much to be gained from comparative analysis of microarray experiments from *in vitro* and *in vivo A. fumigatus* samples. More generally, inter-experimental comparisons of gene expression might significantly enhance understanding of the host-infecting *A. fumigatus* transcriptome. However, major challenges encountered during such analyses are the impenetrable nature of the published datasets, difficulties in accounting for the various experimental designs, and substantial differences in normalisation and definition of differentially expressed genes. Indeed, gene expression from various growth morphologies has been reported relevant to dormant conidia (Lamarre et al. 2008, Alcazar-Fuoli, unpublished data), spores incubated for 1 hour in YPD (Sheppard et al. 2009), germlings grown in YPD (McDonagh et al. 2008) and spores isolated at 4, 8 or 14 hours post infection (Chapter 3). In light of these difficulties, a fuller exploitation of the expanding *A. fumigatus* transcriptional literature is severely limited. Non-ratiometric array normalisation of all the published *A. fumigatus* transcriptional datasets, including those presented in this thesis, might circumvent these difficulties. Work presented in Chapter 3 demonstrates that following non-ratiometric and quantile normalisation, gene expression can be compared between experimental samples without the need for co-hybridisation. Non-ratiometric normalisation of datasets from the studies of Twumasi-Boateng, McDonagh, Alcazar-Fuoli, Chapter 3, among others (e.g. Nierman et al. 2005, Perrin et al. 2007) would effect inter-experimental normalisation and facilitate comparison of gene expression under a variety of *in vitro* and *in vivo* conditions. This might be a major step in harnessing the full power of *A. fumigatus* transcriptional profiling.

Work presented in this thesis supports the hypothesis that fungal secondary metabolites are a defining feature of the early host-pathogen interface. Analysis of deletion and disruption mutants suggest metabolite molecules from the pseurotin A, brevianamide F, *pes3* and *regA* biosynthetic pathways directly or indirectly modulate host-pathogen interactions. Both augmentation (*psoA*/*ftmA*/*regA*) and diminution (*pes3*) of virulence were supported by analyses of gene deletants in murine models of IPA. The *A. fumigatus laeA*-deletant utilised in this study is impaired in gliotoxin production and multiple unknown secondary metabolites as determined by TLC analyses of

laboratory culture (Bok et al. 2004, Bok et al. 2005). Accordingly, the attenuation of Δ*laeA* strains in murine models has been attributed to reduced toxin production during infection, especially gliotoxin (Bok et al. 2005, Sugui et al. 2007, Dagenais et al. 2010). This thesis directly challenges this hypothesis, in that it has demonstrated expression of secondary metabolite genes are comparable in the host between Δ*laeA* and a wild-type isolate. For example, ratiometric comparisons throughout the initiating stages of infection between Δ*laeA* and a wild-type isolate demonstrated secondary metabolite genes were comparably employed. Non-ratiometric analyses have demonstrated secondary metabolites are preferentially employed during the hyphal stage of disease, with 128 and 103 secondary metabolite genes upregulated between 8 – 14 hours in wild-type and Δ*laeA* isolates respectively (Chapter 3). Thus, the role of LaeA in secondary metabolite regulation during infection seems to be minimal. These data pose two interesting questions; (1) how are secondary metabolite loci regulated *in vivo*, and (2) why is Δ*laeA* attenuated?

With regard to secondary metabolite cluster regulation, given that HepA occupancy of the sterigmatocystin gene cluster in *A. nidulans* is inversely correlated with gene expression, it is likely that local euchromatic chromatin is a prerequisite for secondary metabolite gene expression (Reyes-Dominguez et al. 2010). During growth arrest *in vitro*, reversal of heterochromatin is presumably LaeA mediated, as genes at 13 secondary metabolite clusters demonstrated reduced transcript abundance in Δ*laeA* relative to Af293 following 60 hour culture in AMM (Perrin et al. 2007). Upregulation of numerous secondary metabolite genes in Af293 and Δ*laeA* between 8 – 14 hours *in vivo* suggests either of the following: (1) secondary metabolite loci are generally in a euchromatic state in the host, making LaeA function redundant, or (2) heterochromatin formation may be reversed or antagonised at secondary metabolite loci via LaeA-independent mechanisms. The latter hypothesis is strengthened by the observation that several genes which putatively promote gene silencing via epigenetic mechanisms were upregulated during the initiation of infection, suggesting a LaeA independent mechanism of chromatin remodelling is required. For example, a SIR2 family histone deacetylase (Afu3g00520) was upregulated, the orthologue of which in *S. cerevisiae* directs gene silencing at telomeres (Imai et al. 2000). Several other histone deacetylases were upregulated (Afu1g05490, Afu2g03810). Most notably, histone deacetylase *hdaA* (Afu5g01980) was moderately upregulated between 4 and 14 hours post infection. HdaA directs the hypoacetylation of H3 and H4 and is associated with silencing of secondary metabolite loci in *A. fumigatus* (Lee et al. 2009). Indeed, based on the model in which LaeA and HdaA reverse and promote the formation of heterochromatin at secondary metabolite loci respectively, one would predict that in both Δ*laeA* and Af293, secondary metabolite loci would be transcriptionally silenced by epigenetic mechanisms.

Several genes were upregulated during infection which may biosynthesise proteins which reverse or antagonise the formation of heterochromatin. For example, two LaeA-like methyltransferases (Afu3g14920 and Afu2g04380) are moderately upregulated. The role of these proteins in DNA or histone methylation is unknown. Protein kinases upregulated in the host may regulate gene expression at the level of chromatin remodelling, in addition to phosphorylation of transcription factors. In *S. cerevisiae* MAP kinases and protein kinase A subunits, including Hog1, Tpk1, Fus3, and Kss1 become physically associated with the genes that they regulate (Pokholok et al. 2006). Immunoprecipitation of histones in a *S. cerevisiae* Δ*hog1* and wild-type isolates following osmostress demonstrated marked reduction in histone content at the *stl1* gene (a glycerol proton symporter strongly induced when cells are subjected to osmotic shock) was limited to the wild-type isolate, indicating that Hog1 mediates nucleosome reorganisation in response to stress (Mas et al. 2009). Several studies in HeLa cell lines demonstrate that protein kinases have active roles in chromatin remodelling and may reverse or antagonise the formation of transcriptionally silent heterochromatin. Fischle and colleagues used mass spectrometry to suggest that H3 purified from a HeLa cell line contained K9 methylation and serine 9 phosphroylation (Fischle et al. 2005). Therefore, the authors inhibited the cell cycle regulator aurora B kinase with hesperadin. The authors conducted western blots of total chromatin content, and immunfluorescence of HeLa cells using an anti-heterochromatin 1 antibody to demonstrate increased HP1 chromatin binding following hesperadin treatment. Additionally, a florescein-labelled H3K9me3 peptide was used in a fluorescence assay to demonstrate loss of HP1 binding occurred to methylated H3 peptide following phosphorylation, which suggested phosphylation of histone 3 by aurora 1 protein kinase is able to disassociate HP1 from chromatin. In addition to modifying histones, Lomberk and colleagues have demonstrated that phosphorylation, specifically of heterochromatin protein 1, represents a regulatory mechanism for antagonising the H3 K9 epigenetic silencing mark (Lomberk et al. 2006). These authors used immunolocalisation of P-Ser 83-Hp1 and DAPI visualisation of chromatin regions to demonstrate this post translational modification led to Hp1 which was strongly association with euchromatic regions. Further experimentation demonstrated P-Ser 83-HP1 co-localises with RNA Pol II in HeLa cells and was thus located in regions of active transcription. Moreover, ChIP analysis of the human GAPDH gene showed that P-Ser 83-HP1 was present in regions of transcription, but not the promoter region. While the role of protein kinases in *A. fumigatus* chromatin remodelling is not known, these studies demonstrate that the upregulation of several protein kinases during infection may antagonise or reverse heterochromatin at secondary metabolite loci.

It was intriguing to note the high upregulation of the histone acetyltransferase subunit *yaf9* (Afu4g09820) between 4 and 8 hours post infection (Chapter 3). In *S. cerevisiae*, Yaf9 is a

component of the NuA4 histone H4 acetyltransferase complex (Zhang et al. 2004). Acetyltransferases are associated with the formation of euchromatin via the acetylation of histones. *S. cerevisiae* Δ*yaf9* strains display reduced transcription of genes in subtelomeres relative to progenitor strain as determined by microarray analyses of gene expression of *in vitro* culture (Zhang et al. 2004). Additionally, ChIP analyses demonstrated occupancy of the transcriptional silencing protein Sir3 at telomere-proximal regions caused transcriptional silencing in Δ*yaf9* strains.

In *A. fumigatus*, secondary metabolite biosynthesis is not solely regulated at the epigenetic level, but also by pathway specific and broad domain transcription factors. Pathway specific transcription factors which reside in the cluster they putatively regulate, have been of great interest due to their potential to aid metabolite discovery, as in the case of aspyridone A and B biosynthesis by an *A. nidulans* overexpression strain of the transcriptional regulator *apdR* (Bergman et al. 2007). Additionally, these regulators may co-ordinate the expression of toxic food contaminants, as is the case for *aflR*, which controls aflatoxin biosynthesis in *A. flavus*, and *A. paraciticus*, and sterigmatocysin in *A. nidulans* (Brown et al. 1996, Chang et al. 1995, Yu et al. 1996). *aflR* is the best studied pathway specific transcription factor, which binds to the *alfR* binding motif TCG(N_5)CGA in the promoter region of the majority of genes in the aflatoxin and sterigmatocystin biosynthetic clusters (Keller and Yin 2011). The importance of this gene with regard to metabolite biosynthesis is highlighted by deletion of *aflR*, which results in reduced levels of sterigmatocystin production by *A. nidulans in vitro* (Yin et al. 1996). Pathway specific regulatory factors may contribute to virulence of plant and animal pathogens. For example, the epipolythiodioxopiperazine toxin sirodesmin PL augments virulence of the phytopathogen *Leptosphaeria maculans* (Elliott et al. 2007). Genes within the cluster are regulated by the transcription factor *sirZ,* which is required for biosynthesis of the toxin (Fox et al. 2008). Several putative pathway specific transcription factors were upregulated in the wild-type isolate in the host (Chapter 3), including *regA* (Afu1g17640), *gliZ* (Afu3g12890), and other putative transcription factors, (Afu8g00420, Afu3g12890, Afu4g14680). The importance of these regulatory genes with regard to host pathogen interactions and virulence is highlighted by the attenuation of Δ*gliZ* (Bok et al. 2006) and Δ*regA* (Chapter 4).

While these transcription factors are likely to direct the expression of secondary metabolite genes in the host, the upregulation of several broad domain transcription factors which also control secondary metabolite biosynthesis was also observed. For example, the alkaline response transcription factor *pacC*, which was upregulated during infection, links external alkalinity and penicillin production in *A. nidulans* (Espeso et al. 1993). Growth in alkaline pH, or mutation in

PacC reduces biosynthesis of penicillin and transcript abundance of the isopenicillin N synthetase *ipnA*. Accordingly, we hypothesise that LaeA plays a minimal role in regulation of secondary metabolite loci *in vivo*. Work presented in this thesis suggests other chromatin remodelling proteins activate these clusters, and that positive regulation is effected by broad acting transcriptional regulators, pathway specific transcription factors and additionally the developmental regulator StuA.

With regard to elucidating the molecular basis of Δ*laeA* attenuation, several studies have suggested modification in the spore architecture may contribute to the virulence phenotype. For example, Δ*laeA* spores contain 60% less of the hydrophobic protein RodA relative to wild-type spores, which might increase exposure of PAMPs to host PRR and thus contribute to the attenuation of the isolate (Dagenais et al. 2010). Increased macrophage phagocytosis of dormant Δ*laeA* relative to wild-type conidia supports the hypothesis that exposed PAMPs on the conidial surface may result in increased phagocytosis (Bok et al. 2005, Dagenais et al. 2010). Nevertheless, several studies suggest this does not account for the attenuation of Δ*laeA*. For example, a Δ*rodA* isolate is fully virulent in a corticosteroid treated murine model of infection (Thau et al. 1994), whereas Δ*laeA* is attenuated (Sugui et al. 2007b). Perhaps more importantly, the relevance of pathogen-macrophage interactions has recently been questioned by depletion of macrophages in murine model of IPA using clodronate liposomes (Mircescu et al. 2009). These data demonstrate alveolar macrophage depletion did not result in murine susceptibility to intratracheal infection. Moreover, a Δ*laeA* isolate is able to germinate into hyphal filaments during murine infection, suggesting the hydrophobin layer of dormant conidia is not relevant to attenuation. Thus, previous hypotheses which attempt to explain Δ*laeA* attenuation are unsatisfactory. Transcriptional profiling of host and pathogen (Chapter 3 and Chapter 8) has allowed several new and previously unreported hypotheses to be postulated.

Increased transcript abundance of the Th1 associated GPI-anchored *gel1*, and downregulation of the Th2 allergens *mep1* and *alp1* in Δ*laeA* relative to the wild-type might suggest that the host is preferentially stimulated towards a protective Th1 response following infection with the mutant. Given the importance of adaptive immunity in the outcome of IPA (Mehrad et al. 1999, Cenci et al. 1999, Romani 2004), this is an attractive hypothesis. Additionally, innate immune profiling revealed transcriptional downregulation of both TLR-1 and TLR-6 which might recognise carbohydrate or lipopeptide moieties which are expressed and absent on the wild-type and Δ*laeA* cell surface respectively. We hypothesise that IL-10 might be upregulated in wild-type infected animals through the stimulation of these PRR which might downregulate Th1 cytokines such as INF-γ and THN-α, inhibit differentiation of protective Th1 CD4+, and suppress macrophage

function and proliferation. This hypothesis is partially supported by histopathological analysis of the infected lungs, which demonstrate reduced inflammation in Δ*laeA* infected animals relative to infection with the wild-type.

Interestingly, both ratiometric and non-ratiometric analyses suggested downregulation of putative pheromones in Δ*laeA* relative to the wild-type during infection. Prior to the discovery of the *A. fumigatus* sexual cycle (O'Gorman et al. 2009), both MAT1-1 and MAT1-2 mating loci had been identified (Paoletti et al. 2005, Nierman et al. 2005). *A. fumigatus* possesses a heterothallic breading system and a sexual cycle that leads to the production of cleistothecia following 6 months of laboratory culture (O'Gorman et al. 2009). Mating-type, pheromone-precursor, and pheromone-receptor genes *preA* and *preB* are expressed following 4 days growth on solid agar (Paoletti et al. 2005). Between 4 – 14 hours in Af293 various mating associated genes were highly upregulated including mating pheromone *ppgA* (Afu6g06360 rank 15), sexual development protein EsdC, (Afu7g01930, rank 36) and G protein complex alpha subunit *gpaA* (Afu1g13140, rank 40). Additionally, between 8 – 14 hours, a high mobility group (HMG) box gene was highly upregulated (Afu4g12470 rank 47). In Δ*laeA*, only two of these genes was upregulated, yet at a lesser rank than in Af293 (Afu7g01930, 4 – 14 hours, rank 337, Afu6g06360, 4 – 8 hours, rank 1219). The downregulation of mating associated genes in the Δ*laeA* strain was substantiated by ratiometric analysis, as *ppgA* Afu6g06360 was downregulated in Δ*laeA* at 8 and 14 hours post infection. These data are intriguing, given that pheromone signalling controls sexual reproduction and can activate expression of virulence factors in fungal pathogens of humans and plants. For example *C. ablicans* undergoes mating and a sexual or parasexual cycle. Mating competency is regulated by transcription factors *mtla1* and *mtlα2*, and sexual competency is associated with the secretion of sexual pheromones. These pheromones induce polarization, a G1 block and conjugation tube formation in cells of opposite mating type (Sahni et al. 2009). Additionally following response to pheromones, genes related to adhesion are upregulated, possibly as a mechanism to facilitate mating by increased physical proximity of cells. This might facilitate biofilm formation, a putative virulence factor in *C. albicans* infection. In *U. maydis*, the switch from a saprophytic haploid yeast phase to a dikaryotic filamentous phase is essential for pathogenesis (Hartmann et al. 1996). Mating of haploid yeast strains from either *a* or *b* mating-type loci is a prerequisite for generation of the infecting filamentous dikaryon. The *a* locus includes *mfa* and *pra*, which encode secreted pheromone and membrane-spanning pheromone receptors respectively. Pheromone recognition activates a MAP kinase signalling cascade, which results in the morphological switch and virulence. In *A. fumigatus,* the effect of pheromone signalling on development and virulence has not been determined. Nevertheless, downregulation of these enzymes might contribute to the attenuation of Δ*laeA*.

Ratiometric comparisons revealed a striking downregulation of membrane transporters in Δ*laeA* relative to the wild-type at 4 hours post infection. Such a reduction in cell membrane transport at the very early stage of infection might suggest (1) poor pH adaptation of Δ*laeA*, as many membrane transporters rely on the symport of protons which consequently impacts pH of the cytoplasm, or (2) osmotic stress sensitivity of the mutant. *In vitro* phenotypic analyses demonstrated Δ*laeA* was not sensitive to pH, whilst it remains to be seen whether the mutant is sensitive to osmotic stress.

Analysis of Δ*psoA* and Δ*ftmA* isolates in hydrocortisone and neutropenic murine models of infection strongly suggests that the fumitremorgin and pseurotin A biosynthetic pathways augment *A. fumigatus* virulence. With regard to the physical loci of these genes, both reside in a cluster (Afu8g00100 – Afu8g00720), which contains a total of 63 genes, spans 166.1 kb and is located in the subtelomeric left arm of chromosome 8 (Perrin et al. 2007). This locus has been referred to as a secondary metabolite "super cluster" due to the inclusion of three uncharacterised PKSs (Afu8g00270, Afu8g00370, Afu8g00490), in addition to the NRPS *ftmA* (Afu8g00170) and hybrid PKS/NRPS *psoA* (Afu8g00540). The region can be subdivided into three putative secondary metabolite clusters, including the *psoA* cluster (Afu8g00530 – Afu8g00570) the *ftmA* cluster (Afu8g00170 – Afu8g00260) and an uncharacterised cluster encoding a putative metabolite (Afu8g00620 – Afu8g00720 (Perrin et al. 2007, Kato et al. 2009, Maiya et al. 2006, Maiya et al. 2007). The *ftmA* and *psoA* supercluster is intriguing for several reasons. Firstly, it is the largest secondary metabolite cluster in the genome, with the second biggest containing 36 genes (Afu4g14380 - Afu4g14850) and occupying 109.4 kb. Additionally, physical proximity of at least two contiguous metabolite clusters, both of which direct distinct biosynthetic pathways which contribute to *A. fumigatus* infection is rare in pathogenic fungi. While numerous clusters contribute to virulence of both plant and animal fungal pathogens, they are generally not proximal to other functionally distinct pathogenicity clusters. For example, in *U. maydis*, approximately 20% of putatively secreted hydrolytic enzymes occur in 12 physically contiguous clusters composed of 3 – 26 genes (Kamper et al. 2005). Global transcriptional profiling during infection suggested 7 of these clusters were upregulated during infection relative to laboratory culture. Construction of mutants in which several genes per cluster were deleted revealed four mutants with reduced virulence, and one with a hyper-virulent phenotype, leading the authors to describe these regions as biotrophy clusters (Kamper et al. 2005). However, these biotrophy clusters were sparsely distributed among 10 of *U. maydis* 23 chromosomes. Additionally *U. maydis* is able to scavenge iron using both siderophore and a high affinity iron uptake system (Eichhorn et al. 2006). The ferro-oxidase *fer1* and the ferric permease *fir2* of the high affinity iron uptake system are adjacent to each other on the *U. maydis* chromosome and are both required for wild-type virulence

(Eichhorn et al. 2006). Nevertheless, this two gene cluster does not reside in a locus enriched with virulence-associated genes. The *ace1* avirulence cluster in *M. grisea* contains 15 genes which biosynthesise a secondary metabolite product which is putatively recognised by rice cultivars carrying the Pi33 resistance gene (Collemare et al. 2008). The sequencing of the *M. grisea* genome, and targeted sequencing of telomeric regions has demonstrated that avirulence clusters, such as *ace1*, are not locationally enriched at specific regions of the genome (Farman 2007). Several virulence clusters have been identified in *C. albicans*, yet these are not physically linked to with other virulence loci, for example clustered lipase genes on chromosome 1 (*lip1, lip2, lip3, lip6, lip10*) and chromosome 7 (*lip5, lip8, lip9*) or secreted aspartyl proteinases (*sap1, sap4, sap5* and *sap6*) on chromosome 6. Similarly, *A. fumigatus* secondary metabolite clusters which are involved in virulence and host pathogen interactions are generally distributed throughout the genome, for example, the *regA* cluster (Chromosome 1), DHN-melanin cluster (Chromosome 2), *pes3* cluster (Chromosome 5), and gliotoxin cluster (Chromosome 6).

The *psoA* and *ftmA* super cluster is therefore a rare example of locationally proximal, yet pathway distinct secondary metabolite clusters which contribute to fungal virulence. This region is somewhat analogous to prokaryotic pathogenicity islands, the discovery of which revolutionised understanding of the evolutionary mechanisms and molecular basis of bacterial virulence. Prokaryotic pathogenicity islands are a subset of genomic islands, which also include regions associated with symbiosis or antibiotic resistance. While the bacterial conserved “core” genome encodes genes required for essential cellular function, and is homogenous with regard to G + C content, genomic islands have distinct G + C content, are enriched in transposable elements or repeat sequences, and contain non-essential genes associated with niche adaptation and, in the case of pathogenic bacteria, virulence. Genes encoded in these regions may be functionally related, such as the 15 kb *S. aureus* pathogenicity island 1 (SaPI1) which contains three genes encoding secreted endotoxins, *tst*, *sel*, and *sek*. Alternatively, pathogenicity islands may biosynthesise metabolites or organelles required for virulence. For example, the *cag* pathogenicity island of *Helicobacter pylori* is 37 – 40 kb in length and encodes 27 ORFs, which biosynthesise a type-4 secretory system and the secreted effector CagA.

Comparisons between *A. fumigatus* A1163, *N. fischeri* and *A. clavatus* revealed that *A. fumigatus* specific genes cluster at 13 chromosomal islands which display a subtelomeric bias (Federova et al. 2008). Genes at these loci are enriched in functions directing carbohydrate catabolism, transport and secondary metabolite biosynthesis. The *psoA* and *ftmA* supercluster is conserved between *Aspergillus* species. For example, there are *psoA* orthologues in *A. nidulans* (AN8412) and *A. clavatus* (ACLA_023380) and *ftmA* orthologues in *A. nidulans* (AN7884). Approximately 25

putative proteins encoded by genes in the supercluster are very similar to members of the conserved 25 gene sterigmatocystin/aflatoxin synthetic cluster of *A. flavus, A. nidulans*, and *A. parasiticus* (Sheppard et al. 2005). Nevertheless, 7 genes from the cluster (11.1%) including a NRPS (Afu8g00490) are specific to *A. fumigatus*, which equates to a slight increase on the average species specific genes of *A. fumigatus* genome (8.5%, Federova et al. 2008). Given that this cluster resides in the sub-telomere, it is likely several evolutionary mechanisms account for its size and diversity of putative metabolite genes. Firstly, these regions are contain repeat sequences of various lengths, enabling high levels of ectopic recombination and may cause DNA polymerase slip which results in chromosomal rearrangements (Viguera et al. 2001). Additionally, this cluster contained two genes which may be associated with transposition; firstly a reverse transcriptase, which was highly upregulated between 8 – 14 hours (rank 22, Afu8g00330); and secondly a LINE-1 retrotransposon, which was also highly upregulated at this time-point (rank 660, Afu8g00310). This latter gene was of great interest, given that it was one of three LINE-1s in the genome which was not truncated, and did not show evidence of G:C and A:T transitions which are characteristic of repeat induced point (RIP) mutations and gene silencing (Galagan and Selker 2004). We hypothesise that this element may diversify gene content in this region, either by the repeat sequence facilitating homologous recombination with other chromosomes, or by mobilisation, which can can lead to local insertions, deletions, duplications and inversions (Volff 2006). Thus, it seems mobile genetic elements may contribute to *A. fumigatus* genome plasticity and ultimately the virulence of this species.

The principle objective of the thesis was to define disease initiating host-pathogen interactions in murine models of IPA. This objective has been achieved, given that evidence presented suggests a role for the *regA, pes3*, *ftmA,* and *psoA* biosynthetic pathways in *A. fumigatus* virulence. Many additional experiments to further the work presented in this thesis can be proposed, and are summarised below.

Extensive gene expression analyses conducted by the Bignell laboratory has generated the following datasets using global transcriptional profiling: (1) ATCC46645, Ku80, Af293, wild-type isolate (this study), Δ*pacC*, Δ*pabaA*, Δ*laeA*, Δ*crz1* (*in vivo,* neutropenic model, 4, 8, 14 hours post infection); (2) wild-type isolate used in this study (*in vivo,* corticosteroid model, 4, 8, 14, 24, 48, 72 hours post infection); (3) ATCC46645, wild-type isolate (this study), Δ*pacC*, *in vitro* growth, YPD, 4, 8, 14 hours post infection; (4) ATCC46645, wild-type isolate (this study), Δ*pacC*, Δ*laeA,* ATCC46645, (dormant conidia). Every sample consists of at least 1 dye-swap experiment. Thus, at least 88 datasets are available for non-ratiometric quantile normalisation. In addition, we anticipate normalising experiments from published array datasets (e.g. Nierman et al. 2005,

Sheppard et al. 2005, Twumasi-Boateng et al. 2009). This will enable inter-experimental comparisons of gene expression between any of the above samples which will give unparalleled insight into the *A. fumigatus* transcriptome.

Further characterisation of the Δ*psoA,* Δ*ftmA*, and Δ*pes3* mutants relative to the wild-types using *in vitro* assays (e.g. oxidative stress, pH stress), *ex vivo* (e.g. macrophage) and *in vivo* (i.e. *G. mellonella*) in order to further elucidate the molecular basis of Δ*psoA,* Δ*ftmA* and Δ*pes3* attenuation. Additionally, Dr Alcazar-Fuoil has deleted the entire *psoA* and *ftmA* cluster using a deletion cassette generated by the recombineering methodology. Moreover, we intend to generate a Δ*psoA* and Δ*ftmA* double mutant and characterise this isolate in both corticosteroid and neutropenic murine models of infection. We hypothesise that loss of both genes will result in significant attenuation of *A. fumigatus*.

With regard to further characterisation of the Δ*regA* mutant, and identification of the putative metabolite biosynthesised by this cluster, several experiments are currently being pursued or designed:

- Further phenotypic testing with regard to several stressors, such as antibiotic resistance, UV sensitivity and heavy metal tolerance
- Measurement of conidial and hyphal melanin content by the method described in Chai et al 2009.
- Complementation of the Δ*regA* mutant and testing of the strain in murine models of infection
- Construction of a *regA* overexpression mutant using psk379
- HPLC and TLC analyses of conidial and mycelial extracts from overexpression, Δ*regA* and complemented strains

In order to utilise 24 strains putatively expressing a poly-histidine tag for the study of *A. fumigatus* effectors, immunohistochemistry using an anti-his antibody is being conducted on murine lung infected with recombinant isolates. At the time-of writing this thesis, immunohistochemistry is being optimised with animals infected with a Ku80 progenitor strain and an isolate expressing epitope tagged alkaline serine protease Alp1 (Afu4g11800_His_6).

Further standardisation of the ELISPOT assay analysing recombinant Asp F4 and Asp F10 is being conducted by Dr Leonardo Potenza. We hypothesise that these recombinant proteins may perform better than non-standardised spore extracts with regard to eliciting protective host responses and also for diagnostic purposes

In order to elucidate the molecular mechanism for Δ*laeA* attenuation, the following experiments might be useful:

- Analysis of the Δ*laeA* osmotic stress phenotype
- Construction of a Δ*laeA*Δ*gel1* double mutant and characterisation of this isolate in murine models of infection may determine if overexpression of *gel1 in vivo* resulted in a Th1 response
- Establishment of pheromone expression in Δ*laeA* during *in vitro* growth

With regard to determining LINE-1 mobilisation in Af293 clinical isolate, a number of significant steps have been made. Firstly, Af293 gDNA libraries from 14 and 24 hour *in vitro* growth have been generated in the pUC19 plasmid. We are using an internal primer with homology to the conserved region of the LINE-1 elements, and a primer from pUC19 to amplify regions of gDNA which flank the LINE-1. We hypothesise that this may identify gDNA regions into which the LINE-1 element might have integrated.

In summary, host-pathogen interactions have critical implications for the establishment of disease and for determining adaptive immune responses of the host. This study has conducted the first global *A. fumigatus* transcriptional analyses throughout the initiation of murine infection, which has identified hundreds of upregulated genes which putatively biosynthesise products which interact with the host.

The potential of these datasets to futher understanding of host-pathogen interactions and virulence is evidence by attenuation of Δ*ftmA*, Δ*psoA*, and Δ*regA*, and hypervirulence of Δ*pes3* in murine models of infection. However work presented in this thesis represents initial analyses into substantial datasets. A recombineering methodology for the high-throughput construction of gene deletion cassettes represents a promising strategy for analysing *A. fumigatus* genes in the mammalian host. Additionally, the qPCR assay for determining fungal burden will enable more rapid analyses of mutants in murine models of infection.

With regard to Δ*laeA* attenuation, there was no evidence to support the view that defective secondary metabolism is causative of the attenuated virulence phenotype. Work presented in this thesis suggests attenuation of the isolate might be related to upregulation and downregulation of Th1 and Th2 associated antigens respectively, and/or deficiencies in plasma membrane transport relative to wild-type isolates. A hypothesised deficiency in maintenance of genome stability, due to LINE-1 mobilisation in the Δ*laeA* isolate was tested, and subsequently discredited by a discovered lack of isogenicity among the tested strains. Nevertheless, the biological relevance of a putatively

mobile LINE-1 element was substantiated as a strain specific phenomenon, whereby the Af293 clinical isolate demonstrated increased copy number of the transposon. We hypothesise that this might have critical implications for the evolutionary mechanisms of *A. fumigatus* virulence.

10

Addendum

Ratiometric and non-ratiometric comparisons of *A. fumigatus* Af293 and Δ*laeA* during the initation of infection

10.1 Overview

A specific objective of this thesis is to conduct comparative gene expression analyses of Af293 and the attenuated Δ*laeA* strain during the initiation of infection in order to reverse engineer the transcriptional basis of *A. fumigatus* attenuation (Section 1.7.1).

Following the completion of the array experiments described in Chapters 3 and 8, Southern blot analysis was used to interrogate copy number of putative LINE-1 elements in Af293, Af293Δ*laeA*, CEA10 and CEA10Δ*laeA* (Figure 8.11). An unexpected finding evidenced by the distinctive LINE-1 Soutern blot banding pattern of the Af293 and CEA10 isolates demonstrated that the two strains used in Chapters 3 and 8 were not isogenic.

To address the obvious limitations of utilising non-isogenic strains in the comparative analyses described in this thesis, the infection experiments described in Chaper 3 and 8 were repeated with a genotypically confirmed Af293 isolate, which was obtained as a kind gift from Nancy Keller (University of Wisconsin, USA). The Af293 isolate was genotypically validated by Jon Palmer (Nancy Keller's Laboratory, University of Wisconsin) using Southern blot analyses as described in Figure 8.11. Briefly, HindIII digested gDNA was probed using a 592 bp fragment common to putative LINE-1 elements. This revealed distinctive banding patterns which were common to the Af293 background (data not shown). Both non-ratiometric and ratiometric comparisons from the repeat experiments are presented here. Both histology (Chapter 3) and virulence data (Chapter 4 and 5) utilised the confirmed Af293 isolate and are therefore not addressed in this Addendum.

10.2 Materials and methods

10.2.1 Murine infection, microarray data capture and normalisation

Murine infections were conducted as described in section 3.2.2. Groups of 7 mice were infected with either AF293 or Δ*laeA* and culled at 4, 8 and 14 hours post infection. RNA was extracted, amplified and reverse transcribed into labelled cDNA as described in section 3.2.3.

The array platform utilised was the 70-mer oligotide glass slide DNA microarray designed and spotted by the Pathogen Functional Genomics Resource Center (PFGRC, J. Craig Venter Institue, Rockville, USA). On this array platform, 8763 *A. fumigatus* ORFs are represented by duplicate oligotide spots. Data capture was conducted as described in section 3.2.4.

Non-ratiometric and ratiometric normlisations were conducted as described in sections 3.3.1 and 8.3.2 respectively. Quantile normalisation was conducted in Genespring 11.5.0 (Agilent).

10.3 Results

10.3.1 Experimental design

Groups of 7 mice were infected with either AF293 or Δ*laeA* and culled at 4, 8 and 14 hours post infection. RNA was extracted, amplified and reverse transcribed into labelled cDNA as described in section 3.2.3. Labelled cDNA samples were co-hybridised on a dye-swap pair of arrays. Additionally, two technical replicates were included by amplification, reverse transcription and labelling of Δ*laeA* RNA samples reported in Chapter 3 and 8 (Figure 10.1). These samples were co-hybridised with labelled cDNA from the Af293 sample. A single RNA sample (Δ*laeA* replicate 1, 14 hours) failed to amplify RNA to sufficient concentrations for reverse transcription (data not shown). This sample was therefore omitted from the experiment (Figure 10.1). Thus, a total of 6 arrays were used to analyse 4 and 8 hour time points, and 4 arrays used to analyse the 14 hour time-point (Figure 10.1).

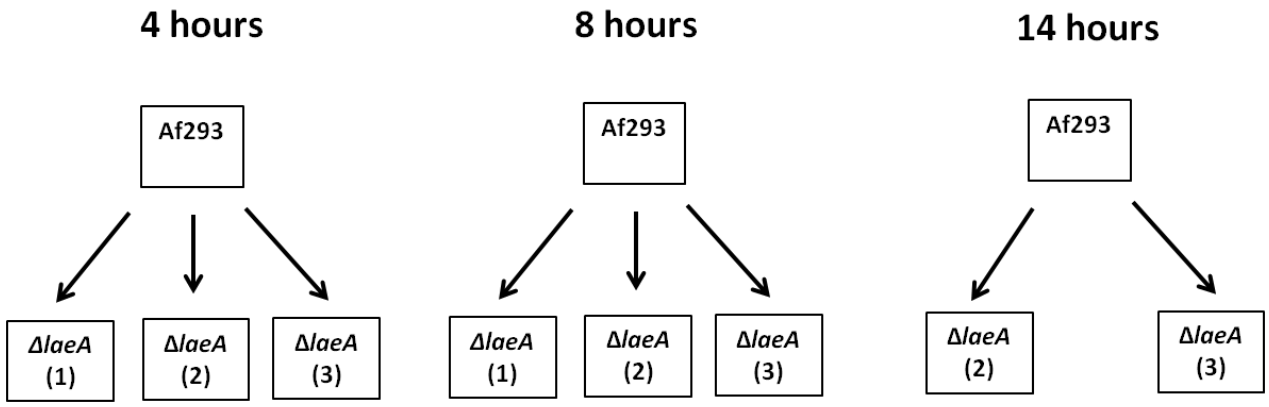


Figure 10.1: Hybridisation scheme for replicated Af293/Δ*laeA* competitive hybridisations. Black arrows indicate co-hybridisations of samples. All co-hybridisations were performed with dye swap replication. RNA was extracted from mice infected with a genotypically validated Af293 isolate was co-hybridised with RNA samples deriving from three independent biological replicates of a Δ*laeA* murine infection. Numbers in parentheses indicate Δ*laeA* biological replicate number. RNA samples, the analysis of which is described in Chapter 3, derived from Δ*laeA*-infected animals were utilised for co-hybridisation (replicates 1 and 2). A further, *de novo*, infection replicate was also performed, (Δ*laeA* replicate 3).

10.3.2 Time-point specific transcriptional profiling of *A. fumigatus* Af293 during the initiation of murine infection

Data were captured from slides using TIGR Spotfinder, and were exported as MEV files. From MEV files (n = 16) intensity channels (n = 32) were grouped into strain and time-point specific cohorts. On the PFGRC *A. fumigatus* arrays used in this experiment, duplicate oligonucleotide spots represent each gene. These spots are identified by a unique gene identification (UID) number. Mean UID spot values were calculated within each array to give an average spot intensity value (aSI) for each gene per channel. Quantile normalisation and $\log_2$ transformation was conducted on aSI data within time-point and strain cohorts, followed by a second quantile normalisation across the entire dataset. Following quantile normalisation, all arrays have identical distribution, and inter-array variance is reduced (Figure 10.2). For each gene, quantile normalised values were averaged within the strain and time specific channel cohorts, producing a single normalised intensity value (nSI) per gene for either Af293 or Δ*laeA* at each time-point. Genes were filtered based on count and standard deviation filtering as described in section 3.3.1. Table 10.1 shows the number of values filtered by count and standard deviation filtering for Af293. Finally, only genes with nSI values at all three time-points were considered in final dataset.

To determine temporal transcriptional profiles throughout infection, nSI ratios were calculated between time-points. nSI ratios are reported relative to an earlier time-point (either 4 hours or 8 hours) and are directional in terms of the temporal gene profile, i.e. > 1 if the gene increases and < 1 if the gene decreases between time-points. From relative nSI values, differentially expressed transcripts between time-points were defined as upregulated or downregulated based on upper and lower quartiles of the relative nSI datasets. All relative nSI datasets were normally distributed around median values approaching 1.0 (Figure 10.3).

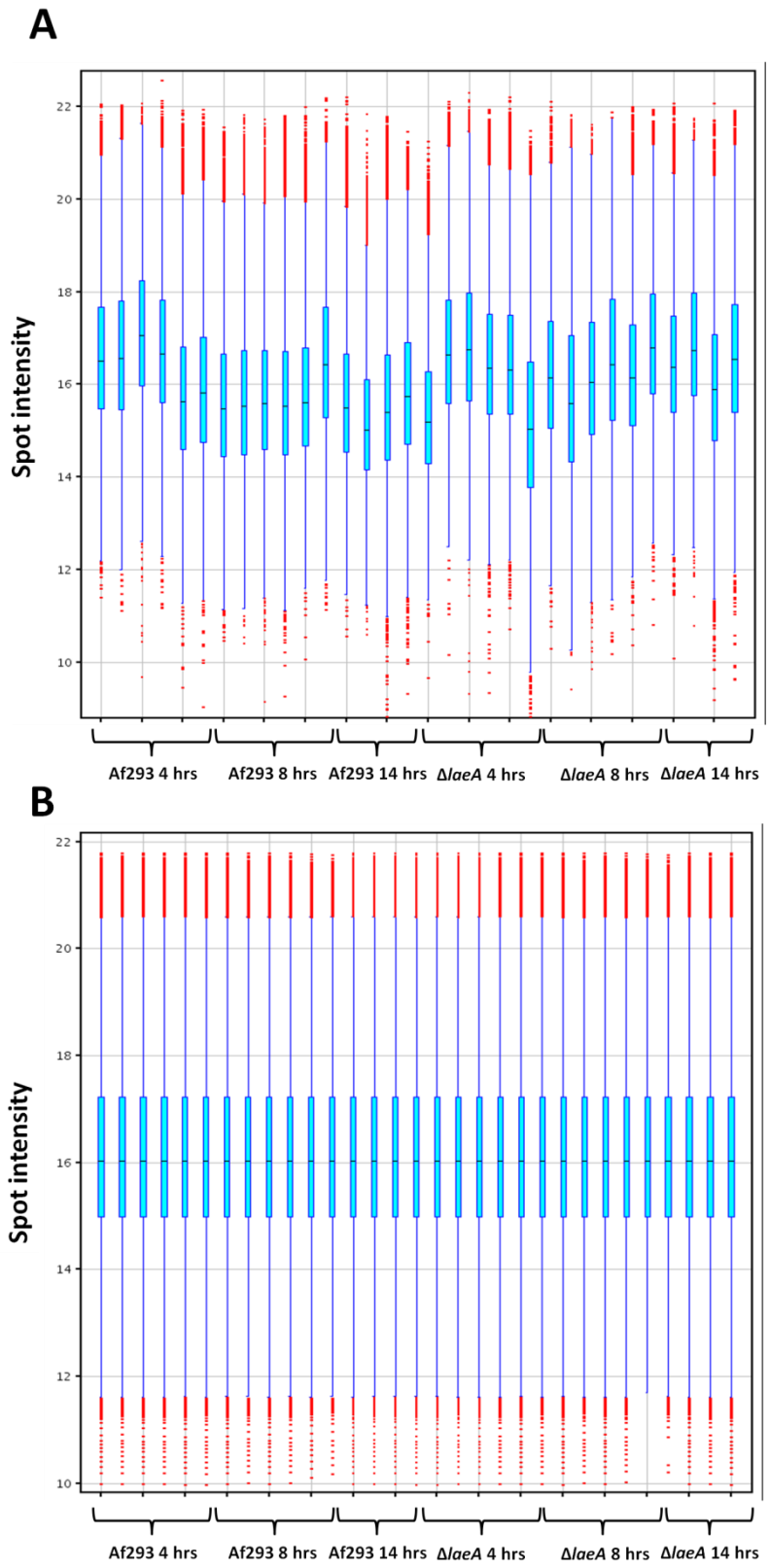


Figure 10.2: Box plots depicting non-ratiometric spot intensity distribution before and after double quantile normalisation for Af293 and Δ*laeA* datasets. Data points represent intensity values (*y* axis) for a single spot on each array. **A.** Distribution of $\log_2$ transformed spot intensity values for every intensity channel (n = 32). Channels were grouped into strain and time-point cohorts. **B.** Distribution of spot intensity values following double quantile normalisation (within time-point and strain cohorts), followed by quantile normalisation across all intensity channels in the experiment. Following the second quantile normalisation, all channels have identical intensity distribution.

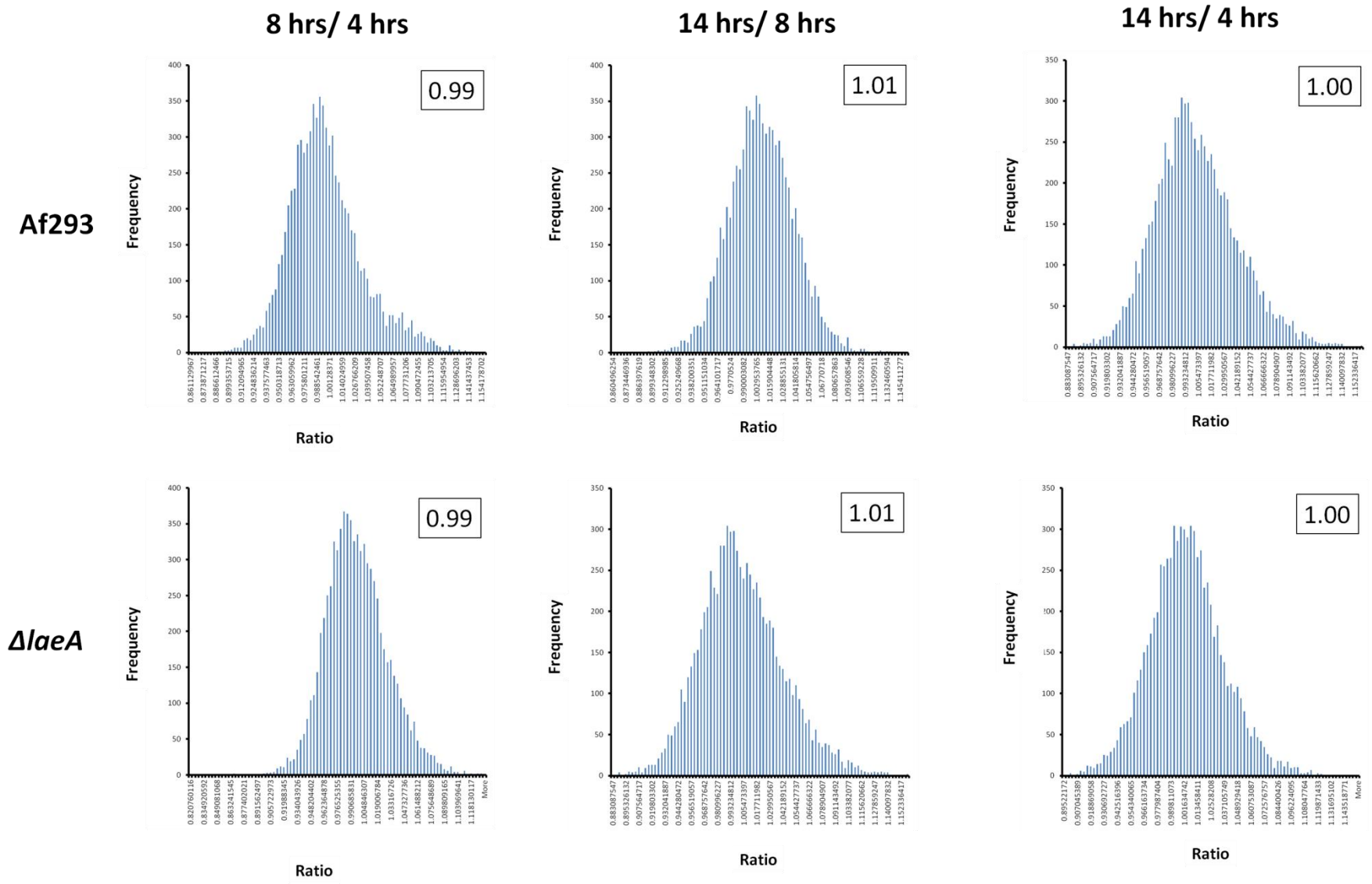


Figure 10.3: Frequency distribution of relative nSI datasets. To determine temporal transcriptional profiles throughout infection, nSI ratios were calculated between time-points. nSI ratios are reported relative to an earlier time-point (either 4 hours or 8 hours) A value of 1 therefore indicates no change between time-points. Median values are shown in black boxes. Upper and lower quartiles were considered increased and decreased gene expression between time-points respectively.

10.3.3 *A. fumigatus* Af293 transcriptional profile during the initiation of murine infection

As summarised in Table 10.1, fluorescence intensities for 8709, 8436 and 8576 out of a possible 8763 represented ORFs passed quality control filtering for 4, 8 and 14 hour time-points respectively. Genes failing to return expression values for all three time-points (due to quality control filtering) were omitted from the dataset, resulting in a total of 8195 gene expression profiles. To determine the temporal basis of transcriptional changes during infection, relative nSI values were calculated between time-points and the upper and lower quartiles of the relative nSI datasets were considered up- and down-expressed transcripts respectively (n = 2049). Up- and down-expressed gene sets were subdivided into three cohorts of high, moderate, and low transcriptional changes between time-points (n = 683) respectively. Table 10.2 summarises upper and lower quartile values at each time-point, and maximal and minimal relative nSI values between time-points.

	4 hrs	8 hrs	14
Count fail	47	204	65
Standard deviation fail	7	123	122
Retained genes	8709	8436	8576
Average nSI	16.22	16.14	16.25
Median nSI	16.05	15.96	16.04
Standard deviation	1.44	1.41	1.54
Minimum nSI value	12.97	12.74	12.29
Maximum nSI value	21.16	21.76	21.51

Table 10.1: Summary statistics for the Af293 non-ratiometric analysis. The number of genes failing count and standard deviation quality control filtering are shown. The total number of genes with expression values common to every time-point and thus retained for analysis was 8195.

	nSI			Relative nSI		
	4 hrs	8 hrs	14 hrs	8 vs 4 hrs	14 vs 8 hrs	4 vs 14 hrs
Lower quartile	15.13	15.10	15.08	0.97	0.99	0.98
Upper quartile	17.12	16.96	17.20	1.02	1.03	1.03
Median	16.05	15.96	16.04	0.99	1.01	1.00
Average	16.22	16.14	16.25	1.00	1.01	1.00
Standard deviation	1.44	1.41	1.54	0.04	0.03	0.04

Table 10.2: Summary statistics for Af293 relative nSI datasets. Relative nSI values were calculated for 8195 genes. Upper and lower quartiles (n = 2049) were used to define up and down expressed genes respectively.

Distribution of the up and down expressed datasets is summarised in 2 and 3-way Venn diagram in Figure 10.4. A comparative analysis of gene cohorts differentially expressed genes between the 4 – 8 and 8 – 14 hours time-points revealed 417 and 287 genes with consistently increased or decreased transcript abundance, respectively. These identified genes also featured in the 4 - 14 hour dataset (Figure 10.4B). Consequently, the 4 – 14 hour comparison is inclusive of all gene expression changes and therefore constitutes the most appropriate cohort for interrogating transcriptional changes across the entire time-course. 4 – 8 and 8 – 14 hour comparisons were used to identify time-point specific transcriptional changes.

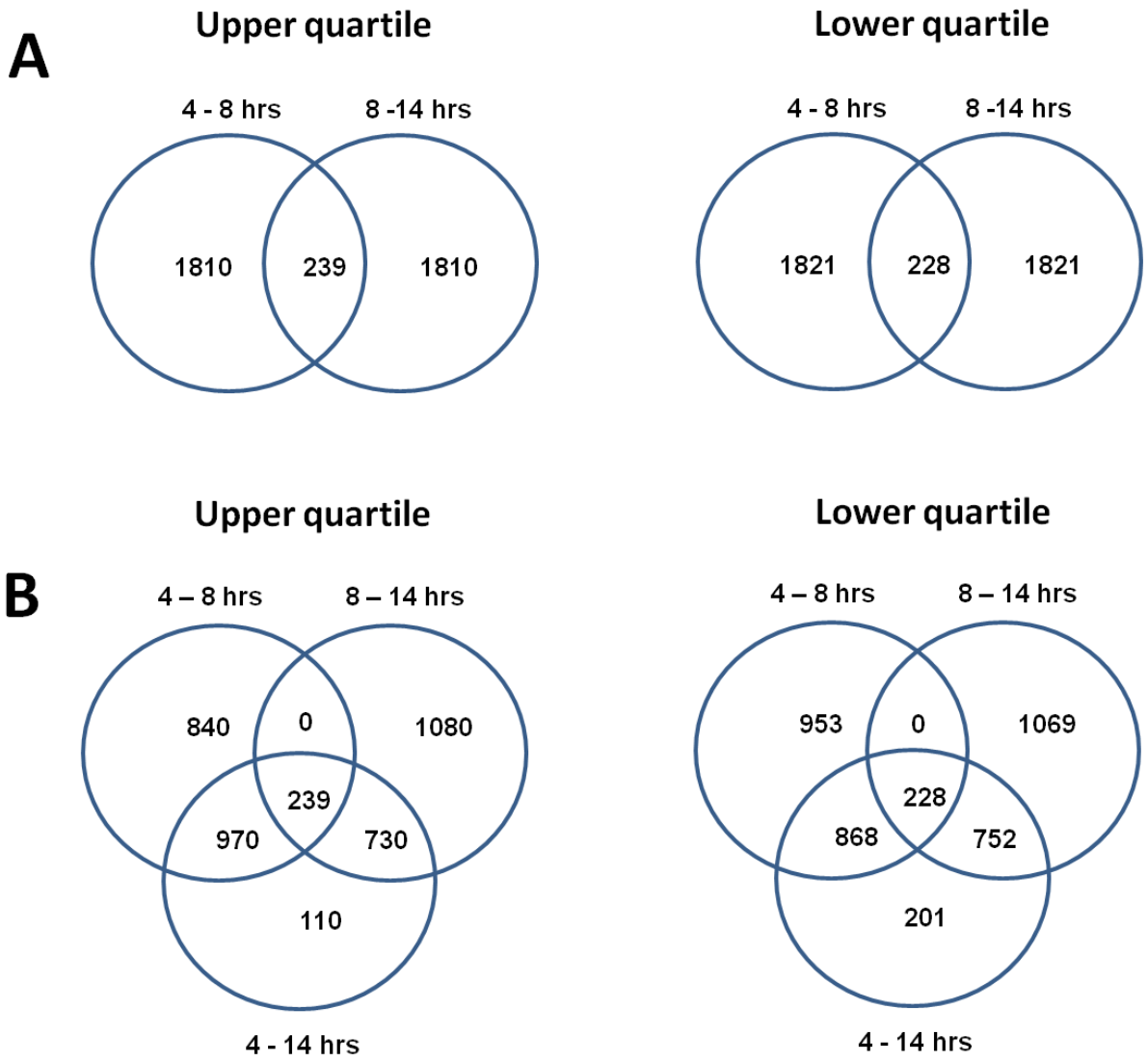


Figure 10.4: Venn diagrams depicting comparisons between relative nSI datasets from the Af293 non-ratiometric analysis. A. 2 way Venn diagram depicting comparisons between time-point specific datasets. **B**. Three-way Venn diagram depicting comparisons between all nSI datasets. Upper and lower quartiles (n =2049) were used to define genes with increase and decrease in expression respectively.

Gene expression profiling of the Af293 isolate between 4 and 14 hours in the murine lung

Initial interpretations of gene expression profiles were conducted on the cohort of genes identified as differentially expressed between 4 – 14 hours post infection. Gene ontology analysis was conducted using Genespring GX 11.5.0 to indentify over represented terms in increased or decreased datasets. No over-representation of GO terms satisfying an arbitrarily imposed corrected p value cut off of ≤ 0.2 was reported. The 200 genes having the greatest increases and 200 genes having the greatest decreases, in transcript abundance between 4 and 14 hours are reported in Tables 10.3 and 10.4.

Table 10.3: 200 genes with greatest nSI increases between 4 and 14 hours post infection. Genes are ranked according to greatest nSI intensity increase between 4 and 14 hours where 1 is the greatest. A one-way ANOVA was conducted on nSI values between time-points, with the null hypothesis that nSI values do not change between time-points. FDR correct *p*-values from this analysis are reported for each gene. Hypothetical proteins (n = 94) were removed.

ORF	Description	Rank	*p-value*	GO Biological Process
Afu6g10550	arrestin domain protein	1	0.048	
Afu7g00360	UDP-galactose 4-epimerase	2	-	
Afu1g02780	L-asparaginase	3	0.032	endoplasmic reticulum///asparagine catabolic process///cellular response to nitrogen starvation///nuclear envelope///cell wall-bounded periplasmic space///asparaginase activity
Afu7g05090	glucuronyl hydrolase	6	0.015	
Afu7g00700	aldo-keto reductase (AKR13), puatative	7	0.029	aldo-keto reductase activity///cytoplasm///nucleus///cellular aldehyde metabolic process
Afu2g10990	chromatin remodeling complex subunit (Arp8)	8	0.014	chromatin remodeling complex
Afu2g17240	C2H2 finger domain protein	10	0.017	
Afu6g05320	purine nucleoside phosphorylase I, inosine and guanosine-specific	12	0.015	cellular component unknown///purine-nucleoside phosphorylase activity///purine nucleoside catabolic process
Afu1g05050	cytosine deaminase	13	0.032	cytosine metabolic process///cytosine deaminase activity///cytoplasm///nucleus///zinc ion binding
Afu1g06000	Ser/Thr protein phosphatase family protein	14	-	
Afu5g02900	SNARE domain protein	15	0.044	
Afu2g13380	GATA transcription factor (AreB)	16	0.023	regulation of nitrogen utilization///negative regulation of transcription from RNA polymerase II promoter///specific RNA polymerase II transcription factor activity///nucleus///zinc ion binding///nitrogen compound metabolic process
Afu3g10320	RING finger domain protein	18	0.033	
Afu5g12730	nonribosomal peptide synthase	20	-	nonribosomal peptide biosynthetic process///catalytic activity///amino acid

					adenylylation by nonribosomal peptide synthase
Afu3g02370	short-chain dehydrogenase/reductase	21	-		oxidoreductase activity///cytoplasm///metabolic process
Afu2g08580	pyridoxine	22		0.045	thiamin biosynthetic process///pyridoxine metabolic process///imidazoleglycerol-phosphate synthase activity///cytoplasm///protein binding
Afu3g06410	Coenzyme Q (ubiquinone) biosynthesis protein Coq4, putative	23	-		ubiquinone metabolic process///mitochondrial inner membrane///molecular function unknown
Afu5g13130	chorismate mutase	24		0.027	chorismate mutase activity///cytoplasm///nucleus///aromatic amino acid family biosynthetic process
Afu4g07140	killer toxin sensitivity protein (IKI3)	25	-		""DNA-directed RNA polymerase II, holoenzyme"""""///transcription elongation factor complex///RNA polymerase II transcription elongation factor activity///regulation of transcription from RNA polymerase II promoter///"histone acetyltransferase activity""
Afu2g08300	DnaJ domain protein	26		0.010	endoplasmic reticulum lumen///co-chaperone activity///protein folding
Afu5g11110	thiamin pyrophosphokinase -related protein	29		0.036	cellular component unknown///biological process unknown///molecular function unknown
Afu6g09170	3-methyl-2-oxobutanoate hydroxymethyltransferase PanB	31			pantothenate biosynthetic process///3-methyl-2-oxobutanoate hydroxymethyltransferase activity///mitochondrion
Afu1g06280	short-chain dehydrogenase/reductase family protein, putative	32		0.008	cellular component unknown///biological process unknown///molecular function unknown
Afu1g06910	arabinogalactan endo-1,4-beta-galactosidase GalA	33			
Afu2g06140	uracil DNA N-glycosylase Ung1	35			DNA repair///base-excision repair///nucleus///uracil DNA N-glycosylase activity///mitochondrion
Afu2g15490	TPR domain protein	36			
Afu2g16490	rhomboid family membrane protein	37			
Afu5g13460	mitochondrial protein	38		0.027	mitochondrial genome maintenance///mitochondrion inheritance///mitochondrion organization///mitochondrial outer membrane///molecular function unknown

Afu5g13580	3-ketosteroid-delta-1-dehydrogenase	39		
Afu6g13570	cytochrome c peroxidase	40	0.023	
Afu3g01950	zinc-containing alcohol dehydrogenase	41	0.010	cellular component unknown///"oxidoreductase activity, acting on the CH-OH group of donors, NAD or NADP as acceptor"""""""///hexose metabolic process"
Afu2g13730	NEDD8 activating enzyme (UbaC)	42		NEDD8 class-dependent protein catabolic process///cytoplasm///protein neddylation during NEDD8 class-dependent protein catabolic process///NEDD8 activating enzyme activity
Afu7g04220	protein required for cell viability Rrp17	43	0.029	
Afu3g07260	esterase/lipase	44		
Afu3g13230	AT DNA binding protein	45		nucleus///AT DNA binding
Afu1g10100	3-oxoacyl-(acyl-carrier-protein) reductase	46		
Afu2g05750	agmatinase	47	0.036	spermidine biosynthetic process///agmatinase activity
Afu2g04380	LaeA-like methyltransferase	48		
Afu6g13880	MFS transporter	51	0.032	plasma membrane///transporter activity///transport
Afu6g03530	glutamine synthetase	53	0.008	glutamine biosynthetic process///glutamate-ammonia ligase activity
Afu5g11130	PAXNEB protein superfamily	54		transcription elongation factor complex///cytoplasm///RNA polymerase II transcription elongation factor activity///regulation of transcription from RNA polymerase II promoter
Afu5g01750	MATH and UCH domain protein, putaitve	55		
Afu7g05790	vacuolar morphogenesis protein AvaB	58		vacuole organization"///vacuolar membrane""///fungal-type vacuole///Rab guanyl-nucleotide exchange factor activity///"homotypic vacuole fusion, non-autophagic"""""
Afu6g14360	cytochrome P450 monooxygenase	59	0.029	
Afu5g02620	P450 family sporulation-specific N-formyltyrosine oxidase Dit2	60	0.032	oxidoreductase activity///cellular component unknown///spore wall assembly (sensu Saccharomyces)///catalytic

					activity///metabolic process
Afu3g09760	peptidyl-tRNA hydrolase domain protein	62			cellular component unknown///biological process unknown///molecular function unknown
Afu4g12280	methyltransferase-like protein 1	63			protein binding///nucleus///tRNA methylation///tRNA (guanine-N7-)-methyltransferase activity
Afu5g11000	small nuclear ribonucleoprotein U2, A'	64	-		"nuclear mRNA splicing, via spliceosome"""""///""pre-mRNA splicing factor activity"///U2 snRNP""///"cytoplasm
Afu4g01520	gentisate 1,2-dioxygenase	65		0.010	
Afu8g01570	ADP-ribosylglycohydrolase family protein	67		0.039	
Afu8g00710	secreted antimicrobial peptide	68	-		
Afu6g08870	nicotinamide mononucleotide adenylyl transferase	69	-		nicotinate-nucleotide adenylyltransferase activity///nucleus///NAD metabolic process
Afu5g10050	cytochrome P450 monooxygenase	71	-		oxidoreductase activity///metabolic process
Afu1g08820	DUF814 domain protein	73	-		cytoplasm///biological process unknown///molecular function unknown
Afu4g11250	carbonic anhydrase Nce103	74	-		cytoplasm///nucleus///biological process unknown///molecular function unknown
Afu5g06680	4-aminobutyrate transaminase GatA	75	-		intracellular///4-aminobutyrate transaminase activity///nitrogen utilization
Afu2g13320	mitochondrial membrane fission protein (Fis1)	77		0.023	
Afu6g12580	anthranilate synthase component I	78		0.049	cytoplasm///anthranilate synthase activity///tryptophan biosynthetic process
Afu4g05980	JmjC domain protein	80		0.033	chromatin remodeling///DNA binding///nucleus
Afu3g01990	DUF636 domain protein	81	-		
Afu2g03150	kinesin family protein	83	-		kinesin complex///microtubule motor activity///establishment of mitotic spindle orientation///cytoplasmic microtubule///microtubule depolymerization///nuclear microtubule
Afu7g05410	thiamine pyrophosphokinase Thi80	84		0.023	thiamin metabolic process///thiamin diphosphokinase activity
Afu5g04030	50S ribosomal protein L27	85		0.042	structural constituent of ribosome///translation///mitochondrial large ribosomal subunit///peptidyltransferase activity

Afu5g02550	RNA polymerase III transcription factor subunit, putative	86	-		transcription initiation from RNA polymerase III promoter///transcription factor TFIIIC complex///RNA polymerase III transcription factor activity
Afu6g02690	C2H2 finger domain protein	87		0.017	DNA binding///nucleus///zinc ion binding
Afu5g10420	nitrate reductase	88	-		endoplasmic reticulum///biological process unknown///molecular function unknown
Afu1g13350	MFS transporter	90	-		membrane///transporter activity///transport
Afu2g04710	cytochrome b5	91		0.023	sterol biosynthetic process///electron transporter activity///microsome///endoplasmic reticulum membrane
Afu1g07750	SWIRM domain protein Fun19	93	-		cellular component unknown///biological process unknown///molecular function unknown
Afu6g09820	vesicle-mediated transport protein Bfr2/Che-1	96		0.011	nucleolus///ER to Golgi vesicle-mediated transport
Afu1g09750	aldehyde reductase (AKR1)	99	-		aldo-keto reductase activity///cytoplasm///nucleus///cellular aldehyde metabolic process
Afu1g14700	MFS allantoate transporter	102	-		allantoate transmembrane transporter activity///plasma membrane///allantoate transport
Afu1g16000	serine/threonine protein kinase	103	-		protein kinase activity
Afu5g00610	oxidase	104		0.006	
Afu4g03585	alpha-galactosidase	105		0.025	
Afu8g03890	peptidyl-prolyl cis-trans isomerase	106	-		peptidyl-prolyl cis-trans isomerase activity///protein folding///mitochondrion
Afu8g02200	proline permease	108		0.049	amino acid transport///plasma membrane///amino acid permease activity///amino acid transmembrane transporter activity
Afu3g00150	short-chain dehydrogenase/oxidoreductase	109		0.042	oxidoreductase activity///cytoplasm///metabolic process
Afu1g04080	GARP complex subunit (Sac2)	110	-		actin filament-based process///Golgi to vacuole transport///protein binding///GARP complex///Golgi apparatus
Afu2g16920	actin monomer binding protein	115		0.044	sequestering of actin monomers///actin polymerization or depolymerization///actin monomer binding///bipolar cellular bud site selection
Afu1g10350	phosphoglycerate kinase PgkA	116	-		phosphoglycerate kinase activity///cytoplasm///cytosol///gluconeogenesis///glycolysis
Afu2g02710	60S ribosomal protein L24b	117	-		structural constituent of ribosome///nucleolus///ribosomal large subunit biogenesis

Afu2g02750	S-adenosylmethionine-dependent methyltransferase, putative	121	0.031	S-adenosylmethionine-dependent methyltransferase activity///cytoplasm///biological process unknown
Afu2g08700	isochorismatase family hydrolase	124	0.039	hydrolase activity///metabolic process
Afu5g06340	BAR domain protein	125	-	
Afu4g03240	cell wall serine-threonine-rich galactomannoprotein Mp1	126	0.034	
Afu8g04050	transcriptional regulator PacG/VIB-1	128	0.029	
Afu1g01850	C6 finger domain protein	129	-	
Afu1g07560	MYB DNA-binding domain protein	131	-	
Afu5g01600	PHP domain protein	134	0.032	
Afu1g14660	regulator of secondary metabolism LaeA	136	-	secondary metabolic process///pathogenesis
Afu3g00720	DUF500 and UBA/TS-N domain protein	137	0.049	cellular component unknown///biological process unknown///molecular function unknown
Afu7g01150	LipA and NB-ARC domain protein	138	0.034	cellular component unknown///nucleotide binding
Afu1g10080	C2H2 transcription factor	139	0.046	specific RNA polymerase II transcription factor activity///regulation of transcription from RNA polymerase II promoter///nucleus///zinc ion binding
Afu5g05560	non-canonical purine NTP pyrophosphatase, rdgB/HAM1 family	140	-	
Afu5g01640	ankyrin repeat protein	141	-	
Afu2g02770	LPXTG-motif cell wall anchor domain protein	142	0.029	
Afu1g11690	proline-rich, actin-associated protein Vrp1	143	-	
Afu1g09230	DUF1000 domain protein	146	-	
Afu3g01980	chromatin structure remodeling complex protein RSC3, putative	148	-	DNA binding///zinc ion binding

Afu2g02960	translation factor pelota	149		0.018	translation///cytoplasm///meiosis///molecular function unknown
Afu3g10060	Dor1-like family protein	150		0.049	
Afu4g00620	cell wall glycosyl hydrolase Dfg5	151		0.048	membrane fraction///fungal-type cell wall biogenesis///anchored to plasma membrane
Afu1g04720	C-8 sterol isomerase (Erg-1)	152	-		endoplasmic reticulum///ergosterol biosynthetic process///C-8 sterol isomerase activity
Afu4g12310	DNA repair protein Rtt107	153	-		"negative regulation of transposition, DNA-mediated"""""""///"molecular function unknown""///""nucleus
Afu1g04940	small monomeric GTPase SarA	154		0.041	SAR small monomeric GTPase activity///ER to Golgi vesicle-mediated transport///COPII vesicle coat
Afu2g09070	DUF221 domain protein	155	-		cellular component unknown///biological process unknown///molecular function unknown
Afu7g05990	5-formyltetrahydrofolate cyclo-ligase	157		0.044	cellular component unknown///5-formyltetrahydrofolate cyclo-ligase activity///folic acid and derivative biosynthetic process
Afu3g07150	succinate-semialdehyde dehydrogenase	158	-		response to oxidative stress///succinate-semialdehyde dehydrogenase [NAD(P)+] activity///cytoplasm///glutamate catabolic process
Afu1g14120	nuclear segregation protein (Bfr1)	159	-		spindle organization///nuclear envelope-endoplasmic reticulum network///regulation of mitosis///polysome///meiosis///RNA binding///cytokinesis
Afu3g11090	Golgi complex component Cog3	162	-		Golgi transport complex///"""""retrograde transport, vesicle recycling within Golgi"""""///""protein transporter activity///intra-Golgi vesicle-mediated transport""///ER to Golgi vesicle-mediated transport"///soluble fraction///"peripheral to membrane of membrane fraction
Afu1g16750	mitochondrial cation transporter	163		0.032	iron ion transport///mitochondrion///integral to membrane///cation transmembrane transporter activity
Afu6g14180	beta-1,4-mannosyltransferase (Alg1)	164	-		protein amino acid N-linked glycosylation///integral to membrane"""///"beta-1,4-mannosyltransferase activity"""""
Afu5g08500	spermine/spermidine synthase family protein	166	-		
Afu1g06410	nuclear localization protein NPL6	167		0.023	protein import into nucleus///nucleus///molecular function unknown

Afu1g12250	mitochondrial hypoxia responsive domain protein	168		0.029	mitochondrion///biological process unknown///molecular function unknown
Afu6g12760	GPI transamidase component (GAA1)	169	-		integral to endoplasmic reticulum membrane///GPI-anchor transamidase activity///attachment of GPI anchor to protein
Afu3g14000	metaphase-anaphase transition protein (Mlo2)	170		0.015	
Afu4g11830	cell cycle control protein (Cwf19)	172	-		
Afu6g10470	zinc finger protein ZPR1	173	-		regulation of progression through cell cycle///cytoplasm///nucleolus///protein binding
Afu3g03410	enoyl-CoA hydratase/isomerase family protein	174		0.045	
Afu6g12130	C6 transcription factor	178		0.032	transcription activator activity///"""""regulation of transcription, DNA-dependent"""""///"galactose metabolic process""///nucleus"
Afu4g11110	C2 domain protein	179	-		cellular component unknown///biological process unknown///molecular function unknown
Afu2g00970	alcohol dehydrogenase, zinc-containing	180	-		oxidoreductase activity///"oxidoreductase activity, acting on the CH-OH group of donors, NAD or NADP as acceptor"///zinc ion binding///metabolic process
Afu4g10340	C6 finger domain protein	182		0.029	DNA binding///zinc ion binding
Afu4g00930	CorA family metal ion transporter	183	-		"di-, tri-valent inorganic cation transport"""""///"magnesium ion transport""///""""""""di-, tri-valent inorganic cation transmembrane transporter activity"""""///plasma membrane
Afu6g11030	RNA binding protein MSSP-2	186	-		
Afu8g06020	glutamate decarboxylase	187	-		response to oxidative stress///cytoplasm///glutamate catabolic process///glutamate decarboxylase activity
Afu5g08230	C3HC4 finger protein	188	-		
Afu3g06210	phosphoribosyl-aminoimidazole-succinocarboxamide synthase	189	-		purine ribonucleotide biosynthetic process///cytoplasm///phosphoribosylaminoimidazolesuccinocarboxamide synthase activity///nucleus///purine base metabolic process
Afu4g07050	L-lactate dehydrogenase	193		0.044	L-lactate dehydrogenase (cytochrome) activity///mitochondrial intermembrane space///electron transport

Afu3g11610	nucleosome binding protein (Nhp6a)	195	-		nuclear chromatin///chromatin binding///regulation of transcription from RNA polymerase III promoter///regulation of transcription from RNA polymerase II promoter///chromatin organization
Afu2g05490	HEAT repeat protein	196	-		cytoplasm///nucleus///biological process unknown///molecular function unknown
Afu8g04150	MFS transporter	197	-		
Afu1g06780	CBS and PB1 domain protein	198	-		
Afu6g11770	NmrA-like family protein	200		0.029	
Afu6g02600	phosphoglycerate mutase family protein	201	-		cytoplasm///nucleus///biological process unknown///molecular function unknown
Afu2g03810	histone deacetylase HosA	204	-		histone deacetylation"///""regulation of transcription, DNA-dependent""///histone deacetylase complex///NAD-dependent histone deacetylase activity///chromatin organization///NAD-independent histone deacetylase activity///""negative regulation of meiosis
Afu5g08160	cyclin	205	-		
Afu1g16150	thioredoxin domain protein	206		0.031	
Afu1g03420	adenylate kinase 2	210		0.049	"nucleobase, nucleoside and nucleotide interconversion"///adenylate kinase activity///mitochondrial inner membrane
Afu2g03600	NUDIX family hydrolase	214	-		hydrolase activity///metabolic process
Afu5g08970	oligosaccharyl transferase subunit (beta)	216	-		oligosaccharyltransferase complex///dolichyl-diphosphooligosaccharide-protein glycotransferase activity///protein amino acid N-linked glycosylation///cell cycle
Afu5g11210	molybdopterin binding domain protein	217	-		catalytic activity///cytoplasm///nucleus///Mo-molybdopterin cofactor biosynthetic process
Afu6g04400	transcription factor TFIIIB component	220		0.049	transcription factor TFIIIB complex///transcription initiation from RNA polymerase III promoter///RNA polymerase III transcription factor activity
Afu6g03620	FAD/FMN-containing isoamyl alcohol oxidase MreA	221	-		
Afu5g07490	steroid monooxygenase (CpmA)	222		0.023	
Afu6g12720	40S ribosomal protein S29	223	-		structural constituent of ribosome///translation///cytosolic small

					ribosomal subunit (sensu Eukaryota)
Afu5g04090	SGT1 and CS domain protein	224		0.023	protein ubiquitination///regulation of progression through cell cycle///ubiquitin ligase complex///co-chaperone activity///centromere and kinetochore complex maturation///protein complex assembly///cAMP-mediated signaling
Afu4g07740	small nuclear ribonucleoprotein SmB	225	-		"nuclear mRNA splicing, via spliceosome""""///""pre-mRNA splicing factor activity"///"small nuclear ribonucleoprotein complex""
Afu5g09430	RNA-directed RNA polymerase	226	-		
Afu2g09810	mandelate racemase/muconate lactonizing enzyme family protein	227	-		
Afu2g01880	low molecular weight phosphotyrosine protein phosphatase	228	-		protein amino acid dephosphorylation///cytoplasm///nucleus///protein tyrosine phosphatase activity
Afu8g06030	alpha-1,3-glucanase	229	-		cellular glucan metabolic process///fungal-type cell wall"///""""""""hydrolase activity, hydrolyzing O-glycosyl compounds"""""
Afu6g13440	choline sulfatase	230	-		sulfuric ester hydrolase activity///metabolic process
Afu3g12270	glutathione peroxidase Hyr1	231		0.045	intracellular///response to oxidative stress///thiol peroxidase activity///glutathione peroxidase activity
Afu3g03060	cell wall protein PhiA	232	-		
Afu2g16880	60S ribosomal protein L37a	233	-		structural constituent of ribosome///translation///cytosolic large ribosomal subunit (sensu Eukaryota)
Afu5g03640	mitochondrial export translocase Oxa1	234	-		protein transporter activity///mitochondrial translocation///mitochondrial inner membrane
Afu4g11260	aldo-keto reductase	235	-		aldo-keto reductase activity///cytoplasm///cellular aldehyde metabolic process
Afu2g01640	tryptophanyl-tRNA synthetase	237	-		cytoplasm///tryptophan-tRNA ligase activity///tryptophanyl-tRNA aminoacylation
Afu4g12110	TPR domain protein	238	-		protein binding
Afu1g07000	DNA repair protein Rad26	239	-		
Afu5g01160	MFS monosaccharide	240	-		mannose transmembrane transporter activity///hexose transport///fructose

	transporter				transmembrane transporter activity///plasma membrane///glucose transmembrane transporter activity
Afu4g06460	pentafunctional AROM polypeptide	242		0.010	3-dehydroquinate synthase activity///3-phosphoshikimate 1-carboxyvinyltransferase activity///cytoplasm///aromatic amino acid family biosynthetic process///shikimate kinase activity///shikimate 5-dehydrogenase activity///3-dehydroquinate dehydratase activity
Afu2g16360	DRAP deaminase (Rib2)	243	-		DRAP deaminase activity///cytoplasm///pseudouridylate synthase activity///riboflavin biosynthetic process
Afu1g12570	RNA binding protein Ligatin/Tma64	246	-		cellular component unknown///RNA binding///biological process unknown
Afu5g03780	L-PSP endoribonuclease family protein Brt1	247		0.049	cytoplasm///cytosol///nucleus///mRNA catabolic process///endoribonuclease activity
Afu5g08680	mitochondrial GTPase (YlqF)	248		0.024	translation///mitochondrial inner membrane///GTPase activity///ribosome assembly
Afu3g12560	allantoicase Alc	249	-		cellular component unknown///allantoicase activity///allantoin catabolic process
Afu1g11280	oxidoreductase	250	-		oxidoreductase activity///metabolic process
Afu4g13550	short chain dehydrogenase/reductase family	252	-		sporulation (sensu Saccharomyces)///fatty acid catabolic process///""""2,4-dienoyl-CoA reductase (NADPH) activity""""""""///"peroxisomal matrix
Afu6g03560	IgE-binding protein	254		0.028	
Afu1g15760	phosphatidylserine decarboxylase	255	-		phosphatidylserine decarboxylase activity///mitochondrial inner membrane///mitochondrion///phosphatidylcholine biosynthetic process
Afu5g09010	conserved glutamic acid rich protein	256	-		
Afu2g04770	autophagy protein Atg13	257	-		
Afu5g06990	O-methyltransferase	258		0.037	O-methyltransferase activity
Afu4g07120	cytochrome c1 heme lyase	259	-		holocytochrome-c synthase activity///cytochrome c-heme linkage///mitochondrial intermembrane space
Afu2g00680	glycosyl hydrolase	260	-		pseudohyphal growth///fungal-type cell wall biogenesis///anchored to plasma membrane///molecular function unknown
Afu2g12440	diphthamide	261	-		cytoplasm

	biosynthesis protein				
Afu4g04730	riboflavin-specific deaminase	262	-		
Afu5g10490	amidase	264	-		amidase activity
Afu2g04320	NADH-dependent flavin oxidoreductase	265	-		NADPH dehydrogenase activity///cytoplasm///nucleus///biological process unknown
Afu1g07220	6-phosphofructo-2-kinase 1	266		0.046	6-phosphofructo-2-kinase activity"///""regulation of glycolysis///"cytoplasm///""""""fructose 2,6-bisphosphate metabolic process"""""""""
Afu4g06070	translation initiation regulator (Gcn20)	267	-		cytosolic ribosome (sensu Eukaryota)///cytosol///regulation of translational elongation///regulation of translational initiation///ATP binding
Afu1g14990	ATP-dependent RNA helicase (Drs1)	268	-		nucleolus///ribosomal large subunit assembly///35S primary transcript processing///ATP-dependent RNA helicase activity
Afu6g00500	chitosanase	269	-		
Afu2g00590	glutathione S-transferase	270		0.027	
Afu6g02000	NCS1 allantoate transporter	275	-		membrane///allantoin uptake transmembrane transporter activity///allantoin transport
Afu6g00770	extracellular arabinanase	277	-		"hydrolase activity, hydrolyzing N-glycosyl compounds"///metabolic process
Afu2g08570	small subunit of nuclear cap-binding protein complex	278	-		pre-mRNA splicing factor activity"///nuclear cap binding complex///""""""nuclear mRNA splicing, via spliceosome""""""""///"commitment complex
Afu2g08920	GDSL Lipase/Acylhydrolase family protein	279	-		""hydrolase activity, acting on ester bonds""""""///"cellular component unknown///acetate metabolic process"""
Afu5g07750	mitochondrial ferrochelatase	280	-		ferrochelatase activity///heme biosynthetic process///mitochondrial inner membrane
Afu6g11570	alpha/beta hydrolase	282	-		hydrolase activity///metabolic process
Afu2g09330	C6 finger domain protein	284	-		
Afu8g03980	cytoplasmic protein required for cell viability, putative	286		0.032	cytoplasm///transcription
Afu6g02560	alpha-galactosidase	288	-		
Afu2g14220	vacuolar protein sorting protein Vps66	290	-		
Afu1g10490	F1F0 ATP synthase assembly protein	291	-		mitochondrial envelope///protein complex assembly///molecular function unknown

	Atp10			
Afu5g02860	integral membrane protein	294	-	

Table 10.4: 200 genes with greatest nSI decrease between 4 and 14 hours post infection. Genes are reported ranked according to greatest nSI intensity increase between 4 and 14 hours where 1 is the greatest. A one-way ANOVA was conducted on nSI values between time-points, with the null hypothesis that nSI values do not change between time-points. FDR correct *p*-values from this analysis are reported for each gene. Hypothetical proteins (n = 41) were removed.

ORF	Description	Rank	*p-value*	GO Biological Process
Afu5g13520	ribosome biogenesis protein Ria1	1	0.023	ribosome biogenesis///cytoplasm///translation elongation factor activity
Afu4g03110	MFS monosaccharide transporter	2	0.033	
Afu2g11380	rRNA assembly protein Mis3	4	0.016	ribosome biogenesis///nucleolus///rRNA processing///molecular function unknown
Afu6g13290	SWI/SNF family DNA-dependent ATPase Ris1	6	0.015	mating type switching///chromatin assembly or disassembly///nucleus///DNA-dependent ATPase activity
Afu7g03760	phosphatidylinositol 4-kinase (STT4)	7	0.017	protein secretion///plasma membrane///phosphatidylethanolamine biosynthetic process///1-phosphatidylinositol 4-kinase activity///MAPKKK cascade///actin cytoskeleton organization
Afu8g00560	cytochrome P450 oxidoreductase	8	-	oxidoreductase activity///metabolic process
Afu6g11250	C2H2 finger domain protein	9	0.034	
Afu8g01560	aldo-keto reductase (YakC)	11	0.015	aldo-keto reductase activity///cytoplasm///nucleus///cellular aldehyde metabolic process
Afu3g11740	RNAPII degradation factor Def1	12	0.032	
Afu7g00130	C6 transcription factor	13	0.023	
Afu2g08650	RING finger membrane protein	14	0.032	ubiquitin-protein ligase activity///mRNA polyadenylation///nuclear envelope
Afu1g15440	alpha-1,3-glucan synthase Ags3	15	0.029	cellular glucan metabolic process///fungal-type cell wall biogenesis///plasma membrane///pathogenesis///"alpha-1,3-glucan synthase activity"///cell morphogenesis
Afu2g12790	MFS	16	0.008	membrane///monocarboxylic acid

	monocarboxylate transporter			transmembrane transporter activity///transporter activity///transport
Afu2g01090	DNA helicase	18	0.014	DNA helicase activity///lagging strand elongation///alpha DNA polymerase:primase complex
Afu3g11760	MFS transporter	20	0.032	transporter activity///transport///integral to membrane
Afu5g09220	Beige/BEACH domain protein	21	0.034	cellular component unknown///response to pH///molecular function unknown
Afu3g12900	MFS transporter	22	0.035	fungal-type vacuole membrane///monocarboxylic acid transmembrane transporter activity///transporter activity///transport
Afu5g04260	arginine transporter	23	-	basic amino acid transmembrane transporter activity///arginine permease activity///lysine permease activity///basic amino acid transport///plasma membrane
Afu5g02410	eukaryotic translation initiation factor eIF-4A subunit	25	-	nucleolus///35S primary transcript processing///ATP-dependent RNA helicase activity
Afu5g11670	Leucine carboxyl methyltransferase family	26	0.029	C-terminal protein carboxyl methyltransferase activity///cytoplasm///biological process unknown
Afu2g06020	mitochondrial respiratory complex I chaperone (Cia84), putative	28	-	
Afu4g10140	glucoamylase/glucan 1,4-alpha-glucosidase	29	-	polysaccharide metabolic process""///"sporulation (sensu Saccharomyces)///fungal-type vacuole"///""""""""glucan 1,4-alpha-glucosidase activity"""""///"""""hydrolase activity, acting on glycosyl bonds"""""
Afu4g10130	alpha-amylase	31	0.029	extracellular region///alpha-amylase activity///polysaccharide catabolic process
Afu5g14860	cytochrome P450	33	0.023	
Afu6g04890	CaaX prenyl proteinase Rce1	34	-	integral to endoplasmic reticulum membrane///protein processing///prenyl-dependent CAAX protease activity///conjugation with cellular fusion///peptide pheromone maturation
Afu2g12780	von Willebrand domain protein	35	0.034	
Afu5g00530	inulinase	36	-	extracellular region///cytoplasm///sucrose catabolic process
Afu2g11870	beta-1,6 glucan synthetase (Kre6)	37	0.011	cell wall organization///"1,6-beta-glucan biosynthetic process"///glucosidase activity///integral to membrane///Golgi cis cisterna

Afu3g12800	clathrin-coated vesiclec protein (Bud7)	38		0.044	cellular bud site selection///clathrin-coated vesicle///molecular function unknown
Afu1g06250	CAIB/BAIF family enzyme	39	-		
Afu7g05860	RING finger domain protein	41	-		
Afu1g06210	N-acetylglucosamine-phosphate mutase	43	-		phosphoacetylglucosamine mutase activity///cytoplasm///N-acetylglucosamine biosynthetic process///nucleus
Afu6g14620	fungal alpha-L-arabinofuranosidase	44		0.045	
Afu6g08100	nucleotide-sugar transporter	45	-		
Afu3g00120	amino acid transporter (Mtr)	46		0.033	
Afu2g17960	NADPH dehydrogenase Oye3	47		0.023	
Afu5g12510	adenylate-forming enzyme AfeA	48		0.049	cytoplasm///AMP binding
Afu3g02120	short-chain dehydrogenase/reductase family protein, putative	49	-		
Afu6g02400	MFS drug efflux pump	50		0.032	transporter activity///transport
Afu6g13680	APSES transcription factor Xbp1	51		0.046	
Afu3g02750	C6 transcription factor	52	-		DNA binding
Afu3g08400	SNF2 family helicase/ATPase	53	-		nucleus///chromosome organization and biogenesis (sensu Eukaryota)///molecular function unknown
Afu2g16600	DNA polymerase delta catalytic subunit Cdc2	56		0.045	leading strand elongation///delta DNA polymerase complex///nucleotide-excision repair///base-excision repair///mutagenesis///lagging strand elongation///delta DNA polymerase activity///mismatch repair///postreplication repair
Afu3g01940	MFS multidrug transporter	57		0.029	transporter activity///transport
Afu8g00440	steroid monooxygenase	58	-		
Afu3g13870	GATA-type sexual development transcription factor NsdD	59	-		transcription factor activity///regulation of developmental process///nucleus///zinc ion binding///regulation of transcription///sporocarp development
Afu8g04290	C2H2 finger	60		0.033	

	domain protein				
Afu4g10100	FAD binding domain protein	61	-		
Afu6g07580	essential cytoplasmic protein Ctr86	62		0.023	cytoplasm///biological process unknown///molecular function unknown
Afu5g12760	CCCH zinc finger DNA binding protein	63		0.050	
Afu2g11170	origin recognition complex subunit Orc4	64	-		nuclear origin of replication recognition complex///DNA replication initiation///DNA replication origin binding///pre-replicative complex assembly
Afu5g00370	amino acid permease	65	-		basic amino acid transmembrane transporter activity///basic amino acid transport///plasma membrane
Afu6g09770	geranylgeranyl diphosphate synthase	66	-		terpenoid biosynthetic process///farnesyltranstransferase activity///mitochondrion
Afu2g02060	aminoacyl-tRNA hydrolase	67		0.031	aminoacyl-tRNA hydrolase activity///metabolic process
Afu2g17540	conidial pigment biosynthesis oxidase Abr1/brown 1	68	-		
Afu3g12450	DIL and Ankyrin domain protein	69	-		cellular component unknown///biological process unknown///molecular function unknown
Afu2g10710	DNA repair protein rad9	71		0.023	
Afu5g08010	protein N-terminal asparagine amidohydrolase	72		0.038	protein catabolic process///protein N-terminal asparagine amidohydrolase activity///protein modification process///mitochondrion
Afu2g01770	GMC oxidoreductase	74		0.038	
Afu7g01640	C6 transcription factor (War1)	76		0.044	transcription factor activity///nucleus///response to acid///regulation of transcription
Afu2g08350	MFS allantoate transporter	77		0.018	allantoate transmembrane transporter activity///plasma membrane///allantoate transport
Afu2g08400	integral membrane protein	78		0.036	
Afu3g07700	glucosyltransferase	80		0.024	"transferase activity, transferring hexosyl groups"///protein amino acid glycosylation///endoplasmic reticulum///dolichol-linked oligosaccharide biosynthetic process
Afu8g05500	COP9 signalosome subunit CsnD	81	-		regulation of developmental process///sporocarp

				development///signalosome
Afu3g01540	MFS monocarboxylate transporter	82	0.044	fungal-type vacuole membrane///monocarboxylic acid transmembrane transporter activity///transporter activity///transport
Afu2g00630	GDSL lipase/acylhydrolase family protein	83	-	lipase activity
Afu2g17970	ergot alkaloid biosynthetic protein A	86		
Afu1g11180	heat shock protein/chaperonin HSP78	88		mitochondrial genome maintenance///mitochondrial translocation///chaperone activity///protein folding///ATP-dependent peptidase activity///mitochondrial matrix///response to stress///heat shock protein activity
Afu3g14320	Golgi transport protein Sly1	89		SNARE binding///endoplasmic reticulum///ER to Golgi vesicle-mediated transport///ER to Golgi transport vesicle///Golgi apparatus
Afu4g01010	C6 transcription factor	90	0.049	transcription activator activity///DNA binding///nucleus///zinc ion binding///regulation of transcription
Afu6g02845	ethanolamine utilization protein (EutQ)	91	0.034	
Afu8g00570	alpha/beta hydrolase	94	0.023	
Afu8g00590	fatty acid desaturase	95	0.032	stearoyl-CoA 9-desaturase activity///fatty acid biosynthetic process
Afu2g09890	NDT80	97		
Afu2g13490	KH domain protein	98	0.029	
Afu7g05580	phospholipase PldA	99	0.044	phospholipase D activity///phospholipid metabolic process///response to osmotic stress
Afu5g00790	ABC multidrug transporter	100	0.017	ATP-binding cassette (ABC) transporter activity///ATP binding///transport
Afu5g12330	WD repeat protein	101	0.033	
Afu6g07070	cellobiohydrolase celD	102	0.032	
Afu4g04070	mucin family signaling protein Msb2	104	0.045	
Afu3g06790	RNA-directed RNA polymerase (Sad-1)	105		RNA-directed RNA polymerase activity///posttranscriptional gene silencing///cytoplasm
Afu7g06150	endoglucanase	106		
Afu1g14510	ankyrin repeat protein	107		molecular function unknown
Afu6g13370	SSU processome	108		maturation of SSU-rRNA///snoRNA

	component Utp10			binding///small nucleolar ribonucleoprotein complex
Afu2g11370	autophagy protein (Atg22)	109	0.010	
Afu3g05580	chitin synthase activator (Chs3)	110	0.025	response to osmotic stress///enzyme activator activity///cell wall chitin biosynthetic process///cytokinesis
Afu4g07700	clathrin heavy chain	111		structural molecule activity///clathrin vesicle coat///vesicle-mediated transport
Afu6g07500	DNA excision repair protein Rad2	112	0.039	single-stranded DNA specific endodeoxyribonuclease activity""///"nucleotide-excision repair, DNA incision, 3'-to lesion"""""///""nucleotide-excision repair factor 3 complex"
Afu4g10120	C6 finger domain protein	114	0.034	DNA binding///zinc ion binding
Afu6g12480	NGG1 interacting factor Nif3	115	0.032	cytoplasm///mitochondrion
Afu1g07160	ubiquitin C-terminal hydrolase	116		protein deubiquitination///cytoplasm///ubiquitin-specific protease activity
Afu4g14790	cytochrome P450 monooxygenase	117	0.008	
Afu4g13810	F-box domain protein	118	0.010	
Afu2g06290	nuclear division Rft1 protein	119		protein amino acid N-linked glycosylation///oligosaccharide transmembrane transporter activity///oligosaccharide transport///endoplasmic reticulum membrane
Afu8g01500	Pfs domain protein	120	0.048	purine-nucleoside phosphorylase activity
Afu4g04090	conserved serine-threonine rich protein	121	0.044	
Afu5g13240	inositol hexaphosphate kinase KCS1	122		inositol or phosphatidylinositol kinase activity///vacuole organization///cytoplasm///response to stress
Afu8g06640	ubiE/COQ5 methyltransferase	123	0.023	methyltransferase activity///metabolic process
Afu8g05170	autophagy protein Apg6	124	0.039	membrane fraction///autophagy///protein targeting to vacuole///molecular function unknown
Afu4g12750	transcription factor	125		3'-5'-exoribonuclease activity///cytoplasm///nuclear-transcribed mRNA poly(A) tail shortening///regulation of transcription from RNA polymerase II promoter///"nuclear-transcribed mRNA catabolic process, deadenylation-dependent decay"///CCR4-NOT core

				complex
Afu1g04270	calcium ion transporter Vcx1	127		calcium ion transport///calcium:hydrogen antiporter activity///fungal-type vacuole///calcium ion transmembrane transporter activity///cellular calcium ion homeostasis///vacuolar membrane
Afu5g03530	class III chitinase	128		cell wall chitin catabolic process///fungal-type cell wall///chitinase activity
Afu2g08040	C6 finger domain protein	129	0.042	DNA binding///nucleus///zinc ion binding
Afu5g00710	GABA permease	130		plasma membrane///choline transport///choline transmembrane transporter activity
Afu2g08420	prenyl cysteine carboxyl methyltransferase Ste14	131		protein-S-isoprenylcysteine O-methyltransferase activity///conjugation with cellular fusion///peptide pheromone maturation///endoplasmic reticulum membrane
Afu4g06000	50S ribosomal protein L3	132	0.032	structural constituent of ribosome///translation///mitochondrial large ribosomal subunit///ribosomal large subunit assembly///peptidyltransferase activity
Afu3g06170	mating type protein MAT1-2-1	133		
Afu5g09460	ABC transporter	134		transporter activity///transport
Afu1g00100	MFS monocarboxylate transporter	135		
Afu4g07000	tyrosine phosphatase family protein	136		protein amino acid dephosphorylation///cytoplasm///response to stress///protein tyrosine phosphatase activity
Afu6g03670	biotin synthase	137		biotin synthase activity///biotin biosynthetic process///mitochondrion
Afu1g17550	HET domain protein	138		
Afu1g09670	HLH transcription factor (GlcD gamma)	139		transcription///transcription factor activity///nucleus
Afu2g04390	cytomegalovirus gH-receptor family protein	140		cellular component unknown///biological process unknown///molecular function unknown
Afu3g13610	oxidoreductase, zinc-binding	141	0.041	
Afu5g11780	TOR signalling pathway regulator (TapA)	142		cellular component unknown///cell growth and/or maintenance///protein binding///signal transduction
Afu4g11690	RNA polymerase II transcription factor related protein	143	0.024	"negative regulation of transcription from RNA polymerase II promoter, mitotic"///holo TFIIH complex///nucleotide-excision repair

			factor 3 complex///nucleotide-excision repair///transcription initiation from RNA polymerase II promoter///general RNA polymerase II transcription factor activity///"nucleotide-excision repair, DNA duplex unwinding"
Afu3g10690	calcium-translocating P-type ATPase(PMCA-type),putative	144	calcium ion transport///cellular calcium ion homeostasis///calcium-transporting ATPase activity
Afu3g14230	BAR adaptor protein RVS167	145	endocytosis///response to osmotic stress///cytoskeletal protein binding///bipolar cellular bud site selection
Afu6g13760	alpha-1,2-mannosidase subfamily	146	
Afu6g00220	fungal specific transcription factor	147	transcription factor activity///nucleus///regulation of transcription
Afu4g12080	ubiquitin conjugating enzyme (MmsB)	148	regulation of DNA repair///ubiquitin-dependent protein catabolic process///ubiquitin cycle///cytoplasm///postreplication repair///nucleus///ubiquitin conjugating enzyme activity
Afu1g10760	CCAAT-box-binding transcription factor	149	nucleolus///nucleus///ribosomal large subunit assembly///molecular function unknown
Afu1g05150	C2H2 transcription factor (TFIIIA)	150	zinc ion binding///transcription initiation from RNA polymerase III promoter///transcription factor complex///RNA polymerase III transcription factor activity
Afu4g14220	C6 finger domain protein	151	
Afu2g01960	UbiA prenyltransferase family protein	152	
Afu4g14230	MFS transporter	155	integral to plasma membrane///transporter activity///transport
Afu6g07860	catabolite repressor protein (CreC)	157	negative regulation of transcription by carbon catabolites
Afu3g12810	transcriptional corepressor of histone genes (Hir3), putative	159	gene silencing///nucleosome assembly///nucleosome///transcription corepressor activity
Afu1g07080	tRNA-specific adenosine-34 deaminase subunit Tad3, putative	160	zinc ion binding

Afu7g02620	DNA-directed RNA polymerases N/8 kDa subunit superfamily	161		DNA-directed RNA polymerase II, core complex""///"DNA-directed RNA polymerase III complex///transcription from RNA polymerase I promoter"///DNA-directed RNA polymerase I complex///transcription from RNA polymerase II promoter///transcription from RNA polymerase III promoter///DNA-directed RNA polymerase activity
Afu1g11770	COPII-coated vesicle protein SurF4/Erv29	162		COPII-coated vesicle///ER to Golgi vesicle-mediated transport
Afu7g02380	ferulic acid esterase (FaeA)	163		
Afu3g12830	RTA1 domain protein	165		
Afu3g08980	threonine synthase Thr4	168		cytoplasm///nucleus///threonine synthase activity///threonine metabolic process
Afu7g05140	class III chitinase	169	0.044	cell wall chitin catabolic process///extracellular region///fungal-type cell wall///chitinase activity///"cytokinesis, completion of separation"
Afu1g16110	arsenic methyltransferase Cyt19	170	0.043	S-adenosylmethionine-dependent methyltransferase activity///response to arsenic///cytoplasm
Afu4g12950	vacuolar targeting protein Atg24	171	0.031	membrane///autophagy///lipid binding///transport
Afu1g01490	NACHT domain protein	172		
Afu1g05330	F-box domain protein	173		
Afu1g09220	SNF7 family protein	175		late endosome to vacuole transport///endosome///cytoplasm///molecular function unknown
Afu4g10660	histone acetylase complex subunit MRG15-2	176	0.014	histone acetyltransferase complex///regulation of transcription from RNA polymerase II promoter///histone acetyltransferase activity///histone acetylation
Afu3g08300	DNA replication factor C subunit Rfc2	177		leading strand elongation///DNA replication factor C complex///DNA clamp loader activity///cell cycle checkpoint///sister chromatid cohesion///mismatch repair///purine nucleotide binding
Afu8g00940	MFS multidrug transporter	178	0.044	response to drug///multidrug transport///integral to plasma membrane///multidrug efflux pump activity
Afu4g13930	CRAL/TRIO domain protein	180		phosphatidylinositol transporter activity///cell wall organization///phospholipid

				transport///cytoplasm///cytosol///microsome
Afu6g14050	FAD binding domain protein	182	0.049	
Afu5g01320	phosphate permease	183	0.032	integral to plasma membrane///inorganic phosphate transmembrane transporter activity///phosphate transport
Afu3g11530	Hsp40 co-chaperone Jid1	184	0.027	protein binding///protein folding///mitochondrion
Afu3g08480	sucrose transporter	185		
Afu5g00300	zinc-binding oxidoreductase	186	0.032	oxidoreductase activity///cellular component unknown///zinc ion binding///metabolic process
Afu6g09300	C2H2 finger domain protein	187		
Afu4g03610	phosphate:H+ symporter	188		
Afu1g04780	peroxisomal ABC transporter (PXA1)	189		integral to peroxisomal membrane///ATP-binding cassette (ABC) transporter activity///fatty acid transport
Afu4g04640	ubiquitin fusion degradation protein (Ufd1)	190	0.019	
Afu5g00470	general amidase GmdB	191		cellular component unknown///amidase activity///biological process unknown
Afu8g01430	oxidoreductase, zinc-binding dehydrogenase family, putative	193		oxidoreductase activity///cellular component unknown///zinc ion binding///metabolic process
Afu4g02760	DUF829 domain protein (PaxU)	194		
Afu4g14820	transferase family protein	195		
Afu5g01980	histone deacetylase HdaA	196		"regulation of transcription, DNA-dependent""""///histone deacetylase activity///"chromatin organization""///histone deacetylase complex///""protein amino acid deacetylation///loss of chromatin silencing during replicative cell aging"
Afu2g10380	eukaryotic translation initiation factor 3 subunit EifCl	197	0.015	translation initiation factor activity///eukaryotic translation initiation factor 3 complex///translational initiation
Afu7g02170	cyclophilin-type peptidyl-prolyl cis-trans isomerase, putative	198		RNA binding
Afu4g01160	von Willebrand domain protein	199		
Afu5g13560	FHA domain protein	200		cytoplasm///biological process unknown///molecular function unknown

Afu1g08830	Golgi matrix protein	201	0.034	ER to Golgi vesicle-mediated transport///molecular function unknown///Golgi apparatus
Afu8g06010	C6 transcription factor	202		transcription factor activity///nucleus///zinc ion binding///regulation of transcription
Afu1g03690	4-carboxymuconolactone decarboxylase family protein	203		4-carboxymuconolactone decarboxylase activity///catechol catabolic process
Afu1g13740	pentafunctional polypeptide (AroM)	204		3-dehydroquinate synthase activity///3-phosphoshikimate 1-carboxyvinyltransferase activity///cytoplasm///aromatic amino acid family biosynthetic process///shikimate kinase activity///shikimate 5-dehydrogenase activity///3-dehydroquinate dehydratase activity
Afu1g03560	peroxisome biosynthesis protein (Peroxin-2)	205	0.043	
Afu3g06160	mating locus protein	206		
Afu3g11900	oxidoreductase, zinc-binding	208	0.008	alcohol metabolic process///soluble fraction///alcohol dehydrogenase (NADP+) activity///cellular aldehyde metabolic process
Afu3g02020	conserved hypothetical protein	209		
Afu5g10310	AflR-like C6 zinc cluster transcription factor, putative	210		DNA binding///transcription factor activity///nucleus///zinc ion binding///regulation of transcription
Afu4g12240	nitrilase, putitive	211		"hydrolase activity, acting on carbon-nitrogen (but not peptide) bonds, in other compounds"
Afu4g13530	alpha,alpha-trehalase TreB/Nth1	212		response to stress""///""cytoplasm///trehalose catabolic process"///cytosol///"alpha,alpha-trehalase activity"""""
Afu6g12040	MFS sugar permease	213		alpha-glucoside:hydrogen symporter activity///membrane fraction///alpha-glucoside transport///trehalose transport///trehalose transmembrane transporter activity///maltose:hydrogen symporter activity
Afu4g14300	dynamin family GTPase	214		
Afu1g03890	alpha/beta hydrolase	215		cellular component unknown///hydrolase activity///metabolic process
Afu4g10830	SNF2 family	216		helicase activity///nucleus///""nucleotide-

	helicase			excision repair, DNA damage recognition""///DNA-dependent ATPase activity
Afu2g11140	50S ribosomal protein L4	218		
Afu3g10350	stress response protein Nst1	219		response to salt stress///cytoplasm///molecular function unknown
Afu1g04670	PSP1 domain protein	220		cytoplasm///biological process unknown///molecular function unknown
Afu3g10880	anion exchange family protein	221		membrane fraction///plasma membrane///anion transmembrane transporter activity///transport
Afu5g14500	MFS transporter	222		integral to plasma membrane
Afu8g01550	oxidoreductase, short chain dehydrogenase/reductase family superfamily	223	0.036	sporulation (sensu Saccharomyces)///fatty acid catabolic process///""""2,4-dienoyl-CoA reductase (NADPH) activity""""""""///"peroxisomal matrix
Afu7g06950	oxidoreductase	224	0.029	
Afu5g03230	stress response RCI peptide	225		response to stress
Afu2g01380	GNAT family N-acetyltransferase	226		N-acetyltransferase activity///metabolic process
Afu1g07180	ribonuclease H	227		ribonuclease H1 activity///ribonuclease H activity///RNA catabolic process///cell wall organization///DNA replication///cell
Afu1g12620	MFS toxin efflux pump (AflT)	228	0.031	response to drug///multidrug transport///multidrug efflux pump activity
Afu5g08150	ABC bile acid transporter	230		ATP-binding cassette (ABC) transporter activity///bile acid transmembrane transporter activity///fungal-type vacuole///bile acid and bile salt transport
Afu6g08480	aquaglyceroporin	231		glycerol transport///water transport///water channel activity///glycerol channel activity///integral to membrane
Afu3g10040	cyclin-like protein (Clg1)	232	0.042	cell cycle///cyclin-dependent protein kinase regulator activity///cyclin-dependent protein kinase holoenzyme complex
Afu6g00230	NmrA-like family protein	233		
Afu2g09530	DUF833 domain protein	234		
Afu5g01540	MFS aflatoxin efflux pump	235	0.037	cellular component unknown///biological process unknown///molecular function unknown
Afu3g00470	endo-1,4-beta-xylanase	237	0.040	xylan metabolic process
Afu5g08040	Exocyst complex component Sec8	238		incipient cellular bud site///exocyst///Golgi to plasma membrane transport///vesicle

				fusion///protein binding///vesicle docking during exocytosis///cytokinesis///bipolar cellular bud site selection///cellular bud tip
Afu6g07190	NmrA-like family protein	239	0.044	
Afu5g02720	phosphoribosylformylglycinamidine synthase	240	0.049	cytoplasm///purine nucleotide biosynthetic process///phosphoribosylformylglycinamidine synthase activity
Afu2g03350	MIZ zinc finger domain protein	241		

10.3.4 Functional classification of differentially expressed genes between 4 and 14 hours post infection in Af293

Differentially expressed genes were grouped into functional categories based on GO Terms and by reference to the *A. fumigatus* literature. A summary of up and down expressed functional categories between 4 and 14 hours is given in Table 10.5.

Table 10.5: Functional classification of selected genes having differential transcript abundance in Af293 between 4 and 14 hours post infection in the murine lung. Increased (red) and decreased (green) are shown for each functional category. Both increasing and decreasing transcripts are sub divided into expression cohorts which are either high, moderate, and low with respect to their expression change. Genes within functional categories ranked according to greatest nSI intensity changes between 4 and 14 hours. A one-way ANOVA was conducted on nSI values between time-points, from which FDR correct *p*-values are reported for each gene.

Functional Category	ORF	Description	Rank	p-value	Magnitude	ORF	Description	Rank	p-value	Magnitude
Cell wall	Afu8g06030	alpha-1,3-glucanase	229	-	UP HIGH	Afu1g15440	alpha-1,3-glucan synthase Ags3	15	0.029	DOWN HIGH
	Afu2g05340	1,3-beta-glucanosyltransferase	498	-	UP HIGH	Afu3g05580	chitin synthase activator (Chs3)	110	0.025	DOWN HIGH
	Afu4g13360	endo-1,3(4)-beta-glucanase	806	-	UP MOD	Afu5g03530	class III chitinase	128		DOWN HIGH
	Afu2g11270	alpha-1,3-glucan synthase Ags2	1290	0.043	UP MOD	Afu7g05140	class III chitinase	169	0.044	DOWN HIGH
	Afu2g00430	exo-beta-1,3-glucanase	1359	-	UP MOD					
	Afu5g08550	Rho guanyl nucleotide exchange factor (Rom2)	1376	-	UP LOW	Afu2g14360	GPI anchored endo-1,3(4)-beta-glucanase	283		DOWN HIGH
	Afu3g10340	Rho GTPase Rho 2	1496	-	UP LOW	Afu1g12560	endoglucanase	321		DOWN HIGH
	Afu6g12400	1,3-beta-glucan synthase catalytic subunit FksP	1639	-	UP LOW	Afu5g03760	class III chitinase ChiA1	372	0.047	DOWN HIGH
	Afu5g00760	chitin synthase C	1682	-	UP LOW	Afu2g14910	alpha-1,6-mannosyltransferase subunit	383	0.029	DOWN HIGH
	Afu8g05620	chitin synthase activator (Chs3)	1703	-	UP LOW	Afu5g02280	endo-1,3(4)-beta-glucanase	420		DOWN HIGH
	Afu1g05290	endo-1,3(4)-beta-glucanase	1730	-	UP LOW	Afu3g11280	class V chitinase	548		DOWN HIGH
	Afu5g14190	beta-glucanase	1881	-	UP LOW	Afu8g02040	glycosyl transferase	569		DOWN HIGH

	Afu1g14450	exo-beta-1,3-glucanase Exg0	2005	-		UP LOW	Afu6g14480	alpha-1,3-mannosyltransferase	628	0.032	DOWN HIGH
							Afu1g12040	chitin biosynthesis protein (Chs7)	764		DOWN MOD
							Afu6g06900	Rho GTPase Rho1	1099	-	DOWN MOD
							Afu8g05630	chitin synthase F	1481	-	DOWN LOW
							Afu5g03960	class V chitinase Chi100	1631	-	DOWN LOW
							Afu8g01410	class V chitinase ChiB1	1903	-	DOWN LOW
Ergosterol biosynthesis	Afu1g04720	C-8 sterol isomerase (Erg-1)	152	-		UP HIGH	Afu5g08960	triglyceride lipase-cholesterol esterase	288	0.032	DOWN HIGH
	Afu4g06380	sterol carrier protein	536	-		UP HIGH	Afu2g03700	HMG-CoA reductase	468		DOWN HIGH
	Afu2g03790	oxysterol binding protein (Osh7)	1192	-		UP MOD	Afu2g17400	C-3 sterol dehydrogenase/C-4 decarboxylase family protein	552	0.037	DOWN HIGH
	Afu4g07780	mevalonate kinase	1384	0.049		UP LOW	Afu1g05720	c-14 sterol reductase	733		DOWN MOD
	Afu5g07780	squalene monooxygenase Erg1	1767	-		UP LOW	Afu1g03950	cytochrome P450 sterol C-22 desaturase, putaitve	1153	-	DOWN MOD
	Afu3g11750	oxysterol binding protein (Osh5)	1944	-		UP LOW	Afu4g12040	lanosterol synthase	1382	-	DOWN LOW
							Afu6g05140	sterol delta 5,6-desaturase ERG3	1633	-	DOWN LOW
							Afu3g05520	oxysterol binding protein (Orp8)	1666	-	DOWN LOW
Microtubule	Afu2g03150	kinesin family protein	83	-		UP HIGH	Afu1g13390	gamma tubulin MipA	363		DOWN HIGH
	Afu1g15240	prefoldin subunit 4	309	-		UP HIGH	Afu6g12980	spindle pole body component	449	0.038	DOWN HIGH
	Afu2g14990	tubulin subunit TubB	804	-		UP MOD	Afu3g11320	spindle pole body component (Alp6)	507		DOWN HIGH
	Afu7g03710	kinesin family protein (KipA)	1019	-		UP MOD	Afu2g15750	gamma-tubulin complex component GCP4	726		DOWN MOD

	Afu1g10740	prefoldin subunit 5	1280	-	UP MOD	Afu6g14220	kinesin family protein (KinA)	747		DOWN MOD
	Afu6g12840	kinesin family protein	1360	-	UP MOD	Afu4g14740	serine/threonine protein kinase (Ark1)	1016	-	DOWN MOD
	Afu2g04140	chromosome segregation protein Spc105	1502	-	UP LOW	Afu1g01640	kinesin family protein	1496	-	DOWN LOW
	Afu3g12820	kinesin family protein	1822	-	UP LOW					
Cell polarity	Afu4g10490	Exocyst complex component Sec6	563	-	UP HIGH	Afu6g06400	Rho GTPase activator (Bem3)	857		DOWN MOD
	Afu4g06180	casein kinase II beta subunit CKB1	867	-	UP MOD	Afu7g05370	septin AspB	1806	-	DOWN LOW
	Afu1g07580	cell polarity protein (Alp11)	1451	-	UP LOW					
	Afu1g04360	Exocyst complex component Sec3	1522	-	UP LOW					
	Afu7g02280	U5 snRNP complex subunit	2026	-	UP LOW					
	Afu6g02300	serine/threonine protein kinase (Kcc4)	2027	-	UP LOW					
Ion transport	Afu4g00930	CorA family metal ion transporter	183	-	UP HIGH	Afu1g04270	calcium ion transporter Vcx1	127	-	DOWN HIGH
	Afu2g09460	potassium transporter	405	-	UP HIGH	Afu5g02290	potassium ion transporter (Trk1)	335	-	DOWN HIGH
	Afu2g09460	potassium transporter	405	-	UP HIGH	Afu8g04010	ZIP family zinc transporter	816	-	DOWN MOD
	Afu2g11330	V-type ATPase F subunit	612	0.032	UP HIGH	Afu4g13540	potassium uptake transporter	1084	-	DOWN MOD
	Afu1g10880	P-type calcium ATPase	1291	-	UP MOD	Afu5g05830	CorA family metal ion transporter	1102	-	DOWN MOD
	Afu6g00470	plasma membrane zinc ion transporter	1370	-	UP LOW	Afu6g14240	calcium sensor (NCS-1)	1285	-	DOWN MOD
	Afu3g08180	Ctr copper transporter family protein	1395	-	UP LOW	Afu1g11110	calcium channel subunit Cch1	1601	-	DOWN LOW
	Afu6g14170	CDF zinc transporter (Msc2), putaitve	1801	-	UP LOW	Afu1g14250	potassium channel	1646	-	DOWN LOW

Iron acquisition	Afu1g16750	mitochondrial cation transporter	163	0.032	UP HIGH	Afu1g16040	ferric-chelate reductase	587	-	DOWN HIGH
	Afu2g10370	iron-sulfur cluster assembly accessory protein Isa2, putative	474	-	UP HIGH	Afu3g01360	siderochrome-iron transporter	710	-	DOWN MOD
	Afu3g03390	siderophore biosynthesis lipase/esterase	1520	-	UP LOW	Afu3g13670	siderochrome-iron transporter	855	-	DOWN MOD
						Afu1g04450	siderophore biosynthesis protein	1265	-	DOWN LOW
						Afu1g17200	nonribosomal siderophore peptide synthase SidC	1531	-	DOWN LOW
						Afu3g03640	MFS siderochrome iron transporter MirB	1809	-	DOWN LOW
Antigen	Afu4g03240	cell wall serine-threonine-rich galactomannoprotein Mp1	126	0.034012	UP HIGH	Afu2g09030	secreted dipeptidyl peptidase DppV	373		DOWN HIGH
	Afu6g11030	RNA binding protein MSSP-2	186	-	UP HIGH	Afu1g09670	HLH transcription factor (GlcD gamma)	139		DOWN HIGH
	Afu5g09210	autophagic serine protease Alp2	512	-	UP HIGH	Afu5g13300	aspartic endopeptidase Pep1/aspergillopepsin F	1999	-	DOWN LOW
	Afu1g06830	60S acidic ribosomal protein P1	922	-	UP MOD					
	Afu5g02040	extracellular lipase	1069	-	UP MOD					
	Afu2g00690	glucan 1,4-alpha-glucosidase	1110	-	UP MOD					
	Afu5g02330	major allergen and cytotoxin AspF1	1398	-	UP LOW					
	Afu2g10100	60S acidic ribosomal protein P2/allergen Asp F 8	1877	-	UP LOW					
	Afu1g07440	molecular chaperone Hsp70	1880	-	UP LOW					
Secreted proteases	Afu3g08930	tripeptidyl peptidase SED3	367	-	UP HIGH	Afu2g09030	secreted dipeptidyl peptidase DppV	373		DOWN HIGH

	Afu4g13750	penicillolysin/deuterolysin metalloprotease	406	-		UP HIGH	Afu6g10250	alkaline serine protease AorO	394			DOWN HIGH
	Afu5g09210	autophagic serine protease Alp2	512	-		UP HIGH	Afu1g07730	metalloprotease MEP1	544			DOWN HIGH
	Afu6g13540	carboxypeptidase CpyA/Prc1	1082	-		UP MOD	Afu3g12210	carboxypeptidase Y	736			DOWN MOD
	Afu2g01250	serine peptidase	1163	-		UP MOD	Afu4g14000	tripeptidyl peptidase A	1262	-		DOWN MOD
	Afu2g17330	extracelular serine carboxypeptidase	1276	-		UP MOD	Afu4g07040	aspartic-type endopeptidase (CtsD)	1483		0.031	DOWN LOW
	Afu4g11150	ADAM family of metalloprotease ADM-B	1385	-		UP LOW	Afu6g05350	aspartic-type endopeptidase (OpsB)	1952	-		DOWN LOW
	Afu4g09400	aspartic-type endopeptidase	1514	-		UP LOW	Afu5g13300	aspartic endopeptidase Pep1/aspergillopepsin F	1999	-		DOWN LOW
	Afu1g17400	peptidase S41 family protein	1705	-		UP LOW						
	Afu5g01200	carboxypeptidase S1	1804	-		UP LOW						
	Afu1g08940	pheromone processing carboxypeptidase KexA	1895	-		UP LOW						
Secretion peptide encoding genes	Afu4g03240	cell wall serine-threonine-rich galactomannoprotein Mp1	126		0.034	UP HIGH	Afu3g07700	glucosyltransferase	80		0.024	DOWN HIGH
	Afu4g00620	cell wall glycosyl hydrolase Dfg5	151		0.048	UP HIGH	Afu5g03530	class III chitinase	128			DOWN HIGH
	Afu3g03060	cell wall protein PhiA	232	-		UP HIGH	Afu7g05140	class III chitinase	169		0.044	DOWN HIGH
	Afu6g03560	IgE-binding protein	254		0.028	UP HIGH	Afu5g02290	potassium ion transporter (Trk1)	335			DOWN HIGH
	Afu2g00680	glycosyl hydrolase	260	-		UP HIGH	Afu4g08720	lysophospholipase Plb1	351		0.029	DOWN HIGH
	Afu6g00500	chitosanase	269	-		UP HIGH	Afu5g14150	lipase	415			DOWN HIGH
	Afu6g00770	extracellular arabinanase	277	-		UP HIGH	Afu3g11280	class V chitinase	548			DOWN HIGH
	Afu3g01660	glycosyl hydrolase, family 43	311		0.029	UP HIGH	Afu8g07060	hydrophobin	720			DOWN MOD
	Afu1g03790	mannosylphosphorylation protein (Mnn4)	669	-		UP HIGH	Afu8g00900	spherulin 4-like cell surface protein	767			DOWN MOD
	Afu1g17250	conidial hydrophobin RodB	915	-		UP MOD	Afu3g14620	extracellular endo-1,5-alpha-L-arabinase	1160	-		DOWN MOD

	Afu5g02040	extracellular lipase	1069	-	UP MOD	Afu5g13090	alpha-1,2-mannosyltransferase	1432	-		DOWN LOW
	Afu2g00690	glucan 1,4-alpha-glucosidase	1110	-	UP MOD	Afu6g07480	endoglucanase	1488	-		DOWN LOW
	Afu7g01710	cholinesterase	1111	-	UP MOD	Afu5g07540	hypothetical protein	1521	-		DOWN LOW
	Afu6g11600	endoglucanase	1267	-	UP MOD	Afu2g00190	hypothetical protein	1593	-		DOWN LOW
	Afu3g02270	mycelial catalase Cat1	1287	-	UP MOD	Afu3g14890	pectate lyase	1605	-		DOWN LOW
	Afu4g09400	aspartic-type endopeptidase	1514	-	UP LOW	Afu1g15130	GPI anchor transamidase	1677	-		DOWN LOW
	Afu1g10590	GPI anchored protein	1550	-	UP LOW	Afu4g02710	hypothetical protein	1724	-		DOWN LOW
	Afu5g10380	pectin lyase	1671	-	UP LOW	Afu6g11820	glycosyl hydrolase family protein	1742	-		DOWN LOW
	Afu4g06820	GPI-anchored cell wall organization protein Ecm33	1727	-	UP LOW	Afu3g02970	aspergillopepsin	1916	-		DOWN LOW
						Afu6g11390	1,3-beta-glucanosyltransferase Gel2	2037	-		DOWN LOW
Pathogenesis	Afu1g14660	regulator of secondary metabolism LaeA	136	-	UP HIGH	Afu1g15440	alpha-1,3-glucan synthase Ags3	15		0.029	DOWN HIGH
	Afu6g09610	nonribosomal peptide synthase	444	-	UP HIGH	Afu6g08520	adenylate cyclase AcyA	590			DOWN HIGH
	Afu3g02270	mycelial catalase Cat1	1287	-	UP MOD	Afu2g17560	conidial pigment biosynthesis 1,3,6,8-tetrahydroxynaphthalene reductase Arp2	1361	-		DOWN MOD
	Afu5g02330	major allergen and cytotoxin AspF1	1398	-	UP LOW	Afu2g04200	4-hydroxyphenylpyruvate dioxygenase	1913	-		DOWN LOW
	Afu5g09250	transcription factor (Snd1/p100)	1590	-	UP LOW	Afu5g13300	aspartic endopeptidase Pep1/aspergillopepsin F	1999	-		DOWN LOW
	Afu8g02750	rRNA processing protein CgrA	1603	-	UP LOW						
	Afu6g13990	acetyltransferase	1698	-	UP LOW						
	Afu8g02310	aldehyde dehydrogenase ALDH	1792	-	UP LOW						

Secondary metabolism	Afu5g12730	nonribosomal peptide synthase pes3	20	-	UP HIGH	Afu8g00560	cytochrome P450 oxidoreductase	8	-		DOWN HIGH
	Afu3g01430	benzodiazepine receptor family protein	303	-	UP HIGH	Afu2g17970	ergot alkaloid biosynthetic protein A	86			DOWN HIGH
	Afu3g14610	cytochrome P450 monooxygenase	327	-	UP HIGH	Afu8g00570	alpha/beta hydrolase	94		0.023	DOWN HIGH
	Afu6g09610	nonribosomal peptide synthase	444	-	UP HIGH	Afu6g12040	MFS sugar permease	213			DOWN HIGH
	Afu8g00350	hypothetical protein	445	-	UP HIGH	Afu8g00100	aspartate-tRNA ligase	278			DOWN HIGH
	Afu8g00200	O-methyltransferase	481	-	UP HIGH	Afu8g00370	polyketide synthase	343			DOWN HIGH
	Afu6g03310	hypothetical protein	558	-	UP HIGH	Afu3g14630	extracellular dioxygenase	425		0.049	DOWN HIGH
	Afu4g14520	toxin biosynthesis protein	833	-	UP MOD	Afu3g01410	polyketide synthase	479		0.048	DOWN HIGH
	Afu3g03190	MFS multidrug transporter	861	-	UP MOD	Afu8g00170	nonribosomal brevianamide peptide synthase FtmA	517			DOWN HIGH
	Afu3g14720	MFS transporter	886	-	UP MOD	Afu6g09730	cytochrome P450 oxidoreductase GliF	745			DOWN MOD
	Afu3g13010	Zn-dependent hydrolase/oxidoreductase family protein, putative	988	-	UP MOD	Afu3g15270	nonribosomal peptide synthase	770			DOWN MOD
	Afu3g15290	C6 transcription factor	1054	-	UP MOD	Afu8g00360	NlpC/P60-like cell-wall peptidase	1369	-		DOWN LOW
	Afu3g14710	toxin biosynthesis proten (Fum3)	1166	-	UP MOD	Afu3g13730	nonribosomal peptide synthase	1402	-		DOWN LOW
	Afu6g12060	MAK1-like monooxygenase	1227	-	UP MOD	Afu6g03490	phenol 2-monooxygenase	1526	-		DOWN LOW
	Afu2g17550	conidial pigment biosynthesis protein Ayg1	1281	-	UP MOD	Afu3g03200	cysteine hydrolase family protein	1651	-		DOWN LOW
	Afu1g17640	C6 transcription factor RegA	1307	-	UP MOD	Afu3g14600	fungal specific transcription factor	1836	-		DOWN LOW

	Afu6g13990	acetyltransferase	1698	-	UP LOW		Afu3g12910	O-methyltransferase GliM-like	1843	-	DOWN LOW
	Afu8g00540	hybrid PKS-NRPS enzyme psoA	1779	-	UP LOW		Afu3g01530	phosphatidylglycerol specific phospholipase	1846	-	DOWN LOW
	Afu3g13630	hypothetical protein	1812	-	UP LOW		Afu4g00180	fatty acid oxygenase	1867	-	DOWN LOW
Ribosome biogenesis and RNA metabolism	Afu2g08320	U3 small nucleolar ribonucleoprotein subunit (Imp3), putative	651	-	UP HIGH		Afu5g13520	ribosome biogenesis protein Ria1	1	0.023	DOWN HIGH
	Afu8g04400	RNA binding protein	783	-	UP MOD		Afu2g11380	rRNA assembly protein Mis3	4	0.016	DOWN HIGH
	Afu1g04070	Eukaryotic translation initiation factor eIF-5A	868	-	UP MOD		Afu3g06790	RNA-directed RNA polymerase (Sad-1)	105		DOWN HIGH
	Afu6g10370	RNA lariat debranching enzyme	888	-	UP MOD		Afu7g02170	cyclophilin-type peptidyl-prolyl cis-trans isomerase, putative	198		DOWN HIGH
	Afu1g17120	translation elongation factor eEF-1B gamma subunit, putative	950	-	UP MOD		Afu2g01900	RNA polymerase II transcription elongation factor Rtf1p	253	0.032	DOWN HIGH
	Afu4g01200	extracellular guanyl-specific ribonuclease	1087	-	UP MOD		Afu1g04980	RNA polymerase III transcription factor TFIIIC subunit (Tfc4)	293	0.034	DOWN HIGH
	Afu1g07600	ribonuclease HI large subunit	1595	-	UP LOW		Afu3g10030	forkhead domain protein	296		DOWN HIGH
	Afu8g02750	rRNA processing protein CgrA	1603	-	UP LOW		Afu5g04240	RNA binding protein Nrd1	302		DOWN HIGH
	Afu8g04820	ribonuclease P complex subunit Pop2	1728	-	UP LOW		Afu2g12150	midasin	434		DOWN HIGH
	Afu2g11810	pre-rRNA processing protein Rrp12	1736	-	UP LOW		Afu4g07580	translation initiation factor EF-2 gamma subunit, putative	444	0.038	DOWN HIGH
	Afu2g08750	mitochondrial inner membrane nuclease Nuc1	1798	-	UP LOW		Afu1g16330	ribosome assembly protein Noc2	469		DOWN HIGH
	Afu6g10320	ribosome biogenesis protein (Rrb1)	1999	-	UP LOW		Afu1g15620	DEAD box RNA helicase HelA	647		DOWN HIGH
							Afu5g07640	RNA 3'-terminal phosphate cyclase	734		DOWN MOD
							Afu7g01550	mitochondrial exoribonuclease Cyt-4	839		DOWN MOD
							Afu5g06510	ribosome biogenesis GTPase Lsg1	849		DOWN MOD

						Afu2g04630	translation elongation factor EF-1 subunit	890			DOWN MOD
						Afu2g10750	RNA helicase (Dbp)	917			DOWN MOD
						Afu5g12100	rRNA methyltransferase Spb1	1008	-		DOWN MOD
						Afu6g12550	mitochondrial carrier protein	1116	-		DOWN MOD
						Afu5g05710	pseudouridylate synthase family protein	1183	-		DOWN MOD
						Afu3g09820	C2H2 transcription factor	1195	-		DOWN MOD
						Afu5g02160	RNA binding protein (Arp)	1238	-		DOWN MOD
						Afu5g09060	RNA binding protein	1508	-		DOWN LOW
						Afu8g03940	ribosome recycling factor	1544	-		DOWN LOW
Sugar transport	Afu5g01160	MFS monosaccharide transporter	240	-	UP HIGH	Afu4g03110	MFS monosaccharide transporter	2		0.033	DOWN HIGH
	Afu1g02530	MFS sugar transporter	505	-	UP HIGH	Afu6g12040	MFS sugar permease	213			DOWN HIGH
	Afu1g11580	MFS quinate transporter QutD	535	-	UP HIGH	Afu3g02890	MFS sugar transporter	320		0.014	DOWN HIGH
	Afu1g16390	MFS hexose transporter	572	-	UP HIGH	Afu4g13080	MFS monosaccharide transporter	441			DOWN HIGH
	Afu2g10910	MFS alpha-glucoside transporter	580	-	UP HIGH	Afu1g07700	MFS monosaccharide transporter	585			DOWN HIGH
	Afu4g00990	MFS quinate transporter	661	-	UP HIGH	Afu6g14442	MFS monosaccharide transporter	593			DOWN HIGH
	Afu6g11920	MFS alpha-glucoside transporter	927	-	UP MOD	Afu2g02110	MFS monosaccharide transporter	719			DOWN MOD
	Afu7g00220	plasma membrane hexose transporter	1212	-	UP MOD	Afu4g01340	MFS monosaccharide transporter	934			DOWN MOD
	Afu6g04270	MFS sugar transporter	1657	-	UP LOW	Afu3g06730	MFS sugar transporter	1028	-		DOWN MOD
	Afu1g11050	MFS sugar transporter	1811	-	UP LOW	Afu3g12170	MFS sugar transporter	1236	-		DOWN MOD

	Afu4g06630	MFS monosaccharide transporter	1873	-	UP LOW	Afu1g03280	MFS alpha-glucoside transporter	1322	-	DOWN MOD
	Afu5g14540	MFS monosaccharide transporter	1888	-	UP LOW	Afu5g01080	MFS monosaccharide transporter	1356	-	DOWN MOD
	Afu3g03240	MFS monocarboxylate transporter	1901	-	UP LOW	Afu6g14590	MFS alpha-glucoside transporter	1433	-	DOWN LOW
						Afu3g01670	MFS hexose transporter	1524	-	DOWN LOW
						Afu2g08120	MFS monosaccharide transporter (Hxt8)	1608	-	DOWN LOW
						Afu5g00280	MFS sugar transporter	1727	-	DOWN LOW
						Afu2g05190	MFS monosaccharide transporter	1739	-	DOWN LOW
						Afu1g03530	MFS sugar transporter	1991	-	DOWN LOW
						Afu1g09910	MFS sugar transporter	2024	-	DOWN LOW
						Afu3g12170	MFS sugar transporter	1236	-	DOWN MOD
						Afu1g03280	MFS alpha-glucoside transporter	1322	-	DOWN MOD
						Afu5g01080	MFS monosaccharide transporter	1356	-	DOWN MOD
						Afu6g14590	MFS alpha-glucoside transporter	1433	-	DOWN LOW
						Afu3g01670	MFS hexose transporter	1524	-	DOWN LOW
Amino acid transport	Afu1g14700	MFS allantoate transporter	102	-	UP HIGH	Afu3g00120	amino acid transporter (Mtr)	46	0.033	DOWN HIGH
	Afu8g02200	proline permease	108	0.049	UP HIGH	Afu5g00370	amino acid permease	65	-	DOWN HIGH

	Afu5g01510	amino acid permease	631	-	UP HIGH	Afu5g00710	GABA permease	130		DOWN HIGH
	Afu2g10560	amino acid permease	863	-	UP MOD	Afu5g02790	amino acid permease	588		DOWN HIGH
	Afu4g01570	amino acid transporter	1057	-	UP MOD	Afu5g09440	amino acid permease	682		DOWN HIGH
	Afu7g01090	proline permease PrnB	1145	-	UP MOD	Afu5g14660	GABA permease	847		DOWN MOD
	Afu4g03370	GABA permease (Uga4)	1203	-	UP MOD	Afu2g00310	amino acid transporter	1047	-	DOWN MOD
	Afu6g03720	MFS allantoate transporter	1363	-	UP MOD	Afu7g04290	amino acid permease (Gap1)	1089	-	DOWN MOD
	Afu3g09710	amino acid permease	1755	-	UP LOW	Afu4g06990	amino acid transporter	1245	-	DOWN MOD
						Afu5g06230	GABA permease	1272	-	DOWN MOD
						Afu2g15470	neutral amino acid permease	1360	-	DOWN MOD
						Afu3g01820	amino acid permease	1615	-	DOWN LOW
						Afu2g08800	amino acid permease (Dip5)	1735	-	DOWN LOW
						Afu8g07200	amino acid transporter	1827	-	DOWN LOW
						Afu4g03220	amino acid permease	1885	-	DOWN LOW
						Afu5g09120	neutral amino acid permease	1898	-	DOWN LOW
						Afu4g00240	amino acid transporter	1901	-	DOWN LOW
						Afu4g10090	GABA permease	1971	-	DOWN LOW
Protein and carbohydrate glycosylation	Afu2g00680	glycosyl hydrolase	260	-	UP HIGH	Afu3g07700	glucosyltransferase	80	0.024	DOWN HIGH
	Afu3g01660	glycosyl hydrolase, family 43	311	0.029	UP HIGH	Afu8g02040	glycosyl transferase	569		DOWN HIGH
	Afu8g02070	glycosyl transferase	562	0.029	UP HIGH	Afu8g01730	glycosyl transferase family protein	1404	-	DOWN LOW
	Afu7g06110	glycosyl hydrolase	769	-	UP MOD	Afu3g03620	glycosyl transferase	1408	-	DOWN LOW

	Afu1g17030	glycosyl transferase	1228	-		UP MOD	Afu4g00390	glycosyl hydrolase	1535	-		DOWN LOW
	Afu3g07860	glycosyl transferase	1233	-		UP MOD	Afu2g11080	glucosyltransferase (Die2)	1570	-		DOWN LOW
	Afu2g03270	glycosyl hydrolase	1245	-		UP MOD	Afu6g11820	glycosyl hydrolase family protein	1742	-		DOWN LOW
	Afu6g05000	Glycosyl hydrolases family 32 superfamily	1629	-		UP LOW	Afu4g02860	glycosyl hydrolase family 88	2042	-		DOWN LOW
	Afu4g13770	glycosyl hydrolase	1685	-		UP LOW						
Transcription factors	Afu5g11390	APSES transcription factor	748	-		UP MOD	Afu3g13870	GATA-type sexual development transcription factor NsdD	59	-		DOWN HIGH
	Afu5g13790	C6 transcription factor (Acr-2)	824	-		UP MOD	Afu7g01640	C6 transcription factor (War1)	76		0.044	DOWN HIGH
	Afu3g04070	bZIP transcription factor HacA	924	-		UP MOD	Afu1g05150	C2H2 transcription factor (TFIIIA)	150			DOWN HIGH
	Afu4g03960	C6 transcription factor Ctf1A	1022	-		UP MOD	Afu5g12900	GATA transcription factor (Ams2)	505			DOWN HIGH
	Afu3g11990	C6 transcription factor (Mut3)	1294	-		UP MOD	Afu5g12020	C6 transcription factor (NirA)	542			DOWN HIGH
	Afu1g06900	C2H2 transcription factor Crz1	1389	-		UP LOW	Afu2g15260	C6 transcription factor (Leu3)	830			DOWN MOD
	Afu4g12180	C6 transcription factor Prf	1416	-		UP LOW	Afu3g12660	C6 finger domain protein Acr-2	1681	-		DOWN LOW
	Afu1g15470	C6 transcription factor (UaY)	1420	-		UP LOW						
	Afu7g05620	APSES transcription factor (MbpA)	1513	-		UP LOW						
	Afu1g03860	C6 transcription factor (AmdR)	1605	-		UP LOW						
Signal transduction	Afu2g17130	MAPKKK cascade protein kinase regulator Ste50	621	-		UP HIGH	Afu2g15050	Rho GTPase activator (Lrg11)	318			DOWN HIGH
	Afu3g05770	RAS small monomeric GTPase	779	-		UP MOD	Afu1g12940	MAP kinase SakA	357			DOWN HIGH
	Afu5g10020	sensor histidine kinase/response regulator	948		0.025	UP MOD	Afu8g05680	serine/threonine protein kinase	598			DOWN HIGH

Afu2g03640	Ras GTPase activating protein	1029	-	UP MOD
Afu5g09100	MAP kinase MpkC	1195	-	UP MOD
Afu4g03100	ras-like GTP-binding protein	1241	-	UP MOD
Afu6g09260	sensor histidine kinase/response regulator	1305	-	UP MOD
Afu2g15570	RAS small monomeric GTPase Rab6	1511	-	UP LOW
Afu2g00660	sensor histidine kinase/response regulator TcsB/Sln1, putative	1530	-	UP LOW
Afu6g06860	regulator of G protein signaling domain protein	1775	-	UP LOW

Afu1g05800	MAP kinase kinase (Mkk2)	620			DOWN HIGH
Afu1g15950	MAP kinase kinase (Pbs2)	633		0.023	DOWN HIGH
Afu6g06400	Rho GTPase activator (Bem3)	857			DOWN MOD
Afu2g13640	serine/threonin protein kinase	886			DOWN MOD
Afu2g01060	Rho GTPase activator (Sac7)	949			DOWN MOD
Afu4g14740	serine/threonine protein kinase (Ark1)	1016	-		DOWN MOD
Afu4g11890	serine/threonine protein kinase	1066	-		DOWN MOD
Afu5g06700	serine/threonine protein phosphatase PPT1	1094	-		DOWN MOD
Afu1g02190	Ras GTPase Rab11	1174	-		DOWN MOD
Afu2g09570	serine/threonine protein kinase	1225	-		DOWN MOD
Afu5g07950	serine/threonine protein kinase	1460	-		DOWN LOW
Afu6g13160	serine/threonine protein kinase	1477	-		DOWN LOW
Afu6g06720	serine/threonine protein kinase	1514	-		DOWN LOW
Afu4g08040	RAB GTPase Ypt5	1594	-		DOWN LOW
Afu6g12820	MAP kinase MpkB	1693	-		DOWN LOW
Afu1g14810	serine/threonine protein kinase (Kin4)	1694	-		DOWN LOW
Afu8g04670	serine/threonine protein kinase	1737	-		DOWN LOW
Afu1g06920	serine/threonine protein kinase	1768	-		DOWN LOW
Afu2g10620	serine/threonine protein kinase (YPK1)	1930	-		DOWN LOW
Afu6g02840	serine/threonine protein kinase	1967	-		DOWN LOW

		Afu3g10740	RAB GTPase Vps21/Ypt51	1979	-	DOWN LOW

10.3.5 Characterisation of differentially expressed genes between 4 and 14 hours: chromosomal loci, lineage specificity and functionality

Given the previously observed over-representation of transcripts encoded by genes of subtelomeric loci (including *A. fumigatus* specific genes, signal peptide encoding genes, and secondary metabolite clusters) during infection relative to laboratory growth (McDonagh et al. 2008) and reported in Chapter 3 of this thesis, distribution of genes demonstrating increased or decreased transcript abundance between 4 and 14 hours was investigated with respect to these cohorts. Statistical significance of enrichment was measured by Chi square analyses, with the null hypothesis that equal numbers of increased and decreased genes would be expected to occur in each cohort (Figure 10.5 and Table 10.6). Transposition associated genes which were identified manually from the genome annotation in Chapter 3 are not represented on the PFGR array.

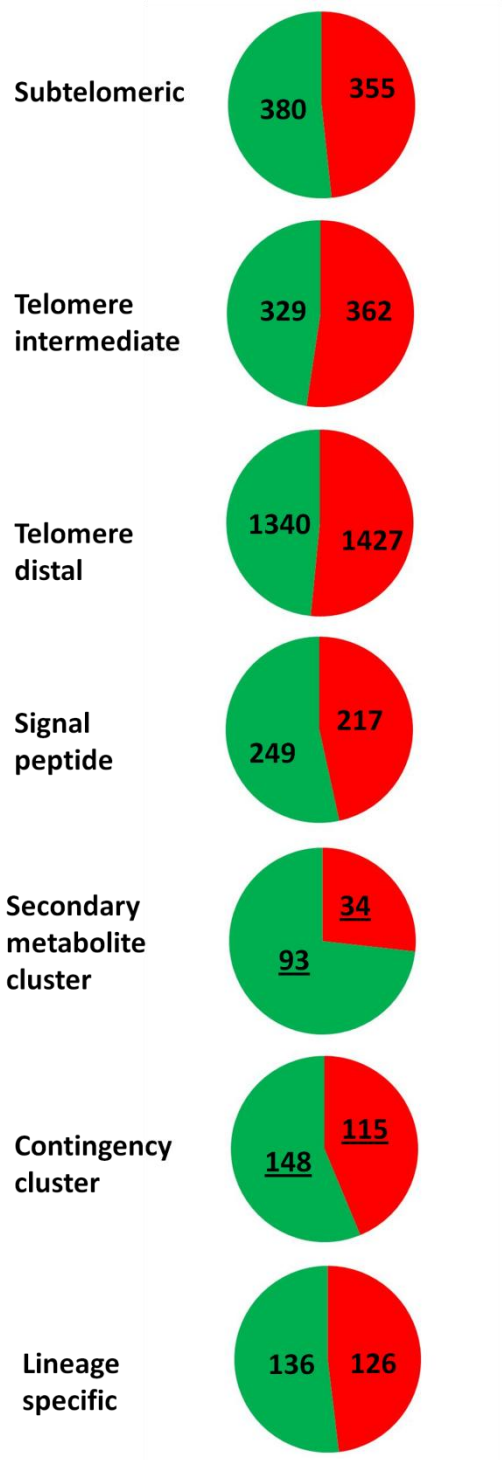


Figure 10.5 Distribution of differentially expressed genes between 4 – 14 hours post infection among the functional cohorts of chromosomal location, signal peptide content, *A. fumigatus* specificity and functional association. Distribution of upregulated (red) and downregulated (green) genes at subtelomeric loci (0 – 300 Kb from telomere, n =1509); telomere intermediate loci (301 - 600 Kb from telomere, n = 1634); telomere distal loci (> 600 Kb from telomere, n =6494). Secondary metabolite clusters (n = 337); Contingency clusters (n = 594); signal peptide cohort (n = 1103); *A. fumigatus* specific genes (n = 596). Underlined values significantly deviate from the null hypothesis that an equal number of upregulated or downregulated genes will occur in each cohort, as tested by Chi-square analysis**.**

	Number of genes	Differentially expressed	Up (observed)	Down (observed)	Up (expected)	Down (expected)	Chi-square	p-value
0-300 kb	1509	735	355	380	367.5	367.5	0.85	0.356
301- 600 kb	1634	691	362	329	345.5	345.5	1.57	0.209
>600 kb	6373	2767	1427	1340	1383.5	1383.5	2.73	0.098
Signal P	1103	466	217	249	233	233	2.19	0.138
Secondary metabolism	337	127	34	93	63.5	63.5	27.4	<0.001
Contingency cluster	594	263	115	148	131.5	131.5	4.14	0.041
Aspergillus specific	596	262	126	136	131	131	0.38	0.536

Table 10.6: Distribution and Chi-square analysis of differentially expressed genes categorised by chromosomal location, signal peptide content, *A. fumigatus* specificity and annotation at 4 – 14 hours post infection. Chi-square analysis with one degree of freedom was used to test the distribution of upper and lower quartiles with respect to cohorts of interest to this study, with the null hypothesis that even numbers of upregulated or downregulated genes occur in each group.

10.3.6 Time-point specific gene expression profiling of the Af293 isolate in the murine lung

To determine gene expression profiles specific to each time-point of infection relative nSI datasets, representing gene expression changes 4 – 8 and 8 – 14 hours post infection, were analysed and top 200 genes with greatest increase and decrease between time-points are listed in tables 10.7 – 10.10.

Table 10.7: 200 genes with greatest nSI increase between 4 and 8 hours post infection. Genes are reported ranked according to greatest nSI intensity increase between 4 and 14 hours where 1 is the greatest. Hypothetical proteins (n = 91) were removed.

ORF	Description	Rank	GO Biological Process
Afu6g03420	trehalose synthase, pseudogene, similar to GB:AAC64285.1: clock-controlled gene-9 protein [Neurospora crassa]	3	
Afu2g03150	kinesin family protein	4	kinesin complex///microtubule motor activity///establishment of mitotic spindle orientation///cytoplasmic microtubule///microtubule depolymerization///nuclear microtubule

Afu6g10550	arrestin domain protein	5	
Afu3g13230	AT DNA binding protein	6	nucleus///AT DNA binding
Afu5g02900	SNARE domain protein	7	
Afu7g00360	UDP-galactose 4-epimerase	8	
Afu7g05790	vacuolar morphogenesis protein AvaB	10	vacuole organization"///vacuolar membrane""///fungal-type vacuole///Rab guanyl-nucleotide exchange factor activity///"homotypic vacuole fusion, non-autophagic"""""
Afu5g12730	nonribosomal peptide synthase	11	nonribosomal peptide biosynthetic process///catalytic activity///amino acid adenylylation by nonribosomal peptide synthase
Afu5g08500	spermine/spermidine synthase family protein	12	
Afu3g08930	tripeptidyl peptidase SED3	13	protein catabolic process///tripeptidyl-peptidase activity
Afu2g04380	LaeA-like methyltransferase	14	
Afu3g13010	Zn-dependent hydrolase/oxidoreductase family protein, putative	15	
Afu5g09010	conserved glutamic acid rich protein	18	
Afu4g07140	killer toxin sensitivity protein (IKI3)	20	""DNA-directed RNA polymerase II, holoenzyme"""""///transcription elongation factor complex///RNA polymerase II transcription elongation factor activity///regulation of transcription from RNA polymerase II promoter///"histone acetyltransferase activity""
Afu6g13140	3,4-dihydroxy-2-butanone 4-phosphate synthase	22	cytosol///riboflavin biosynthetic process"///""aerobic respiration///mitochondrial intermembrane space""///"3,4-dihydroxy-2-butanone-4-phosphate synthase activity"""""
Afu1g04720	C-8 sterol isomerase (Erg-1)	23	endoplasmic reticulum///ergosterol biosynthetic process///C-8 sterol isomerase activity
Afu3g02370	short-chain dehydrogenase/reductase	25	oxidoreductase activity///cytoplasm///metabolic process
Afu1g14730	cell division cycle protein Cdc20	26	ubiquitin-dependent protein catabolic process///anaphase-promoting complex///mitotic metaphase/anaphase transition///cyclin catabolic process///mitotic sister chromatid segregation///mitotic spindle elongation///enzyme activator activity
Afu2g08580	pyridoxine	28	thiamin biosynthetic process///pyridoxine metabolic process///imidazoleglycerol-phosphate synthase activity///cytoplasm///protein binding

Afu4g05980	JmjC domain protein	30	chromatin remodeling///DNA binding///nucleus
Afu3g01980	chromatin structure remodeling complex protein RSC3, putative	31	DNA binding///zinc ion binding
Afu3g01990	DUF636 domain protein	35	
Afu3g09690	extracellular thaumatin domain protein	38	
Afu2g08700	isochorismatase family hydrolase	40	hydrolase activity///metabolic process
Afu6g04400	transcription factor TFIIIB component	44	transcription factor TFIIIB complex///transcription initiation from RNA polymerase III promoter///RNA polymerase III transcription factor activity
Afu6g09170	3-methyl-2-oxobutanoate hydroxymethyltransferase PanB	46	pantothenate biosynthetic process///3-methyl-2-oxobutanoate hydroxymethyltransferase activity///mitochondrion
Afu8g06030	alpha-1,3-glucanase	50	cellular glucan metabolic process///fungal-type cell wall"///""""""""hydrolase activity, hydrolyzing O-glycosyl compounds"""""
Afu8g05840	fungal specific transcription factor	54	transcription factor activity///regulation of transcription
Afu6g13440	choline sulfatase	55	sulfuric ester hydrolase activity///metabolic process
Afu8g04400	RNA binding protein	56	rRNA metabolic process///nucleolus///RNA binding
Afu1g05040	protein mitochondrial targeting protein (Mas1), putative	58	Hsp70/Hsc70 protein regulator activity///cytosol///protein targeting to mitochondrion///chaperone regulator activity///ATPase activator activity
Afu1g09230	DUF1000 domain protein	60	
Afu4g08410	mannose-6-phosphate isomerase, class I	62	mannose-6-phosphate isomerase activity///protein amino acid glycosylation///cytoplasm///GDP-mannose biosynthetic process///nucleus///cell wall mannoprotein biosynthetic process
Afu2g09340	fungal specific trascription factor	64	
Afu2g07440	thioesterase family protein	65	CoA hydrolase activity///fatty acid metabolic process
Afu7g02550	xylitol dehydrogenase	67	cellular component unknown///L-iditol 2-dehydrogenase activity///fructose metabolic process///mannose metabolic process
Afu1g07750	SWIRM domain protein Fun19	69	cellular component unknown///biological process unknown///molecular function unknown
Afu7g05800	fructose-2,6-bisphosphatase	70	6-phosphofructo-2-kinase activity"///""fructose-2,6-bisphosphate 2-phosphatase activity""///""cytosol///gluconeogenesis
Afu5g13580	3-ketosteroid-	72	

	delta-1-dehydrogenase		
Afu4g13360	endo-1,3(4)-beta-glucanase	73	fungal-type cell wall///"""hydrolase activity, hydrolyzing O-glycosyl compounds""///""1,3-beta-glucan metabolic process"""
Afu6g05320	purine nucleoside phosphorylase I, inosine and guanosine-specific	74	cellular component unknown///purine-nucleoside phosphorylase activity///purine nucleoside catabolic process
Afu2g12890	small nucleolar ribonucleoprotein complex subunit, putative	75	maturation of SSU-rRNA///snoRNA binding///small nucleolar ribonucleoprotein complex
Afu6g02670	G2-specific protein kinase NimA	76	regulation of transcription involved in G2-phase of mitotic cell cycle///chromosome segregation///protein kinase activity
Afu3g00150	short-chain dehydrogenase/oxidoreductase	77	oxidoreductase activity///cytoplasm///metabolic process
Afu1g16000	serine/threonine protein kinase	78	protein kinase activity
Afu2g13730	NEDD8 activating enzyme (UbaC)	79	NEDD8 class-dependent protein catabolic process///cytoplasm///protein neddylation during NEDD8 class-dependent protein catabolic process///NEDD8 activating enzyme activity
Afu6g12760	GPI transamidase component (GAA1)	80	integral to endoplasmic reticulum membrane///GPI-anchor transamidase activity///attachment of GPI anchor to protein
Afu7g01420	isoleucyl-tRNA synthetase	81	isoleucyl-tRNA aminoacylation///translation///isoleucine-tRNA ligase activity///mitochondrion
Afu3g07670	transcription elongation factor S-II	82	reciprocal meiotic recombination///RNA elongation from RNA polymerase II promoter///nucleoplasm///positive transcription elongation factor activity
Afu6g06850	DUF647 domain protein	83	
Afu5g02240	NAD dependent epimerase/dehydratase family protein	84	
Afu2g09330	C6 finger domain protein	85	
Afu1g06270	zinc metallopeptidase	86	
Afu5g01640	ankyrin repeat protein	87	
Afu3g06410	Coenzyme Q (ubiquinone) biosynthesis protein Coq4, putative	92	ubiquinone metabolic process///mitochondrial inner membrane///molecular function unknown
Afu3g02250	3-beta hydroxysteroid	94	oxidoreductase activity///methylglyoxal reductase (NADH-dependent)

	dehydrogenase/isomerase family protein		activity///cytoplasm///nucleus///response to stress
Afu2g06060	transcriptional co-activator (Hfi1/Ada1)	95	
Afu5g02440	20S cyclosome subunit (APC8)	96	ubiquitin-dependent protein catabolic process///ubiquitin-protein ligase activity///anaphase-promoting complex///mitotic metaphase/anaphase transition///protein binding///mitotic sister chromatid segregation///mitotic spindle elongation
Afu3g07260	esterase/lipase	97	
Afu4g10490	Exocyst complex component Sec6	98	endocytosis///establishment of cell polarity (sensu Saccharomyces)///exocyst///Golgi to plasma membrane transport///actin cap (sensu Saccharomyces)///vesicle fusion///vesicle docking during exocytosis///cytokinesis///bipolar cellular bud site selection///molecular function unknown
Afu2g16692	vacuolar sorting protein SNF7 family protein	99	
Afu6g14360	cytochrome P450 monooxygenase	101	
Afu1g04330	Ser/Thr protein phosphatase family protein	102	
Afu2g17870	short chain dehydrogenase	103	cytoplasm///""L-serine metabolic process"///"oxidoreductase activity, acting on the aldehyde or oxo group of donors, NAD or NADP as acceptor"""""""
Afu4g12600	phosphoribosyl-aminoimidazole carboxylase	105	phosphoribosylaminoimidazole carboxylase activity///cytoplasm///purine base metabolic process
Afu5g13790	C6 transcription factor (Acr-2)	106	transcription factor activity///nucleus///regulation of transcription
Afu5g06340	BAR domain protein	107	
Afu1g06650	actin filament organization protein App1-like	109	actin filament organization///actin cortical patch (sensu Saccharomyces)///actin cytoskeleton organization///molecular function unknown///actin cytoskeleton
Afu2g01680	monooxygenase	110	
Afu2g05750	agmatinase	111	spermidine biosynthetic process///agmatinase activity
Afu5g10050	cytochrome P450 monooxygenase	112	oxidoreductase activity///metabolic process
Afu6g13880	MFS transporter	115	plasma membrane///transporter activity///transport
Afu4g00620	cell wall glycosyl hydrolase Dfg5	116	membrane fraction///fungal-type cell wall biogenesis///anchored to plasma membrane
Afu8g03890	peptidyl-prolyl cis-trans isomerase	117	peptidyl-prolyl cis-trans isomerase activity///protein folding///mitochondrion
Afu3g06210	phosphoribosyl-aminoimidazole-	118	purine ribonucleotide biosynthetic process///cytoplasm///phosphoribosylaminoimidazoles

	succinocarboxamide synthase		uccinocarboxamide synthase activity///nucleus///purine base metabolic process
Afu6g00500	chitosanase	119	
Afu2g15440	integral membrane protein	122	
Afu5g11110	thiamin pyrophosphokinase -related protein	123	cellular component unknown///biological process unknown///molecular function unknown
Afu4g11250	carbonic anhydrase Nce103	125	cytoplasm///nucleus///biological process unknown///molecular function unknown
Afu1g12380	WD repeat protein	129	protein binding
Afu6g03620	FAD/FMN-containing isoamyl alcohol oxidase MreA	130	
Afu1g13300	GTP cyclohydrolase II	131	GTP cyclohydrolase II activity///cytoplasm///nucleus///riboflavin biosynthetic process
Afu3g07380	oligo-1,6-glucosidase	132	cellular component unknown"///"biological process unknown""///""""hydrolase activity, hydrolyzing O-glycosyl compounds"""""
Afu5g14640	haloacid dehalogenase, type II	134	
Afu2g11780	C2H2 transcription factor (Crea)	135	specific RNA polymerase II transcription factor activity///cytoplasm///regulation of transcription from RNA polymerase II promoter///nucleus///zinc ion binding///glucose metabolic process
Afu2g09150	adenosine deaminase	136	cytoplasm///adenine catabolic process///nucleus///adenine deaminase activity
Afu1g10100	3-oxoacyl-(acyl-carrier-protein) reductase	137	
Afu1g13750	C2H2 transcription factor (Rpn4)	138	transcription activator activity///DNA binding///zinc ion binding
Afu2g09810	mandelate racemase/muconate lactonizing enzyme family protein	139	
Afu5g09430	RNA-directed RNA polymerase	141	
Afu4g14620	RING finger protein	142	
Afu5g13130	chorismate mutase	143	chorismate mutase activity///cytoplasm///nucleus///aromatic amino acid family biosynthetic process
Afu1g14690	ubiquitin-protein ligase Sel1/Ubx2	144	
Afu8g03930	Hsp70 chaperone (HscA)	146	chaperone activity///translation///polysome///cytoplasm///ATPase activity
Afu5g00910	MBL2-like secreted	149	

	peptide		
Afu1g14940	protein translocation complex componenet (Npl1), putative	150	SRP-dependent cotranslational protein targeting to membrane, translocation""///"protein transporter activity///endoplasmic reticulum membrane"
Afu1g14660	regulator of secondary metabolism LaeA	151	secondary metabolic process///pathogenesis
Afu1g06000	Ser/Thr protein phosphatase family protein	152	
Afu4g07050	L-lactate dehydrogenase	153	L-lactate dehydrogenase (cytochrome) activity///mitochondrial intermembrane space///electron transport
Afu4g12110	TPR domain protein	154	protein binding
Afu6g08110	DNA (apurinic or apyrimidinic site) lyase, endon uclease	156	DNA-(apurinic or apyrimidinic site) lyase activity///DNA repair///base-excision repair///nucleus///mitochondrion
Afu1g01850	C6 finger domain protein	158	
Afu1g09750	aldehyde reductase (AKR1)	159	aldo-keto reductase activity///cytoplasm///nucleus///cellular aldehyde metabolic process
Afu5g12270	rRNA processing protein (Ebp2)	160	nucleolus///rRNA processing///molecular function unknown
Afu2g14560	dihydrodipicolinate synthetase family protein	162	catalytic activity///metabolic process
Afu6g03980	hexokinase	163	fructose metabolic process///cytosol///nucleus///hexokinase activity
Afu7g02400	alcohol dehydrogenase, zinc-containing	166	cytoplasm///nucleus///biological process unknown///molecular function unknown
Afu3g00380	beta-galactosidase	167	
Afu3g03410	enoyl-CoA hydratase/isomera se family protein	168	
Afu2g12190	mitochondrial intermembrane space translocase subunit Tim13	169	mitochondrial intermembrane space protein transporter complex///protein transporter activity///mitochondrial translocation///mitochondrial intermembrane space
Afu2g01640	tryptophanyl-tRNA synthetase	172	cytoplasm///tryptophan-tRNA ligase activity///tryptophanyl-tRNA aminoacylation
Afu6g12580	anthranilate synthase component I	174	cytoplasm///anthranilate synthase activity///tryptophan biosynthetic process
Afu2g16360	DRAP deaminase (Rib2)	176	DRAP deaminase activity///cytoplasm///pseudouridylate synthase activity///riboflavin biosynthetic process

Afu5g08160	cyclin	177	
Afu3g07290	SD08430p	178	cellular component unknown///biological process unknown///molecular function unknown
Afu5g10620	histone-like transcription factor	179	
Afu8g05010	C2H2 finger domain protein	180	DNA binding///nucleus///zinc ion binding
Afu5g03780	L-PSP endoribonuclease family protein Brt1	183	cytoplasm///cytosol///nucleus///mRNA catabolic process///endoribonuclease activity
Afu6g08870	nicotinamide mononucleotide adenylyl transferase	184	nicotinate-nucleotide adenylyltransferase activity///nucleus///NAD metabolic process
Afu2g17330	extracelular serine carboxypeptidase	185	
Afu1g05470	3-oxo-5-alpha-steroid 4-dehydrogenase	186	cellular component unknown///pseudohyphal growth///molecular function unknown
Afu5g01780	cell differentiation and development protein Fsr1	187	sexual reproduction///developmental process
Afu1g12950	Avl9 protein	188	
Afu2g04910	proteasome component Pup1	189	proteasome core complex///endopeptidase activity"""///"""""proteasome core complex, beta-subunit complex"""""///"ubiquitin-dependent protein catabolic process
Afu5g12910	small nuclear ribonucleoprotein SmD2	191	"nuclear mRNA splicing, via spliceosome"""""///""pre-mRNA splicing factor activity"///"small nuclear ribonucleoprotein complex""
Afu7g04120	DUF636 domain protein	193	
Afu5g09100	MAP kinase MpkC	194	cytoplasm///protein amino acid phosphorylation///MAP kinase activity///hyperosmotic response
Afu4g12310	DNA repair protein Rtt107	195	"negative regulation of transposition, DNA-mediated"""""///"molecular function unknown""///""nucleus
Afu6g12750	rhomboid family protein	197	COPI-coated vesicle///serine-type peptidase activity///protein processing///integral to membrane///Golgi apparatus
Afu5g11130	PAXNEB protein superfamily	200	transcription elongation factor complex///cytoplasm///RNA polymerase II transcription elongation factor activity///regulation of transcription from RNA polymerase II promoter
Afu6g14180	beta-1,4-mannosyltransferase (Alg1)	203	protein amino acid N-linked glycosylation///integral to membrane"""///"beta-1,4-mannosyltransferase activity"""""
Afu7g04220	protein required for cell viability Rrp17	205	
Afu2g06140	uracil DNA N-	207	DNA repair///base-excision repair///nucleus///uracil

	glycosylase Ung1		DNA N-glycosylase activity///mitochondrion
Afu7g03780	YT521-B-like splicing factor	208	
Afu2g03600	NUDIX family hydrolase	209	hydrolase activity///metabolic process
Afu2g05180	NF-X1 finger and helicase domain protein	210	DNA binding///DNA helicase activity///nucleus///zinc ion binding///RNA helicase activity
Afu8g04070	glucosamine-6-phosphate deaminase	211	glucosamine-6-phosphate deaminase activity///N-acetylglucosamine catabolic process
Afu5g08970	oligosaccharyl transferase subunit (beta)	212	oligosaccharyltransferase complex///dolichyl-diphosphooligosaccharide-protein glycotransferase activity///protein amino acid N-linked glycosylation///cell cycle
Afu1g08820	DUF814 domain protein	213	cytoplasm///biological process unknown///molecular function unknown
Afu5g05670	transporter	214	
Afu2g05880	ammonium transporter MeaA	215	plasma membrane///ammonium transport///ammonium transmembrane transporter activity
Afu2g01660	mitochondrial outer membrane translocase receptor (TOM70)	216	protein transporter activity///mitochondrial outer membrane translocase complex///mitochondrial outer membrane///protein binding///protein targeting to mitochondrion
Afu4g11830	cell cycle control protein (Cwf19)	217	
Afu4g07870	2-hydroxychromene-2-carboxylate isomerase	218	
Afu3g08820	glycosyl hydrolase	219	cytoplasm///biological process unknown///molecular function unknown
Afu5g06680	4-aminobutyrate transaminase GatA	220	intracellular///4-aminobutyrate transaminase activity///nitrogen utilization
Afu7g05990	5-formyltetrahydrofolate cyclo-ligase	221	cellular component unknown///5-formyltetrahydrofolate cyclo-ligase activity///folic acid and derivative biosynthetic process
Afu2g16920	actin monomer binding protein	223	sequestering of actin monomers///actin polymerization or depolymerization///actin monomer binding///bipolar cellular bud site selection
Afu8g06020	glutamate decarboxylase	224	response to oxidative stress///cytoplasm///glutamate catabolic process///glutamate decarboxylase activity
Afu7g04270	3'-5' exonuclease/helicase (Wrn)	225	
Afu6g04120	short chain dehydrogenase/reductase family protein	226	oxidoreductase activity///metabolic process
Afu5g01870	DNA replication factor C subunit	227	leading strand elongation///DNA replication factor C complex///DNA clamp loader activity///sister

	Rfc3		chromatid cohesion///mismatch repair///nucleus///ATPase activity
Afu2g14840	glucose oxidase	228	oxidoreductase activity///metabolic process
Afu5g09170	C2H2 finger domain protein	230	"regulation of transcription, DNA-dependent"///transcription factor activity///nucleus///zinc ion binding
Afu3g10060	Dor1-like family protein	231	
Afu1g08790	exportin KapK	232	mRNA export from nucleus///protein export from nucleus///nucleus///ribosomal large subunit export from nucleus///protein transmembrane transporter activity
Afu3g11700	ubiquitin C-terminal hydrolase	233	protein deubiquitination///cytoplasm///ubiquitin-specific protease activity
Afu1g15910	C6 transcription factor RosA-like	234	RNA polymerase II transcription factor activity///nucleus///regulation of transcription
Afu1g13350	MFS transporter	235	membrane///transporter activity///transport
Afu5g06840	class V chitinase	236	
Afu5g11320	thioredoxin TrxA	238	thiol-disulfide exchange intermediate activity///DNA-dependent DNA replication///response to oxidative stress///regulation of cell redox homeostasis///fungal-type vacuole///"vacuole fusion, non-autophagic"""""""///cytosol///vacuole inheritance"
Afu1g17030	glycosyl transferase	239	"transferase activity, transferring glycosyl groups"
Afu1g14780	BAP31 domain protein	240	programmed cell death///endoplasmic reticulum///molecular function unknown
Afu2g02350	MYB DNA-binding domain protein	241	nucleolus///biological process unknown///molecular function unknown
Afu5g03740	isopenicillin N-CoA epimerase	242	secondary metabolic process
Afu5g10760	alpha-1,2-mannosyltransferase (Kre2)	243	Golgi apparatus""///protein amino acid O-linked glycosylation"///cell wall mannoprotein biosynthetic process///"alpha-1,2-mannosyltransferase activity"""""///""N-glycan processing
Afu5g02470	thiamine biosynthesis protein (Nmt1)	244	thiamin biosynthetic process///cellular component unknown///molecular function unknown
Afu8g06180	DOC family protein	245	nucleic acid binding///catalytic activity///programmed cell death
Afu1g14400	hydroxyisocaproate dehydrogenase	246	oxidoreductase activity, acting on the CH-OH group of donors, NAD or NADP as acceptor"""///cytoplasm///nucleus///metabolic process///""NAD or NADH binding
Afu3g09960	aureobasidin resistance protein Aur1	247	inositol phosphoceramide synthase activity///sphingolipid metabolic process///Golgi apparatus
Afu1g16150	thioredoxin domain protein	248	
Afu4g00930	CorA family metal ion transporter	249	"di-, tri-valent inorganic cation transport"""""///"magnesium ion transport""///""""""""di-, tri-valent inorganic cation transmembrane transporter activity"""""""///plasma membrane

Afu5g11000	small nuclear ribonucleoprotein U2, A'	250	"nuclear mRNA splicing, via spliceosome""""///""pre-mRNA splicing factor activity"///U2 snRNP""///"cytoplasm
Afu2g02840	TBC domain protein	252	
Afu2g01880	low molecular weight phosphotyrosine protein phosphatase	253	protein amino acid dephosphorylation///cytoplasm///nucleus///protein tyrosine phosphatase activity
Afu1g06280	short-chain dehydrogenase/reductase family protein, putative	255	cellular component unknown///biological process unknown///molecular function unknown
Afu3g09970	vacuolar iron transporter Ccc1	256	membrane fraction///cellular manganese ion homeostasis///cellular calcium ion homeostasis///cellular iron ion homeostasis///Golgi apparatus
Afu4g10180	signal recognition particle protein	258	signal sequence binding///protein targeting to ER///""signal recognition particle, endoplasmic reticulum targeting""
Afu5g11210	molybdopterin binding domain protein	259	catalytic activity///cytoplasm///nucleus///Mo-molybdopterin cofactor biosynthetic process
Afu7g05220	mitochondrial carrier protein	260	mitochondrial inner membrane///transporter activity///transport
Afu8g00410	methionine aminopeptidase, type II	263	proteolysis///methionyl aminopeptidase activity///cytoplasm
Afu6g07430	pyruvate kinase	265	cytosol///pyruvate metabolic process///pyruvate kinase activity///glycolysis
Afu1g10080	C2H2 transcription factor	267	specific RNA polymerase II transcription factor activity///regulation of transcription from RNA polymerase II promoter///nucleus///zinc ion binding
Afu7g04930	alkaline serine protease (PR1)/allergen F18-like	268	protein catabolic process///cellular component unknown///peptidase activity
Afu3g01430	benzodiazepine receptor family protein	269	
Afu4g11260	aldo-keto reductase	270	aldo-keto reductase activity///cytoplasm///cellular aldehyde metabolic process
Afu2g16880	60S ribosomal protein L37a	272	structural constituent of ribosome///translation///cytosolic large ribosomal subunit (sensu Eukaryota)
Afu2g02070	CCR4-NOT transcription complex, subunit 3	273	3'-5'-exoribonuclease activity///cytoplasm///nuclear-transcribed mRNA poly(A) tail shortening///regulation of transcription from RNA polymerase II promoter///CCR4-NOT core complex
Afu4g03740	MFS transporter	274	
Afu8g04160	folylpolyglutamate	275	cytoplasm///tetrahydrofolylpolyglutamate synthase

	synthetase		activity///mitochondrion///one-carbon metabolic process
Afu3g03060	cell wall protein PhiA	276	
Afu1g11690	proline-rich, actin-associated protein Vrp1	277	
Afu8g05190	Myb-like DNA-binding domain protein	278	
Afu5g11640	secretory pathway protein Ssp120	279	protein secretion///cytoplasm///molecular function unknown
Afu6g00490	DUF521 domain protein	285	
Afu5g07160	DUF636 domain protein	287	
Afu3g13470	sulfate transporter	289	endoplasmic reticulum
Afu3g02910	dihydroxy-acetone synthase	290	cytoplasm///pentose-phosphate shunt///transketolase activity
Afu5g14880	mitochondria protein Fmp29	291	mitochondrion///biological process unknown///molecular function unknown

Table 10.8: 200 genes with greatest nSI decrease between 4 and 8 hours post infection. Genes are reported ranked according to greatest nSI intensity decrease between 4 and 8 hours where 1 is the greatest. Hypothetical proteins (n = 78) were removed

ORF	Description	Rank	GO Biological Process
Afu2g09710	protein kinase (NpkA)	1	regulation of progression through cell cycle///G1/S transition of mitotic cell cycle///regulation of meiosis///cytoplasm///S phase of mitotic cell cycle///protein amino acid phosphorylation///nucleus///cyclin-dependent protein kinase activity///G2/M transition of mitotic cell cycle///protein kinase activity
Afu5g01900	heat shock transcription factor Hsf1	2	response to heat///transcription factor activity///regulation of transcription from RNA polymerase II promoter///nucleus///response to stress
Afu6g08100	nucleotide-sugar transporter	3	
Afu2g17050	nuclear export protein Noc3	4	DNA replication initiation///chromatin binding///nucleolus///rRNA processing///protein binding///nucleus
Afu6g00230	NmrA-like family protein	5	
Afu6g05220	BET3 family protein	8	
Afu6g04950	mitochondrial GTPase (Mss1)	11	translation///GTP binding///mitochondrial inner membrane
Afu2g03700	HMG-CoA reductase	12	hydroxymethylglutaryl-CoA reductase (NADPH) activity///mitochondrial matrix///ergosterol biosynthetic process///endoplasmic reticulum membrane///nuclear envelope
Afu5g14500	MFS transporter	14	integral to plasma membrane

Afu2g17480	amino acid transporter	15	
Afu1g03150	c-14 sterol reductase	18	endoplasmic reticulum///ergosterol biosynthetic process///C-14 sterol reductase activity
Afu1g16540	WD40 domain protein	19	
Afu4g07640	40S ribosomal protein S13	20	cytoplasm///mitochondrion///biological process unknown///molecular function unknown
Afu1g14080	integral membrane protein Pth11-like	21	
Afu5g09480	ABC transporter	22	membrane///ATP-binding cassette (ABC) transporter activity///transport
Afu5g14490	MFS transporter	23	
Afu2g04550	MFS sugar transporter	24	
Afu5g08210	dolichyl-phosphate beta-glucosyltransferase	27	protein amino acid N-linked glycosylation///dolichyl-phosphate beta-glucosyltransferase activity///endoplasmic reticulum membrane
Afu6g00300	serine palmitoyltransferase 1	30	serine C-palmitoyltransferase complex///membrane fraction///sphingolipid biosynthetic process///microsome///serine C-palmitoyltransferase activity
Afu1g03550	mitochondrial dihydroxy acid dehydratase	31	dihydroxy-acid dehydratase activity///branched chain family amino acid biosynthetic process///mitochondrion
Afu8g04320	NADH-ubiquinone oxidoreductase 178 kDa subunit, putative	32	
Afu6g12010	glycosyl hydrolase family protein	33	carbohydrate metabolic process"///"hydrolase activity, hydrolyzing O-glycosyl compounds"""""""
Afu2g00140	FAD monooxygenase	35	cellular aromatic compound metabolic process
Afu5g02800	C6 transcription factor	36	RNA polymerase II transcription factor activity///nucleus///zinc ion binding///regulation of transcription
Afu5g03230	stress response RCI peptide	37	response to stress
Afu3g03430	ABC multidrug transporter SitT	38	ATP-binding cassette (ABC) transporter activity///ATP binding///transport
Afu7g05550	sugar transporter family protein	39	lactate transmembrane transporter activity///lactate transport///plasma membrane
Afu2g17360	MFS monocarboxylate transporter (Mct)	40	fungal-type vacuole membrane///monocarboxylic acid transmembrane transporter activity///transporter activity///transport
Afu3g07170	phosphatidylinositol:UDP-GlcNAc transferase PIG-C	41	GPI anchor biosynthetic process///endoplasmic reticulum///molecular function unknown
Afu3g02470	amidase family protein	43	allophanate hydrolase activity///urea metabolic process///cytoplasm///urea carboxylase activity
Afu5g01700	C6 transcription factor	44	transcription factor activity///nucleus///zinc ion binding///regulation of transcription

Afu7g05130	O-methyltransferase	46	
Afu3g08530	MFS drug transporter	47	response to drug///multidrug transport///multidrug efflux pump activity
Afu4g07100	nuclear envelope protein	48	
Afu4g04700	F-box domain protein	49	
Afu1g06920	serine/threonine protein kinase	51	cytoplasm///protein amino acid phosphorylation///protein kinase activity
Afu2g13490	KH domain protein	52	
Afu1g16040	ferric-chelate reductase	53	ferric-chelate reductase activity///integral to plasma membrane///ferrous iron transport///cellular iron ion homeostasis
Afu3g10570	haemolysin-III channel protein Izh2	54	nonselective channel activity///integral to membrane
Afu2g04390	cytomegalovirus gH-receptor family protein	55	cellular component unknown///biological process unknown///molecular function unknown
Afu1g16840	TCTP family protein	56	cytoplasm///biological process unknown///molecular function unknown
Afu3g04020	conserved mitochondrial protein	58	
Afu7g06960	monooxygenase	60	
Afu3g03180	NAD binding Rossmann fold oxidoreductase	61	oxidoreductase activity///metabolic process
Afu3g08300	DNA replication factor C subunit Rfc2	63	leading strand elongation///DNA replication factor C complex///DNA clamp loader activity///cell cycle checkpoint///sister chromatid cohesion///mismatch repair///purine nucleotide binding
Afu2g17890	RTA1 domain protein	67	fatty acid transport///plasma membrane///endoplasmic reticulum///integral to membrane
Afu6g09310	class V chitinase	68	chitinase activity///chitin catabolic process
Afu4g08140	threonine dehydratase, biosynthetic	69	branched chain family amino acid biosynthetic process///L-threonine ammonia-lyase activity///mitochondrion
Afu8g05270	C6 transcription factor	70	
Afu2g17810	RTA1 domain protein	71	
Afu2g17170	Na+/H+ antiporter Nha1	72	cellular monovalent inorganic cation homeostasis///plasma membrane///cation:cation antiporter activity
Afu1g10990	ribosomal RNA processing protein	73	
Afu3g06080	multicopy suppressor of stt4 mutation	74	plasma membrane///1-phosphatidylinositol-4-phosphate 5-kinase activity///actin cable formation///actin cytoskeleton organization

Afu1g16440	ABC ATPase	75	
Afu6g07020	SAM and PH domain protein (Boi1)	76	Rho protein signal transduction///phospholipid binding///cell morphogenesis
Afu4g08440	Patatin family phospholipase	78	lipid particle///molecular function unknown
Afu6g13780	MFS multidrug transporter	79	integral to plasma membrane///multidrug transporter activity///response to toxin
Afu4g12270	LIM domain protein	80	
Afu4g11140	DNA polymerase iota	81	UV protection
Afu2g13240	V-type ATPase, B subunit	82	cytoplasm///"""""vacuolar proton-transporting V-type ATPase, V1 domain"""""""///"vacuolar acidification///"""""""proton-transporting ATPase activity, rotational mechanism"""""""
Afu4g13290	HAD superfamily hydrolase	84	cytoplasm///nucleus///hydrolase activity///metabolic process
Afu8g01180	MFS sugar transporter	85	membrane///transporter activity///transport
Afu8g02600	short-chain dehydrogenase/reductase 2	86	cellular component unknown///biological process unknown///molecular function unknown
Afu2g04690	nucleoside transporter	87	vitamin or cofactor transporter activity///plasma membrane///vitamin or cofactor transport
Afu1g10790	alpha-1,2-mannosidase family protein	88	
Afu5g02790	amino acid permease	89	
Afu6g11310	bifunctional pyrimidine biosynthesis protein (PyrABCN), putative	90	membrane///aspartate carbamoyltransferase activity///cytoplasm///carbamoyl-phosphate synthase activity///pyrimidine base biosynthetic process
Afu2g00410	amidase family protein	91	
Afu1g02830	endoplasmic reticulum and nuclear membrane proteinc Npl4	92	nuclear envelope-endoplasmic reticulum network///ER-associated protein catabolic process///endoplasmic reticulum
Afu6g03030	phenol monooxygenase	95	FAD binding
Afu2g05860	calcium/mangenease P-type ATPase	96	manganese-transporting ATPase activity///manganese ion transport///calcium ion transport///calcium-transporting ATPase activity///Golgi apparatus
Afu6g08860	sugar isomerase, KpsF/GutQ	97	
Afu1g02140	glycogen debranching enzyme Gdb1	98	4-alpha-glucanotransferase activity///glycogen catabolic process"///cytoplasm///"""amylo-alpha-1,6-glucosidase activity""
Afu8g05780	NACHT and Ankyrin	99	GTP binding///protein binding

	domain protein		
Afu4g11880	splicing factor 3a subunit 2	101	spliceosome assembly///RNA binding///U2 snRNP
Afu8g04702	MFS transporter	103	plasma membrane///transporter activity///transport
Afu2g10710	DNA repair protein rad9	104	
Afu5g03000	Impact family protein	106	regulation of cellular amino acid metabolic process///cytoplasm///nucleus
Afu1g17160	MFS transporter	111	membrane///transporter activity///transport
Afu3g05450	glutamate carboxypeptidase	113	metallopeptidase activity///proteolysis///cytoplasm///mitochondrion
Afu5g01300	integral membrane protein	114	
Afu4g08570	regulatory protein Ral2	115	
Afu5g12330	WD repeat protein	116	
Afu7g01300	mannosyltransferase (PIG-M)	117	GPI anchor biosynthetic process///endoplasmic reticulum membrane///mannosyltransferase activity
Afu4g03280	short-chain dehydrogenase/reductase family protein, putative	118	
Afu5g12510	adenylate-forming enzyme AfeA	119	cytoplasm///AMP binding
Afu6g07440	1-phosphatidylinositol-3-phosphate 5-kinase (Fab1), putative	120	vacuole organization///phospholipid metabolic process///1-phosphatidylinositol-3-phosphate 5-kinase activity///response to stress///vacuolar membrane
Afu6g03140	oligopeptide transporter	122	oligopeptide transporter activity///integral to plasma membrane///oligopeptide transport
Afu1g07260	NUDIX family hydrolase	123	hydrolase activity///metabolic process
Afu3g12910	O-methyltransferase GliM-like	125	S-adenosylmethionine-dependent methyltransferase activity///O-methyltransferase activity
Afu7g00710	oxalate/formate antiporter	126	membrane///monocarboxylic acid transmembrane transporter activity///transporter activity///transport
Afu5g05750	protein kinase	127	cytoplasm///protein kinase activity
Afu2g11380	rRNA assembly protein Mis3	128	ribosome biogenesis///nucleolus///rRNA processing///molecular function unknown
Afu5g02880	C6 transcription factor	130	transcription factor activity///regulation of transcription
Afu2g09700	superoxide dismutase copper chaperone Lys7	131	removal of superoxide radicals///superoxide metabolic process///superoxide dismutase copper chaperone activity///cytosol///intracellular copper ion transport
Afu8g01010	thermophilic desulfurizing enzyme family protein	135	
Afu3g02460	serine protein	137	

	kinase		
Afu5g06580	MFS multidrug transporter	138	drug transport///drug transporter activity///integral to membrane
Afu2g09860	purine-cytosine permease	139	purine transport///cytosine transport///cytosine-purine permease activity///plasma membrane
Afu1g07300	tetracycline transporter	141	transporter activity///transport
Afu3g14700	polyketide synthase	143	polyketide biosynthetic process///polyketide synthase activity
Afu6g10780	carboxylesterase	144	
Afu5g08180	cell wall protein	146	
Afu2g03230	alpha-amylase AmyA	149	
Afu5g13270	pH signal transduction protein PalH	150	
Afu3g13610	oxidoreductase, zinc-binding	152	
Afu2g01900	RNA polymerase II transcription elongation factor Rtf1p	153	Cdc73/Paf1 complex///transcription elongation factor complex///RNA elongation from RNA polymerase II promoter///RNA polymerase II transcription elongation factor activity///transcription from RNA polymerase II promoter
Afu5g01320	phosphate permease	154	integral to plasma membrane///inorganic phosphate transmembrane transporter activity///phosphate transport
Afu1g15610	oxidoreductase, zinc-binding dehydrogenase family, putative	157	oxidoreductase activity///cytoplasm///zinc ion binding///metabolic process
Afu4g10660	histone acetylase complex subunit MRG15-2	158	histone acetyltransferase complex///regulation of transcription from RNA polymerase II promoter///histone acetyltransferase activity///histone acetylation
Afu6g11800	RTA1 domain protein	160	
Afu8g01430	oxidoreductase, zinc-binding dehydrogenase family, putative	161	oxidoreductase activity///cellular component unknown///zinc ion binding///metabolic process
Afu1g12550	membrane-tethered transcription factor (SPT23), putative	163	transcription activator activity///response to cold///fatty acid metabolic process///endoplasmic reticulum membrane///positive regulation of transcription from RNA polymerase II promoter
Afu6g09630	C6 finger domain protein GliZ	164	
Afu1g04450	siderophore biosynthesis protein	166	
Afu1g13250	1-phosphatidylinositol-4,5-bisphosphate	167	phosphoinositide phospholipase C activity///pseudohyphal growth///cell growth and/or maintenance///nucleus///signal

	phosphodiesterase Plc1		transduction///condensed nuclear chromosome kinetochore
Afu3g13670	siderochrome-iron transporter	170	siderophore-iron transport///siderophore-iron (ferrioxamine) uptake transmembrane transporter activity///integral to membrane///cellular iron ion homeostasis
Afu2g08040	C6 finger domain protein	171	DNA binding///nucleus///zinc ion binding
Afu6g07500	DNA excision repair protein Rad2	172	single-stranded DNA specific endodeoxyribonuclease activity""///"nucleotide-excision repair, DNA incision, 3'-to lesion"""""///""nucleotide-excision repair factor 3 complex"
Afu2g17960	NADPH dehydrogenase Oye3	173	
Afu5g12020	C6 transcription factor (NirA)	174	""regulation of transcription, DNA-dependent"""""///transcription factor activity///"cellular amino acid catabolic process""///nucleus"
Afu2g12010	pentatricopeptide repeat protein	175	
Afu8g00520	integral membrane protein	177	
Afu7g01840	membrane bound C2 domain protein (vp115)	178	calcium ion binding///membrane///biological process unknown
Afu5g09750	nucleoside transporter	179	nucleoside transport///nucleoside transmembrane transporter activity
Afu8g02430	zinc-binding alcohol dehydrogenase	180	alcohol metabolic process///soluble fraction///zinc ion binding///alcohol dehydrogenase (NADP+) activity
Afu1g12850	nitrate transporter CrnA	181	nitrate transmembrane transporter activity///nitrate transport///integral to plasma membrane
Afu3g01410	polyketide synthase	182	3-oxoacyl-[acyl-carrier-protein] synthase activity///polyketide synthase activity
Afu4g14680	C6 transcription factor	183	
Afu1g01920	plasma membrane protein Pth11-like	184	
Afu3g15170	molybdenum cofactor biosynthesis protein (MoeA), putative	185	catalytic activity///Mo-molybdopterin cofactor biosynthetic process
Afu1g15790	CDP-diacylglycerol-inositol 3-phosphatidyltransferase PIS	186	CDP-diacylglycerol-inositol 3-phosphatidyltransferase activity///endoplasmic reticulum///phosphatidylinositol biosynthetic process
Afu1g15970	aldo-keto reductase (AKR13)	189	aldo-keto reductase activity///cytoplasm///cellular aldehyde metabolic process
Afu1g09370	pentatricopeptide repeat protein	191	

Afu6g08020	ABC transporter	192	ATP-binding cassette (ABC) transporter activity///transport///integral to membrane
Afu3g10650	glutamate carboxypeptidase Tre2	193	metallopeptidase activity///proteolysis///protein targeting to vacuole
Afu5g11990	alpha-1,3-mannosyltransferase (Alg3)	196	protein amino acid glycosylation"///dolichol-linked oligosaccharide biosynthetic process///endoplasmic reticulum///"alpha-1,3-mannosyltransferase activity"""""""
Afu5g04390	cytokinesis regulator (Byr4)	197	
Afu8g05740	RTA1 domain protein	198	biological process unknown///molecular function unknown///integral to membrane
Afu4g01090	Zn2+ dependent hydrolase	199	
Afu2g02550	Phosducin family protein	200	positive regulation of transcription from RNA polymerase II promoter by pheromones///cytoplasm///GTPase inhibitor activity
Afu3g13650	integral membrane protein	201	
Afu2g01500	ABC bile acid transporter	202	ATP-binding cassette (ABC) transporter activity///bile acid transmembrane transporter activity///fungal-type vacuole///bile acid and bile salt transport
Afu4g12950	vacuolar targeting protein Atg24	205	membrane///autophagy///lipid binding///transport
Afu2g11870	beta-1,6 glucan synthetase (Kre6)	206	cell wall organization///"1,6-beta-glucan biosynthetic process"///glucosidase activity///integral to membrane///Golgi cis cisterna
Afu5g13090	alpha-1,2-mannosyltransferase	207	Golgi apparatus""///""protein amino acid glycosylation"///"alpha-1,2-mannosyltransferase activity"""""
Afu1g17380	3-oxoacyl-(acyl-carrier-protein) reductase	208	
Afu8g00660	solute transporter	209	
Afu2g01860	integral membrane protein	212	
Afu6g06960	MFS quinate transporter	213	
Afu6g12020	C2H2 finger domain protein	214	DNA binding///nucleus///zinc ion binding
Afu5g11900	guanine nucleotide exchange factor (Gea2)	215	Golgi-associated vesicle///ER to Golgi vesicle-mediated transport///ARF guanyl-nucleotide exchange factor activity///intra-Golgi vesicle-mediated transport
Afu1g14140	DUF409 domain protein	216	cellular component unknown///biological process unknown///molecular function unknown
Afu1g15100	EBP domain protein	217	
Afu4g14840	transferase family protein	218	
Afu1g14240	Golgi membrane protein (Coy1)	219	Golgi vesicle transport///Golgi membrane///molecular function unknown

Afu4g12240	nitrilase, putitive	220	"hydrolase activity, acting on carbon-nitrogen (but not peptide) bonds, in other compounds"
Afu2g02570	F-box domain protein	221	ubiquitin-dependent protein catabolic process///ubiquitin ligase complex///protein binding
Afu4g07660	ATP dependent RNA helicase (Dbp1)	222	cytoplasm///RNA helicase activity///translational initiation
Afu6g05140	sterol delta 5,6-desaturase ERG3	223	C-5 sterol desaturase activity///endoplasmic reticulum///ergosterol biosynthetic process
Afu1g02070	cytochrome C1/Cyt1	224	"electron transporter, transferring electrons within CoQH2-cytochrome c reductase complex activity"///mitochondrial respiratory chain complex III///mitochondrial inner membrane///mitochondrial respiratory chain///oxidative phosphorylation///"mitochondrial electron transport, ubiquinol to cytochrome c"
Afu5g02290	potassium ion transporter (Trk1)	225	cellular potassium ion homeostasis///plasma membrane///potassium ion transmembrane transporter activity
Afu3g12970	DUF580 domain protein Pns1	226	
Afu5g14560	cellulase family protein	227	
Afu3g00310	extracellular phytase	229	phosphate metabolic process///extracellular region///acid phosphatase activity
Afu2g11230	nuclear pore protein (SEH1)	230	tRNA export from nucleus///mRNA export from nucleus///NLS-bearing substrate import into nucleus///nuclear pore///structural molecule activity///rRNA export from nucleus///protein export from nucleus///mRNA-binding (hnRNP) protein import into nucleus///nuclear pore organization///ribosomal protein import into nucleus///snRNA export from nucleus///snRNP protein import into nucleus
Afu2g06020	mitochondrial respiratory complex I chaperone (Cia84), putative	231	
Afu8g04240	origin recognition complex subunit 3	233	
Afu2g13910	EBP domain protein	234	
Afu1g13950	short-chain oxidoreductase	235	oxidoreductase activity///metabolic process
Afu8g00370	polyketide synthase	236	3-oxoacyl-[acyl-carrier-protein] synthase activity///polyketide synthase activity
Afu1g13660	phenol 2-monooxygenase	239	cellular aromatic compound metabolic process///monooxygenase activity
Afu1g05010	MFS multidrug transporter	240	ascospore formation///integral to plasma membrane///signal transduction///transport
Afu5g09670	RNase III domain protein	241	

Afu7g05340	cellular morphogenesis protein (Rax2)	243	membrane///cellular bud scar///cellular bud neck///cellular bud site selection///molecular function unknown
Afu1g17360	bZIP transcription factor (BACH2)	244	transcription///transcription factor activity///nucleus
Afu5g00280	MFS sugar transporter	245	membrane///transporter activity///transport
Afu6g03350	GNAT family N-acetyltransferase	247	N-acetyltransferase activity///metabolic process
Afu4g00120	MFS transporter	248	
Afu5g07770	pentatricopeptide repeat protein	249	
Afu6g09440	tetrahydrofolylpoly glutamate synthase	251	
Afu4g07800	CaaX farnesyltransferase alpha subunit Ram2	252	protein geranylgeranyltransferase activity///protein amino acid farnesylation///protein amino acid geranylgeranylation///protein farnesyltransferase complex///protein farnesyltransferase activity///conjugation with cellular fusion///peptide pheromone maturation
Afu4g00550	MFS transporter	253	
Afu1g04890	translocon protein Sec61beta	254	protein transporter activity///cotranslational protein targeting to membrane///Sec61 translocon complex
Afu1g02810	mRNA cleavage and polyadenylation specificity factor complex subunit	255	cleavage and polyadenylylation specificity factor activity///mRNA cleavage and polyadenylation specificity factor complex///mRNA polyadenylation///mRNA cleavage
Afu8g01550	oxidoreductase, short chain dehydrogenase/reductase family superfamily	256	sporulation (sensu Saccharomyces)///fatty acid catabolic process///"""""2,4-dienoyl-CoA reductase (NADPH) activity""""""""///"peroxisomal matrix
Afu3g06300	Rho GTPase Rac	257	Rho protein signal transduction///signal transducer activity///Rho small monomeric GTPase activity///invasive growth///plasma membrane///pheromone-dependent signal transduction involved in conjugation with cellular fusion///soluble fraction///exocytosis
Afu7g06610	isochorismatase family hydrolase	259	
Afu2g16320	MFS multidrug transporter	260	integral to plasma membrane///multidrug transporter activity///response to toxin
Afu3g10350	stress response protein Nst1	262	response to salt stress///cytoplasm///molecular function unknown
Afu2g00630	GDSL lipase/acylhydrolase family protein	263	lipase activity
Afu3g02750	C6 transcription factor	267	DNA binding
Afu6g07220	sreptomyces cyclase/dehydrase	268	

	family protein		
Afu8g06310	Patatin-like serine hydrolase	269	
Afu2g01770	GMC oxidoreductase	270	
Afu3g14560	MFS multidrug transporter	271	transporter activity///transport
Afu4g12040	lanosterol synthase	273	lipid particle///plasma membrane///endoplasmic reticulum///ergosterol biosynthetic process///lanosterol synthase activity
Afu5g01950	histone H2A	274	chromatin assembly complex///nuclear chromatin///chromatin binding///regulation of transcription from RNA polymerase II promoter
Afu6g10580	GPI anchored CFEM domain protein	278	

Table 10.9: 200 genes with greatest nSI increase between 8 and 14 hours post infection. Genes are reported ranked according to greatest nSI intensity increase between 8 and 14 hours. Hypothetical proteins (n = 71) were removed.

ORF	Description	Rank	GO Biological Process
Afu6g07020	SAM and PH domain protein (Boi1)	1	Rho protein signal transduction///phospholipid binding///cell morphogenesis
Afu5g01900	heat shock transcription factor Hsf1	2	response to heat///transcription factor activity///regulation of transcription from RNA polymerase II promoter///nucleus///response to stress
Afu6g00770	extracellular arabinanase	3	"hydrolase activity, hydrolyzing N-glycosyl compounds"///metabolic process
Afu2g15490	TPR domain protein	6	
Afu3g01880	fungal specific transcription factor	7	transcription factor activity///regulation of transcription
Afu6g13390	FAD dependent oxidoreductase	8	oxidoreductase activity///FAD binding///metabolic process
Afu7g05090	glucuronyl hydrolase	11	
Afu6g13570	cytochrome c peroxidase	13	
Afu6g09550	RTA1 domain protein	14	biological process unknown///molecular function unknown///integral to membrane
Afu2g17240	C2H2 finger domain protein	15	

Afu1g10990	ribosomal RNA processing protein	16	
Afu1g05050	cytosine deaminase	17	cytosine metabolic process///cytosine deaminase activity///cytoplasm///nucleus///zinc ion binding
Afu6g11770	NmrA-like family protein	18	
Afu5g14490	MFS transporter	19	
Afu2g17480	amino acid transporter	20	
Afu1g02070	cytochrome C1/Cyt1	21	"electron transporter, transferring electrons within CoQH2-cytochrome c reductase complex activity"///mitochondrial respiratory chain complex III///mitochondrial inner membrane///mitochondrial respiratory chain///oxidative phosphorylation///"mitochondrial electron transport, ubiquinol to cytochrome c"
Afu1g17240	C6 transcription factor	22	transcription factor activity///nucleus///regulation of transcription
Afu2g04550	MFS sugar transporter	23	
Afu2g00400	cell wall cysteine-rich protein	25	
Afu8g01180	MFS sugar transporter	27	membrane///transporter activity///transport
Afu4g12250	exosome complex exonuclease exoribonuclease (Rrp44), putative	28	3'-5'-exoribonuclease activity///nuclear exosome (RNase complex)///mRNA catabolic process///cytoplasmic exosome (RNase complex)///35S primary transcript processing
Afu1g02780	L-asparaginase	29	endoplasmic reticulum///asparagine catabolic process///cellular response to nitrogen starvation///nuclear envelope///cell wall-bounded periplasmic space///asparaginase activity
Afu7g00700	aldo-keto reductase (AKR13), puatative	30	aldo-keto reductase activity///cytoplasm///nucleus///cellular aldehyde metabolic process
Afu2g15150	choline transport protein	31	plasma membrane///choline transport///choline transmembrane transporter activity
Afu2g17050	nuclear export protein Noc3	32	DNA replication initiation///chromatin binding///nucleolus///rRNA processing///protein binding///nucleus
Afu4g00990	MFS quinate transporter	33	mannose transmembrane transporter activity///hexose transport///fructose transmembrane transporter activity///plasma membrane///glucose transmembrane transporter activity
Afu3g00880	extracellular conserved serine-rich protein	34	
Afu5g08560	vacuolar ATPase proteolipid subunit c	37	"vacuolar proton-transporting V-type ATPase, V0 domain""""""""///"vacuolar acidification///""""""""proton-transporting ATPase activity, rotational mechanism"""""""
Afu3g02290	arylsulfatase	38	sulfuric ester hydrolase activity///metabolic process

Afu2g02710	60S ribosomal protein L24b	39	structural constituent of ribosome///nucleolus///ribosomal large subunit biogenesis
Afu3g14430	NEDD8 conjugating enzyme (UbcL)	40	NEDD8 conjugating enzyme activity///NEDD8 class-dependent protein catabolic process///cytoplasm///protein neddylation during NEDD8 class-dependent protein catabolic process
Afu2g11040	U-box domain protein	41	
Afu2g09070	DUF221 domain protein	44	cellular component unknown///biological process unknown///molecular function unknown
Afu2g05540	cell division control protein (Cdc5)	45	pre-mRNA splicing factor activity"///""""nuclear mRNA splicing, via spliceosome"""""""///"spliceosomal complex
Afu5g08210	dolichyl-phosphate beta-glucosyltransferase	47	protein amino acid N-linked glycosylation///dolichyl-phosphate beta-glucosyltransferase activity///endoplasmic reticulum membrane
Afu1g03150	c-14 sterol reductase	48	endoplasmic reticulum///ergosterol biosynthetic process///C-14 sterol reductase activity
Afu4g11460	aminotransferase, classes I and II	49	
Afu3g01950	zinc-containing alcohol dehydrogenase	50	cellular component unknown///"oxidoreductase activity, acting on the CH-OH group of donors, NAD or NADP as acceptor"""""""///hexose metabolic process"
Afu2g08300	DnaJ domain protein	53	endoplasmic reticulum lumen///co-chaperone activity///protein folding
Afu2g09710	protein kinase (NpkA)	55	regulation of progression through cell cycle///G1/S transition of mitotic cell cycle///regulation of meiosis///cytoplasm///S phase of mitotic cell cycle///protein amino acid phosphorylation///nucleus///cyclin-dependent protein kinase activity///G2/M transition of mitotic cell cycle///protein kinase activity
Afu3g13240	aldose 1-epimerase	57	hexose metabolic process///racemase and epimerase activity
Afu5g09910	nitroreductase family protein	60	negative regulation of fatty acid metabolic process///cytoplasm///nucleus///molecular function unknown
Afu2g10320	SH3 domain protein	62	actin cortical patch (sensu Saccharomyces)///actin cytoskeleton organization///myosin I binding
Afu5g02400	catabolite degradation protein	63	cytoplasm///nucleus///molecular function unknown///negative regulation of gluconeogenesis
Afu1g14140	DUF409 domain protein	64	cellular component unknown///biological process unknown///molecular function unknown
Afu5g13460	mitochondrial protein	65	mitochondrial genome maintenance///mitochondrion inheritance///mitochondrion organization///mitochondrial outer membrane///molecular function unknown
Afu4g07100	nuclear envelope protein	66	
Afu6g04950	mitochondrial	67	translation///GTP binding///mitochondrial inner

	GTPase (Mss1)		membrane
Afu2g17890	RTA1 domain protein	68	fatty acid transport///plasma membrane///endoplasmic reticulum///integral to membrane
Afu6g12010	glycosyl hydrolase family protein	70	carbohydrate metabolic process"///"hydrolase activity, hydrolyzing O-glycosyl compounds"""""""
Afu2g15370	MFS transporter family protein	71	cellular component unknown///autophagy///protein targeting to vacuole///molecular function unknown
Afu7g01300	mannosyltransferase (PIG-M)	73	GPI anchor biosynthetic process///endoplasmic reticulum membrane///mannosyltransferase activity
Afu5g00550	endoglycoceramidase	75	
Afu2g02580	HAD superfamily hydrolase	79	mitochondrion///biological process unknown///molecular function unknown
Afu4g11880	splicing factor 3a subunit 2	80	spliceosome assembly///RNA binding///U2 snRNP
Afu6g10470	zinc finger protein ZPR1	83	regulation of progression through cell cycle///cytoplasm///nucleolus///protein binding
Afu4g00970	IMP-specific 5'-nucleotidase (Isn1)	84	
Afu2g05860	calcium/mangenease P-type ATPase	87	manganese-transporting ATPase activity///manganese ion transport///calcium ion transport///calcium-transporting ATPase activity///Golgi apparatus
Afu5g05900	protein kinase (Chm1)	89	protein serine/threonine kinase activity///protein amino acid phosphorylation///cytokinesis
Afu5g07750	mitochondrial ferrochelatase	90	ferrochelatase activity///heme biosynthetic process///mitochondrial inner membrane
Afu7g04150	cochaperone Pam16	91	mitochondrion///protein import into mitochondrial matrix///molecular function unknown
Afu3g01660	glycosyl hydrolase, family 43	92	carbohydrate metabolic process///"hydrolase activity, hydrolyzing N-glycosyl compounds"
Afu3g00480	RTA1 domain protein	93	
Afu4g01520	gentisate 1,2-dioxygenase	94	
Afu2g15140	MFS drug transporter	95	integral to plasma membrane///transporter activity///transport
Afu4g09140	L-ornithine aminotransferase Car2	96	arginine catabolic process///cytoplasm///nucleus///ornithine-oxo-acid transaminase activity
Afu4g06630	MFS monosaccharide transporter	102	integral to plasma membrane///transporter activity///transport
Afu7g01520	BolA domain protein	104	
Afu4g07280	cAMP-mediated signaling protein Sok1	105	nucleus///cAMP-mediated signaling///molecular function unknown
Afu7g06200	ankyrin repeat protein	106	
Afu3g03180	NAD binding Rossmann fold	107	oxidoreductase activity///metabolic process

	oxidoreductase		
Afu5g06780	carbamoyl-phosphate synthase, small subunit	109	arginine biosynthetic process///cytosol///carbamoyl-phosphate synthase (glutamine-hydrolyzing) activity
Afu2g16490	rhomboid family membrane protein	110	
Afu2g01500	ABC bile acid transporter	111	ATP-binding cassette (ABC) transporter activity///bile acid transmembrane transporter activity///fungal-type vacuole///bile acid and bile salt transport
Afu3g03430	ABC multidrug transporter SitT	113	ATP-binding cassette (ABC) transporter activity///ATP binding///transport
Afu5g11450	arginine metabolism regulation protein iii	117	inositol or phosphatidylinositol kinase activity///phosphorylation///arginine metabolic process///nucleus
Afu2g04320	NADH-dependent flavin oxidoreductase	118	NADPH dehydrogenase activity///cytoplasm///nucleus///biological process unknown
Afu1g01180	isoamyl alcohol oxidase	120	FAD binding
Afu1g14080	integral membrane protein Pth11-like	121	
Afu1g04070	Eukaryotic translation initiation factor eIF-5A	122	ribosome///translation initiation factor activity///translational initiation
Afu7g05130	O-methyltransferase	124	
Afu8g04050	transcriptional regulator PacG/VIB-1	125	
Afu6g08630	mitochondrial protein	127	mitochondrion///biological process unknown///molecular function unknown
Afu3g14990	alpha/beta hydrolase	128	lipid particle///cytoplasm///biological process unknown///molecular function unknown
Afu1g14610	lipin Smp2	129	
Afu4g11110	C2 domain protein	130	cellular component unknown///biological process unknown///molecular function unknown
Afu3g14000	metaphase-anaphase transition protein (Mlo2)	131	
Afu4g04730	riboflavin-specific deaminase	132	
Afu5g00730	H	133	manganese-transporting ATPase activity///manganese ion transport///calcium ion transport///calcium-transporting ATPase activity///secretory pathway///Golgi apparatus
Afu2g07750	haloacid dehalogenase, type II	134	

Afu6g11370	Exocyst complex component Exo84	135	"nuclear mRNA splicing, via spliceosome"""""///molecular function unknown""///Golgi to plasma membrane transport///actin cap (sensu Saccharomyces)///vesicle fusion///vesicle docking during exocytosis///bipolar cellular bud site selection"///""establishment of cell polarity (sensu Saccharomyces)///cytokinesis///"exocyst
Afu5g06410	C2H2 transcription factor (AmdA)	136	RNA polymerase II transcription factor activity///negative regulation of transcription from RNA polymerase II promoter///nucleus///zinc ion binding
Afu4g09620	WD repeat protein	137	protein binding
Afu1g17130	F-box domain protein	140	
Afu4g12390	cell differentiation protein (Rcd1)	141	regulation of transcription from RNA polymerase II promoter///CCR4-NOT complex///molecular function unknown
Afu7g06420	NADH-dependent flavin oxidoreductase	142	NADPH dehydrogenase activity///cytoplasm///nucleus///biological process unknown
Afu7g00710	oxalate/formate antiporter	143	membrane///monocarboxylic acid transmembrane transporter activity///transporter activity///transport
Afu8g00962	cytochrome P450	144	
Afu5g08230	C3HC4 finger protein	147	
Afu5g10420	nitrate reductase	148	endoplasmic reticulum///biological process unknown///molecular function unknown
Afu2g03640	Ras GTPase activating protein	149	actin filament organization///response to osmotic stress///cytoskeletal protein binding///cytokinesis
Afu3g10310	acetolactate synthase, large subunit	150	valine biosynthetic process///isoleucine biosynthetic process///branched chain family amino acid biosynthetic process///acetolactate synthase complex///mitochondrion///acetolactate synthase activity
Afu8g05270	C6 transcription factor	152	
Afu1g11330	lactonohydrolase	153	
Afu1g07300	tetracycline transporter	155	transporter activity///transport
Afu6g11030	RNA binding protein MSSP-2	156	
Afu3g10320	RING finger domain protein	157	
Afu5g03000	Impact family protein	158	regulation of cellular amino acid metabolic process///cytoplasm///nucleus
Afu3g11690	fructose-bisphosphate aldolase, class II	159	
Afu1g16840	TCTP family protein	160	cytoplasm///biological process unknown///molecular function unknown
Afu2g08840	terminal deoxynucleotidyl	161	nucleotidyltransferase activity

	transferase		
Afu1g15570	ubiquitin-conjugating enzyme	162	
Afu5g09210	autophagic serine protease Alp2	163	cellular response to starvation///serine-type endopeptidase activity///fungal-type vacuole///programmed cell death///autophagy///vacuolar protein catabolic process///sporulation resulting in formation of a cellular spore
Afu1g03210	MYB family conidiophore development protein FlbD, putative	164	
Afu6g09450	LipA and NB-ARC domain protein	166	cellular component unknown///nucleotide binding
Afu2g10990	chromatin remodeling complex subunit (Arp8)	167	chromatin remodeling complex
Afu4g11210	pheromone-regulated multispanning membrane protein Prm1	168	plasma membrane fusion///mating projection///molecular function unknown///integral to membrane
Afu8g02070	glycosyl transferase	169	fungal-type vacuole"///biological process unknown""///"transferase activity, transferring glycosyl groups"""""
Afu8g02310	aldehyde dehydrogenase ALDH	170	polyamine catabolic process///cytoplasm///3-chloroallyl aldehyde dehydrogenase activity///beta-alanine biosynthetic process///cellular aldehyde metabolic process
Afu3g00780	cAMP receptor (Car4)	171	
Afu2g00970	alcohol dehydrogenase, zinc-containing	172	oxidoreductase activity///"oxidoreductase activity, acting on the CH-OH group of donors, NAD or NADP as acceptor"///zinc ion binding///metabolic process
Afu3g00100	flavin-containing amine oxidase	173	
Afu7g02030	cytochrome c oxidase assembly protein (Pet117), putative	174	
Afu2g12180	lectin family integral membrane protein	176	
Afu8g04150	MFS transporter	179	
Afu2g04700	RNA binding effector protein Scp160	180	nuclear envelope-endoplasmic reticulum network///polysome///chromosome segregation///intracellular mRNA localization///RNA binding///endoplasmic reticulum membrane

Afu3g01640	C6 finger domain protein	181	zinc ion binding///regulation of transcription
Afu5g01160	MFS monosaccharide transporter	182	mannose transmembrane transporter activity///hexose transport///fructose transmembrane transporter activity///plasma membrane///glucose transmembrane transporter activity
Afu5g08390	response regulator	183	cytoplasm///enzyme activator activity///osmosensory signaling pathway via two-component system///two-component response regulator activity
Afu7g01580	molybdopterin synthase small subunit CnxG	184	
Afu6g06960	MFS quinate transporter	186	
Afu1g04940	small monomeric GTPase SarA	187	SAR small monomeric GTPase activity///ER to Golgi vesicle-mediated transport///COPII vesicle coat
Afu4g13750	penicillolysin/deuterolysin metalloprotease	189	
Afu5g01260	ankyrin repeat protein	190	
Afu2g17840	MFS transporter	192	plasma membrane///transporter activity///transport
Afu6g12800	uroporphyrinogen-III synthase (UroS)	193	cellular component unknown///uroporphyrinogen-III synthase activity///heme biosynthetic process
Afu5g01450	NADH-dependent flavin oxidoreductase	194	cellular component unknown///NADPH dehydrogenase activity///biological process unknown
Afu3g08270	pyruvate dehydrogenase complex component Pdx1	196	protein binding///acetyl-CoA biosynthetic process from pyruvate///mitochondrion///mitochondrial pyruvate dehydrogenase complex
Afu7g05650	glutamine-serine rich protein MS8	197	
Afu2g00430	exo-beta-1,3-glucanase	198	fungal-type cell wall///"""hydrolase activity, hydrolyzing O-glycosyl compounds""///""1,3-beta-glucan metabolic process"""
Afu1g06350	pathogenesis associated protein Cap20	199	
Afu6g05220	BET3 family protein	200	
Afu6g04790	proteasome component Pre5	201	proteasome core complex///endopeptidase activity"""///"""proteasome core complex, alpha-subunit complex"""///"ubiquitin-dependent protein catabolic process
Afu1g01010	polyketide synthase	202	polyketide synthase activity
Afu3g02180	AM-toxin synthetase	203	
Afu8g02280	C6 transcription factor	204	transcription cofactor activity///nucleus///regulation of transcription
Afu3g00440	F-box domain protein	205	

Afu5g01600	PHP domain protein	206	
Afu3g12840	Signal peptidase I	207	signal peptide processing///signal peptidase complex///endoplasmic reticulum///signal peptidase activity
Afu5g08180	cell wall protein	208	
Afu7g02080	RNA polymerase I subunit Rpa43	209	
Afu5g13320	UV radiation resistance protein (UVRAG)	210	programmed cell death
Afu6g11520	C6 transcription factor	211	
Afu4g14840	transferase family protein	212	
Afu1g17250	conidial hydrophobin RodB	213	cell wall organization
Afu3g07120	MFS transporter	216	plasma membrane///transporter activity///transport
Afu2g02780	KH domain RNA-binding protein	217	telomere maintenance via telomerase"///intracellular mRNA localization///cytoplasm///mRNA binding///"nuclear chromosome, telomeric region"""""""
Afu7g06040	integral membrane protein	218	
Afu7g02280	U5 snRNP complex subunit	219	establishment of cell polarity (sensu Saccharomyces)///cytoplasm///maturation of SSU-rRNA///cytokinesis///snoRNA binding///small nucleolar ribonucleoprotein complex
Afu2g12820	polyketide synthase	221	oxidoreductase activity///metabolic process
Afu5g00760	chitin synthase C	222	chitin synthase activity///chitin biosynthetic process///cytokinesis
Afu1g12640	zinc metalloproteinase	223	
Afu1g06910	arabinogalactan endo-1,4-beta-galactosidase GalA	225	
Afu5g04030	50S ribosomal protein L27	227	structural constituent of ribosome///translation///mitochondrial large ribosomal subunit///peptidyltransferase activity
Afu2g02570	F-box domain protein	228	ubiquitin-dependent protein catabolic process///ubiquitin ligase complex///protein binding
Afu1g14990	ATP-dependent RNA helicase (Drs1)	231	nucleolus///ribosomal large subunit assembly///35S primary transcript processing///ATP-dependent RNA helicase activity
Afu1g13250	1-phosphatidylinositol-4,5-bisphosphate phosphodiesterase Plc1	233	phosphoinositide phospholipase C activity///pseudohyphal growth///cell growth and/or maintenance///nucleus///signal transduction///condensed nuclear chromosome kinetochore
Afu3g12270	glutathione peroxidase Hyr1	234	intracellular///response to oxidative stress///thiol peroxidase activity///glutathione peroxidase activity

Afu3g00750	short-chain dehydrogenase/reductase	235	oxidoreductase activity///metabolic process
Afu6g00370	aminotransferase	236	cytoplasm///nucleus///biological process unknown///molecular function unknown
Afu1g06460	BCAS2 family protein	237	
Afu8g04430	oligosaccharyl transferase subunit (Stt3)	238	oligosaccharyltransferase complex///dolichyl-diphosphooligosaccharide-protein glycotransferase activity///protein amino acid N-linked glycosylation
Afu5g14380	alpha-glucuronidase	240	
Afu5g01230	RTA1 domain protein	241	fatty acid transport///phospholipid-translocating ATPase activity///plasma membrane///endoplasmic reticulum///integral to membrane
Afu6g09630	C6 finger domain protein GliZ	242	
Afu1g15580	acetylserotonin methytransferase-like protein (ASMTL), putative	243	
Afu2g10150	peroxisome biosynthesis protein (PAS1/Peroxin-1), putative	244	ATPase activity///peroxisome organization///peroxisome
Afu6g12130	C6 transcription factor	246	transcription activator activity///""""regulation of transcription, DNA-dependent""""///"galactose metabolic process""///nucleus"
Afu5g03240	pyruvate dehydrogenase kinase	247	mitochondrion///biological process unknown///protein kinase activity
Afu3g01840	MFS transporter	248	transporter activity///transport///integral to membrane
Afu3g14330	mating-type alpha-pheromone receptor PreB	249	response to pheromone during conjugation with cellular fusion///integral to plasma membrane///mating-type alpha-factor pheromone receptor activity///cell projection assembly
Afu3g14040	RNA polymerase II mediator complex subunit Soh1, putative	250	
Afu3g08200	alpha-mannosidase	251	carbohydrate metabolic process///alpha-mannosidase activity///vacuolar membrane
Afu1g17000	Sin3-associated polypeptide Sap18	253	
Afu6g11310	bifunctional pyrimidine biosynthesis protein (PyrABCN), putative	255	membrane///aspartate carbamoyltransferase activity///cytoplasm///carbamoyl-phosphate synthase activity///pyrimidine base biosynthetic process
Afu1g10790	alpha-1,2-mannosidase	256	

	family protein		
Afu5g11060	WD repeat protein	257	
Afu7g00380	GNAT family acetyltransferase	258	
Afu2g01180	cellobiose dehydrogenase	259	oxidoreductase activity///metabolic process
Afu7g05340	cellular morphogenesis protein (Rax2)	260	membrane///cellular bud scar///cellular bud neck///cellular bud site selection///molecular function unknown
Afu5g04190	HLH transcription factor (PalcA)	263	regulation of phosphorus utilization///transcription///transcription factor activity///nucleus///response to stress
Afu3g14700	polyketide synthase	264	polyketide biosynthetic process///polyketide synthase activity
Afu4g13770	glycosyl hydrolase	265	
Afu3g02585	integral membrane protein	266	
Afu7g01200	aspergillopepsin, putaitve	267	
Afu6g02170	metalloreductase transmembrane component	268	copper ion import///plasma membrane///"oxidoreductase activity, oxidizing metal ions"
Afu1g16540	WD40 domain protein	269	
Afu1g02140	glycogen debranching enzyme Gdb1	270	4-alpha-glucanotransferase activity///glycogen catabolic process"///cytoplasm///"""amylo-alpha-1,6-glucosidase activity""
Afu5g14250	DNA repair family protein	271	oxidoreductase activity///metabolic process

Table 10.10: 200 genes with greatest nSI decrease between 8 and 14 hours post infection. Genes are reported ranked according to greatest nSI intensity decrease between 8 and 14 hours where 1 is the greatest. Hypothetical proteins (n = 55) were removed.

ORF	Description	Rank	GO Biological Process
Afu4g03110	MFS monosaccharide transporter	1	
Afu8g00410	methionine aminopeptidase, type II	2	proteolysis///methionyl aminopeptidase activity///cytoplasm
Afu6g03420	trehalose synthase, pseudogene, similar to GB:AAC64285.1: clock-controlled gene-9 protein [Neurospora	3	

	crassa]		
Afu5g04260	arginine transporter	6	basic amino acid transmembrane transporter activity///arginine permease activity///lysine permease activity///basic amino acid transport///plasma membrane
Afu3g01030	RTA1 domain protein	7	biological process unknown///molecular function unknown///integral to membrane
Afu5g04300	WD repeat protein	8	
Afu6g08520	adenylate cyclase AcyA	9	pathogenesis///adenylate cyclase activity"///"G-protein signaling, coupled to cAMP nucleotide second messenger"""""""
Afu5g13520	ribosome biogenesis protein Ria1	10	ribosome biogenesis///cytoplasm///translation elongation factor activity
Afu1g07730	metalloprotease MEP1	11	
Afu3g09690	extracellular thaumatin domain protein	12	
Afu6g05030	polysaccharide deacetylase family protein	13	
Afu2g09890	NDT80	14	
Afu8g00560	cytochrome P450 oxidoreductase	15	oxidoreductase activity///metabolic process
Afu6g04890	CaaX prenyl proteinase Rce1	16	integral to endoplasmic reticulum membrane///protein processing///prenyl-dependent CAAX protease activity///conjugation with cellular fusion///peptide pheromone maturation
Afu7g00130	C6 transcription factor	17	
Afu7g04930	alkaline serine protease (PR1)/allergen F18-like	18	protein catabolic process///cellular component unknown///peptidase activity
Afu5g14150	lipase	19	
Afu3g08820	glycosyl hydrolase	20	cytoplasm///biological process unknown///molecular function unknown
Afu4g10140	glucoamylase/glucan 1,4-alpha-glucosidase	21	polysaccharide metabolic process""///"sporulation (sensu Saccharomyces)///fungal-type vacuole"///""""""""glucan 1,4-alpha-glucosidase activity"""""///"""""hydrolase activity, acting on glycosyl bonds"""""
Afu5g11910	DNA repair and transcription protein (Xab2)	22	cell cycle///"spliceosomal complex///"""""nuclear mRNA splicing, via spliceosome"""""""
Afu3g12320	lipase/serine esterase	23	lipid particle///biological process unknown///molecular function unknown
Afu2g05180	NF-X1 finger and helicase domain protein	24	DNA binding///DNA helicase activity///nucleus///zinc ion binding///RNA helicase activity
Afu5g14640	haloacid	25	

	dehalogenase, type II		
Afu8g04220	rRNA maturation protein (Nop14)	26	nucleolus///nucleus///maturation of SSU-rRNA///snoRNA binding///small nucleolar ribonucleoprotein complex
Afu1g04670	PSP1 domain protein	28	cytoplasm///biological process unknown///molecular function unknown
Afu1g04330	Ser/Thr protein phosphatase family protein	29	
Afu3g02120	short-chain dehydrogenase/reductase family protein, putative	30	
Afu2g13820	SAP domain protein	31	DNA binding
Afu7g05800	fructose-2,6-bisphosphatase	32	6-phosphofructo-2-kinase activity"///""fructose-2,6-bisphosphate 2-phosphatase activity""///""cytosol///gluconeogenesis
Afu8g00440	steroid monooxygenase	33	
Afu1g03380	UDP-N-acetylglucosaminyltransferase	34	
Afu3g08780	nuclear import and export protein Msn5	35	protein binding///protein export from nucleus///nucleus///importin-alpha export receptor activity
Afu8g05480	CCCH zinc finger protein	38	
Afu1g15910	C6 transcription factor RosA-like	39	RNA polymerase II transcription factor activity///nucleus///regulation of transcription
Afu5g14860	cytochrome P450	40	
Afu6g02960	NADH-ubiquinone oxidoreductase 105 kDa subunit	44	
Afu1g06250	CAIB/BAIF family enzyme	45	
Afu2g11780	C2H2 transcription factor (Crea)	47	specific RNA polymerase II transcription factor activity///cytoplasm///regulation of transcription from RNA polymerase II promoter///nucleus///zinc ion binding///glucose metabolic process
Afu4g06210	JmjC domain protein	48	DNA binding
Afu1g06030	AP-1 adaptor complex subunit gamma	49	AP-1 adaptor complex///clathrin binding///vesicle-mediated transport
Afu4g04540	C4-dicarboxylate transporter/malic acid transport protein	50	
Afu1g01530	GrpB domain protein	51	

Afu2g11170	origin recognition complex subunit Orc4	52	nuclear origin of replication recognition complex///DNA replication initiation///DNA replication origin binding///pre-replicative complex assembly
Afu2g05430	uridine kinase	53	pyrimidine salvage///cytoplasm///uridine kinase activity///nucleus
Afu1g08800	cytochrome P450 phenylacetate hydroxylase	54	oxidoreductase activity///metabolic process
Afu6g02030	aminotransferase	55	
Afu2g14750	endo-arabinase	56	
Afu8g01560	aldo-keto reductase (YakC)	57	aldo-keto reductase activity///cytoplasm///nucleus///cellular aldehyde metabolic process
Afu5g12760	CCCH zinc finger DNA binding protein	58	
Afu5g00530	inulinase	59	extracellular region///cytoplasm///sucrose catabolic process
Afu3g12900	MFS transporter	61	fungal-type vacuole membrane///monocarboxylic acid transmembrane transporter activity///transporter activity///transport
Afu3g03820	MFS nicotinic acid transporter Tna1	63	nicotinamide mononucleotide transport///nicotinamide mononucleotide permease activity///integral to plasma membrane
Afu3g11740	RNAPII degradation factor Def1	64	
Afu4g14300	dynamin family GTPase	66	
Afu1g05330	F-box domain protein	67	
Afu2g05880	ammonium transporter MeaA	69	plasma membrane///ammonium transport///ammonium transmembrane transporter activity
Afu1g14730	cell division cycle protein Cdc20	70	ubiquitin-dependent protein catabolic process///anaphase-promoting complex///mitotic metaphase/anaphase transition///cyclin catabolic process///mitotic sister chromatid segregation///mitotic spindle elongation///enzyme activator activity
Afu6g13790	flavin-binding monooxygenase	72	
Afu6g09770	geranylgeranyl diphosphate synthase	73	terpenoid biosynthetic process///farnesyltranstransferase activity///mitochondrion
Afu1g04062	RNA polymerase I specific transcription initiation factor Rrn7	74	
Afu3g13010	Zn-dependent hydrolase/oxidoreductase family	75	

	protein, putative		
Afu3g05350	histone H2B	76	nuclear nucleosome///DNA binding///chromatin assembly or disassembly
Afu1g05040	protein mitochondrial targeting protein (Mas1), putative	77	Hsp70/Hsc70 protein regulator activity///cytosol///protein targeting to mitochondrion///chaperone regulator activity///ATPase activator activity
Afu8g05170	autophagy protein Apg6	79	membrane fraction///autophagy///protein targeting to vacuole///molecular function unknown
Afu1g05560	GTP binding protein	80	GTP binding///cytoplasm///biological process unknown
Afu7g02170	cyclophilin-type peptidyl-prolyl cis-trans isomerase, putative	81	RNA binding
Afu4g13060	zinc knuckle transcription factor (CnjB)	83	
Afu6g12940	metallo-beta-lactamase domain protein	84	catalytic activity///metabolic process
Afu1g05800	MAP kinase kinase (Mkk2)	85	MAP kinase kinase activity///protein amino acid phosphorylation///signal transduction
Afu1g08790	exportin KapK	86	mRNA export from nucleus///protein export from nucleus///nucleus///ribosomal large subunit export from nucleus///protein transmembrane transporter activity
Afu4g10830	SNF2 family helicase	87	helicase activity///nucleus///""nucleotide-excision repair, DNA damage recognition""///DNA-dependent ATPase activity
Afu3g06790	RNA-directed RNA polymerase (Sad-1)	90	RNA-directed RNA polymerase activity///posttranscriptional gene silencing///cytoplasm
Afu3g07290	SD08430p	91	cellular component unknown///biological process unknown///molecular function unknown
Afu6g07910	PH domain protein	92	cellular component unknown///biological process unknown///molecular function unknown
Afu3g11830	phosphoglucomutase PgmA	93	glucose 1-phosphate utilization///cytosol///glucose 6-phosphate utilization///phosphoglucomutase activity
Afu4g10180	signal recognition particle protein	94	signal sequence binding///protein targeting to ER///""signal recognition particle, endoplasmic reticulum targeting""
Afu4g13270	unfolded protein response protein Orm1	98	endoplasmic reticulum///response to unfolded protein///molecular function unknown
Afu4g14630	FAD binding oxidoreductase	99	
Afu5g06840	class V chitinase	100	
Afu2g09150	adenosine deaminase	101	cytoplasm///adenine catabolic process///nucleus///adenine deaminase activity
Afu1g12950	Avl9 protein	102	
Afu1g04980	RNA polymerase III	103	protein binding///transcription initiation from RNA

	transcription factor TFIIIC subunit (Tfc4)		polymerase III promoter///transcription factor TFIIIC complex///RNA polymerase III transcription factor activity
Afu4g12830	vacuolar protein sorting-associated protein Vps5, putative	105	
Afu6g04080	conserved hypotetical protein	108	biological process unknown///molecular function unknown
Afu1g07080	tRNA-specific adenosine-34 deaminase subunit Tad3, putative	109	zinc ion binding
Afu1g15950	MAP kinase kinase (Pbs2)	110	MAP kinase kinase activity///activation of MAPK activity involved in osmosensory signaling pathway///osmosensory signaling pathway///protein amino acid phosphorylation
Afu1g15440	alpha-1,3-glucan synthase Ags3	111	cellular glucan metabolic process///fungal-type cell wall biogenesis///plasma membrane///pathogenesis///"alpha-1,3-glucan synthase activity"///cell morphogenesis
Afu6g07580	essential cytoplasmic protein Ctr86	112	cytoplasm///biological process unknown///molecular function unknown
Afu5g13190	kinesin family protein	113	kinesin complex///microtubule motor activity///establishment of mitotic spindle orientation///cytoplasmic microtubule///nuclear migration along microtubule///microtubule depolymerization///nuclear microtubule///mitotic spindle organization in nucleus
Afu6g07730	plasma membrane antiporter	114	cellular monovalent inorganic cation homeostasis///plasma membrane///cation:cation antiporter activity
Afu6g14390	extracelular cellulose binding protein (Cip2)	115	
Afu2g01090	DNA helicase	116	DNA helicase activity///lagging strand elongation///alpha DNA polymerase:primase complex
Afu1g00100	MFS monocarboxylate transporter	117	
Afu3g12450	DIL and Ankyrin domain protein	119	cellular component unknown///biological process unknown///molecular function unknown
Afu2g12780	von Willebrand domain protein	120	
Afu4g06400	pH signal transduction protein PalA	121	proteolysis///invasive growth///protein processing///cytoplasm///nucleus///sporulation resulting in formation of a cellular spore///molecular function unknown
Afu6g10620	nuclear pore complex subunit	122	nuclear pore///protein import into nucleus///nuclear envelope organization///nuclear pore organization///ribosomal protein import into nucleus///mRNA export from nucleus///tRNA export

			from nucleus///NLS-bearing substrate import into nucleus///structural molecule activity///rRNA export from nucleus///protein export from nucleus///mRNA-binding (hnRNP) protein import into nucleus///snRNA export from nucleus///snRNP protein import into nucleus
Afu5g10760	alpha-1,2-mannosyltransferase (Kre2)	123	Golgi apparatus""///protein amino acid O-linked glycosylation"///cell wall mannoprotein biosynthetic process///"alpha-1,2-mannosyltransferase activity"""""///""N-glycan processing
Afu7g05580	phospholipase PldA	124	phospholipase D activity///phospholipid metabolic process///response to osmotic stress
Afu1g09820	DUF1339 domain protein	125	
Afu6g10680	XAP5 domain protein	126	
Afu2g06060	transcriptional co-activator (Hfi1/Ada1)	129	
Afu1g15940	Auxin Efflux Carrier superfamily	130	endoplasmic reticulum///biological process unknown///molecular function unknown
Afu4g05850	malonyl CoA-acyl carrier protein transacylase	131	
Afu7g02620	DNA-directed RNA polymerases N/8 kDa subunit superfamily	133	DNA-directed RNA polymerase II, core complex""///"DNA-directed RNA polymerase III complex///transcription from RNA polymerase I promoter"///DNA-directed RNA polymerase I complex///transcription from RNA polymerase II promoter///transcription from RNA polymerase III promoter///DNA-directed RNA polymerase activity
Afu4g06200	flavin-binding monooxygenase	134	
Afu1g12080	RING finger ubiquitin ligase (Tul1)	135	intracellular///ligase activity///protein transport
Afu4g13810	F-box domain protein	136	
Afu2g09030	secreted dipeptidyl peptidase DppV	138	proteolysis///serine-type peptidase activity
Afu6g07860	catabolite repressor protein (CreC)	139	negative regulation of transcription by carbon catabolites
Afu3g11760	MFS transporter	140	transporter activity///transport///integral to membrane
Afu3g06170	mating type protein MAT1-2-1	141	
Afu4g14350	kelch repeat protein	142	
Afu6g12040	MFS sugar permease	143	alpha-glucoside:hydrogen symporter activity///membrane fraction///alpha-glucoside transport///trehalose transport///trehalose transmembrane transporter

			activity///maltose:hydrogen symporter activity
Afu6g09240	protein kinase	144	
Afu4g10130	alpha-amylase	145	extracellular region///alpha-amylase activity///polysaccharide catabolic process
Afu7g03760	phosphatidylinositol 4-kinase (STT4)	146	protein secretion///plasma membrane///phosphatidylethanolamine biosynthetic process///1-phosphatidylinositol 4-kinase activity///MAPKKK cascade///actin cytoskeleton organization
Afu2g14710	arsenite resistance protein Ars2	147	
Afu6g09300	C2H2 finger domain protein	148	
Afu3g03330	mitochondrial enoyl reductase	149	aerobic respiration///fatty acid biosynthetic process///mitochondrion///enoyl-[acyl-carrier-protein] reductase activity
Afu6g11250	C2H2 finger domain protein	150	
Afu3g07670	transcription elongation factor S-II	152	reciprocal meiotic recombination///RNA elongation from RNA polymerase II promoter///nucleoplasm///positive transcription elongation factor activity
Afu2g13310	RING finger domain protein	153	zinc ion binding
Afu6g05150	transcriptional repressor TupA/RocA	155	negative regulation of transcription///nucleus///general transcriptional repressor activity
Afu3g05400	DnaJ and TPR domain protein	156	peripheral to membrane of membrane fraction///co-chaperone activity///endoplasmic reticulum///protein folding///karyogamy during conjugation with cellular fusion
Afu1g08770	C6 finger domain protein	157	zinc ion binding
Afu2g10430	AAR2 family protein	159	
Afu1g04210	IQ and HECT domain protein	160	ubiquitin-protein ligase activity///cytoplasm///protein polyubiquitination///protein monoubiquitination///nucleus
Afu2g15030	C-3 sterol dehydrogenase/C-4 decarboxylase	161	C-3 sterol dehydrogenase (C-4 sterol decarboxylase) activity///endoplasmic reticulum///ergosterol biosynthetic process///endoplasmic reticulum membrane
Afu5g00670	beta-galactosidase	163	
Afu6g08560	NRPS-like enzyme	164	oxidoreductase activity///nonribosomal peptide biosynthetic process///amino acid activation for nonribosomal peptide biosynthetic process///cytoplasm///amino acid adenylylation by nonribosomal peptide synthase
Afu2g11220	proline permease	166	plasma membrane///neutral amino acid transmembrane transporter activity///neutral amino acid transport///amino acid permease activity
Afu5g09460	ABC transporter	167	transporter activity///transport

Afu6g11200	DENN (AEX-3) domain protein	168	
Afu4g01020	sensor histidine kinase/response regulator	170	protein histidine kinase activity///protein amino acid phosphorylation///two-component sensor activity
Afu3g05760	C6 transcription factor (Fcr1)	173	transcription factor activity///nucleus///zinc ion binding///regulation of transcription
Afu4g12750	transcription factor	174	3'-5'-exoribonuclease activity///cytoplasm///nuclear-transcribed mRNA poly(A) tail shortening///regulation of transcription from RNA polymerase II promoter///"nuclear-transcribed mRNA catabolic process, deadenylation-dependent decay"///CCR4-NOT core complex
Afu1g03230	ABC multidrug transporter	175	
Afu8g04060	beta-N-acetylglucosaminidase	176	beta-N-acetylglucosaminidase activity///N-acetylglucosamine catabolic process
Afu5g00370	amino acid permease	177	basic amino acid transmembrane transporter activity///basic amino acid transport///plasma membrane
Afu2g15340	AflR-like C6 transcription factor	178	
Afu6g13290	SWI/SNF family DNA-dependent ATPase Ris1	179	mating type switching///chromatin assembly or disassembly///nucleus///DNA-dependent ATPase activity
Afu5g11780	TOR signalling pathway regulator (TapA)	180	cellular component unknown///cell growth and/or maintenance///protein binding///signal transduction
Afu1g09670	HLH transcription factor (GlcD gamma)	181	transcription///transcription factor activity///nucleus
Afu2g05850	double-strand-break repair protein rad21	182	nuclear cohesin complex///mitotic sister chromatid cohesion///mitotic chromosome condensation///molecular function unknown
Afu5g14660	GABA permease	183	plasma membrane///choline transport///choline transmembrane transporter activity
Afu1g01110	polyketide synthase	184	
Afu5g08910	3-methylcrotonyl-CoA carboxylase subunit alpha (MccA), putative	185	cytoplasm///leucine catabolic process
Afu2g13780	splicing factor 3B subunit 1	187	
Afu4g04720	nuclear pore protein (Nic96)	188	
Afu5g00470	general amidase GmdB	189	cellular component unknown///amidase activity///biological process unknown
Afu5g08580	alpha-1,6-mannosyltransferase subunit (Och1)	191	cell wall mannoprotein biosynthetic process""///""""""""alpha-1,6-mannosyltransferase complex"""""///N-glycan processing///substituted

			mannan metabolic process///"alpha-1,6-mannosyltransferase activity"""""
Afu5g06470	serine/threonine protein kinase	192	protein serine/threonine kinase activity///protein amino acid phosphorylation///nucleus
Afu6g07190	NmrA-like family protein	194	
Afu1g07690	protein O-mannosyl transferase	195	endoplasmic reticulum///dolichyl-phosphate-mannose-protein mannosyltransferase activity///protein amino acid O-linked glycosylation
Afu3g13460	F-box domain protein	197	
Afu2g09960	mitochondrial Hsp70 chaperone (Ssc70)	198	protein transporter activity///mitochondrial translocation///mitochondrial inner membrane///enzyme regulator activity///protein folding///ATPase activity///mitochondrion///heat shock protein activity
Afu6g13680	APSES transcription factor Xbp1	199	
Afu2g02110	MFS monosaccharide transporter	200	membrane///transporter activity///transport
Afu4g14570	metallo-beta-lactamase domain protein	201	catalytic activity///metabolic process
Afu1g07540	26S proteasome regulatory particle subunit Rpn8, putative	202	endopeptidase activity""///"proteasome regulatory particle, lid subcomplex"""""///""ubiquitin-dependent protein catabolic process"
Afu5g12990	Snf1 protein kinase complex subunit Snf4	203	
Afu3g14110	nicotinamide N-methyltransferase Nnt1	205	nicotinamide N-methyltransferase activity///nicotinamide metabolic process///chromatin silencing at rDNA///cytoplasm
Afu5g04270	AMP-binding enzyme	206	N-terminal protein myristoylation///lipid metabolic process///peroxisome///long-chain-fatty-acid-CoA ligase activity
Afu1g00440	DUF895 domain membrane protein	207	integral to membrane
Afu2g06080	GTPase activating protein (Gyp1)	209	
Afu4g14790	cytochrome P450 monooxygenase	210	
Afu4g10120	C6 finger domain protein	212	DNA binding///zinc ion binding
Afu4g07110	SNARE domain protein	213	Golgi to vacuole transport///endosome///t-SNARE activity///Golgi apparatus
Afu7g01640	C6 transcription factor (War1)	214	transcription factor activity///nucleus///response to acid///regulation of transcription
Afu4g13080	MFS monosaccharide transporter	216	membrane///transporter activity///transport

Afu2g03360	polarized growth protein (Boi2)	217	Rho protein signal transduction///phospholipid binding///cell morphogenesis
Afu8g05860	aromatic amino acid and leucine permease	218	amino acid transport///plasma membrane///amino acid permease activity///amino acid transmembrane transporter activity
Afu2g13430	chitin synthase	219	chitin synthase activity///chitin biosynthetic process
Afu3g11220	ribonuclease T2 family	220	RNA catabolic process///extracellular region///endoribonuclease activity///cell morphogenesis
Afu5g07760	tetracycline-efflux transporter	221	cellular component unknown///biological process unknown///molecular function unknown
Afu5g08960	triglyceride lipase-cholesterol esterase	222	lipase activity///lipid particle///lipid metabolic process
Afu5g07160	DUF636 domain protein	223	
Afu2g00150	catecholamine-O-methyltransferase	225	
Afu4g06990	amino acid transporter	226	endoplasmic reticulum///transporter activity///transport
Afu3g07050	WSC domain protein	230	
Afu8g02040	glycosyl transferase	231	N-linked glycoprotein maturation///"transferase activity, transferring glycosyl groups"
Afu1g06650	actin filament organization protein App1-like	233	actin filament organization///actin cortical patch (sensu Saccharomyces)///actin cytoskeleton organization///molecular function unknown///actin cytoskeleton
Afu5g08010	protein N-terminal asparagine amidohydrolase	234	protein catabolic process///protein N-terminal asparagine amidohydrolase activity///protein modification process///mitochondrion
Afu3g08030	tRNA (guanine) methyltransferase Trm5	235	tRNA (guanine) methyltransferase activity///cytoplasm///nucleus///tRNA methylation
Afu2g04720	ubiquitin C-terminal hydrolase	236	protein deubiquitination///cytoplasm///ubiquitin-specific protease activity
Afu5g00710	GABA permease	237	plasma membrane///choline transport///choline transmembrane transporter activity
Afu7g03800	C2 domain protein	240	
Afu8g05960	integral membrane protein	241	
Afu4g04070	mucin family signaling protein Msb2	242	
Afu1g12940	MAP kinase SakA	243	osmosensory signaling pathway///protein amino acid phosphorylation///response to stress///MAP kinase activity///positive regulation of transcription from RNA polymerase II promoter
Afu1g14690	ubiquitin-protein ligase Sel1/Ubx2	245	
Afu6g09930	bZIP transcription factor AP-1/Yap1	246	response to drug///response to oxidative stress///cytoplasm///transcription///transcription

			factor activity///nucleus
Afu3g02330	chromatin remodeling complex subunit (Arp9)	247	chromatin remodeling///nucleosome remodeling complex///RSC complex///regulation of transcription///SWI/SNF complex
Afu5g02150	proteasome component Pre6	248	proteasome core complex///endopeptidase activity"""///"""proteasome core complex, alpha-subunit complex"""///"ubiquitin-dependent protein catabolic process
Afu2g00880	C6 finger domain protein	250	
Afu1g17550	HET domain protein	251	
Afu1g07140	c-24(28) sterol reductase	254	delta24(24-1) sterol reductase activity///endoplasmic reticulum///ergosterol biosynthetic process
Afu4g08410	mannose-6-phosphate isomerase, class I	255	mannose-6-phosphate isomerase activity///protein amino acid glycosylation///cytoplasm///GDP-mannose biosynthetic process///nucleus///cell wall mannoprotein biosynthetic process

10.3.7 Functional classification of time-point specifc datasets for Af293 murine infection

Differentially expressed genes were grouped into functional categories based on GO Terms and by reference to the *A. fumigatus* literature. A summary of up and down expressed functional categories identified for 4 – 8 and 8 – 14 hours post infection are reported in Tables 10.11 and 10.12 respectively.

Table 10.11: Functional classification of selected genes having differential transcript abundance in Af293 between 4 and 8 hours post infection in the murine lung. Upregulated (red) and downregulated genes (green) are shown for each functional category. Both increasing and decreasing transcripts are sub divided into expression cohorts which are either high, moderate, or low with respect to their expression change. Genes within functional categories are ranked according to greatest nSI intensity changes between 4 and 8 hours.

Functional Category	ORF	Description	Rank	Magnitude	ORF	Description	Rank	Magnitude
Cell wall	Afu8g06030	alpha-1,3-glucanase	50	UP HIGH	Afu6g09310	class V chitinase	68	DOWN HIGH
	Afu4g13360	endo-1,3(4)-beta-glucanase	73	UP HIGH	Afu5g11990	alpha-1,3-mannosyltransferase (Alg3)	196	DOWN HIGH
	Afu5g08580	alpha-1,6-mannosyltransferase subunit (Och1)	553	UP HIGH	Afu7g05140	class III chitinase	309	DOWN HIGH
	Afu2g05340	1,3-beta-glucanosyltransferase	626	UP HIGH	Afu6g14480	alpha-1,3-mannosyltransferase	319	DOWN HIGH
	Afu2g13430	chitin synthase	658	UP HIGH	Afu6g10430	chitin deacetylase	532	DOWN HIGH
	Afu5g14190	beta-glucanase	743	UP MOD	Afu2g06160	alpha-1,3-glucanase/mutanase	616	DOWN HIGH
	Afu2g01170	1,3-beta-glucanosyltransferase Gel1	848	UP MOD	Afu7g01540	endo-1,4-beta-glucanase	636	DOWN HIGH
	Afu7g08510	extracellular alpha-1,3-glucanase/mutanase	1082	UP MOD	Afu3g05580	chitin synthase activator (Chs3)	753	DOWN MOD
	Afu8g00700	class III chitinase ChiA2	1429	UP LOW	Afu1g00310	class V chitinase	897	DOWN MOD
	Afu3g06690	Rho GTPase Rho3	1430	UP LOW	Afu8g01410	class V chitinase ChiB1	936	DOWN MOD

	Afu6g02510	chitin biosynthesis protein (Chs5)	1604	UP LOW	Afu1g12600	chitin synthase D	938	DOWN MOD
	Afu4g09940	polysaccharide deacetylase family protein	1612	UP LOW	Afu5g03530	class III chitinase	1047	DOWN MOD
	Afu2g12850	1,3-beta-glucanosyltransferase Gel3	1986	UP LOW	Afu1g15440	alpha-1,3-glucan synthase Ags3	1075	DOWN MOD
					Afu5g03940	alpha-1,3-glucanase	1154	DOWN MOD
					Afu1g04260	endo-1,3-beta-glucanase Engl1	1391	DOWN LOW
					Afu6g12410	1,3-beta-glucanosyltransferase	1429	DOWN LOW
					Afu5g00760	chitin synthase C	1554	DOWN LOW
					Afu1g01380	alpha-1,6-mannosyltransferase subunit (Hoc1)	1816	DOWN LOW
Ergosterol biosynthesis	Afu1g04720	C-8 sterol isomerase (Erg-1)	23	UP HIGH	Afu2g03700	HMG-CoA reductase	12	DOWN HIGH
	Afu3g11750	oxysterol binding protein (Osh5)	486	UP HIGH	Afu1g03150	c-14 sterol reductase	18	DOWN HIGH
	Afu2g15030	C-3 sterol dehydrogenase/C-4 decarboxylase	608	UP HIGH	Afu6g05140	sterol delta 5,6-desaturase ERG3	223	DOWN HIGH
	Afu2g03790	oxysterol binding protein (Osh7)	749	UP MOD	Afu4g12040	lanosterol synthase	273	DOWN HIGH
	Afu4g07780	mevalonate kinase	888	UP MOD	Afu2g17400	C-3 sterol dehydrogenase/C-4 decarboxylase family protein	1885	DOWN LOW
	Afu7g02480	oxysterol binding protein (Osh1)	932	UP MOD				
	Afu2g02220	UDP-glucose:sterol	947	UP MOD				

		glycosyltransferase					
	Afu4g09190	S-adenosyl-methionine-sterol-C-methyltransferas	992	UP MOD			
	Afu4g06380	sterol carrier protein	998	UP MOD			
	Afu1g11140	Sterol desaturase family	1240	UP MOD			
	Afu1g07140	c-24(28) sterol reductase	1264	UP MOD			
Microtubule	Afu2g03150	kinesin family protein	4	UP HIGH	Afu2g15750	gamma-tubulin complex component GCP4	596	DOWN HIGH
	Afu2g14990	tubulin subunit TubB	357	UP HIGH	Afu2g14730	kinesin family protein	1911	DOWN LOW
	Afu4g07630	microtubule associated protein (Ytm1)	634	UP HIGH				
	Afu5g13190	kinesin family protein	683	UP HIGH				
	Afu7g00250	tubulin beta subunit	740	UP MOD				
	Afu2g08190	tubulin-specific chaperone Rbl2	1384	UP LOW				
	Afu5g11940	tubulin-specific chaperone D	1562	UP LOW				
	Afu1g04850	dynein light chain type 1	2040	UP LOW				
Cell polarity	Afu1g07580	cell polarity protein (Alp11)	1099	UP MOD	Afu7g02280	U5 snRNP complex subunit	1156	DOWN MOD
	Afu1g09950	casein kinase 2 beta' regulatory subunit Ckb2	1399	UP LOW	Afu5g12850	cell morphogenesis protein Las1	1462	DOWN LOW

	Afu5g09710	separin	1448	UP LOW				
	Afu5g08540	septin AspA	1514	UP LOW				
Ion transport	Afu3g13790	cation transporting ATPase	314	UP HIGH	Afu2g05860	calcium/mangenease P-type ATPase	96	DOWN HIGH
	Afu3g13790	cation transporting ATPase	314	UP HIGH	Afu1g17470	high affinity nitrate transporter NrtB	475	DOWN HIGH
	Afu2g09460	potassium transporter	334	UP HIGH	Afu2g08740	ZIP metal ion transporter	569	DOWN HIGH
	Afu6g00470	plasma membrane zinc ion transporter	345	UP HIGH	Afu8g04010	ZIP family zinc transporter	828	DOWN MOD
	Afu6g00470	plasma membrane zinc ion transporter	345	UP HIGH	Afu3g10690	calcium-translocating P-type ATPase(PMCA-type),putative	1712	DOWN LOW
	Afu6g14170	CDF zinc transporter (Msc2), putaitve	1080	UP MOD	Afu1g11110	calcium channel subunit Cch1	1924	DOWN LOW
	Afu3g12740	copper resistance-associated P-type ATPase	1842	UP LOW	Afu1g04270	calcium ion transporter Vcx1	2017	DOWN LOW
	Afu7g06350	sodium/phosphate symporter	1901	UP LOW	Afu3g13660	Ctr copper transporter family protein	2038	DOWN LOW
Iron acquisition	Afu3g09970	vacuolar iron transporter Ccc1	256	UP HIGH	Afu1g16040	ferric-chelate reductase	53	DOWN HIGH
	Afu7g06060	siderochrome-iron transporter Sit1	698	UP MOD	Afu1g04450	siderophore biosynthesis protein	166	DOWN HIGH
	Afu3g03390	siderophore biosynthesis lipase/esterase	1492	UP LOW	Afu3g13670	siderochrome-iron transporter	170	DOWN HIGH
	Afu3g10820	ferric-chelate reductase	1526	UP LOW	Afu3g01360	siderochrome-iron transporter	337	DOWN HIGH

	Afu5g03800	high-affinity iron transporter FtrA	1853	UP LOW	Afu7g04730	siderochrome-iron transporter	547	DOWN HIGH
					Afu5g03790	ferrooxidoreductase Fet3	684	DOWN MOD
					Afu4g03940	ferric-chelate reductase	933	DOWN MOD
					Afu3g03640	MFS siderochrome iron transporter MirB	1485	DOWN LOW
					Afu5g11260	siderophore transcription factor SreA	1711	DOWN LOW
Antigen	Afu7g04930	alkaline serine protease (PR1)/allergen F18-like	268	UP HIGH	Afu5g13300	aspartic endopeptidase Pep1/aspergillopepsin F	737	DOWN MOD
	Afu1g07440	molecular chaperone Hsp70	507	UP HIGH	Afu6g02280	allergen Asp F3	904	DOWN MOD
	Afu5g01440	allergen	528	UP HIGH	Afu2g11850	60S ribosomal protein L3	1749	DOWN LOW
	Afu7g05740	malate dehydrogenase, NAD-dependent	1204	UP MOD				
	Afu4g03240	cell wall serine-threonine-rich galactomannoprotein Mp1	1221	UP MOD				
	Afu4g09090	thioredoxin	1310	UP MOD				
	Afu6g11430	aldehyde dehydrogenase AldA	1368	UP LOW				
	Afu5g02040	extracellular lipase	1566	UP LOW				
	Afu1g12610	Hsp70 chaperone Hsp88	1962	UP LOW				

629

Secreted proteases	Afu3g08930	tripeptidyl peptidase SED3	13	UP HIGH	Afu3g12210	carboxypeptidase Y	375	DOWN HIGH
	Afu2g17330	extracelular serine carboxypeptidase	185	UP HIGH	Afu4g14000	tripeptidyl peptidase A	722	DOWN MOD
	Afu1g17400	peptidase S41 family protein	499	UP HIGH	Afu5g07330	carboxypeptidase S1	727	DOWN MOD
	Afu1g07730	metalloprotease MEP1	795	UP MOD	Afu5g13300	aspartic endopeptidase Pep1/aspergillopepsin F	737	DOWN MOD
	Afu2g01250	serine peptidase	934	UP MOD	Afu8g04120	carboxypeptidase S1	929	DOWN MOD
	Afu1g08940	pheromone processing carboxypeptidase KexA	1045	UP MOD				
	Afu3g11400	aspartic endopeptidase Pep2	1299	UP MOD				
	Afu6g13540	carboxypeptidase CpyA/Prc1	1328	UP MOD				
	Afu4g12970	pheromone processing endoprotease KexB	1500	UP LOW				
	Afu4g12970	pheromone processing endoprotease KexB	1500	UP LOW				
	Afu2g00220	aminopeptidase	1576	UP LOW				
	Afu4g03490	tripeptidyl-peptidase (TppA)	1710	UP LOW				
Secretion peptide encoding genes	Afu6g12760	GPI transamidase component (GAA1)	80	UP HIGH	Afu6g09310	class V chitinase	68	DOWN HIGH

Afu4g00620	cell wall glycosyl hydrolase Dfg5	116	UP HIGH	Afu5g08180	cell wall protein	146	DOWN HIGH
Afu6g00500	chitosanase	119	UP HIGH	Afu6g10580	GPI anchored CFEM domain protein	278	DOWN HIGH
Afu3g03060	cell wall protein PhiA	276	UP HIGH	Afu8g02060	glycan biosynthesis protein (PigL)	300	DOWN HIGH
Afu1g13760	cell wall anchored protein	405	UP HIGH	Afu7g05140	class III chitinase	309	DOWN HIGH
Afu3g13880	extracellular lipase	543	UP HIGH	Afu2g00400	cell wall cysteine-rich protein	380	DOWN HIGH
Afu2g05340	1,3-beta-glucanosyltransferase	626	UP HIGH	Afu4g06640	acid sphingomyelinase	460	DOWN HIGH
Afu1g09650	GPI anchored protein	719	UP MOD	Afu4g01070	acid phosphatase	497	DOWN HIGH
Afu1g09650	GPI anchored protein	719	UP MOD	Afu6g09540	endoglucanase	761	DOWN MOD
Afu2g01170	1,3-beta-glucanosyltransferase Gel1	848	UP MOD	Afu6g09910	glutaminase	780	DOWN MOD
Afu6g09520	lipase/esterase family protein	924	UP MOD	Afu4g08280	glutaminyl cyclase	1027	DOWN MOD
Afu3g01800	GPI anchored dioxygenase	1205	UP MOD	Afu5g03530	class III chitinase	1047	DOWN MOD
Afu3g01800	GPI anchored dioxygenase	1205	UP MOD	Afu6g03230	cell wall glucanase/allergen F16-like	1259	DOWN MOD
Afu5g14150	lipase	1212	UP MOD	Afu2g17540	conidial pigment biosynthesis oxidase Abr1/brown 1	1331	DOWN MOD
Afu8g00700	class III chitinase ChiA2	1429	UP LOW	Afu6g12410	1,3-beta-glucanosyltransferase	1429	DOWN LOW
Afu3g08990	cell surface protein	1452	UP LOW	Afu8g06830	endoglucanase	1439	DOWN LOW
Afu5g02040	extracellular lipase	1566	UP LOW	Afu5g01330	acid phosphatase AphA	1559	DOWN LOW
Afu6g03560	IgE-binding	1695	UP LOW	Afu2g03870	FKBP-type peptidyl-prolyl	1717	DOWN

631

		protein				isomerase		LOW
	Afu3g12010	high-affinity hexose transporter	1704	UP LOW	Afu1g03630	GPI anchored serine-threonine rich protein	1961	DOWN LOW
	Afu3g12010	high-affinity hexose transporter	1704	UP LOW				
Pathogenesis	Afu1g14660	regulator of secondary metabolism LaeA	151	UP HIGH	Afu5g13300	aspartic endopeptidase Pep1/aspergillopepsin F	737	DOWN MOD
	Afu3g02270	mycelial catalase Cat1	406	UP HIGH	Afu6g02280	allergen Asp F3	904	DOWN MOD
	Afu6g08520	adenylate cyclase AcyA	684	UP MOD	Afu1g15440	alpha-1,3-glucan synthase Ags3	1075	DOWN MOD
	Afu3g12960	cytochrome P450 monooxigenase GliC-like	1229	UP MOD				
	Afu6g10240	sensor histidine kinase/response regulator Fos-1/TcsA	1332	UP MOD				
	Afu6g04820	para-aminobenzoate synthase PabaA	1347	UP MOD				
	Afu8g02750	rRNA processing protein CgrA	1489	UP LOW				
Secondary metabolism	Afu5g12730	nonribosomal peptide synthase	11	UP HIGH	Afu3g12910	O-methyltransferase GliM-like	125	DOWN HIGH
	Afu8g00350	hypothetical protein	641	UP HIGH	Afu3g14700	polyketide synthase	143	DOWN HIGH
	Afu8g00710	secreted antimicrobial peptide	742	UP MOD	Afu6g09630	C6 finger domain protein GliZ	164	DOWN HIGH

	Afu3g02590	C6 transcription factor	835	UP MOD	Afu3g01410	polyketide synthase	182	DOWN HIGH
	Afu2g17580	conidial pigment biosynthesis scytalone dehydratase Arp1	1067	UP MOD	Afu4g14680	C6 transcription factor	183	DOWN HIGH
	Afu6g09720	methyltransferase GliN	1068	UP MOD	Afu8g00370	polyketide synthase	236	DOWN HIGH
	Afu3g12890	C6 transcription factor GliZ-like	1089	UP MOD	Afu1g17710	C6 transcription factor	329	DOWN HIGH
	Afu3g12960	cytochrome P450 monooxigenase GliC-like	1229	UP MOD	Afu8g00170	nonribosomal brevianamide peptide synthase FtmA	526	DOWN HIGH
	Afu6g03390	glutathione S-transferase family protein	1402	UP LOW	Afu3g12940	C6 transcription factor	716	DOWN MOD
	Afu3g13750	hypothetical protein	1434	UP LOW	Afu4g14590	C6 transcription factor	829	DOWN MOD
	Afu3g14710	toxin biosynthesis proten (Fum3)	1512	UP LOW	Afu2g17970	ergot alkaloid biosynthetic protein A	1140	DOWN MOD
	Afu4g14520	toxin biosynthesis protein	1543	UP LOW				
	Afu6g09650	membrane dipeptidase GliJ	1568	UP LOW				
	Afu7g00160	polyketide synthase	1665	UP LOW				
	Afu8g00130	hypothetical protein	1789	UP LOW				
	Afu3g14740	hypothetical protein	1805	UP LOW				
Ribosome biogenesis and RNA metabolism	Afu5g12270	rRNA processing protein (Ebp2)	160	UP HIGH	Afu4g07640	40S ribosomal protein S13	20	DOWN HIGH

Afu2g16880	60S ribosomal protein L37a	272	UP HIGH
Afu1g12570	RNA binding protein Ligatin/Tma64	395	UP HIGH
Afu6g10320	ribosome biogenesis protein (Rrb1)	476	UP HIGH
Afu1g09200	ribosome biogenesis protein Erb1	513	UP HIGH
Afu3g04110	rRNA processing protein Bystin	518	UP HIGH
Afu5g10830	RNA helicase-like splicing factor (HRH1)	547	UP HIGH
Afu6g05200	60S ribosomal protein L28	607	UP HIGH
Afu3g06960	60S ribosomal protein L21	722	UP MOD
Afu1g04062	RNA polymerase I specific transcription initiation factor Rrn7	736	UP MOD
Afu6g10370	RNA lariat debranching enzyme	805	UP MOD
Afu3g14550	RNA polymerase II general transcription and DNA repair factor TFIIH component Tfb5	874	UP MOD

Afu1g10990	ribosomal RNA processing protein	73	DOWN HIGH
Afu2g01900	RNA polymerase II transcription elongation factor Rtf1p	153	DOWN HIGH
Afu4g07570	60S ribosome biogenesis protein Mak11	413	DOWN HIGH
Afu4g03650	ribosome associated DnaJ chaperone Zuotin	469	DOWN HIGH
Afu5g04240	RNA binding protein Nrd1	525	DOWN HIGH
Afu8g05280	RNA interference and gene silencing protein (Qde2), putative	568	DOWN HIGH
Afu5g09060	RNA binding protein	598	DOWN HIGH
Afu3g06250	RNA polymerase II mediator complex component Srb8, putative	613	DOWN HIGH
Afu3g13310	ribosomal protein S15	642	DOWN HIGH
Afu3g05840	RNA binding protein Rnp24	822	DOWN MOD
Afu3g06640	40S ribosomal protein S27	824	DOWN MOD

Afu1g02630	rRNA processing protein Pwp1	915	UP MOD
Afu3g11820	RNA exonuclease Rex2	1058	UP MOD
Afu2g04130	40S ribosomal protein S11	1078	UP MOD
Afu2g10300	40S ribosomal protein S17	1150	UP MOD
Afu8g02730	RNA binding protein Tma22	1195	UP MOD
Afu2g03590	40S ribosomal protein S21	1224	UP MOD
Afu6g02440	60S ribosomal protein L24a	1261	UP MOD
Afu2g10440	40S ribosomal protein S11	1441	UP LOW
Afu8g02750	rRNA processing protein CgrA	1489	UP LOW
Afu4g08190	ribosome biogenesis protein Pescadillo	1513	UP LOW

Afu5g02160	RNA binding protein (Arp)	944	DOWN MOD
Afu2g07460	RNA polymerase II transcriptional coactivator	997	DOWN MOD
Afu4g11690	RNA polymerase II transcription factor related protein	1005	DOWN MOD
Afu1g14410	60S ribosomal protein L17	1024	DOWN MOD
Afu5g08330	RNA binding protein	1036	DOWN MOD
Afu1g04660	60S ribosomal protein L15	1124	DOWN MOD
Afu6g13330	RNA binding protein	1195	DOWN MOD
Afu2g13350	RNA polymerase II transcription mediator complex subunit Srb7	1213	DOWN MOD
Afu1g05990	ribosomal protein L16a	1214	DOWN MOD
Afu2g09200	60S ribosomal protein L30	1336	DOWN MOD
Afu2g02150	40S ribosomal protein S10a	1350	DOWN MOD
Afu4g08360	RNA polymerase II mediator complex component Med8, putative	1546	DOWN LOW
Afu6g09060	60S ribosomal protein L6	1607	DOWN LOW
Afu2g11850	60S ribosomal protein L3	1749	DOWN LOW
Afu1g02210	60S ribosome biogenesis protein Brx1	1878	DOWN LOW

					Afu1g06770	40S ribosomal protein S26	1890	DOWN LOW
					Afu2g08170	RNA polymerase II transcription factor SIII (Elongin) subunit A	1940	DOWN LOW
Sugar transport	Afu1g02530	MFS sugar transporter	1020	UP MOD	Afu6g08100	nucleotide-sugar transporter	3	DOWN HIGH
	Afu3g12580	MFS sugar transporter protein	1083	UP MOD	Afu2g04550	MFS sugar transporter	24	DOWN HIGH
	Afu4g03110	MFS monosaccharide transporter	1355	UP MOD	Afu7g05550	sugar transporter family protein	39	DOWN HIGH
	Afu1g16390	MFS hexose transporter	1365	UP MOD	Afu8g01180	MFS sugar transporter	85	DOWN HIGH
	Afu2g15410	MFS sugar transporter	1596	UP LOW	Afu5g00280	MFS sugar transporter	245	DOWN HIGH
	Afu3g12010	high-affinity hexose transporter	1704	UP LOW	Afu7g01740	sugar transporter	286	DOWN HIGH
	Afu3g00200	hexose transporter protein	1744	UP LOW	Afu1g03280	MFS alpha-glucoside transporter	342	DOWN HIGH
	Afu1g11050	MFS sugar transporter	1868	UP LOW	Afu4g00150	MFS maltose transporter	368	DOWN HIGH
					Afu2g08120	MFS monosaccharide transporter (Hxt8)	377	DOWN HIGH
					Afu4g01340	MFS monosaccharide transporter	430	DOWN HIGH
					Afu3g12720	sugar transporter-like protein	489	DOWN HIGH
					Afu3g01670	MFS hexose transporter	563	DOWN HIGH

					Afu3g06730	MFS sugar transporter	654	DOWN HIGH
					Afu4g06630	MFS monosaccharide transporter	706	DOWN MOD
					Afu7g05190	MFS alpha-glucoside transporter	863	DOWN MOD
					Afu3g02890	MFS sugar transporter	875	DOWN MOD
					Afu8g06870	MFS sugar transporter	919	DOWN MOD
					Afu3g01700	MFS alpha-glucoside transporter	963	DOWN MOD
					Afu7g06390	MFS maltose permease MalP	1045	DOWN MOD
					Afu6g14590	MFS alpha-glucoside transporter	1165	DOWN MOD
					Afu5g02840	MFS sugar transporter	1204	DOWN MOD
					Afu1g07700	MFS monosaccharide transporter	1450	DOWN LOW
					Afu3g13980	MFS glucose transporter	1758	DOWN LOW
					Afu3g00220	MFS sugar transporter	1959	DOWN LOW
Amino acid transport	Afu1g14700	MFS allantoate transporter	485	UP HIGH	Afu2g17480	amino acid transporter	15	DOWN HIGH
	Afu4g00830	MFS peptide transporter	498	UP HIGH	Afu5g02790	amino acid permease	89	DOWN HIGH
	Afu2g10560	amino acid permease	657	UP HIGH	Afu3g01820	amino acid permease	402	DOWN HIGH
	Afu5g01510	amino acid permease	675	UP HIGH	Afu4g03220	amino acid permease	403	DOWN HIGH

	Afu2g11220	proline permease	681	UP HIGH	Afu3g00120	amino acid transporter (Mtr)	501	DOWN HIGH
	Afu8g02200	proline permease	1008	UP MOD	Afu5g09300	amino acid transporter	595	DOWN HIGH
	Afu4g01570	amino acid transporter	1353	UP MOD	Afu7g04290	amino acid permease (Gap1)	609	DOWN HIGH
	Afu7g05910	purine permease	1443	UP LOW	Afu1g12310	GABA permease	752	DOWN MOD
	Afu6g08780	proline utilization protein PrnX	1521	UP LOW	Afu2g08800	amino acid permease (Dip5)	1185	DOWN MOD
	Afu2g00220	aminopeptidase	1576	UP LOW	Afu2g17790	amino acid transporter	1699	DOWN LOW
	Afu7g01090	proline permease PrnB	1684	UP LOW	Afu8g06580	amino acid permease	1701	DOWN LOW
	Afu3g07990	GABA permease GabA	1701	UP LOW	Afu2g00310	amino acid transporter	1781	DOWN LOW
					Afu3g11490	GABA permease	1856	DOWN LOW
					Afu6g00412	amino acid permease	1871	DOWN LOW
					Afu4g00240	amino acid transporter	1900	DOWN LOW
Transcription factors	Afu5g13790	C6 transcription factor (Acr-2)	106	UP HIGH	Afu6g09630	C6 finger domain protein GliZ	164	DOWN HIGH
	Afu2g11780	C2H2 transcription factor (Crea)	135	UP HIGH	Afu5g12020	C6 transcription factor (NirA)	174	DOWN HIGH
	Afu1g13750	C2H2 transcription factor (Rpn4)	138	UP HIGH	Afu1g17360	bZIP transcription factor (BACH2)	244	DOWN HIGH
	Afu2g10770	C2H2 transcription factor (Con7)	377	UP HIGH	Afu6g03010	C2H2 finger domain protein (Zms1)	321	DOWN HIGH
	Afu3g04070	bZIP transcription factor HacA	489	UP HIGH	Afu2g02540	bZIP transcription factor (Fcr3)	666	DOWN HIGH

	Afu6g09930	bZIP transcription factor AP-1/Yap1	492	UP HIGH	Afu1g05150	C2H2 transcription factor (TFIIIA)	1023	DOWN MOD
	Afu1g15470	C6 transcription factor (UaY)	585	UP HIGH	Afu3g09820	C2H2 transcription factor	1052	DOWN MOD
	Afu3g05760	C6 transcription factor (Fcr1)	739	UP MOD	Afu3g09670	C6 transcription factor OefC	1403	DOWN LOW
	Afu1g16460	bZIP transcription factor (LziP)	1079	UP MOD	Afu3g12660	C6 finger domain protein Acr-2	1574	DOWN LOW
	Afu3g12890	C6 transcription factor GliZ-like	1089	UP MOD	Afu2g00100	C6 transcription factor Aro80	1678	DOWN LOW
Signal transduction	Afu1g16000	serine/threonine protein kinase	78	UP HIGH	Afu2g09710	protein kinase (NpkA)	1	DOWN HIGH
	Afu5g09100	MAP kinase MpkC	194	UP HIGH	Afu3g06300	Rho GTPase Rac	257	DOWN HIGH
	Afu5g06470	serine/threonine protein kinase	332	UP HIGH	Afu5g07430	Rho guanyl nucleotide exchange factor	391	DOWN HIGH
	Afu4g03100	ras-like GTP-binding protein	446	UP HIGH	Afu5g05900	protein kinase (Chm1)	428	DOWN HIGH
	Afu2g12200	cAMP-dependent protein kinase catalytic subunit PkaC1	495	UP HIGH	Afu2g15050	Rho GTPase activator (Lrg11)	464	DOWN HIGH
	Afu3g05770	RAS small monomeric GTPase	644	UP HIGH	Afu3g10740	RAB GTPase Vps21/Ypt51	987	DOWN MOD
	Afu1g08960	cAMP-regulated phosphoprotein family protein Igo1, putative	697	UP MOD	Afu1g02190	Ras GTPase Rab11	1662	DOWN LOW
	Afu3g11080	MAP kinase kinase kinase (Bck1)	931	UP MOD	Afu4g04810	Rab GTPase SrgA	1964	DOWN LOW
	Afu5g11230	RAS small monomeric GTPase RasA	1126	UP MOD				

Afu3g06690	Rho GTPase Rho3	1430	UP LOW	
Afu3g10080	serine/threonine protein kinase	1557	UP LOW	
Afu5g05960	serine/threonine protein kinase	1580	UP LOW	
Afu3g06280	Rho GTPase activator (Rgd1)	1740	UP LOW	
Afu3g05900	MAP kinase kinase Ste7	1840	UP LOW	
Afu3g01190	serine/threonine protein kinase	1845	UP LOW	
Afu1g05800	MAP kinase kinase (Mkk2)	1849	UP LOW	

Table 10.12: Functional classification of selected genes having differential transcript abundance in Af293 between 8 and 14 hours post infection in the murine lung. Upregulated (red) and downregulated genes (green) are shown for each functional category. Both increasing and decreasing transcripts are sub divided into expression cohorts which are either high, moderate, or low with respect to their expression change. Genes within functional categories are ranked according to greatest nSI intensity changes between 8 and 14 hours.

Functional Category	ORF	Description	Rank	Magnitude		ORF	Description	Rank	Magnitude
Cell wall	Afu5g00760	chitin synthase C	222	UP HIGH		Afu1g15440	alpha-1,3-glucan synthase Ags3	111	DOWN HIGH
	Afu6g09310	class V chitinase	290	UP HIGH		Afu5g08580	alpha-1,6-mannosyltransferase subunit (Och1)	191	DOWN HIGH
	Afu1g00310	class V chitinase	322	UP HIGH		Afu2g13430	chitin synthase	219	DOWN HIGH
	Afu5g11990	alpha-1,3-mannosyltransferase (Alg3)	621	UP HIGH		Afu8g02040	glycosyl transferase	231	DOWN HIGH

Afu1g12600	chitin synthase D	720	UP MOD
Afu5g08550	Rho guanyl nucleotide exchange factor (Rom2)	727	UP MOD
Afu2g06160	alpha-1,3-glucanase/mutanase	852	UP MOD
Afu6g10430	chitin deacetylase	898	UP MOD
Afu1g04260	endo-1,3-beta-glucanase Engl1	1254	UP MOD
Afu5g14060	Rho GTPase Rho4	1437	UP LOW
Afu1g05290	endo-1,3(4)-beta-glucanase	1489	UP LOW
Afu8g05620	chitin synthase activator (Chs3)	1518	UP LOW
Afu7g01540	endo-1,4-beta-glucanase	1529	UP LOW
Afu2g11270	alpha-1,3-glucan synthase Ags2	1563	UP LOW
Afu3g03080	endo-1,3(4)-beta-glucanase	1671	UP LOW
Afu5g03940	alpha-1,3-glucanase	1982	UP LOW
Afu3g10340	Rho GTPase Rho 2	2008	UP LOW

Afu8g05630	chitin synthase F	320	DOWN HIGH
Afu2g14910	alpha-1,6-mannosyltransferase subunit	412	DOWN HIGH
Afu4g13360	endo-1,3(4)-beta-glucanase	418	DOWN HIGH
Afu1g12560	endoglucanase	472	DOWN HIGH
Afu1g12040	chitin biosynthesis protein (Chs7)	522	DOWN HIGH
Afu5g02280	endo-1,3(4)-beta-glucanase	529	DOWN HIGH
Afu3g11280	class V chitinase	598	DOWN HIGH
Afu6g06900	Rho GTPase Rho1	606	DOWN HIGH
Afu5g03760	class III chitinase ChiA1	661	DOWN HIGH
Afu7g08510	extracellular alpha-1,3-glucanase/mutanase	672	DOWN HIGH
Afu2g14360	GPI anchored endo-1,3(4)-beta-glucanase	715	DOWN MOD
Afu5g03530	class III chitinase	913	DOWN MOD
Afu3g05580	chitin synthase activator (Chs3)	1104	DOWN MOD
Afu3g06690	Rho GTPase Rho3	1127	DOWN MOD
Afu8g06030	alpha-1,3-glucanase	1553	DOWN LOW
Afu5g03960	class V chitinase Chi100	1619	DOWN

641

								LOW
					Afu5g14190	beta-glucanase	1682	DOWN LOW
Ergosterol biosynthesis	Afu1g03150	c-14 sterol reductase	48	UP HIGH	Afu2g15030	C-3 sterol dehydrogenase/C-4 decarboxylase	161	DOWN HIGH
	Afu2g03700	HMG-CoA reductase	550	UP HIGH	Afu5g08960	triglyceride lipase-cholesterol esterase	222	DOWN HIGH
	Afu5g07780	squalene monooxygenase Erg1	789	UP MOD	Afu1g07140	c-24(28) sterol reductase	254	DOWN HIGH
	Afu6g05140	sterol delta 5,6-desaturase ERG3	1292	UP MOD	Afu2g02220	UDP-glucose:sterol glycosyltransferase	265	DOWN HIGH
	Afu4g12040	lanosterol synthase	1759	UP LOW	Afu4g14770	squalene-hopene-cyclase	757	DOWN MOD
	Afu1g11230	HMG-CoA reductase	1880	UP LOW	Afu3g11750	oxysterol binding protein (Osh5)	814	DOWN MOD
					Afu1g11140	Sterol desaturase family	1004	DOWN MOD
					Afu7g02480	oxysterol binding protein (Osh1)	1095	DOWN MOD
					Afu1g04720	C-8 sterol isomerase (Erg-1)	1302	DOWN MOD
					Afu1g03950	cytochrome P450 sterol C-22 desaturase, putaitve	1439	DOWN LOW
					Afu2g17400	C-3 sterol dehydrogenase/C-4 decarboxylase family protein	1576	DOWN LOW
Microtubule	Afu6g12840	kinesin family protein	802	UP MOD	Afu5g13190	kinesin family protein	113	DOWN HIGH
	Afu7g01400	kinesin family protein (BimC)	862	UP MOD	Afu1g06650	actin filament organization protein App1-like	233	DOWN HIGH
	Afu7g03710	kinesin family protein (KipA)	1203	UP MOD	Afu2g01200	actin polymerization protein Bzz1	303	DOWN HIGH
	Afu6g07150	actin binding protein	1327	UP MOD	Afu6g14220	kinesin family protein (KinA)	305	DOWN HIGH

	Afu3g04300	actin cytoskeleton organization and biogenesis protein, putative	1461	UP LOW	Afu7g00250	tubulin beta subunit	566	DOWN HIGH
	Afu2g02310	actin cortical patch protein Sur7	1908	UP LOW	Afu1g13390	gamma tubulin MipA	623	DOWN HIGH
	Afu8g04460	dynein intermediate chain	2003	UP LOW	Afu2g03150	kinesin family protein	844	DOWN MOD
	Afu3g09370	spindle-pole body protein (Pcp1)	1592	UP LOW	Afu5g11810	dynein heavy chain	1372	DOWN LOW
Cell polarity	Afu1g08850	septin	1631	UP LOW				
Ion transport	Afu2g05860	calcium/mangenease P-type ATPase	87	UP HIGH	Afu7g06350	sodium/phosphate symporter	270	DOWN HIGH
	Afu1g10880	P-type calcium ATPase	415	UP HIGH	Afu4g13540	potassium uptake transporter	350	DOWN HIGH
	Afu3g12740	copper resistance-associated P-type ATPase	614	UP HIGH	Afu1g04270	calcium ion transporter Vcx1	389	DOWN HIGH
	Afu1g16750	mitochondrial cation transporter	689	UP MOD	Afu3g10690	calcium-translocating P-type ATPase(PMCA-type),putative	570	DOWN HIGH
	Afu2g01460	ZIP Zinc transporter, putaitve	841	UP MOD	Afu2g12050	ZIP metal ion transporter	634	DOWN HIGH
	Afu5g06220	sodium/hydrogen exchanger 3	994	UP MOD	Afu2g05320	calcium-proton exchanger	706	DOWN MOD
	Afu1g12090	cation efflux family protein family	1059	UP MOD	Afu4g09560	ZIP Zinc transporter	719	DOWN MOD
	Afu8g01480	potassium channel	1451	UP LOW	Afu6g00470	plasma membrane zinc ion transporter	894	DOWN MOD
					Afu5g05840	calcium channel subunit Mid1	940	DOWN

								MOD
					Afu1g13190	copper-activated transcription factor GRISEA	1831	DOWN LOW
Iron acquisition	Afu7g04730	siderochrome-iron transporter	754	UP MOD	Afu5g03800	high-affinity iron transporter FtrA	793	DOWN MOD
	Afu1g04450	siderophore biosynthesis protein	1334	UP MOD	Afu7g06060	siderochrome-iron transporter Sit1	1159	DOWN MOD
	Afu6g12870	ABC iron exporter Atm1	1637	UP LOW				
	Afu3g03660	siderophore esterase IroE-like	1683	UP LOW				
	Afu3g13670	siderochrome-iron transporter	1932	UP LOW				
Antigen	Afu6g11030	RNA binding protein MSSP-2	156	UP HIGH	Afu2g09030	secreted dipeptidyl peptidase DppV	138	DOWN HIGH
	Afu5g09210	autophagic serine protease Alp2	163	UP HIGH	Afu1g09670	HLH transcription factor (GlcD gamma)	181	DOWN HIGH
	Afu1g06830	60S acidic ribosomal protein P1	301	UP HIGH	Afu1g07440	molecular chaperone Hsp70	916	DOWN MOD
	Afu6g02280	allergen Asp F3	374	UP HIGH	Afu1g12610	Hsp70 chaperone Hsp88	1117	DOWN MOD
	Afu4g03240	cell wall serine-threonine-rich galactomannoprotein Mp1	388	UP HIGH	Afu5g04170	molecular chaperone and allergen Mod-E/Hsp90/Hsp1	1542	DOWN LOW
	Afu2g00690	glucan 1,4-alpha-glucosidase	927	UP MOD	Afu4g09090	thioredoxin	1578	DOWN LOW
	Afu2g10100	60S acidic ribosomal protein P2/allergen Asp F 8	1406	UP LOW	Afu6g11430	aldehyde dehydrogenase AldA	1659	DOWN LOW

	Afu5g02330	major allergen and cytotoxin AspF1	1439	UP LOW	Afu2g03830	allergen Asp F4	1930	DOWN LOW
	Afu2g11850	60S ribosomal protein L3	1737	UP LOW				
Secreted proteases	Afu5g09210	autophagic serine protease Alp2	163	UP HIGH	Afu1g07730	metalloprotease MEP1	11	DOWN HIGH
	Afu4g13750	penicillolysin/deuterolysin metalloprotease	189	UP HIGH	Afu2g09030	secreted dipeptidyl peptidase DppV	138	DOWN HIGH
	Afu5g01200	carboxypeptidase S1	652	UP HIGH	Afu6g10250	alkaline serine protease AorO	306	DOWN HIGH
	Afu5g07330	carboxypeptidase S1	1394	UP LOW	Afu3g08930	tripeptidyl peptidase SED3	314	DOWN HIGH
	Afu2g08790	zinc carboxypeptidase	1618	UP LOW	Afu1g17400	peptidase S41 family protein	1051	DOWN MOD
	Afu4g09030	aminopeptidase	1688	UP LOW	Afu2g18070	metalloproteinase	1189	DOWN MOD
					Afu4g03490	tripeptidyl-peptidase (TppA)	1332	DOWN MOD
					Afu6g05350	aspartic-type endopeptidase (OpsB)	1355	DOWN MOD
					Afu3g11400	aspartic endopeptidase Pep2	1947	DOWN LOW
Secretion peptide encoding genes	Afu1g03150	c-14 sterol reductase	48	UP HIGH	Afu5g14150	lipase	19	DOWN HIGH
	Afu7g01200	aspergillopepsin, putaitve	267	UP HIGH	Afu3g12340	hypothetical protein	60	DOWN HIGH
	Afu6g09310	class V chitinase	290	UP HIGH	Afu6g07200	hypothetical protein	65	DOWN HIGH
	Afu1g00310	class V chitinase	322	UP HIGH	Afu5g06840	class V chitinase	100	DOWN HIGH
	Afu4g03240	cell wall serine-threonine-rich	388	UP HIGH	Afu2g17540	conidial pigment biosynthesis oxidase Abr1/brown 1	361	DOWN HIGH

		galactomannoprotein Mp1						
	Afu4g01070	acid phosphatase	503	UP HIGH	Afu3g11280	class V chitinase	598	DOWN HIGH
	Afu4g03210	cutinase	572	UP HIGH	Afu8g02530	extracellular lipase	614	DOWN HIGH
	Afu5g12160	alpha-1,2-mannosyltransferase (Kre5)	601	UP HIGH	Afu4g03660	acid phosphatase	753	DOWN MOD
	Afu4g09470	cytochrome P450 monooxygenase	703	UP MOD	Afu1g13760	cell wall anchored protein	827	DOWN MOD
	Afu6g08510	cell wall glucanase	1228	UP MOD	Afu6g00430	IgE-binding protein	1209	DOWN MOD
	Afu4g03500	GPI anchored protein	1346	UP MOD	Afu1g06890	alpha-1,2-mannosyltransferase (Alg11)	1219	DOWN MOD
	Afu5g14410	cysteine dioxygenase	1411	UP LOW	Afu1g09650	GPI anchored protein	1351	DOWN MOD
	Afu2g08500	carboxylesterase	1704	UP LOW	Afu2g03120	cell wall glucanase (Utr2)	1452	DOWN LOW
	Afu5g01330	acid phosphatase AphA	1760	UP LOW	Afu1g01300	GPI anchored protein	1642	DOWN LOW
	Afu2g09540	cytochrome P450 family protein	1766	UP LOW	Afu8g07120	beta-1,6-glucanase Neg1	1725	DOWN LOW
	Afu4g06640	acid sphingomyelinase	1916	UP LOW	Afu2g14420	cutinase	1759	DOWN LOW
	Afu1g10590	GPI anchored protein	1938	UP LOW	Afu2g12850	1,3-beta-glucanosyltransferase Gel3	1778	DOWN LOW
					Afu2g01170	1,3-beta-glucanosyltransferase Gel1	1780	DOWN LOW
Pathogenesis	Afu6g09610	nonribosomal peptide synthase	369	UP HIGH	Afu6g08520	adenylate cyclase AcyA	9	DOWN HIGH
	Afu6g02280	allergen Asp F3	374	UP HIGH	Afu1g15440	alpha-1,3-glucan synthase Ags3	111	DOWN HIGH
	Afu6g13990	acetyltransferase	876	UP MOD	Afu2g12200	cAMP-dependent protein kinase catalytic subunit PkaC1	302	DOWN HIGH

	Afu5g02330	major allergen and cytotoxin AspF1	1439	UP LOW	Afu2g04200	4-hydroxyphenylpyruvate dioxygenase	631	DOWN HIGH
	Afu8g01670	bifunctional catalase-peroxidase Cat2	1523	UP LOW	Afu6g04820	para-aminobenzoate synthase PabaA	811	DOWN MOD
	Afu3g10000	cAMP-dependent protein kinase regulatory subunit PkaR	1611	UP LOW	Afu6g10240	sensor histidine kinase/response regulator Fos-1/TcsA	902	DOWN MOD
					Afu3g02270	mycelial catalase Cat1	1195	DOWN MOD
					Afu7g05060	MgtC/SapB family membrane protein	1781	DOWN LOW
					Afu2g03830	allergen Asp F4	1930	DOWN LOW
Secondary metabolism	Afu6g09630	C6 finger domain protein GliZ	242	UP HIGH	Afu8g00560	cytochrome P450 oxidoreductase	15	DOWN HIGH
	Afu3g14700	polyketide synthase	264	UP HIGH	Afu6g09770	geranylgeranyl diphosphate synthase	73	DOWN HIGH
	Afu4g14590	C6 transcription factor	286	UP HIGH	Afu4g14630	FAD binding oxidoreductase	99	DOWN HIGH
	Afu8g00540	hybrid PKS-NRPS enzyme	297	UP HIGH	Afu5g00370	amino acid permease	177	DOWN HIGH
	Afu2g17550	conidial pigment biosynthesis protein Ayg1	361	UP HIGH	Afu4g14790	cytochrome P450 monooxygenase	210	DOWN HIGH
	Afu6g09610	nonribosomal peptide synthase	369	UP HIGH	Afu2g17580	conidial pigment biosynthesis scytalone dehydratase Arp1	337	DOWN HIGH
	Afu6g03480	nonribosomal peptide synthase	460	UP HIGH	Afu6g03430	C6 finger domain protein	366	DOWN HIGH
	Afu8g00710	secreted antimicrobial	534	UP HIGH	Afu3g03250	aldehyde dehydrogenase family protein	368	DOWN HIGH

	peptide						
Afu5g00120	cytochrome P450 oxidoreductase/alkane hydroxylase, putative	567	UP HIGH	Afu3g12950	FAD binding domain protein	384	DOWN HIGH
Afu8g00660	solute transporter	594	UP HIGH	Afu3g12890	C6 transcription factor GliZ-like	429	DOWN HIGH
Afu8g00380	DltD N-terminal domain protein	624	UP HIGH	Afu3g01510	C6 transcription factor	518	DOWN HIGH
Afu3g12910	O-methyltransferase GliM-like	634	UP HIGH	Afu2g17970	ergot alkaloid biosynthetic protein A	579	DOWN HIGH
Afu6g13990	acetyltransferase	876	UP MOD	Afu3g15270	nonribosomal peptide synthase	585	DOWN HIGH
Afu3g15290	C6 transcription factor	923	UP MOD	Afu6g09720	methyltransferase GliN	616	DOWN HIGH
Afu1g17710	C6 transcription factor	1048	UP MOD	Afu8g00590	fatty acid desaturase	679	DOWN HIGH
Afu1g17640	C6 transcription factor RegA	1063	UP MOD	Afu2g18010	cytochrome P450 monooxygenase	963	DOWN MOD
Afu8g00220	cytochrome P450	1201	UP MOD	Afu8g00100	aspartate-tRNA ligase	1007	DOWN MOD
Afu3g12940	C6 transcription factor	1260	UP MOD	Afu6g09730	cytochrome P450 oxidoreductase GliF	1072	DOWN MOD
Afu4g14830	cytochrome P450 monooxygenase	1382	UP LOW	Afu3g13640	extracellular serine-rich protein	1724	DOWN LOW
Afu3g13600	C6 transcription factor	1399	UP LOW	Afu8g00240	cytochrome P450 monooxygenase	1768	DOWN LOW
Afu6g13920	adenylate-forming enzyme	1427	UP LOW	Afu4g14850	extracellular 3-ketosteroid 1-dehydrogenase	1789	DOWN LOW
Afu8g00620	dimethylallyl tryptophan synthase	1734	UP LOW	Afu8g00700	class III chitinase ChiA2	1790	DOWN LOW

	Afu3g02700	C6 transcription factor	1804	UP LOW	Afu8g00530	alpha/beta hydrolase	1794	DOWN LOW
	Afu8g00250	dimethylallyl tryptophan synthase	1960	UP LOW	Afu6g09690	glutathione S-transferase GliG	1828	DOWN LOW
Ribosome biogenesis and RNA metabolism	Afu1g10990	ribosomal RNA processing protein	16	UP HIGH	Afu5g13520	ribosome biogenesis protein Ria1	10	DOWN HIGH
	Afu2g02710	60S ribosomal protein L24b	39	UP HIGH	Afu8g04220	rRNA maturation protein (Nop14)	26	DOWN HIGH
	Afu6g11030	RNA binding protein MSSP-2	156	UP HIGH	Afu1g04062	RNA polymerase I specific transcription initiation factor Rrn7	74	DOWN HIGH
	Afu7g02080	RNA polymerase I subunit Rpa43	209	UP HIGH	Afu1g04980	RNA polymerase III transcription factor TFIIIC subunit (Tfc4)	103	DOWN HIGH
	Afu5g04030	50S ribosomal protein L27	227	UP HIGH	Afu1g01990	ribosome biogenesis protein Rsa4	273	DOWN HIGH
	Afu3g14040	RNA polymerase II mediator complex subunit Soh1, putative	250	UP HIGH	Afu1g09200	ribosome biogenesis protein Erb1	278	DOWN HIGH
	Afu1g06830	60S acidic ribosomal protein P1	301	UP HIGH	Afu2g11140	50S ribosomal protein L4	280	DOWN HIGH
	Afu4g03650	ribosome associated DnaJ chaperone Zuotin	450	UP HIGH	Afu3g14550	RNA polymerase II general transcription and DNA repair factor TFIIH component Tfb5	329	DOWN HIGH
	Afu1g06770	40S ribosomal protein S26	494	UP HIGH	Afu4g06000	50S ribosomal protein L3	347	DOWN HIGH

Afu6g11260	ribosomal protein L26	558	UP HIGH
Afu1g05630	40S ribosomal protein S3	632	UP HIGH
Afu5g12800	50S ribosomal protein L4	663	UP HIGH
Afu2g07380	60S ribosomal protein L18	791	UP MOD
Afu7g04490	Ribosomal protein S28e	817	UP MOD
Afu3g14100	RNA polymerase II Elongator complex associated protein Kti12	916	UP MOD
Afu5g08330	RNA binding protein	1045	UP MOD
Afu4g09750	50S ribosomal protein L12	1085	UP MOD
Afu1g04230	50S ribosomal protein YmL27	1197	UP MOD
Afu2g13090	RNA polymerase II subunit 3	1242	UP MOD
Afu6g12720	40S ribosomal protein S29	1250	UP MOD
Afu3g06840	40S ribosomal protein S4	1352	UP MOD
Afu2g10100	60S acidic ribosomal protein P2/allergen Asp F 8	1406	UP LOW

Afu3g10120	RNA polymerase I and III transcription factor complex component Tbp	377	DOWN HIGH
Afu5g12270	rRNA processing protein (Ebp2)	625	DOWN HIGH
Afu5g10830	RNA helicase-like splicing factor (HRH1)	641	DOWN HIGH
Afu6g10320	ribosome biogenesis protein (Rrb1)	748	DOWN MOD
Afu4g00950	RNA polymerase II mediator complex component SRB4, putative	784	DOWN MOD
Afu3g04110	rRNA processing protein Bystin	846	DOWN MOD
Afu1g06230	ribosome biogenesis protein Ssf2	883	DOWN MOD
Afu5g12100	rRNA methyltransferase Spb1	884	DOWN MOD
Afu4g12170	50S ribosomal protein L2	903	DOWN MOD
Afu8g02730	RNA binding protein Tma22	941	DOWN MOD
Afu4g11690	RNA polymerase II transcription factor related protein	1053	DOWN MOD
Afu2g10510	50S ribosomal protein L13	1236	DOWN MOD
Afu1g05940	RNA polymerase II mediator complex protein Nut2, putative	1414	DOWN LOW

650

	Afu3g06250	RNA polymerase II mediator complex component Srb8, putative	1434	UP LOW	Afu8g05430	ribosome biogenesis protein Noc4	1595	DOWN LOW
	Afu2g07650	RNA binding protein	1505	UP LOW	Afu4g09000	60S ribosomal protein L25	1650	DOWN LOW
	Afu6g08430	RNA binding protein Pym	1574	UP LOW	Afu6g06830	RNA polymerase II mediator complex subunit Srb5, putative	1862	DOWN LOW
					Afu2g10750	RNA helicase (Dbp)	1894	DOWN LOW
					Afu6g04320	RNA binding protein	1897	DOWN LOW
					Afu2g06180	RNA polymerase II holoenzyme/mediator complex component Rgr1	1979	DOWN LOW
Sugar transport	Afu2g04550	MFS sugar transporter	23	UP HIGH	Afu4g03110	MFS monosaccharide transporter	1	DOWN HIGH
	Afu8g01180	MFS sugar transporter	27	UP HIGH	Afu6g12040	MFS sugar permease	143	DOWN HIGH
	Afu4g06630	MFS monosaccharide transporter	102	UP HIGH	Afu2g02110	MFS monosaccharide transporter	200	DOWN HIGH
	Afu5g01160	MFS monosaccharide transporter	182	UP HIGH	Afu4g13080	MFS monosaccharide transporter	216	DOWN HIGH
	Afu7g01740	sugar transporter	331	UP HIGH	Afu3g12580	MFS sugar transporter protein	1337	DOWN MOD
	Afu6g11920	MFS alpha-glucoside transporter	347	UP HIGH	Afu6g14442	MFS monosaccharide transporter	1463	DOWN LOW
	Afu2g10910	MFS alpha-glucoside transporter	544	UP HIGH	Afu3g00200	hexose transporter protein	1663	DOWN LOW

	Afu8g00770	sugar transporter family protein	796	UP MOD	Afu3g02890	MFS sugar transporter	2018	DOWN LOW
	Afu6g04270	MFS sugar transporter	873	UP MOD				
	Afu7g05550	sugar transporter family protein	1039	UP MOD				
	Afu5g00280	MFS sugar transporter	1287	UP MOD				
	Afu5g14540	MFS monosaccharide transporter	1351	UP MOD				
	Afu7g05190	MFS alpha-glucoside transporter	1481	UP LOW				
	Afu8g06870	MFS sugar transporter	1603	UP LOW				
	Afu1g16390	MFS hexose transporter	1657	UP LOW				
	Afu2g08120	MFS monosaccharide transporter (Hxt8)	1845	UP LOW				
	Afu8g05710	MFS sugar transporter Stl1	1886	UP LOW				
Amino acid transport	Afu2g17480	amino acid transporter	20	UP HIGH	Afu5g00370	amino acid permease	177	DOWN HIGH
	Afu8g02200	proline permease	474	UP HIGH	Afu5g14660	GABA permease	183	DOWN HIGH
	Afu8g06580	amino acid permease	493	UP HIGH	Afu4g06990	amino acid transporter	226	DOWN HIGH
	Afu5g09300	amino acid transporter	585	UP HIGH	Afu5g00710	GABA permease	237	DOWN HIGH
	Afu7g01490	MFS peptide transporter Ptr2	793	UP MOD	Afu3g07990	GABA permease GabA	681	DOWN HIGH

	Afu8g02260	neutral amino acid permease	904	UP MOD	Afu3g00120	amino acid transporter (Mtr)	760	DOWN MOD
	Afu3g09710	amino acid permease	1038	UP MOD	Afu5g09440	amino acid permease	813	DOWN MOD
	Afu4g03220	amino acid permease	1627	UP LOW	Afu8g07200	amino acid transporter	1058	DOWN MOD
	Afu8g05070	neutral amino acid permease	1679	UP LOW	Afu5g06230	GABA permease	1200	DOWN MOD
	Afu5g02790	amino acid permease	1749	UP LOW	Afu6g11100	amino acid permease	1404	DOWN LOW
	Afu3g01820	amino acid permease	1923	UP LOW	Afu4g10090	GABA permease	1518	DOWN LOW
					Afu1g10770	neutral amino acid permease	1941	DOWN LOW
Transcription factors	Afu5g06410	C2H2 transcription factor (AmdA)	136	UP HIGH	Afu2g11780	C2H2 transcription factor (Crea)	47	DOWN HIGH
	Afu6g09630	C6 finger domain protein GliZ	242	UP HIGH	Afu3g05760	C6 transcription factor (Fcr1)	173	DOWN HIGH
	Afu4g03960	C6 transcription factor Ctf1A	304	UP HIGH	Afu7g01640	C6 transcription factor (War1)	214	DOWN HIGH
	Afu1g06900	C2H2 transcription factor Crz1	365	UP HIGH	Afu3g12890	C6 transcription factor GliZ-like	429	DOWN HIGH
	Afu1g03860	C6 transcription factor (AmdR)	506	UP HIGH	Afu5g13790	C6 transcription factor (Acr-2)	534	DOWN HIGH
	Afu5g11390	APSES transcription factor	542	UP HIGH	Afu2g15260	C6 transcription factor (Leu3)	873	DOWN MOD
	Afu2g07900	APSES transcription factor StuA	1062	UP MOD	Afu1g13750	C2H2 transcription factor (Rpn4)	912	DOWN MOD
	Afu1g17640	C6 transcription factor RegA	1063	UP MOD	Afu1g05150	C2H2 transcription factor (TFIIIA)	1082	DOWN MOD
	Afu3g02320	C2H2 finger	1153	UP MOD	Afu6g11170	C2H2 finger domain protein	1272	DOWN

		domain protein (Kin17)				(Ezf)		MOD
	Afu4g09080	C2H2 transcription factor (Seb1)	1739	UP LOW	Afu6g08790	C6 transcription factor (PrnA)	1462	DOWN LOW
Signal transduction	Afu2g03640	Ras GTPase activating protein	149	UP HIGH	Afu1g05800	MAP kinase kinase (Mkk2)	85	DOWN HIGH
	Afu5g10020	sensor histidine kinase/response regulator	333	UP HIGH	Afu1g15950	MAP kinase kinase (Pbs2)	110	DOWN HIGH
	Afu2g17130	MAPKKK cascade protein kinase regulator Ste50	495	UP HIGH	Afu5g06470	serine/threonine protein kinase	192	DOWN HIGH
	Afu6g09260	sensor histidine kinase/response regulator	858	UP MOD	Afu1g12940	MAP kinase SakA	243	DOWN HIGH
	Afu4g13720	MAP kinase MpkA	1425	UP LOW	Afu4g08040	RAB GTPase Ypt5	344	DOWN HIGH
	Afu5g14060	Rho GTPase Rho4	1437	UP LOW	Afu2g02850	serine/threonine protein kinase	524	DOWN HIGH
	Afu3g12550	sensor histidine kinase/response regulator	1468	UP LOW	Afu5g09100	MAP kinase MpkC	548	DOWN HIGH
	Afu3g13340	Rho-like small GTPase	1499	UP LOW	Afu6g06900	Rho GTPase Rho1	606	DOWN HIGH
	Afu3g07130	sensor histidine kinase/response regulator	1535	UP LOW	Afu3g05900	MAP kinase kinase Ste7	710	DOWN MOD
	Afu3g10340	Rho GTPase Rho 2	2008	UP LOW	Afu2g01060	Rho GTPase activator (Sac7)	716	DOWN MOD

10.3.8 Characterisation of Af293 time-point specific datasets: chromosomal loci, lineage specificity and functionality

Functional enrichment of increased and decreased datasets was investigated among gene categories of interest by Chi-square analyses, with the null hypothesis that equal numbers of upregulated and downregulated genes occur in each cohort (Figure 10.6, Tables 10.13 and 10.14)

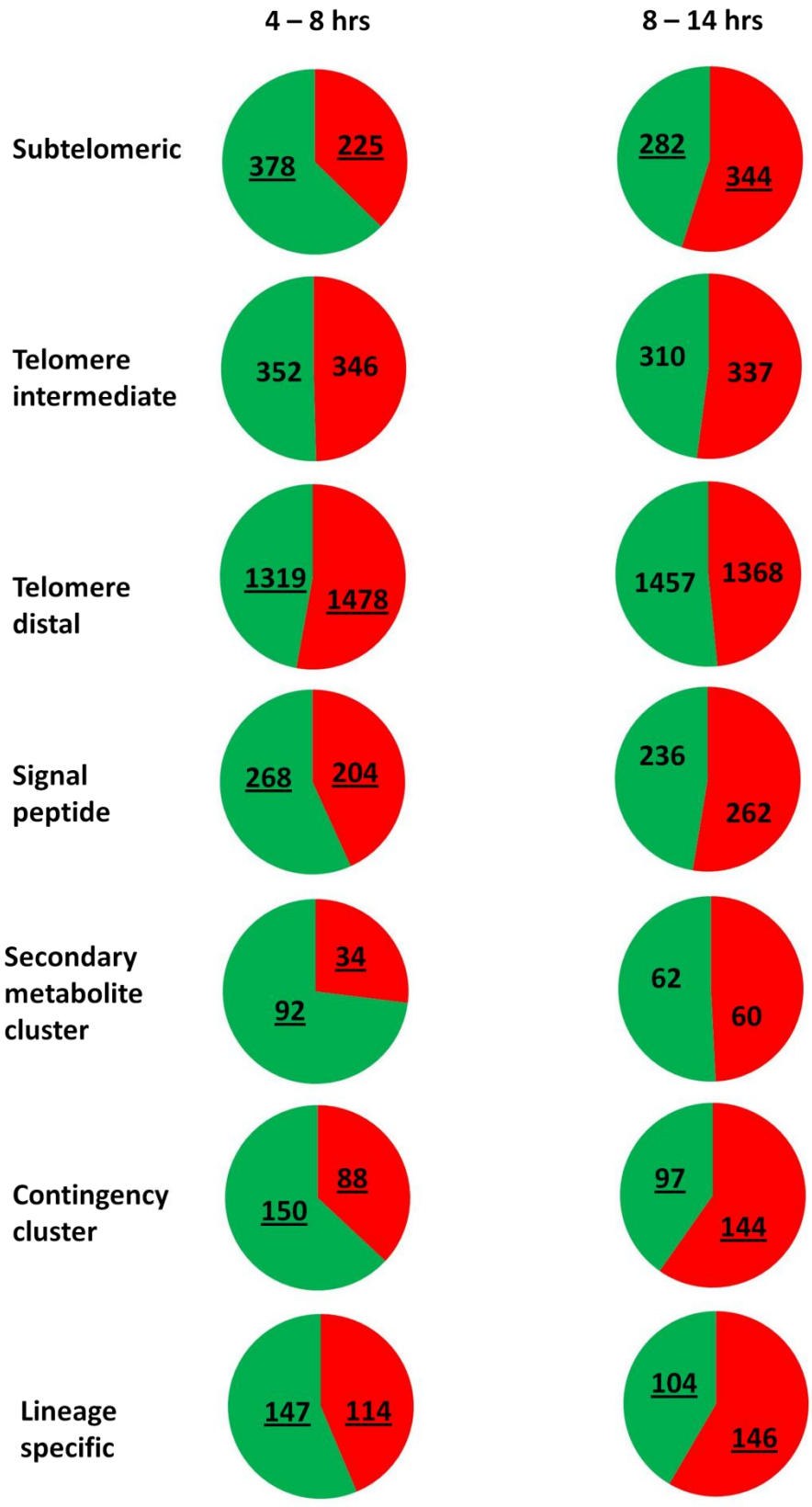


Figure 10.6: Distribution of differentially expressed genes between 4 – 8, and 8 - 14 hours post infection among the functional cohorts of chromosomal location, signal peptide content, and *A. fumigatus* specificity. Distribution of genes in upregulated (red) and downregulated (green) datasets among gene cohorts of interest to this study. Underlined values significantly deviate from the null hypothesis that an equal number of upregulated or downregulated genes will occur in each cohort, as tested by Chi-square analysis.

	Number of genes	Differentially expressed	Up (observed)	Down (observed)	Up (expected)	Down (expected)	Chi-square	p-value
0-300 kb	1509	603	225	378	301.5	301.5	38.82	0.0000
301- 600 kb	1634	698	346	352	349	349	0.05	0.8203
>600 kb	6373	2797	1478	1319	1398.5	1398.5	9.03	0.0026
Signal P	1103	472	204	268	236	236	8.67	0.0032
Secondary metabolism	337	126	34	92	63	63	26.69	0.0000
Infection cluster	594	238	88	150	119	119	16.15	0.0001
Aspergillus specific	596	261	114	147	130.5	130.5	4.17	0.0411

Table 10.13: Distribution and Chi-square analysis of differentially expressed genes categorised by chromosomal location, signal peptide content, *A. fumigatus* specificity and annotation at 4 - 8 hours post infection. Chi square analysis with one degree of freedom was used to test the distribution of upper and lower quartiles with respect to cohorts of interest to this study, with the null hypothesis that even numbers of upregulated or downregulated genes occur in each group.

	Number of genes	Differentially expressed	Up (observed)	Down (observed)	Up (expected)	Down (expected)	Chi-square	p-value
0-300 kb	1509	626	344	282	313	313	4.39	0.0132
301- 600 kb	1634	647	337	310	323.5	323.5	1.12	0.2885
>600 kb	6373	2825	1368	1457	1412.5	1412.5	2.8	0.0940
Signal P	1103	498	262	236	249	249	1.35	0.2440
Secondary metabolism	337	122	60	62	61	61	0.03	0.8563
Infection cluster	594	241	144	97	120.5	120.5	9.16	0.0025
Aspergillus specific	596	250	146	104	125	125	7.05	0.0079

Table 10.14: Distribution and Chi-square analysis of differentially expressed genes categorised by chromosomal location, signal peptide content, *A. fumigatus* specificity and annotation at 8 - 14 hours post infection. Chi square analysis with one degree of freedom was used to test the distribution of upper and lower quartiles with respect to cohorts of interest to this study, with the null hypothesis that even numbers of upregulated or downregulated genes occur in each group.

10.3.10 Ratiometric comparisons of *A. fumigatus* Af293 and Δ*laeA* during murine infection

Ratiometric normalisation was conducted as described in section 8.3.2. Figure 10.5 depicts box plots summarising data adjustments at each stage of the normalisation process. A reduction in variance among $\log_2$ ratios is effected among the 16 un-normalised MEV input files (Figure 10.7A) and 8 LOWESS, flip dye checked MIDAS files (Figure 10.7B). Averaging between the replicate experiments (Figure 10.7C) further reduces $\log_2$ ratio variation between time-points. Robust gene expression values were defined as genes for which the normalised value which did not vary more than a standard deviation of 1.5 between the replicates. Following normalisation, datasets at each time-point were filtered based on $\log_2$ ratios, where a cut-off of ±1.5 was applied. This cut-off was too stringent, as evidenced by the filtering of all upregulated genes at 8 hours post infection (Table 10.13). For interpretations of the datasets presented in this addendum, the top 100 genes upregulated or downregulated in LaeA at each time-point were considered differentially expressed. These genes are presented in Tables 10.16 - 10.21.

	4 hr	8 hr	14 hr
Observations	8267	8118	8307
Minimum	-1.706	-2.007	-1.824
Maximum	1.920	1.133	2.053
Mean	0.038	0.008	-0.009
Median	0.037	0.008	-0.006
Standard deviation	0.021	0.007	0.004
Outliers	0.353	0.194	0.361

Table 10.15: Summary statistics for the Δ*laeA* versus Af293 time course during initiation of murine infection. Statistics are based on Genespring 11.5.0 files. Mean and median $\log_2$ ratios approximate zero, which are consistent with the hypothesis that the majority of genes are not differentially expressed between isolates.

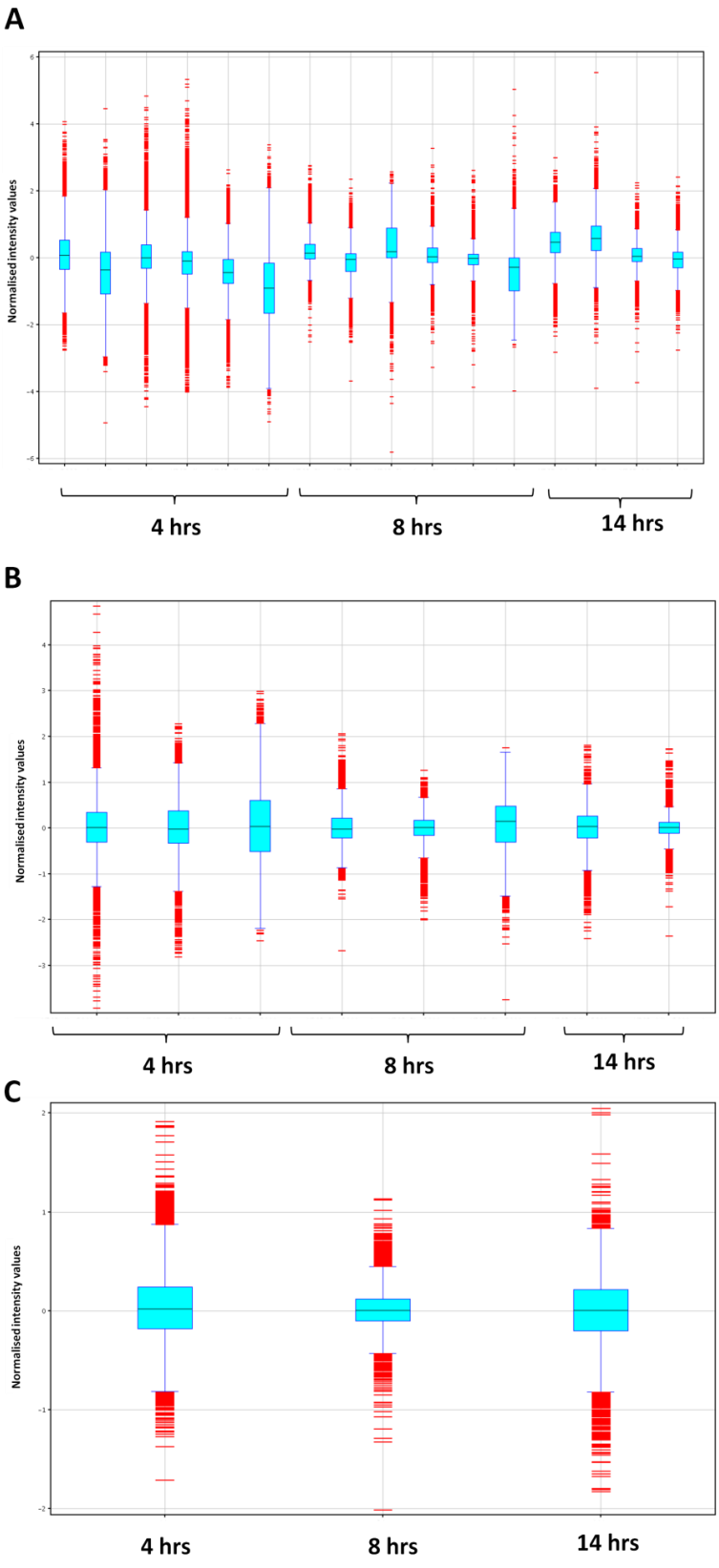


Figure 10.7: Box whisker plots depicting the effect of sequential data normalisations. Variance among data distributions is effected by LOWESS normalisation and flip-dye checking (B) and after averaging of replicates at each time point (C). Sample medians are depicted in the middle of the box, which also display the 25th quartile and the 75th quartile. The whiskers are 1.5 times the interquartile and red points outside the whiskers are outliers.

Table 10.16: 100 genes with greatest log_2 ratios (Δ*laeA*:Af293) at 4 hrs post infection. Genes are reported ranked according to greatest log_2 ratios at 4 hours where 1 is the greatest.

ORF	Description	Rank	GO Biological Process
Afu5g10490	amidase	1	amidase activity
Afu1g09430	hypothetical protein	2	
Afu2g01680	monooxygenase	3	
Afu4g09740	t-complex protein 1, theta subunit	4	chaperone activity///cytoplasm///protein folding///cytoskeleton organization///cytoskeleton
Afu3g06140	cytoskeleton assembly control protein Sla2	5	endocytosis///actin filament organization///incipient cellular bud site///cell wall organization///exocytosis///structural constituent of cytoskeleton///bipolar cellular bud site selection
Afu4g08910	hypothetical protein	6	
Afu6g08950	hypothetical protein	7	
Afu3g03295	hypothetical protein	8	
Afu2g14030	arginyl-tRNA synthetase	9	translation///cytoplasm///arginine-tRNA ligase activity
Afu4g09770	hypothetical protein	10	
Afu3g01990	DUF636 domain protein	11	
Afu3g11200	vacuolar assembly protein	12	high-affinity iron ion transport///endosome///""homotypic vacuole fusion, non-autophagic""///fungal-type vacuole///protein transport///Rab guanyl-nucleotide exchange factor activity///vacuolar membrane"///"vacuole organization
Afu6g03660	onanonoxo-7-onima-8-eninoihtemlysoneda	13	adenosylmethionine-8-amino-7-oxononanoate transaminase activity///cytoplasm///biotin biosynthetic process
Afu5g11560	Arp2/3 complex subunit (Arp3)	14	Arp2/3 protein complex///actin filament organization///actin binding///structural constituent of cytoskeleton
Afu3g09530	cytochrome P450	15	
Afu3g14310	hypothetical protein	16	
Afu5g07730	hypothetical protein	17	
Afu4g06070	translation initiation regulator (Gcn20)	18	cytosolic ribosome (sensu Eukaryota)///cytosol///ATP binding///regulation of translational initiation///regulation of translational elongation
Afu1g07000	DNA repair protein Rad26	19	
Afu3g11380	ARID/BRIGHT domain protein (SWI1)	20	chromatin remodeling///nucleosome remodeling complex///general RNA polymerase II transcription factor activity
Afu6g09360	proline-glycine rich protein	21	
Afu5g11880	PP-loop family protein	22	

Afu6g13890	hypothetical protein	23	
Afu5g11000	small nuclear ribonucleoprotein U2, A'	24	cytoplasm///""nuclear mRNA splicing, via spliceosome""///U2 snRNP"///"pre-mRNA splicing factor activity
Afu1g13200	hypothetical protein	25	
Afu4g11570	G-patch domain protein (TFIP11)	26	cytoplasm///nucleus///RNA binding///biological process unknown
Afu4g02830	aldehyde dehydrogenase	27	
Afu6g03590	citrate synthase Cit1	28	"propionate metabolic process, methylcitrate cycle"///mitochondrion///2-methylcitrate synthase activity///mitochondrial matrix
Afu8g06020	glutamate decarboxylase	29	response to oxidative stress///cytoplasm///glutamate catabolic process///glutamate decarboxylase activity
Afu6g02340	hypothetical protein	30	
Afu3g01980	chromatin structure remodeling complex protein RSC3, putative	31	DNA binding///zinc ion binding
Afu2g16880	60S ribosomal protein L37a	32	structural constituent of ribosome///translation///cytosolic large ribosomal subunit (sensu Eukaryota)
Afu8g03910	hypothetical protein	33	
Afu2g16920	actin monomer binding protein	34	sequestering of actin monomers///actin monomer binding///actin polymerization or depolymerization///bipolar cellular bud site selection
Afu1g17750	nicotinamide N-methyltransferase	35	nicotinamide metabolic process///nicotinamide N-methyltransferase activity///chromatin silencing at rDNA///cytoplasm
Afu3g00640	hypothetical protein	36	
Afu5g09690	hypothetical protein	37	
Afu6g03530	glutamine synthetase	38	glutamine biosynthetic process///glutamate-ammonia ligase activity
Afu1g03730	MFS transporter	39	integral to plasma membrane///transporter activity///transport
Afu4g03740	MFS transporter	40	
Afu3g09730	hypothetical protein	41	
Afu3g05550	OTU-like cysteine protease	42	protein catabolic process///cysteine-type peptidase activity///cytoplasm///nucleus
Afu7g02400	alcohol dehydrogenase, zinc-containing	43	cytoplasm///nucleus///biological process unknown///molecular function unknown
Afu1g15120	dsDNA-dependent ATPase (Rad54b)	44	reciprocal meiotic recombination///DNA binding///mitotic recombination///nucleus///DNA-dependent ATPase activity
Afu6g14450	hypothetical protein	45	

Afu5g11210	molybdopterin binding domain protein	46	catalytic activity///cytoplasm///nucleus///Mo-molybdopterin cofactor biosynthetic process
Afu7g03850	oxidoreductase, 2-nitropropane dioxygenase family, putative	47	oxidoreductase activity///metabolic process
Afu3g01430	benzodiazepine receptor family protein	48	
Afu5g13460	mitochondrial protein	49	mitochondrial genome maintenance///mitochondrion inheritance///mitochondrial outer membrane///mitochondrion organization///molecular function unknown
Afu7g06750	phosphoglycerate mutase family protein	50	
Afu3g08820	glycosyl hydrolase	51	cytoplasm///biological process unknown///molecular function unknown
Afu2g04890	TAM domain methyltransferase	52	
Afu5g02380	hypothetical protein	53	
Afu4g07467	hypothetical protein	54	
Afu4g11830	cell cycle control protein (Cwf19)	55	
Afu6g04220	hypothetical protein	56	cytoplasm///biological process unknown///molecular function unknown
Afu1g01580	hypothetical protein	57	
Afu6g11670	flavin-containing amine oxidasedehydrogenase	58	
Afu2g11770	hypothetical protein	59	
Afu1g01970	VeA-like protein	60	
Afu3g11440	glutamyl-tRNA(Gln) amidotransferase, B subunit	61	aerobic respiration///translation///mitochondrion organization///mitochondrion///molecular function unknown
Afu1g13280	mannose-6-phosphate isomerase, class I	62	mannose-6-phosphate isomerase activity///protein amino acid glycosylation///cytoplasm///nucleus///GDP-mannose biosynthetic process///cell wall mannoprotein biosynthetic process
Afu3g02370	short-chain dehydrogenase/reductase	63	oxidoreductase activity///cytoplasm///metabolic process
Afu6g11070	DEAD box RNA helicase (Hca4)	64	nucleolus///35S primary transcript processing///ATP-dependent RNA helicase activity
Afu1g16720	hypothetical protein	65	
Afu4g09450	hypothetical	66	

	protein		
Afu2g17820	O-methyltransferase	67	
Afu6g03630	very-long-chain acyl-CoA synthetase family protein (CefD1)	68	lipid particle///plasma membrane///very-long-chain fatty acid metabolic process///peroxisome///microsome///long-chain fatty acid transporter activity///long-chain-fatty-acid-CoA ligase activity///lipid transport
Afu6g13090	hypothetical protein	69	
Afu1g15390	DUF1014 domain protein	70	
Afu3g09120	hypothetical protein	71	
Afu6g00500	chitosanase	72	
Afu2g13140	meiosis induction protein kinase (Ime2)	73	regulation of meiosis///nucleus///protein amino acid phosphorylation///protein kinase activity
Afu6g13440	choline sulfatase	74	sulfuric ester hydrolase activity///metabolic process
Afu2g02960	translation factor pelota	75	translation///cytoplasm///meiosis///molecular function unknown
Afu1g05400	hypothetical protein	76	
Afu3g08670	integral membrane protein	77	
Afu1g10670	Vacuolar ATP synthase subunit H	78	vacuolar acidification///""vacuolar proton-transporting V-type ATPase, V1 domain"""///fungal-type vacuole membrane///"""proton-transporting ATPase activity, rotational mechanism""
Afu7g05790	vacuolar morphogenesis protein AvaB	79	homotypic vacuole fusion, non-autophagic""///fungal-type vacuole///Rab guanyl-nucleotide exchange factor activity///vacuolar membrane"///"vacuole organization
Afu3g10860	hypothetical protein	80	
Afu4g03530	hypothetical protein	81	
Afu5g08300	alpha-actinin, sarcomeric (f-actin cross linking protein)	82	
Afu4g12350	hypothetical protein	83	
Afu5g11060	WD repeat protein	84	
Afu4g13130	hypothetical protein	85	
Afu4g12110	TPR domain protein	86	protein binding
Afu5g11640	secretory pathway protein Ssp120	87	cytoplasm///protein secretion///molecular function unknown
Afu2g15800	hypothetical protein	88	
Afu2g08300	DnaJ domain protein	89	endoplasmic reticulum lumen///co-chaperone activity///protein folding

Afu3g07380	oligo-1,6-glucosidase	90	biological process unknown"///""hydrolase activity, hydrolyzing O-glycosyl compounds""///"cellular component unknown
Afu1g06270	zinc metallopeptidase	91	
Afu5g13320	UV radiation resistance protein (UVRAG)	92	programmed cell death
Afu5g14970	hypothetical protein	93	
Afu2g03040	ribosomal protein L34 protein	94	structural constituent of ribosome///translation///ribosome biogenesis///cytosolic large ribosomal subunit (sensu Eukaryota)
Afu1g14730	cell division cycle protein Cdc20	95	ubiquitin-dependent protein catabolic process///anaphase-promoting complex///mitotic metaphase/anaphase transition///mitotic sister chromatid segregation///cyclin catabolic process///mitotic spindle elongation///enzyme activator activity
Afu2g13730	NEDD8 activating enzyme (UbaC)	96	NEDD8 class-dependent protein catabolic process///cytoplasm///NEDD8 activating enzyme activity///protein neddylation during NEDD8 class-dependent protein catabolic process
Afu6g10640	hypothetical protein	97	
Afu2g12570	peptidase family M20/M25/M40 protein	98	
Afu6g14100	mitochondrial carnitine:acyl carnitine carrier, putative	99	carnitine:acyl carnitine antiporter activity///mitochondrial inner membrane///mitochondrion///fatty acid metabolic process
Afu1g05050	cytosine deaminase	100	cytosine metabolic process///cytosine deaminase activity///cytoplasm///nucleus///zinc ion binding

Table 10.17: 100 genes with lowest log_2 ratios (Δ*laeA*:Af293) at 4 hrs post infection. Genes are reported ranked according to lowest log_2 ratios at 4 hours where 1 is the greatest.

ORF	Description	Rank	GO Biological Process
Afu2g11380	rRNA assembly protein Mis3	1	ribosome biogenesis///nucleolus///rRNA processing///molecular function unknown
Afu5g01900	heat shock transcription factor Hsf1	2	response to heat///transcription factor activity///nucleus///regulation of transcription from RNA polymerase II promoter///response to stress
Afu7g01300	mannosyltransferase (PIG-M)	3	GPI anchor biosynthetic process///mannosyltransferase activity///endoplasmic reticulum membrane
Afu3g12810	transcriptional corepressor of histone genes (Hir3), putative	4	gene silencing///nucleosome assembly///nucleosome///transcription corepressor activity
Afu2g17480	amino acid transporter	5	
Afu8g00290	hypothetical protein	6	

Afu3g13210	protein kinase domain-containing protein	7	protein kinase activity
Afu5g10210	hypothetical protein	8	
Afu3g07590	ER-Golgi SNARE complex subunit (Sed5)	9	retrograde vesicle-mediated transport, Golgi to ER"""///cis-Golgi network///ER to Golgi vesicle-mediated transport///t-SNARE activity///"vesicle fusion///intra-Golgi vesicle-mediated transport
Afu2g00470	C6 transcription factor	10	RNA polymerase II transcription factor activity///nucleus///regulation of transcription
Afu2g03460	C6 transcription factor (Leu3)	11	specific RNA polymerase II transcription factor activity///leucine biosynthetic process///nucleus///regulation of transcription from RNA polymerase II promoter
Afu5g09200	ubiquitin conjugating enzyme (UbcC)	12	ubiquitin-protein ligase activity///ubiquitin-dependent protein catabolic process///G1/S transition of mitotic cell cycle///cytoplasm///nucleus///ubiquitin conjugating enzyme activity///G2/M transition of mitotic cell cycle///nuclear ubiquitin ligase complex
Afu1g03150	c-14 sterol reductase	13	endoplasmic reticulum///ergosterol biosynthetic process///C-14 sterol reductase activity
Afu5g13680	hypothetical protein	14	
Afu1g11830	MFS sugar transporter	15	plasma membrane///transporter activity///transport
Afu6g01940	dienelactone hydrolase family protein	16	
Afu7g04250	protein-ER retention protein (Erd1)	17	protein retention in ER lumen///integral to membrane
Afu7g04860	dimethyladenosine transferase	18	nucleolus///"rRNA (adenine-N6,N6-)-dimethyltransferase activity"///rRNA modification///35S primary transcript processing
Afu5g06090	integral membrane protein (Ytp1)	19	membrane///biological process unknown///molecular function unknown
Afu3g02720	MFS transporter	20	
Afu4g00290	succinyl-CoA synthetase beta subunit	21	tricarboxylic acid cycle///succinate-CoA ligase (ADP-forming) activity///mitochondrion///succinyl-CoA metabolic process
Afu3g07000	hypothetical protein	22	
Afu2g09300	hypothetical protein	23	
Afu2g00140	FAD monooxygenase	24	cellular aromatic compound metabolic process
Afu4g06280	hypothetical protein	25	
Afu7g01130	hypothetical protein	26	
Afu2g08690	nuclear distribution protein NudE	27	

Afu2g08110	hexokinase family protein	28	cytoplasm///biological process unknown///molecular function unknown
Afu6g07370	hypothetical protein	29	
Afu6g12370	hypothetical protein	30	cytoplasm///biological process unknown///molecular function unknown
Afu1g06920	serine/threonine protein kinase	31	cytoplasm///protein amino acid phosphorylation///protein kinase activity
Afu5g05750	protein kinase	32	cytoplasm///protein kinase activity
Afu2g01630	MSF1 domain protein	33	biological process unknown///mitochondrion///molecular function unknown
Afu6g09570	hypothetical protein	34	
Afu6g09020	GPI transamidase component Gpi16	35	integral to endoplasmic reticulum membrane///GPI-anchor transamidase activity///attachment of GPI anchor to protein///GPI-anchor transamidase complex
Afu6g11310	bifunctional pyrimidine biosynthesis protein (PyrABCN), putative	36	membrane///aspartate carbamoyltransferase activity///cytoplasm///carbamoyl-phosphate synthase activity///pyrimidine base biosynthetic process
Afu3g03180	NAD binding Rossmann fold oxidoreductase	37	oxidoreductase activity///metabolic process
Afu2g05050	hypothetical protein	38	
Afu3g12910	O-methyltransferase GliM-like	39	S-adenosylmethionine-dependent methyltransferase activity///O-methyltransferase activity
Afu4g13290	HAD superfamily hydrolase	40	cytoplasm///nucleus///metabolic process///hydrolase activity
Afu2g17210	hypothetical protein	41	
Afu2g04390	cytomegalovirus gH-receptor family protein	42	cellular component unknown///biological process unknown///molecular function unknown
Afu1g07300	tetracycline transporter	43	transporter activity///transport
Afu5g10710	hypothetical protein	44	
Afu7g01220	farnesyl-diphosphate farnesyltransferase	45	farnesyl-diphosphate farnesyltransferase activity///endoplasmic reticulum///ergosterol biosynthetic process
Afu6g14170	CDF zinc transporter (Msc2), putaitve	46	membrane///cellular zinc ion homeostasis///nucleus///endoplasmic reticulum///cation:cation antiporter activity
Afu1g11820	MFS transporter	47	integral to plasma membrane///transporter activity///transport
Afu4g11690	RNA polymerase II transcription factor related protein	48	"negative regulation of transcription from RNA polymerase II promoter, mitotic"///nucleotide-excision repair factor 3 complex///holo TFIIH complex///nucleotide-excision repair///transcription initiation from RNA polymerase II promoter///general RNA polymerase II transcription factor

			activity///"nucleotide-excision repair, DNA duplex unwinding"
Afu5g13750	calcium binding protein Caleosin	49	
Afu5g13240	inositol hexaphosphate kinase KCS1	50	inositol or phosphatidylinositol kinase activity///vacuole organization///cytoplasm///response to stress
Afu2g09420	F-box domain protein	51	
Afu6g13210	oxidoreductase, short-chain dehydrogenase/reductase family	52	
Afu4g06060	hypothetical protein	53	
Afu4g03980	chromosome segregation protein (Pcs1)	54	
Afu5g05690	chorismate mutase/prephenate dehydratase	55	
Afu8g01120	hypothetical protein	56	
Afu2g13490	KH domain protein	57	
Afu6g10940	hypothetical protein	58	
Afu2g03780	hypothetical protein	59	cytoplasm///biological process unknown///molecular function unknown
Afu3g07960	alpha-ketoglutarate-dependent taurine dioxygenase	60	cellular component unknown///sulfur metabolic process///sulfonate dioxygenase activity
Afu3g08110	cell wall protein	61	
Afu6g06510	extracellular triacylglycerol lipase	62	cellular component unknown///lipase activity///biological process unknown
Afu7g06610	isochorismatase family hydrolase	63	
Afu5g09480	ABC transporter	64	ATP-binding cassette (ABC) transporter activity///membrane///transport
Afu3g07120	MFS transporter	65	plasma membrane///transporter activity///transport
Afu2g12410	hypothetical protein	66	cytoplasm///biological process unknown///molecular function unknown
Afu2g14490	endoglucanase	67	
Afu1g09370	pentatricopeptide repeat protein	68	
Afu1g09570	hypothetical protein	69	
Afu5g02770	hypothetical protein	70	
Afu6g04790	proteasome component Pre5	71	ubiquitin-dependent protein catabolic process///""proteasome core complex, alpha-subunit complex""///"proteasome core

			complex///endopeptidase activity"
Afu7g02500	polysaccharide synthase Cps1	72	carbohydrate metabolic process///"transferase activity, transferring glycosyl groups"
Afu4g12950	vacuolar targeting protein Atg24	73	membrane///autophagy///lipid binding///transport
Afu1g14540	oxidoreductase, short-chain dehydrogenase/reductase family	74	
Afu1g03550	mitochondrial dihydroxy acid dehydratase	75	dihydroxy-acid dehydratase activity///branched chain family amino acid biosynthetic process///mitochondrion
Afu5g06580	MFS multidrug transporter	76	drug transport///drug transporter activity///integral to membrane
Afu4g04190	hypothetical protein	77	
Afu6g11720	hypothetical protein	78	
Afu3g02470	amidase family protein	79	allophanate hydrolase activity///urea metabolic process///cytoplasm///urea carboxylase activity
Afu2g17170	Na+/H+ antiporter Nha1	80	cellular monovalent inorganic cation homeostasis///plasma membrane///cation:cation antiporter activity
Afu6g11190	protein kinase (VPS15)	81	Golgi membrane///protein serine/threonine kinase activity///vacuolar transport///protein retention in Golgi apparatus///protein binding///protein amino acid phosphorylation///protein targeting to vacuole
Afu8g04580	hypothetical protein	82	
Afu1g12880	epoxide hydrolase	83	metabolic process///hydrolase activity
Afu8g00580	glutathione S-transferase	84	cytosolic ribosome (sensu Eukaryota)///regulation of translational elongation///translation elongation factor activity
Afu6g03030	phenol monooxygenase	85	FAD binding
Afu5g08210	dolichyl-phosphate beta-glucosyltransferase	86	protein amino acid N-linked glycosylation///dolichyl-phosphate beta-glucosyltransferase activity///endoplasmic reticulum membrane
Afu1g04780	peroxisomal ABC transporter (PXA1)	87	ATP-binding cassette (ABC) transporter activity///integral to peroxisomal membrane///fatty acid transport
Afu2g17050	nuclear export protein Noc3	88	DNA replication initiation///chromatin binding///nucleolus///protein binding///rRNA processing///nucleus
Afu2g12510	hypothetical protein	89	
Afu5g09750	nucleoside transporter	90	nucleoside transmembrane transporter activity///nucleoside transport
Afu6g07220	sreptomyces cyclase/dehydrase family protein	91	
Afu8g05300	RNA polymerase II subunit 7	92	transcription from RNA polymerase II promoter///"DNA-directed RNA polymerase II, core complex"///DNA-directed RNA polymerase activity
Afu2g02540	bZIP transcription	93	response to drug///transcription factor

	factor (Fcr3)		activity///transcription///nucleus
Afu4g08480	26S proteasome regulatory subunit Rpn2	94	ubiquitin-dependent protein catabolic process///endopeptidase activity///proteasome regulatory particle///receptor activity
Afu8g00520	integral membrane protein	95	
Afu4g09860	C6 transcription factor	96	transcription factor activity///nucleus///zinc ion binding///regulation of transcription
Afu1g10300	hypothetical protein	97	
Afu1g06840	vacuolar membrane PQ loop repeat protein	98	fungal-type vacuole membrane///cytoplasm///biological process unknown///molecular function unknown
Afu3g12170	MFS sugar transporter	99	membrane///transporter activity///transport
Afu5g02710	hypothetical protein	100	

Table 10.18: 100 genes with greatest log_2 ratios (Δ*laeA*:Af293) at 8 hrs post infection. Genes are reported ranked according to greatest log_2 ratios at 8 hours where 1 is the greatest.

ORF	Description	Rank	GO Biological Process
Afu1g09660	mitochondrial 2-oxodicarboxylate carrier protein, putative	1	mitochondrial transport///intracellular transporter activity///mitochondrial inner membrane///organic acid transmembrane transporter activity
Afu2g13530	translation elongation factor EF-2 subunit	2	
Afu2g09710	protein kinase (NpkA)	3	regulation of progression through cell cycle///G1/S transition of mitotic cell cycle///regulation of meiosis///S phase of mitotic cell cycle///cytoplasm///nucleus///protein amino acid phosphorylation///cyclin-dependent protein kinase activity///G2/M transition of mitotic cell cycle///protein kinase activity
Afu4g06060	hypothetical protein	4	
Afu4g11130	hypothetical protein	5	
Afu6g10500	hypothetical protein	6	
Afu6g03890	spore-specific catalase CatA	7	intracellular immature spore///response to oxidative stress///cytoplasm///catalase activity
Afu5g09750	nucleoside transporter	8	nucleoside transmembrane transporter activity///nucleoside transport
Afu3g06080	multicopy suppressor of stt4 mutation	9	plasma membrane///1-phosphatidylinositol-4-phosphate 5-kinase activity///actin cable formation///actin cytoskeleton organization
Afu6g08020	ABC transporter	10	ATP-binding cassette (ABC) transporter activity///transport///integral to membrane
Afu1g16540	WD40 domain	11	

	protein		
Afu6g03700	hypothetical protein	12	
Afu4g08380	hypothetical protein	13	
Afu4g04440	conserved leucine-rich repeat protein	14	
Afu6g14170	CDF zinc transporter (Msc2), putaitve	15	membrane///cellular zinc ion homeostasis///nucleus///endoplasmic reticulum///cation:cation antiporter activity
Afu1g17350	CP2 transcription factor	16	
Afu5g03010	hypothetical protein	17	
Afu6g14250	endosomal integral membrane protein (P24a)	18	membrane fraction///biological process unknown///molecular function unknown
Afu3g14420	chitin synthase ChsG	19	chitin synthase activity///plasma membrane///chitin biosynthetic process///pathogenesis
Afu8g00410	methionine aminopeptidase, type II	20	proteolysis///methionyl aminopeptidase activity///cytoplasm
Afu4g11510	mannose-1-phosphate guanylyltransferase	21	protein amino acid glycosylation///cytoplasm///GDP-mannose biosynthetic process///mannose-1-phosphate guanylyltransferase activity///cell wall mannoprotein biosynthetic process
Afu5g03130	chromatin assembly factor 1 subunit C	22	chromatin silencing at telomere///H3/H4 histone acetyltransferase activity///chromatin assembly or disassembly///cytoplasm///nucleus
Afu8g01260	hypothetical protein	23	
Afu2g09300	hypothetical protein	24	
Afu5g05500	D-3-phosphoglycerate dehydrogenase	25	phosphoglycerate dehydrogenase activity///cytoplasm///serine family amino acid biosynthetic process
Afu6g11170	C2H2 finger domain protein (Ezf)	26	DNA binding///nucleus///zinc ion binding
Afu1g13250	1-phosphatidylinositol-4,5-bisphosphate phosphodiesterase Plc1	27	phosphoinositide phospholipase C activity///pseudohyphal growth///cell growth and/or maintenance///nucleus///signal transduction///condensed nuclear chromosome kinetochore
Afu4g00320	sensor histidine kinase/response regulator	28	protein histidine kinase activity///two-component sensor activity///protein amino acid phosphorylation
Afu2g16040	rRNA biogenesis protein RRP5	29	nucleolus organizer region///nucleolus///rRNA processing///RNA binding///maturation of SSU-rRNA///snoRNA binding
Afu1g02070	cytochrome C1/Cyt1	30	"electron transporter, transferring electrons within CoQH2-cytochrome c reductase complex activity"///mitochondrial

			respiratory chain complex III///mitochondrial inner membrane///mitochondrial respiratory chain///oxidative phosphorylation///"mitochondrial electron transport, ubiquinol to cytochrome c"
Afu3g07120	MFS transporter	31	plasma membrane///transporter activity///transport
Afu7g04580	TBC domain protein	32	
Afu1g17230	hypothetical protein	33	
Afu6g04300	hypothetical protein	34	
Afu7g06960	monooxygenase	35	
Afu4g01560	MFS myo-inositol transporter	36	myo-inositol transport///membrane///myo-inositol transmembrane transporter activity
Afu6g02680	ankyrin repeat and BTB/POZ domain protein	37	cytoplasm///biological process unknown///molecular function unknown
Afu7g04060	hypothetical protein	38	
Afu1g03610	hypothetical protein	39	
Afu6g12370	hypothetical protein	40	cytoplasm///biological process unknown///molecular function unknown
Afu4g08610	calcium homeostasis protein Regucalcin	41	cellular component unknown
Afu1g01190	hypothetical protein	42	
Afu2g07350	gamma-glutamyl phosphate reductase	43	proline biosynthetic process///cytoplasm///glutamate-5-semialdehyde dehydrogenase activity///nucleus
Afu4g04810	Rab GTPase SrgA	44	
Afu1g14260	TGF beta receptor associated protein 1	45	
Afu3g06100	hypothetical protein	46	
Afu1g12580	hypothetical protein	47	
Afu1g06860	protein phophatase 2C family protein	48	cellular component unknown///protein phosphatase type 2C activity///biological process unknown
Afu2g09700	superoxide dismutase copper chaperone Lys7	49	removal of superoxide radicals///superoxide metabolic process///superoxide dismutase copper chaperone activity///cytosol///intracellular copper ion transport
Afu4g01290	endo-chitosanase, pseudogene	50	
Afu1g06300	proteasome regulatory particle subunit (RpnF), putative	51	proteasome regulatory particle, lid subcomplex""///endopeptidase activity"///"ubiquitin-dependent protein catabolic process
Afu5g12350	ribonucleotide reductase small	52	DNA replication///ribonucleoside-diphosphate reductase activity///cytoplasm///nucleus

	subunit RnrA		
Afu3g09640	camp independent regulatory protein	53	cytoplasm///nucleus///biological process unknown///molecular function unknown
Afu3g11030	histone chaperone ASF1	54	chromatin assembly complex///nucleosome assembly///programmed cell death///histone binding
Afu3g14970	thioredoxin Trx1	55	DNA-dependent DNA replication///electron transport"///""vacuole fusion, non-autophagic""///response to oxidative stress///cytoplasm///fungal-type vacuole///regulation of cell redox homeostasis///"thiol-disulfide exchange intermediate activity///vacuole inheritance
Afu2g03950	serine/threonine protein phosphatase	56	cellular component unknown///cellular sodium ion homeostasis///protein serine/threonine phosphatase activity
Afu3g13210	protein kinase domain-containing protein	57	protein kinase activity
Afu6g08860	sugar isomerase, KpsF/GutQ	58	
Afu1g02380	hypothetical protein	59	
Afu5g11330	hypothetical protein	60	
Afu7g05880	hypothetical protein	61	
Afu2g12380	intracellular protein transport protein (Sat1), putative	62	intracellular protein transport///guanyl-nucleotide exchange factor activity///Golgi apparatus
Afu4g06210	JmjC domain protein	63	DNA binding
Afu8g04950	transcription initiation factor TFIID subunit TSM1/127kD	64	transcription initiation from RNA polymerase II promoter///regulation of transcription involved in G1 phase of mitotic cell cycle///general RNA polymerase II transcription factor activity///transcription factor TFIID complex
Afu6g11500	dipeptidase	65	
Afu6g07540	t-complex protein 1, epsilon subunit	66	chaperone activity///cytoplasm///protein folding///cytoskeleton organization///cytoskeleton
Afu3g07710	nucleolin protein Nsr1	67	ribosomal small subunit assembly///single-stranded DNA binding///nucleolus///rRNA processing///nucleus///programmed cell death///RNA binding
Afu5g14330	12-oxophytodienoate reductase	68	NADPH dehydrogenase activity///cytoplasm///nucleus///biological process unknown
Afu5g08210	dolichyl-phosphate beta-glucosyltransferase	69	protein amino acid N-linked glycosylation///dolichyl-phosphate beta-glucosyltransferase activity///endoplasmic reticulum membrane
Afu3g06280	Rho GTPase activator (Rgd1)	70	osmosensory signaling pathway///Rho GTPase activator activity
Afu2g17050	nuclear export protein Noc3	71	DNA replication initiation///chromatin binding///nucleolus///protein binding///rRNA processing///nucleus
Afu2g03540	extracellular	72	

	threonine rich protein		
Afu7g08530	hypothetical protein	73	
Afu1g03530	MFS sugar transporter	74	hexose transport///mannose transmembrane transporter activity///fructose transmembrane transporter activity///plasma membrane///glucose transmembrane transporter activity
Afu1g08870	hypothetical protein	75	
Afu2g05320	calcium-proton exchanger	76	calcium ion transport///calcium:hydrogen antiporter activity///fungal-type vacuole///calcium ion transmembrane transporter activity///cellular calcium ion homeostasis///vacuolar membrane
Afu2g12260	cytochrome c oxidase assembly protein Cox11	77	aerobic respiration///mitochondrial inner membrane///molecular function unknown
Afu7g00340	metallo-beta-lactamase domain protein	78	catalytic activity///metabolic process
Afu3g06560	lipoic acid synthetase precursor	79	catalytic activity///mitochondrion///fatty acid metabolic process
Afu1g17550	HET domain protein	80	
Afu8g01430	oxidoreductase, zinc-binding dehydrogenase family, putative	81	cellular component unknown///oxidoreductase activity///metabolic process///zinc ion binding
Afu7g08620	hypothetical protein	82	
Afu6g12440	hypothetical protein	83	
Afu5g03220	microsomal signal peptidase subunit (gp23)	84	
Afu5g02770	hypothetical protein	85	
Afu3g08030	tRNA (guanine) methyltransferase Trm5	86	tRNA (guanine) methyltransferase activity///cytoplasm///nucleus///tRNA methylation
Afu5g03240	pyruvate dehydrogenase kinase	87	biological process unknown///mitochondrion///protein kinase activity
Afu3g11400	aspartic endopeptidase Pep2	88	aspartic-type endopeptidase activity///protein catabolic process///extracellular region///fungal-type cell wall
Afu6g09020	GPI transamidase component Gpi16	89	integral to endoplasmic reticulum membrane///GPI-anchor transamidase activity///attachment of GPI anchor to protein///GPI-anchor transamidase complex
Afu4g06490	DNA mismatch repair protein	90	reciprocal meiotic recombination///mismatch repair///nucleus///molecular function unknown

	(Mlh3)		
Afu3g11660	DUF221 domain protein	91	cellular component unknown///biological process unknown///molecular function unknown
Afu3g02470	amidase family protein	92	allophanate hydrolase activity///urea metabolic process///cytoplasm///urea carboxylase activity
Afu2g14850	enoyl-CoA hydratase/isomerase family protein	93	
Afu3g13310	ribosomal protein S15	94	
Afu1g10240	hypothetical protein	95	
Afu6g09100	hypothetical protein	96	
Afu6g13530	UPF0023 family protein	97	cytoplasm///nucleus///35S primary transcript processing///molecular function unknown
Afu3g03810	hypothetical protein	98	
Afu4g07590	CaaX prenyl protease Ste24	99	integral to endoplasmic reticulum membrane///metalloendopeptidase activity///prenyl-dependent CAAX protease activity///conjugation with cellular fusion///peptide pheromone maturation
Afu5g06660	UPF0187 domain membrane protein	100	

Table 10.19: 100 genes with lowest log_2 ratios (Δ*laeA*:Af293) at 8 hrs post infection. Genes are reported ranked according to lowest log_2 ratios at 8 hours where 1 is the greatest.

ORF	Description	Rank	GO Biological Process
Afu6g08570	DNA damage repair protein Mus42	1	DNA-directed DNA polymerase activity///DNA-dependent DNA replication///DNA repair///nucleus
Afu3g13010	Zn-dependent hydrolase/oxidoreductase family protein, putative	2	
Afu1g15910	C6 transcription factor RosA-like	3	RNA polymerase II transcription factor activity///nucleus///regulation of transcription
Afu6g02670	G2-specific protein kinase NimA	4	regulation of transcription involved in G2-phase of mitotic cell cycle///chromosome segregation///protein kinase activity
Afu1g12700	hypothetical protein	5	
Afu6g03420	trehalose synthase, pseudogene, similar to GB:AAC64285.1: clock-controlled gene-9 protein [Neurospora crassa]	6	

Afu2g06060	transcriptional co-activator (Hfi1/Ada1)	7	
Afu3g01030	RTA1 domain protein	8	biological process unknown///molecular function unknown///integral to membrane
Afu5g06460	C6 finger domain protein	9	zinc ion binding
Afu8g04220	rRNA maturation protein (Nop14)	10	nucleolus///nucleus///maturation of SSU-rRNA///small nucleolar ribonucleoprotein complex///snoRNA binding
Afu6g04830	HATPase_c domain protein	11	ATP binding
Afu4g14350	kelch repeat protein	12	
Afu2g02650	hypothetical protein	13	
Afu7g02230	mRNA binding post-transcriptional regulator (Csx1), putative	14	commitment complex///mRNA splice site selection"///""nuclear mRNA splicing, via spliceosome""///RNA binding///mRNA binding///"U1 snRNP
Afu5g13790	C6 transcription factor (Acr-2)	15	transcription factor activity///nucleus///regulation of transcription
Afu5g11590	glycerophosphocholine phosphodiesterase Gde1	16	phospholipid catabolic process///cytoplasm///glycerophosphodiester phosphodiesterase activity
Afu4g14660	hypothetical protein	17	
Afu5g01000	oxidoreductase, 2OG-Fe(II) oxygenase family	18	oxidoreductase activity///metabolic process
Afu3g02140	ion channel	19	nonselective channel activity///ion channel activity///transport
Afu1g02750	hypothetical protein	20	
Afu1g08800	cytochrome P450 phenylacetate hydroxylase	21	oxidoreductase activity///metabolic process
Afu1g15900	importin beta-2 subunit	22	cell cycle///protein import into nucleus///nuclear localization sequence binding///cytosol///mRNA-binding (hnRNP) protein import into nucleus
Afu6g13060	hypothetical protein	23	
Afu5g14640	haloacid dehalogenase, type II	24	
Afu5g03880	signal recognition particle protein SRP54	25	signal sequence binding///"signal recognition particle, endoplasmic reticulum targeting"///protein targeting to ER
Afu8g07225	hypothetical protein	26	
Afu1g01070	hypothetical protein	27	
Afu1g03130	hypothetical	28	

	protein		
Afu7g05770	hypothetical protein	29	
Afu6g01850	hypothetical protein	30	
Afu2g09930	hypothetical protein	31	
Afu5g14660	GABA permease	32	plasma membrane///choline transmembrane transporter activity///choline transport
Afu1g03590	importin 11	33	nuclear pore///cytoplasm///protein import into nucleus///structural constituent of nuclear pore
Afu2g04720	ubiquitin C-terminal hydrolase	34	ubiquitin-specific protease activity///cytoplasm///protein deubiquitination
Afu7g01270	DNA-directed polymerase kappa	35	
Afu6g01940	dienelactone hydrolase family protein	36	
Afu6g03900	F-box domain protein	37	
Afu4g04560	GTP binding protein	38	
Afu2g14340	hypothetical protein	39	
Afu7g06450	hypothetical protein	40	
Afu4g03990	membrane-spanning ATPase	41	
Afu1g12490	sexual development activator VeA	42	antibiotic biosynthetic process///secondary metabolic process///sporocarp development
Afu2g04780	WD repeat protein	43	cellular component unknown///biological process unknown
Afu2g12570	peptidase family M20/M25/M40 protein	44	
Afu6g09670	cytochrome P450 oxidoreductase GliC	45	oxidoreductase activity///metabolic process
Afu3g13230	AT DNA binding protein	46	nucleus///AT DNA binding
Afu3g09100	hypothetical protein	47	
Afu5g05680	peptide chain release factor eRF/aRF, subunit 1	48	translation release factor activity, codon specific"""///translational termination///"cytosol
Afu8g06890	extracellular exo-polygalacturonase	49	pectin catabolic process///extracellular region///polygalacturonase activity
Afu3g00380	beta-galactosidase	50	
Afu7g01090	proline permease PrnB	51	plasma membrane///neutral amino acid transmembrane transporter activity///neutral amino acid transport///amino acid permease activity
Afu1g09880	hypothetical	52	

	protein		
Afu1g09770	La domain family	53	
Afu6g11440	pyridoxamine phosphate oxidase family protein	54	
Afu7g04930	alkaline serine protease (PR1)/allergen F18-like	55	peptidase activity///cellular component unknown///protein catabolic process
Afu7g06480	hypothetical protein	56	
Afu5g03710	hypothetical protein	57	
Afu6g08770	ankyrin repeat protein	58	
Afu8g04400	RNA binding protein	59	rRNA metabolic process///nucleolus///RNA binding
Afu6g11610	1,4-beta-D-glucan-cellobiohydrolyase	60	
Afu2g10300	40S ribosomal protein S17	61	structural constituent of ribosome///ribosomal small subunit assembly///translation///cytosolic small ribosomal subunit (sensu Eukaryota)
Afu2g04450	HECT domain protein	62	cellular component unknown///ubiquitin-protein ligase activity///protein polyubiquitination///protein monoubiquitination
Afu1g11810	hypothetical protein	63	
Afu3g00420	acetyl xylan esterase (Axe1)	64	cellulose binding///xylan metabolic process///acetylxylan esterase activity
Afu3g07640	plasma membrane H+-ATPase Pma1	65	proton transport"///plasma membrane///regulation of pH///"""hydrogen-exporting ATPase activity, phosphorylative mechanism""
Afu3g04160	Ser/Thr protein phosphatase family	66	fungal-type vacuole///biological process unknown///molecular function unknown
Afu3g11300	proteasome component Prs2	67	proteasome core complex, alpha-subunit complex""///endopeptidase activity"///"ubiquitin-dependent protein catabolic process
Afu8g06090	amino acid permease	68	plasma membrane///choline transmembrane transporter activity///choline transport
Afu4g02940	bZIP transcription factor	69	
Afu1g01990	ribosome biogenesis protein Rsa4	70	cellular component unknown///biological process unknown///molecular function unknown
Afu2g12520	hypothetical protein	71	
Afu8g04500	mannosyltransferase PMTI	72	endoplasmic reticulum///dolichyl-phosphate-mannose-protein mannosyltransferase activity///protein amino acid O-linked glycosylation
Afu6g12910	dsDNA-dependent ATPase Rad54	73	chromatin remodeling///DNA supercoiling activity///telomere maintenance via recombination///double-strand break repair via synthesis-dependent strand annealing///nucleus///double-

			strand break repair via single-strand annealing///DNA-dependent ATPase activity///double-strand break repair via break-induced replication///heteroduplex formation
Afu6g07700	chromosomal organization and DNA repair protein Mms21, putative	74	
Afu2g03150	kinesin family protein	75	kinesin complex///microtubule motor activity///establishment of mitotic spindle orientation///cytoplasmic microtubule///microtubule depolymerization///nuclear microtubule
Afu2g12340	hypothetical protein	76	
Afu6g00480	hypothetical protein	77	
Afu2g16030	WD repeat protein	78	
Afu7g06290	Pfs, NACHT, and Ankyrin domain protein	79	purine-nucleoside phosphorylase activity///GTP binding///protein binding///programmed cell death
Afu1g11920	SH3 domain protein	80	protein binding
Afu1g00320	hypothetical protein	81	
Afu5g03960	class V chitinase Chi100	82	extracellular region///chitinase activity///chitin binding///chitin catabolic process
Afu6g09720	methyltransferase GliN	83	
Afu5g11720	26S proteasome regulatory subunit Mts4	84	ubiquitin-dependent protein catabolic process///cytoplasm///endopeptidase activity///endoplasmic reticulum///proteasome regulatory particle///receptor activity
Afu5g04270	AMP-binding enzyme	85	N-terminal protein myristoylation///peroxisome///lipid metabolic process///long-chain-fatty-acid-CoA ligase activity
Afu3g06170	mating type protein MAT1-2-1	86	
Afu7g00620	hypothetical protein	87	
Afu4g12070	endosomal peripheral membrane protein (Mon2)	88	endosome///protein targeting to vacuole///transport
Afu8g05850	FAD dependent oxidoreductase superfamily	89	
Afu6g11850	hypothetical protein	90	
Afu3g03670	ABC multidrug transporter	91	ATP-binding cassette (ABC) transporter activity///ATP binding///transport
Afu4g06430	hypothetical protein	92	
Afu2g03500	sugar transporter	93	
Afu1g14550	Mn superoxide dismutase MnSOD	94	manganese superoxide dismutase activity///oxygen and reactive oxygen species metabolic

			process///mitochondrion///mitochondrial matrix
Afu2g14240	hypothetical protein	95	
Afu3g01530	phosphatidylglycerol specific phospholipase	96	
Afu4g14640	low affinity iron transporter	97	iron ion transmembrane transporter activity///low-affinity iron ion transport///integral to plasma membrane///intracellular copper ion transport
Afu1g01530	GrpB domain protein	98	
Afu3g04010	MFS transporter	99	nicotinamide mononucleotide permease activity///nicotinamide mononucleotide transport///integral to plasma membrane
Afu2g17720	PAF acetylhydrolase family protein	100	

Table 10.20: 100 genes with greatest log_2 ratios (Δ*laeA*:Af293) at 14 hrs post infection. Genes are reported ranked according to greatest log_2 ratios at 14 hours where 1 is the greatest.

ORF	Description	Rank	GO Biological Process
Afu3g03780	hypothetical protein	1	
Afu6g08570	DNA damage repair protein Mus42	2	DNA-directed DNA polymerase activity///DNA-dependent DNA replication///DNA repair///nucleus
Afu6g07370	hypothetical protein	3	
Afu5g00470	general amidase GmdB	4	cellular component unknown///amidase activity///biological process unknown
Afu4g03110	MFS monosaccharide transporter	5	
Afu6g11250	C2H2 finger domain protein	6	
Afu1g12360	hypothetical protein	7	
Afu5g11350	Ndc80 complex component Nuf2	8	
Afu5g12310	pseudouridine synthase	9	
Afu2g08820	hypothetical protein	10	
Afu6g00640	integral membrane protein	11	
Afu6g03420	trehalose synthase, pseudogene, similar to GB:AAC64285.1: clock-controlled gene-9 protein [Neurospora crassa]	12	
Afu6g07420	F-box domain protein	13	
Afu6g08330	hypothetical protein	14	
Afu6g09356	hypothetical protein	15	
Afu3g06170	mating type protein	16	

	MAT1-2-1		
Afu2g09310	Mitochondrial ATP synthase epsilon chain domain-containing protein	17	
Afu3g12830	RTA1 domain protein	18	
Afu2g05180	NF-X1 finger and helicase domain protein	19	DNA binding///DNA helicase activity///nucleus///zinc ion binding///RNA helicase activity
Afu8g01970	extracellular endo-polygalacturonase	20	pectin catabolic process///pseudohyphal growth///extracellular region///polygalacturonase activity
Afu6g09570	hypothetical protein	21	
Afu4g12440	sulfate transporter family protein	22	fungal-type vacuole///biological process unknown///molecular function unknown
Afu8g06820	dihydrofolate reductase family protein	23	
Afu1g02450	hypothetical protein	24	
Afu6g14610	alfa-L-rhamnosidase	25	
Afu1g13340	DUF6 domain protein	26	biological process unknown///molecular function unknown///integral to membrane
Afu1g00320	hypothetical protein	27	
Afu7g01890	C6 transcription factor	28	transcription factor activity///regulation of transcription
Afu5g08330	RNA binding protein	29	cytoplasm///RNA binding///regulation of cell size
Afu1g00150	IBR finger domain protein	30	
Afu2g04920	nuclear pore complex subunit Nup159	31	mRNA export from nucleus///ribosomal subunit export from nucleus///structural molecule activity///nuclear pore///rRNA export from nucleus///nuclear pore organization
Afu1g08830	Golgi matrix protein	32	ER to Golgi vesicle-mediated transport///molecular function unknown///Golgi apparatus
Afu1g02660	F-box domain protein	33	
Afu5g14640	haloacid dehalogenase, type II	34	
Afu2g08640	hypothetical protein	35	
Afu6g07580	essential cytoplasmic protein Ctr86	36	cytoplasm///biological process unknown///molecular function unknown
Afu6g00690	hypothetical protein	37	
Afu2g08800	amino acid permease (Dip5)	38	amino acid transport///plasma membrane///amino acid transmembrane transporter activity///amino acid permease activity
Afu3g14810	pathogenesis associated protein Pep2	39	
Afu1g17700	short chain dehydrogenase	40	oxidoreductase activity///metabolic process
Afu2g17810	RTA1 domain protein	41	
Afu5g14860	cytochrome P450	42	
Afu3g11020	CFIA complex component Rna14	43	cleavage and polyadenylylation specificity factor activity///mRNA cleavage factor complex///nucleus///mRNA polyadenylation///mitochondrion///mRNA cleavage
Afu6g04500	Snf1 kinase complex beta-subunit Gal83	44	AMP-activated protein kinase activity///nucleus///protein amino acid phosphorylation///signal transduction///cell

			adhesion///filamentous growth
Afu1g11360	aldehyde reductase II	45	cellular component unknown///dihydrokaempferol 4-reductase activity///biological process unknown
Afu3g02800	lipase/esterase	46	
Afu6g06840	hypothetical protein	47	
Afu6g10250	alkaline serine protease AorO	48	
Afu3g10660	hydroxymethylglutaryl-CoA synthase Erg13	49	hydroxymethylglutaryl-CoA synthase activity///endoplasmic reticulum///mitochondrion///ergosterol biosynthetic process
Afu7g06620	integral membrane protein Pth11-like	50	
Afu4g14840	transferase family protein	51	
Afu5g03960	class V chitinase Chi100	52	extracellular region///chitinase activity///chitin binding///chitin catabolic process
Afu3g12910	O-methyltransferase GliM-like	53	S-adenosylmethionine-dependent methyltransferase activity///O-methyltransferase activity
Afu3g01360	siderochrome-iron transporter	54	siderophore-iron transport///siderophore-iron transmembrane transporter activity///integral to membrane
Afu6g12340	GTPase activating protein (BUD2/CLA2)	55	GTPase activator activity///intracellular///signal transducer activity///small GTPase mediated signal transduction///Ras GTPase activator activity
Afu1g08800	cytochrome P450 phenylacetate hydroxylase	56	oxidoreductase activity///metabolic process
Afu2g01060	Rho GTPase activator (Sac7)	57	intracellular///signal transducer activity///small GTPase mediated signal transduction///actin filament reorganization during cell cycle///Rho GTPase activator activity
Afu6g12230	hypothetical protein	58	
Afu5g01620	extracellular proline-rich protein	59	
Afu2g15840	HET-C domain protein HetC	60	programmed cell death///signal transduction
Afu5g10080	hypothetical protein	61	
Afu4g06790	ubiquinol-cytochrome c reductase complex 14 kDa protein	62	aerobic respiration///mitochondrial respiratory chain complex III///"respiratory chain complex III assembly///ubiquinol-cytochrome-c reductase activity///""mitochondrial electron transport, ubiquinol to cytochrome c"""
Afu1g15670	laccase TilA	63	high-affinity iron ion transport///plasma membrane///ferroxidase activity
Afu4g03850	protein kinase Yak1	64	
Afu6g02670	G2-specific protein kinase NimA	65	regulation of transcription involved in G2-phase of mitotic cell cycle///chromosome segregation///protein kinase activity
Afu6g12980	spindle pole body component	66	spindle pole body///microtubule nucleation///microtubule binding///structural constituent of cytoskeleton
Afu8g05640	WD repeat protein	67	
Afu3g09690	extracellular thaumatin domain protein	68	
Afu4g08230	aldehyde reductase	69	aldo-keto reductase activity///cytoplasm///cellular aldehyde metabolic process
Afu4g10460	homocitrate synthase	70	lysine biosynthetic process via aminoadipic

			acid///nucleus///homocitrate synthase activity
Afu8g04230	hypothetical protein	71	
Afu7g06470	hypothetical protein	72	
Afu6g09630	C6 finger domain protein GliZ	73	
Afu4g14440	NRPS-like enzyme	74	CoA-ligase activity///nonribosomal peptide biosynthetic process///cytoplasm
Afu2g17960	NADPH dehydrogenase Oye3	75	
Afu2g15820	SNARE complex subunit (Syn8)	76	
Afu4g03900	peroxisomal multifunctional beta-oxidation protein (MFP)	77	
Afu5g10960	hypothetical protein	78	
Afu5g08870	hypothetical protein	79	
Afu7g05960	C2H2 finger domain protein	80	DNA binding///cytoplasm///nucleus///zinc ion binding
Afu1g03080	ribosomal protein/carboxylic ester hydrolase (Ppe1), putative	81	cellular component unknown///carboxylic ester hydrolase activity///protein modification process
Afu6g03440	fructosyl amino acid oxidase	82	
Afu5g15140	hypothetical protein	83	
Afu6g07490	WD repeat protein	84	cytoplasm///biological process unknown///molecular function unknown
Afu1g00550	hypothetical protein	85	
Afu7g06800	glutamyl-tRNA(Gln) amidotransferase, subunit A	86	
Afu6g01850	hypothetical protein	87	
Afu2g12850	1,3-beta-glucanosyltransferase Gel3	88	cell wall organization///"1,3-beta-glucanosyltransferase activity"///fungal-type cell wall
Afu2g07800	GPI anchored protein	89	
Afu2g14060	NADH-cytochrome b5 reductase	90	cytochrome-b5 reductase activity///microsome///electron transport
Afu1g09260	acetyltransferase, GNAT family family	91	
Afu2g00820	extracellular GDSL-like lipase/acylhydrolase	92	lipase activity
Afu1g09880	hypothetical protein	93	
Afu8g02780	vacuolar protein sorting protein	94	signal sequence binding///vacuolar transport///protein targeting to vacuole///Golgi apparatus
Afu5g11910	DNA repair and transcription protein (Xab2)	95	cell cycle///""nuclear mRNA splicing, via spliceosome"""///"spliceosomal complex
Afu2g10690	MFS phosphate transporter	96	integral to plasma membrane///inorganic phosphate transmembrane transporter activity///phosphate transport

Afu8g04702	MFS transporter	97	plasma membrane///transporter activity///transport
Afu6g03030	phenol monooxygenase	98	FAD binding
Afu5g11170	nucleosome remodeling complex ATPase subunit (Snf2h), putative	99	chromatin remodeling///ISW2 complex///nucleosome remodeling complex///nucleoplasm///NURF complex///DNA replication-dependent nucleosome assembly///ATPase activity///regulation of transcription
Afu6g00600	hypothetical protein	100	

Table 10.21: 100 genes with lowest log_2 ratios (Δ*laeA*:Af293) at 14 hrs post infection. Genes are reported ranked according to lowest log_2 ratios at 14 hours where 1 is the greatest.

ORF	Description	Rank	GO Biological Process
Afu1g05610	protein phosphotase 2a 65kd regulatory sububit	1	actin filament organization///protein amino acid dephosphorylation///spindle pole body///translation///cellular bud neck///protein phosphatase type 2A complex///nucleus///protein phosphatase type 2A activity///cellular bud tip///mating projection///mitotic cell cycle spindle assembly checkpoint///cytoplasm///budding cell bud growth
Afu8g03930	Hsp70 chaperone (HscA)	2	chaperone activity///polysome///translation///cytoplasm///ATPase activity
Afu5g12350	ribonucleotide reductase small subunit RnrA	3	DNA replication///ribonucleoside-diphosphate reductase activity///cytoplasm///nucleus
Afu2g13730	NEDD8 activating enzyme (UbaC)	4	NEDD8 class-dependent protein catabolic process///cytoplasm///NEDD8 activating enzyme activity///protein neddylation during NEDD8 class-dependent protein catabolic process
Afu7g00700	aldo-keto reductase (AKR13), puatative	5	aldo-keto reductase activity///cytoplasm///nucleus///cellular aldehyde metabolic process
Afu1g09280	protein phosphatase PTC2	6	protein amino acid dephosphorylation///DNA damage checkpoint///G1/S transition of mitotic cell cycle///inactivation of MAPK activity involved in osmosensory signaling pathway///cytoplasm///nucleus///regulation of cyclin-dependent protein kinase activity///response to unfolded protein///protein phosphatase type 2C activity
Afu5g01750	MATH and UCH domain protein, putaitve	7	
Afu3g07790	argininosuccinate lyase	8	arginine biosynthetic process///cytosol///argininosuccinate lyase activity
Afu1g02780	L-asparaginase	9	endoplasmic reticulum///asparagine catabolic process///cellular response to nitrogen starvation///nuclear envelope///asparaginase activity///cell wall-bounded periplasmic space
Afu3g07150	succinate-semialdehyde dehydrogenase	10	response to oxidative stress///succinate-semialdehyde dehydrogenase [NAD(P)+] activity///cytoplasm///glutamate catabolic process
Afu5g09690	hypothetical protein	11	

Afu5g08970	oligosaccharyl transferase subunit (beta)	12	dolichyl-diphosphooligosaccharide-protein glycotransferase activity///oligosaccharyltransferase complex///protein amino acid N-linked glycosylation///cell cycle
Afu1g09970	eukaryotic translation initiation factor 3 subunit EifCh	13	translation initiation factor activity///eukaryotic translation initiation factor 3 complex///translational initiation
Afu1g05400	hypothetical protein	14	
Afu1g13350	MFS transporter	15	membrane///transporter activity///transport
Afu3g07260	esterase/lipase	16	
Afu2g01880	low molecular weight phosphotyrosine protein phosphatase	17	protein amino acid dephosphorylation///cytoplasm///nucleus///protein tyrosine phosphatase activity
Afu1g16500	small monomeric GTPase (Gtr2)	18	cytoplasm///nucleus///biological process unknown///small monomeric GTPase activity
Afu2g13380	GATA transcription factor (AreB)	19	regulation of nitrogen utilization///negative regulation of transcription from RNA polymerase II promoter///specific RNA polymerase II transcription factor activity///nucleus///zinc ion binding///nitrogen compound metabolic process
Afu1g15760	phosphatidylserine decarboxylase	20	phosphatidylserine decarboxylase activity///mitochondrial inner membrane///mitochondrion///phosphatidylcholine biosynthetic process
Afu2g01240	beta-fructofuranosidase	21	extracellular region///cytoplasm///beta-fructofuranosidase activity///sucrose catabolic process
Afu3g15010	hypothetical protein	22	
Afu1g05080	60S ribosomal protein P0	23	structural constituent of ribosome///translation///translational elongation///ribosomal large subunit assembly///cytosolic large ribosomal subunit (sensu Eukaryota)
Afu5g01510	amino acid permease	24	plasma membrane///neutral amino acid transmembrane transporter activity///neutral amino acid transport///amino acid permease activity
Afu6g11240	hypothetical protein	25	
Afu3g08320	hypothetical protein	26	
Afu5g09080	transcription factor (SPT8)	27	transcription cofactor activity///chromatin modification///SAGA complex///nucleus///histone acetylation
Afu2g14030	arginyl-tRNA synthetase	28	translation///cytoplasm///arginine-tRNA ligase activity
Afu8g06020	glutamate decarboxylase	29	response to oxidative stress///cytoplasm///glutamate catabolic process///glutamate decarboxylase activity
Afu1g10130	adenosylhomocysteinase	30	adenosylhomocysteinase activity///cytoplasm///selenocysteine metabolic process///methionine metabolic process
Afu2g04840	BSD domain protein	31	
Afu1g01850	C6 finger domain protein	32	
Afu1g12570	RNA binding	33	cellular component unknown///RNA binding///biological

	protein Ligatin/Tma64		process unknown
Afu5g05960	serine/threonine protein kinase	34	cellular component unknown///G1/S transition of mitotic cell cycle///cellular cation homeostasis///protein kinase activity
Afu4g01430	hypothetical protein	35	
Afu5g11130	PAXNEB protein superfamily	36	transcription elongation factor complex///cytoplasm///regulation of transcription from RNA polymerase II promoter///RNA polymerase II transcription elongation factor activity
Afu2g11470	hypothetical protein	37	biological process unknown///molecular function unknown
Afu3g09530	cytochrome P450	38	
Afu1g11730	ADP-ribosylation factor	39	ARF small monomeric GTPase activity///Golgi-associated vesicle///cytosol///ER to Golgi vesicle-mediated transport///intra-Golgi vesicle-mediated transport
Afu1g11500	hypothetical protein	40	
Afu8g04330	hypothetical protein	41	S-adenosylmethionine-dependent methyltransferase activity///cytoplasm///nucleus///biological process unknown
Afu1g01980	IgE binding protein	42	
Afu1g16360	hypothetical protein	43	
Afu3g10320	RING finger domain protein	44	
Afu2g04770	autophagy protein Atg13	45	
Afu5g10480	molybdenum cofactor biosynthetic protein (CnxF), putative	46	Mo-molybdopterin cofactor sulfurase activity///URM1 activating enzyme activity///cytoplasm///protein modification process///Mo-molybdopterin cofactor biosynthetic process
Afu5g07230	carboxyphosphono enolpyruvate phosphonomutase-like protein	47	
Afu3g08380	inorganic diphosphatase	48	phosphate metabolic process///inorganic diphosphatase activity///cytosol
Afu5g02900	SNARE domain protein	49	
Afu6g04430	ARD/ARD family protein	50	cytoplasm///nucleus///biological process unknown///molecular function unknown
Afu1g14590	hypothetical protein	51	
Afu7g05090	glucuronyl hydrolase	52	
Afu2g01920	glutaminyl-tRNA synthetase	53	glutamine-tRNA ligase activity///cytoplasm///tRNA aminoacylation for protein translation
Afu7g00380	GNAT family acetyltransferase	54	
Afu4g10110	homeobox transcription factor	55	cellular copper ion homeostasis///transcription initiation from RNA polymerase II promoter///specific RNA polymerase II

			transcription factor activity///nucleus
Afu4g02830	aldehyde dehydrogenase	56	
Afu2g16620	protein kinase	57	protein amino acid phosphorylation///protein kinase activity
Afu1g15240	prefoldin subunit 4	58	tubulin complex assembly///cytoplasm///tubulin binding
Afu1g12590	RNA-binding La domain protein	59	nucleoplasm///nucleolus///nucleus///RNA binding///tRNA processing
Afu2g09850	oxidoreductase, 2-nitropropane dioxygenase family, putative	60	oxidoreductase activity///metabolic process
Afu3g11310	hypothetical protein	61	
Afu1g05910	hypothetical protein	62	
Afu5g03640	mitochondrial export translocase Oxa1	63	protein transporter activity///mitochondrial translocation///mitochondrial inner membrane
Afu2g05550	hypothetical protein	64	nucleolus///nucleus///biological process unknown///molecular function unknown
Afu8g03950	hypothetical protein	65	
Afu5g04030	50S ribosomal protein L27	66	structural constituent of ribosome///translation///mitochondrial large ribosomal subunit///peptidyltransferase activity
Afu1g06910	arabinogalactan endo-1,4-beta-galactosidase GalA	67	
Afu5g02470	thiamine biosynthesis protein (Nmt1)	68	cellular component unknown///thiamin biosynthetic process///molecular function unknown
Afu2g08580	pyridoxine	69	pyridoxine metabolic process///thiamin biosynthetic process///imidazoleglycerol-phosphate synthase activity///cytoplasm///protein binding
Afu7g02490	mitochondrial molecular chaperone (Atp12)	70	chaperone activity///protein complex assembly///mitochondrial matrix
Afu4g04440	conserved leucine-rich repeat protein	71	
Afu5g10780	UDP-glucose 4-epimerase	72	cellular component unknown///molecular function unknown///galactose metabolic process
Afu1g15930	choline kinase	73	choline kinase activity///cytosol///phosphatidylcholine biosynthetic process
Afu1g13420	phosphotyrosyl phosphatase activator	74	cell fraction///response to osmotic stress///cytosol///protein phosphatase type 2A regulator activity///mitotic spindle organization
Afu1g04530	Ribosomal L18ae protein family	75	structural constituent of ribosome///translation///cytosolic large ribosomal subunit (sensu Eukaryota)
Afu6g07890	telomere silencing protein Zds1	76	
Afu1g13320	6-phosphogluconate	77	

	dehydrogenase family protein		
Afu5g11030	acyltransferase	78	acyltransferase activity///metabolic process
Afu4g09740	t-complex protein 1, theta subunit	79	chaperone activity///cytoplasm///protein folding///cytoskeleton organization///cytoskeleton
Afu7g05470	electron transfer flavoprotein alpha subunit	80	electron carrier activity///mitochondrion///electron transport
Afu2g06140	uracil DNA N-glycosylase Ung1	81	DNA repair///base-excision repair///uracil DNA N-glycosylase activity///nucleus///mitochondrion
Afu1g14990	ATP-dependent RNA helicase (Drs1)	82	nucleolus///ribosomal large subunit assembly///35S primary transcript processing///ATP-dependent RNA helicase activity
Afu6g12390	serine palmitoyl CoA transferase subunit LcbA	83	serine C-palmitoyltransferase complex///membrane fraction///sphingolipid biosynthetic process///serine C-palmitoyltransferase activity///microsome
Afu3g03760	hypothetical protein	84	
Afu4g00830	MFS peptide transporter	85	peptide transporter activity///plasma membrane///peptide transport
Afu1g06190	histone H4 arginine methyltransferase RmtA	86	mRNA export from nucleus///peptidyl-arginine modification///nucleus///protein-arginine N-methyltransferase activity
Afu3g00740	2-dehydropantoate 2-reductase family protein	87	2-dehydropantoate 2-reductase activity///cytoplasm///nucleus///FAD binding
Afu2g16480	DHHC zinc finger membrane protein	88	
Afu5g05560	non-canonical purine NTP pyrophosphatase, rdgB/HAM1 family	89	
Afu2g08300	DnaJ domain protein	90	endoplasmic reticulum lumen///co-chaperone activity///protein folding
Afu1g05280	Golgi complex component (Vps8)	91	membrane fraction///late endosome to vacuole transport///molecular function unknown
Afu2g01640	tryptophanyl-tRNA synthetase	92	tryptophan-tRNA ligase activity///cytoplasm///tryptophanyl-tRNA aminoacylation
Afu5g10550	ATP synthase F1, beta subunit	93	hydrogen ion transporting ATP synthase activity, rotational mechanism""///soluble fraction///"ATP synthesis coupled proton transport///""mitochondrial proton-transporting ATP synthase, catalytic core"""///age-dependent general metabolic decline during replicative cell aging
Afu2g09210	60S ribosomal protein L10	94	structural constituent of ribosome///translation///ribosomal large subunit assembly///cytosolic large ribosomal subunit (sensu Eukaryota)
Afu4g11830	cell cycle control protein (Cwf19)	95	
Afu2g02810	alcohol dehydrogenase, zinc-containing	96	cellular component unknown///"oxidoreductase activity///""oxidoreductase activity, acting on the CH-OH group of donors, NAD or NADP as acceptor"""///metabolic process///zinc ion binding
Afu5g03720	chromatin	97	

	assembly factor 1 subunit A		
Afu3g01920	acyl-CoA dehydrogenase	98	phospholipid catabolic process///fatty acid catabolic process///acyl-CoA dehydrogenase activity
Afu3g06980	hypothetical protein	99	
Afu3g05550	OTU-like cysteine protease	100	protein catabolic process///cysteine-type peptidase activity///cytoplasm///nucleus

10.3.9 Functional classification of differentially expressed genes in Δ*laeA*:Af293

Table 10.22 lists functional categories of interest amoung the 100 most up and downregulated genes.

Table 10.22: Functional classification of selected genes with the greatest log_2 ratio increase and decrease in Δ*laeA* mutant relative to Af293 during the initiation of murine infection. Rank of each gene in either upregulated or down regulated co-horts is given, with the lowest values representing the greatest change.

	Upregulated					Down regulated				
Functional category	**Time-point**	**ORF**	**Description**	**Rank**	**GO annotation**	**Time-point**	**ORF**	**Description**	**Rank**	**GO annotation**
Actin/ microtubule	4 hrs	Afu4g09740	t-complex protein 1, theta subunit	4	chaperone activity///cytoplasm///protein folding///cytoskeleton organization///cytoskeleton	**14 hrs**	Afu1g13420	phosphotyrosyl phosphatase activator	74	cell fraction///response to osmotic stress///cytosol///protein phosphatase type 2A regulator activity///mitotic spindle organization
		Afu5g11560	Arp2/3 complex subunit (Arp3)	14	Arp2/3 protein complex///actin filament organization///actin binding///structural constituent of cytoskeleton					
		Afu2g16920	actin monomer binding protein	34	sequestering of actin monomers///actin monomer binding///actin polymerization or depolymerization///bipolar cellular bud site selection					
	8 hrs	Afu6g07540	t-complex protein 1, epsilon subunit	66	chaperone activity///cytoplasm///protein folding///cytoskeleton organization///cytoskeleton					
		Afu3g06280	Rho GTPase activator (Rgd1)	70	osmosensory signaling pathway///Rho GTPase activator activity					
	14 hrs	Afu5g11350	Ndc80 complex component Nuf2	8						
		Afu2g01060	Rho GTPase activator (Sac7)	57	intracellular///signal transducer activity///small GTPase mediated signal transduction///actin filament reorganization during cell cycle///Rho GTPase activator activity					
		Afu6g12980	spindle pole body component	66	spindle pole body///microtubule nucleation///microtubule binding///structural constituent of cytoskeleton					

ER/ Vacuole/ Golgi/ endosome	4 hrs	Afu3g11200	vacuolar assembly protein	12	high-affinity iron ion transport///endosome///""homotypic vacuole fusion, non-autophagic""///fungal-type vacuole///protein transport///Rab guanyl-nucleotide exchange factor activity///vacuolar membrane"///"vacuole organization
		Afu1g10670	Vacuolar ATP synthase subunit H	78	vacuolar acidification///""vacuolar proton-transporting V-type ATPase, V1 domain"""///fungal-type vacuole membrane///"""proton-transporting ATPase activity, rotational mechanism""
		Afu2g08300	DnaJ domain protein	89	endoplasmic reticulum lumen///co-chaperone activity///protein folding
	8 hrs	Afu6g14250	endosomal integral membrane protein (P24a)	18	membrane fraction///biological process unknown///molecular function unknown
		Afu3g14970	thioredoxin Trx1	55	DNA-dependent DNA replication///electron transport"///""vacuole fusion, non-autophagic""///response to oxidative stress///cytoplasm///fungal-type vacuole///regulation of cell redox homeostasis///"thiol-disulfide exchange intermediate activity///vacuole inheritance
4 hrs		Afu7g01300	mannosyltransferase (PIG-M)	3	GPI anchor biosynthetic process///mannosyltransferase activity///endoplasmic reticulum membrane
		Afu3g07590	ER-Golgi SNARE complex subunit (Sed5)	9	retrograde vesicle-mediated transport, Golgi to ER"""///cis-Golgi network///ER to Golgi vesicle-mediated transport///t-SNARE activity///"vesicle fusion///intra-Golgi vesicle-mediated transport
		Afu7g04250	protein-ER retention protein (Erd1)	17	protein retention in ER lumen///integral to membrane
		Afu6g09020	GPI transamidase component Gpi16	35	integral to endoplasmic reticulum membrane///GPI-anchor transamidase activity///attachment of GPI anchor to protein///GPI-anchor transamidase complex
		Afu4g12950	vacuolar targeting protein Atg24	73	membrane///autophagy///lipid binding//transport

		Afu5g08210	dolichyl-phosphate beta-glucosyltransferase	69	protein amino acid N-linked glycosylation///dolichyl-phosphate beta-glucosyltransferase activity///endoplasmic reticulum membrane
		Afu5g03220	microsomal signal peptidase subunit (gp23)	84	
		Afu3g11400	aspartic endopeptidase Pep2	88	aspartic-type endopeptidase activity///protein catabolic process///extracellular region///fungal-type cell wall
		Afu6g09020	GPI transamidase component Gpi16	89	integral to endoplasmic reticulum membrane///GPI-anchor transamidase activity///attachment of GPI anchor to protein///GPI-anchor transamidase complex
	14 hrs	Afu1g08830	Golgi matrix protein	32	ER to Golgi vesicle-mediated transport///molecular function unknown///Golgi apparatus
		Afu3g10660	hydroxymethylglutaryl-CoA synthase Erg13	49	hydroxymethylglutaryl-CoA synthase activity///endoplasmic reticulum///mitochondrion///ergosterol biosynthetic process
		Afu8g02780	vacuolar protein sorting protein	94	signal sequence binding///vacuolar transport///protein targeting to vacuole///Golgi apparatus

	Afu6g11190	protein kinase (VPS15)	81	Golgi membrane///protein serine/threonine kinase activity///vacuolar transport///protein retention in Golgi apparatus///protein binding///protein amino acid phosphorylation///protein targeting to vacuole
	Afu5g08210	dolichyl-phosphate beta-glucosyltransferase	86	protein amino acid N-linked glycosylation///dolichyl-phosphate beta-glucosyltransferase activity///endoplasmic reticulum membrane
8 hrs	Afu2g04720	ubiquitin C-terminal hydrolase	34	ubiquitin-specific protease activity///cytoplasm///protein deubiquitination
	Afu5g11720	26S proteasome regulatory subunit Mts4	84	ubiquitin-dependent protein catabolic process///cytoplasm///endopeptidase activity///endoplasmic reticulum///proteasome regulatory particle///receptor activity
	Afu4g12070	endosomal peripheral membrane protein (Mon2)	88	endosome///protein targeting to vacuole///transport
14 hrs	Afu8g03930	Hsp70 chaperone (HscA)	2	chaperone activity///polysome///translation///cytoplasm//ATPase activity
	Afu5g08970	oligosaccharyl transferase subunit (beta)	12	dolichyl-diphosphooligosaccharide-protein glycotransferase activity///oligosaccharyltransferase complex///protein amino acid N-linked glycosylation///cell cycle
	Afu1g11730	ADP-ribosylation factor	39	ARF small monomeric GTPase activity///Golgi-associated vesicle///cytosol///ER to Golgi vesicle-mediated transport///intra-Golgi vesicle-mediated transport
	Afu2g04770	autophagy protein	45	

Chromatin remodelling	4 hrs	Afu3g11380	ARID/BRIGHT domain protein (SWI1)	20	chromatin remodeling///nucleosome remodeling complex///general RNA polymerase II transcription factor activity
	8 hrs	Afu3g11030	histone chaperone ASF1	54	chromatin assembly complex///nucleosome assembly///programmed cell death///histone binding
Stress response	8 hrs	Afu2g09700	superoxide dismutase copper chaperone Lys7	49	removal of superoxide radicals///superoxide metabolic process///superoxide dismutase copper chaperone activity///cytosol///intracellular copper ion transport
		Afu2g03950	serine/threonine protein phosphatase	56	cellular component unknown///cellular sodium ion homeostasis///protein serine/threonine phosphatase activity

		Atg13		
	Afu2g08300	DnaJ domain protein	89	endoplasmic reticulum lumen///co-chaperone activity///protein folding
	Afu1g05280	Golgi complex component (Vps8)	91	membrane fraction///late endosome to vacuole transport///molecular function unknown
4hrs	Afu2g17050	nuclear export protein Noc3	88	DNA replication initiation///chromatin binding///nucleolus///protein binding///rRNA processing///nucleus
8 hrs	Afu2g06060	transcriptional co-activator (Hfi1/Ada1)	7	
14 hrs	Afu5g09080	transcription factor (SPT8)	27	transcription cofactor activity///chromatin modification///SAGA complex///nucleus///histone acetylation
	Afu1g16500	small monomeric GTPase (Gtr2)	18	cytoplasm///nucleus///biological process unknown///small monomeric GTPase activity
	Afu5g03720	chromatin assembly factor 1 subunit A	97	
4 hrs	Afu5g01900	heat shock transcription factor Hsf1	2	response to heat///transcription factor activity///nucleus///regulation of transcription from RNA polymerase II promoter///response to stress
	Afu2g17170	Na+/H+ antiporter Nha1	80	cellular monovalent inorganic cation homeostasis///plasma membrane///cation:cation antiporter activity

	14 hrs	Afu6g04500	Snf1 kinase complex beta-subunit Gal83	44	AMP-activated protein kinase activity///nucleus///protein amino acid phosphorylation///signal transduction///cell adhesion///filamentous growth		**14 hrs**	Afu5g05960	serine/threonine protein kinase	34	cellular component unknown///G1/S transition of mitotic cell cycle///cellular cation homeostasis///protein kinase activity

10.4 Discussion

Comparisons between transcriptional datasets generated from *in vitro* growth (Lamarre et al. 2008, Sheppard et al. 2005, Twumasi-Boateng et al. 2009, Alcazar-Fuoli et al, unpublished) with those from the host niche (section 10.3.2) enables the identification of genes whose differential expression is limited to infection. These genes are of considerable interest, as they might enable the discrimination between obligatory growth and differentiation processes which occur both inside and outside of the host with virulence strategies specifically employed by *A. fumigatus* to facilitate infection. Comparisons of the Af293 stage specific transcriptional profile presented in section 10.3.2 with the aforementioned *in vitro* datasets (Chapter 9, Alcazar-Fuoli et al. unpublished (Lamarre et al. 2008, Sheppard et al. 2005, Twumasi-Boateng et al. 2009) reveals intriguing commonalities and divergences between growth inside and outside the host.

With regard to infection, many virulence associated genes are upregulated during both *in vivo* and *in vitro* growth. For example, an IgE-binding protein (Afu6g03560), mycelial catalase Cat1 (Afu3g02270), para-aminobenzoate synthase *pabaA* (Afu6g04820), allergen Asp F3 (Afu6g02280), allergen Asp F1 (Afu5g02330) are upregulated in the host and also during *in vitro* growth. Therefore it is likely that these virulence associated genes are upregulated during infection due to their role in growth and differentiation, rather than as specific strategies employed to colonise the mammalian host.

The increased transcript abundance of genes encoding secreted proteases between 4 – 8 hours post infection reported in Chapter 3 (Table 3.19) was supported in stage specific profiling of Af293 (Table 10.11). 12 genes encoding putative proteases with signal peptides were upregulated in Af293 between 4 and 8 hours post infection (Table 10.11). None of these genes were upregulated in any of the interrogated *in vitro* datasets. Six other putatively secreted proteases demonstrated downregulation following 24 hours growth in YPD (tripeptidyl peptidase SED3 Afu3g08930, extracellular serine carboxypeptidase Afu2g17330, peptidase S41 family protein Afu1g17400, metalloprotease MEP1 Afu1g07730, serine peptidase Afu2g01250, pheromone processing carboxypeptidase KexA Afu1g08940, Alcazar-Fuoli et al. unpublished). These data support the preferential use of these enzymes in the proteinaceous lung when compared to nitrogen rich *in vitro* media, and highlight them as potential aggressive strategies employed by *A. fumigatus*, either for nutrient acquisition, host immune attack, or both.

In order to compare *A. fumigatus* transcriptional responses following growth in nitrogen rich and limiting conditions, Hartmann and co-workers extracted RNA from mycelium which had been shifted into media supplemented with either ammonium tartrate or BSA as the sole nitrogen source (Hartmann et al. 2011). Microarray analyses revealed upregulation of 27 putatively secreted proteases in the low nitrogen medium relative to the nitrogen rich medium. When compared to the 12 proteases upregulated between 4 – 8 hours post infection, 7 were common to both analyses. For example, the extra-cellular serine carboxypeptidase (Afu2g17330) was highly upregulated between 4 – 8 hours post infection, and demonstrated a 4.5 fold-increase in growth with protein as the sole nitrogen source relative to the growth in nitrogen-replete media (Hartmann et al. 2011, Table 10.11). Thus, it seems likely that rapid upregulation of these genes in the host represents a pathogen strategy for acquisition of nitrogen from the lung. These data might support the use of endogenous protease inhibitors for the prophylaxis of ABPA or IPA, to both reduce allergic responses and inhibit nutrient acquisition by the pathogen in the host. For example, antileukoprotease is a cationic antiprotease found in mucous secretions of the respiratory tract. Exposure of swollen *A. fumigatus* conidia to recombinantly expressed antileukoprotease demonstrated toxicity to *in vitro* spores at concentrations of 2 μM (Tomee et al. 1997). However, it seems unlikely that protease inhibition will be a useful strategy for the treatment of IPA, given that analyses of the extracellular protease regulator Δ*prtT* in a neutropenic model of infection demonstrated comparable levels of virulence to the wild-type (Bergmann et al. 2009, Sharon et al. 2009). Nevertheless, the observation that ungerminated spores in the host niche may biosynthesise enzymes which are known to cause allergic Th2 responses is of particular relevance to ABPA, an allergic condition in which spores do not necessarily germinate in the lung. Isolation of human $CD4^+$ T-cells from healthy human PBMC and pulsing with recombinant Mep1p and DppVp activated IL-4-producing clones, thus suggesting an unfavourable Th2 response to these enzymes (Bozza et al. 2009). The exploitation of the reliance of *A. fumigatus* on secreted proteases in the host might therefore be a pathogen strategy which is therapeutically exploitable for ABPA by using protease inhibitors.

Notably, there were distinct differences in the secreted proteases upregulated in the isolates studied and reported in Chapter 3, and in Af293, this section. Of the 12 and 16 secreted protease genes upregulated between 4 – 8 hours in the unknown *A. fumigatus* isolate (Chapter 3) and AF293 (this addendum) respectively, only 1 was common to both analyses (serine peptidase Afu2g01250). These data challenge the relevance of PtrT regulated proteases during the initiation of infection in the Af293 isolate. Sharon and co-workers demonstrated reduced transcription of six out of forty seven proteases in the Af293Δ*ptrT* relative to the wild-type throughout a time-series of

in vitro growth (Sharon et al. 2009). These included Alp1 (Afu4g11800), Mep (Afu8g07080), CpdS (Afu4g11800), Dpp4 (Afu4g09320), extracellular serine carboxypeptidase (Afu2g17330) and putative serine protease *sedE* (Afu7g06220). Fascinatingly, only one of these genes (extracellular serine carboxypeptidase Afu2g17330) was employed in Af293 during the initiation of infection. These data suggest the wild-type virulence of Af293Δ*ptrT* in murine models of infection (Sharon et al. 2009) might be due to PtrT independent secreted protease employment in this isolate rather than redundancy of secreted proteases *per se*.

Additionally, one may speculate that the striking downregulation of secreted proteases Alp1, Mep, and a putative carboxypeptidase reported from ratiometric analyses conducted between the unknown isolate and Af293Δ*laeA* (Table 8.8) is due to the isogenic differences between strains, rather than a LaeA regulatory phenomenon. Indeed, this is supported by the absence of differentially expressed secreted proteases presented in ratiometric analyses presented in this addendum. Differences between the inventories of secreted proteases between isolates during the initiation of infection might therefore be a confounding factor in reports of the functional redundancy of these enzymes with regards to host colonisation. Of great value would be deletion of *ptrT* and virulence analyses in the unknown isolate used in Chapter 3. More generally, these data reinforce the necessity of working in multiple *A. fumigatus* isolates in order to comprehensively determine gene function in the host.

With regard to secondary metabolism during infection, interrogation of the 34 and 60 secondary metabolite genes which increase between 4 – 8 and 8 – 14 hours respectively (Figure 10.4) reveals that the majority of these genes are also upregulated during *in vitro* growth. For example, 18 and 31 of the upregulated genes between 4 – 8 and 8 – 14 hours respectively demonstrated increased transcript abundance in at least one of the *in vitro* datasets. These data support the strong link between secondary metabolite biosynthesis and cell growth and differentiation (Keller et al. 2005). Interrogation of genes upregulated uniquely during host colonisation does not suggest enrichment of specific metabolite clusters, but do reinforce the role of key biosynthetic or regulatory enzymes, such as *pes3* and *regA*. These genes were highly and moderately upregulated in the 4 – 8 and 8 – 14 hour datasets respectively (Tables 10.9 and 10.10) and not upregulated in any *in vitro* dataset. Indeed, *regA* is downregulated during *in vitro* growth in two studies (Lamarre et al. 2008, Alcazar-Fuoli et al. unpublished). Genes which are also uniquely upregulated *in vivo* between 4 – 8 hours include a polyketide synthase (Afu7g00160) and a putative pathway specific transcription factor (Afu3g02590). Finally, a polyketide synthase (Afu3g14700) was upregulated between 8 – 14 hours which was not differentially expressed in

any *in vitro* dataset. In light of the *regA* and *pes3* expression profiles, combined with their putative role in modulating host-pathogen interactions in corticosteroid treated murine models of infection (Chapters 4 and 5) we hypothesise that the uncharacterised secondary metabolite genes Afu7g00160, Afu3g02590 and Afu3g14700 are outstanding candidates for deletion and analyses with regards to host-pathogen interactions and virulence.

Notwithstanding the fact that the hybrid PKS/NRPS *psoA* is upregulated in two *in vitro* analyses (Alcazar-Fuoli et al. unpublished, Sheppard et al. 2005) this gene was highly upregulated between 8 – 14 hours post infection for both wild-type isolates analysed in this thesis (Chapter 3, this addendum). This finding is significant given the remarkable differences in transcriptional profiles between isolates, and supports the hypothesis that the augmentation of virulence by *psoA* is maintained among isolates of differing genetic backgrounds. Moreover, *psoA* upregulation occurs at the invasive stage of disease for both isolates, which might support the putative role of this gene product in epithelial toxicity and/or hyphal penetration of the epithelial cell layer (Chapter 4). Recent work conducted in our laboratory has generated a Δ*psoA* mutant in the *A. fumigatus* Ku80 background, which demonstrates attenuation in a *G. mellonella* model of infection relative to the wild-type (Alcazar-Fuoli, unpublished data). The attenuation of Δ*psoA* mutants in two genetic backgrounds, and in both invertebrate and mammalian models of infection strongly supports a role for *psoA* and the pseurotin A biosynthetic pathway in host-pathogen interactions and *A. fumigatus* virulence.

Comparison of the brevianamide F synthetase *ftmA* (Afu8g00170) expression profile between Chapter 3 and microarray analyses conducted in this addendum identifies the limitations with regard to interpreting isolated microarray studies from the host niche. In the first wild-type experiment, the *ftmA* gene demonstrated low increase between 8 – 14 hours post infection (Table 3.20). However in the repeat experiment, *ftmA* demonstrated high downregulation between 4 – 8 hours post infection, and also between 4 – 14 hours (Tables 10.4 and 10.9). Two possibilities can be offered to explain this discrepancy: (A) differential expression of this gene between experiments is attributable to differences in genetic backgrounds; (B) expression of this gene cannot be reproduced between biological replicates and/or using a different array platform.

Notwithstanding the fact that the Δ*ftmA* isolate demonstrated a reduction in fungal burden (Chapter 4), we suggest that these data highlight the importance of conducting transcriptional profiles of different strain backgrounds during the initiation of host infection. This is supported by analyses of the three genes which are reproducibly upregulated during infection using the

methods described in this thesis (*psoA, pes3* and *regA*), all of which putatively contribute to host-pathogen interactions and virulence (Chapter 4 and 5). Genes which impact host-pathogen interactions irrespective of genetic background represent the most promising target for *A. fumigatus* anti-fungal development. The non-ratiometric normalisation for array datasets generated from isolates Af293, ATCC46645, wild type isolate (Chapter 3) and Ku80 at 4, 8 and 14 hours post infection is being completed at the time of writing this addendum.

Data presented in Chapter 3 demonstrated the majority of differentially expressed secondary metabolite genes decreased in transcript abundance between 4 – 8 hours (n = 96), followed by a notable trend towards their upregulation between 8 – 14 hours post infection (n = 128, Figure 3.11). In the experiment utilising Af293 described in this addendum, the number of these genes decreasing between 4 – 8 hours was comparable (n = 92) yet under half as many were found to increase in between 8 - 14 hours (n = 60, Figure 10.4). Certainly, the decrease in the number of upregulated secondary metabolite genes may be attributed to the array platform, as 18 of the 128 previously described upregulated secondary metabolite genes are not represented on the PFGRC array (data not shown). Nevertheless, one can suggest that in general the upregulation of secondary metabolite genes between 8 – 14 hours was notably reduced in the Af293 isolate when compared to the unknown isolate. While full interrogation of the discrepancies in secondary metabolite gene upregulation in the host between the two wild-type isolates is beyond the scope of this addendum, it is notable that genes specifically upregulated in Af293 (n = 41) do not cluster at physically linked secondary metabolite loci. This is interesting given the high upregulation of *laeA* (Afu1g14660, Table 10.2 and 10.9) in this isolate. Indeed, in the wild-type isolate tested in Chapter 3, more secondary metabolite genes were upregulated yet *laeA* was not differentially expressed during infection. These data further challenge the role of LaeA in regulation of secondary metabolite loci during the initiation of infection (Chapter 9).

In addition to focusing on genes which are only upregulated *in vivo*, a second approach which will likely enhance our understanding of host-pathogen interactions is the analysis of upregulated genes which are *A. fumigatus* specific. These candidates might therefore both contribute to the establishment of IPA, and also account for the prevalence of *A. fumigatus* as the etiological agent of aspergillosis. A striking feature of the stage specific Af293 transcriptional profile *in vivo* was the upregulation of hypothetical genes (4 – 8 hours, n = 545, 4 – 14 hours, n = 595, data not shown). These genes reveal no known domains following bioinformatic analyses. *In silico* comparative genomic analyses between *A. fumigatus* and seven other *Aspergilli* revealed that of the 377 genes specific to *A. fumigatus,* 97 % were hypothetical proteins (Gastebois et al 2009). Further

analyses of upregulated hypothetical genes during the initiation of infection reveals that 61 (4 – 8 hours) and 108 (8 – 14 hours) were specific to *A. fumigatus*. The pressing need to characterise the role of genes encoding hypothetical proteins in virulence is highlighted by a comparative genomic study, which identified 17 such genes which were conserved in the human pathogens *Yersinia pestis*, *Neisseria gonorrhoeae*, *Helicobacter pylori*, *Borrelia burgdorferi*, *Streptococcus pneumoniae*, and *Treponema pallidum* (Garbom et al. 2004). Subsequent deletion of these genes in *Yersinia pseudotuberculosis* and analyses of the mutant isolates in an oral murine infection model demonstrated reduced virulence relative to wild-type isolates in 5 of the mutants (Garbom et al. 2004). Given the large numbers of genes which encode hypothetical proteins which were upregulated during *A. fumigatus* infection, the high-throughput recombineering approach for generating deletion constructs (Chapter 5) and rapid virulence assay (Chapter 4) developed in this thesis both represent attractive strategies for the analysis of these genes with respect to *A. fumigatus* virulence.

With regard to reverse engineering the molecular basis of Δ*laeA* attenuation, transcriptional profiles were compared between the mutant and Af293 at 4, 8 and 14 hours post infection using a ratiometric normalisation protocol. Initial interpretations of these datasets demonstrate that cell wall associated genes 1, 3-beta-glucanosyltransferase Gel1 (Afu2g01170), cell surface protein Mas1 (Afu8g00610), cell wall biogenesis protein (Afu2g04880) and a GPI anchored protein (Afu1g01300) are not differentially expressed between the isolates. Additionally, comparable expression of secreted proteases and transport processes is reported in this addendum. These data are in contrast to transcriptional comparisons presented in Chapter 8 (Table 8.8). We therefore hypothesise that these genes do not contribute to the attenuation of Δ*laeA* in murine models of infection.

Nevertheless, interrogation of the 100 most up or down regulated genes presented in Tables 10.16 - 10.21 suggest other explanations for the attenuation of Δ*laeA* in murine models of infection. For example, many genes associated with the endoplasmic reticulum, vacuole, endocytosis and cytoskeletal elements are differentially expressed in the Δ*laeA* isolate during infection which is suggestive of elevated secretory stress in the mutant (Table 10.22).

Secretion of hydrolytic enzymes and subsequent absorption of products produced from enzymatic reactions is fundamental to a saprophytic lifestyle and is relevant to host colonisation, as evidenced by transcriptional profiling conducted in this thesis (Table 3.19, 10.9). The secretion of hydrolytic enzymes involves several organelles, including the endoplasmic reticulum and Golgi

apparatus which post translationally modify proteins. Proteins are delivered to the vacuole, appropriate to the functions of this organelle, which include maintenance of cytosolic homeostasis, storage and degradation of proteins. Rapid translation of proteins during germination in the host may result in the accumulation of unfolded proteins, a stress which is compensated by the unfolded protein response (UPR) and endoplasmic reticulum associated pathway (ERAD). These processes adjust the folding capacity of the ER and dispose of miss-folded proteins respectively (see section 1.2.8). The relevance of the UPR and ERAD pathways with regard to infection is suggested by the attenuation of Δ*hacA* and Δ*derA* isolates in murine models of infection respectively (Ritchie et al. 2009, Richie et al. 2011). Accordingly, it was interesting to note the upregulation and downregulation of genes associated with the endoplasmic reticulum, vacuole, Golgi apparatus, and endocytosis in the Δ*laeA* mutant (Table 10.22). This included the downregulation at 14 hours post infection of a putative protein phosphatase Ptc2 (Afu1g09280), which downregulates the UPR in *S. cerevisiae* by dephosphorylation of the transmembrane serine/threonine kinase Ire1p. The downregulation of other ER genes, including Sed5 (Afu3g07590, SNARE complex subunit), vaculolar targeting protein Atg24 (Afu4g12950) and actin and microtubule associate proteins (e.g. t-complex protein 1, theta subunit Afu4g09740), which might be associated with vesicle transport reinforces a state of secretory stress in Δ*laeA* during the initiation of infection.

What is the physiological cue for the putative secretory stress in Δ*laeA*? An interesting observation was the downregulation of a putative heat shock transcription factor Hsf1 (Afu5g01900) at 4 hours post infection in Δ*laeA* relative to Af293 (Table 10.22). In *S. cerevisiae*, heat shock impairs protein and membrane folding in the ER, which initiates the UPR via Ire1p. Indeed, heat shock response induced artificially by introduction of constitutively active Hsf1 is able to relieve ER stress in *S. cerevisiae* Δ*ire1* (Liu and Chang 2008). We hypothesise that Δ*laeA* might be attenuated in the host niche due to a greater secretory stress in the mutant, which possibly occurs via a miss-regulated response to mammalian body temperature via Hsf1 at 4 hours post infection. We are currently conducting phenotypic tests to assess response of Δ*laeA* to elevated temperature and secretory stress (i.e. following growth on the reducing agent dithiothreitol).

Intriguingly, two genes were differentially expressed in Δ*laeA* which are putatively involved in the Spt/Ada/Gcn5 acetyltransferase (SAGA) complex, a histone acetyltransferase-coactivator involved in regulation of gene expression at the level of nucleosome remodelling in *S. cerevisiae* (Roberts and Winston 1997). A transcriptional co-activator Hfi1/Ada1 (Afu2g06060) and a transcription

factor Spt8 (Afu5g09080) were downregulated in Δ*laeA* at 8 and 14 hours post infection respectively (Table 10.22). A recent study by Nützmann and co-workers demonstrated that the SAGA complex is required for prokaryote induced natural product formation in *A. nidulans* (Nützmann et al. 2011). Deletion of 36 *A. nidulans* histone acetyltransferases identified a single mutant which was impaired in the ability to produce the polyketide orsellinic acid following co-incubation with *Streptomyces rapamycinicus*. The mutant lacked the *gcnE* gene, which is homoglous to *S. cerevisiae* Gcn5. Further characterisation demonstrated SAGA complex was also required for induction of sterigmatocystin, terrequinone and penicillin. These authors demonstrated that *laeA* deletion does not impact biosynthesis of orsellinic acid, suggesting it is not required for bacteria-induced activation of this cluster. Nevertheless, differential expression of SAGA complex and other chromatin associated genes (e.g. Afu5g03720, chromatin assembly factor 1 subunit A, Table 10.22) might result in significant modifications to chromatin architecture and gene expression in the Δ*laeA* mutant during infection. Any direct or indirect interaction of LaeA with the SAGA complex remains to be determined.

The experiments presented in this addendum have generated extensive gene expression datasets which require comprehensive bioinformatic interrogation. Nevertheless, initial analyses presented in this addendum demonstrate interesting aspects of the Af293 and Δ*laeA* host infecting transcriptome which provide insights into host-pathogen interactions during the initiation of infection, and identify new lines of inquiry for establishing the molecular basis of Δ*laeA* attenuation.

Appendix A

Gene expression datasets

The tables listed in this appendix are contained in the supplementary data CD attached to this thesis. Data files are contained in folders which are named according to each Chapter.

The file name and a summary of the contents are given below:

Folder name: Chapter 3

File name: Af293 relative nSI (size 3200 kb)

All genes passing count and standard deviation filtering for non-ratiometric analysis of the wild type are given in this file. ORF, nSI values, FDR corrected p values are given as detailed in Chapter 3.

File name: LaeA relative nSI (size 3200 kb)

All genes passing count and standard deviation filtering for non-ratiometric analysis of Δ*laeA* are given in this file. ORF, nSI values, FDR corrected p values are given as detailed in Chapter 3.

File name: Af293 differentially expressed (size 3700 kb)

Differentially expressed genes in the wild-type between the three time points of infection using non-ratiometric analysis (Chapter 3). The file is in Excel format, and tabs denote the time-point comparision and the direction of expression change, e.g. “4 – 8 Upregulated”

File name: LaeA differentially expressed (size 3700 kb)

Differentially expressed genes in the Δ*laeA* isolate between the three time points of infection using non-ratiometric analysis (Chapter 3). The file is in Excel format, and tabs denote the time-point comparision and the direction of expression change, e.g. “4 – 8 Upregulated”.

File name: Extended GO Annotation (size 805 kb)

Extended GO annotation for STEM analysis reported in Chapter 3. This file also lists the *A. fumigatus* specific genes, secondary metabolite genes, signal peptide genes, transposition associated genes and telomeric proximity

Folder name: Chapter 8

File name: LaeA vs Af293 ratiometric analysis (size 1420 kb)

Differentially expressed genes between wild-type and Δ*laeA* isolates at three time points of infection using ratiometric normalisation (Chapter 8). The file is in Excel format, and each tab denotes a time-point e.g. “4 hours”. Ratios are reported relative Δ*laeA*:Af293 as detailed in Chapter 8.

File name: Host-qRT-PCR (size 36 kb)

Differentially expressed genes between mice infected with wild-type, Δ*laeA* or saline relative to saline incoluated immunocompetent control mice (Chapter 8). The file is in Excel format, and each tab denotes a time-point e.g. “4 hours”. Ratios are reported relative Δ*laeA*:Af293 as detailed in Chapter 8. Additionally, full list of gene names and RefSeq annotations are given.

Folder name: Chapter 10

File name: Non-ratiometric Af293 Differentially regulated (Addendum)

Differentially expressed genes in the Af293 between the three time points of infection using non-ratiometric analysis (Chapter 10). The file is in Excel format, and tabs denote the time-point comparision and the direction of expression change, e.g. “4 – 8 Upregulated”

Folder name: Ratiometric dataset LaeA-Af293 (Addendum)

Differentially expressed genes between wild-type and Δ*laeA* isolates at three time points of infection using ratiometric normalisation (Chapter 10). The file is in Excel format, and each tab denotes a time-point e.g. “4 hours”. Ratios are reported relative Δ*laeA*:Af293 as detailed in Chapter 8.

References

't Hoen PAC, Turk R, Boer JM, Sterrenburg E, de Menezes RX, van Ommen G-JB, den Dunnen JT. 2004. Intensity-based analysis of two-colour microarrays enables efficient and flexible hybridization designs. Nucl. Acids Res. 32: e41-.

Agranoff, et al. 2006. Identification of diagnostic markers for tuberculosis by proteomic fingerprinting of serum. Lancet 368: 1012-1021.

Aimanianda V, et al. 2009. Surface hydrophobin prevents immune recognition of airborne fungal spores. Nature 460: 1117-1121.

Alanio A, Cordonnier C, Bretagne S. 2011. Azole Resistance in *Aspergillus fumigatus*—Current Epidemiology and Future Perspectives. Current Fungal Infection Reports 5: 168-178.

Albrecht D, Guthke R, Brakhage AA, Kniemeyer O. 2010. Integrative analysis of the heat shock response in *Aspergillus fumigatus*. BMC Genomics 11: 32.

Alcazar-Fuoli L, Mellado E, Garcia-Effron G, Lopez JF, Grimalt JO, Cuenca-Estrella JM, Rodriguez-Tudela JL. 2008. Ergosterol biosynthesis pathway in Aspergillus fumigatus. Steroids 73: 339-347.

Alspaugh JA, Perfect JR, Heitman J. 1997. Cryptococcus neoformans mating and virulence are regulated by the G-protein alpha subunit GPA1 and cAMP. Genes Dev 11: 3206-3217.

Amitani R, Murayama T, Nawada R, Lee WJ, Niimi A, Suzuki K, Tanaka E, Kuze F. 1995. Aspergillus culture filtrates and sputum sols from patients with pulmonary aspergillosis cause damage to human respiratory ciliated epithelium in vitro. Eur Respir J 8: 1681-1687.

Amutan M, Nyyssonen E, Stubbs J, Diaz-Torres MR, Dunn-Coleman N. 1996. Identification and cloning of a mobile transposon from *Aspergillus niger* var. awamori. Curr Genet 29: 468-473.

Armstrong-James, Shaunak S, Teo IA, Shrivastava S, Petrou MA, Taube D, Dorling A. 2010. Exogenous Interferon-gamma Immunotherapy for Invasive Fungal Infections in Kidney Transplant Patients. American Journal of Transplantation 10: 1796-1803.

Armstrong-James, Turnbull SA, Teo I, Stark J, Rogers NJ, Rogers TR, Bignell E, Haynes K. 2009. Impaired interferon-gamma responses, increased interleukin-17 expression, and a tumor necrosis factor-alpha transcriptional program in invasive aspergillosis. J Infect Dis 200: 1341-1351.

Asami Y, Kakeya H, Komi Y, Kojima S, Nishikawa K, Beebe K, Neckers L, Osada H. 2008. Azaspirene, a fungal product, inhibits angiogenesis by blocking Raf-1 activation. Cancer Science 99: 1853-1858.

Baber I, Tamby JP, Manoukis NC, Sangaré D, Doumbia S, Traoré SF, Maiga MS, Dembélé D. 2011. A python module to normalize microarray data by the quantile adjustment method. Infection, Genetics and Evolution 11: 765-768.

Balloy V, Huerre M, Latge JP, Chignard M. 2005. Differences in patterns of infection and inflammation for corticosteroid treatment and chemotherapy in experimental invasive pulmonary aspergillosis. Infect Immun 73: 494-503.

Banerjee B, Kurup VP. 2003. Molecular biology of Aspergillus allergens. Front Biosci 8: s128-139.

Banerjee B, Kurup VP, Phadnis S, Greenberger PA, Fink JN. 1996. Molecular cloning and expression of a recombinant *Aspergillus fumigatus* protein Asp f II with significant immunoglobulin E reactivity in allergic bronchopulmonary aspergillosis. J Lab Clin Med 127: 253-262.

Barry JD, Ginger ML, Burton P, McCulloch R. 2003. Why are parasite contingency genes often associated with telomeres? International Journal for Parasitology 33: 29-45.

Bayram O, Braus GH. 2011. Coordination of secondary metabolism and development in fungi: the velvet family of regulatory proteins. FEMS Microbiol Rev.

Bayram O, et al. 2008. VelB/VeA/LaeA complex coordinates light signal with fungal development and secondary metabolism. Science 320: 1504-1506.

Beaumier DL, Caldwell MA, Holbein BE. 1984. Inflammation triggers hypoferremia and de novo synthesis of serum transferrin and ceruloplasmin in mice. Infect. Immun. 46: 489-494.

Beffa T, et al. 1998. Mycological control and surveillance of biological waste and compost. Med Mycol 36 Suppl 1: 137-145.

Behnsen J, Lessing F, Schindler S, Wartenberg D, Jacobsen ID, Thoen M, Zipfel PF, Brakhage AA. 2010. Secreted *Aspergillus fumigatus* protease Alp1 degrades human complement proteins C3, C4, and C5. Infect Immun 78: 3585-3594.

Bellocchio S, Montagnoli C, Bozza S, Gaziano R, Rossi G, Mambula SS, Vecchi A, Mantovani A, Levitz SM, Romani L. 2004. The Contribution of the Toll-Like/IL-1 Receptor Superfamily to Innate and Adaptive Immunity to Fungal Pathogens In Vivo. The Journal of Immunology 172: 3059-3069.

Ben-Ami R, Lewis RE, Kontoyiannis DP. 2010. Enemy of the (immunosuppressed) state: an update on the pathogenesis of *Aspergillus fumigatus* infection. British Journal of Haematology 150: 406-417.

Ben-Ami R, Lewis RE, Leventakos K, Kontoyiannis DP. 2009. *Aspergillus fumigatus* inhibits angiogenesis through the production of gliotoxin and other secondary metabolites. Blood 114: 5393-5399.

Bergmann, Hartmann T, Cairns T, Bignell EM, Krappmann S. 2009. A regulator of *Aspergillus fumigatus* extracellular proteolytic activity is dispensable for virulence. Infect Immun 77: 4041-4050.

Bergmann S, Funk AN, Scherlach K, Schroeckh V, Shelest E, Horn U, Hertweck C. 2010. Activation of a Silent Fungal Polyketide Biosynthesis Pathway through Regulatory Cross Talk with a Cryptic Nonribosomal Peptide Synthetase Gene Cluster. Applied and Environmental Microbiology 76: 8143-8149.

Bernard M, Latge JP. 2001. *Aspergillus fumigatus* cell wall: composition and biosynthesis. Med Mycol 39 Suppl 1: 9-17.

Bhabhra R, Miley MD, Mylonakis E, Boettner D, Fortwendel J, Panepinto JC, Postow M, Rhodes JC, Askew DS. 2004. Disruption of the *Aspergillus fumigatus* Gene Encoding Nucleolar Protein CgrA Impairs Thermotolerant Growth and Reduces Virulence. Infect. Immun. 72: 4731-4740.

Bhatti MF, Jamal A, Petrou MA, Cairns TC, Bignell EM, Coutts RH. 2011. The effects of dsRNA mycoviruses on growth and murine virulence of *Aspergillus fumigatus*. Fungal Genet Biol.

Bignell E, Negrete-Urtasun S, Calcagno AM, Haynes K, Arst HN, Jr., Rogers T. 2005. The Aspergillus pH-responsive transcription factor PacC regulates virulence. Mol Microbiol 55: 1072-1084.

Birch, Denning DW, Robson GD. 2004. Comparison of extracellular phospholipase activities in clinical and environmental *Aspergillus fumigatus* isolates. Med Mycol 42: 81-86.

Birch, Boevink PC, Gilroy EM, Hein I, Pritchard L, Whisson SC. 2008. Oomycete RXLR effectors: delivery, functional redundancy and durable disease resistance. Current Opinion in Plant Biology 11: 373-379.

Bok, Keller NP. 2004. LaeA, a regulator of secondary metabolism in Aspergillus spp. Eukaryot Cell 3: 527-535.

Bok, Noordermeer D, Kale SP, Keller NP. 2006a. Secondary metabolic gene cluster silencing in Aspergillus nidulans. Molecular Microbiology 61: 1636-1645.

Bok, Balajee SA, Marr KA, Andes D, Nielsen KF, Frisvad JC, Keller NP. 2005. LaeA, a regulator of morphogenetic fungal virulence factors. Eukaryot Cell 4: 1574-1582.

Bok, Chung D, Balajee SA, Marr KA, Andes D, Nielsen KF, Frisvad JC, Kirby KA, Keller NP. 2006b. GliZ, a transcriptional regulator of gliotoxin biosynthesis, contributes to *Aspergillus fumigatus* virulence. Infect Immun 74: 6761-6768.

Bolker M, Basse CW, Schirawski J. 2008. *Ustilago maydis* secondary metabolism - From genomics to biochemistry. Fungal Genetics and Biology 45: S88-S93.

Bolstad BM, Irizarry RA, Astrand M, Speed TP. 2003. A comparison of normalization methods for high density oligonucleotide array data based on variance and bias. Bioinformatics 19: 185-193.

Borish LC, Steinke JW. 2003. 2. Cytokines and chemokines. J Allergy Clin Immunol 111: S460-475.

Bossers, Ylstra B, Brakenhoff RH, Smeets SJ, Verhaagen J, van de Wiel MA. 2010a. Intensity-based analysis of dual-color gene expression data as an alternative to ratio-based analysis to enhance reproducibility. BMC Genomics 11: 112.

Bossers, Wirz KTS, Meerhoff GF, Essing AHW, van Dongen JW, Houba P, Kruse CG, Verhaagen J, Swaab DF. 2010b. Concerted changes in transcripts in the prefrontal cortex precede neuropathology in Alzheimer's disease. Brain 133: 3699-3723.

Bowman JC, Abruzzo GK, Anderson JW, Flattery AM, Gill CJ, Pikounis VB, Schmatz DM, Liberator PA, Douglas CM. 2001. Quantitative PCR Assay To Measure *Aspergillus fumigatus* Burden in a Murine Model of Disseminated Aspergillosis: Demonstration of Efficacy of Caspofungin Acetate. Antimicrob. Agents Chemother. 45: 3474-3481.

Bozza S, Gaziano R, Spreca A, Bacci A, Montagnoli C, di Francesco P, Romani L. 2002. Dendritic cells transport conidia and hyphae of *Aspergillus fumigatus* from the airways to the draining lymph nodes and initiate disparate Th responses to the fungus. J Immunol 168: 1362-1371.

Bozza S, et al. 2009. Immune sensing of *Aspergillus fumigatus* proteins, glycolipids, and polysaccharides and the impact on Th immunity and vaccination. J Immunol 183: 2407-2414.

Brakhage AA, Schroeckh V. 2011. Fungal secondary metabolites – Strategies to activate silent gene clusters. Fungal Genetics and Biology 48: 15-22.

Brieland JK, et al. 2001. Cytokine networking in lungs of immunocompetent mice in response to inhaled *Aspergillus fumigatus*. Infect Immun 69: 1554-1560.

Brown, Yu JH, Kelkar HS, Fernandes M, Nesbitt TC, Keller NP, Adams TH, Leonard TJ. 1996. Twenty-five coregulated transcripts define a sterigmatocystin gene cluster in *Aspergillus nidulans*. Proceedings of the National Academy of Sciences of the United States of America 93: 1418-1422.

Brown JS, Aufauvre-Brown A, Brown J, Jennings JM, Arst H, Jr., Holden DW. 2000. Signature-tagged and directed mutagenesis identify PABA synthetase as essential for *Aspergillus fumigatus* pathogenicity. Mol Microbiol 36: 1371-1380.

Bruns, Seidler M, Albrecht D, Salvenmoser S, Remme N, Hertweck C, Brakhage AA, Kniemeyer O, Muller FM. 2010a. Functional genomic profiling of *Aspergillus fumigatus* biofilm reveals enhanced production of the mycotoxin gliotoxin. Proteomics 10: 3097-3107.

Bruns, Kniemeyer O, Hasenberg M, Aimanianda V, Nietzsche S, Thywißen A, Jeron A, Latgé J-P, Brakhage AA, Gunzer M. 2010b. Production of Extracellular Traps against *Aspergillus fumigatus In Vitro* and in Infected Lung Tissue Is Dependent on Invading Neutrophils and Influenced by Hydrophobin RodA. PLoS Pathog 6: e1000873.

Buades C, Moya A. 1996. Phylogenetic analysis of the isopenicillin-N-synthetase horizontal gene transfer. Journal of Molecular Evolution 42: 537-542.

Butchko RA, Adams TH, Keller NP. 1999. *Aspergillus nidulans* mutants defective in stc gene cluster regulation. Genetics 153: 715-720.

Cagas SE, Jain MR, Li H, Perlin DS. 2011. Profiling the *Aspergillus fumigatus* proteome in response to caspofungin. Antimicrob Agents Chemother 55: 146-154.

Cairns T, Minuzzi F, Bignell E. 2010. The host-infecting fungal transcriptome. FEMS Microbiology Letters.

Calera, Haas. 2009. Cations: Zinc and iron. Washington DC: ASM.

Cardenas ME, Cutler NS, Lorenz MC, Di Como CJ, Heitman J. 1999. The TOR signaling cascade regulates gene expression in response to nutrients. Genes & Development 13: 3271-3279.

Casadevall A, Steenbergen JN, Nosanchuk JD. 2003. 'Ready made' virulence and 'dual use' virulence factors in pathogenic environmental fungi — the *Cryptococcus neoformans* paradigm. Current Opinion in Microbiology 6: 332-337.

Cenci, Romani L, Mencacci A, Spaccapelo R, Schiaffella E, Puccetti P, Bistoni F. 1993. Interleukin-4 and interleukin-10 inhibit nitric oxide-dependent macrophage killing of Candida albicans. Eur J Immunol 23: 1034-1038.

Cenci, Perito S, Enssle KH, Mosci P, Latge JP, Romani L, Bistoni F. 1997. Th1 and Th2 cytokines in mice with invasive aspergillosis. Infect Immun 65: 564-570.

Cenci, Mencacci A, Fe d'Ostiani C, Del Sero G, Mosci P, Montagnoli C, Bacci A, Romani L. 1998. Cytokine- and T helper-dependent lung mucosal immunity in mice with invasive pulmonary aspergillosis. J Infect Dis 178: 1750-1760.

Cenci, et al. 1999. Interleukin-4 Causes Susceptibility to Invasive Pulmonary Aspergillosis through Suppression of Protective Type I Responses. Journal of Infectious Diseases 180: 1957-1968.

Chai, Netea MG, Sugui J, Vonk AG, van de Sande WWJ, Warris A, Kwon-Chung KJ, Jan Kullberg B. 2010. *Aspergillus fumigatus* Conidial Melanin Modulates Host Cytokine Response. Immunobiology 215: 915-920.

Chai, Netea MG, Vonk AG, Kullberg BJ, Verweij PE, Verschueren I, van der Meer JWM, Joosten LAB, Latge JP. 2011. *Aspergillus fumigatus* cell wall components differentially modulate host TLR2 and TLR4 responses. Microbes and Infection 13: 151-159.

Chan W, Costantino N, Li R, Lee SC, Su Q, Melvin D, Court DL, Liu P. 2007. A recombineering based approach for high-throughput conditional knockout targeting vector construction. Nucleic Acids Res 35: e64.

Chang, Yu J, Bhatnagar D, Cleveland TE. 2000. Characterization of the *Aspergillus parasiticus* major nitrogen regulatory gene, areA. Biochim Biophys Acta 1491: 263-266.

Chang, Ehrlich KC, Yu JJ, Bhatnagar D, Cleveland TE. 1995. Increased Expression of Aspergillus-Parasiticus Aflr, Encoding a Sequence-Specific DNA-Binding Protein, Relieves Nitrate Inhibition of Aflatoxin Biosynthesis. Applied and Environmental Microbiology 61: 2372-2377.

Chang, Bien CM, Lee H, Espenshade PJ, Kwon-Chung KJ. 2007. Sre1p, a regulator of oxygen sensing and sterol homeostasis, is required for virulence in *Cryptococcus neoformans*. Mol Microbiol 64: 614-629.

Chaudhary N, Staab JF, Marr KA. 2010. Healthy human T-Cell Responses to *Aspergillus fumigatus* antigens. PLoS ONE 5: e9036.

Chaveroche MK, Ghigo JM, d'Enfert C. 2000. A rapid method for efficient gene replacement in the filamentous fungus *Aspergillus nidulans*. Nucleic Acids Res 28: E97.

Chen D, Toone WM, Mata J, Lyne R, Burns G, Kivinen K, Brazma A, Jones N, Bahler J. 2003. Global transcriptional responses of fission yeast to environmental stress. Mol Biol Cell 14: 214-229.

Cheng J, Park TS, Fischl AS, Ye XS. 2001. Cell cycle progression and cell polarity require sphingolipid biosynthesis in *Aspergillus nidulans*. Mol Cell Biol 21: 6198-6209.

Choi W, Dean RA. 1997. The adenylate cyclase gene MAC1 of *Magnaporthe grisea* controls appressorium formation and other aspects of growth and development. Plant Cell 9: 1973-1983.

Chow LP, Liu SL, Yu CJ, Liao HK, Tsai JJ, Tang TK. 2000. Identification and expression of an allergen Asp f 13 from *Aspergillus fumigatus* and epitope mapping using human IgE antibodies and rabbit polyclonal antibodies. Biochem J 346 Pt 2: 423-431.

Clemons KV, Stevens DA. 2005. The contribution of animal models of aspergillosis to understanding pathogenesis, therapy and virulence. Med Mycol 43 Suppl 1: S101-110.

Clemons KV, Grunig G, Sobel RA, Mirels LF, Rennick DM, Stevens DA. 2000. Role of IL-10 in invasive aspergillosis: increased resistance of IL-10 gene knockout mice to lethal systemic aspergillosis. Clin Exp Immunol 122: 186-191.

Collemare J, Pianfetti M, Houlle A-E, Morin D, Camborde L, Gagey M-J, Barbisan C, Fudal I, Lebrun M-H, Böhnert HU. 2008. *Magnaporthe grisea* avirulence gene ACE1 belongs to an infection-specific gene cluster involved in secondary metabolism. New Phytologist 179: 196-208.

Colot HV, Park G, Turner GE, Ringelberg C, Crew CM, Litvinkova L, Weiss RL, Borkovich KA, Dunlap JC. 2006. "A high-throughput gene knockout procedure for Neurospora reveals functions for multiple transcription factors" (vol 103, pg 10352, 2006). Proceedings of the National Academy of Sciences of the United States of America 103: 16614-16614.

Court DL, Sawitzke JA, Thomason LC. 2002. Genetic engineering using homologous recombination. Annual Review of Genetics 36: 361-388.

Cramer. 2011. Secretion stress and fungal pathogenesis: A new, exploitable chink in fungal armor? Virulence 2: 1-3.

Cramer, Rivera A, Hohl TM. 2011. Immune responses against *Aspergillus fumigatus*: what have we learned? Current Opinion in Infectious Diseases 24: 315-322 310.1097/QCO.1090b1013e328348b328159.

Cramer, Perfect BZ, Pinchai N, Park S, Perlin DS, Asfaw YG, Heitman J, Perfect JR, Steinbach WJ. 2008. Calcineurin Target CrzA Regulates Conidial Germination, Hyphal Growth, and Pathogenesis of *Aspergillus fumigatus*. Eukaryotic Cell 7: 1085-1097.

Cramer, et al. 2006. Disruption of a nonribosomal peptide synthetase in *Aspergillus fumigatus* eliminates gliotoxin production. Eukaryot Cell 5: 972-980.

D'Souza C, Alspaugh J, Yue C, Harashima T, Cox G, Perfect J, Heitman J. 2001. Cyclic AMP-dependent protein kinase controls virulence of the fungal pathogen *Cryptococcus neoformans*. Mol Cell Biol 21: 3179 - 3191.

da Silva Ferreira ME, Kress MR, Savoldi M, Goldman MH, Hartl A, Heinekamp T, Brakhage AA, Goldman GH. 2006. The akuB(KU80) mutant deficient for nonhomologous end joining is a powerful tool for analyzing pathogenicity in *Aspergillus fumigatus*. Eukaryot Cell 5: 207-211.

Dagenais TRT, Keller NP. 2009. Pathogenesis of *Aspergillus fumigatus* in Invasive Aspergillosis. Clin. Microbiol. Rev. 22: 447-465.

Dagenais TRT, Giles SS, Aimanianda V, Latge J-P, Hull CM, Keller NP. 2010. *Aspergillus fumigatus* LaeA-Mediated Phagocytosis Is Associated with a Decreased Hydrophobin Layer. Infect. Immun. 78: 823-829.

de Jonge HJM, Fehrmann RSN, de Bont ESJM, Hofstra RMW, Gerbens F, Kamps WA, de Vries EGE, van der Zee AGJ, te Meerman GJ, ter Elst A. 2007. Evidence Based Selection of Housekeeping Genes. PLoS ONE 2: e898.

De las Penas A, Pan SJ, Cormack BP, Castano I, Alder J, Cregg R. 2003. Virulence-related surface glycoproteins in the yeast pathogen *Candida glabrata* are encoded in subtelomeric clusters and subject to RAP1- and SIR-dependent transcriptional silencing. Genes & Development 17: 2245-2258.

De Wit PJ, Mehrabi R, Van den Burg HA, Stergiopoulos I. 2009. Fungal effector proteins: past, present and future. Mol Plant Pathol 10: 735-747.

Delgado N, Xue J, Yu JJ, Hung CY, Cole GT. 2003. A recombinant beta-1,3-glucanosyltransferase homolog of *Coccidioides posadasii* protects mice against coccidioidomycosis. Infect Immun 71: 3010-3019.

Demain AL, Fang A. 2000. The natural functions of secondary metabolites. Adv Biochem Eng Biotechnol 69: 1-39.

Denning. 2001. Chronic forms of pulmonary aspergillosis. Clin Microbiol Infect 7 Suppl 2: 25-31.

Denning, Pleuvry A, Cole DC. 2010. P183 Global burden of allergic bronchopulmonary aspergillosis (ABPA) complicating asthma. Thorax 65: A155.

Denning, et al. 2011. High-frequency Triazole Resistance Found In Nonculturable *Aspergillus fumigatus* from Lungs of Patients with Chronic Fungal Disease. Clinical Infectious Diseases 52: 1123-1129.

Depont F, et al. 2007. Drug-drug interactions with systemic antifungals in clinical practice. Pharmacoepidemiol Drug Saf 16: 1227-1233.

Diamond DL, Kimball JR, Krisanaprakornkit S, Ganz T, Dale BA. 2001. Detection of beta-defensins secreted by human oral epithelial cells. J Immunol Methods 256: 65-76.

Dixon MS, Jones DA, Keddie JS, Thomas CM, Harrison K, Jones JD. 1996. The tomato Cf-2 disease resistance locus comprises two functional genes encoding leucine-rich repeat proteins. Cell 84: 451-459.

Do JH, Yamaguchi R, Miyano S. 2009. Exploring temporal transcription regulation structure of *Aspergillus fumigatus* in heat shock by state space model. BMC Genomics 10: 306.

Doyle S. 2011. Fungal proteomics: from identification to function. FEMS Microbiol Lett.

Dubourdeau M, Athman R, Balloy V, Huerre M, Chignard M, Philpott DJ, Latgé J-P, Ibrahim-Granet O. 2006. *Aspergillus fumigatus* Induces Innate Immune Responses in Alveolar Macrophages through the MAPK Pathway Independently of TLR2 and TLR4. The Journal of Immunology 177: 3994-4001.

Eichhorn H, Lessing F, Winterberg B, Schirawski J, Kamper J, Muller P, Kahmann R. 2006. A ferroxidation/permeation iron uptake system is required for virulence in *Ustilago maydis*. Plant Cell 18: 3332-3345.

Eliahu N, Igbaria A, Rose MS, Horwitz BA, Lev S. 2007. Melanin biosynthesis in the maize pathogen *Cochliobolus heterostrophus* depends on two mitogen-activated protein kinases, Chk1 and Mps1, and the transcription factor Cmr1. Eukaryot Cell 6: 421-429.

Elias JA, Homer RJ, Hamid Q, Lee CG. 2005. Chitinases and chitinase-like proteins in TH2 inflammation and asthma. Journal of Allergy and Clinical Immunology 116: 497-500.

Elliott CE, Gardiner DM, Thomas G, Cozijnsen A, A VDW, Howlett BJ. 2007. Production of the toxin sirodesmin PL by Leptosphaeria maculans during infection of *Brassica napus*. Mol Plant Pathol 8: 791-802.

Ernst J, Bar-Joseph Z. 2006. STEM: a tool for the analysis of short time series gene expression data. BMC Bioinformatics 7: 191.

Espeso EA, Tilburn J, Arst HN, Penalva MA. 1993. Ph Regulation Is a Major Determinant in Expression of a Fungal Penicillin Biosynthetic Gene. Embo Journal 12: 3947-3956.

Farman ML. 2007. Telomeres in the rice blast fungus *Magnaporthe oryzae*: the world of the end as we know it. FEMS Microbiology Letters 273: 125-132.

Fedorova N, et al. 2008. Genomic islands in the pathogenic filamentous fungus *Aspergillus fumigatus*. PLoS Genetics 4: e1000046.

Feng B, Wang X, Hauser M, Kaufmann S, Jentsch S, Haase G, Becker JM, Szaniszlo PJ. 2001. Molecular Cloning and Characterization of WdPKS1, a Gene Involved in Dihydroxynaphthalene Melanin Biosynthesis and Virulence in *Wangiella (Exophiala) dermatitidis*. Infect. Immun. 69: 1781-1794.

Fischer, Timberlake WE. 1995. *Aspergillus nidulans* apsA (anucleate primary sterigmata) encodes a coiled-coil protein required for nuclear positioning and completion of asexual development. J Cell Biol 128: 485-498.

Fischer, Müller T, Schwalbe R, Ostrowski R, Dott W. 2000. Species-specific profiles of mycotoxins produced in cultures and associated with conidia of airborne fungi derived from biowaste. International Journal of Hygiene and Environmental Health 203: 105-116.

Fischle W, Tseng BS, Dormann HL, Ueberheide BM, Garcia BA, Shabanowitz J, Hunt DF, Funabiki H, Allis CD. 2005. Regulation of HP1-chromatin binding by histone H3 methylation and phosphorylation. Nature 438: 1116-1122.

Fontana MF, Banga S, Barry KC, Shen X, Tan Y, Luo Z-Q, Vance RE. 2011. Secreted Bacterial Effectors That Inhibit Host Protein Synthesis Are Critical for Induction of the Innate Immune Response to Virulent *Legionella pneumophila*. PLoS Pathog 7: e1001289.

Fox EM, Gardiner DM, Keller NP, Howlett BJ. 2008. A Zn(II)2Cys6 DNA binding protein regulates the sirodesmin PL biosynthetic gene cluster in *Leptosphaeria maculans*. Fungal Genet Biol 45: 671-682.

Freitas-Junior LH, et al. 2005. Telomeric heterochromatin propagation and histone acetylation control mutually exclusive expression of antigenic variation genes in malaria parasites. Cell 121: 25-36.

Fukuchi Y, Kumagai T, Ebina K, Yokota K. 1996. Apolipoprotein B inhibits the hemolytic activity of Asp-hemolysin from *Aspergillus fumigatus*. Biological & Pharmaceutical Bulletin 19: 547-550.

Fukuda T, Boeckh M, Carter RA, Sandmaier BM, Maris MB, Maloney DG, Martin PJ, Storb RF, Marr KA. 2003. Risks and outcomes of invasive fungal infections in recipients of allogeneic hematopoietic stem cell transplants after nonmyeloablative conditioning. Blood 102: 827-833.

Gacser A, Stehr F, Kroger C, Kredics L, Schafer W, Nosanchuk JD. 2007. Lipase 8 Affects the Pathogenesis of *Candida albicans*. Infect. Immun. 75: 4710-4718.

Galagan, Selker EU. 2004. RIP: the evolutionary cost of genome defense. Trends Genet 20: 417-423.

Galagan, et al. 2005. Sequencing of Aspergillus nidulans and comparative analysis with *A. fumigatus* and *A. oryzae*. Nature 438: 1105-1115.

Garbom S, Forsberg Å, Wolf-Watz H, Kihlberg B-M. 2004. Identification of Novel Virulence-Associated Genes via Genome Analysis of Hypothetical Genes. Infection and Immunity 72: 1333-1340.

Gardiner DM, Waring P, Howlett BJ. 2005. The epipolythiodioxopiperazine (ETP) class of fungal toxins: distribution, mode of action, functions and biosynthesis. Microbiology 151: 1021-1032.

Garlanda C, et al. 2002. Non-redundant role of the long pentraxin PTX3 in anti-fungal innate immune response. Nature 420: 182-186.

Gautam P, Shankar J, Madan T, Sirdeshmukh R, Sundaram CS, Gade WN, Basir SF, Sarma PU. 2008. Proteomic and transcriptomic analysis of *Aspergillus fumigatus* on exposure to amphotericin B. Antimicrob Agents Chemother 52: 4220-4227.

Geunes-Boyer S, Heitman J, Wright JR, Steinbach WJ. 2010. Surfactant protein D binding to *Aspergillus fumigatus* hyphae is calcineurin-sensitive. Medical Mycology 48: 580-588.

Gomez BL, Nosanchuk JD. 2003. Melanin and fungi. Curr Opin Infect Dis 16: 91-96.

Goncalves, Pombeiro-Sponchiado SR. 2005. Antioxidant activity of the melanin pigment extracted from *Aspergillus nidulans*. Biological & Pharmaceutical Bulletin 28: 1129-1131.

Gonzales DA, et al. 2010. Protein expression profiles distinguish between experimental invasive pulmonary aspergillosis and *Pseudomonas pneumonia*. Proteomics 10: 4270-4280.

Gout L, Fudal I, Kuhn ML, Blaise F, Eckert M, Cattolico L, Balesdent MH, Rouxel T. 2006. Lost in the middle of nowhere: the AvrLm1 avirulence gene of the Dothideomycete *Leptosphaeria maculans*. Mol Microbiol 60: 67-80.

Grahl N, Puttikamonkul S, Macdonald JM, Gamcsik MP, Ngo LY, Hohl TM, Cramer RA. 2011. *In vivo* Hypoxia and a Fungal Alcohol Dehydrogenase Influence the Pathogenesis of Invasive Pulmonary Aspergillosis. PLoS Pathog 7: e1002145.

Gravelat FN, Ejzykowicz DE, Chiang LY, Chabot JC, Urb M, Macdonald KD, al-Bader N, Filler SG, Sheppard DC. 2010. *Aspergillus fumigatus* MedA governs adherence, host cell interactions and virulence. Cell Microbiol 12: 473-488.

Greenbaum D, Colangelo C, Williams K, Gerstein M. 2003. Comparing protein abundance and mRNA expression levels on a genomic scale. Genome Biol 4: 117.

Grundmann A, Kuznetsova T, Afiyatullov SS, Li S-M. 2008. FtmPT2, an N-Prenyltransferase from *Aspergillus fumigatus*, Catalyses the Last Step in the Biosynthesis of Fumitremorgin B. Chembiochem 9: 2059-2063.

Hammond TM, Andrewski MD, Roossinck MJ, Keller NP. 2008. Aspergillus mycoviruses are targets and suppressors of RNA silencing. Eukaryot Cell 7: 350-357.

Harris. 2006. Cell Polarity in Filamentous Fungi: Shaping the Mold. Pages 41-77 in Kwang WJ, ed. International Review of Cytology, vol. Volume 251 Academic Press.

Hartmann, Kahmann R, Bolker M. 1996. The pheromone response factor coordinates filamentous growth and pathogenicity in *Ustilago maydis*. Embo Journal 15: 1632-1641.

Hartmann, Cairns TC, Olbermann P, Morschhäuser J, Bignell EM, Krappmann S. 2011. Oligopeptide transport and regulation of extracellular proteolysis are required for growth of *Aspergillus fumigatus* on complex substrates but not for virulence. Molecular Microbiology 82: 917-935.

Hawksworth. 2001. The magnitude of fungal diversity: the 1.5 million species estimate revisited. Mycological Research 105: 1422-1432.

Henriet SSV, Hermans PWM, Verweij PE, Simonetti E, Holland SM, Sugui JA, Kwon-Chung KJ, Warris A. 2011. Human Leukocytes Kill *Aspergillus nidulans* by Reactive Oxygen Species-Independent Mechanisms. Infect. Immun. 79: 767-773.

Hensel M, Arst HN, Jr., Aufauvre-Brown A, Holden DW. 1998. The role of the *Aspergillus fumigatus* areA gene in invasive pulmonary aspergillosis. Mol Gen Genet 258: 553-557.

Herrera ML, Vallor AC, Gelfond JA, Patterson TF, Wickes BL. 2009. Strain-Dependent Variation in 18S Ribosomal DNA Copy Numbers in *Aspergillus fumigatus*. J. Clin. Microbiol. 47: 1325-1332.

Hershenson MB. 2007. Proteases and Protease-activated receptors signalling: at the crossroads of acquired and innate immunity. Clinical & Experimental Allergy 37: 963-966.

Hilgers V, Parker R, Teixeira D. 2006. Translation-independent inhibition of mRNA deadenylation during stress in *Saccharomyces cerevisiae*. Rna-a Publication of the Rna Society 12: 1835-1845.

Houterman PM, Cornelissen BJC, Rep M. 2008. Suppression of Plant Resistance Gene-Based Immunity by a Fungal Effector. PLoS Pathog 4: e1000061.

Howard, Ferrari MA. 1989. Role of melanin in appressorium function. Experimental Mycology 13: 403-418.

Howard, Valent B. 1996. Breaking and entering: host penetration by the fungal rice blast pathogen *Magnaporthe grisea*. Annu Rev Microbiol 50: 491-512.

Hu, Cheng PY, Sham A, Perfect JR, Kronstad JW. 2008. Metabolic adaptation in Cryptococcus neoformans during early murine pulmonary infection. Mol Microbiol 69: 1456-1475.

Hu, et al. 2007. Essential Gene Identification and Drug Target Prioritization in *Aspergillus fumigatus*. PLoS Pathog 3: e24.

Hudson DL, Layton AN, Field TR, Bowen AJ, Wolf-Watz H, Elofsson M, Stevens MP, Galyov EE. 2007. Inhibition of type III secretion in *Salmonella enterica serovar Typhimurium* by small-molecule inhibitors. Antimicrob Agents Chemother 51: 2631-2635.

Hughes AL, Todd BL, Espenshade PJ. 2005. SREBP Pathway Responds to Sterols and Functions as an Oxygen Sensor in Fission Yeast. Cell 120: 831-842.

Hutchens TW, Yip TT. 1993. New Desorption Strategies for the Mass-Spectrometric Analysis of Macromolecules. Rapid Communications in Mass Spectrometry 7: 576-580.

Ibrahim-Granet O, Philippe B, Boleti H, Boisvieux-Ulrich E, Grenet D, Stern M, Latge JP. 2003. Phagocytosis and intracellular fate of *Aspergillus fumigatus* conidia in alveolar macrophages. Infect Immun 71: 891-903.

Imai S, Guarente L, Armstrong CM, Kaeberlein M. 2000. Transcriptional silencing and longevity protein Sir2 is an NAD-dependent histone deacetylase. Nature 403: 795-800.

Ioannidis JP. 2005. Microarrays and molecular research: noise discovery? Lancet 365: 454-455.

Isberg RR, O'Connor TJ, Heidtman M. 2009. The *Legionella pneumophila* replication vacuole: making a cosy niche inside host cells. Nature Reviews Microbiology 7: 12-24.

Ishikawa M, Ninomiya T, Akabane H, Kushida N, Tsujiuchi G, Ohyama M, Gomi S, Shito K, Murata T. 2009. Pseurotin A and its analogues as inhibitors of immunoglobuline E production. Bioorganic & Medicinal Chemistry Letters 19: 1457-1460.

Jenuwein T, Allis CD. 2001. Translating the histone code. Science 293: 1074-1080.

Jeu L, Piacenti FJ, Lyakhovetskiy AG, Fung HB. 2003. Voriconazole. Clinical Therapeutics 25: 1321-1381.

Jung WH, Hu G, Kuo W, Kronstad JW. 2009. Role of ferroxidases in iron uptake and virulence of *Cryptococcus neoformans*. Eukaryot Cell 8: 1511-1520.

Kami M, et al. 2002. The Gastrointestinal Tract Is a Common Target of Invasive Aspergillosis in Patients Receiving Cytotoxic Chemotherapy for Hematological Malignancy. Clinical Infectious Diseases 35: 105-107.

Kamper J, et al. 2006. Insights from the genome of the biotrophic fungal plant pathogen *Ustilago maydis*. Nature 444: 97-101.

Karas M, Hillenkamp F. 1988. Laser desorption ionization of proteins with molecular masses exceeding 10,000 daltons. Anal Chem 60: 2299-2301.

Kato N, Suzuki H, Takagi H, Asami Y, Kakeya H, Uramoto M, Usui T, Takahashi S, Sugimoto Y, Osada H. 2009. Identification of Cytochrome P450s Required for Fumitremorgin Biosynthesis in *Aspergillus fumigatus*. Chembiochem 10: 920-928.

Kauppi AM, Nordfelth R, Uvell H, Wolf-Watz H, Elofsson M. 2003. Targeting Bacterial Virulence: Inhibitors of Type III Secretion in Yersinia. Chemistry & Biology 10: 241-249.

Keller, Hohn TM. 1997. Metabolic pathway gene clusters in filamentous fungi. Fungal Genet Biol 21: 17-29.

Keller, Yin WB. 2011. Transcriptional Regulatory Elements in Fungal Secondary Metabolism. Journal of Microbiology 49: 329-339.

Keller, Turner G, Bennett JW. 2005. Fungal secondary metabolism- from biochemistry to genomics. Nat Rev Micro 3: 937-947.

Kesh S, Mensah NY, Peterlongo P, Jaffe D, Hsu K, M VDB, O'Reilly R, Pamer E, Satagopan J, Papanicolaou GA. 2005. TLR1 and TLR6 polymorphisms are associated with susceptibility to invasive aspergillosis after allogeneic stem cell transplantation. Ann N Y Acad Sci 1062: 95-103.

Keyser P, Elofsson M, Rosell S, Wolf-Watz H. 2008. Virulence blockers as alternatives to antibiotics: type III secretion inhibitors against Gram-negative bacteria. Journal of Internal Medicine 264: 17-29.

Khoufache K, Puel O, Loiseau N, Delaforge M, Rivollet D, Coste A, Cordonnier C, Escudier E, Botterel F, Bretagne S. 2007. Verruculogen associated with *Aspergillus fumigatus* hyphae and conidia modifies the electrophysiological properties of human nasal epithelial cells. BMC Microbiol 7: 5.

Kimura K, Miyazaki S, Tateda K, Matsumoto T, Tsujimoto S, Yamaguchi K. 1999. Factors affecting the course and severity of transnasally induced *Staphylococcus aureus* pneumonia in mice. J Med Microbiol 48: 1005-1010.

Kniemeyer O, Lessing F, Brakhage AA. 2009. Proteome analysis for pathogenicity and new diagnostic markers for *Aspergillus fumigatus*. Med Mycol 47 Suppl 1: S248-254.

Kniemeyer O, Lessing F, Scheibner O, Hertweck C, Brakhage AA. 2006. Optimisation of a 2-D gel electrophoresis protocol for the human-pathogenic fungus *Aspergillus fumigatus*. Curr Genet 49: 178-189.

Kogan TV, Jadoun J, Mittelman L, Hirschberg K, Osherov N. 2004. Involvement of Secreted *Aspergillus fumigatus* Proteases in Disruption of the Actin Fiber Cytoskeleton and Loss of Focal Adhesion Sites in Infected A549 Lung Pneumocytes. Journal of Infectious Diseases 189: 1965-1973.

Komagata D, Fujita S, Yamashita N, Saito S, Morino T. 1996. Novel neuritogenic activities of pseurotin A and penicillic acid. J Antibiot (Tokyo) 49: 958-959.

Kozel TR, Wilson MA, Farrell TP, Levitz SM. 1989. Activation of C3 and binding to *Aspergillus fumigatus* conidia and hyphae. Infect Immun 57: 3412-3417.

Krappmann S, Bignell EM, Reichard U, Rogers T, Haynes K, Braus GH. 2004. The *Aspergillus fumigatus* transcriptional activator CpcA contributes significantly to the virulence of this fungal pathogen. Mol Microbiol 52: 785-799.

Kubodera T, Yamashita N, Nishimura A. 2002. Transformation of Aspergillus sp. and Trichoderma reesei Using the Pyrithiamine Resistance Gene (ptrA) of *Aspergillus oryzae*. Bioscience, Biotechnology, and Biochemistry 66: 404-406.

Kumar A, Ahmed R, Singh PK, Shukla PK. 2011. Identification of virulence factors and diagnostic markers using immunosecretome of *Aspergillus fumigatus*. Journal of Proteomics 74: 1104-1112.

Kurup VP, Xia JQ, Shen HD, Rickaby DA, Henderson JD, Fink JN, Chou H, Kelly KJ, Dawson CA. 2002. Alkaline serine proteinase from *Aspergillus fumigatus* has synergistic effects on Asp-f-2-induced immune response in mice. International Archives of Allergy and Immunology 129: 129-137.

Kwon-Chung, Polacheck I, Popkin TJ. 1982. Melanin-Lacking Mutants of *Cryptococcus neoformans* and Their Virulence for Mice. Journal of Bacteriology 150: 1414-1421.

Kwon MJ, Arentshorst M, Roos ED, van den Hondel CA, Meyer V, Ram AF. 2011. Functional characterization of Rho GTPases in *Aspergillus niger* uncovers conserved and diverged roles of Rho proteins within filamentous fungi. Mol Microbiol 79: 1151-1167.

Lamarre C, Sokol S, Debeaupuis JP, Henry C, Lacroix C, Glaser P, Coppee JY, Francois JM, Latge JP. 2008. Transcriptomic analysis of the exit from dormancy of *Aspergillus fumigatus* conidia. BMC Genomics 9: 417.

Lambou K, Lamarre C, Beau R, Dufour N, Latge JP. 2010. Functional analysis of the superoxide dismutase family in *Aspergillus fumigatus*. Mol Microbiol 75: 910-923.

Land CJ, Hult K, Fuchs R, Hagelberg S, Lundstrom H. 1987. Tremorgenic Mycotoxins from *Aspergillus fumigatus* as a Possible Occupational-Health Problem in Sawmills. Applied and Environmental Microbiology 53: 787-790.

Langfelder K, Philippe B, Jahn B, Latge JP, Brakhage AA. 2001. Differential expression of the *Aspergillus fumigatus* pksP gene detected in vitro and in vivo with green fluorescent protein. Infection and Immunity 69: 6411-6418.

Langfelder K, Jahn B, Gehringer H, Schmidt A, Wanner G, Brakhage AA. 1998. Identification of a polyketide synthase gene of *Aspergillus fumigatus* involved in conidial pigment biosynthesis and virulence. Medical Microbiology and Immunology 187: 79-89.

Lass-Florl C. 2009. The changing face of epidemiology of invasive fungal disease in Europe. Mycoses 52: 197-205.

Latge. 1999. *Aspergillus fumigatus* and Aspergillosis. Clin. Microbiol. Rev. 12: 310-350.

—. 2001. The pathobiology of *Aspergillus fumigatus*. Trends Microbiol 9: 382 - 389.

Latgé J-P, Calderone R. 2002. Host–microbe interactions: fungi invasive human fungal opportunistic infections. Current Opinion in Microbiology 5: 355-358.

Lee I, Oh JH, Shwab EK, Dagenais TR, Andes D, Keller NP. 2009. HdaA, a class 2 histone deacetylase of *Aspergillus fumigatus*, affects germination and secondary metabolite production. Fungal Genet Biol 46: 782-790.

Leidich SD, et al. 1998. Cloning and Disruption of caPLB1, a Phospholipase B Gene Involved in the Pathogenicity of *Candida albicans*. Journal of Biological Chemistry 273: 26078-26086.

Lessing F, Kniemeyer O, Wozniok I, Loeffler J, Kurzai O, Haertl A, Brakhage AA. 2007. The *Aspergillus fumigatus* transcriptional regulator AfYap1 represents the major regulator for defense against reactive oxygen intermediates but is dispensable for pathogenicity in an intranasal mouse infection model. Eukaryot Cell 6: 2290-2302.

Levdansky E, Romano J, Shadkchan Y, Sharon H, Verstrepen KJ, Fink GR, Osherov N. 2007. Coding tandem repeats generate diversity in *Aspergillus fumigatus* genes. Eukaryot Cell 6: 1380-1391.

Levels JH, Bleijlevens B, Rezaee F, Aerts JM, Meijers JC. 2007. SELDI-TOF mass spectrometry of High-Density Lipoprotein. Proteome Sci 5: 15.

Levitz, Farrell T. 1990. Human neutrophil degranulation stimulated by *Aspergillus fumigatus*. Journal of Leukocyte Biology 47: 170-175.

Levitz SM, Diamond RD. 1985. Mechanisms of resistance of *Aspergillus fumigatus* Conidia to killing by neutrophils in vitro. J Infect Dis 152: 33-42.

Linden A, Laan M, Anderson GP. 2005. Neutrophils, interleukin-17A and lung disease. European Respiratory Journal 25: 159-172.

Liu, Chang A. 2008. Heat shock response relieves ER stress. EMBO J 27: 1049-1059.

Liu, Nizet V. 2009. Color me bad: microbial pigments as virulence factors. Trends in Microbiology 17: 406-413.

Liu, Wu F. 2010. Global burden of aflatoxin-induced hepatocellular carcinoma: a risk assessment. Environ Health Perspect 118: 818-824.

Lomberk G, Bensi D, Fernandez-Zapico ME, Urrutia R. 2006. Evidence for the existence of an HP1-mediated subcode within the histone code. Nature Cell Biology 8: 407-U462.

Luberto C, Toffaletti DL, Wills EA, Tucker SC, Casadevall A, Perfect JR, Hannun YA, Del Poeta M. 2001. Roles for inositol-phosphoryl ceramide synthase 1 (IPC1) in pathogenesis of *C. neoformans*. Genes & Development 15: 201-212.

Luther K, Torosantucci A, Brakhage AA, Heesemann J, Ebel F. 2007. Phagocytosis of Aspergillus fumigatus conidia by murine macrophages involves recognition by the dectin-1 beta-glucan receptor and Toll-like receptor 2. Cell Microbiol 9: 368-381.

Madan T, Eggleton P, Kishore U, Strong P, Aggrawal SS, Sarma PU, Reid KB. 1997. Binding of pulmonary surfactant proteins A and D to *Aspergillus fumigatus* conidia enhances phagocytosis and killing by human neutrophils and alveolar macrophages. Infect Immun 65: 3171-3179.

Madan T, Kishore U, Singh M, Strong P, Hussain EM, Reid KB, Sarma PU. 2001. Protective role of lung surfactant protein D in a murine model of invasive pulmonary aspergillosis. Infect Immun 69: 2728-2731.

Maiya S, Grundmann A, Li SM, Turner G. 2006. The fumitremorgin gene cluster of *Aspergillus fumigatus*: identification of a gene encoding brevianamide F synthetase. Chembiochem 7: 1062-1069.

Maiya S, Grundmann A, Li X, Li SM, Turner G. 2007. Identification of a hybrid PKS/NRPS required for pseurotin A biosynthesis in the human pathogen *Aspergillus fumigatus*. Chembiochem 8: 1736-1743.

Maniatis. 1982. Molecular cloning : a laboratory manual Cold Spring Harbor, N.Y. :: Cold Spring Harbor Laboratory.

MAQC-Consortium. 2006. The MicroArray Quality Control (MAQC) project shows inter- and intraplatform reproducibility of gene expression measurements. Nat Biotech 24: 1151-1161.

Marichal P, Gorrens J, Vanden Bossche H. 1985. The action of itraconazole and ketoconazole on growth and sterol synthesis in *Aspergillus fumigatus* and *Aspergillus niger*. Medical Mycology 23: 13-21.

Markaryan A, Morozova I, Yu H, Kolattukudy PE. 1994. Purification and characterization of an elastinolytic metalloprotease from *Aspergillus fumigatus* and immunoelectron microscopic evidence of secretion of this enzyme by the fungus invading the murine lung. Infect Immun 62: 2149-2157.

Marshall E. 2004. Getting the noise out of gene arrays. Science 306: 630-631.

Mas G, de Nadal E, Dechant R, de la Concepcion MLR, Logie C, Jimeno-Gonzalez S, Chavez S, Ammerer G, Posas F. 2009. Recruitment of a chromatin remodelling complex by the Hog1 MAP kinase to stress genes (vol 28, pg 326, 2009). Embo Journal 28: 1191-1191.

Mattoo S, Lee YM, Dixon JE. 2007. Interactions of bacterial effector proteins with host proteins. Current Opinion in Immunology 19: 392-401.

McCormick A, Heesemann L, Wagener J, Marcos V, Hartl D, Loeffler J, Heesemann J, Ebel F. 2010. NETs formed by human neutrophils inhibit growth of the pathogenic mold *Aspergillus fumigatus*. Microbes Infect 12: 928-936.

McDonagh A, et al. 2008. Sub-Telomere Directed Gene Expression during Initiation of Invasive Aspergillosis. PLoS Pathog 4: e1000154.

Mehrad B, Strieter RM, Standiford TJ. 1999. Role of TNF-alpha in pulmonary host defense in murine invasive aspergillosis. J Immunol 162: 1633-1640.

Meier A, Kirschning CJ, Nikolaus T, Wagner H, Heesemann J, Ebel F. 2003. Toll-like receptor (TLR) 2 and TLR4 are essential for Aspergillus-induced activation of murine macrophages. Cell Microbiol 5: 561-570.

Mezger, Kneitz S, Wozniok I, Kurzai O, Einsele H, Loeffler J. 2008a. Proinflammatory Response of Immature Human Dendritic Cells is Mediated by Dectin-1 after Exposure to *Aspergillus fumigatus* Germ Tubes. Journal of Infectious Diseases 197: 924-931.

Mezger, et al. 2008b. Polymorphisms in the chemokine (C-X-C motif) ligand 10 are associated with invasive aspergillosis after allogeneic stem-cell transplantation and influence CXCL10 expression in monocyte-derived dendritic cells. Blood 111: 534-536.

Mircescu MM, Lipuma L, van Rooijen N, Pamer EG, Hohl TM. 2009. Essential Role for Neutrophils but not Alveolar Macrophages at Early Time Points following *Aspergillus fumigatus* Infection. Journal of Infectious Diseases 200: 647-656.

Miroux B, Walker JE. 1996. Over-production of proteins in *Escherichia coli*: mutant hosts that allow synthesis of some membrane proteins and globular proteins at high levels. J Mol Biol 260: 289-298.

Monroy F, Sheppard DC. 2005. Taf1: a class II transposon of *Aspergillus fumigatus*. Fungal Genet Biol 42: 638-645.

Moreno MÁ, Ibrahim-Granet O, Vicentefranqueira R, Amich J, Ave P, Leal F, Latgé J-P, Calera JA. 2007. The regulation of zinc homeostasis by the ZafA transcriptional activator is essential for *Aspergillus fumigatus* virulence. Molecular Microbiology 64: 1182-1197.

Morgenstern DE, Gifford MAC, Li LL, Doerschuk CM, Dinauer MC. 1997. Absence of Respiratory Burst in X-linked Chronic Granulomatous Disease Mice Leads to Abnormalities in Both Host Defense and Inflammatory Response to *Aspergillus fumigatus*. The Journal of Experimental Medicine 185: 207-218.

Mosquera G, Giraldo MC, Khang CH, Coughlan S, Valent B. 2009. Interaction transcriptome analysis identifies *Magnaporthe oryzae* BAS1-4 as Biotrophy-associated secreted proteins in rice blast disease. Plant Cell 21: 1273-1290.

Mouyna I, et al. 2005. Deletion of GEL2 encoding for a β(1–3)glucanosyltransferase affects morphogenesis and virulence in *Aspergillus fumigatus*. Molecular Microbiology 56: 1675-1688.

Nagappan V, Deresinski S. 2007. Reviews of anti-infective agents: posaconazole: a broad-spectrum triazole antifungal agent. Clin Infect Dis 45: 1610-1617.

Nair PK, Melnick SJ, Ramachandran R, Escalon E, Ramachandran C. 2006. Mechanism of macrophage activation by (1,4)-alpha-D-glucan isolated from *Tinospora cordifolia*. Int Immunopharmacol 6: 1815-1824.

Nakae S, Komiyama Y, Nambu A, Sudo K, Iwase M, Homma I, Sekikawa K, Asano M, Iwakura Y. 2002. Antigen-Specific T Cell Sensitization Is Impaired in IL-17-Deficient Mice, Causing Suppression of Allergic Cellular and Humoral Responses. Immunity 17: 375-387.

Nascimento AM, Goldman GH, Park S, Marras SAE, Delmas G, Oza U, Lolans K, Dudley MN, Mann PA, Perlin DS. 2003. Multiple Resistance Mechanisms among *Aspergillus fumigatus* Mutants with High-Level Resistance to Itraconazole. Antimicrob. Agents Chemother. 47: 1719-1726.

Natarajan K, Meyer MR, Jackson BM, Slade D, Roberts C, Hinnebusch AG, Marton MJ. 2001. Transcriptional Profiling Shows that Gcn4p Is a Master Regulator of Gene Expression during Amino Acid Starvation in Yeast. Mol. Cell. Biol. 21: 4347-4368.

Netea MG, van de Veerdonk F, Verschueren I, van der Meer JW, Kullberg BJ. 2008. Role of TLR1 and TLR6 in the host defense against disseminated candidiasis. FEMS Immunol Med Microbiol 52: 118-123.

Neuveglise C, Sarfati J, Latge JP, Paris S. 1996. Afut1, a retrotransposon-like element from *Aspergillus fumigatus*. Nucleic Acids Res 24: 1428-1434.

Nierman W, et al. 2005. Genomic sequence of the pathogenic and allergenic filamentous fungus *Aspergillus fumigatus*. Nature 438: 1151 - 1156.

Nishimura M, Fukada J, Moriwaki A, Fujikawa T, Ohashi M, Hibi T, Hayashi N. 2009. Mstu1, an APSES Transcription Factor, Is Required for Appressorium-Mediated Infection in *Magnaporthe grisea*. Bioscience Biotechnology and Biochemistry 73: 1779-1786.

Nota B, Verweij RA, Molenaar D, Ylstra B, van Straalen NM, Roelofs D. 2010. Gene expression analysis reveals a gene set discriminatory to different metals in soil. Toxicol Sci 115: 34-40.

Nützmann H-W, Reyes-Dominguez Y, Scherlach K, Schroeckh V, Horn F, Gacek A, Schümann J, Hertweck C, Strauss J, Brakhage AA. 2011. Bacteria-induced natural product formation in the fungus *Aspergillus nidulans* requires Saga/Ada-mediated histone acetylation. Proceedings of the National Academy of Sciences 108: 14282-14287.

Nygaard V, Hovig E. 2006. Options available for profiling small samples: a review of sample amplification technology when combined with microarray profiling. Nucleic Acids Res 34: 996-1014.

O'Brien HE, Parrent JL, Jackson JA, Moncalvo J-M, Vilgalys R. 2005. Fungal Community Analysis by Large-Scale Sequencing of Environmental Samples. Applied and Environmental Microbiology 71: 5544-5550.

O'Gorman CM, Fuller HT, Dyer PS. 2009. Discovery of a sexual cycle in the opportunistic fungal pathogen *Aspergillus fumigatus*. Nature 457: 471-474.

O'Hanlon KA, Cairns T, Stack D, Schrettl M, Bignell EM, Kavanagh K, Miggin SM, O'Keeffe G, Larsen TO, Doyle S. 2011. Targeted Disruption of Non-Ribosomal Peptide Synthetase pes3 Augments the Virulence of *Aspergillus fumigatus*. Infect. Immun.: IAI.00192-00111.

Odds FC, Brown AJ, Gow NA. 2003. Antifungal agents: mechanisms of action. Trends Microbiol 11: 272-279.

Orbach MJ, Farrall L, Sweigard JA, Chumley FG, Valent B. 2000. A Telomeric Avirulence Gene Determines Efficacy for the Rice Blast Resistance Gene Pi-ta. The Plant Cell Online 12: 2019-2032.

Osherov N. 2009. Conidial germination in *Aspergillus fumigatus*. Washington DC: ASM.

Owen KA, Bouton AH, Thomas KS. 2007. The differential expression of *Yersinia pseudotuberculosis* adhesins determines the requirement for FAK and/or Pyk2 during bacterial phagocytosis by macrophages. Cellular Microbiology 9: 596-609.

Pain A, et al. 2004. Insight into the genome of *Aspergillus fumigatus*: analysis of a 92.2 kb region encompassing the nitrate assimilation gene cluster. Fungal Genetics and Biology 41: 443-453.

Palmer JM, Perrin RM, Dagenais TRT, Keller NP. 2008. H3K9 Methylation Regulates Growth and Development in *Aspergillus fumigatus*. Eukaryotic Cell 7: 2052-2060.

Panepinto JC, Oliver BG, Fortwendel JR, Smith DLH, Askew DS, Rhodes JC. 2003. Deletion of the *Aspergillus fumigatus* Gene Encoding the Ras-Related Protein RhbA Reduces Virulence in a Model of Invasive Pulmonary Aspergillosis. Infect. Immun. 71: 2819-2826.

Paoletti M, Rydholm C, Schwier EU, Anderson MJ, Szakacs G, Lutzoni F, Debeaupuis J-P, Latgé J-P, Denning DW, Dyer PS. 2005. Evidence for Sexuality in the Opportunistic Fungal Pathogen *Aspergillus fumigatus*. Current Biology 15: 1242-1248.

Paolo W, Dadachova E, Mandal P, Casadevall A, Szaniszlo P, Nosanchuk J. 2006. Effects of disrupting the polyketide synthase gene WdPKS1 in *Wangiella [Exophiala] dermatitidis* on melanin production and resistance to killing by antifungal compounds, enzymatic degradation, and extremes in temperature. BMC Microbiology 6: 55.

Papadopoulos MC, et al. 2004. A novel and accurate diagnostic test for human African trypanosomiasis. Lancet 363: 1358-1363.

Pardo J, et al. 2006. The mitochondrial protein Bak is pivotal for gliotoxin-induced apoptosis and a critical host factor of *Aspergillus fumigatus* virulence in mice. The Journal of Cell Biology 174: 509-519.

Paris, Latge. 2001. Afut2, a new family of degenerate gypsy-like retrotransposon from *Aspergillus fumigatus*. Med Mycol 39: 195-198.

Paris, Boisvieux-Ulrich E, Crestani B, Houcine O, Taramelli D, Lombardi L, Latge J. 1997. Internalization of *Aspergillus fumigatus* conidia by epithelial and endothelial cells. Infect. Immun. 65: 1510-1514.

Paris, Wysong D, Debeaupuis JP, Shibuya K, Philippe B, Diamond RD, Latge JP. 2003. Catalases of *Aspergillus fumigatus*. Infect Immun 71: 3551-3562.

Park, Mehrad B. 2009. Innate Immunity to Aspergillus Species. Clin. Microbiol. Rev. 22: 535-551.

Park, Myers CL, Sheppard DC, Phan QT, Sanchez AA, J EE, Filler SG. 2005. Role of the fungal Ras-protein kinase A pathway in governing epithelial cell interactions during oropharyngeal candidiasis. Cell Microbiol 7: 499-510.

Penalva MA, Arst HN, Jr. 2004. Recent advances in the characterization of ambient pH regulation of gene expression in filamentous fungi and yeasts. Annu Rev Microbiol 58: 425-451.

Perrin RM, Fedorova ND, Bok JW, Cramer RA, Wortman JR, Kim HS, Nierman WC, Keller NP. 2007. Transcriptional regulation of chemical diversity in *Aspergillus fumigatus* by LaeA. PLoS Pathog 3: e50.

Perruccio K, et al. 2005. Transferring functional immune responses to pathogens after haploidentical hematopoietic transplantation. Blood 106: 4397-4406.

Pfaffl MW. 2001. A new mathematical model for relative quantification in real-time RT-PCR. Nucleic Acids Res 29: e45.

Philippe B, Ibrahim-Granet O, Prevost MC, Gougerot-Pocidalo MA, Sanchez Perez M, Van der Meeren A, Latge JP. 2003. Killing of *Aspergillus fumigatus* by Alveolar Macrophages Is Mediated by Reactive Oxidant Intermediates. Infect. Immun. 71: 3034-3042.

Pihet M, Vandeputte P, Tronchin G, Renier G, Saulnier P, Georgeault S, Mallet R, Chabasse D, Symoens F, Bouchara JP. 2009. Melanin is an essential component for the integrity of the cell wall of *Aspergillus fumigatus* conidia. BMC Microbiology 9.

Pinel C, Arlotto M, Issartel JP, Berger F, Pelloux H, Grillot R, Symoens F. 2011. Comparative proteomic profiles of *Aspergillus fumigatus* and *Aspergillus lentulus* strains by surface-enhanced laser desorption ionization time-of-flight mass spectrometry (SELDI-TOF-MS). BMC Microbiology 11.

Plasterk RHA. 2002. RNA Silencing: The Genome's Immune System. Science 296: 1263-1265.

Pokholok DK, Young RA, Zeitlinger J, Hannett NM, Reynolds DB. 2006. Activated signal transduction kinases frequently occupy target genes. Science 313: 533-536.

Potenza L, et al. 2007. Diagnosis of invasive aspergillosis by tracking Aspergillus-specific T cells in hematologic patients with pulmonary infiltrates. Leukemia 21: 578-581.

Quackenbush J. 2002. Microarray data normalization and transformation. Nat Genet 32 Suppl: 496-501.

Ramanan N, Wang Y. 2000. A high-affinity iron permease essential for *Candida albicans* virulence. Science 288: 1062-1064.

Ramaprakash H, Hogaboam CM, Ito T, Standiford TJ, Kunkel SL. 2009. Toll-Like Receptor 9 Modulates Immune Responses to *Aspergillus fumigatus* Conidia in Immunodeficient and Allergic Mice. Infection and Immunity 77: 108-119.

Reichard U, Buttner S, Eiffert H, Staib F, Ruchel R. 1990. Purification and characterisation of an extracellular serine proteinase from *Aspergillus fumigatus* and its detection in tissue. J Med Microbiol 33: 243-251.

Reiss J. 1982. Development of *Aspergillus parasiticus* and Formation of Aflatoxin-B1 under the Influence of Conidiogenesis Affecting Compounds. Archives of Microbiology 133: 236-238.

Reyes-Dominguez, Bok JW, Berger H, Shwab EK, Basheer A, Gallmetzer A, Scazzocchio C, Keller N, Strauss J. 2010. Heterochromatic marks are associated with the repression of secondary metabolism clusters in *Aspergillus nidulans*. Mol Microbiol.

Richardson MD, Shankland GS, Gray CA. 1991. Opsonizing Activity of C-Reactive Protein in Phagocytosis of *Aspergillus fumigatus* Conidia by Human Neutrophils. Mycoses 34: 141-143.

Richie, Feng X, Krishnan K, Askew DS. 2011. Secretion stress and antifungal resistance: An Achilles' heel of *Aspergillus fumigatus*? Medical Mycology 49: S101-S106.

Richie, et al. 2009. A role for the unfolded protein response (UPR) in virulence and antifungal susceptibility in *Aspergillus fumigatus*. PLoS Pathog 5: e1000258.

Riley PA. 1994. Free radicals in biology: oxidative stress and the effects of ionizing radiation. Int J Radiat Biol 65: 27-33.

Rivera A, Hohl TM, Collins N, Leiner I, Gallegos A, Saijo S, Coward JW, Iwakura Y, Pamer EG. 2011. Dectin-1 diversifies *Aspergillus fumigatus*-specific T cell responses by inhibiting T helper type 1 CD4 T cell differentiation. J Exp Med 208: 369-381.

Roberts SM, Winston F. 1997. Essential Functional Interactions of SAGA, a *Saccharomyces cerevisiae* Complex of Spt, Ada, and Gcn5 Proteins, With the Snf/Swi and Srb/Mediator Complexes. Genetics 147: 451-465.

Roilides E, Sein T, Roden M, Schaufele RL, Walsh TJ. 2001. Elevated serum concentrations of interleukin-10 in nonneutropenic patients with invasive aspergillosis. J Infect Dis 183: 518-520.

Roilides E, Dimitriadou A, Kadiltsoglou I, Sein T, Karpouzas J, Pizzo PA, Walsh TJ. 1997. IL-10 exerts suppressive and enhancing effects on antifungal activity of mononuclear phagocytes against *Aspergillus fumigatus*. J Immunol 158: 322-329.

Romani L. 2004. Immunity to fungal infections. Nat Rev Immunol 4: 11-24.

Romero-Martinez R, Wheeler M, Guerrero-Plata A, Rico G, Torres-Guerrero H. 2000. Biosynthesis and Functions of Melanin in *Sporothrix schenckii*. Infect. Immun. 68: 3696-3703.

Rooney HCE. 2005. Cladosporium Avr2 inhibits tomato Rcr3 protease required for Cf-2-dependent disease resistance. Science 310: 54-54.

Rosas A, Casadevall A. 1997. Melanization affects susceptibility of *Cryptococcus neoformans* to heat and cold. FEMS Microbiol Lett 153: 265 - 272.

Rosas A, Nosanchuk J, Feldmesser M, Cox G, McDade H, Casadevall A. 2000. Synthesis of polymerized melanin by *Cryptococcus neoformans* in infected rodents. Infect Immun 68: 2845 - 2853.

Rosenberg E, Koren O, Reshef L, Efrony R, Zilber-Rosenberg I. 2007. The role of microorganisms in coral health, disease and evolution. Nat Rev Micro 5: 355-362.

Roth AH, Dersch P. 2010. A novel expression system for intracellular production and purification of recombinant affinity-tagged proteins in *Aspergillus niger*. Appl Microbiol Biotechnol 86: 659-670.

Rouabhia M, Mukherjee PK, Lattif AA, Curt S, Chandra J, Ghannoum MA. 2011. Disruption of sphingolipid biosynthetic gene IPT1 reduces *Candida albicans* adhesion and prevents activation of human gingival epithelial cell innate immune defense. Med Mycol 49: 458-466.

Saeed AI, et al. 2003. TM4: a free, open-source system for microarray data management and analysis. Biotechniques 34: 374-378.

Sahni N, Yi S, Daniels KJ, Srikantha T, Pujol C, Soll DR. 2009. Genes Selectively Up-Regulated by Pheromone in White Cells Are Involved in Biofilm Formation in *Candida albicans*. PLoS Pathog 5: e1000601.

Schmaler-Ripcke J, Sugareva V, Gebhardt P, Winkler R, Kniemeyer O, Heinekamp T, Brakhage AA. 2009. Production of pyomelanin, a second type of melanin, via the tyrosine degradation pathway in *Aspergillus fumigatus*. Appl Environ Microbiol 75: 493-503.

Schmeda-Hirschmann G, Hormazabal E, Rodriguez JA, Theoduloz C. 2008. Cycloaspeptide A and pseurotin A from the endophytic fungus *Penicillium janczewskii*. Z Naturforsch C 63: 383-388.

Schmidt S, Tramsen L, Hanisch M, Latgé J-P, Huenecke S, Koehl U, Lehrnbecher T. 2011. Human Natural Killer Cells Exhibit Direct Activity Against *Aspergillus fumigatus* Hyphae, But Not Against Resting Conidia. Journal of Infectious Diseases 203: 430-435.

Schmittgen TD, Livak KJ. 2008. Analyzing real-time PCR data by the comparative CT method. Nat. Protocols 3: 1101-1108.

Schrettl, Bignell E, Kragl C, Joechl C, Rogers T, Arst HN, Haynes K, Haas H. 2004. Siderophore Biosynthesis But Not Reductive Iron Assimilation Is Essential for *Aspergillus fumigatus* Virulence. The Journal of Experimental Medicine 200: 1213-1219.

Schrettl, Bignell E, Kragl C, Sabiha Y, Loss O, Eisendle M, Wallner A, Arst HN, Jr., Haynes K, Haas H. 2007. Distinct roles for intra- and extracellular siderophores during *Aspergillus fumigatus* infection. PLoS Pathog 3: 1195-1207.

Schrettl, Carberry S, Kavanagh K, Haas H, Jones GW, O'Brien J, Nolan A, Stephens J, Fenelon O, Doyle S. 2010. Self-protection against gliotoxin--a component of the gliotoxin biosynthetic cluster, GliT, completely protects *Aspergillus fumigatus* against exogenous gliotoxin. PLoS Pathog 6: e1000952.

Schroeckh V, Scherlach K, Nutzmann HW, Shelest E, Schmidt-Heck W, Schuemann J, Martin K, Brakhage AA. 2009. Intimate bacterial-fungal interaction triggers biosynthesis of archetypal polyketides in *Aspergillus nidulans*. Proceedings of the National Academy of Sciences of the United States of America 106: 14558-14563.

Schué M, Maurin D, Dhouib R, N′Goma J-CB, Delorme V, Lambeau G, Carrière F, Canaan S. 2010. Two cutinase-like proteins secreted by *Mycobacterium tuberculosis* show very different lipolytic activities reflecting their physiological function. The FASEB Journal 24: 1893-1903.

Schweigert FJ, Wirth K, Raila J. 2004. Characterization of the microheterogeneity of transthyretin in plasma and urine using SELDI-TOF-MS immunoassay. Proteome Sci 2: 5.

Schwienbacher M, Israel L, Heesemann J, Ebel F. 2005. Asp f6, an Aspergillus allergen specifically recognized by IgE from patients with allergic bronchopulmonary aspergillosis, is differentially expressed during germination. Allergy 60: 1430-1435.

Sehgal A, Lee CY, Espenshade PJ. 2007. SREBP controls oxygen-dependent mobilization of retrotransposons in fission yeast. PLoS Genet 3: e131.

Serrano-Gomez D, Leal JA, Corbi AL. 2005. DC-SIGN mediates the binding of *Aspergillus fumigatus* and keratinophylic fungi by human dendritic cells. Immunobiology 210: 175-183.

Shaaban M, Palmer JM, El-Naggar WA, El-Sokkary MA, Habib el SE, Keller NP. 2010. Involvement of transposon-like elements in penicillin gene cluster regulation. Fungal Genet Biol 47: 423-432.

Shabab M, Shindo T, Gu C, Kaschani F, Pansuriya T, Chintha R, Harzen A, Colby T, Kamoun S, van der Hoorn RAL. 2008. Fungal Effector Protein AVR2 Targets Diversifying Defense-Related Cys Proteases of Tomato. The Plant Cell Online 20: 1169-1183.

Shao, Dixon JE, Merritt PM, Bao ZQ, Innes RW. 2002. A Yersinia effector and a pseudomonas avirulence protein define a family of cysteine proteases functioning in bacterial pathogenesis. Cell 109: 575-588.

Sharon H, Hagag S, Osherov N. 2009. Transcription Factor PrtT Controls Expression of Multiple Secreted Proteases in the Human Pathogenic Mold *Aspergillus fumigatus*. Infect. Immun. 77: 4051-4060.

Sheppard DC, Doedt T, Chiang LY, Kim HS, Chen D, Nierman WC, Filler SG. 2005. The *Aspergillus fumigatus* StuA protein governs the up-regulation of a discrete transcriptional program during the acquisition of developmental competence. Mol Biol Cell 16: 5866-5879.

Shi, Perkins RG, Fang H, Tong W. 2008a. Reproducible and reliable microarray results through quality control: good laboratory proficiency and appropriate data analysis practices are essential. Curr Opin Biotechnol 19: 10-18.

Shi, et al. 2005. Cross-platform comparability of microarray technology: Intra-platform consistency and appropriate data analysis procedures are essential. BMC Bioinformatics 6: S12.

—. 2008b. The balance of reproducibility, sensitivity, and specificity of lists of differentially expressed genes in microarray studies. BMC Bioinformatics 9 Suppl 9: S10.

Shwab, Bok JW, Tribus M, Galehr J, Graessle S, Keller NP. 2007. Histone deacetylase activity regulates chemical diversity in Aspergillus. Eukaryotic Cell 6: 1656-1664.

Siemann M, Koch-Dörfler M, Gaude M. 1998. False-positive results in premature infants with the Platelia®Aspergillus sandwich enzyme-linked immunosorbent assay. Mycoses 41: 373-377.

Smith JM, Tang CM, Van Noorden S, Holden DW. 1994. Virulence of *Aspergillus fumigatus* double mutants lacking restriction and an alkaline protease in a low-dose model of invasive pulmonary aspergillosis. Infect Immun 62: 5247-5254.

Soubani AO, Chandrasekar PH. 2002. The clinical spectrum of pulmonary aspergillosis. Chest 121: 1988-1999.

Steele C, Rapaka RR, Metz A, Pop SM, Williams DL, Gordon S, Kolls JK, Brown GD. 2005. The Beta-Glucan Receptor Dectin-1 Recognizes Specific Morphologies of *Aspergillus fumigatus*. PLoS Pathog 1: e42.

Stoldt VR, Sonneborn A, Leuker CE, Ernst JF. 1997. Efg1p, an essential regulator of morphogenesis of the human pathogen *Candida albicans*, is a member of a conserved class of bHLH proteins regulating morphogenetic processes in fungi. EMBO J 16: 1982-1991.

Sugui JA, Kim HS, Zarember KA, Chang YC, Gallin JI, Nierman WC, Kwon-Chung KJ. 2008. Genes differentially expressed in conidia and hyphae of *Aspergillus fumigatus* upon exposure to human neutrophils. PLoS ONE 3: e2655.

Sugui JA, Pardo J, Chang YC, Zarember KA, Nardone G, Galvez EM, Mullbacher A, Gallin JI, Simon MM, Kwon-Chung KJ. 2007a. Gliotoxin is a virulence factor of *Aspergillus fumigatus*: gliP deletion attenuates virulence in mice immunosuppressed with hydrocortisone. Eukaryot Cell 6: 1562-1569.

Sugui JA, et al. 2007b. Role of laeA in the Regulation of alb1, gliP, Conidial Morphology, and Virulence in *Aspergillus fumigatus*. Eukaryot Cell 6: 1552-1561.

Szewczyk E, Nayak T, Oakley CE, Edgerton H, Xiong Y, Taheri-Talesh N, Osmani SA, Oakley BR. 2006. Fusion PCR and gene targeting in *Aspergillus nidulans*. Nat Protoc 1: 3111-3120.

Takano Y, Kubo Y, Shimizu K, Mise K, Okuno T, Furusawa I. 1995. Structural analysis of PKS1, a polyketide synthase gene involved in melanin biosynthesis in *Colletotrichum lagenarium*. Mol Gen Genet 249: 162-167.

Takeda K, Takeuchi O, Akira S. 2002. Recognition of lipopeptides by Toll-like receptors. J Endotoxin Res 8: 459-463.

Tan PK, Downey TJ, Spitznagel EL, Jr., Xu P, Fu D, Dimitrov DS, Lempicki RA, Raaka BM, Cam MC. 2003. Evaluation of gene expression measurements from commercial microarray platforms. Nucleic Acids Res 31: 5676-5684.

Tang N, Tornatore P, Weinberger SR. 2004. Current developments in SELDI affinity technology. Mass Spectrom Rev 23: 34-44.

Taylor LH, Latham SM, woolhouse MEJ. 2001. Risk factors for human disease emergence. Philosophical Transactions of the Royal Society of London. Series B: Biological Sciences 356: 983-989.

Tekaia F, Latge JP. 2005. *Aspergillus fumigatus*: saprophyte or pathogen? Curr Opin Microbiol 8: 385-392.

Terpe K. 2003. Overview of tag protein fusions: from molecular and biochemical fundamentals to commercial systems. Appl Microbiol Biotechnol 60: 523-533.

Teutschbein J, Albrecht D, Pötsch M, Guthke R, Aimanianda V, Clavaud Cc, Latgé J-P, Brakhage AA, Kniemeyer O. 2010. Proteome Profiling and Functional Classification of Intracellular Proteins from Conidia of the Human-Pathogenic Mold *Aspergillus fumigatus*. Journal of Proteome Research 9: 3427-3442.

Thau N, Monod M, Crestani B, Rolland C, Tronchin G, Latge JP, Paris S. 1994. Rodletless Mutants of *Aspergillus fumigatus*. Infection and Immunity 62: 5706-5706.

Then Bergh K, Brakhage AA. 1998. Regulation of the *Aspergillus nidulans* penicillin biosynthesis gene acvA (pcbAB) by amino acids: implication for involvement of transcription factor PACC. Appl Environ Microbiol 64: 843-849.

Thewes S, Kretschmar M, Park H, Schaller M, Filler SG, Hube B. 2007. In vivo and ex vivo comparative transcriptional profiling of invasive and non-invasive *Candida albicans* isolates identifies genes associated with tissue invasion. Mol Microbiol 63: 1606-1628.

Thomas PA. 2003. Current perspectives on ophthalmic mycoses. Clin Microbiol Rev 16: 730-797.

Thywiben A, Heinekamp T, Dahse H-M, Schmaler-Ripcke J, Nietsche S, Zipfel PF, Brakhage AA. 2011. Conidial dihydroxynaphthalene melanin of the human pathogenic fungus *Aspergillus fumigatus* interferes with the host endocytosis pathway. Frontiers in Microbiology 2.

Timberlake WE, Marshall MA. 1989. Genetic engineering of filamentous fungi. Science 244: 1313-1317.

Tkalcevic J, Novelli M, Phylactides M, Iredale JP, Segal AW, Roes J. 2000. Impaired immunity and enhanced resistance to endotoxin in the absence of neutrophil elastase and cathepsin G. Immunity 12: 201-210.

Todd BL, Stewart EV, Burg JS, Hughes AL, Espenshade PJ. 2006. Sterol Regulatory Element Binding Protein Is a Principal Regulator of Anaerobic Gene Expression in Fission Yeast. Mol. Cell. Biol. 26: 2817-2831.

Tomee JF, Hiemstra PS, Heinzel-Wieland R, Kauffman HF. 1997. Antileukoprotease: an endogenous protein in the innate mucosal defense against fungi. J Infect Dis 176: 740-747.

Tramsen L, et al. 2009. Clinical-scale generation of human anti-Aspergillus T cells for adoptive immunotherapy. Bone Marrow Transplantation 43: 13-19.

Triantafilou M, Gamper FG, Haston RM, Mouratis MA, Morath S, Hartung T, Triantafilou K. 2006. Membrane sorting of toll-like receptor (TLR)-2/6 and TLR2/1 heterodimers at the cell surface determines heterotypic associations with CD36 and intracellular targeting. J Biol Chem 281: 31002-31011.

Tsai HF, Wheeler MH, Chang YC, Kwon-Chung KJ. 1999. A developmentally regulated gene cluster involved in conidial pigment biosynthesis in *Aspergillus fumigatus*. J Bacteriol 181: 6469-6477.

Tsai HF, Chang YC, Washburn RG, Wheeler MH, Kwon-Chung KJ. 1998. The developmentally regulated alb1 gene of *Aspergillus fumigatus*: its role in modulation of conidial morphology and virulence. J Bacteriol 180: 3031-3038.

Tsuji G, Kenmochi Y, Takano Y, Sweigard J, Farrall L, Furusawa I, Horino O, Kubo Y. 2000. Novel fungal transcriptional activators, Cmr1p of *Colletotrichum lagenarium* and pig1p of *Magnaporthe grisea*, contain Cys2His2 zinc finger and Zn(II)2Cys6 binuclear cluster DNA-binding motifs and regulate transcription of melanin biosynthesis genes in a developmentally specific manner. Mol Microbiol 38: 940-954.

Twumasi-Boateng K, Sheppard DC, Yu Y, Chen D, Gravelat FN, Nierman WC. 2009. Transcriptional Profiling Identifies a Role for BrlA in the Response to Nitrogen Depletion and for StuA in the Regulation of Secondary Metabolite Clusters in *Aspergillus fumigatus*. Eukaryotic Cell 8: 104-115.

Valiante V, Jain R, Heinekamp T, Brakhage AA. 2009. The MpkA MAP kinase module regulates cell wall integrity signaling and pyomelanin formation in *Aspergillus fumigatus*. Fungal Genet Biol 46: 909-918.

Vallor AC, Kirkpatrick WR, Najvar LK, Bocanegra R, Kinney MC, Fothergill AW, Herrera ML, Wickes BL, Graybill JR, Patterson TF. 2008. Assessment of *Aspergillus fumigatus* Burden in Pulmonary Tissue of Guinea Pigs by Quantitative PCR, Galactomannan Enzyme Immunoassay, and Quantitative Culture. Antimicrob. Agents Chemother. 52: 2593-2598.

van Esse HP, Van't Klooster JW, Bolton MD, Yadeta KA, van Baarlen P, Boeren S, Vervoort J, de Wit PJ, Thomma BP. 2008. The Cladosporium fulvum virulence protein Avr2 inhibits host proteases required for basal defense. Plant Cell 20: 1948-1963.

Vasil ML, Stonehouse MJ, Vasil AI, Wadsworth SJ, Goldfine H, Bolcome RE, 3rd, Chan J. 2009. A complex extracellular sphingomyelinase of *Pseudomonas aeruginosa* inhibits angiogenesis by selective cytotoxicity to endothelial cells. PLoS Pathog 5: e1000420.

Viguera E, Canceill D, Ehrlich SD. 2001. Replication slippage involves DNA polymerase pausing and dissociation. EMBO J 20: 2587-2595.

Vodisch M, Scherlach K, Winkler R, Hertweck C, Braun HP, Roth M, Haas H, Werner ER, Brakhage AA, Kniemeyer O. 2011. Analysis of the *Aspergillus fumigatus* proteome reveals metabolic changes and the activation of the pseurotin A biosynthesis gene cluster in response to hypoxia. J Proteome Res 10: 2508-2524.

Volff J-N. 2006. Turning junk into gold: domestication of transposable elements and the creation of new genes in eukaryotes. Bioessays 28: 913-922.

Walker LA, Maccallum DM, Bertram G, Gow NA, Odds FC, Brown AJ. 2009. Genome-wide analysis of *Candida albicans* gene expression patterns during infection of the mammalian kidney. Fungal Genet Biol 46: 210-219.

Walsh TJ, McEntee C, Dixon DM. 1987. Tissue homogenization with sterile reinforced polyethylene bags for quantitative culture of *Candida albicans*. J Clin Microbiol 25: 931-932.

Walton JD. 2000. Horizontal gene transfer and the evolution of secondary metabolite gene clusters in fungi: an hypothesis. Fungal Genet Biol 30: 167-171.

Wang, Casadevall A. 1994. Decreased Susceptibility of Melanized *Cryptococcus neoformans* to UV-Light. Applied and Environmental Microbiology 60: 3864-3866.

Wang, Aisen P, Casadevall A. 1995. *Cryptococcus neoformans* melanin and virulence: mechanism of action. Infect Immun 63: 3131-3136.

Wang, Wang XF, Liu J, Ishii M, Igarashi Y, Cui ZJ. 2007. Effect of oxygen concentration on the composting process and maturity. Compost Science & Utilization 15: 184-190.

Wartenberg D, Lapp K, Jacobsen ID, Dahse H-M, Kniemeyer O, Heinekamp T, Brakhage AA. 2011. Secretome analysis of *Aspergillus fumigatus* reveals Asp-hemolysin as a major secreted protein. International Journal of Medical Microbiology 301: 602-611.

Warwas ML, Watson JN, Bennet AJ, Moore MM. 2007. Structure and role of sialic acids on the surface of *Aspergillus fumigatus* conidiospores. Glycobiology 17: 401-410.

Waugh DS. 2005. Making the most of affinity tags. Trends in Biotechnology 23: 316-320.

Wenke J, Anke H, Sterner O. 1993. Pseurotin-a and 8-O-Demethylpseurotin-a from *Aspergillus fumigatus* and Their Inhibitory Activities on Chitin Synthase. Bioscience Biotechnology and Biochemistry 57: 961-964.

Werner JL, Metz AE, Horn D, Schoeb TR, Hewitt MM, Schwiebert LM, Faro-Trindade I, Brown GD, Steele C. 2009. Requisite role for the dectin-1 beta-glucan receptor in pulmonary defense against *Aspergillus fumigatus*. J Immunol 182: 4938-4946.

Wezensky SJ, Cramer RA. 2011. Implications of hypoxic microenvironments during invasive aspergillosis. Medical Mycology 49: S120-S124.

Willger SD, Puttikamonkul S, Kim K-H, Burritt JB, Grahl N, Metzler LJ, Barbuch R, Bard M, Lawrence CB, Cramer RA, Jr. 2008. A Sterol-Regulatory Element Binding Protein Is Required for Cell Polarity, Hypoxia Adaptation, Azole Drug Resistance, and Virulence in *Aspergillus fumigatus*. PLoS Pathog 4: e1000200.

Williams RB, Henrikson JC, Hoover AR, Lee AE. 2008. Epigenetic remodeling of the fungal secondary metabolome. Organic & Biomolecular Chemistry 6: 1895-1897.

Yamazaki M, Suzuki S, Kukita KI. 1979. Neurotoxical Studies on Fumitremorgin-a, a Tremorgenic Mycotoxin, on Mice. Journal of Pharmacobio-Dynamics 2: 119-125.

Yang Z, Jaeckisch SM, Mitchell CG. 2000. Enhanced binding of *Aspergillus fumigatus* spores to A549 epithelial cells and extracellular matrix proteins by a component from the spore surface and inhibition by rat lung lavage fluid. Thorax 55: 579-584.

Yeghen T, Kibbler CC, Prentice HG, Berger LA, Wallesby RK, McWhinney PHM, Lampe FC, Gillespie S. 2000. Management of Invasive Pulmonary Aspergillosis in Hematology Patients: A Review of 87 Consecutive Cases at a Single Institution. Clinical Infectious Diseases 31: 859-868.

Yu JH, Keller N. 2005. Regulation of secondary metabolism in filamentous fungi. Annu Rev Phytopathol 43: 437-458.

Yu JH, Butchko RAE, Fernandes M, Keller NP, Leonard TJ, Adams TH. 1996. Conservation of structure and function of the aflatoxin regulatory gene aflR from *Aspergillus nidulans* and *A. flavus*. Current Genetics 29: 549-555.

Zhang, Richardson DO, Roberts DN, Utley R, Erdjument-Bromage H, Tempst P, Cote J, Cairns BR. 2004. The Yaf9 component of the SWR1 and NuA4 complexes is required for proper gene expression, histone H4 acetylation, and Htz1 replacement near telomeres. Mol Cell Biol 24: 9424-9436.

Zhang, et al. 2002. Contribution of human alpha-defensin 1, 2, and 3 to the anti-HIV-1 activity of CD8 antiviral factor. Science 298: 995-1000.

Zhu Z, Zheng T, Homer RJ, Kim YK, Chen NY, Cohn L, Hamid Q, Elias JA. 2004. Acidic mammalian chitinase in asthmatic Th2 inflammation and IL-13 pathway activation. Science 304: 1678-1682.

Zmeili OS, Soubani AO. 2007. Pulmonary aspergillosis: a clinical update. QJM 100: 317-334.

Acknowledgements

I am hugely indebted to my supervisor, Dr Elaine Bignell, for the support, hard work, patience and inspiration. I am deeply grateful for her dedication to both my project and academic development, and I thank her for making the four years in her laboratory such a fantastic and enjoyable experience.

My sincere thanks also go to the following people:

All members of the Bignell, Haynes and Arst laboratories for continued help and friendship throughout my PhD.

Margherita Bertuzzi, Laura Alcazar-Fuoli and Hwen-yee Chea for uncountable acts of kindness

Professor Ken Haynes, for friendship and inspiration

My oldest friend James Osborn, for unquestionable companionship, loyalty and hilarity

Special thanks to my mum, dad and brothers Benny, Matt and Mike

I thank Vicky Bond for love, support, and so many other things, not least introducing me to Ginger (who never left my side for a single hour of writing)

This thesis is submitted with sadness that a young chemist and friend, Mark Dare, passed away before he had the opportunity to do the same.